Development of methods to predict the discharge capacity in model and prototype meandering compound channels

by

Alasdair Breac MacLeod, B.Eng.

UNIVERSITY
of
GLASGOW

Thesis submitted to the University of Glasgow
in candidature for the degree of
Doctor of Philosophy

Department of Civil Engineering
University of Glasgow

December 1997

ABSTRACT

This thesis summarises the work undertaken by the author whilst employed at Glasgow University as part of a research team contracted to the EPSRC Series B extension programme. The main remit of this programme was to investigate flow behaviour in small-scale meandering compound channel models and to develop improved methods for predicting the discharge capacity of uniform channels and non-uniform channels. The Series B extension programme ran between October 1993 and November 1996 and was funded by EPSRC grant GR/J41048. The research team was comprised of researchers from three collaborating Institutions:- the University of Glasgow, the University of Aberdeen and the University of Bristol.

The research team shared responsibility for investigating the influence of 11 geometric and geomorphic parameters on meandering compound channel flow. The author built and tested models to investigate the influence of 7 parameters on flow behaviour in meandering compound channels. These parameters were: relative overbank flow depth, relative meander belt width, main channel side slope, model scale, relative roughness between the flood plain and main channel, main channel shape and main channel aspect ratio (width/depth). The team in Aberdeen University investigated the influence of 5 parameters: relative overbank flow depth, relative roughness, main channel side slope, main channel shape and main channel sinuosity. The team in Bristol University built and investigated the influence of 5 parameters: longitudinal flood plain slope, lateral flood plain slope, relative meander belt width, relative depth, and flood bank sinuosity; unfortunately they had not published their results at the time of writing this thesis. Fifty-six small scale models in total were built and tested in Glasgow and Aberdeen Universities and detailed schedules of the global and local flow data which were collected by the author in Glasgow are tabulated in Appendices A1 and A2.

The author identified how the relative variation in flow state in the main and flood plain channels at different flow depths affects the nature of the flow interaction mechanisms between these two layers in meandering compound channels. An hypothesis is forwarded which explains how these changes in interaction mechanism are linked to the creation of the characteristic 4 flow regions which are revealed in meandering compound channel flow by plotting relative depth versus the non dimensional discharge

parameter known as F*. The use of the F* parameter enables the influence of bed friction to be stripped away in order to reveal the magnitude of flow resistance generated by the layer interactions. The nature of the interaction mechanisms in different scale models was shown to be similar in comparable flow regions. The author was therefore able to combine flow data from various scale models when developing the improved discharge capacity prediction methods.

The author developed two methods for predicting the discharge capacity of uniform meandering compound channels. The first method utilised an Artificial Neural Network (ANN) functional approximator which was taught to replicate the relationship between 9 of the key parameters and the magnitude of F* which was exhibited by the flow data gathered during the Series B extension (1993-1996) programme. The ANN approximator was constructed using a 'Matlab' software environment and was supported on a PC. The second method consisted of a semi-physical / semi-empirical method which was named the Enhanced zonal method. This method comprised formulations which explicitly determined the discharge capacity of the 3 individual flow zones in meandering compound channels whilst accounting for differences induced by the characteristic 4 flow region behaviour.

The author demonstrated that both of these methods produce more accurate discharge capacity predictions than the James and Wark [1] [1992] method for the majority of available flow data sets. The James and Wark [1] [1992] method was the optimal method prior to the Series B extension (1993-1996) programme. The ANN approximator gave the most accurate predictions when the parameters of the compound channels to which it was applied fell within the range of the parameters incorporated in the ANN training data set. However, the author demonstrated that the Enhanced zonal method is the most reliable discharge capacity prediction method over the full range of uniform meandering compound channel configurations.

The author developed two refined one-dimensional (1D) numerical models (for application to both steady and unsteady flow conditions) which incorporated the Ackers [1991] and James and Wark [1] [1992] methods to determine the conveyance characteristics at representative uniform cross-sections in natural meandering compound

channels. The author demonstrated, using a case study of the River Dane, that these refined 1D models were able to predict the water surface profiles in natural channels to a high degree of accuracy. They explicitly account for the layer interactions in the river channels and are therefore able to give more reliable predictions than are traditionally achievable. This is especially significant when the available calibration data is suspect or sparsely defined which makes the classic friction factor adjustment approach to accounting for extra sources of head loss less than reliable. The author notes that these models and their descendants will be of considerable benefit to the Hydraulic Engineering community, once they have been comprehensively validated and incorporated into a commercially available model, such as Hec-RAS. However this will take time and will require further work. In anticipation the author developed a 10 point design procedure with Dr A. Ervine to assist River Engineers with their design of compound channel flood protection works whilst making use of the benefits offered by the author's refined 1D numerical models.

ACKNOWLEDGEMENTS

The author is very grateful for the insight, encouragement, supervision and friendship which he received from Professor Alan Ervine during the Series B extension programme and the writing of this thesis. The memories of our time and work together in Glasgow will always be important to me. I also offer many thanks to Dr Gareth Pender whose observations and comments greatly assisted me with my research.

In addition I owe a considerable debt of gratitude to the other members of the Series B extension programme which included Professor R H J Sellin and Catherine Wilson from Bristol University and Professor B B Willetts and Paresh Rameshwaran from Aberdeen University. Their professionalism, conceptual observations and teamwork ensured the programme ran smoothly and successfully. The quarterly meetings which were held throughout the course of the programme were always stimulating, intellectually challenging and rewarding. I look forward to maintaining contact in the future and I hope that we will have the opportunity to collaborate together once again.

I also want to thank my other colleagues and friends who coincided with me during my time in Glasgow. In particular I remember my fellow researchers: Dr Waseem Khalifa, Dr Jason Beith, Dr Mahmood Alsayed, Francesco Basile and Alistair Nisbet. I thank them for being there to discuss the issues of the day both academic and social. Many thanks are also offered to Dr Yen Liu and Professor David Murray-Smith from the Department of Electrical Engineering at the University of Glasgow for introducing me to the fascinating world of Artificial Neural Networks which eventually comprised a significant proportion of my thesis. In addition all the contributions made by the technical and computer support staff within the Department of Civil Engineering were greatly appreciated. Special thanks must go to Mr Ken McColl, Mr Stuart Mclean and Mr Alan Burnett. Thanks are also due to the Department of Civil Engineering at Glasgow University, headed by Dr Graham Herbertson, for making the facilities available for me to pursue my research and for introducing me to the cut-throat world of inter-departmental academic 5-a-side football. I hope that all my team-mates' hamstrings stay stretched and viable for many years to come.

Finally and most importantly I extend my thanks to my wife and family whose support and humour have buoyed me through the difficult times and whose friendship has enhanced the good times. I thank my father, brother and sister who were continually encouraging. It is a pleasure to share my life with them. I thank Ceridwen Mavis (Mum) who was always there for me, whether the times were good or bad. From the start, to first turn on the pumps, right through to the present with her good-natured chivvying pressing me to finally submit. As my adviser she is much more valued than she can ever realise and she is a great friend. She has revealed countless opportunities and insights to me during this life and I am eternally grateful.

To conclude however my greatest vote of thanks is offered to Joey Boger MacLeod, my wife, to whom I dedicate this thesis. I will always remember her invigorating optimism and support throughout all the times when I was a research hermit. I love you and I look forward with great hope to our life together.

TABLE OF CONTENTS

5. THE DEVELOPMENT OF AN ARTIFICIAL NEURAL NETWORK TO PREDICT THE DISCHARGE CAPACITY OF MEANDERING COMPOUND CHANNELS 269

NOTATION

α	energy coefficient
β	momentum coefficient
φ	main channel cross-sectional shape
τ_b	bed shear stress
θ_m	mean angle between flood plain centre line and main channel
θ_{sk}	slot skew angle
ϕ_{SS}	main channel side slope
S_S	main channel side slope
a	meander amplitude
A	cross-sectional area
AR	aspect ratio
B	top width of main channel
b	the neuron bias in an Artificial Neural Network
$B_{1,2}$	blockage effect for Ackers [1991] method
C	Chezy bed friction parameter
c	coefficient in the James and Wark [1] [1992] equation for the zone 1 adjustment factor
C_{sl}	length coefficient for expansion and contraction losses, zone 2
C_{sse}	side slope coefficient for contraction loss, zone 2
C_{sse}	side slope coefficient for expansion loss, zone 2
C_{wc}	combined contraction head loss coefficient, zone 2
C_{wd}	shape coefficient for expansion and contraction losses, zone 2
C_{we}	combined expansion head loss coefficient, zone 2
D	the local depth of flow
f'	relative Reynolds number
f , λ	Darcy-Weisbach friction factor due to bed friction only
F	General flow region parameter
F_{B1}	Flow region parameter for Zone B1
F_{B2}	Flow region parameter for Zone B2
F*	a non-dimensional measure of discharge capacity
$F_{1,2}$	flow parameters to account for slot resistance
Fr	Froude number
g	the gravitational acceleration
h	hydraulic depth of main channel, = A/B
$h_{1,2}$	the elevation of the free water surface
h_f	head loss due to bed friction
h_L	head loss through a bend
K_T	total head loss adjustment coefficient in the James and Wark [1] [1992]
K_c	contraction coefficient
K_e	expansion coefficient

K_{meas}	measured head loss adjustment coefficient
L , λ_m	meander wavelength
L_r	the length scale ratio in a model
m	coefficient in the James and Wark [1] [1992] equation for the zone 1 adjustment factor
M_w	relative meander belt width
n	Manning's friction parameter bed friction only
n'	Manning's friction parameter including bend losses
$n_{1,2}$	number of laterally spaced dowel rods
$N_{1,2}$	number of longitudinally spaced dowel rods
O_1	output values from an ANN
P	wetted perimeter
P_1	input values from an ANN
Q_A'	adjustment factor for Zone A discharge
$Q_{A, B, C}$	the discharge capacity of Zones A, B or C.
Q_{bf}	main channel bankfull discharge
Q_{calc}	calculated discharge
Q_{meas}	measured discharge
r	main channel sinuosity
R	Hydraulic radius
r_b	flood bank sinuosity
R_c	mean radius of curvature
RD	relative depth
Re	Reynolds number
Re'	Relative Reynolds number
S_L	lateral flood plain slope
S_o	flood plain gradient
T_1	ANN target values for training ANNs
V	average velocity
v	point velocity
v	The kinematic viscosity of a fluid
v_t	The kinematic eddy viscosity
w_1	The numerical weighting applied to an ANN neuron
W_T	width of the flood plain
y_2	flood plain flow depth
y'	a non-dimensional flow depth on flood plain, = $y_2/(A/B)$

TABLE OF FIGURES

Chapter 1

Chapter 2

Chapter 3

Chapter 4

Chapter 5

Chapter 6

Chapter 7

LIST OF TABLES

Chapter 2

Chapter 3

Chapter 4

Chapter 5

Chapter 6

Chapter 7

Chapter 1

1. An introduction

1.1 River flooding and compound channels

When flood water over-tops the banks of the main river channel and inundates the flood plains the repercussions can be devastating, especially if man has decided to inhabit these integral components of the natural river channel. Figure 1.1 shows a photograph of the market area in Netheravon, near Salisbury, Wiltshire which was taken in January 1915. Unfortunately Netheravon has been built in the flood plain of the River Avon.

Figure 1.1 Netheravon, near Salisbury, Wiltshire (January 1915)

Normally, if man does not intervene, the surplus discharge which is created in the time of a flood will use the flood plains to provide the extra storage capacity that is required to facilitate the transmission of the flood waters down the river corridor to the sea. A

compound channel is formed such as the one shown in Figure 1.2. The total flood discharge is contained within a combination of the lower, main river channel and the upper, flood plain channel.

Figure 1.2 A natural compound channel, the River Wylye near Salisbury (May 1979)

Throughout history however, humans have had an unfortunate tendency to establish settlements within these naturally-occurring compound channels (on the flood plains of a river) despite the risk of periodic flooding and the ensuing danger posed to countless lives and assets. It is a River Engineer's responsibility to predict the impact of flooding on these settlements and to develop strategies / flood defence schemes (with an appropriate cost to benefit ratio) in order to protect against such flooding.

The magnitude of the damage and hence cost which is suffered in the event of a flood depends on the extent of flood plain inundation. The level of the water surface will dictate the extent of this inundation. The water surface level adjusts until the channel area provided is adequate to pass a certain volume of flood water down a river corridor. The channel area required depends on the flow velocity in the channel which in turn depends on the resistance to flow exerted by bed friction and other head loss

mechanisms. There are many methods available to the River Engineer with which to determine the discharge capacity of a compound channel.

1.2 Discharge capacity prediction methods for compound channels

For nearly 50 years various researchers have explored the nature of flow in compound channels. They have developed a number of discharge capacity prediction methods with which to determine the impact of flooding on communities and to design methods to protect these communities against flooding. These prediction methods have fallen into three broad categories:-

- **Hand calculation / Deterministic methods**

The most accurate of these are:- Ackers [1991] for straight compound channels and James and Wark [1992] for meandering compound channels. These deterministic methods apply empirical adjustments to basic theoretical models.

- **Simple turbulence models**

These explicitly determine the magnitude of lateral turbulent shear which is the dominant mechanism resulting from the layer interaction in straight compound channels. This method has been employed by Knight *et al* [1989] in an analytical method and by Wark et al [1990] using a finite difference method. Such models predict the depth-averaged velocity which is integrated to obtain discharge capacity at any flow depth.

- **Navier-Stokes flow equation models**

Many attempts have been made over the years to solve the three dimensional Navier-Stokes flow equations when applied to rivers. The one-dimensional numerical models for steady and unsteady flow, which are obtained by simplifying the basic Navier-Stokes equations, have proved to be very popular with the engineering community. They have had widespread use and have been shown to be capable of producing excellent estimates for the relationship between water surface level and discharge rate in most natural channels. However they are limited because the flow characteristics at each cross-section are obtained by simply averaging the flow velocity over the whole channel cross-section area. Consequently they do not model the true three-dimensional nature of flow in the channels. Although the one-dimensional models have been used with a great deal of success, engineers are attracted by the extra information about local flow fields which would be provided by the two and three dimensional numerical models.

Two and three dimensional flow field information would enable an engineer to judge with more accuracy the impact of various flows on the geomorphology of erosion-prone river channels and to determine local fluctuations in water level. Various attempts have been made to develop improved two and three-dimensional models often based on adaptations of the Navier-Stokes equations. Such models have included Algebraic stress models and Reynolds stress models which both attempt to model the local flow velocities and turbulence fields. However these models are cumbersome to apply to natural channels because they are computationally burdensome and consequently they can not easily be practically or economically implemented. Developments in computing power may facilitate their more widespread use in the future.

1.3 The SERC Series A and B experimental programmes (1985-1992)

With the results of so much independent research into compound channel behaviour being available prior to 1985, a River Engineer was often faced with the difficult task of sorting through the available options in order to find the discharge capacity prediction method which was most suitable and reliable for his/her particular problem. Consequently, the Science and Engineering Research Council (SERC) decided to fund the Series A (1985-1988) and Series B (1989-1992) research programmes which were intended to produce high quality, larger scale model flow data which could be used to:

1. Refine the general understanding of flow behaviour in compound channels
2. Appraise existing prediction methods
3. Facilitate the development of improved discharge capacity prediction methods.

The Series A programme concentrated on straight and skew meandering compound channels and the Series B programme concentrated on meandering compound channels. The two optimal methods for predicting discharge capacity which were produced as a result of the Series A and B programmes were: Ackers [1991] for straight compound channels and James and Wark [1992] for meandering compound channels. They were published by the National Rivers Authority in NRA [1993]. The James and Wark [1992] method does represent the optimum deterministic method that is available for predicting the discharge capacity of a meandering compound channel but it still suffers from a number of limitations. It was devised using a limited range of flow data which did not

make allowance for every influential geometric and flow state parameter which influence meandering compound channel flow. Therefore it can not be completely relied upon for application to compound channels with configurations significantly different to the ones used to develop it. Consequently the Series B extension (1993-1996) programme was commissioned with a remit to build and test a large number of small scale physical models. The results that were produced were intended to:

1. Fill in the gaps in the existing flow data set that were left after the Series B (1989-1992) programme.
2. To facilitate the production of improved discharge capacity prediction methods
3. To assist with the development of a technique for applying these discharge capacity prediction methods for uniform channels to natural non-uniform rivers.

1.4 The scope of the EPSRC Series B extension (1993-1996) programme

The Series B extension programme ran between 1993 and 1996 and was funded at Glasgow through an EPSRC grant (GR/J41048) with parallel grants at Bristol and Aberdeen. The members of the programme postulated that eleven parameters influence flow behaviour in meandering compound channels. The three Institutions co-ordinated their physical modelling programmes so that the responsibility for testing all eleven was shared between them. Each Institution had access to all the flow data which was produced in order to develop their own individual discharge capacity prediction methods. However, the methods devised in Aberdeen and Bristol are not reviewed in this thesis because they were either unfinished or unpublished at the time of writing.

1.5 The scope of this thesis

Chapter 2 initially describes why interest in compound channels has grown in recent years because of their viability as environmentally sensitive flood defence solutions. However a number of the features of these channels which have limited their widespread implementation are also identified. The rest of the chapter is dedicated to presenting a review of the literature, which documents the significant advances towards divulging the nature of compound channel flow behaviour, made by the Engineering Community from 1953 to the present day. The relative merits of the various deterministic discharge capacity prediction methods and numerical models that have

been developed are discussed. All the existing meandering compound channel flow data which is accompanied by reliable bed friction calibration data was compiled and analysed.

Chapter 3 details the physical modelling methods, the channel configurations and the flow measurement techniques which were used in all the meandering compound channel and slot model tests which were performed at University of Glasgow during the Series B extension (1993-1996) programme.

Chapter 4 presents the flow data which was obtained from the meandering compound channel model tests in Glasgow are presented. The influence of 11 key parameters on the layer interaction mechanisms and resulting flow resistance is highlighted. Plots of relative depth versus Global F* (a non-dimensional discharge coefficient for the whole channel) were used in order to illustrate that 4 flow regions are typically generated in meandering compound channel flow. The author demonstrates that the flow behaviour in channels of different scales is similar in nature. Finally, the results obtained from some additional slot model experiments are presented. The influence of 5 key parameters on this head loss was demonstrated.

Chapter 5 details the steps taken by the author in the development of an Artificial Neural Network (ANN) to predict the discharge capacity in a meandering compound channel. The novel ANN model was designed (trained) to predict the discharge capacity of any meandering compound channel by approximating the functional relationship exhibited by the flow results gathered during the Series B extension (1993-1996) programme, which related the water surface level to the discharge capacity (measured using the non-dimensional discharge parameter, F*) of a meandering compound channel. The final ANN model was tested against an independent set of flow data and its accuracy was assessed.

Chapter 6 concentrates on the development and testing of the Enhanced zonal method for predicting discharge capacity in a meandering compound channel. The author developed this method by enhancing the original James and Wark discharge prediction method for meandering compound channels using the data gathered during the Series B

extension (1993-1996) programme. This method incorporates separate discharge capacity prediction methods for 3 flow zones in a meandering compound cross-section and explicitly accounts for the differences in flow behaviour between the 4 flow regions which characterise meandering compound channel flow. The accuracy of the Enhanced zonal method was tested using a number of independent flow data sets which were collected during the Series B extension programme. Finally, the Enhanced zonal method predictions are compared and contrasted with the corresponding predictions obtained using the ANN method and the original James and Wark [1992] method.

Chapter 7 describes the development of a refined one-dimensional (1D) numerical model for predicting the relationship between water surface level and discharge rate in natural channels. It was soluble for both steady and unsteady flows. The 1D model was tested against two sets of flooding calibration data for the River Dane, Cheshire and the results are compared with those obtained using a traditional 1D model, Mike 11 from a previous study. The relative merits of the traditional and refined numerical models are discussed. A number of design proposals are suggested for distant flood bank schemes which might possibly meet the Environment Agency's development control criteria and therefore enable development to proceed on the flood plains of the River Dane, outwith the constructed flood banks. A 10 point design procedure was developed to assist River Engineers with their design of compound channel flood protection works whilst making use of the benefits offered by a refined 1D numerical model.

Chapter 8 presents a summary of the author's conclusions regarding the nature of flow behaviour in meandering compound channels and an assessment of the relative performance of the various discharge capacity methods which were developed and tested by the author during the Series B extension (1993-1996) programme.

Chapter 9 presents the recommendations made by the author for future research in the field of meandering compound channels.

Chapter 2

2. Compound channels: A literature review

2.1 Introduction

Natural river channels behave like compound channels. In summer the water levels normally remain below the bankfull level of the main channel forming a simple channel. However, in winter, prolonged periods of heavy rainfall regularly result in the main channel being unable to carry the volume of run-off issuing from the whole river catchment. The excess water spills over the main river channel banks and inundates the flood plains (forming a compound channel) which in combination can provide the extra capacity to pass these large volumes of water down the river corridor to the sea. The flood plains are an integral part of the river itself. One such typical river is shown in Figure 2.1.

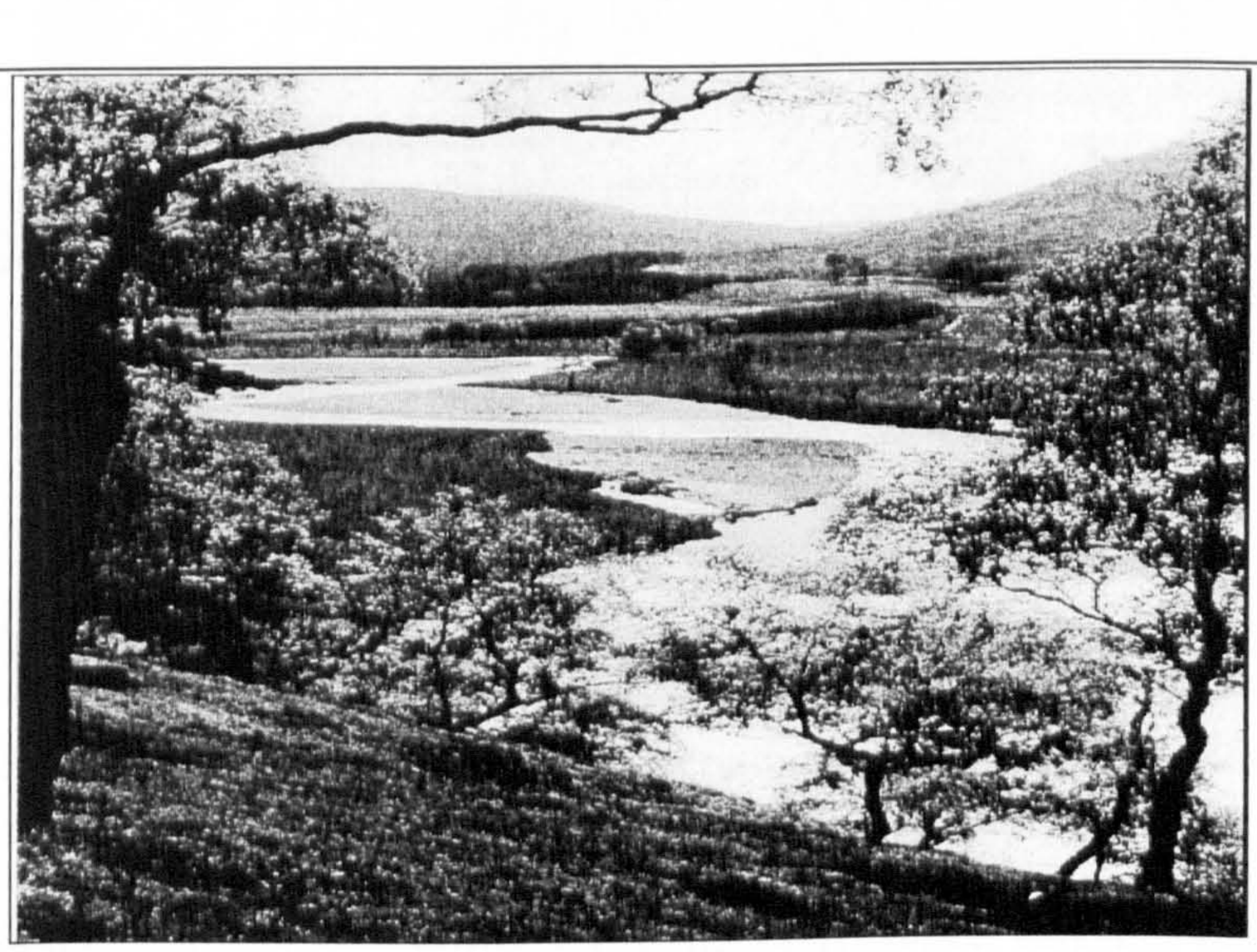

Figure 2.1 Natural flood plains and main channel of the River Dee (after Sellin [1996])

In recent times development pressures resulting from an ever-growing human population have resulted in encroachment of man-made constructions into the flood plains as space and opportunity on other sites becomes more and more scarce. However there is a penalty to pay for this approach. Not only will the properties themselves be at

risk from flooding, but because their presence will lead to a reduction in conveyance and volume storage capacity of the river there will be an increased level of risk to third parties. Flood plains act as temporary flood water storage areas reducing the peak of the passing flood wave and providing extra local conveyance capacity.

To maintain the conveyance capacity of a river and protect the assets and lives at risk in the flood plain, engineers have traditionally tended to straighten, widen, dredge and even build up the banks of the main channels. Flood plains have become disconnected from the main river channel which has caused damage to local wetlands, and previously stable river geomorphologies have been made unstable and consequently unsustainable. In order to avoid this detrimental impact, in recent years there has been a tendency to create artificial compound channels by building flood banks offset from the banks of the main river channel as shown in Figure 2.2.

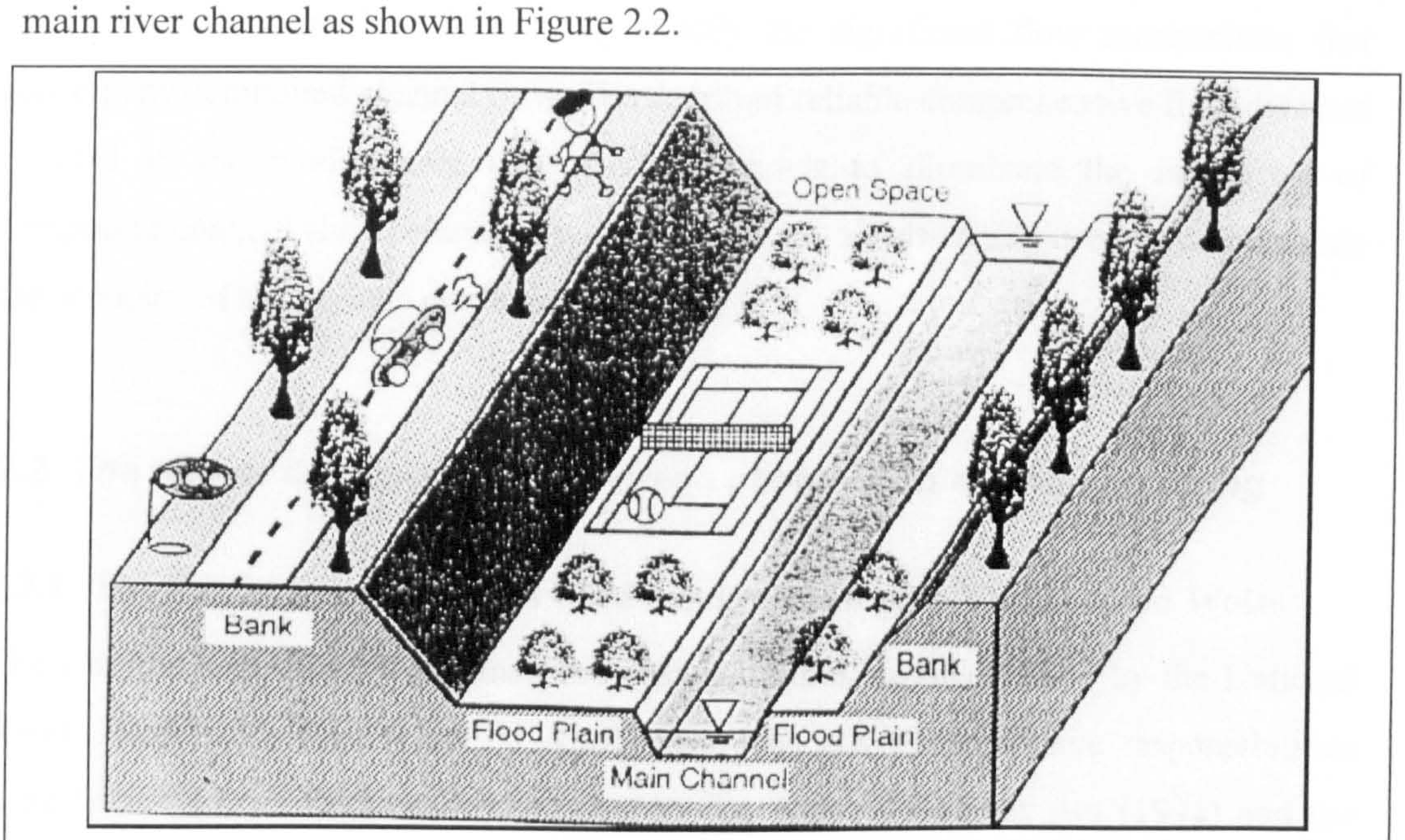

Figure 2.2 Artificial flood banks creating a compound channel (after Nezu [1994])

These compound channels still utilise the extra conveyance carrying capacity of the flood plains which are left naturally connected to the main river channel, although this capacity is reduced to an extent determined by the area of flood plains which are cut-off from the main channel. The artificial compound channels are more geomorphologically stable and environmentally sensitive because the main channel is left untouched during their construction. The author suggests that in addition to the obvious difficulties of lack

of land availability and the potential cost implications, the absence of reliable methods for predicting the discharge capacity of these channels has hindered the widespread implementation of these environmentally-beneficial schemes.

This chapter elaborates the general difficulties which must be overcome under current restraints to enable the successful implementation of compound channel flood defence schemes in England and Wales from the perspective of the Environment Agency and sets these difficulties off against the benefits afforded to the community by their implementation. The Environment Agency is responsible for the management and safeguarding of every river and watercourse in England and Wales. The attempts made by various researchers to overcome the technical difficulties and produce a reliable method for predicting the discharge capacity of such channels are also reviewed. Much of the work has involved identifying exactly the significant flow mechanisms that accompany compound channel flow. The dearth of reliable comprehensive field data has resulted in the predominant use of scale models to illuminate the intricacies of compound channel flow behaviour with the field test results being used to demonstrate the accuracy of the various prediction methods.

2.2 The role of compound / multi-stage channels in river engineering

2.2.1 The Environment Agency's flood defence strategy in England and Wales

The Environment Agency assumed the responsibilities originally held by the National Rivers Authority's (NRA) on 1st April 1996. The NRA's legislative responsibilities were founded on a framework stipulated by the Water Resources Act (1991) and the Land Drainage Act (1991). They were conferred with three primary duties:-

1. To exercise supervision over all matters relating to flood defence (river or coastal).
2. To be responsible for issuing consents for construction of any works on, in, or under all main rivers and some water courses.
3. To further conservation in all its functions.

The EA is a Non Departmental Government Body and consequently its underpinning legislation and flood defence strategies reflect the demands of the influential environmental lobby groups which became increasingly powerful during the late 1980s and early 1990s. It became politically essential that public bodies demonstrated

environmental sensitivity in the execution of all their duties. The survey reported in House and Sangster [1991] details the typical concerns and requirements of the public relating to the conservation of the river corridor environment.

Prior to the formation of the NRA, responsibility for river corridor management fell to the local authorities in England and Wales. Each authority was only responsible for managing the catchment within their own limited boundaries. Consequently they tended to assess the viability of individual flood defence projects on their individual merits using cost - benefit analysis and gave scant regard to the impact of the works on the areas managed by other authorities. The cost-benefit analysis method presented by Penning - Rowsell and Chatterton [1977] was typically used. Unfortunately this method did not include an explicit provision for setting the benefit of the scheme, measured in terms of the cost/benefit ratio against the detrimental environmental impact. The analysis tended to be applied only to the area close to the flood defence works and the full impact, on the whole catchment, upstream and downstream from local flood defence works was often overlooked. In a number of cases the flooding problems were simply transferred along the river system.

In an attempt to meet all their legislative duties the old NRA devised a new approach for assessing the viability of any flood defence proposals. They conceived the concept of Catchment Management Planning (CMP) which was outlined in NRA [1993], the Flood Defence Strategy report. The philosophy of CMP was that all future flood defence schemes should exhibit positive cost - benefit results and simultaneously minimise the environmentally detrimental impact of the scheme on the whole catchment. These dual criteria were conceived in an attempt to ensure that the environmental integrity of a river corridor is maintained at all times, whatever flood protection schemes were implemented. Consequently it is important for the River Engineer to consider that the design solutions for a particular flood defence problem will fall into two different categories:

1. Traditional solutions which simply lower the risk of local flooding.
2. Environmentally sensitive solutions which minimise the impact of the flood defence works on local habitat whilst simultaneously lowering the risk of local flooding.

2.2.2 Traditional flood defence options

Traditional flood defence options typically utilised the 'improved drain' principle, as described by Purseglove [1989]. The discharge capacity of the main river channel was increased and therefore the frequency and severity of overbank flooding was reduced. Although these 'improved drain' methods caused the water level to be reduced locally, the flood peak was not attenuated to the same extent as before, because a smaller percentage of the flow was temporarily stored on the flood plain. Consequently there could be serious flooding repercussions because a greater peak discharge than before would be transmitted to areas downstream. These traditional methods were only accepted in the past because the negative repercussions on the local environment and the neighbouring river reaches were deemed to be unavoidable or were simply neglected. Three examples of these options are outlined below with their incumbent drawbacks.

2.2.2.1 Channel dredging or widening

Widening or dredging the main channel as shown in Figure 2.3, results in the removal of the river's natural habitats and vegetation.

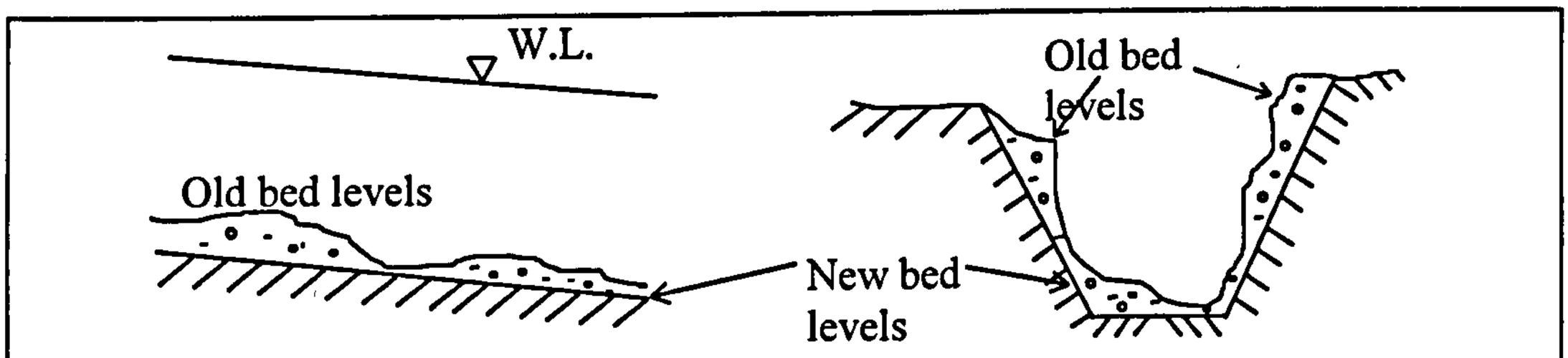

Figure 2.3 Dredged or Widened main river channel

The increased conveyance capacity of the channels tends to be short-lived because the river channel may re-deposit sediment. Although the water level is reduced temporarily the magnitude of the flood peak is not.

2.2.2.2 Removing meanders and straightening the main channels

Removing meanders and straightening the main channels as shown in Figure 2.4, damages local habitats and vegetation. The river channel is locally steepened and the

sediment transport regime is altered. The attenuation of the flood peak due to temporary flood plain storage is also reduced.

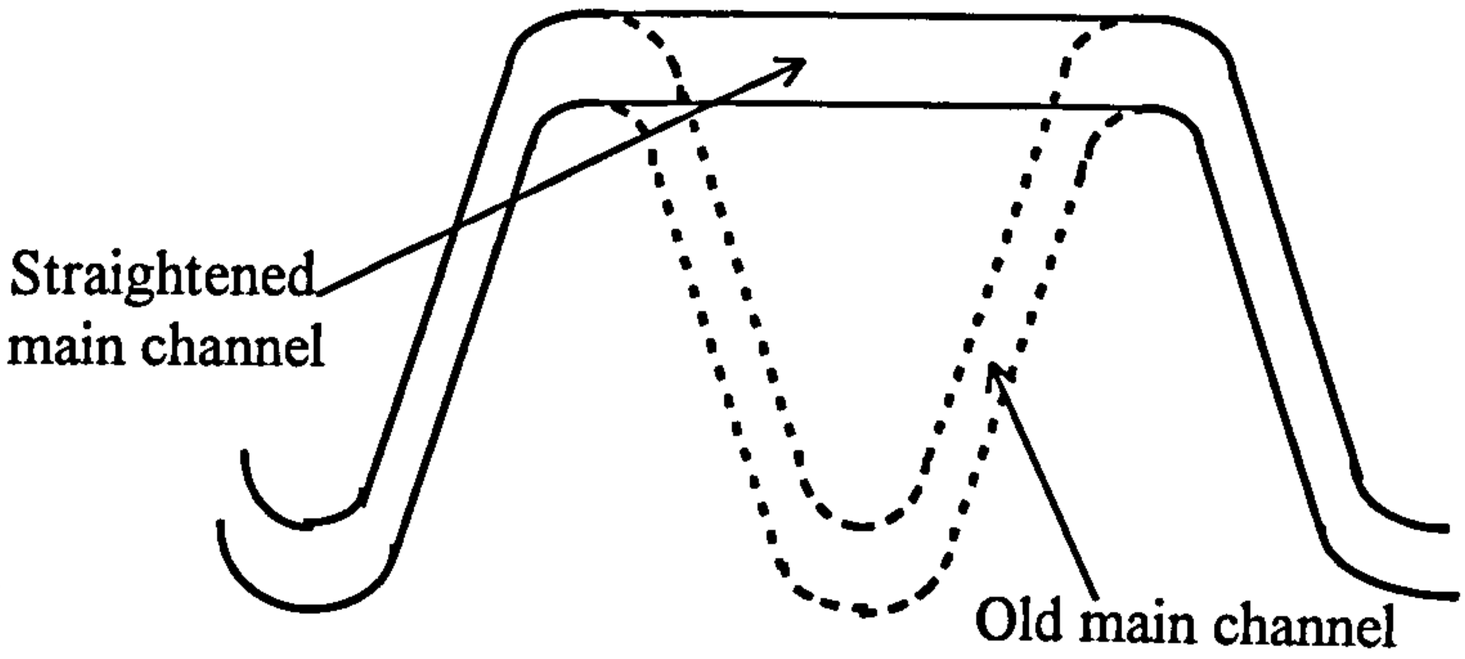

Figure 2.4 Straightened main river channel

2.2.2.3 Construction of flood banks [levees] at the river edge

Constructing flood banks at the river edge, as shown in Figure 2.5, causes a loss in the visual amenity of the river itself, the flood plain is forcibly cut-off from the river and greater flood peaks are transmitted downstream due to loss of temporary storage on the flood plains.

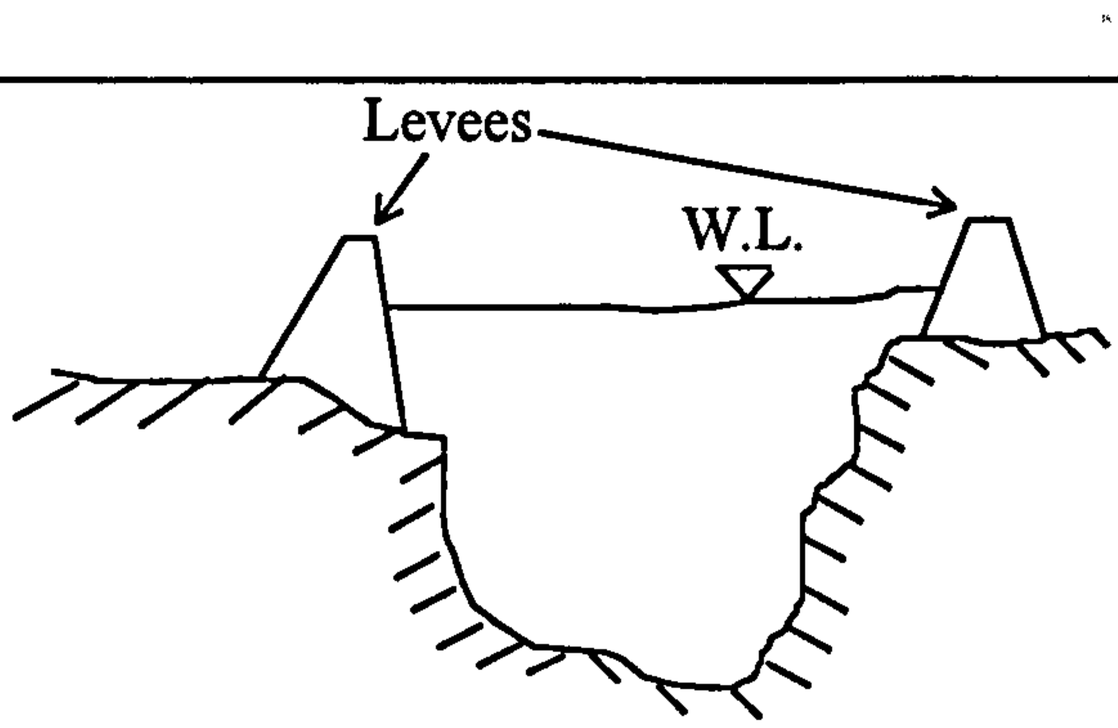

Figure 2.5 Flood banks [Levees] on main river channel banks

2.2.3 Environmentally-sensitive flood defence options

2.2.3.1 Flood relief channels

A sketch of a typical flood relief channel is shown in Figure 2.6 for a proposed scheme at the River Thames, Maidenhead, UK. In essence a second river is created and the original river remains intact. A similar flow regime to the original river is maintained, however, some of the flow may be drawn off into the flood relief channel if a minimum level of

vegetation and provide new recreation areas. During peak flow events it provides extensive temporary storage to reduce the flood peak and extra conveyance capacity to reduce the flood level. The main drawback of this type of scheme is that it tends to be expensive because of the land take required and the construction costs. The 12 km Maidenhead channel was 30-45m wide and cost an estimated £75 million.

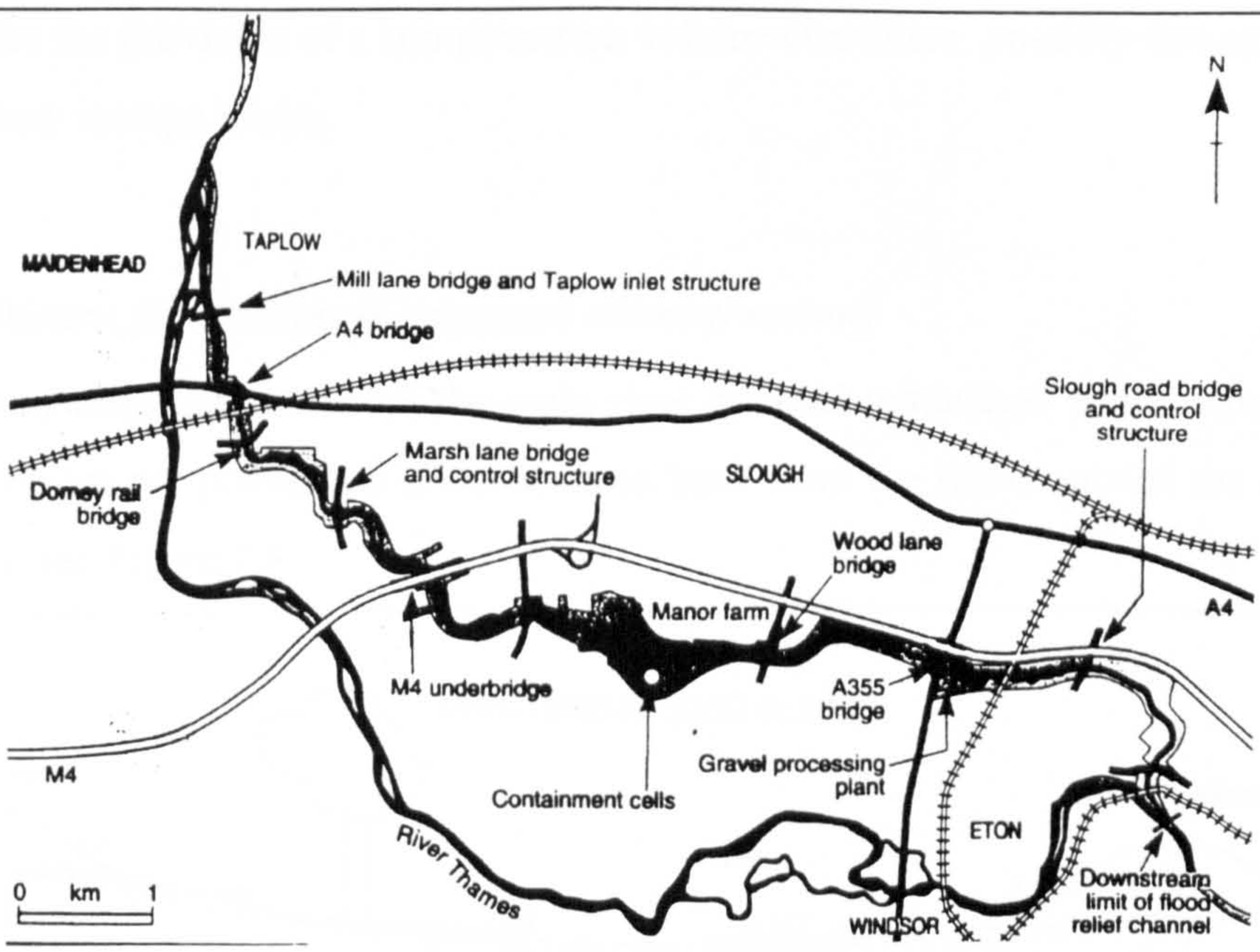

Figure 2.6 Flood relief channels [Maidenhead]

2.2.3.2 Flood plain temporary storage basins

A temporary flood plain storage basin is sketched in Figure 2.7.

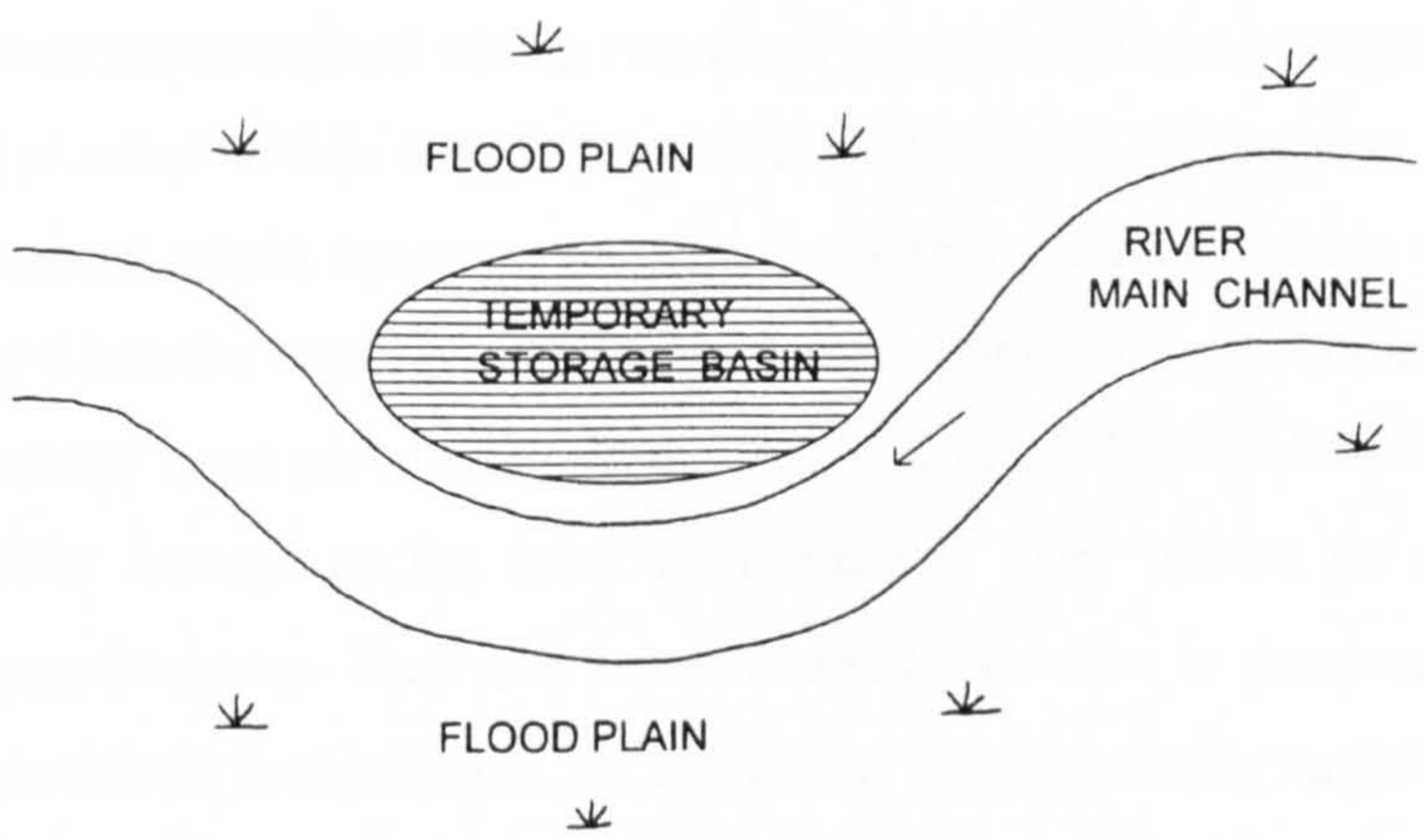

Figure 2.7: Temporary storage pond

A proportion of the flood is diverted to the basin and released once the flood has receded. This is an attractive option provided the volume required for temporary storage is not excessive. It seems that temporary storage basins are set to become more popular in the UK following NRA [1993] which outlines national guidelines for flood compensation. Any loss of flood water volume storage due to flood plain development will require the provision of a compensation volume elsewhere, possibly through the use of temporary storage basins.

2.2.3.3 Distant flood banks [Compound channel option]

This type of construction leaves the main river channel untouched while natural flood banks or levees are positioned some distance back from the river, outside the meander belt width, see Figure 2.8.

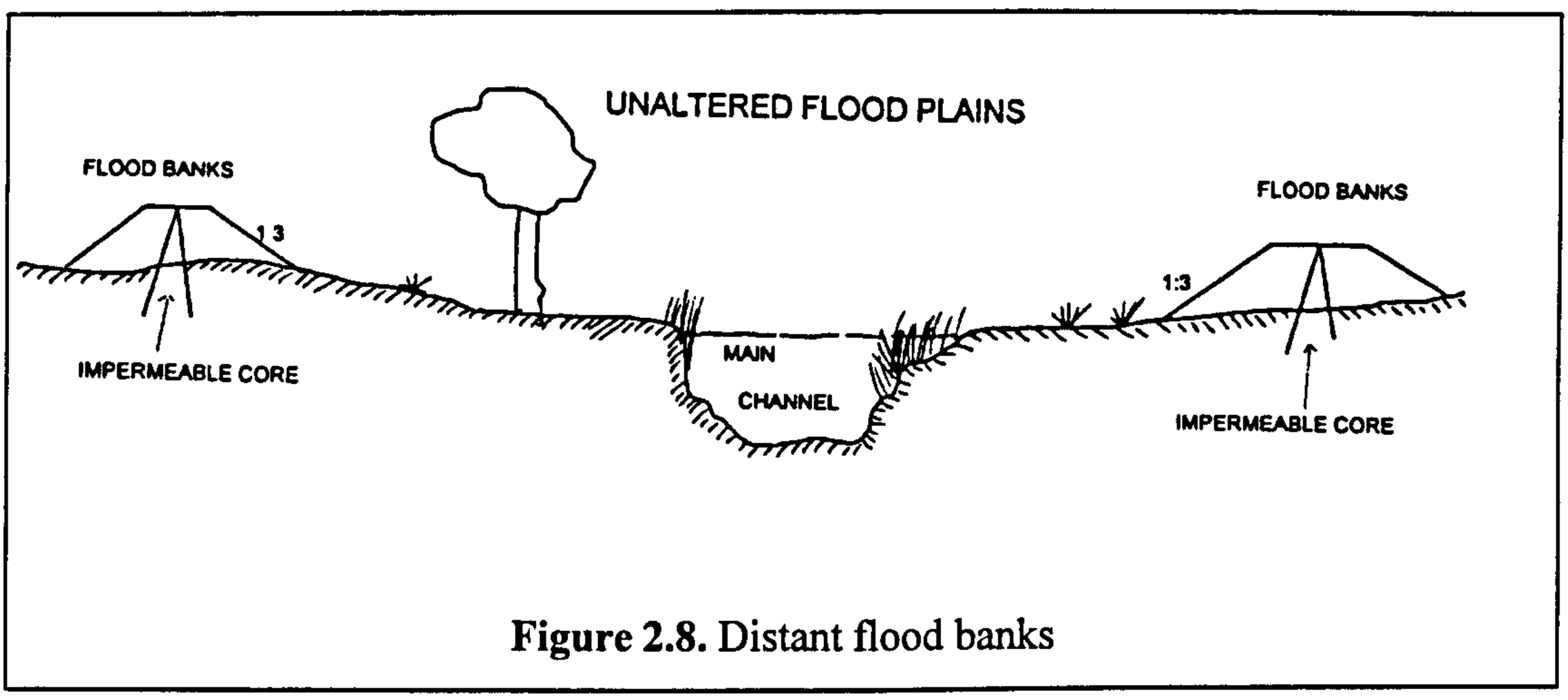

Figure 2.8. Distant flood banks

The flood waters are contained within two flood banks forming a compound channel. A lower [main] channel which runs below bankfull for most of the year and the upper flood plain channel which becomes inundated possibly once or twice a year. On those rare occasions when the water overflows the lower channel it is still contained with the rigid bounds of the flood plain banks so damage is limited. Distant flood bank channels inflict negligible damage to the local environment. They induce no change to the sediment transport regime. They may cause a small reduction in temporary flood plain storage but this can be compensated for elsewhere. They generally cause a rise in flood water level due to flood plain confinement. The flood plain sometimes comprises a

number of distinct tiers, set at different levels, forming what are known as multi-stage channels.

2.2.3.4 Two-stage channels [Compound channel option]

A two-stage channel is a special type of compound channel. It varies from distant flood banks, mainly in the sense that a "slice" is taken off the flood plain as shown in Figures 2.9 and 2.10.

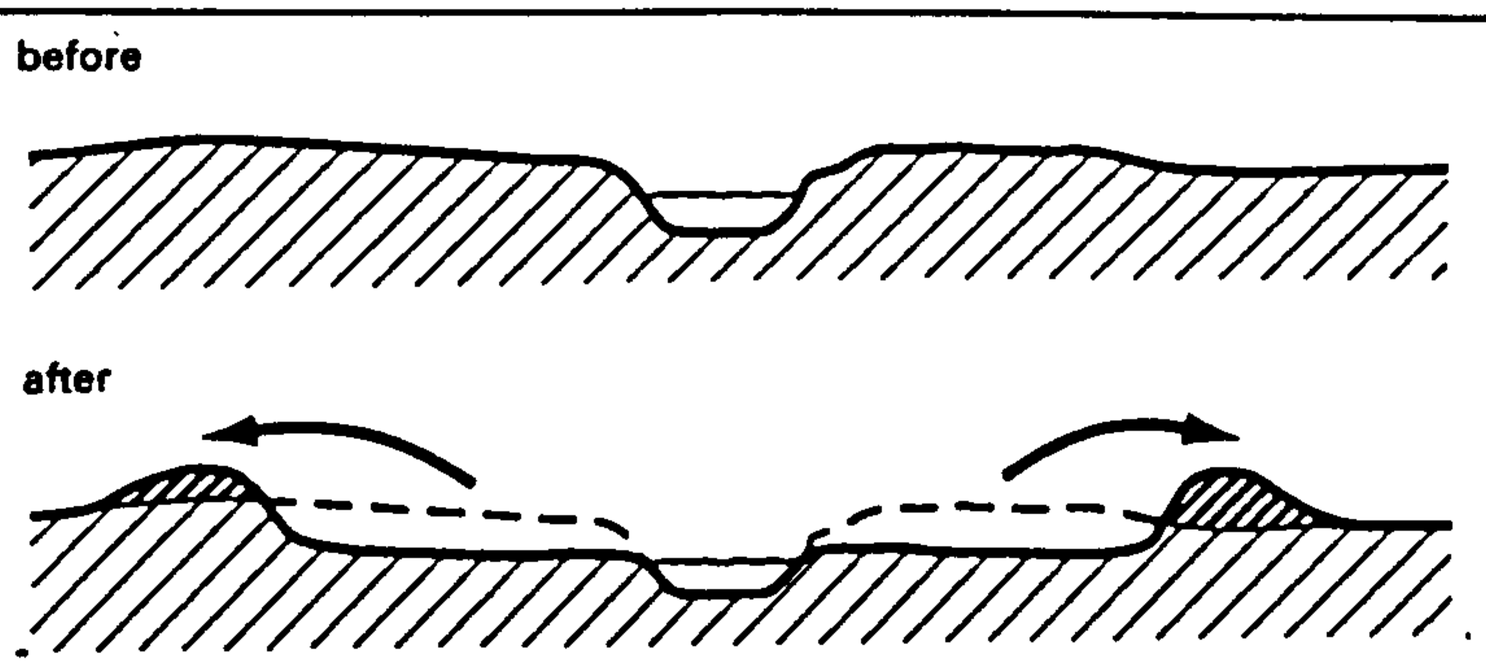

Figure 2.9. Two-stage channels [Cross-section]

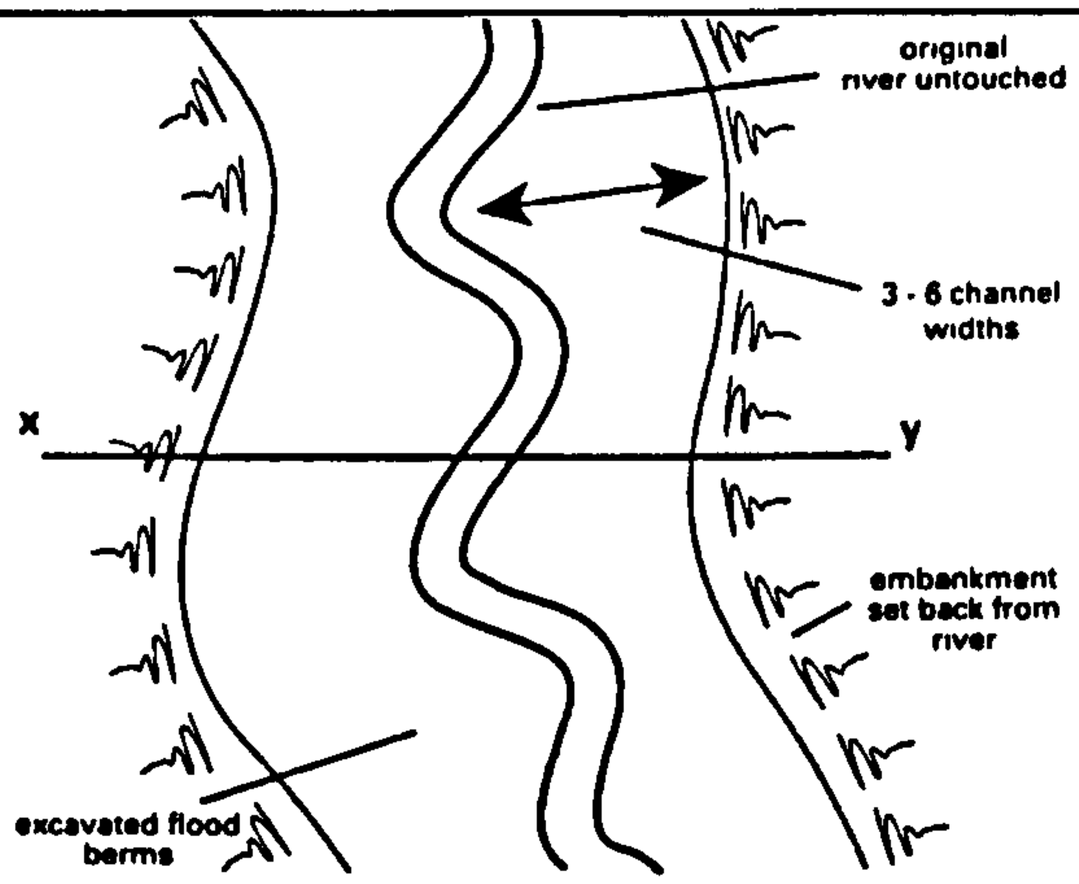

Figure 2.10. Two-stage channels [Plan]

The slice reduces flood levels and generates extra temporary storage. Such schemes have been investigated by Sellin [1990] at the River Roding, Essex, and recently the River Blackwater (Hampshire). In these schemes the bank full depth is effectively lowered. The river goes overbank more frequently but is contained within the distant flood banks. Flood plains can be re-vegetated or form a linear park. Hey [1990] noted that the reduced flood plain level may interact more with the water table level, which would be more suitable for the creation of meadows/wetland rather than a linear park for

recreation. The additional storage created by a two-stage channel may compensate for storage lost outside the flood banks.

2.3 The viability of the compound channel flood defence options

The Environment Agency's adherence to the Catchment Management Planning approach for assessing flood defence schemes has resulted in recent years in the rejection of many traditionally favoured flood defence schemes. Their tendency to inflict unacceptable damage on the environment has counted against them even when it is demonstrated that they adequately alleviate the local flooding problems. Nowadays, the EA actively promote the implementation of more environmentally sensitive schemes, however, to date, only a limited number of compound channel schemes have been built. There are a number of drawbacks which prevent their widespread implementation.

Although compound channel schemes can potentially provide environmentally-sensitive solutions to the problems of flood defence, only a very limited number of such schemes have been built in recent years. Compound channels schemes currently fail to meet one of the EA's primary flood defence assessment criteria. They contravene the EA's fundamental 'Level for Level' flood volume storage compensation criterion. Previous unrestricted flood plain development has tended to cause a loss of temporary flood plain storage during floods. The flood peaks have not been attenuated as much as they were previously and therefore higher flood levels and more extensive inundation has resulted. The EA have reacted to this phenomenon by requiring that any loss in temporary storage volume which is induced by a new development or defence works must be provided for elsewhere in the catchment. Significantly this replacement storage must be provided on a 'level-for-level' basis, as illustrated in Figure 2.11.

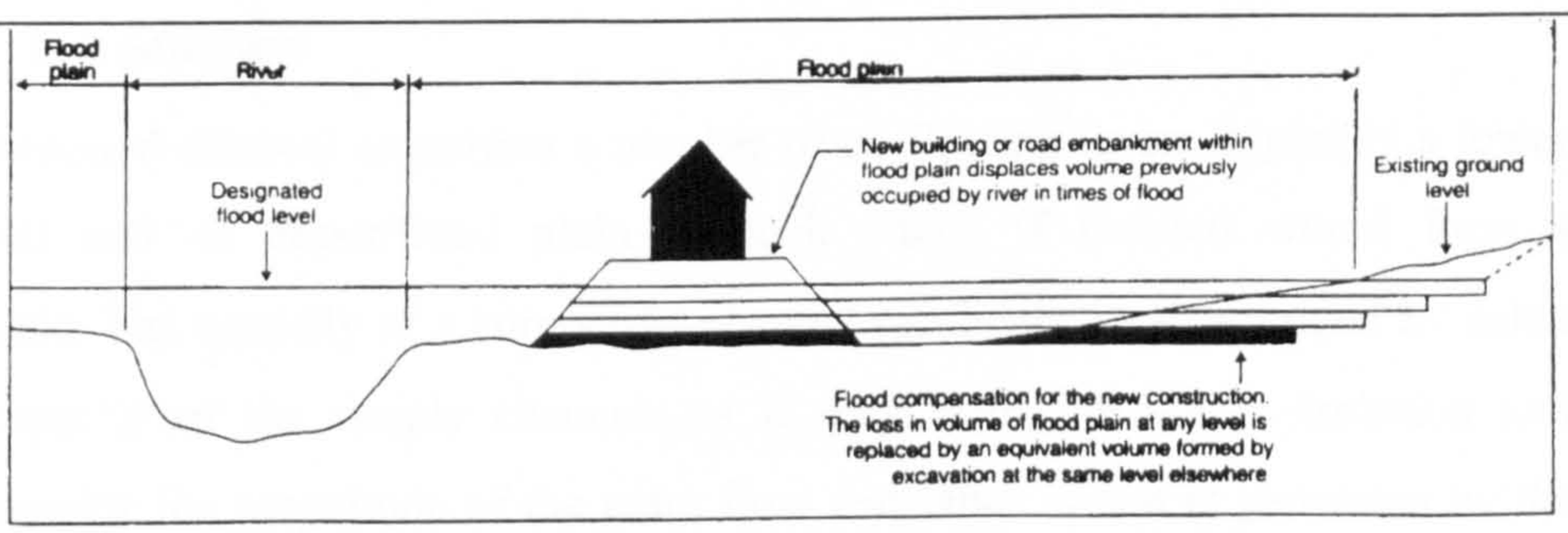

Figure 2.11. The 'level for level' criterion

In other words, the loss of volume of flood plain at any level is to be replaced by an equivalent volume formed by excavation at the same level on a nearby site which is still connected to the main channel during times of flood. Although it may always be possible to provide extra volume within the confines of the compound channel by incorporating temporary storage ponds or by excavating flood plain berms, these may be inappropriate or impossible to implement on a strict level-for-level basis. Often the failure of an compound channel solution to meet the level-for-level compensation criterion introduces an obstacle to an otherwise viable flood control solution.

The likelihood of gaining approval for any compound channel solution will depend, to some extent, on the rigidity of the EA's imposition of the flood compensation criterion. The situation may arise when in order to implement a compound channel solution a practising Engineer may have to rely on the EA accepting the 'spirit' of the flood compensation requirement rather than adhering to the 'letter of the law'. The requirement of level-for-level compensation ensures that a large factor of safety is effectively applied to the discharge capacity predictions. Whatever is constructed or altered on the flood plain none of the volume available to flow is lost. However, depending on the political climate, there may well be additional features associated with compound channel schemes which may make them potentially more appropriate than other schemes, even if 'level for level' compensation can not be readily provided. Clearly if any relaxation is to be feasible then the methods must be available to accurately predict the discharge capacity of the compound channels.

2.4 Traditional discharge capacity prediction methods for simple channels

2.4.1 Introduction

A compound channel comprises a number of co-flowing layers, typically a lower/main channel and an upper/flood plain channel, which if isolated would form simple channels. The capacity of a compound channel can hence be determined by calculating the capacity of the simple channels as if they were flowing in isolation and then determining the magnitude of the extra flow resistance which is generated by the flow layer given a particular set of geometric and flow state conditions. Three resistance formulae are commonly used by River Engineers to predict the discharge capacity of

simple channels. These are the Chezy, Manning and Colebrook-White formulae. Such relationships are not applicable to compound channels when treated as a single channel because they assume uniform flow in a channel with the same average velocity adjacent to each of the model surfaces. In compound channels there is considerable variation in average velocity throughout the channel cross-section.

2.4.2 Derivation of the standard resistance formulae

2.4.2.1 The Chezy and Manning formulae

The standard resistance formulae are derived by assuming that uniform flow conditions exist in the channel. This infers that the net force acting on any water element in the channel is equal to zero, the component of water weight when resolved down the channel slope is balanced by an opposing force generated by bed shear stress. The system of equations defined in Equation 2.1 was derived by assuming that the average flow velocity in the cross-section is equal to $\overline{U}$, and that the bed shear stress, τ_b, is constant all around the wetted perimeter, P, and can be related to a river's mean kinetic energy per unit volume (by means of dimensional analysis).

$$\tau_b \delta x P = \frac{\rho U^2 f}{8} P \delta x = \rho g A S_o \qquad [2.1]$$

δx is the length of the water element contained in the channel, A is the channel's cross-sectional area and f is a roughness parameter. Equation 2.2, commonly known as Chezy's formula, is derived by re-arranging Equation 2.1.

$$\overline{U} = C\sqrt{RS_o} \qquad [2.2]$$

Where R = A/P is the hydraulic radius and C is the Chezy friction coefficient. The Chezy formula can be related to the Manning's n formula which is shown in Equation 2.3 where $C = R^{1/6}/n$ and the expression for $\overline{U}$ is back-substituted into $Q = \overline{U}A$.

$$Q = \frac{1}{n} A R^{\frac{2}{3}} \sqrt{S_o} \qquad [2.3]$$

Extensive data sets have been derived by researchers such as Chow [1959] which define values for n for a huge variety of channel bed surface roughness for both main channels and flood plains. The Manning's formula is strictly only appropriate for straight, sloping, prismatic channels with uniform roughness throughout the wetted perimeter.

2.4.2.2 The Colebrook-White formula

The Colebrook-White formula was developed for application to pipe flow but has been adapted so that it can be applied to simple open channels. Equation 2.4 demonstrates the relationship between the pipe friction factor, λ, flow state and the geometry of an open channel for transitional flow states, between rough turbulent and smooth turbulent flow.

Rough turbulent component — Smooth component

$$\frac{1}{\sqrt{\lambda}} = -2\log\left(\frac{k_s}{14.8R} + \frac{0.6275}{\mathrm{Re}\sqrt{\lambda}}\right) \qquad [2.4]$$

k_S is the roughness height, Re is the Reynolds number of the flow, Re=4UR/ν, R is the hydraulic radius. For predominantly rough turbulent flow the pipe friction factor, λ can be related to Chezy C, Manning's n or the Darcy-Weisbach friction factor, f using the definitions in Equation 2.5.

$$C = \sqrt{\frac{2g}{f}} \quad \text{where } f = \frac{\lambda}{4} \quad \text{and} \quad \lambda^{-1/2} = -2\log(14.8R/k_s) \qquad [2.5]$$

The calibrated values for Manning's n, Chezy C and k_S were derived from investigations of rough turbulent flow. They are dimensional and can not be extended for application to smooth channels with flow in the laminar-turbulent region. The Darcy-Weisbach friction factor, f, is non-dimensional and has been shown to be related to the Reynolds number of flow. It has been reliably applied as a measure of roughness coefficient in smooth turbulent flow

2.4.3 The influence of flow conditions on bed friction effects

Many compound channel scale models which have been built over the years have incorporated smooth surfaces and the flow has tended towards laminar conditions. The Stanford conference in 1968 concluded that a modified smooth turbulent formulation could be used to relate the Darcy-Weisbach friction factor f, to the Reynolds number of the flow in models with smooth surfaces, as shown in Equation 2.6.

$$\frac{1}{\sqrt{f}} = \mathrm{C}\cdot Log_{10}\left(\mathrm{Re}\sqrt{f}\right) - \mathrm{D} \qquad [2.6]$$

Ackers [1991] observed that a value for C of 2.03 is common for all smooth turbulent flow. Myers and Brennan [1990] identified that C was equal to 2.02 for the Series A tests. The value of D in a modified smooth turbulent equation indicates different levels

of bed friction resistance. A value for D of 1.38 for most smooth model channels was established by Ackers [1991]. D was found to be equal to 1.42 for the Series A and B tests. Modified smooth law is not applicable in laminar flow conditions consequently its use must be confined to flow states where the Reynolds number, Re is greater than 2000.

2.4.4 Determining roughness coefficients for channels with variable bed surfaces

2.4.4.1 Introduction

Natural rivers never exhibit uniform channel surface characteristics. A number of methods have been developed to supplement basic roughness coefficients so that representative values can be determined for all channel configurations. The identification of reliable methods for catering for variable bed surfaces was essential to enable the bed friction contribution to be accurately calculated when analysing the compound channel flow in the Series B extension models. Where the flood plain flow passes over the main channel, no bed friction losses will generated. The standard resistance formulae must be adapted to account for this gap (lateral variation) in the wetted perimeter.

2.4.4.2 Natural channels: Lateral variations

Horton [1933], Lotter [1933], Einstein and Banks [1950] and Krishnamurthy and Christensen [1972] all developed formulations for deriving a weighted mean roughness coefficient, n_{av}, for simple channels with sections of wetted perimeter with different roughness characteristics as shown in Figure 2.12. The formulations are given in Equations 2.7 - 2.10 respectively.

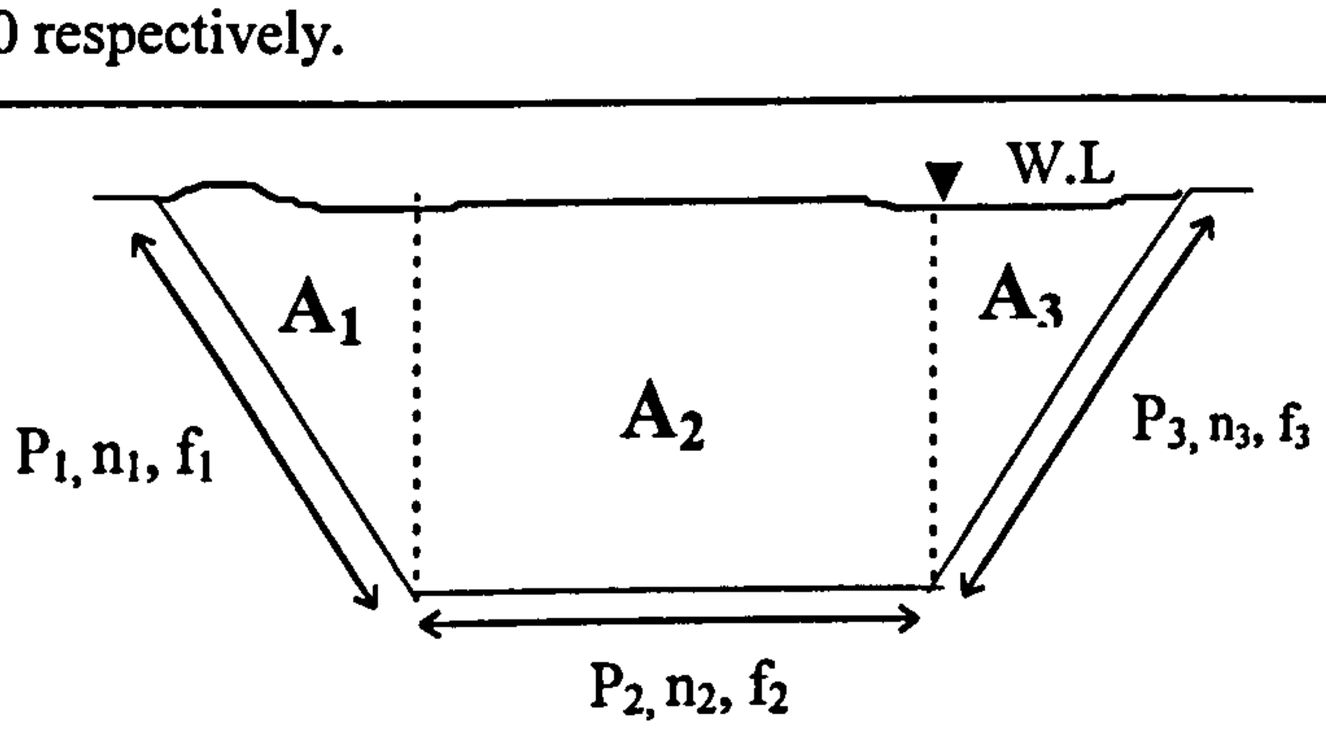

Figure 2.12 Lateral variation of roughness on the wetted perimeter

$$n_{av} \equiv \left(\sum_{i}^{n} P_i\left(n_i^{3/2}\right)\right)^{2/3} / P^{2/3} \qquad \text{Horton [1933]} \qquad [2.7]$$

$$n_{av} \equiv PR^{5/3} / \sum_{i}^{n}\left(\left(P_i R_i^{5/3}\right) / n_i\right) \qquad \text{Lotter [1933]} \qquad [2.8]$$

$$n_{av} \equiv \left(\sum_{i}^{n} P_i\left(n_i^{2}\right)\right)^{1/2} / P^{1/2} \qquad \text{Einstein and Banks [1950]} \qquad [2.9]$$

$$Ln(n) \equiv \left(\sum_{1}^{n} P_i Ln\left(n_i\right)\right) / P \qquad \text{Krishnamurthy [1972]} \qquad [2.10]$$

Horton [1933] assumed that the mean velocity is the same in each section. Lotter [1933] assumed that the sum of the area discharge was equal to the total discharge and that the surface shear stress was the constant along the whole perimeter. Einstein and Banks [1950] assumed that the total force resisting flow over the whole area of the channel was equal to the forces resisting flow in each area. He also assumed that the surface shear stress was the constant along the whole perimeter. Krishnamurthy and Christensen [1972] assumed that the cross-section was wide and shallow so that the hydraulic radius of each area could be approximated by vertical depth, d_i and that the average flow velocity followed a logarithmic distribution law.

The Krishnamurthy and Christensen [1972] method is most accurate for large Aspect ratio channels like the Mississippi but not for channels with smaller aspect ratios as in the Series B and Series B extension tests. In these channels the mean velocity in the different flow areas did not vary very much and the surface shear stress varied between the sloping sides and bed of the channel. Consequently the author decided that the Horton [1933] method was the most appropriate equation to use to determine the effect of wetted perimeter variations when analysing the flow results from the Series B extension (1993-1996) models.

2.4.4.3 Natural channels: Longitudinal variations

Chow [1959] produced tables specifying roughness coefficients for natural channels with constant roughness characteristics along a full river reach. However in any one reach these characteristics may vary considerably. Cowan [1956] produced a procedure

adapted to incorporate the effect of longitudinal variation. Cowan [1956] proposed calculating n_{av} which is defined by Equation 2.11.

$$n_{av}=[n_b+n_1+n_2+n_3+n_4]m \qquad [2.11]$$

where

n_b = a base value for n for a straight, uniform, smooth channel in natural materials.

n_1 = a correction factor for the effect of main and flood plain channel surface irregularity.

n_2 = a value for variations in shape and size of the channel cross-section.

n_3 = a value for obstructions

n_4 = a value for vegetation and flow conditions

m = a correction factor for the meandering of the channels

This equation can be applied to both the flood plain and main channels and consequently provides much more flexibility and accuracy than can be achieved using Chow [1959] in isolation. Work done by Aldridge [1973] and Acrement and Schneider [1989] have updated this approach. Aldridge [1973] derived a rationalised set of basic roughness values (base values, n_b) for application to typical channels. Acrement and Schneider [1989] developed a formulation for n_4 which could account for heavily vegetated flood plains. Despite its advantages the Acrement and Schneider [1989] method is not appropriate for application in model channels. The flow resistance can usually be determined using carefully applied standard resistance formulae.

2.4.4.4 Physical models

A limited number of experimental programmes have included scale models of compound channels which have been built with specially roughened flood plains. The Vicksburg [1956] experimental programme used expanded metal sheets to roughen the flood plains. However, only one value for Manning's n calibration data was presented even though it would have varied with flow depth.

In the Series A (1985-1988) and Series B (1989-1992) experimental programmes the flood plains were roughened with dowel rods which penetrated the free water surface at all flow depths. They were positioned in a formation with the dowel rods at the apices of a repeating pattern of equilateral triangles as shown in Figures 2.13 and 2.14.

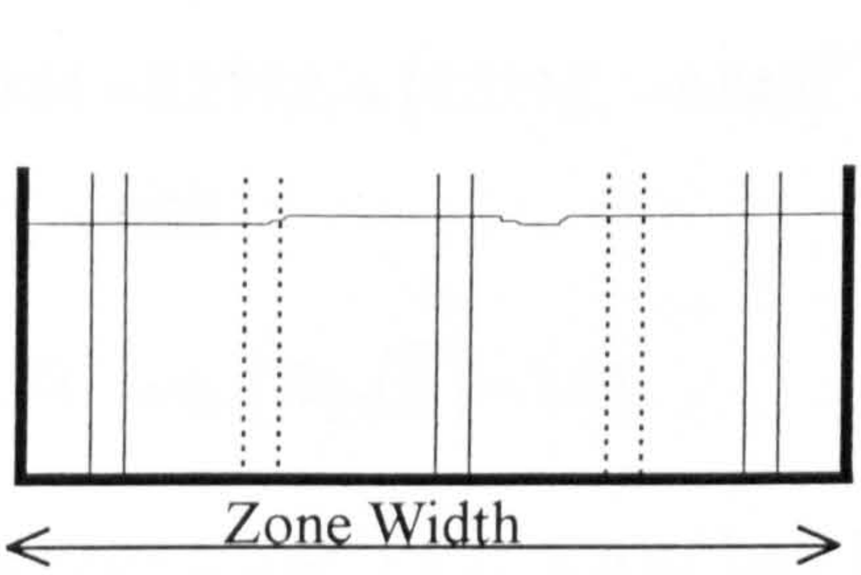

Figure 2.13 Cross-section view

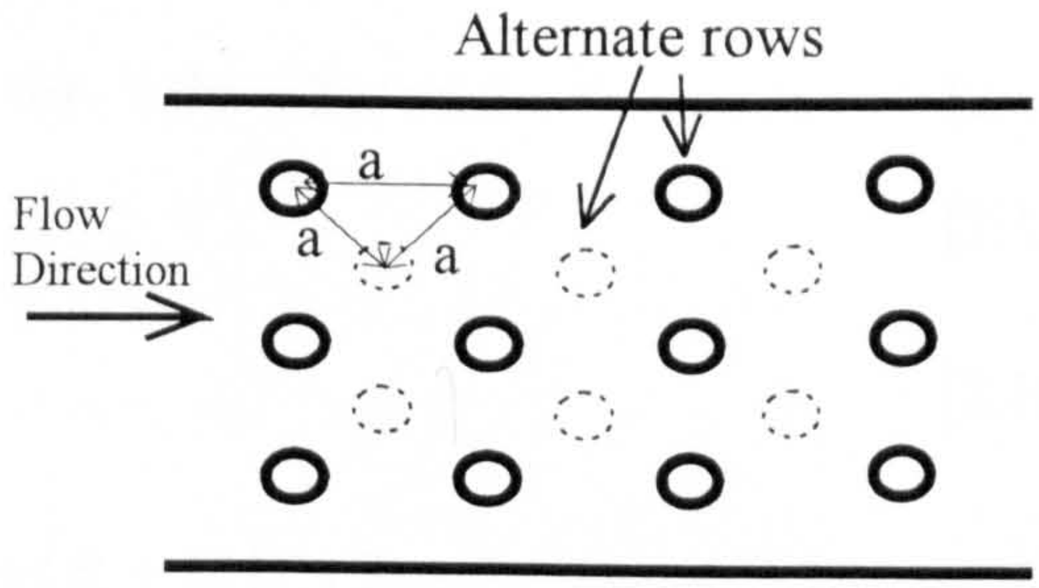

Figure 2.14 Plan view

The dowel rods typically generated a variation of flow resistance (Manning's n) with flow depth, as shown schematically in Figure 2.15, which would be generated on the flood plains of natural rivers only if the flood plains were heavily planted with trees. The majority of natural flood plains by contrast are actually composed of grassland vegetation. On these flood plains the flow resistance would be large and increase only until the majority vegetation was overtopped. Subsequently the flow resistance would steadily decrease as shown schematically in Figure 2.16. Thus dowels are not a good simulation of typical flood plain roughness.

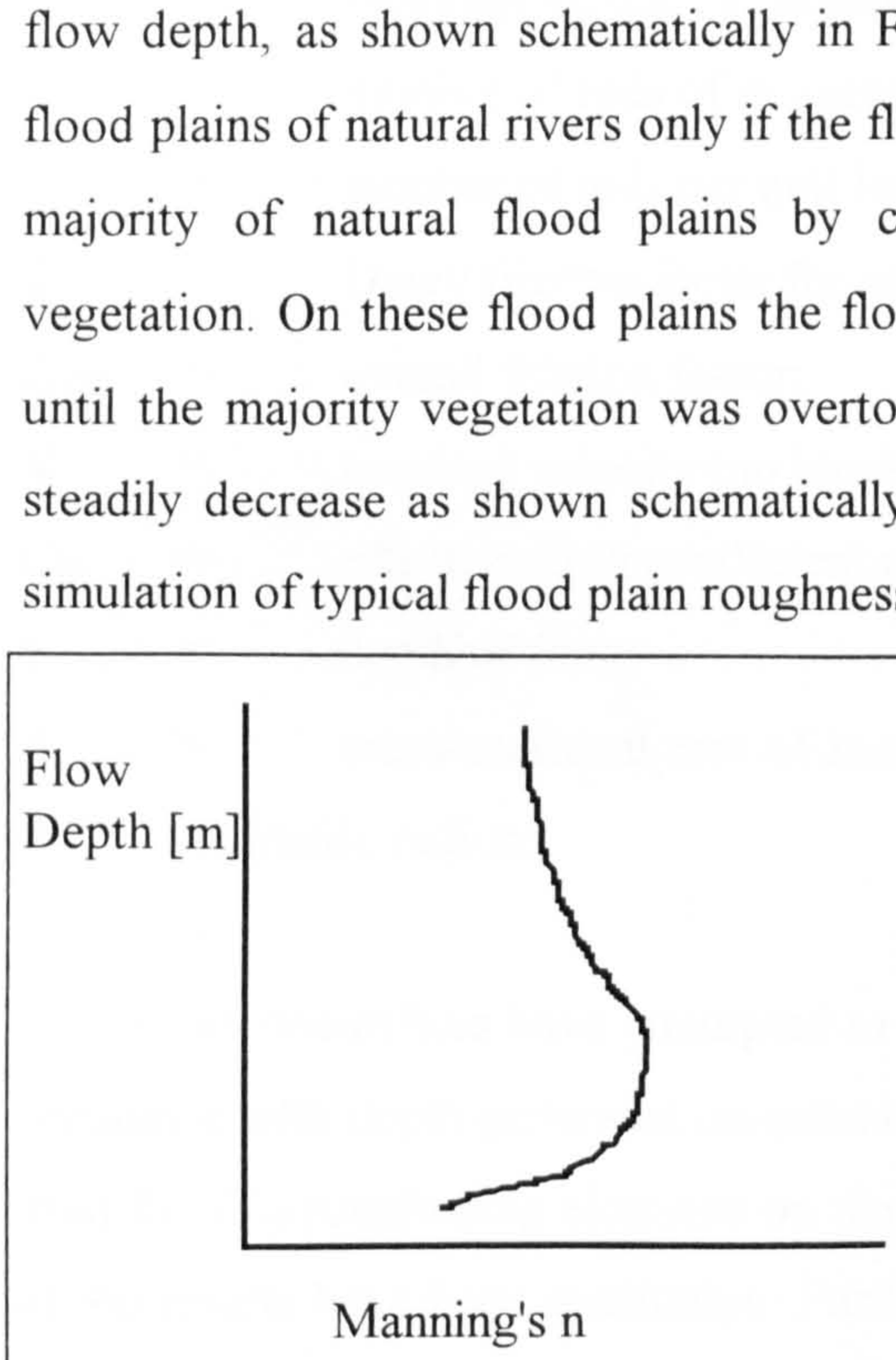

Figure 2.15 Roughness variation : Natural

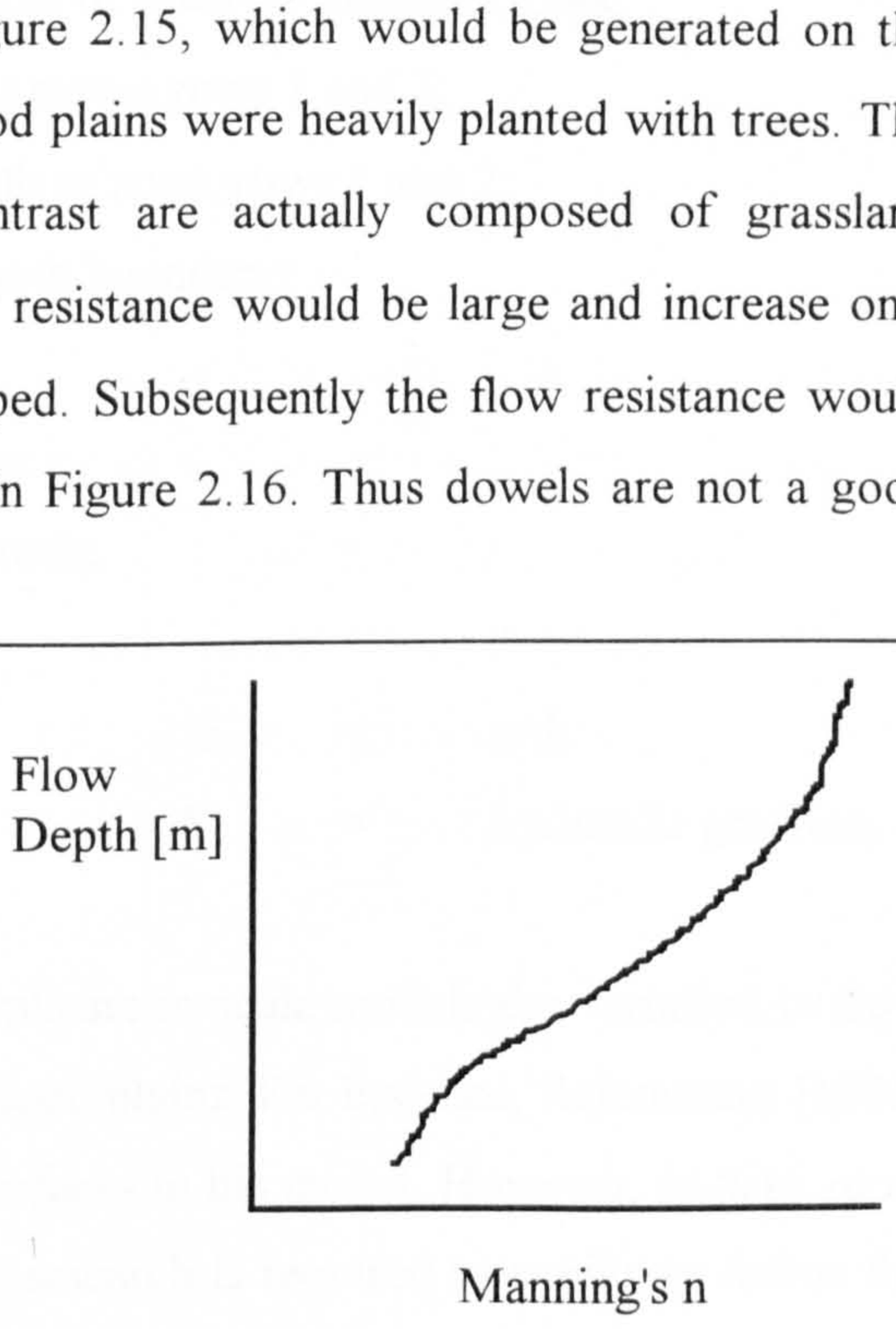

Figure 2.16 Roughness variation: Dowels

Ackers [1991] devised a set of formulae to predict the flow resistance generated by dowel rods arranged in the Series A and B configuration. The Darcy f coefficient was

used as an alternative to Manning's n for these scale models. Ackers [1991] formulae are described in Equations 2.12 -2.17.

$$B_1 = \left(1 - n_1 zd/A\right)^{-2} \qquad [2.12]$$

$$B_2 = \left(1 - n_2 zd/A\right)^{-2} \qquad [2.13]$$

$$\alpha C_D = 1.184 - 0.277 Z_* + \left(0.529 Z_* - 0.843\right)^{0.5} \quad \text{for} \quad 1.75 < Z_* < 6.6 \qquad [2.14]$$

$$\text{else} \quad \alpha C_D = 0.95 \qquad [2.15]$$

$$\frac{1}{\sqrt{f_s}} = 2.02 \cdot Log_{10}\left(\mathrm{Re}\sqrt{f_s}\right) - 1.38 \qquad [2.16]$$

$$f_{tot} = 8gRS/V^2 = 4\alpha C_D\left(B_1 N_1 + B_2 N_2\right)dz/P + \left(B_1 + B_2\right)f_s/2 \qquad [2.17]$$

Where:

Re = Reynolds number of blocked channel = $2VR\left(B_1^{0.5} + B_2^{0.5}\right)/\nu$;

$B_{1,2}$ = blockage effect, i.e. square area of rows for alternate rows;

$n_{1,2}$ = number of rods of diameter d across rows 1 and 2;

$N_{1,2}$ = number of rods per unit length of zone, rows 1 and 2;

f_s = Darcy friction factor for smooth boundary;

f_{TOT} = overall friction factor;

V = nominal velocity (no blockage);

C_D = effective drag coefficient of rods;

z = depth of flow;

A = cross-sectional area of zone; Z_* = z/d;

R hydraulic radius; S = hydraulic gradient.

Numerous researchers have attempted to replicate in scale models the variation in flow resistance with depth generated on natural flood plains. For instance, Rajaratnam [1981] used flexible roughening elements on the surfaces in his model. However, to date, most of the results have been qualitative. Further research is required to explicitly define the magnitude of flow resistance generated by these flexible elements and to use the results to investigate the resulting effect on flow behaviour in compound channels. It is particularly important that similarity between the velocity profiles in natural and model channels is achieved.

2.4.5 Adjustment of roughness coefficients to account for secondary circulation

2.4.5.1 Introduction

When water flows round the bends in a meandering (sinuous) main channel, secondary currents are established due to the differences in centripetal acceleration experienced by water at different levels in the channel. Currents are created towards the outside of the bend at the water surface and towards the inside of the bend at bed level. A super-elevation in the water surface profile is induced at each bend apex which balances the non-uniform lateral pressure distribution which is introduced by the secondary currents. The extra head loss is generated because the levels of turbulence intensity are increased and a lateral component of bed shear is generated by the secondary currents. This results in an increase in the overall resistance to flow. Consequently the discharge capacity of meandering channels is lower than in a straight channel with identical dimensions for an equal depth of flow.

In meandering channels the bends are not isolated, one bend turning one way is followed by another turning in a opposite direction. Any residual secondary currents in the flow (as it leaves one bend) will be countered by centripetal forces which generate secondary currents with an opposite sense of rotation. The energy loss due to secondary currents in a meandering channel will be affected by how the currents, generated in consecutive bends, interact. The extra flow resistance created will depend on the length of transition between alternate bends as well as the tightness of the bends. The parameter, Sinuosity, can be used as a combined measure for both of these separate parameters. It is defined as the ratio between the thalweg distance (the distance between two points A and B along the centre line of the main channel), as is shown in Figure 2.17 and the straight line distance between A and B.

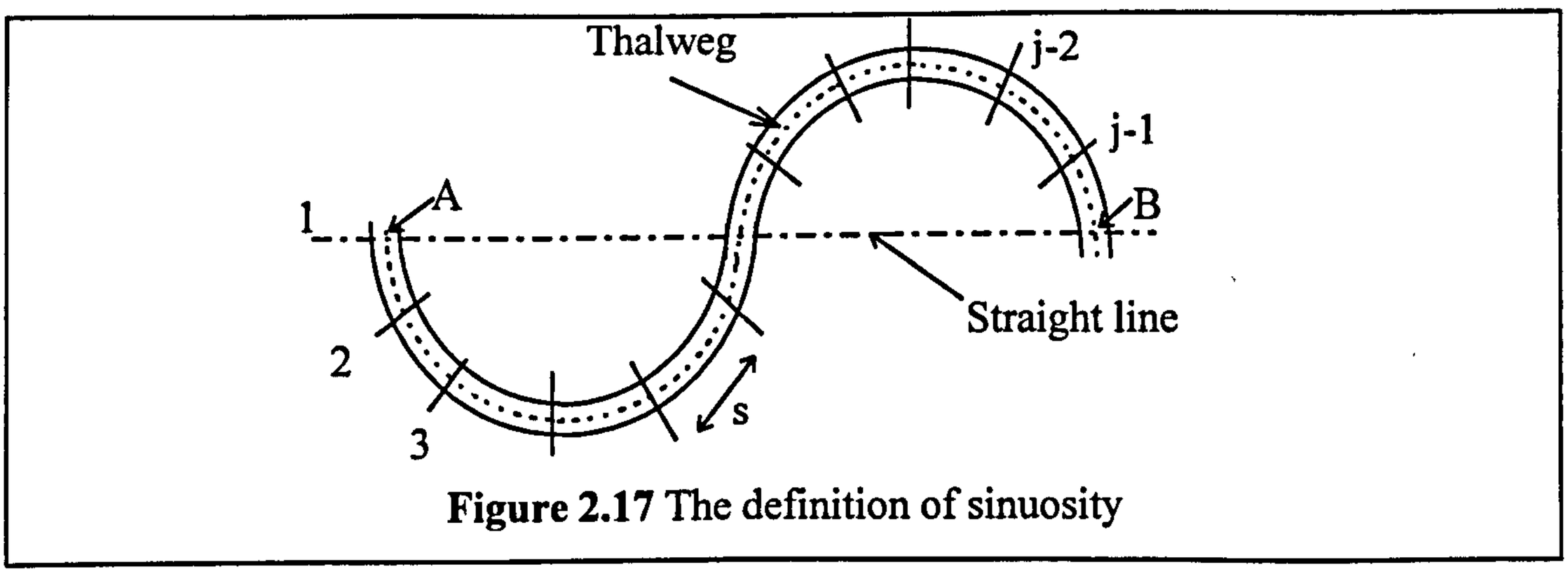

Figure 2.17 The definition of sinuosity

James [1994] compared the accuracy of various methods which had been developed over the years to predict the discharge capacity prediction of simple meandering channels. The methods incorporated an allowance for the extra head losses generated by the secondary circulation in the flow. Some of the models were empirically based and some theoretically based. James [1994] demonstrated that the two most accurate methods were the linearised version of the Soil Conservation Service method (SCS) [1963] and the modified Chang [1984] method.

2.4.5.2 Modified Chang Method [1984]

Chang [1984] predicts the discharge capacity of the test channels with a bend, with greater accuracy than the LSCS method. It directly accounts for bend radius and variations in bend radius along the length of a channel. The transverse velocity, v_{rc}, at the water surface along the centre line through a bend is defined using Equation 2.18.

$$(v_{rc})_{j+1} = \overbrace{\left((v_{rc})_j + (f/2)^{1/2}\left(10/3 - (1/\kappa)(5/9)(f/2)^{1/2}\right)\exp\left((\kappa/y)(f/2)^{1/2}\Delta s\right)\Delta s\right)}^{\text{Growth term}} \overbrace{*\exp\left(-(\kappa/y)(f/2)^{1/2}\right)\Delta s}^{\text{Decay term}} \quad [2.18]$$

The subscript, j, is the cross-section index as shown in Figure 2.17, Δs is the distance between adjacent sections j and j+1, f is the friction factor calculated by neglecting head losses associated with secondary circulation, y is the flow depth (uniform flow), V is the mean velocity calculated using the Darcy-Weisbach formula and κ is the Von Karman constant. The full equation is applied to cross-sections through a bend but the growth term is discarded in the straight between adjacent bends.

First the mean velocity is calculated by neglecting the head losses generated by secondary circulation. Subsequently $[v_{rc}]_1$ is set to zero and substituted with the other values into Equation 2.18 to calculate the initial distribution of v_{rc} through one complete wavelength. The value for $[v_{rc}]_j$ in the last section is substituted for $[v_{rc}]_1$ in the first section and the distribution is calculated iteratively along a wavelength until the value for v_{rc} at the first and last sections are identical within a specified tolerance. This

corresponds to uniform conditions through a series of meanders. The average value of v_{rc}, $[v_{rc}]_{av}$ through a wavelength is calculated using Equation 2.19.

$$\left(v_{rc}\right)_{av} = \left(\sum_{1}^{j} v_{rc}\Delta s\right) \Big/ \left(\sum_{1}^{j} \Delta s\right) \qquad [2.19]$$

The mean flow is subsequently recalculated using Equation 2.20 which accounts for the losses associated with secondary circulation.

$$V = \left(\left(gS_o\right) \Big/ \left(\left(f/_{8R}\right) + K\right)\right)^{1/2} \qquad [2.20]$$

where
$$K = \left(\frac{\left(2.86 f^{1/2} + 2.07 f\right)}{\left(0.565 + f^{1/2}\right)} \right) \left(y/_{R_c}\right)^2 \left(B/_A\right) \left(v_{rcav}/_{v_{rcfd}}\right) \qquad [2.21]$$

and
$$v_{rcfd}/_V = \left(y/_{R_c}\right)\left(\frac{1}{\kappa}\right)\left(10/_3 - \left(\frac{1}{\kappa}\right)\left(V_*/_V\right)\left(10/_9\right)\right) \qquad [2.22]$$

with $S_f = S_o$ for uniform flow and $V_* = \left(gRS_f\right)^{1/2}$

The recalculated mean velocity is then used in Equation 2.18 to compute a new distribution of v_{rc} through the wavelength. The procedure is repeated until the recalculated mean velocity is the same as the previous one, within a specified tolerance.

The modified Chang [1984] method is based on the assumption that the channel is wide compared to its depth and therefore it is inappropriate for use with the majority of model channels used in the Series A, B and B extension model tests. It is also difficult to apply the method to natural channels because of their variable configuration. In some instances the Modified Chang method will give more accurate, physically justifiable results however in most circumstances the more simple LSCS method will be more appropriate.

2.4.5.3 Linearised SCS method (LSCS) [1963]

The original Soil Conservation Service [SCS] [1963] method consisted of an empirically-based model which incorporates the extra flow resistance generated by secondary circulation resulting from the influence of a channels sinuosity by adjusting the roughness coefficients which are used in the standard resistance formulae as shown in Equations 2.23 - 2.25 where n' is the modified Manning's n value and n is the Manning's n value in an equivalent straight channel.

$$n' / n = [f'/f]^{1/2} = 1.0 \quad \text{for } s<1.2 \quad [2.23]$$

$$n' / n = [f'/f]^{1/2} = 1.15 \quad \text{for } 1.2=< s< 1.5 \quad [2.24]$$

$$n' / n = [f'/f]^{1/2} = 1.3 \quad \text{for } s >= 1.5 \quad [2.25]$$

James and Wark [1992] replaced the step function defined above with a linear function to avoid the implicit discontinuity. This linear function is described in Equations 2.26 and 2.27.

$$n' / n = 0.43*s + 0.57 \quad \text{for } s<1.7 \quad [2.26]$$

$$n' / n = 1.3 \quad \text{for } s>=1.7 \quad [2.27]$$

This method was easy to apply and yields the results which were almost as accurate as the Modified Chang [1984] method, although it does not account for the influence of bend radius on the losses generated in the channel. It was used to analyse flow data during the Series B extension programme.

2.4.5.4 The influence of scale on energy loss in bend due to secondary circulation

Chang [1984, 1988] demonstrated that the Reynolds number, Re, of the flow and the ratio of the bend radius, R_c to the main channel depth, h_a 'tightness', significantly effects the ratio of secondary circulation energy loss slope, S" to bed friction energy loss slope, S'. In small scale physical models of natural channels the bend radius is often scaled at a different rate to the channel depth in order to maintain similarity of flow conditions between the full size channel and the scale model. The main channel is often deepened to ensure that turbulent conditions prevail in the model channels thus ensuring that flow mechanisms which are comparable with those in the larger channels are maintained. Figure 2.18 shows the relationship between the ratio of the secondary circulation losses in a meandering channel and the bed friction losses , S"/S', and the magnitude of the ratio of bend radius and main channel depth, R_c/h, after Fares [1989]. The head losses

are measured in terms of the friction slope values. The ratio S"/ S' increases exponentially with the decreasing magnitude of [R_c/h].

Figure 2.18 indicates that if the scale reduction in channel depth is reduced then the magnitude of secondary losses generated in the simple meandering channel will be increased, which will counter the increase in mean bankfull velocity caused by the decrease in hydraulic radius. Any alteration to the mean bankfull velocity will have the potential to influence the magnitude flow interaction losses generated in meandering compound channels. No researcher to date has obtained any evidence to demonstrate explicitly the influence of scale on secondary circulation losses on the flow resistance in meandering compound channels.

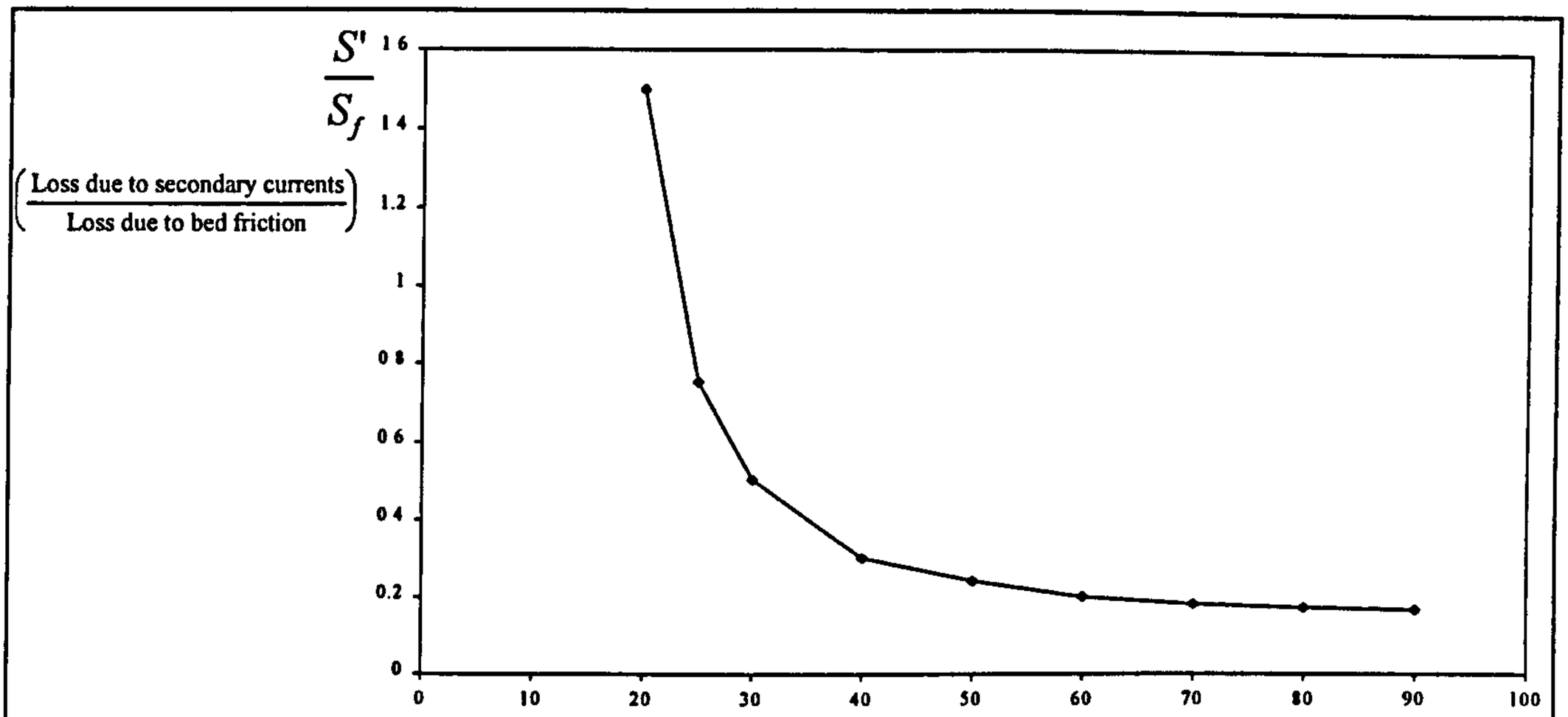

Figure 2.18 Secondary circulation/friction losses versus R_c/h (after Fares [1989])

2.5 Traditional discharge capacity prediction methods for compound channels

2.5.1 Introduction

The most commonly used method is a one-dimensional numerical river model ignoring interaction between the main channel and flood plain. Simple and divided channel methods (the traditional tools of River Engineers when determining the discharge capacity of compound channels) are typically used to produce flow tables for inclusion in one-dimensional numerical models. Even though they do not accurately cater for all the sources of head loss in a compound channel and only quantify the head loss due to bed friction the discrepancy is initially overlooked because of the manner in which they

are subsequently adjusted. During the process of numerical model building, the water surface levels produced by the model are adjusted by systematically varying the basic roughness coefficients in the numerical model until it fits the available calibration data. This method has been shown to work but there are difficulties.

2.5.2 Simple channel method

Treating a compound channel as a simple channel (one complete channel) causes a problem when applying Manning's formula. There is a discontinuity in the values of P and R when the river flows just overbank. If values for discharge and water level are known then back calculation using Manning's formula reveals that the value for Manning's n appears to drop dramatically when the water levels change from inbank to overbank. Knight et al [1989] demonstrated this behaviour clearly in their analysis of data from the River Severn at Montford. A dramatic decrease in the value of n such as the one observed would appear to imply that the overall resistance to flow instantaneously reduces as the water flows overbank. However, the opposite has proved to be true. The disproportionately large increase in the length of wetted perimeter exposed to the flow compared with the increase in flow area would, in reality, induce an increase of flow resistance. The use of hydraulic radius is not appropriate for compound channels.

2.5.3 The Divided channel method

The usual approach adopted to avoid discontinuities in P and R is to divide the compound channel into zones as shown in Figure 2.19. The flow velocity in the individual zones is assumed to be uniform and prone only to flow resistance due to bed friction and secondary circulation. The assumption underlying this method is that the dividing lines coincide with lines of zero shear stress.

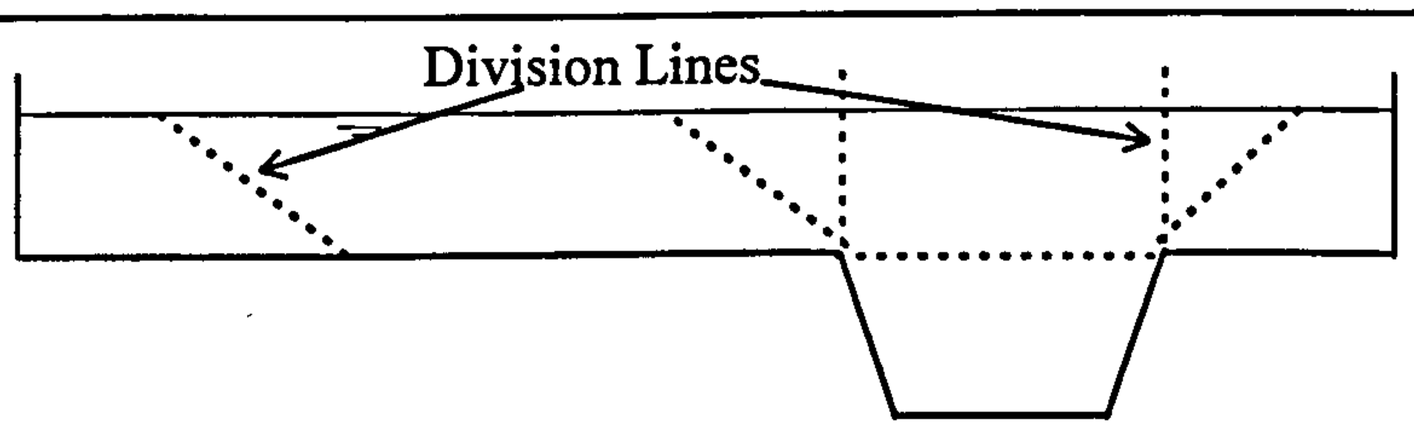

Figure 2.19 Typical division lines

The flow zones created by the division lines are assumed to exert no force on each other. Various methods have been proposed to select the orientation of the division lines depending on the configuration of the compound channel. Some methods require that the division lines themselves are included as wetted perimeter values. This approach allows for the flow resistance generated as a result of momentum transfer between zones to be catered for by arbitrarily increasing the resistance due to bed friction.

2.5.4 Computational modelling

One dimensional computational water models are the Water Industry's main tool for assessing the hydraulic performance of natural rivers and flood alleviation schemes. Mike 11, HEC-RAS and Flucomp 1 & 2 are among the most popular 1D models used in the UK at present. A 1D model is created by dividing a river reach into a number of representative cross-sections. Conveyance tables are constructed to describe the flow characteristics for all possible water levels at each individual cross-section. Conveyance, K is a function of discharge, Q, where $Q = K\sqrt{S_o}$ and S_0 is the bed slope. The flow characteristics in adjacent cross-sections can be related using the St Venant equations which are solved to determine the actual variation of water levels between the cross-sections for different upstream and downstream boundary conditions. The accuracy of the models is very dependent on the accuracy of the methods used for predicting the discharge capacity at each cross-section.

Typically the extra flow resistance generated by the turbulence and momentum transfer between the layers in a compound channel is not explicitly determined during the compilation of the conveyance tables. The extra flow resistance is incorporated during the calibration of the 1D models against known water surface levels and corresponding discharge rates in overbank flow. The conveyance tables are calculated for individual reaches using, for example, the divided channel method which incorporates the Engineer's estimates for the flow resistance generated by friction and secondary circulation. Comparison with calibration data acquired from measured flood events generally shows that the model underestimates the water levels achieved for the known discharge because it does not allow for the interaction losses. As a result the Engineer is

forced to adjusted the friction resistance coefficients until the predicted water levels tally with those obtained from the calibration event. These artificial friction coefficients are subsequently used to determine the water levels for a given discharge whatever the configuration of natural channel or flood alleviation scheme, even though they are only reliable for the same configuration of river channel which existed when the calibration data was gathered. Consequently Engineers have adopted designs for various flood defence schemes which have been very conservative in order to ensure that very few problems were created as a result of this shortcoming which is universally recognised by the Water Industry.

In order to ensure a conservative design traditional flood defence schemes have been commonly implemented. These traditional schemes are often favoured because they guarantee an overall lowering of basic flow resistance from that exhibited by the calibration events. Alternative Environmentally sensitive flood defence schemes, such as compound channels, could only be realistically promoted when the causes for the interaction head losses were better understood and explicitly included in reliable prediction methods. The following sections outline the research performed in recent years to elaborate the flow behaviour of compound channels and describe the various prediction methods which have been developed.

2.6 Flow behaviour in straight compound channels

2.6.1 Introduction

Straight compound channels are idealised forms of compound channel. They do not tend to occur naturally but are usually produced as the result of man's intervention. Figure 2.20 shows the cross-sectional configuration of a typical straight compound channel.

This section presents a limited review of the significant research performed to date which has revealed the intricacies of their flow behaviour and has produced methods which can predict the characteristics of this flow behaviour. Wark [1993] should be consulted for a more comprehensive review.

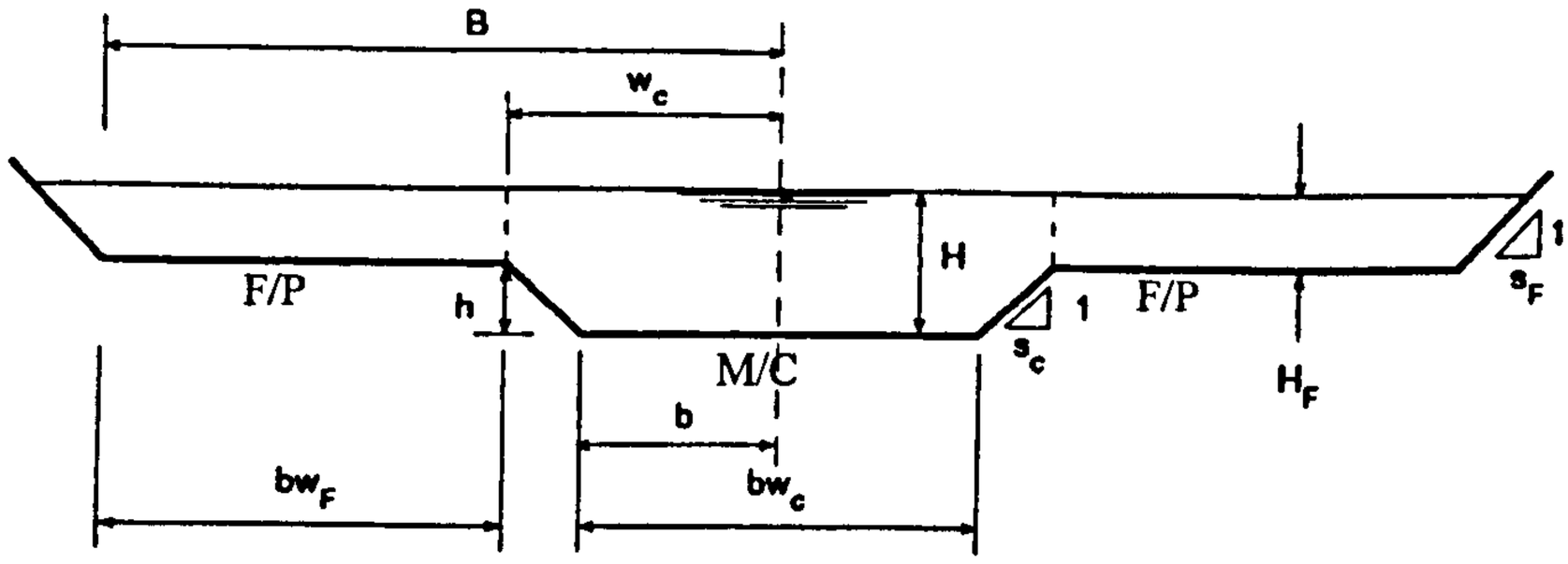

Figure 2.20 Geometric parameters after Ackers [1991]

2.6.2 Flow characteristics and mechanisms

2.6.2.1 Stage and Discharge relationship

Sellin [1964] performed some of the first documented laboratory experiments that investigated flow behaviour in straight compound channels. He measured the stage and discharge of the channels and demonstrated an anomaly in flow behaviour of the straight compound channels when the water flowed just overbank. At this flow depth the discharge capacity of the compound channel was actually less than when the main channel was flowing at bankfull levels. He also noted that for all levels of flow on the flood plain the discharge capacity was less than was expected if bed friction was the only source of flow resistance. He concluded that this was evidence for the existence of interaction mechanisms which generate extra flow resistance.

A number of researchers including Bhowmik and Demissie [1982] and Knight et al [1989] have produced field data for the Salt Creek river in Greenview, Illinois and the River Severn at Montford bridge respectively which have corroborated that this characteristic stage and discharge behaviour is exhibited by natural rivers.

2.6.2.2 Velocity Distribution

Sellin [1964] took point velocities readings for a number of different channel configurations. He demonstrated that the average flow velocity on the flood plains was lower than in the main channel. Zheleznyakov [1965] suggested that the flow behaviour

exhibited by straight compound channels can be divided into two different regions depending on flow depth. At low overbank stages he showed that the main channel velocity initially decreased and then, after a certain depth is reached started to increase once again. He also showed that main channel velocity was reduced more when the flood plain was rougher. Myers [1978] demonstrated that the relative velocity between the two flow regions (main channel and flood plain) depended on the relative flow depth, [H-h]/H. Rajaratnam and Ahmadi [1979, 1981] investigated the dimensions of the lateral width over which a shear layer is developed between the two flow regions and derived an empirical relationship between the width of the shear layer and the main channel depth as shown in Equations 2.28-2.30.

$$B_{slt}=5.97h \quad [2.28]$$

$$B_{slm}=4.37h \quad [2.29]$$

$$B_{slf}=1.6h \quad [2.30]$$

where B_{slt} is the total shear layer and B_{slm} and B_{slf} are the shear layer widths in the main channel and flood plain respectively. Baird and Ervine [1982, 1984] demonstrated that relative velocity depended on relative flow depth and Aspect ratio of the two channels. Knight, Demetriou and Hamed [1983] demonstrated that the relative velocity depended on relative flow depth, Aspect ratio of the main channel and flood plain region, $[2*w_c/h]$ and $[[bw_f+h*s_f]/h]$ respectively, and the relative roughness of the flood plains and main channel, f_f and f_c respectively. Pasche and Rouve [1985] demonstrated that for smooth flood plain channels the main channel side slopes effect the magnitude of the channel interaction but the effect was less significant when the flood plains were heavily roughened.

A series of large scale straight compound channels were also built and tested between 1986 and 1989 as part of the Series A experimental programme. The models were built at the Flood Channel Facility (FCF) at HR Wallingford. Eleven models with different configurations were built. The influence of the four significant parameters identified by previous researchers: relative flow depth, channel width, relative roughness and main channel side slope were investigated. The data also demonstrated the effect of scale on the interactions in a straight compound channel and provided enough data to facilitate the production of a definitive discharge prediction method.

2.6.2.3 Boundary shear stress distribution and Turbulence measurements

Significant results demonstrating the influence of various parameters on the distribution and magnitude of boundary shear stress and local turbulence have been obtained by a number of researchers. Myers [1978], Rajaratnam and Ahmadi [1981], Knight and Hamed [1984] and Knight and Lai [1985] all demonstrated how shear stress varies along the channel boundary in different model configurations and for varying flow states. Prinos et al [1985] and Knight and Cao [1994] confirmed that local boundary stresses are strongly influenced by the lateral transfer of momentum between the main channel and flood plain flows and hence depend on the four parameters: relative flow depth, the channel widths, the relative roughness and the main channel side slope. They showed that the longitudinal and vertical turbulence intensities were significantly higher in the area where there was a lateral transfer of momentum between the fast flowing main channel and the slower flood plain. Knight and Cao [1994] demonstrated that the local boundary shear stress on the flood plains was some 42% larger than the expected two-dimensional value, given by $\rho g(H-h)S_O$ in the lateral shear zone (probably because of the turbulence effects from the secondary circulation and vorticity). They also demonstrated that the slope of the main channel side slopes had a significant effect. For vertical slopes the maximum shear stress occurs near the top of the wall, for 1:1 slopes the maximum shear stress just below the mid-point of wall, for 1:2 slopes the maximum shear stress occurs close to the bed of the main channel.

As the research focus turned towards the development of numerical simulation of the turbulence-driven secondary currents in compound channels further refined measurements were taken in order to establish the magnitude of local turbulence. Prinos et al [1985] and Tominaga et al [1989] used hot-film anemometry. Recently Knight and Shiono [1991] (as part of the Series A programme) and Tominaga and Nezu [1991] used Laser Doppler anemometry. Both the Series A data and the data produced by Tominaga and Nezu [1991] have been used extensively to validate various numerical models.

2.6.2.4 Interaction mechanisms

Sellin [1964] used photographic methods, with aluminium powder floating on the water surface, in order to show that vortices with vertical axes were established at the interface

between these fast and slow flowing regions, as shown in Figure 2.21. Water was exchanged between the two regions of flow causing a transfer of momentum. and resultant head loss.

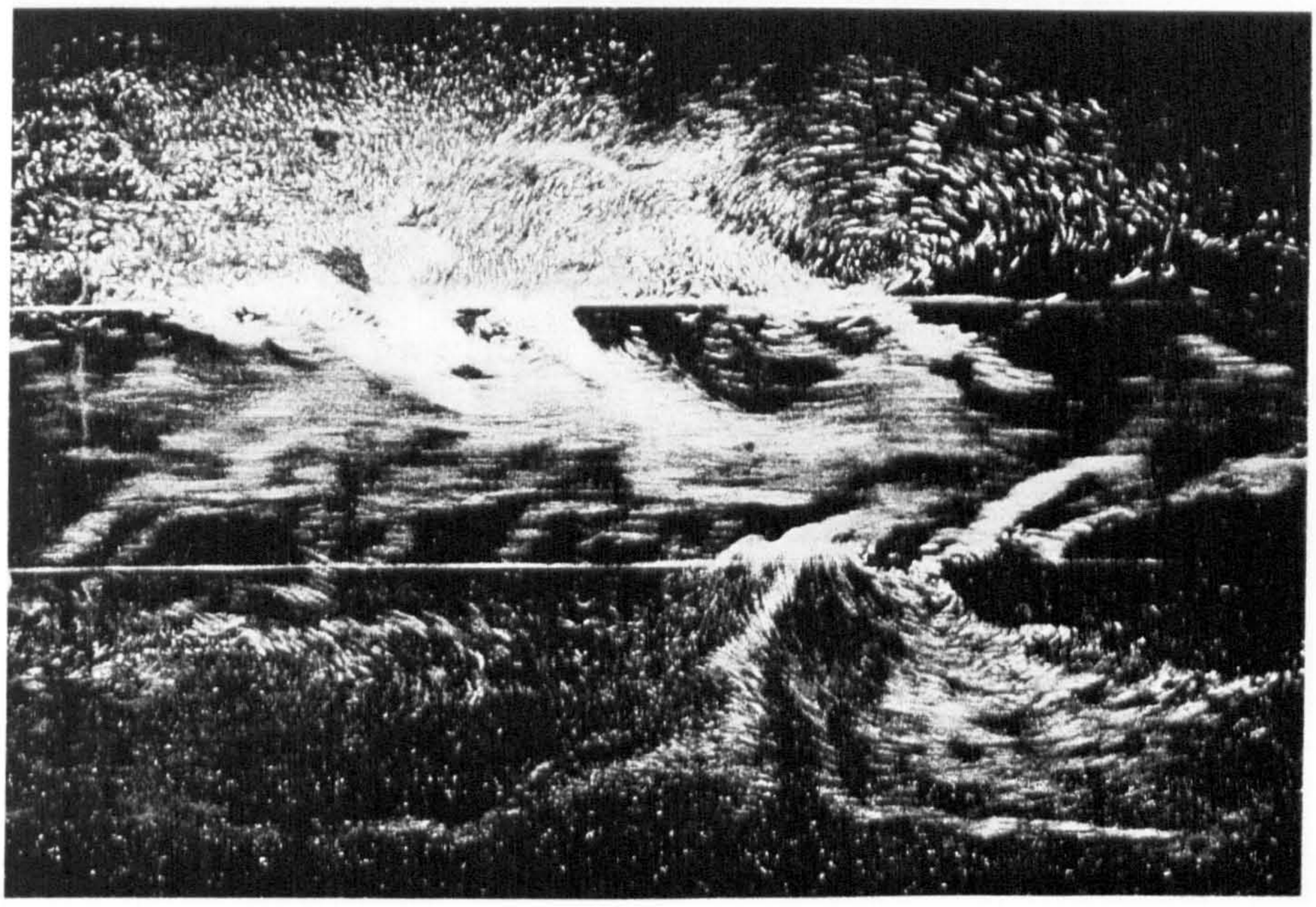

Figure 2.21 Vortices between main channel and flood plain flow (after Sellin [1964])

He showed that the relative roughness of the flood plain to the main channel had a major effect on the size of interaction losses and he attempted to develop a relationship linking the pitch (centres) of the vortices to the overall discharge capacity of the channel. This was not successful and there have been no subsequent attempts to extend this work. He also investigated ways of decreasing the interaction between the main channel and flood plains using a slotted wall at their boundary. He demonstrated that an effective increase in the discharge capacity of the overall channel was only possible if the extra frictional resistance produced by the walls was insignificant compared to the flow resistance induced by momentum transfer.

In subsequent years many researchers demonstrated the presence of a shear layer at the interface between the flood plain and main channel. The extent of the shear layer was distinguished by the area of steep gradient on a plot showing the distribution of the depth averaged longitudinal velocity. The gradients were steepest at lower depth ratios.

During the early 1990s the development and application of LDA enabled Tominaga and Nezu [1991] to show that secondary currents with axes parallel to longitudinal axes of the channel were also generated at the interface between the main channel and the flood plain and contributed to the transfer of momentum, as shown in Figure 2.22.

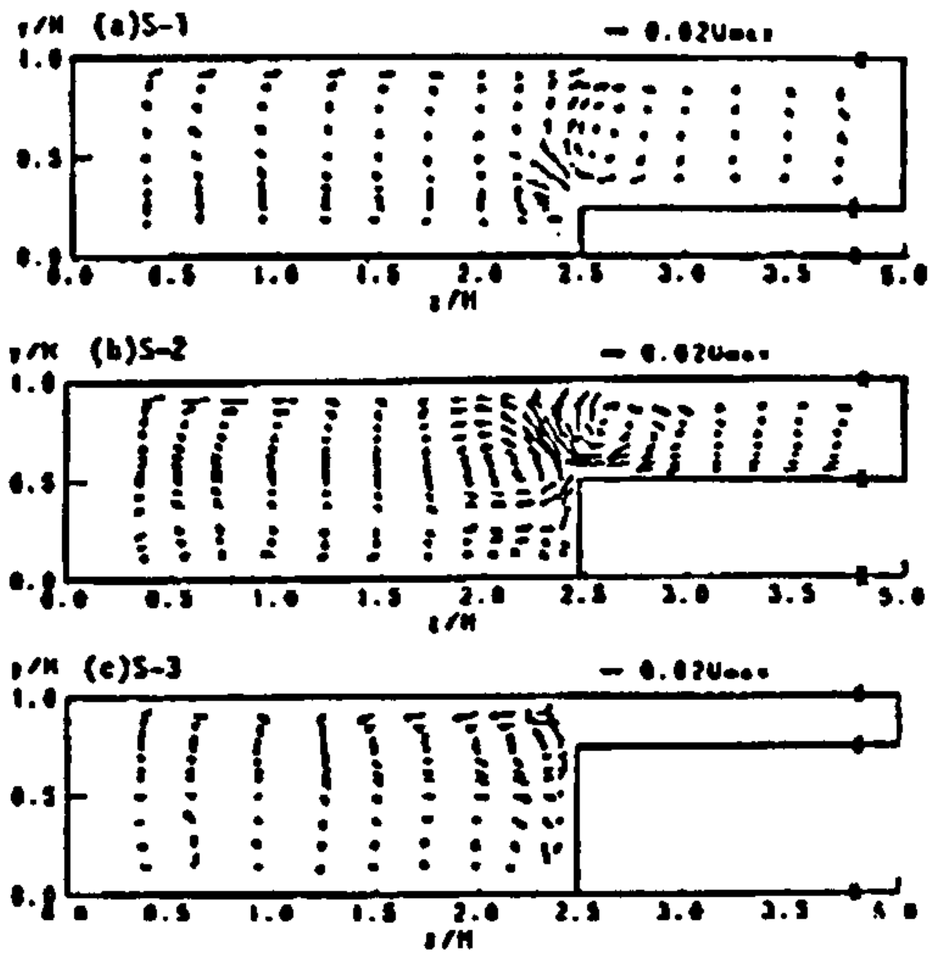

Figure 2.22 Secondary current distributions (after Tominaga et al [1989, 1991])

Kawahara and Tamai [1989] suggested that the mechanism of momentum transfer consists of a combination of two main components, advection by secondary flow and turbulent diffusion. They demonstrated that the advection was small compared with the diffusion component at low flood plain depths but became increasingly insignificant for increasing flow depths.

Nazu and Rodi [1985] observed that for certain flows, turbulent eddies do not have sufficient energy to break the water surface and therefore break down into smaller ones, redistributing the velocity fluctuations.

2.6.2.5 Unsteady flow in straight compound channels

Recently a number of investigations into the flow behaviour of straight compound channels when subjected to unsteady flow have been performed. Nezu et al [1993] demonstrated that the boundary shear stress was considerably larger in the rising stage than in the falling stage in open channels. Tominaga et al [1994] demonstrated that the

unsteady flow characteristics of a compound channel are different to those in rectangular channels.

Tominaga et al [1994] used a 13m long, 0.6m wide, 0.4 m deep and 1:1000 slope tilting flume with a main channel 0.2m wide and 0.059m deep. The unsteady flow was set with a base flow of $0.003m^3/s$, a peak flow of $0.02m^3/s$, time to peak, T_P equal to 60s (large unsteadiness) and 120s (small unsteadiness) and a peak period equal to $T_P/6$. The velocity was measured using mini-propellers at a sampling rate of 180s and 320s for T_P equal to 60 and 120secs respectively. In the main channel the velocity varies drawing a clear loop and the difference in velocity is extremely large between the rising and falling stages, as shown in Figure 2.23.

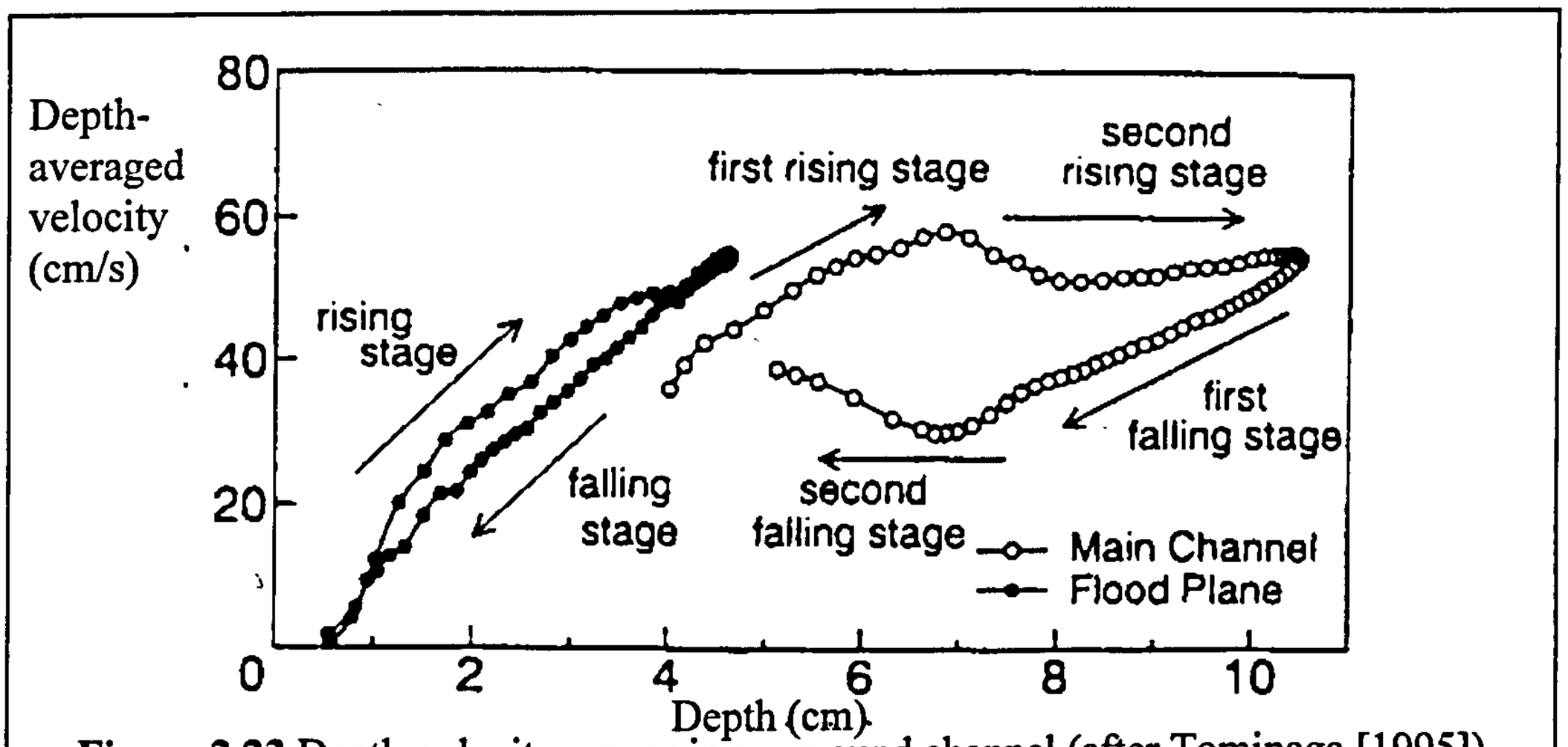

Figure 2.23 Depth-velocity curves in compound channel (after Tominaga [1995])

Tominaga [1995] noted that the whole process of depth-velocity variation can be divided into four stages: the first and second rising stage and the first and second falling stage. In the flood plain the loop property is less significant than in the main channel. Many point velocity measurements (in 2-dimensions) were taken by Tominaga [1995] and he demonstrated that there is a considerable difference between the flow structures in compound and rectangular channels for unsteady flow. They showed that when the unsteadiness was large the peak value of velocity occurred earlier in the main channel than in the single cross-section rectangular channels. In the flood plain the unsteadiness was smaller than in the main channel. When the unsteadiness was mild the main channel velocity decreases in the second rising stage because of the effects of mixing between the main channel and flood plain flows.

Tu et al [1995] reported their findings using an asymmetric compound channel. The flume was 24m long, 1m wide, at a slope of 1:2000 and with a lower channel 0.4m wide and 0.05m deep. Two electromagnetic probes were used to measure three components of velocity at 5cm intervals across the flume and at 5mm in the vertical. Tu et al [1995] observed that the velocities (mainly longitudinal) were reduced close to the interface between the flood plain and the main channel and at flood plain height. The measurements for transverse velocity component (w) showed that in the main channel close to the interface the secondary flow towards the main channel is much stronger during the rising stage while at the centre of the main channel the w-component is almost zero. The log law for vertical velocity distribution is only valid below the flood plain height. The longitudinal velocity component's distribution across the compound channel section is highly non-uniform in the rising stage while it becomes much more uniform in the falling stage. Tu et al [1995] observed that the conclusion drawn from these experiments may not be true for other hydrographs. Further experiments are required to confirm.

A second paper by Tu et al [1995] also reported results for unsteady flow when the upper flood plain channel was vegetated. They used the same basic flume with rigid wooden cylinders set at the apices of a square acrylic resin plate (with dimensions of 2.5cm by 2.5cm) to model the vegetation. The thickness of the resin plate was 1.45cm so the depth of the lower channel became 0.0645m. They concluded that the roughness of the flood plain, due to vegetation, increases the flow resistance and raises the water level on the flood plain (excluding the interactive zone) while decreasing the velocity, thus enhancing the difference between the flood plain and main channel velocities in a similar way as is observed in steady flow. Unlike smooth compound channel flow velocity distribution in the transverse direction is highly non-uniform in both rising and receding stages. This indicates that in the contact zone flow pattern reverses from rising to receding stage and outside of the contact zone, there is a clockwise secondary flow in the main channel.

2.6.3 Deterministic methods for predicting discharge capacity

2.6.3.1 The Division Line method

These methods divide the cross-section of a compound channel into several units separated by lines of supposedly zero stress as shown in Figure 2.24.

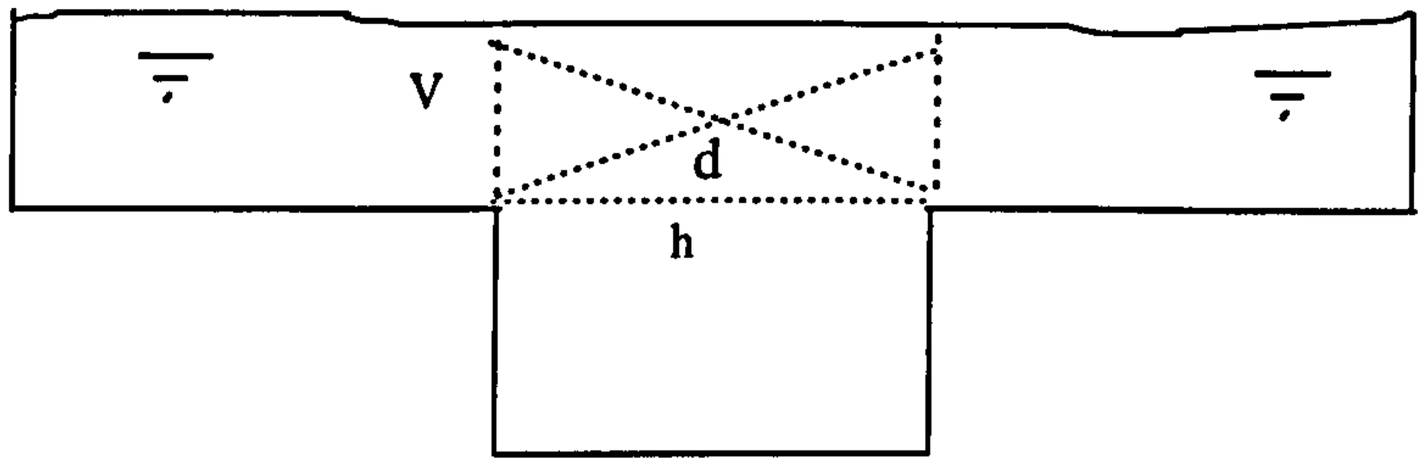

Figure 2.24 Channel cross-section showing alternative division lines

Various methods have been proposed and involve choosing pertinent dividing lines which demarcate planes of zero shear stress. Typically these have coincided with the top bank of the main channel and have been either vertical, v, horizontal, h, or diagonal, d. These methods typically require that some of the length of the division lines are included in the wetted perimeter values in order to account for the flow resistance due to the momentum transfer between flow zones, by artificially increasing the frictional resistance that is imposed. Ramsbottom [1989] reviewed eight of these methods and showed that a vertical division method which included the division in the wetted perimeter of the flood plains and not the main channel worked most effectively. Wormleaton *et al* [1982] developed the Apparent shear stress ratio (ASSR), λ_i. He demonstrated that λ_i could be used as a criterion for selecting whether or not to include the wetted perimeter in the discharge calculation. Holden and James [1988] proposed methods in which they attempted to develop empirical adjustments to either the flow area or the wetted perimeter lengths in the division line method. They demonstrated that the 'modified k method' with vertical division lines which involved deriving an adjusted wetted perimeter, P_c' for the main channel according to Equation 2.31. The Holden and James [1988] method generated fairly reliable results but all these methods were limited by the artificiality of the division line designation and the absence of an allowance for the real interaction mechanisms within the flow.

$$P_c'=P_c+2kd \qquad [2.31]$$

where

$$\log(k)=1.274(v_c/v_{fp})-2.235 \qquad [2.32]$$

v_c and v_{fp} are the average velocities in the main channel and flood plain respectively and, d, is the flood plain flow depth.

The division line methods incorporate no recognition of the real interaction mechanisms that may be encountered in compound channel flow. Different division lines are clearly more appropriate at different flow depths. Consequently they should only ever be used with great care to determine discharge capacity.

2.6.3.2 Apparent Shear stress method and correction factors methods

Further experimental programmes confirmed the dependency of the flow behaviour on various parameters. Prinos and Townsend [1984], Wormleaton *et al* [1985], Knight and Lai [1985] and Holden and James [1988, 1989] produced more raw data that demonstrated that apparent shear stresses are dependant on a combination of the following parameters: relative flow depth, channel width, relative roughness and main channel side slope.

A number of authors such as Baird and Ervine [1982], Radojkovic and Djordjevic [1985] and Wormleaton and Merrett [1990] have suggested that the influence of the interaction mechanism in straight compound channel flow can be represented by an apparent shear stress acting on the division lines in the channel. Formulations for Apparent Shear stress have often been used as the basis for deriving correction factors such as the Radojkovic indices, ϕ which relate the predicted discharge in each flow zone allowing for bed friction only to the actual discharge in a straight compound channel as shown in Equation 2.33.

$$Q_T=Q_C\phi_C^{(1/2)}+Q_{fp}\phi_{fp}^{(1/2)} \qquad [2.33]$$

The indices are related to Apparent shear stress assuming fully turbulent flow by Equation 2.34

$$\phi_C=\tau'_C/\tau_C=(V'_C/V_C)^2 \qquad [2.34]$$

where $\tau_C = \frac{\rho g A_C}{2y_{fp}}(1-\phi_C)$ and $\tau_{fp} = \frac{\rho g A_{fp}}{2y_{fp}}(\phi_{fp}-1)$ [2.35]

Various formulations have been developed by the authors listed above which define Apparent shear stress in terms of various geometric and flow parameters and have been

obtained from a number of experiments. These are summarised in Wark [1993]. The author has reservations about the use of Apparent shear force methods. Analysis is only realistically possible in laboratory scale channels because shear forces require great care in their measurement and τ_C' must be averaged over the whole river cross-section.

General correction factor methods have similar limitations to the division line methods. They incorporate no recognition of the real interaction mechanisms that may be encountered in compound channel flow and may only be appropriate for the model on which they were based. They should only ever be used with great care to determine discharge capacity.

2.6.3.3 Ackers Method

Introduction

Ackers [1991] devised an empirical discharge capacity prediction method based mainly on the large scale model tests conducted at the Flood Channel Facility (FCF) in HR Wallingford (1986-1989). He produced adjustment factors based on two main parameters, Coherence and DISADF.

Coherence is a measure of interaction between the main channel and flood plain flows and depends on the comparability of the hydraulic conditions in these zones. It is the ratio of the conveyance calculated by treating the channel as a single unit (with perimeter of friction factors) to that calculated by summing the conveyance of the individual zones and is defined in Equation 2.45

$$COH = \frac{\sum_{i=1}^{i=n} A_i \sqrt{\sum_{i=1}^{=n} A_i \Big/ \sum_{i=1}^{=n} (f_i P_i)}}{\sum_{i=1}^{=n} \left[A_i \sqrt{A_i / f_i P_i} \right]} \qquad [2.36]$$

DISADF is a non-dimensional measure of discharge and is defined as the ratio of the actual discharge capacity of a straight compound channel, Q, divided by the theoretical discharge, Q_{TB} , which is equal to the sum of the discharges in the two zones created by the vertical division lines shown in Figure 2.24: the main channel, Q_{CB}, and the flood plain, Q_{FB}. The further DISADF falls below one, the greater the interaction losses between the main and flood plain channels.

$$DISADF = \frac{Actual\ discharge,\ Q_A}{Theoretically\ determined\ discharge\ (Q_{CB} + Q_{FB})} \quad [2.37]$$

A typical plot of relative depth H*=(H-h)/H versus DISADF is shown in Figure 2.25. It reveals 4 flow regions which represent 4 changes in the dominance of different interaction mechanisms.

Ackers [1991] used the available results obtained during Series A to develop empirical equations to give the best estimate for the discharge in each flow region. The method did not rely on the modelling of the precise interaction behaviour. The best estimate for flow in Region 1 is obtained from Equation 2.38

$$Q_{R1}=Q_{TB}-(Q_{*2C}+N_FQ_{*2F})(V_C-V_F)Hh^*ARF \quad [2.38]$$

If the flow was in region 2, 3,4 then the best estimate is obtained from Equation 2.39

$$Q_{R2,3\ or\ 4}=DISADF_{R2,\ 3\ or\ 4}*Q_{TB} \quad [2.39]$$

ARF is equal to 2b/10h unless b/h>20 then ARF=2. The unknowns in Equations 2.38 and 2.39:- $DISADF_{R2,\ 3\ or\ 4}$, Q_{*2C}, Q_{*2F}, were empirically determined using data gathered from the Series A experiments.

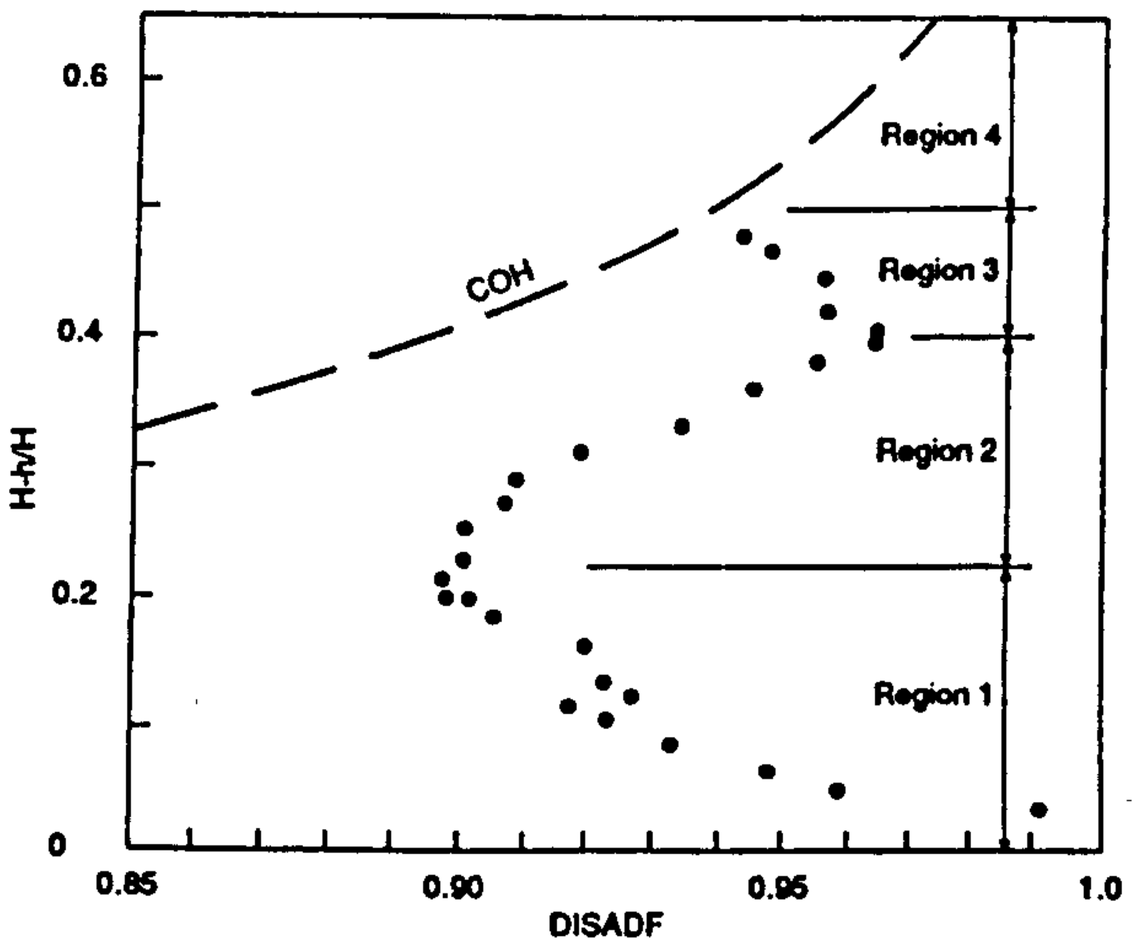

Figure 2.25 The variation of DISADF with relative depth after Ackers [1991]

Region 1

Figure 2.25 shows that in Region 1 where the flow depth are relatively shallow the interference effects increase progressively with depth. The Ackers [1991] formulation utilises a discharge deficit, Q_{*2}, normalised by the product $(V_C-V_F)Hh$ to relate the theoretically determined discharge capacity of the channel (assuming the only source of

flow resistance was bed friction) to the actual discharge capacity. The discharge deficit is then deducted from the theoretical discharge, as shown in Equation 2.38, using the separate deficits for flood plains and main channel which are defined in Equations 2.40 and 2.41. An additional adjustment for aspect ratio is also included.

$$Q_{*2F}= -1.0H^*(f_c/f_f) \quad [2.40]$$

$$Q_{*2C}= -1.24+0.395B/W_c+GH^* \quad [2.41]$$

A lower limit for $Q_{*2C}=0.5$ with ($Q_{*2F}=0$) was set to provide some minimum interaction effect and the magnitude of G is defined in Equations 2.42 and 2.43.

For $s_C>1.0$ $G=10.42+0.17f_F/f_C$ [2.42]

For $s_C<1.0$ $G=10.42+0.17\ s_C\ f_F/f_C+0.34(1-s_C)$ [2.43]

Region 2

Figure 2.25 also shows that from a minimum value of DISADF at the end of region 1 the interference effects in region 2 reduce again, DISADF increases. Ackers [1991] demonstrated that DISADF can be related to the magnitude of coherence (COH) with the coherence value shifted to an increased depth as shown in Equation 2.44

$$DISADF(H^*)=COH(H^*+shift) \quad [2.44]$$

The magnitude of shift is defined in Equations 2.43 and 2.44.

For $s_c>1.0$ $shift=0.05+0.05N_F$ [2.45]

For $s_c<1.0$ $shift=-0.01+0.05N_F+0.06s_c$ [2.46]

Region 3

Figure 2.25 shows that at high flow depth in Region 3 the flow resistance due to interference starts to increase once again over a short range of flow depths. Ackers [1991] derived empirically a definition for DISADF in Region 3 in terms of Coherence, as shown in Equation 2.47.

$$DISADF=1.567-0.667*COH \quad [2.47]$$

Region 4

In this region Ackers [1991] noted that the coherence of the cross-section is such that it may be treated as a single section when calculating overall flow, with perimeter weighting of friction factors. DISADF was therefore defined as shown in Equation 2.48.

$$DISADF=COH \quad [2.48]$$

Choice of region

The logic behind the selection of the appropriate region, given in Equations 2.49 - 2.51, and hence which set of equations to apply depends on the relative magnitude of the discharge calculated using each set of equations.

If $Q_{R1} \geq Q_{R2}$ then $Q = Q_{R1}$ [2.49]

If $Q_{R1} < Q_{R2}$ and $Q_{R2} \leq Q_{R3}$ then $Q = Q_{R2}$ [2.50]

If $Q_{R1} < Q_{R2}$ and $Q_{R3} < Q_{R2}$ then $Q = Q_{R3}$ unless $Q_{R4} > Q_{R3}$ when $Q = Q_{R4}$ [2.51]

Limitations of the Ackers [1991] method

The Ackers [1991] method is the most reliable hand calculation method yet developed for predicting the discharge capacity of straight compound channels. It is applied to each zone separately so that shear stress can be measured and the critical state of flow can be determined. However the Ackers [1991] formulation was not based on the conceptual modelling of the physical phenomenon. It was purely based on empirical results. There is scope to use the results to investigate further the nature of flows corresponding to the 4 flow regions which may lead to the refinement of the prediction method.

2.6.4 Computational models for predicting flow behaviour

2.6.4.1 Introduction

Two other approaches to modelling flow behaviour in straight compound channels have been adopted, as alternatives to the one-dimensional methods described in the previous sections, in which the effect of flow interaction is determined on the fluid in the complete cross-section. One method is based on the solution of depth-averaged or integrated equations of flow with a free surface, known as the Lateral Distribution Method (LDM). The other is based on three dimensional models which incorporate turbulence modelling.

2.6.4.2 Lateral Distribution Method (LDM)

These methods involve evaluating the integral for Q given in Equation 2.52 using an equation which specifies the lateral variation of the velocity component, U.

$$Q = \int u_s dA \qquad [2.52]$$

The depth-wise variation of u is assumed to be of some standard form, say logarithmic. The longitudinal dynamic equation is integrated through depth to give Equation 2.53.

$$gDS + Bf\frac{U^2}{8} = \frac{\delta}{\delta y}\left[\varepsilon\frac{\delta DU}{\delta y}\right] \qquad [2.53]$$

where U is the depth-averaged velocity, D is the flow depth, f is the Darcy friction factor, ε is a turbulence exchange parameter and B is a factor depending on the transverse slope. This exchange parameter models the momentum exchange through turbulence between the main channel and flood plain flows. It is related to the primary flow variables and the geometric properties of the cross-section and effectively introduces a correction factor linked closely to the physics of the flow. For most definitions of ε, Equation 2.53 is not amenable to direct solution but numerical methods with the aid of a computer are used. Ramsbottom [1989], Wormleaton *et al* [1988], Knight *et al* [1989] and Wark *et al* [1993] have demonstrated that this approach produces accurate predictions for the variation of span-wise depth-averaged velocity which can be used to derive predictions for discharge capacity with the same level of accuracy as the Ackers [1991] method. Samuels [1988] and Shiono and Knight [1988] developed analytical solutions to the basic equation by imposing a number of assumptions which are described in more detail in Wark [1993].

2.6.4.3 Turbulence models for straight compound channels

Krishnappan and Lau [1985] and Prinos [1990] have developed algebraic stress models which can calculate 3-dimensional flow fields and apparent shear stresses. Naot et al [1993] and latterly Nezu et al [1995] developed an algebraic stress model that can simulate secondary currents in compound open channel flows. The algebraic stress model is derived from the full stress transport model assuming local equilibrium where the production of turbulence, π is balanced by the dissipation, ε. Figure 2.26 shows the isovel lines of the mean primary velocity U(y,z) normalised by the maximum velocity U_{Max} at D/H=0.25, 0.5 and 0.75 (where D equals flood plain depth and H equals main channel depth) from the experimental data obtained by Tominaga and Nezu [1991] and the numerical predictions using the algebraic stress model. Figure 2.27 shows the patterns of secondary currents at D/H=0.25, 0.5 and 0.75. The numerical simulation

produces very similar results to the experimental ones both qualitatively and quantitatively.

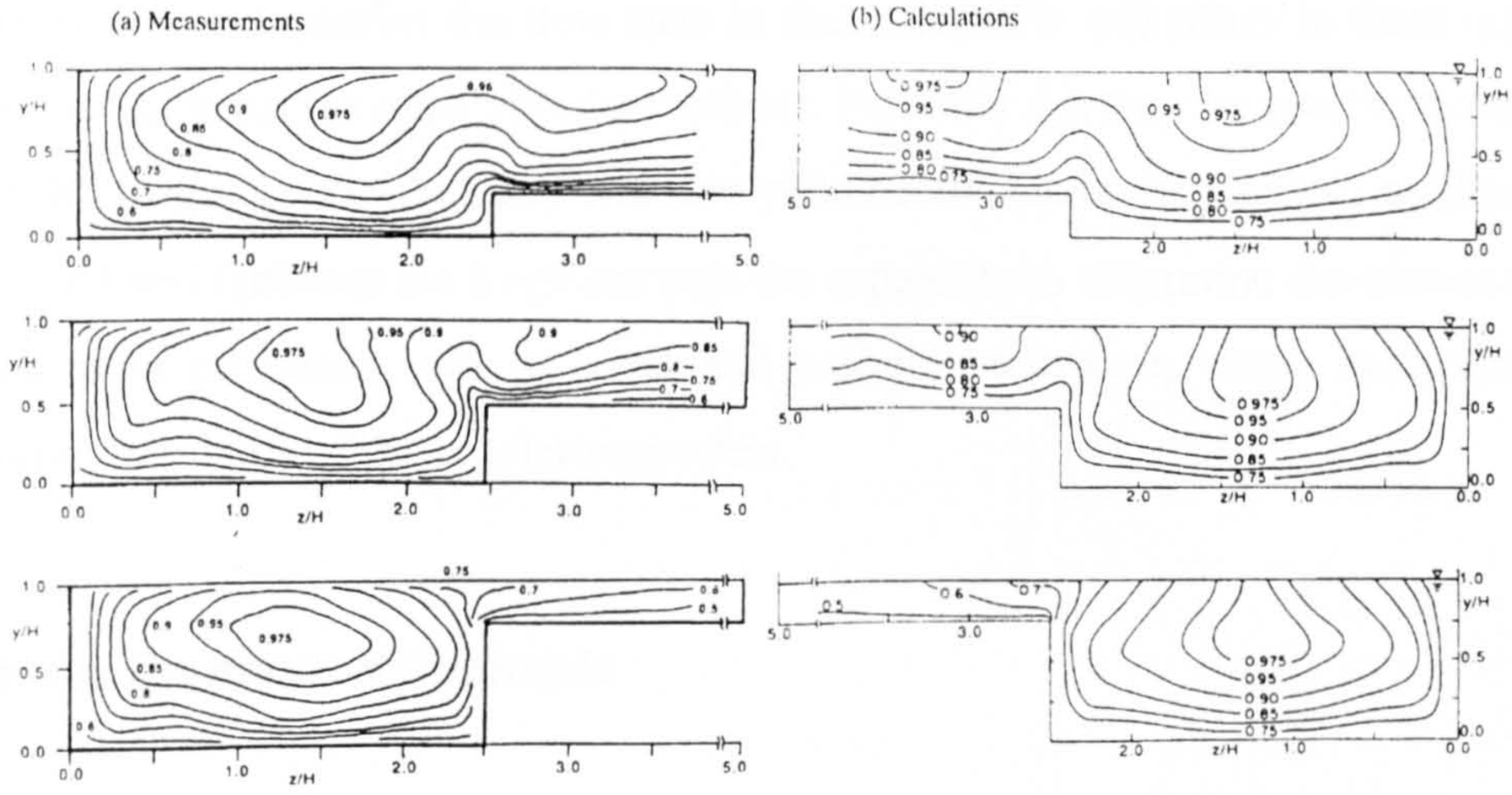

Figure 2.26 Isovels at D/H=0.25, 0.5 and 0.75 (after Nezu [1994])

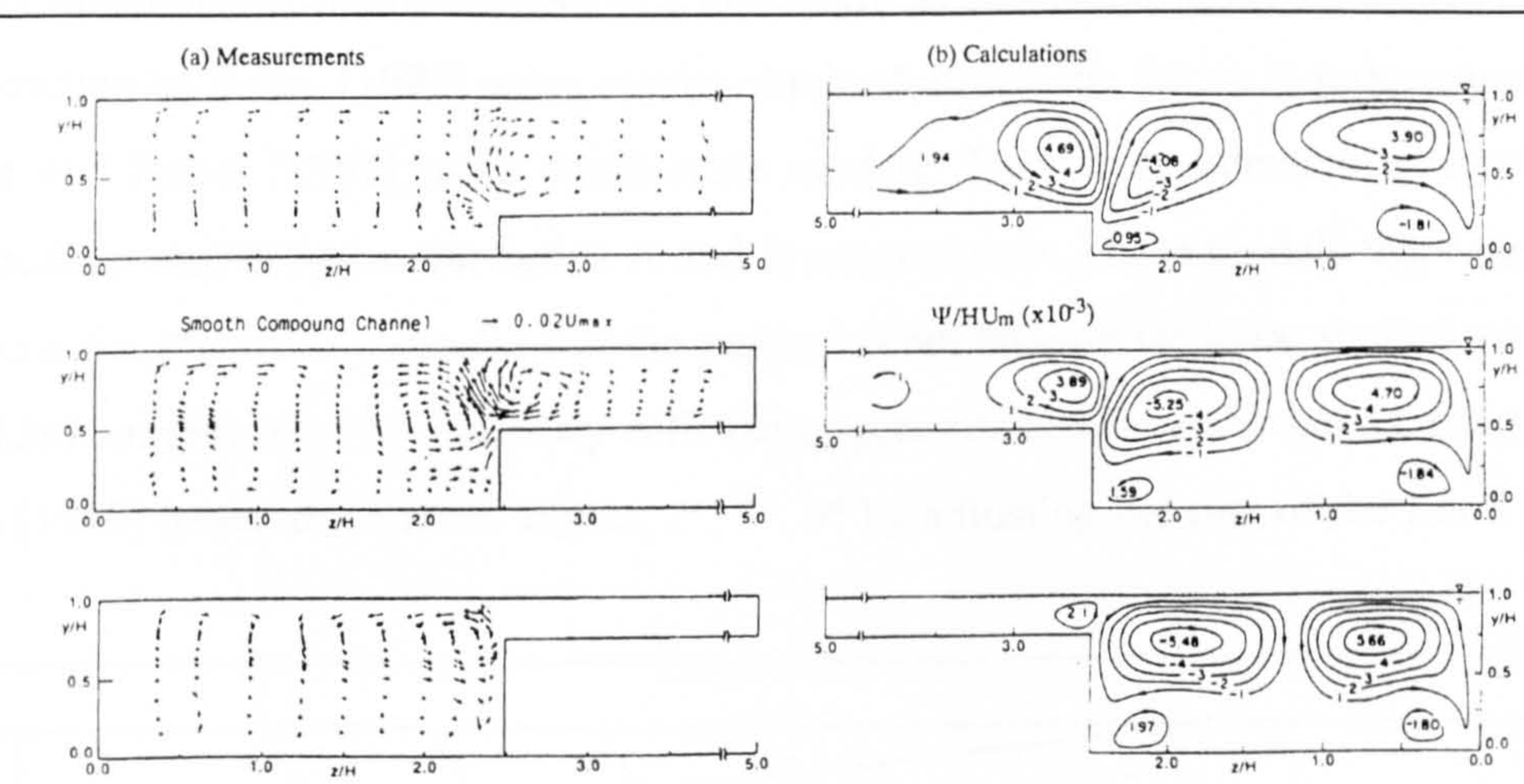

Figure 2.27 Secondary currents at D/H=0.25, 0.5 and 0.75 (after Nezu [1994])

Thomas and Williams [1995] report the production of a Large Eddy Simulation (LES) of turbulent flow in symmetric straight compound channels from the Series A experimental programme. The level of agreement is similar to that obtained using algebraic stress models.

The computational difficulties of extending the three dimensional models described above will for the time-being severely limit the use of these models by the Engineering

community as a whole. However if these problems can be resolved then the ability of the models to actually replicate the physical processes observed in straight compound channel flow and to predict the flow state in these channels will result in these types of models replacing all the other simpler methods. Not only can they be used to accurately predict discharge capacity but they will also yield details about the intrinsic mechanisms of flow and will facilitate the Engineer with the capability to determine the impact of the flow on other processes such as scour and pollution transport, vastly increasing the scope and usefulness of the predictive models.

2.7 Skew Compound Channels

2.7.1 Introduction

Skew compound channels consist of a straight lower channel which cuts across a straight upper (flood plain) channel at a low angle as shown in Figure 2.28. They have been studied by Sellin [1995] using results obtained during the Series A programme and Ervine and Jasem [1995] using small scale models. They were intended to create an intermediate step between the Series A and B programmes. These models were devised to enable the effects of cross-flow at the main channel boundaries to be studied without the added complication of secondary cells being generated by meander bends. Elliot and Sellin [1988] tested three skew angles, 2°, 5°, 9° by adjusting the line of the flood plain walls.

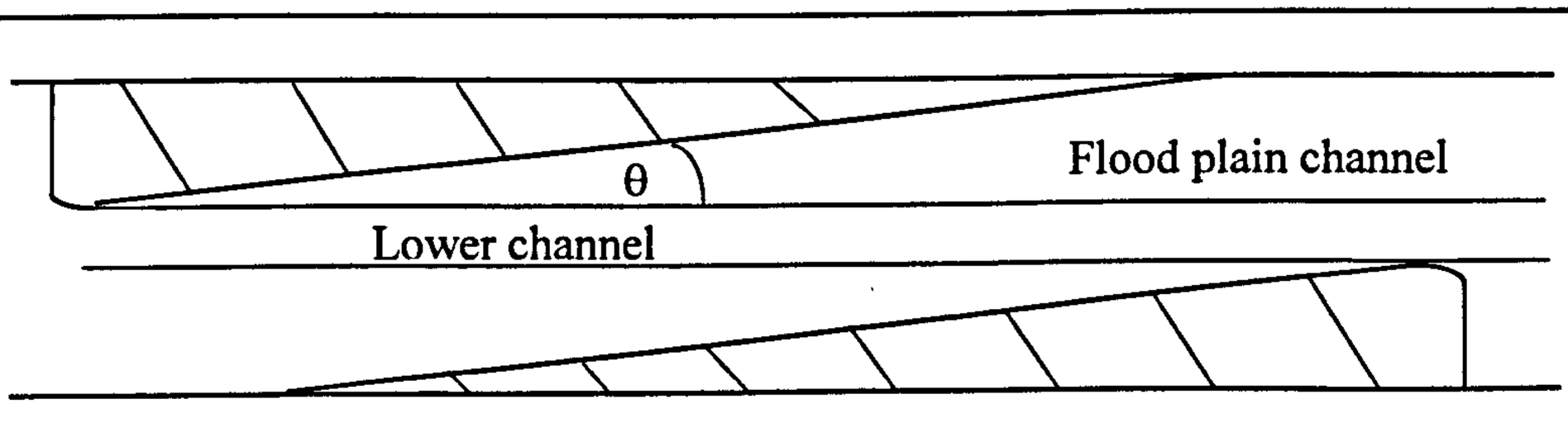

Figure 2.28 Plan of skew channel, skew angle = θ

Sellin and Elliot [1990] and Sellin [1995] attempted to develop a method to apply a simple division line discharge capacity prediction method to skew channels. Ackers [1991] introduced a linear modification in his straight channel method to account for the

flow behaviour of skew channels with skew angles, θ, between 1°-10° as described by Equation 2.55.

2.7.2 Flow characteristics and mechanisms

2.7.2.1 Stage and Discharge relationship

The skew compound channel models which were built at the FCF during Series A and were analysed by Sellin [1995] were 5.6m wide, 60m long with a main channel 1.2m wide, 0.15m deep and at a skew angle of: 2.1°, 5.1°, and 9.2°, and with three side slope angles; s_c=0, 1, 2. Sellin [1995] demonstrated that the loss of discharge in a skew compound channel compared with a straight channel rises to a value of 10% at H*=0.25 and then falls to a minimum of 2% at H*=0.4. He also demonstrated that variation in skew angle had a minor effect on this behaviour but the side slope angle had a major effect with almost no loss in discharge capacity in the 5% skew channel with side slopes equal to s_c=2 but as much as 20% loss for s_c=0 (rectangular channel).

Ervine and Jasem [1990] used a non-dimensional measure of discharge F* to illustrate flow behaviour in skew compound channels. F* is defined in Equation 2.54

$$F^* \equiv \frac{\text{ACTUAL MEASURED DISCHARGE (Qmeas)}}{\text{THEORETICAL DISCHARGE (BED FRICTION LOSSES ONLY (Qf))}} \qquad [2.54]$$

They showed that for smooth flood plains the value of F* for small scale model tests with low Aspect ratio is significantly lower than that for large scale tests with larger Aspect ratios.

2.7.2.2 Boundary shear stress distribution and turbulence measurements

Sellin [1995] reported the boundary shear stress magnitude which was measured using a Preston tube at a number of cross-sections over the test reach in the Series A models. At low relative depths very high values were measured at the top of the submerged bank on the receiving flood plain side. The high values persisted onto the flood plain for a distance approximately equal to the main channel width. At high relative depths the boundary shear values were greater although much more uniformly spread across the

whole channel. Sharp peaks and troughs were always visible in the shear values at the top and bottom corners of the submerged banks.

Sellin and Elliott [1990] combined the values for boundary shear stresses and zonal velocities using a momentum balancing technique in order to isolate Apparent Shear Force (ASF) from the cross-flow momentum transfer due to the transverse net flow across the longitudinal boundaries. They showed that the ASF term is relatively more important at low flow depth ratios while the cross-flow component appears to suppress it at higher flow depths.

2.7.2.3 Velocity Distribution

Detailed point velocity data was obtained at two cross-sections and two relative flow depths H*=0.15 and 0.49 in each of the skew compound channels tested in the Series A experiments. Ervine and Jasem [1990] measured point velocity at 6 relative depths; 0.15, 0.2, 0.25, 0.3, 0.35, 0.4 in a 5.2° small scale channel. Longitudinal velocity values were to be consistently higher on the receiving flood plain compared with the upstream flood plain. In the central section of the channel the high velocity zone was located towards the expanding flood plain. These effects were stronger at the downstream sections. Transverse velocities were found to be consistent with the skew angle on the flood plains. In the central section the transverse velocities were far more complex revealing the presence of multi-cell secondary circulation mechanisms, as shown in Figure 2.29.

The secondary cells in the main channel had mean circulating velocities of around 20-30% of the flood plain velocity. For a skew angle of between 5° and 6° the secondary cell velocities are up to 5 to 6 times bigger than in the straight compound channels. The longitudinal velocity distribution reveals higher velocities and a wider shear layer for the flood plain receiving flow from the main channel.

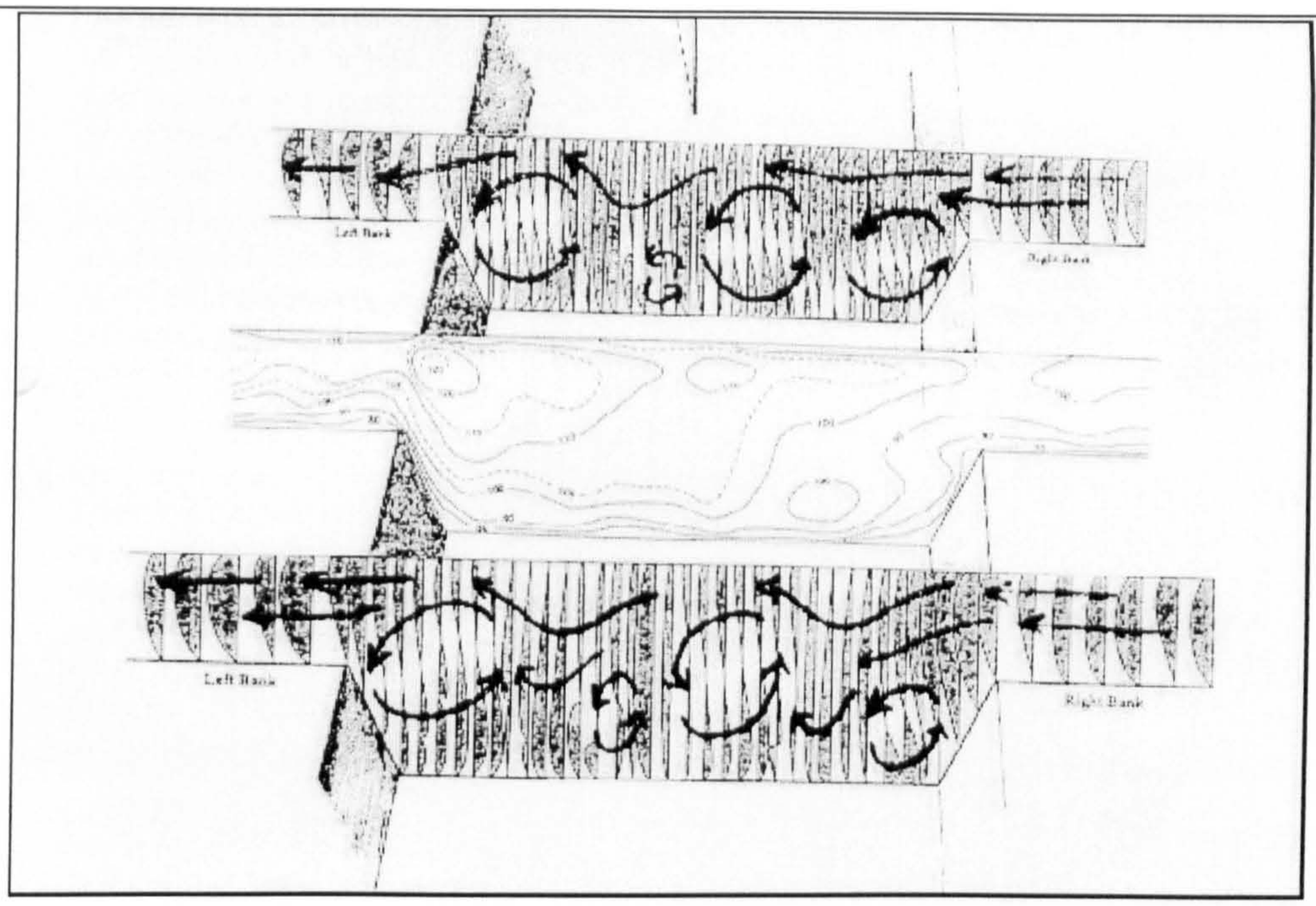

Figure 2.29 Longitudinal / transverse velocities in Series A model (after Sellin [1995])

2.7.2.4 Interaction mechanisms

Neither Sellin [1995] nor Ervine and Jasem [1990] propose any clear interaction mechanism for low depths apart from observing that the ASF term is more important at low depths. They both present evidence for the generation of secondary circulation in the main channel. Sellin [1995] found that three co-rotating parallel cells can be distinguished as well as a weaker one as shown in Figure 2.29. He could find no evidence of these cells moving onto the flood plain although the central area of high longitudinal velocity is carried well onto the downstream flood plain.

2.7.3 Deterministic methods for predicting discharge capacity

Sellin [1995] demonstrated that the divided channel method (DCM) overestimates the discharge capacity of a skew compound channel because it makes no allowance for the strong momentum transfer between flow zones. Ackers [1991] has developed the only viable method so far for skew channels. He derived a linear modification to DISADF (for flow regions 2, and 3) in his straight channel method (based on the Series A data) to account for the flow behaviour of skew channels with skew angles, θ, between 1°-10° as shown in Equation 2.54

$$DISADF_{SKEW}=DISADF_{STRAIGHT}*(1.03+0.074\theta) \quad [2.55]$$

2.7.4 Computational models for predicting flow behaviour

The author's literature review did not uncover any specific computational models for skew compound channels.

2.8 Meandering Compound Channels

2.8.1 Introduction

Natural river channels characteristically adopt a meandering pattern in the bottom of a river corridor. Consequently when the main channel over-tops its banks and spills onto the flood plain a meandering compound channel is formed. This section presents a review of the significant research performed to date on these channels.

Reliable field data relating to meandering compound channels is so rare that laboratory experiments have been used as the main tool for developing an understanding of meandering compound flow. A large data set was collated as part of the Series B extension programme (1989-1992) which consisted of all those experimental programmes performed world-wide which provide reliable surface roughness calibration data along with the raw flow data. This compilation continues the work begun by James and Wark [1992].

All the existing flow data was also reviewed in order to identify which geometric and flow state parameters had been investigated previously by other researchers and to determine whether they were shown to influence flow behaviour in meandering compound channels. All the parameters which were identified as being influential were noted and the relevant data was gathered for comparison with the results obtained during the Series B extension (1993-1996) programme.

2.8.2 Modelling the morphology of the main river channel

2.8.2.1 Introduction

The space limitations in small scale physical models has induced a number of researchers to build meandering compound channels in which the main channel meander configuration is dissimilar to any configuration that has ever been found in nature. Any results obtained from these types of experiments must be treated cautiously. Although they might provide valuable information about the general nature of flow behaviour in meandering compound channels, the results they yield may not easily be extrapolated to predict the flow behaviour in a natural channel, small or large scale. Various researchers have demonstrated with empirical evidence that most natural rivers exhibit configurations for which their specific geometric ratios tend to fall within a set range of values as described in Section 2.8.2.2.

2.8.2.2 The geometric ratios which identify natural channels

A number of parameters have been used by researchers such as Hey [1988] to classify the morphology of any river channel. Figure 2.30 illustrates the following: meander wavelength, λ_m, channel top width, B_c, bend radius of curvature, R_c, meander amplitude, a_m. An additional parameter is often utilised: channel depth, h_a, which is averaged for a particular cross-section (A/B), where A is cross-sectional area.

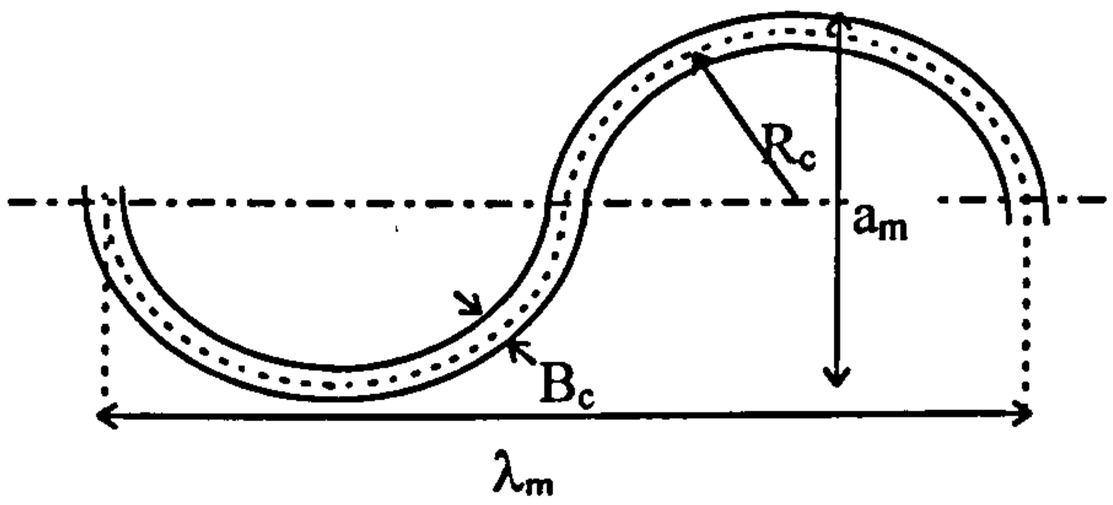

Figure 2.30 The geomorphologic parameters in a meandering river channel

The dimensions of a natural channel are often quoted as an averaged over one, typical meander wavelength. Leopold *et al* [1960] analysed many rivers to determine the geometric ratios which correspond to typical rivers. They suggested that Equations 2.56-2.59 represent the relationships between geometric parameters in a natural river.

$$\lambda_m = 10.9B_c^{1.01} \quad [2.56]$$

$$a = 2.7B_c^{1.1} \quad [2.57]$$

$$\lambda_m = 4.7R_c^{0.98} \quad [2.58]$$

$$R_c = 2.4B_c \quad [2.59]$$

Ervine and Ellis [1987] synthesised the geometric ratio evidence accumulated by other authors, including Hey [1978]. They identified a set of key geometric ratios which surveys had been shown to satisfactorily approximate the geometric ratios in most natural river channels in the UK. They are described in Equations 2.60-2.63.

$$\lambda_m / B_c = 10 \quad [2.60]$$

$$a/\lambda_m = 0.5 \quad \text{when } 5 > B_c/h > 20 \quad h_a = A/B_c \quad [2.61]$$

$$\lambda_m / R_c = 4.6 \quad [2.62]$$

$$R_c/B_c = 2.4 \quad [2.63]$$

A number of the model meandering compound channels tested over the years included morphologies which did not conform to these ratios. Flow data and behaviour which were identified using these models were treated with caution. Especially when they contradicted findings derived from channels with natural geomorphologies.

2.8.2.3 Modelling natural channel shape

In natural channels the depth of the main channel varies periodically along adjacent wavelengths of channel. At a bend the cross-section of channel is asymmetric, scouring deepens the outside of the bend and deposition builds up the inside of the bend, as shown in Figure 2.31. At the cross over, the intersection between one bend and the next, the cross-section is basically symmetrical, almost trapezoidal as shown in Figure 2.32.

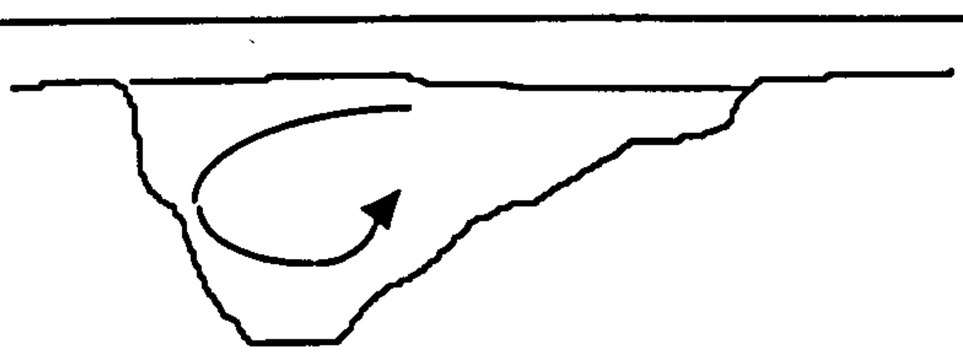

Figure 2.31 Apex Cross-section

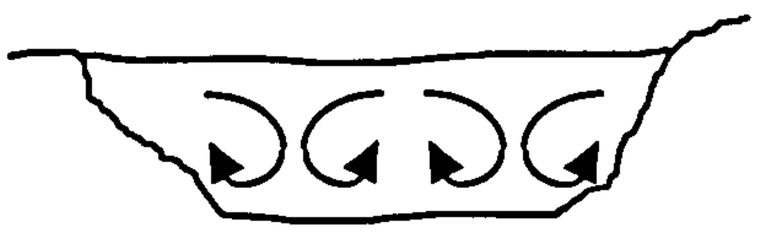

Figure 2.32 Cross-over cross section

Most experimental tests were performed using main channels which did not possess natural cross-sections. Although the results from these channels can be used to give an indication about the effect of different parameters, care must be taken when extending

the observed results to apply to natural channels. Only recently have some researchers built models with quasi-natural channels such as Willetts and Hardwick [1993] and Lorena [1993]. Willetts and Hardwick [1993] produced self-forming channels made using stabilised Bakelite. Lorena [1993] fabricated quasi-natural channels using channel insets which were placed inside a simple trapezoidal channel during the Series B (1989-1992) programme.

Lorena [1993] carried out a survey of 17 river bends (world-wide) to establish the overall dimensions for a quasi-natural channel. He established that in a natural channel the typical apex shape changed orientation between consecutive apices and varied linearly in between. A trapezoidal channel with a maximum depth almost half that found at the apex is established at the cross-over point. It is likely that there will be a dramatic difference between the flow behaviour of natural channels compared with trapezoidal channels. This is significant because most meandering compound channel programmes to date have used trapezoidal main channels.

2.8.3 Experimental details/associated findings (Reliable bed roughness data)

2.8.3.1 Introduction

The experimental programmes described below have produced results describing the flow behaviour of meandering compound channels and have also provided reliable bed friction calibration data which can be used to facilitate the confident re-analysis of the original flow data. Those associated papers which presented analysis and discussion of the original flow results are also reviewed.

2.8.3.2 United States (US) Army, Vicksburg [1956]

The US army built and tested 44 meandering compound channel models in a 30.5m long by 9.2m wide flume in Vicksburg, Mississippi, USA. The discharge capacity of these models at various overbank flow depths was measured and the influence of various geometric and roughness parameters was assessed. The influence of the following parameters was assessed: flood plain roughness, meander belt width, main channel sinuosity, the radius of curvature of the bends and the relative flow depth.

Thirty models were built which contained a trapezoidal main channel with a top width of 0.457m and a depth of 0.152m with 63.4° side slopes. The aspect ratio of these channels, B/h = 3 however was lower than the minimum found in natural rivers, B/h>5. The US Army were dissatisfied with the results which they felt were inconclusive so they built and tested an additional set of 14 meandering compound channel models which incorporated main channels with an aspect ratio equal to 5. The top width was 0.762m the depth was 0.152m and the side slope angles were 63.4°. Each of these models consisted of 3.5 meander wavelengths which were 7.315m long. The flood plain walls were built using temporary brick walls. Channels with 3 different sinuosities were built: r = 1.57, 1.4 and 1.2. Figure 2.33 shows the plan and cross-section of the Vicksburg [1956] flume with a sinuosity, r, equal to 1.2.

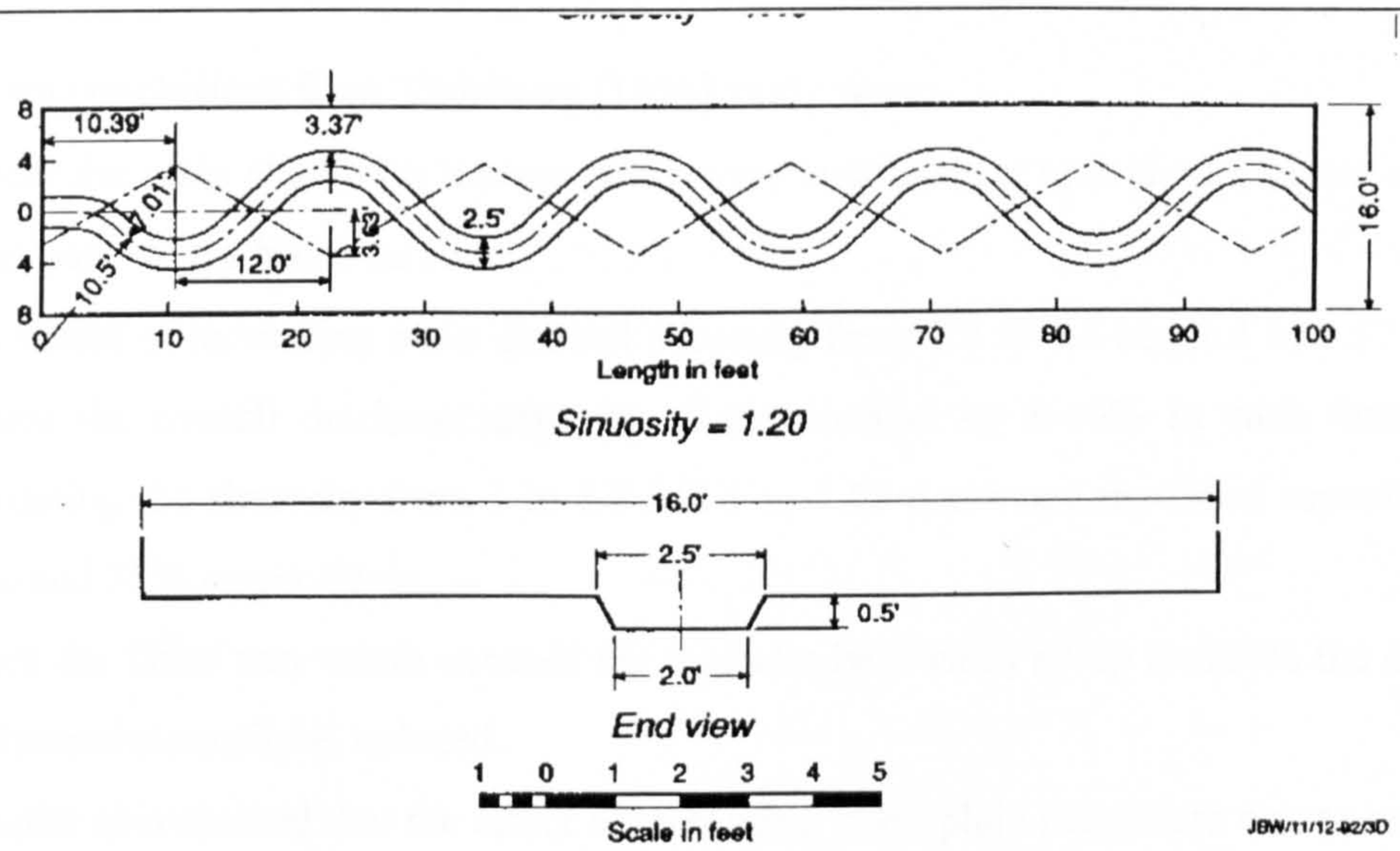

Figure 2.33 Vicksburg [1956] flume (Sinuosity, r = 1.2) (after Wark [1993])

The brushed concrete surfaces in the main channel and on the flood plains were stated to possess a Manning's n value of 0.012. The flood plain was assigned two additional roughness configurations which were obtained by covering the surfaces with expanded metal sheets. These sheets were aligned either parallel or perpendicular to the main flow direction and the Manning's n values were stated as 0.025 and 0.035 respectively. The temperature of the water was assumed to be equal to 15°C. Table 2.1 shows the inter-relationship between the 3 geometric and roughness parameters which were varied in 11 models. The stage and discharge relationship for each model was determined at three overbank flow depths. These are listed in detail in Wark [1993].

Ref. No.	Flood plain Manning n	Sinuosity	Meander belt width	Flood way width
SDVB201	0.012	1.571	4.420	4.877
SDVB202	0.025	1.571	4.420	4.877
SDVB203	0.035	1.571	4.420	4.877
SDVB204	0.012	1.400	3.761	4.877
SDVB205	0.025	1.400	3.761	4.877
SDVB206	0.035	1.400	3.761	4.877
SDVB207	0.012	1.200	2.822	4.877
SDVB208	0.025	1.200	2.822	4.877
SDVB209	0.035	1.200	2.822	4.877
SDVB210	0.035	1.200	2.822	9.144
SDVB211	0.035	1.571	4.42	9.144

Table 2.1 The parameters tested in Vicksburg [1956]

The main conclusions from Vicksburg [1956] study were:-

- Where the main channel is narrow with a very small aspect ratio the influence of the other parameters becomes small.
- The effect of increasing main channel sinuosity from 1.2 to 1.4 and 1.4 to 1.57 is to reduce the overall discharge capacity of the channel by 8-10% in each instance. Increasing the sinuosity from 1 to 1.2 and 1 to 1.57 decreased the flood capacity by 20% and 35% respectively.
- When the flood way width exceeds the meander belt width by up to 300% the effect of channel sinuosity is reduced.

The results also showed that the effect of increasing flood plain roughness was to reduce the total discharge capacity of the channel. The method they used to analyse the results split the channel into two zones dived by vertical lines at the top of the main channel. They did distinguish how to split the channels at high and low depths, depending on the flow behaviour of the channel, nor did they investigate the method vigorously. It was only used as another way to display the results. No point velocity measurement results were presented. They did not confirm the nature of the flow structures in a meandering compound channel or explain the dependency of these flow structure on the configuration of the channels. Any attempt to re-analyse the data nowadays is limited by the fact that only 3 flow depths were tested for every model. There is not enough information to determine precisely the exact influence of depth variations on the flow in the Vicksburg [1956] channels. In addition the bed friction calibration must be treated

cautiously. Constant Manning's n values were derived to describe the friction coefficient of the surfaces. This assumption may be adequate for the concrete surfaces at certain flow depths. However at this scale the magnitude would certainly vary with flow depth for the surfaces roughened by the expanded metal grating. The bed friction calibration was re-defined during the Series B extension programme by assuming that the concrete surfaces would have exhibited modified smooth law behaviour where C=2.02 and D=1.38. No refinement of the roughness definitions for the two other surfaces was possible because of the limited scope of suitable calibration data. Any future analysis which attributes a constant Manning's n to these roughened surfaces must be treated with scepticism.

2.8.3.3 Toebes and Sooky [1967]

Toebes and Sooky [1967] performed an extensive series of laboratory experiments in which the influence of channel roughness, flood plain slope and channel depth on the discharge capacity of a meandering compound channel was investigated. Many of their findings were useful for practising Engineers. They proposed a number of ideas explaining the way by which meandering compound channel flow influences the geomorphology of a channel. They provided evidence that deposition would occur in the deep parts of the channel and that scour would occur at the cross-over and the inside of the bends causing the river to straighten. In addition they measured the local velocity and water surface levels in the compound channel with the stated intent of linking the observed global behaviour to the local flow mechanisms.

They used a 7.3m long by 1.18m wide flume. The main channel was constructed out of Styrofoam sheets which were crafted to produce a rectangular cross-section and a sinusoidal meander waveform consisting of 5.5 wavelengths. The meander belt was 0.462m wide and the flood way was 1.184m wide in all the models. A sinuosity of 1.09 was set for all the models which meant that the key parameters of these models were dissimilar to the key parameters in natural river channels. Figure 2.34 shows the plan and cross-section of the Toebes and Sooky [1967] flume with a main channel depth equal to 0.076m.

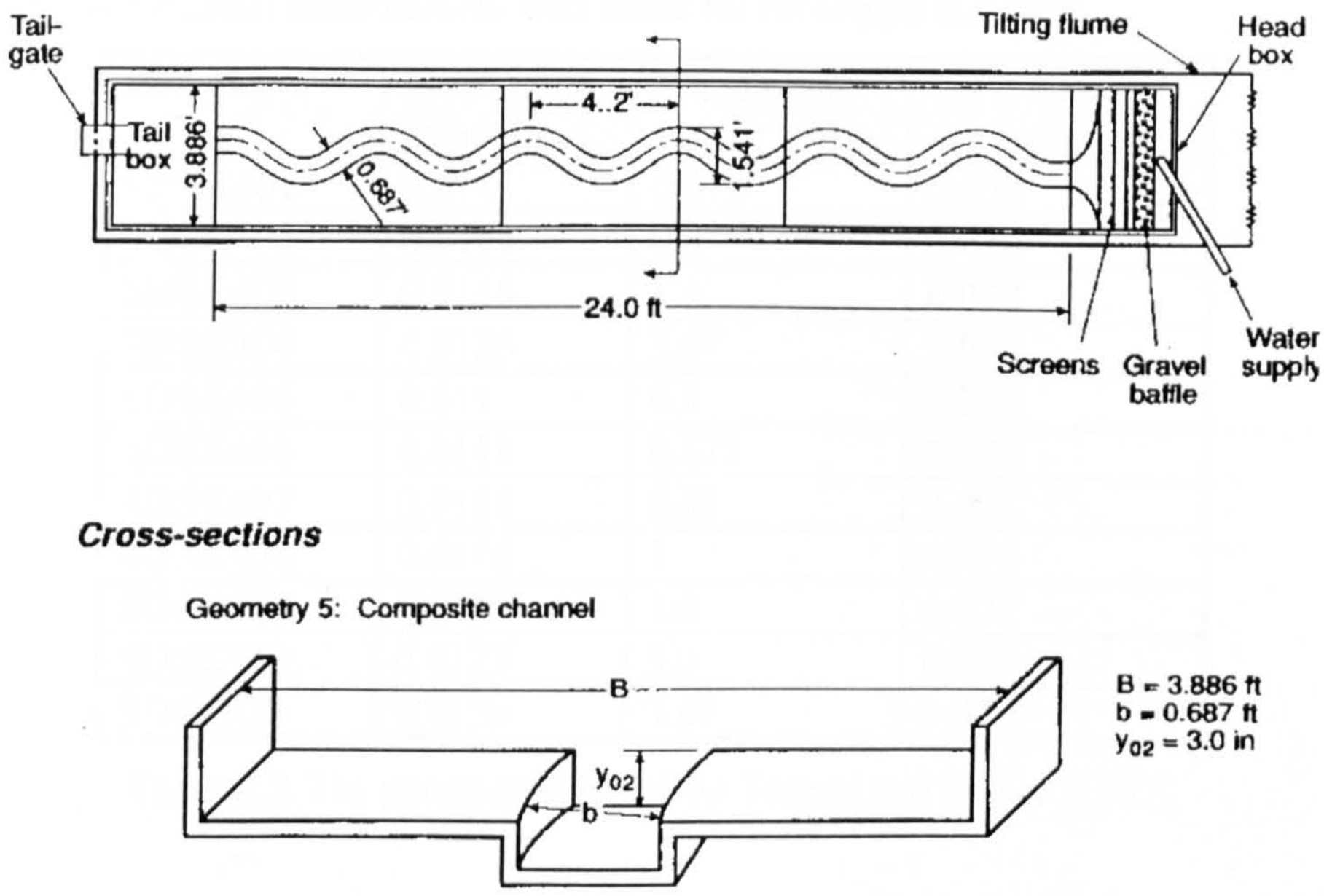

Figure 2.34 Sooky [1967] flume (h=0.076m) (after Wark [1993])

Consequently the flow results will not necessarily replicate real river behaviour, however they can be assumed to give a good insight into general flow behaviour and the dependency of meandering compound channels on longitudinal slope and channel aspect ratio. Calibration flow data from some inbank straight channel tests were available to enable the frictional resistance coefficients, Manning's n to be calculated for the various flood plain slopes. A modified smooth law was also established for the smooth model surfaces with C=2.02 and D=1.3. The configurations of the various models tested are shown in Table 2.2. Point velocity measurements taken by Toebes and Sooky [1967] showed that the secondary, helicoidal, cells that were developed in the main channel when the main channel flow first overtopped its banks. These cells rotated in an opposite direction to the cells developed by centripetal forces during inbank flow.

They showed that the magnitude of interaction losses (assessed by measuring the relationship between stage and discharge) was dependent upon the mean flow velocity in the compound channel and overbank flow depth and that they decrease with decreasing Aspect ratio. They did not draw any conclusions about the effect of

longitudinal slope. They also questioned, but did not resolve, how to compare the flow results from the small scale models with those for prototype channels,

Ref. No.	Flood plain Manning n	Flood plain slope $*10^{-3}$	Main Channel depth [m]
SDSK401	0.0111	0.675	0.038
SDSK402	0.0114	0.87	0.038
SDSK403	0.0118	1.6	0.038
SDSK404	0.0126	3.67	0.038
SDSK405	0.011	0.3	0.076
SDSK406	0.0111	0.675	0.076
SDSK407	0.0114	0.87	0.076
SDSK408	0.0116	1	0.076
SDSK409	0.0118	1.6	0.076
SDSK410	0.0123	3.0	0.076
SDSK411	0.0126	3.67	0.076

Table 2.2 The parameters tested by Toebes and Sooky [1967]

2.8.3.4 River Roding, Oxfordshire (1983-1987)

Only a few sets of field data have been collected over the years which are comprehensive and accurate enough to demonstrate the full intricacies of flow behaviour in full scale, natural, meandering compound channels. It is often prohibitively expensive to acquire the cross-sectional data and difficult to determine accurately the friction coefficients relating to the natural channels. In addition it is sometimes dangerous and often costly to accurately measure flood water level, discharge and point velocities for rivers in flood. Unfortunately all this information is required if useful quantitative and qualitative results are to be gathered for natural channels which can subsequently be used to further our understanding and develop models of the flow behaviour.

The best available field data for meandering compound channel flow was obtained from a stretch of the River Roding in Hampshire which was studied by Sellin et al between 1985 and 1989. Figure 2.35 shows the general planform arrangement of the channel.

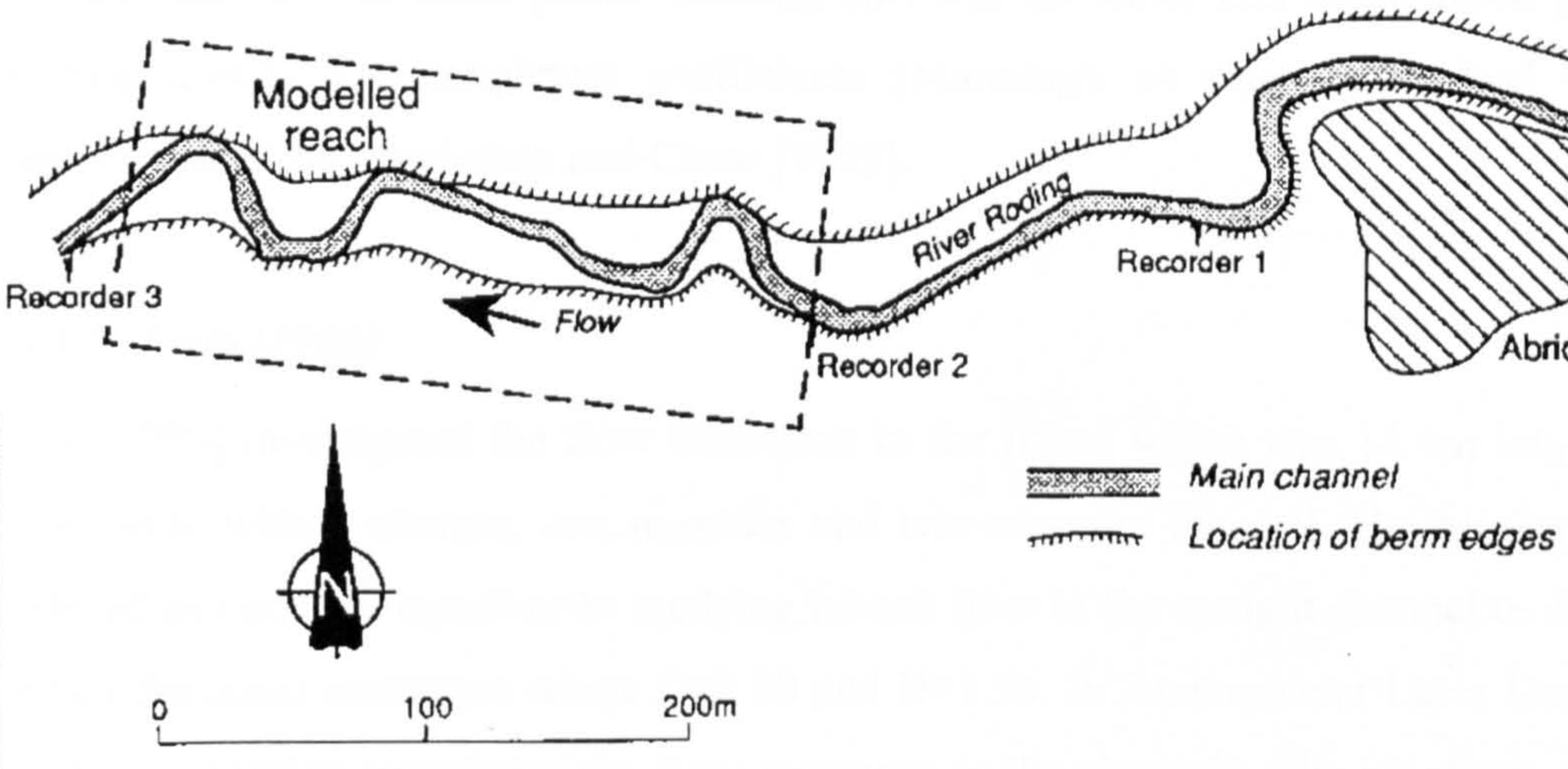

Figure 2.35 Planform of the River Roding (after Sellin [1990])

Searle [1985] presented the details of the preparatory model study and Sellin, Giles and van Beesten [1990] presented the final appraisal of the implementation of the full prototype. Table 2.3 details the range of geometric dimensions and roughness characteristics of the two channel configurations. The stage and discharge data obtained for each channel is given in Table 2.4.

Model		RD	Re'	n_c	n_f	r	FL	Mw	AR	SS
Roding	Min.	0.12	0.60	0.038	0.035	1.38	0.0014	1.00	9.51	0.55
cut	Max.	0.57	17.2	0.038	0.035	1.38	0.0014	1.00	9.51	0.55
Roding	Min.	0.12	0.31	0.038	0.05	1.38	0.0014	1.00	9.51	0.55
uncut	Max.	0.60	10.3	0.038	0.05	1.38	0.0014	1.00	9.51	0.55

Table 2.3 Range of geometries and roughness characteristics for the River Roding

River Roding Cut flood plains				River Roding Uncut flood plains			
F/P Flow depth (m)	Q (m^3/sec)	A (m^2)	P (m)	F/P Flow depth (m)	Q (m^3/sec)	A (m^2)	P (m)
0.1	2.5	4.2	35.8	0.1	2.5	4.2	35.8
0.2	3.8	6.4	44.3	0.2	3.8	6.4	44.3
0.3	6.3	9.2	46.3	0.3	5.5	9.2	48.3
0.4	8.5	12.1	48.5	0.4	7.3	12.1	48.5
0.5	11.3	15.0	49.6	0.5	8.8	15.0	49.6
0.6	14.0	17.9	49.8	0.6	10.5	17.9	49.8
0.7	16.5	20.9	50.3	0.7	12.2	20.9	50.3
0.8	19.0	23.9	50.6	0.8	14.5	23.9	50.6
0.9	22.5	27.0	51.7	0.9	16.0	27.0	51.7
1.0	25.8	30.0	52.7	1.0	17.5	30.0	52.7
1.1	29	33.2	53.7				

Table 2.4 Flow data for R. Roding

One channel had cut flood plains (Roding cut) and the other had uncut flood plains (Roding uncut). The roughness coefficients (Manning's n) were determined using photographs of the flood plain and Chow [1959].

2.8.3.5 Kiely [1989]

Kiely [1989] investigated the flow behaviour in the flume which was 14.4m long and 1.2 m wide with a straight, one meander and two meander channel. He developed a modified smooth law equation by studying inbank flow in the straight channel to define the bed frictional resistance where C=2.10 and D=1.56. A 2-component Laser Doppler system was used to investigate the flow structures in the channels. The planform shape and bed friction calibration data was accurate so the author had the confidence to use the results to develop and test further methods for predicting flow behaviour in meandering compound channels. A summary of the range of values describing the geometric and roughness parameters in Kiely's meandering compound channel are listed in Table 2.5. Figure 2.36 shows a plan and cross-section of the Kiely [1989] flume with multiple meander wavelengths.

Model			F*	RD	Re'	f'	r'	FL	Mw	AR	SS
SDKI 301		Min.	0.670	0.09	0.58	0.91	1.22	0.0010	1.56	4.00	1.00
		Max.	0.784	0.44	24.0	2.69	1.22	0.0010	1.56	4.00	1.00

Table 2.5 Geometric configuration and roughness characteristics for Kiely [1989]

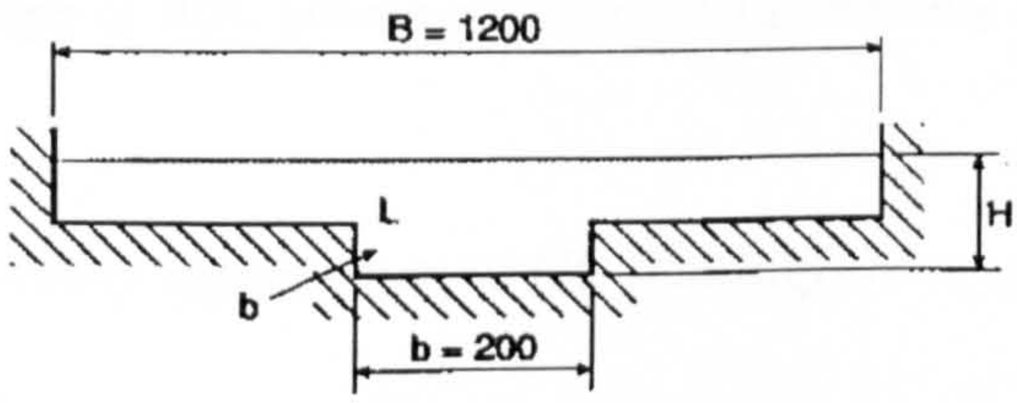

Multiple meander compound channel

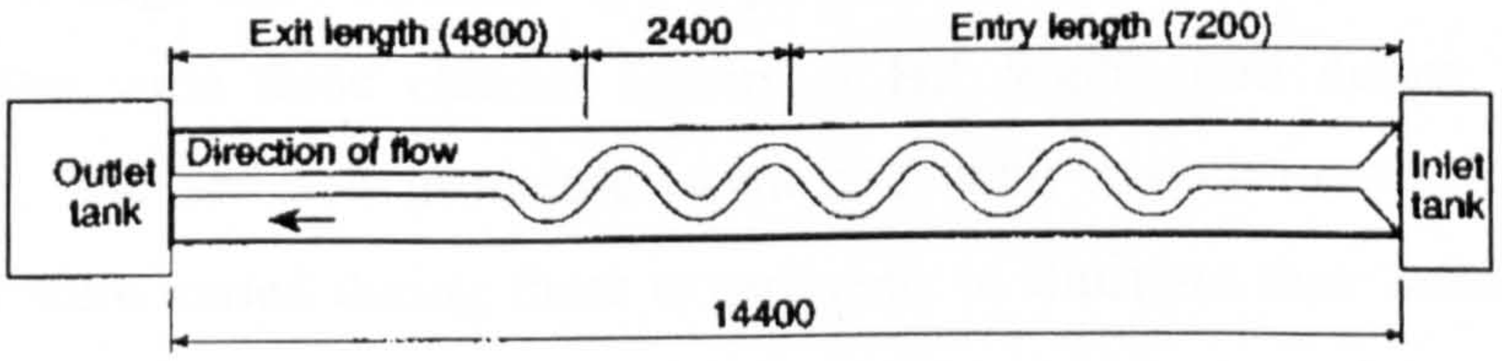

Figure 2.36 Kiely [1989] flume (h=0.076m) (after Wark [1993])

Kiely [1989] used the stage and discharge data and point velocities results to make some observations about meandering compound channel flow. He confirmed the observations made by Toebes and Sooky [1967] regarding the secondary cell flow reversal in the main channel during overbank flow and showed that water was exchanged between the main channel and the flood plain. He also presented new evidence which showed that there was a change in direction of the local flow between above main channel bankfull level. He postulated that this indicated that there is horizontal shear layer established between the main channel and flood plain channels.

Kiely's [1989] important conclusion from these observations was that a basic expansion and contraction model would generate similar flow processes between the main and flood plain channels as he observed in his experiments. This was important further evidence to justify the use of an expansion and contraction model to predicate the head losses in the flood plain flow (above the meander belt). This assumption had formed the basis of a number of recently developed discharge prediction models such as Yen and Yen [1983] and Ervine and Ellis [1987].

However, Kiely's [1989] results were obtained for relatively high flow depths and using smooth flood plains. The author questions whether similar flow behaviour would indeed be observed in natural channels which would range over much lower flow depths and would possess almost stagnant flood plain flow. Further experiments are required to replicate and study the type of flow behaviour which is more likely in natural channels.

2.8.3.6 Series B (1989-1991) experiments at HR Wallingford

2.8.3.6.1 Experimental programme

A number of large scale meandering compound channel models were built in the 50m long by 10m wide flood channel facility at HR Wallingford during the Series B programme. The Series B geometries were built with smooth mortar. The following parameters were varied during these experiments to illustrate their influence on flow behaviour; relative depth, relative roughness, sinuosity, main channel Aspect ratio/shape and relative meander belt width. The flood plain width was equal to 10m for most models with the meander belt width equalling 6.667 and 8.560m for main channels with

sinuosities of 1.374 and 2.043 respectively. Figure 2.37 shows a plan of the flume with a sinuosity equal to 2.043.

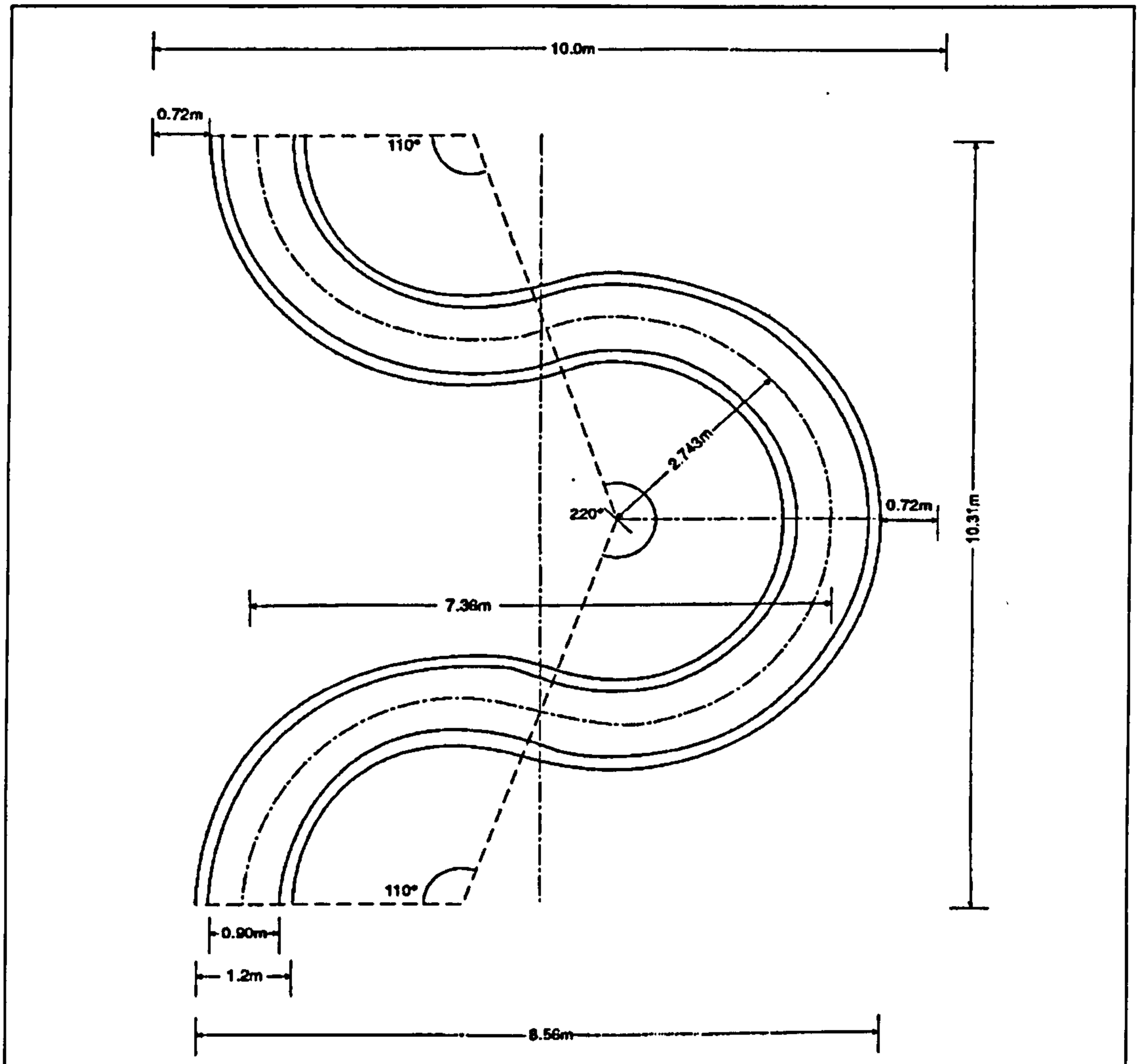

Figure 2.37 Plan view of the Series B flume , r=2.043 (after Wark [1993])

For two models the flood plain width was set equal to the meander belt width. The longitudinal flood plain slopes were $0.996*10^{-3}$ and $1.021*10^{-3}$ respectively. The main channels all had a top breadth equal to 1.2m, 45° side slope angles and a maximum depth equal to 0.15. The majority of the main channels were given quasi-natural shapes, Aspect ratio was equal to 14.6, based on the findings of Lorena [1993] with a vertical distortion of 2:1. One model incorporated a trapezoidal main channel which had an Aspect ratio equal to 9.142. The flood plains were roughened using dowel rods or bricks placed on the flood plain surface. For the smooth mortar surfaces a modified smooth law equation was developed which defined the roughness coefficient in variable flow

conditions. It was derived using inbank flow data obtained from specific straight channel tests. The coefficients were determined to be equal to C=2.02 and D=1.38. The roughness coefficients for the flood plains blocked by doweling rods were defined for variable flow conditions using Equations 2.12-2.17. No roughness coefficient calibration was performed for flood plains blocked by bricks consequently the results could not be used in future analysis

Further details of the model geometries used in the Series B experiments can be found in Wark [1993]. Table 2.6 lists the values of the parameters varied in the models for which extensive discharge measurements were taken at many relative flow depths and for which there is reliable bed friction calibration.

Ref. No.	Flood plain roughening, f_f	Sinuosity, r	Floodway width (m), FW	Belt width (m), BW	Aspect ratio, AR
SDB21	smooth	1.374	10	6.107	9.142
SDB25	smooth	1.374	10	6.107	14.6
SDB31	smooth	1.374	6.107	6.107	14.6
SDB34	dowels	1.374	10	6.107	14.6
SDB39	smooth	2.043	10	8.56	14.6
SDB43	dowels	2.043	10	8.56	14.6
SDB47	smooth	2.043	8.56	8.56	14.6

Table 2.6 The parameters tested during the Series B programme (1989-1992)

Table 2.7 lists the values of the parameters varied in the models for which discharge, point velocity, and boundary shear stress measurements were taken at either 2 or 3 overbank flow depths.

Ref. No	Flow Depths (mm)	f_f	r	FW	BW	Aspect Ratio
SDB23, 24	50.5 100.9	smooth	1.374	10	6.107	9.142
SDB28, 29, 30	15.2, 50.0, 99.7	smooth	1.374	10	6.107	14.6
SDB35, 36, 37	15.3, 50.1, 101.0	dowels	1.374	10	6.107	14.6
SDB41, 42	15.0, 50.8	smooth	2.043	10	8.560	14.6
SDB44, 45	15.6, 50.3	smooth	2.043	10	8.560	14.6

Table 2.7 The parameters tested during the Series B programme (1989-1992)

The measurements of stage-discharge were taken for all the model configurations. The measurements of point velocity (magnitude and direction), boundary shear stress data, turbulence and dispersion were taken for various model configurations. The point

velocities for the main channel (perpendicular to the main channel and extending 300mm onto the flood plain) were taken at eleven cross-sections along a quarter of a wavelength of the 1.374 sinuosity channel and at fourteen cross-sections over half a wavelength of the 2.043 sinuosity channel. Measurements were taken on a grid with horizontal spacing of 150mm or 50mm and vertical spacing of 15mm. On the flood plain measurements were made at thirteen (sinuosity=1.374) and eleven (sinusoity=2.043) traverses covering half a wavelength. readings were taken at spacing of 0.5m laterally and 10mm vertically.

The raw data gathered in the Series B programme has been published en masse in twelve volumes referenced under Series B [1994]. Consequently a number of authors have been able to analyse the data and publish their findings in many separate reports.

2.8.3.6.2 Knight D W, Yuan Y M and Fares [1992]

Knight et al [1992] presented their findings and conclusions for the investigations performed during Series B into the shear stress on the boundaries of quasi-natural meandering compound channels and the nature of turbulence. A two-component Laser Doppler Anemometer was used to measure turbulence, a Preston tube was used to measure shear stress and dye visualisation tests were used to confirm the nature of the flow behaviour.

Knight et al [1992] demonstrated that the boundary shear stress, τ_b, in the main channel initially decreases when the flow first goes overbank compared with inbank flows (over half a meander wavelength) and subsequently increases for increasing overbank flow depths. The magnitude of shear stress was larger in the low sinuosity channels at all the flow depths that were tested. Figures 2.38 and 2.39 show the variation of boundary shear stress versus theta (the angle between the centre line of main and flood plain channels at adjacent cross-sections over half a meander wavelength) in SDB25 and SDB39 respectively. SDB25 and SDB39 have sinuosities equal to 1.374 and 2.043 respectively. The measurements were taken for one inbank flow depth, 140mm, and two overbank flow depths, 165mm and 200mm. The main channel was 150mm deep.

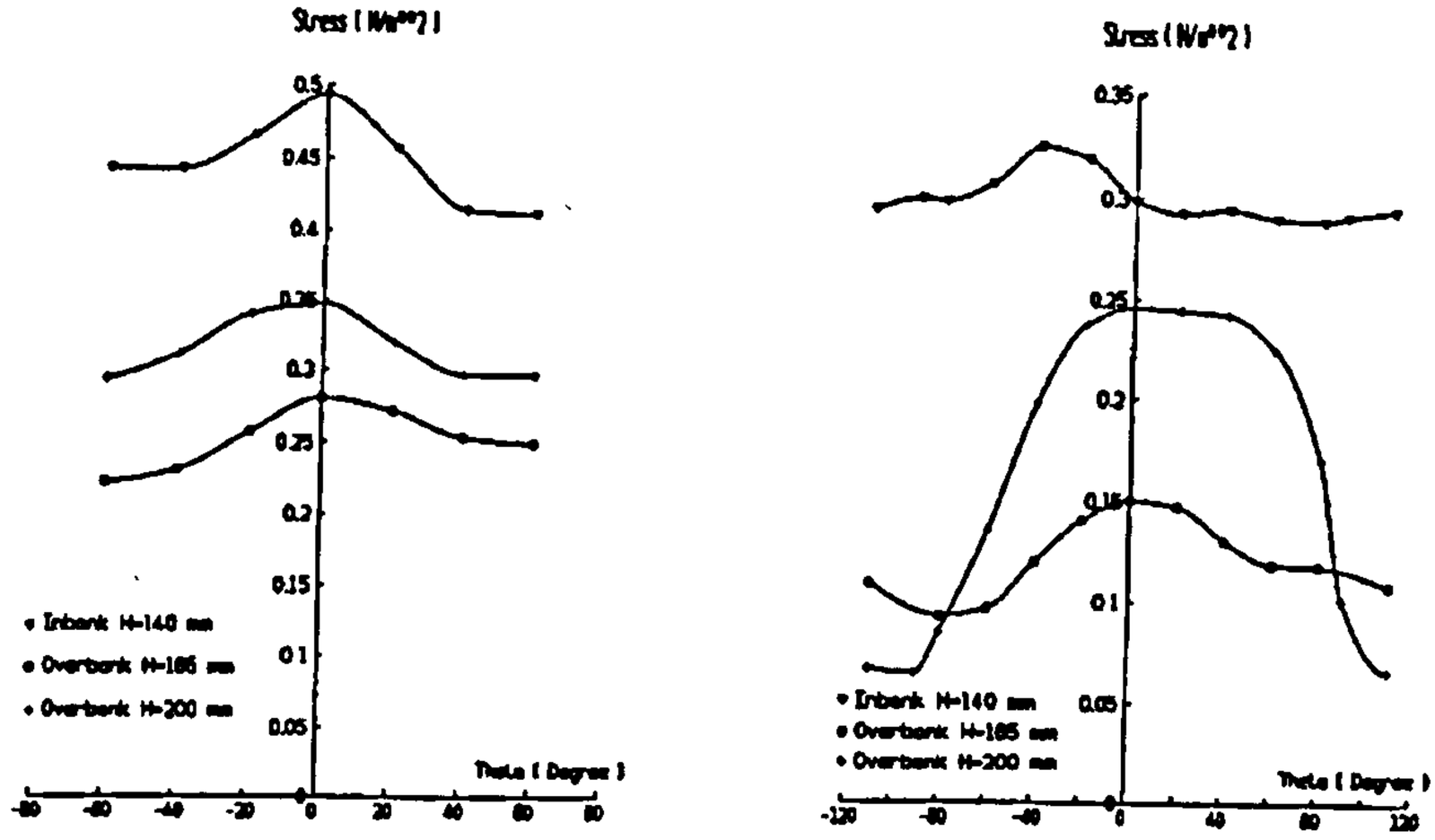

Figure 2.38 Average main channel boundary shear stress (after Knight et al [1992])

Figure 2.39 shows plots of the sectional average shear stress on the flood plain at a flow depth equal to 200mm over half a wavelength for both main channel sinuosities.

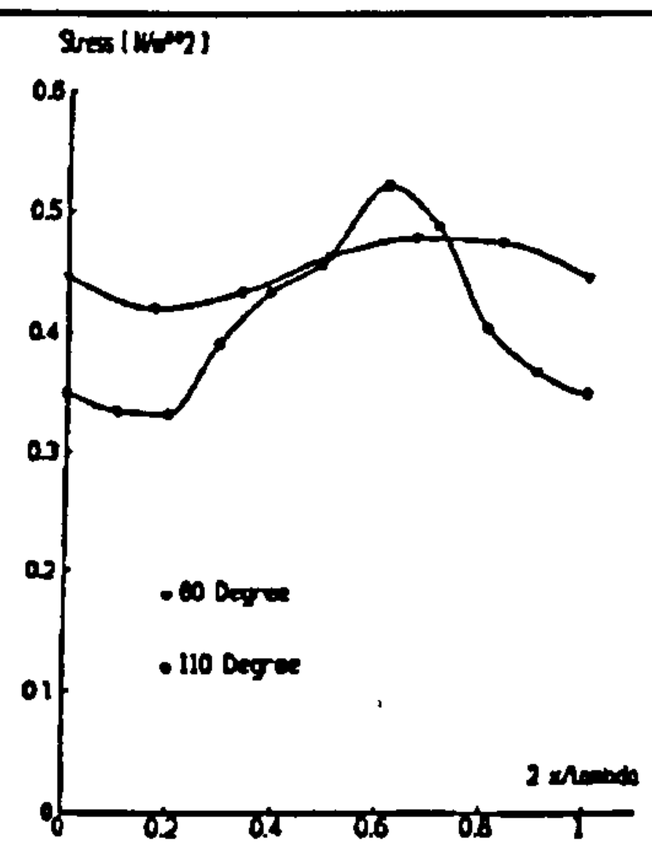

Figure 2.39 Average flood plain boundary shear stress (after Knight et al [1992])

Clearly the sinuosity does not have a significant effect on the average shear stress on the flood plain. It is also apparent that the shear stresses on the flood plain and main channel are similar in magnitude at this flow depth. This implies that the erosive potential is similar for both which will have a significant effect on the distribution of erosion and deposition between the main channel and flood plain at times of overbank flow. Although the flood plain shear stress (overbank flow) is nearly uniform in the valley slope direction because of the two-dimensional nature of the flow, in the areas where

three dimensional flow mechanisms dominate, the shear stresses do tend to exhibit a significant increase in the magnitude of shear stress.

2.8.3.6.3 Sellin, Ervine, and Willetts [1993]

Sellin et al [1993] examined the point velocity and flow visualisation results obtained from the Series B experiments in order to extend the observations made by Knight et al [1992] and others and to clarify the important aspects of flow behaviour in meandering compound channel. The primary velocities in the main and flood plain channels are skewed across each other and a significant proportion of flow enters the main channel from the upstream flood plain and travels across the channels in a skew path to leave the channel before the next bend. Significant volumes of water plunge down of the flood plain into the main channel and become entrained, while similarly significant volumes of water are displaced onto the flood plain. The entrainment appears to be assisted by secondary cells which are formed in the main channel.. The secondary currents were shown to be stronger in the trapezoidal channels rather than the quasi-natural ones. Also sinuosity was shown to effect the magnitude of the interaction losses but no analysis was presented to indicate how exactly this interaction varied with flow depth. The point velocities were only measured at a limited number of depths, a maximum of three. Sellin et al [1993] acknowledged the need for measurements at additional flow depths to resolve this issue. They inferred the nature of the general flow interaction mechanisms using the above observations and they illustrated the mechanisms using Figure 2.40. Once again however smooth flood plains were used in the majority of the tests analysed by Sellin et al [1993]. The author doubts whether these flow mechanisms would actually be generated in a natural channel where over the most likely range of expected flow depths the flood plain flow will almost be stagnant.

Sellin, Ervine, and Willetts [1993] also presented stage and discharge data collected from eight of the models tested during Series B. They attempted to demonstrate the effects of the meandering channel on overbank flow by presenting the distribution of total Manning's n and Darcy friction factor. Unfortunately these traditional methods did not facilitate the separation of the various sources of head loss in meandering compound

channel flow so an explanation for the direct influence of parameter variations on the layer interaction mechanisms were not forthcoming.

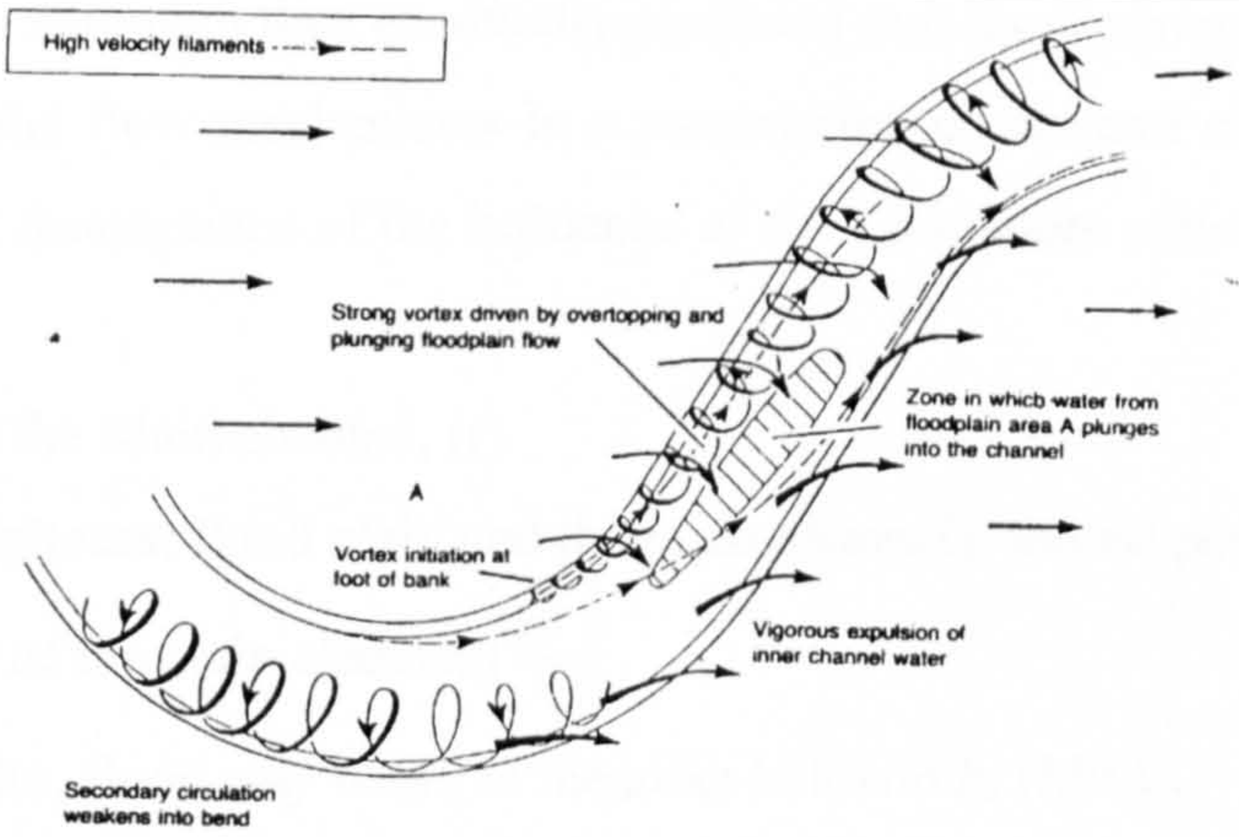

Figure 2.40 Flow mechanisms in a meandering compound channel (after Ervine[1993])

2.8.3.6.4 Ervine, Sellin, Willetts and Lorena [1993]

Ervine *et al* [1993] presented a novel method for analysing stage and discharge data which avoided the limitation of Manning's n where all the head losses were combined. The effect of varying parameter on the interaction losses in a meandering compound channel was isolated by using a non-dimensional measure of discharge called F* which is defined in Equation 2.64:-

$$F^* \equiv \frac{\text{ACTUAL MEASURED DISCHARGE (Qmeas)}}{\text{THEORETICAL DISCHARGE (BED FRICTION LOSSES ONLY (Qf))}} \qquad [2.64]$$

F* was an adaptation of the DISADF factor used by Ackers [1991] in straight compound channels. Different divisions were used because 3 co-flowing zones appeared to be created in meandering channels whereas only 2 co-flowing zones were identified in straight compound channels. Theoretical discharge was determined by applying the standard resistance formulae to a cross-section divided into these 3 zones. The vertical lines of zero stress which were assumed to separate the zones as shown in Figure 2.41

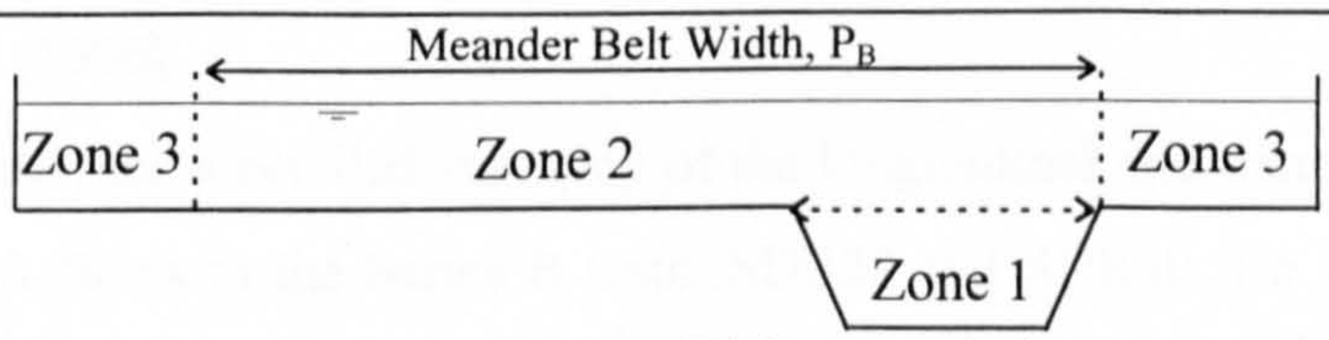

Figure 2.41 Zonal divisions to calculate F* in meandering compound channels

Ervine *et al* [1993] re-analysed the Series B data presented in Sellin *et al* [1993] using F* to demonstrate the effect of several key parameters on the magnitude of the interaction losses. Although they eventually predicted that the 8 parameters listed below would influence the flow mechanisms in a meandering compound channel flow, their data only allowed descriptions of the influence of the parameters which have an asterisk next to them.

1. Sinuosity of the Main channel, (r) (*)
2. Relative roughness: flood plain and the main channel's wetted perimeter (f') (*)
3. Aspect ratio of the main channel ($\frac{B^2}{A}$) (*)
4. Relative width, flood way width to meander belt width, (Mw) (*)
5. Relative depth of flow on flood plain compared to main channel, (y') (*)
6. Side slopes of main channel, (s)
7. Flood plain topography, the lateral slope on the flood plains, (L)
8. Flood plain slope (S)

2.8.3.6.5 Willetts, Ervine, and Sellin [1993]

Willetts *et al* [1993] present comparisons between the flow mechanisms in meandering compound channels with regular planform as in the Series B models and one with irregular planform, such as the River Backwater as described by Naish [1995]. Although the overall flow mechanisms were shown to be approximately the same in the two types of channel the nature of site specific features, like sinuous flood plain channels, was acknowledged to be significant. The authors stated that as a consequence of there being so many factors which influence meandering compound channel flow there is an urgent need to develop a sound theoretical model of the flow processes so that the effects of geometrical peculiarities can be explored with more flexibility.

2.8.3.6.6 Sellin [1995]

Sellin [1995] presented a detailed summary of the longitudinal and transverse velocities for two overbank flows in the Series B tests: SDB28 and SDB30. He showed that the longitudinal velocity in the main channel is less effected at low flow depths than at high flow depths. In high flow a concentrated high velocity zone is generated downstream

from the apices parallel to the outside of the bends. This high velocity zone is related to the strong flow out of the inner channel at this point and tallies with the observations of Knight et al [1991] showing large values of τ_b in the same location. Sellin [1995] concluded that the flow mechanisms proposed in Figure 2.40 are valid at certain flow depths but will alter for varying flow depths.

2.8.3.7 Hardwick and Willetts [1993]

Three meandering compound channel models were built by Hardwick and Willetts [1993] in a 11m long by 1.2 m wide flume in Aberdeen to complement the Series B results. The meander belt width ratio and aspect ratio of the trapezoidal channels were set equal to 1.0 and 3.837 respectively. Hardwick and Willetts [1993] investigated the nature of the velocity fields in meandering compound channels and the effect of varying longitudinal flood plain slope, main channel sinuosity on discharge capacity. The flood plains in each model were smooth and a modified smooth law was derived where C=2.48 and D=2.91. The values of the parameters varied by Hardwick and Willetts [1993] are listed in Table 2.8. Figure 2.42 shows the overall planform and cross-section dimensions of the meandering compound channels which were built.

Ref. No.	Flood plain slope	Sinuosity
SDAB101	0.001	1.215
SDAB102	0.001	1.406
SDAB104	0.000621	2.041

Table 2.8 The parameters tested by Hardwick and Willetts [1993]

The influence of natural channels was also studied. Hardwick and Willetts [1993] reporting on experiments they performed at Aberdeen in 1991, presented further evidence for the large scale flow features associated with meandering channel flow. The vigorous exchange of water between the main and flood plain channels in and beyond the downstream half of each bend was demonstrated with dye visualisation techniques. The flood plain water entering the main channel was shown to penetrate to its full depth providing evidence that the secondary circulation occupies the whole cross-section.

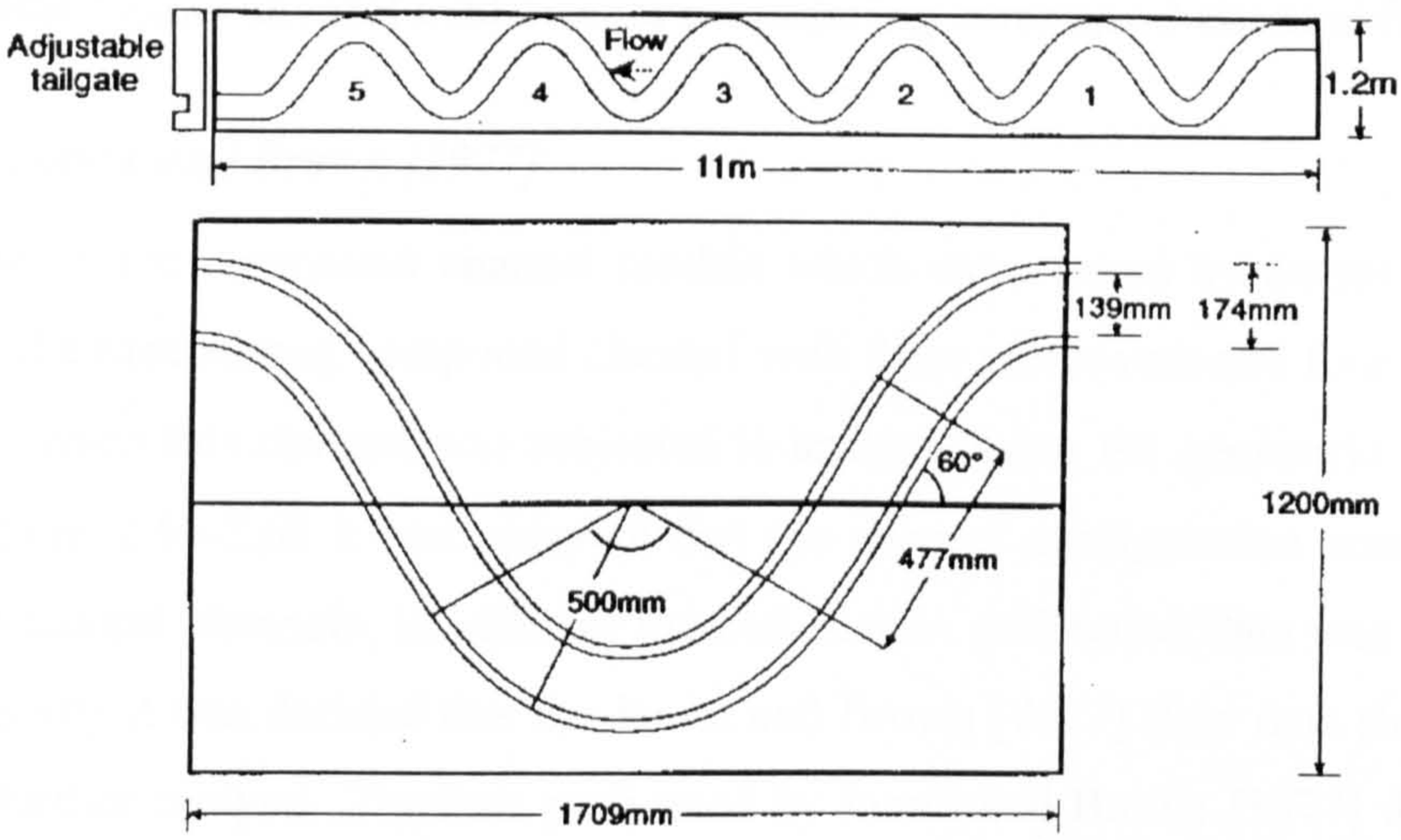

Figure 2.42 Planform and cross-section of Aberdeen (1991) model (after Wark [1993])

Also provided was supplementary evidence that conveyance capacity decreases with increasing sinuosity. They also observed that this influence is moderated by the adoption of natural geometry for the channel bed. However this observation was based on very little evidence and the results could also have been effected by the change in Aspect ratio between the trapezoidal and natural channels caused by the method of bed formation as shown in Figure 2.43.

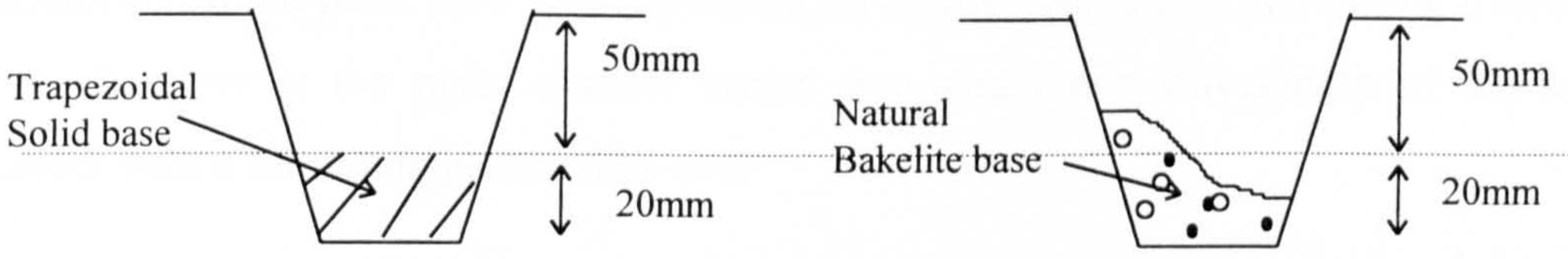

Figure 2.43 Trapezoidal versus natural channels (after Hardwick and Willetts [1993])

The bed shape is formed by passing bankfull inbank flows over Bakelite granules then fixing the shape which evolves with cement powder. Hardwick and Willetts [1993] stated a perception held by a number of authors that attempts to develop predictive methods based on the correlation of geometric and flow parameters may always be frustrated by the shear number of such parameters and a deterministic description of the physics of flow is more likely to lead to a useful method. The author acknowledges this point and has attempted to base his new methods on the observed physics of the flow.

2.8.4 Other experimental evidence on meandering compound channel flows

2.8.4.1 James and Brown [1977]

Only one of the compound channel models which were tested by James and Brown resembled a meandering compound channel with three crossovers and four tight bends. However when this channel was subjected to analysis using the geometric ratios given in Equations 2.60-2.63 it was apparent that the channel configuration was unlike any found in natural channels. In addition the bed friction calibration data was inadequate. Consequently it was decided that the James and Brown [1977] flow data should not be used in further analysis. The tests performed by James and Brown [1977] did however provide some useful evidence to demonstrate that the discharge capacity of a meandering compound channel reduces for increasing sinuosity.

2.8.4.2 Smith [1978]

Smith [1978] performed stage-discharge experiments for three channels, a straight compound channel, a meandering compound channel and the flood plain alone. The calibration data provided was unreliable and can not be used to develop further models. However he did confirm that head loss caused by the interaction between the main channel and flood plain flow was dependant on relative depth and that during overbank flow, the flow in the main channel varied throughout one wavelength of the main channel with a minimum at the cross-over

2.8.4.3 Stein and Rouve [1989]

Stein and Rouve [1989] concentrated on investigating the three-dimensional structure of flow in a meandering compound channel. They used Laser Doppler anemometry to measure all three point velocity components within the flow for one water and discharge rate. They confirmed that secondary currents in the main channel rotate in the opposite direction to those for inbank flow. They presented evidence for the exchange of water between the main channel and flood plain flow and the associated slowing of flood plain velocities. They suggested that their results demonstrated that a horizontal shear layer exists between the main channel and flood plain flow. Figure 2.44 shows the flow mechanisms that they inferred by analysing local flow velocity data.

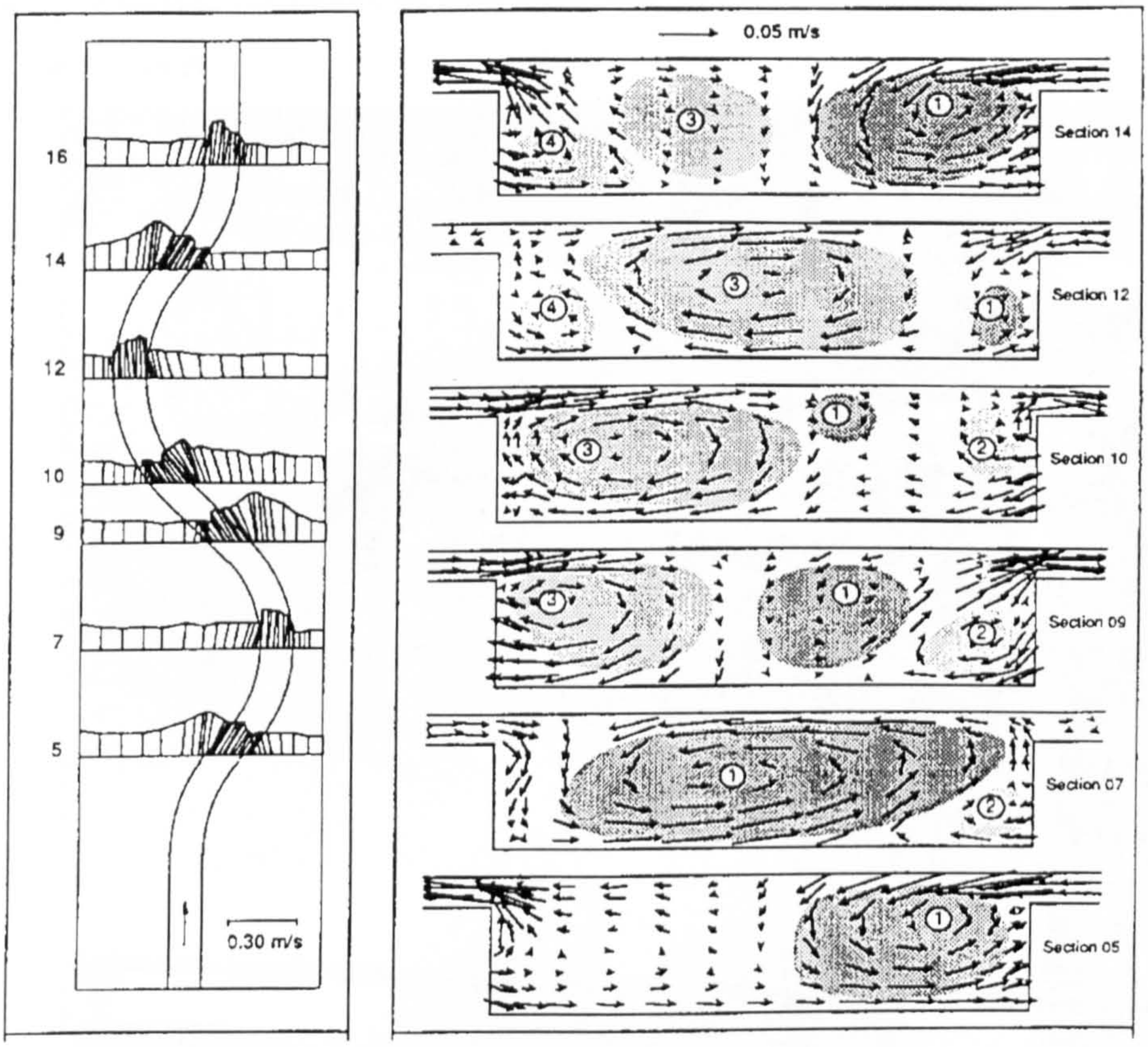

Figure 2.44 Flow mechanisms: planform and sectional view (after Stein et al [1989])

2.8.4.4 River Blackwater, Hampshire (1993-1997) (Model studies)

2.8.4.4.1 NRA [1996]

NRA [1996] reports the experimental details and findings from the investigation into the hydraulic performance of a 1:5 scale model of the River Backwater which was built in HR Wallingford. This report summarises many of the initial findings which were reported in Naish and Sellin [1994]. The model was 56m long and 10m wide with a flood plain slope of 1:1000. The planform configuration adopted is shown in Figure 2.45.

Stage, discharge, point velocity and boundary shear stress measurements were taken. Plots of Manning's n, the Darcy-Weisbach factor and a DISADF equivalent (calculated by dividing the measured discharge by the theoretical channel discharge determined by using the Ackers [1991] divided channel method) versus flow/relative flow depth were

plotted to illustrate the nature of flow behaviour and magnitude of flow resistance in the Blackwater model.

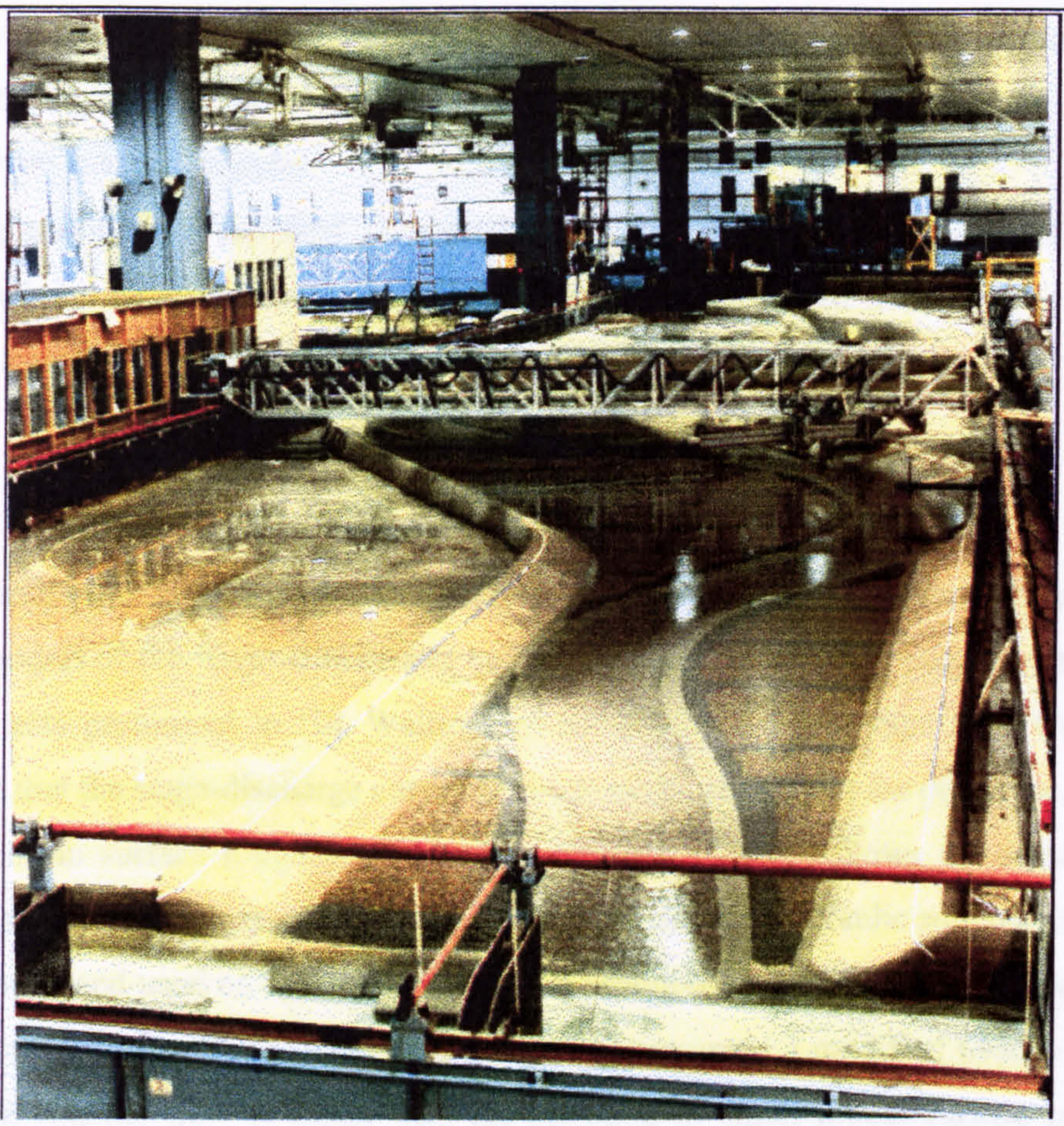

Figure 2.45 The 1:5 scale model of the River Blackwater (after NRA[1996])

The analysis presented in NRA [1996] demonstrated that:

- At high flow depths the channel with horizontal berms conveyed more water than the channel with inclined berms.
- At low flow depths the absence of direct and unobstructed flow paths across the inclined berms constrain the flow over them. This reduces the flood plain /main channel interaction and associated momentum losses. There was a consequent increase in capacity at low flow depths.
- At low overbank flow depths the roughness of the flood plain berm had very little effect on overall flow resistance. As depth increases however the berm roughness becomes more important. High berm roughness induces greater overall flow resistance at high flow depths.

- The maximum velocity filament in the main channel moves from the outside of the bend to the inner bank when flow transits between inbank and overbank flow. The average velocity in the flood plain channel typically increases with increasing flow depth until reaching a magnitude similar and sometimes greater than the main channel average velocity.

No explanation for the flow velocity behaviour in terms of flow mechanisms was proffered and no attempt was made to separate the effect of bed friction from the effect of the layer interaction mechanisms using techniques such as F* analysis.

2.8.4.4.2 Naish and Sellin [1995]

Naish and Sellin [1995] presented details of the experimental programmes for the 1:25 scale models of the River Blackwater built in Bristol University to complement the 1:5 model tests performed in HR Wallingford as well as the prototype field tests. They showed that the stage-discharge curves for both model scales and the prototype, with the difference in surface roughness taken into account, closely follows the same profile. They also illustrated that care must be taken when scaling hydraulic roughness because the 0.4mm sand used on the 1:25 scale model produced higher scale roughness than the 8mm gravel used on the 1:5 model. Finally they presented a modified Moody diagram for open channel flow to assist with the selection of small model surface roughness values to accurately reproduce prototype scale data. No flow results for the River Blackwater have been made available to the general Hydraulic Engineering community at the time of writing this thesis.

2.8.5 Methods for predicting discharge capacity in meandering compound flows

2.8.5.1 Toebes and Sooky [1967]

Toebes and Sooky accounted for the extra flow resistance generated by layer interaction in a meandering compound channel by including an additional boundary surface (wetted perimeter) when applying the standard resistance formulae to determine discharge capacity in a divided channel. This boundary surface was horizontal and capped the main channel at bankfull level as shown in Figure 2.46.

Analysis of the available experimental data was performed to determine the appropriate magnitude of the extra boundary resistance that had to exerted by the hypothetical wetted perimeter.

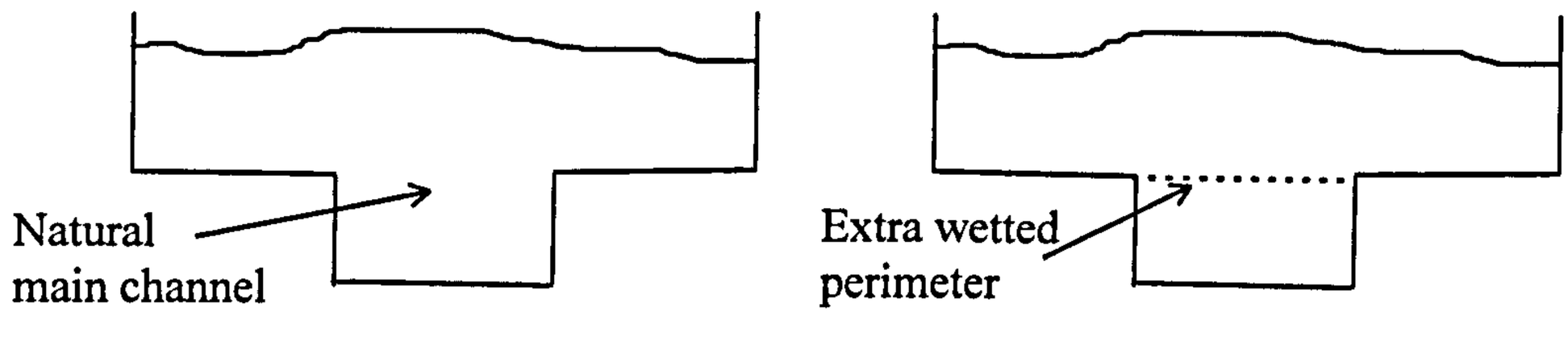

Figure 2.46 Extra wetted perimeter by Toebes and Sooky [1967]

The magnitude of the extra boundary resistance was shown to vary in a rather complex way with overbank flow depth, main channel depth, and channel gradient. Toebes and Sooky [1967] did not actually propose any practically useful relationship for defining the boundary resistance in terms of these parameters.

2.8.5.2 James and Brown [1977]

James and Brown proposed that the flow layer interaction losses in straight and meandering compound channels could be accounted for by developing predictive formulae which implemented empirically adjusted values for Manning's n and incorporated layer interaction losses as well as bed friction resistance. These adjusted Manning's n values were applied using standard resistance formulae an used to determine the discharge capacity in meandering compound channels when treated as simple channels Using their experimental results they developed a formula for predicting this Manning's n value which was dependent on relative flow depth and the ratio of flood plain width to main channel width, by fitting their formulation to the measured results. Although James and Brown [1977] obtained a prediction formula for discharge capacity, it was based on a limited range of experimental data and can not reliably be applied to models other than those used to develop it.

2.8.5.3 Yen and Yen [1983]

Yen and Yen [1983] treated the meandering compound channel cross-section as a unit (simple channel) and included the main channel solely as a resistance element, as shown

schematically in Figure 2.47. They proposed a Darcy Weisbach type resistance coefficient in order to account for the flow resistance induced by the layer interaction. Their model did not account for flow in the main channel. The definition of the additional resistance coefficient relied on empirical information obtained for closed conduits which is unverified for open channel flow over backward and forward facing steps. The methods fit the stage and discharge distributions exhibited by the models used to develop the methods themselves but are less reliable than other prediction methods when applied to models outside the development set.

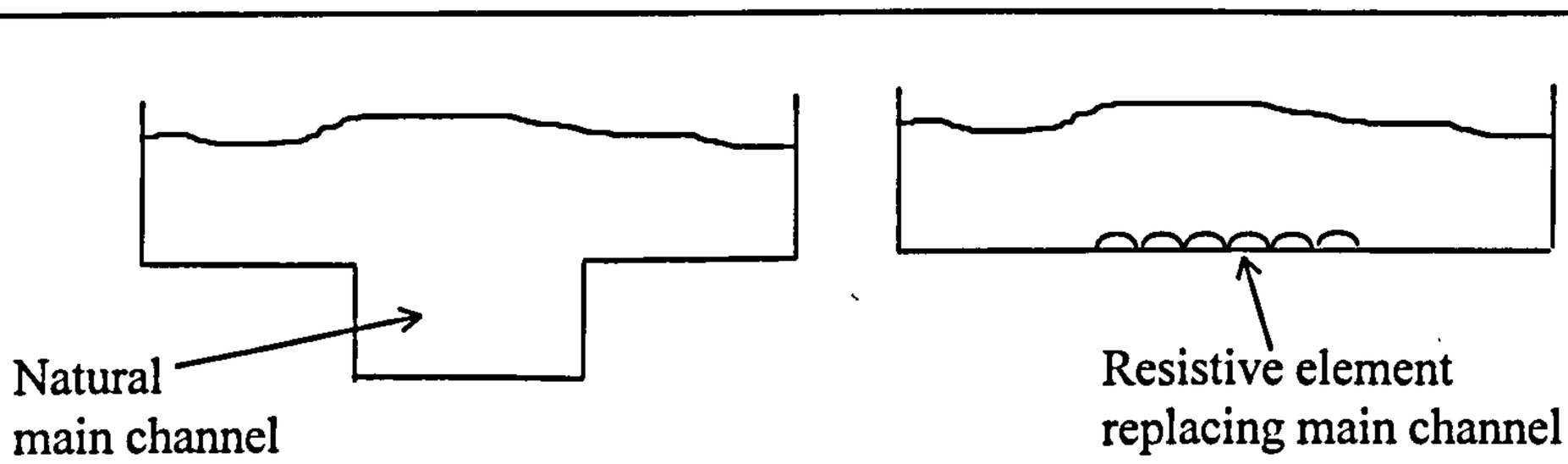

Figure 2.47 An equivalent channel with resistive element by Yen and Yen [1983]

2.8.5.4 Ervine and Ellis [1987]

Ervine and Ellis [1987] developed a stage - discharge prediction method based on classic open channel flow theory and the division of the cross-section into three zones. Zone 1: the main channel below bankfull level, Zone 2: the flood plain within the meander width, and Zone 3: the flood plain beyond the meander belt. They identified the major sources of energy losses in each of these zones.

In Zone 1 these were:

- Friction on the wetted perimeter.
- Boundary reliance due to transverse shear and internal friction associated with secondary currents induced by the meander bends.
- The turbulent shear stress generated by the velocity difference between the main channel and the collinear component of the flood plain flow at the horizontal interface at bankfull level.
- Bed form resistance associated with the undulating riffle-pool sequence.

In Zone 2 these were:

- Friction on the wetted perimeter.

- Expansion of the flow as it enters the main channel.
- Contraction of the flow as it re-enters the flood plain.

In Zone 3 only bed friction on the wetted perimeter was assumed to contribute to energy loss.

Ervine and Ellis [1987] proposed a model for predicting stage-discharge relationships by quantifying the more important of these loss mechanisms. They applied their model to the experimental results obtained by the US Army Corps of Engineers, Vicksburg [1956] and Toebes and Sooky [1967] and they obtained reasonable accuracy. Figure 2.48 shows the results for Vicksburg [1956].

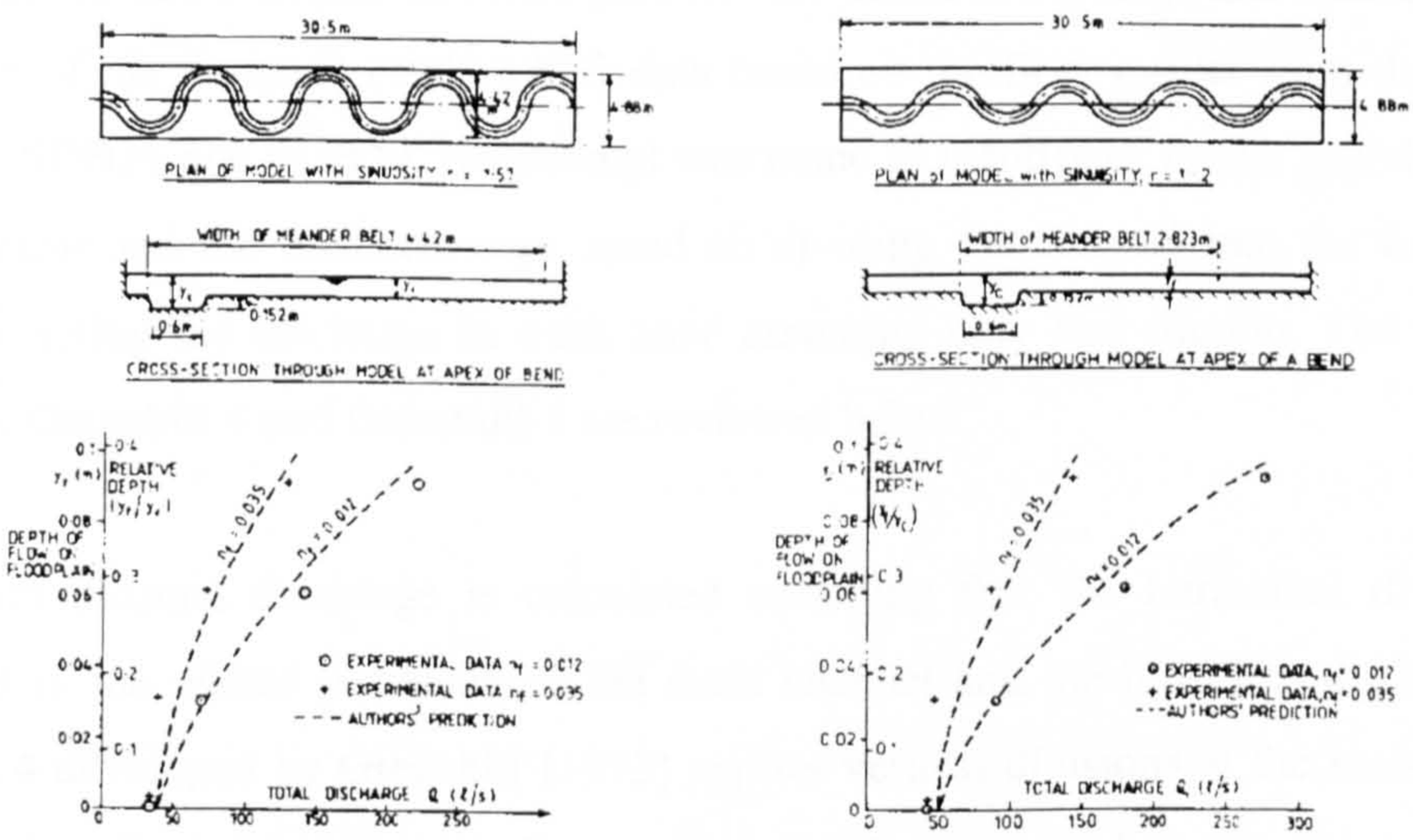

Figure 2.48 Stage - discharge plots from Toebes [1967} (after Ervine and Ellis [1987])

Surface friction losses were estimated using the Darcy-Weisbach equation with the friction factor given by the Colebrook-White equation. Losses associated with secondary currents in the main channel are estimated using the method proposed by Chang [1984] for fully developed circulation in wide, rectangular channels. Subsequent experimental observations have shown the secondary circulation to be generally opposite in sense for overbank flows compared with inbank flows. This is because it is driven by the horizontal shear at the bankfull level, rather than by centripetal acceleration. The method developed by Chang [1984] was derived for inbank flow in the main channel and is therefore inappropriate for overbank cases. Ervine and Ellis account for the growth and decay of secondary currents by applying only half of the head loss predicted by Chang [1984] model.

Expansion losses to the flood plain flow are determined by application of the force-momentum principle, and contraction losses by using loss coefficient values presented by Rouse [1950] and used by Yen and Yen [1983]. Overall the Ervine and Ellis [1997] method has a fairly sound physical basis but there is potential for refinement when more experimental data reveals further details about the nature of the zonal flow. In the interim, however, it does yield fairly reliable predictions for the discharge capacity of a number of meandering compound channels for which there is flow data available.

2.8.5.5 Greenhill [1992]

Greenhill produced various different methods for determining stage and discharge for a selection of the Series B (1989-1992) data based on the flow results from the models SDB25, SDB31 and SDB39. No attempt was made to identify or model individual loss mechanisms and the methods were based on dividing the channel into the four zones and calculating the discharge in each zone assuming only bed friction. The two best methods Greenhill 4 and Greenhill 5 are reviewed below.

The main channel discharge is calculated assuming that the horizontal division is included in the wetted perimeter of the main channel and the inner flood plain zone. Method 4 developed by Greenhill [1993] applies vertical divisions at the meander belt edges and method 5 is based on division lines inclined outward at 45°. These division lines are included in the wetted perimeter of the inner flood plain zone but not the outer zones. The main channel hydraulic slope [S_o/r] is used when calculating the main channel and meander belt discharges while the flood plain gradient [So] is used in calculating the outer flood plain flows. The methods fit the stage and discharge distributions exhibited by the models used to develop the methods themselves, but are less reliable than other prediction methods when applied to models outside this development set.

2.8.5.6 James and Wark [1] [1992]

2.8.5.6.1 Introduction

James and Wark [1992] devised the most accurate method to date for predicting the discharge capacity of meandering compound channels. They refined the method proposed by Ervine and Ellis [1987] using the recently acquired Series B data. Their method consists of semi-physical / semi-empirical formulations for predicting the discharge capacities of the 4 flow zones in a meandering channel.

2.8.5.6.2 Zone 1

James and Wark [1992] developed an empirical formulation, given in Equation 2.65 to determine the correct flow in Zone 1, Q_1.

$$Q_1 = Q_{bf} * Q_1' \qquad [2.65]$$

The bankfull discharge Q_{bf} could be calculated accurately using the standard resistance formulae coupled with either the LSCS method or the Modified Chang method to determine the extra losses due to secondary circulation. The experimental results for the Series B tests were used to determine equations to define the adjustment factor Q_1' for various flow depths. The available experimental data was limited in scope, so two linear expressions referring to two ranges of flow depths were empirically derived. The adjustment factor was defined as the greater of Equations 2.66 or 2.67:

$$Q_1' = 1.0 - 1.69y' \qquad [2.66]$$

or

$$Q_1' = my' + Kc \qquad [2.67]$$

where

$$m = 0.0147\, B^2/A + 0.032\, f' + 0.169 \qquad [2.68]$$

$$c = 0.0132\, B^2/A - 0.302\, s + 0.851 \qquad [2.69]$$

$$K = 1.14 - 0.136\, f' \qquad [2.70]$$

$$y' = y_2 / [A/B] \qquad [2.71]$$

$$f' = f_2 / f_1 \qquad [2.72]$$

The Zone 1 discharge capacity which was predicted using these equations fitted the observed behaviour from the Series B tests well, however it is unlikely that it will be as accurate for other model configurations. In Equation 2.66 Q_1' is defined to be only dependant on the relative depth. Other parameters such as aspect ratio and the absolute

Reynolds number of the flow might affect the Zone 1 capacity at flow depths. Further testing will be required to ascertain the accuracy of Equation 2.66 for other models.

In addition the assumption that the relationship between Q_1' and relative depth is linearly dependant at higher flow depths, as exhibited in Equation 2.67, is unlikely to be shown to be accurate when more flow data becomes available. James and Wark [1992] were forced to make this assumption because of the limited amount of reliable data that was available at the time. Further testing will be required to ascertain whether this linear form of equation can be applied to all meandering compound channels.

2.8.5.6.3 Zone 2

James and Wark [1992] adopted Ervine and Ellis' [1987] assumption that the head loss generated in flood plain flow as it passes over a trench formed by a meandering channel in the flood plain floor can be simulated using two simple trenches, as shown in Figures 2.49 and 2.50.

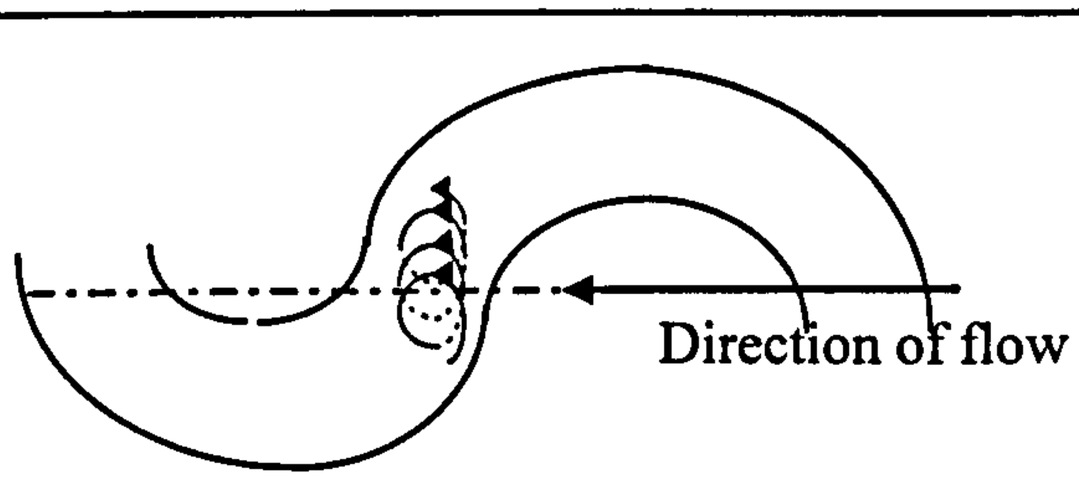

Figure 2.49 Meandering trench channel

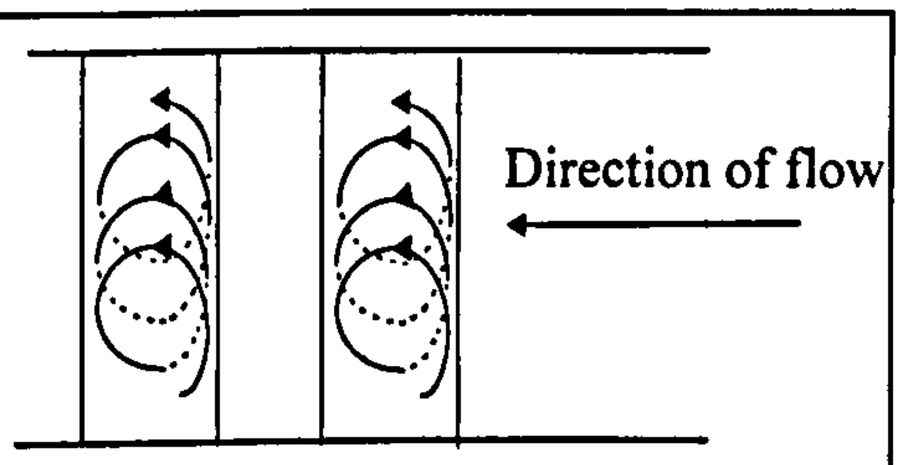

Figure 2.50 Simple trench channel

James and Wark [1992] developed an semi-empirical / semi-physical formulation to determine head loss in Zone 2 based on this assumption. They assumed that the total energy lost over one meander wavelength, L, was equal to the sum of the friction and expansion and contraction head losses, h_f, h_e and h_c. They combined the expansion and contraction terms into one term, h_l where

$$h_l = he + hc \qquad [2.73]$$

Under uniform flow conditions the gradient of the energy line associated with Zone 2 was assumed to be equal to the flood plain gradient, S_o so that

$$h_f + h_l = S_o L \qquad [2.74]$$

They combined expressions for h_f and h_l to derive a formulation for defining the average Zone 2 velocity V_2 which is given in Equation 2.75.

They combined expressions for h_f and h_l to derive a formulation for defining the average Zone 2 velocity V_2 which is given in Equation 2.75.

$$V_2 = \left(\frac{2gS_0L}{(f_2L)/4R_2 + K_T} \right)^{1/2} \qquad [2.75]$$

Term 1 Term 2

Term 1 is obtained by re-arranging the Darcy - Weisbach friction loss expression where f_2 is the Darcy friction factor for the flood plain in Zone 2, L is the meander wavelength, and R_2 [$=A_2/P_2$] is the hydraulic radius of Zone 2 (A_2 is equal to the flow area of Zone 2 and P_2 is equal to the length of wetted perimeter in the average cross-section of Zone 2).

Term 2 is equal to K_T which is an energy loss coefficient [defined as the sum of the expansion and contraction head loss coefficients] which apply to backward facing and forward facing steps which combine to form a slot, as shown in Figure 2.51. h is equal to the step depth and y_2 is equal to the upper channel flow depth.

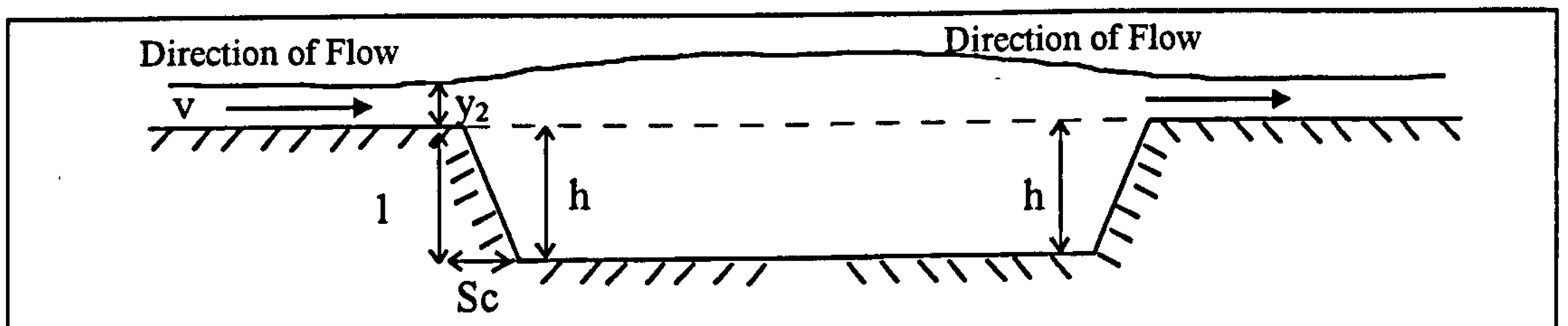

Figure 2.51 Illustration of backward and forward facing steps

K_T is defined in Equation 2.76 and is based on the same theoretical head loss equations used by Ervine and Ellis [1987] which are adjusted using empirically derived coefficients.

Term a Term b

$$K_T = C_{sl}\, C_{wd}\, [C_{ssc}[1 - y_2[y_2 + h]]^2 + C_{ssc}K_c] \qquad [2.76]$$

Term a, $[1 - y_2[y_2 + h]]^2$ (K_e) is equal to the theoretical head loss for the expansion over a backward facing step with infinite length of reach in front and behind it. Term b, K_c, is the theoretical head for the contraction over a backward facing step with infinite length of reach in front and behind it. James and Wark [1992] used data derived by Jasem [1990] and others in order to determine adjustment factors, C, which relate the theoretical expansion and contraction head losses for steps, K_e and K_c respectively, with the head loss actually generated in flow over slots. The adjustment factors are identified in Equation 2.76, the variable of K_{meas} is equal to the actual magnitude of head loss generated in flow over slots which was measured by Jasem [1990]

$$C = \frac{K_{meas}}{K_{e,c}} \qquad [2.77]$$

The coefficient, C_{sl} is an adjustment coefficient which James and Wark [1992] included in order to relate the complicated meandering trench configuration formed by the meandering main channel to two equivalent simple trenches over one wavelength. The two equivalent trenches are shown in Figure 2.51. Their definition for C_{sl} is given in Equation 2.78.

$$C_{sl} = 2\,[W_2 - B] / W_2 \qquad [2.78]$$

However this arbitrary definition assumes that the expansion and contraction mechanisms are not generated over the whole width, W_2, of Zone 2 but only occur over a width equal to $[W_2\text{-}B]$.

The adjustment coefficients C_{ssc} [expansion] and C_{ssc} [contraction] given in Equations 2.79 and 2.80 account for the fact that both steps may be sloping whereas the theoretical head loss values were calculated by assuming that the steps were orthogonal to the main flow direction. The parameter S is equal to the tangent of the average side slope angle.

$$C_{ssc} = 1.0 - S_s / 5.7 \qquad [2.79]$$

$$C_{ssc} = 1.0 - S_s / 2.5 \qquad [2.80]$$

C_{wd} accounts for the influence of aspect ratio on the theoretical energy loss coefficients and indicates the relative proximity of the backward and forward facing steps.

$$C_{wd} = 0.02\,[B_2 / A] + 0.69 \qquad [2.81]$$

Two additional adjustment factors F_1 and F_2 were also applied to K_T. These account for the discrepancies encountered when comparing the measured Zone 2 velocity in the meandering compound channel results from Series B (1989-1992) and Willetts and Hardwick [1993] results and those predicted using the basic James and Wark [1992] formulation which was defined in Equation 2.75. Equation 2.82 demonstrates how F_1 and F_2 are applied.

$$V_2 = \left(\frac{2gS_0L}{(f_2L)/4R_2 + F_1F_2K_T} \right)^{1/2} \qquad [2.82]$$

The induced definitions for F_1 and F_2 are given in Equations 2.83 -2.85.

$$F_1 = 0.1\,B^2 / A \text{ for } B^2 / A < 10 \qquad [2.83]$$

$$F_1 = 1 \text{ for } B^2 / A > 10 \qquad [2.84]$$

$$F_2 = 1.4 / s \qquad [2.85]$$

The author notes that a number of the assumptions underpinning the formulation of the expansion and contraction head loss component of the Zone 2 discharge prediction expression are difficult to justify when considering the nature of the physics of the flow layer interaction. Firstly, the F_1 and F_2 adjustments are unlikely to be accurate for the full range of possible meandering compound channels. Their derivation was based on a limited set of data. Secondly, the adjustment coefficients C_{ssc} and C_{ssc} were initially derived by Formica [1955] based on the lateral expansion and contraction of flows, as shown in Figure 2.52. Further assessment is required to confirm whether it was a valid assumption that Formica's [1955] formulations for lateral expansion can be applied successfully to vertical steps comprising a flood plain slot.

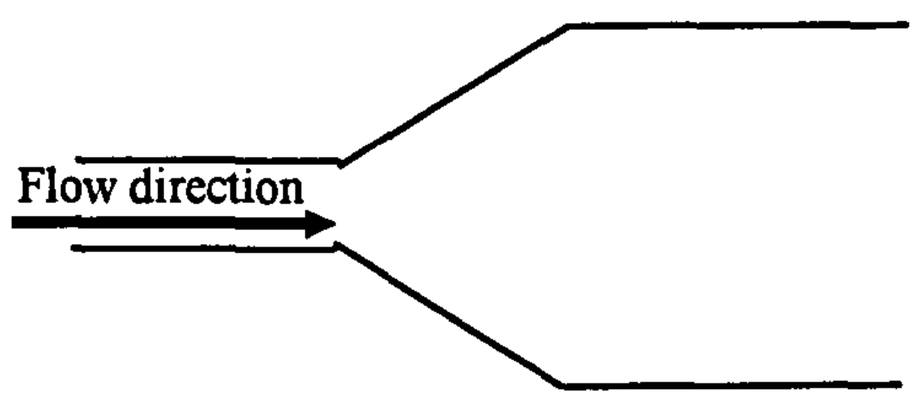

Figure 2.52 Plan view of Formica's flume (Lateral expansion and contraction)

Thirdly, the author suggests that an enhanced adjustment coefficient, similar to C_{wd} may be more appropriate for use in the Zone 2 discharge prediction equation instead of James and Wark's [1992] coefficient. Their original C_{wd} was defined only in terms of aspect ratio and it is likely that the magnitude of expansion and contraction loss will also be affected by other parameters, such as relative flow depth, relative roughness, slot skew angle.

Fourthly, the author notes that there is little evidence to justify the formulation of the step width correction factor, C_{sl}, which discounts the contribution of expansion and contraction head losses over a width of Zone 2 equal to the main channel. Inspection of the depth-averaged velocity results from the Series B tests, for example SDB21 in Figure 2.53, actually demonstrates that it would be more appropriate to treat Zone 2 as two 'newly-defined' sub-areas, Zones B1 and B2, because the average flow velocity distribution appears to be divided into two distinct regions. In these two sub-zones there is clearly considerably greater head loss experienced in Zone B1 compared to Zone B2.

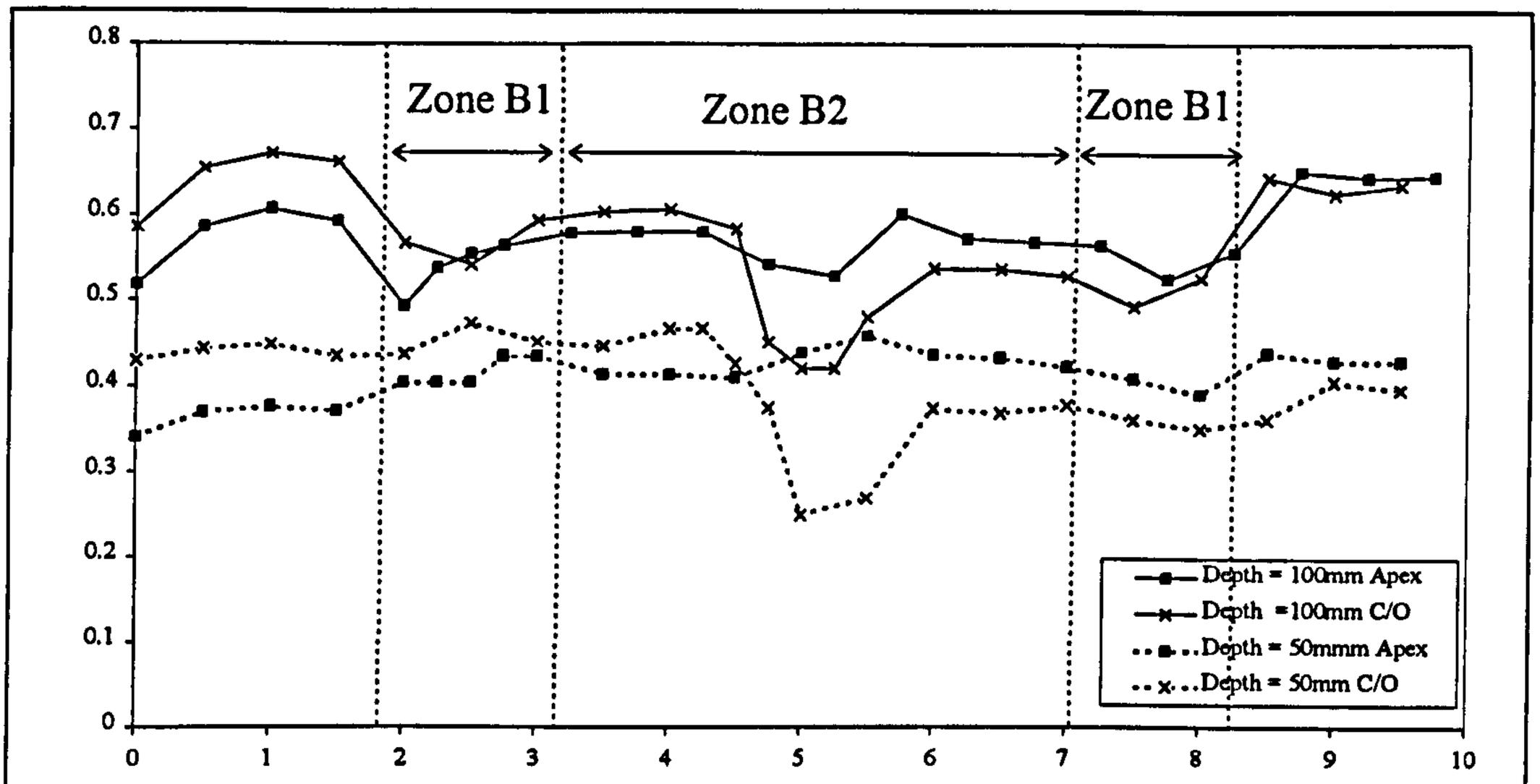

Figure 2.53 Depth averaged velocity for SDB21 [Series B], 50 and 100mm flow depths

Finally, the fundamental basis of the expansion and contraction term in James and Wark's [1992] Zone 2 formulation is that the nature of flow in Zone 1 does not influence the processes of expansion and contraction in Zone 2 thus facilitating the application of the standard formulae for simple steps to the meandering compound channel (slot) situation. However this assumption is unlikely to be accurate. Further experiments are needed to assess exactly what the influence of Zone 1 flow will be on the expansion and contraction processes both qualitatively and quantitatively.

2.8.5.6.4 Zones 3 and 4

James and Wark [1992] concurred with Ervine and Ellis' [1987] original assumption which stated that the outer flood plain zones, Zones 3 and 4, were solely influenced by bed friction effects. The zonal discharge is therefore determined by using the appropriate standard resistance equations, as shown in Equations 2.86 and 2.87 with a division line (with no frictional contribution) separating Zones 3 and 4 from Zone 2.

$$Q_3 = A_3 V_3 \qquad [2.86]$$

$$Q_3 = A_3 V_3 \qquad [2.87]$$

where

$$V_3 = [8 g R_3 S_0 / f_3]^{1/2} \qquad [2.88]$$

$$V_4 = [8 g R_4 S_0 / f_4]^{1/2} \qquad [2.89]$$

James and Wark [1992] showed that this assumption appeared to have no detrimental effect on the overall accuracy of discharge predictions produced by their model for the case studies they presented. However the author notes that it is likely that there will be another source of head loss experienced by Zone 3 and 4 due to the likely transfer of momentum between Zone 2 and Zones 3 and 4 due to the difference in velocity of the flow in the three zones. Further testing will be required to ascertain whether this mechanism might indeed be significant and will require calculation.

2.8.5.7 James and Wark[2] [1992]

This method implements the same formulation for Zones 1, 3 and 4 as in James and Wark [1] but replaces the semi-empirical / semi physical formulation with a simple empirically-derived formula for Zone 2 which was obtained by analysing the zonal flow data obtained during Series B. An multiplicative adjustment factor, Q_2', which related the basic Zone 2 discharge (allowing for bed friction losses only), Q_{2bf}, to the actual measured discharge, Q_2, was determined as shown in Equation 2.90.

$$Q_2 = Q_2' * Q_{2bf} \qquad [2.90]$$

Q_2' was defined in terms of relative depth, aspect ratio and sinuosity and its value was equal to the lesser of Equations 2.91 and 2.92

$$Q_2' = 6.0y' \qquad [2.91]$$

$$Q_2' = (1.02s^{-0.915}) * y'^{(-0.81(B2/A)-0.477)} \qquad [2.92]$$

This method did not perform as well as James and Wark [1] [1992]when tested against experimental data. This is due to the limited data available to develop the relationships and the exclusion of other influential parameters like relative roughness, main channel side slope and relative meander width. It will be possible to refine the James and Wark [2] [1992] method further once additional Zone 2 flow data is produced. Figure 2.54 shows the differences between the measured discharges for the River Roding study and the predicted discharges using the James and Wark methods which were presented in Wark [1993].

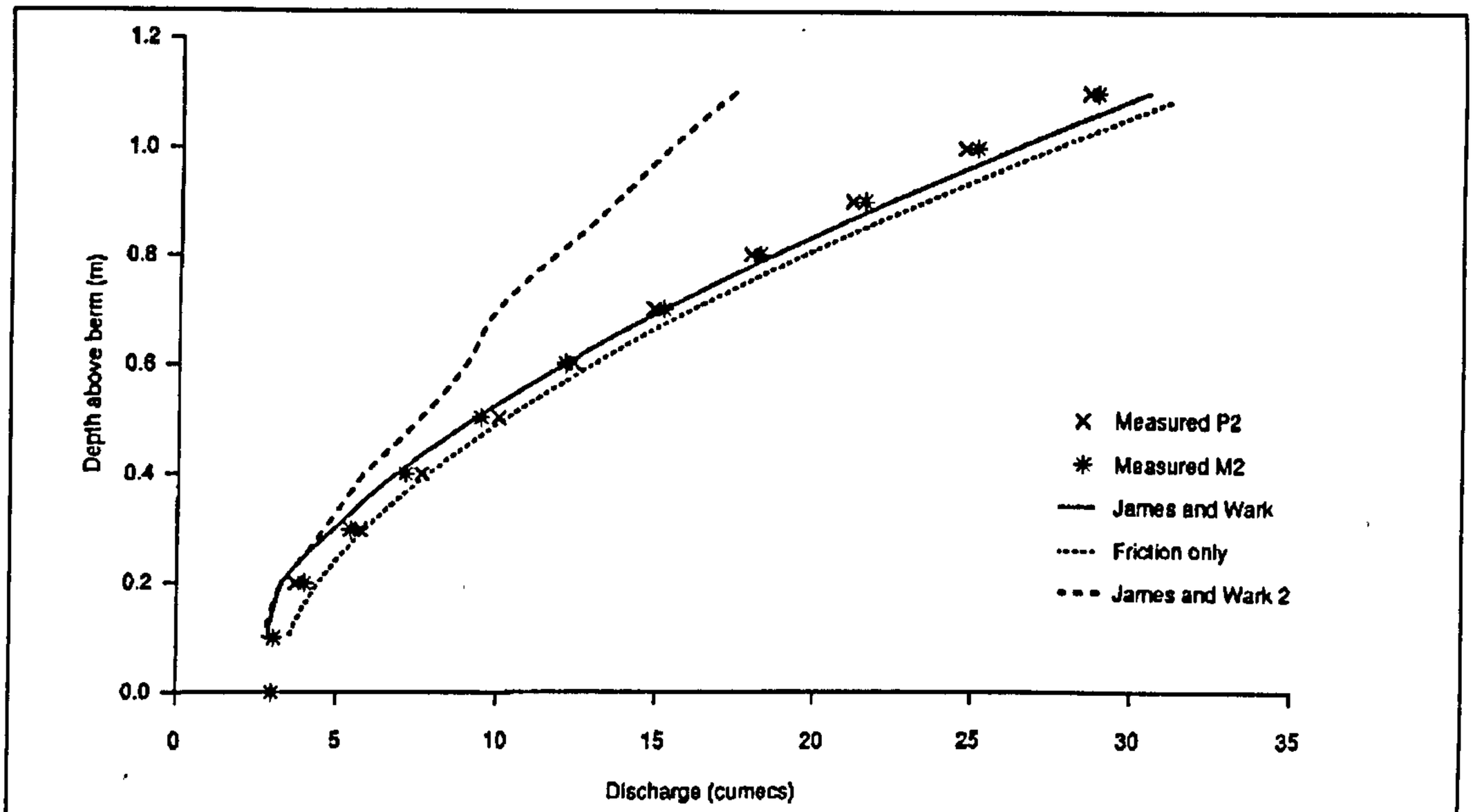

Figure 2.54 Predicted stage and discharge curves for River Roding (after Wark [1993])

2.8.5.8 Naish [1995]

Naish [1995] divided the cross-section flow in a meandering compound channel into two zones: the main channel and the flood plain. This method did not distinguish the flood plain outwith the meander belt (Zone 2). It was not necessary for the River Blackwater on which this method was predominantly based, because it did not possess an outer flood plain. However, this was an oversight because to extend this method to other meandering channels some allowance for the difference in flow between Zones 2 and 3 would be necessary. Naish [1995] used Equation 2.93 to predict the average main channel flow velocity. R_{MC} and S_{MC} are equal to the main channel slope and hydraulic radius respectively. n_{MC} is the main channel, Manning's n, adjusted for the effect of sinuosity using the linearised SCS method as shown in Equations 2.23 - 2.25.

$$V_{MC} = \frac{1}{n_{MC}} R_{MC}^{2/3} \sqrt{S_{MC}} \qquad [2.93]$$

Naish [1995] also defined an novel formulation for sinuosity for use in Equations 2.23 and 2.24 which is shown in Equation 2.94. This formulation combines the sinuosity of the flood plain channel, s_{fp}, and the main channel, s_{mc}, to create an average sinuosity, s. There was little evidence to support the use of this arbitrary definition of sinuosity and it may possibly introduce additional errors

Naish [1995] used the same sinuosity value to predict the mean velocity in the flood plain. He introduced an empirically derived Manning's n correction factor, FPnCF, to the basic Manning's equation as shown in Equation 2.95 in order to account for layer interaction head losses and any computational errors.

$$V_{FP} = \frac{1}{n_{FP}(FPnCF)} R_{FP}^{2/3} \sqrt{S_{FP}} \qquad [2.95]$$

FPnCF was defined in terms of roughness ratio, RRF and flood plain berm inclination ratio, BIF. Two different formulations were derived because Naish [1995] demonstrated that at low flow depths, when the main channel flow was significantly retarded by interaction losses, FPnCF had to be negative. However eventually FPnCF became positive (demonstrated using the River Blackwater tests). The author notes that although it was possible, when fitting the formulation to the River Blackwater data to determine when FPnCF would be negative or positive Naish [1995] did not clarify how this was to be done when the method was applied to other channels. In addition the basic formula was derived using such a limited set of data that when it was applied to test results, James and Brown [1977], large errors were encountered. Two adjustment factors were introduced to adjust the model so that it also fitted the James and Brown [1977] data. These were the geometric ratio, GRF and the corrected depth formulation given in Equation 2.96.

$$Corrected\ depth = \frac{flood\ plain\ flow\ depth}{RRF * GRF * BIF} \qquad [2.96]$$

FPnCF was defined according to Equations 2.96 and 2.97.

$$\text{if FPnCF is -ve then } FPnCF = FPnCF*(RRF*GRF*BIF^2) \qquad [2.97]$$

$$\text{if FPnCF is +ve then } FPnCF = (FPnCF-1)*(RRF*GRF*BIF^2)+1 \qquad [2.98]$$

The method developed by Naish [1995] will predict the discharge capacity of the models which provided the development data but can not be extended reliably to other meandering compound channels.

2.8.6 Computational models for predicting flow behaviour

2.8.6.1 Stein and Rouve [1989]

Stein and Rouve [1989] produced a 2D depth-averaged model to predict flow behaviour in a compound meandering channel. The basic three dimensional equation system was

reduced by integration over depth and neglected velocities and gradients in the z-direction. An equation system was formulated by considering conservation of momentum in the x- and y- directions and conservation of mass by defining the depth-averaged stress tensor in two dimensions. Lack of closure led to bottom shear stress and the depth-averaged stress tensor being parameterised. An approximate numerical solution of the equation system was achieved using a finite element technique which combined a 'front' equation solver and a Newton-Raphson iteration scheme. Boundary conditions were determined from the test set provided by Stein and Rouve [1988]. For inflow, a velocity distribution was used. For outflow, a water level profile was used. Wall boundaries were assumed to exhibit free slip (only velocities parallel to the wall are considered. Some stagnation points were fixed; u=v=0.

The model predicted water level with an error of up to 2%. Predictions for velocity distribution were not so good. However the main fluid exchange between the main channel and flood plain was replicated. Stein and Rouve [1989] predicted that their future attempts to develop and incorporate a k-ε turbulence model in the basic model will produce more accurate results .

2.8.6.2 Manson [1994]

Manson [1994] implemented a k-ε turbulence model in a set of 3D flow equations and tested it against results obtained from Kiely [1989]. The model was used to predict the water levels and zonal velocities for the models tested by Kiely [1989].

Computational power limitations however prevent the application of the method to complete and complex natural river systems. Consequently as a everyday tool for River Engineers, for modelling the stage and discharge behaviour of a natural river, it is not yet viable. However Manson's [1994] model is also able to predict the nature and magnitude of the local turbulence fields in simple compound channels. Consequently when a problem can be suitably simplified to enable the application of Manson's [1994] model then it will be very useful to the River Engineer in order to help determine the impact of the flow on the geomorphology of the river channel.

2.9 Chapter 2: Summary and conclusions

- The author concluded that a number of researchers have investigated the flow behaviour in meandering compound channels and determined the influence of various parameters. However, only a few of them have attempted to precisely relate the changes in layer interaction mechanism which occur at various flow depths to the observed flow behaviour.
- The author noted that the Ackers [1991] method provides the most reliable stage and discharge prediction method for the straight and skew compound channels.
- The author noted that the James and Wark [1] [1992] method provides the most reliable stage and discharge prediction method for meandering compound channels for a limited range of channel configurations.
- The author recognised that the limited scope of pertinent flow data for meandering compound channels has hampered the development of reliable methods for general meandering compound channel configurations to some extent.
- The author noted that the James and Wark [1] [1992] method does not account for all key parameters which influence flow behaviour. Consequently it is not completely reliable when applied to meandering compound channels which were not included in the data sets used to develop it.
- The author notes that of all the various approaches that have been devised for analysing meandering compound channel flow, the novel non-dimensional discharge parameter, F*, introduced by Ervine et al [1993] is the most useful for developing new discharge capacity prediction methods. Its ability to strip away the influence of bed friction (which is significantly affected by scale difference) and hence reveal the influence of layer interaction provided the author with the opportunity to assess the influence of model scale solely on the layer interaction mechanisms.
- The author recognised that the use of F* may be vital for the successful development of new prediction methods. In order to obtain enough data to determine the influence of all the key parameters that influence meandering compound channel flow, it was essential to enable the combination of results from different scale models and especially to utilise the flexibility of small scale models.
- The author noted that in traditional approaches to flow analysis the influence of the parameters on layer interaction had often been obscured by the significant differences in bed friction resistance in different scale models.

- The author identified that only five data sets possessed reliable enough bed friction calibration data to facilitate F* analysis. These five data sets were collated and prepared for analysis as part of the Series B extension (1993-1996) programme in Glasgow. These five data sets were:

  1) Vicksburg [1956]
  2) Toebes and Sooky [1967]
  3) Kiely [1989]
  4) Series B (1989-1992) (see Ervine *et al* [1993])
  5) Aberdeen (1991) (see Willetts and Hardwick [1993])

Chapter 3

3. The Series B extension physical model details and testing programme

3.1 Introduction

Chapter 1 highlighted the broad rationale for this research programme. At its core is the idea that meandering compound channel flows are influenced by eleven key parameters which were identified during the literature review and are noted below:-

1. The scale of the model, (L_r)
2. The relative depth of flow, (RD)
3. The relative roughness of the main channel / flood plain, (f')
4. The sinuosity of the main channel, (r)
5. The longitudinal bed slope, (S_o)
6. The relative width of the meander belt and floodway, (M_w)
7. The aspect ratio of the main channel, (AR)
8. The sides slope angles of the main channel, (S_S)
9. The cross-sectional shape of the main channel, (φ)
10. The sinuosity of the flood plain banks, (r_u)
11. The lateral flood plain slope towards the main channel, (S_L)

It was unrealistic to expect one Institution to determine the influence of all eleven parameters. A three-way split was agreed between Glasgow, Aberdeen and Bristol Universities as outlined in Table 3.1. The significance of each parameter was determined by testing model configurations in which 10 parameters were kept constant while the other one was varied. Seven parameters were investigated in Glasgow. These were, model scale, relative depth, relative roughness, relative meander belt width, main channel aspect ratio, shape and side slope. Thirty different model configurations were constructed in Glasgow in order to demonstrate the influence of each parameter. The geometric configurations and surface roughness details of each model are outlined in Table 3.8 on page 128. In Aberdeen, 24 model configurations were tested and these are

outlined in Table 3.9 on page 129. Bristol had not completed their tests when this thesis was written and therefore details of their configurations have not been included.

Glasgow		Aberdeen		Bristol	
Relative roughness	(1)	Relative roughness	(1)	Relative roughness	(1)
Main channel shape	(2)	Main channel shape	(2)	Main channel shape	(2)
Effects of Scale	(3)	M/C Sinuosity	(7)	Floodway channel width	(6)
M/C Side slope	(4)	Longitudinal Slope	(8)	Sinuosity of Flood banks	(9)
Main Channel Aspect ratio	(5)	Sinuosity of Flood banks	(9)	Lateral flood plain slope	(10)
Floodway channel width	(6)				

Table 3.1. The geometric and roughness characteristics of the physical models

The compatibility and repeatability of the models and results was assured by building and testing an identical model configuration in each Institution (the common test). Comparisons between the results from the common tests, were used to co-ordinate the experimental techniques of each Institution and ensure compatibility. Frequent inter-Institutional meetings were also held to facilitate compatibility. The intention was that the Institutions would be able to freely combine all the flow results on completion of the experimental programme.

The author conducted an additional set of experiments to compliment the basic meandering compound channel tests. The head loss due to the expansion and contraction of flow passing over a slot (or trench) in a channel bed was measured for various slot configurations. These slot tests were devised to simulate the flow mechanisms which are generated within flood plain flow as it passes over a deeper main channel in a meandering compound channel. Although the analogy with compound channel flow is not exact, the tests were devised to be a useful adjunct and to relate the magnitude of the expansion and contraction head losses to slot parameters replicated in meandering compound channels. The results obtained added to the data set obtained by Jasem [1990] who investigated the influence of flow depth and slot length (aspect ratio) on the magnitude of head loss generated by these mechanisms. The author compared Jasem's [1990] experimental results for 80mm wide slots with slots of a similar configuration but 300mm wide. In addition the influence of three extra parameters on slot flow was investigated. These parameters included: slot side slope, the relative

boundary roughness upstream and downstream of the slot, and the angle (skew) of the slot to the oncoming flow.

3.2 The Meandering Compound Channel tests

3.2.1 Choice of model dimensions

The range of possible model configurations was constrained by the dimensions of the flumes at each institution as shown in Table 3.2 and Table 3.3. To enable comparison between the Series B (1989-1992) data from HR Wallingford and the extension tests, a scale model of the Series B model SDB21, was adopted as the basic common shape for all Series B extension models. The HR Wallingford configuration was reduced in scale by a factor 1:6 so that the meander belt width and wavelength could be incorporated into each flume with enough wavelengths to ensure fully developed flow.

Location	Flume Width
Aberdeen	1.2m
Glasgow	1.65m
Bristol	2.0m

Table 3.2 Flume Widths

Location	Flume Length
Aberdeen	11m
Glasgow	8m
Bristol	10m

Table 3.3 Flume lengths

Kiely [1989] demonstrated that a minimum of two repeating wavelengths was required to establish developed flow patterns. The SDB21 planform configuration was scaled at a ratio of 1:6 in order to obtain a meander wavelength of 2m which facilitated the inclusion of more than 2 meander wavelengths in the models at each Institution. The Glasgow flume was the shortest and comprised 3.5 wavelengths. Table 3.4 lists the number of wavelengths possible in all the flumes.

Location	No. of Wavelengths
Glasgow	3.5
Aberdeen	4.5
Bristol	4.5

Table 3.4. Number of Wavelengths in each flume

A common model was built and tested at each Institution. The common model consisted of a 1:6 scale model (planform and cross-sectional) of the Series B model SDB21. Figures 3.1(a), (b), and (c). show the planform configuration for the common model in

each of the three flumes. The models are identical apart from the number of wavelengths fitted into each flume.

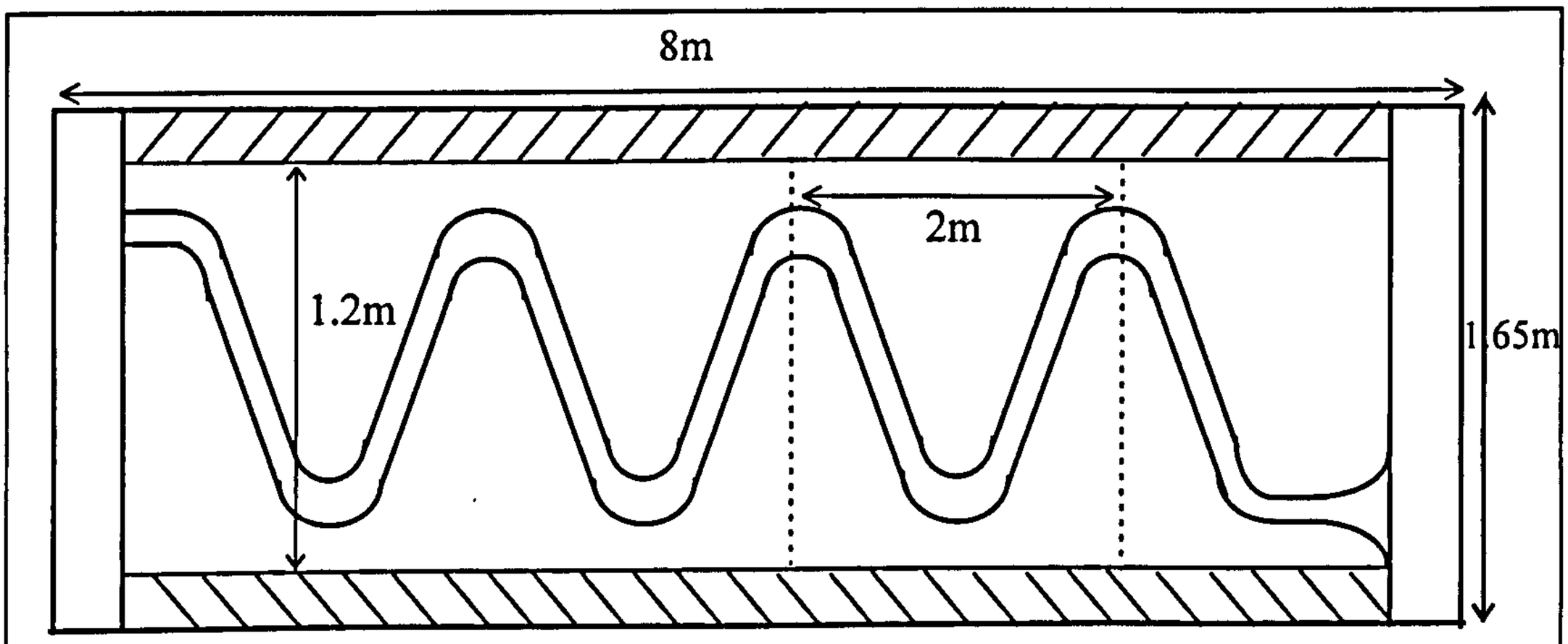

Figure 3.1(a) The common test planform configuration for Glasgow

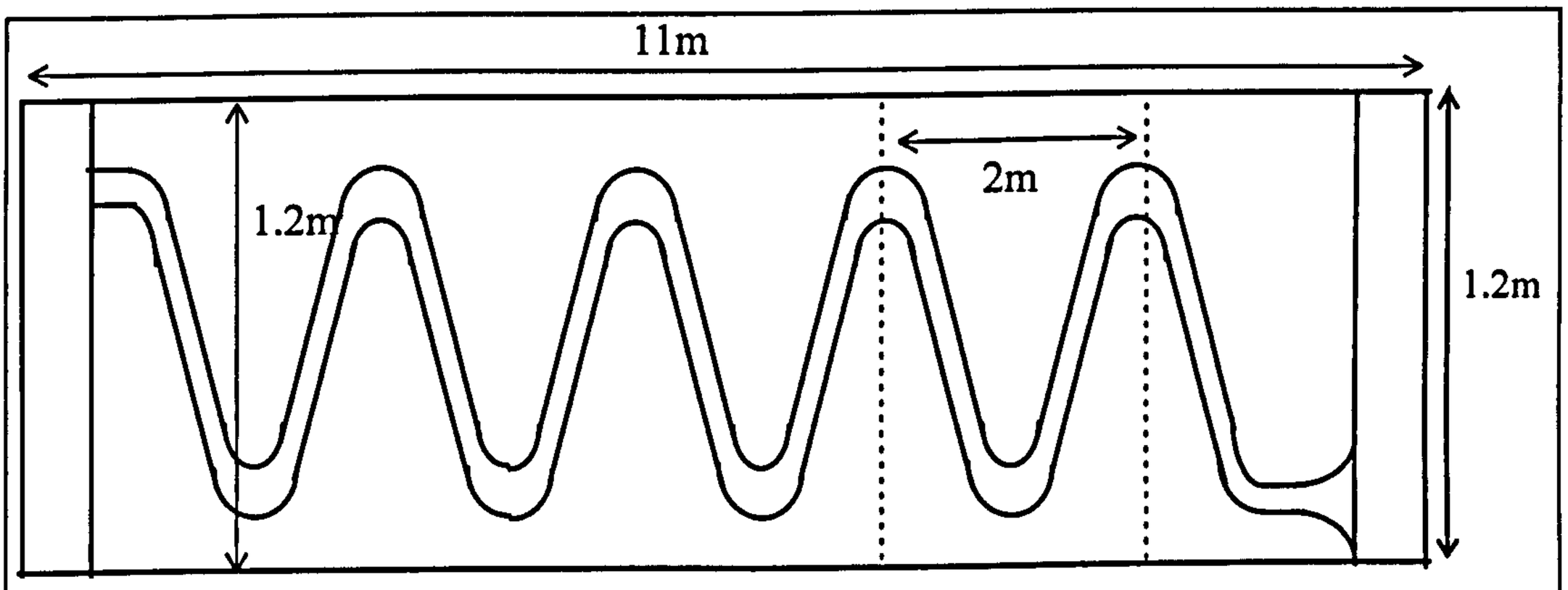

Figure 3.1(b) The common test planform configuration for Aberdeen

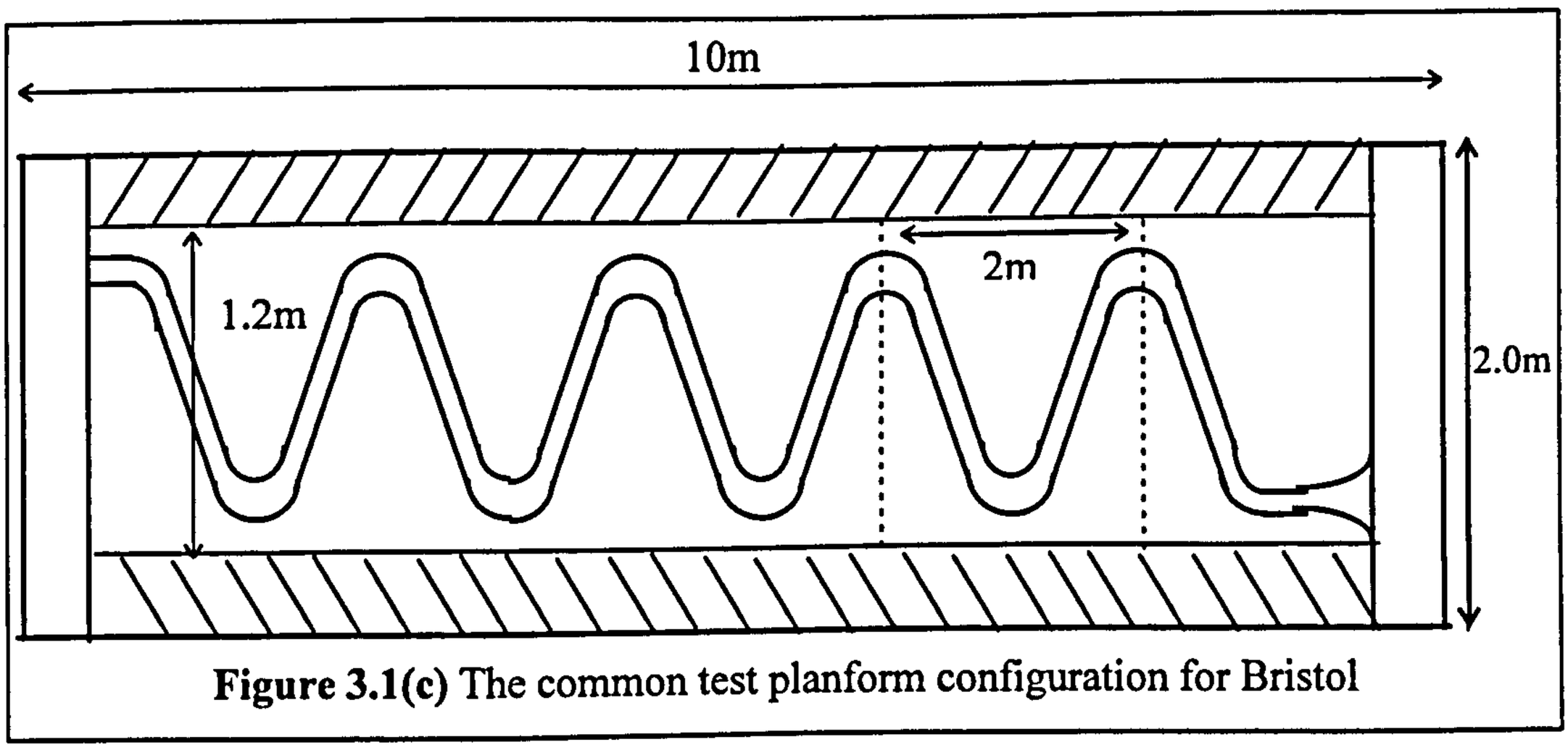

Figure 3.1(c) The common test planform configuration for Bristol

The narrowest width of flume available in the three Institutions was the 1.2m wide flume in Aberdeen which consequently dictated the flume width in the common test. The flood plain width of the common test was reduced from a width of 1.65m (determined by direct 1:6 scaling) to a width of 1.2m to enable the common model to be fitted in each flume. The wider Glasgow and Bristol flumes were narrowed to create the correct flood plain widths by placing polystyrene inserts on the inside walls of the flumes. These inserts were glued on top of the existing model surface and held down using weights and clamps. Great care was taken to ensure the inlet and outlet conditions and the friction characteristics of the model surfaces were the same in each flume.

3.2.2 Model fabrication techniques

High density polystyrene was used to created the models in Glasgow. Band saws and hot-wire cutters were used to cut the basic polystyrene sheets. The cutting equipment was designed specifically for this project. Eighteen identical polystyrene pieces were cut to create the flood plains of a meandering compound channel, as shown in Figure 3.2.

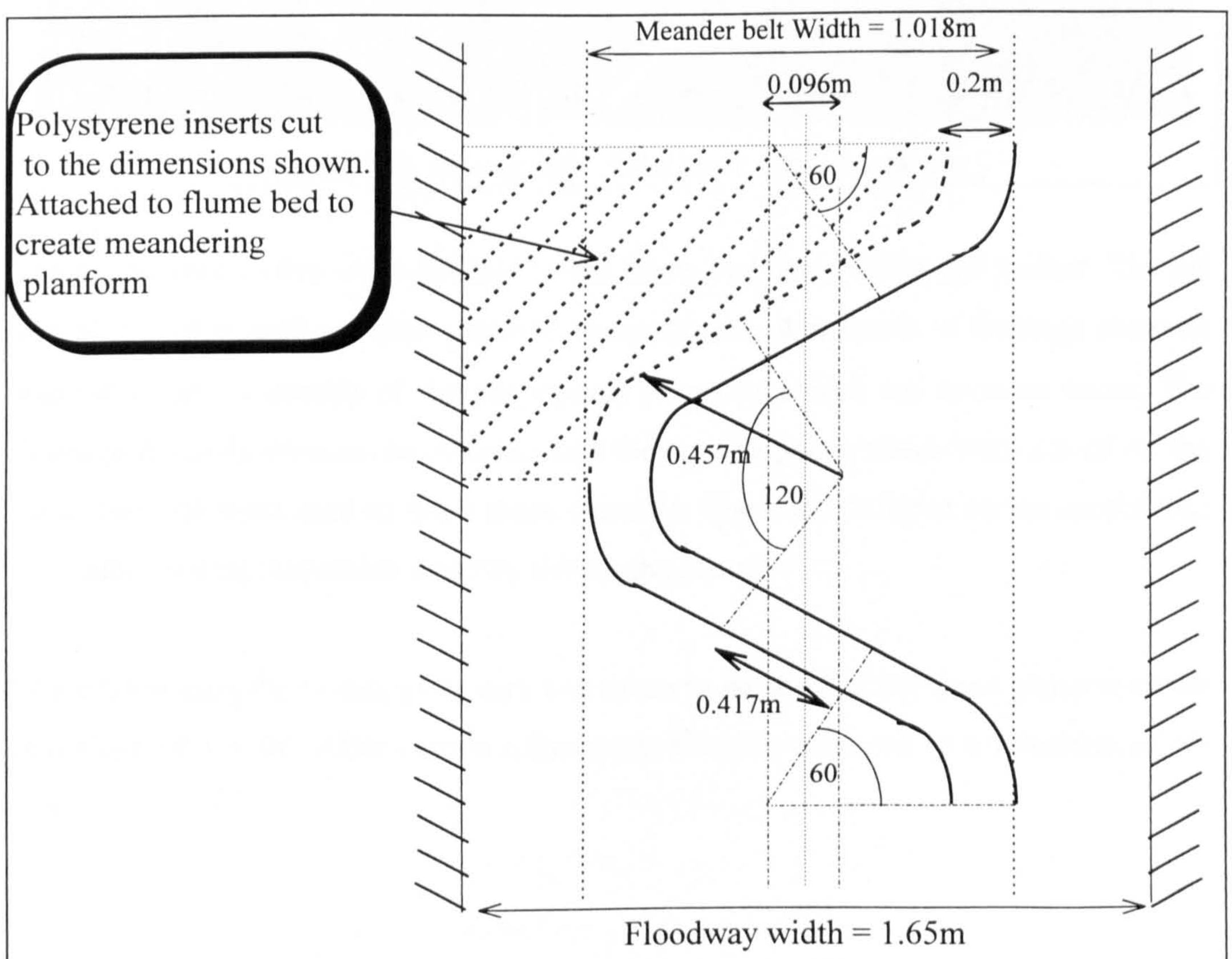

Figure 3.2 Planform dimensions of the Glasgow models

The main channel was formed by the gaps that are left between the eighteen polystyrene pieces. A couple of extra polystyrene pieces were cut to create the special transition pieces at the inlet and outlet ends. The dimensions of the 1:6 scale model planform of the SDB21 test were defined using a combination of straight lengths and circles with varying radii, as sketched in Figure 3.2. Figure 3.3 shows a photograph of a basic meandering compound channel which was constructed in Glasgow. It had a 1.65m wide floodway and a main channel sinuosity of 1.374.

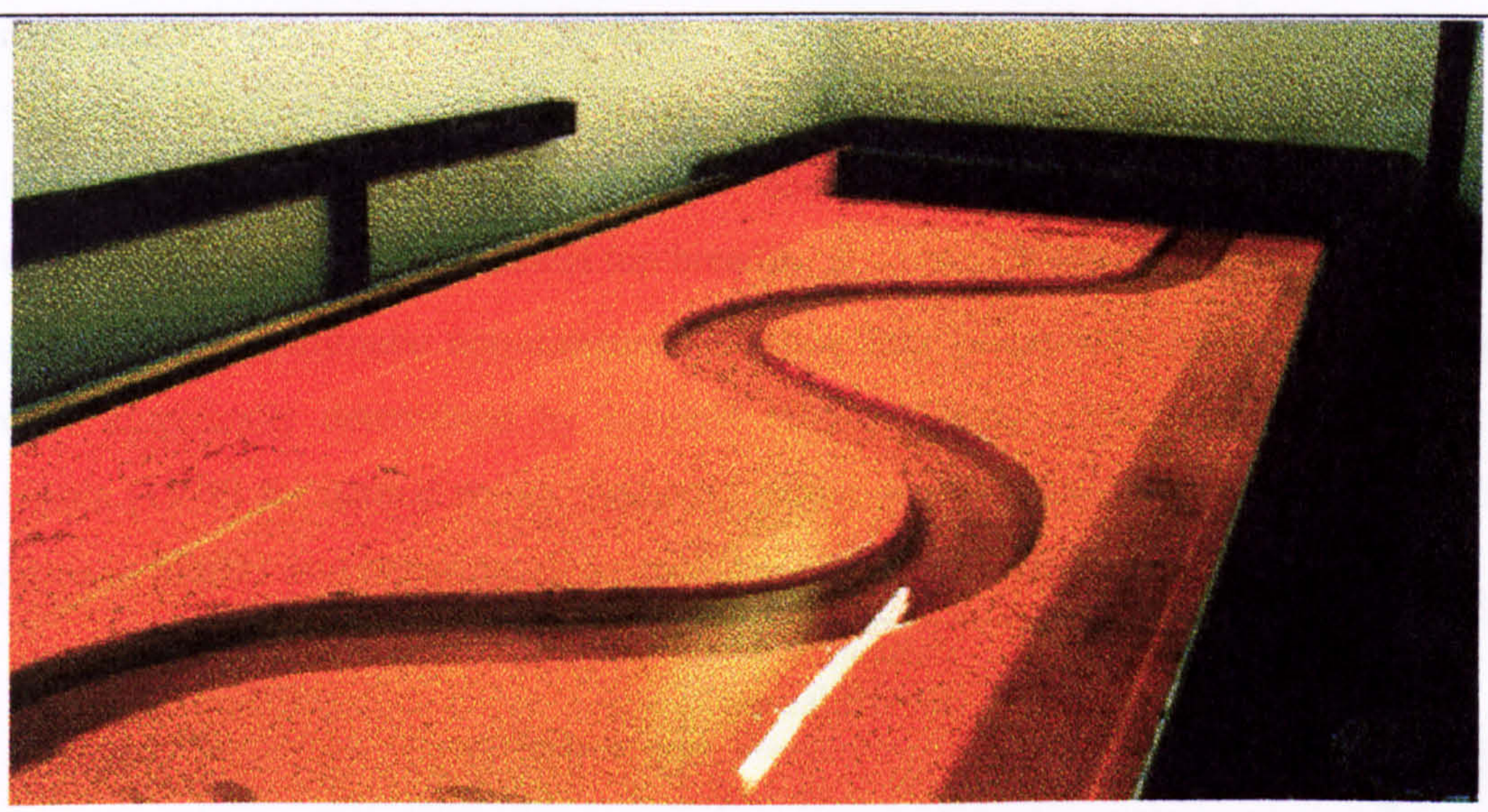

Figure 3.3. Photograph of the basic Glasgow flume

The polystyrene pieces were attached to the flume bed using silicon gel sealant. The gel was also used to seal any gaps prone to water ingress. A network of drainage channels was cut on the underside of the polystyrene pieces to collect any invasive water. The drainage channels were cut to coincide with the tapping points which were placed on the flume bed and were used to drain these channels. The buoyant force on the model was maintained within reasonable limits by this arrangement.

While fabricating the model, great care was taken to ensure that the flood plains were set at a slope of 1:1000. After careful adjustment, this was achieved to a tolerance of +/- 0.5mm.

3.2.3 Details of the planform configurations

3.2.3.1 The Glasgow models

The majority of the physical models built in Glasgow were 1:6 planform scale models of the Series B test, SDB21. The width of the flood plain was varied in a few models. The configuration of the main channel in SDB21 was chosen to be similar to a typical configuration found in natural rivers in order to increase the likelihood of similar flow mechanisms being generated in both. When designing SDB21 the main channel sinuosity was first set equal to 1.374, a typical natural river sinuosity. Subsequently four other geomorphic parameters:- meander amplitude, A, bend radius, R_c, meander wavelength, λ_m, and main channel top breadth, B_c, were chosen so that when they were analysed using particular non-dimensional ratios their values were similar to those that were empirically determined by Leopold [1960], Chang [1988], Zeller [1967] and Jansen [1979] for natural rivers. Table 3.5 shows a comparison between the parameter ratios in SDB21 and in natural rivers thus demonstrating their final similarity.

Key Indicators SDB21	Key Indicators Natural Rivers
$\lambda_m / B_c = 10$	$\lambda_m / B_c = 10$ Zeller [1967]
$R_c / B_c = 2.3$	$R_c / B_c = 2.3$ Chang [1988]
$\lambda_m / R_c = 4.38$	$\lambda_m / R_c = 4.4$ Leopold[(1960]
$A / \lambda_m = 0.4$	$A / \lambda_m = 0.4$ Jansen [1979]

Table 3.5. Comparison of the Glasgow model and the key indicators

3.2.3.2 The Aberdeen models

The Aberdeen group built some models with sinuosities other than the standard 1.374 in order to investigate the influence of sinuosity on discharge capacity. In these models the other non-dimensional parameter ratios were maintained at similar values as were set in the models with 1.374 sinuosity. This was done in an attempt to isolate the influence of one parameter, sinuosity and to keep the configuration similar to those in naturally occurring channels. The two alternative sinuosities tested were r= 1.772 and r=1.110. The values of the non-dimensional parameter ratios for these two sinuosities are given in Tables 3.6a and 3.6b. The channels with a sinuosity 1.722 had a wavelength, λ, equal to 1.4m, and average bend radius, R_c, equal to 0.3554m and a meander belt width, M_w,

equal to 1.034m. The channels with a sinuosity 1.110 had a wavelength, λ_m, equal to 2.4m, and average bend radius, R_c, equal to 0.8485m and a meander belt width, M_w, equal to 0.697m. The main channel top width, B_c was maintained at 0.2m for all the model tests.

Key Indicators Aberdeen r = 1.772	Key Indicators Natural rivers
$\lambda_m/B_c = 7$	$\lambda_m/B_c = 10.7$
$R_c/B_c = 1.8$	$R_c/B_c = 2.3$
$\lambda_m/R_c = 3.9$	$\lambda_m/R_c = 4.4$
$A/\lambda_m = 0.7$	$A/\lambda_m = 0.4$

Table 3.6a. r=1.772 (Aberdeen)

Key Indicators Aberdeen r = 1.110	Key Indicators Natural rivers
$\lambda_m/B_c = 12$	$\lambda_m/B_c = 10.7$
$R_c/B_c = 4.2$	$R_c/B_c = 2.3$
$\lambda_m/R_c = 2.8$	$\lambda_m/R_c = 4.4$
$A/\lambda_m = 0.42$	$A/\lambda_m = 0.4$

Table 3.6b. r=1.110 (Aberdeen)

3.2.4 Preparation of the model surfaces

A combination of rubberised cement screeding and gloss paint was used to treat any irregular or rough surfaces produced during the modelling phase in order to produce hydraulically smooth finishes which were used in some of the meandering compound channel models tested during the Series B extension programme. Smooth flood plains and main channels were only used in a small number of test runs. For most of the Series B extension tests the flood plain surfaces were roughened using mapping pins in an effort to reproduce more realistic variation of flood plain roughness with depth. Spherical headed mapping pins, with 5mm diameter heads, were used. The mapping pins were arranged in triangular patterns. The triangles were equilateral and the pins were placed at the apex of these triangles. The lengths of the sides, x mm, were varied to give different frictional resistance characteristics with depth. Figure 3.4 shows the general arrangement of the push-pins and the orientation of the pins to the longitudinal component of flood plain flow.

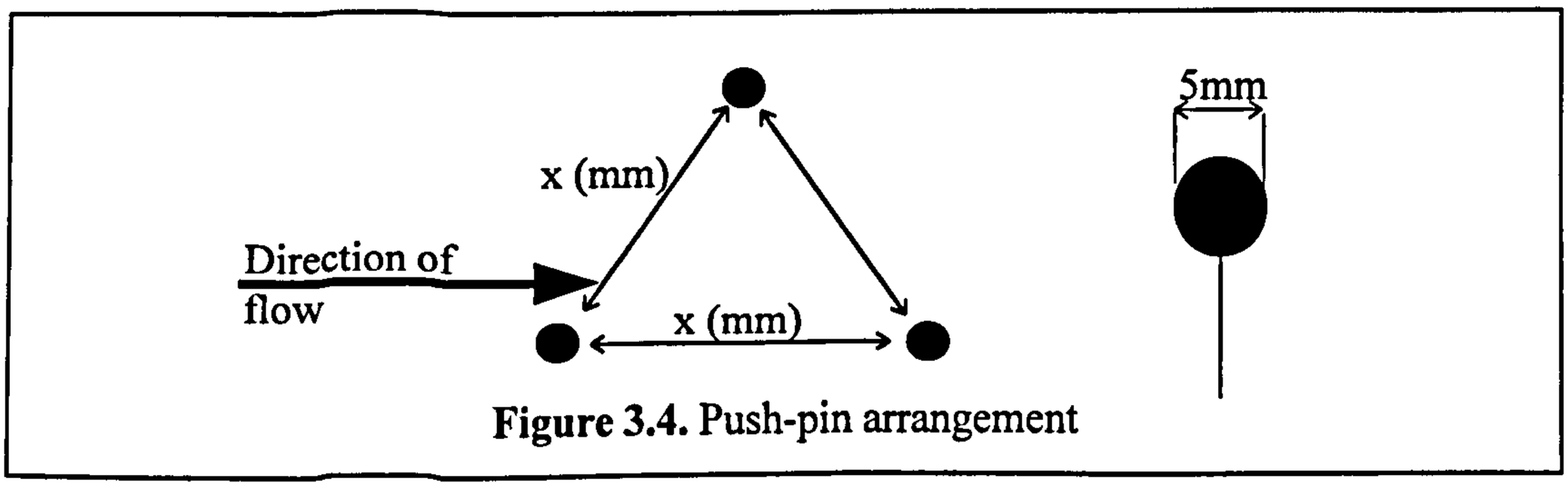

Figure 3.4. Push-pin arrangement

Both Glasgow and Aberdeen carried out flow resistance calibration tests on the smooth and roughened surfaces in simple rectangular flumes. The different lateral push-pin spacings that were tested are listed in Table 3.7. In Glasgow a 1.65m wide flume with painted side walls was used whilst in Aberdeen a 0.3m wide flume with glass side walls was used. Only the flume beds were roughened, the side walls were left hydraulically smooth. Stage and discharge readings were taken over a range of flow depths which corresponded to the range of flow depths that were to be tested in the meandering compound channel models during the Series B extension programme. The calibration results that were obtained are presented in Section 4.3.

Originator	Aberdeen	Glasgow	Aberdeen	Glasgow	Aberdeen
Spacing	60mm	50mm	30mm	25mm	15mm

Table 3.7. Push-pin spacing

Analysis of the results from all the calibration tests persuaded the members of the Series B extension programme to use two lateral pin spacings of 60mm and 30mm to roughen the surfaces in the meandering compound channel models. The variation of relative boundary roughness (f_f/f_c) with flow depth for these push-pin spacings exhibited similar patterns of behaviour to those that are observed in natural rivers. The 60mm push-pin spacing arrangement is later referred to as 'Rough A' and the 30mm push-pin spacing arrangement is later referred to as 'Rough B'.

3.2.5 Fabrication of the main channel geometries

3.2.5.1 Introduction

The main channel cross-sections in the Series B extension models all had a top width of 200mm. Their maximum depth was dependent on the thickness of the polystyrene sheets used for making the flood plains. The Glasgow main channel was 75mm deep and in Aberdeen and Bristol it was 52.5mm deep. The various main channel shapes, either trapezoidal or quasi-natural, were moulded by in-filling the cross-sections.

3.2.5.2 Forming the quasi-natural channels in Aberdeen

In Aberdeen natural channels were created from Bakelite using self forming methods. A layer of Bakelite was placed on the bed of the existing channels. Typically this was

25mm deep. Water was passed down the main channel at bankfull level to develop the appropriate bed forms. A Bakelite grain size of d_{50}≈1-2mm was chosen so only the macro bed form characteristics were generated in the main channel. The other smaller scale bed forms such as dunes, ripples and pools were avoided because these would complicate the flow mechanisms generated during the tests. Extra Bakelite was fed from the upstream end until equilibrium conditions were achieved. Cement was then sprinkled on the surface to fix the Bakelite in position and after hardening was painted with 2 coats of gloss paint to make it hydraulically smooth.

The bedform configuration changed with each channel sinuosity and set of flow conditions at bankfull. This complicated the quantitative analysis of the flow results because it was not possible to maintain the same natural bed configurations as sinuosity was varied. Also because an in-filling technique was used and the top width of the main channel was kept constant it was never possible to produce quasi-natural channels with exactly the same aspect ratio as the trapezoidal channels. Figure 3.5a and 3.5b show pictorially the in-filling used to create both trapezoidal and quasi-natural channels respectively.

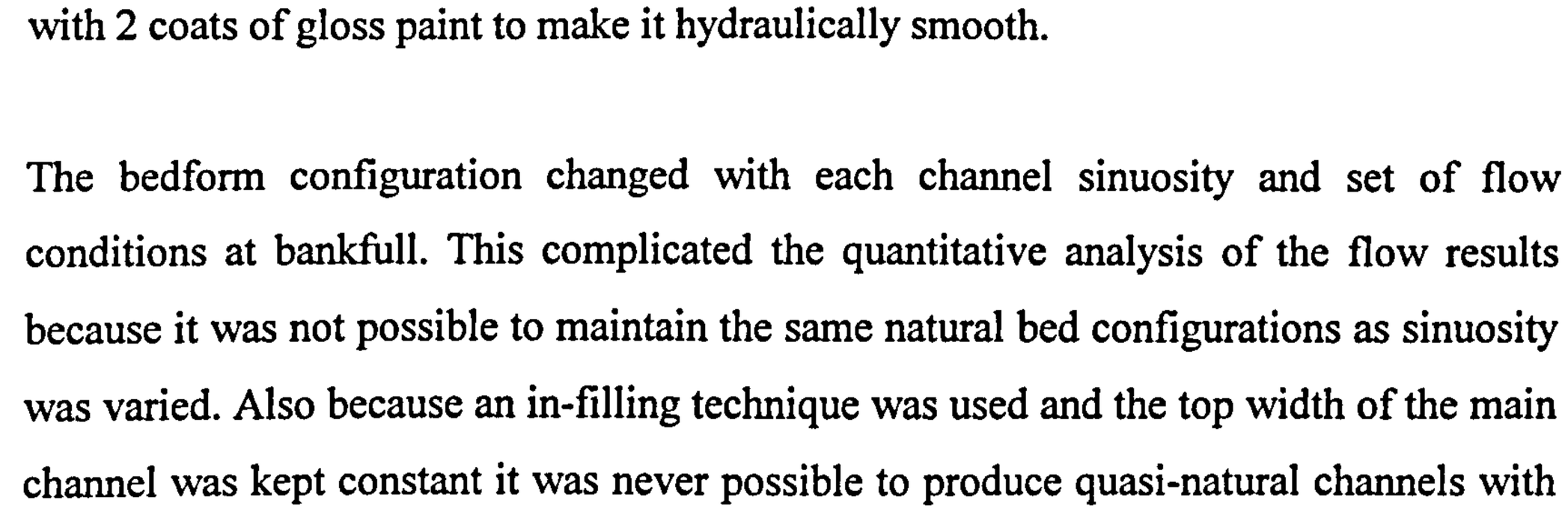

Figure 3.5a Trapezoidal channel

Figure 3.5b Natural channel

3.2.5.3 Forming the quasi-natural channels in Glasgow

In Glasgow a different method was used to fabricate quasi-natural main channel shapes. These channels were modelled by hand and were not self-formed. They were based on an analysis of 17 river bends and crossovers in natural channels which was conducted by Lorena [1993]. The Glasgow models were fabricated to be linear approximations of Lorena's [1993] natural channels. Because Lorena's average channel was assumed to be independent of sinuosity, the same shape was used for main channels with any sinuosity.

The linear approximation of Lorena's channels produced triangular sections at the meander apex sections. The maximum depth of the channel was positioned on the outside of the bend. Trapezoidal sections were fabricated at the cross-over sections. The depth at the cross-over was approximately half the maximum depth at the apex. Figure 3.6 shows how the linear approximation compares with the natural sections identified by Lorena [1993] at the apex of the river meanders.

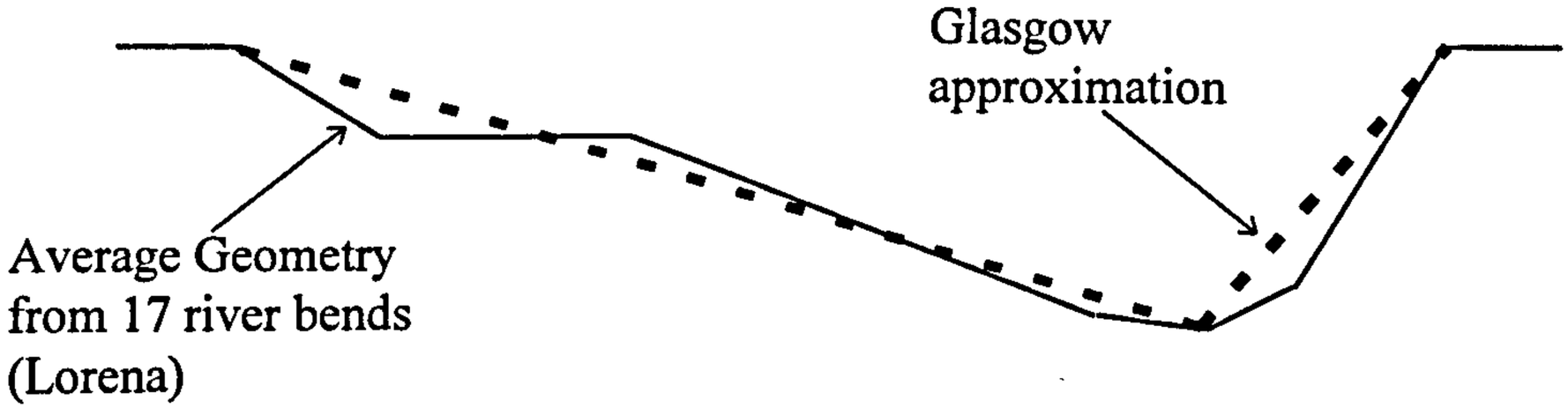

Figure 3.6. The main channel apex approximation and a typical channel

A combination of wet Loch Aline sand, $D_{50} = 2mm$, rubberised cement screed and two layers of gloss paint were used to model the natural channels. Templates were used to first mould the sand into the correct shapes. Then the screed and paint were added to fix the channel bed. The bed forms varied linearly between each apex and cross-over section. Figures 3.7a and 3.7b shows the bedform configuration for a main channel model which was 50mm maximum depth at the apex and 25mm deep at the cross-over section with 60° side slopes. This is the 'natural' channel referred to as G50N60R in Table 3.8.

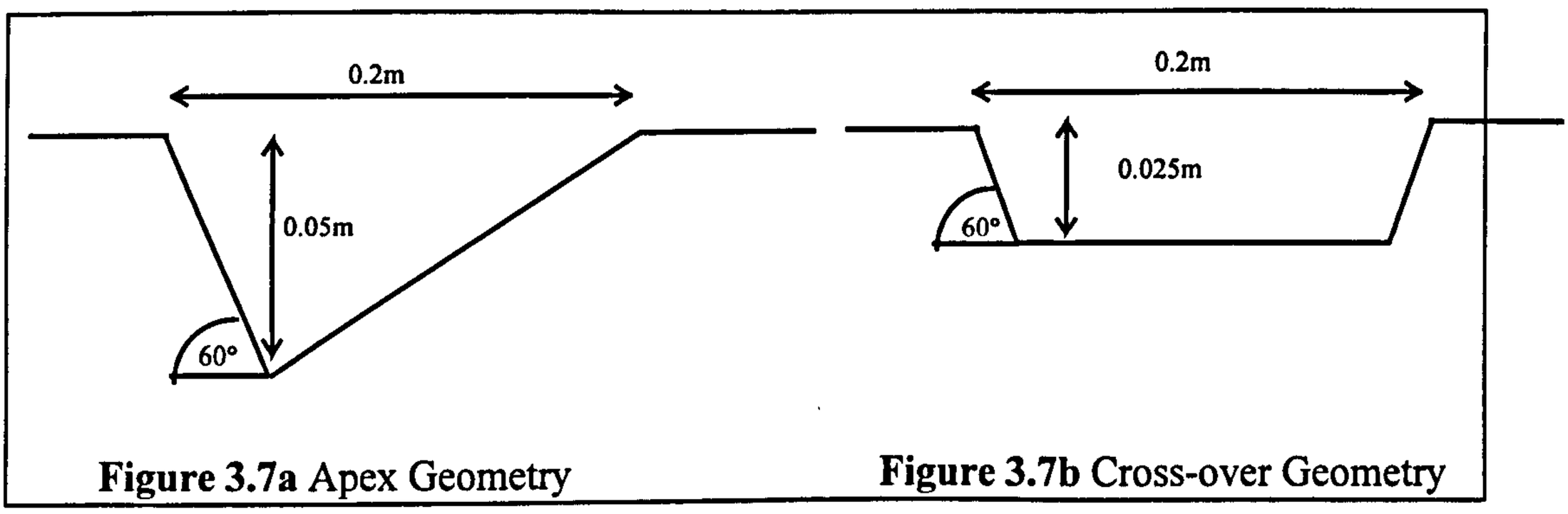

Figure 3.7a Apex Geometry **Figure 3.7b** Cross-over Geometry

The aspect ratio of Lorena's typical main channel (the ratio between the channel width and its average depth, B^2/A) and that of the linear approximation shown in Figure 3.7a, and adopted in Glasgow, differed by only 6% when measured from a datum of bankfull

level. This was only a small difference and therefore the adoption of this linear approximation was judged satisfactory. However unfortunately the quasi-natural channels were not totally compatible at the two Institutions.

Keller [1995] presents a new numerical model for predicting the evolution of meander planforms in natural rivers. The model accurately predicts the migration of meanders in a number of naturally occurring rivers, notably the Buma-Putra, in Bangladesh. In his model, Keller [1995] adopted the same linear approximation for the main channel cross-section as in the Glasgow physical models. The success of his method when predicting the migration of meanders tends to reinforce the validity of a linear approximation for channel shape.

3.2.6 Models built and referencing systems adopted

Tables 3.8 and 3.9 list the basic geometric and roughness characteristics of the models which were built by Glasgow and Aberdeen respectively for the Series B extension programme. The Bristol models have not been included because the results were not complete at the time of writing. Figure 3.8 below shows how the reference number systems adopted for the Glasgow models can be used at a glance to identify the configuration of the model.

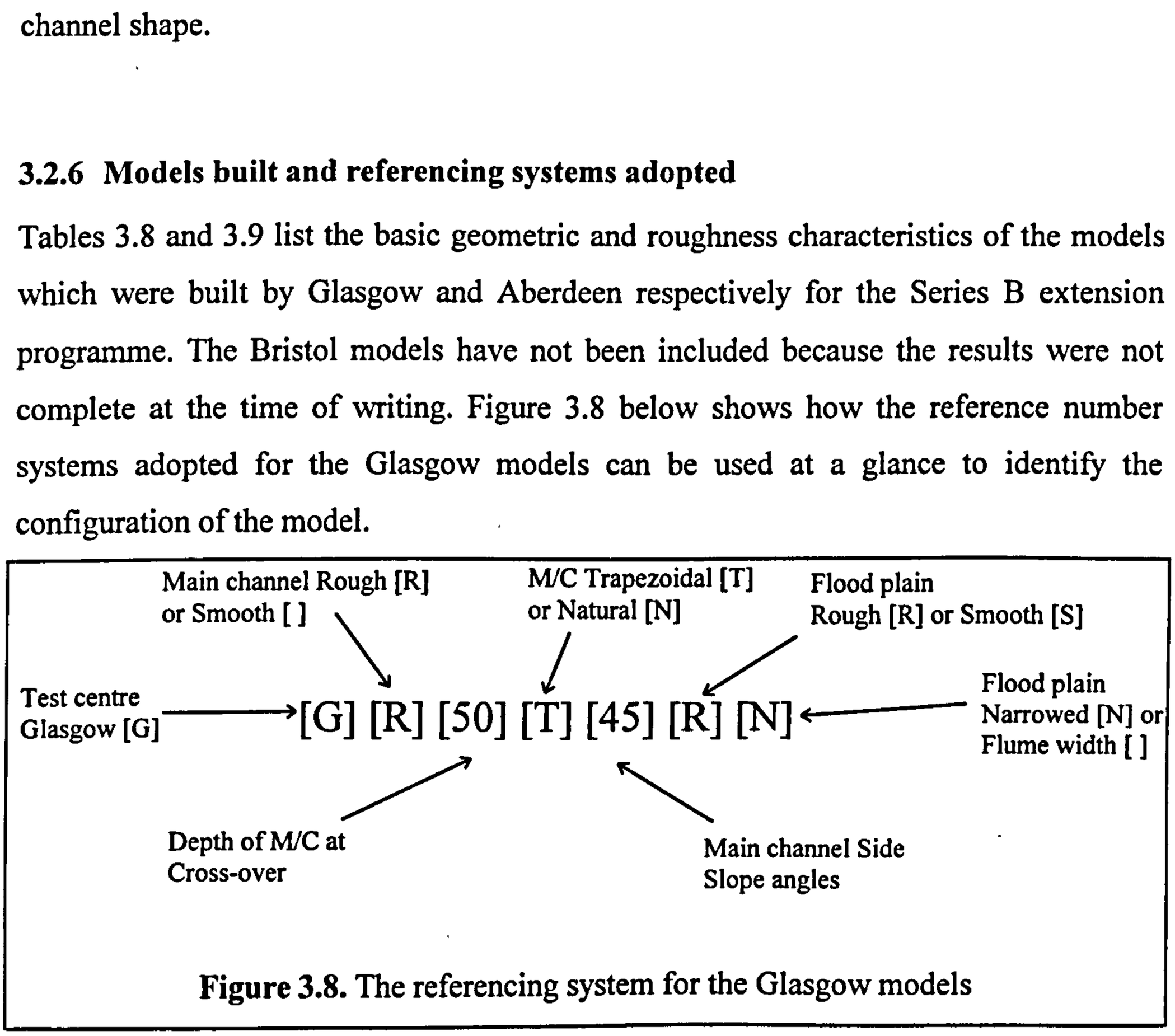

Figure 3.8. The referencing system for the Glasgow models

Figure 3.9 shows how the reference number systems adopted for the Aberdeen models can be used at a glance to identify the configuration of the models.

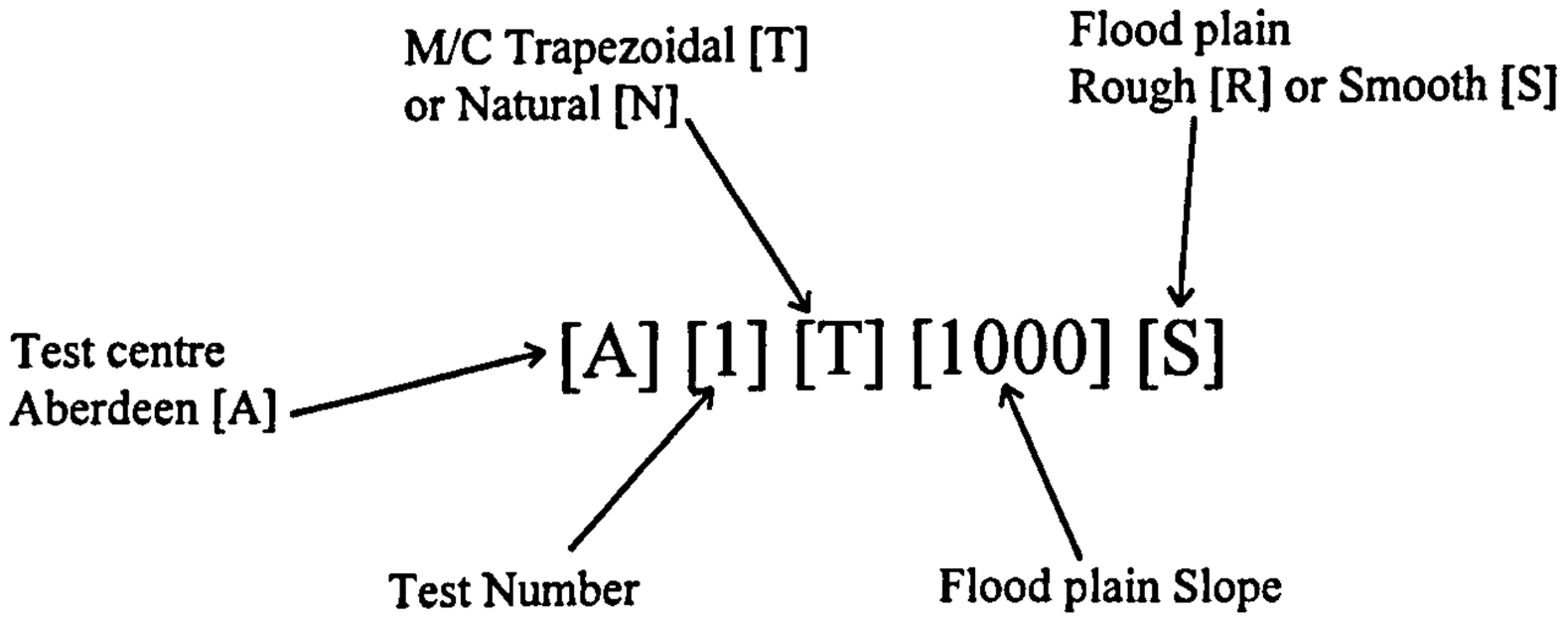

Figure 3.9 The referencing system for the Aberdeen models

Test No.	Reference Number	Aspect Ratio	Date of Test	Bankfull Depth (mm)	M/C Shape	M/C side Slope	F/P Manning's 'n'	M/C Manning's 'n'	Total F/P Width
1	G75T90S	2.670	Sum. '94	75.0	Trap.	90	S	SM	1.650
2	G75T90R	2.670	Sum. '94	75.0	Trap.	90	B	SM	1.650
3	GR75T90R	2.670	Aut. '95	75.0	Trap.	90	B	B	1.650
4	G75T60R	3.400	Spr. '95	75.0	Trap.	60	B	SM	1.650
5	G75T45R	4.260	Sum. '95	75.0	Trap.	45	B	SM	1.018
6	G75T45RN	4.260	Aut. '95	75.0	Trap.	45	B	SM	1.650
7	G75T37R	5.270	Win. '95	75.0	Trap.	60	B	SM	1.650
8	G50T90R	4.000	Aut. '94	50.0	Trap.	90	B	SM	1.650
9	G50T60RA	4.490	Spr. '95	52.5	Trap.	60	B	SM	1.200
10	G50T60R	4.670	Spr. '95	50.0	Trap	60	B	SM	1.650
11	G50T45R	5.330	Sum. '95	50.0	Trap	45	B	SM	1.650
12	GDA50T37R	5.990	Spr. '96	75.0	Trap	37	B	0.019	1.650
13	G50T37R	5.990	Spr. '96	50.0	Trap	37	B	SM	1.650
14	G50T30R	7.050	Aut. '95	50.0	Trap	30	B	SM	1.650
15	G50N90R	4.570	Aut. '94	50.0	Nat	90	B	SM	1.650
16	G50N60R	4.980	Spr. '95	50.0	Nat	60	B	SM	1.650
17	G50N45R	5.330	Sum. '95	50.0	Nat	45	B	SM	1.650
18	G50N37R	5.640	Win. '95	50.0	Nat	37	B	SM	1.650
19	G25T90R	8.000	Win. '94	25.0	Trap	90	B	SM	1.650
20	G25T60R	8.621	Sum. '95	25.0	Trap	60	B	SM	1.650
21	G25T45R	9.143	Sum. '95	25.0	Trap	45	B	SM	1.650
22	G25T45S	9.143	Aut. '95	25.0	Trap	45	S	SM	1.650
23	G25T45SN	9.143	Aut. '95	25.0	Trap	45	S	SM	1.018
24	G25T45RN	9.143	Aut. '95	25.0	Trap	45	B	SM	1.018
25	G25T30R	10.26	Win. '95	25.0	Trap	30	B	SM	1.650
26	G25N90R	8.000	Win. '94	25.0	Nat	90	B	SM	1.650
27	G25N60R	8.300	Spr. '95	25.0	Nat	60	B	SM	1.650
28	G25N45R	8.530	Sum. '95	25.0	Nat	45	B	SM	1.650
29	G25N30R	8.970	Win. '95	25.0	Nat	30	B	SM	1.650
30	G10N60R	15.69	Sum. '95	12.5	Nat	60	B	SM	1.650

Table 3.8. The models built and tested in Glasgow

Test No.	Reference Number	Aspect Ratio (M/C)	F/P Slope	Date of Test	Depth Bankfull (mm)	M/C Shape	Temp° C	F/P Manning's 'n'	M/C Manning's 'n'
1	A1T1000S	4.49	1:1000	Sum. '94	52.5	Trap.	20.5	SM	SM
2	A1T750S	4.49	1:750	Aut. '94	52.5	Trap.	20	SM	SM
3	A1T750A	4.49	1:750	Aut '94	52.5	Trap.	19.5	A	SM
4	A1T1000A	4.49	1:1000	Aut. '94	52.5	Trap.	20.5	A	SM
5	A1T1000B	4.49	1:1000	Aut. '94	52.5	Trap.	20	B	SM
6	A1T750B	4.49	1:750	Aut. '94	52.5	Trap.	20	B	SM
7	A1N1000B	7.236	1:1000	Win. '95	28	Nat.	18.5	B	SM
8	A1N750B	7.236	1:750	Win. '95	28	Nat.	18.5	B	SM
9	A2T1000S	4.49	1:1000	Spr. '95	52.5	Trap.	19	SM	SM
10	A2T750S	4.49	1:750	Spr. '95	52.5	Trap.	20	SM	SM
11	A2N1000S	5.26	1:1000	Spr. '95	38	Nat.	18.5	SM	SM
12	A2N750S	5.26	1:750	Spr. '95	38	Nat.	18	SM	SM
13	A2N750A	5.26	1:750	Spr. '95	38	Nat.	18.5	A	SM
14	A2N1000A	5.26	1:1000	Spr. '95	38	Nat.	19	A	SM
15	A2N1000B	5.26	1:1000	Sum. '95	38	Nat.	19	B	SM
16	A2N750B	5.26	1:750	Sum. '95	38	Nat.	18	B	SM
17	A3T1000S	4.49	1:1000	Sum. '95	52.5	Nat.	18	SM	SM
18	A3T750S	4.49	1:750	Sum. '95	52.5	Nat.	19	SM	SM
19	A3N1000S	4.57	1:1000	Aut. '95	44	Nat.	20	SM	SM
20	A3N750S	4.57	1:750	Aut. '95	44	Nat.	20	SM	SM
21	A3N750A	4.57	1:750	Aut. '95	44	Nat.	19.5	A	SM
22	A3N1000A	4.57	1:1000	Aut. '95	44	Nat.	19	A	SM
23	A3N1000B	4.57	1:1000	Aut. '95	44	Nat.	19.5	B	SM
24	A3N750B	4.57	1:750	Aut. '95	44	Nat.	19.5	B	SM

Table 3.9. The models built and tested in Aberdeen

3.2.7 Discharge measurement techniques

3.2.7.1 Measuring the total discharge capacity

The Glasgow flume is a re-circulating system with two storage tanks, a pump, connecting main, and a 1.65m wide flume. The pump could deliver a maximum discharge of 60 litres/sec to the model. The total discharge was measured using an Orifice plate meter. The general arrangement of the meandering compound channel flume is shown in Figure 3.10. The head difference across the Orifice plate was measured using a combination of differential mercury and water manometers (sloping and upright). Velocity integration methods were used to check the discharge calibration for the Orifice plate.

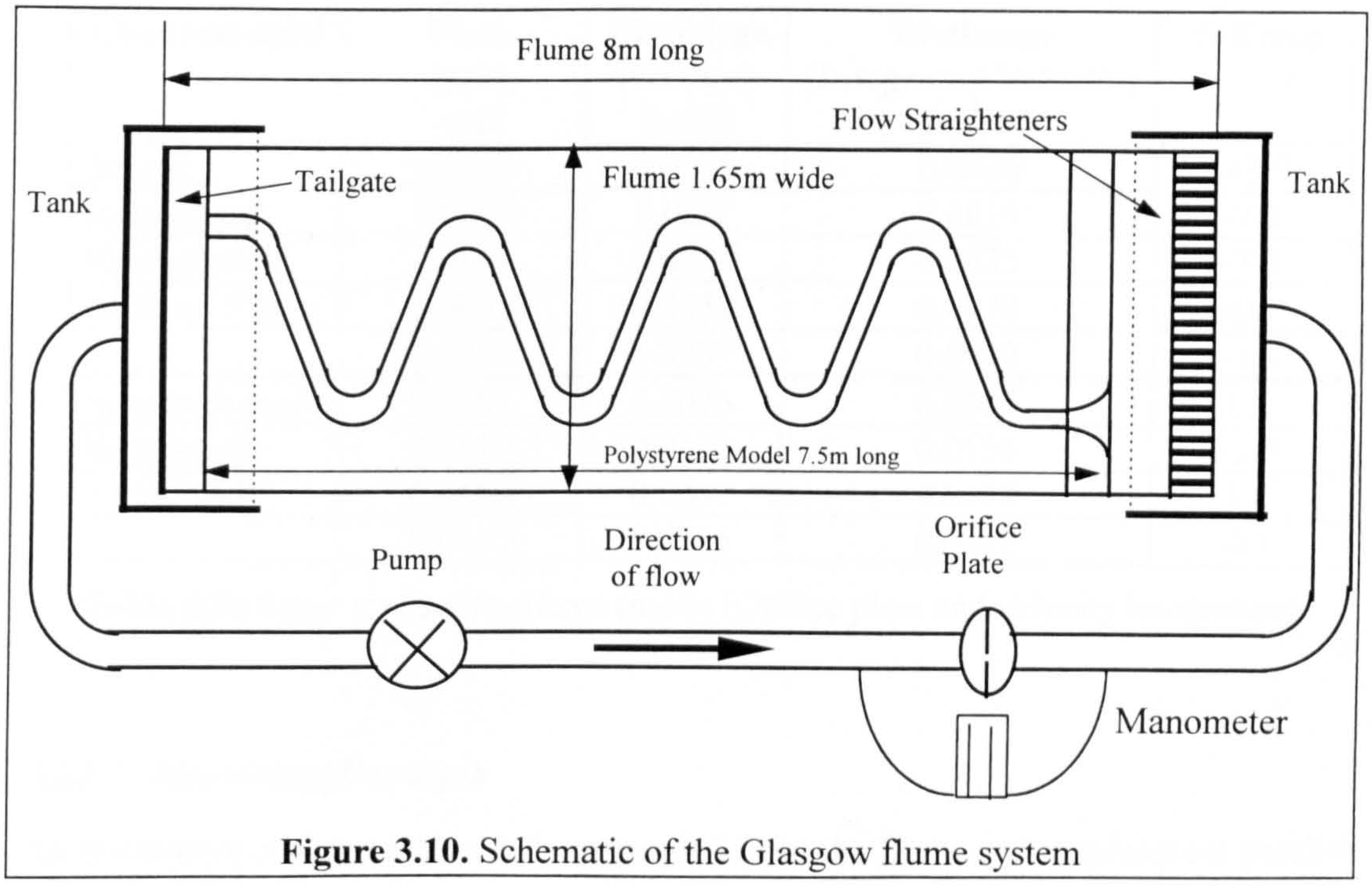

Figure 3.10. Schematic of the Glasgow flume system

The results are compared with the British standard, BS1042 for orifice plates as shown in Figure 3.11. Table 3.10 shows the comparisons for 10 depths of flow. The larger discharges were checked in the 1.65m wide rectangular flume.

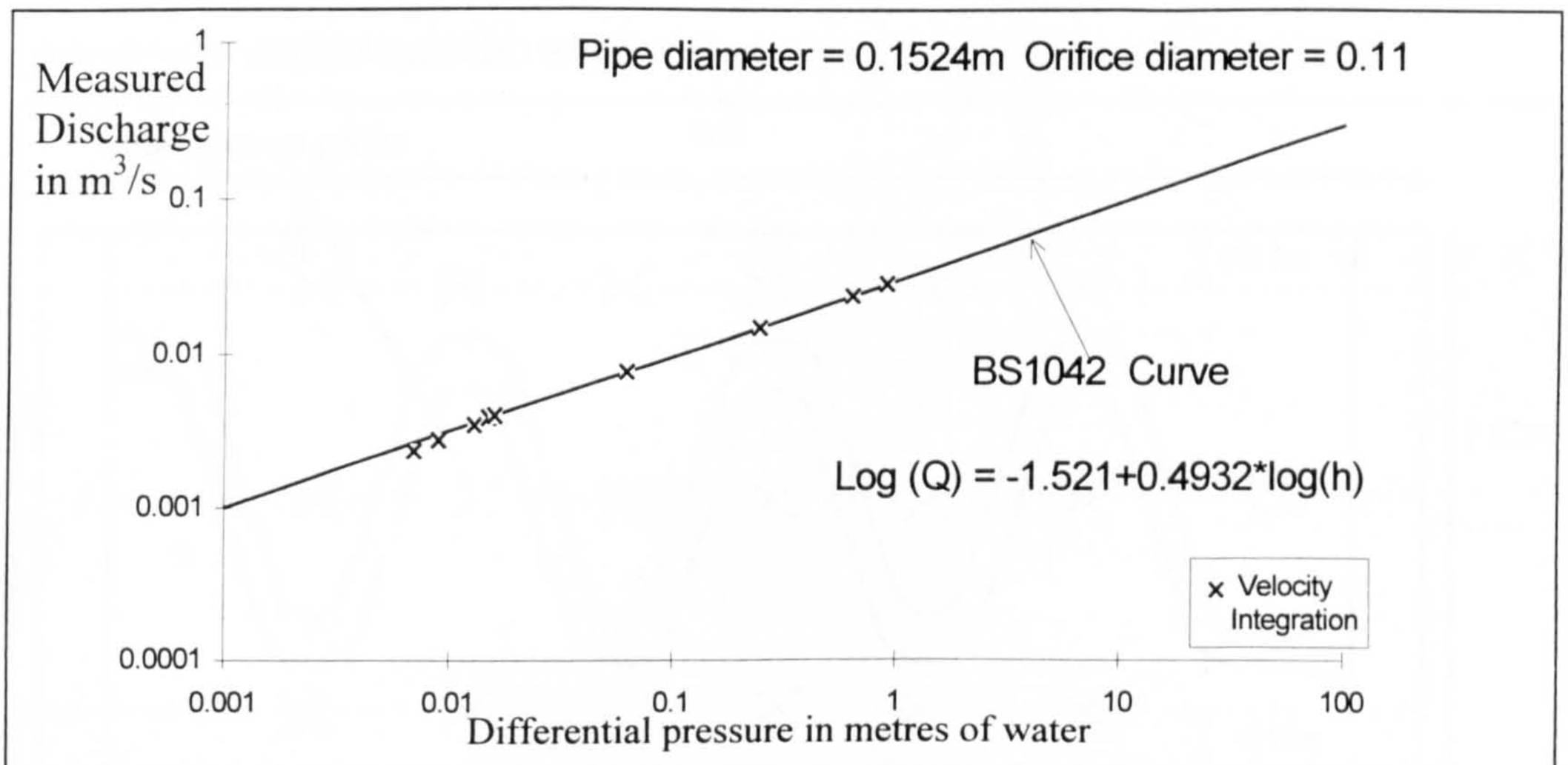

Figure 3.11 The Orifice meter:- Head versus Discharge calibration chart

The lower discharges were checked by running the water inbank in the meandering channel model. An accuracy of at least ±4% was achieved for all discharges greater than 3 l/s. The orifice meter predictions were not reliable for discharges less than 2 l/s.

Channels used	Flow depth (m)	Discharge (Orifice) (m^3/s)	Discharge (Integrated Velocity) (m^3/s)	% Error
Inbank	0.0529	0.0023	0.0026	-11.9
meandering	0.0570	0.0027	0.0029	-7.1
Rect. channel	0.0655	0.0034	0.0035	-3.8
200mm*75mm	0.0690	0.0038	0.0038	-0.1
	0.0715	0.0039	0.0040	-1.9
Simple channel	0.0201	0.0076	0.0076	0.2
Rectangular	0.0310	0.0150	0.0156	-3.7
1.65m wide	0.0400	0.0240	0.0237	1.6
	0.0455	0.0286	0.0292	-2.0

Table 3.10 Stage versus Discharge (m3/s) (Orifice plate and velocity integration)

3.2.7.2 Measuring flow depth

An instrument carriage ran on rails suspended from the flume and carefully set parallel to the slope of the flood plains. The water levels and bed levels were measured using a pointer gauge mounted from this carriage. The pointer gauge could be read accurately to the nearest +/- 0.1mm. Bed and water level measurements were taken along three parallel lines at 18 grid points as shown in Figure 3.12. Measurements taken at these points were used to establish when uniform flow conditions had been achieved.

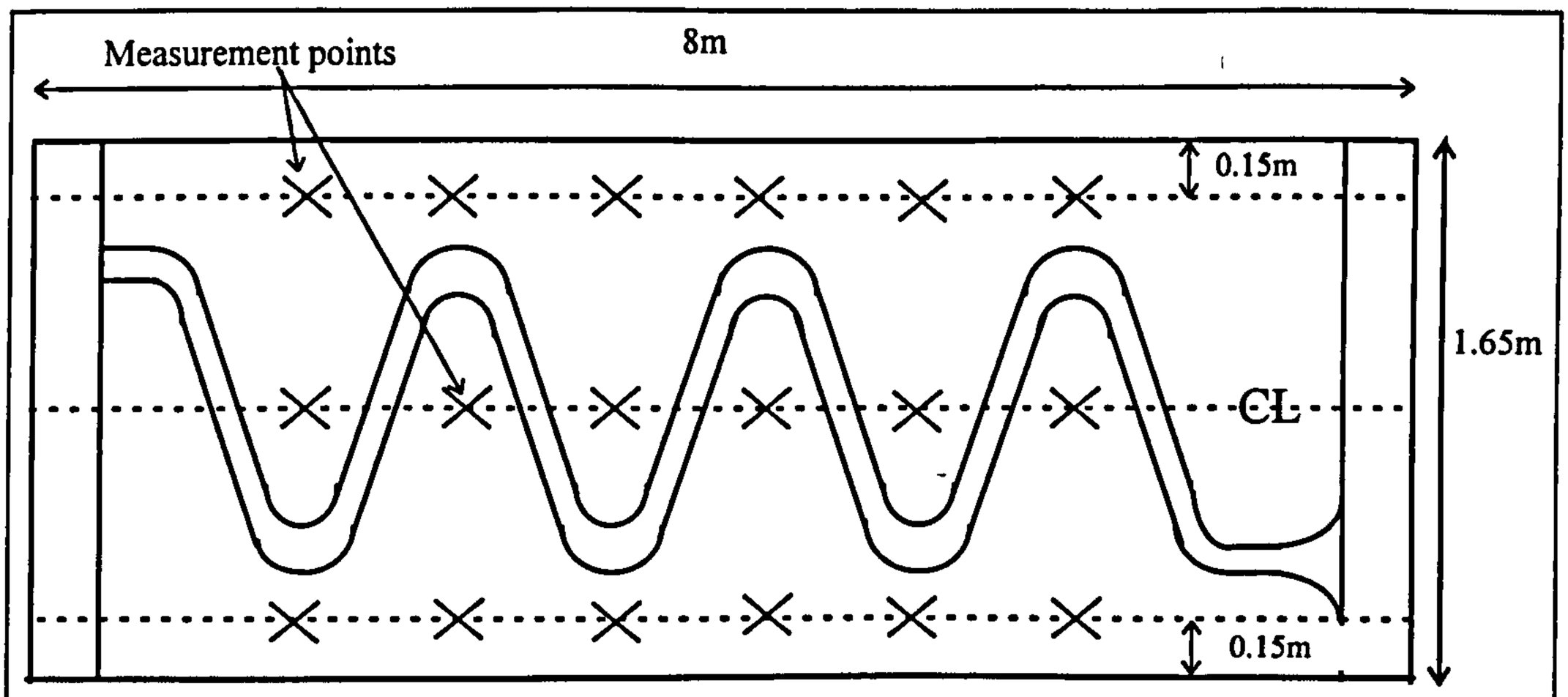

Figure 3.12. Flow depth measurement points

3.2.7.3 Setting uniform flow in the Series B extension flumes

The Series B extension experimental programme was founded on the principle of assessing the hydraulic performance of the meandering compound channel models when

steady uniform flow conditions had been established. It is only feasible to determine 'quasi-uniform flow' in a model of a meandering compound channel. There were considerable local variations in water level. To accurately establish when uniform flow depth had been achieved the water surface slope was measured along the three parallel lines in the flume, one down the centre line and two down lines on opposite sides of the flume in Zone 3, as seen in Figure 3.12. The flow down the centre line was different in character to the flow in Zone 3. Down the centre line it was very turbulent with variable depth. In Zone 3 the flow was much less turbulent with only small variations in depth. Uniform flow was identified when the average of the water surface slopes down all three lines is equal to the flood plain slope. The depth of flow was then measured across the flume and an average of these flow depths was assumed to correspond to the uniform flow depth.

A graphical technique was used to identify which tailgate setting will give uniform flow for a known discharge. This technique is as follows:-

1. First set the discharge rate and measure it.
2. Record the elevation of the tailgate position.
3. Measure the water surface levels.
4. Calculate the best fit average water surface slope.
5. Chose another tailgate setting and calculate the new surface slope. These first two water surface measurement position should be located within the M2 backwater curve, as shown in Figure 3.13, where the tail gate is set slightly low.
6. Set two more tailgate settings in the M1 backwater curve with the tailgate slightly high.

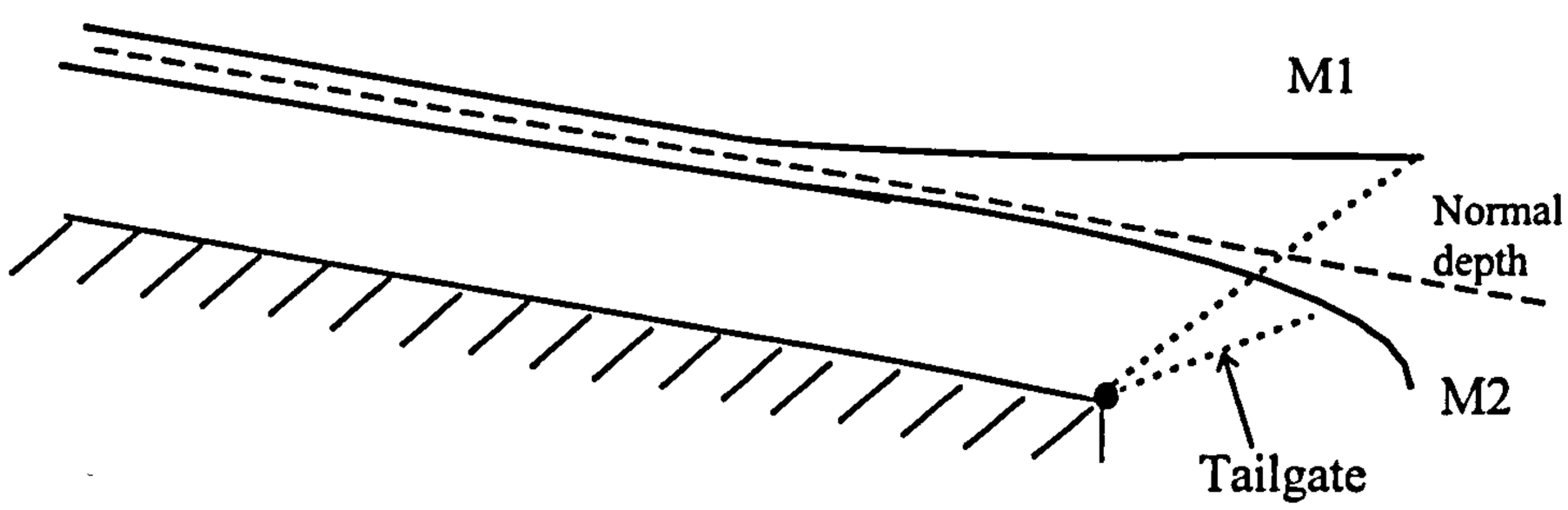

Figure 3.13. Tailgate settings to produce M1 and M2 backwater curves

7. Once the water surface slopes for these have also been calculated, the magnitude of water surface slope should be plotted against tailgate height and water depth as shown in Figure 3.14.
8. The tailgate height required to achieve a uniform flow depth for the particular discharge rate can be interpolated from the graph in Figure 3.14 and coincides with depth at which the water surface slope equals the flood plain slope.
9. Finally set the tailgate height at the interpolated value and check that this does in fact result in uniform flow conditions being established.

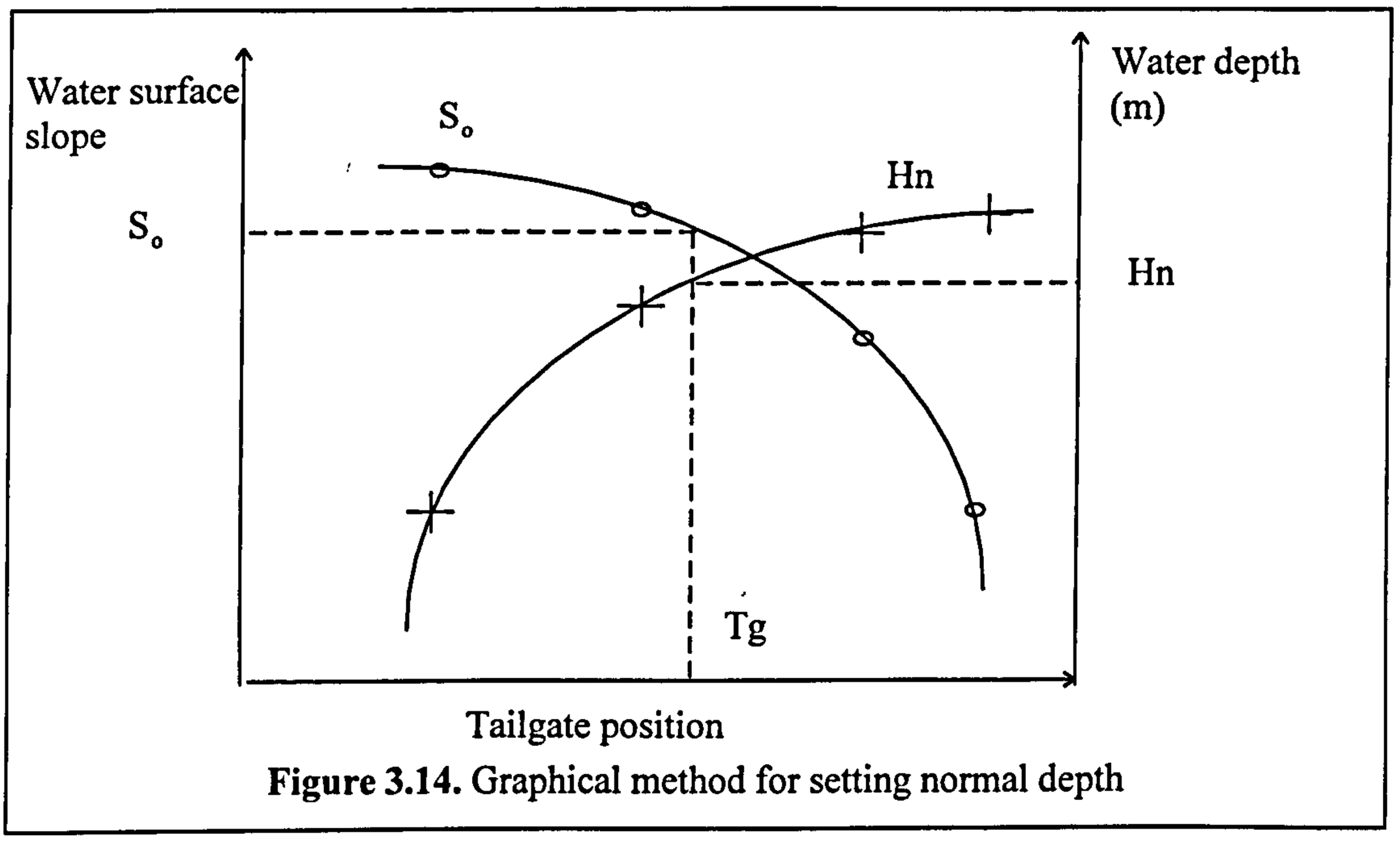

Figure 3.14. Graphical method for setting normal depth

3.2.7.4 The Stage versus Discharge (Rating) curve

A unique rating curve for each model geometry tested was obtained from two experimental runs. The first run produced a rating curve obtained by increasing discharges and flow depths. The second run produced a rating curve obtained by decreasing discharge and flow depths. For all the tests two compatible runs had to be produced before the rating curve was accepted.

Between 2 and 5 inbank stage and discharge measurements were taken for every model geometry. Although similar techniques were adopted for finding the normal depth in many cases the discharge had to be calculated using velocity integration methods because the Orifice plate predictions were unreliable at lower discharges.

3.2.7.5 Water temperature measurement

Before the stage and discharge experiments commenced, the water in the feeder tanks were left for up to 3 to 4 days. The flume was left running for at least 16 - 20 hours during that period to allow the water to warm to room temperature. The temperature of the water was measured using a mercury thermometer in the downstream tank. This procedure maintained the flume water a fairly constant temperature of 26°C. Subsequently the water temperature would only fluctuate by +/- 2 °C during the experiments. It was very important to stabilise the water temperature in all the experiments because large variations in water temperature could cause significant variations in the absolute viscosity of the water and therefore bias the test results.

3.2.8 Local velocity measurement techniques

3.2.8.1 Introduction

Figure 3.15 shows the instrument carriage which was used to support and position the flow measurement devices over the flume.

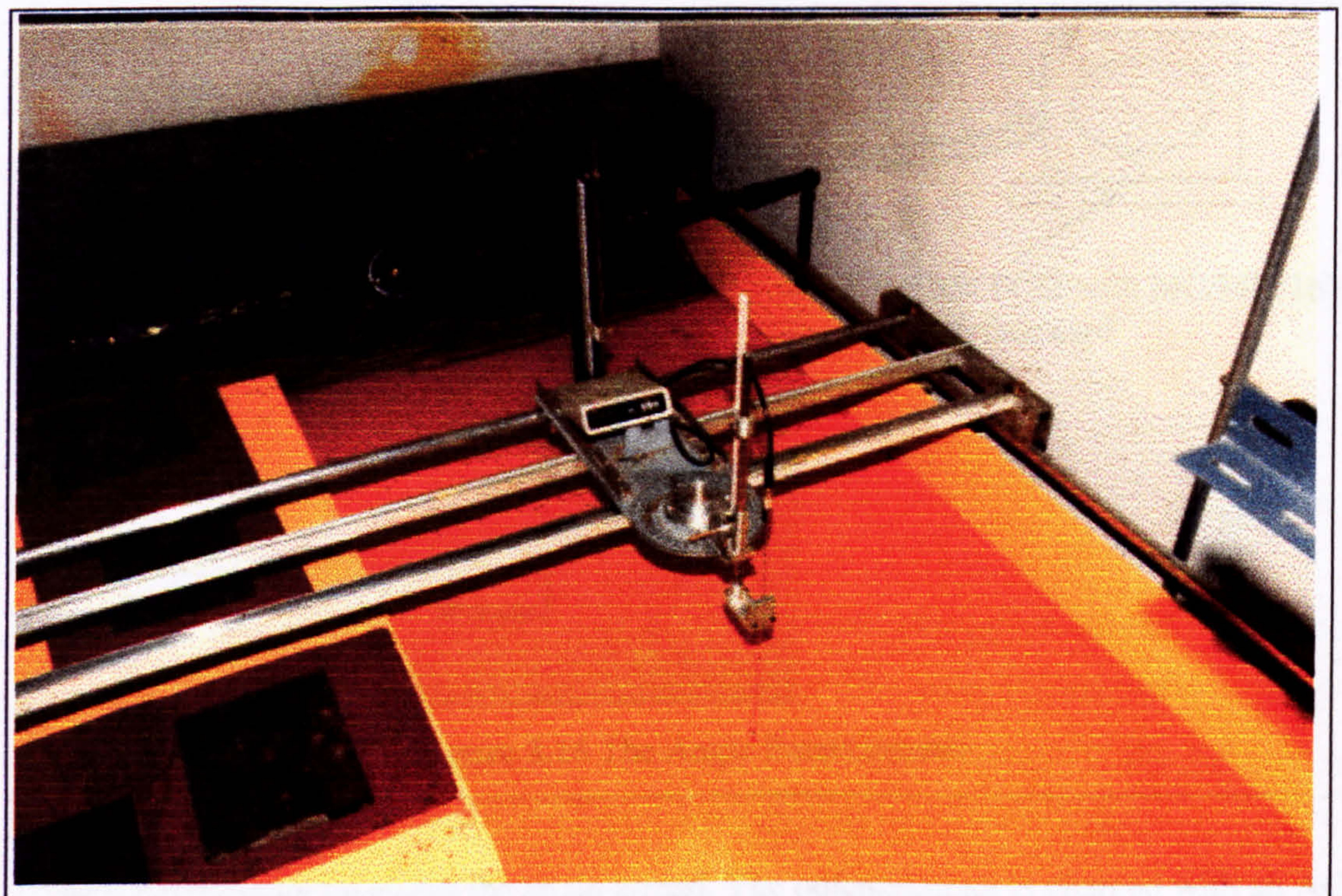

Figure 3.15 The instrument carriage

A combination of mini-propeller meters, pitot tubes and angle potentiometers were used to measure local flow velocity at two different cross-sections for all the Series B extension model geometries which were tested. Some flow visualisation tests were also performed using time-lapse photography and different coloured dye traces at the same locations to help divulge the nature of the interaction mechanisms.

3.2.8.2 The Angle Potentiometer

Pitot tubes and mini-propeller meters were used to measure flow velocity in these experiments. However these instruments exhibited significant errors if they were mis-aligned to the main streamline component of flow. Angles greater than 10° between streamline and instrument can induce gross error. Therefore in the Series B extension programme angle potentiometers were used to measure the angle of incidence of the main component of flow first, prior to any velocity measurement.

Figure 3.16 shows the angle potentiometer, spindle and the vane. The vane on the end of a long thin spindle is placed in the flow and aligns with the main component of velocity.

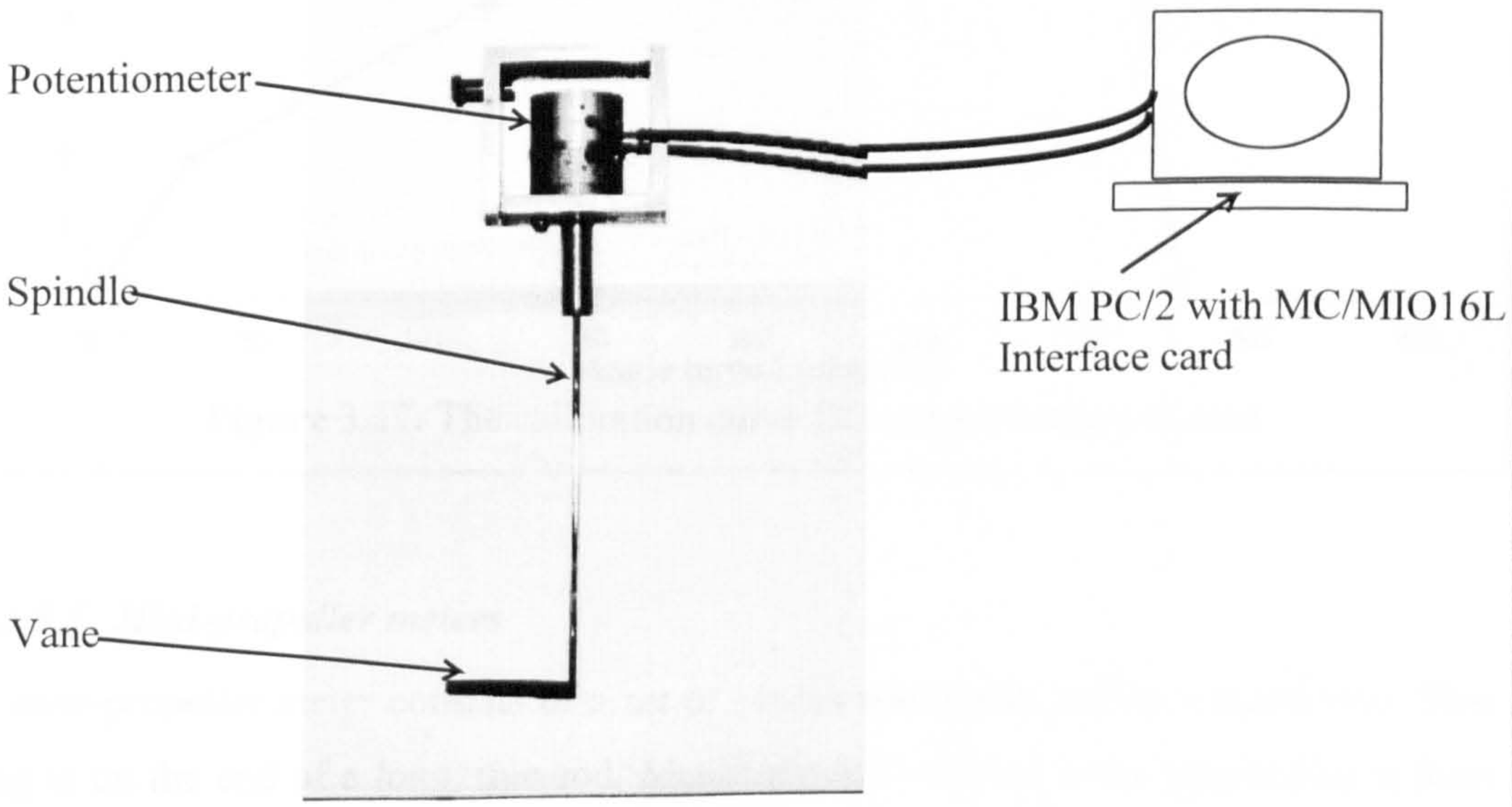

Figure 3.16 The Angle Potentiometer

The potentiometer measures the angle turned. The potentiometer is charged with an AC voltage. This induces a DC voltage response which shows linear behaviour (between 0 and 10 volts) over an angle of 300° turned by the vane. The potentiometer was

suspended from the instrument carriage. An IBM personal computer, version PS/2, with a Hewlett Packard MC/MIO16L analogue interface card was used to log the DC voltage data. The Labtech Notebook; version 6, software package with an Iconview graphical interface was used to process the data. A sample rate of 5Hz was used for 20 seconds to obtain an appropriate DC voltage average.

The potentiometer was calibrated manually against known angles measured with a protractor over a suitable operating range. The calibration relationship that was derived is shown in Figure 3.17. During operation the potentiometer was initially aligned with the vane parallel to the centre line of the flume. The potentiometer was set to give a DC output mid-way in its operating range. This procedure ensured that the potentiometer remained in the linear response range for all angles encountered.

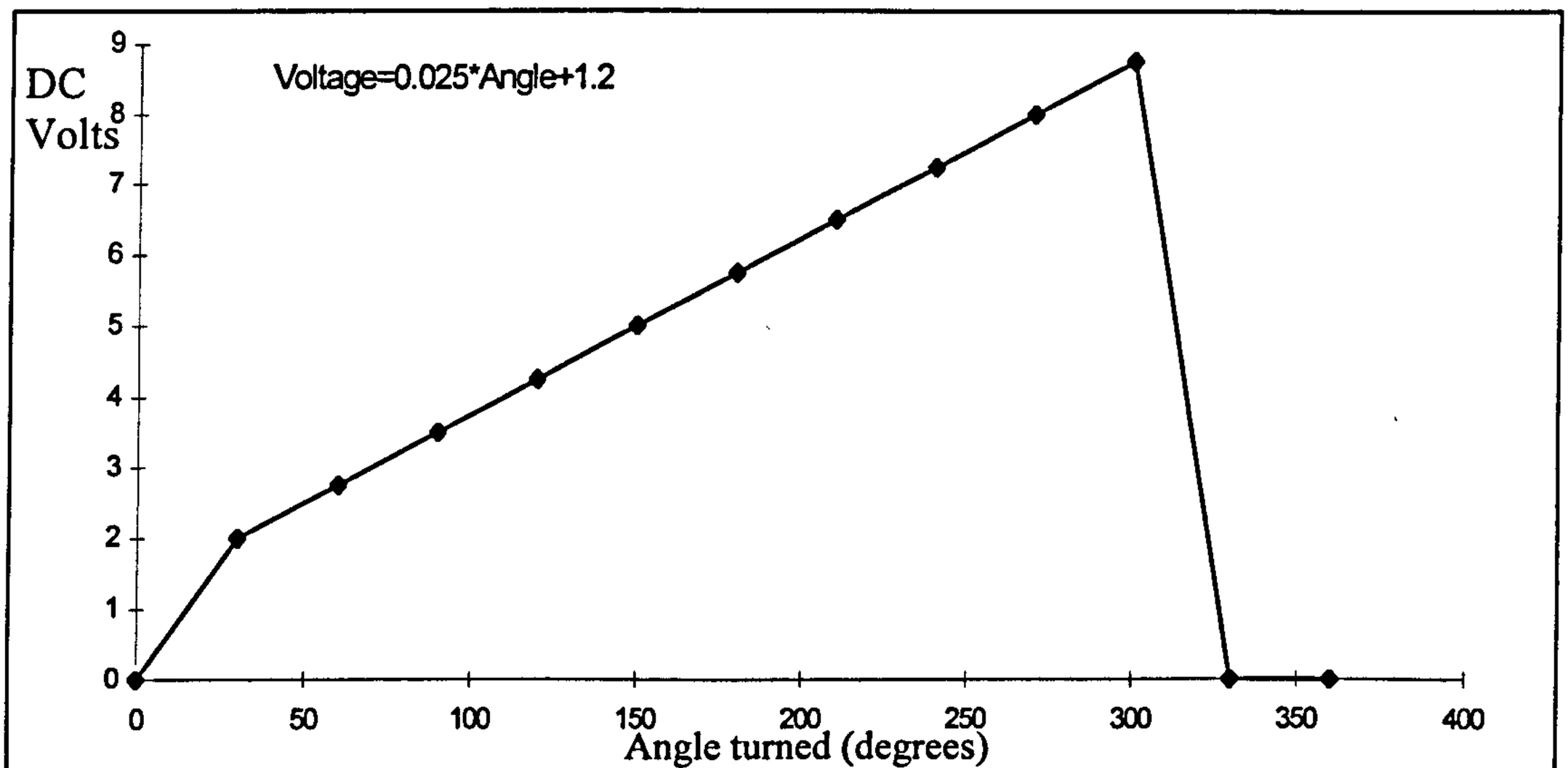

Figure 3.17. The calibration curve DC output to angle turned

3.2.8.3 Mini-propeller meters

A mini-propeller meter consists of a set of blades which turn inside a metal ring. This ring is on the end of a long, thin rod. Measurements were taken by suspending it from the instrument carriage and aligning the blades' longitudinal axis with the maximum component of velocity through the relevant measurement, see Figure 3.18.

The propeller meter rotates and yields a reading measured in Hertz. It is calibrated to relate the reading in Hertz to the value of local flow velocity. The mini-propeller No.

1372 was used throughout the Glasgow tests. The calibration chart is presented in Figure 3.19. This mini-propeller had to be regularly checked to ensure accuracy of the calibration was maintained.

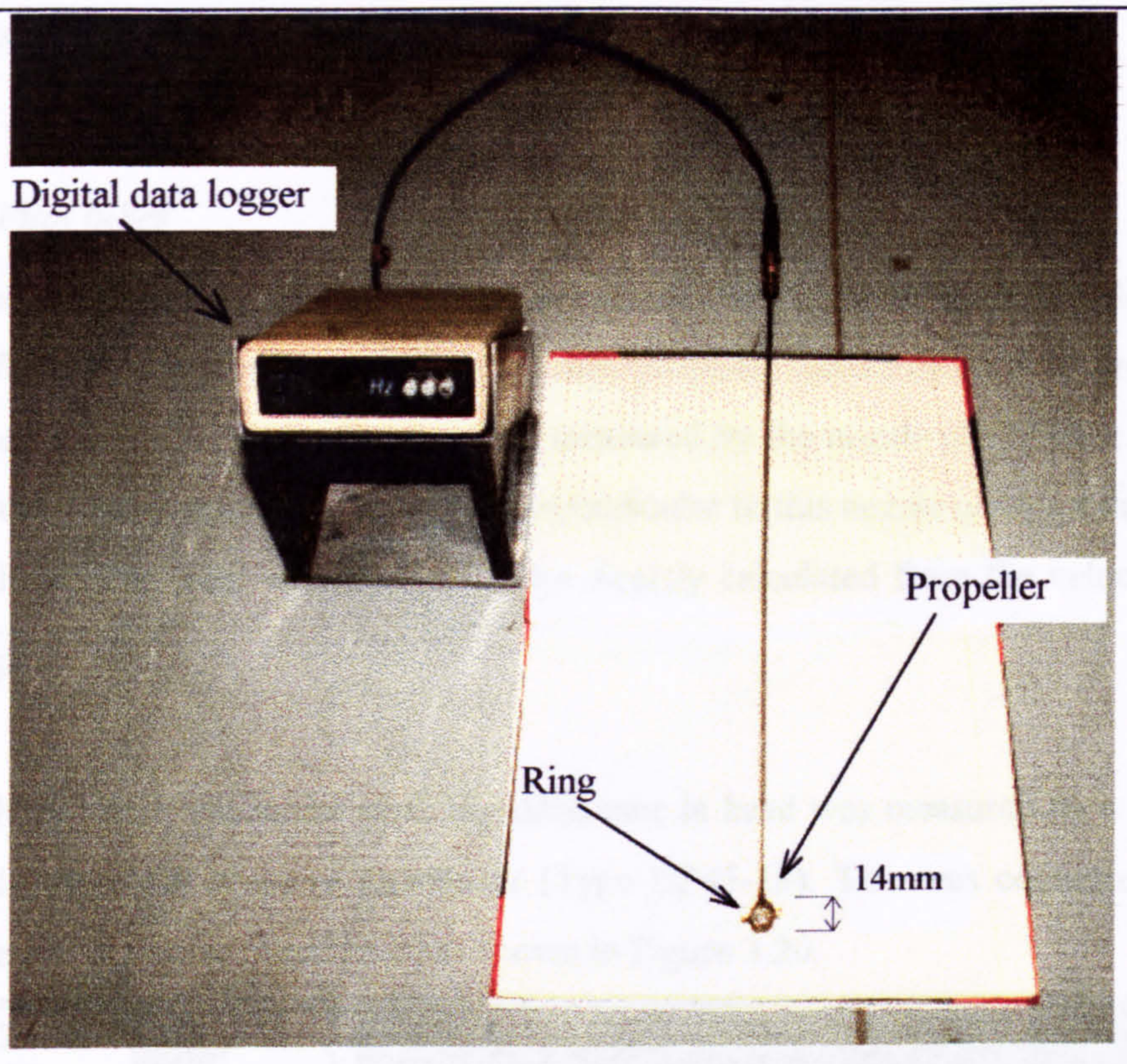

Figure 3.18. The Mini-propeller meter

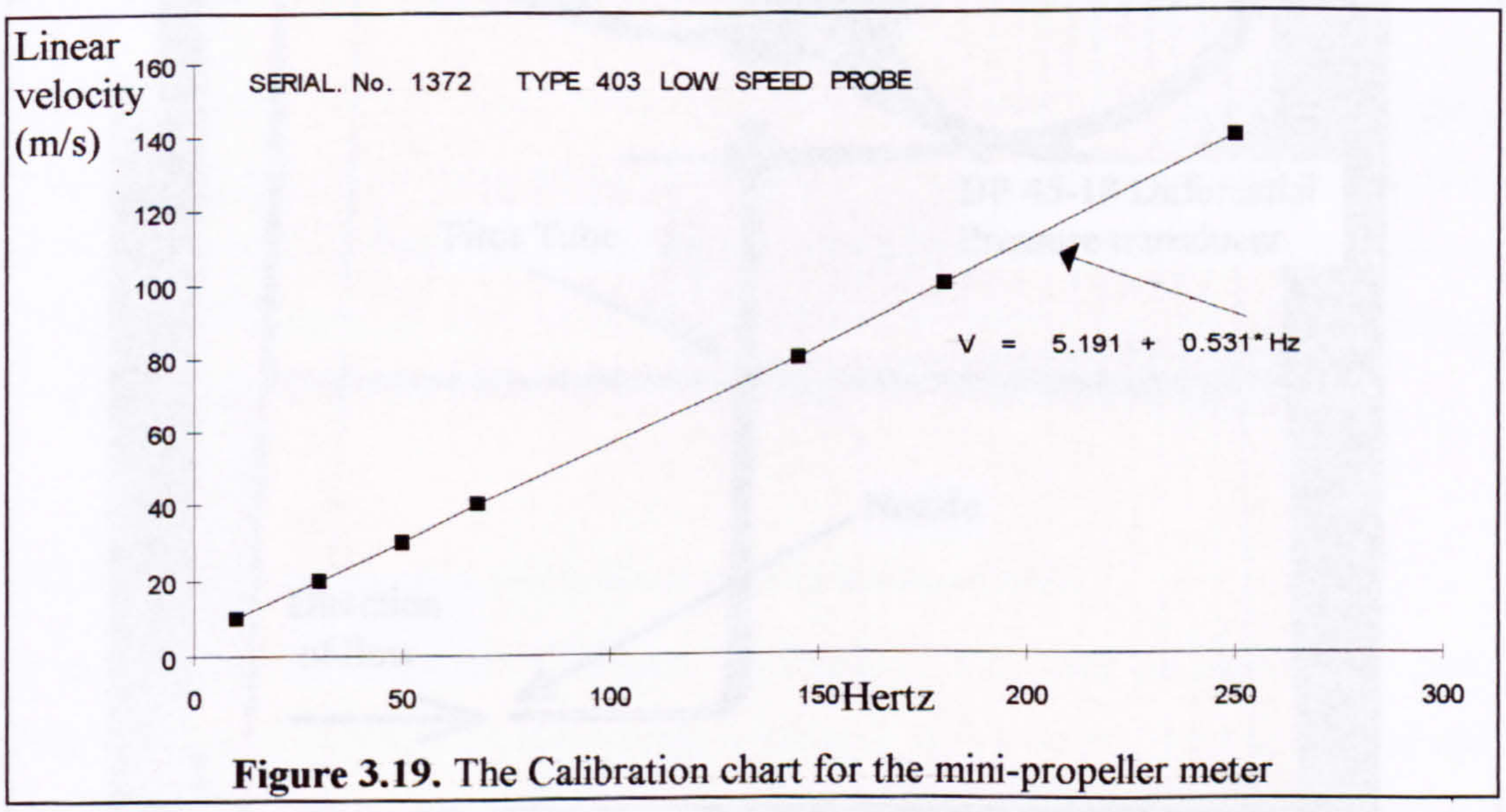

Figure 3.19. The Calibration chart for the mini-propeller meter

The whole of the ring, which is 14mm in diameter must be immersed in water for the mini-propeller meter to function accurately,. This creates the correct form of magnetic field. The mini-propeller meter was not used for any flow which was less than 14mm deep throughout the Glasgow tests.

3.2.8.4 Pitot tubes

Pitot tubes with 4mm heads were used to measure low magnitude flow velocities in shallow flow, in flow conditions where the mini-propeller meters could not operate. The difference between the stagnation pressure measured by the nozzle of the pitot tube and the pressure head measured by the holes perpendicular to this nozzle gives a value for the velocity head. The local velocity, U, can be directly calculated from the velocity head, $U = \sqrt{2gh}$.

During the Series B extension work the difference in head was measured by a Validyne low head differential pressure transducer (Type DP45-18). This was connected to the pitot tube by two water filled tubes, as shown in Figure 3.20.

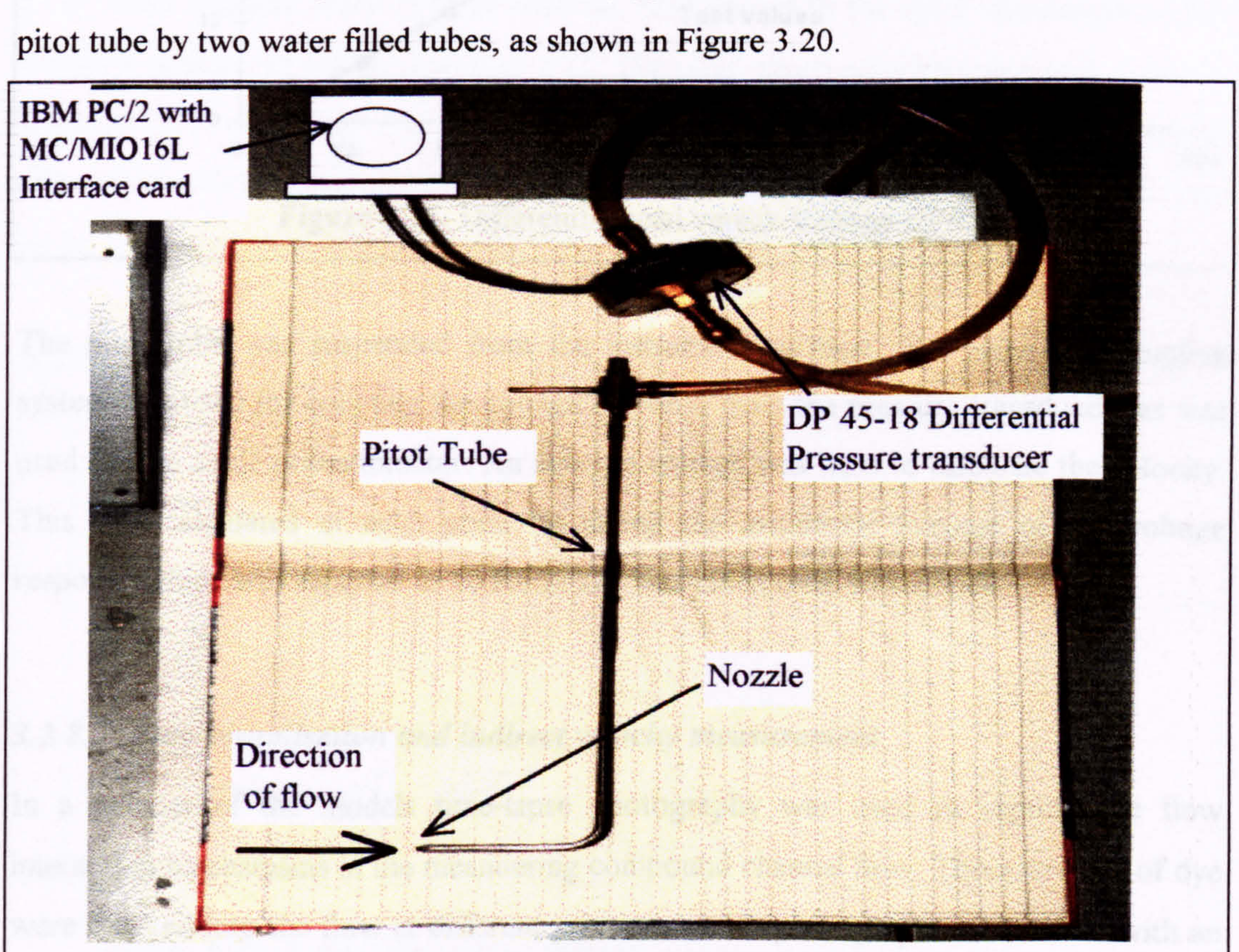

Figure 3.20 The pitot tube and pressure transducer

The transducer's operating range was between 0mm and 54mm which is equal to velocities of between 0 m/s and 1 m/s. However, the pitot tube characteristics were only reliable for velocities greater than 0.15 m/s.

The transducers were calibrated for their differential head to voltage relationship using a variable head manometer built in the Glasgow Laboratories. The calibration results for the pressure transducer DP 45-18 which was used is shown in Figure 3.21.

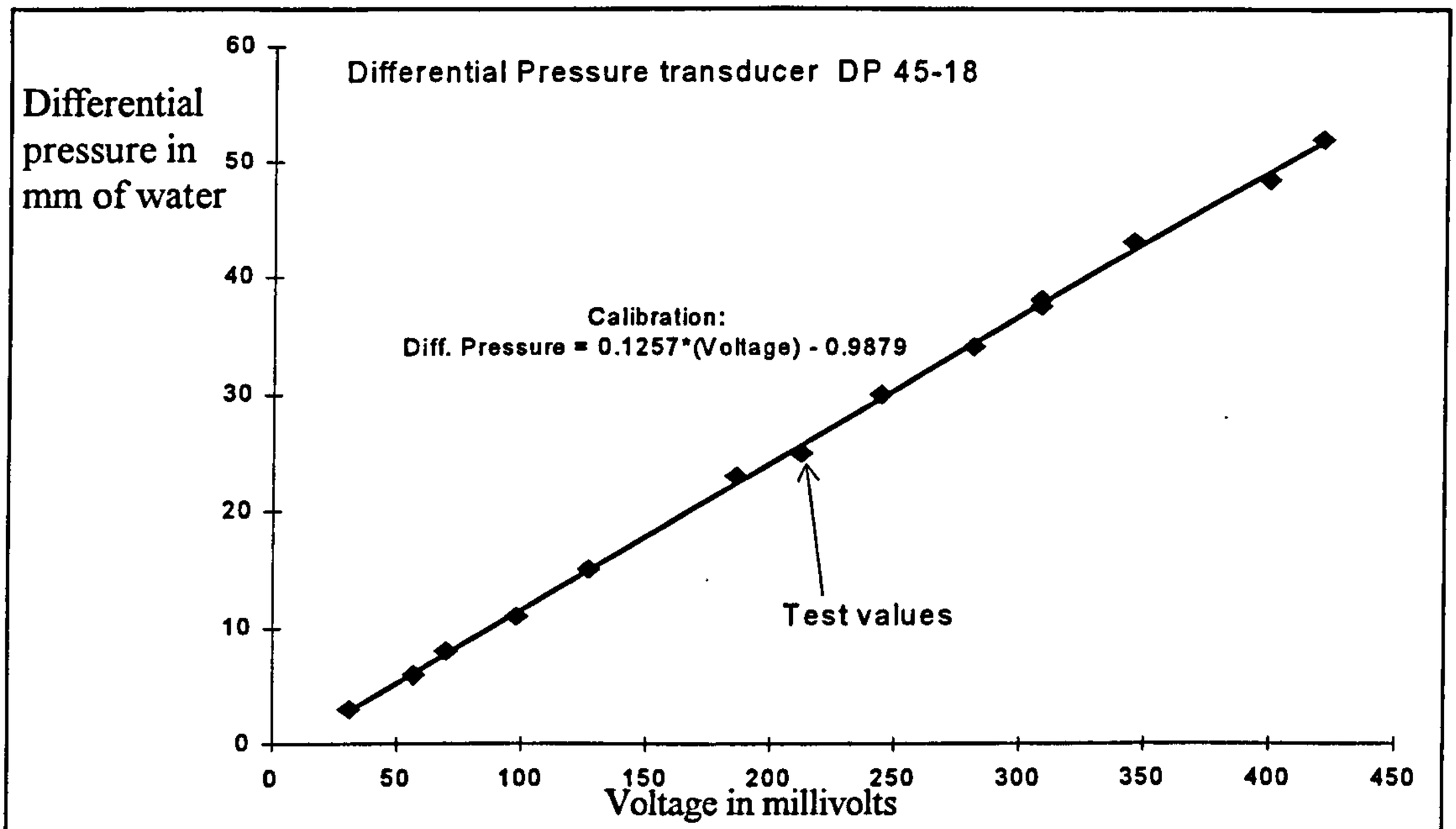

Figure 3.21. Differential head versus Voltage DP45-18

The pitot tube was suspended from the instrument carriage. The same data logging system was used for collating the voltage response from the pressure transducers as was used for the angle potentiometer. An average voltage was used to calculate the velocity. This was calculated at each point by taking the arithmetic average of the voltage response which was sampled at 10 Hertz and was taken over 30 seconds.

3.2.8.5 Flow visualisation and indirect velocity measurement

In a number of the models time-lapse photography was used to capture the flow interaction mechanisms in the meandering compound channel flow. Three streams of dye were injected into the flow at different positions and 3 photographs were taken with an interval of 3 seconds between them.

Time-lapse photography was also used to check the velocity of flood plain flow for depths less than 14mm. A slug of dye was placed manually in the water across the flood plain. Two photographs were taken separated by a 3 second interval. The average distance travelled by the dye front in that time was measured by comparing its relative positions in the two photographs using the ruler which was suspended within view. The average velocity was calculated by dividing the distance travelled by the time taken. An amount was subtracted to allow for the molecular diffusion of the dye.

3.2.9 Flow measurement positions

3.2.9.1 Introduction

Local flow measurements were taken at two sections down the flume. One section was perpendicular to the centre line of the flume and positioned at the Apex. In the other section, the Cross-over section, the flood plain sections were perpendicular to the centre line of the flume. However over the main channel the sections were taken perpendicular to the main channel. Both of these sections were placed in the third wavelength of the Glasgow models, as shown in Figure 3.22. The other group members also took velocity measurements at similar Apex and Cross-over sections but they were positioned at different wavelengths down the flume. They did however take readings at similar flow depths and measurement grid resolutions.

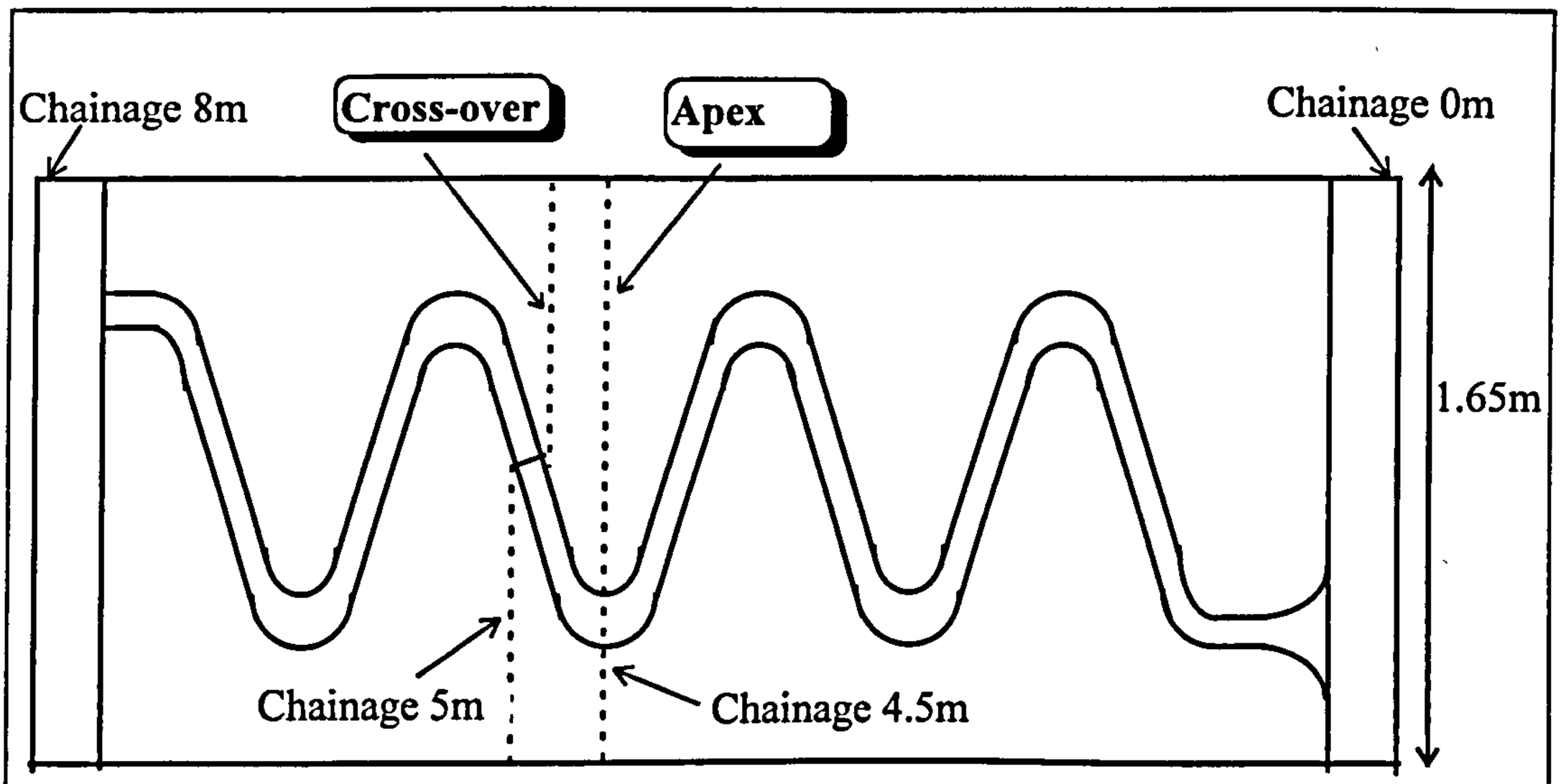

Figure 3.22. A plan view of the velocity measurement sections (Glasgow)

3.2.9.2 Point velocity measurements: Flood plains

The number of point velocity measurements taken corresponded to the complexity of flow mechanisms in that area and the suitability of the instrumentation. Enough measurements were taken to enable accurate values of zonal discharge to be calculated as well as to enable clarification of the form and magnitude of the local flow patterns. The flow velocities on the flood plains were measured at the same lateral offset positions across the flume for every model tested. The number of measurements taken vertically on the flood plain depended on the depth of flow. For flow depths less than 20mm only one velocity measurement was taken. This velocity may be measured directly using either a pitot tube or a mini-propeller meter, or indirectly using time-lapse photography and dye traces.

For flow depths greater than 20mm but less than 30mm, two velocity measurements were taken and velocity is measured using a mini-propeller meter with one reading at the bed and one at the water surface. For flow depths greater than 30mm then a maximum of 3 velocity measurements were taken. Velocity was measured using a mini-propeller meter with one reading at the bed and one at the water surface and one half-way. Figures 3.23a and 3.23b show the offset and depth measurement positions at the apex and cross-over respectively.

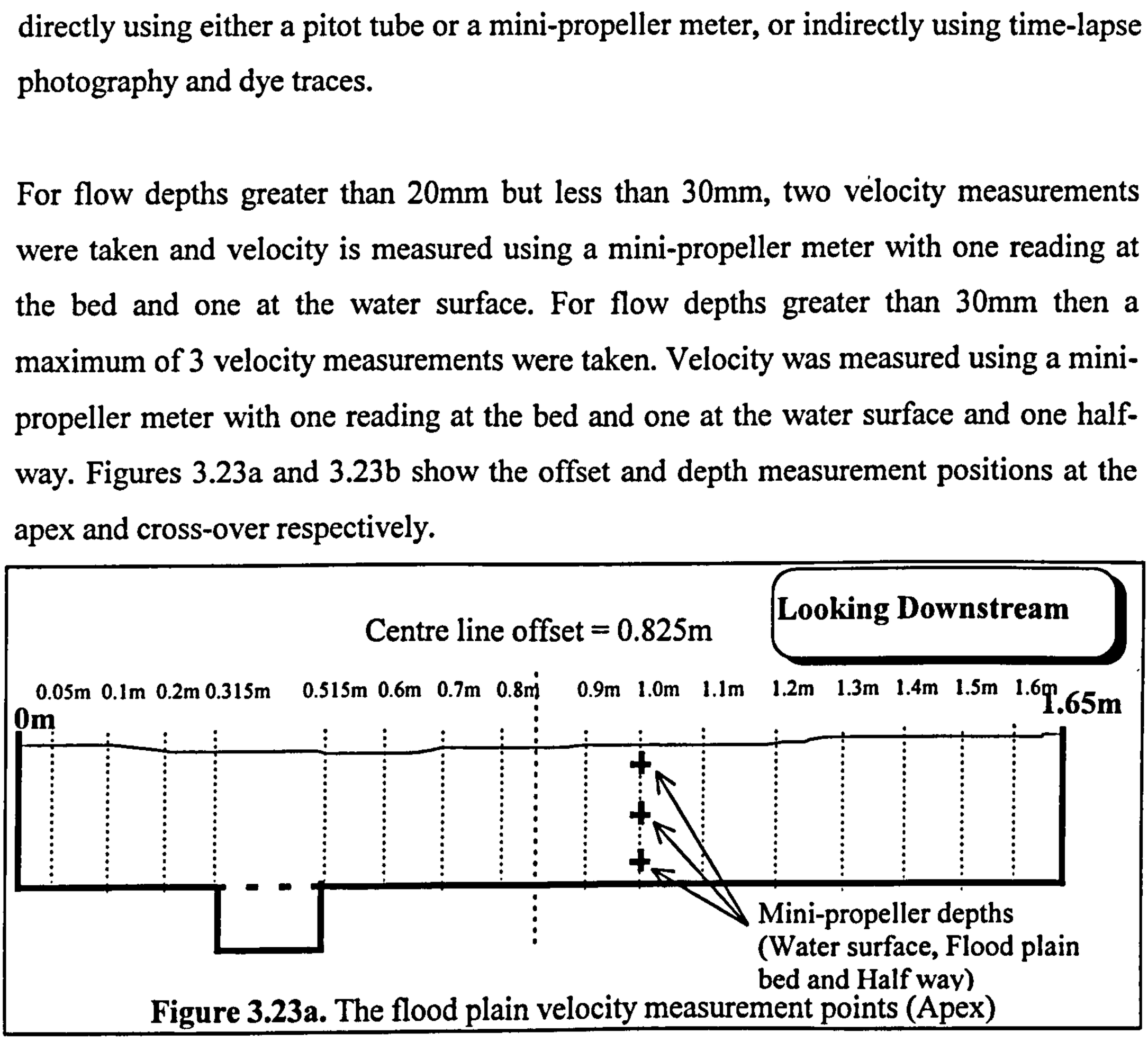

Figure 3.23a. The flood plain velocity measurement points (Apex)

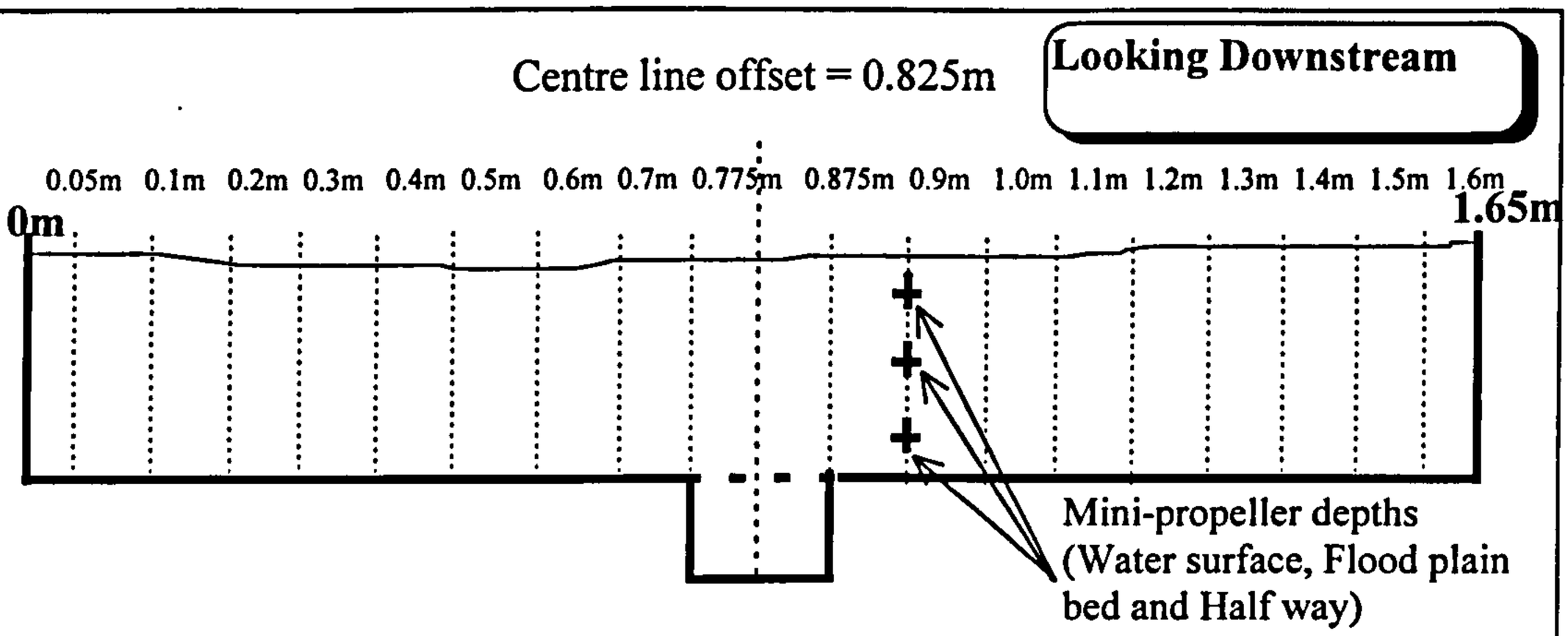

Figure 3.23b. The flood plain velocity measurement points (Cross-over)

3.2.9.3 Point velocity measurements: Main channel

Figure 3.24 shows the measurement point grid for a 50mm deep rectangular channel with 50mm flood plain flow depth.

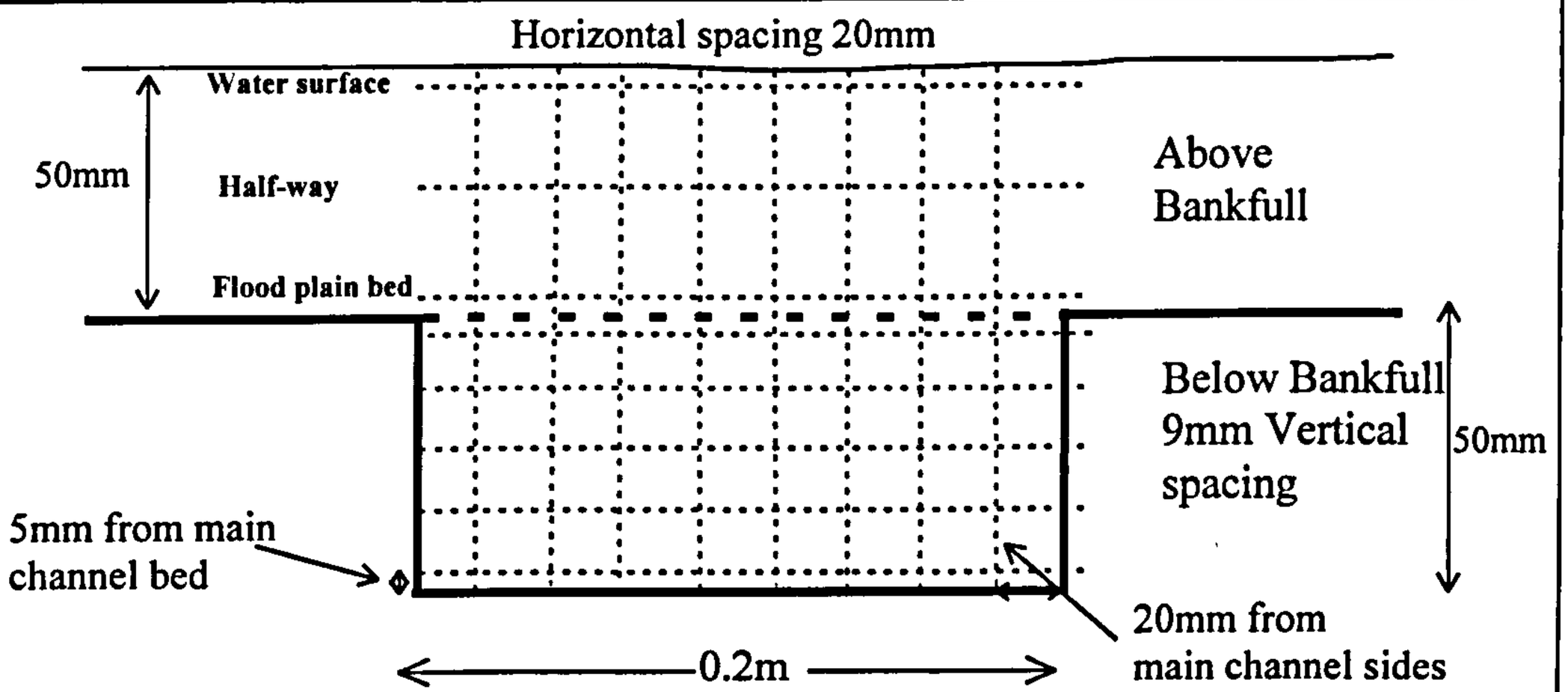

Figure 3.24 Measurement grid for 50mm deep main channel and flood plain

The vertical spacing of the flow measurements above bank full depth coincide with those taken on the rest of the flood plain. In the main channel velocity readings were taken every 20mm across the channel and, every 8mm vertically for 25mm deep channels, 10mm vertically for 50mm deep channels and 13mm vertically for 75mm deep channels.

3.2.10 Zonal velocities and flood plain flow depths

Table 3.11 lists the depths of flood plain flow for each of the models tested in Glasgow for which zonal velocity readings were taken.

Test	Reference		8mm	12mm	16.7m	25m	33.3-37.5mm	50m	75m
1	G75T90S		x			x		x	
2	G75T90R		x			x	x	x	
3	GR75T90R		x		x	x	x	x	
4	G75T60R		x			x	x	x	
5	G75T45R		x			x	x	x	x
6	G75T45RN		x			x		x	
7	G75T37R		x		x	x	x	x	
8	G50T90R		x		x	x	x		
9	G50T60RA		x		x	x		x	
10	G50T60R		x		x	x	x	x	
11	G50T45R		x		x	x	x	x	
12	GDA50T37R		x		x	x	x	x	
13	G50T37R		x		x	x	x	x	
14	G50T30R		x		x	x	x	x	
15	G50N90R		x		x	x	x	x	
16	G50N60R		x			x	x	x	
17	G50N45R		x		x	x	x	x	x
18	G50N37R		x		x	x	x	x	
19	G25T90R		x		x	x	x	x	
20	G25T60R		x		x	x	x	x	
21	G25T45R		x		x	x		x	
22	G25T45S		x		x	x		x	
23	G25T45SN		x		x	x		x	
24	G25T45RN		x		x	x		x	
25	G25T30R		x		x	x		x	
26	G25N90R		x	x	x	x	x		
27	G25N60R		x		x	x	x	x	
28	G25N45R		x		x	x	x		
29	G25N30R		x	x	x	x	x		
30	G10N60R		No readings taken						

Table 3.11 The Flow depths at which zonal velocity data is obtained

3.2.10.1 Main channel Flow visualisation

Flow visualisation records were obtained for two flood plain flow depths: 8mm and 50mm. Three dye traces were injected in the corners and down the centre line of the main channels at both the Apex and the cross-over, see Figure 3.25. Photographs were taken when the dye was injected at three depths in the main channel; the channel bed, the water surface and the bankfull depth. The G50T90R channel is used to illustrate these positions with 50mm flood plain flow, as shown in Figure 3.26.

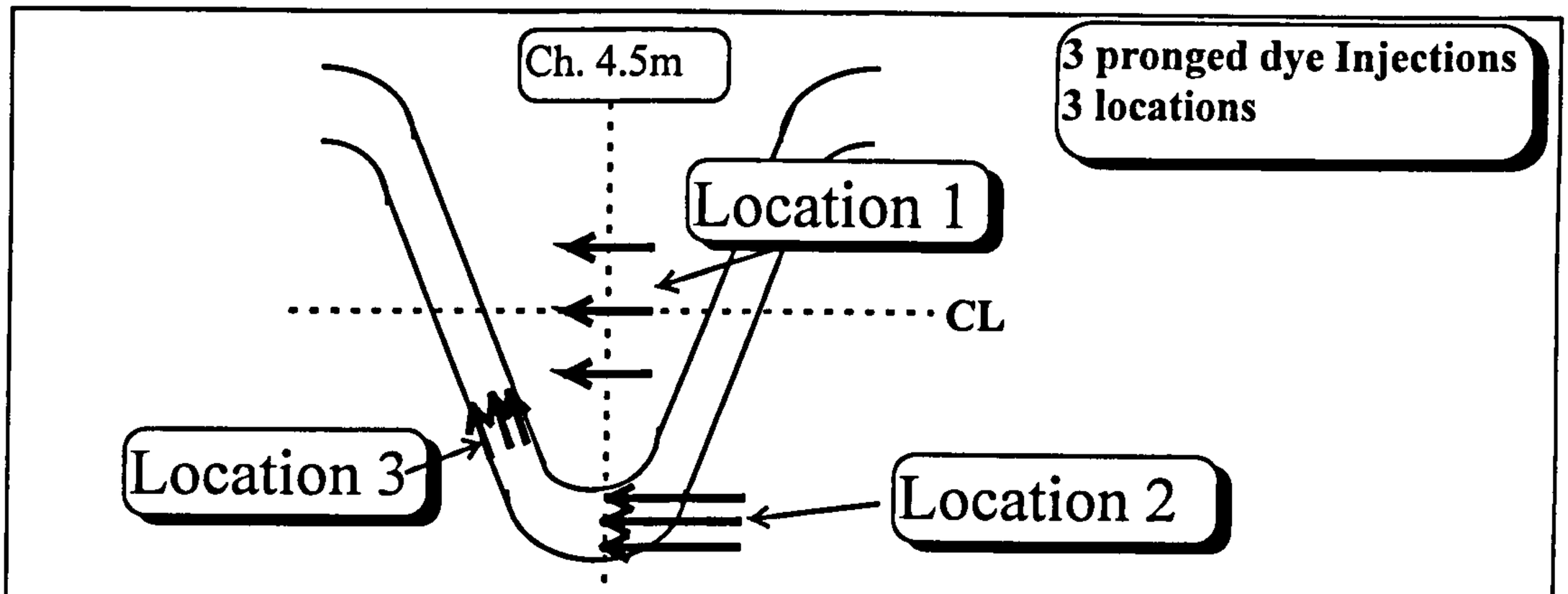

Figures 3.25 Dye injection locations (Plan view)

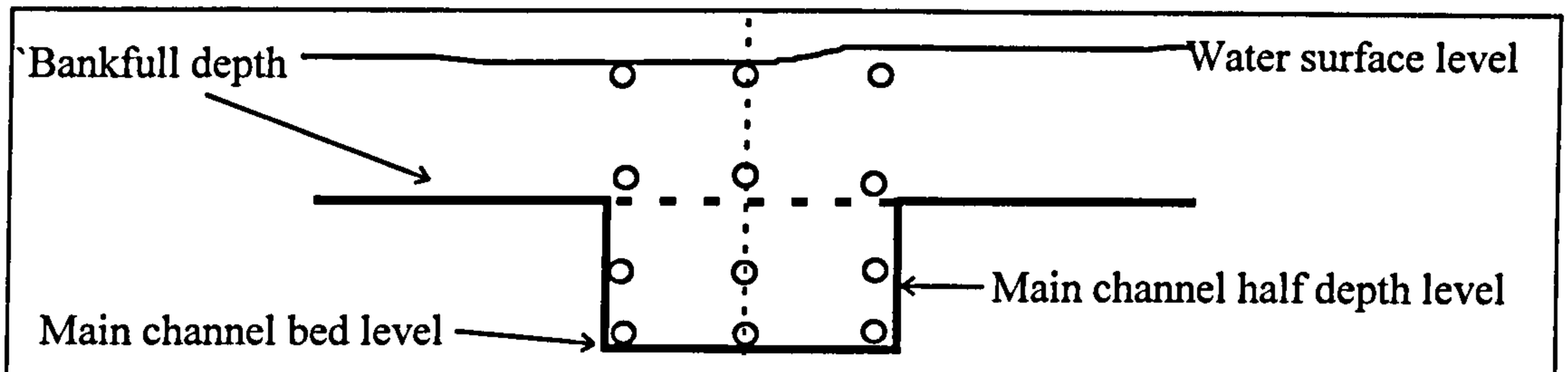

Figures 3.26 Dye injection locations (Cross - Section)

3.3 Investigating flow over a slot in a channel bed

3.3.1 Introduction

A series of experiments were performed by the author in Glasgow as part of the Series B extension programme in order to investigate the flow mechanisms generating head loss in flow over a slot or trench in the flood plain channel bed. The flood plain flow typically expands and contracts as it passes over a lower slot channel which generates head loss. A number of authors had suggested that the flood plain flow in a meandering compound channel as it passes over the main channel experiences an interaction mechanism and consequently head loss magnitude which is very similar to the expansion and contraction mechanism in flow over a simple slot.

The author attempted to relate the magnitude of head loss generated by the main channel and flood plain interaction in a meandering compound channel to its configuration. The effect of five parameters on flow over simple slots was investigated. These parameters were: relative flow depth, aspect ratio, side slope, relative main and flood plain channel

roughness and the incident angle of the slot to the main component of flood plain flow. These parameters were chosen so that they were pertinent to the main channel configuration in a meandering compound channel. The basic slot which was initially constructed is shown in Figure 3.27.

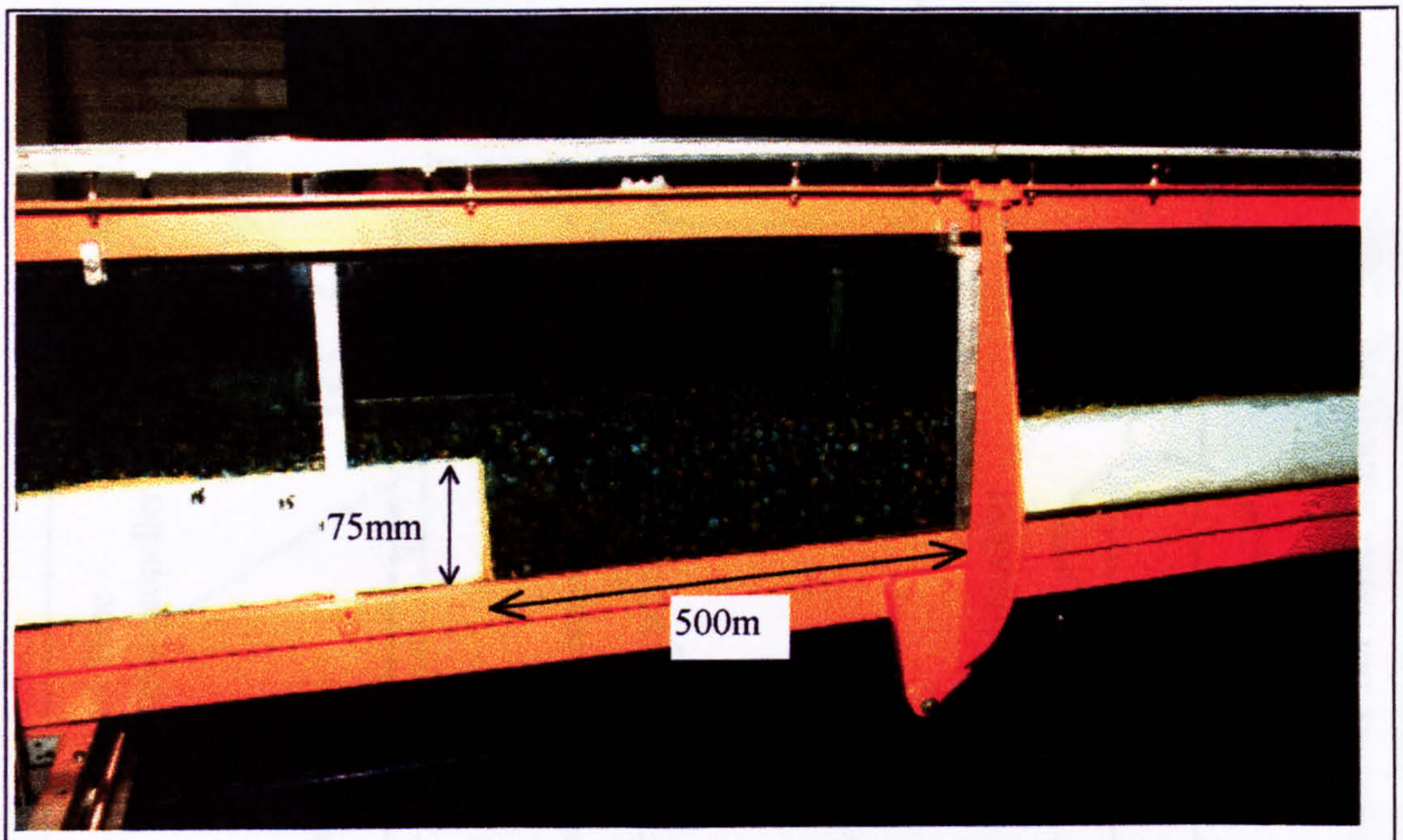

Figure 3.27. Fabrication of different slot configurations

The basic slot configuration was rectangular and 500mm long by 75mm deep. Marbles have been inserted into the slot as part of a subsequent experiment.

3.3.2 Details of the slot models

The slot model was contained within a tilting Armfield flume which was 5m long by 0.3m wide and was fabricated by inserting smooth polystyrene inserts into the flume. The Armfield flume was supplied with water from two end feeder tanks, in a closed system as shown in Figure 3.28.

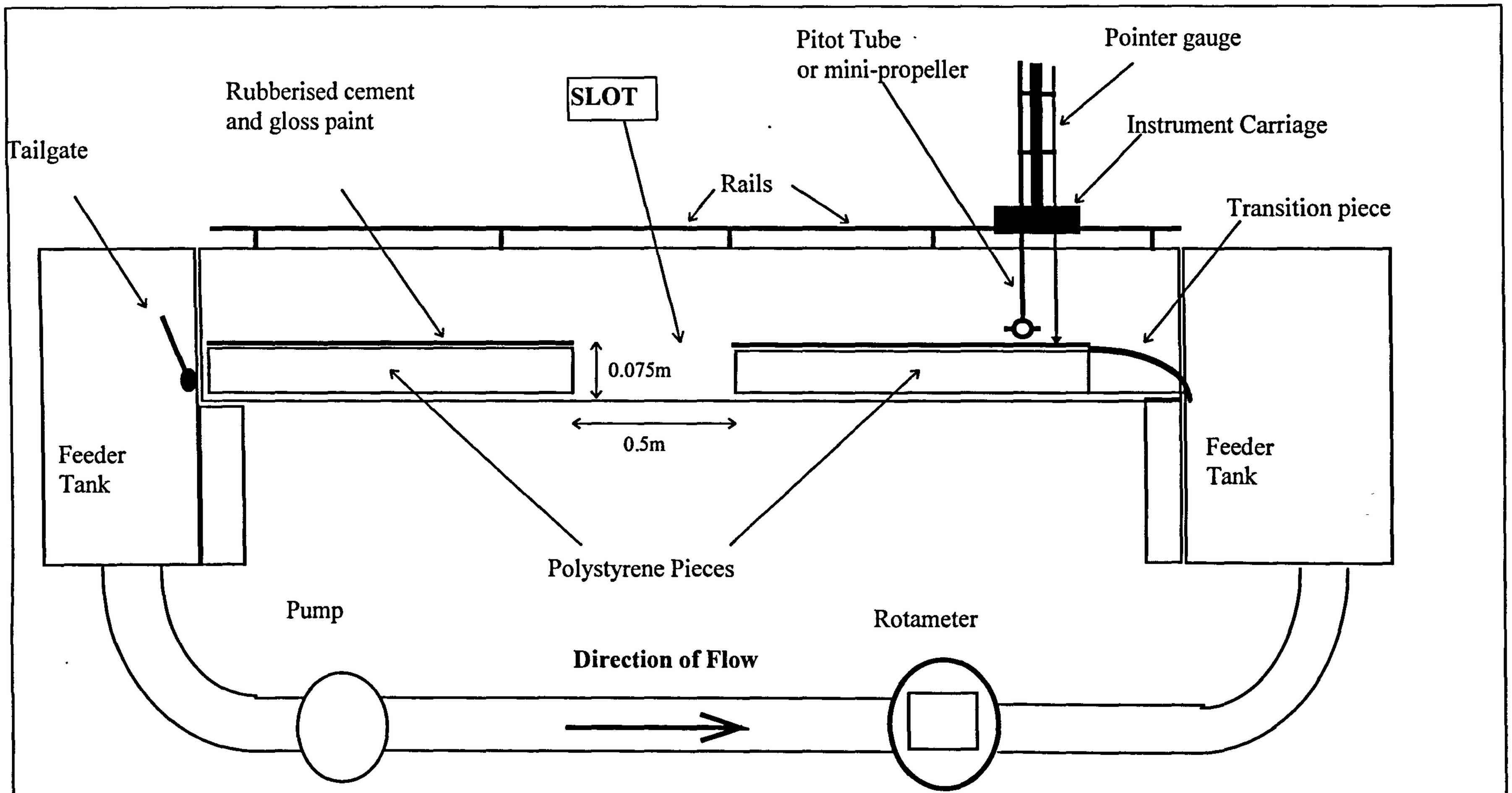

Figure 3.28 The tilting Armfield flume and basic slot model flume (Long section)

An on-line pump was capable of delivering a maximum discharge rate of 30L/s. Flow straighteners and a transition piece at the inflow end were used to calm the flow. A rotameter on the feeder pipe measured the discharge rate. The rotameter was calibrated using velocity integration techniques. Polystyrene pieces were cut and fixed using silicon gel within the basic slot in order to create the various slot configurations as shown in Figure 3.29. These were designed to vary slot side slope and width/depth (aspect) ratio. A number of models were also built with the slot skewed to the main component of flow. A couple of tests were performed using simple triangular inserts but this reduced the slot length and altered the skew angle, as shown in Figure 3.30.

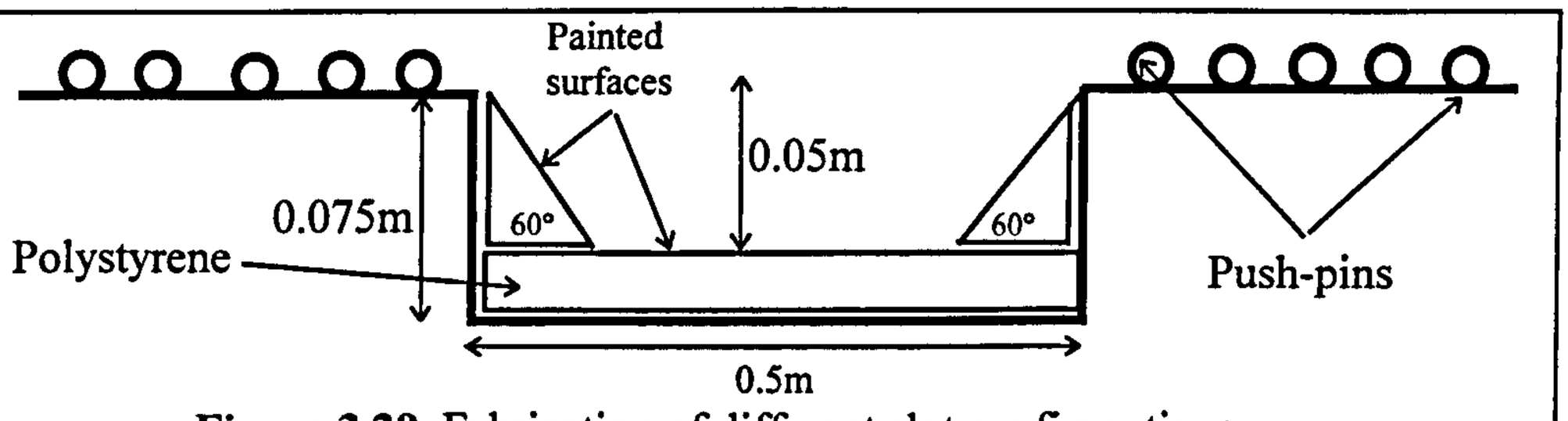

Figure 3.29. Fabrication of different slot configurations

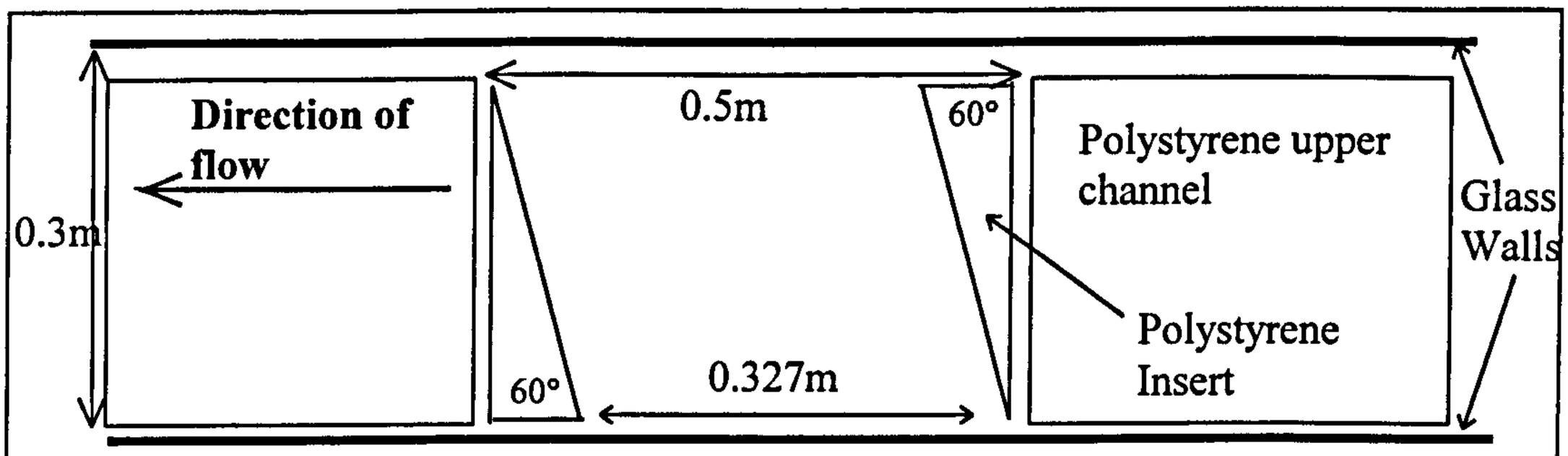

Figure 3.30. Skewed slot: Simple inserts (Plan view)

Further tests were performed which cut back the original polystyrene pieces which formed the upper channel before the skewed inserts were placed. This method ensured that the top width was maintained at a constant 500mm.

3.3.3 Model surface roughness

Both the upper channel (flood plain) and lower channel (slot) surfaces were fabricated to be hydraulically smooth. Any irregularities were treated using a combination of

rubberised cement screed and layers of gloss paint. The modified smooth law relationship for the model surfaces was calibrated and given in Equation 3.1.

$$\frac{1}{\sqrt{f_b}} = 2.02 Log\left(\mathrm{Re}\sqrt{f_b}\right) - 1.38 \qquad [3.1]$$

The flume walls were made of glass and were assigned a value of Manning's n equal to 0.01. The flood plain and the slot were roughened using push-pins. Rough A and Rough B triangular patterns were used to replicate the roughened surfaces that were tested during the Series B extension tests.

3.3.4 Model details and referencing system

Twenty different slot geometries were built and tested over a two year period. An upper channel slope of 1:1000 was used for all the tests. A schedule of all the models which were tested and their respective geometric and roughness characteristics is given in Table 3.12.

Test No.	Ref. No.	Slot depth (mm)	Slot width (mm)	Side slope angle	Upper Channel roughness	Lower Channel roughness	Slot skew angle
1	S7G9S	75	500	90	Smooth	Smooth	90
2	S7G6S	75	500	60	Smooth	Smooth	90
3	S7G4S	75	500	45	Smooth	Smooth	90
4	S7G3S	75	500	30	Smooth	Smooth	90
5	S5G9S	50	500	90	Smooth	Smooth	90
6	S5G6S	50	500	60	Smooth	Smooth	90
7	S5G4S	50	500	45	Smooth	Smooth	90
8	S5G3S	50	500	30	Smooth	Smooth	90
9	S2G9S	25	500	90	Smooth	Smooth	90
10	S2G6S	25	500	60	Smooth	Smooth	90
11	S2G4S	25	500	45	Smooth	Smooth	90
12	S2G3S	25	500	30	Smooth	Smooth	90
13	B2G4S	25	500	45	Smooth	Rough B	90
14	S7G9B	75	500	90	Rough B	Smooth	90
15	S7G9A	75	500	90	Rough A	Smooth	90
16	S7G9S4	75	250	90	Smooth	Smooth	45
17	S7G9S7	75	390	90	Smooth	Smooth	70
18	S7G9S6	75	500	90	Smooth	Smooth	60
19	S5G9S6	50	500	90	Smooth	Smooth	60
20	S5G9S4	50	500	90	Smooth	Smooth	45

Table 3.12 The slot test model configurations

3.3.5 Measurement of the flow characteristics

3.3.5.1 *Cross-sectional measurement grid in the slot area*

The flow depths and velocities were measured along three parallel lines at each cross-section. One of these lines was aligned with the centre line of the flume and the other two lines, which were offset by 100mm, on either side of the centre line. The point velocity readings in and over the slot were taken at depth intervals of 5mm for the 25mm and 50mm deep channels and at depth intervals of 10mm for 75mm channels. The point velocity readings were taken at depth intervals of 5mm for flow depths less than 40mm and at depth intervals of 10mm for flows greater than 40mm. The velocity measurement points in a 25mm deep channel, with a 50mm flow on flood plain flow, are shown in Figure 3.32.

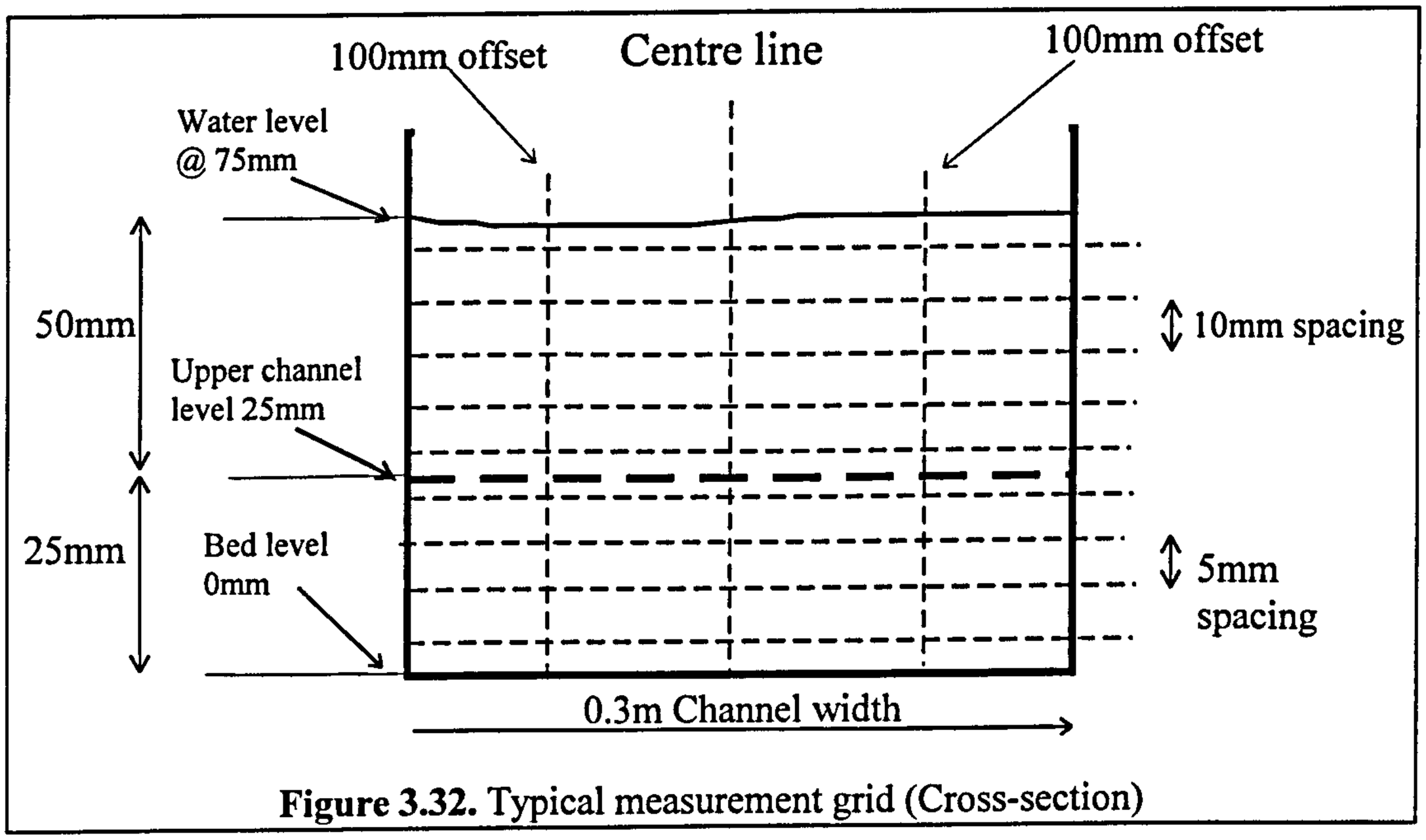

Figure 3.32. Typical measurement grid (Cross-section)

3.3.5.2 *Longitudinal measurement positions*

Point velocity readings and flow depths were measured at 20 cross-sections along the length of the flume as shown in Figure 3.33.

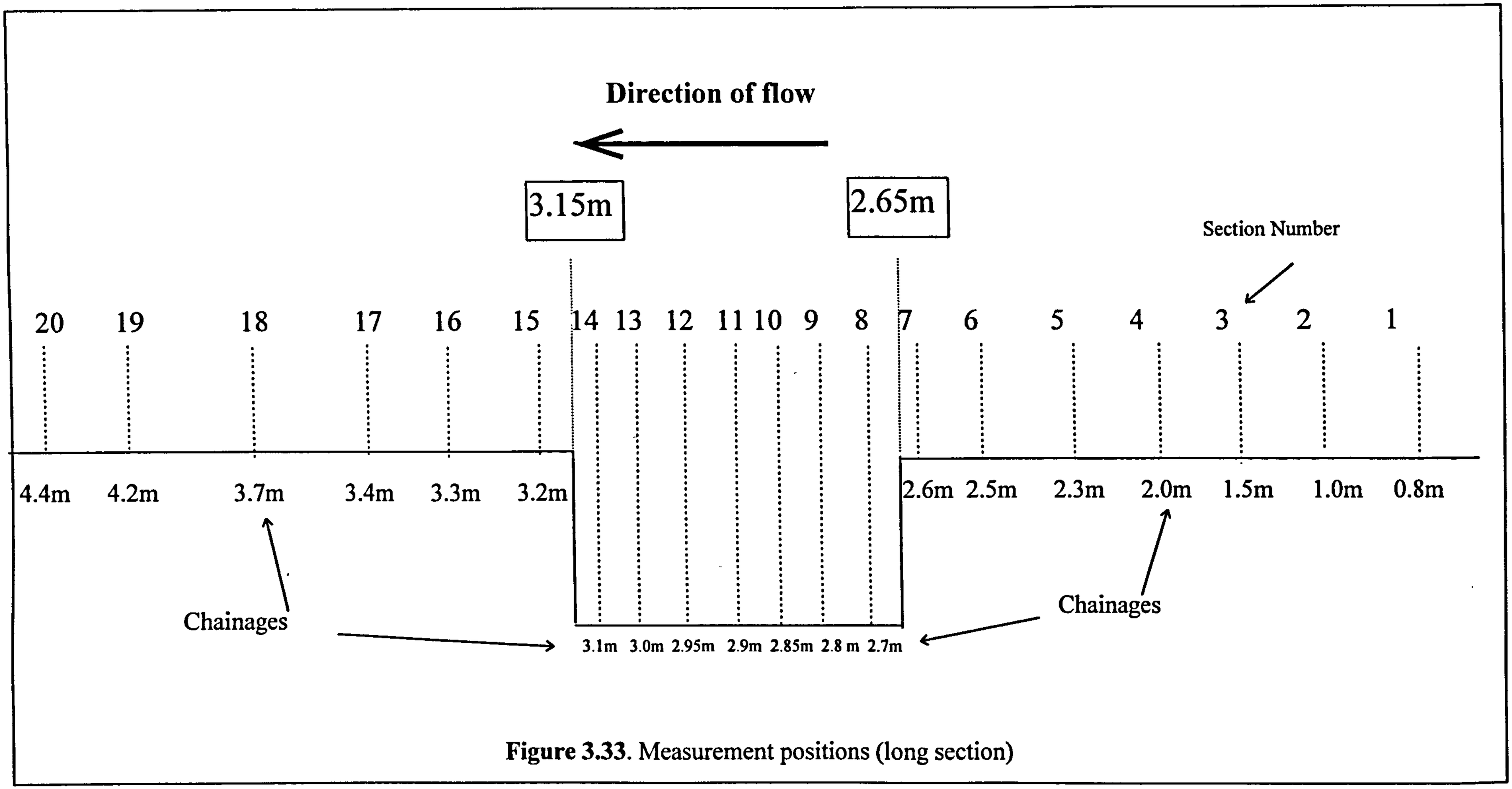

Figure 3.33. Measurement positions (long section)

3.3.5.3 The flow readings taken

An instrument carriage ran on rails on the top of the flume. The rails carriage were set parallel to the flume bed. A pointer gauge was attached to a carriage that ran on these rails. It was used to measure difference between bed level and water surface level The pointer gauge was accurate to +/-0.1mm.

An angle potentiometer was used to determine the principal component of velocity in the skew channel tests only. A initial series of experiments were performed to confirm that the principal component of velocity was parallel to the centre line of the flume when the slot was aligned perpendicular to the flow.

Pitot tubes and mini-propeller meters were used to measure point velocities in all tests. The same instruments which were used in the meandering channel tests were also used in the slot tests.

3.3.6 Specific Energy line analysis

3.3.6.1 Introduction

The velocity and flow depth readings were used to determine the total energy line. A Specific Energy line was generated for each flow depth tested in every model. They were created by plotting the Specific Energy of the flow against the corresponding longitudinal model chainage, as shown in Figure 3.34. The Specific Energy at each cross-section was calculated using Equation 3.2.

$$E.L. = W.L. + \frac{\alpha V^2}{2g} \qquad [3.2]$$

E.L. is the Specific Energy level, W.L. is the measured water level, V is the average velocity for any cross-section and α is the energy coefficient at each cross-section which is defined in Equation 3.3

$$\alpha = \frac{\int v^3 dA}{V^3 A} = \frac{\sum v^3 dA}{V^3 A} \qquad [3.3]$$

v is the point velocity and dA is the area over which a particular point velocity acts. The point velocity, v, is positive in the downstream direction. A is the cross-sectional area which is equal to the sum of all dA.

3.3.6.2 Setting Normal depth

The complete set of flow depth and velocity readings at each cross-section which was required to produce a full energy line was only taken once normal flow depth was established in the model. Normal depth was identified as the state of flow for which the slope of the Specific Energy line at the extreme ends of the flume was parallel with the model's bed. Four or five normal flow depths, ranging between 12mm and 100mm were investigated for each model. A suitable discharge rate was established in the flume and then the tailgate was adjusted until the slope of Specific Energy line at the test points, at both ends of the flume, were equal to the model's upper bed slope, as shown in Figure 3.34. The upstream points which were used to check for normal depth were 1, 2 & 3 and the downstream points were 18, 19, & 20.

3.3.7 Determining the magnitude of expansion and contraction head loss

3.3.7.1 Introduction

The graphical technique described below was used to interpret the Specific Energy line which was created for each normal depth setting and model configuration. This technique was used to determine the magnitude of the expansion and contraction head losses which were generated in the flow over the slot. Figure 3.34 shows an idealised plot of the Energy Line and water surface level plots which are obtained in a typical model and demonstrates the application of the graphical method to establish normal depth and the magnitude of energy losses.

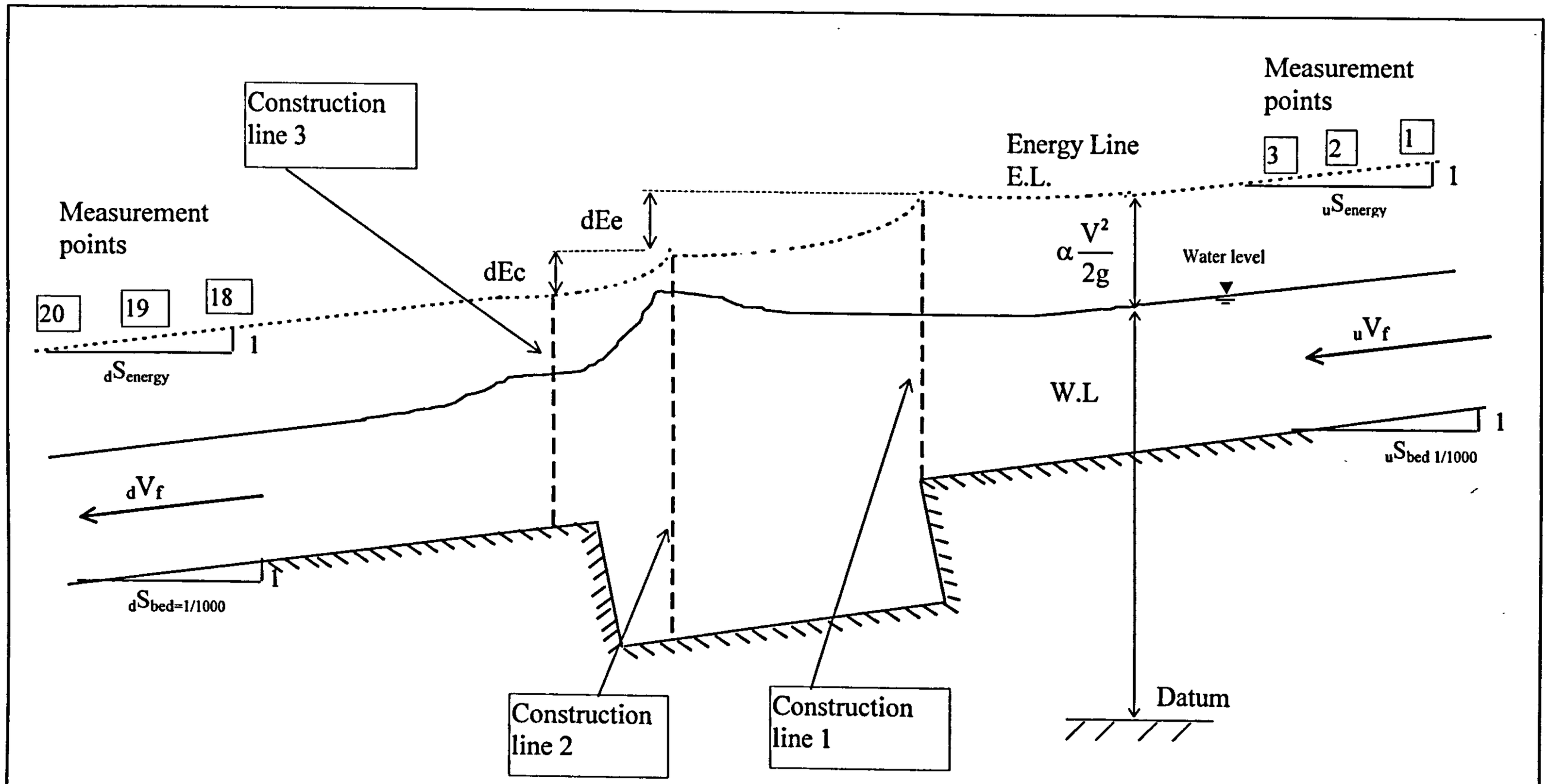

Figure 3.34 Water level and Energy line versus Longitudinal offset (Graphical energy loss calculation technique)

3.3.7.2 Graphical technique for determining specific energy

1) The tailgate level setting is altered until the energy line slope at the upstream the down stream test points is equal to the bed slope, ${}_dS_{energy} = {}_uS_{bed}$ and ${}_uS_{energy}$ and ${}_uS_{bed}$
2) The head loss due to flow expansion is defined as the difference between the Specific energy of the flow at construction line 1 and construction line 2. Construction line 1 coincides with the corner of the backward facing step. Construction line 2 is drawn to coincide with peak water level.
3) The head loss due to flow contraction is defined as the difference between the Specific energy of the flow at construction line 2 and construction line 3. Construction line 3 coincides with the peak water level once the water passes over the forward facing step.

3.3.7.3 Definition of head loss coefficient, K

The theoretical expansion and contraction head loss coefficients, K_e and K_c were calculated for each model and flow depth by back-substituting the measured values for head loss, h and average upper channel flow velocity, V_f into Equations 3.4 and 3.5. The magnitude of bed friction loss was assumed to be equal to zero.

$$h_e = K_e \frac{{}_uV_f^2}{2g} \qquad [3.4]$$

$$h_c = K_c \frac{{}_dV_f^2}{2g} \qquad [3.5]$$

The subscripts e and c indicate expansion and contraction values and u and d represent upstream and downstream values. The adjustment coefficients were calculated by dividing the values for K_e and K_c, thus obtained by the theoretical head loss coefficients which were equal to $[1-y_2[y_2+h]]^2$ and the Rouse [1950] definition for K_c for expansion and contraction respectively.

3.4 Statistical measures of the performance of regression models

3.4.1 Multi-variate regression analysis

The author used the computer program 'Sigmaplot' produced by Jandel Scientific Corporation to perform the multi-variate regression analysis of the flow data obtained

during the Series B extension programme. The one dependant variable (typically a flow parameter) is related to a number of independent variables (typically the geomorphic and roughness parameters characterising the meandering compound channel) by determining the values of various parameters (coefficients and constants) which produce the best fit. The quality of the regression fit results and the accuracy of these coefficients and constants was assessed in terms of three statistical measures:

1. Standard error of the mean of the parameters,
2. Coefficients of variation, CV (expressed as a percentage),
3. Parameter dependency.

Standard error, STERR is defined in Equation 3.6. The coefficients of variation, CV% (the normalised version of the standard errors) is defined in Equation 3.7. Parameter dependency is defined by Equation 3.8.

$$STERR = \left[\left({}^{1}/_{n-1} \right) \sum_{i=1}^{n} \left(x_i - \bar{x} \right)^2 \right]^{0.5} \Big/ \sqrt{n} \qquad [3.6]$$

$$CV\% = standard\ error * \frac{100}{parameter\ value} \qquad [3.7]$$

$$Dependency = 1 - \frac{\left(variance\ of\ the\ parameter, other\ parameters\ constant \right)}{\left(variance\ of\ the\ parameter, other\ parameters\ changing \right)} \qquad [3.8]$$

The values obtained for STERR and CV% enable the general accuracy of various regression fits to be compared. Parameter with dependencies near to 1 are strongly dependant on one another. This indicates that the equations used are too complicated and 'over-parameterised' - too many parameters are being used. A model with fewer parameters may be better.

The relative values of the above measures guided the author towards identifying the optimal regression fit. The final assessment however was made by directly comparing the derived model function with the experimental (training) data, which is comprised of n data pairs, and determining the mean error.

3.4.2 Determination of 'error' between a regression fit and experimental data

Many researchers have used the value of the 'mean error' as defined in Equation 3.9 to assess the quality of fit between the model predictions and the experimental data.

$$Mean\ error,\ \bar{x} = \frac{\sum_{i=1}^{n}\left(x_i - \bar{x}\right)}{n} \qquad [3.9]$$

However if the mean error for a set of points are both positive and negative, then on summation they will counteract each other and give a false impression of the level of accuracy. If the fit under-predicted the dependant variable over a range of independent parameters and over-predicted the dependant variable over a different range then the error mean may tend towards zero thus obscuring the nature and overall magnitude of the error. To overcome this drawback the author used a measure of Root Mean Square (RMS) error to assess fit quality as defined in Equation 3.10.

$$RMS = \frac{\sum\left(\left(x_i - \bar{x}\right)^2\right)^{0.5}}{n} \qquad [3.10]$$

The RMS error for all data points is positive so negative error does not counteract positive error on summation and a representative picture of overall accuracy is obtained.

The author typically determines the mean and RMS percentage differences in discharge capacity for each model (averaged over all flow depths) when determining the accuracy of a prediction model. Mean percentage difference, Q%, is defined as in Equation 3.11.

$$Q\% = 100*(Q_{Pred} - Q_{meas})/\ Q_{meas} \qquad [3.12]$$

Q_{meas} is the measured discharge capacity and Q_{Pred} is the predicted discharge capacity. When Q% is positive the predicted discharge is greater than the measured discharge.

3.5 Summary and conclusions

- A total of 54 meandering compound channel models were built and tested in Glasgow (30) and Aberdeen (24) as part of the Series B extension (1993-1996) programme. The results obtained were combined with existing data sets to produce a large and comprehensive data set which demonstrated the relationship between 9 of the 11 key geometric and roughness parameters which influence flow behaviour in

meandering compound channels. These 11 parameters are listed below and the 2 untested parameters are asterisked:-

1) The scale of the model, (L_r)
2) The relative depth of flow, (RD)
3) The relative roughness of the main channel / flood plain, (f')
4) The sinuosity of the main channel, (r)
5) The longitudinal bed slope, (S_o)
6) The relative width of the meander belt and floodway, (M_w)
7) The aspect ratio of the main channel, (AR)
8) The sides slope angles of the main channel, (S_S)
9) The cross-sectional shape of the main channel, (φ)
10) The sinuosity of the flood plain banks, (r_u) *
11) The lateral flood plain slope towards the main channel, (S_L) *

- 20 slot (trench) models were built and tested in Glasgow as part of the Series B extension (1993-1996) programme. The results obtained were compared with data produced by Jasem [1990] and Formica [1955]. A large and comprehensive data set was produced which demonstrated the relationship between 5 geometric and roughness parameters and the magnitude of head loss generated by the expansion and contraction of flow as it passes over a slot. These 5 parameters are listed below:-
  1) relative depth
  2) main channel aspect ratio
  3) main channel side slope
  4) the relative boundary roughness upstream and downstream of the slot
  5) the angle (skew) of the slot to the oncoming flow.
- The modelling and measurement techniques used by the three teams in the Series B extension (1993-1996) programme were co-ordinated so that they were as similar as possible.
- Point velocity measurements were performed in both Institutions to directly measure the local velocity in individual flow zones and hence divulge the nature of flow layer interaction mechanisms.
- Dye visualisation tests were performed in both Institutions in order to elucidate the flow mechanisms in individual flow zones as well as providing an indirect measurement technique for assessing flow velocity in flow zones where the depth

was so shallow that conventional direct measurement devices, such as Pitot tubes and mini-propellers, were unsuitable.

Chapter 4

4. Experimental results for the meandering compound channel and slot tests

4.1 Introduction

This chapter presents an in-depth analysis of the flow data which were obtained during the 3 year Series B extension experimental programme at Glasgow. Comparisons are made with data obtained from previous experimental programmes. The sets of existing data which had bed friction calibration data reliable enough to make re-analysis feasible were identified in Section 2.8. A complete summary of the model configurations tested during the Series B experimental programme at Glasgow and Aberdeen, together with the existing data set configurations were given in Tables 3.7 and 3.8 and Section 2.8 respectively.

Chapter 4 is structured so that it is divided into 9 further sections. Section 4.2 details the results from the bed friction calibration tests on the typical smooth and push pin roughened surfaces which were used in the meandering compound channel models. Section 4.3 presents an analysis of the results from the common tests performed by each Institution co-operating in the Series B extension programme. Section 4.4 presents an assessment of the relative merits of a number of different discharge measurement parameters when they are applied to both the complete (Global) cross-section of a meandering compound channel and the individual zones comprising the cross-section. Section 4.5 presents the findings from the models tested in Glasgow and Aberdeen during the Series B extension programme which demonstrate the influence of 11 key parameters on the layer interaction head loss / flow resistance which is generated in a complete meandering compound channel. A measure of Global F* is defined in order to quantify the magnitude of interaction flow resistance. Section 4.6 presents the findings from the models tested in Glasgow during the Series B extension programme which demonstrated the influence of six key parameters on the flow mechanisms and head loss

/ flow resistance in the individual zones comprising the complete cross-section of a meandering compound channel. Local F* measurements are used to quantify the magnitude of interaction flow resistance. In Section 4.7 the author identifies the flow mechanism which generate the interaction flow resistance in meandering compound channels using the results obtained for Global and local F* in Sections 4.5 and 4.6. A novel explanation for the influence of channel scale on the flow mechanisms in a meandering compound channel is also proposed using references to the 4 flow region behaviour which was shown to be characteristic of meandering compound channel flow and the critical Threshold values for the relative flow states in the main and flood plain channels. Section 4.8 details the results gathered from an additional series of slot model tests which were performed in Glasgow during the Series B extension programme in order to investigate the flow interaction mechanisms which generate head loss in flow over slots in the bottom of a flood plain channel. The influence of five key geometric and roughness parameters on these flow mechanisms was assessed and empirical formulations to predict the magnitude of head loss generated were developed. Section 4.9 summarises all the findings described in Chapter 4 and draws together the important conclusions.

4.2 The calibration of the model surfaces in terms of bed friction

4.2.1 Introduction

The characteristic frictional resistance of the various model surface finishes which were used for the Series B extension models was measured in terms of standard resistance coefficients such as Manning's, n, Darcy friction factor, f, and Colebrook-White, Ks. Two tilting flumes were commissioned to perform the calibration tests. A 0.3m wide by 5m long flume was used in Aberdeen and a 1.65m wide by 8m long flume was used in Glasgow. The boundary roughness was only varied on the bed of the two flumes. The discharge capacity of these flumes was measured over a range of flow depths and bed roughness types. The range of flow depths tested matched the range of flow depths to be implemented in the meandering compound channel tests. The relationship between the magnitude of the friction coefficients and the flow depth was determined. The magnitude of the roughness coefficients (flow resistance) was significantly influenced by the flow depth in the small scale models.

4.2.2 Smooth model surfaces

Flow depth and the corresponding discharge capacity data were collected from the calibration tests on the models with smooth surfaces and were used to calculate frictional resistance in terms of Darcy, f and Reynolds number, Re. The frictional resistance coefficient of the flume bed, f_b ,was calculated by subtracting the contribution of the channel walls, f_w, from the total frictional resistance, f. A method proposed by French [1986] and shown in Equation 4.1 was used to relate the magnitude of frictional resistance between the total resistance and the bed and side wall resistance.

$$f_b = \frac{P}{P_b} f - \frac{P_w}{P_b} f_w \qquad [4.1]$$

P_b is the wetted perimeter of the walls, P_w is the wetted perimeter of the flume and P is the total wetted perimeter of the whole channel ($P = P_b + P_w$). Ackers [1991] and others have successfully used a modified smooth law to relate f_b to Re in previous small scale models with smooth flood plains. A linear regression fit was performed on the results obtained for f_b and Re which were extracted from the Series B extension tests and an equation of the form shown in Equation 4.2 was derived.

$$\frac{1}{\sqrt{f_b}} = \mathrm{C} \cdot Log\left(Re\sqrt{f_b}\right) - \mathrm{D} \qquad [4.2]$$

Plots showing the flow data and the linear regression fit equations are shown in Figure 4.1. Ackers [1991] observed that a value for, C, of 2.03 has been commonly derived for smooth turbulent flow. Myers and Brennan [1990] determined that C was equal to 2.02 in the Series A tests. The values of the coefficients, C and D, which were derived for the Glasgow and Aberdeen tests were compared with those obtained from the Series A and B calibration tests. The value of C was set equal to 2.02 when analysing the Glasgow and Aberdeen flow data because smooth turbulent behaviour was anticipated. The corresponding value of D was calculated. The values for D obtained and the corresponding Coefficient of Determination values, R^2 (which indicate the accuracy of the regression fitting of the straight line equations) are listed in Table 4.1. They are compared with the equivalent values obtained for the Series A and B experiments.

Experimental Series	C	D	R^2 value
Series A & B (1986-1992)	2.02	1.42	0.97
Series B Ext. (Glasgow)	2.02	1.30	0.97
Series B Ext. (Aberdeen)	2.02	0.91	0.93

Table 4.1 Coefficients for the Smooth Turbulent equation derived experimentally

The best fit lines produced an R^2 value greater than 0.93 for both the Glasgow and Aberdeen calibration data, which was similar in magnitude to the values obtained for the Series A and B flow data. The Stanford Conference in 1968 agreed that the variation in the value of, D, in a modified smooth turbulent equation indicated different levels of bed friction resistance. The results listed in Table 4.1 indicate that the Aberdeen model surfaces were slightly smoother than those in the Series A, Series B and Series B extension (Glasgow) models.

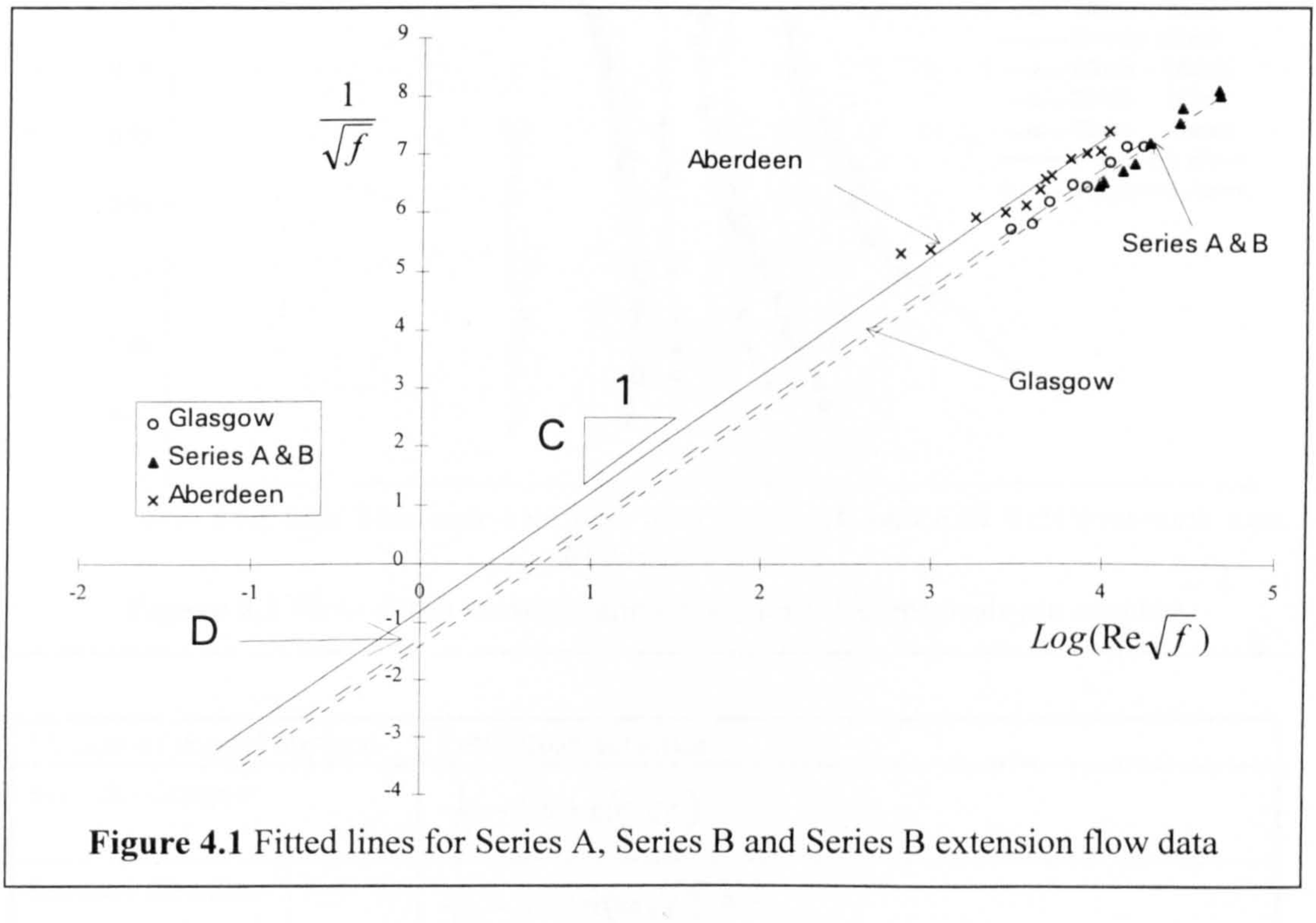

Figure 4.1 Fitted lines for Series A, Series B and Series B extension flow data

4.2.3 Roughened model surfaces

In order to ensure that the values for the relative roughness between the main channel and the flood plains were similar to naturally occurring values, the flood plain surfaces were roughened in most of the Series B extension models. Plots of Manning's n versus flow depth, which were obtained for the 5 different model surface roughnesses tested

during the Series B extension programme are shown in Figure 4.2. Only three model surface roughnesses were used in the meandering compound channels, these were: Smooth (no push-pins), 60mm push-pin spacing and 30mm push-pin spacing.

Polynomial regression equations, order 2, were determined to model the observed relationships between Manning's n and flow depth for the roughened surfaces with the 30mm and 60mm push-pin spacing. Table 4.2 lists the modified smooth law and polynomial expressions which were derived for the three surfaces.

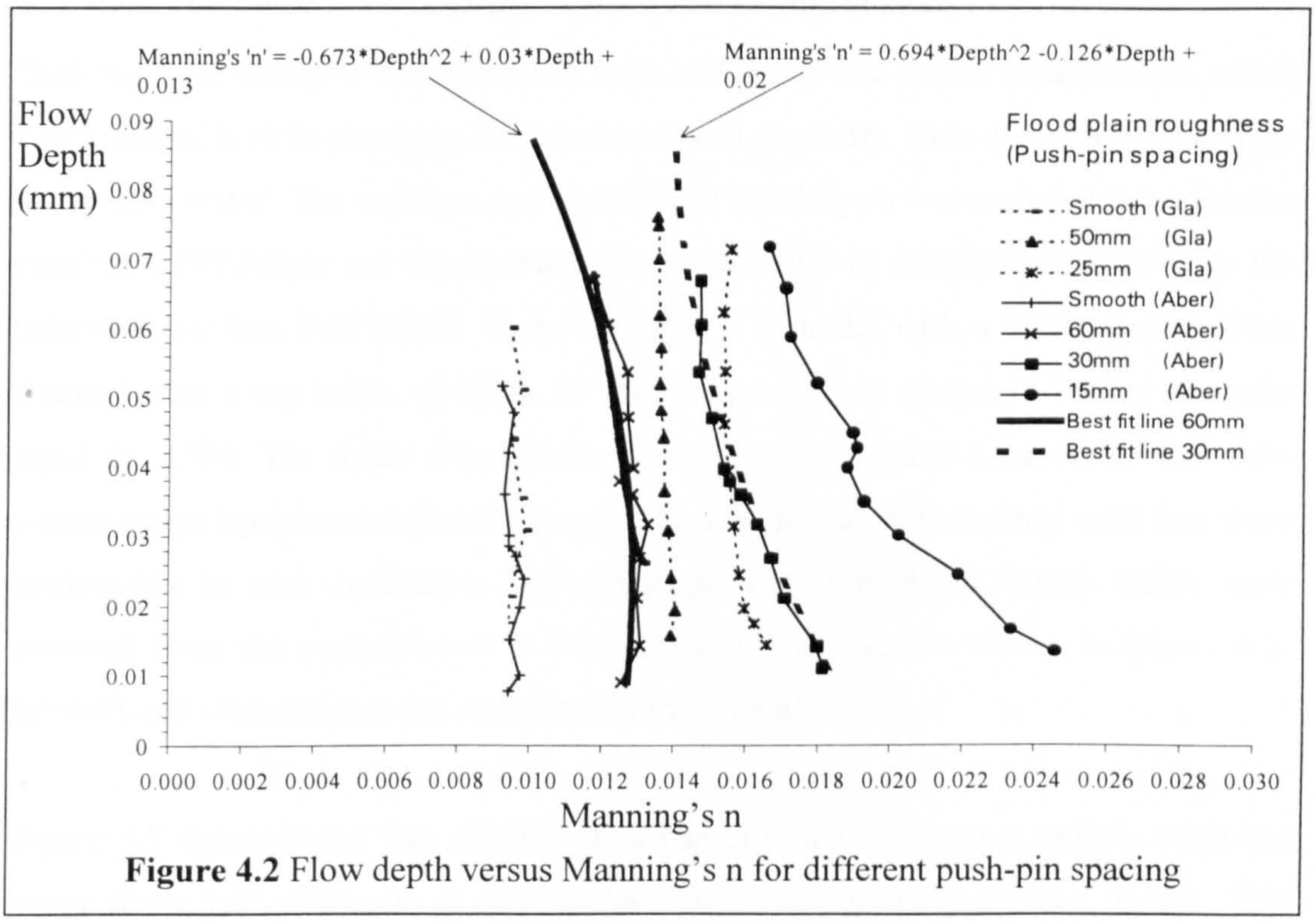

Figure 4.2 Flow depth versus Manning's n for different push-pin spacing

Nature of model surface	Prediction formula
Smooth:- Glasgow	$\frac{1}{\sqrt{f}} = 2.02.\log\left(\mathrm{Re}\sqrt{f}\right) - 1.3$
Smooth:- Aberdeen	$\frac{1}{\sqrt{f}} = 2.02.\log\left(\mathrm{Re}\sqrt{f}\right) - 0.81$
Rough A (60mm spacing)	Manning's 'n' =-0.673*Depth^2 + 0.03*Depth + 0.012
Rough B (30mm spacing)	Manning's 'n' = 0.694*Depth^2 - 0.126*Depth + 0.02

Table 4.2 Expressions relating frictional resistance to flow depth (Series B extension)

Additional experiments were performed in Aberdeen to determine whether changing the slope of a channel had any significant effect on the frictional characteristics of the

channels. Channel slopes of 1:750, 1:1000 and 1:1500 were tested. Analysis of the flow results demonstrated that the magnitude of channel slope had a negligible effect on the relationship between frictional resistance and flow depth at these model scales and over the range of slopes which were tested. Consequently the expressions derived relating frictional resistance to flow depth for the 1:1000 slopes were used to analyse the flow results obtained from all the models that were tested.

4.3 The common meandering compound channel test

Both teams in Glasgow and Aberdeen built and tested one model configuration which was identical both in planform and cross-sectional geometry. This model was known as: 'the common test'. The common test model built in Glasgow was assigned the reference number, G50T60RA, and the common test model built in Aberdeen was assigned the reference number, A1T1000B. Essentially this is a model with a 52.5mm deep main channel with a top width of 0.2m, 60° side slopes which meanders with a sinuosity equal to 1.374. The upper flood plain channel is smooth and 1.2m wide. The flow measurement equipment and model construction techniques were refined until they were comparable in each Institution. The discharge and flow depth curves which were obtained from the common test in Glasgow and Aberdeen are shown in Figure 4.3. Bristol's common test was not completed at the time of writing.

Figure 4.3 demonstrates that the discharge capacity of the Glasgow model, when the water flows just overbank, is slightly less than that for the Aberdeen model. This difference increases with flow depth. The discharge capacity of the Glasgow flume averaged over all the measured depths of overbank flow is 5% (RMS average) less than the Aberdeen flume. This small difference was attributed to the fact that the Aberdeen model surfaces were proven to be slightly smoother than those in the Glasgow model in the calibration tests.

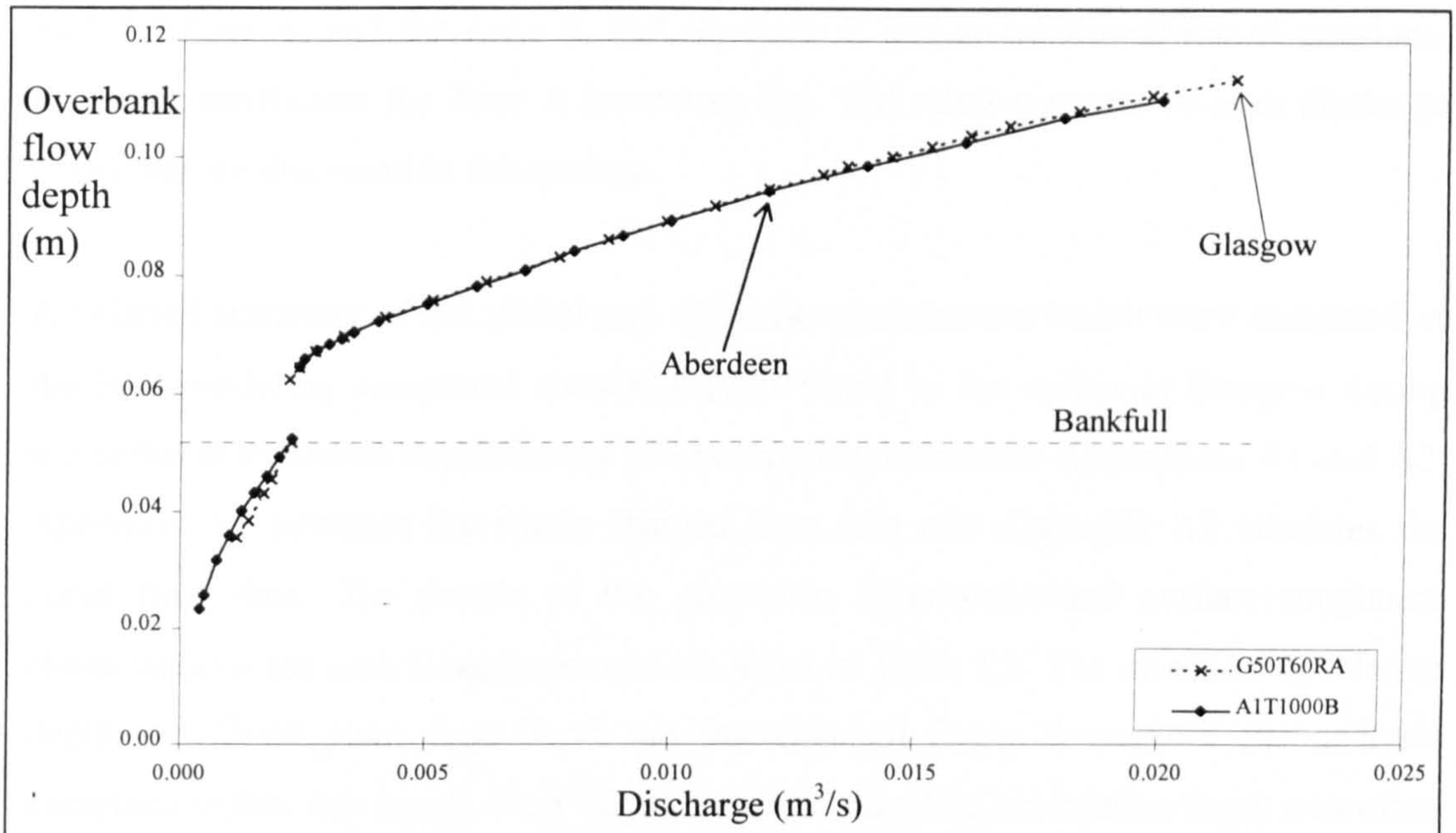

Figure 4.3 Discharge capacity versus overbank flow depth (The common test)

The difference in the number of relative meander wavelengths in the two models appears to have only a minimal effect on the relative flow performance which corroborates the observations made by Kiely [1989]. Kiely [1989] presented evidence indicating that when the number of identical main channel wavelengths in each compound channel model increases above 2 there is no significant change in type and magnitude of flow mechanisms that are generated. Further studies are required in order to confirm how this phenomenon might be related to the specific flow conditions that are required to develop a turbulent boundary layer within a meandering compound channel.

4.4 The discharge parameters used to analyse flow behaviour

4.4.1 Introduction

The author identified a number of discharge parameters which could be used to measure the influence of the 11 key geometric and roughness parameters on the flow behaviour in the meandering compound channels tested during the Series B extension programme (for both whole cross-sections and different flow zones). These parameters include: Discharge rate, Q, Manning's n, Darcy f, Colebrook-White, K_s, a non-dimensional global discharge coefficient, Global F*, non-dimensional local discharge coefficients,

$F_{A,}$* for Zone A, F_B* for Zone B, F_C* for Zone C and an additional non-dimensional discharge coefficient for Zone A known as $Q_A^{/}$. The relative merits of each discharge parameter are discussed in this section.

A detailed summary of the global and zonal flow parameters which were measured in the 30 meandering compound channel models tested by the author in Glasgow during the Series B extension experimental programme is tabulated in Appendices A1 and A2. Appendix A1 tabulates the whole channel flow data and Appendix A2 tabulates the zonal flow data. The details of the geometric dimensions and surface roughness characteristics for each Glasgow model are listed in Table 3.8. The measures of relative depth and flood plain flow depth are interchanged freely throughout the analysis contained within this report. Flow depth is easy to visualise but relative depth was often used as an alternative in order to facilitate comparison between flow results obtained from model tests performed at different scales.

4.4.2 Discharge parameters for the complete cross-section

4.4.2.1 Global discharge capacity

Figure 4.4 shows plots of flow depth versus discharge capacity from G75T90R, G50T90R and G25T90R, which were typical of the models tested during the Series B extension programme.

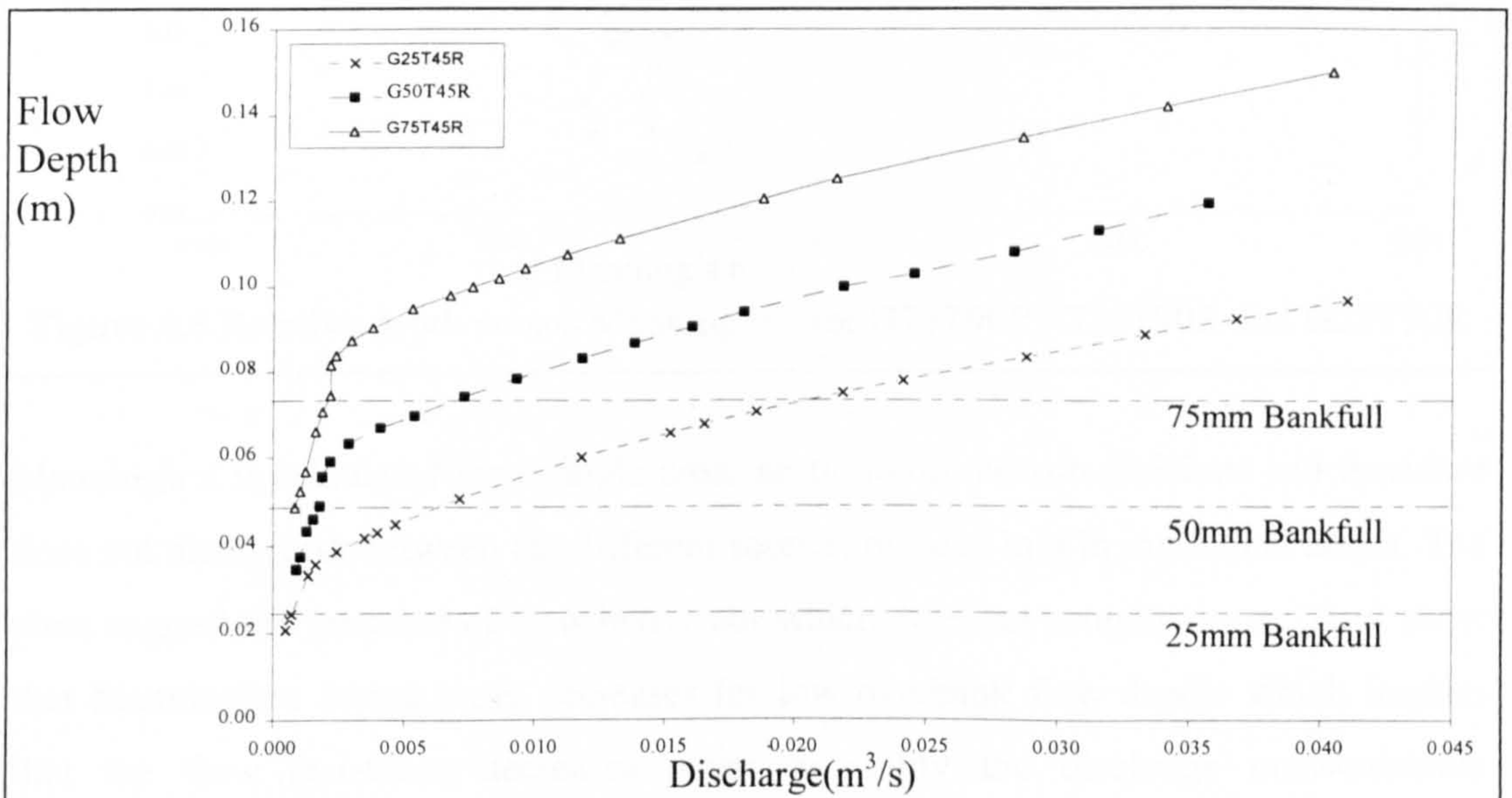

Figure 4.4 Flow depth versus Discharge rate for G75T90R, G50T90R and G25T90R

In each plot a significant discontinuity is observed at the transition point between inbank and overbank flow. The discharge capacity of the compound channel when it is flowing just overbank is slightly less than when the flow is inbank. This provides clear evidence that a significant additional source of head loss is generated when the flow is steady and overbank. The Glasgow model tests demonstrated that for meandering compound channels these discontinuities are most pronounced in the models with small main channel aspect ratios (width/depth). It was not possible to distinguish clearly the influence of each of the 11 geometric and flow state parameters on the flow behaviour purely from stage-discharge plots. Consequently other methods were considered.

4.4.2.2 Manning's n and flow depth

Figure 4.5 plots relative flow depth versus Manning's n for flow in the whole channel for models G75T90R, G50T90R and G25T90R from the Series B programme.

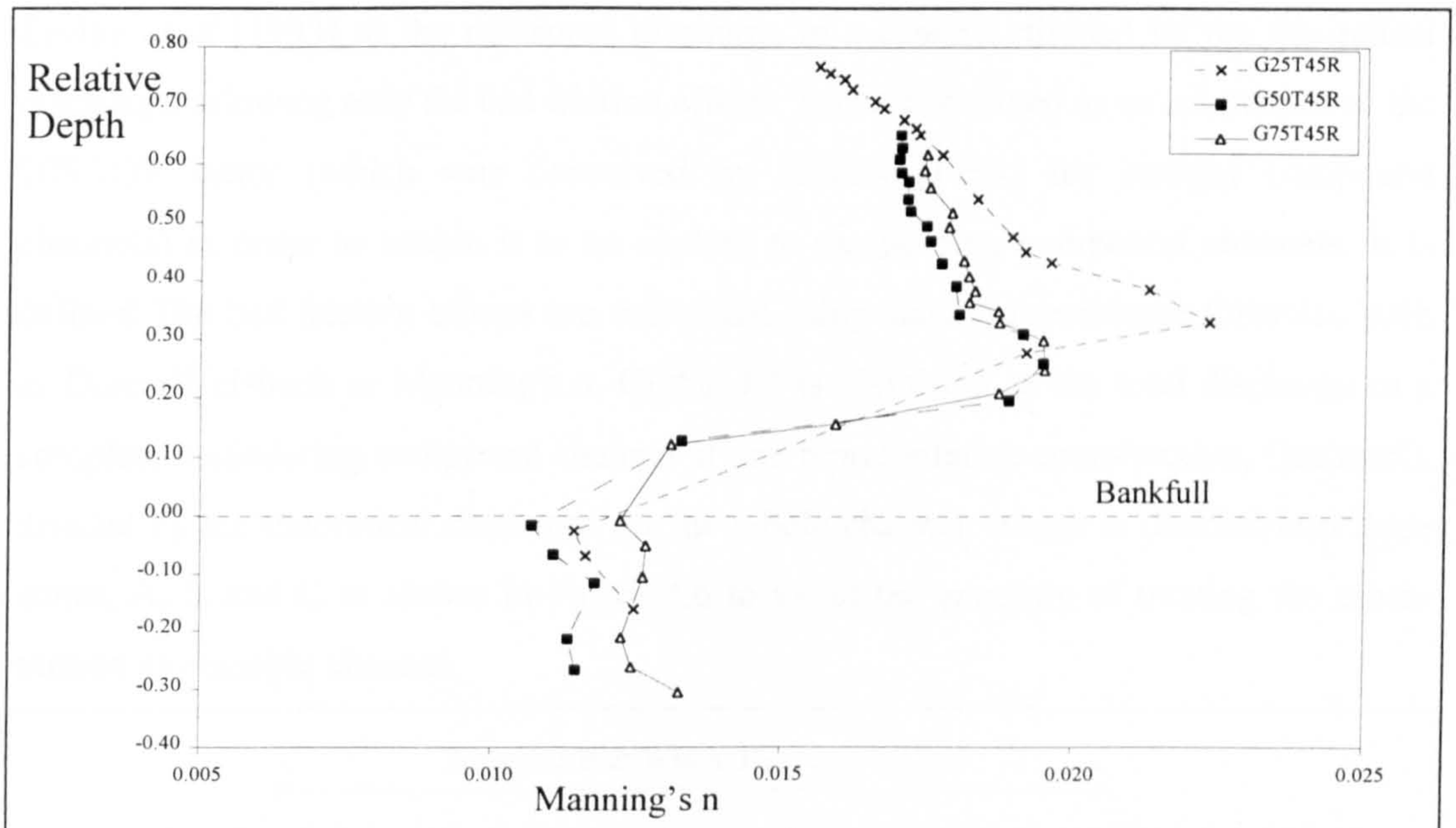

Figure 4.5 Relative depth versus Manning's n for G75T90R, G50T90R and G25T90R

Manning's n is calculated for a single cross-section with no sub-divisions and therefore does not distinguish between the different sources of head loss in individual zones. The plots suggest the presence of flow behaviour which does not actually occur. They show that Manning's n dramatically decreases for low overbank flow depths which implies that the flow resistance decreases when in reality the discharge measurements demonstrate that the flow resistance increases. This anomalous behaviour is attributable

to a mathematical anomaly whereby the hydraulic radius increases rapidly compared with the cross-sectional area when the water first passes overbank resulting in an unrealistically small value for Manning's n. The author concluded therefore that it would be unwise to use variation in Manning's n (or any other standard resistance formulae (such as Chezy, Darcy-Weisbach and Colebrook-White) to elucidate the effect of the key parameters.

4.4.2.3 Discharge adjustment coefficient, (Global F)*

The author decided to adopt a variable, first used in the analysis of Series B (1989-1992) data by Ervine et al [1993], namely the discharge adjustment coefficient, F*. This parameter separates the influence of the proportion of flow resistance generated by bed friction and therefore enables the proportion of flow resistance generated by layer interaction in a meandering compound channel to be quantified. F* was defined by Ervine *et al* [1993] as the measured discharge in a channel divided by the theoretical discharge, allowing only for bed friction effects. It was conceived as an adaptation of the DISADF factor (which was conceived by Ackers [1991] for straight compound channels) in order to enable it to be applied to meandering compound channels. It is defined The bed friction effects are calculated using standard resistance formulae such as Darcy-Weisbach or Manning's n. Global F* is identified as the total discharge in a complete meandering compound channel at one representative cross-section, Qm(total), divided by the theoretical discharge for the whole channel, which is divided into three zones, A, B and C as shown in Figure 4.6 to avoid the anomaly of treating the cross-section as a simple channel.

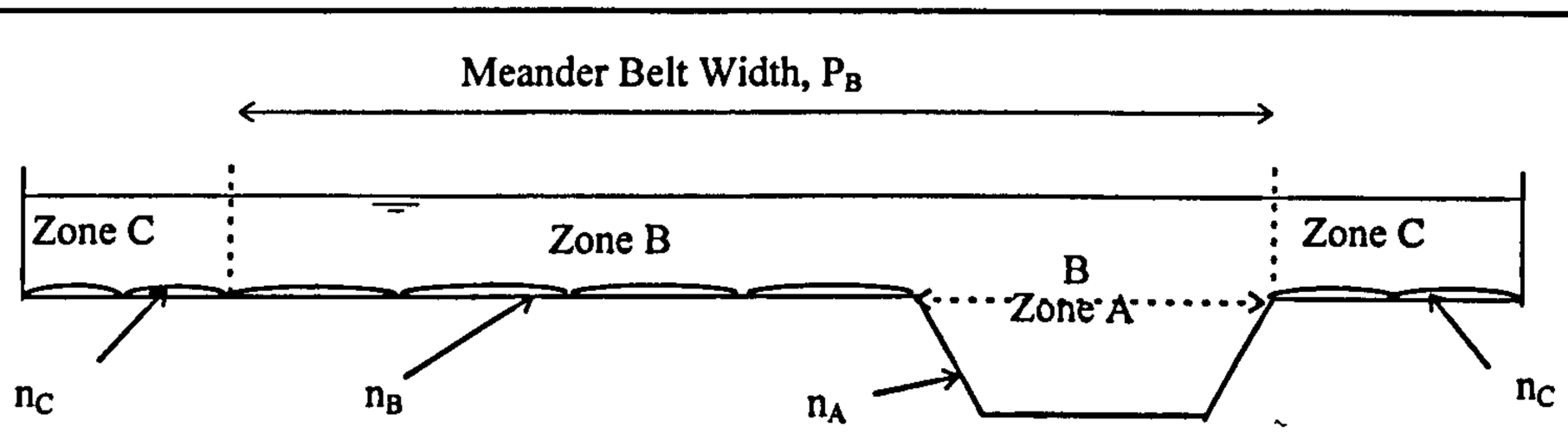

Figure 4.6 Compound channel Zonal divisions for computation

The theoretical discharges in Zones A, B and C are labelled Q_A, Q_B and Q_C. Global F* is defined in Equation 4.3.

$$\text{Global } F^* \equiv \frac{\text{Actual measured discharge}(Q_m)}{\text{Theoretical discharge based on bed friction only } (Q_A + Q_B + Q_C)} \quad [4.3]$$

The magnitude of Global F* varies between 1 and zero. When F* is equal to 1 then the implication is that the only resistance to flow is generated by bed friction. The implication when F* reduces to values significantly less than one is that a larger proportion of the flow resistance is being generated in the flow layer interaction between the main channel and the flood plain water.

4.4.3 Discharge parameters for individual flow zones

4.4.3.1 Zonal F (for Zones A, B and C)*

When the acquisition of comprehensive local flow velocity measurements, enables the discharge capacity of each zone in a meandering compound channel to be calculated, a zonal discharge coefficient, $F_{A,B,C}^*$, can be determined separately for each flow zone in a meandering compound channel. The formulation defined in Equation 4.4 is used.

$$F_{A,B,C}^* \equiv \frac{\text{Actual measured discharge}(Q_{mA,mB,mC})}{\text{Theoretical discharge based on bed friction only } (Q_{A,B,C})} \quad [4.4]$$

The measured discharge capacity, Q_{mA}, in each zone is divided by the theoretical discharge capacity of each zone, Q_A, which is calculated by assuming that only bed friction contributes to flow resistance.

4.4.3.2 Zone A discharge measured using the adjustment coefficient, Q_A'

James and Wark [1992] investigated variations in the discharge capacity of Zone A in overbank flow. They used an alternative non-dimensional measure of discharge which was known as the adjustment coefficient, Q_A'. During overbank flow the discharge in Zone A is less than bankfull discharge, Q_{bf}, for the majority of flow depths encountered. The average Zone A discharge during overbank flow, Q_A, can be related to the bankfull discharge by a non-dimensional adjustment coefficient, Q_A', as shown in Equation 4.5.

$$Q_A = Q_A' * Q_{bf} \quad [4.5]$$

James and Wark [1992] developed linear regression models to model the relationship between Q_A' and 4 meandering compound channel parameters: relative depth, RD, aspect ratio, AR, relative roughness, f', and sinuosity, r.

*4.5 The influence of 11 key parameters on Global flow resistance, Global F**

4.5.1 Introduction

The author identified 11 key non-dimensional parameters in the literature review which were thought to influence the nature and magnitude of the layer interaction mechanisms in meandering compound channels. The analysis presented in this section has adopted the measure of Global F* to separate the contribution of bed friction flow resistance from the flow resistance generated by interaction between the main and flood plain channels. Plots of relative depth and/or flow depth versus Global F* were used to explicitly reveal the magnitude and variation of the layer interaction losses with each parameter.

4.5.2 The influence of relative depth on global flow resistance

4.5.2.1 Introduction

Figure 4.7 shows the relationship between relative depth and Global F* which was obtained in three typical models tested in Glasgow during the Series B extension programme:- G75T90R, GR75T90R, G25T45R.

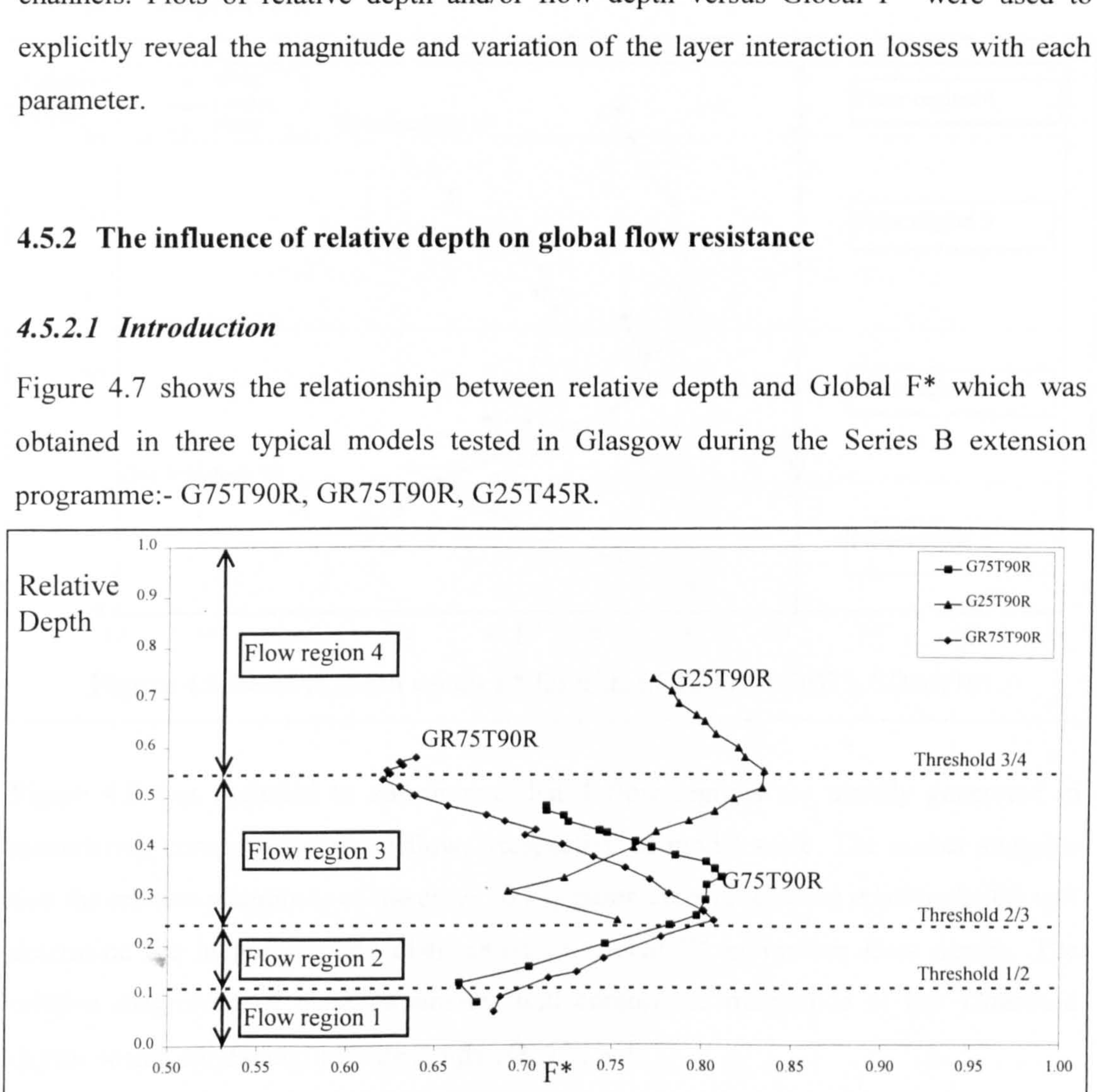

Figure 4.7 Relative depth versus F* for tests G75T90R, G25T90R and GR75T90R

Three distinct regions of flow, sometimes four, can be identified in each of the plots. Within each of these flow regions the rate of increase or decrease of Global F* remains

approximately constant with increasing relative depth. The flow depths which mark the transition depth at the interface between flow regions 1 and 2, 2 and 3 and 3 and 4. The author named these interface depths: Thresholds 1/2, 2/3, 3/4 respectively.

Figure 4.8 shows 3 plots of relative depth versus Global F* which were selected from existing flow data sets collected during the Series B extension programme. These plots were taken from:- SDB25 (Series B (1989-1992)), SDAB102 (Aberdeen [1991]), and SDKI301 (Kiely [1989]). The parameter details of each model are given in Tables 2.6, 2.8 and 2.5 respectively.

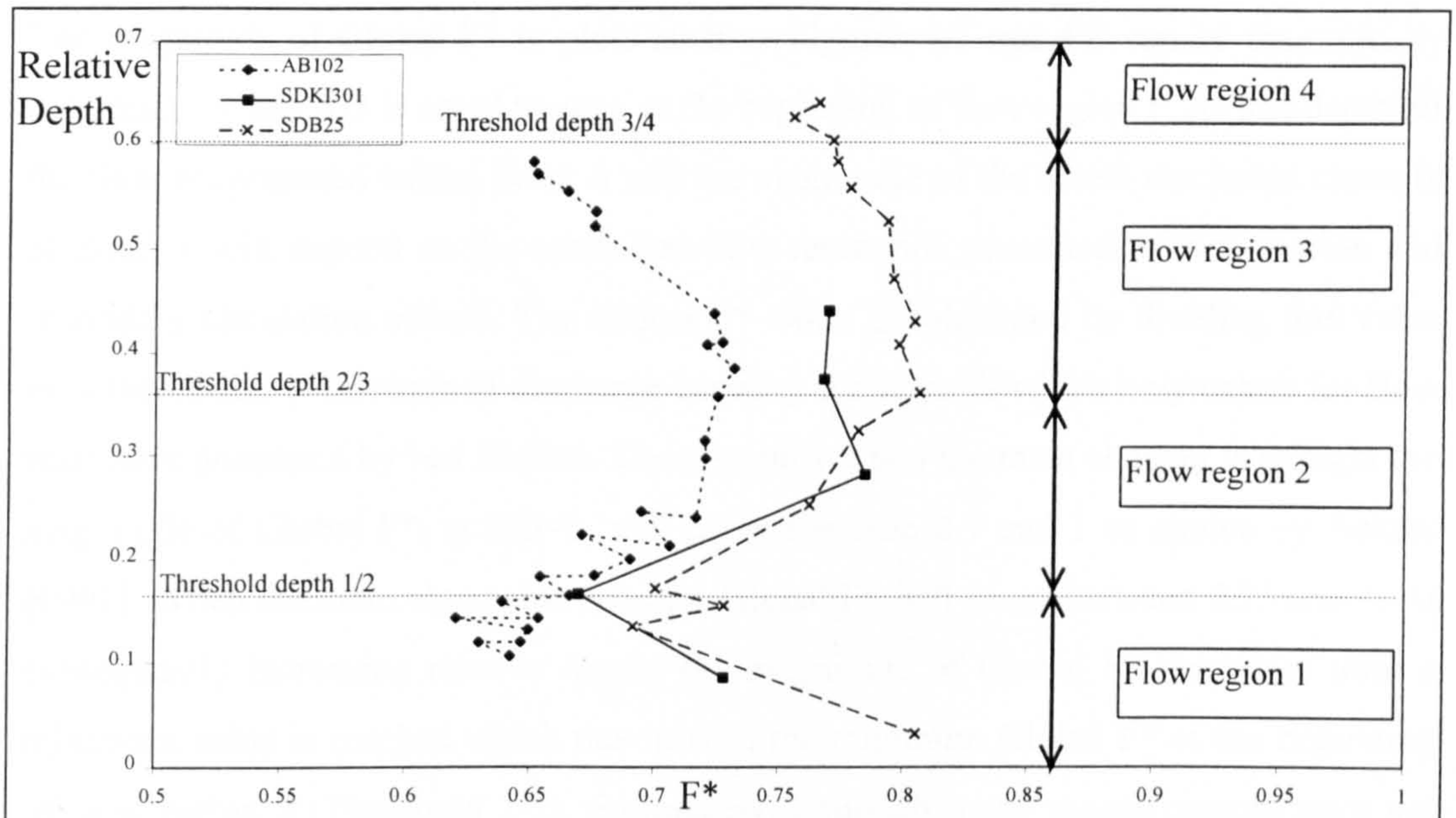

Figure 4.8 Relative depth versus F* for tests SDKI301, SDB25, SDAB101.

Figure 4.8 was included to corroborate that 4 flow regions are usually generated in meandering compound channel flow, irrespective of model scale. The author suggests that the relative magnitude of the other 10 key parameters (excluding relative depth) will determine the magnitude and distribution of Global F* at various flow depths. The relative magnitude of these parameters will control the magnitude of the Threshold depths which correspond to Thresholds 1/2, 2/3, 3/4.

4.5.2.2 The characteristics of flow region 1

In Glasgow (during the Series B extension experiments) special attention was given to obtaining flow data at low relative flow depths in acknowledgement of the

recommendations made by James and Wark [1992]. The majority of natural flood events occur at low flood plain flow depths so it was vital to ensure that, during the Series B extension programme the nature of flow behaviour in flow region 1 was investigated further. A range of Global F* measurements was difficult to obtain in these scale models in flow region 1 because it typically extended over such a limited range of flow depths. As a result the majority of the significant new information was gathered to demonstrate zonal flow behaviour data at these flow depths, data which was in short supply prior to the Series B extension programme.

The magnitude of Global F* in plots such as Figures 4.7 and 4.8 can be theoretically determined when RD is equal to zero, at the beginning of flow region 1. At this depth all the flow is contained within Zone A and the magnitude of the actual discharge capacity of Zone A will depend on the combined flow resistance generated by bed friction and secondary circulation effects. The Global F* value is calculated by dividing this value by a theoretically-determined discharge capacity for Zone A which only caters for flow resistance generated by bed friction. Consequently when the main channel is straight the magnitude of Global F*, at RD=0, will range between 0.9 and 1 as shown by Ackers [1991]. When the main channel is sinuous, Global F* will range between 0.75 and 1. At subsequently increasing relative depths the magnitude of Global F* decreases until a minimum value is reached which ties-in with the minimum Global F* at the beginning of flow region 2 (Threshold 1/2). Fortunately, although many measurements were not obtained within flow region 1, the majority of model tests did reveal evidence for the onset of the changing Global F* behaviour in the vicinity of Threshold 1/2 thus fixing the other end of flow region 1.

The rapid decrease in magnitude of Global F* over a small range of increasing relative flow depths in flow region 1, indicates that the proportion of flow resistance caused by flood plain / main channel (layer) interference rapidly increases with increasing relative depth. The lowest Global F* value yet observed in experiments (which coincides with Threshold 1/2) is equal to 0.4. This indicates that the total discharge rate is only 40% of that computed using bed friction alone.

4.5.2.3 The characteristics of flow region 2

Figures 4.7 and 4.8 illustrate the typical behaviour of flow region 2 which is exhibited after Threshold 1/2 has been attained. Global F* increases throughout flow region 2 for increasing flow depths. This indicates that the proportion of flow resistance which is attributable to flow layer interaction steadily decreases. The end of flow region 2 is distinguished by Global F* attaining a maximum value at Threshold 2/3.

4.5.2.4 The characteristics of flow region 3

Figures 4.7 and 4.8 illustrate the typical flow behaviour of flow region 3 which is exhibited after the Threshold 2/3 has been attained. Over flow region 3 Global F* decreases again for increasing flow depths. This indicates that the proportion of flow resistance generated by layer interaction is again steadily increasing. The magnitude of Global F* decreases steadily until Threshold 3/4 is reached. Threshold 3/4 corresponds to the flow depth at which Global F* stops decreasing and starts to increase once again.

4.5.2.5 The characteristics of flow region 4

The plot of relative depth versus Global F* for GR75T90R in Figure 4.7 presents an indication of the existence of the fourth flow region which is initiated after Threshold 3/4 has been attained. The author suggests that in flow region 4 the magnitude of Global F* tends towards 1 as relative flow depth tends towards 1. The increase in Global F* magnitude indicates that the proportion of flow resistance contributed by layer interaction decreases in comparison with the bed friction effects. The compound channel is beginning to behave like a simple channel (with no interaction losses). Ackers [1991] introduced a parameter called coherence (defined in Equation 2.45) which was a measure of the similarity between the flow resistance generated in a compound channel and a simple channel, a measure similar to Global F*. Figure 4.9 shows a plot of relative depth versus Global F* for G25T45S.

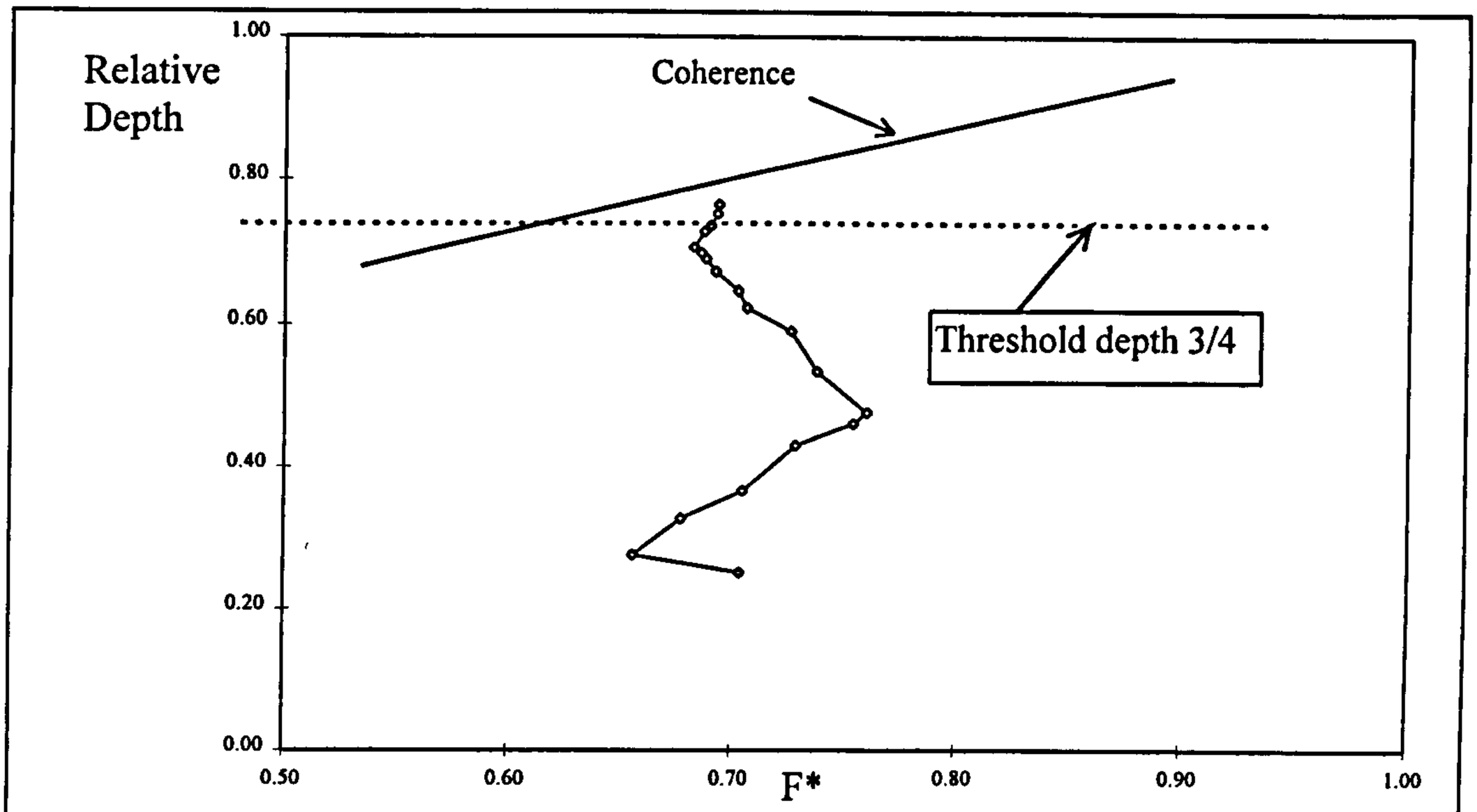

Figure 4.9 Relative depth versus Global F* for G25T45S

The plot of relative depth versus Global F* also indicates the presence of flow region 4 behaviour. The Global F* plot is combined with a plot of relative depth versus coherence and both parameters appear to illustrate the onset of simple channel-like flow behaviour by meandering compound channels at high flow depths.

4.5.2.6 A comparison between meandering and straight compound channels

Similar patterns of 4 flow region behaviour were observed in the both the straight compound channels, described by Ackers [1991], and the meandering compound channels. The magnitude of the extra flow resistance, caused by the interaction mechanisms in straight compound channels, was assessed using a quantity called DISADF which was defined a similar way to Global F* as shown in Section 2.6.3.3. Figures 4.10 and 4.11 show the typical variation of relative depth with Global F* and DISADF for both channel types.

The minimum value of Global F* measured was significantly less than the minimum value of DISADF. The interaction mechanisms in meandering compound channels have a more significant effect than in the straight compound channel. However, the similarity in the pattern of behaviour indicates that there may be certain similarities between the

critical flow conditions which must prevail in order to obtain the changes in interaction behaviour which are indicated by the presence of the Threshold depths.

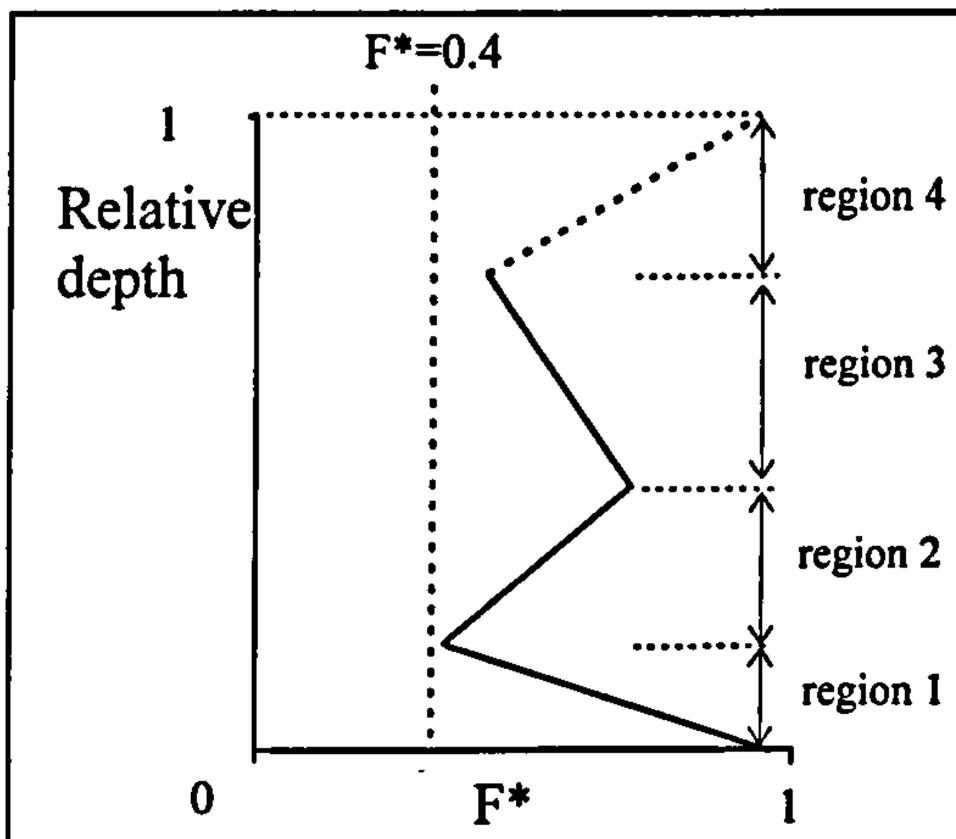

Figure 4.10 Meandering compound channel

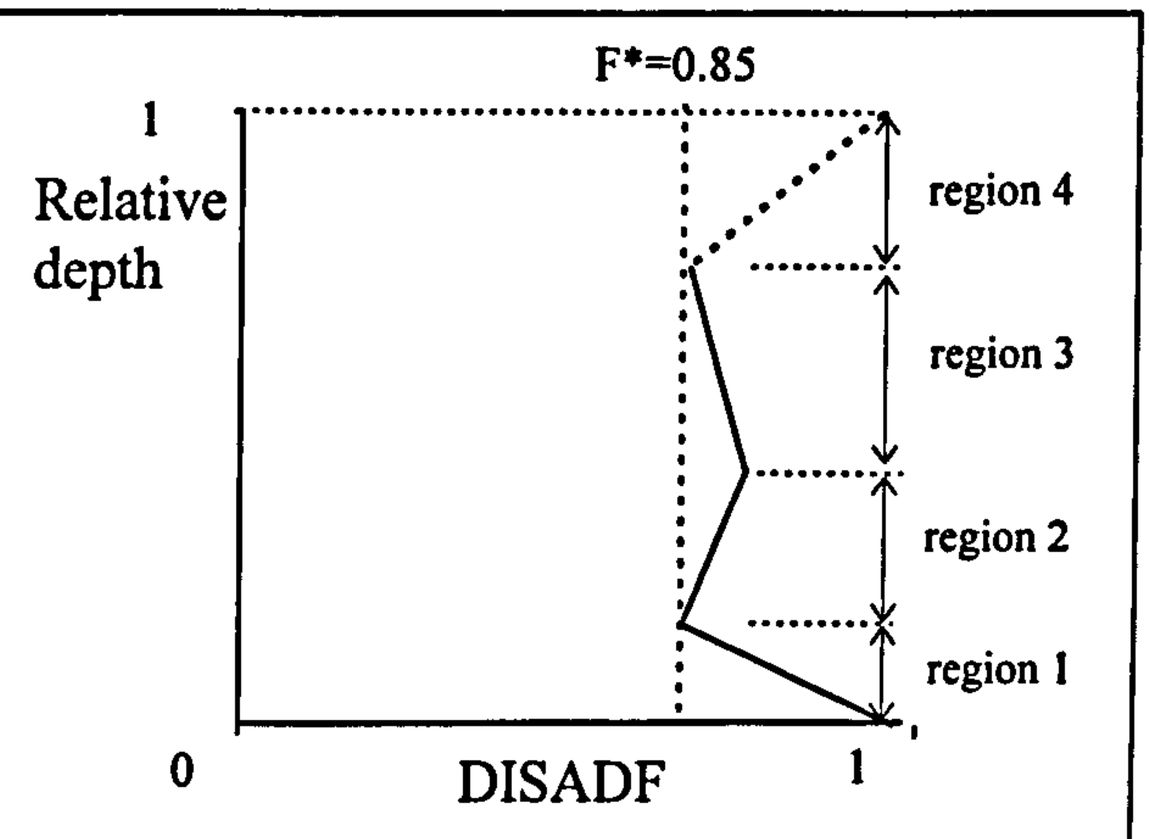

Figure 4.11 Straight compound channel

4.5.3 The influence of model scale on global flow resistance

4.5.3.1 The influence of model scale on discharge capacity

The use of small scale models during the Series B extension programme meant that it was possible to test many more model configurations than were tested during the Series B programme (1989-1992). However the programme's participants were concerned that these scale differences might drastically affect the flow behaviour in the models irrespective of the similarities in overall planform and cross-sectional configuration, making it difficult to compare, contrast and eventually combine the flow results obtained from different scale models in order to produce quantitative discharge capacity prediction methods. Consequently the influence of scale was explicitly assessed as part of the Series B extension programme by comparing the flow results from the Series B model SDB21 and an exact 1:6 cross-sectional and planform scale model which was built in Glasgow, namely G25T45S. Both scales of model were built with hydraulically smooth surfaces for which similar modified smooth law equations had been derived (as shown in Tables 4.1 and 4.2). These equations can be used to determine accurate predictions for the flow resistance generated by bed friction that is exerted by each of the model surfaces.

The length scale ratio, L_r, between the models was equal to 6/1 which resulted in the Reynolds number scale ratio, Re_r being equal to $(6)^{3/2}$ in the larger scale models. The

modified smooth equation showed that an increase in Reynolds number results in a lowering of the bed frictional resistance. Consequently the flow in a smaller scale model will experience greater frictional resistance at the same relative depth compared with the flow in a larger scale model, even if the same model surface is used. The impact of this phenomenon can be clearly seen by comparing the Manning's n values in the two models. Both models register Manning's n values for the smooth surfaces equal to 0.01, at most relative depths. However, because the Manning's n is also scaled by $L_r^{1/6}$ = 1.348, where the Manning's n in G25T45S is equal to 0.01, this is equivalent to a Manning's n equal to 0.01348 in SDB21.

Figure 4.12 shows the impact of the bed friction discrepancies. It shows plots of relative depth versus the theoretical and measured discharge capacities for both scales of model.

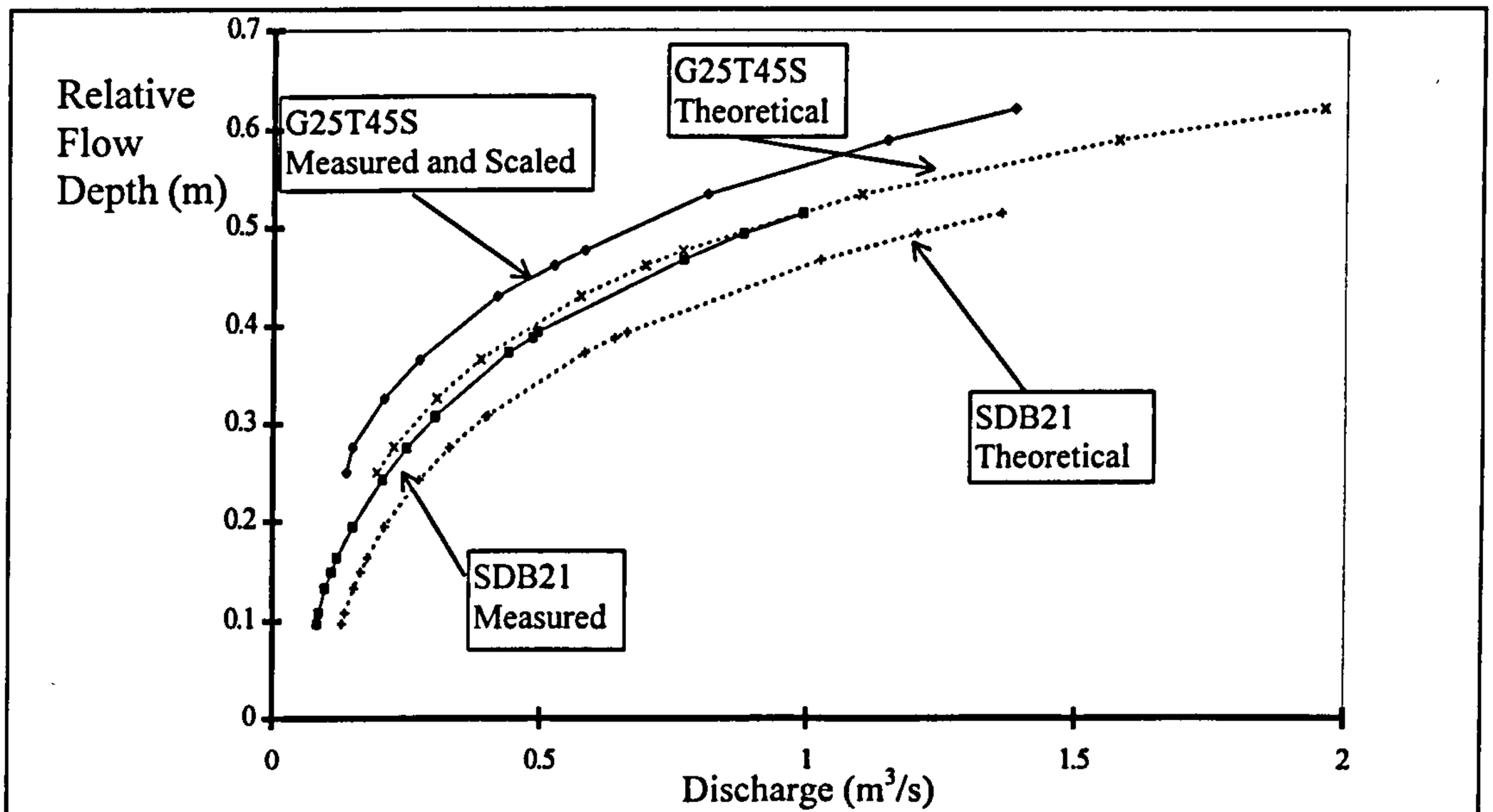

Figure 4.12 Flow depth versus Discharge capacity: Different scale models

The discharge values for G25T45S were scaled using the discharge scale ratio, Q_r , which was equal to $(6)^{5/2}$. The theoretical discharge was calculated by dividing the meandering compound channels into zones using the vertical division line method and only accounting for bed friction.

The disparity between the theoretical and measured discharges of the two scale models appears to be about the same magnitude, between 20% and 35%, which is attributable to the interaction mechanisms between the flow layers in meandering compound channels

causing extra head loss. The significant difference between the two measured discharge values is mainly due to the discrepancy in scaled Manning's n and obscures the evidence illustrating the presence of different layer interaction mechanisms in the two different scale models. Consequently the author produced plots of relative depth versus Global F* in order to strip out the bed friction effects and to facilitate an explicit comparison between the relative influence of layer interaction in meandering compound channel models with scaled geometric configurations.

4.5.3.2 Global F versus relative depth: The influence of model scale*

Figure 4.13 shows a plot of relative depth versus Global F* for two models: SDB21 and G25T45S. Similar patterns of overall flow behaviour are demonstrated in both plots.

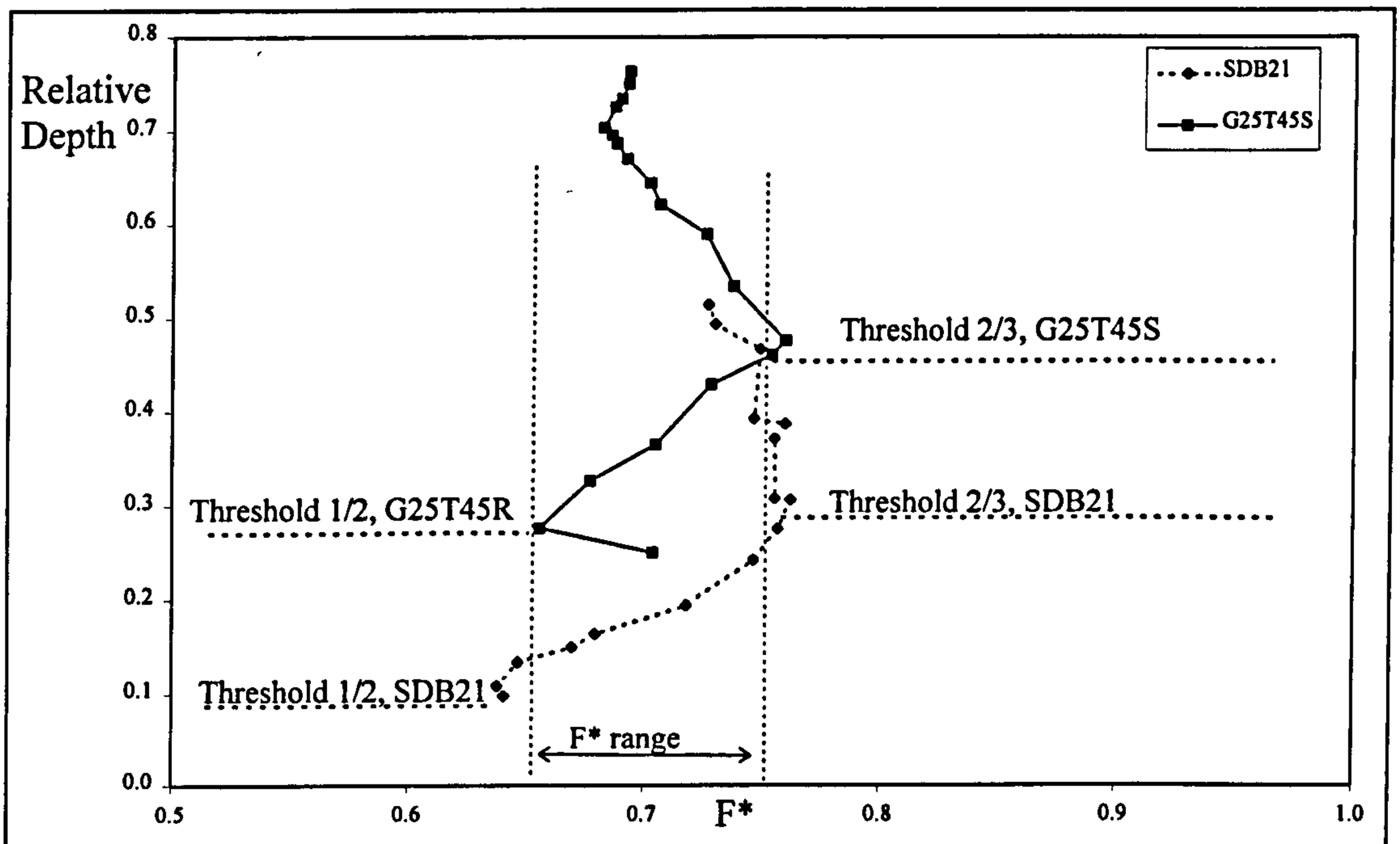

Figure 4.13 Relative depth versus Global F* for G25T45S and SDB21

Both sets of model results demonstrate the characteristic 3 - 4 flow region behaviour, which were exhibited in Figures 4.8 and 4.9 and are characteristic of meandering compound channel flow. The Threshold depths can also be clearly observed. Figure 4.14 plots overbank flow depth versus Global F* for SDB21 and G25T45S. The flow depths which correspond to the Threshold depths can once again be clearly identified together with the familiar 3 - 4 flow region behaviour.

Significantly the minimum Global F* value at the end of flow region 1 (Threshold 1/2) and the maximum Global F* value at the end of flow region 2 (Threshold 2/3) are shown to be similar in magnitude for both scales of model, G25T45S and SDB21. The similarity in Global F* magnitude implies that proportion of flow resistance generated by layer interaction is similar in magnitude in both scales of model. Consequently the author inferred that similar dominant flow interaction mechanisms are generated in each flow region, irrespective of scale, which meant that it was possible to compare flow results form different scale models.

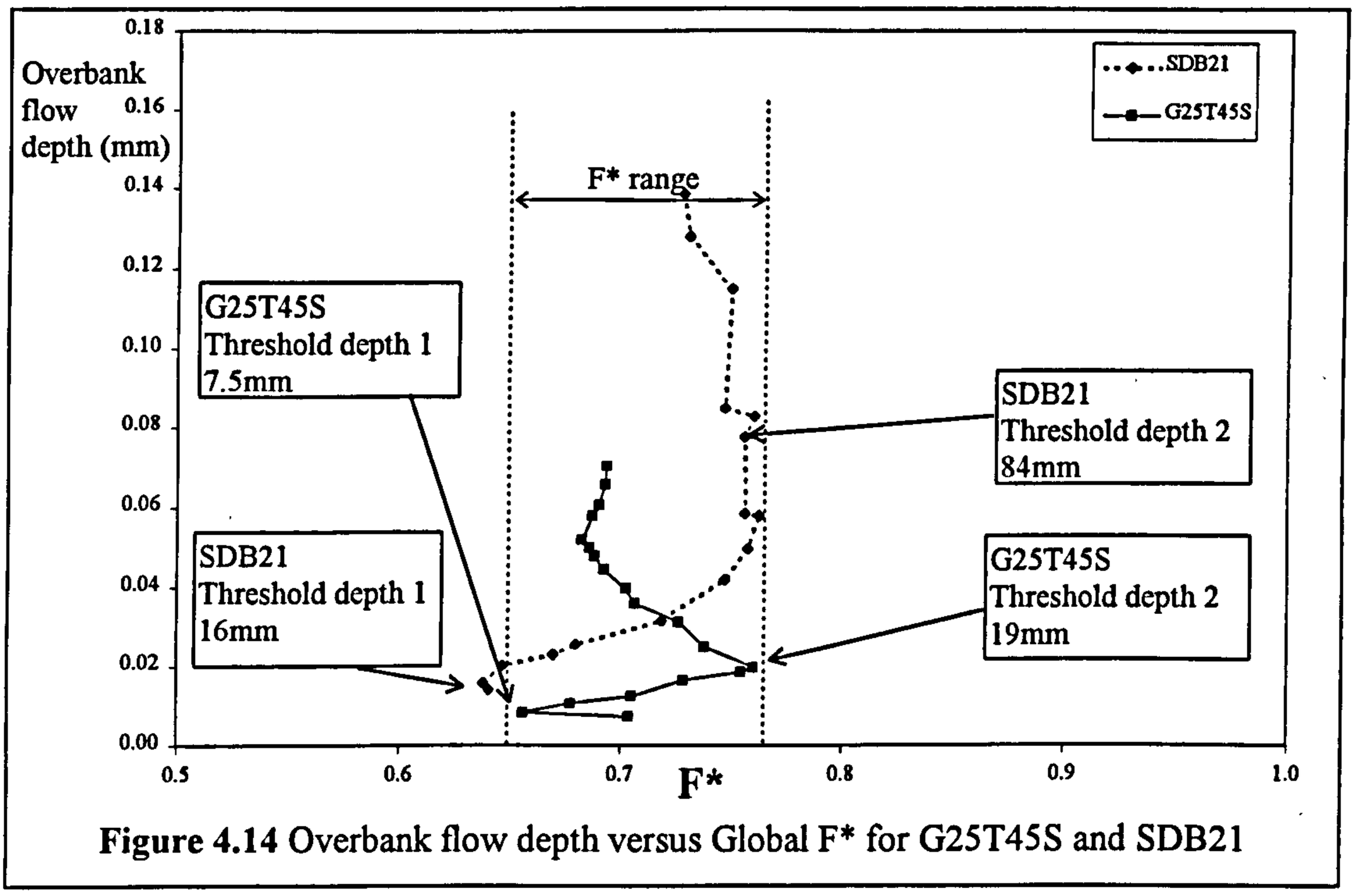

Figure 4.14 Overbank flow depth versus Global F* for G25T45S and SDB21

However the author also noted that there were differences in the Threshold depths, marking the onset of each flow region, in each model. The author postulated that the onset of different interaction mechanisms caused the creation of the different flow regions and that the depth at which each interaction mechanism was initiated was dependant on the relative flow state between the main and flood plain channels. The author suggests that the Threshold depths simply corresponded to the relative depths and/or flow depths at which critical relative flow states were established.

The significant differences in the magnitude of bed friction resistance exerted by the flood plains at the same relative flow depths in different scale models and the greater energy levels associated with Zone A flow in large scale models were thought to cause

the relative flow states to vary with relative depth in the different scale models. The author notes that the influence of the other key parameters will influence the relative flow state at different relative depths.

4.5.4 The influence of relative roughness on global flow resistance, Global F*

4.5.4.1 Introduction

Over the years, two substantial sets of flow data have been produced, by the Vicksburg [1956] and the Series B (1989-1992) programmes, to demonstrate the influence of relative roughness on flow behaviour in meandering compound channels. The original analyses of these data sets predominantly concentrated upon demonstrating the effect of relative roughness on total discharge capacity and overall flow resistance. They demonstrated that the flow resistance in a meandering compound channel generally increases for increasing relative roughness. They did not separate bed friction effects from the layer interaction effects. Consequently the author re-analysed the original data using plots of flow depth (and relative flow depth) versus Global F* in order to determine explicitly the influence of relative roughness on the extra flow resistance caused by layer interaction. The results from the existing data sets were compared with those obtained during the Series B extension programme.

4.5.4.2 Existing flow data sets

The Vicksburg [1956] data required cautious analysis because the roughness calibration data which was supplied with the published stage-discharge data was limited and unreliable. One value of Manning's n was supplied for each of the three flood plain surfaces. All the surfaces, especially those with the expanded metal sheets will have actually demonstrated Manning's n values that will have varied with flow depth. Consequently it was decided that that the Vicksburg [1956] data should not be used for developing prediction methods based on Global F* because the accuracy of the F* methods depends so much on accuracy of the friction calibration. Consequently, the Vicksburg [1956] data was used predominantly as a test set. Figure 4.15 shows plots of overbank flow depth versus Global F* for 4 models from the Series B (1989-1992) tests: SDB25, SDB34, SDB39 and SDB43. SDB25 had smooth flood plains and SDB34 had

dowel rod roughened flood plains. They had identical planform and cross-sectional configurations with main channel sinuosities equal to 1.374. Similarly SDB39 had smooth flood plains and SDB43 had dowel rod roughened flood plains. They also had identical planform and cross-sectional configurations but with main channel sinuosities equal to 2.043.

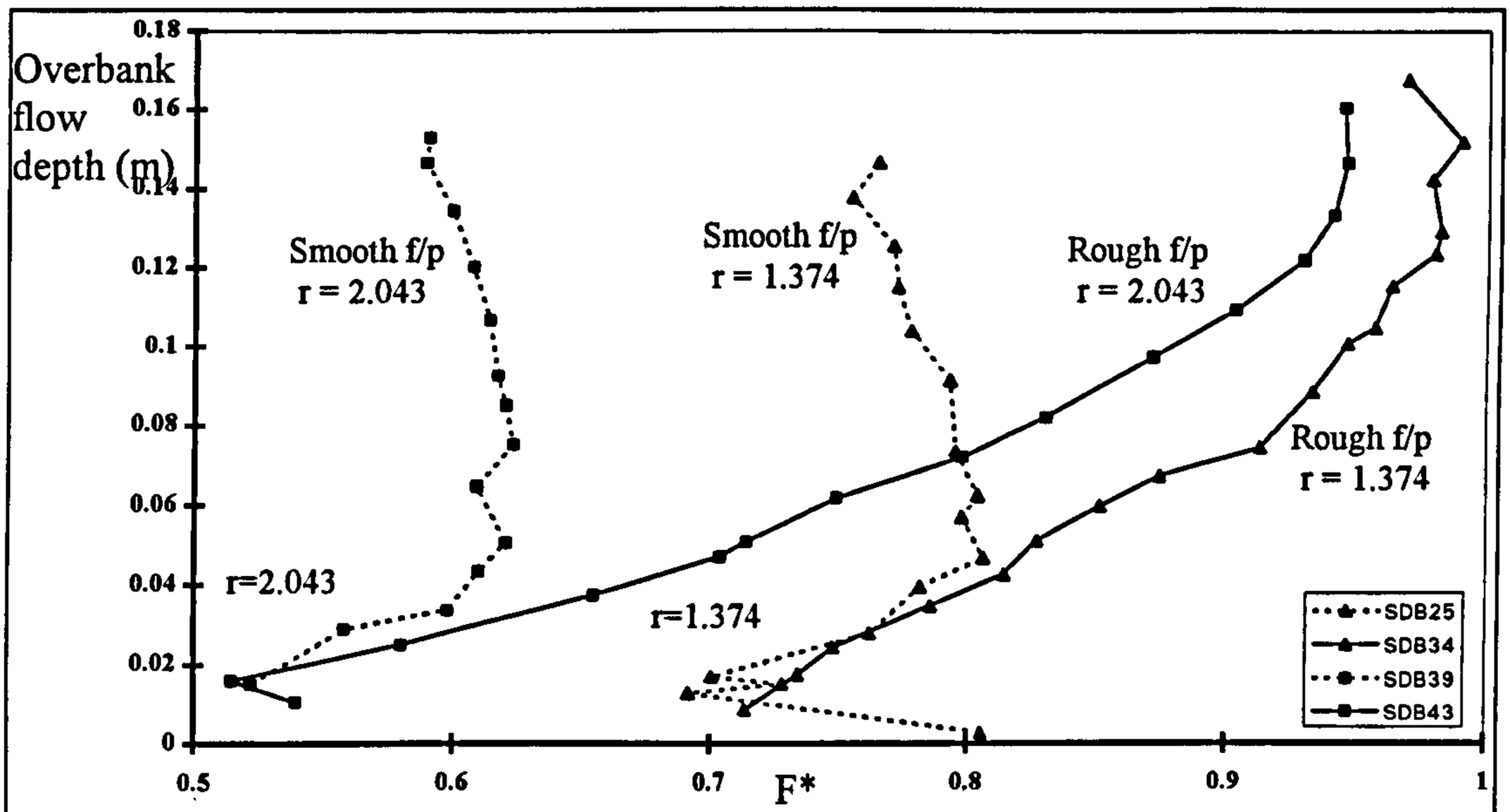

Figure 4.15 Flow depth versus Global F* for SDB25, SDB34, SDB39 and SDB43

The combination of smooth surfaces, on the flood plains and in the main channel, for SDB25 and SDB39, generated a relative roughness, f' (where $f' = f_{fp}/f_{mc}$) close to 1 at most flow depths. This ratio is unrepresentative of natural channels where the flood plains are generally much rougher than the main channel. Consequently SDB34 and SDB43 were built during the Series B (1989-1992) programme with their flood plain surfaces roughened with dowel rods, in an attempt to produce a relative roughness which was more similar to those encountered in nature.

Figure 4.15 shows that the trends in the relative depth versus Global F* plots caused by varying relative roughness in the two sets of models are similar at all flow depths, irrespective of the sinuosity of the main channel. Relative roughness has a limited influence in flow regions 1 and 2 but variations in relative roughness has a significant effect in flow region 3. The reduction in magnitude of Global F* with increasing flow depth in flow region 3, which is observed in the majority of model results, is not

developed in the models with dowel rod roughened flood plains and high relative roughness. The author deduces that in models with highly roughened flood plains, the significant layer interaction mechanisms which are typically generated in flow region 3 are either not generated or if they are, they are overwhelmed by the dominant influence bed friction effects

The author decided that results obtained from models with dowel rod roughened flood plains, although interesting were unlikely to replicate common flow behaviour in nature. Dowel rods will only simulate a flood plain covered in closely spaced trees for which the flow resistance, caused by bed friction and blocking, increases monotonically with increasing flow depth. In many natural channels the flood plains are predominantly grassy and dowel rods do not accurately model the variation of bed roughness. Grassy flood plains will exhibit large flow resistance at low flow depths but because the flow depth increases, eventually, the majority of the vegetation will be over-topped. The grass will be flattened by the weight of water and an ever-increasing depth of unimpeded flow will be developed over the top of the grass level, causing a reduction in the proportion of frictional resistance to flow, and the measure of flow resistance (Manning's n) will decrease to a constant minimum value. The typical variation of flow resistance with flow depth was illustrated in Figures 2.15 and 2.16.

The Series B extension tests were conceived so that the majority of models which were built with roughened flood plains exhibited variations of flow resistance with flow depth which were more typical of grass dominated flood plains. This was achieved by roughening the flood plain with push-pins.

4.5.4.3 The Series B extension results (Aberdeen)

Five millimetre diameter push-pins were used in the models that were built during the Series B extension programme in order to replicate the variation in flow resistance with flow depth found on natural flood plains. The push-pins were arranged in triangular configurations to generate particular relationships between the flow depth and Manning's n. Figure 4.16 shows a plot of Manning's n versus flow depth for push-pins with 60mm spacing. The flow characteristics are similar to those found with natural

flood plains. Manning's n increases for increasing flow depth over low flow depths until it reaches a maximum value and then decreases for further increases in flow depth.

The team in Aberdeen had the primary responsibility for investigating the influence of relative roughness. They investigated the effect of changing flood plain roughness. However, some tests were also performed in Glasgow where the relative roughness was altered by changing both flood plain and main channel roughness. There was a free exchange of data between Glasgow and Aberdeen during the Series B extension programme and so both sets of results are presented.

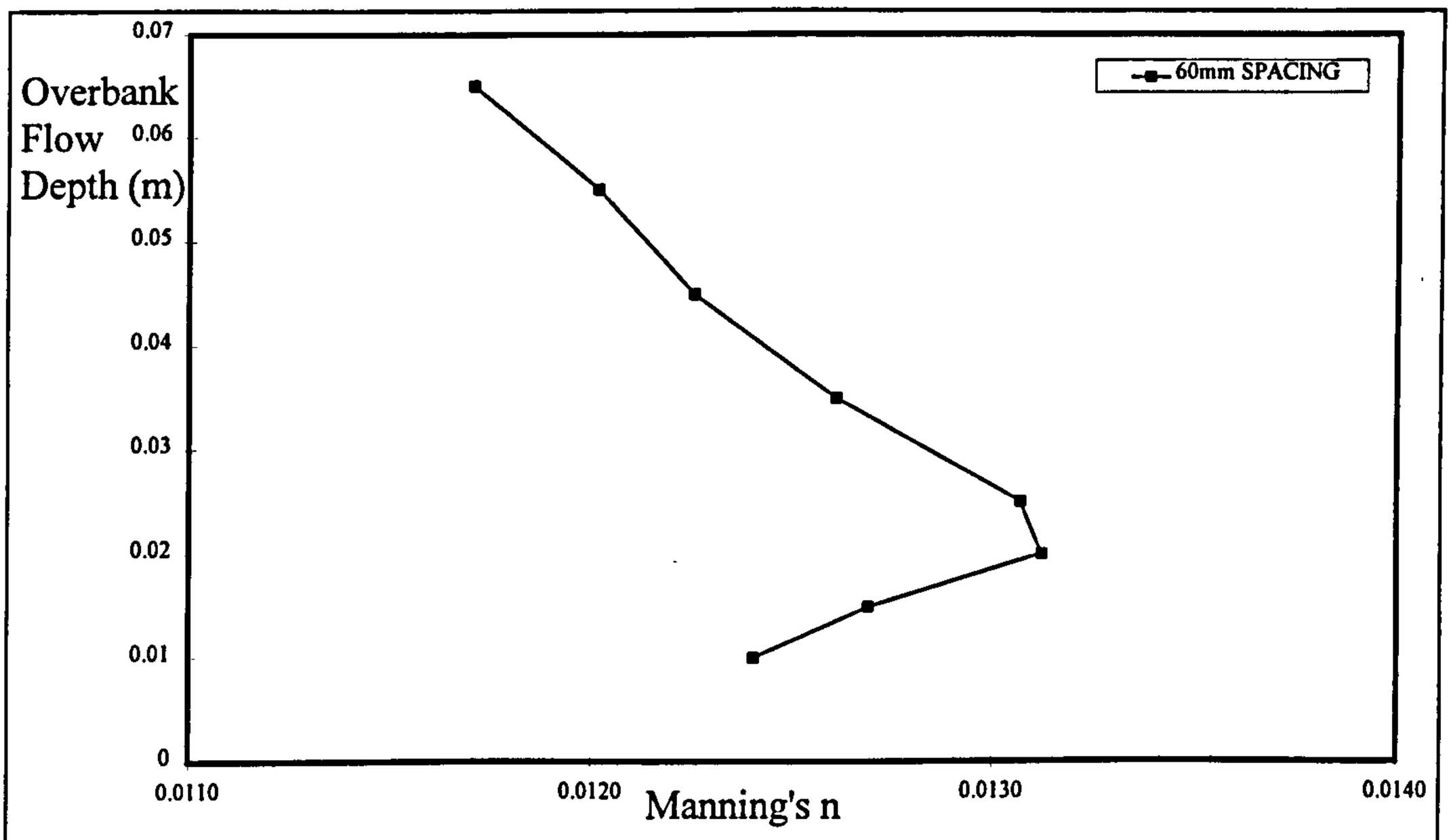

Figure 4.16 Flow depth versus Manning's n for 60mm spaced push-pins

Figures 4.17 plots overbank flow depth versus Global F* for 2 sets of the Aberdeen model tests: A2N1000S, A2N1000A, A2N1000B which had sinuosities of 1.774 and Smooth, Rough A and Rough B flood plain surfaces, and A3N1000S, A3N1000A and A3N1000B which had sinuosities of 1.111 and the same flood plain surfaces. Figure 4.17 reveals that the variation of overbank flow depth with Global F* is similar in flow region 1 and 2, irrespective of the relative roughness of the model, which concurred with the Series B (1989-1992) results. However, unlike the Series B results Aberdeen models, with roughened flood plains, clearly exhibited the presence of flow region 3 behaviour. In addition there is evidence to demonstrate that flow region 3 is initiated at higher flow depths in models with higher relative roughness (e.g. Rough B) and that the

magnitude of Global F* is greater (and the rate of reduction of Global F* is marginally smaller in models) in models with high relative roughness (e.g. Rough B).

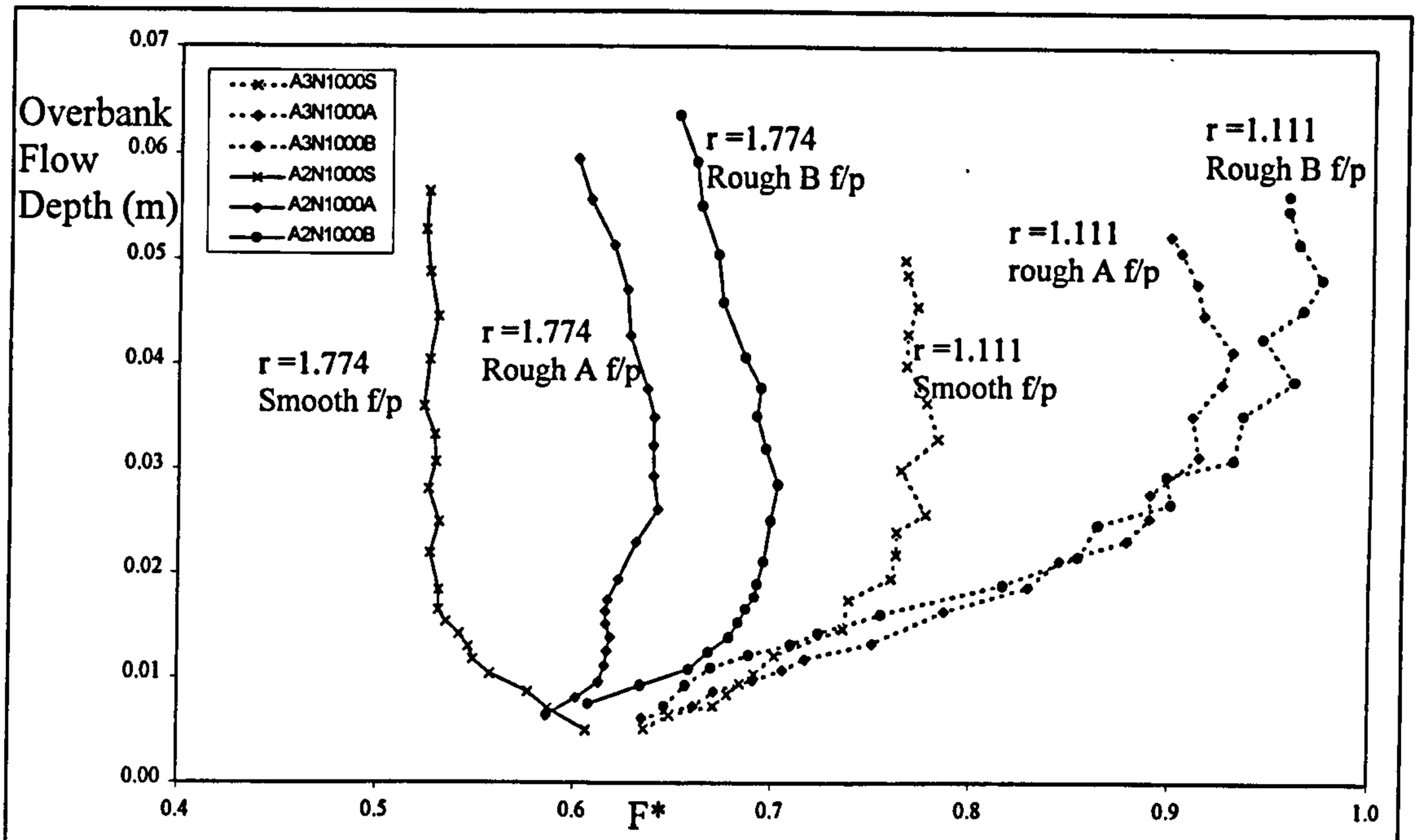

Figure 4.17 Flow depth versus Global F* for variable Relative Roughness (Aberdeen)

The plot of overbank flow depth versus Global F* for A2N1000S produces one significantly anomalous result. Flow region 1 is indistinguishable from flow region 3. There is no evidence for the existence of flow region 2. The author postulates that Thresholds 1/2 and 2/3 occur at such similar depths that flow region 2 becomes insignificant and therefore does not show in the plots of relative depth versus Global F*.

4.5.4.4 The Series B extension results (Glasgow)

Figures 4.18 plots overbank flow depth versus Global F* for G75T90S, G75T90R and GR75T90R Both the flood plain and main channel roughnesses were altered in these models. G75T90S had a smooth main channel and flood plains, G75T90R had a smooth main channel and Rough B flood plains and GR75T90R had a Rough B main channel and flood plains. Figure 4.18 further illustrates the influence of relative roughness on Global F* and largely concurs with the Aberdeen results. Flow regions 1 and 2 show similar patterns of flow behaviour for all the models. The magnitude of Global F* is however marginally smaller in the model with smooth flood plains compared with the models with rough flood plains. Flow region 3 is initiated at different flow depths for

models with different flood plain roughness, G75T90S and G75T90R but at a similar flow depth for models with similar relative roughnesses at all flow depths, G75T90S and GR75T90R, even though the absolute roughnesses of the main channel and flood plains were very different.

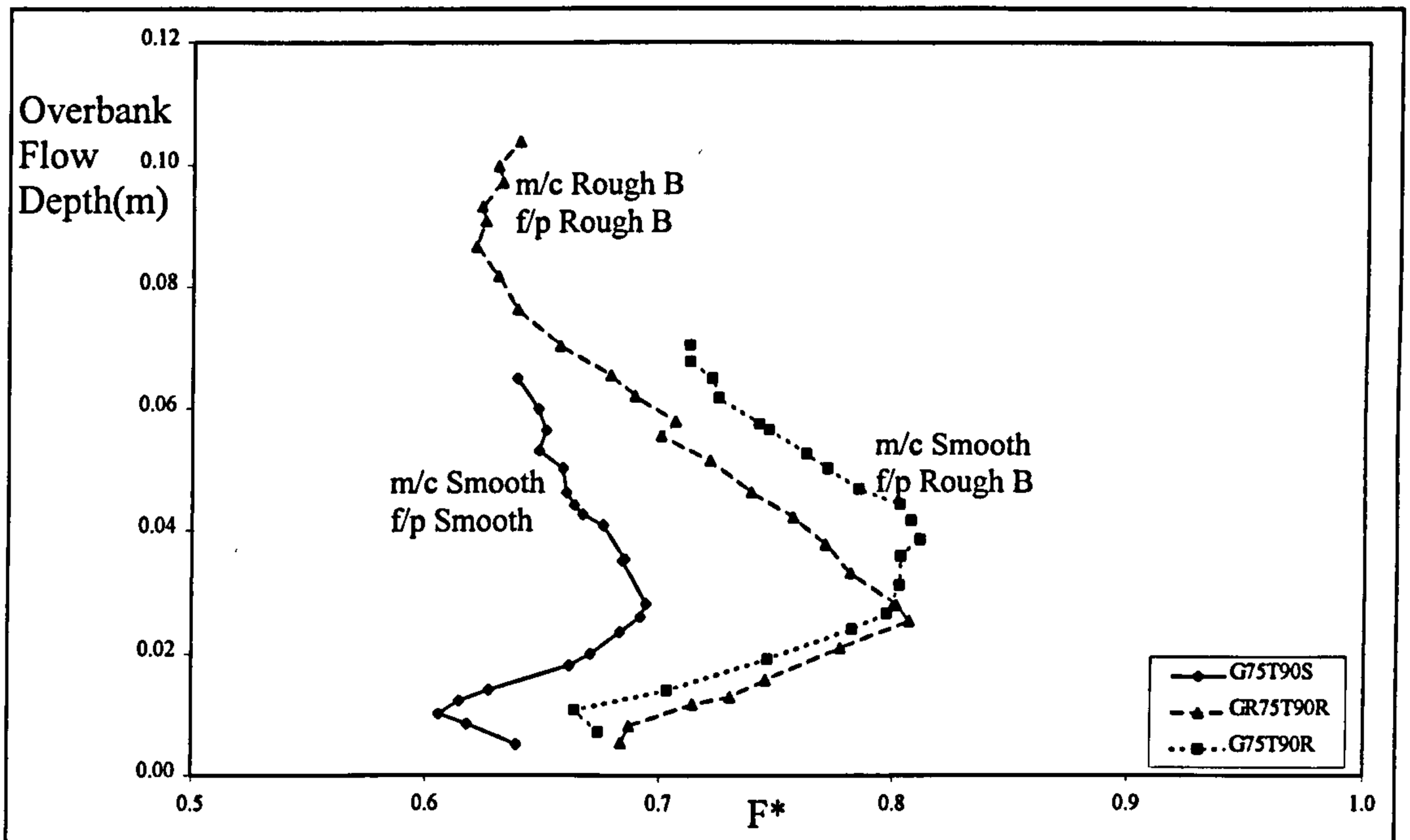

Figure 4.18 Flow depth versus Global F* for G75T90S, G75T90R, GR75T90S

The rate of reduction of Global F* in flow region 3 is greater for GR75T90R than for G75T90S even though it has been shown in the Aberdeen models that the rate of reduction of Global F* with flow depth was greater for the models with smooth flood plains. The author suggests that the roughening of the main channel (reduction of the bankfull main channel velocity) causes the layer interaction mechanism in flow region 3 to be more significant in models with rough rather than smooth main channels.

The results from the relative roughness tests provide further corroboratory evidence for the author's conjecture that the relative flow state in the main and flood plain channels control the relative dominance of various flow mechanisms. The author postulates that the transition between these flow mechanisms is signalled by the Threshold depths which occur at different flow depths depending on the relative flow state.

4.5.5 The influence of main channel aspect ratio on global flow resistance

4.5.5.1 Introduction

The influence of main channel aspect ratio (width/depth) on meandering compound channel flow has been investigated in two previous experimental programmes: Toebes and Sooky [1967] and Series B (1989-1992). The boundary roughness calibration data for Toebes and Sooky [1967] was unreliable which meant that any retrospective analysis using Global F* may be inaccurate. Consequently the author's back-analysis of the effect of aspect ratio on the variation of flow depth versus Global F* concentrated on the Series B (1989-1992) results

4.5.5.2 Existing flow data sets

Figure 4.19 plots overbank flow depth versus Global F* for SDB21 and SDB25 from the Series B (1989-1992) programme. SDB21 had a trapezoidal main channel with an aspect ratio equal to 9.14 and SDB25 had a quasi-natural main channel with an aspect ratio equal to 14.6. Otherwise they had identical planform and cross-sectional configurations.

The author observed that the magnitude of Global F* was greater for the natural channel at all flow depths. Ervine et al [1993] postulated that this behaviour resulted from the different flow behaviour mechanisms generated in trapezoidal and natural channels. The author acknowledged that this was a possibility but observed that because the natural channels had been constructed by placing inserts into the trapezoidal channel the aspect ratio of the natural channel was considerably larger than that of the trapezoidal channel, which is likely to have been influential. The Series B extension programme was devised to investigate the effect of aspect ratio and channel shape independently in order to clarify the precise effect of these two parameters on flow behaviour.

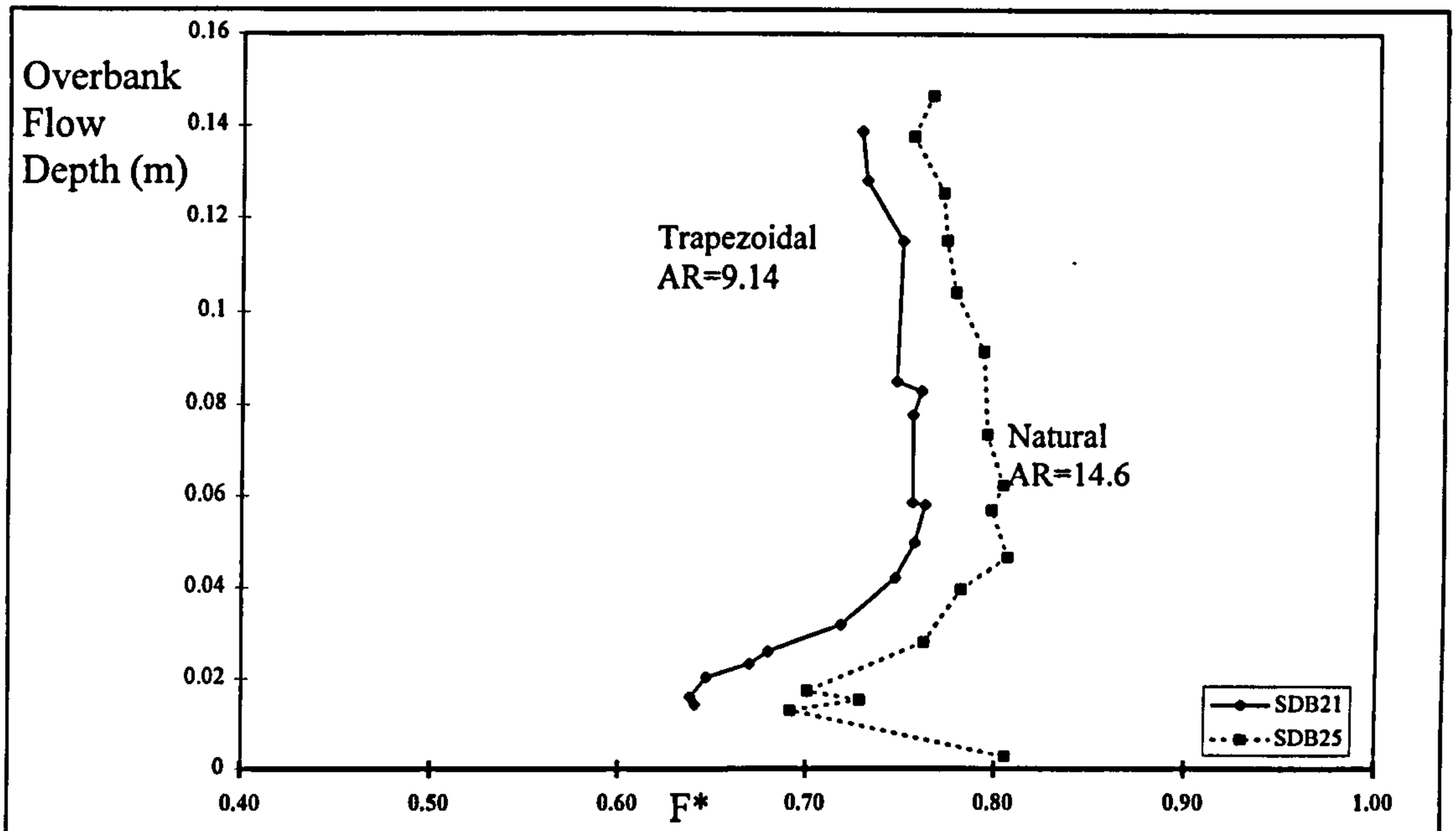

Figure 4.19 Flow depth versus Global F* for aspect ratios equal to 9.143 and 14.6

4.5.5.3 Series B extension results

Some results from the work performed in Glasgow during the Series B extension programme are shown in Figures 4.20 and 4.21 which plot overbank flow depth versus Global F* for two sets of trapezoidal channels with varying aspect ratios. One set had 90° side slopes and the other had 45° side slopes. The aspect ratio of the main channel was varied by raising the bed level of the main channel so that the maximum depth of the channels was equal to either 75mm, 50mm or 25mm. The models in Figure 4.20: G75T90R, G50T90R, G25T90R had aspect ratios equal to 2.7, 4.0, 8.0 respectively. The models in Figure 4.21: G75T45R, G50T45R, G25T45R, had aspect ratios equal to 4.3, 5.33 and 9.14.

The magnitude of Global F* was smaller for a main channels with a low aspect ratio equal to 4.3. This indicated that the flow resistance generated by layer interaction was smaller in low aspect ratio channels. This has significant implications for the small scale laboratory models used in the Series B extension programme which had relatively small aspect ratios compared with real rivers (large aspect ratios). There may be a tendency for the smaller AR models to overstate the flow resistance caused by layer interaction.

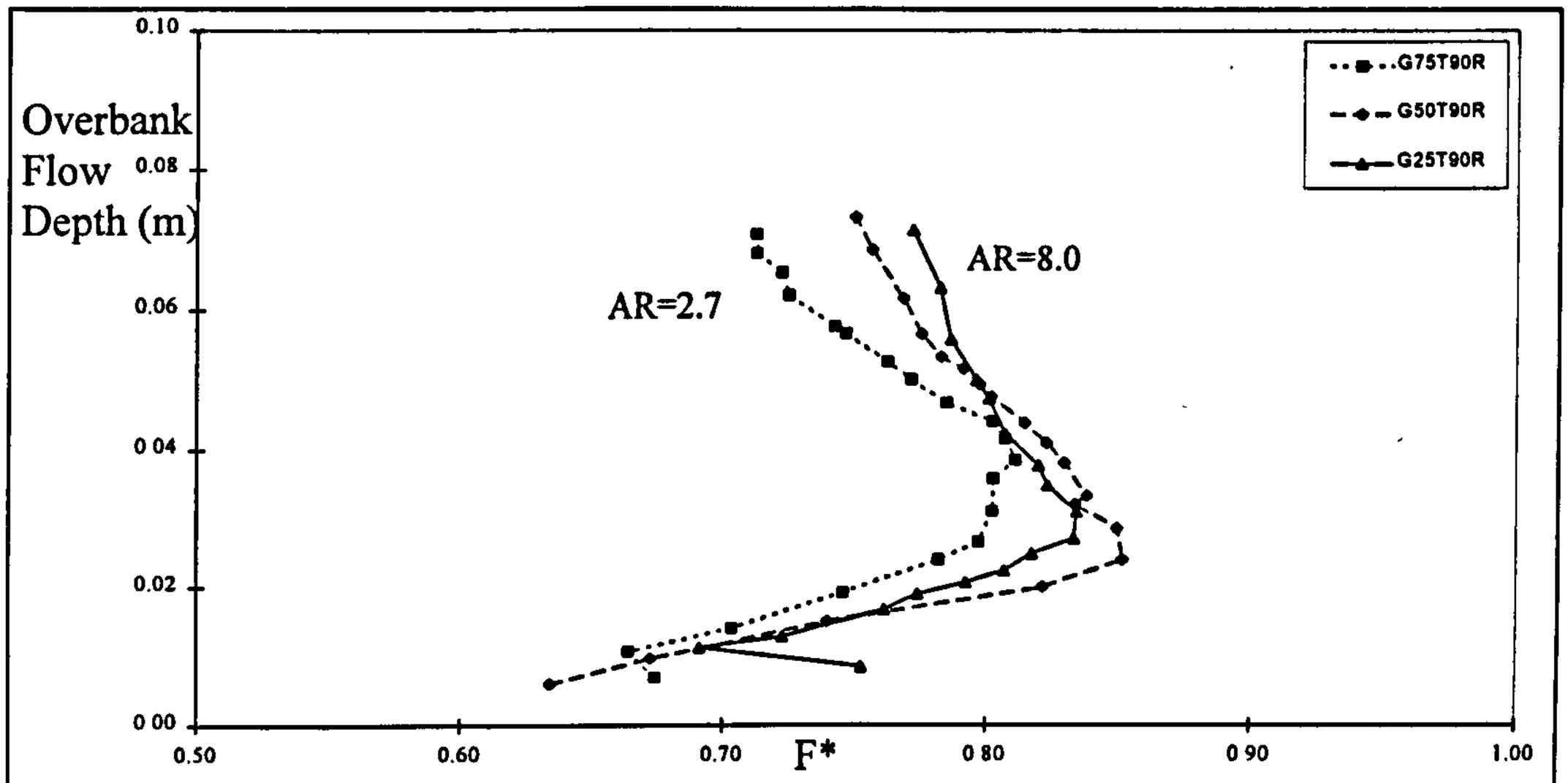

Figure 4.20 Flow depth versus F* for various aspect ratios (90 degree side slopes)

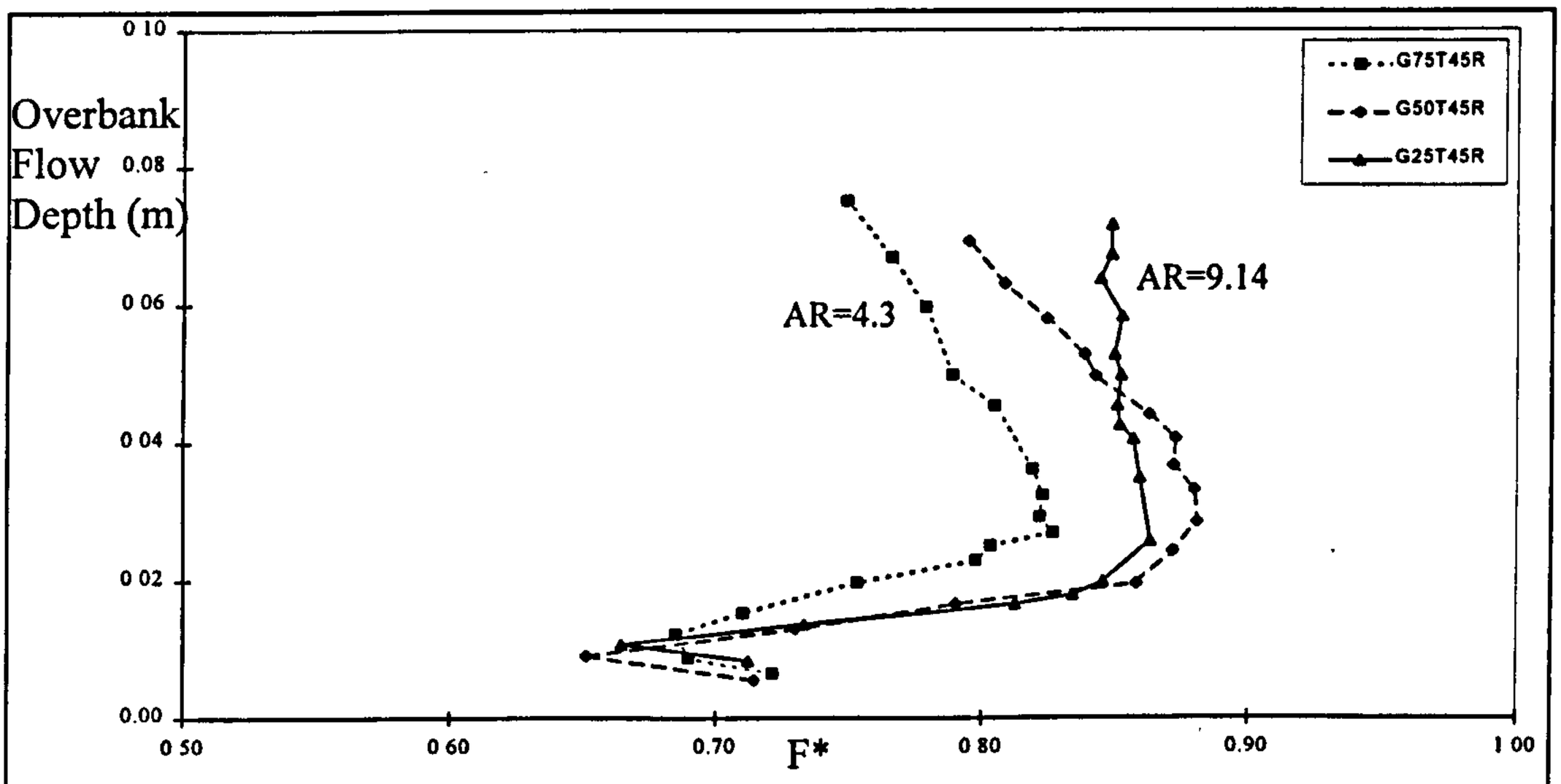

Figure 4.21 Flow depth versus F* for various aspect ratios (45 degree side slopes)

4.5.6 The influence of relative meander belt width on global flow resistance

4.5.6.1 Introduction

Only one previous experimental programme, Series B (1989-1992) attempted to demonstrate the influence of relative meander belt width, Mw (flood way width/meander belt width), on flow behaviour in meandering compound channels without varying other parameters. Ervine et al [1993] in their analysis of the Series B data demonstrated the effect of relative meander belt width on total discharge capacity

and overall flow resistance. They demonstrated that the flow resistance in a meandering compound channel increased for increasing relative meander belt width, Mw, over a limited range of flow depths but offered no explanation in terms of flow mechanisms for the observed flow behaviour

The author re-analysed the original Series B data using plots of overbank flow depth versus Global F* in order to isolate the influence of relative meander belt width on flow layer interaction losses from the bed friction losses. The Series B (1989-1992) flow data was compared with the flow data from the Series B extension (1993-1996) programme.

4.5.6.2 Existing flow data sets

Figure 4.22 presents plots of overbank flow depth versus Global F* which were obtained from the Series B models: SDB25 and SDB31. Both SDB25 and SDB31 had sinuosities equal to 1.374 but possessed different relative meander belt widths, Mw, which were equal to 1.64 and 1.0 respectively. SDB39 and SDB43 both had sinuosities equal to 2.043 and relative meander belt widths, Mw, equal to 1.18 and 1.0 respectively.

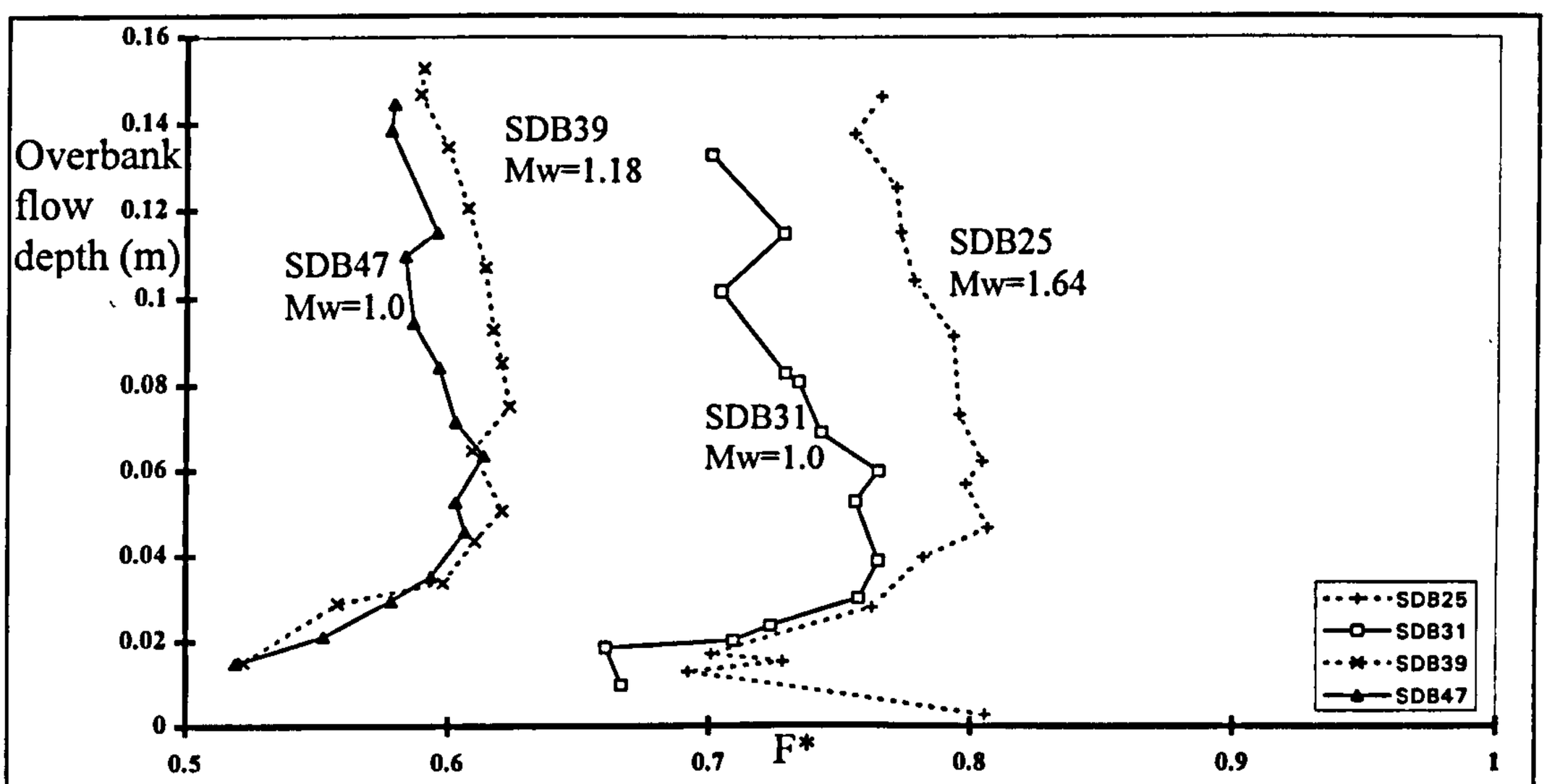

Figure 4.22 Flow depth versus Global F* for tests SDB25, SDB31, SDB39 and SDB47

Figure 4.22 shows that the magnitude and variation of overbank flow depth with Global F* is similar in flow regions 1 and 2, irrespective of relative meander belt width. It shows that flow region 3 is initiated at similar flow depths irrespective of relative meander belt width. However Figure 4.22 also shows that Global F* is smaller in flow

region 3 for models with smaller relative meander belt widths. This implies that greater interaction losses are produced in channels with smaller relative meander belt widths. Additional experiments were performed in Glasgow as part of the Series B extension programme in order to determine whether similar flow behaviour is exhibited in smaller scale models.

4.5.6.3 Series B extension results

Figure 4.23 shows plots of overbank flow depth versus Global F* which were obtained from the Series B extension models: G25T45R and G25T45RN were both 25mm deep and had relative meander belt width ratios, Mw, equal to 1.64 and 1.0 respectively. G75T45R and G75T45RN were both 75mm deep and had relative meander belt ratios, Mw, equal to 1.64 and 1.0 respectively.

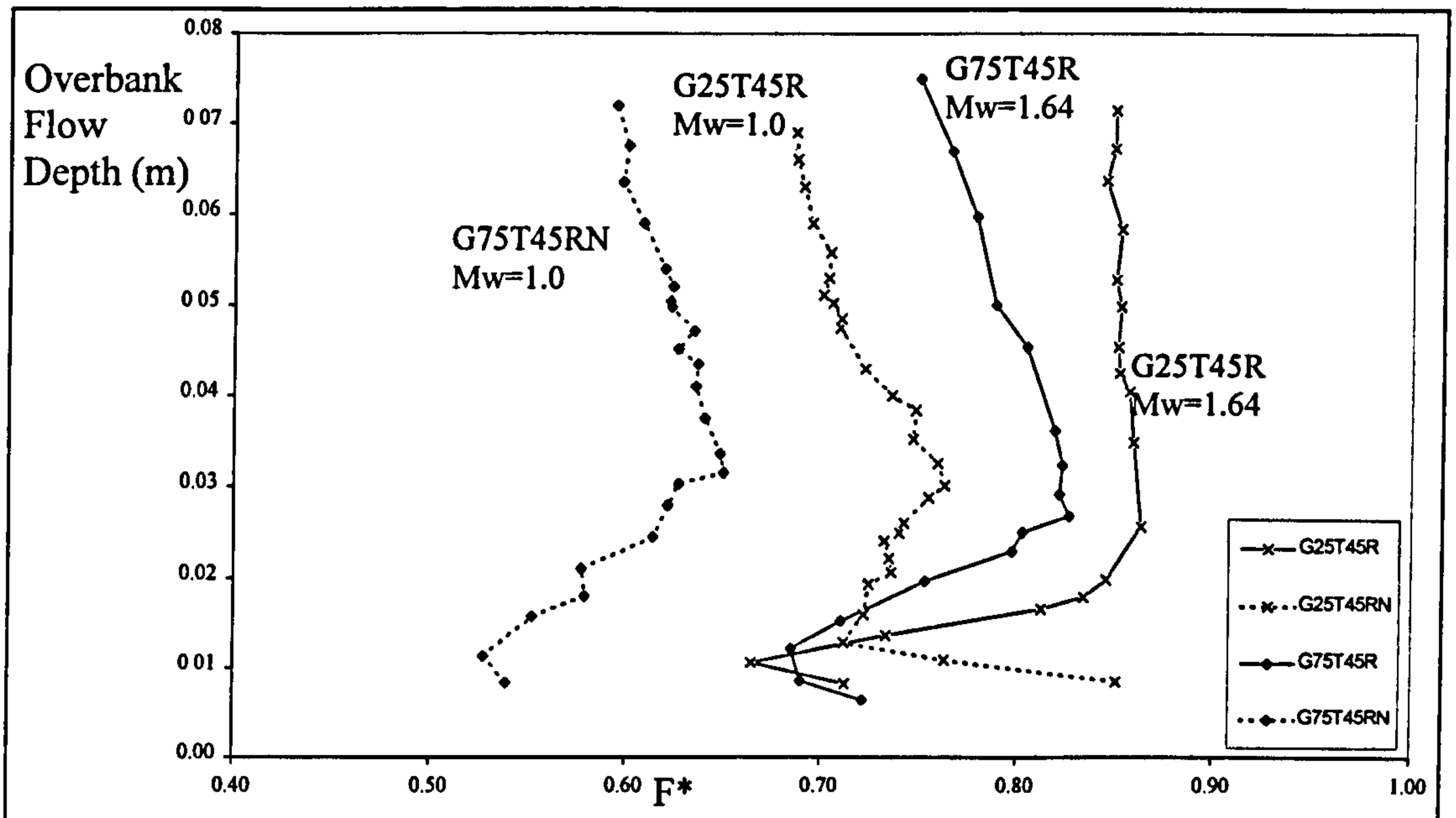

Figure 4.23 Flow depth versus F*: G25T45R, G25T45RN, G75T45R, G75T45RN

Comparing Figure 4.23 with Figure 4.22 demonstrates that relative meander belt width ratio appears to effect the layer interaction mechanisms in meandering compound channels differently in different scale channels. Global F* is smaller in channels with smaller relative meander belt widths in flow regions 1 and 2, which contradicts the observations from the Series B (1989-1992) results. However similarities still exist in flow region 3. In flow region 3 Global F* remains smaller in the channels with smaller relative mender belt width, Mw=1.0, mirroring the behaviour that was exhibited by the

larger Series B (1989-1992) models, although the difference in Global F* magnitude was greater in the small scale channels with different relative meander belt widths. Significantly the Threshold depths were still initiated at similar flow depths in the large and small scale models, irrespective of relative meander belt width. The author suspects that this may indicate that the flow mechanisms are not different in the different scale models but that the observed behaviour may be related to the formulation of Global F*. The zonal data presented in Section 4.6 had to be used to explain this phenomenon.

4.5.7 The influence of main channel sinuosity on global flow resistance

4.5.7.1 Introduction

The influence of sinuosity, in isolation, on flow behaviour in meandering compound channels has been investigated in two previous experimental programmes the Series B (1989-1992) and Vicksburg [1956] programmes. Of these only the Series B (1989-1992) has produced reliable bed friction calibration data which can facilitate a full re-analysis of the flow data using Global F*. Ervine et al [1993], Willetts et al [1993] and Sellin et al [1993] demonstrated that the flow resistance in a meandering compound channel increases with increasing main channel sinuosity. The author re-analysed the original data using plots of overbank flow depth versus Global F* and compared the results with the results obtained during the Series B extension programme.

4.5.7.2 Existing data sets

Figure 4.24 shows plots of overbank flow depth versus Global F* for two compound channels from the Series B programme: SDB25 and SDB39. Both models possessed quasi-natural main channels, with common aspect ratios equal to 14.6, but they had different main channel sinuosities equal to 1.374 and 2.043 respectively.

The magnitude of Global F* is smaller in the high sinuosity channel when compared at all flow depths. This indicates that greater interaction losses are generated in the high sinuosity channels. In addition the Thresholds 1/2 and 2/3 occur at lower overbank flow depths in the high sinuosity channel. The rate of change of Global F* in flow region 3 is

similar in both models which indicates that the head loss due to the interaction mechanisms is similar in both channels despite their different sinuosities.

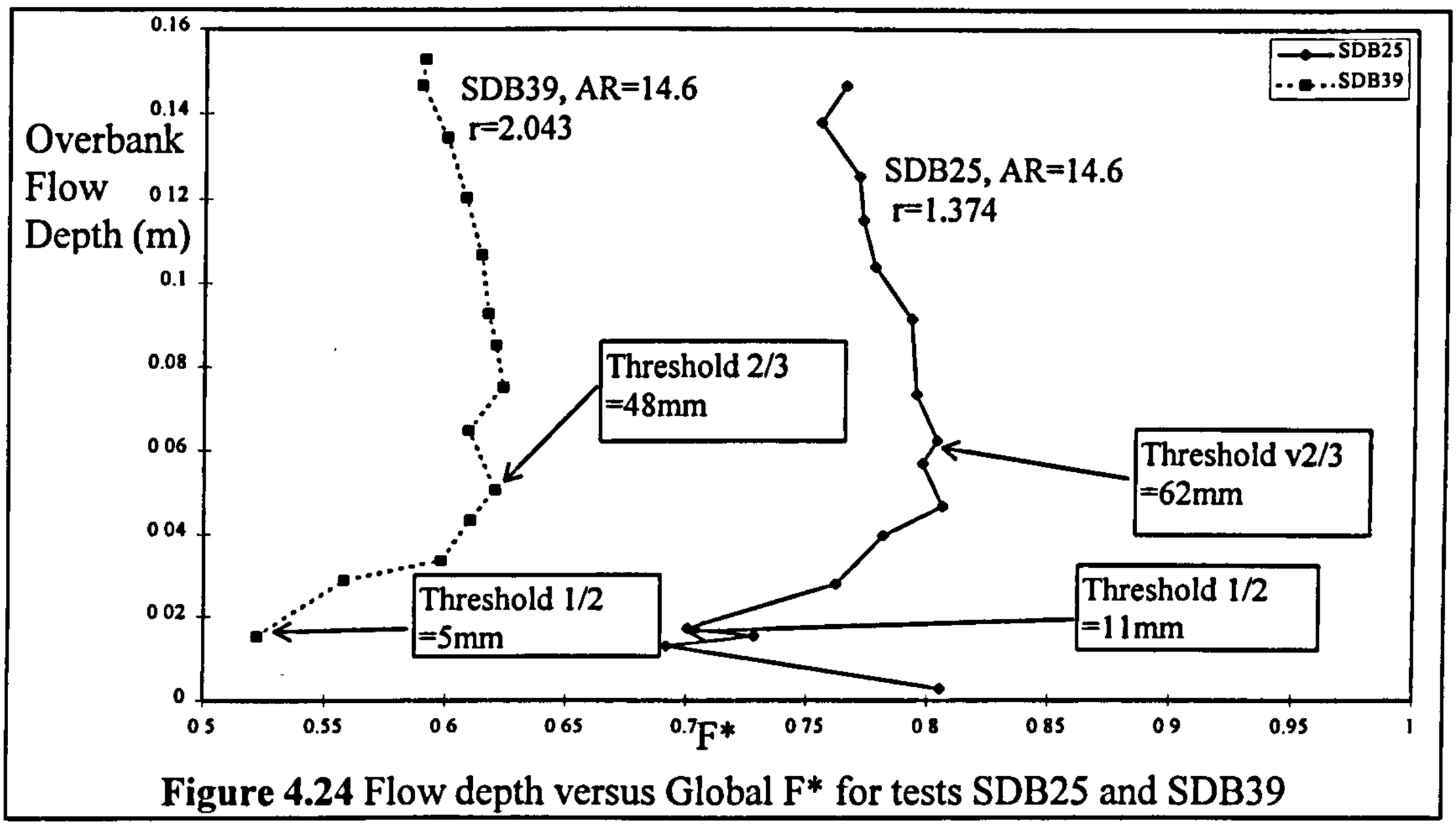

Figure 4.24 Flow depth versus Global F* for tests SDB25 and SDB39

Both the Series B models had smooth flood plain channels and were built at a larger scale than the Series B extension models. The Series B extension models were built to determine if similar flow mechanisms were generated in smaller scale models and when flood plains with different roughness were used.

4.5.7.3 Series B extension results

During the Series B extension (1993-1996) programme further tests were performed in Aberdeen to demonstrate the effect of sinuosity on meandering compound channel flow. There was a free exchange of data between Glasgow and Aberdeen. Figures 4.25 and 4.26 show plots of overbank flow depth versus Global F* for two sets of meandering compound channels. Each set consisted of three models with different main channel sinuosities. Each set had different flood plain roughness. Figure 4.25 shows the plots for A3T1000S, A1T1000S, A2T1000S which had respective sinuosities of 1.111, 1.374 and 1.778 and smooth flood plains. Figure 4.26 shows the plots for A3N1000B, A1N1000B, A2N1000B which had respective sinuosities of 1.111, 1.374 and 1.778, marginally different aspect ratios and Rough B flood plains. The two models A3T1000S and A3N1000B had a larger Zone C width than the other two models in order to produce a low sinuosity channel which possessed features which were similar to natural rivers.

Figure 4.25 demonstrates that the smaller scale Series B extension models with smooth flood plains exhibit a dependency between Global F* and sinuosity which is similar to that observed in the Series B experiments. The high sinuosity models generated lower values for Global F* at all flow depths indicating that greater layer interaction losses were generated. However, unlike the larger scale models the Thresholds 1/2 and 2/3 occurred at similar flow depths in different sinuosity channels with smooth flood plains.

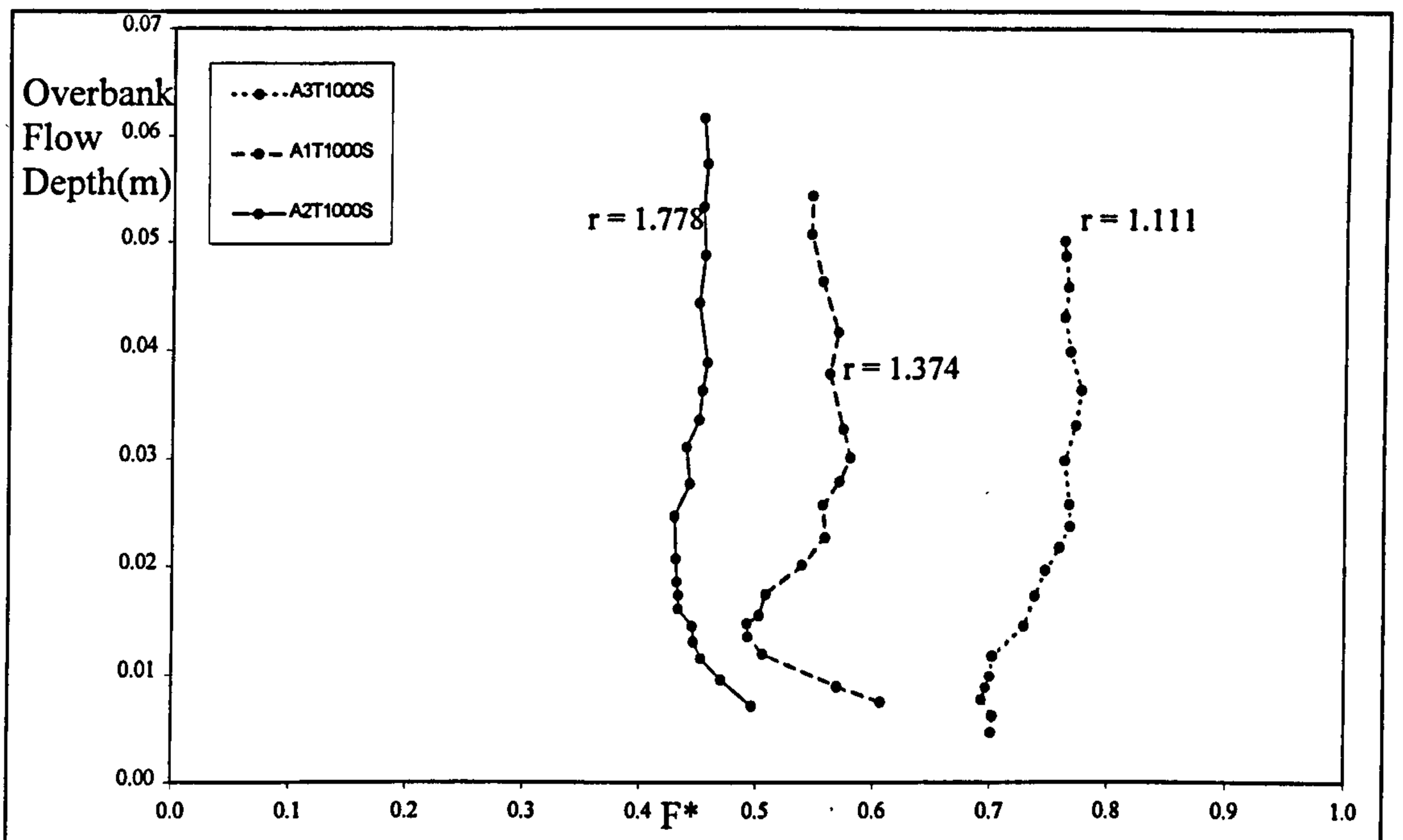

Figure 4.25 Relative depth versus F* for tests A3T1000S, A1T1000S, A2T1000S

Figure 4.26 clearly shows that variations in the main channel sinuosity only have a minor effect on the magnitude of Global F* in flow region 1 and 2 for the models with Rough B flood plains. This differs from the results shown for similar models with smooth flood plains and the Series B results. However in flow region 3 the higher sinuosity channels do exhibit much lower Global F* values than in the lower sinuosity channels. This indicates that there are greater interaction losses generated in the higher sinuosity channels only in flow region 3.

The Thresholds 1/2 and 2/3 occurred at similar flow depths in the models with different sinuosity main channels and rough B flood plains as they did in the models with smooth flood plains. However they both differed from the Series B results which exhibited

significant differences in Thresholds 1/2 and 2/3 for models with different main channel sinuosity. Unfortunately Aberdeen had not published the zonal flow results for these channels at the time of writing so the author was not able to develop an explanation for this deviation in flow behaviour based on the zonal flow behaviour

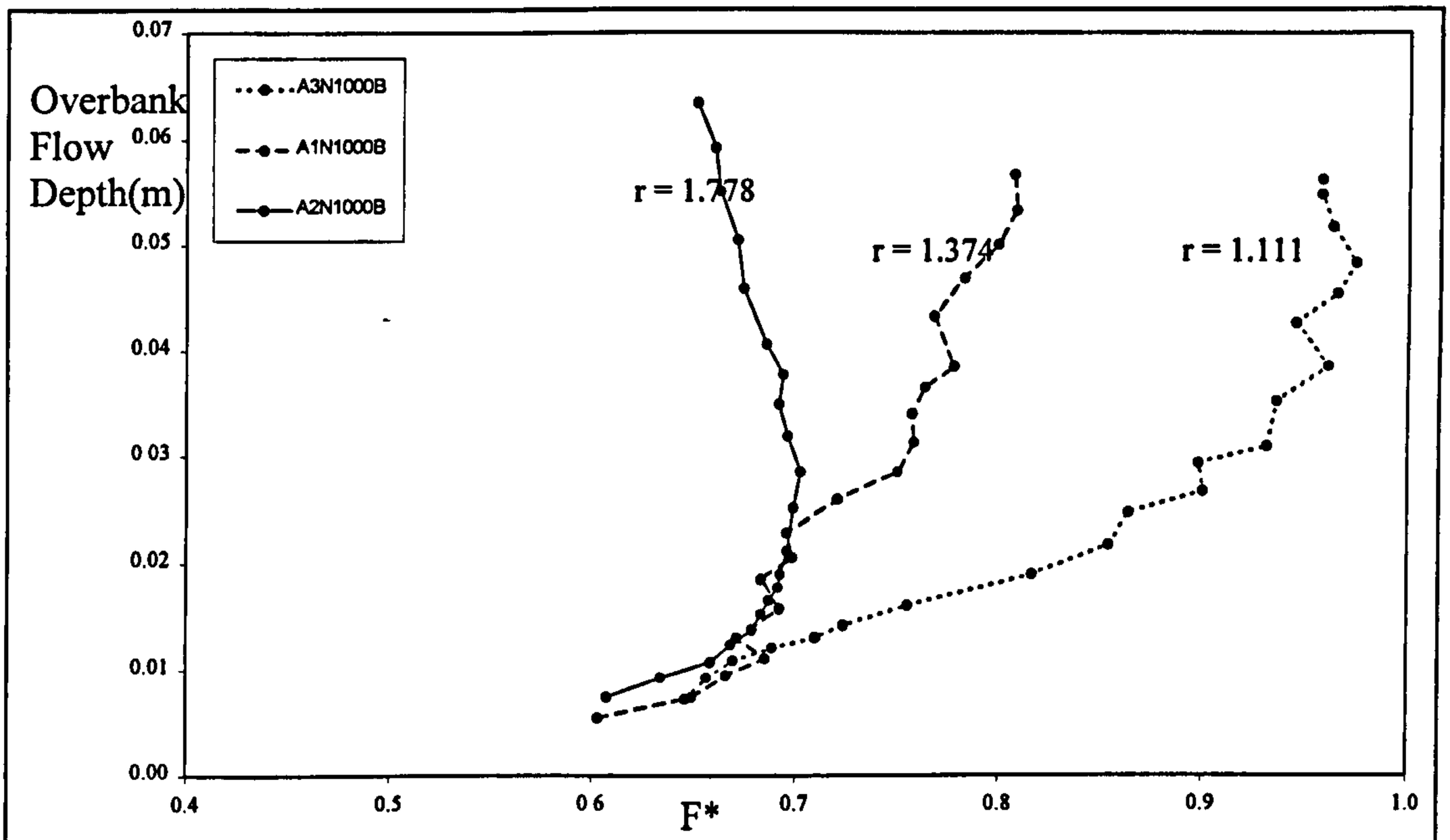

Figure 4.26 Relative depth versus F* for tests A3N1000B, A1N1000B, A2N1000B

4.5.8 The influence of main channel shape on global flow resistance

4.5.8.1 Introduction

The Series B (1989-1992) programme has provided the only reliable flow data to date which has attempted to illustrate the influence of channel shape on flow behaviour. However, the aspect ratio of the main channel was altered as well as its shape so further experiments were performed during the Series B extension programme in order to further investigate the influence of channel shape independently from aspect ratio.

4.5.8.2 Existing flow data sets

Figure 4.27 plots overbank flow depth versus Global F* for SDB21 and SDB25 from the Series B programme (1989-1991). Global F* was greater for the natural channel at all flow depths. However SDB21 had an aspect ratio equal to 9.143 and a trapezoidal main channel whereas SDB25 had an aspect ratio of 14.6 and a quasi-natural main

channel. There was not enough data to separate the influences of channel shape from aspect ratio.

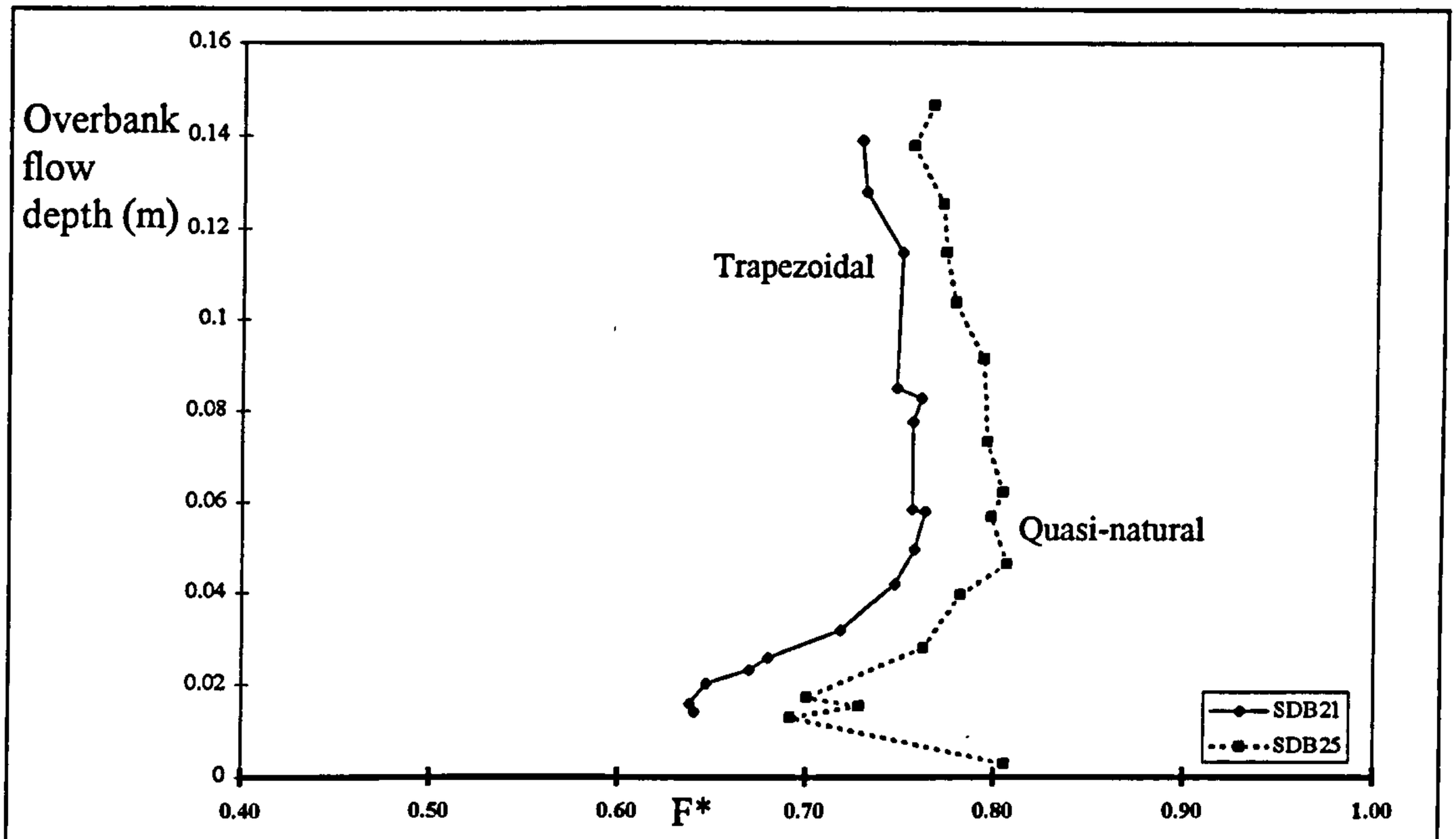

Figure 4.27 Flow depth versus F* for aspect ratios equal to 9.143 and 14.57

The Series B extension tests were devised to investigate the influence of channel shape on the layer interaction proportion of global flow resistance independently from aspect ratio.

4.5.8.3 Series B extension results (Aberdeen)

Figure 4.28 shows plots of overbank flow depth versus Global F* for A1T1000B, A1N1000B, A2T1000S, A1N1000S which were constructed in Aberdeen during the Series B extension programme. They were formed by passing water over Bakelite powder which was placed inside the original main channel. Unfortunately the channels formed in this way had larger aspect ratios than their equivalent trapezoidal channels. The aspect ratios of A1T1000B, A1N1000B, A2T1000S, A2N1000S were 4.49, 7.24, 4.49 and 5.26 respectively.

The trapezoidal and quasi-natural channels tested in Aberdeen suffered from the same problems as the Series B tests in that the aspect ratio varies as well as the channel shape. The high aspect ratio channels exhibited the higher Global F* values at all flow depths

thus following the typical trend first identified using the Series B experimental results where the effect of channel shape was difficult to distinguish from that due to the aspect ratio.

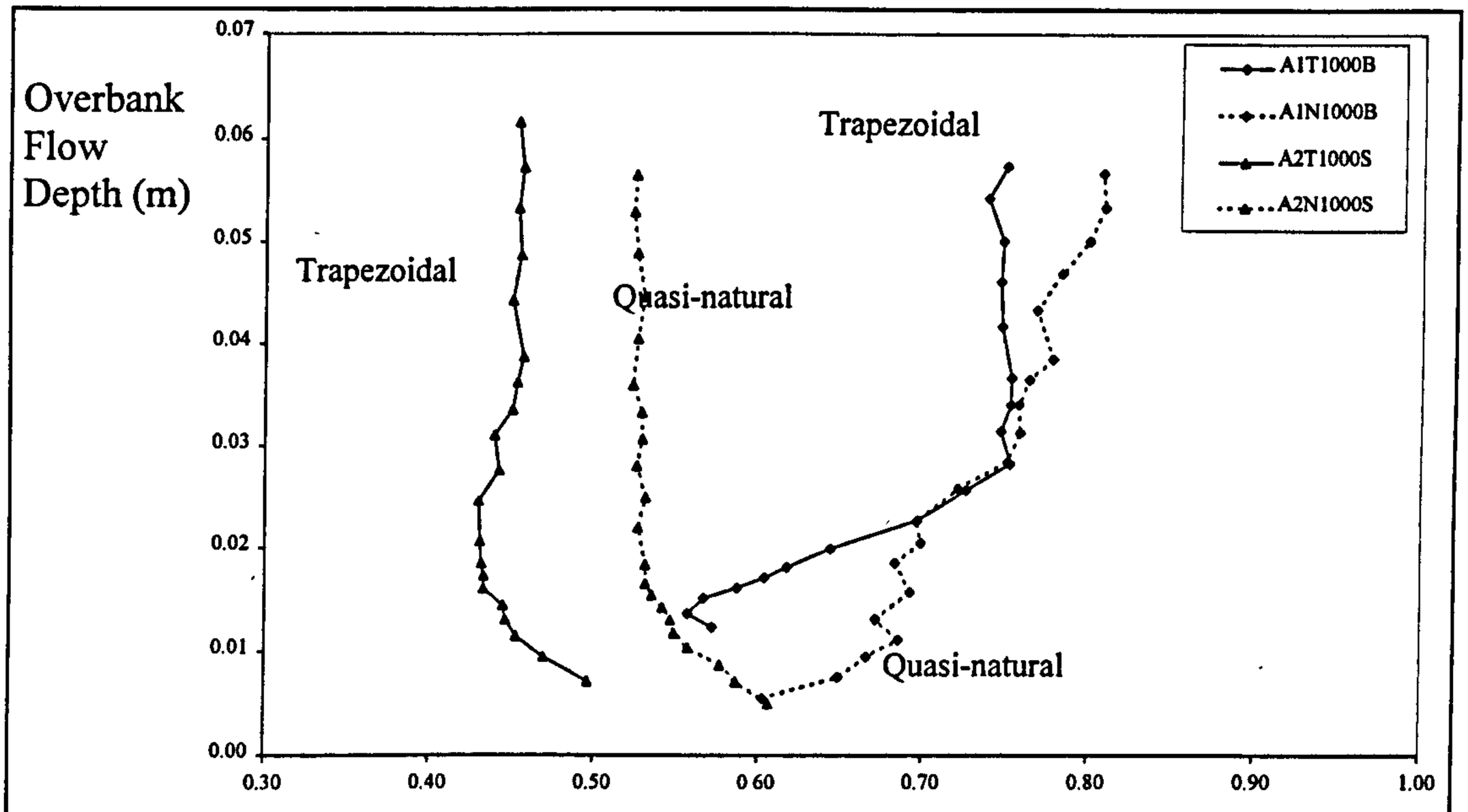

Figure 4.28 Flow depth versus Global F^* for A1T1000B, A1N1000B, A2T1000S, A2N1000S

4.5.8.4 Series B extension results (Aberdeen and Glasgow)

Two types of model with either trapezoidal or quasi-natural main channels were built in Glasgow during the Series B extension programme. They were used to explicitly distinguish the influence of channel shape because they were fabricated to have the same aspect ratio averaged along one wavelength. Figure 4.29 shows plots of overbank flow depth versus Global F* for G25T90R and G25N90R which had aspect ratios equal to 8.0 and trapezoidal and quasi-natural main channel shapes respectively.

Figure 4.30 shows plots of flow depth versus Global F* for G50T45R and G50N45R which had aspect ratios equal to 5.33 and trapezoidal and quasi-natural main channel shapes respectively.

The magnitude of Global F* was greater at all flow depths in the trapezoidal channel which indicates that natural channels experience greater layer interaction losses than trapezoidal channels during overbank flow.

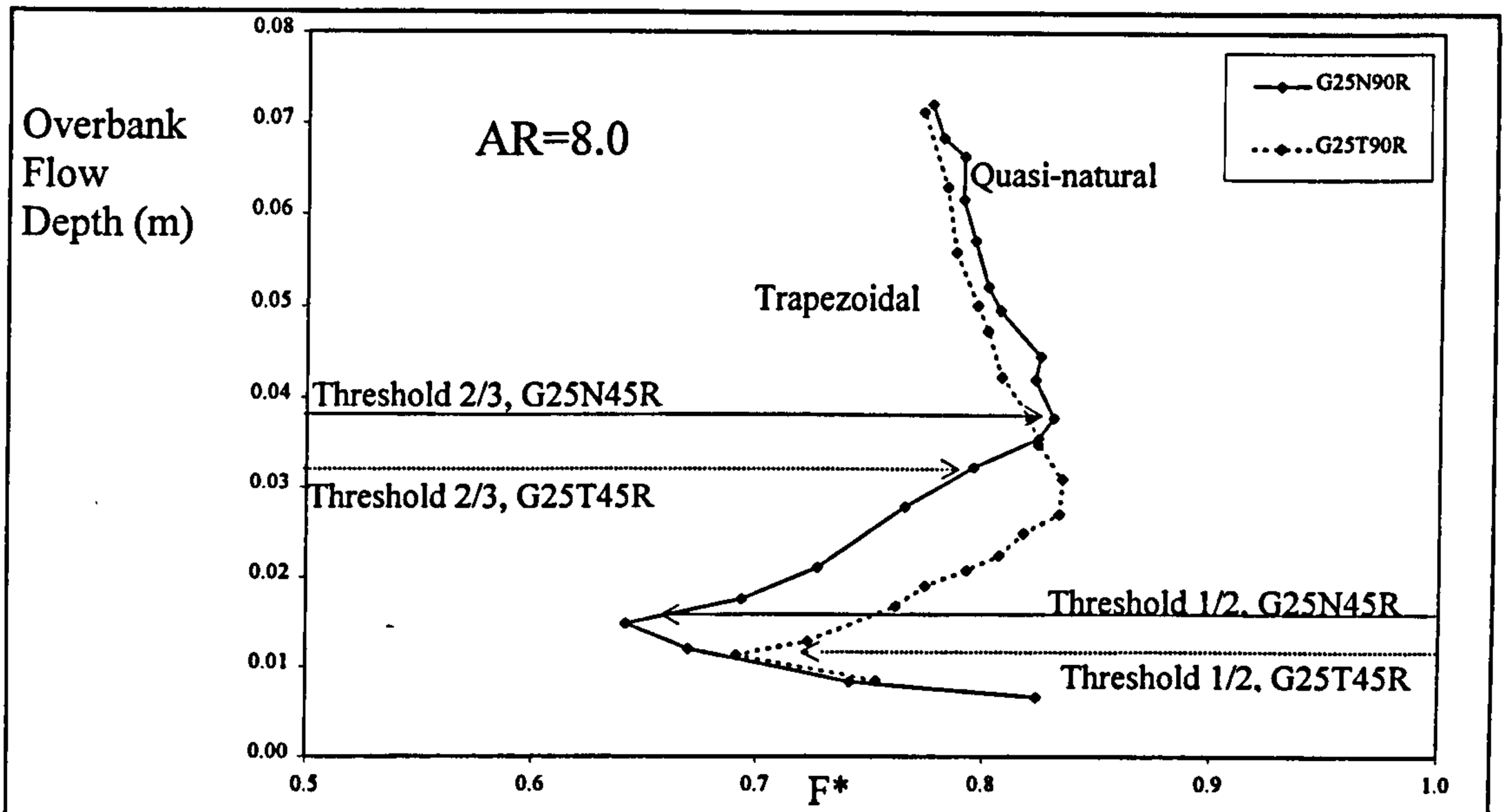

Figure 4.29. Flow depth versus Global F* for G25N90R, G25T90R

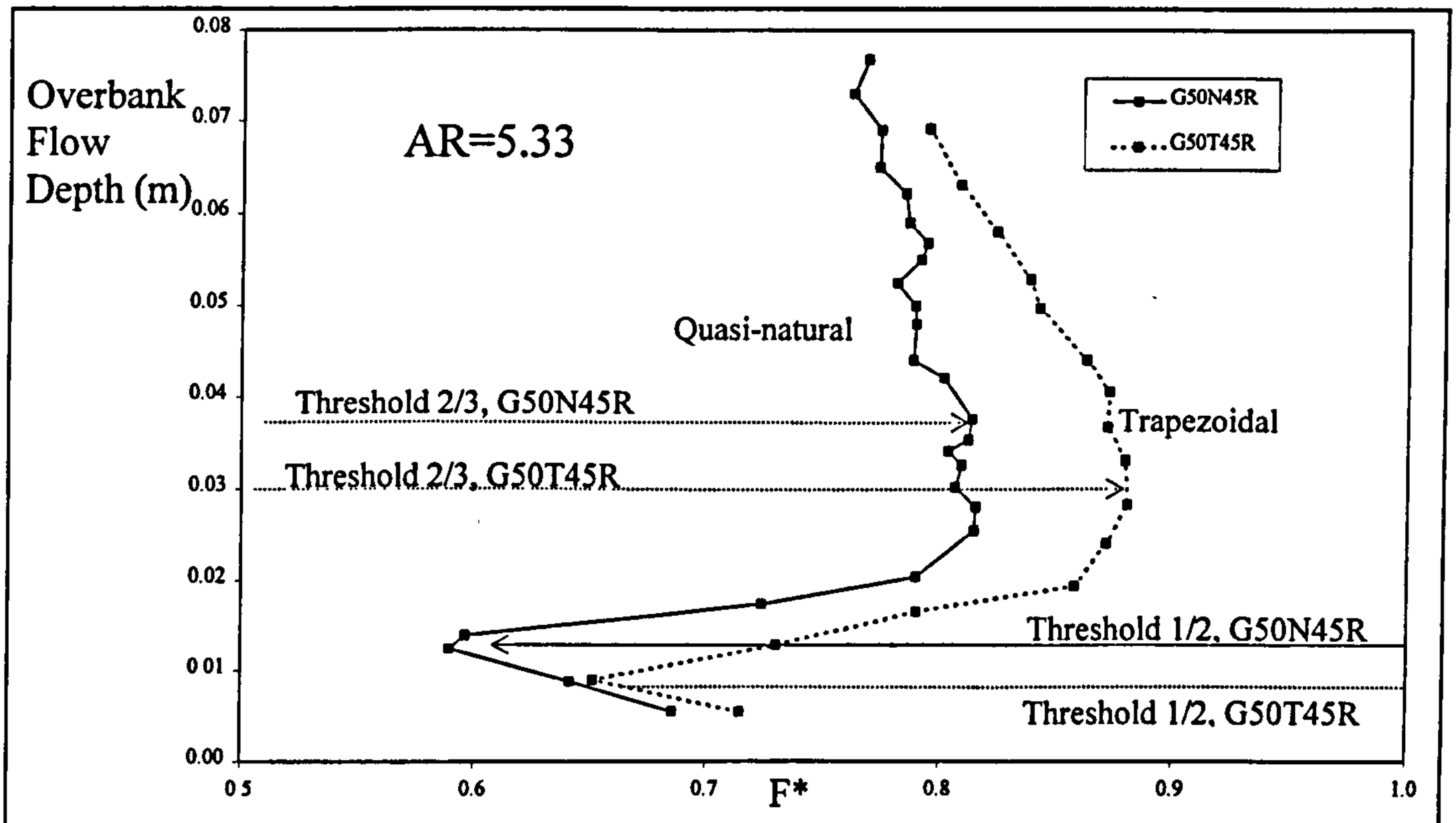

Figure 4.30. Flow depth versus Global F* for G50N45R, G50T45R

The Thresholds 1/2 and 2/3 occur at slightly greater flow depths in the natural channel than in the trapezoidal channel. The trapezoidal and natural channels have identical shapes at the cross-over sections but a deeper cross-section at the apex section as shown in Figures 3.7a and 3.7b. This will decrease the aspect ratio of the channel at this point. The author suggests that this will increase the potential interaction losses but only over

the deeper section, a potential sub-zone in Zone B. The zonal data must be examined to obtain further corroboratory data but this seems to be a valid initial conjecture.

4.5.9 The influence of main channel side slope angle on global flow resistance

4.5.9.1 Introduction

Sellin [1995] demonstrated that the side slope angle of the main channel had a significant effect on the flow resistance of skew compound channels. Before the Series B extension (1993-1996) experiments were performed in Glasgow, no results had been reported describing the effect of side slope angle on the layer interaction proportion of flow resistance in meandering compound channels.

4.5.9.2 Series B extension results

Figures 4.31, 4.32 and 4.33 show plots of overbank flow depth versus Global F* for three sets of meandering compound channel models containing main channels with maximum main channel depths equal to 75mm, 50mm and 25mm respectively. Each set contained models with 3 side slopes angles equal to 90°, 45° and 30° degrees.

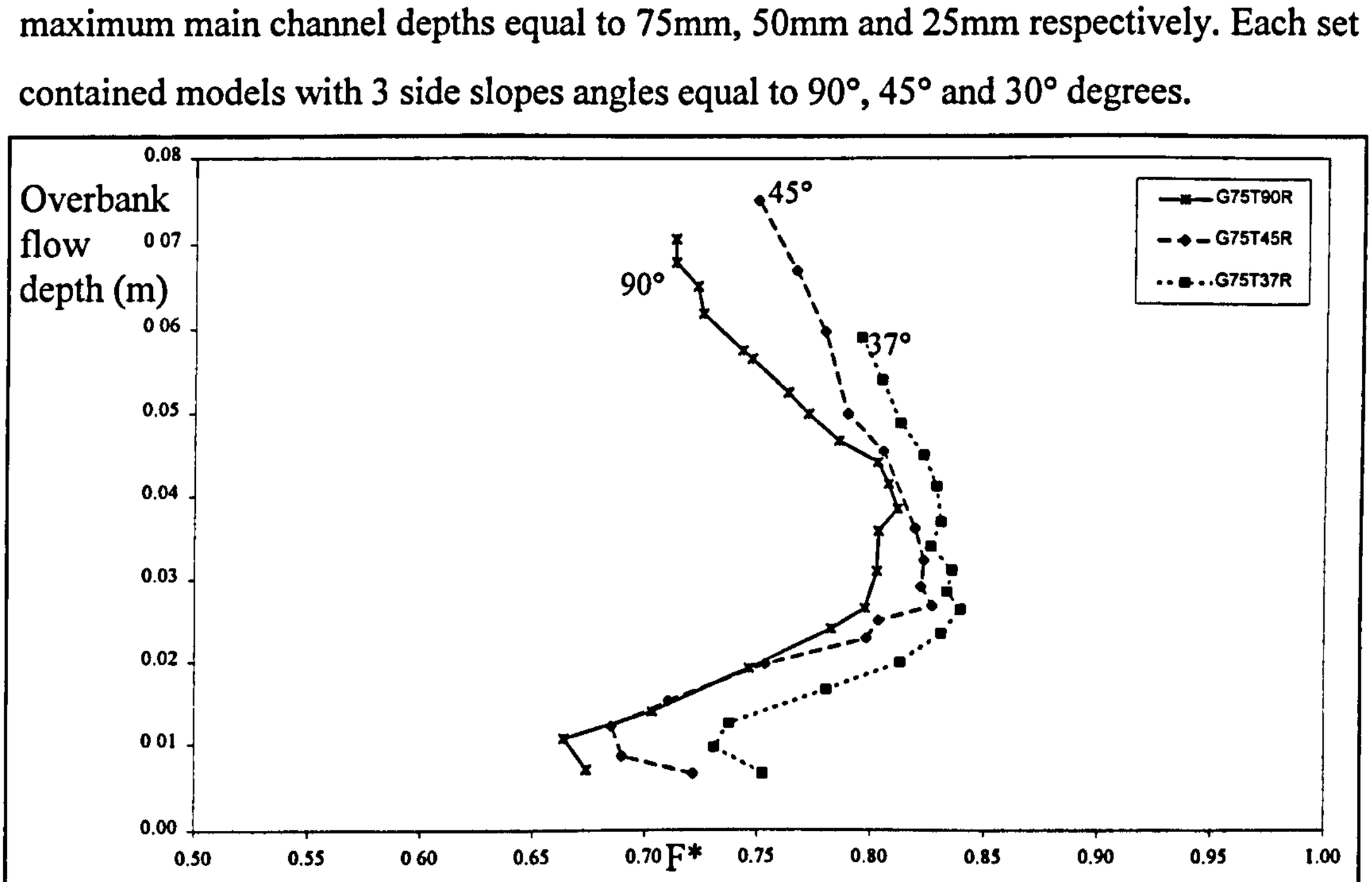

Figure 4.31. Flow depth versus Global F* (G75T90R, G75T60R and G75T37R)

Figures 4.31, 4.32 and 4.33 demonstrate that the magnitude of Global F* is similar in flow regions 1 and 2 but in flow region 3 Global F* increases with decreasing main channel side slope angle. This flow behaviour indicates that the layer interaction increases with main channel side slope in flow region 3. Variation in main channel side slope only has a minimal influence on the flow depth corresponding to Thresholds 1/2 and 2/3.

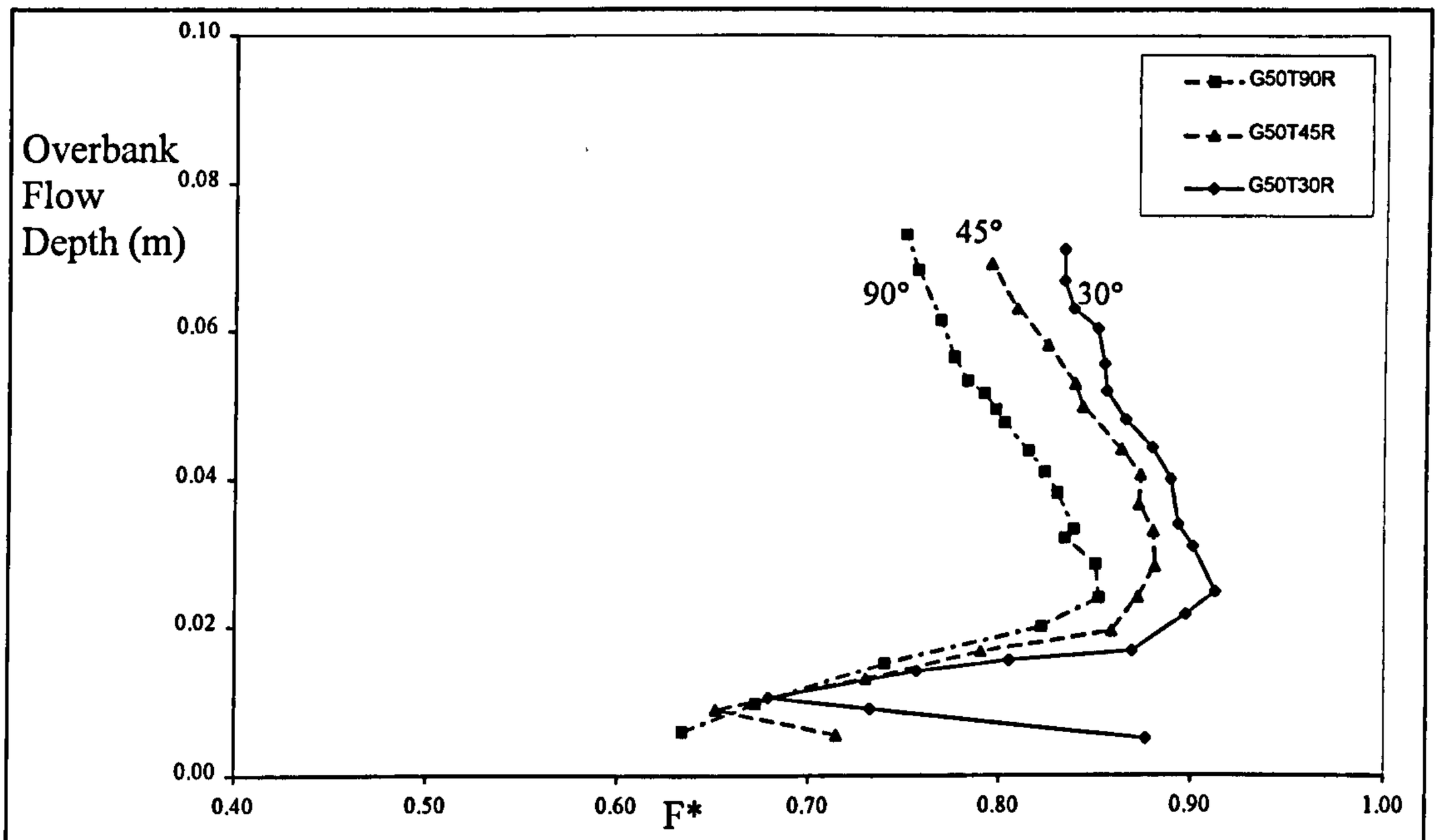

Figure 4.32 Flow depth versus Global F* (G50T90R, G50T45R, G50T30R)

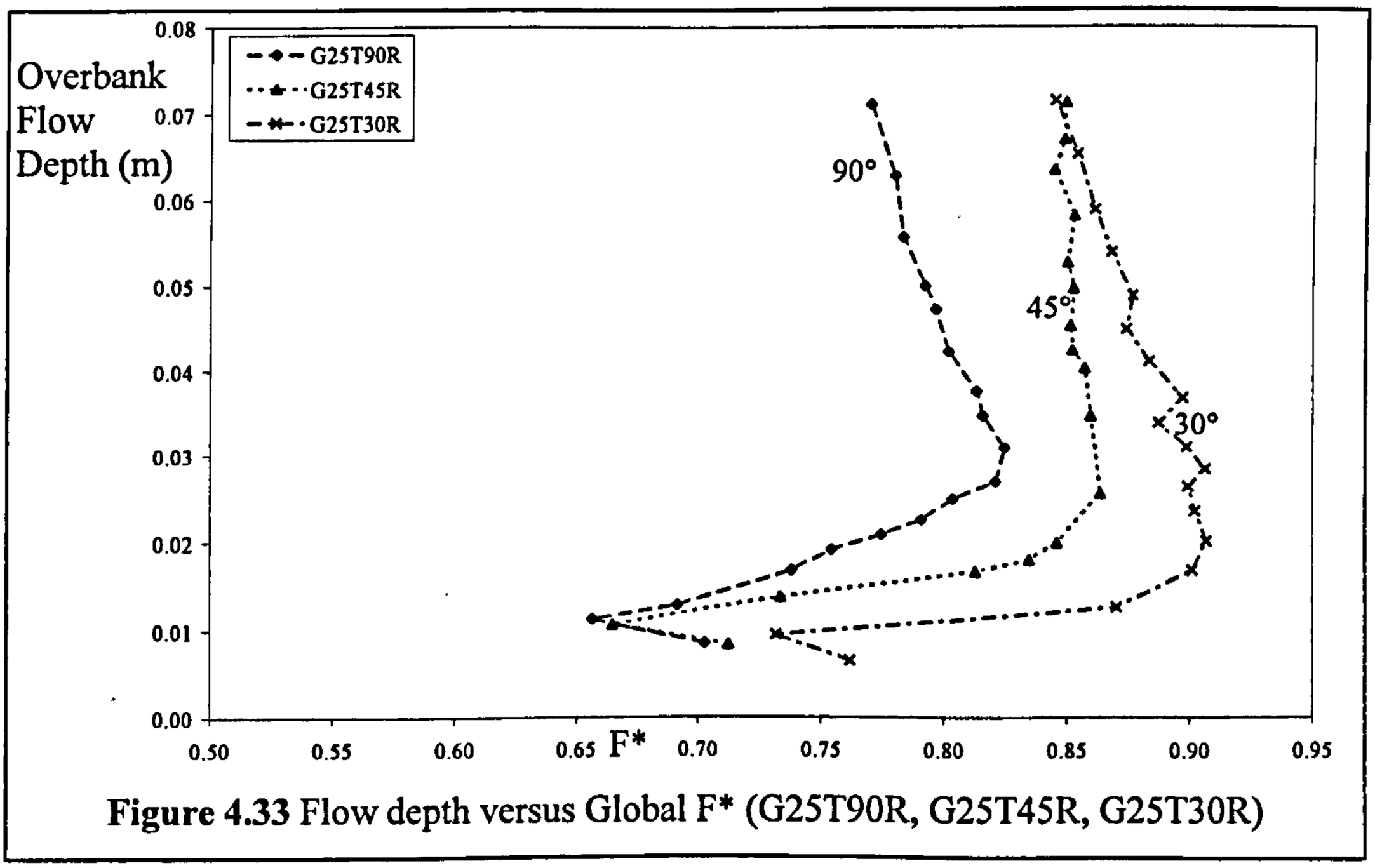

Figure 4.33 Flow depth versus Global F* (G25T90R, G25T45R, G25T30R)

4.5.10 The influence of longitudinal flood plain slope on global flow resistance

4.5.10.1 Introduction

Increasing the flood plain slope in the model tests automatically resulted in a pro-rata increase in the main channel slope. Toebes and Sooky [1967] are the only researchers to date who have reported an investigation into the effect of flood plain slope on flow behaviour in meandering compound channels. Their results were re-analysed in terms of Global F* in order to determine the influence of longitudinal flood plain slope on the layer interaction proportion of flow resistance. The unreliable friction calibration which is available with the Toebes and Sooky [1967] data meant that a degree of caution had to be exercised when re-analysing their results.

4.5.10.2 Existing flow data sets

Figure 4.34 shows a plot of overbank flow depth versus Global F* for 4 models investigated by Toebes and Sooky [1967]: SDSK401, SDSK402, SDSK403, SDSK404. The planform and cross-sectional geometries were identical apart from having different flood plain slopes which were equal to : 1/1470, 1/1150, 1/625 and 1/275 respectively.

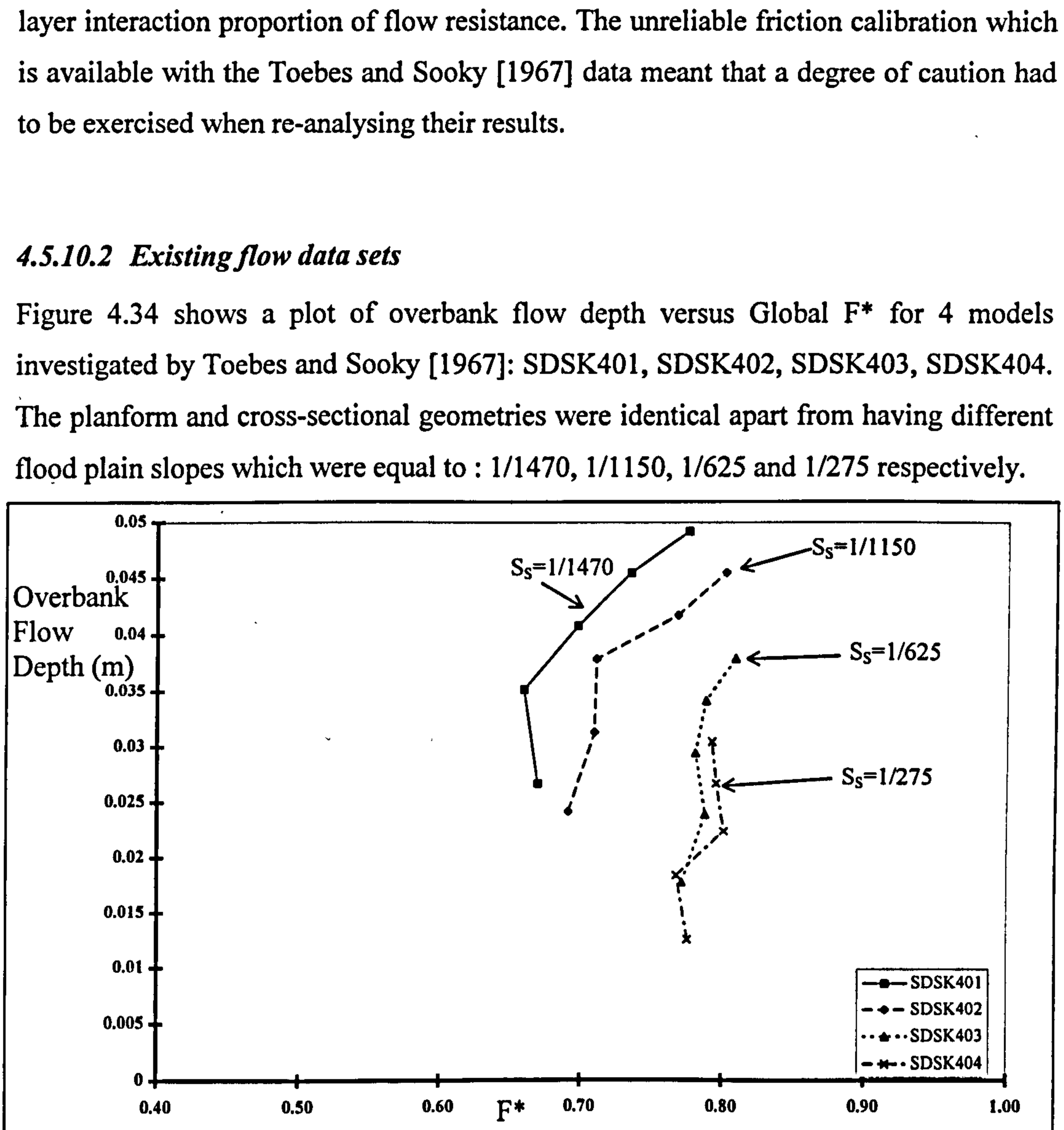

Figure 4.34 Flow depth versus Global F* for various flood plain slopes (Sooky [1967])

Analysis of the Toebes and Sooky [1967] results in Figure 4.34 demonstrates that the magnitude of Global F* is smaller at all flow depths for steeper flood plain slopes which implies the interaction losses decrease with increasing slope. However the 4 flow region behaviour which normally characterises meandering compound channel flow can not be observed. The author suggests that this was because the Toebes and Sooky [1967] model configurations were dissimilar to natural rivers judging by the geometric ratios given in Equations 2.59-2.62. However it could also have been because only a limited number of flow data points were taken in each model. The Series B extension (1993-1996) programme incorporated models to enable the further study of the influence of longitudinal flood plain slope on flow resistance in meandering compound channels.

4.5.10.3 Series B extension results

The influence of flood plain slope on flow behaviour in meandering compound channels was tested in Aberdeen as part of the Series B extension programme. Figure 4.35 plots overbank flow depth versus Global F* for models: A1T1000S A1T750S, A1N750B and A1N750B which had longitudinal flood plain slopes of 1/1000, 1/750, 1/750 and 1/1000 respectively.

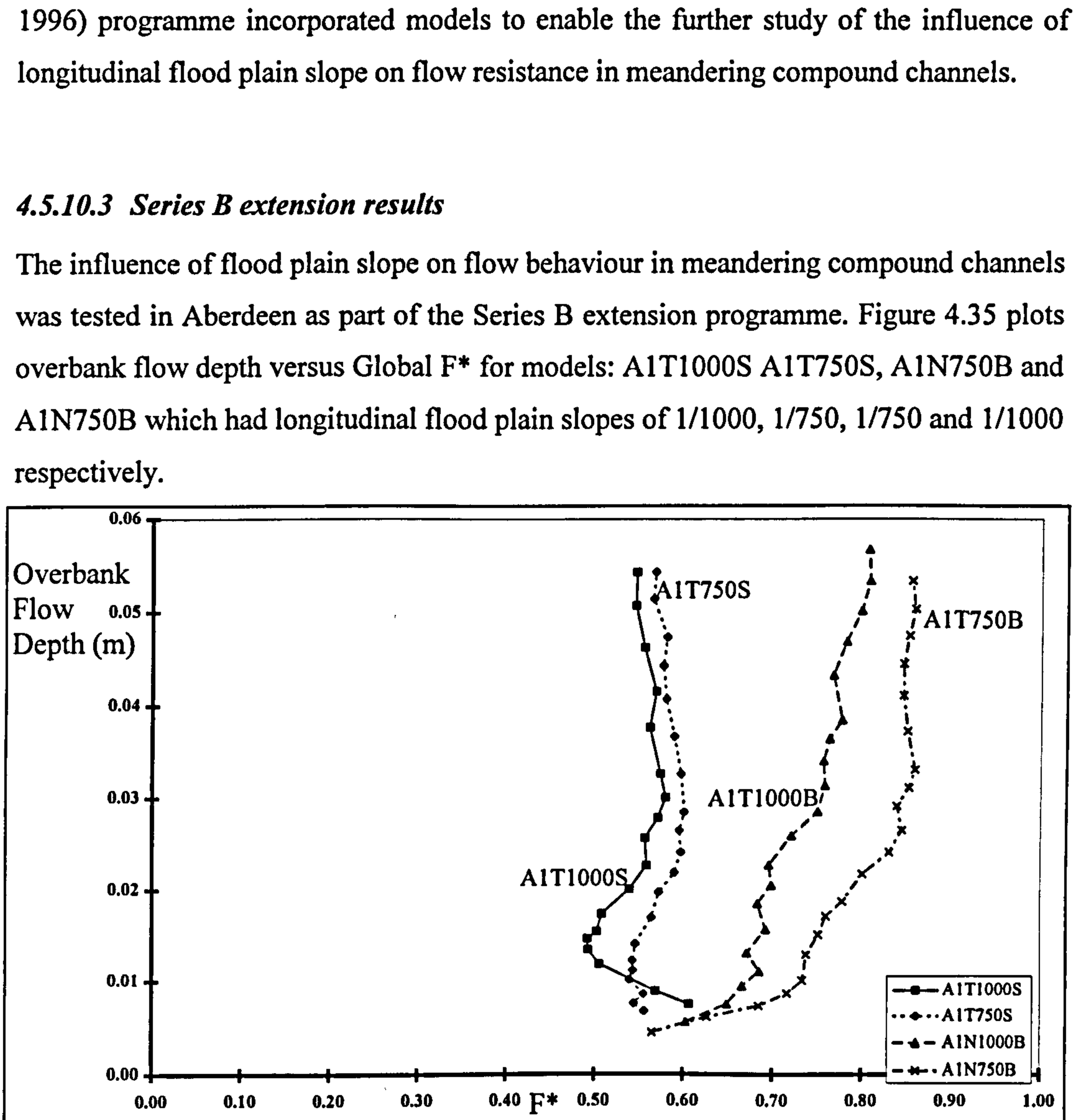

Figure 4.35 Flow depth versus Global F* for flood plain slopes

Figure 4.35 demonstrates that 4 flow region behaviour is generated in these models and confirm the results obtained from the Toebes and Sooky [1967] data. The magnitude of Global F* is larger at all flow depths for the larger flood plain slopes indicating that the layer interaction losses become smaller when the longitudinal flood plain slope increases. Significantly Thresholds 1/2 and 2/3 appear to occur at similar flow depths in the different models. This was expected because the relative flow state appears to influence Threshold depths and this is unchanged by flood slope variations because changes in flood plain slope are automatically reflected on a pro-rata basis to the changes in main channel slope.

4.5.11 The influence of flood plain bank sinuosity on global flow resistance

The team in Bristol were programmed to perform tests in order to determine the influence of flood plain sinuosity of the head losses generated by layer interaction in meandering compound channels. Unfortunately the results were not available at the time of writing.

4.5.12 The influence of flood plain lateral slope on global flow resistance

The team in Bristol were programmed to perform tests in order to determine the influence of lateral flood plain slope of the head losses generated by layer interaction in meandering compound channels. Unfortunately the results were not available at the time of writing.

*4.6 The influence of 7 key parameters on local flow resistance, Zonal F**

4.6.1 Introduction

Point velocity and the corresponding zonal discharge measurements were obtained for each Zone A, B and C in all the 30 models tested in Glasgow during the Series B extension programme. The influence of seven key parameters on zonal flow resistance (Zonal F*) was investigated by the author. These parameters were: relative flow depth, model scale, relative roughness, relative meander belt width, main channel shape, main channel side slope and aspect ratio. The two other Institutions participating in the Series B extension programme were scheduled to test 4 additional and 3 similar parameters. The 4 additional parameters were: main channel sinuosity, flood bank sinuosity, longitudinal flood plain slope and lateral flood plain slope. The 3 similar parameters were: relative depth, relative roughness and main channel shape.

The author also investigated the inter-relationship between zonal flow resistance, measured using Zonal F* and the global flow resistance, measured using Global F*. Similar threshold depths to the ones observed in the Global F* plots, marking significant changes in the flow behaviour, also occur in the Zonal F* plots. In order to distinguish between the thresholds in the two types of plot, the zonal F* thresholds are labelled 'Threshold A' for zone A and 'Threshold B' for zones B and C. While the original system is maintained for Global F* with Thresholds 1/2, 2/3 and 3/4.

4.6.2 The relationship between Zonal F* and Global F*

The influence of each Zonal F* value on Global F* will be controlled by the relative proportion of flow capacity that is contained within each zone. Global F* is defined in terms of Zonal F* using Equation 4.6 where Q_A, Q_B, and Q_C are the zonal discharge capacities and F_A^*, F_B^*, F_C^* are the magnitudes of F* determined for each zone.

$$Global\ F^* = \left(\frac{F_A^*.Q_A + F_B^*.Q_B + F_C^*.Q_C +}{Q_A + Q_B + Q_C} \right) \qquad [4.6]$$

Inspection of Equation 4.6 demonstrates that the magnitude of Global F* at low flow depths will be similar to the magnitude of F_A^* because at these flow depths the majority of discharge capacity is provided by Zone A. At high flow depths the magnitude of

Global F* will be similar to the magnitude of F_B* and F_C* because a greater proportion of total channel discharge capacity is provided by Zones B and C at these depths. The relative magnitude of discharge capacity in Zone B, compared with Zone C, will determine the relative influence of F_B* and F_C* on Global F*.

4.6.3 The influence of relative depth on local flow resistance

4.6.3.1 Local F for Zone A and its variation with relative depth*

The magnitude of F* in Zone A, F_A*, was determined at between 3 and 6 relative depths in all the 30 models which were built in Glasgow during the Series B extension programme. F_A* is defined as Q_{MEAN}/Q_{ATH} where Q_{MEAN} is the average Zone A discharge capacity over one wavelength as defined in Equation 4.7 and Q_{AI} is the measured discharge at each component cross-section, n, over one wavelength.

$$Q_{MEAN} = \frac{\sum_{I=1}^{n} Q_{AI}}{n} \qquad [4.7]$$

The subscript, I, represents the relative position of the cross-section along a wavelength as shown in Figure 2.17 and Q_{ATH} is the Zone A discharge which was theoretically determined by assuming that bed friction was the only source of flow resistance.

James and Wark [1992] showed that the measured discharge capacity of Zone A varies sinusoidally along one main channel wavelength using data gathered during the Series B programme (1989-1992). Figure 4.36 shows two typical plots of Q_{AI}/Q_{MEAN} versus $2x/\lambda$ which they produced for meandering compound channels which vary in channel shape and relative roughness at two flow depths.

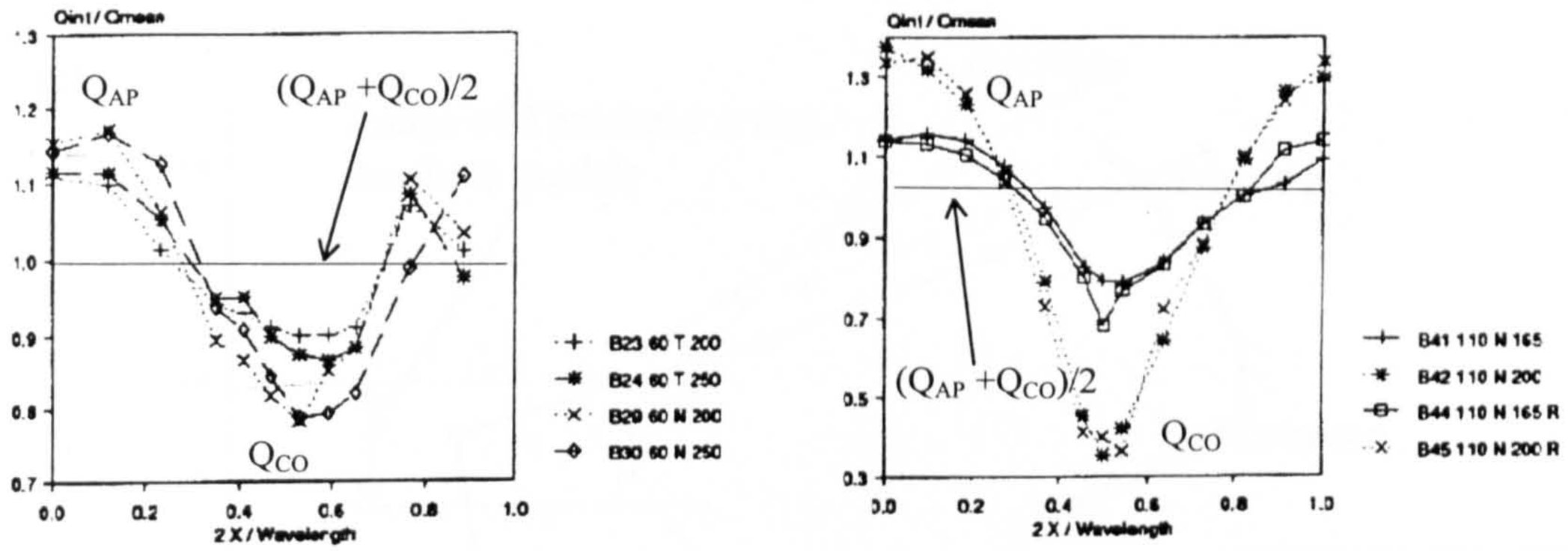

Figure 4.36 Variation of main channel discharge along a meander

The geometries are defined in Table 2.6. Figure 4.36 shows that the arithmetic average of the measured discharge at the apex, Q_{AP}, and cross-over, Q_{CO}, of a meandering channel produces a reliable measure of the average discharge over one wavelength, Q_A, at identical flow depths on the flood plain.

Figure 4.37 shows plots of relative flow depth versus F_A* for the models: G75T45R, G50T45R and G25T45R which were built and tested in Glasgow during the Series B extension programme. The geometries of each model are defined in Table 3.8. They had different maximum main channel depths, equal to 75mm, 50mm and 25mm respectively but their configurations were identical in every other respect. Figure 4.37 also contains a plot of relative depth versus Global F* for model: G75T45R. so that the F_A* variation can be put into context with the flow regions that are exhibited in the Global F* plot.

Figure 4.37 shows that F_A* varies with relative depth in each model with two regions being evident. Over low flow depths F_A* decreases rapidly up to a critical threshold depth, Threshold A. Threshold A often occurs at a slightly different flow depth to Threshold 1/2 in the Global F* plot. Above Threshold A, F_A* begins to increase once again with increasing flow depths in each of the models. The author noted that this general pattern of flow behaviour was similar in each of the other 27 models that were tested.

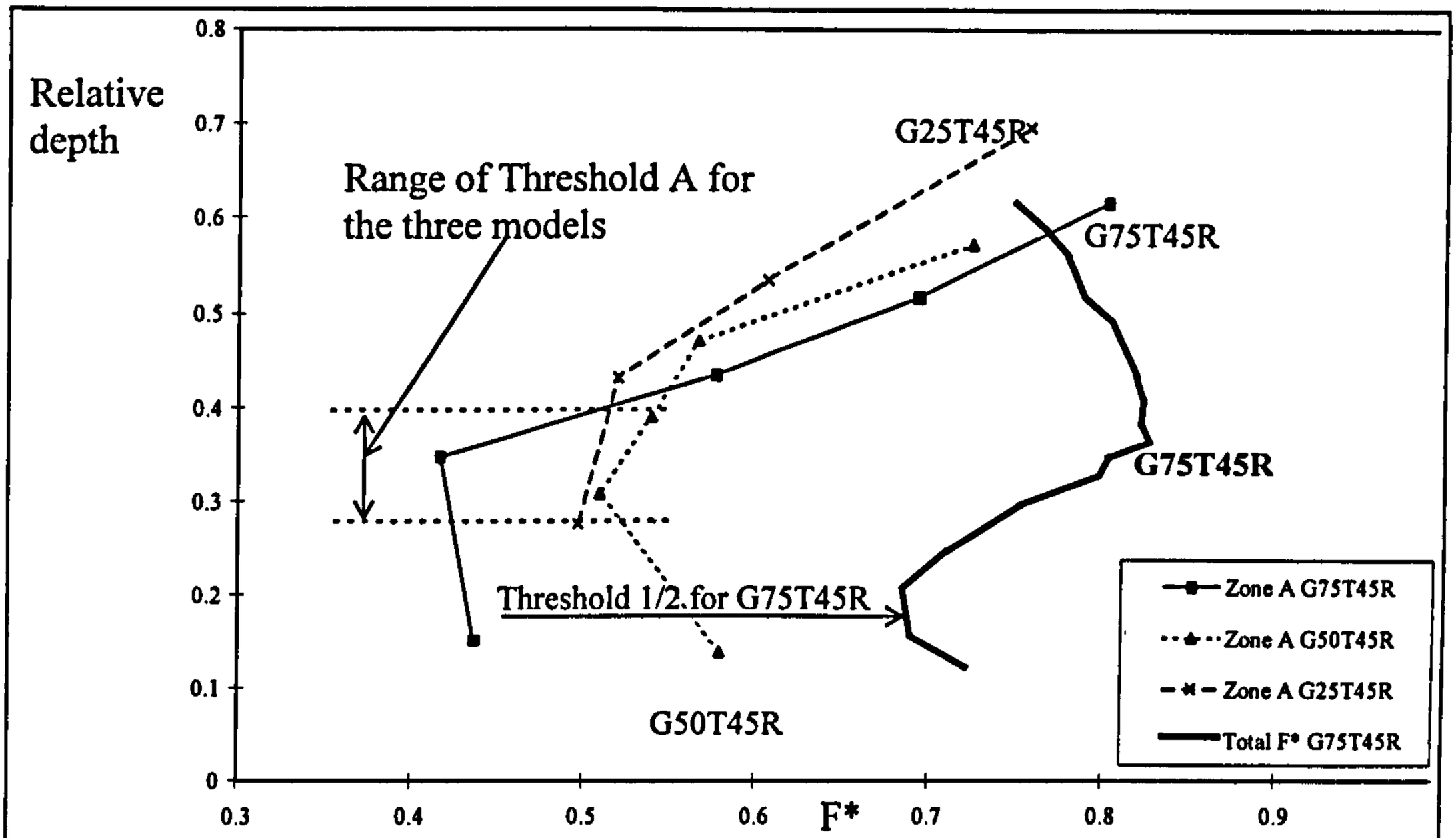

Figure 4.37 Relative depth versus F_A^* for G75T45R, G50T45R and G25T45R.

The author notes that the magnitude of F_A^* (Q_{MEAN}/Q_{AT}) will be less than 1 at relative depth equal to 0 because two sources of flow resistance, bed friction and secondary cell circulation, combine to determine the magnitude of the actual Zone A discharge, Q_{MEAN}, whereas Q_{AT} (the theoretical discharge) was determined by assuming that bed friction was the sole source of flow resistance. The subsequent decrease in F_A^* as relative depth increases towards Threshold A implies that the proportion of flow resistance in Zone A which is attributable to the interaction between the flow layers in Zone A and Zone B is increasing rapidly. At these low flow depths the majority of flow is contained in Zone A so the Global F* plot reflects the F_A^* plot and also rapidly decreases.

After Threshold A is achieved F_A^* stops decreasing. As flow depths subsequently increase the magnitude of F_A^* also starts to increase. This behaviour indicates that the flow resistance in Zone A generated by layer interaction decreases for increasing flow depths. However the distinctive rapid increase in Global F* can not be attributed solely to the increases in F_A^*, which are often significantly less rapid over flow region 2. At these flow depths, while a large proportion of the flow is still contained within Zone A, an increasing proportion of flow is contained within Zones B and C which means that the magnitudes of F_B^* and F_C^* will have an increasing influence on the magnitude of Global F*. Significantly the Threshold A occurs at slightly different relative depths in

each model. Extending the observations made in Section 4.5 the author postulates that the relative depth corresponding to Threshold A will be controlled by the relative flow states in Zones A and B achieving a critical threshold value which will be dependant on the configuration of the main and flood plain channels.

Figure 4.37 also demonstrates that F_A^* continues to increase at higher flow depths (in flow region 3) but the rate of increase diminishes slightly. In certain models the value of F_A^* actually rises above 1. This implies that an acceleration of the Zone A flow is induced where Zone B flow shears over the top and Zone A actually conveys more discharge than would be expected if the only source of flow resistance was bed friction. It is significant that the magnitude of F_A^* does not exhibit the rapid decrease in magnitude that is observed in the Global F* plot (characterising flow region 3). At these flow depths the majority of the flow is contained within Zones B and C and so the Global F* plot reflects the flow behaviour in Zones B and C (measured in terms of F_B^* and F_C^*) and the influence of F_A^* is to some extent be swamped.

4.6.3.2 Local F for Zone B and its variation with relative depth*

The magnitude of F* in Zone B, F_B^*, was calculated at between 3 and 6 relative depths in all 30 models which were built in Glasgow during the Series B extension programme. F_B^* was defined as the arithmetic mean of the discharge in Zone B which was measured at the apex and cross-over section, Q_B, divided by the predicted discharge allowing for bed friction losses only, Q_{TB}. The measured discharge at each cross-section was determined by integrating the point velocities over the area of Zone B.

A combination of photographic and direct measurement techniques were used to determine the average velocity in Zones B and C. At low flow depths, notably 8.33mm, a time-lapse photography technique was adopted to determine the magnitude of local flow velocities and the corresponding discharge capacity in Zones B and C. The other, direct methods for measuring point velocity (Pitot tubes and mini-propeller meters) were unreliable at these low flow depths. The average velocity was determined using the photographic techniques described below.

1. The combined discharge contained within Zones B and C was first calculated by subtracting the discharge capacity of Zone A from the total discharge capacity. The total discharge was measured accurately using an orifice plate and differential pressure manometer. The Zone A discharge capacity was measured accurately using a Pitot tube or mini-propeller meter to determine point velocities which were integrated over the Zone A area in order to determine the discharge capacity.
2. The discharge deficit (which was obtained by subtracting the Zone A discharge from the total discharge) was divided between Zones B and C. The proportion of discharge in each zone was determined by analysing time-lapse photographs in order to determine the relative magnitude of flow velocity in each zone. Two photographs were taken over a two second intervals. A sample of the type of photographs which were obtained are shown in Figure 4.38.
3. The average distance travelled by a number of points at different lateral offsets on the dye front in two seconds was measured (using a graduated rule which was included in two photographs). The local flow velocity at each of these points was therefore calculated. Two sample photographs taken from G25T45R are shown in Figure 4.38.
4. Once the relative velocities in Zones B and C had been determined, the proportion of the discharge deficit conveyed within Zones B and C respectively was calculated.

Although diffusion contributed to the distance travelled by the dye front in two seconds, there was no need to determine the diffusion coefficient for the dye because the photographic technique was only used to obtain a measure of the relative flow velocities in Zone B and C. It was not used to determine absolute measures of velocity.

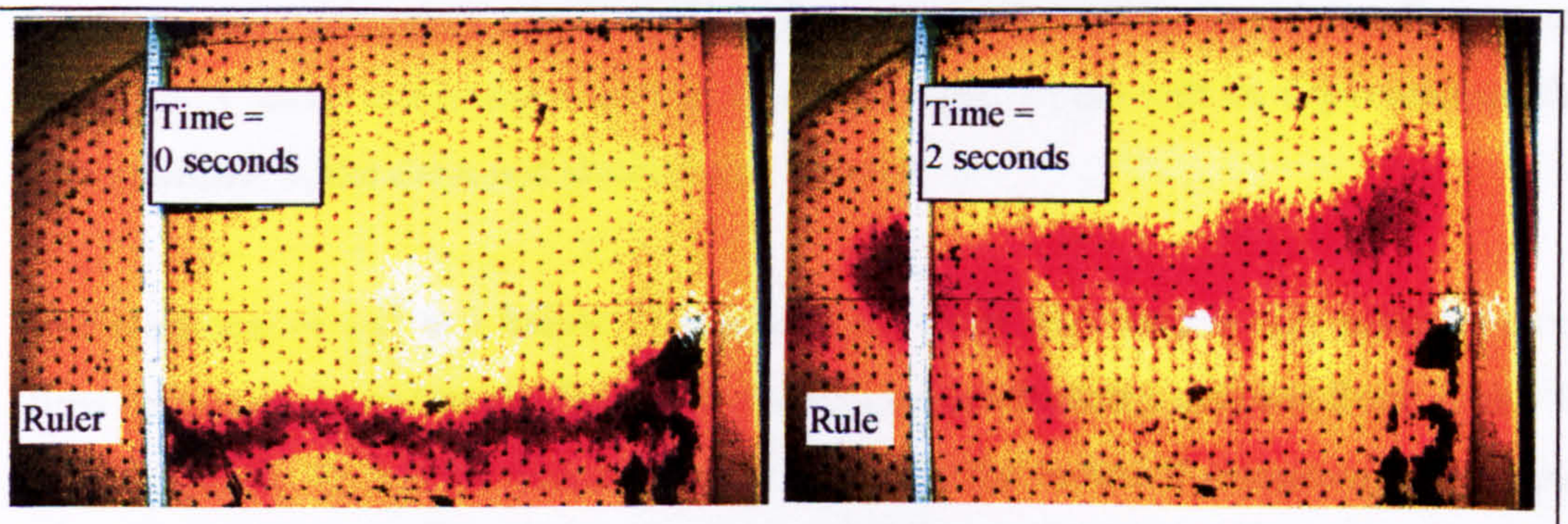

Figure 4.38 Measurement of flow velocity for depth = 8.33mm

Figure 4.39 shows the plots of relative depth versus F_B* which were obtained for three models, namely G75T45R, G50T45R and G25T45R. The same models were used to illustrate the variation of relative depth with F_A*. Figure 4.39 also contains a plot of relative depth versus Global F* for G75T45R so that the F_B* variation can be put into context with the flow regions that are exhibited in the Global F* plot.

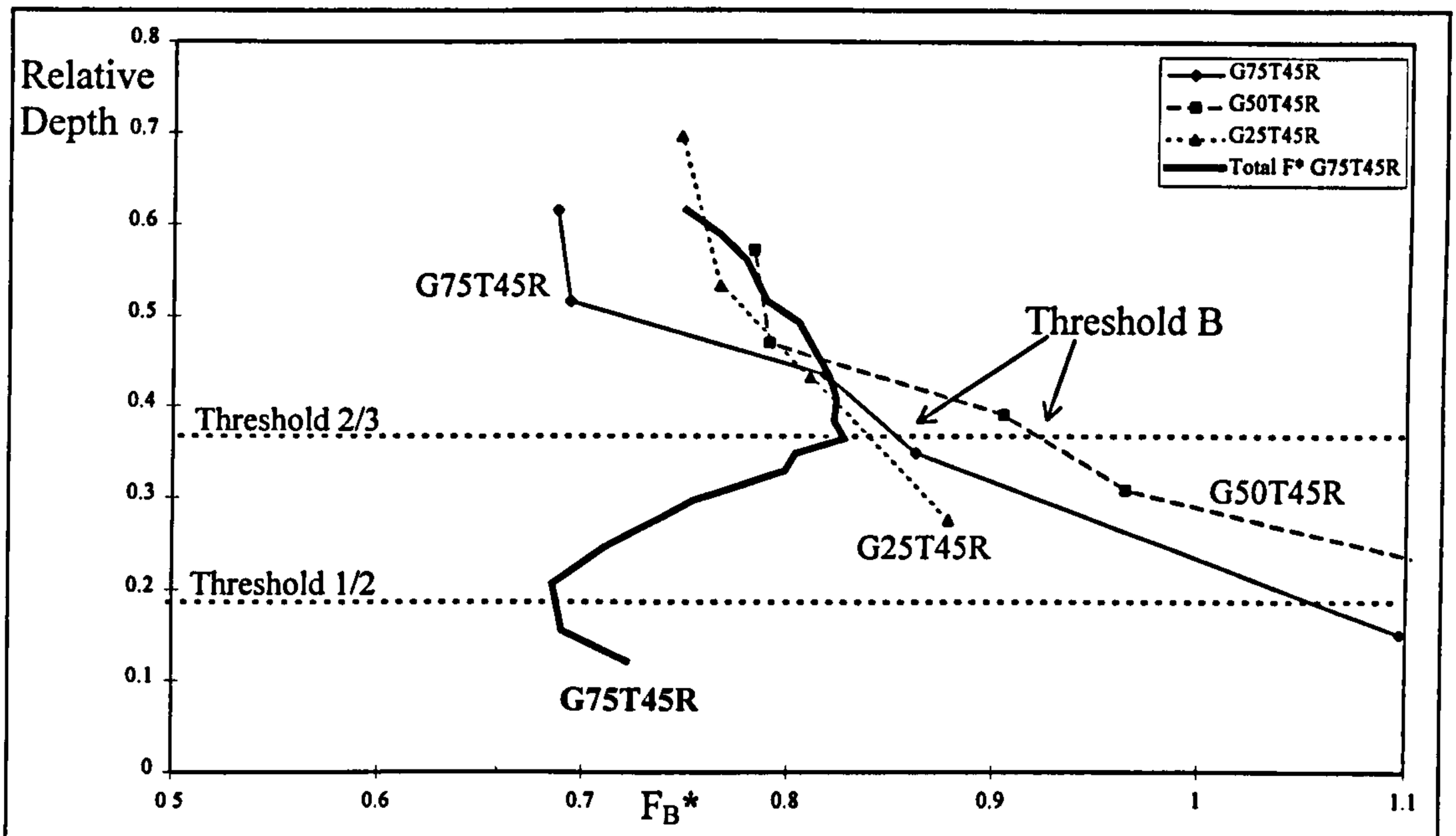

Figure 4.39 Relative depth versus F_B* for G75T45R, G50T45R and G25T45R.

Significantly Threshold 2/3 in the Global F* plot corresponds closely with Threshold B in the F_B* plots. Below Threshold B, in flow regions 1 and 2, F_B* is close to 1. Above Threshold B the magnitude of F_B* rapidly decreases. Significantly the Threshold B occurs at slightly different relative depths in each model. The author postulates that the relative depth corresponding to Threshold B will be controlled by the relative flow states in Zones A and B achieving a critical threshold value which will be dependant on the configuration of the main and flood plain channels.

The closeness of F_B* to 1 below Threshold B indicates that there is only minimal extra flow resistance caused by the flow layer interaction mechanisms between Zone A and B. In some of the 30 models tested in Glasgow during the Series B extension programme F_B* was marginally greater than 1 which indicates that the flow in Zone B is being accelerated by the fast flowing water in Zone A at low flow depths. However, by contrast, other model tests produced results for F_B* which were marginally smaller than

1. This indicated that the interaction of Zone B with Zone A at these flow depths generates extra flow resistance in Zone B flow. However, because there were large experimental variations encountered when measuring the flow velocity at low flow depths (which were attributable to the variability of the results provided by the indirect flow velocity measurements) additional research will be needed to clarify the impact of the Zone A and B interactions at low flow depths. Irrespective of these results, the magnitude of F_B* was always considerably larger than Global F* at low flow depths and in the vicinity of 1. Figure 4.39 shows that the closeness of F_B* to 1 does not significantly affect the Global F* plot in flow region 1 where Global F* exhibits a significant decrease in magnitude over these depths in line with F_A*. This was expected because Zone B only contributes a small proportion of the flow capacity at these depths. However the increasing closeness of F_B* to 1 as flow depths increase in flow region 2 does explain why Global F* shows a dramatic increase in magnitude at these depths. An increasingly large proportion of flow capacity is provided by Zone B as flow depths increase, the magnitude of Global F* becomes more dominated by the magnitude of F_B* in flow region 2.

The rapid decrease in F_B* above Threshold B indicates that a particular flow interaction mechanism, which was not dominant at lower flow depths, is making a more significant contribution to the flow resistance in Zone B at these flow depths. At these flow depths the majority of the conveyance capacity of the whole channel is provided by Zone B so consequently the Global F* reflect the decrease in F_B* magnitude in flow region 3.

Figure 4.39 also provides evidence to indicate that the rate of decrease in F_B* reduces at higher flow depths. The author suggests that this results from the flow resistance generated by layer interaction comprising a smaller proportion of the overall flow resistance in Zone B at high flow depths.

4.6.3.3 Local F for Zone C and its variation with relative depth*

The magnitude of F* in Zone C, F_C*, was calculated at between 3 and 6 relative depths in all 30 models which were built in Glasgow during the Series B extension programme. F_C* was defined as the arithmetic mean of the discharge in Zone B which was measured

at the apex and cross-over section, Q_C, divided by the predicted discharge allowing for bed friction losses only, Q_{TC}. The measured discharge at each cross-section was determined by integrating the point velocities over the area of Zone C. Figure 4.40 shows the plots of relative depth versus F_C^* which were obtained for three models, namely G75T45R, G50T45R and G25T45R. The same models were used to illustrate the variation of relative depth with F_A^* and F_B^*.

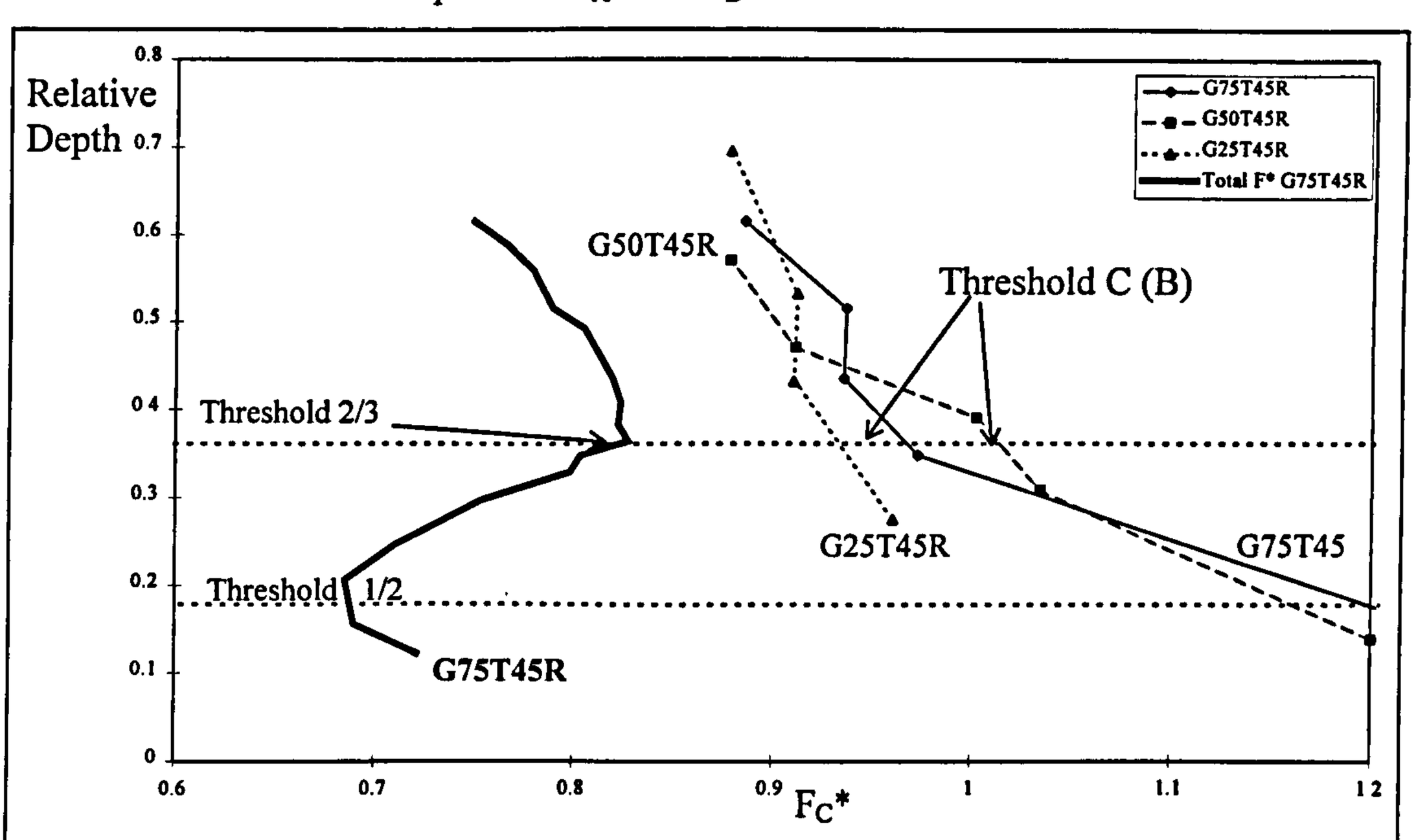

Figure 4.40 Relative depth versus F_C^* for G75T45R, G50T45R and G25T45R.

Figure 4.40 also contains a plot of relative depth versus Global F* for G75T45R so that the F_C^* variation can be put into context with the flow regions that are exhibited in the Global F* plot. Threshold 2/3 in the Global F* plot corresponds closely with Threshold C in the F_C^* plots. Below Threshold C, in flow regions 1 and 2, F_C^* is close to 1. Above Threshold C the magnitude of F_C^* rapidly decreases.

The Series B extension (1993-1996) results gathered in Glasgow demonstrated that the flow depth corresponding to the Threshold in Zone C was identical to that in Threshold B in every model which was tested. Consequently the author adopted the same label, Threshold B to mark the Thresholds in both Zones B and C for the rest of this thesis.

The closeness of F_B^* to 1 below Threshold B indicates that there is no extra flow resistance caused by the flow layer interaction mechanisms between Zone B and C. The

decrease in F_C^* above Threshold B indicates that a significant flow interaction mechanisms (and hence flow resisting force) is initiated at this depth.

The author notes that up to Threshold B, the mean velocity in Zones B and C is similar, which was indicated by similarity in the magnitude of F_B^* and F_C^*. However the magnitude of the mean Zone B velocity significantly reduces above Threshold B, because the interaction mechanisms between Zone A and B are initiated. Consequently, a momentum transfer zone, Zone C2, will be established between the slower flowing Zone B flow and the unaffected part of the Zone C flow, Zone C1, as shown in Figure 4.41. In Zone C1 the only source of flow resistance will be bed friction. This explains why the Threshold depth in Zones B and C are so similar.

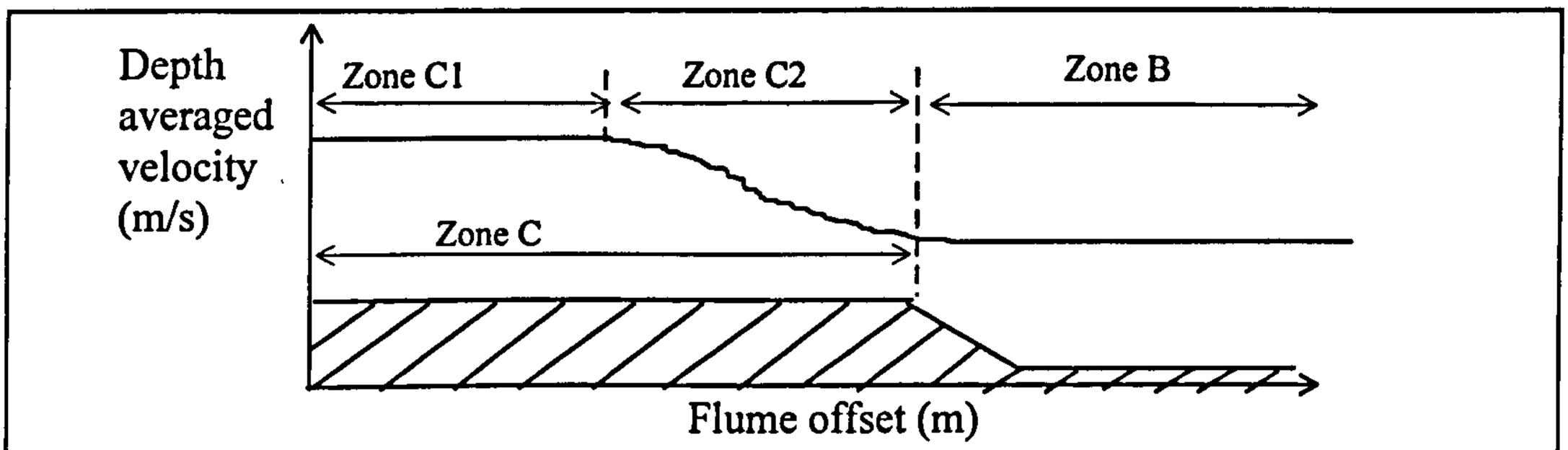

Figure 4.41 The shear zone between Zones B1 and C

The variation of F_C^* with relative depth follows a similar pattern to that exhibited by F_B^* with relative depth. The majority of the conveyance capacity of the whole channel is contained within Zones B and C at these depths so the magnitudes of F_B^* and F_C^* dominate the magnitude of Global F*. The simultaneous reduction in the magnitudes of F_B^* and F_C^* with increasing relative depth above Threshold B is reflected by the rapid decrease in the magnitude of Global F* above Threshold 2/3. The Series B extension (1993-1996) results gathered in Glasgow demonstrated that Threshold 2/3 corresponds closely to Threshold B in every model which was tested.

4.6.3.4 The influence of relative depth on the adjustment coefficient, Q_A'

Figure 4.42 presents plots of Q_A' versus relative flow depth which were obtained for G75T45R, G50T45R and G25T45R. Inspection of Figure 4.42 demonstrates that each model exhibits a relationship between Q_A' and relative depth which is non-linear and appears to be divided into two separate flow regions, flow regions A1 and A2. Flow

region A1 begins at a relative depth equal to 0 where Q_A' is equal to 1 by definition. Flow region A1 subsequently exhibits decreasing magnitude in Q_A' as relative depth increases, which implies that the flow resistance exerted on Zone A is increasing. Flow region A2 is initiated when Q_A' achieves a minimum value and begins to increase with increasing relative depth. This implies that the flow resistance exerted on Zone A is decreasing. Although the rate of increase in Q_A' diminishes with increasing relative depth it appears that the magnitude of Q_A' may achieve values greater than 1.

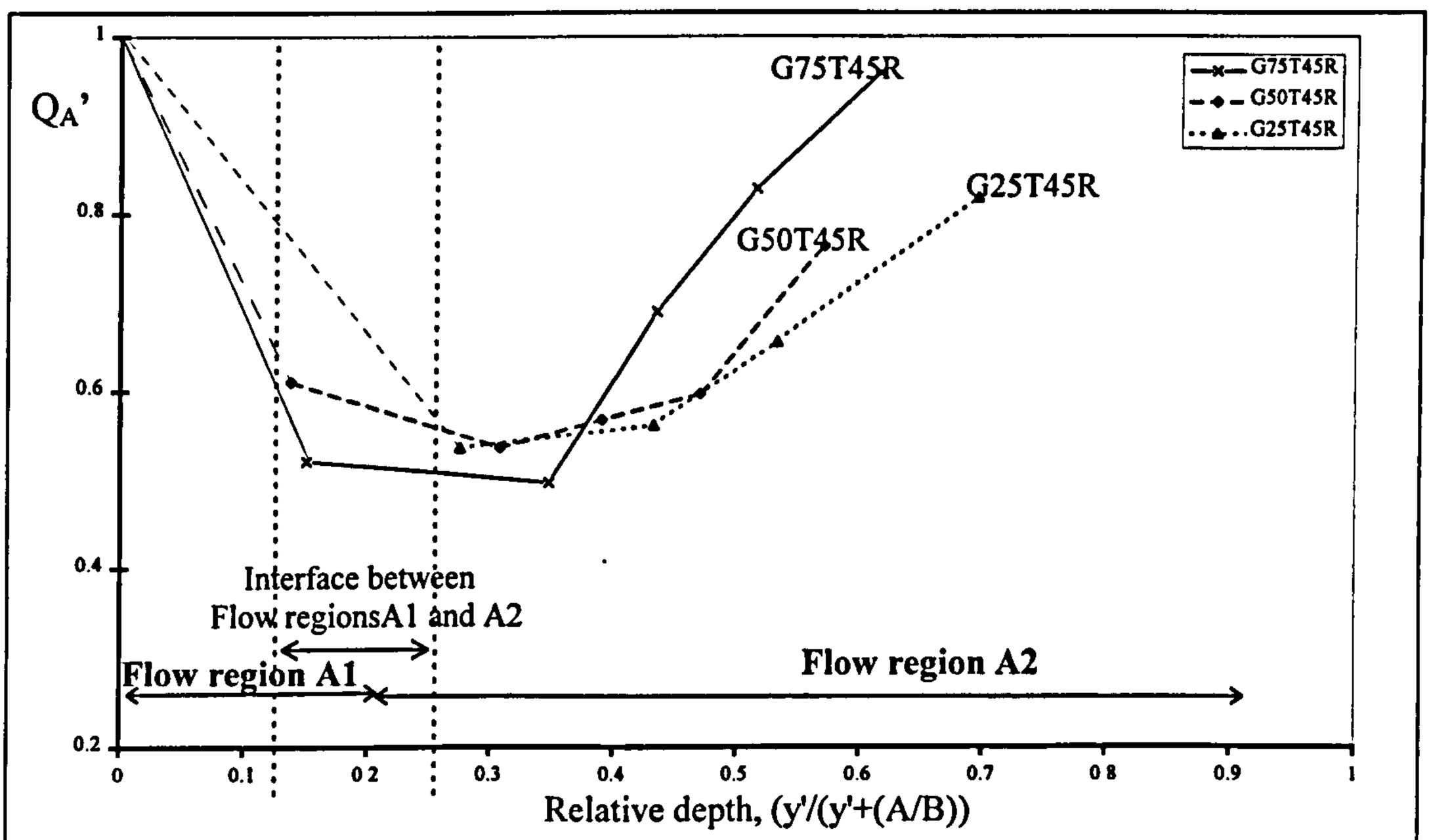

Figure 4.42 Q_A' versus relative depth for G75T45R, G50T45R and G25T45R (RD)

4.6.4 The influence of model scale on zonal flow resistance

4.6.4.1 Local F for Zone A and its variation with model scale*

Figure 4.43 plots relative depth versus F_A* and Global F* for two models: SDB21 and G25T45S, which were tested during the Series B (1989-1992) and Series B extension (1993-1996) programmes respectively. G25T45S was an exact 1:6 scale model of SDB21.

Figure 4.43 demonstrates that although the magnitude of F_A* is different at the same relative depths for each model, the magnitude of F_A* is similar in both models when the values are compared at similar points within the same flow regions (assessed using the Global F* plots). For example both SDB21 and G25T45S register a magnitude of F_A*

approximately equal to 0.64 at the beginning of flow region 3. This similarity is repeated at other points within the flow regions.

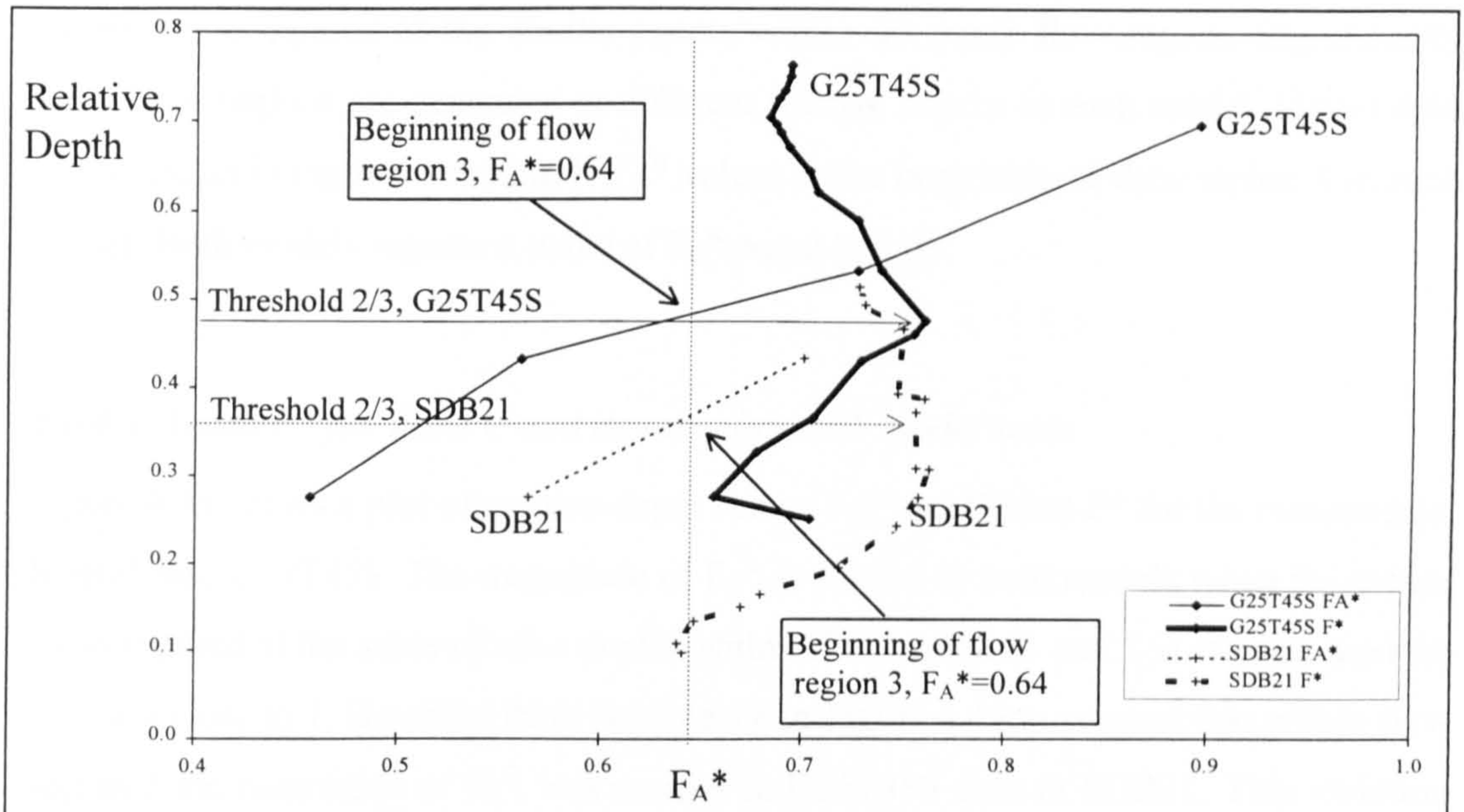

Figure 4.43 Relative depth versus zonal F* (Zone A) for G25T45S and SDB21

4.6.4.2 Local F for Zone B and its variation with model scale*

Figure 4.44 shows a plot of relative depth versus F_B* and Global F* for the two models: SDB21 and G25T45S.

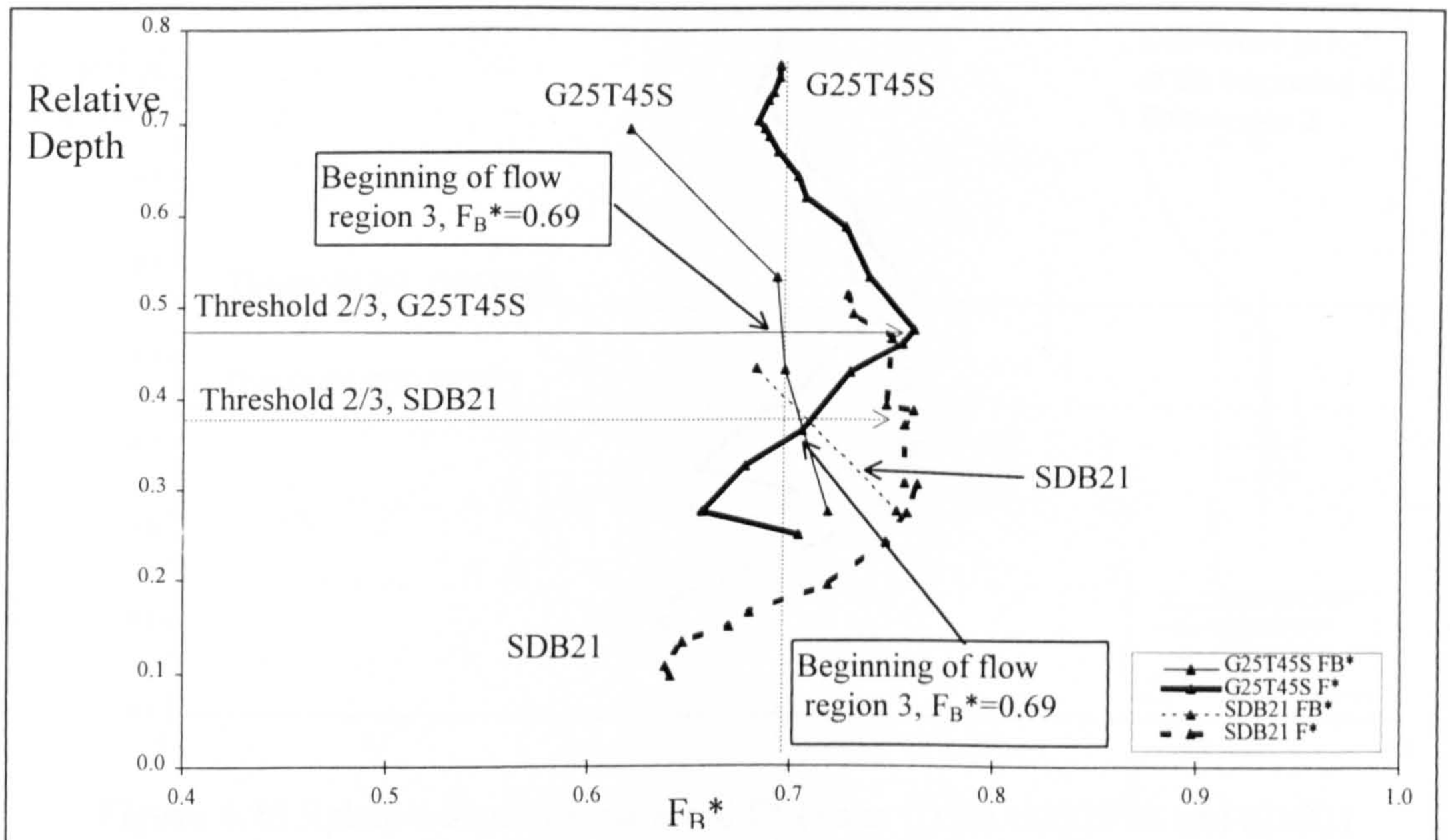

Figure 4.44 Relative depth versus zonal F* (Zone B) for G25T45S and SDB21

Figure 4.44 demonstrates that although the magnitude of F_B* is different at the same relative depths for each model, the magnitude of F_B* is similar in both models when the values are compared at the similar points within the same flow region. Significantly these flow regions are generated at different relative depths in each model. Figure 4.44 is marked showing the comparable F_B* values at the beginning of flow region 3 in each model. Both models register a value of F_B* equal to 0.69.

4.6.4.3 Local F for Zone C and its variation with model scale*

Figure 4.45 shows a plot of relative depth versus F_C* and Global F* for the two models: SDB21 and G25T45S. The magnitude of F_C* is similar in both models when the values are compared at the same relative depths within flow regions 1 and 2 in the two models, both are close to 1. However there is evidence in Figure 4.45 to suggest that within flow region 3 the magnitude of F_C* was smaller in G25T45S than in SDB21. This variation in F_C* magnitude influences the Global F* magnitude because Zone C contributes a significant proportion of the discharge capacity at these flow depths. The author suggests that F_C* is smaller in G25T45S because the shear zone width in Zone C has a disproportionately large influence on the magnitude of overall flow resistance in Zone C for smaller scale models.

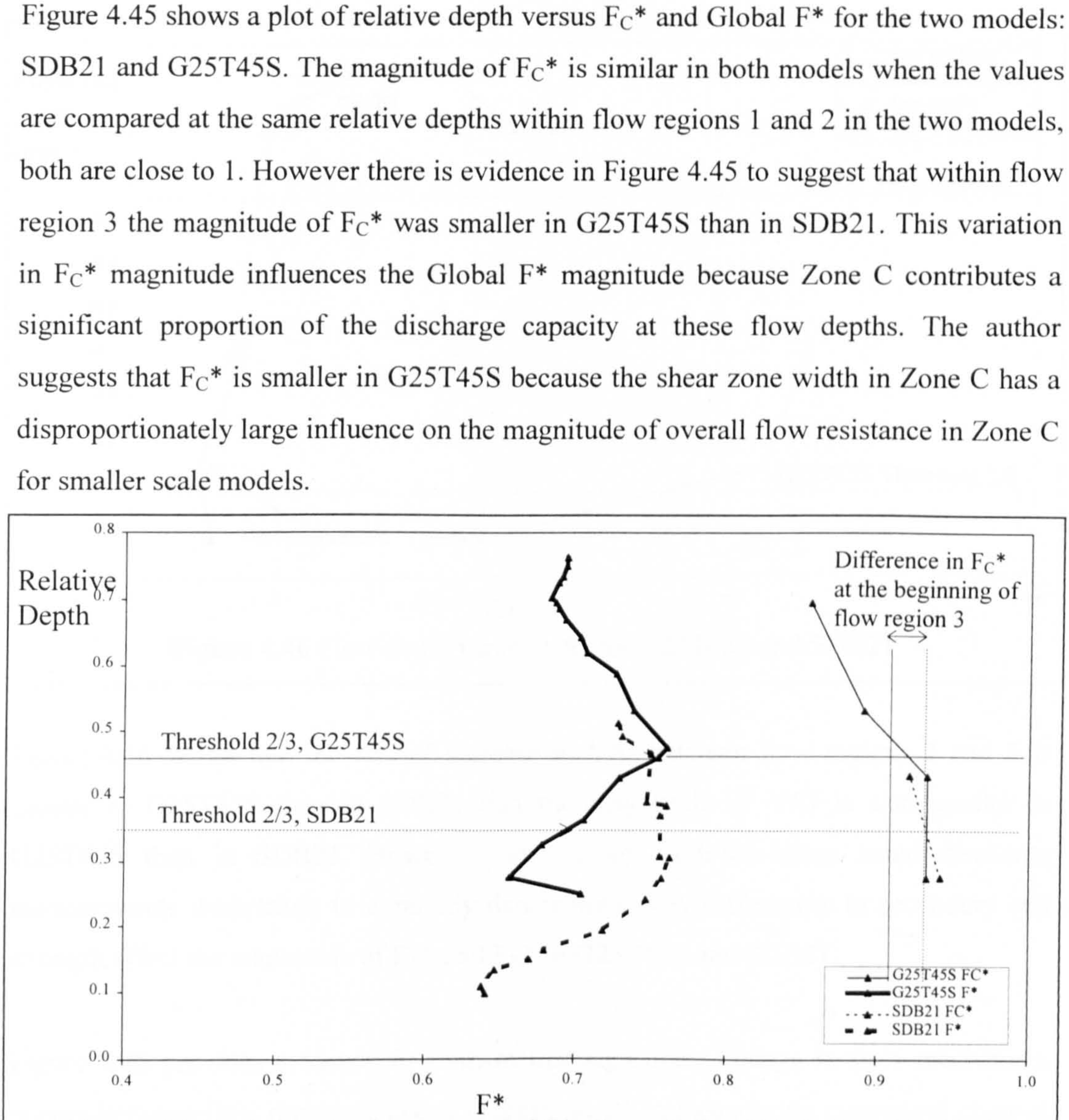

Figure 4.45 Relative depth versus zonal F* (Zone C) for G25T45S and SDB21

4.6.4.4 Variation of secondary circulation cells with model scale in Zone A

The author also investigated the effect of scale difference on the secondary circulation cells that are generated in Zone A during overbank flow. The cells rotate in a direction contrary to the secondary cells that are generated during inbank flow. Their magnitude was measured by dividing the average transverse velocity, V (resolved orthogonally to the centre line of the main channel), by the average longitudinal velocity, U (resolved along the centre line of the main channel). Large values of V/U indicate that strong secondary cells are present. Figure 4.46 shows plots of flow depth versus V/U for G25T45S and SDB21 in the main channel (Zone A).

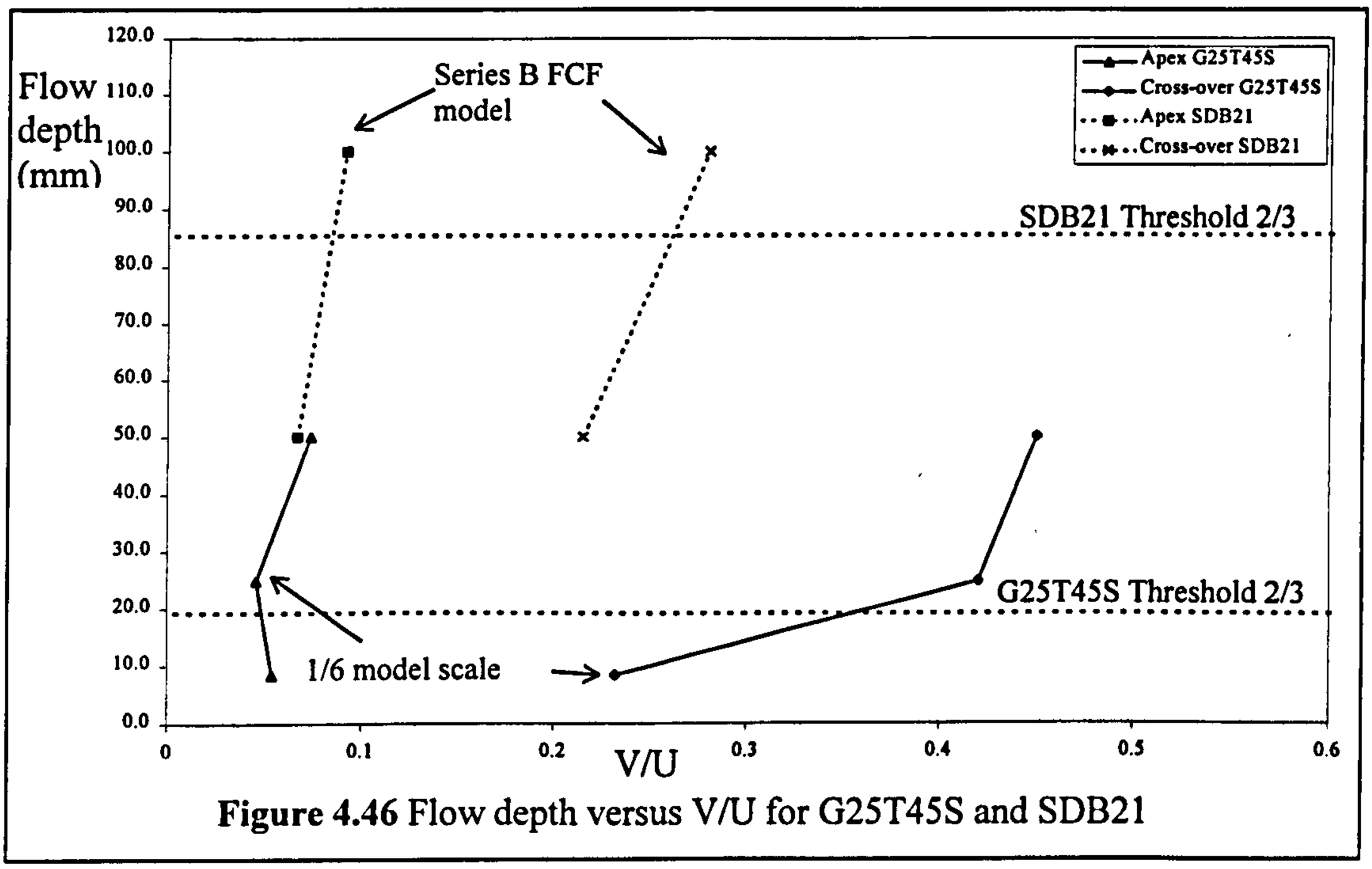

Figure 4.46 Flow depth versus V/U for G25T45S and SDB21

Figure 4.46 shows that the rate of increase in V/U between flow regions 2 and 3 is greater in G25T45S than in SDB21 and the magnitude of V/U is also greater in G25T45S than in SDB21. However, not enough high-resolution zonal discharge measurements were taken to explicitly demonstrate how differences in secondary cell strength affect the magnitude of F_A^* and F_B^* in G25T45S and SDB21.

Figure 4.46 provides evidence to confirm that significant change in flow mechanism occurs between flow regions 2 and 3 (Threshold B) in meandering compound channel flow. The secondary cells in flow region 2 for both models are relatively weak. However, as soon as flow region 3 is achieved they increase rapidly in strength. Various

researchers, such as Ervine and Ellis [1987], have suggested that the contra-rotating secondary cells may be driven by the flow mechanisms associated with the expansion and contraction of the flood plain flow as it passes over the main channel. These results indicate that until flow region 3 (Threshold B) is established there may be some resistance to the creation of secondary cells but, after flow region 3 is established, there is less resistance.

4.6.4.5 The influence of model scale on the adjustment coefficient, Q_A'

Figure 4.47 shows a plot of Q_A' versus relative depth for two models G25T45S and SDB21. There is a significant difference between the plots for the two models, Q_A' is greater for SDB21 than G25T45S at all relative depths. The Reynolds numbers associated with flow in their main channels, Re_{CH}, were equal to $1.78*10^4$ in G25T45S and $2.75*10^5$ in SDB21. Ten of the 11 key parameters were identical. Relative roughness differed, but only slightly at the same relative depths indicating small differences in the bed friction effects in the main channel and on the flood plains. The difference in Re_{CH} , by contrast, was significant, an order of 10 in magnitude difference.

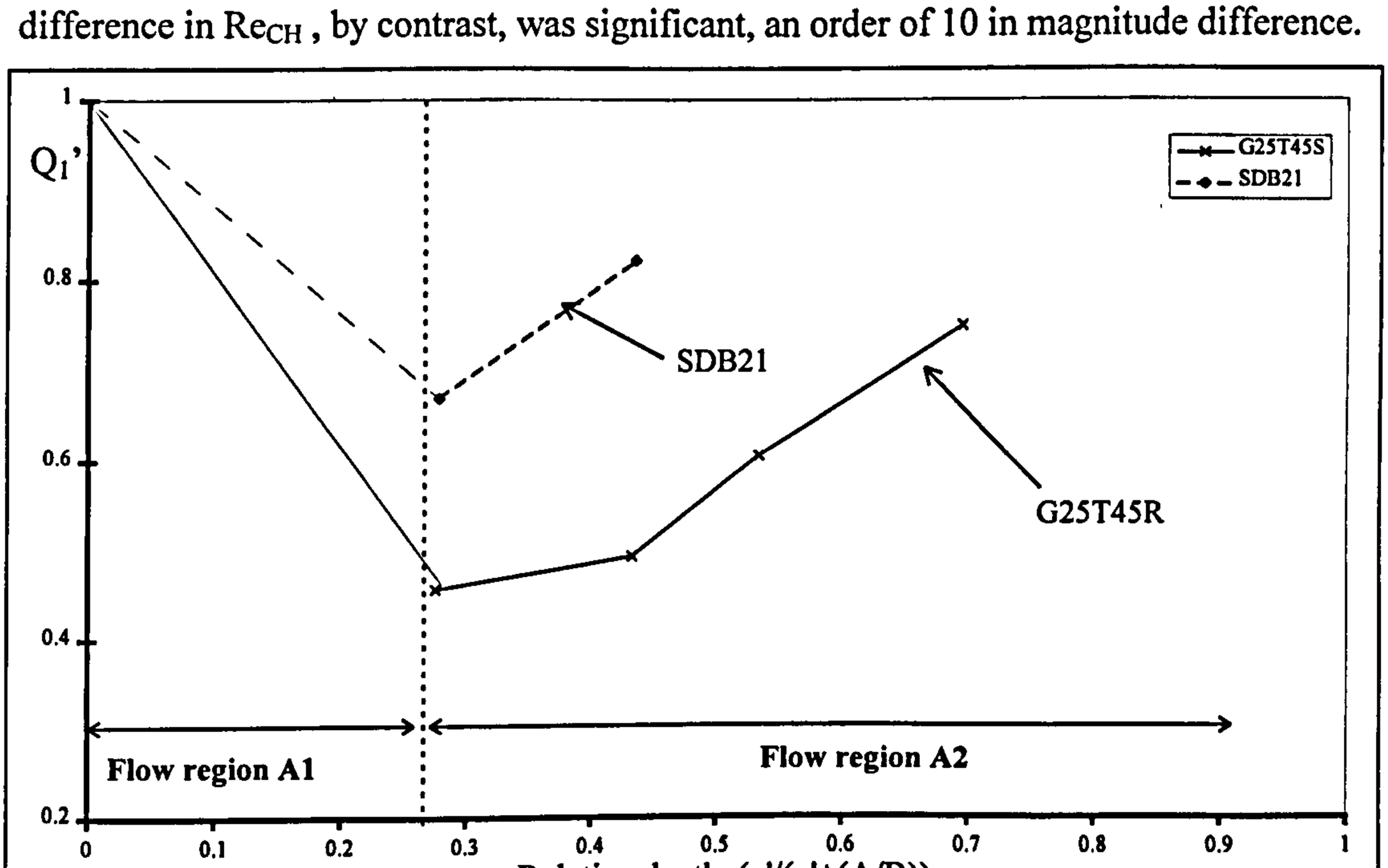

Figure 4.47 Q_A' versus relative depth for SDB21 and G25T45S (Re_{CH})

The author postulates that Q_A' is larger in the larger scale models because the main channels with high energy states are less susceptible to interaction with Zone B.

Consequently the author suggests that a measure of Reynolds number, Re_{CH} would be a good additional parameter to study to link scale difference to flow resistance.

Unfortunately flow data from only two exact scale models was available during the Series B extension programme, but the author attempted to overcome this deficiency by varying the magnitude of Re_{CH} within a number of the smaller models which were tested in Glasgow; Re_{CH} ranged between $1.78*10^4$ and $6.43*10^4$ in these models. The influence of Re_{CH} was explicitly analysed and was shown to have a consistent affect in these models. The author concluded that Re_{CH} could potentially be used as a parameter for predicting the influence of scale differences in meandering compound channels.

4.6.5 The influence of relative roughness on zonal flow resistance

4.6.5.1 Local F for Zone A and its variation with relative roughness*

Aberdeen had not published their zonal flow results at the time of writing this thesis. Consequently the analysis has concentrated upon the Glasgow results to demonstrate the influence of relative roughness on zonal F*. Figures 4.48 shows a plot of overbank flow depth versus F_A* for model tests: G75T90S, G75T90R and GR75T90R.

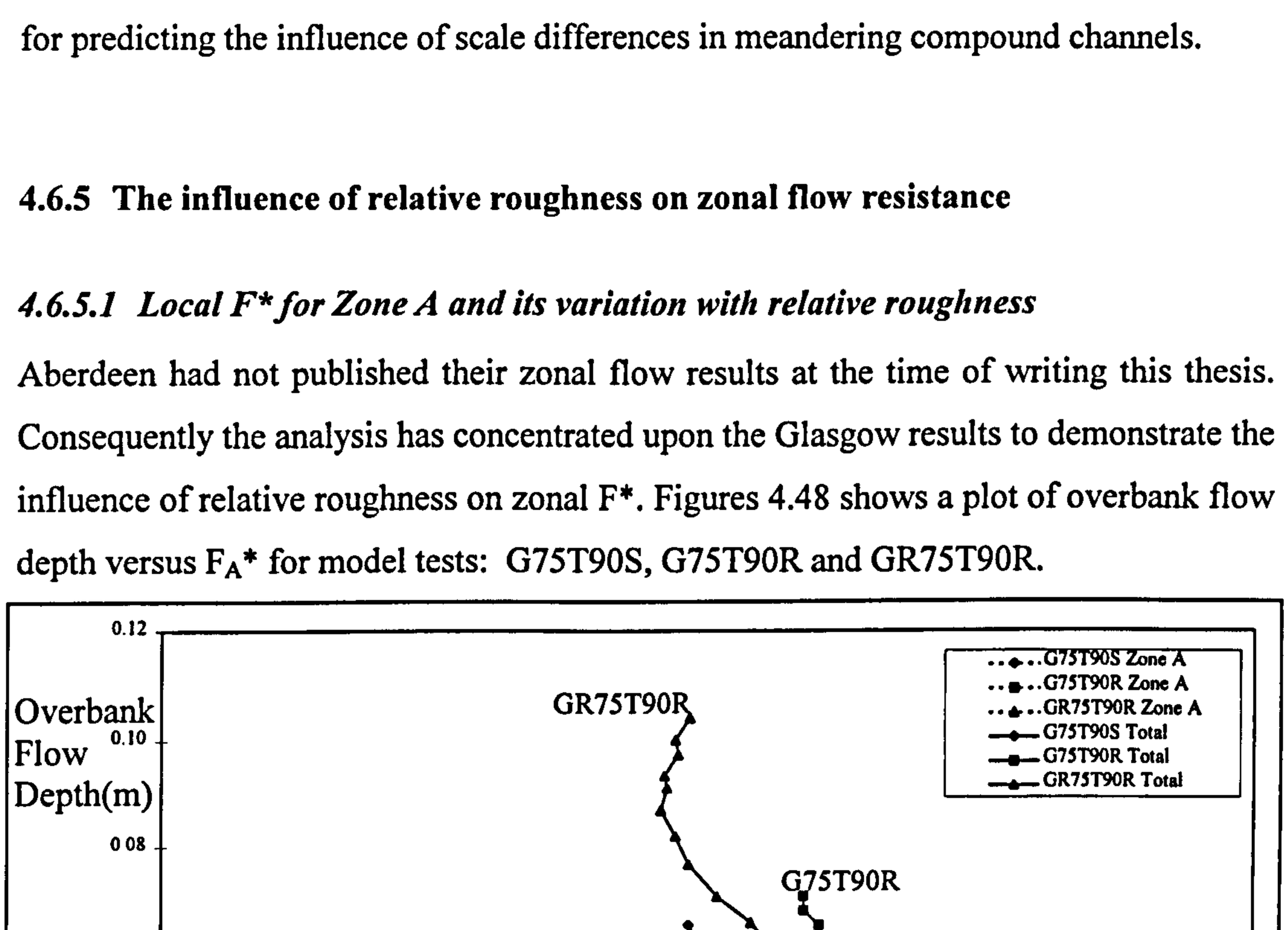

Figure 4.48 Flow depth versus F* and F_A* (Zone A)

It demonstrates that at low flow depths, flow regions 1 and 2, increasing the relative roughness, f_f/f_c, by increasing the flood plain roughness between G75T90S and G75T90R has a negligible effect on F_A*. However decreasing the relative roughness, f_f/f_c, by increasing the main channel roughness and leaving the flood plain roughened in G75T90R and GR75T90R, causes a decrease in the magnitude of F_A*. The author notes that Re_{CH} does not change between G75T90S and G75T90R and there is little change in the magnitude of F_A* in flow region 1, whereas Re_{CH} does significantly decrease between G75T90S and GR75T90R which appears to induce a correspondingly significant decrease in the magnitude of F_A*. Once again the variations in flow state in the main channel (which are affected by its roughness) are shown to have considerable influence on the magnitude of F_A* in flow region 1, up to Threshold A. The flow depth corresponding to Threshold A varies in the plots for different relative roughnesses.

Figure 4.48 also demonstrates that at higher flow depths (above Threshold A) the magnitude for Global F_A* steadily increases and attains a similar magnitude for each of the models irrespective of relative roughness and the main channel Reynolds number, Re_{CH}.

The author postulates that Relative roughness has a significant effect on meandering channel flow because it influences the relative flow state in the main channel and on the flood plains and therefore controls the flow depths at which critical relative flow states are initiated. The author suggests that different interaction mechanism become dominant at these critical flow states.

4.6.5.2 Local F for Zone B and its variation with relative roughness*

Figure 4.49 shows plots of overbank flow depth versus F_B* for model tests G75T90S, G75T90R and GR75T90R. It illustrates that the magnitude of F_B* is close 1 throughout flow regions 1 and 2 irrespective of the relative roughness of the model.

At the onset of flow region 3 however F_B* dramatically decreases with increasing flow depth but the rate of change is similar for each model irrespective of relative roughness. However the depth at which the decrease in F_B* is first observed (which coincides with

Threshold 2/3 in the Global F* plot or Threshold B in the F_B* plot) is different for each model. The author predicts that the flow mechanisms associated with the onset of flow region 3 may be triggered when the relative flow state of the main channel and flood plains achieve a Threshold value which will be influenced by the relative roughness of the main and flood plain channels.

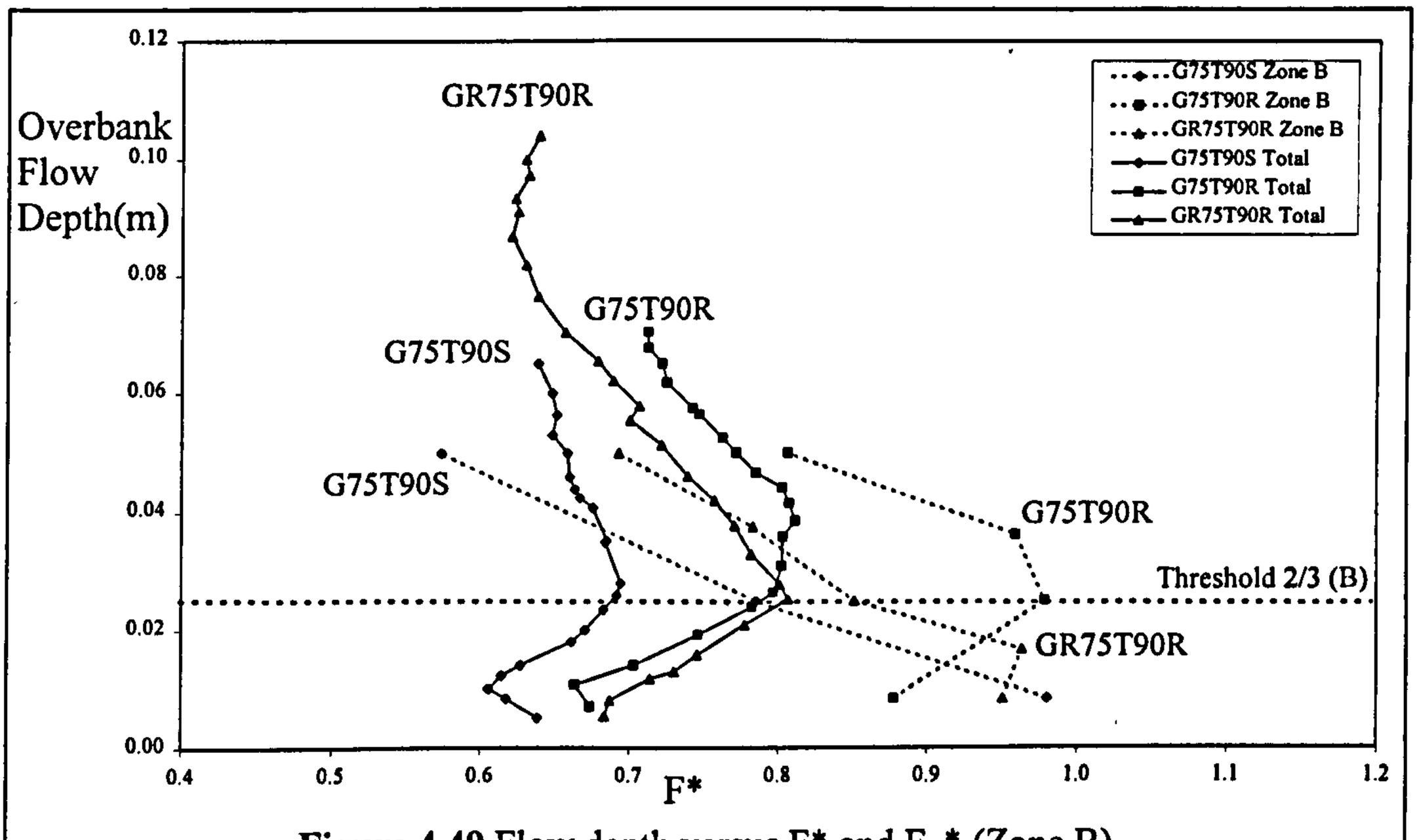

Figure 4.49 Flow depth versus F* and F_B* (Zone B)

4.6.5.3 Local F for Zone C and its variation with relative roughness*

Figures 4.50 shows plots of overbank flow depth versus F_C* for model tests: G75T90S, G75T90R and GR75T90R.

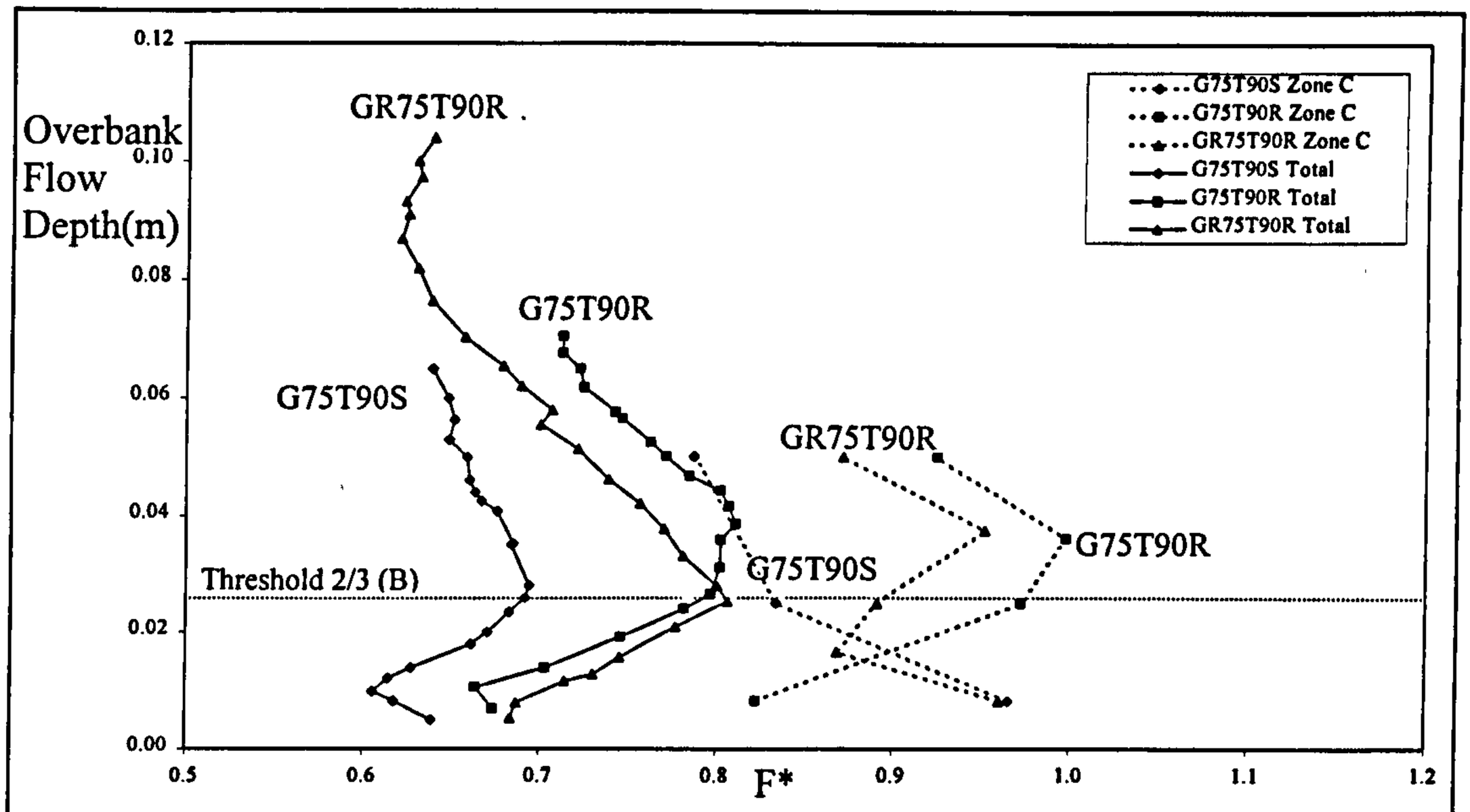

Figure 4.50 Flow depth versus F_C^* and Global F* (Zone C)

Figure 4.50 illustrates that the magnitude of F_C^* is close to 1 throughout flow regions 1 and 2, irrespective of the relative roughness of the channel. At the onset of flow region 3 however, F_C^* starts to decrease with increasing flow depth. The decreasing values for F_C^* are initiated at different flow depths in each model but at similar flow depths to the ones at which F_B^* started to decrease in each model. The author attributes the reduction of F_C^* to the onset of a momentum transfer mechanism between Zones B and C (Zone C2).

The magnitude of F_C^* in flow region 3 is similar for the two channels with roughened flood plains: GR75T90R and G75T90R. However the magnitude of F_C^* is significantly less for G75T90S with smooth flood plains. This behaviour reflects the Zone B behaviour where F_B^* is smaller for G75T45S (the velocity reduction is greater) than for the models with roughened plains.

4.6.5.4 The influence of relative roughness on the adjustment coefficient, Q_A'

Figure 4.51 shows a plot of Q_A' versus relative depth for two models with different relative roughness: G25T45R and G25T45S, which were tested in Glasgow during the Series B extension programme.

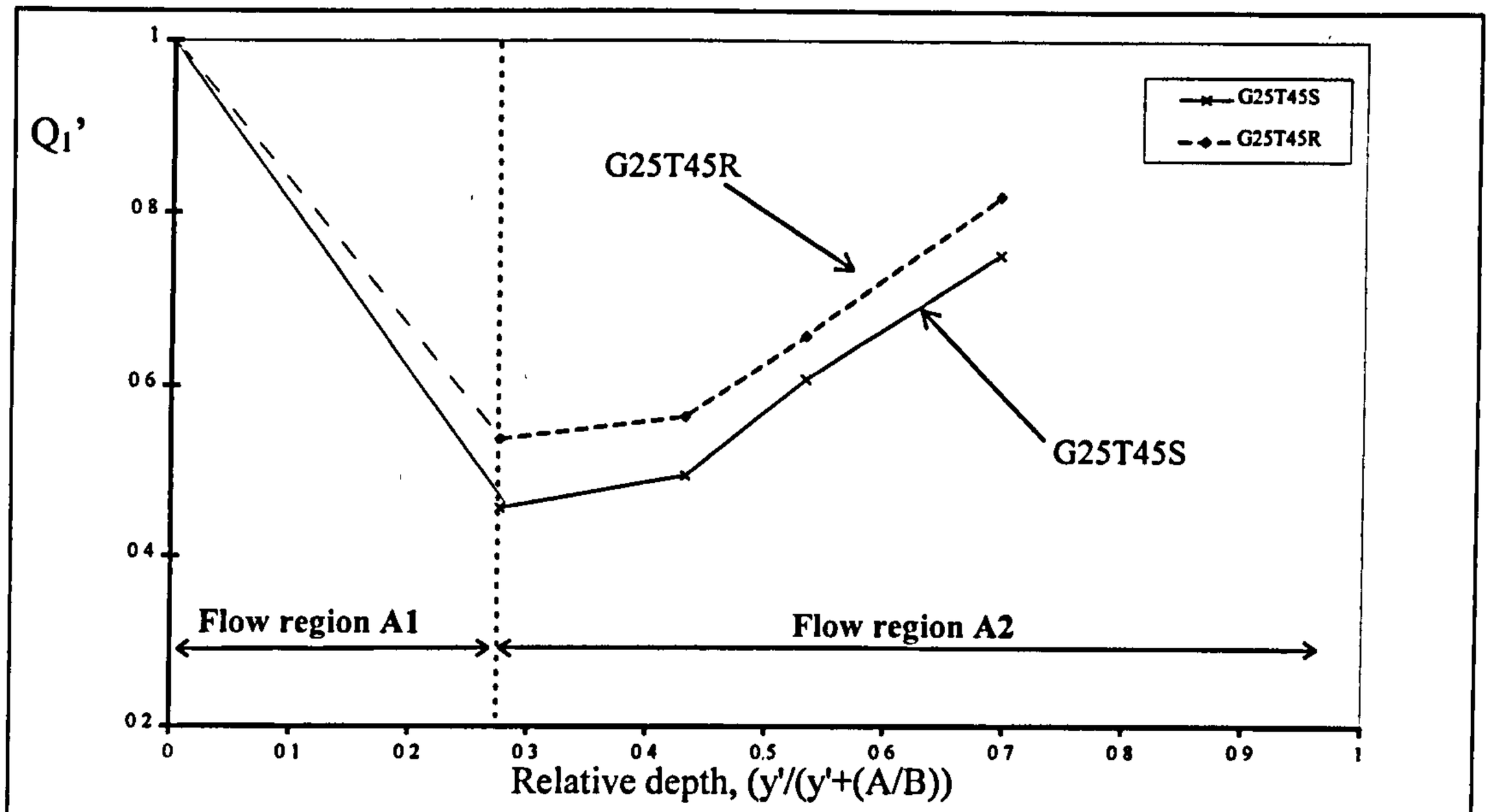

Figure 4.51 Q_A' versus relative depth for G25T45R and G25T45S (f').

G25T45S has smooth flood plains with Manning's n tending towards 0.01 at high flow depths (low relative roughness). G25T45R has roughened flood plains with Manning's n tending towards 0.014 at high flow depths (high relative roughness). The magnitude of Q_A' is greater for G25T45R than for G25T45R at all relative depths. The author suggests that the interaction losses are smaller in G25T45R (resulting in higher Q_A') because the Zone B velocity is lower in G25T45R than in G25T45S at the same flood plain flow depth. The author demonstrated that a similar pattern of behaviour is observed for all the models with similar variations in relative roughness.

4.6.6 The influence of main channel aspect ratio on zonal flow resistance

4.6.6.1 Local F for Zone A and its variation with aspect ratio*

Figure 4.52 shows plots of overbank flow depth versus F_A* and Global F* for G75T45R and G25T45R which had aspect ratios equal to 5.3 and 8.0 respectively.

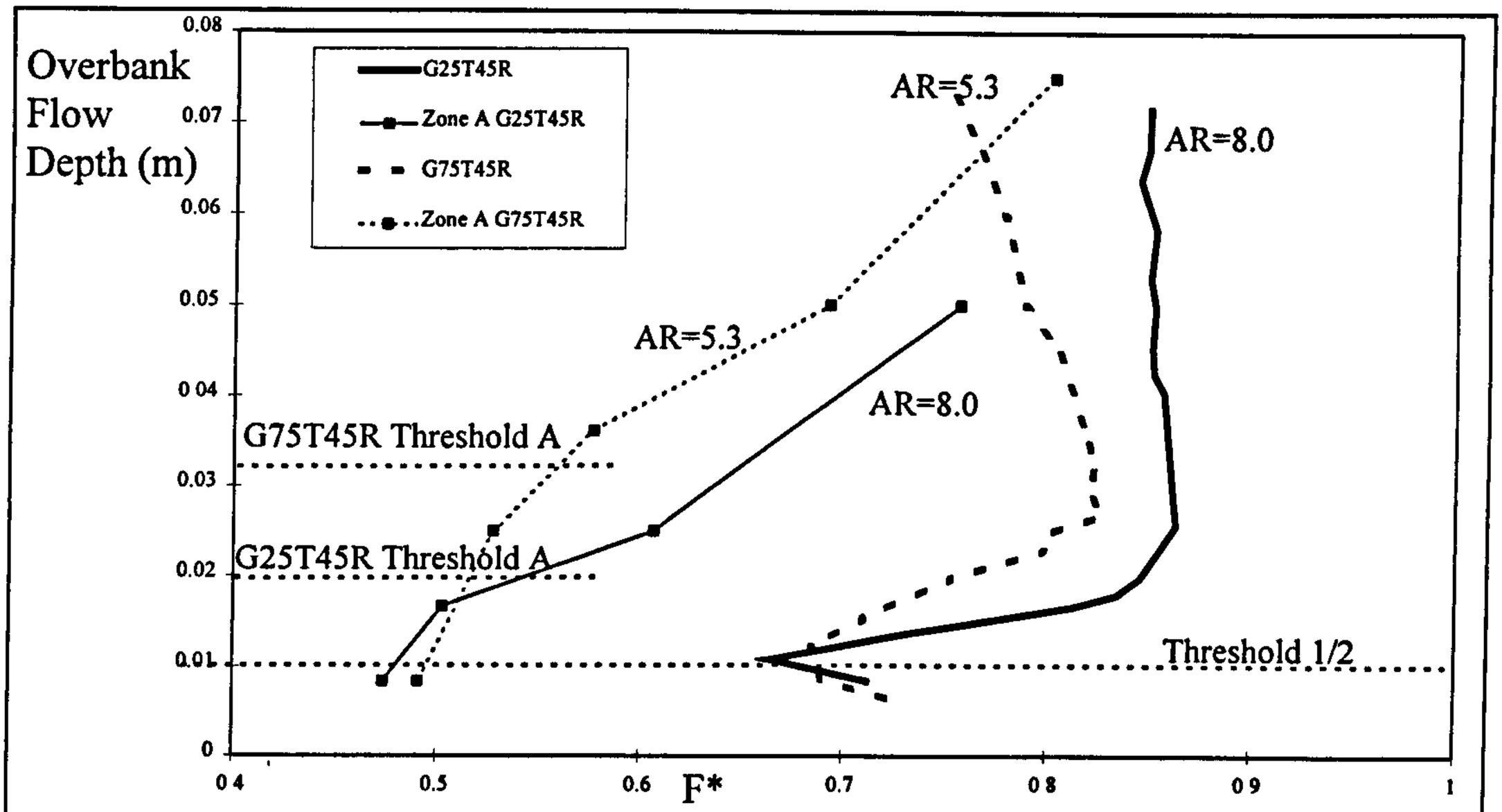

Figure 4.52 Flow depth versus F_A* and Global F* for G25T45R and G75T45R

Figure 4.52 provides evidence that F_A* is slightly smaller in G25T45R (AR=8.0) than in G75T45R (AR=5.3) at low flow depths, up to Threshold A. This indicates that greater flow resistance is generated in the larger aspect ratio channels at low flow depths. Analysis of the other 28 models corroborated this behaviour although the differences in F* are typically small. The similarity of F_A* between the models at low flow depths is reflected by the Global F* plot which also exhibit similar magnitudes at low depths. This was expected because the majority of flow capacity is provided by Zone A.

By contrast, for all higher flow depths the magnitude of F_A* is larger for G25T45R. This indicates that greater flow resistance is generated in the smaller aspect ratio channels at higher flow depths. The difference in F_A* for G25T45R and G75T45R is reflected in the plots of Global F* which is greater for G25T45R than for G75T45R at higher flow depths. However the author notes that this indicates that the flow resistance is smaller in Zones B and C as well as for Zone A at high flow depths (for small aspect ratio channels) because the majority of the flow capacity is provided by Zones B and C at these flow depths.

4.6.6.2 Local F for Zone B and its variation with aspect ratio*

Figure 4.53 shows plots of overbank flow depth for F_B* and Global F* for G75T45R and G25T45R which had aspect ratios equal to 5.3 and 8.0 respectively.

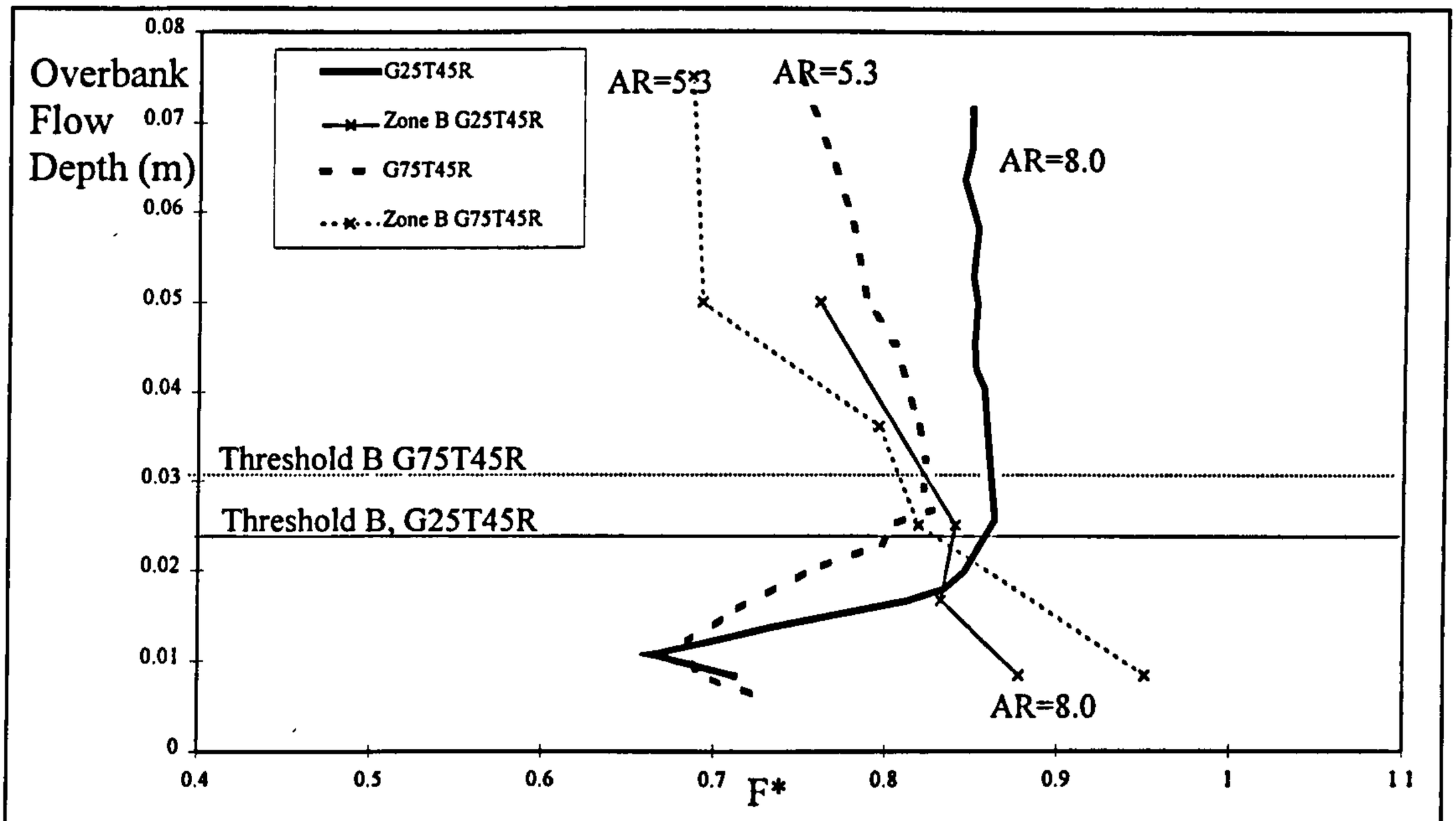

Figure 4.53 Flow depth versus F_B* and Global F* for G25T45R and G75T45R

Figure 4.53 shows that the magnitude of aspect ratio does not significantly affect the magnitude of F_B* in flow regions 1 and 2 (below Threshold B). By contrast in flow region 3 (above Threshold B) it confirms that the magnitude of F_B* is smaller for G75T45R than G25T45R and that the difference becomes greater with increasing flow depths. This indicates that main channels with smaller aspect ratios cause a greater flow resistance to be generated in Zone B.

4.6.6.3 Local F for Zone C and its variation with aspect ratio*

Figure 4.54 shows plots of overbank flow depth versus F_C* and Global F* for G75T45R and G25T45R which had aspect ratios equal to 5.3 and 8.0 respectively.

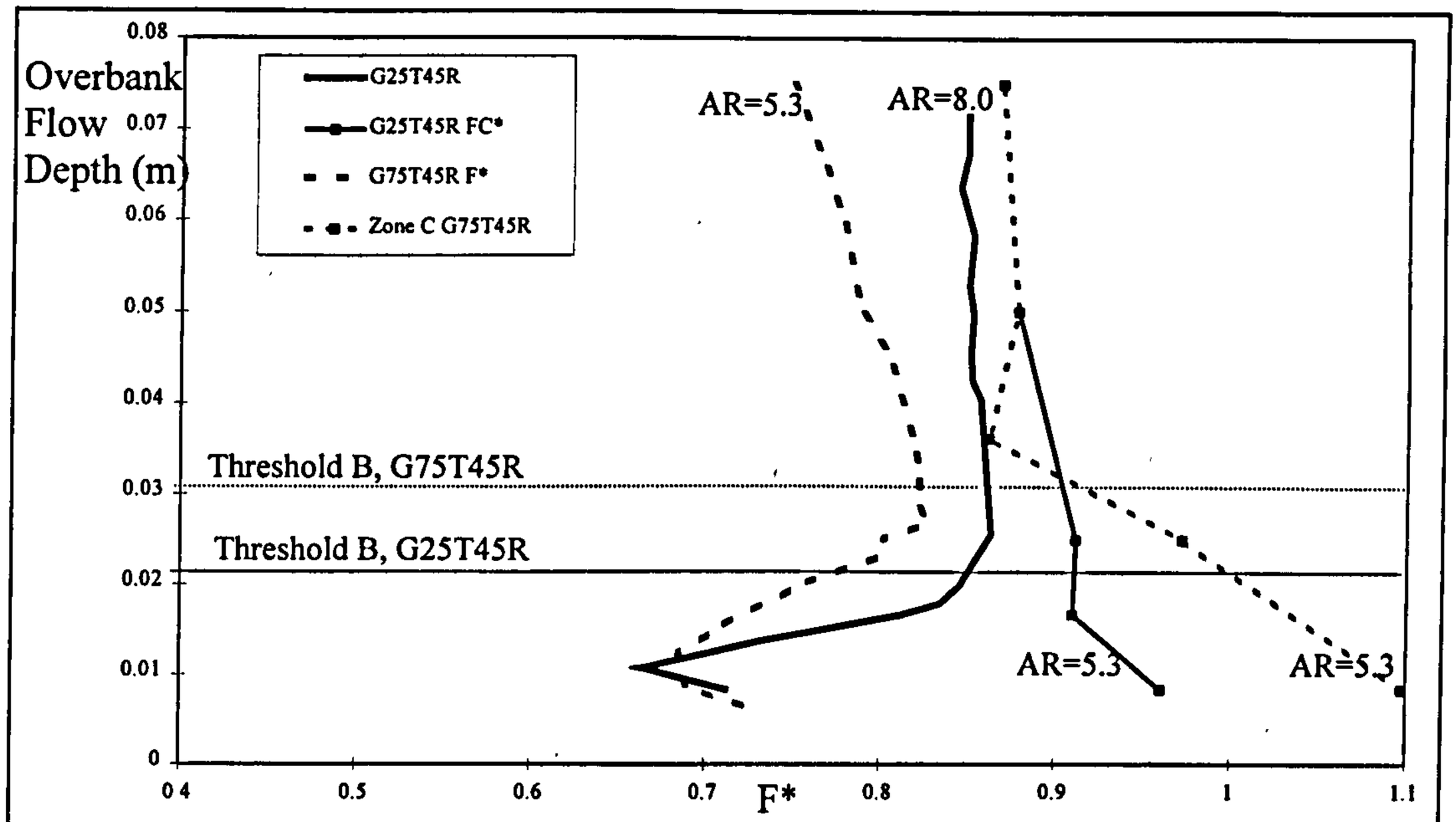

Figure 4.54 Flow depth versus F_C* and Global F* for G25T45R and G75T45R

Figure 4.54 shows that the magnitude of F_C* is close to 1 in flow regions 1 and 2 (below Threshold B), irrespective of the magnitude of the model's aspect ratio. It also shows that in flow region 3 (above Threshold B) the magnitude of F_C* is not significantly affected by variations in the aspect ratio. The difference in F_B* values illustrated in Figure 4.53 indicated that the mean depth-averaged velocities in Zone B were smaller in G75T45R than in G25T45R (at the same overbank flow depth). However it appears that the difference is too small to significantly affect the average velocity in the momentum transfer zone of Zone C and therefore alter the magnitude of F_C* between the models.

4.6.6.4 The influence of aspect ratio on expansion and contraction losses in Zone B

A number of researchers have proposed that the extra flow resistance in Zone B can be attributed to the head losses generated by the expansion and contraction of the Zone B flow as it passes over Zone A. The author used some results from the additional slot model tests which were performed in Glasgow during the Series B extension (1993-1996) programme in order to demonstrate whether the influence of aspect ratio on F_B* behaviour could be explained by identifying the influence of aspect ratio on the expansion and contraction head losses in flow over a slot. Figures 4.55 and 4.56 show plots of the expansion and contraction head loss versus flow depth for slots with 90

degree side slopes: S7G9S, S5G9S and S2G9S. The geometric configurations of these models are listed in Table 3.12.

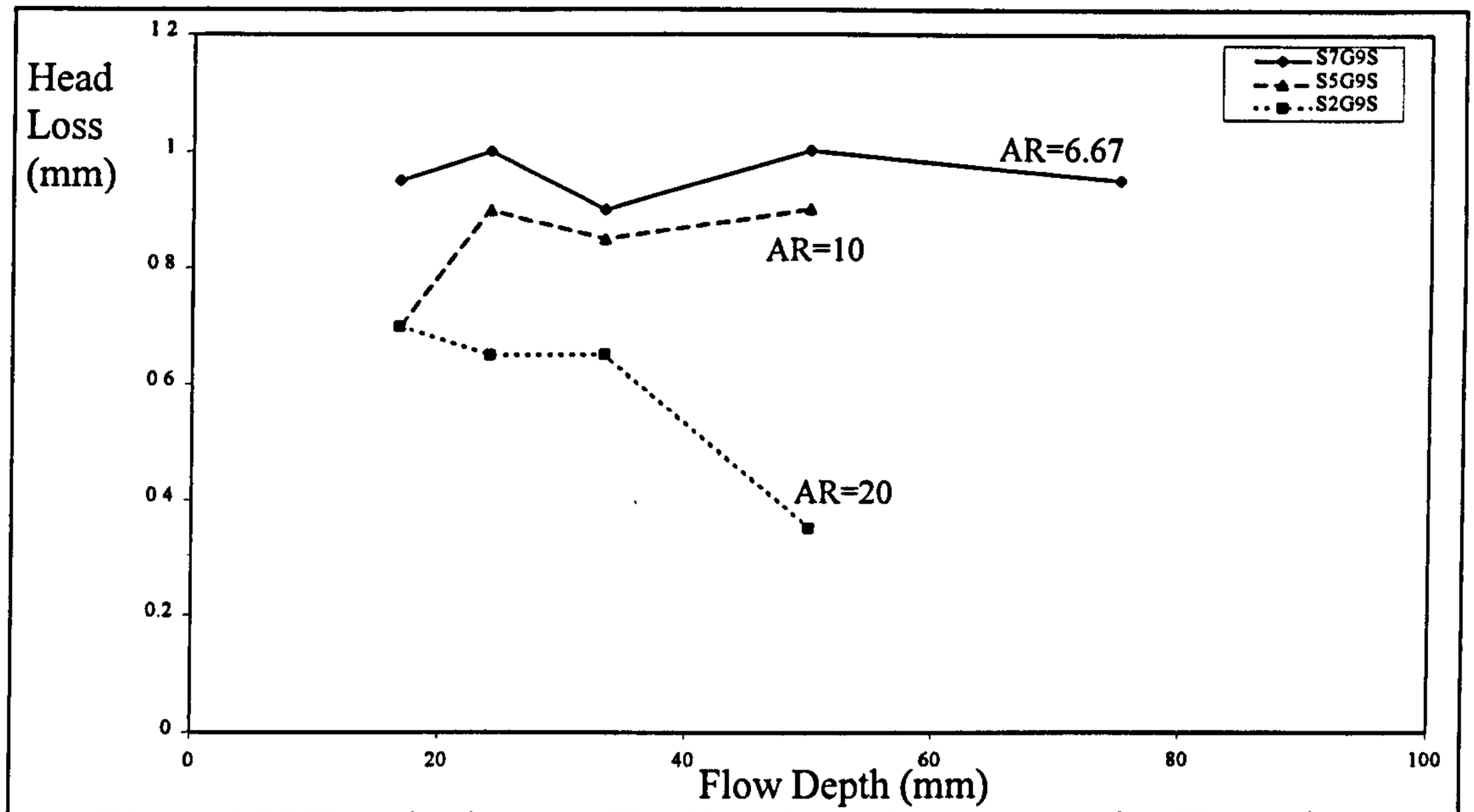

Figure 4.55 Flow depth versus Head loss for various aspect ratios (Expansion)

Figure 4.55 shows a clear trend which demonstrates that the expansion head losses are larger in the small aspect ratio channels (AR=6.67, S7G9S) at all flow depths which explains why F_B* is larger in G75T45R (AR=5.33) than in G25T45R (AR=8.0).

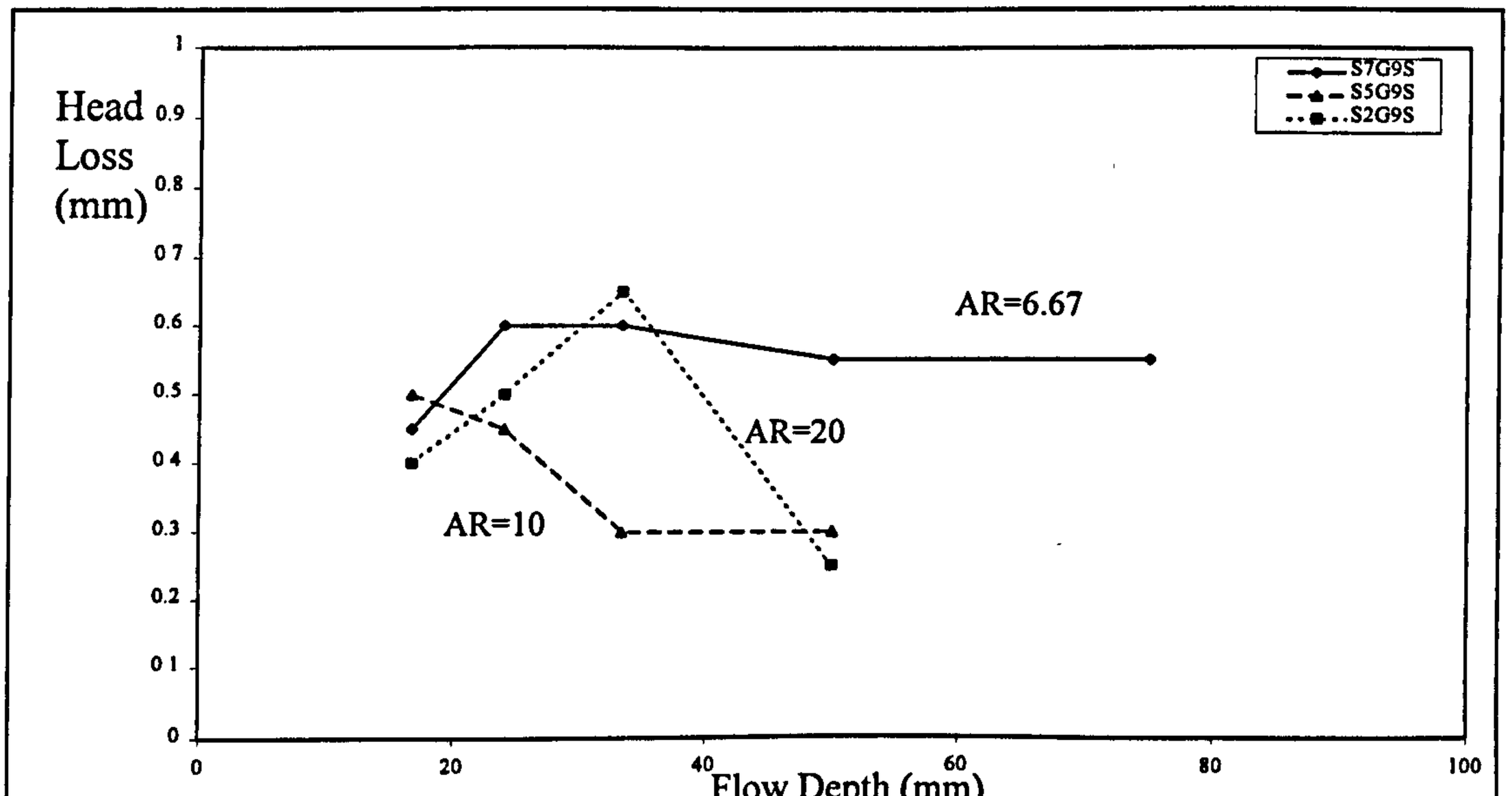

Figure 4.56 Flow depth versus Head loss for various aspect ratio (Contraction)

The results in Figure 4.56 are less conclusive. They do provide limited evidence to demonstrate that the magnitude of contraction head loss is also marginally greater in the

small aspect ratio channels (AR=6.67, S7G9S) at all flow depths thus reinforcing the evidence to explain why F_B* is larger in G75T45R (AR=5.33) than in G25T45R (AR=8.0).

4.6.6.5 The influence of aspect ratio on the adjustment coefficient, Q_A'

Figure 4.57 presents plots of Q_A' versus relative depth which were obtained for G75T45R, G50T45R and G25T45R which had aspect ratios equal to 2.67, 5.33 and 9.13 respectively.

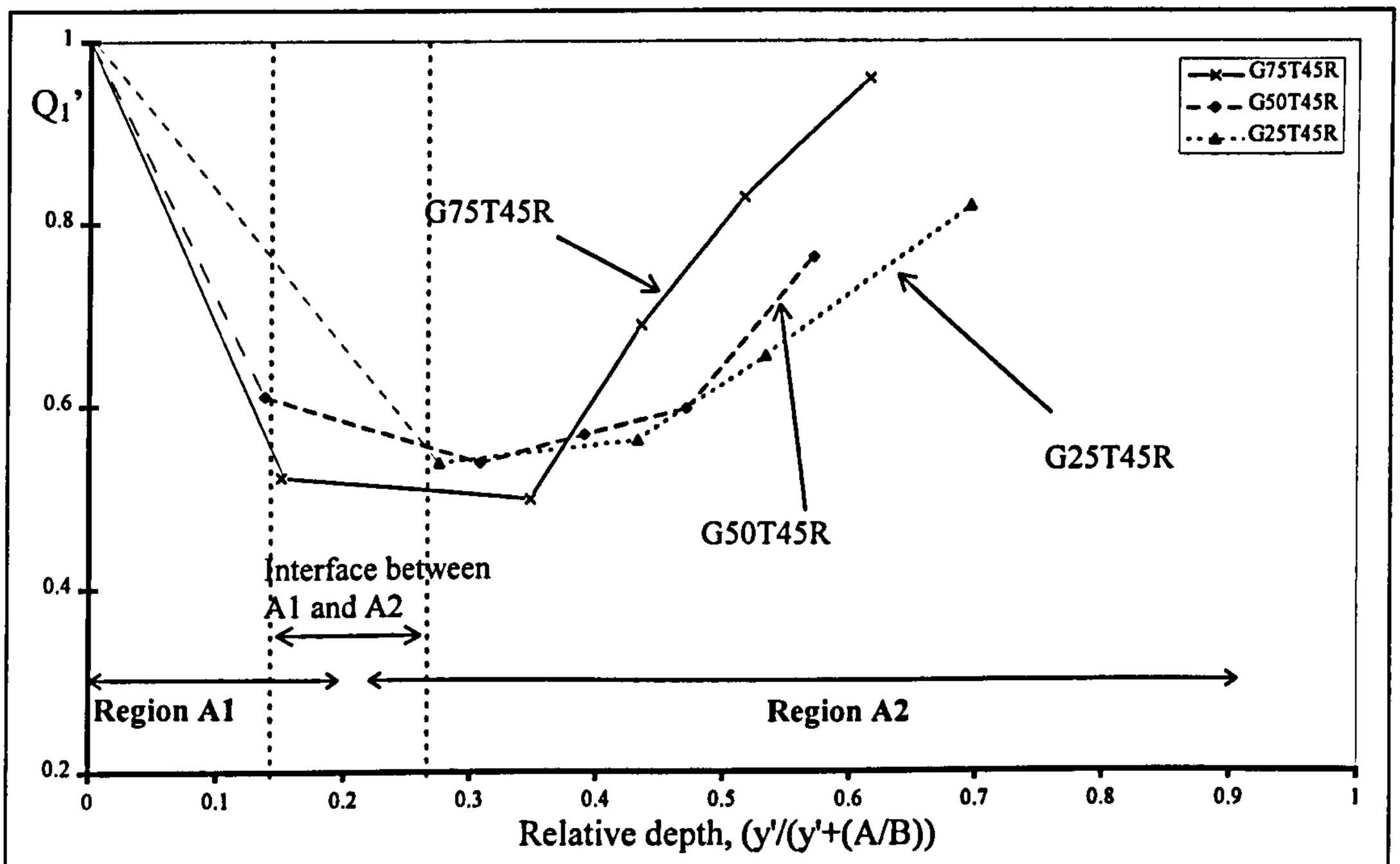

Figure 4.57 Q_A' versus relative depth for G75T45R, G50T45R and G25T45R (AR)

Figure 4.57 shows that the magnitude of aspect ratio influences not only the relative depth at the end of flow region A1 but also the rate of change of Q_A' with relative depth in flow region A2. The relative depth which corresponds to the end of flow region A1 is greater for the large aspect ratio channels (G25T45R) than for the small aspect ratio channels. The rate of increase of Q_A' with relative depth is greater in small aspect ratio channels.

4.6.7 The influence of main channel shape on local flow resistance

4.6.7.1 Local F for Zone A and its variation with channel shape*

Figure 4.58 shows plots of overbank flow depth versus F_A* and Global F* for the models: G50T45R (trapezoidal) and G50N45R (natural) which were tested in Glasgow during the Series B extension programme. They both had main channel aspect ratios equal to 5.33.

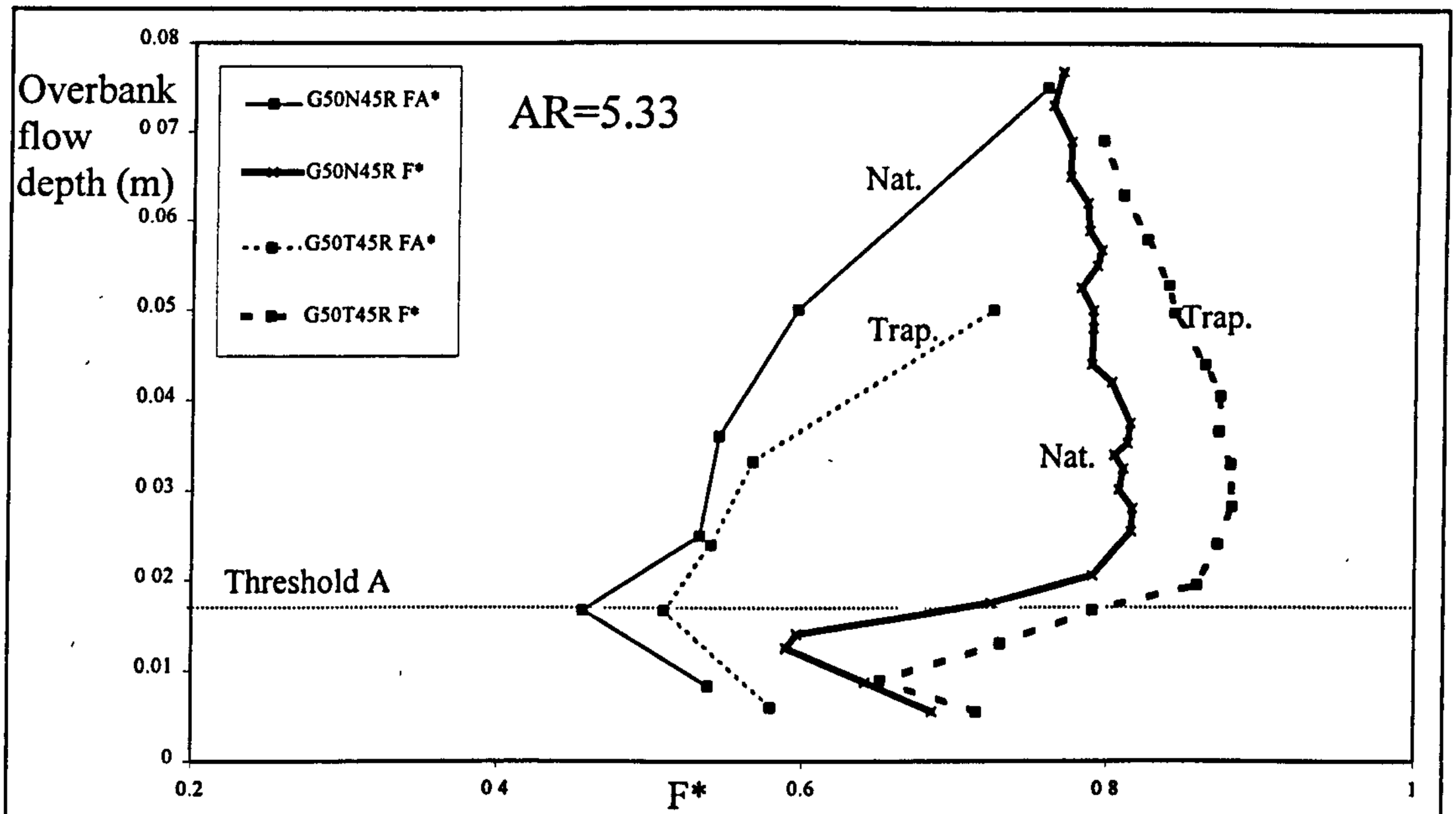

Figure 4.58 Flow depth versus F_A* and F* for G50N45R and G50T45R

Figure 4.58 demonstrates that the magnitude of F_A* is similar in G50T45R and G50N45R at low depths, in the region of Threshold A. There is no evidence that Threshold A occurs at different flow depths in the two models. By contrast for all higher flow depths the magnitude of F_A* is larger for G50T45R which indicates that the flow resistance is lower than in G50N45R.

The author postulates that this behaviour is caused by the maximum depth of the channel at the apex in the natural channel (G50N45R) being greater than the maximum depth at the cross-over, as shown in Figures 3.7a and 3.7b, even though their aspect ratios have the same magnitude. The author notes that the interaction mechanisms are likely to be similar between Zones A and B2 in the two models, as shown in Figure 4.59, because the main channel had almost identical configurations. The author

postulates however that F_A* was lower in G50N90R than in G50T90R there is increased flow resistance generated between Zones A and B1 in G50N45R than in G50T45R because the aspect ratio of the long slot channel below Zone B1, as shown in Figure 4.59 will be smaller in G50N45R than in G50T45R. The author demonstrated in Section 4.6.6 that a reduction in main channel aspect ratio will induce greater flow resistance due to zonal interaction. The aspect ratio in Zone A below Zone B1 reduces over a limited width of Zone A between G50N45R and G50T45R because the natural configuration of G50N45R has a deeper maximum flow depth at the apex in G50N45R than in G50T45R.

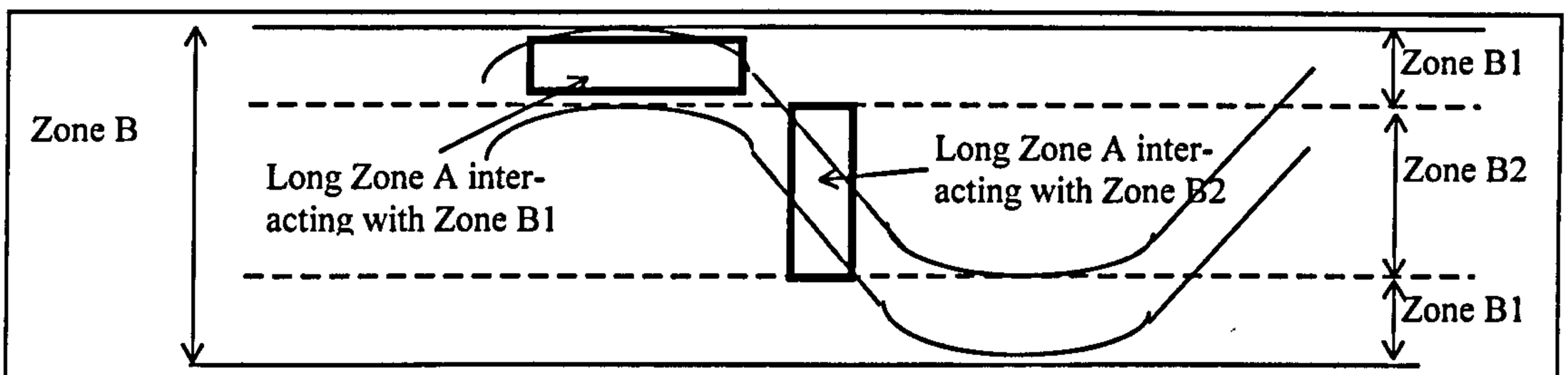

Figure 4.59 Sub-zones in Zone B

Also the author suggests that natural shape of the main channel under Zone B1 , with no inaccessible corners as in the trapezoidal channels, may facilitate the exchange of flow between Zone A and B1 in flow region 3. If more of the water is exchanged this is likely to induce greater flow resistance and lower Zone A and B1 velocities which would therefore lower the magnitude of F_A* in the manner observed in Figure 4.58.

4.6.7.2 Local F for Zone B and its variation with channel shape*

Figure 4.60 shows plots of overbank flow depth versus F_B* and Global F* for G50T45R (trapezoidal) and G50N45R (natural). The magnitude of F_B* is larger for G50T45R than G50N45R at all flow depths. The author postulates that this behaviour is caused by the maximum depth of the channel at the apex in the natural channel (G50N45R) being greater than the maximum depth at the cross-over, as shown in Figures 3.7a and 3.7b even though their aspect ratios have the same magnitude. It is thought that the deeper channel induces greater interaction losses and therefore lower values for F_B*. Also the potentially increased ability to exchange flow between Zones A and B1 due to the shape of the natural channel may have contributed to the lowering of Zone B1 velocities and the reduction in magnitude of F_B*.

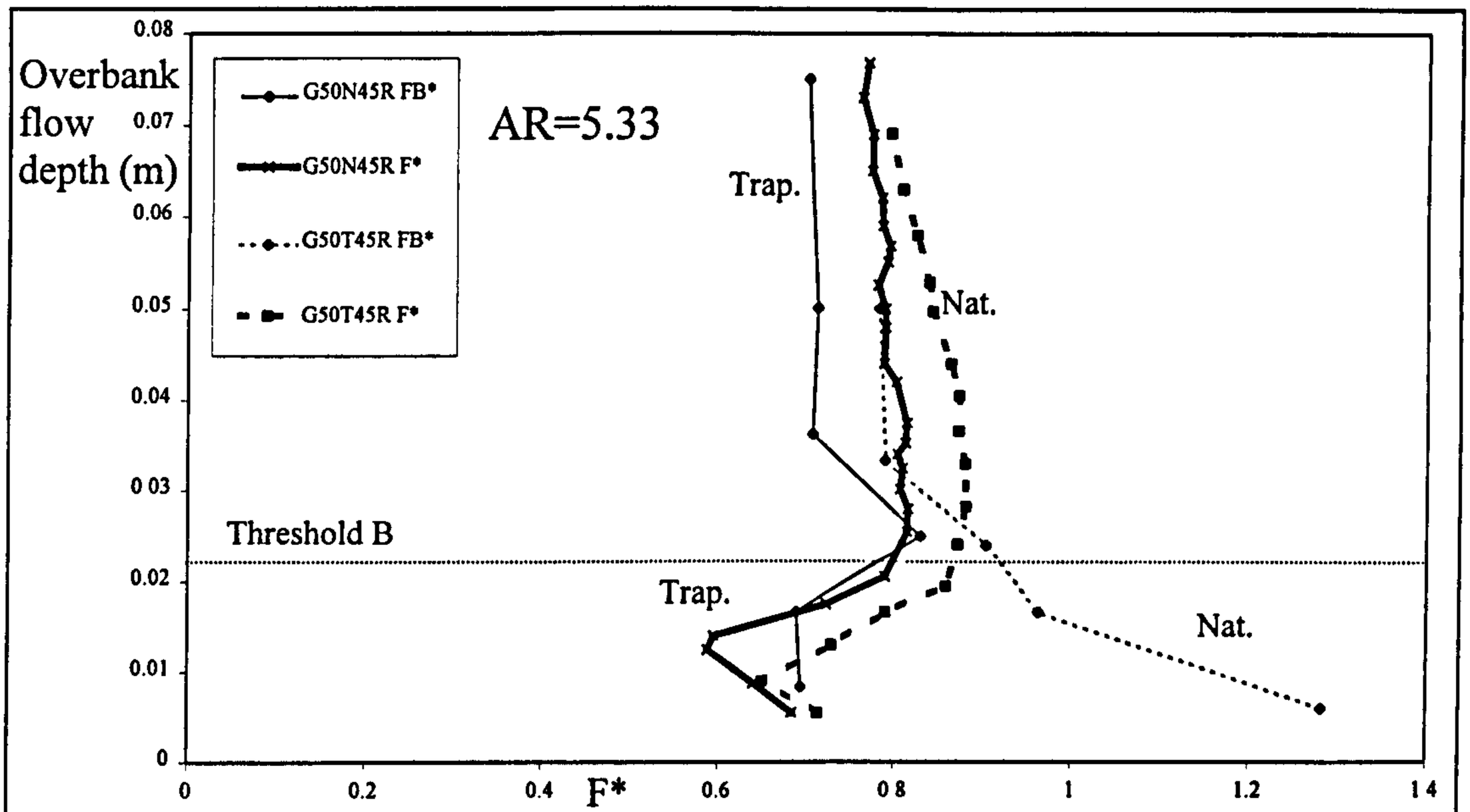

Figure 4.60 Flow depth versus F_B* and F* for G50N45R and G50T45R

4.6.7.3 Local F for Zone C and its variation with channel shape*

Figure 4.61 shows plots of overbank flow depth versus F_C* and Global F* for G50T45R (trapezoidal) and G50N45R (natural).

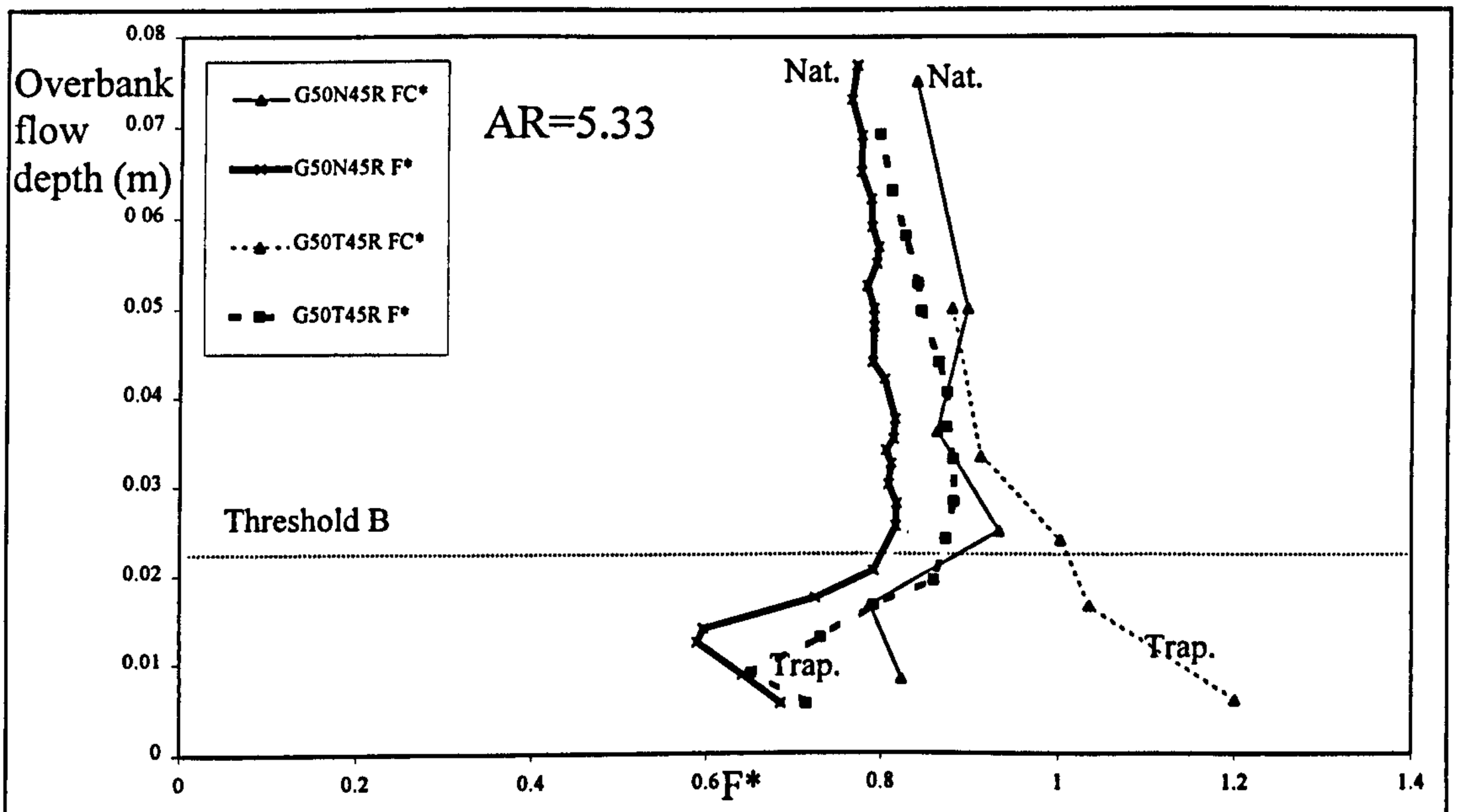

Figure 4.61 Flow depth versus F_A* and Global F* for G50N45R and G50T45R

Both models had main channel aspect ratios equal to 5.33. There is no discernible difference in the magnitude of F_C* between G50T45R and G50N45R apart from the difference attributed, in main, to experimental variations at low flow depths.

4.6.7.4 The influence of main channel shape on the adjustment coefficient, Q_A'

The author suggests that variations in main channel shape influences the magnitude of the aspect ratio and Reynolds number associated with a particular main channel. The author has demonstrated the influence of these two parameters on Q_A' in previous sections.

4.6.8 The influence of main channel side slope angle on flow resistance

4.6.8.1 Local F for Zone A and its variation with main channel side slope*

Figures 4.62 shows plots of overbank flow depth versus F_A* and Global F* for G50T90R and G50T30R in order to demonstrate the influence of main channel side slope on flow resistance. Figure 4.62 shows that F_A* is smaller in G50T90R than G50T30R in all flow regions.

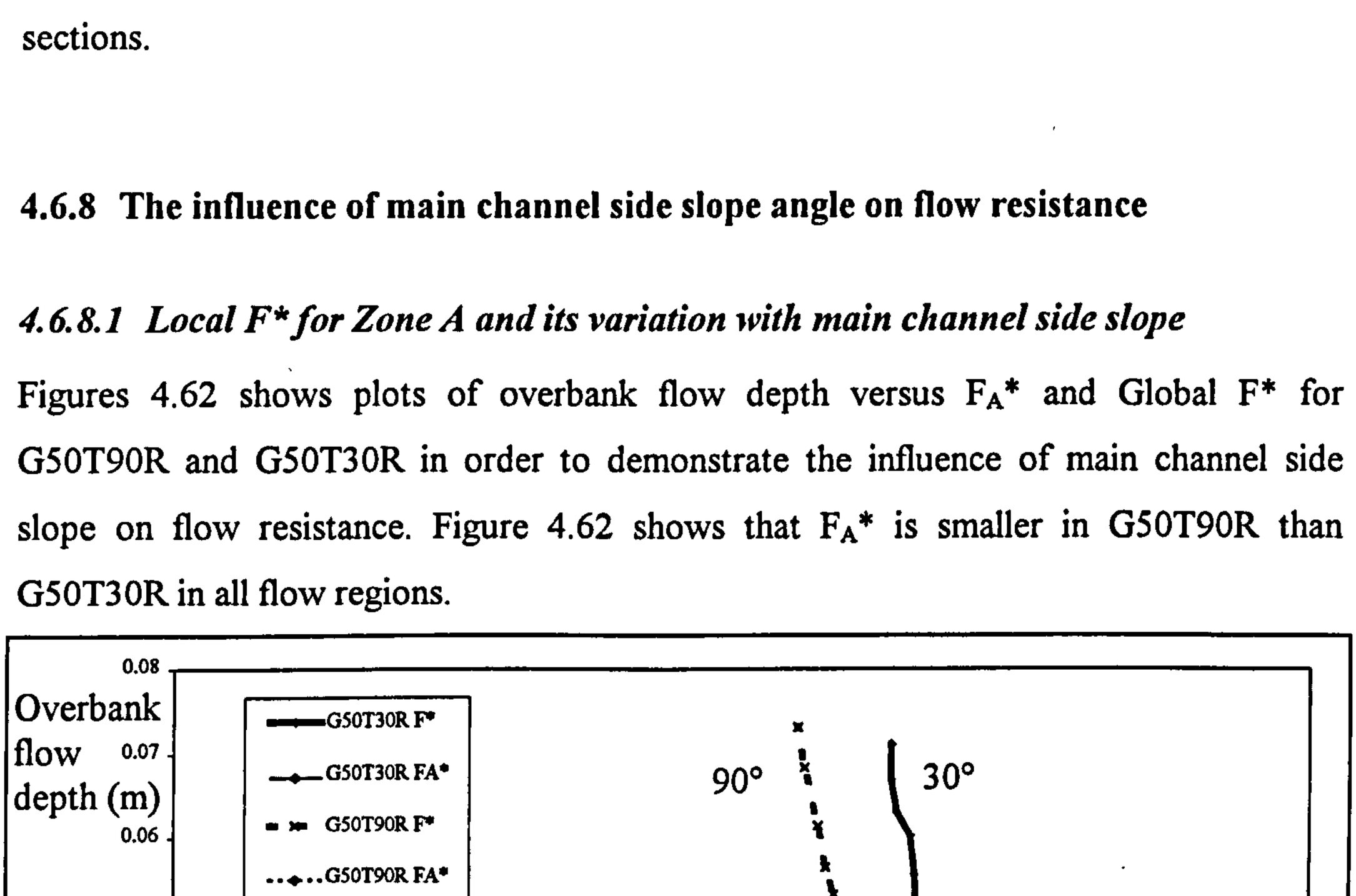

Figure 4.62 Overbank flow depth versus F_A* and Global F* for G50T90R and G50T30R

This indicates that the flow resistance generated by flow layer interaction decreases as the main channel side slope angle reduces. The rate of increase in the magnitude of F_A*, with increasing flow depth after Threshold A, is greater in G50T30R with the shallow side slope angles than in G50T90R.

4.6.8.2 Local F for Zone B and its variation with main channel side slope*

Figures 4.63 shows plots of overbank flow depth versus F_B* and Global F* for G50T90R and G50T30R in order to demonstrate the influence of main channel side slope on flow resistance.

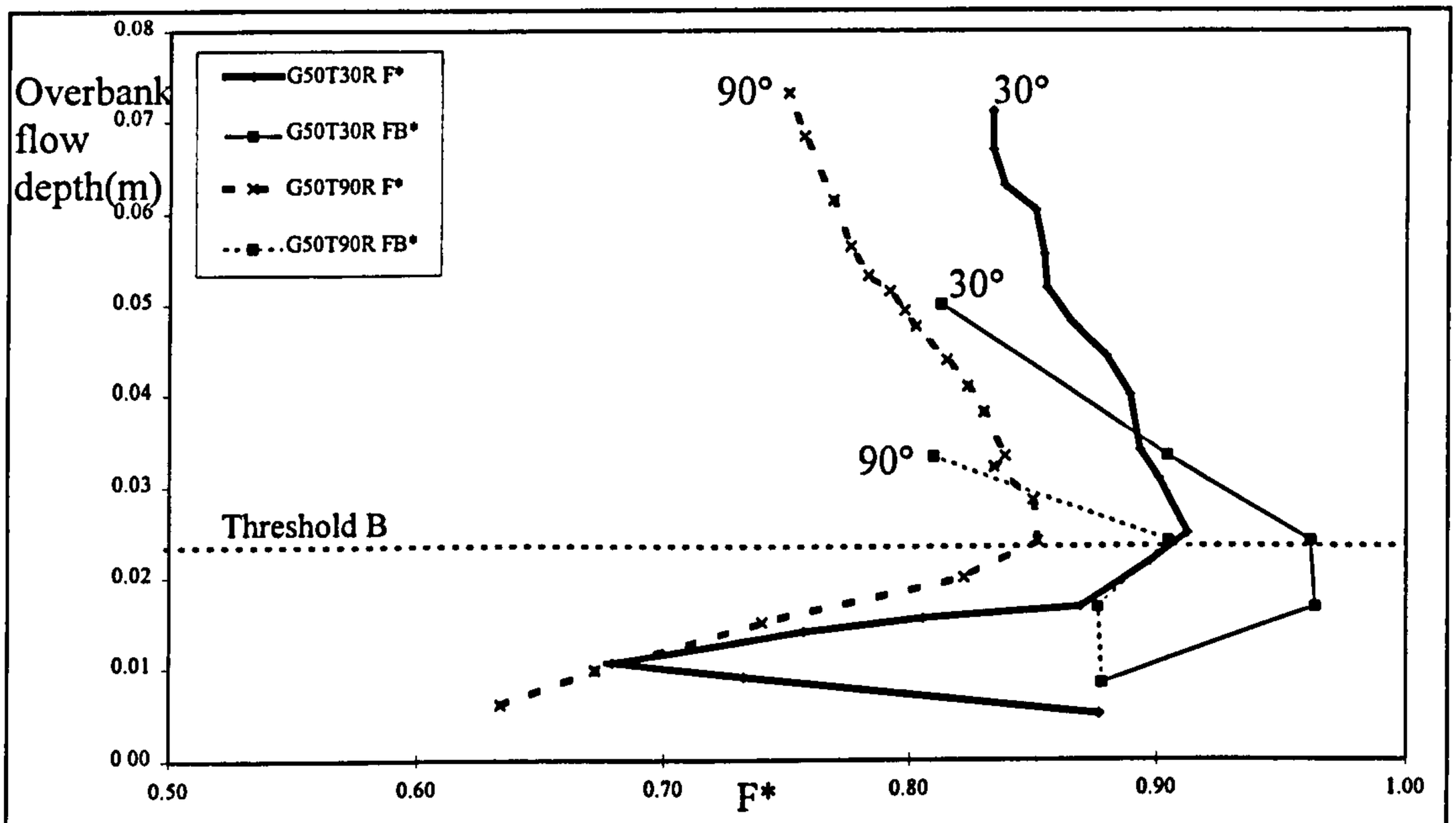

Figure 4.63 Overbank flow depth versus F_B* and Global F* for G50T90R and G50T30R

Figure 4.63 demonstrates that F_B* is close to 1 for both G50T90R and G50T30R in flow regions 1 and 2. This indicates that the side slope angle has a negligible influence on flow resistance at these flow depths. Significant differences in the magnitude of F_B* only become apparent after the onset of flow region 3 where F_B* is smaller in G50T90R than in G50T30R. This indicates that the flow layer interaction mechanism generate flow resistance in Zone B which decreases as the main channel side slope angle becomes shallower.

4.6.8.3 Local F for Zone C and its variation with main channel side slope*

Figure 4.64 shows plots of overbank flow depth versus F_C* and Global F* for G50T90R and G50T30R in order to demonstrate the influence of main channel side slope on flow resistance. It shows that F_C* is close to 1 at all flow depths and similar for both models. This implies that side slope angle has very little influence on the momentum transfer mechanisms between Zones B and C despite reducing the Zone B velocity in channels with steeper main channel side slopes. The author suggests that shallow side slopes may facilitate greater interaction between Zones B and C, which may to some extent counterbalance the influence of the greater velocity differences between Zones B and C for main channels with steep side slopes. Further intricate study of the flow fields in the vicinity of the Zone B and C interface is required before this conjecture can be developed further.

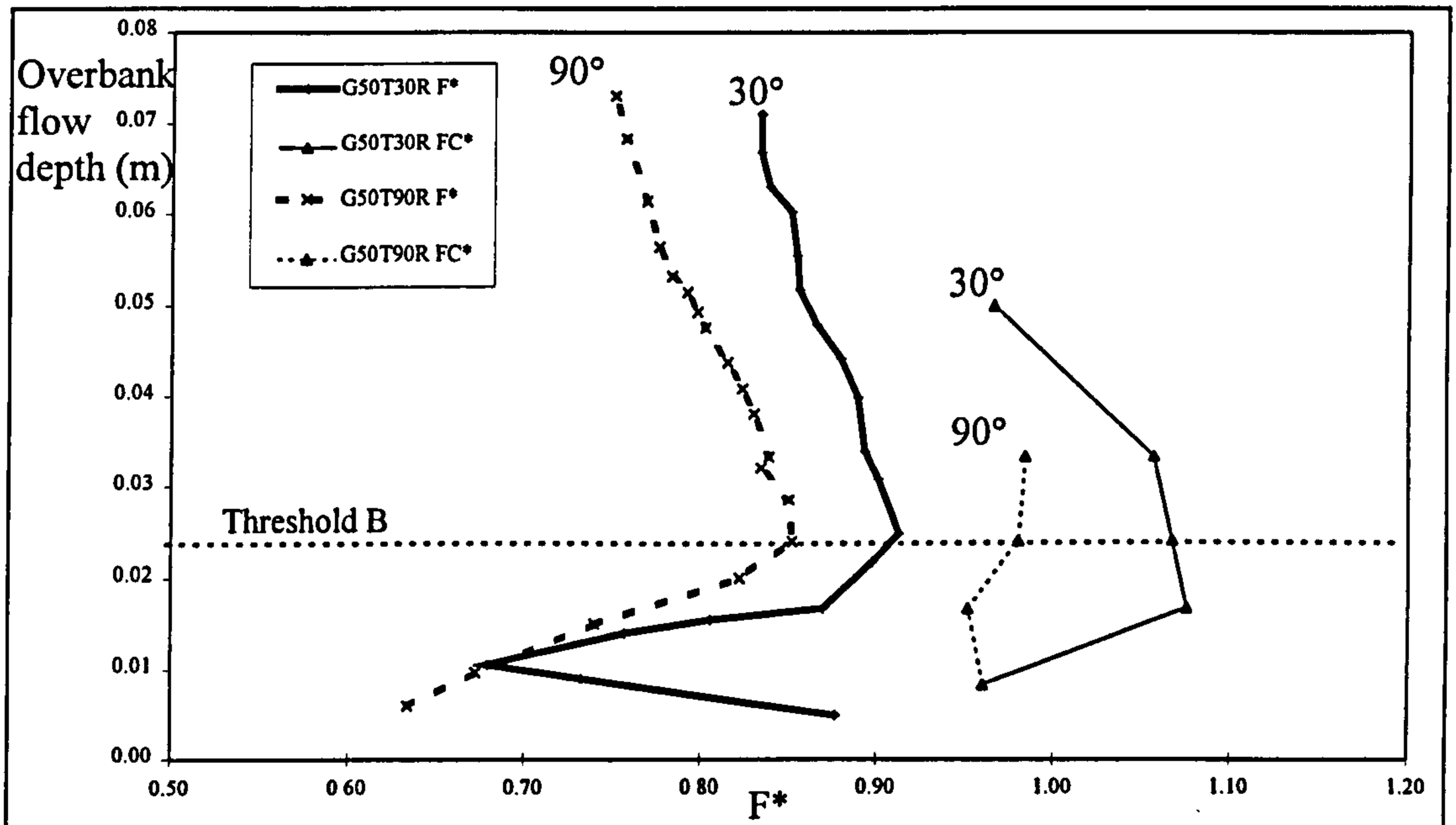

Figure 4.64 Overbank flow depth versus F_C* and F* for G50T90R and G50T30R

4.6.8.4 The influence of side slope on expansion and contraction losses in Zone B

A number of researchers have proposed that the extra flow resistance in Zone B can be attributed to the head losses generated by the expansion and contraction of the Zone B flow as it passes over Zone A. The author used some results from the additional slot tests which were performed in Glasgow during the Series B extension (1993-1996) programme in order to demonstrate the link between F_B* behaviour and variations in

main channel side slope angle which have been shown to influence the magnitude of expansion and contraction head loss in flow over slots.

Figure 4.65 and 4.66 show plots of expansion and contraction head loss versus flow depth for 4 models: S2G9S, S2G6S, S2G4S and S2G3S which had side slope angles equal to: 90°, 60°, 45°, 30° respectively. The geometric configurations of these models are listed in Table 3.12. Despite the scatter in the results, the slot test results demonstrate that the expansion and contraction head losses were smaller in channels with shallower side slopes at the majority of flow depths. However the differences were most significant at higher flow depths. The increase in magnitude of F_B* in models with main channels with shallow side slopes was therefore due to this reduction in head losses in Zone B.

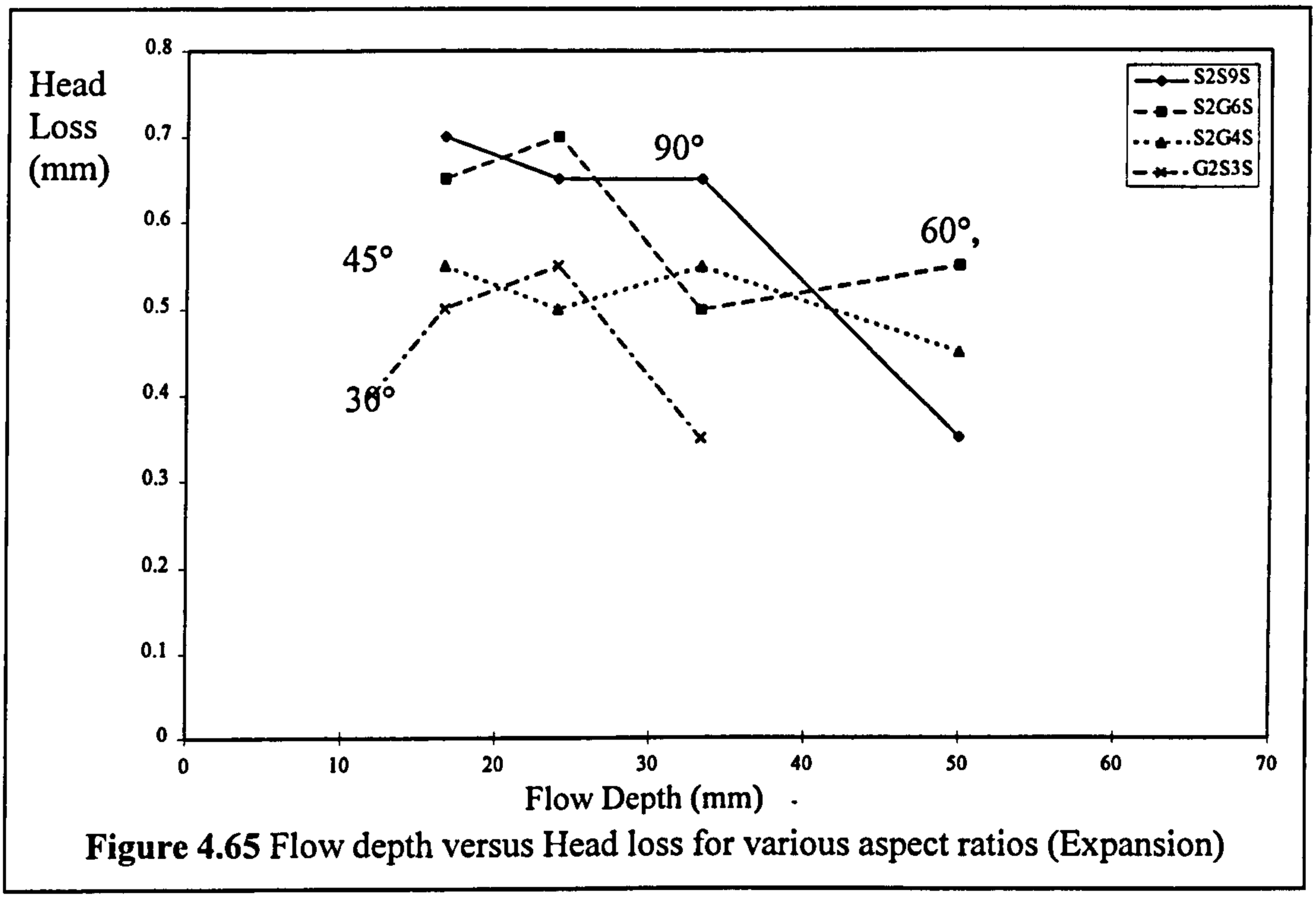

Figure 4.65 Flow depth versus Head loss for various aspect ratios (Expansion)

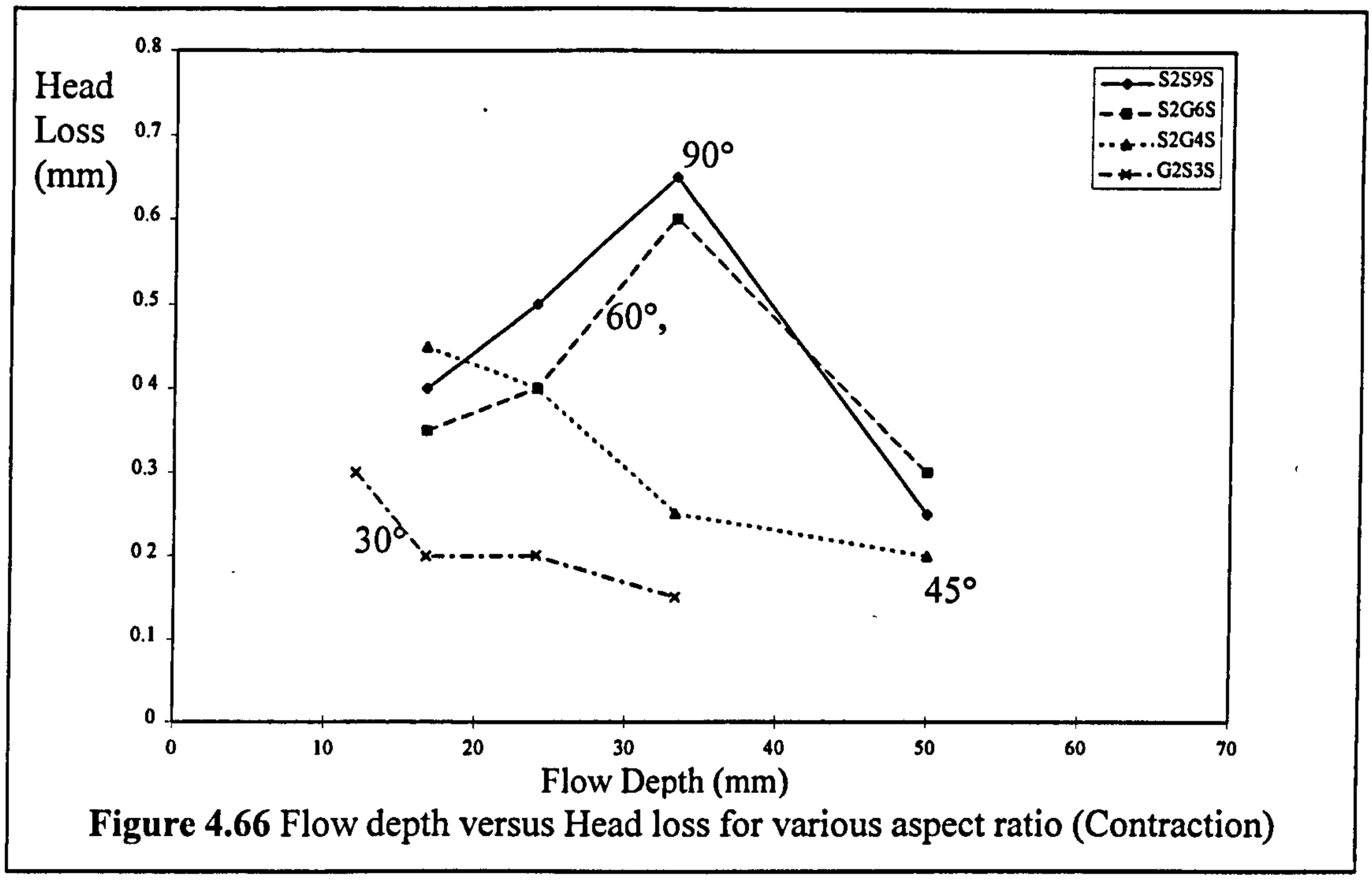

Figure 4.66 Flow depth versus Head loss for various aspect ratio (Contraction)

4.6.8.5 The influence of main channel side slope on the adjustment coefficient, Q_A'

Figure 4.67 presents plots of Q_A' versus relative depth which were obtained for models: G50T90R, G50T60R and G50T45R, which had side slopes equal to 90°, 60°, 45° and 30° respectively.

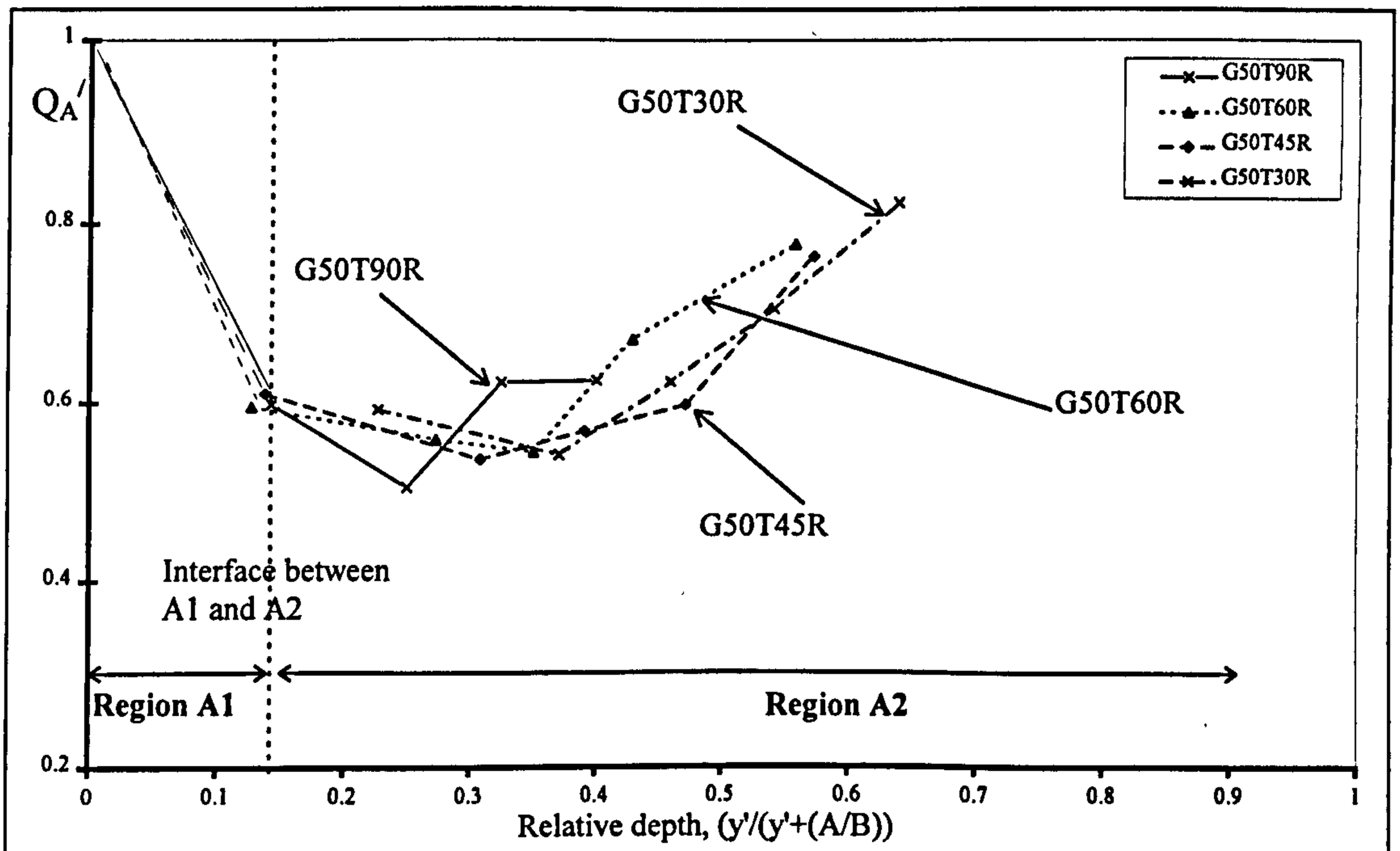

Figure 4.67 Q_A' versus relative depth G50T90R, G50T60R, G50T45R, G50T30R (S_S).

Figure 4.67 shows that the rate of change of the magnitude of Q_A' with relative depth slightly increases with increasing side slope angle at higher relative depths. Variations in the side slope angle appear to have little effect at low relative depths. The other data sets gathered during the Series B extension programme confirmed this observation.

4.6.9 The influence of relative meander belt width on flow resistance

4.6.9.1 Local F for Zone A and its variation with relative meander belt width*

Figure 4.68 shows plots of overbank flow depth versus F_A* and Global F* for G75T45R (Mw=1.62) and G75T45RN (Mw=1.0). The magnitude of F_A* in G75T45RN is smaller than in G75T45R for all flow depths.

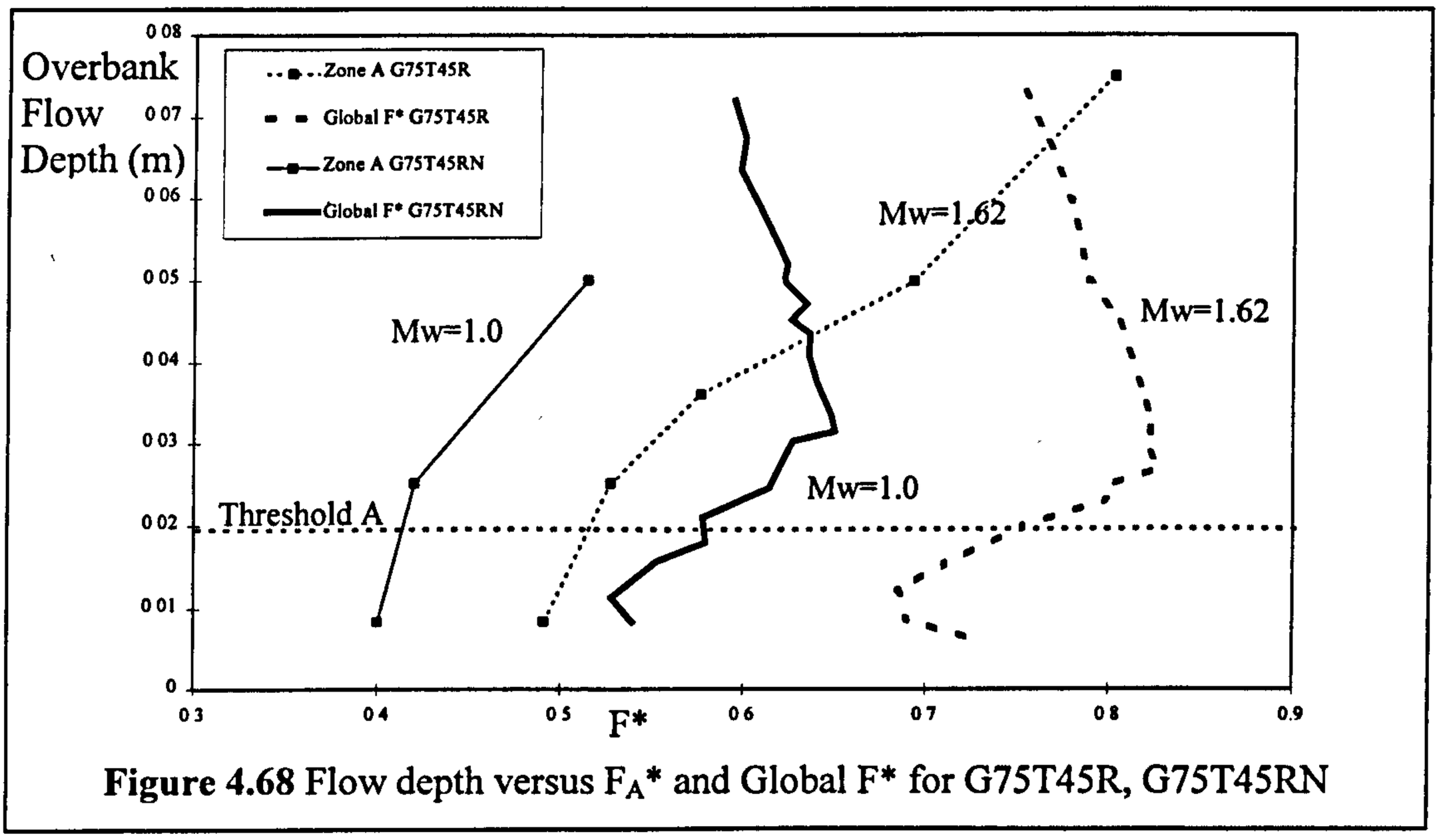

Figure 4.68 Flow depth versus F_A* and Global F* for G75T45R, G75T45RN

The author postulates that this behaviour is attributable to the proximity of the flood plain side wall in G75T45RN, which significantly increases the frictional flow resistance exerted on Zone B and slows the flood plain flow, thus generating increased layer interaction head losses (flow resistance) in Zone A. A similar pattern of flow behaviour was demonstrated by G25T45RN, G25T45R, G25T45SN and G25T45S. The flow depths corresponding to Threshold A do not show any dependence on the relative meander belt width.

4.6.9.2 Local F for Zone B and its variation with relative meander belt width*

Figure 4.69 shows plots of overbank flow depth versus F_B* and Global F* for G75T45R (Mw=1.62) and G75T45RN (Mw=1.0). The magnitude of F_B* in G75T45R is smaller than in G75T45R for all flow depths. The author postulates that this behaviour is attributable to the proximity of the flood plain side wall in G75T45RN which significantly increases the frictional flow resistance exerted on Zone B which slows the flood plain flow. A similar pattern of flow behaviour was also demonstrated by G25T45RN and G25T45R. The flow depths corresponding to Threshold B do not show any dependence on the relative meander belt width.

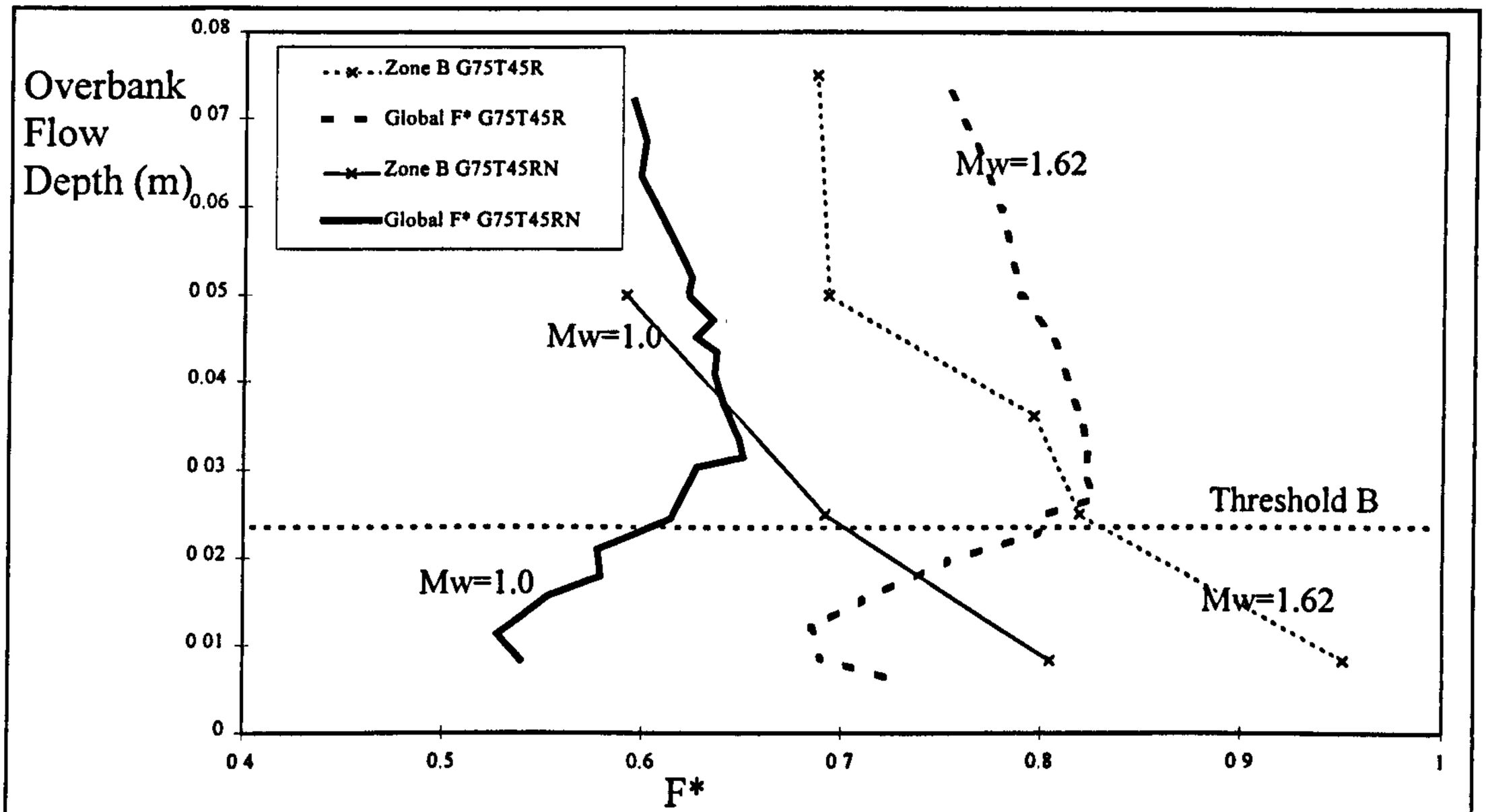

Figure 4.69 Flow depth versus F_B* and Global F* for G75T45R, G75T45RN

4.6.9.3 Local F for Zone C and its variation with relative meander belt width*

Figures 4.70 shows a plot of overbank flow depth versus F_A*, F_B*, F_C* and Global F* for G75T45R (Mw=1.62) and G75T45RN (Mw=1.0).

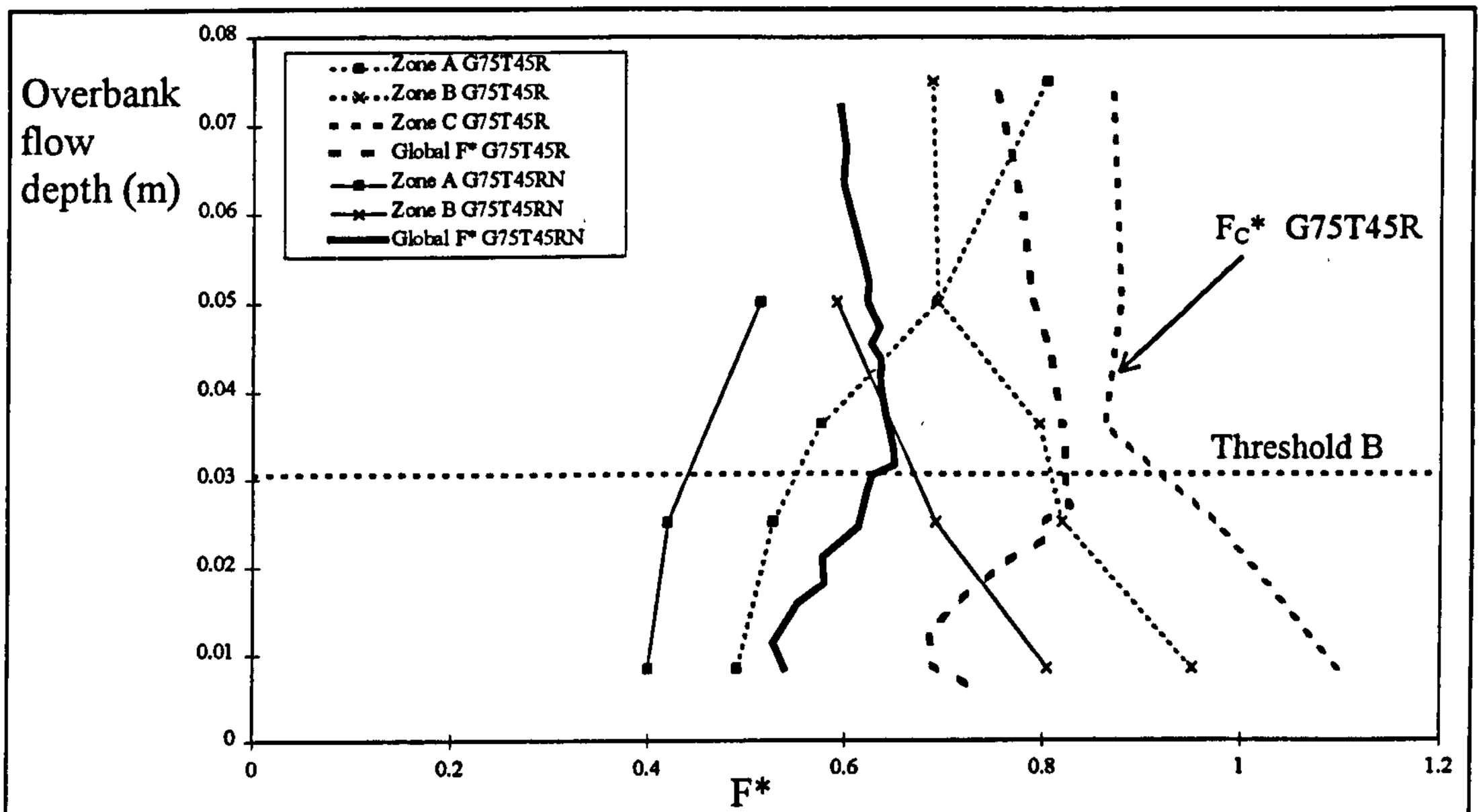

Figure 4.70 Flow depth versus F_A^*, F_B^*, F_C^* and Global F* for G75T45R, G75T45RN

Only G75T45R provides a plot for F_C^* because only it possesses a Zone C. The closeness of this F_C^* value to 1 has significant impact of the magnitude of Global F*. When F_C^* is combined with the other zonal F* values, it will significantly increase the magnitude of Global F* because it is close to 1. The proportion of flow contained within Zone A for each flow depth is diminished when Zone C is included. Consequently the reductive effect of the small F_A^* values will have a smaller contribution to make on the Global F* value in G75T45R so Global F* will be increased in G75T45R at all flow depths in the manner displayed in Figure 4.70. Even when F_C^* starts to decrease above Threshold B it still possess a magnitude which is large compared to F_A^* or F_B^*. Also in the Global F* plot for G75T45RN where there is no addition of F_C^* the magnitude of Global F* will be much reduced compared with the Global F* in G75T45R.

4.6.9.4 The influence of meander belt width on the adjustment coefficient, Q_A'

Figure 4.71 shows plots of Q_A' versus relative depth which were obtained for G75T45R and G75T45RN.

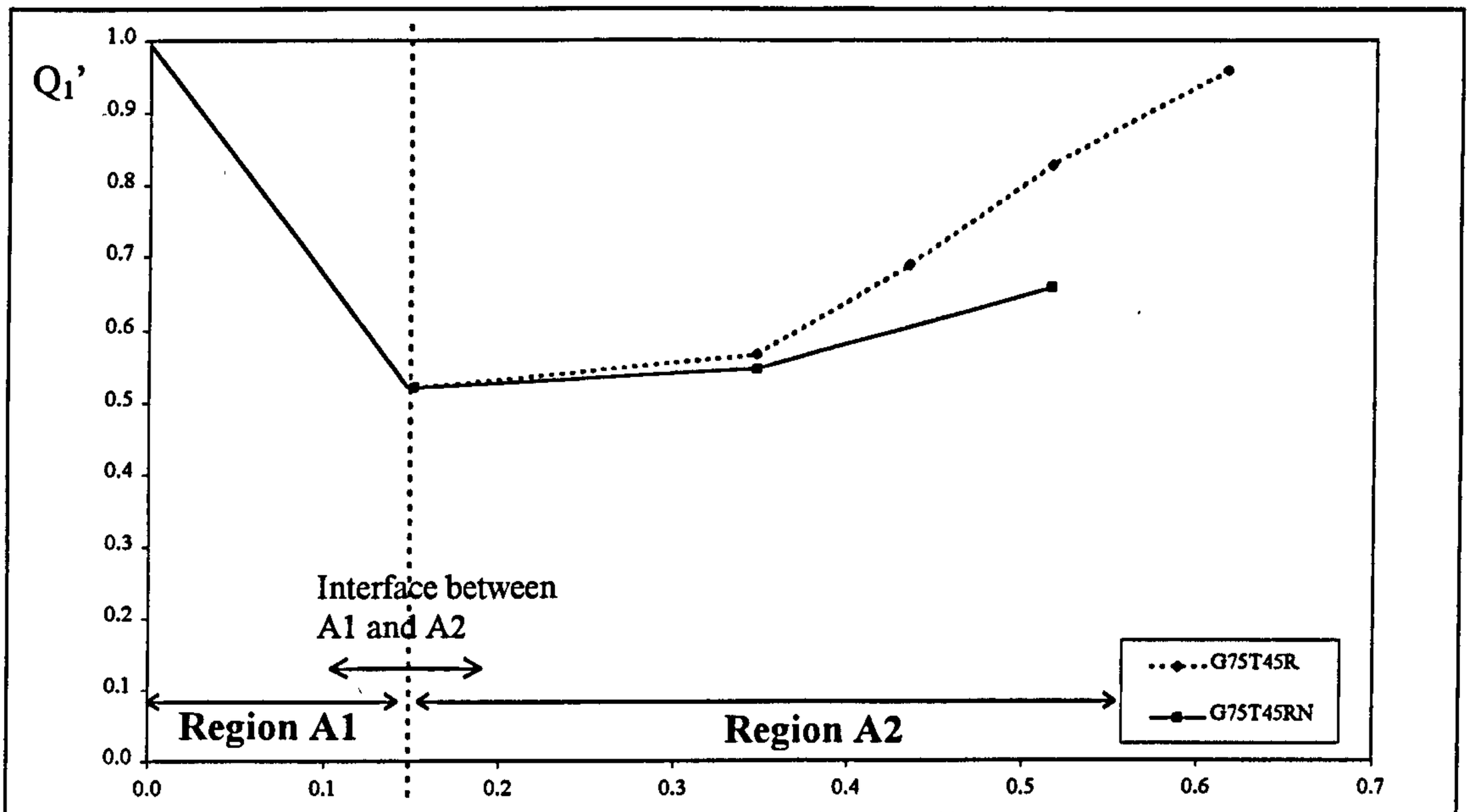

Figure 4.71 Q_A' versus relative depth for G75T45R, and G75T45RN (Mw)

G75T45R and G75T45RN had relative meander belt widths equal to 1.62 and 1.0 respectively. Figure 4.71 shows that the magnitude of Q_A' is smaller for smaller relative meander belt widths at all flow depths thus corroborating the findings from the F_A* plots.

*4.7 Links between the interaction flow mechanisms and Global / Zonal F**

4.7.1 Introduction

The flow visualisation results which were captured on photograph for G75T45R (a typical meandering compound channel model that was tested in Glasgow during the Series B extension (1993-1996) are presented in Figures 4.72a, b, & c and 4.73a, b & c. Each photograph was taken at 3 second intervals and they show the evolution of three dye traces once which were injected in the bottom of the main channel. The dominant flow paths in Zone A and B were traced and consequently the varying nature of the interaction mechanisms at different relative flow depths was illustrated.

Each figure corresponds to a different flood plain flow depth. The flow visualisation test in Figure 4.72a, b, & c was performed at a flow depth equal to 8.33mm which is

equivalent to RD=0.195. The flow visualisation test in Figure 4.73a, b, & c was performed at a flow depth equal to 25mm which is equivalent to RD=0.347.

Illustration of the exchange of flow between the main channel and flood plain

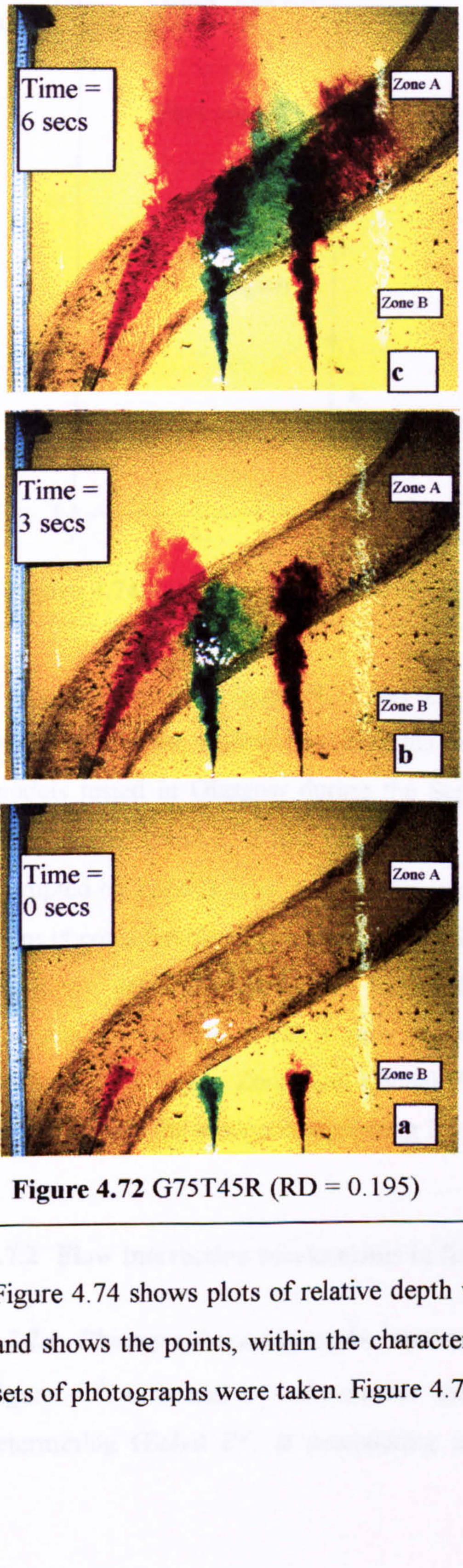

Figure 4.72 G75T45R (RD = 0.195)

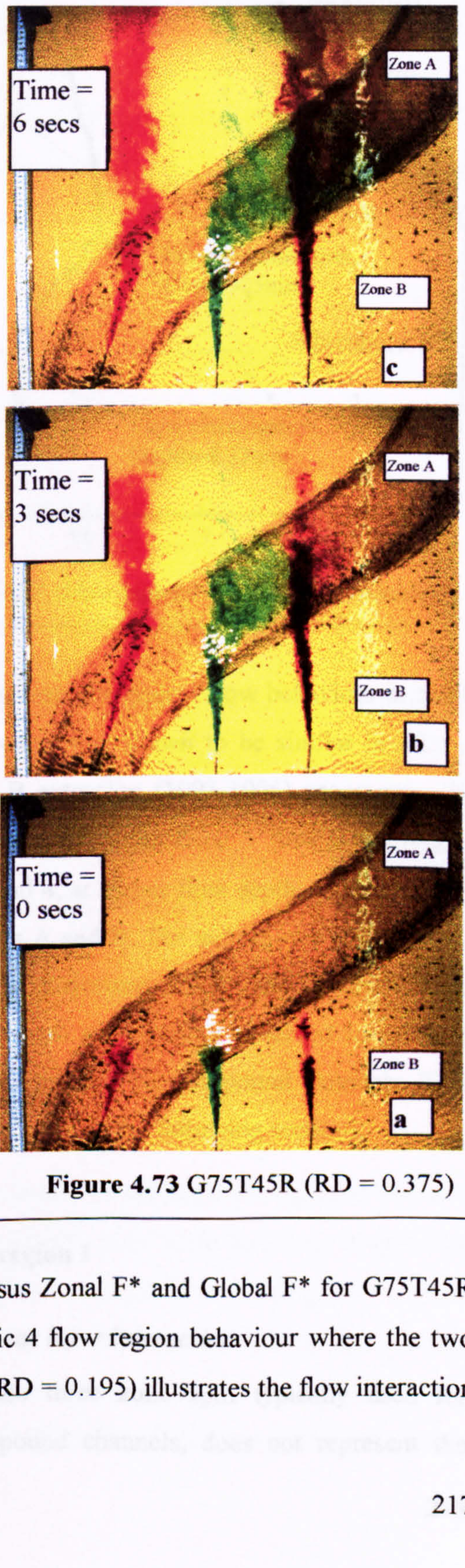

Figure 4.73 G75T45R (RD = 0.375)

Figure 4.74 shows plots of relative depth versus Zonal F* and Global F* for G75T45R and shows the points, within the characteristic 4 flow region behaviour where the two sets of photographs were taken. Figure 4.72 (RD = 0.195) illustrates the flow interaction

mechanisms near Threshold 1/2. Figure 4.73 (RD = 0.375) illustrates the flow interaction mechanisms near Threshold 2/3.

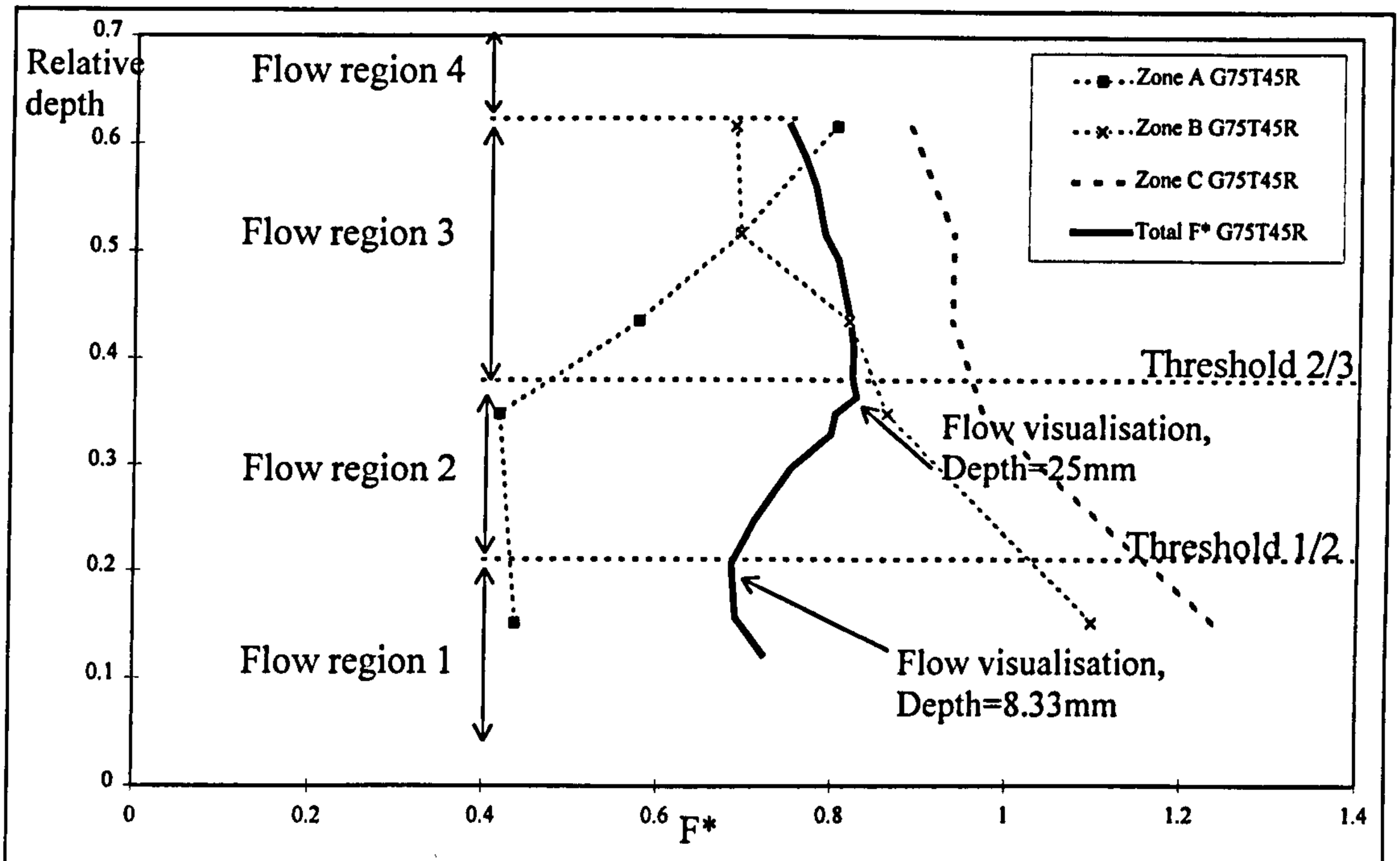

Figure 4.74 Relative depth versus F*: G75T45R (Flow regions / measurement positions)

The photographs in Figures 4.72 and 4.73 illustrate the typical flow behaviour at these points within the 4 flow regions. This behaviour was shown to be similar in all the models tested in Glasgow during the Series B extension (1993-1996) programme. In flow regions 1 and 2, at low flow depths (Figure 4.72), the Zone A flow is minimally disrupted by Zone B flow. In flow regions 3 and 4, at higher flow depths (Figure 4.73), there is considerable interaction between Zones A and B. The author uses these results and more detailed observations to develop a conjecture linking the observed flow interaction behaviour to the 4 flow regions which are typically observed in plots of relative depth versus Zonal and Global F* for meandering compound channels. This conjecture and the evidence supporting it are outlined in the following sections.

4.7.2 Flow interaction mechanisms in flow region 1

4.7.2.1 Photographic evidence for vertical shear layer interaction

Figure 4.72a, b and c demonstrates that the three zone split typically used for determining Global F*, in meandering compound channels, does not represent the

physical reality of the flow behaviour in flow region 1 (near Threshold 1/2). In reality the water in Zone A combines with the water directly above bankfull level, effectively blocking the flow within Zone B. The flow effectively splits into 2 zones as shown in Figure 4.75. Two vertical shear layers are created along the two planes, aa' and bb'. These are coincidental with the top of the main channel's banks. Figure 4.76 shows schematic representation (plan view) of the velocity vectors in Zones 1 and 2. The fast flowing Zone 1 flow forces a passage through the slow flowing Zone 2 water on the flood plains.

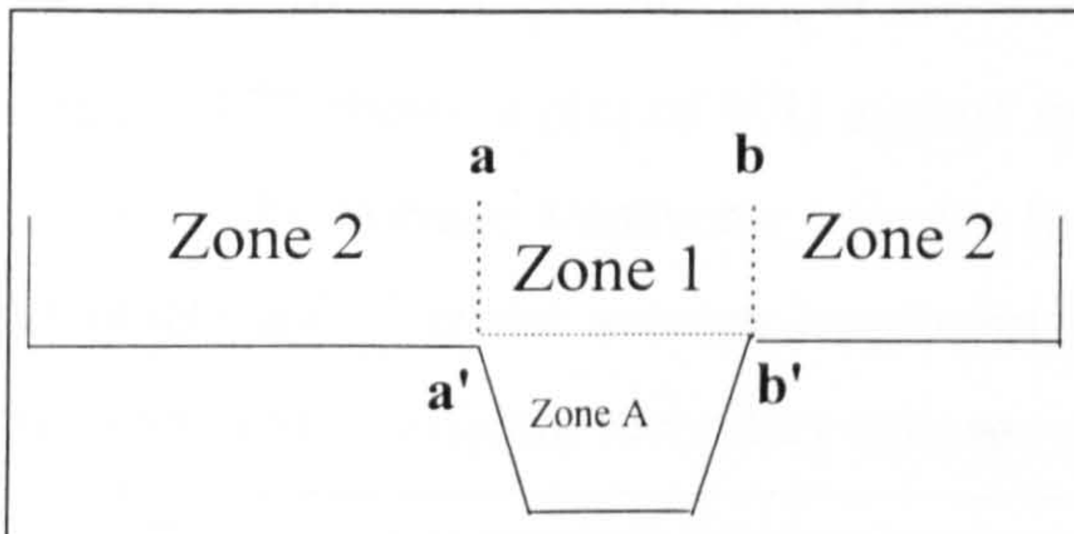

Figure 4.75 Two zone split

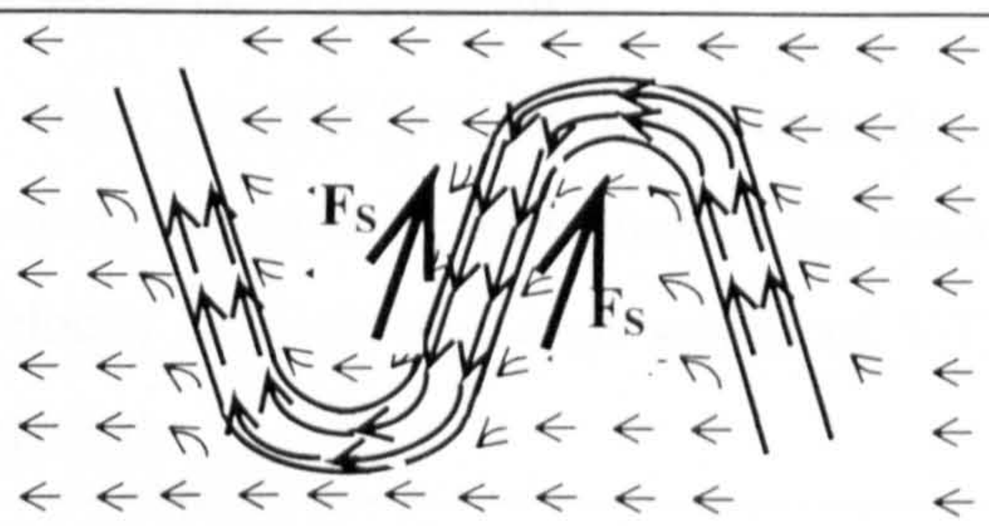

Figure 4.76 Velocity vectors in Zones 1 and 2

The author postulates that the high levels of flow resistance exhibited in flow region 1, (indicated by small values of F_A* and consequently Global F*) are attributable to the vertical shear stress, F_S, which is generated between Zones 1 and 2 along the aa' and bb' planes and which is transferred to Zone A. This layer interaction mechanism has not been traditionally associated with meandering compound channel flows. Researchers such as Ervine et al [1993], who were limited by the lack of availability of suitable data, have previously described the mechanisms of layer interaction and head loss generation predominantly in terms of the secondary cells that are generated when the flood plain flow has enough energy to shear across the top of Zone A and create significant secondary cells as shown in Figure 2.40.

Significantly similar interaction mechanisms to the ones shown in Figures 4.75 and 4.76 (with a 2 zone split) were generated at all flow depths in the heavily roughened Series B (1989-1992) models, SDB34 and SDB43. Dowel rods were used as roughening elements and imposed increasing blockage flow resistance at increasing flow depths. Consequently the flood plain water, Zone 2, was slowed so much that the fast flowing water in Zone 1 had to force its way through creating large vertical shear forces between Zones 1 and 2. The author postulates that the layer interaction behaviour in these models

is therefore similar to the interaction mechanisms generated at very low flow depths in all meandering compound channels. Even when the flood plain is relatively smooth, the effective flood plain roughness will be comparatively high due to the low Reynolds number associated with flow which will result in the 2 zone split. The author recognises that the flow depths over which this high flood plain roughness will extend will depend on the scale of the channel geometry and the roughening elements.

4.7.2.2 Point velocity evidence for the vertical shear layer mechanism

Figure 4.77 shows a plot of V/U against flow depth for G75T45R averaged over Zone A. V is the average transverse velocity (perpendicular to the centre line of the main channel) and U is the average longitudinal velocity in Zone A. Large values of V/U indicate that significant secondary cells are generated.

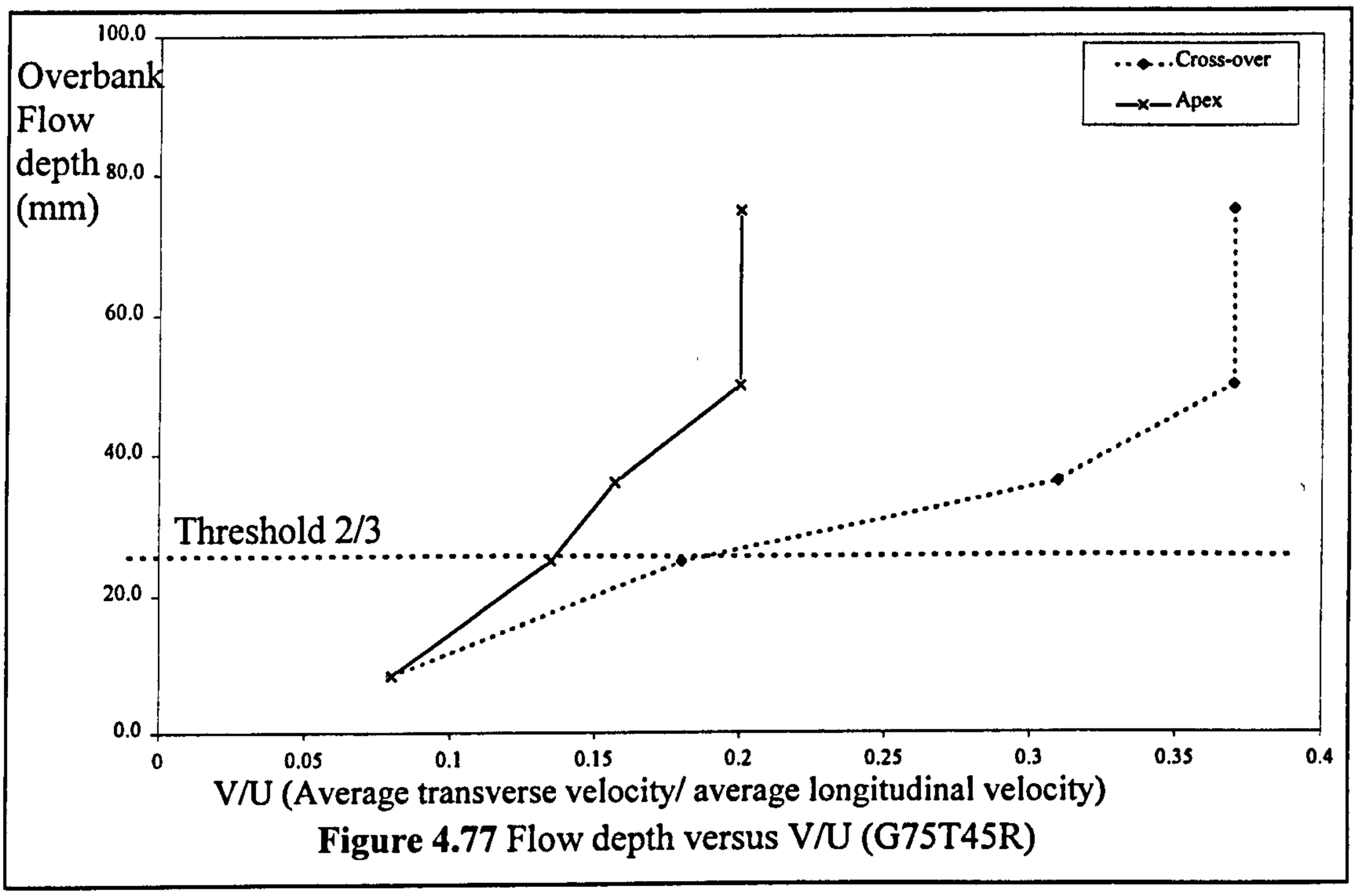

Figure 4.77 Flow depth versus V/U (G75T45R)

Figure 4.77 shows that once Threshold 2/3 (which coincides with Threshold B) is reached the average transverse velocity can be as much as 20%-40% of the longitudinal velocity and consequently will generate a significant amount of extra head loss. due to secondary cell action. However Figure 4.77 also shows that under Threshold 2/3 the magnitude of V/U is much reduced and equal to between 5%-15% of the longitudinal velocity which is much less significant and because Global F*. The author concludes

that because the secondary cells are small in flow region 1 the vertical shear interaction mechanisms must provide a significant source of interaction flow resistance because the magnitude of Global F* can achieve values as little as 0.4 in flow region 1.

Further evidence for the absence of significant secondary cell generation in flow region 1 is provided by looking at the depth-averaged velocities for Zone B and C. Figure 4.78 shows a plot of the depth-averaged velocity (in Zones B and C) across the full flume width for G75T45R at a flow depth on the flood plain equal to 25mm (RD=0.25). The cross-over measurement section was upstream of the apex measurement section. The point velocity measurements were taken where the apex was on the left hand side of the flume. Figure 4.78 demonstrates that at 25mm flow depth the depth-averaged velocities in Zones B and C (V_B and V_C) are the same as the velocity which is predicted by assuming that only bed friction head losses are generated ($V_B = V_C$ =0.157m/s). This indicates that F_B* and F_C* have values close to 1, which implies that there are no additional interaction mechanisms causing head loss (like the expansion and contraction of flood plain flow over Zone A causing secondary cells and head loss).

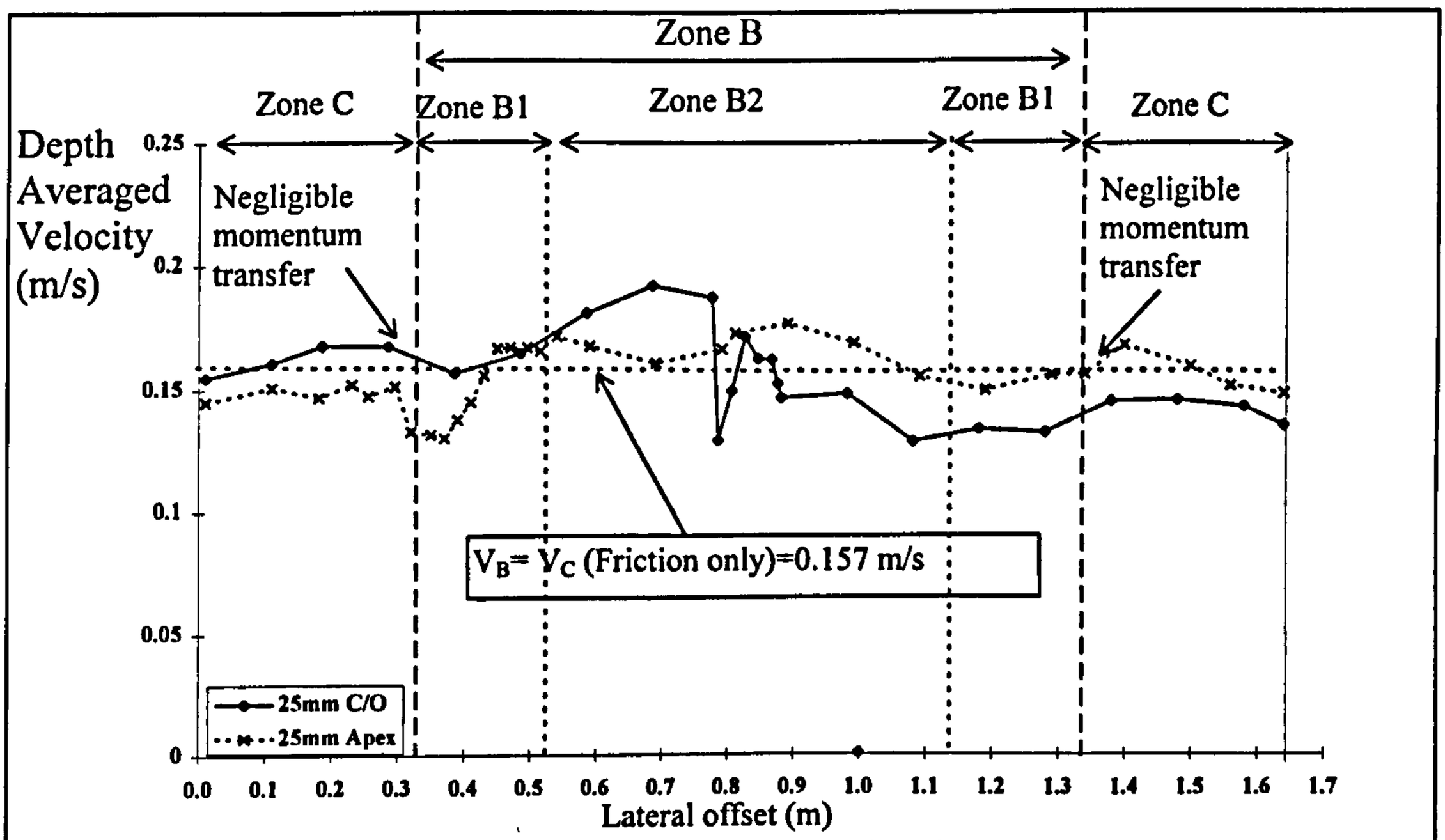

Figure 4.78 Depth averaged velocity versus flume offset for G75T45R, Depth = 25mm

It is important to note that Figure 4.78 displays results for 25mm flow depth which falls within Flow region 2. The results for 25mm flow depth were only used because it was not possible to directly measure flood plain velocity for 8.33mm flood plain flow.

However the author inferred that there would be even less expansion and contraction in the 8.33mm deep flood plain flow than in the 25mm deep flow, because it possesses even less energy to drive secondary cells in Zone A.

4.7.2.3 Significance of the vertical shear layer interaction mechanism

Over the years a number of researchers have observed that the scale models which have been tested have predominantly studied the flow behaviour in meandering compound channels with flood plain flow velocities which have been relatively high compared to the main channel flow velocities. They have correctly stated that these tests do not represent the majority of flow situations in natural channels and are of more theoretical rather than practical importance.

Relatively high flood plain velocities will generate large secondary circulation cells in the main channel but this type of interaction is unlikely to occur in natural channels where in most common flooding situations the flood plain water will simply stagnate on the flood plain when it flows overbank. In these situations the interaction between the main and flood plain channels will only generate limited secondary cells but will generate significant vertical shear interaction as the fast flow main channel water pushes its way through stagnant flood plain water. The flood plain flow in reality will not achieve high flow velocities until a severe flood occurs.

Consequently, during the Series B extension (1993-1996) programme the author produced significant number of flow results to demonstrate the nature of these vertical shear layer interaction mechanisms which will occur when flood plain flow stagnates as it just flow overbank. The author envisages the possibility of deriving explicit predictive methods for quantifying the magnitude of vertical shear loss in the future but accepts that further experimental data will be required to attain this goal. In the interim the author developed a method to predict the Threshold 1/2 (Threshold A) flow depth so that an allowance can be made for the presence of vertical shear interaction (flow region 1 behaviour) in the enhanced semi-physical, semi-empirical prediction method which was developed by the author during the Series B extension programme. The development of this method is reported in Chapter 6.

4.7.3 The identification of Threshold 1/2

The author postulated that the presence of vertical shear layers adjacent to Zone 1 at low flood plain flow depths is dependant upon the ability of Zone 1 to resist the passage of the flood plain flow over Zone A which is significantly retarded at low flow depths because of the high roughness of the flood plains. Consequently the relative flow state in Zones 1 and 2 determines whether the 2 zone behaviour is replaced by 3 zone behaviour. Once flood plain flow achieves a certain state then the flood plain flow will be able to disrupt the Zone 1 flow, force its way over Zone A creating a horizontal shear layer and consequently start to generate secondary circulation cells in Zone A.

The author investigated techniques for gauging the relative flow states in Zones 1 and 2. Dimensional analysis was used to demonstrate that Shear force per unit length, F_S, is proportional to the square of velocity difference between two flow zones multiplied by the height of the vertical shear zone (a length term), as defined in Equation 4.8. For flow in flow region 1 the flood plain flow depth was equal to the height of the vertical shear zone.

$$F_S = C*(V_1 \bullet \cos(\theta_w) - V_2)^2 \bullet y_f \qquad [4.8]$$

C is the proportionality constant and is unknown but is likely to be influenced by many of the 11 key parameters associated with meandering compound channel flow. V_2 is the theoretical flood plain velocity in Zone 2 (assuming only bed friction resistance acts). V_1 is the theoretical Zone 1 velocity (assuming bed friction and secondary circulation losses and that the imaginary dividing planes (Zone 1 to Zone 2) exert no friction force) which is resolved through angle θ so as to be parallel to the main component of flood plain. The angle θ_w was defined as the angle between the flood plain flow and the centre line of the main channel averaged over one meander wavelength.

The author postulated that the relative magnitude of shear force, F_S might be a critical measure of the relative flow state in Zones 1 and 2 and that when the maximum shear stress was achieved this would indicate the greatest flow state differential between Zone 1 flow and Zone 2 flow. At this critical relative flow state the 2 flow zone behaviour, as shown in Figure 4.75, is likely to be disrupted and the 3 flow zone behaviour, as shown in Figure 4.6, is likely to be initiated, with a horizontal shear plane created between

Zones A and B. The Zone 2 flow gains enough energy to force a passage over Zone A. The author decided to investigate the variation of relative magnitude of F_S with flow depth and not the absolute value of F_S. Consequently C was set equal to an arbitrary value of 1.

Figures 4.79 and 4.80 show plots of overbank flow depth versus relative F_S which were derived for a representative selection of models which were tested during the Series B extension (1993-1996) and Series B (1989-1992) programmes respectively.

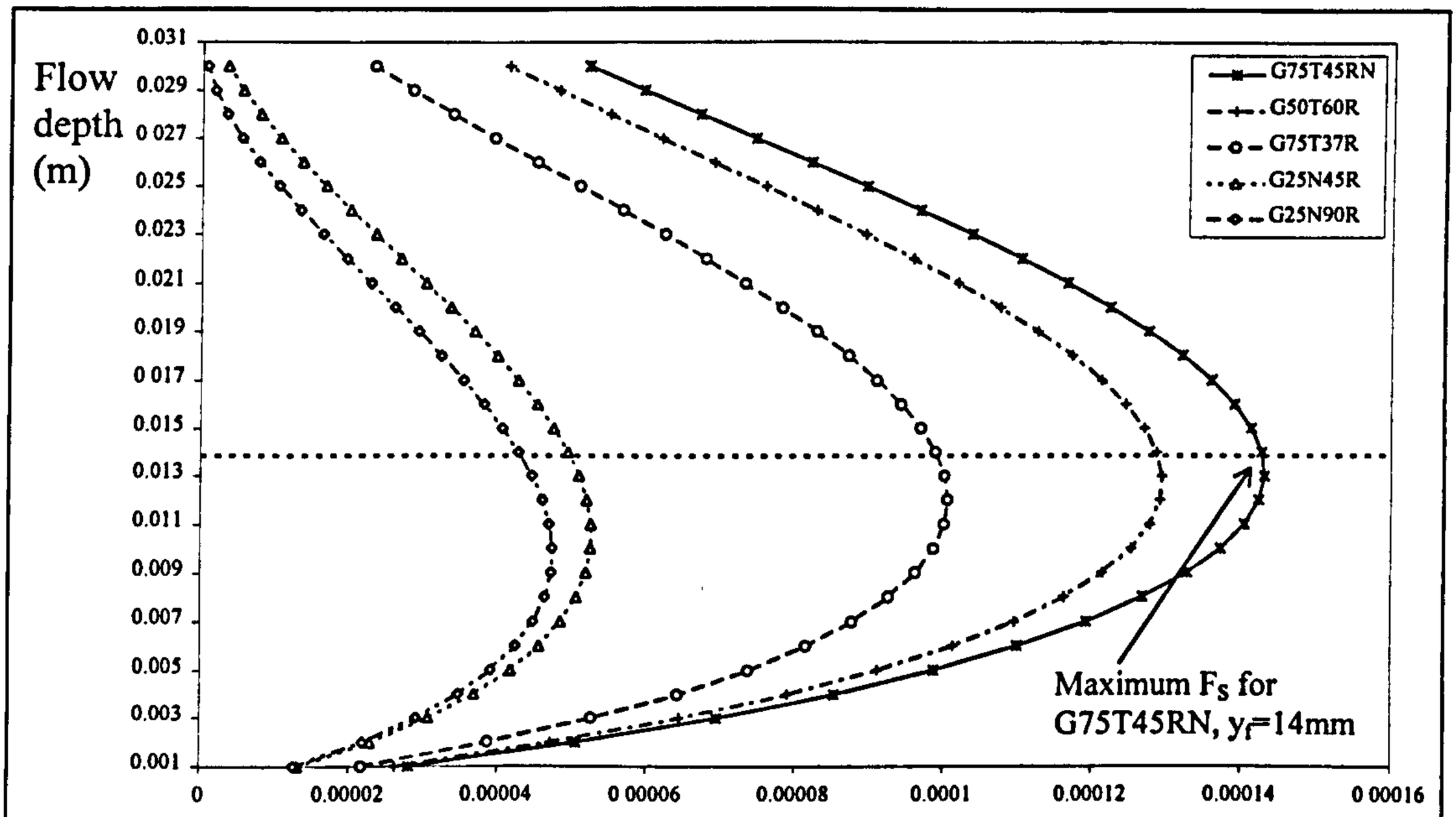

Figure 4.79 Overbank flow depth versus relative shear force, F_S (Series B extension)

Table 4.3 lists the flow depths which correspond to the maximum value of relative shear force, F_S, as predicted using Equation 4.8. It also shows the flow depths corresponding to the end of flow region 1 taken from plots of the overbank flow depth versus Global F* for the same selection of models to which the vertical shear equation was applied.

The predicted flow depths for maximum relative shear force, F_S, were similar to the experimentally measured flow depths which correspond to the end of flow region 1 (Transition 1/2) for both the Series B and Series B extension models.

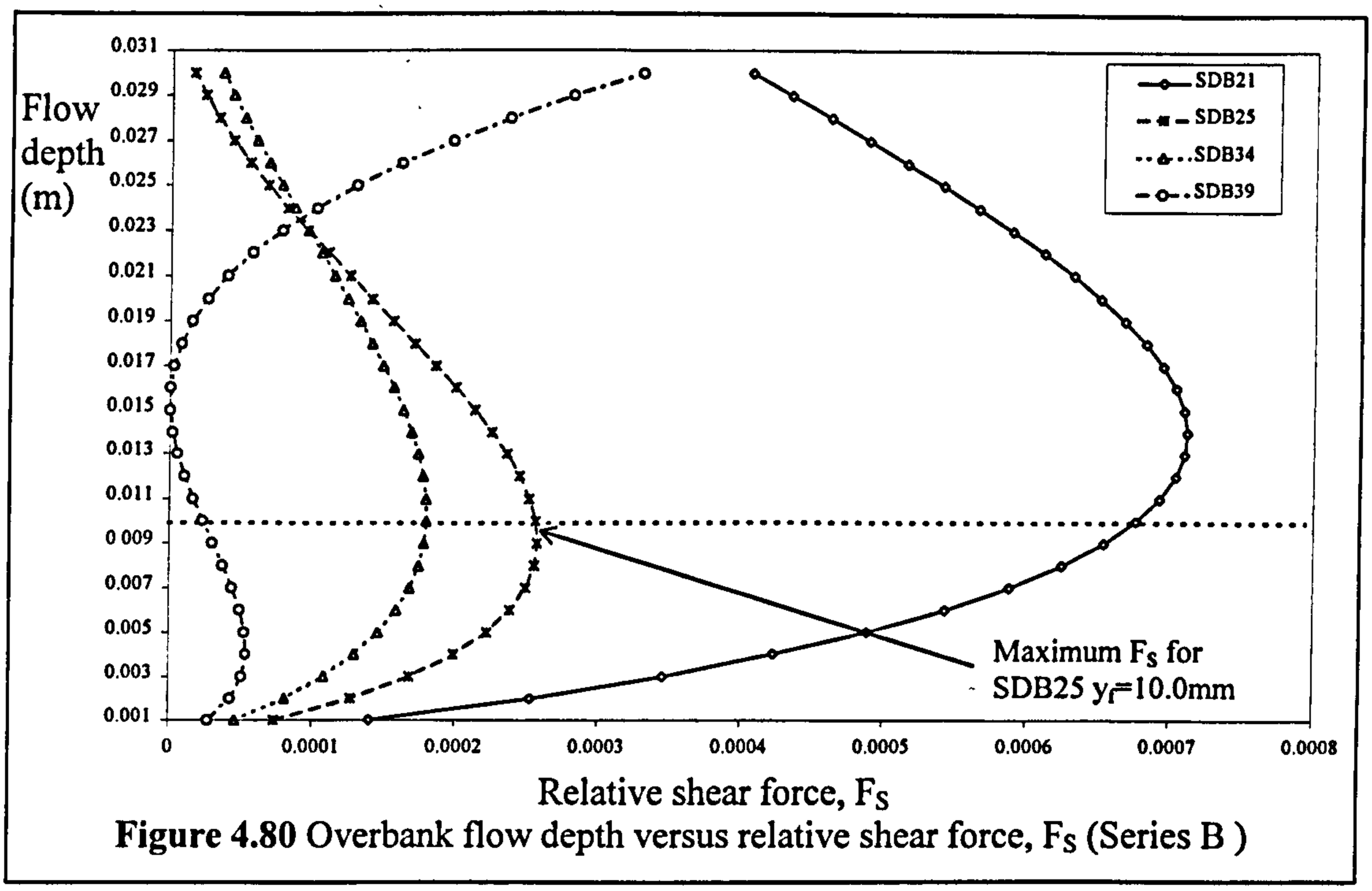

Figure 4.80 Overbank flow depth versus relative shear force, F_S (Series B)

Series B extension			Series B		
Ref. No.	y_f (mm), VS (Predicted)	y_f (mm), F* (Measured)	Ref. No.	y_f (mm), VS (Predicted)	y_f (mm), F* (Measured)
G75T45RN	14	12	SDB21	15	16
G75T37R	14	12	SDB25	10	12
G50T60R	12.5	15	SDB34	10	9
G25N60R	11	13	SDB39	5	(15)
G25N45R	9	8			

Table 4.3 Comparison between the predicted and measured flow depth (Region 1)

The prediction method gave reliable predictions for the measured Transition 1/2. Further testing is required to confirm that the prediction method is reliable for all channel configurations One anomalous result was obtained for SDB39. This result was attributed to the fact that no measurements were taken for this model at a low enough flow depth to precisely reveal Transition 1/2. The flow depth which was measured, and was assumed to correspond to Transition 1/2 was actually only the minimum value of Global F* that was taken. It is likely that the value of Global F* corresponding to Threshold 1/2 would have been generated at lower flow depth than at which it was measured. Consequently the comparison between the predicted and measured minimum flow depths is invalid and so the SDB39 result did not refute the Vertical shear force prediction method.

Any future anomalies that are identified when using this prediction method are likely to exist because of the method used to define Global F*. At low flow depth the majority of the flow is contained within Zone A and so Threshold A in the zonal F_A* plot is likely to correspond closely to Transition 1/2 in the Global F* plot. However, depending on the configuration and relative conveyance contained within Zones A, B and C this might not be the case for all channels. Although the difference is unlikely to be significant the author postulates that the flow depth corresponding to the maximum vertical shear value is likely to relate more accurately to the Zone A flow, measured using F_A*, rather than Global F*. The author suggests that future improvements of the prediction method will include its checking with overbank flow depth versus F_A* plots instead of Global F*. The checking with F_A* plots was not done during the Series B extension programme because the zonal flow measurements were not taken at a high enough resolution of flow depths to facilitate the precise identification of the flow depth corresponding to Threshold A.

4.7.4 Flow interaction mechanisms in flow region 2

Figures 4.74 a, b and c illustrate the flow behaviour in G75T45R for a flow depth equal to 25mm (RD=0.347) which is within flow region 2. The flow paths followed by the dye trails clearly demonstrate that the flow in Zone B shears across the top of Zone A. Some of the dye passes straight over Zone A and some becomes entrained in the flow. In these flow conditions the classic 3 zone split, as shown in Figure 4.6 is more representative of real flow conditions. The vertical shear layer is disrupted and a horizontal shear layer replaces it.

Despite Figure 4.74a, b and c presenting evidence for the presence of minor secondary cells, the author only measured a small increase in the magnitude of V/U over flow region 2. In reality the magnitude of these cells do not increase significantly. The depth-averaged velocities for Zones B and C in flow region 2, as shown in Figure 4.78, confirms this by demonstrating that there are minimal interaction losses experienced by the flow on the flood plain in flow region 2. The magnitudes of F_B* and F_C* remain close to that expected if only bed friction acts and therefore close to a value of 1.

Significantly the magnitude of F_A* is maintained immediately above Threshold 1/2. This indicates that the flow resistance cause by the horizontal shear, after the vertical shear planes are disrupted by Zone B flow, generates a similar magnitude of flow resistance in Zone A to that caused by the vertical shear stress just below Threshold 1/2. The author notes that F_A* begins to rise for further increases in flow depth, as the mean velocities in Zones A and B become more similar. The author postulates that F_A* increases because the magnitude of shear stress decreases, because shear stress is proportional to the square of velocity difference multiplied by a length term (which in this case is equal to the top width of the main channels). The author observes that once the mean flood plain flow velocity becomes greater than the mean main channel flow velocity the magnitude of horizontal shear stress will increase once again. However at these depth it may act to accelerate the flow in Zone A and F_A* will tend to values greater than 1 which is shown by many of the Series B extension (1993-1996) models.

F_A* retains a relatively small magnitude in flow region 2 due to the horizontal shearing action, because F_B* and F_C* are close to 1. Consequently, Global F* increases rapidly as flow depth increases and more of the conveyance capacity of the channel is provided by Zones B and C.

4.7.5 Identification of Threshold 2/3

At Threshold 2/3 in the Global F* plot, or Threshold B in the Zonal F* plots, further significant interaction mechanisms between Zones A and B become initiated with the associated creation of large secondary cells which extend from Zone A into Zone B. At the same depth the reduction in Zone B velocity compared with Zone C velocity induces interaction between the zones in the form of a vertical momentum transfer zone (shear layer) between Zones B and C.

The author postulated that the relative state of flow in Zones A and B was likely to control the onset of this further interaction between Zones A and B. The author investigated different measures of relative flow state in an attempt to identify the Threshold criteria which corresponded to the onset of flow region 3 behaviour.

During this process, the author noted that Reynolds number, Re, where Re=4VR/ν, is often used to assess the flow state in individual channels. The author decided to investigate whether a measure of Relative Reynolds number, Re', could be used to measure relative flow state and thus predict Threshold 2/3. Relative Reynolds number, Re' was defined using Equation 4.9. The Reynolds numbers for Zone A flow, Re_A, and Zone B flow, Re_B, were theoretically determined by assuming that only bed friction resists flow in each zone. Consequently they could be determined for any channel if its geometry and roughness characteristics were known.

$$\text{Relative Reynolds number, } Re' = \left(\frac{Re_B}{Re_A}\right) = \frac{4V_B R_B / \upsilon}{4V_A \cos(\theta_{sk}) R_A / \upsilon} \qquad [4.9]$$

V_A is the component of average velocity in the main channel which is resolved over the average skew angle θ_{SK} (averaged over one wavelength) to be parallel with the main component of flood plain velocity. R_A is the hydraulic radius of the main channel at bankfull. V_B and R_B are the average velocity and hydraulic radius of the flood plain flow in Zone B. For low flow depths Re' is less than 1. When the resolved Reynolds number of the main channel is lower than the flood plain then Re' is greater than 1. The author tested whether there was any particular value of Relative Reynolds number which corresponded to the onset of Threshold 2/3.

Figures 4.81 and 4.82 show plots of overbank flow depth versus Relative Reynolds number, Re', for a selection of Series B extension and Series B models.

Table 4.4 compares the flow depths which generate a Relative Reynolds number, Re', equal to 1 (theoretically calculated) and the measured flow depths from relative depth versus Global F* plots which demonstrate the presence of Threshold 2/3 at the beginning of flow region 3.

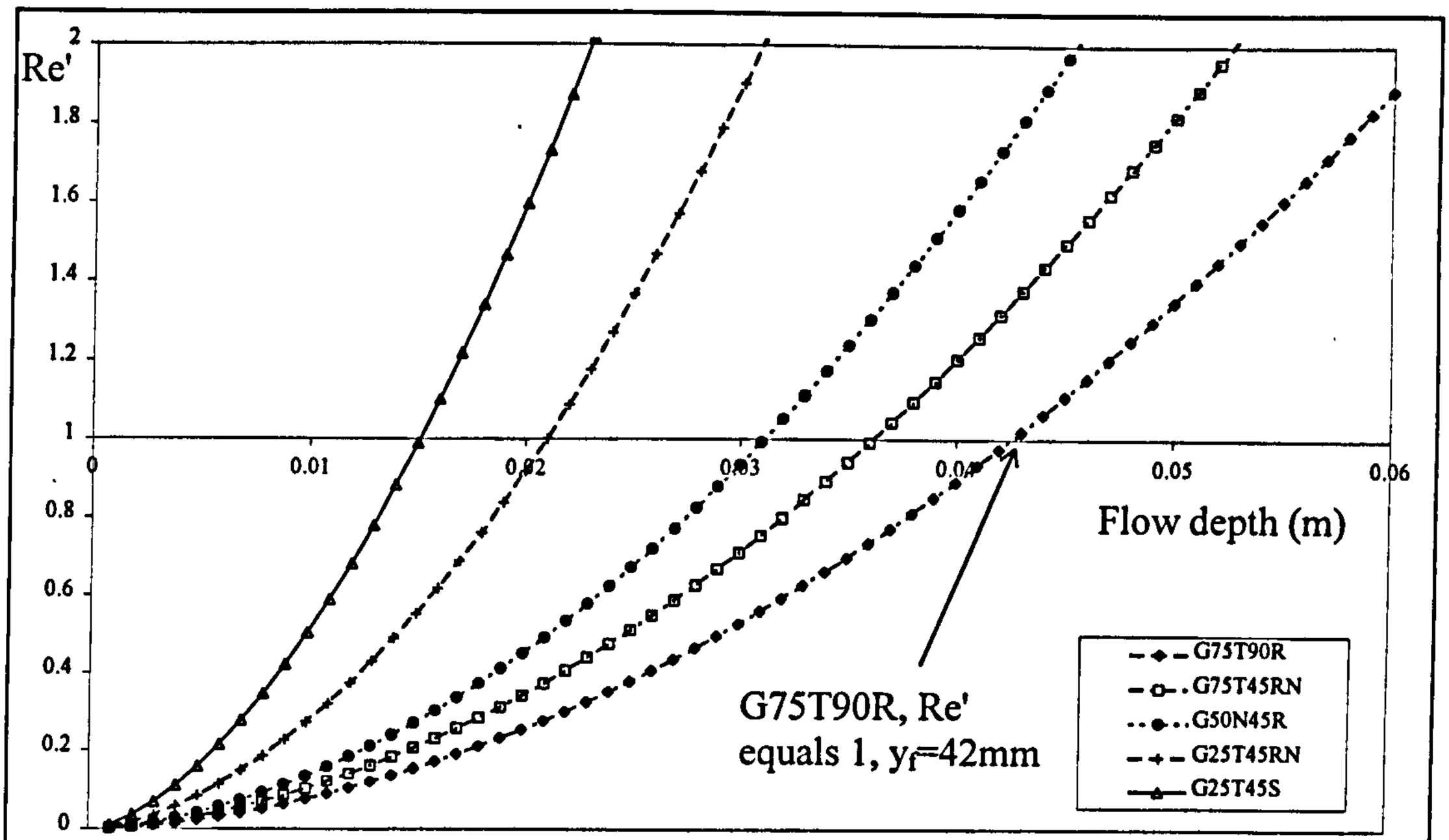

Figure 4.81 Relative Reynolds number versus flood plain flow depth (Series B ext.)

The results in Table 4.4 demonstrate that the flow depths at which the Relative Reynolds number, Re', is equal to 1 do coincide with the start of flow region 3 (Threshold 2/3) for the models tested. Only SDB34 does not fit this pattern. In fact SDB34 does not demonstrate a flow region 3 at all. The unrealistic surface roughening technique which was adopted resulted in the flow velocity in Zone B not increasing sufficiently to generate significant secondary cell mechanisms and so flow region 3 was not established. Overall however, the author concluded that the Relative Reynolds number technique did produce reliable predictions for the onset of flow region 3.

Series B extension (1993-1996)			**Series B (1989-1992)**		
Ref. No.	yf (mm) Predicted	yf (mm) Measured	Ref. No.	yf (mm) Predicted	yf (mm) Measured
G75T90R	42	40	SDB21	91	84
G75T45R	36	34	SDB25	59	62
G50N45R	31	34	SDB34	70	N/A
G25T45RN	21	24	SDB39	46	48
G25T45S	16	19			

Table 4.4 Comparison between the predicted and measured flow depth (Regions 2 & 3)

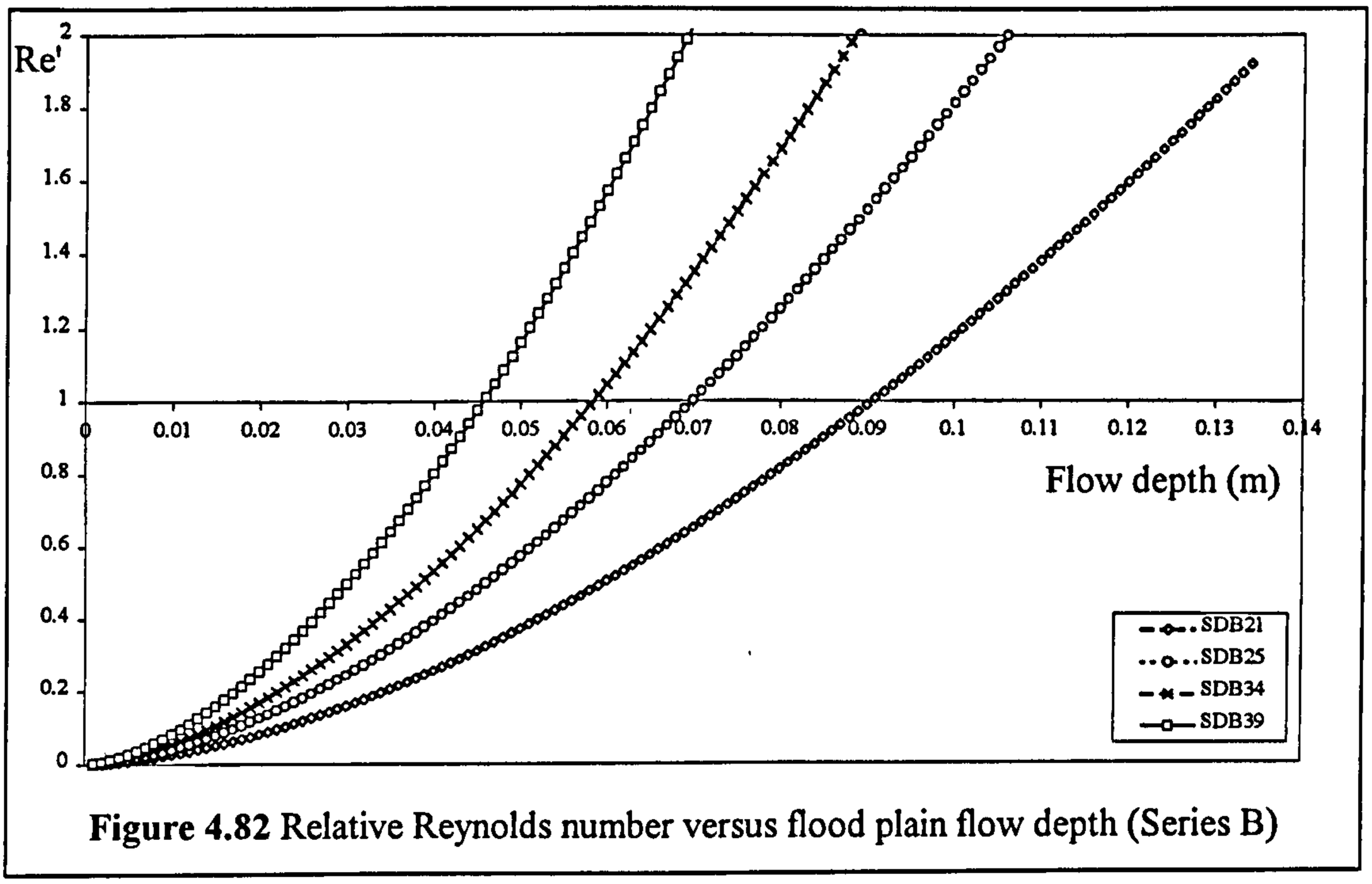

Figure 4.82 Relative Reynolds number versus flood plain flow depth (Series B)

4.7.6 Flow interaction mechanisms in flow region 3

4.7.6.1 The general interaction between Zones A, B and C

The author's prediction for the Relative Reynolds number, Re' which corresponded to Threshold 2/3 in G75T45R coincided with the measured Threshold 2/3 and was equal to a flow depth of 35mm. Figure 4.77 shows a plot of overbank flow depth versus V/U for G75T45R. The change point from relatively small values of V/U to rapidly increasing values of V/U occurs in the vicinity of the same flow depth, about 35mm. This provides evidence that the significant secondary circulation cells are generated by the horizontal shearing of the flood plain water over the main channel above Transition 2/3.

Figure 4.83 shows a plot of the depth averaged velocity in Zones B and C across the full width of the flume for G75T45R at a flood plain flow depth equal to 50mm (RD=0.515) in flow region 3. The impact of the additional interaction mechanisms on the local depth-averaged velocities can be seen clearly. Zone B comprises two distinct sub-zones, B1 and B2 , as shown in Figure 4.84, instead of the one simple Zone B which was postulated by James and Wark [1] [1992].

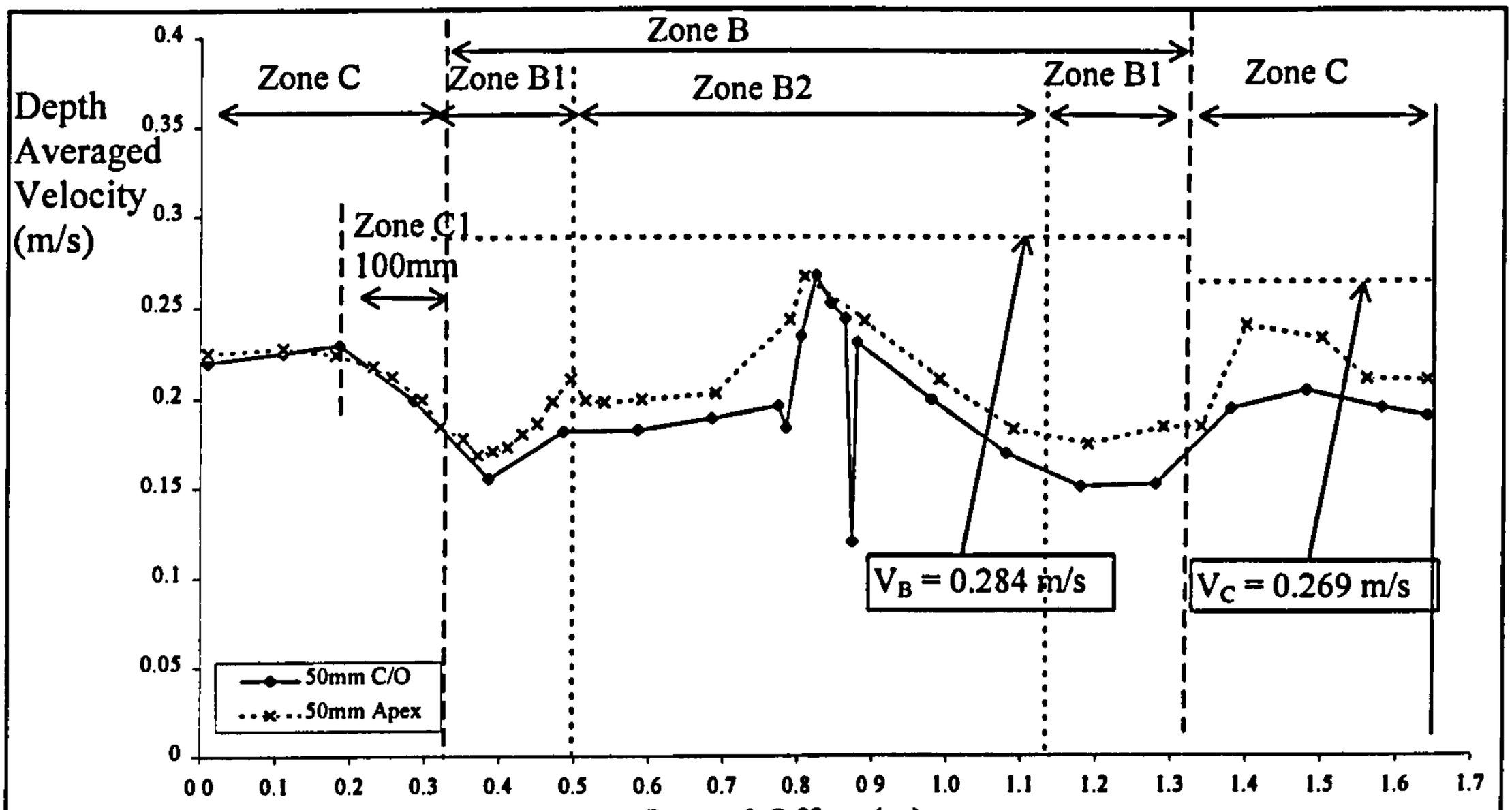

Figure 4.83 Depth averaged velocity versus flume offset for G75T45R, Depth = 50mm

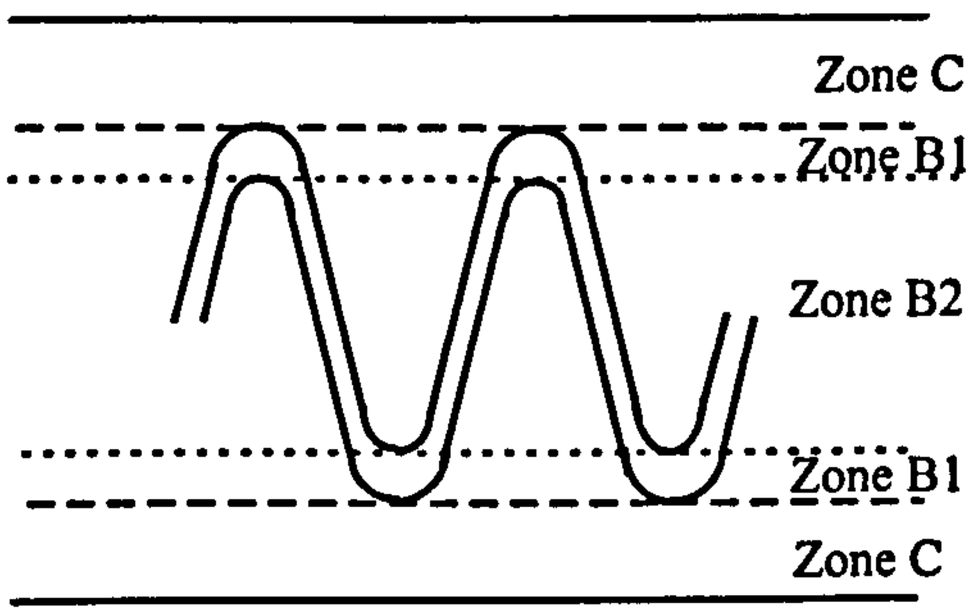

Figure 4.84 The novel Zone B split

Zone B1 lies above the line of the main channel and Zone B2 consists of the remaining width of the channel and aligns with the cross-over section of the main channel. The flow in Zone B1 is characterised by a significant local reduction in depth-averaged velocity compared with Zone B2. Figure 4.83 shows the mean depth-averaged velocities in Zones B1 and B2 in flow region 3, this is typical of the general trend observed in all the model tests. The mean velocity is lower in Zone B than in Zone B2.

Figure 4.83 also demonstrates that a significant vertical shear zone is established between Zones B1 and C. The width of the shear zone depends on the difference in velocity between Zones B1 and C and the frictional characteristics of the Zone C bed surface. In Zone C, outwith the shear zone, the flow was subjected only to bed friction

and therefore the standard resistance formulae can be used. As the width of Zone C1 becomes larger the magnitude of F_C* reduces.

In flow region 3 Zone A will be influenced by a combination of flow mechanisms. The onset of large secondary circulation cells will result in increased flow resistance but the horizontal shear action will tend to accelerate the flow in Zone A. Observations of the Zone A plots for the Series B extension (1993-1996) models reveals that F_A* tends to values greater than 1 as flow depths increase which therefor implies that of the two counter mechanisms the shearing action dominates. Despite the increases in F_A* the magnitude of Global F* decreases in line with F_B* and F_C* because at these flow depths the majority of the flow capacity is provided by Zones B and C.

4.7.6.2 An explanation for the difference in Zone B1 and B2 behaviour

The author demonstrated, using flow visualisation results obtained during the Series B extension (1993-1996) programme, that the majority of the water within Zone A, at the crown of the Apex, is expelled from the main channel and deposited onto the flood plain before it leaves Zone B1, thus confirming the findings of Hardwick and Willetts [1993]. Figure 4.85 clearly shows this exchange for the Series B extension (1993-1996) model: G75T45R. The flood plain flow depth is 25mm deep and in flow region 3. The photographs were taken over a 3 second interval.

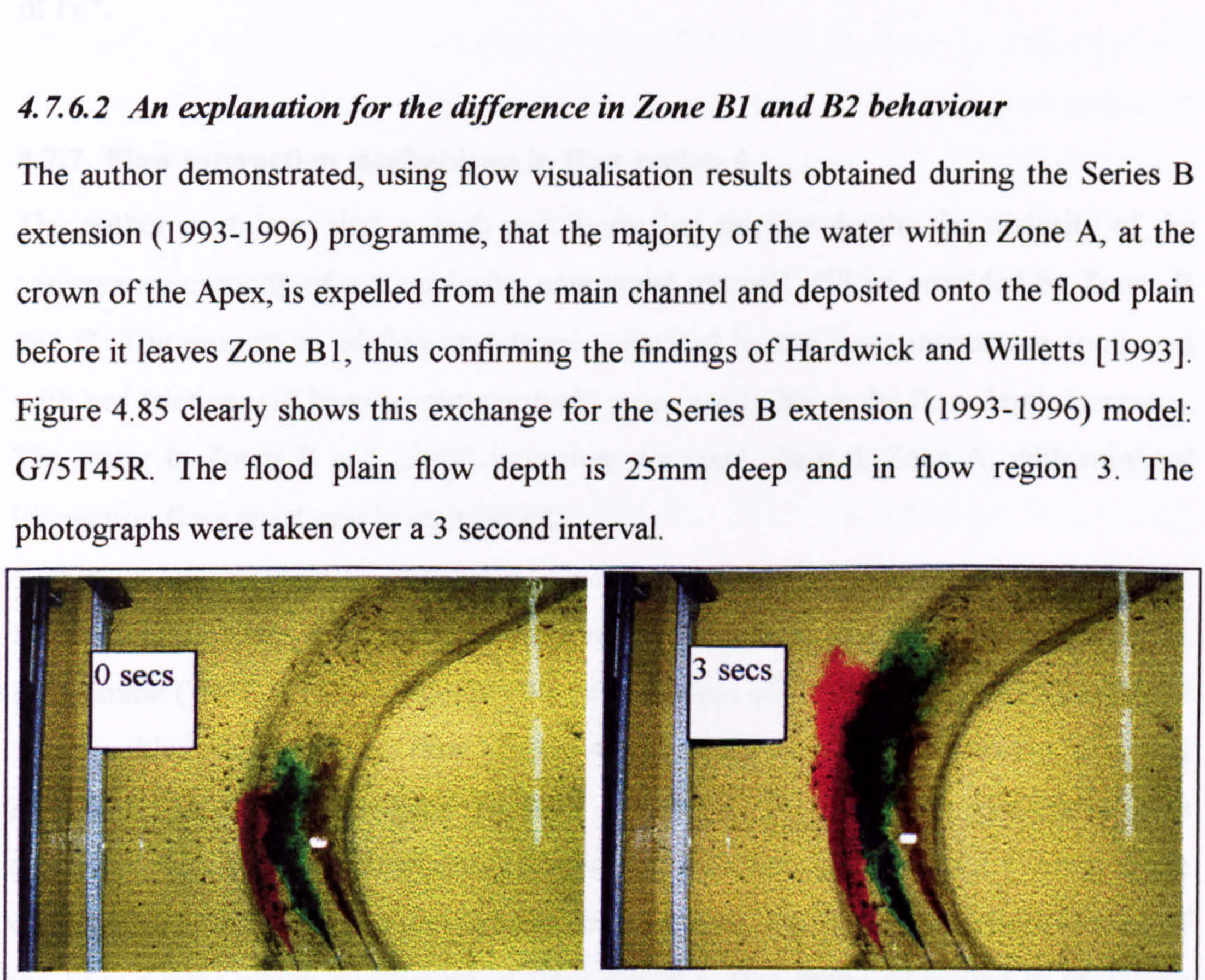

Figure 4.85 Flow exchange between Zones A and B1 (G75T45S, f/p depth=25mm)

By contrast in Zone A below Zone B2 (the cross-over), the secondary cells remain ostensibly undisrupted and although some flow is expelled the majority is retained within Zone A, as demonstrated in Figure 4.73. The author suggests that when the discrete

secondary cells in Zone A (under Zone B2) pass down the main channel and enter the area under Zone B1, they become part-aligned with the main component of Zone B1 flow and consequently increase the forces driving the expansion and contraction of flow in Zone B1 and A, dragging large amounts of the Zone A flow into Zone B1. Consequently the flow in Zone A, under Zone B1, never reaches the section of Zone A under the next stretch of Zone B2.

The author postulates that it is this flow exchange which generates a significant extra source of head loss in Zone B1 and causes the mean velocity in Zone B1 to be significantly less than the mean velocity in Zone B2. Large reductions in mean velocity of Zones B1 and B2 in flow region 3 were reflected by large reductions in the magnitude of F_B*.

4.7.7 Flow interaction mechanisms in flow region 4

The author postulates that at high and increasing relative depths the majority of the conveyance capacity of a meandering compound channel will be provided by Zones B and C. The proportion of flow resistance generated by the layer interaction compared with bed friction will become progressively more negligible as the flow depth increases. The water in Zones B and C will pass over the main channel, Zone A, with minimal interaction flow resistance being exerted.

Insufficient data was gathered at the high relative depths during the Series B extension programme (1993-1996), to facilitate the development of a method to predict Threshold 3/4 (marking the onset of flow region 4). The author does not believe that this represented a major drawback because the Series B extension programme was conceived with the clear intention of developing a pragmatic method for predicting the discharge capacity of a meandering compound channel. As there is very little chance of the flow depths which correspond to flow region 4 ever being generated in prototype channels the author concluded that it was unessential to develop a method to predict Threshold 3/4 now or in the future.

4.7.8 Anomalies in the four flow region behaviour

The plot of relative depth versus Global F* for model: A2T1000S in Figure 4.25 unusually provides no evidence for the existence of flow region 2. The author checked the flow depth corresponding to Threshold 2/3 in this model. The predicted Threshold 2/3 was equal to 15mm. The author postulates that because Threshold 2/3 was so low, the flow readings were not taken at a high enough resolution to distinguish flow region 2 and so it appears that flow regions 1 and 3 merge.

4.7.9 A prediction for the influence of untested key parameters on flow behaviour

4.7.9.1 The influence of flood plain bank sinuosity on flow resistance

The team in Bristol were programmed to perform tests in order to determine the influence of flood plain sinuosity on the head losses generated by layer interaction in meandering compound channels. Unfortunately the results were not available at the time of writing. Nevertheless the author has used the understanding gained from the Series B extension (1993-1996) work to make general predictions for the flow behaviour in meandering compound channels with sinuous flood banks.

Increasing flood bank sinuosity will reduce the mean velocity of flood plain flow compared with models with straight flood banks. Either the linearised SCS [1963] method or the Chang [1988] method, could be used to determine the extra flow resistance resulting from the flood bank sinuosity. Significantly the flood bank sinuosity will not reduce the flood plain velocity by much at low flood plain flow depths and so the author predicts that its influence on the interaction mechanisms will be minimal at a low flow depth, in flow regions 1 and 2.

However the author postulates that the reduction in average flood plain velocity from that in a similar meandering compound channel with straight flood banks will raise Threshold 2/3. It will reduce the increases in interaction flow resistance generated by the expansion and contraction of Zone B because the interaction flow resistance is proportional to the square of flood plain velocity which is reduced. The rate of decrease of F_A* will be reduced. The relative Vertical shear force method and the Relative

Reynolds number methods can be used to determine the Thresholds. The author eagerly awaits the Bristol results in order to confirm his predictions.

4.7.9.2 The influence of flood plain lateral slope on flow resistance

The team in Bristol were programmed to perform tests in order to determine the influence of lateral flood plain slope on the head losses generated by layer interaction in meandering compound channels. Unfortunately the results were not available at the time of writing. The author has used the understanding gained from the Series B extension (1993-1996) work to make general predictions for the flow behaviour in meandering compound channels with sinuous flood banks.

The author predicts that lateral flood plain slope will increase the magnitude of interaction flow resistance in flow regions 1 and 2 because the average flood plain velocity will be lower in the channels with lateral flood plain slopes, at the same flow depths (measured from the top of the main channel banks). Consequently the vertical shear forces in flow regions 1 and 2 are likely to be greater, implying that F_A^* will be reduced. However in flow region 3, the reduction in interaction flow resistance, due to the decrease in the horizontal shearing due the alignment of the flood plain flow to the main channel, will counter the effect of the reduction of the mean flood plain velocity.

The difference in flood plain velocity at equivalent flow depths will effect the Threshold depths. The relative Vertical shear force method and the Relative Reynolds number method can be used to determine the Thresholds. Further work is needed to determine the effect of aligning the flood plain flow in flow region 3 thus reducing the horizontal shearing. The author eagerly awaits the Bristol results in order to confirm his Threshold predictions and to determine precisely the effect that the aligning flood plain flow with Zone A will have on the horizontal shearing mechanism (interaction mechanisms) between Zones A and B.

4.8 Analysis of the slot model experimental results

4.8.1 Introduction

Ervine and Ellis [1987] and James and Wark [1992] have derived semi-physical semi-empirical models for predicting the mean flow velocity in Zone B (flood plain flow within the meander belt) of a meandering compound channel. They have assumed that the additional flow resistance supplementing bed friction head losses in these channels can be determined by assuming that a simple expansion and contraction model for flow over a slot will produce the same magnitude of head loss and flow resistance that is generated within the compound channel. These existing models however have only catered for variations in 3 key parameters: relative depth, RD, and to some extent aspect ratio, AR, and main channel side slope, ϕ_{SS}. The author proposed that the data on which these models were based was limited and that 2 other key parameters, relative roughness, f', and main channel skew angle, θ_{SK}, also have an effect. Consequently he built and tested 20 slot models as part of the Series B extension programme in Glasgow in order to further determine the influence of all 5 parameters and to develop an enhanced expansion and contraction model.

The expansion and contraction head losses, h_E and h_C, were measured using the energy line method described in section 3.3 at each flow depth for each of the 20 slot models. Subsequently the adjustment coefficients, C_{WE} and C_{WC}, were determined in order to relate the theoretical head loss coefficients for flow over steps, $[1-y_2[y_2+h]]^2$ for expansion and K_c (Rouse [1950]) for contraction, to those determined using the experimental results obtained from the slot experiments using Equations 4.10 and 4.11.

$$h_E = C_{WE}\left[1-\frac{y_2}{y_2+h}\right]^2\frac{V^2}{2g} \qquad [4.10]$$

$$h_e = C_{WC}K_C\frac{V^2}{2g} \qquad [4.11]$$

The adjustment coefficients are non-dimensional and it is therefore possible to apply them to models of various scales. Table 4.5 lists the magnitudes of C_{WE} and C_{WC} which were determined for a number of flow depths in 20 slot models. The geometric

configurations and surfaces roughness for each model, referred to by their tests number: such as S7S9S, are given in Table 3.12.

Test No.	Flow Depth	C_{we}	C_{wc}	Test No.	Flow Depth	C_{we}	C_{wc}	Test No.	Flow Depth	C_{we}	C_{wc}
	(mm)				(mm)				(mm)		
S7G9S	13	0.71	0.45	S5G9S	16.7	0.66	0.54	S2G9S	16.7	0.96	0.52
	25	0.57	0.43		24	0.64	0.39		24	0.86	0.54
	36	0.42	0.32		33.3	0.53	0.27		33.3	0.78	0.42
	50	0.39	0.22		50	0.53	0.20		50	0.56	0.30
	75	0.38	0.19								
S7G6S	13	0.51	0.51	S5G6S	16.7	0.52	0.54	S2G6S	16.7	0.96	0.53
	25	0.45	0.39		24	0.53	0.39		24	0.86	0.42
	36	0.35	0.29		33.3	0.53	0.27		33.3	0.65	0.31
	50	0.33	0.22		50	0.47	0.20		50	0.63	0.25
	75	0.32	0.15								
S7G4S	13	0.67	0.45	S5G4S	16.7	0.52	0.48	S2G4S	16.7	0.81	0.53
	25	0.39	0.31		24	0.57	0.35		24	0.73	0.42
	36	0.40	0.26		33.3	0.50	0.24		33.3	0.72	0.21
	50	0.30	0.13		50	0.44	0.20		50	0.63	0.20
	75	0.26	0.10								
S7G3S	13	0.44	0.45	S5G3S	16.7	0.42	0.36	S2G3S	16.7	0.69	0.50
	25	0.42	0.35		24	0.49	0.22		24	0.73	0.30
	36	0.35	0.21		33.3	0.49	0.17		33.3	0.73	0.24
	50	0.33	0.11		50	0.47	0.14		50	0.52	0.21
	75	0.30	0.08								
S7G9S4	16.7	0.47	0.23	S5G9S6	16.7	0.66		S7G9B	16.7	0.62	0.71
	24	0.37	0.30		24	0.61			24	0.52	0.57
	33.3	0.24	0.22		33.3	0.53			33.3	0.20	0.40
	50	0.37	0.16		50	0.56			50	0.15	0.41
S7G9S7	16.7	0.26	0.71	S5G9S4	16.7	0.67		S7G9A	16.7	0.52	0.75
	24	0.46	0.24		24	0.67			24	0.50	0.58
	33.3	0.35	0.08		33.3	0.51			33.3	0.28	0.21
	50	0.11	0.04		50	0.28			50	0.13	0.10
S7G9S6	16.7	0.73	0.92	B2G4S	16.7	0.59					
	24	0.50	0.55		24	0.40					
	33.3	0.28	0.48		33.3	0.59					
	50	0.22	0.22		50	0.56					

Table 4.5 Adjustment coefficients, C_{we} and C_{wc}, for 20 slot models

4.8.2 The influence of Aspect ratio

Figures 4.86 and 4.87 show plots of aspect ratio versus the adjustment coefficients, C_{we} and C_{wc} for slots: S7G9S, S5G9S, and S2G9S which are 500mm long with vertical sides

and are 75mm, 50mm and 25mm deep respectively. All the other parameters were kept constant in each slot. The results for different relative depths were plotted separately to illustrate that the relative depth of flow does have a significant influence and that the approach taken by James and Wark [1] [1992] ignoring relative depth was in fact erroneous.

Figures 4.86 demonstrates that for the low aspect ratios the values for C_{we} was much lower than 1 which implies that full expansion was not occurring. C_{we} would equal 1 if the forward facing step was isolated and full expansion was occurring.

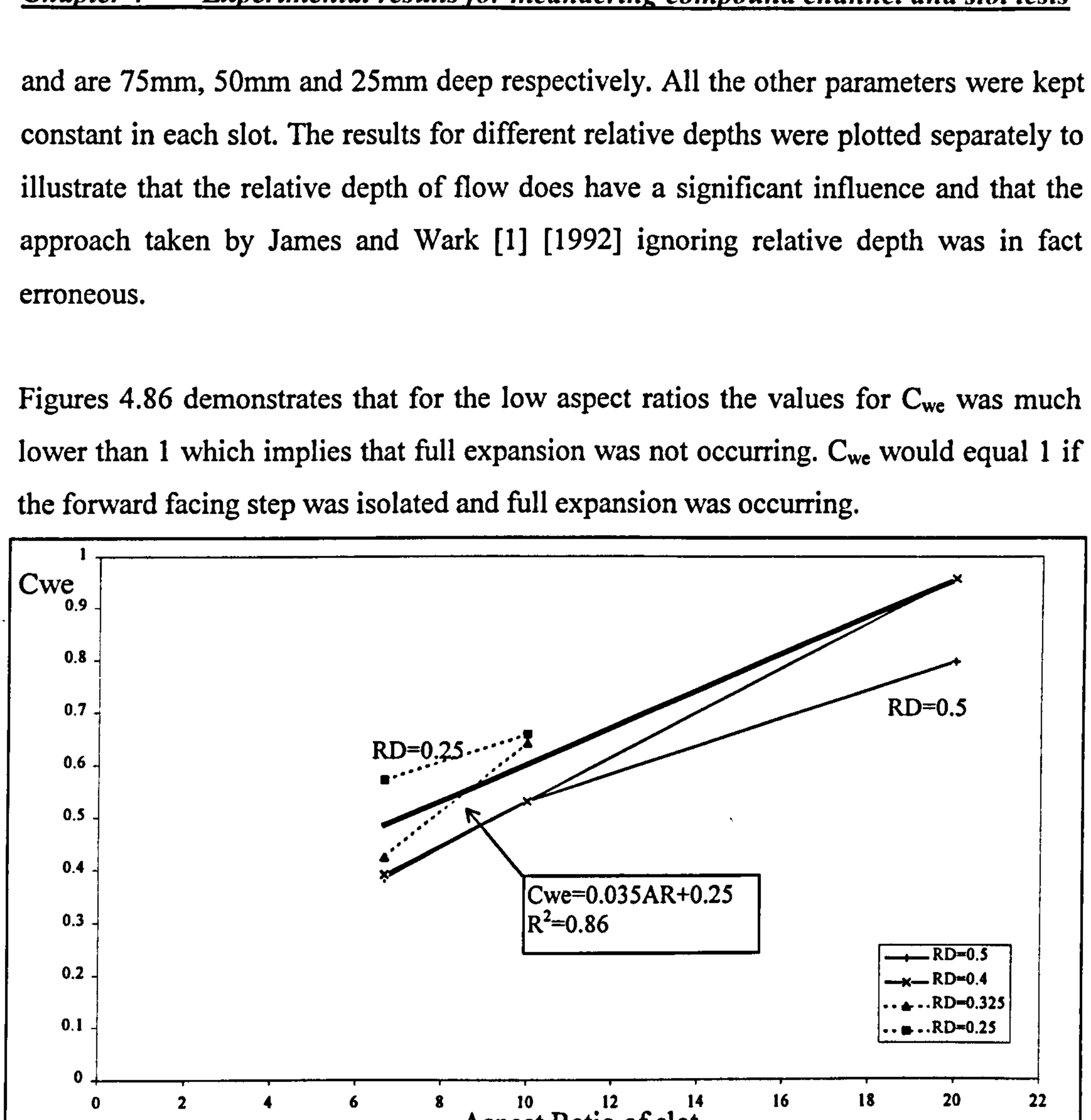

Figure 4.86 Plots of Cwe (Expansion) versus aspect ratio (S7G9S, S5G9S, and S2G9S)

Figure 4.87 demonstrates that for the low aspect ratios, the values for C_{wc} were also much lower than 1 which implies that full contraction was not occurring. C_{wc} would equal 1 if the backward facing step was isolated and full contraction was occurring. Figures 4.86 and 4.87 also demonstrate that as the aspect ratio of the channels becomes larger the magnitude of C_{we} and C_{wc} both tend towards 1.

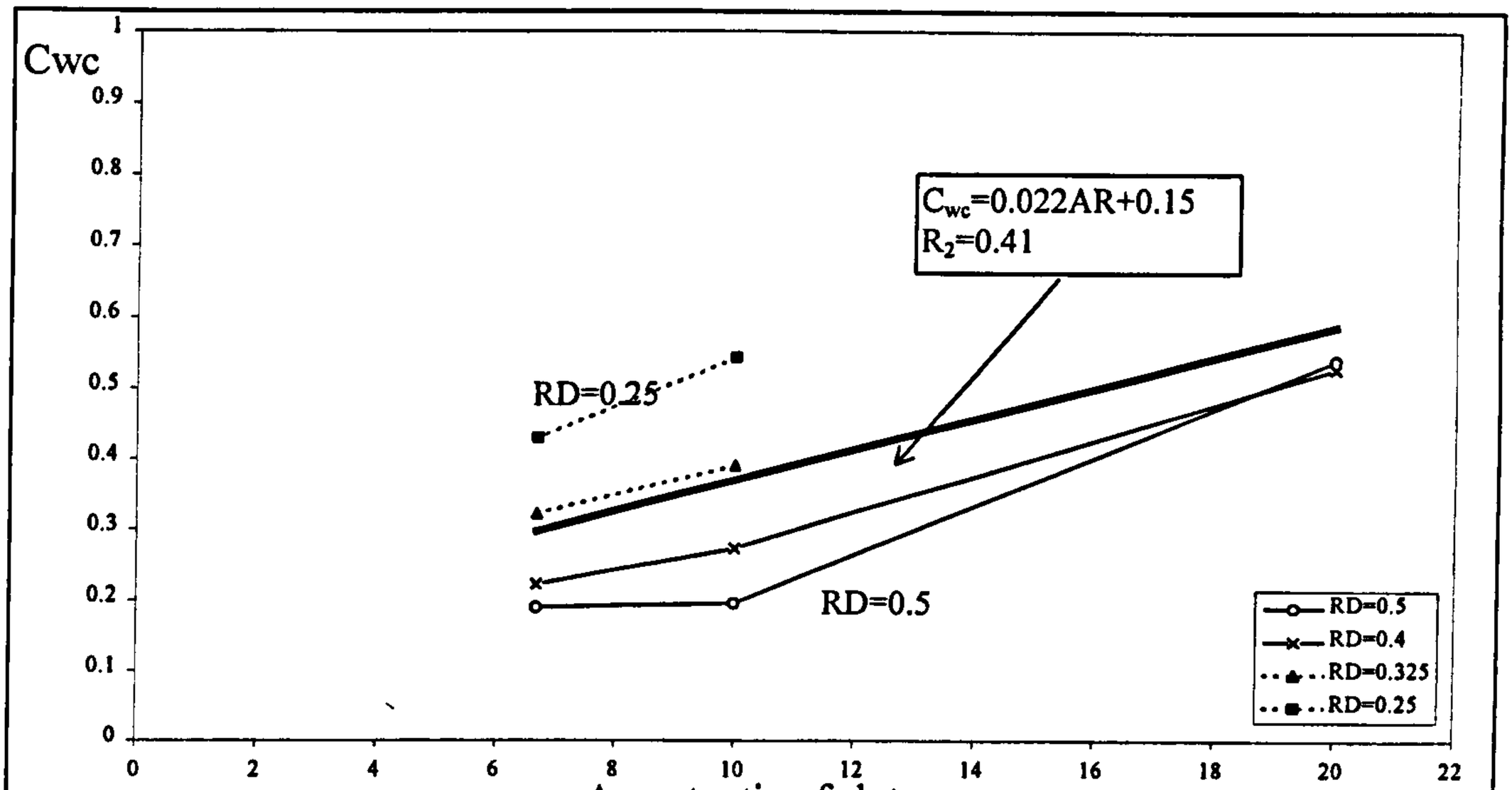

Figure 4.87 Plots of Cwc (Contraction) versus aspect ratio (S7G9S, S5G9S, and S2G9S)

This behaviour can be explained visually using Figures 4.88a, b, c. When the aspect ratio of a slot is very small as in Figure 4.88a the flood plain flow will pass over the slot with only minimal influence on flood plain flow component. As the aspect ratio of the slot increases, increasing amounts of flow separation will occur at the forward facing step and larger, more significant secondary cells will be generated.

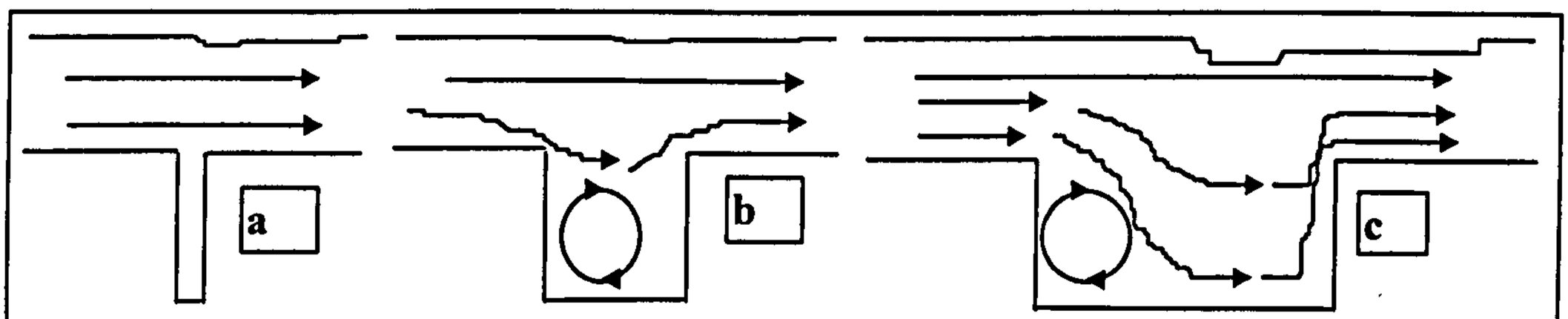

Figure 4.88 Flow vectors in slots with increasing aspect ratio

In channels with relatively small aspect ratios the cell is likely to fill the complete slot width, as shown in Figure 4.88b . Consequently only minimal forward momentum will be gained by the water in the slot and as a result minimal flow contraction (and therefore head losses) will be generated by the slot water flowing back onto the flood plain. The energy expended creating the cell will effectively represent the expansion head losses.

Channels with larger aspect ratios will eventually become large enough so that a finite size of secondary cell will be created by the flow separation in the knuckle of the forward facing step and 're-attachment' will occur. The re-attachment length denotes the

longitudinal chainage where the flow in the slot, adjacent to the bed, changes from flowing backwards a part of the secondary cell, to flowing forwards as shown in Figure 4.88c. The interrelationship between aspect ratio and flow re-attachment length critically influences the magnitude of head losses generated in flow over a slot.

If the flow contained within the slot at all flow depths has a main component of flow towards the backward facing step, the flow over the whole depth will have to contract to re-enter the flood plain, as shown in Figure 4.88c and consequently the magnitude of contraction head loss will large. Much larger than if only a smaller proportion of the slot depth is aligned parallel to the flood plain flow, so less flow has to contract back onto the flood plain as shown in Figure 4.88a.

The re-attachment length (RL) for every model tested during the Series B extension programme was determined by analysing the width-averaged longitudinal velocity vector plots. Figure 4.89 shows a typical plot velocity vector for S5G9S at a relative depth equal to 0.4.

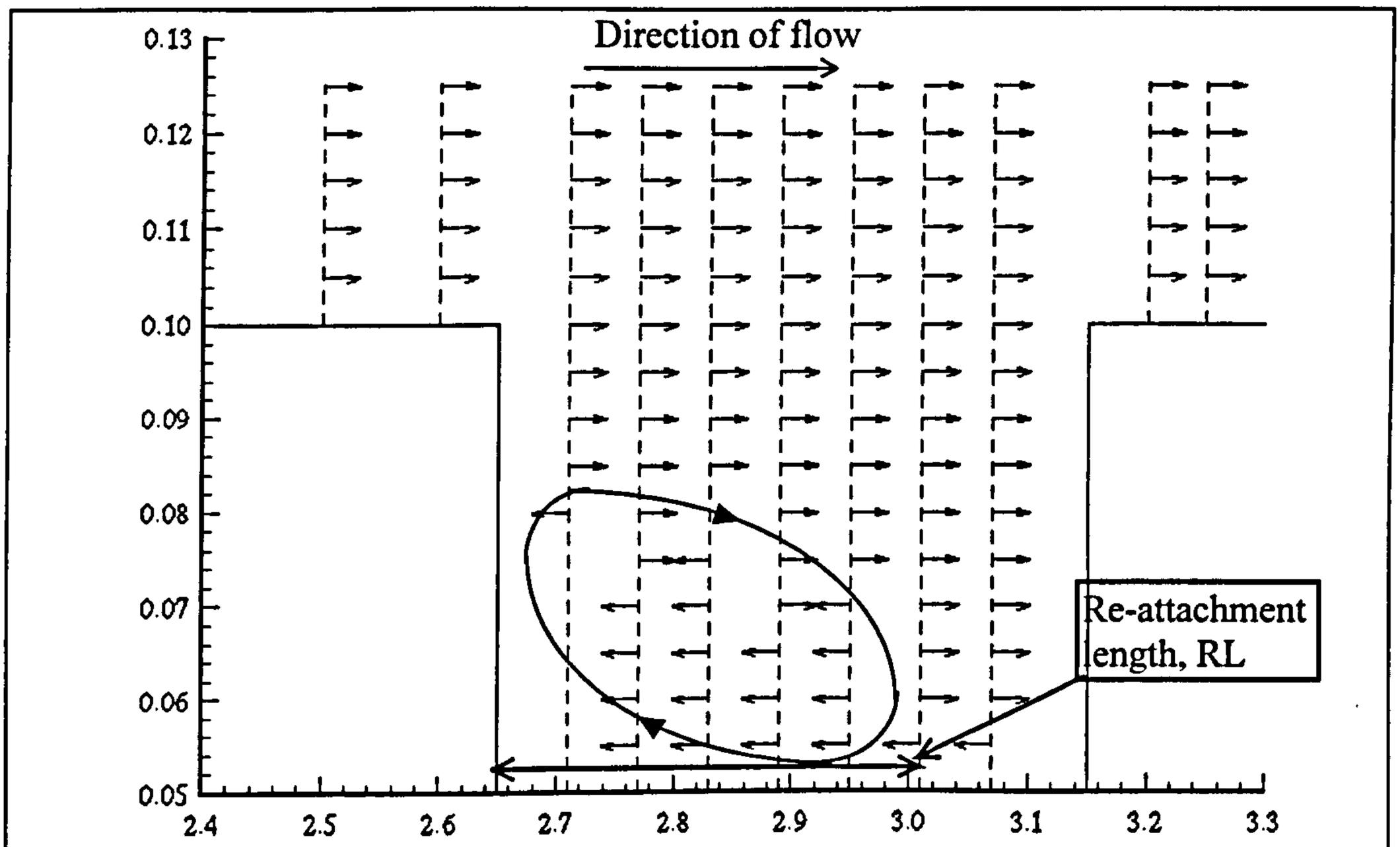

Figure 4.89 Longitudinal velocity profile for slot flume (S5G9S, RD=0.4)

The re-attachment point occurs between the two chainages at which the velocity vector changes direction, adjacent to the bed. The re-attachment length was determined by

using quadratic interpolation of the velocity vectors either side of the re-attachment point. Table 4.6 lists the re-attachment lengths which were measured for models with zero skew, smooth flood plain surfaces and variable relative depths.

In 1980 Kim et al [1980] demonstrated that re-attachment length may not in fact distinguish the end of the expansion region. They used a series of wind tunnel experiments on turbulent flow over a backward facing step to show that for a long distance past the point of reattachment considerable extra turbulence is generated causing extra head loss. Further experimental data must be collected to assess whether similar behaviour is demonstrated in water filled slots where the flow is smooth turbulent as in the Series B extension models. The author assumed that in the interim it is justifiable to use the traditional definition of the re-attachment length to give a first indication of the extent of the full expansion phase that is generated in a slot.

Test No.	Flow Depth	Re-attach. length	Test No.	Flow Depth	Re-attach. length	Test No.	Flow Depth	Re-attach length
	(mm)	(mm)		(mm)	(mm)		(mm)	(mm)
S7G9S	13	N/A	S5G9S	16.7	340	S2G9S	16.7	180
	25	N/A		24	350		24	190
	36	N/A		33.3	340		33.3	200
	50	N/A		50	390		50	200
	75	N/A						
S7G6S	13	N/A	S5G6S	16.7	360	S2G6S	16.7	150
	25	N/A		24	390		24	160
	36	N/A		33.3	390		33.3	180
	50	N/A		50	350		50	200
	75	N/A						
S7G4S	13	N/A	S5G4S	16.7	320	S2G4S	16.7	100
	25	N/A		24	380		24	150
	36	N/A		33.3	380		33.3	160
	50	N/A		50	325		50	160
	75	N/A						
S7G3S	13	N/A	S5G3S	16.7	340	S2G3S	16.7	160
	25	N/A		24	300		24	175
	36	N/A		33.3	320		33.3	175
	50	N/A		50	330		50	150
	75	N/A						

Table 4.6 Re-attachment lengths in the slot

The re-attachment length results obtained by the author provided corroboratory evidence to support the findings of Fujita et al [1991] and Manson [1994]. Fujita et al [1991] suggested that it was incorrect to assume that re-attachment occurs in slots with aspect ratios greater than 5 which has been previously postulated. Manson [1994] even suggested that re-attachment does not even occur at an aspect ratio of 10. The S7 series models had an aspect ratio equal to 6.67 and demonstrated no re-attachment length but the S5 and S2 series models with aspect ratios equal to 10 and 20 respectively did exhibit a re-attachment length. This was further evidence to support the theory that a re-attachment length is usually generated in slots with aspect ratios between 5 and 10 which can be inferred from the findings of Fujita et al [1991] and Manson [1994].

4.8.3 The influence of relative depth of flow

Relative flow depth was defined as the depth of the flood plain flow divided by the depth of the flood plain flow and the main channel. Figures 4.90 and 4.91 show the relationships between the adjustments coefficient and relative flow depth which were obtained for 75mm deep slots: S7G9S S7G6S S7G4S and S7G3S. They were each 500mm long with side slope angles equal to 90°, 60°, 45° and 30° respectively with all other parameters kept the same.

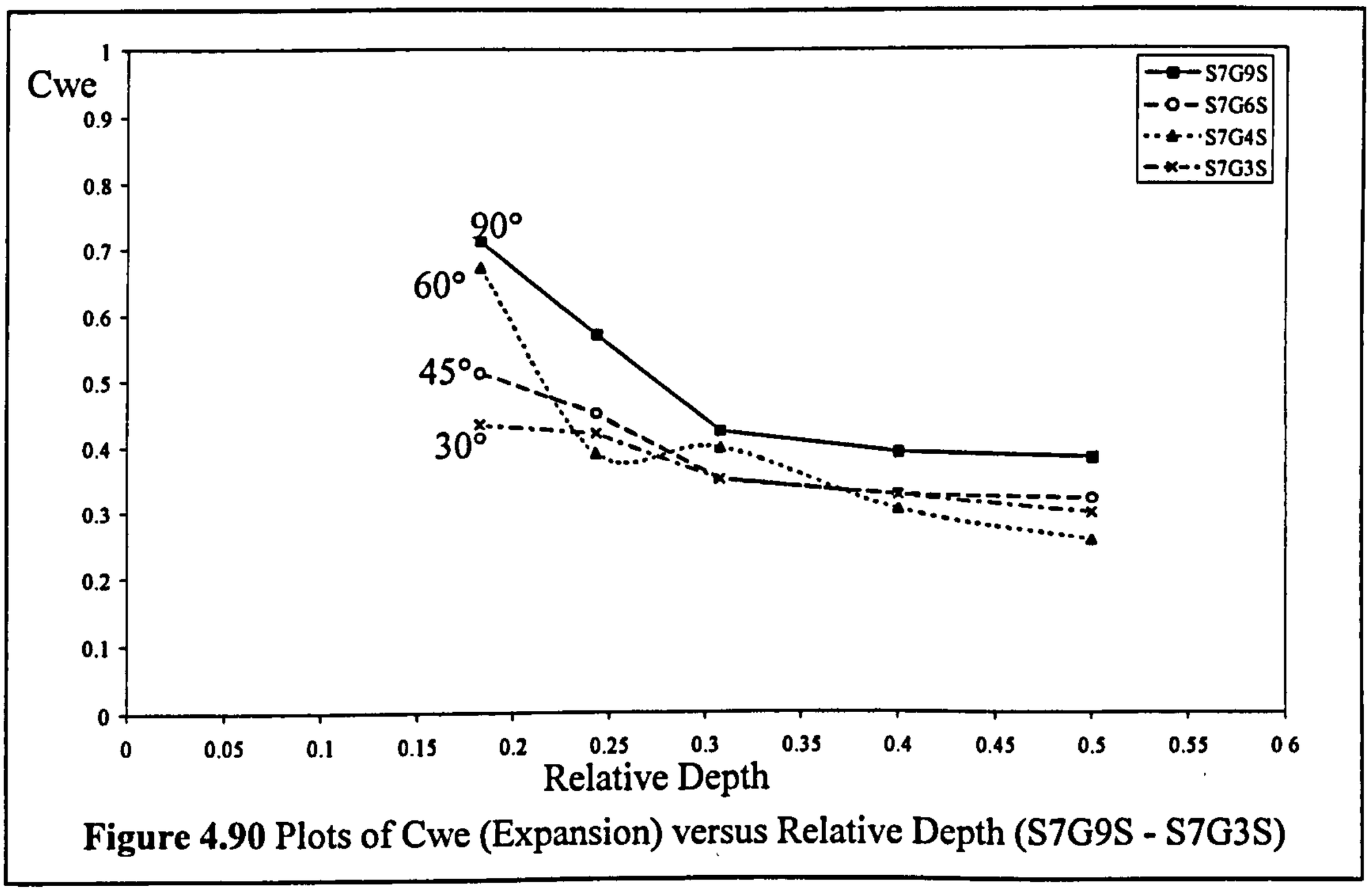

Figure 4.90 Plots of Cwe (Expansion) versus Relative Depth (S7G9S - S7G3S)

Figure 4.90 shows that the rate of decrease of the expansion loss coefficient, C_{we}, is initially large at low relative depths and becomes smaller with increasing relative depth. A similar relationship is exhibited by all the models whatever their side slope angle. Figure 4.91 shows that the rate of decrease of contraction loss coefficient, C_{wc}, is large over the full range of increasing relative depths. It is also clear that a similar relationship is exhibited by all the models whatever their side slope angle.

The decrease in the magnitude of C_{we} and C_{wc} with increasing relative depths was expected because the coefficients are inversely proportional to the square of upper channel (flood plain) velocity which increases with relative depth. The author suggests that the magnitude of C_{wc} decreases more rapidly than C_{we} because no re-attachment occurs in these channels as is demonstrated in Table 4.6. There is greater likelihood that a larger percentage of the flow will pass over the slot without being effected by contraction and so the magnitude of contraction head loss will therefore decrease. As the relative flow depth increases the average flood plain flow velocity will increase which will control the amount of flow separation and re-attachment length and hence the magnitude of expansion and contraction head losses that are generated.

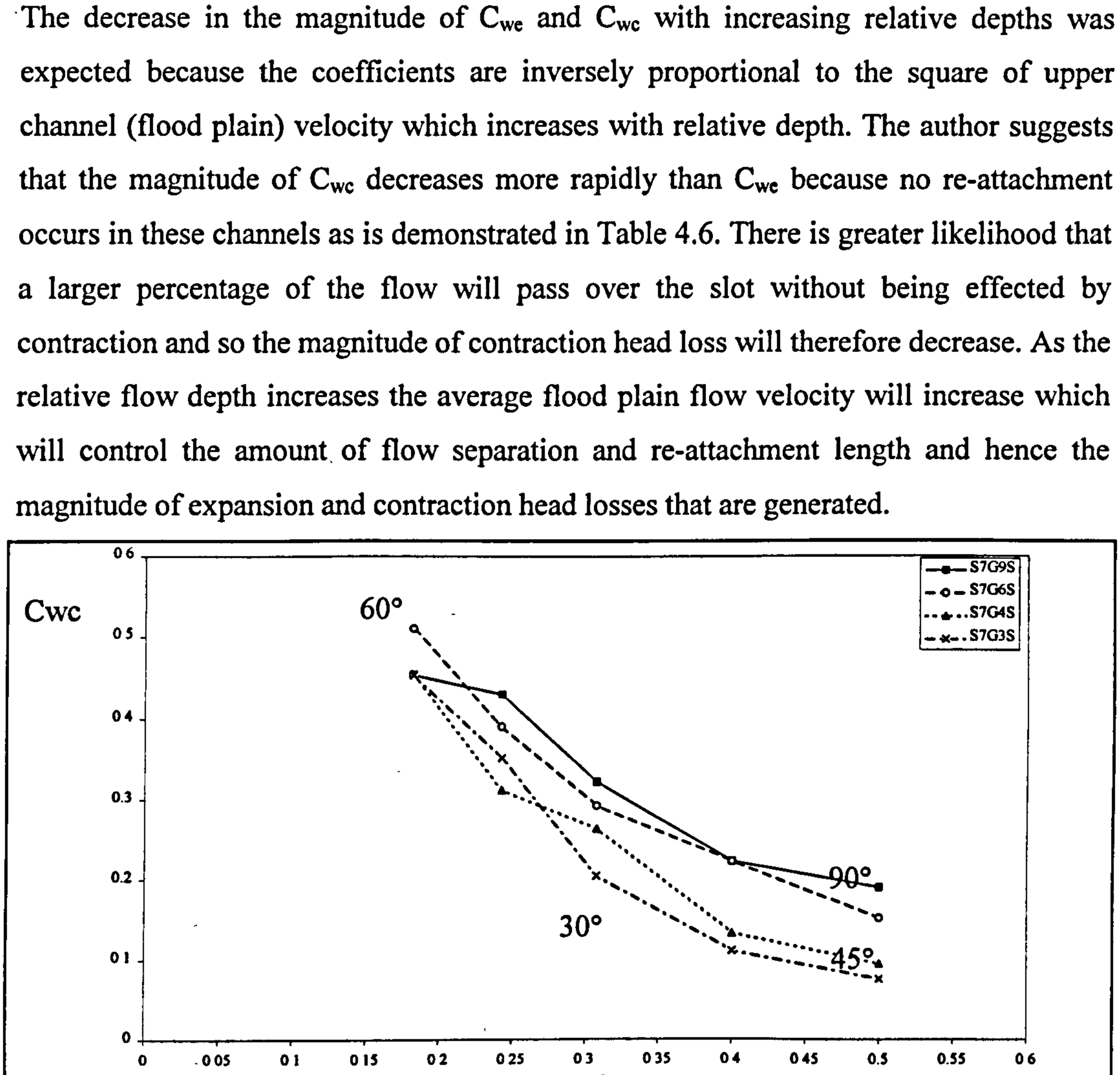

Figure 4.91 Plots of Cwc versus Relative Depth (S7G9S - S7G3S)

The combination of the increase in velocity squared values with the decrease in the magnitude of head loss causes the magnitude of C_{wc} to decrease rapidly. By contrast the expansion head loss is likely to increase steadily because the intensity of the cell driven

as a result of the flow separation will increase steadily with increasing flood plain velocity. Consequently the decrease in the rate of change of C_{we} with relative depth is observed.

Figures 4.92 and 4.93 show the relationship between the adjustments coefficients and relative flow depth which were obtained for 25mm deep slots; S2G9S, S2G6S, S2G4S and S2G3S. They were 500mm long with side slope angles equal to 90°, 60°, 45°, 30° respectively with the other parameters all kept the same.

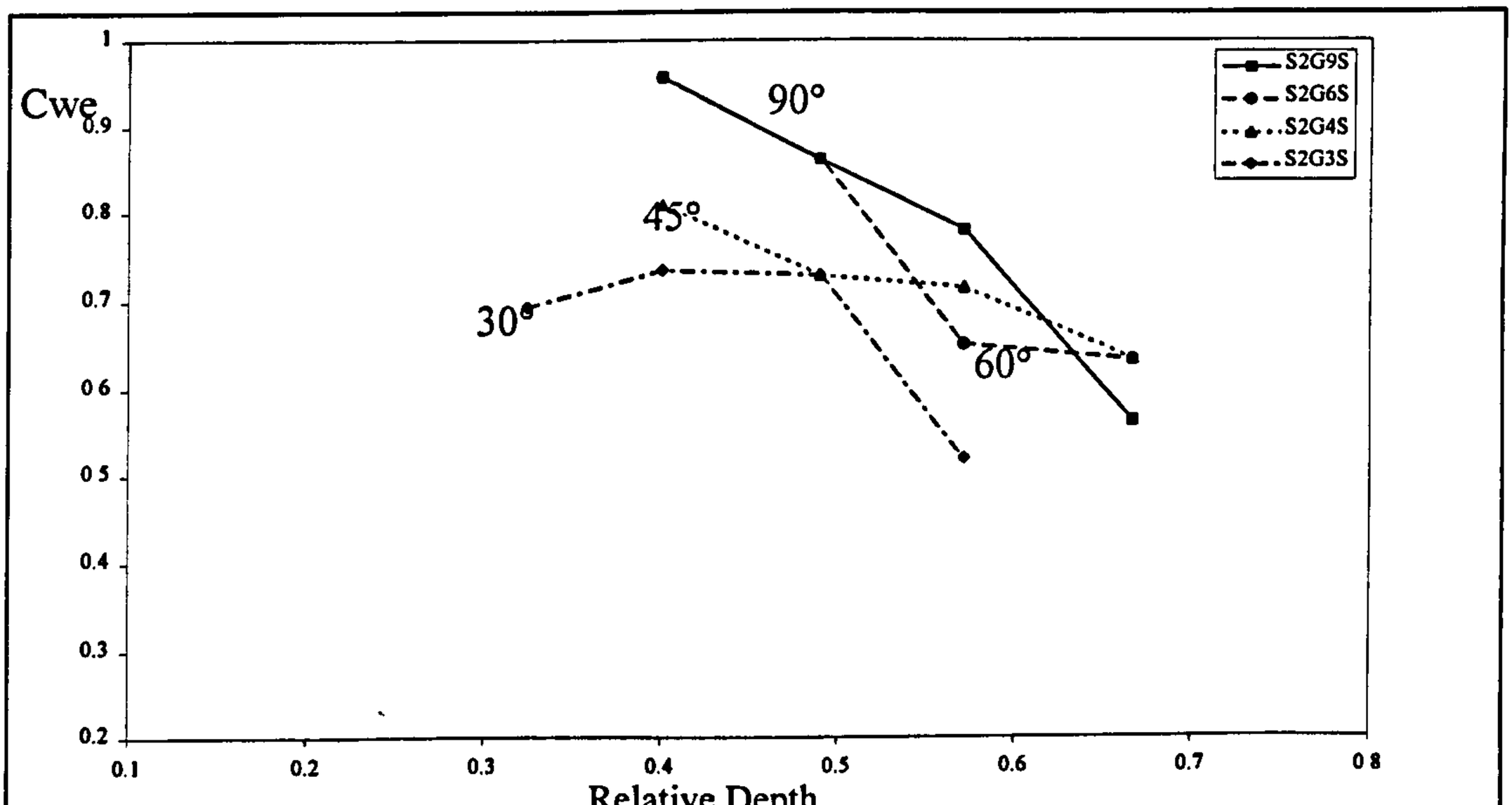

Figure 4.92 Plots of Cwe versus Relative Depth (S2G9S - S2G3S)

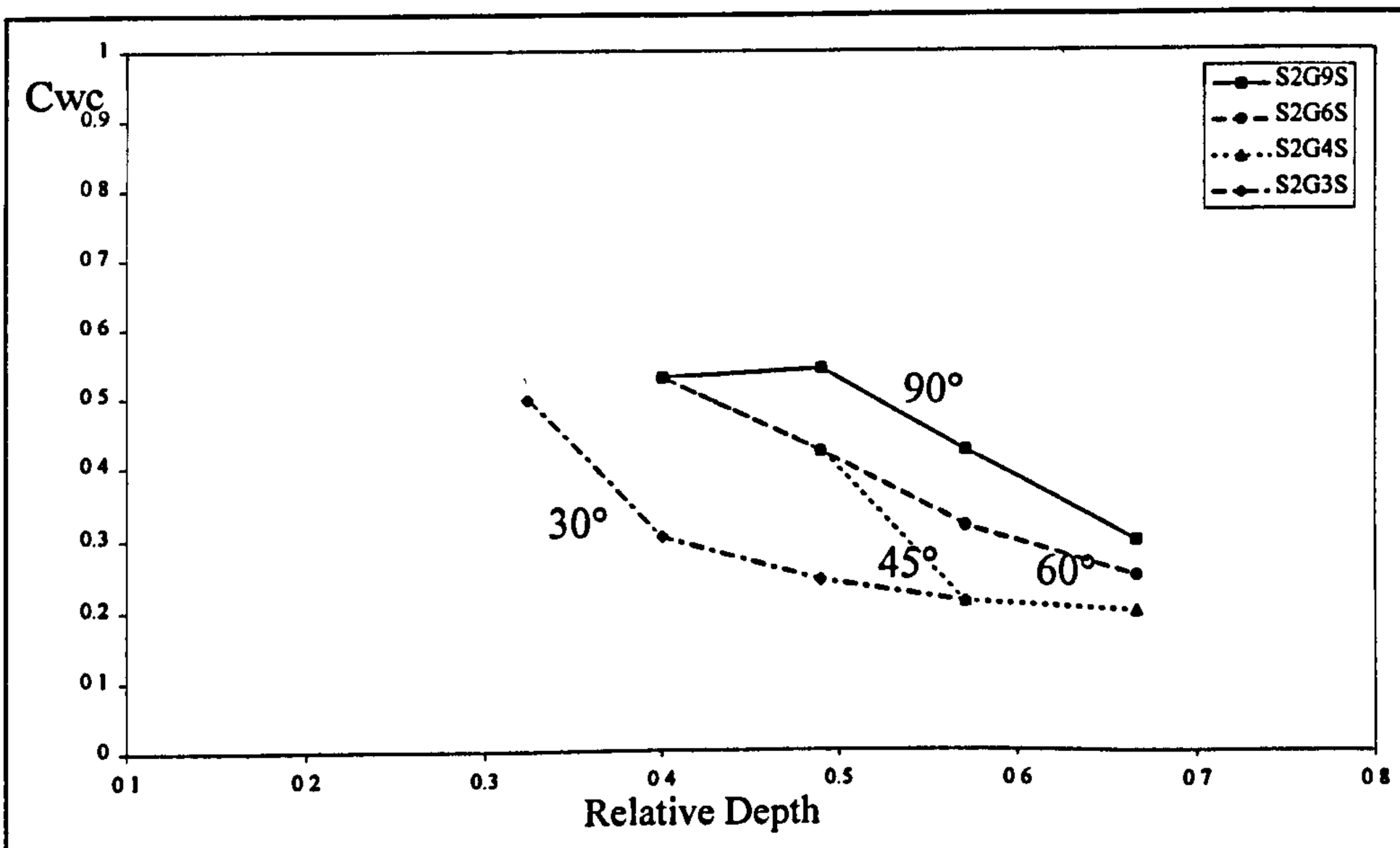

Figure 4.93 Plots of Cwc versus Relative Depth (S2G9S - S2G3S)

In these channels, like the 50mm deep channels, re-attachment does occur so although the velocity squared term increases, the magnitude of expansion and contraction losses does not rapidly decrease so the rates of change in C_{wc} and C_{we} respectively are more similar to each other than occurred in the 75mm deep slots. Both sets of model results for 25mm and 75mm deep slots demonstrated that relative depth a significant influence on the magnitude of the adjustment coefficients. The interrelationship between aspect ratio and relative depth was clearly demonstrated.

4.8.4 The influence of Side slope

Figures 4.94 and 4.95 show the relationship between the adjustments coefficients, C_{wc} and C_{we}, and the reciprocal of the tangent of the side slope angle for S2G9S S2G6S S2G4S and S2G3S where each slot is 500mm long with side slope angles equal to 90°, 60°, 45° and 30° respectively with all other parameters kept the same.

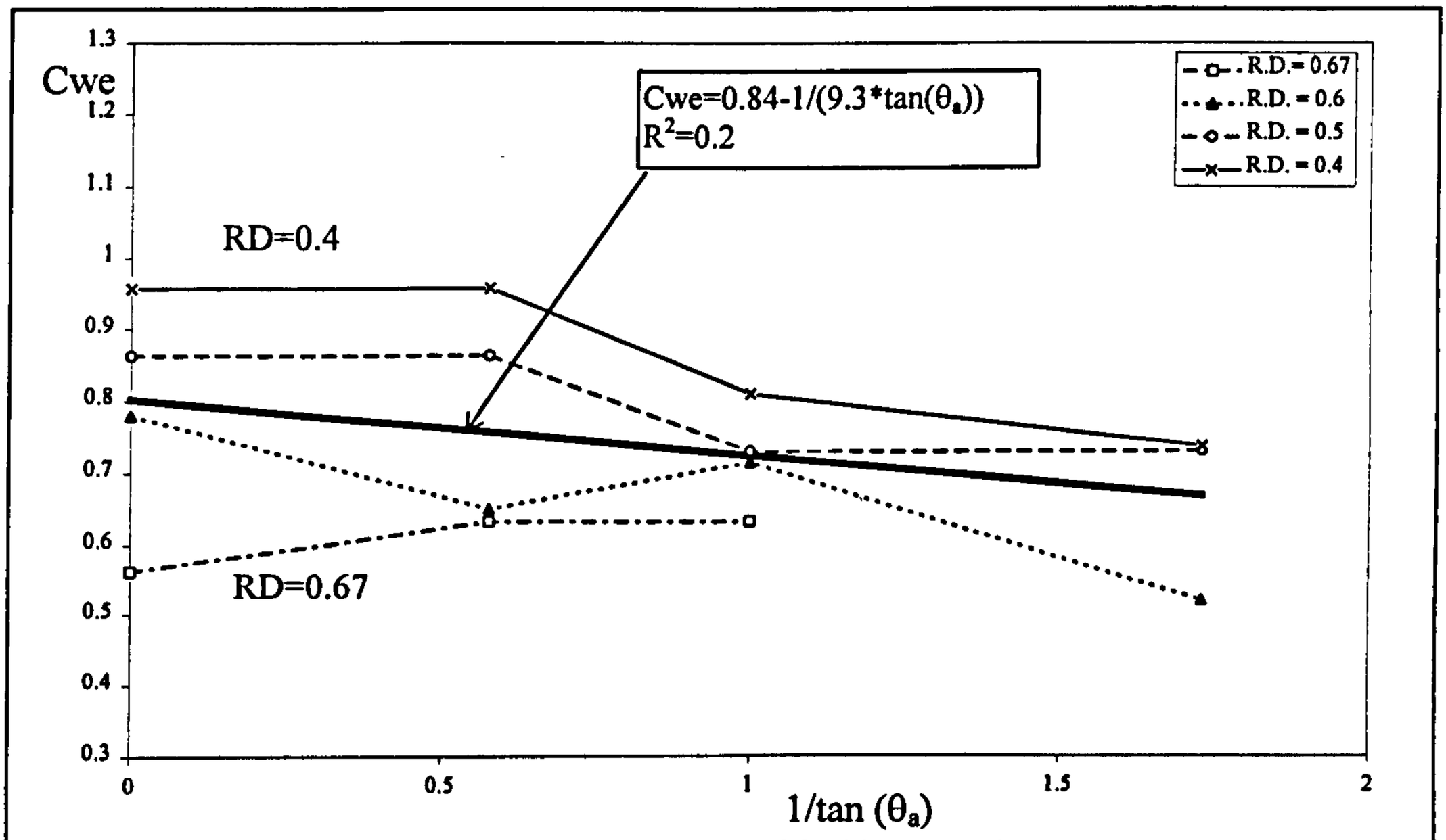

Figure 4.94 Plots of Cwe versus 1/tan(Side Slope angle) (S2G9S-S2S3S)

Figures 4.94 and 4.95 clearly show that the adjustment coefficients C_{we} and C_{wc} decrease for decreasing slot side slope angle. When the slot sides are vertical pronounced flow separation will take place as shown in Figure 4.88b. However when the side slopes have shallower angles as in Figure 4.96 then the flow lines are more likely to follow the profile of the slot and there will be less flow separation, smaller cells

will be generated and consequently there will be smaller expansion head losses generated. The effect of the decreasing expansion head loss is reflected by the magnitude of C_{we} decreasing with decreasing side slope angle.

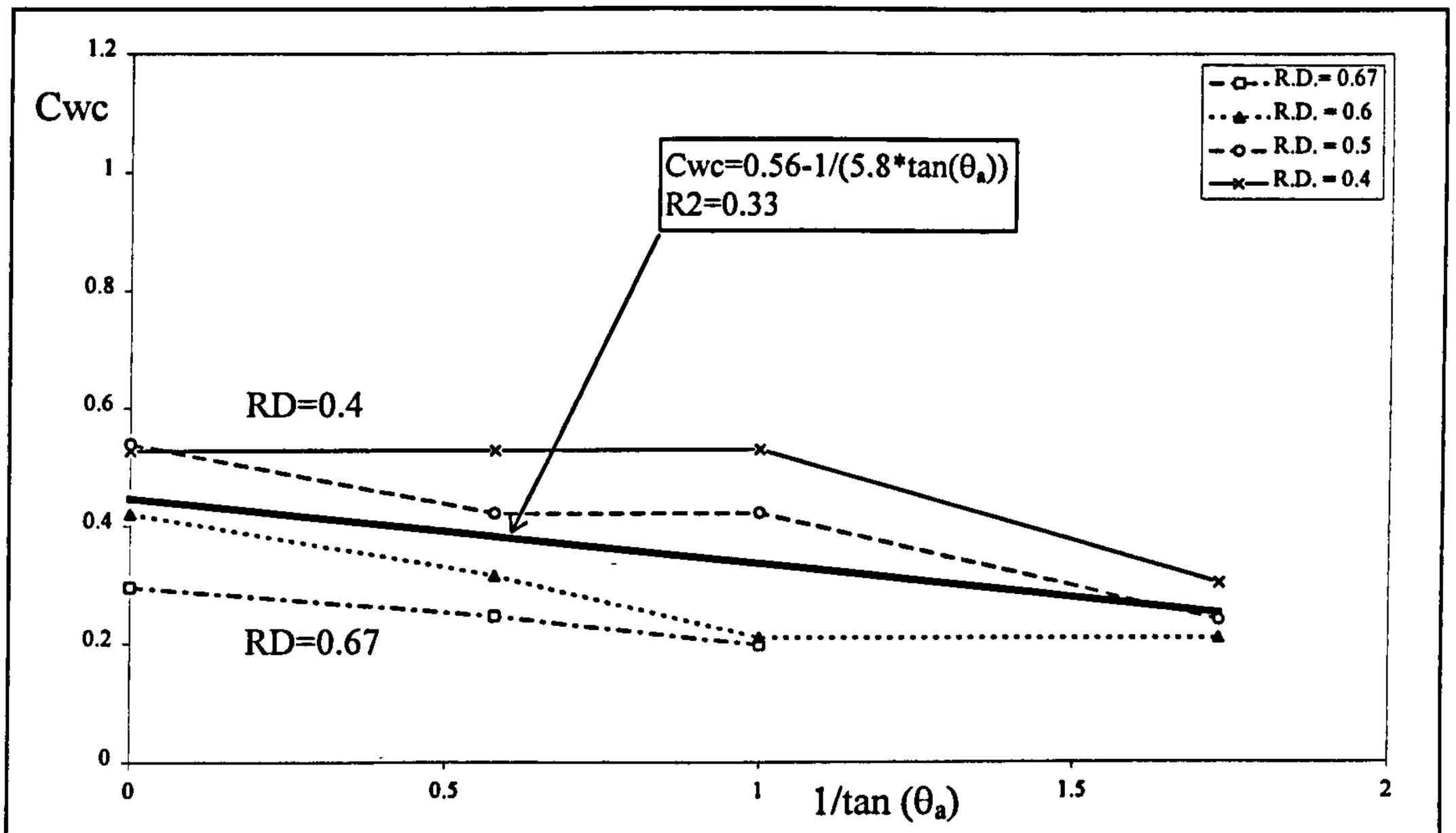

Figure 4.95 Plots of Cwe versus 1/tan(Side Slope angle) (S2G9S-S2S3S)

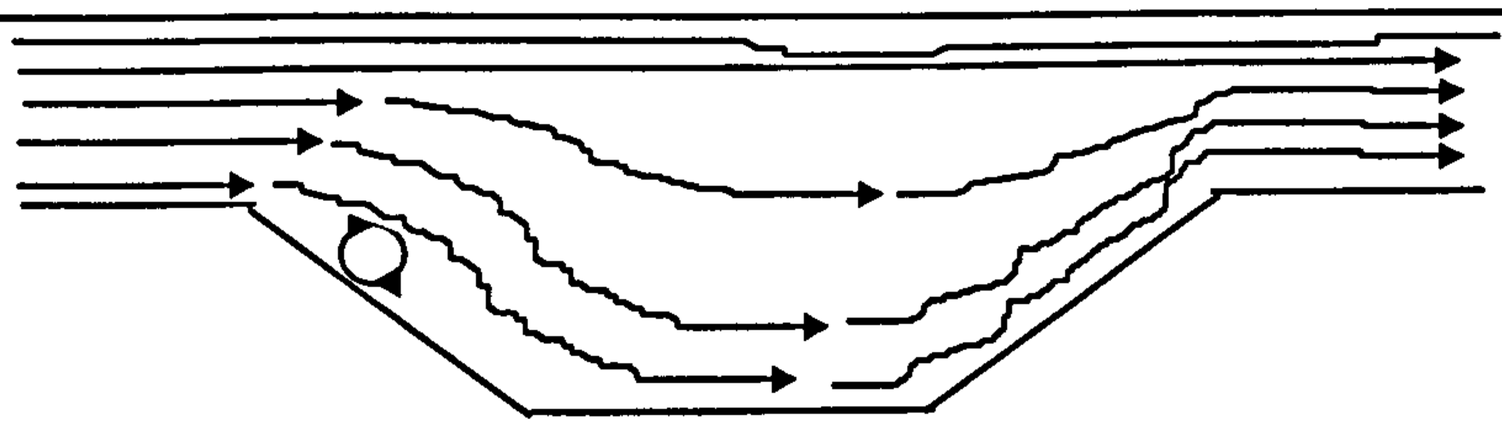

Figure 4.96 Flow vectors in slots with increasing aspect ratio

In addition because the backward facing slope is also sloping this will relieve the opposition to the slot flow passing back onto the flood plain and consequently the contraction losses will be less. The effect of the decreasing contraction head loss is reflected by the magnitude of C_{wc} decreasing with decreasing side slope angle.

4.8.5 The influence of relative roughness (flood plain /main channel)

Relative roughness, n' is defined as the minimum value for the flood plain using Manning's n (measured at high flow depths) divided by the minimum value for the Manning's n of the slot (measured slot bankfull depth). Figures 4.97 and 4.98 show the

relationship between the adjustments coefficients, C_{wc} and C_{we}, and relative roughness, n', for S7G9S, S7G9A and S7G9B which had flood plain roughness equal to smooth, Rough A and Rough B. The plots show that C_{we} decreases with increasing relative roughness for all relative depths. The author proposes that as a flood plain becomes progressively rougher the flow at the level where flow separation takes place (at the entry to the backward facing step) become more and more disrupted. Consequently the shear forces which drive the secondary cell in the knuckle of the bend becomes progressively smaller. As a result the magnitude of head loss generated reduces which is reflected by the decrease in the magnitude of C_{we} which is demonstrated in Figure 4.97.

By contrast C_{wc} increases with increasing relative roughness for all relative depths. The author proposes that as a flood plain becomes progressively rougher the flow over the slot where it forces its way back onto the flood plain (the backward facing step) is forced through a progressively smaller flow area because the roughening elements restrict flow in the area on the flood plain surface at the top of the backward facing step.

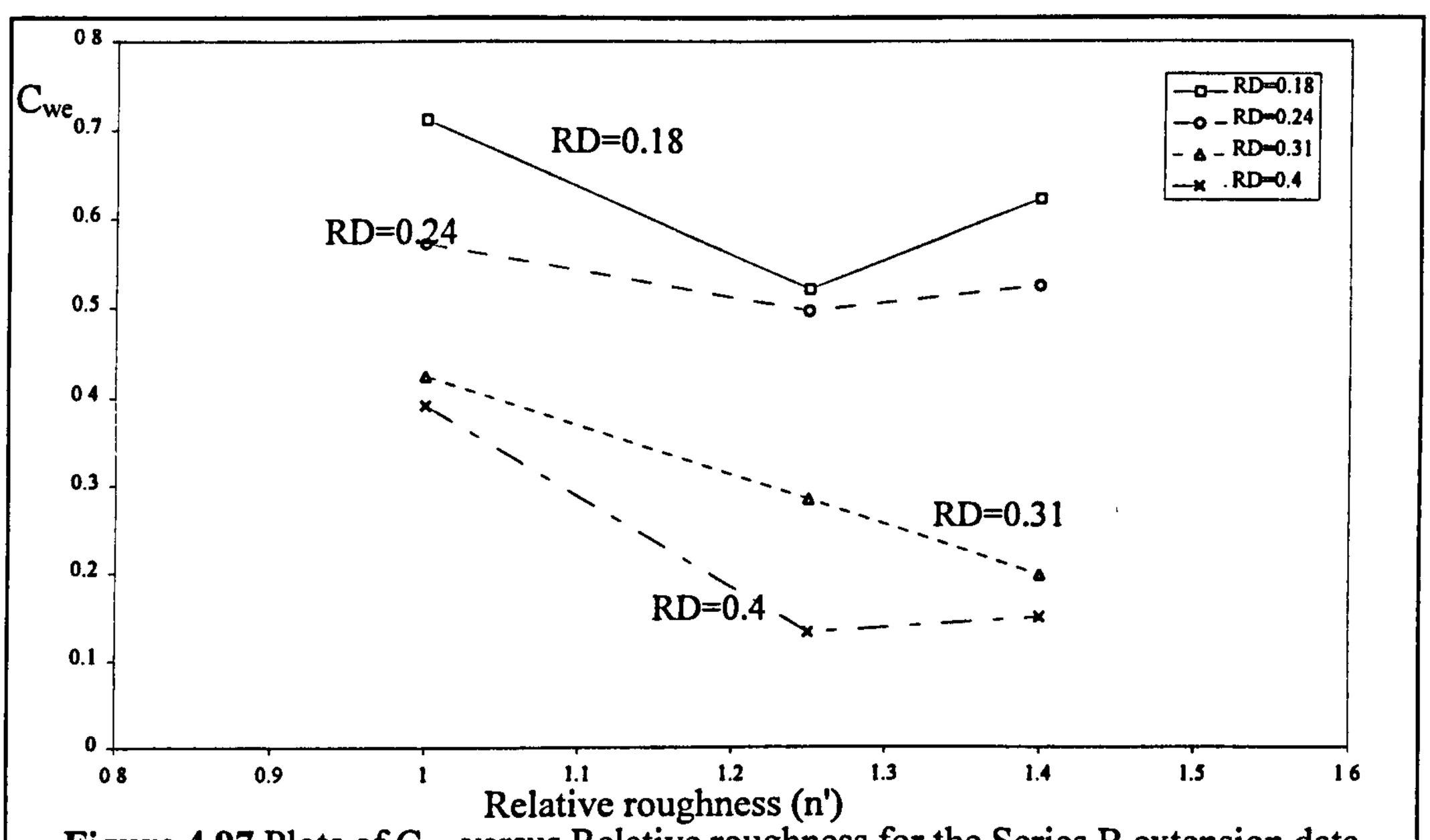

Figure 4.97 Plots of C_{we} versus Relative roughness for the Series B extension data

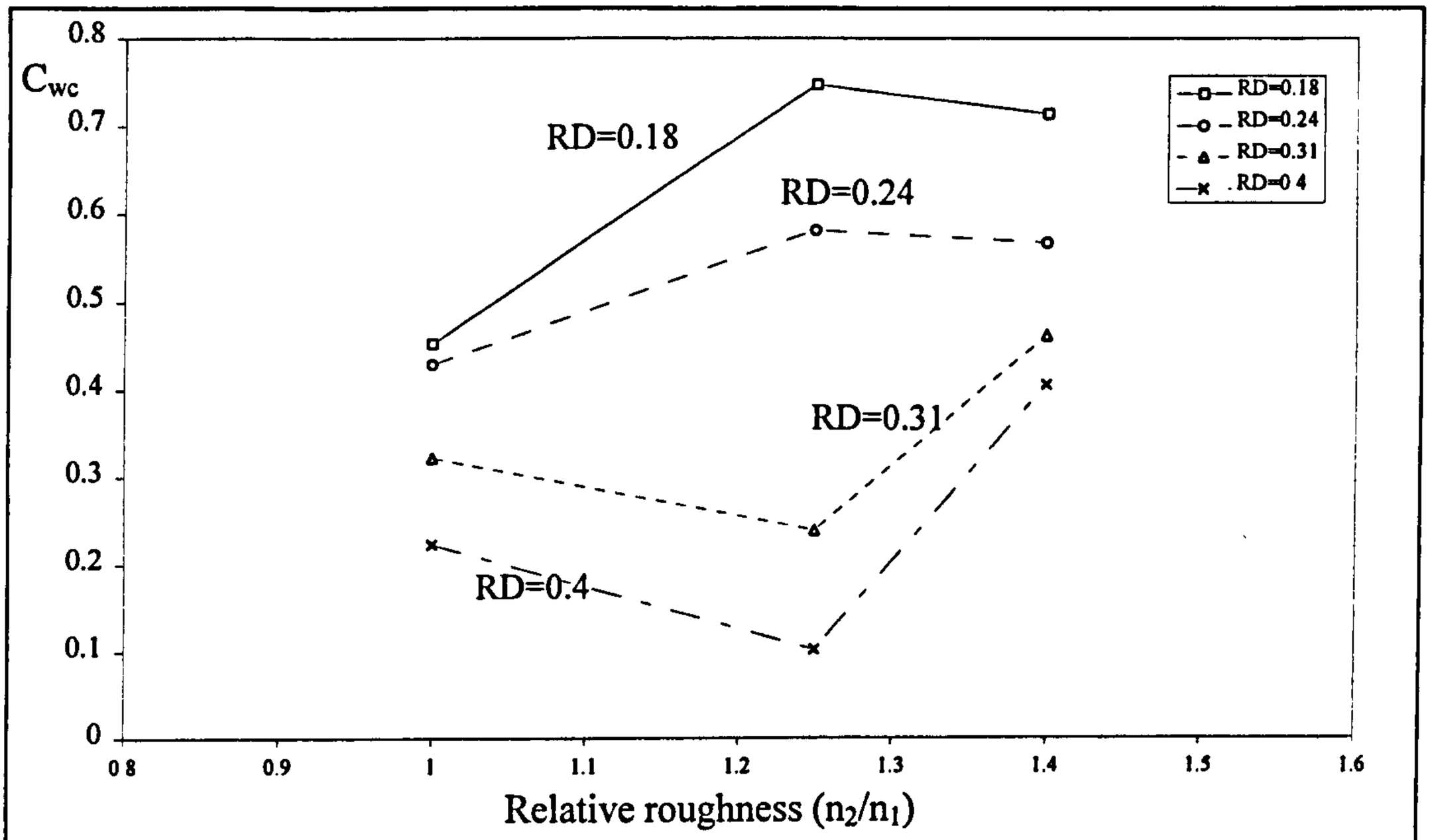

Figure 4.98 Plots of C_{wc} versus Relative roughness for the Series B extension data

4.8.6 The influence of main channel (slot) skew angle

Figures 4.100 and 4.101 show the relationship between the adjustments coefficients, C_{we} and C_{wc}, and the Skew angle, θ_s of the slot (expressed in terms of $1/\text{Tan}(\theta_s)$) for three, 50mm deep channels; S5G9S, S5G9S6 and S5G9S4 which were all 500mm long and with had skew angles equal to 90°, 60° and 45° respectively with all other parameters kept the same. Figure 4.99 shows a schematic representation of the slot skew angles.

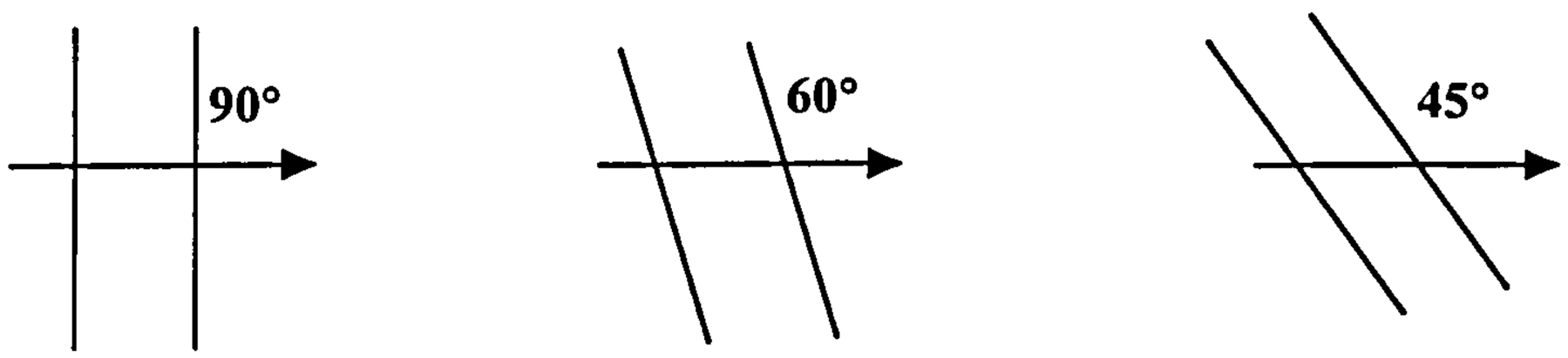

Figure 4.99 Angles of skew of the slot to the flood plain flow

The plots show that C_{we} is approximately constant with decreasing skew angle (increasing $1/\text{Tan}(\theta_s)$) for all relative depths. By contrast C_{wc} increases with decreasing skew angle (increasing $1/\text{Tan}(\theta_s)$) for all relative depths.

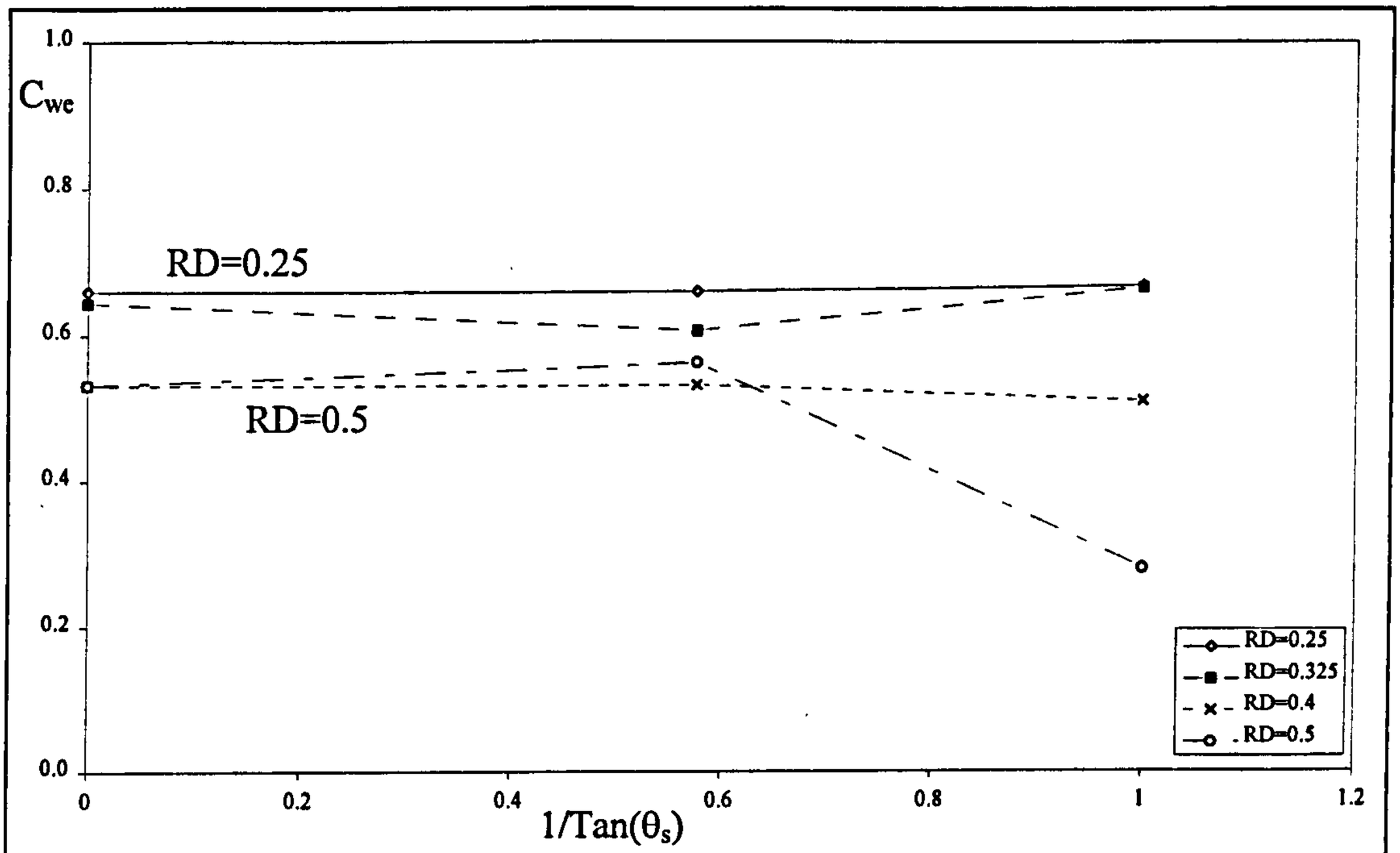

Figure 4.100 Plots of C_{we} versus COS.(skew angle, θ_{sk}) for the Series B extension data

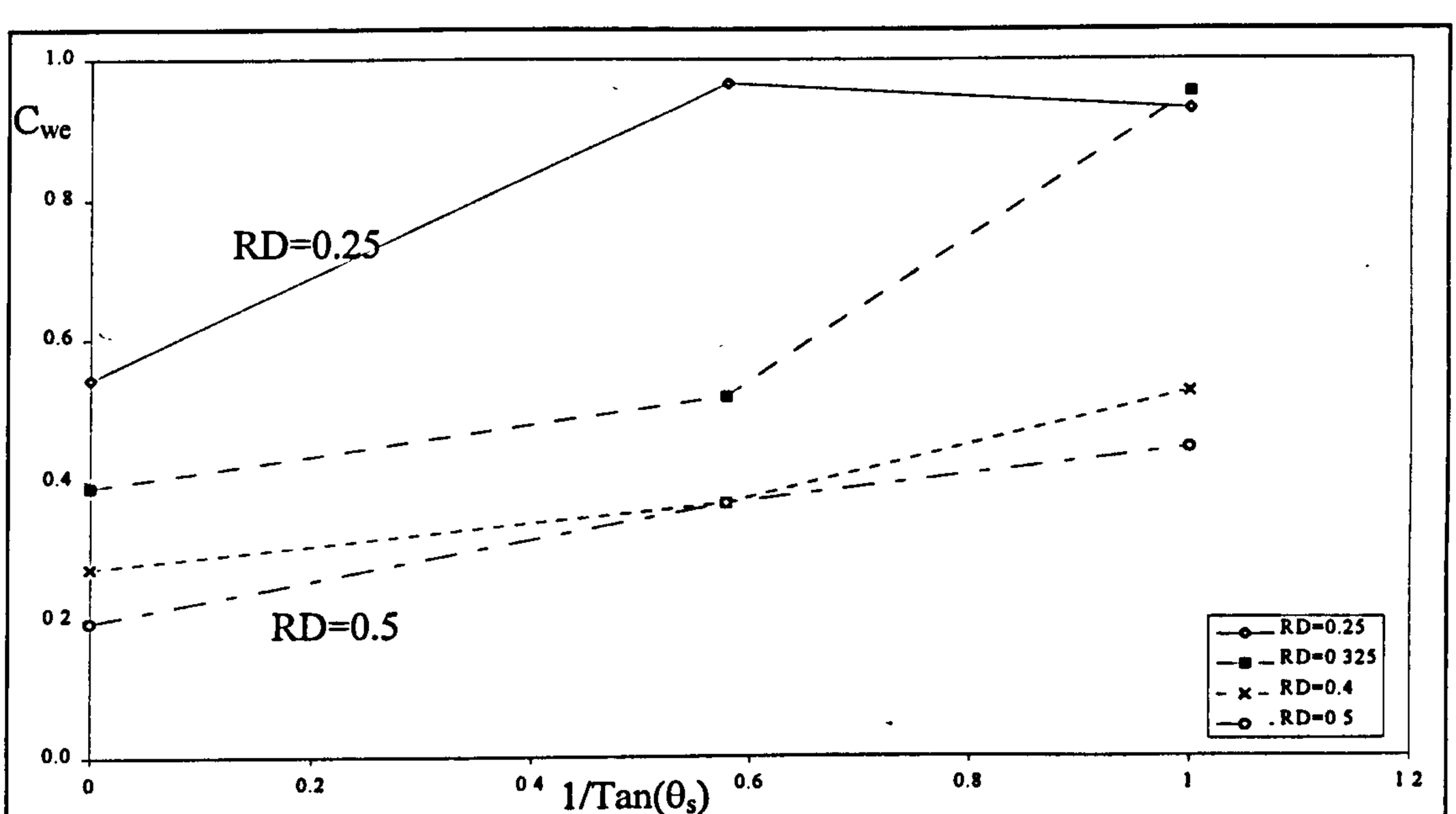

Figure 4.101 Plots of C_{we} versus COS.(skew angle, θ_{sk}) for the Series B extension data

The author proposes that as the slot angle changes the structure of the secondary cell will alter. The secondary cell is generated in the knuckle of the bend as the flood plain flow expands over the slot. The sub-cells (with off-set centre lines as shown in Figure 4.102b) will be generated across the width of the slot. By contrast in the 90° skew slot, which is perpendicular to the main component of flood plain (maximum skew angle),

one large coherent cell was created, as shown in Figure 4.102a. Each adjacent sub-cell was positioned on the same centre line across the width of the slot. However because the results show that C_{we} does not alter with changing skew angle these differences in secondary cell structure clearly do not significantly affect the magnitude of head losses generated in expanding flow over a slot.

In addition the author suggests that when the slot becomes less skew (increasing values for $1/\text{Tan}(\theta_s)$) and the flow in the slot forces its way back onto the flood plain (contracts), the additional lateral interference between the parallel stream lines in the contracting flow will generate increased head loss which is reflected in the increasing magnitude of C_{wc}.

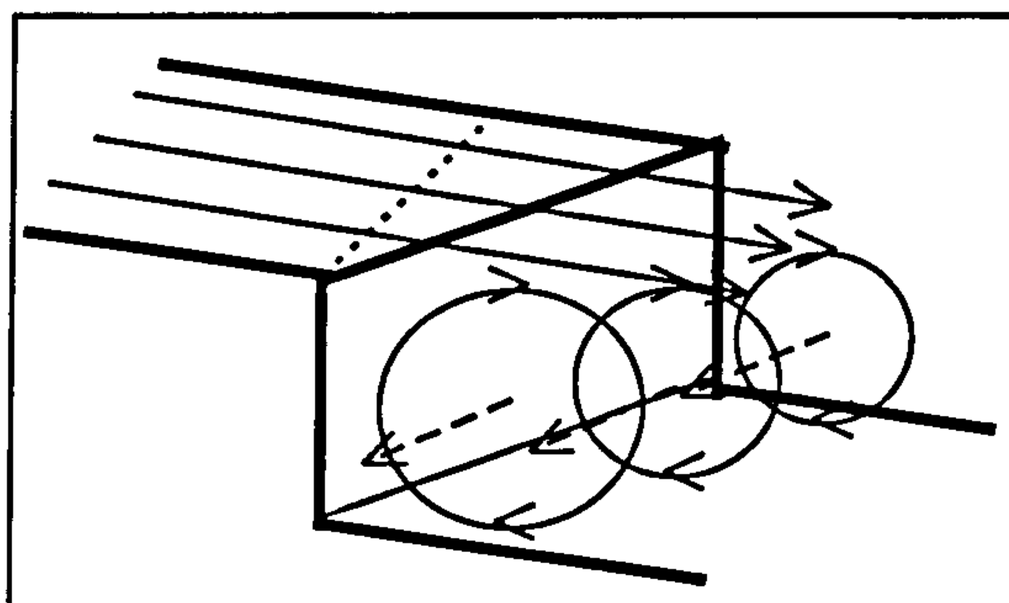

Figure 4.102a 45° skew

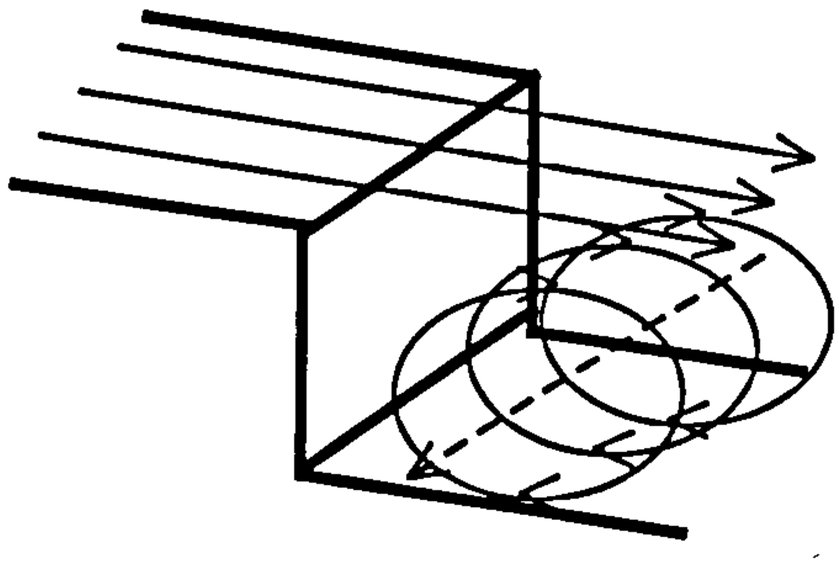

Figure 4.102b 90° skew

Further experiments are required to confirm the precise reasons for the observed relationship between the expansion and contraction adjustment factors and slot skew angle. These additional experiments are also required to check the repeatability of the results and to provide a larger enough data set so that the parameter of the slot skew angle, θ_{SK} can be included in any future formulation of a predictive model for the head loss generated in flow over a slot.

4.8.7 Limitations of the James and Wark [1] [1992] and Jasem [1990] approaches

4.8.7.1 Aspect ratio and relative depth

The original James and Wark [1] [1992] formulations were tested against the experimental results from the Series B experiments. Figures 4.103 and 4.104 show plots

of aspect ratio versus the adjustment coefficients, C_{we} and C_{wc}, for S7G9S, S5G9S, and S2G9S.

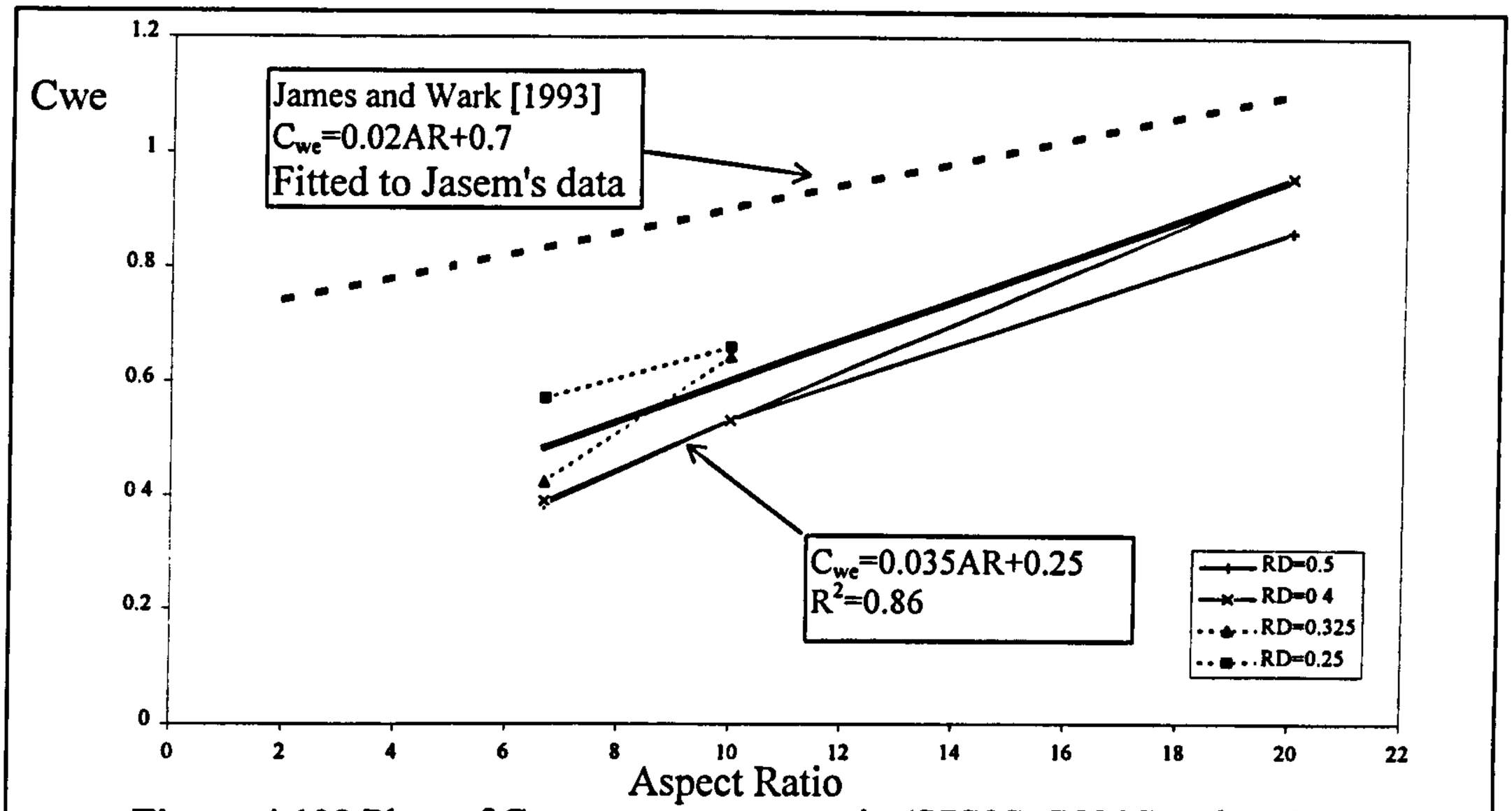

Figure 4.103 Plots of Cwe versus aspect ratio (S7S9S, S5S9S and S2D9S)

The slots in these models were vertical so according to the James and Wark [1] [1992] formulation predicting the influence of side slope angle C_{sse} and C_{ssc} will equal 1. Consequently if the James and Wark [1] [1992] formulations which define: C_{we} and C_{wc}, in terms of aspect ratio were correct, they would be expected to reliably predict the values measured in the models. Figures 4.103 and 4.104 clearly show that the James and Wark [1] [1992] formulation generally over-predicts the magnitude of C_{we} and C_{wc} and takes no account of the influence of relative depth which can be seen to be influential.

Interestingly comparison between the linear best fit equations derived using regression analysis on the results from S7S9S, S5S9S and S2S9S and the James and Wark [1] [1992] formulation (assuming that relative depth does not influence the adjustment factors (the James and Wark [1] [1992] assumption)) demonstrates that similar rates of change in the magnitude of C_{we} and C_{wc} are obtained. This indicates that the experiments performed by Jasem [1990] which were used to develop the James and Wark [1] [1992] formulation did illustrate the general influence of aspect ratio but gave possibly erroneous results for the absolute magnitude of the expansion and contraction losses.

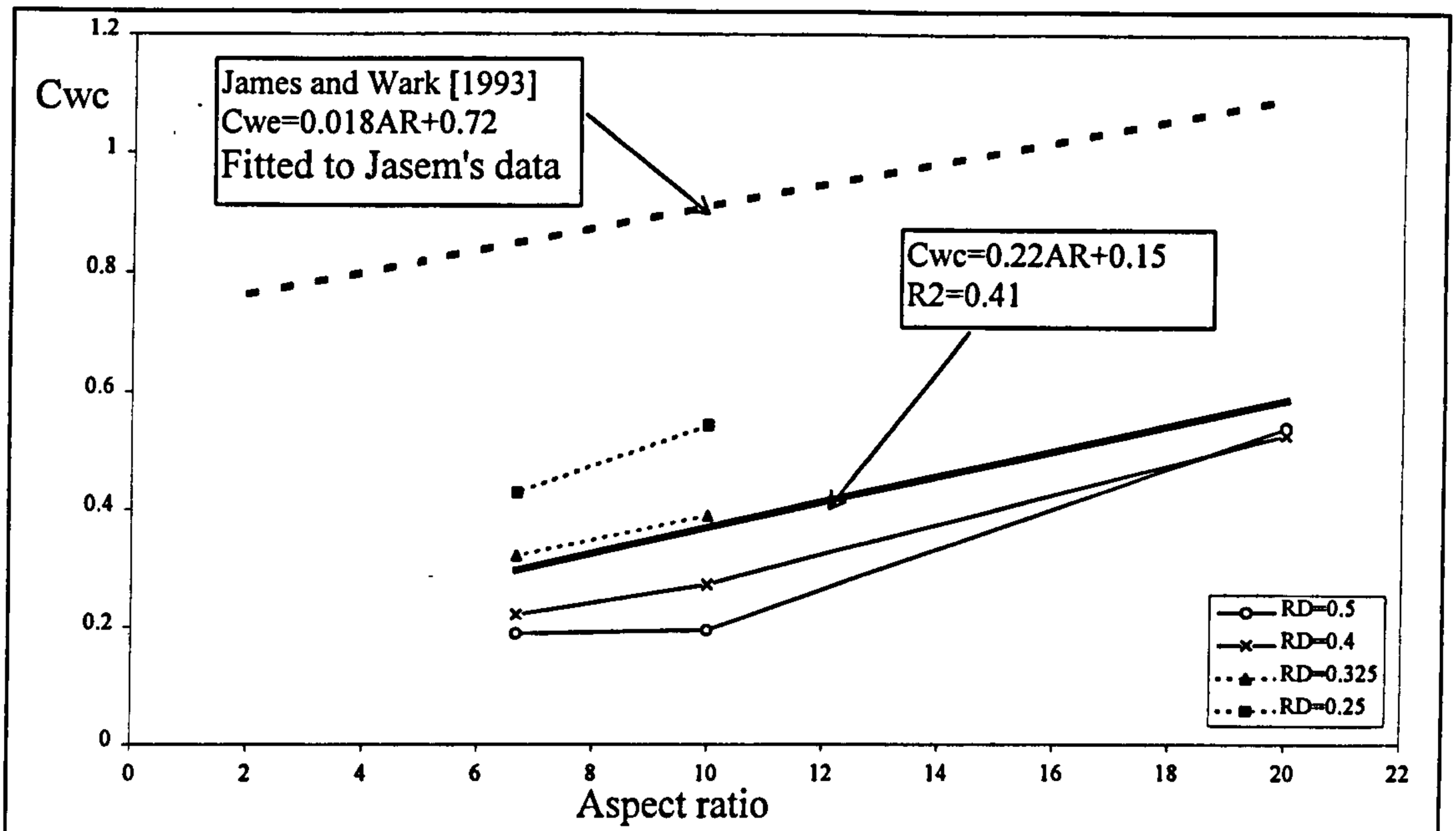

Figure 4.104 Plots of Cwc versus aspect ratio (S7S9S, S5S9S and S2D9S)

The author attributes the difference in the magnitude of head loss to the difference in flume width and flood plain roughness between the two experimental programmes. Tests S7G9S, S5G9S, and S2G9S each had rectangular slots, with 90 degree skew angle, variable relative flow depths, a relative roughness of 1 and a flume width equal to 300mm. Jasem's models had rectangular slots, with 90 degree skew angle, variable relative flow depth, a relative roughness of 1.4 and a flume width equal to only 80mm. The side wall effects in the narrow flume used by Jasem [1990] could have potentially interfered with the contraction and expansion mechanisms in the flow over the slot causing increased local turbulence and associated head loss. Further experiments would be required to elucidate the precise influence of the side wall effects. The author decided that the results from the wider, Series B extension tests were more likely to simulate the expansion and contraction mechanisms found in flow in natural channels where the side wall effect would be negligible therefore reinforcing their reliability.

The relative roughness values were greater in the Jasem [1990] models than in the Series B extension models. The results obtained during the Series B extension (1993-1996) experiments demonstrated that the magnitude of relative roughness does effect the magnitude of the head losses in flow over slots. This might explain the differences

in the magnitude of C_{we} and C_{wc} in the models tested by Jasem [1990] and during Series B extension (1993-1996) programme.

4.8.7.2 Side slope angle

James and Wark [1] [1992] used a formulation proposed by Formica [1955] to relate additional adjustment coefficients, C_{sse} and C_{ssc} to the influence of side slope angle, θ_a, which is defined in Equation 2.10. The expressions were derived using flow data which was obtained from flume tests on open channels with contraction and expansion areas created by using sloping side walls, as shown in Figure 4.105a.

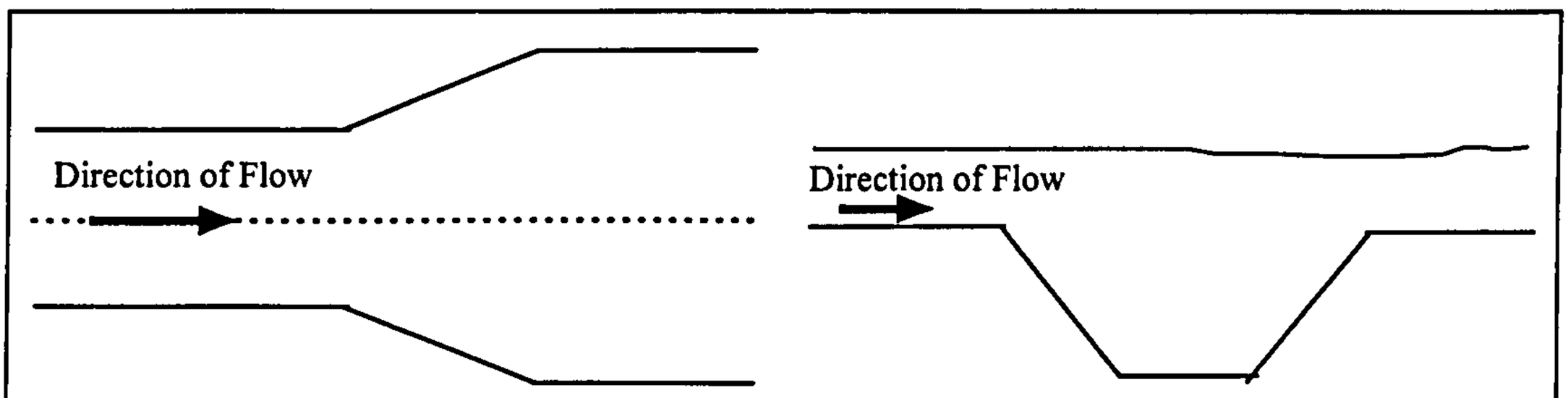

Figure 4.105a Formica (Plan) **Figure 4.105b** Series B extension (Elevation)

During the Series B extension programme the slot side slopes (as shown in Figure 4.105b) were varied. Figures 4.106 and 4.107 show the relationship between the adjustment coefficients, C_{wc} and C_{we} and the reciprocal of the tangent of the side slope angle for S2G9S, S2G6S, S2G4S and S2G3S. All the other parameters were kept constant. Also included is a comparison between the linear regression fit to this Series B extension data and James and Wark's [1] [1992] formulation of C_{ssc} and C_{sse} using Formica's [1955] formulation. The figures show that the intercept value when $1/\tan(\theta_a)$ is equal to zero is smaller for the Series B extension results than for the Formica [1955] expression. This was expected because the Formica [1955] expression did not account for the influence of the other parameters which influence the flow data obtained during the Series B extension tests. Ideally the influence of slot side slope should have been tested using isolated steps but these tests were not included in the experimental programme. The author alternatively used the results from the 25mm deep slot tests in an attempt to determine the influence of side slope angle.

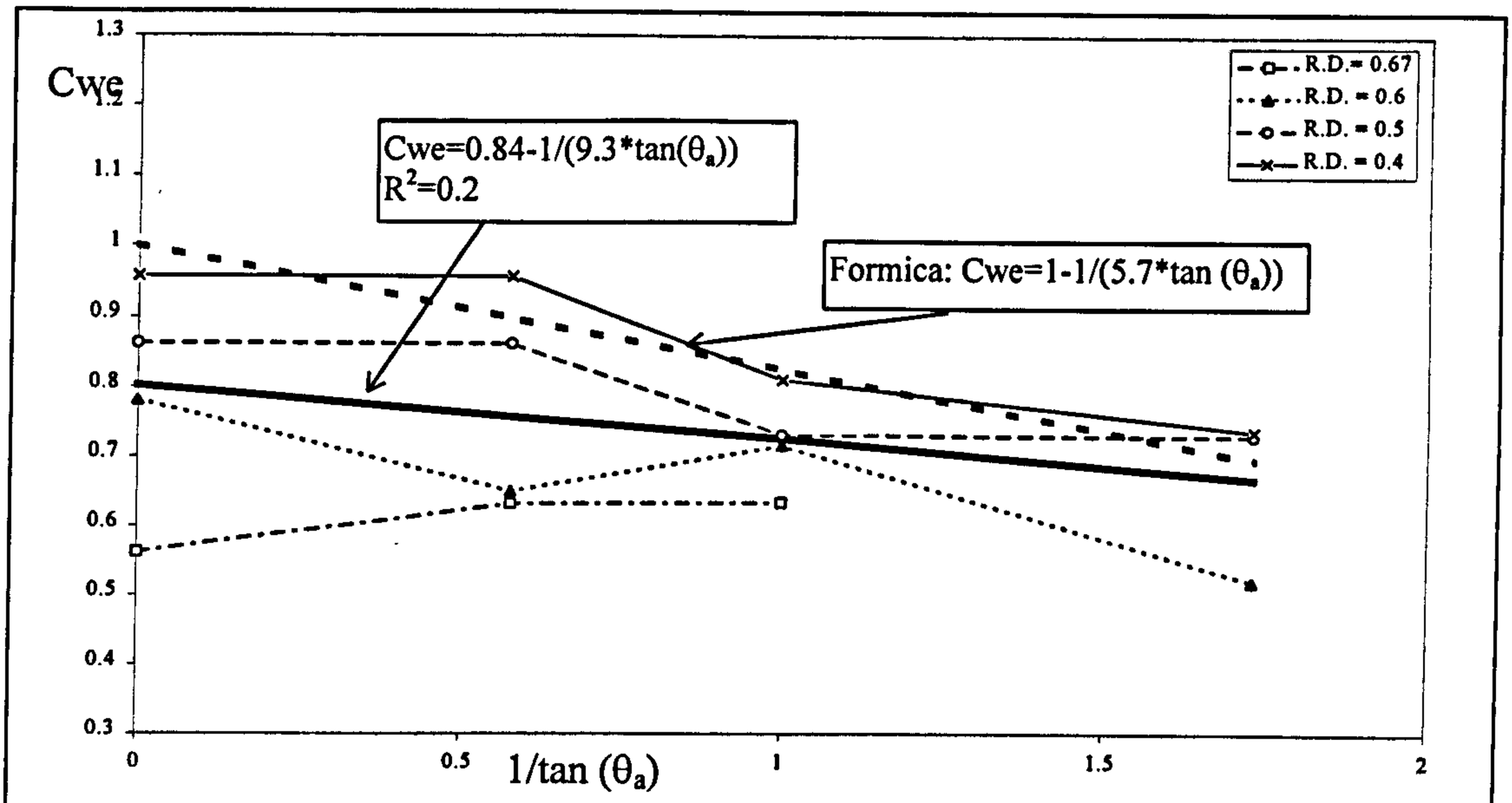

Figure 4.106 Plots of Cwe versus 1/tan(θ_a) (S2G9S S2G6S S2G4S and S2G3S)

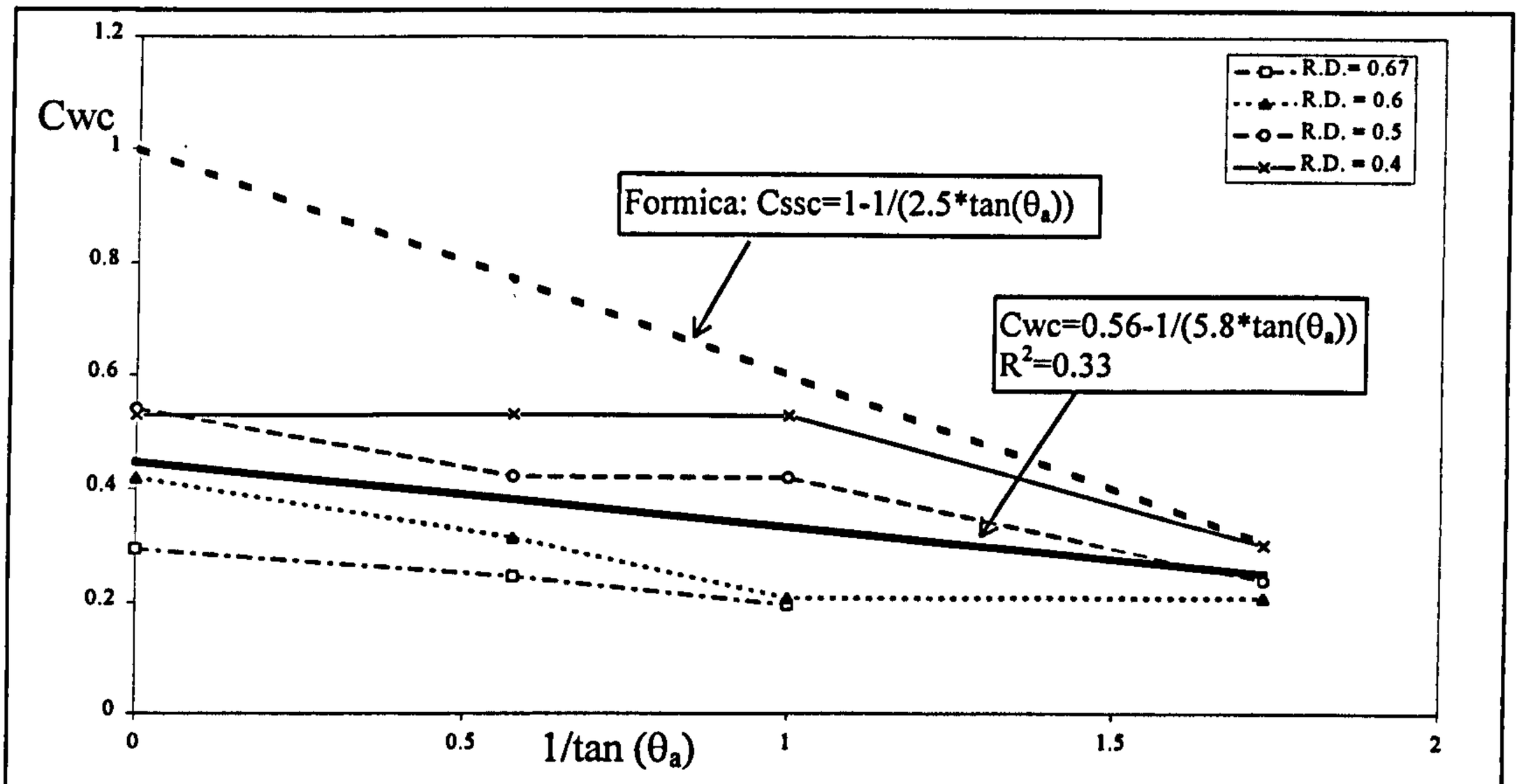

Figure 4.107 Plots of Cwc versus 1/tan(θ_a) (S2G9S S2G6S S2G4S and S2G3S)

Equivalent results from the model with deeper channel depths which were tested were inconclusive with regard to the influence of side slope because other parameters dominate the flow interactions. James and Wark [1] [1992] accounted for aspect ratio by also applying the multiplicative factor C_{wd}.

Figures 4.106 and 4.107 demonstrate that there is a distinct difference in the rates of change of the adjustment coefficients with the reciprocal of the tangent of side slope

angle between those given by Formica [1955] and the best fit line through the Series B extension data. The rate of change is almost twice as great in the Formica [1955] expression compared with that obtained from the Series B extension experiments. The author expected that the Formica [1955] expression would over-estimate by 2 times the rate of change because the channels used to develop Formica's expression effectively incorporates 2 sloping sides in the test channels which consequently were likely to generate twice the head losses associated with expansion and contraction in a slot.

4.8.8 Proposed empirical methods for predicting head losses in flow over a slot

The author has developed two new expressions which relate the expansion and contraction adjustment factors for slots to 5 non-dimensional parameters and were derived using regression analysis. The Series B extension data was used but it was not combined with the Jasem [1990] data which was deemed to incorporate to many side wall effects. The author intended that the inclusion of the 5 influential parameters obtained from slot experiments would produce more reliable results than were produced using the James and Wark [1] [1992] method. The five parameters which were included are: relative depth, RD, aspect ratio, AR, relative roughness, n', channel side slope angle, ϕ_{SS}, and slot skew angle, θ_{SK}. Figure 4.90 and 4.91 illustrated that the adjustment coefficients decrease exponentially with increasing relative depth so the variable RD was incorporated using an exponential function. The author postulated that the relationship would take the form of a basic geometric progression as defined in Equations 4.12 and 4.13.

$$C_{we} = a1 * e^{(-a2*RD)} * AR^{a3} * \left(1/\tan\phi_{SS}\right)^{a4} * n'^{a5} * \left(1/\tan\theta_{sk}\right)^{a6} \quad [4.12]$$

$$C_{we} = b1 * e^{(-b2*RD)} * AR^{b3} * \left(1/\tan\phi_{SS}\right)^{b4} * n'^{b5} * \left(1/\tan\theta_{sk}\right)^{b6} \quad [4.13]$$

where a1,a2, a3, a4, a5, a6, b1, b2, b3, b4, b5 and b6 are constants.

The parameters: relative roughness and channel skew angle were removed after a preliminary regression analysis of the relationships defined in Equations 4.12 and 4.13 demonstrated that the magnitude of StdErr and CV% (as well as the RMS percentage error between the output of the regression equations and the training data) was in fact smaller when they were removed. The author suggests that additional experiments should be performed in order to provide more data which can elaborate the influence of

relative roughness and channel skew angle on the magnitude of C_{we}. and C_{wc} and facilitate its inclusion in the regression analysis.

Tables 4.7 and 4.8 list the statistical values which were obtained by regression fitting the rationalised relationships defining C_{we}. and C_{wc} (which only included aspect ratio, side slope and relative depth) to the flow data obtained from the Series B extension slot tests.

Parameter	Value	StdErr	CV(%)	Dependencies
a1	1.81E-01	1.67E-02	9.24E+00	0.971
a2	1.27E+00	1.59E-01	1.25E+01	0.949
a3	3.36E-01	6.37E-02	1.89E+01	0.513
a4	7.19E-01	4.36E-02	6.07E+00	0.981

Table 4.7 Statistical values for the regression fit on C_{we}.

Parameter	Value	StdErr	CV(%)	Dependencies
b1	2.40E-01	2.61E-02	1.09E+01	0.967
b2	3.41E+00	2.27E-01	6.66E+00	0.949
b3	4.97E-01	8.11E-02	1.63E+01	0.486
b4	7.56E-01	5.76E-02	7.62E+00	0.981

Table 4.8 Statistical values for the regression fit on C_{wc}.

The final formulations which were obtained are detailed in Equations 4.14 and 4.15 where C_{WE} is the formulation for the actual coefficient of expansion and C_{WC} is the formulation for the actual coefficient of contraction.

$$C_{WE} = 0.206e^{(-1.31*RD)}(1/\tan\phi_{SS})^{0.369} AR^{0.693} \quad [4.14]$$

$$C_{WC} = 0.189e^{(-3.68*RD)}(1/\tan\phi_{SS})^{0.455} AR^{0.926} \quad [4.15]$$

Tables 4.7 and 4.8 demonstrate that there are no strong parameter dependencies which show that the formulation is not over-parameterised. The parameter values, standard deviations and CV% values are smaller than for any other parameter combinations that were tested by the author. Figures 4.108 and 4.109 show the measured values for C_{we} and C_{wc} against the values predicted by Equations 4.14 and 4.15 for the slot tests performed in Glasgow during the Series B extension programme which did not vary relative roughness and channel skew angle.

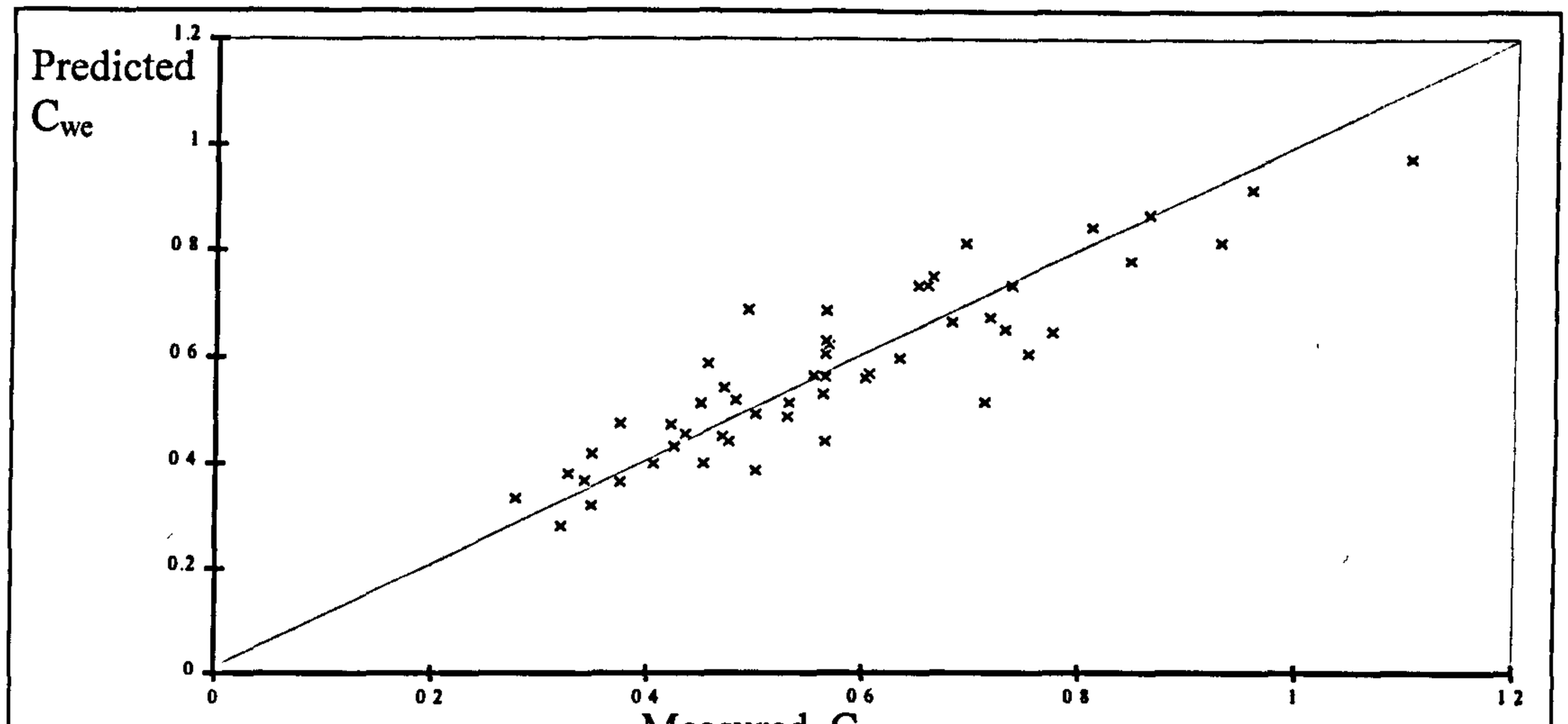

Figure 4.108 Predicted versus measured expansion adjustment coefficient C_{we}

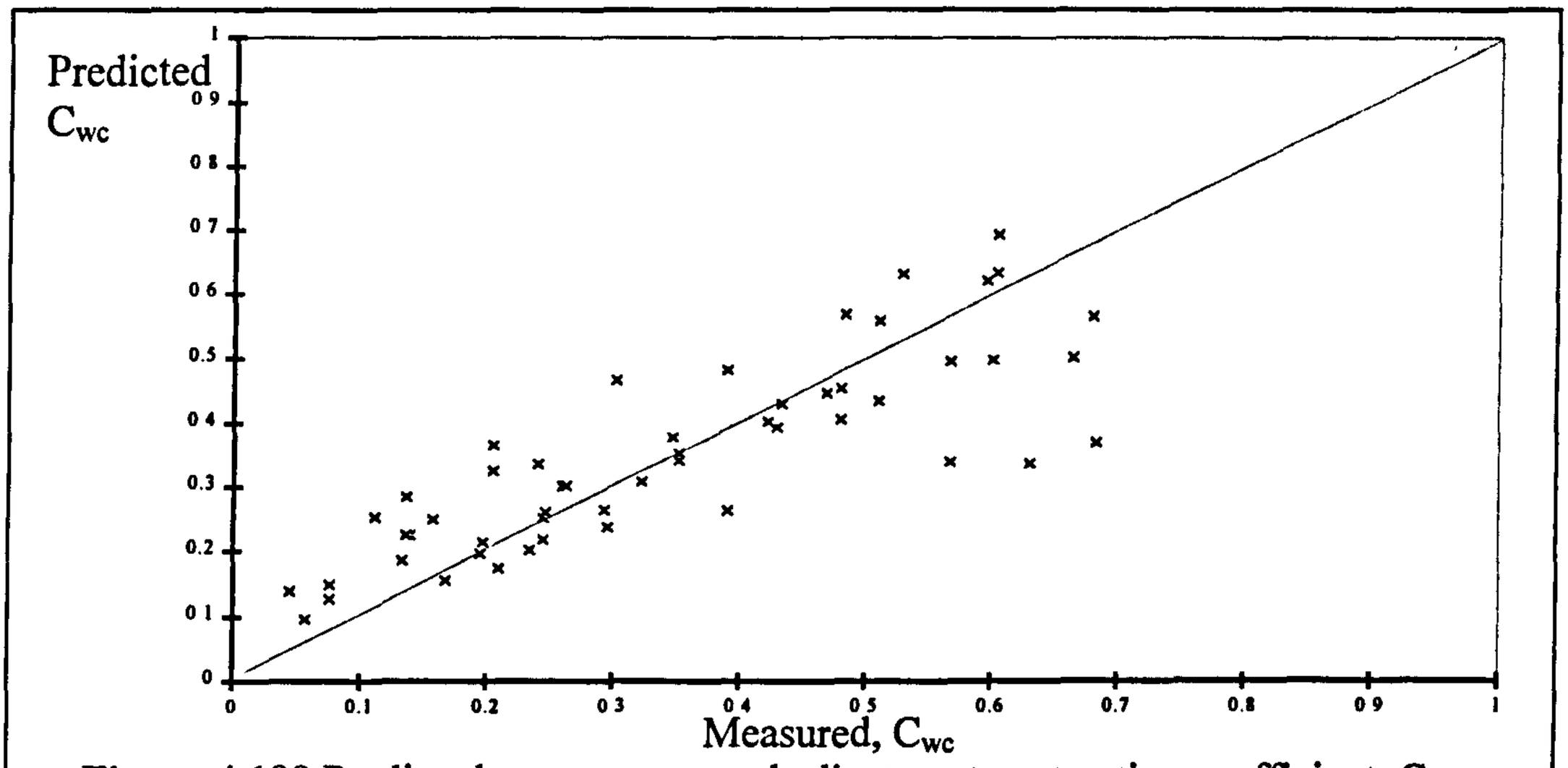

Figure 4.109 Predicted versus measured adjustment contraction coefficient, Cwc

The RMS percentage error and standard deviation for C_{we} were equal to 9.1% and 7.8% respectively. The RMS percentage error and standard deviation for C_{wc} were equal to 13.1% and 11.2% respectively.

4.9 Summary and conclusions

4.9.1 The significance of the Series B extension (1993-1996) programme

- The large range and scope of the flow data gathered during the Series B extension (1993-1996) programme has demonstrated the benefits of using small scale models to investigate flow behaviour in meandering compound channels.
- The author built and tested 30 small scale model channels over the three year period and demonstrated the influence of 7 out of 11 key parameters on meandering compound channel flow. The Series B (1989-1992) programme which was conducted over the same time period, but utilised larger scale models, lacked the flexibility offered by small scale channels and only 7 models were built. In these 7 models, the influence of only 5 key parameters was investigated.
- The author demonstrated that mapping pins, 'push-pins', can be used to roughen small scale model surfaces, thus producing a similar pattern for the variation of frictional resistance with flow depth to that generated on the grassy flood plains of natural channels.
- The author noted that the use of mapping pins as roughening elements facilitated the production of relative roughness values between the main channel and the flood plain which were similar to those found in natural channels.

4.9.2 The general relationship between the layer interaction mechanisms and relative depth

- The author demonstrated that Global F* and Zonal F*, non-dimensional measures of discharge, can be used to separate the influence of bed frictional flow resistance and reveal the proportion of flow resistance generated by layer interaction.
- Two types of zonal split were shown to represent the dominant flow areas which are generated in meandering compound channel flow over two discrete flow depth ranges. These were:-

  1) At high flow depths a 3 zone split is appropriate. Zone A representing the main channel flow below bankfull, Zone B representing the flood plain between the extremes of the meander belt and Zone C representing the flood plain outwith the meander belt.

2) At low flow depths a 2 zone split is appropriate. Zone 1 is bounded by the crest of the main channel banks and includes flow both above and below bankfull level. Zone 2 encompasses the remains of the flood plain.

- The author distinguished 4 distinct flow regions in plots of Global F* versus flood plain flow depth or relative depth. The divisions between flow regions were labelled: Thresholds 1/2, 2/3 and 3/4.
- The author recognised that the 4 flow regions observed in meandering compound channels followed a similar pattern to the 4 flow regions observed in straight compound channels by Ackers [1991] who plotted relative depth versus DISADF (a similar measure of non dimensional discharge capacity like Global F*).

4.9.3 Flow mechanisms within flow region 1

- By analysing the results obtained during the Series B extension (1993-1996) programme, the author concluded that in flow region 1:-

1. For low flow depths up to Threshold 1/2, the meandering compound channel flow separates into two dominant flow zones: Zone 1 which encompasses the flow area in and above the main channel; and Zone 2 which comprises the remaining flood plain areas.
2. Planes of vertical shear stress are generated at the interaction interface between these two zones where Zone 1 forces its way through Zone 2.
3. A significant proportion of the total flow resistance acting on Zone 1 (and hence Zone A) is generated by this vertical shear stress action, so the magnitude of Zonal F* for Zone A is often significantly less than 1.
4. By contrast bed friction contributes the majority of the total flow resistance acting on Zone 2 (and hence Zones B and C), so the magnitude of Zonal F* for Zones B and C is close to 1.
5. Global F* decreases (from a maximum value when the relative depth was equal to zero) for increasing flow depths, in line with the decreases in Zonal F_A*.
6. The author postulated that Threshold 1/2 marked the start of flow region 2 and the flow depth at which the flood plain flow attains enough momentum to disrupt Zone 1 and to start shearing over the main channel, creating 3 dominant flow zones.

7. The author noted that the flow depth at which F_A* achieves a maximum value, which is known as Threshold A, occurs at a similar flow depth to that corresponding to Threshold 1/2.
8. A 'vertical shear force' prediction method based on Equation 4.8 was developed by the author in order to determine the flow depth that corresponds to Threshold 1/2. Threshold 1/2 was shown to occur when the magnitude of vertical shear force attains a maximum value.

4.9.4 Flow mechanisms within flow region 2

- By analysing the results obtained during the Series B extension (1993-1996) programme, the author concluded that in flow region 2:-
  1. The magnitude of F_A* below Threshold 1/2 maintains similar values compared to the magnitude of F_A* above Threshold 1/2.
  2. The author postulated that a significant proportion of the flow resistance in Zone A is generated by the horizontal shearing action within Zone B which replaces the vertical shear stress as the source of flow resistance for Zone A.
  3. The author notes that in flow region 2, the main channel is able, to a large extent, to resist the typical expansion and contraction flow mechanisms which would usually occur in flood plain flow (Zone B) over a slot at these flow depths.
  4. Consequently bed friction still contributes the major proportion of the total flow resistance acting on Zones B and C, so the Zonal F* value for Zones B and C remains close to 1.
  5. Global F* increases monotonically with increasing flow depth, characterising flow region 2 behaviour and reflecting the contribution of Zones B and C as they start to contain a greater proportion of the overall capacity of the channel.

4.9.5 Flow mechanisms within flow region 3

- By analysing the results obtained during the Series B extension (1993-1996) programme, the author concluded that in flow region 3:-
  1. The onset of flow region 3 corresponds to the onset of significant expansion and contraction head losses in Zone B and is marked by Threshold 2/3 in the relative

depth versus Global F* plot.

2. These losses contribute a significant proportion of the overall flow resistance in Zone B and result in a decrease in the mean Zone B velocity. Consequently the magnitude of F_B* decreases with increasing flow depth.
3. Greater flow resistance is generated in sub-zone Zone B1, which extends over the apex of the main channel compared with sub-zone B2 which extends over the cross-over section of the main channel. The author attributed this to the significant exchange of flow between Zones A and B1. This greater flow resistance is reflected by the local reduction of flow velocity in Zone B1 and causes greater decreases in the magnitude of F_B* when flow depth increases.
4. The significant decreases in the mean Zone B1 velocity generate a vertical shear layer at the interface between Zones B1 and C.
5. The onset of the vertical shear layer coincides with the onset of the velocity reduction in Zone B and the corresponding flow depth coincides with Threshold B.
6. The additional flow resistance caused by this vertical shearing contributes a significant proportion of the overall flow resistance in Zone C. Consequently the magnitude of F_C* decreases significantly with increasing flow depth in flow region 3.
7. The author demonstrated that the onset of Threshold B in Zones B and C coincides with the onset of Threshold 2/3. This is because in flow region 3 the majority of the flow is conveyed by Zones B and C and relative depth versus Global F* behaviour reflects this.
8. The author demonstrated that the onset of the significant expansion and contraction mechanisms, which generate increased head loss and result in the flow velocity reduction in Zone B, corresponded to the flow depth at which the relative flow states in Zones A and B reached a critical threshold value.
9. The author presented a Relative Reynolds number technique as a measure of relative flow state. It was determined theoretically using Equation 4.9 which only accounted for flow resistance generated by bed friction in its formulation.

The author showed that the magnitude of Relative Reynolds number was less than 1 below Threshold 2/3 and greater than 1 above Threshold 2/3. Consequently

Threshold 2/3 was shown to correspond to the flow depth at which Relative Reynolds number equals 1.

4.9.6 Flow mechanisms within flow region 4

- By analysing the results obtained during the Series B extension (1993-1996) programme, the author concluded that:-

  1. A fourth flow region existed at high flow depths (tending towards relative depths equal to 1).
  2. In flow region 4 the 'Coherence' of the meandering compound channel flow tends to 1 which implies that the channel behaves like a simple channel and the interaction losses are less significant. No flow data was gathered to determine the flow depths corresponding to Threshold 3/4 because these flow depths corresponded to unrealistic relative depths in natural channels.

4.9.7 The influence of the other 10 key parameters

4.9.7.1 Scale difference, L_r

- The author showed that when the differences in flow resistance due to bed friction variation are removed by using plots of Global F*, the magnitude of flow resistance due to layer interaction mechanisms are similar in both large and small scale meandering compound channels.
- The differences between the flow depths corresponding to Thresholds 1/2 and 2/3, in the different scale models, were shown by the author to be attributable to differences in the relative flow state in the models at the same relative depths. However once threshold relative flow states were generated in each model then similar interaction mechanisms were shown to exist in each flow region.

4.9.7.2 Relative roughness, f'

- The author showed that in flow regions 1 and 2, increasing the relative roughness by increasing flood plain roughness had a negligible influence on Global F*. Hence the flow resistance, caused by layer interaction at the same flow depths is negligible.

- In flow regions 3 and 4, increasing the relative roughness by increasing flood plain roughness increases the magnitude of Global F*. Hence the magnitude of flow resistance generated by layer interaction at the same flow depths decreases.
- In flow regions 1 and 2, increasing the relative roughness by decreasing main channel roughness has a negligible influence on Global F*. Hence the flow resistance caused by layer interaction at the same flow depths is negligible.
- In flow regions 3 and 4, increasing the relative roughness by decreasing main channel roughness decreases the magnitude of Global F*. Hence the magnitude of flow resistance generated by layer interaction at the same flow depths increases.

4.9.7.3 Aspect ratio, AR

- The author showed that in flow regions 1 and 2, decreasing aspect ratio slightly decreases the magnitude of Global F*. Hence the magnitude of flow resistance generated by layer interaction at the same flow depths slightly increases.
- In flow regions 3 and 4, decreasing aspect ratio significantly decreases the magnitude of Global F*. Hence the magnitude of flow resistance generated by layer interaction at the same flow depths significantly increases.

4.9.7.4 Relative meander belt width, M_w

- The author showed that in flow regions 1 and 2, decreasing the relative meander belt width slightly decreases the magnitude of Global F*. Hence the magnitude of flow resistance generated by layer interaction at the same flow depths slightly increases.
- In flow regions 3 and 4, decreasing the relative meander belt width significantly decreases the magnitude of Global F*. Hence the magnitude of flow resistance generated by layer interaction at the same flow depths significantly increases.
- The author demonstrated that the influence of relative meander belt width which was analysed using plots of relative depth versus Global F* was exaggerated by the way that F* is defined. Reducing the width of Zone C alters the relative contributions of F_A* and F_B* which can give the impression of the flow interaction mechanisms are generating significantly greater flow resistance (using the normal interpretation of

F*). In reality the observed variation is predominantly attributable to this change in relative zonal contribution.

- The relative meander belt width was shown to increase the overall flow resistance in a meandering compound channel if it is reduced to a small enough width in small scale models. When the flood banks are brought in close proximity with Zone B then this will induce further frictional resistance to be exerted on Zone B. This has repercussions on the relative flow states that are achieved at the same flow depths in models where only relative meander belt width changes. The increased frictional resistance on Zone B will generate a change in flow velocity and consequently will affect the magnitude of flow resistance that is generated by the interaction mechanisms.
- The influence of relative meander belt width was shown to be more significant in small scale models than in larger scale models. The author postulated that this was attributable to the smaller percentage increase in the wetted perimeter which is induced by placing flood banks close to Zone B in the larger scale models compared with the small scale models.

4.9.7.5 Main channel sinuosity, r

- The author noted that in flow regions 1 and 2, decreasing the main channel sinuosity slightly increases the magnitude of Global F*. Hence the magnitude of flow resistance generated by layer interaction at the same flow depths slightly decreases.
- In flow regions 3 and 4, decreasing the main channel sinuosity significantly increases the magnitude of Global F*. Hence the magnitude of flow resistance generated by layer interaction at the same flow depths significantly decreases.

4.9.7.6 Main channel shape, φ

- The author showed that in flow regions 1 and 2, changing the main channel shape from trapezoidal (often used in scale models) to a quasi-natural shape, while maintaining the aspect ratio, marginally decreases the magnitude of Global F*. Hence the magnitude of flow resistance generated by layer interaction at the same flow depths marginally increases.

- In flow regions 3 and 4, changing the main channel shape from trapezoidal (often used in scale models) to a quasi-natural shape, while maintaining the aspect ratio significantly decreases the magnitude of Global F*. Hence the magnitude of flow resistance generated by layer interaction at the same flow depths significantly increases.
- The author postulated that the characteristic shape of the natural channel at the apex (deeper than the average depth on the outside of the bend) induces these additional interaction losses.

4.9.7.7 Main channel side slope, S_S

- The author showed that in flow regions 1 and 2, decreasing the main channel side slope marginally increases the magnitude of Global F*. Hence the magnitude of flow resistance generated by layer interaction at the same flow depths marginally decreases.
- In flow regions 3 and 4, decreasing the main channel side slope significantly increases the magnitude of Global F*. Hence the magnitude of flow resistance generated by layer interaction at the same flow depths significantly decreases.

4.9.7.8 Flood plain slope, S_o

- The author noted that in flow regions 1 and 2, decreasing the flood plain slope does not alter the magnitude of Global F*. Consequently the magnitude of flow resistance generated by layer interaction at the same flow depths does not alter.
- In flow regions 3 and 4, decreasing the flood plain slope significantly increases the magnitude of Global F*. Hence the magnitude of flow resistance generated by layer interaction at the same flow depths significantly decreases.

4.9.7.9 Sinuosity of the flood plain banks, r_u

- No flow data was available at the time of writing this thesis to demonstrate the influence of lateral flood plain slope. However, the author postulated its influence based on a general understanding of flow behaviour developed during the Series B extension programme.

- In flow regions 1 and 2, increasing the flood bank sinuosity will not significantly alter the magnitude of Global F* nor the flow resistance generated by layer interaction at the same flow depths because the flood bank sinuosity will have an negligible effect on Zones B and C velocities.
- By contrast in flow regions 3 and 4, the author predicts that increasing the flood bank sinuosity will increase the magnitude of Global F* and hence decrease the flow resistance generated by layer interaction at the same flow depths.
- The flood bank sinuosity will reduce the Zone B velocity which will result in a reduction of flow resistance because the significant head losses in Zone B, at these flow depths, are proportional to the square of Zone B velocity.
- The change in relative velocities between Zones A and B will alter the relative flow states at the same depths and hence Threshold depths in similar models.

4.9.7.10 Lateral flood plain slope, S_L

- No flow data was available at the time of writing this thesis to demonstrate the influence of lateral flood plain slope. However, the author postulated its influence based on a general understanding of flow behaviour developed during the Series B extension programme.
- In flow regions 1 and 2, increasing the lateral flood plain slope is likely to decrease the magnitude of Global F* and hence increase the flow resistance generated by layer interaction at the same flow depths.
- The lateral flood plain slope will reduce the increases in Zone B velocity with increasing flow depth because of the relatively large lengths of wetted perimeter compared with flow area in these channels. In addition it will alter the relative flow states at the same depths and hence Threshold depths in similar models.
- By contrast, in flow regions 3 and 4 increasing the lateral flood plain slope is likely to increase the magnitude of Global F* and hence decrease the magnitude of flow resistance generated by layer interaction at the same flow depths.
- The lateral flood plain slope will reduce the Zone B velocity because of the relatively large lengths of wetted perimeter compared with flow area in these channels. However this effect will be less significant in flow regions 3 and 4 compared with flow regions 1 and 2. The reduction in Zone B velocity will slightly reduce the

significant head losses in Zone B, at these flow depths, which are proportional to the square of Zone B velocity.

- The change in relative velocities between Zones A and B will alter the relative flow states at the same depth and hence the Threshold depths.
- In addition the author postulates that the lateral flood plain slope will direct the Zone B flow more in line with Zone A so the horizontal shearing of Zone B2 flow over Zone B will be reduced and hence the head losses associated with the expansion and contraction of flow will decrease. The flow resistance will correspondingly decrease.

4.9.8 Expansion and contraction of flow over slots

- The author demonstrated that 5 geometric and roughness parameters:- aspect ratio, relative depth, side slope angle, relative roughness and slot skew angle influence the magnitude of head loss generated in the expansion and contraction of flow as it passes over a slot
- The author decided that the adjustment coefficients, C_{we} and C_{wc}, which were devised by James and Wark [1] [1992] were useful for relating the head losses for isolated backward and forward facing steps to the head losses in flow over steps which could be determined theoretically.
- Increases in the aspect ratio generated increases in the magnitude of C_{we} and C_{wc}.
- Increases in relative depth generated decreases in the magnitude of C_{we} and C_{wc}.
- Increases in the side slope angle of the slot generated increases in the magnitude of C_{we} and C_{wc}.
- Increases in the relative roughness between the slot and upper channel generated decreases in the magnitude of C_{we} and increases in the magnitude of C_{wc}.
- Increases in the skew angle of the slot had no noticeable effect on the magnitude of C_{we} but generated decreases in the magnitude of C_{wc}.
- The author presented evidence that demonstrated that the flow data gathered by Jasem [1990], with regard to the head losses in flood plain flow over slots, was significantly influenced by the side wall effects in the narrow flume which was used.
- The author presented evidence that demonstrated that using the formulation derived by Formica [1955] results in the 2 fold over-estimation of the influence of side slope in slot channels.

- Insufficient data was collected to enable the influence of relative roughness and slot skew angle to be included in the regression formulation.
- Two formulations defining C_{we} and C_{wc} in terms of aspect ratio, side slope angle and relative depth (as shown in Equations 4.14 and 4.15) were determined by the author using regression analysis of the Series B extension (1993-1996) slot data.

Chapter 5

5. Development of an Artificial Neural Network model to predict the discharge capacity of meandering compound channels

5.1 Introduction

The flow data obtained during the Series B extension (1993-1996) programme was combined with data gathered during previous experimental programmes. This provided extensive evidence to demonstrate the typical relationship between the non dimensional measure of discharge capacity in a meandering compound channel, Global F*, and the 9 key geometric and roughness parameters listed in Table 5.1. These relationships were illustrated graphically in Chapter 4..

Ref. No.	Parameter Description	Abbreviation
1	Sinuosity of the main channel	r
2	Relative roughness of the Zone B / Zone A	f'
3	The meander belt relative to the total floodway width.	M_w
4	The aspect ratio of the main channel.	AR
5	The sides slopes of the main channel.	S_S
6	Cross-sectional shape of the main channel.	φ
7	The longitudinal flood plain slope	So
8	Relative flow depth	RD
9	Relative Reynolds number, Re (Zone A) / Re (Zone B)	Re'

Table 5.1 The nine parameters

This chapter recounts the author's attempts to train a special type of Artificial Neural Network (ANN), a Multi-Layer Perceptron (MLP), to approximate the observed complex multi-variate functional relationship between Global F* and the 9 key parameters, as shown in Equation 5.1.

$$Global\ F^* = f\left(r, f', Mw, AR, SS, XS, FL, RD, \mathrm{Re}'\right) \qquad [5.1]$$

All the parameters were converted into a non dimensional form so that results from different scale models could be realistically compared. The use of Global F* has the benefit of separating the influence of bed friction, which is significantly influenced by model scale and demonstrates the influence of layer interaction in isolation. It ranges

between 0 and 1 which aids comparison between results from different scale models and the Global F* plot was shown to exhibit similar 4 flow region behaviour, irrespective of parameter value, thus facilitating the development of a Global F* approximator.

5.2 The basic structure and functional characteristics of an ANN

Artificial Neural Networks (ANNs) can be created using software run on computers. Programmes are written and constructed so that the basic architecture and functional characteristics of the biological neuron matrix found in the human brain is replicated mathematically. A simplified version of the basic neural structure is shown in Figure 5.1. This structure combines in vast numbers to create the human brain structure. The human brain demonstrates a prodigious ability to learn suitable responses to the myriad of different stimuli. The knowledge / information stored within the neuron matrix enables the brain to deliberately replicate the desired response to a certain stimulus because, during a lifetime of trial and error, the optimal responses to various stimuli have been learnt, remembered (stored) and subsequently retrieved.

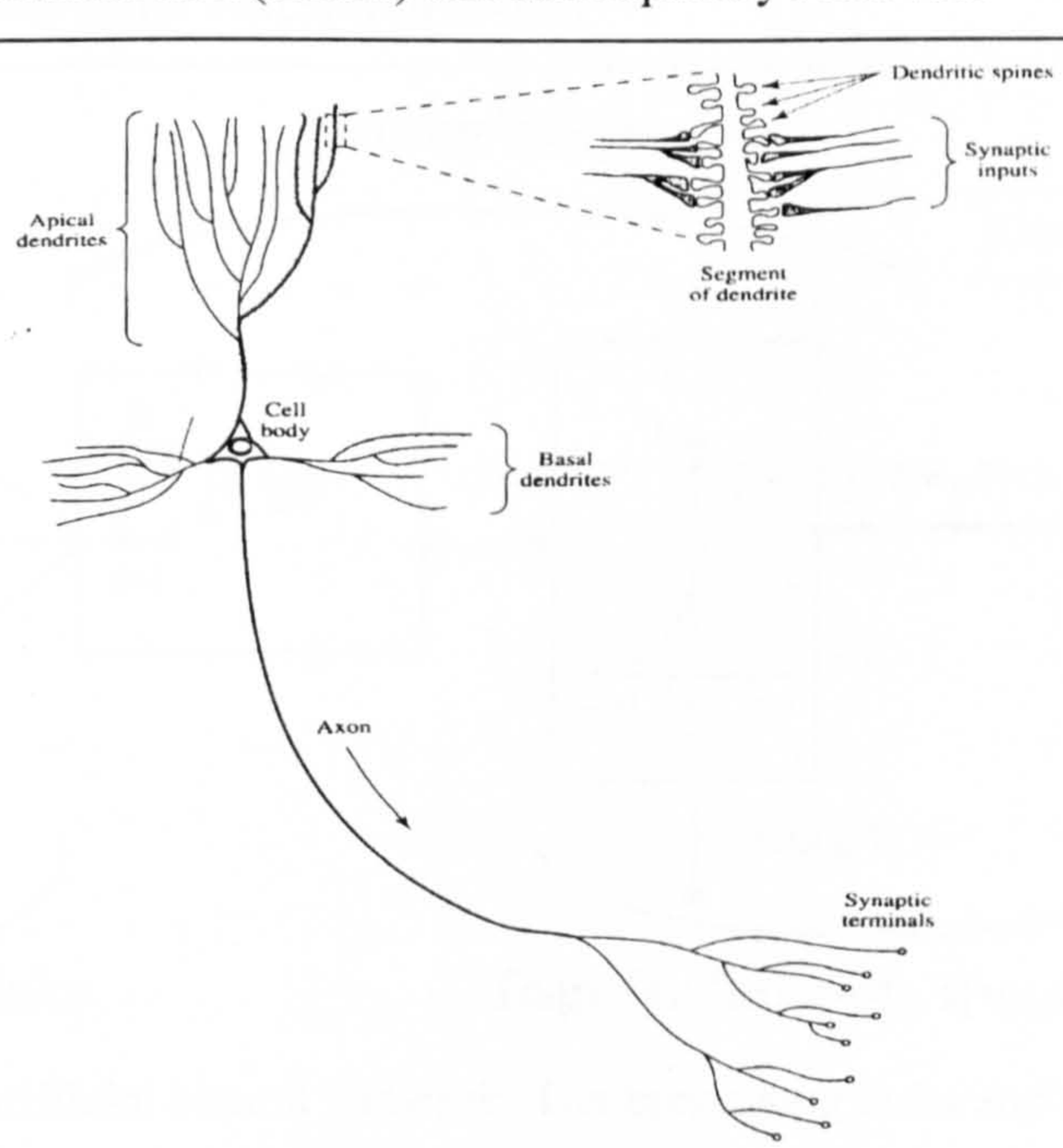

Figure 5.1 Representation Of A Biological Neural Network (After Haykin 1994)

ANNs were conceived in an attempt to simulate this ability to learn reliable responses to a complex set of stimuli (at a vastly diminished level of complexity). With this ability they have proved to be very useful tools for approximating various physical systems.

They function in a way which is mathematically analogous to the function of the brain where the stimuli are replaced by numeric inputs and the responses are replaced by targets or outputs. The biological neurons are represented by simple processing units (nodes) and the synapses by simple functional links, as shown in Figure 5.2. The functional links which represent the synapses are created using a combination of multiplicative *weights*, w_i, and additive *biases*, b, which modulate the input signal, P_i.

The inputs, P_i, are multiplied by the weights, w_i, and added to by the bias, b, (w_iP_i+b,) and then integrated. The resulting values are passed through a transfer function where the output, O_i, is squashed into the required range, which for Global F* would be between 0 and 1. An ANN with one node and one of the common transfer functions can replicate many linear functional relationships. A combination of nodes arranged in multiple layers with many weighted connections can replicate many complex, discontinuous non-linear functions. The most commonly implemented ANN to date with this form of configuration (where the nodes are arranged in layers) is known generically as a Multi-Layer Perceptron (MLP).

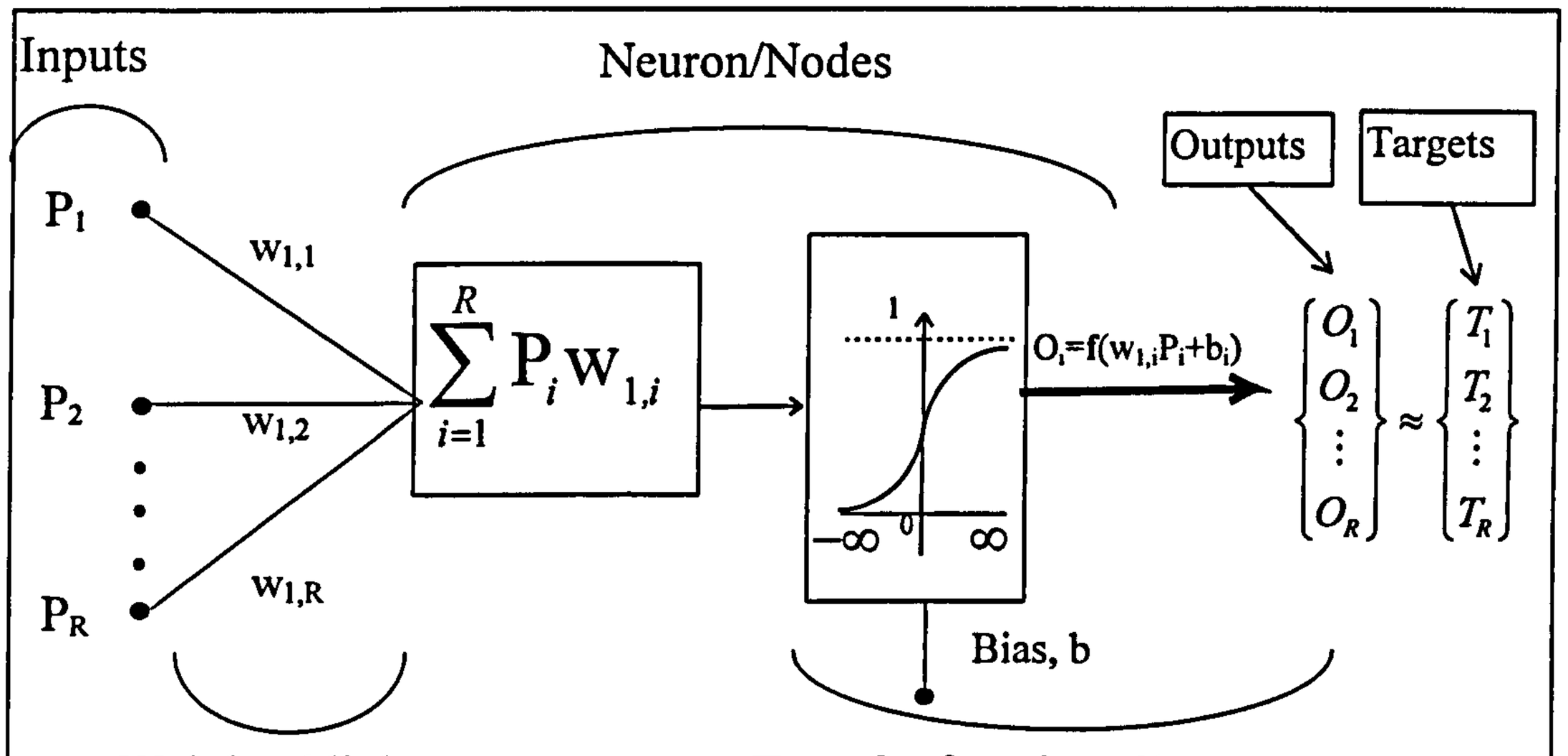

Figure 5.2 An Artificial Neural Network: The processing units and functional links

5.3 A brief history of ANNs

The development of the ANN from its theoretical conception through to its modern form with its capacity for performing complex functional approximation has been rapid

and has drawn on the expertise of many illustrious researchers. There follows a brief synopsis of the developmental history of the ANN. If required a more comprehensive history can be found in Haykin [1995].

McCulloch and Pitts [1943] devised the first logical calculus for ANNs which was based on a simple architecture with a node and link couplet as illustrated in Figure 5.2. However, it was a number of years before a methodology was developed which could be used to train the weight parameters thus enabling a ANN to accurately learn the relationship between a specific input parameter and target pairs. In 1949 Hebb published his ground-breaking book "The Organisation of Behaviour" which gave the first explicit statement of the physiological rule for '*synaptic modification*' by the process of learning. Hebb's new 'Postulate of Learning' stated that the effectiveness of a variable synapse between two neurons is increased by the repeated activation of one neuron by the other across that synapse. Hebb's concept has inspired the development of many computational models of adaptive systems in the years that followed.

During the 1950's the basic McCulloch and Pitt node and link couplets were implemented in simple single layer networks and basic computational learning processes were developed. Subsequently Rochester [1956] first used a computer to test Hebb's neural theory and Uttley [1956] demonstrated a neural network with modifiable synapses being applied to a real world problem. Uttley [1956] taught his ANN to learn to classify simple binary patterns. In 1958 Rosenblatt [1958] developed a simple form of neural network machine called the "Perceptron" to deal with pattern recognition. The perceptron functioned by subjecting a set of input values to the transformation performed by the node and link calculus and then comparing the output with the pertinent target vectors. Combinations of these simple perceptrons form the basis of many of the complex ANNs developed in recent years.

Perceptrons proved to be vital new components in the development of neural networks. Many new applications for these perceptrons were developed. For example Gabor [1960] used a perceptron as a sophisticated Input-Output mapping system, a functional approximator. There were however alternatives to perceptrons developed at about the same time. Widrow and Hoff [1960] introduced the adaptive linear element (Adaline),

which was an advance on the perceptron, and functioned by using a new training procedure "The least square algorithm". Throughout the 1960's ANNs with one layer of perceptrons, Single Layer Perceptrons (SLPs), and Adalines were widely studied and implemented. It was not until 1969 that Minsky and Papert [1969] explicitly demonstrated that the one-layer networks were limited in their range of applications. They showed that that both single layer networks and Adalines could only solve fairly simple problems. Consequently, in the early 1970's enthusiasm for Single Layer Perceptron networks (SLPs) diminished and interest grew in the development of Multi-Layer Perceptrons networks (MLPs). MLPs could be distinguished from (SLPs) because they had a 'hidden' layer of neurons as well as the input and output ones as shown in Figure 5.3.

By the beginning of the 1970's is was widely accepted that MLPs would be much better able than SLPs to model the more complex Stimuli / Response relationships. However the technology to implement MLP networks took nearly 15 years to develop. The computational power needed to deal, with the extra computations generated within an MLP, when passing the vast quantities of data, could not be provided easily at the time and there were not even any suitable training algorithms available. In fact it was left to Hopfield [1982] to kick-start further neural network development. He proposed a new type of recurrent, dynamically stable, neural network which incorporated the feedback of data through the original network to aid the training process. This new class of networks is known by the generic title of Hopfield Networks.

Subsequently, in 1986, the most significant advance in neural network theory in recent years took place, Rumelhart and McCelland [1986] reported the development of a training algorithm which was particularly suited to MLPs, the back-propagation learning algorithm. History has demonstrated that MLP networks trained with the back-propagation algorithm can model hundreds of real-world systems across a multitude of disciplines provided that:-

- The system can be simplified to an input and target mapping situation
- The system involves a classification problem in which the input parameters describe an object requiring recognition and the desired output is an identification of the class or category to which the object belongs..

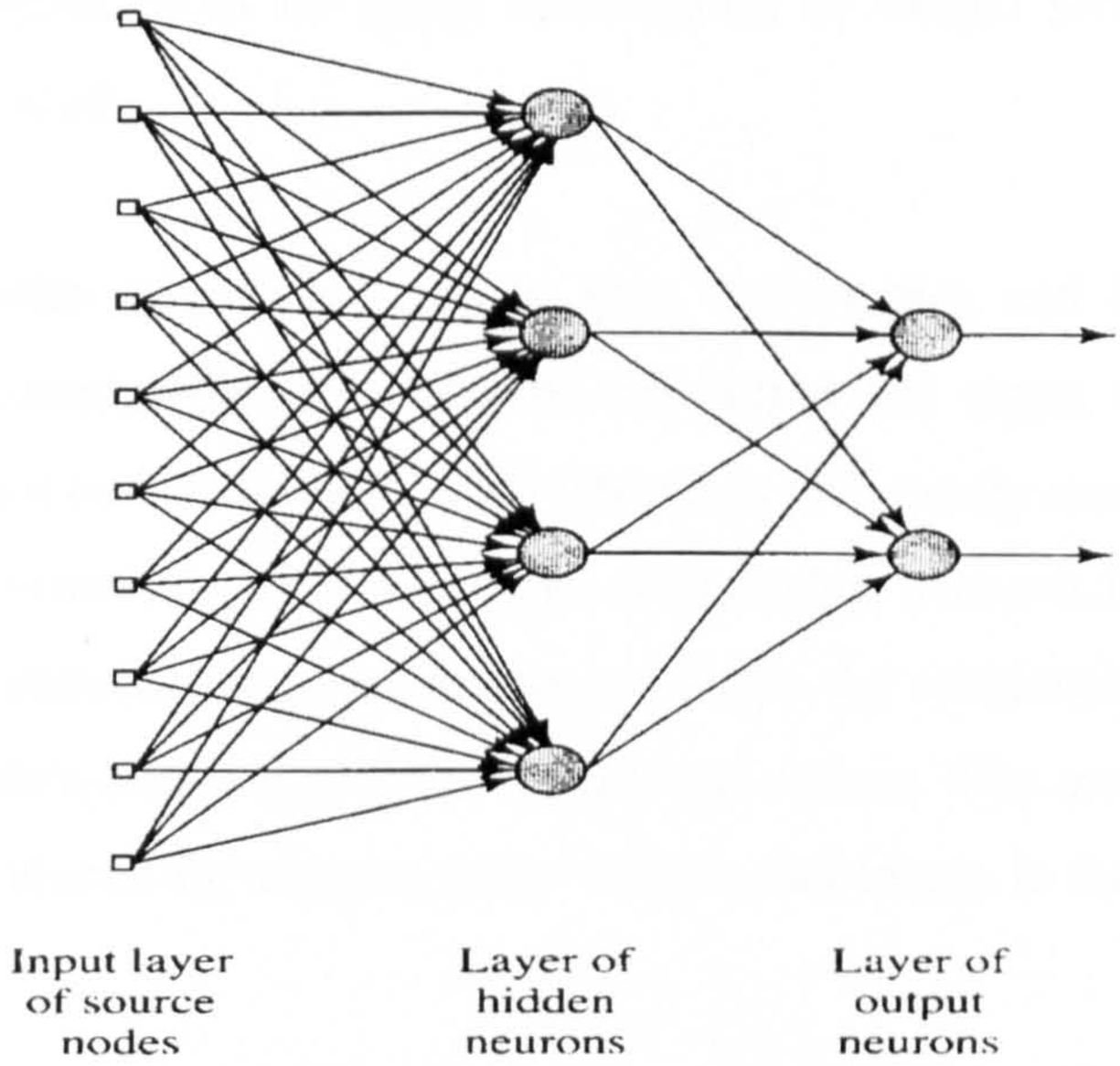

Figure 5.3 A Multi-Layer Perceptron

In recent years new learning algorithms have been developed such as the 'Boltzmann' and 'Reinforced learning' algorithms as well as other new types of layered feed forward and recurrent neural such as Radial Basis networks, Broomhead [1988]. Some of these network and training algorithm combinations have been shown to perform with almost as much reliability as MLPs, such the Radial Basis network, as shown in Mason *et al* [1996]. However, notwithstanding these developments much of the continued research in the field of ANNs has concentrated upon developing the scope of MLPs trained with the back-propagation algorithm because of their flexibility and the plethora of successful applications that there have been found for them.

5.4 The operational characteristics of an ANN

5.4.1 Introduction

When data is gathered from a set of experiments and analysed, it often exhibits a complex functional relationship between the independent signals (Input parameters) and the dependant signals (Target parameters). The combination of input and associated target parameters is collectively known as the training pair. The output generated when the input parameters from a training pair are presented to the first ANN configuration

chosen by a designer (with its initial combination of weight settings) is unlikely to match the target values.

A training algorithm has to be used to tune the weights and biases in the ANN architecture to minimise the error between the output and target values. The average error is obtained for each training pair and when it is sufficiently small this indicates that an efficient approximator of the functional relationship between the input and target values has been created. The approximator replicates the relationship demonstrated by the raw training data between the input and target values. The most efficient training algorithm yet developed for training these weights and biases is the 'back-propagation' algorithm.

5.4.2 The back-propagation training algorithm

The detailed function of the back-propagation algorithm is described in Haykin [1995]. There follows a short summary:

1. An MLP is built with a chosen number of layers and nodes
2. All the weights are initialised and attributed low random values

   Start the cycle
3. A single set of input parameter values from one training pair is chosen at random.
4. The parameter values are inserted into the input layer.
5. The MLP is cycled so that the signal from the input generates an output in the other layers.
6. The error derivative is calculated between the output and target values which correspond to each training data pair.
7. The summed product of the weights and errors is back-propagated in the output layer in order to calculate the error on the intermediate/hidden layers.
8. Update the weights associated with each node according to the measured error on that nodes which were calculated during back-propagation.

Repeat the cycle until the error is sufficiently low or the MLP output settles.

5.4.3 Choice of a particular ANN architecture

Swingler [1996] and the Department of Trade and Industry (DTI) [1996] independently confirmed that no methodology has been developed which can be used to explicitly determine the optimal ANN architecture to give minimised error values after back-propagation. Different architectures give different results and levels of error for each set of training pairs used and types of training algorithms adopted. All ANNs are capable of learning to approximate the training data to a limited extent, however the viability of any final ANN approximator will not be assessed on its ability to learn training data, but will be assessed on the ability of the trained approximator to generalise its response to independent sets of test data. The nature of the ANN architecture, the size and balance of the training data set and the type of training algorithms must be traded-off against each other to produce an MLP in a reasonable length of time which can generalise the functional relationship exhibited by the training data with a high level of accuracy.

5.4.4 Transfer functions

Transfer functions perform mapping operations on input values to produce outputs which are constrained over a certain output range. Many different transfer functions can be used to describe the processing capabilities of the many nodes which comprise each layer in an ANN. The back-propagation training algorithm, which is favoured for use with ANNs, can only work if these transfer functions are differentiable. Figures 5.4a-c illustrate a selection of differentiable transfer functions which are commonly used in ANNs:-

f(n) = Purelin(n)

(a)

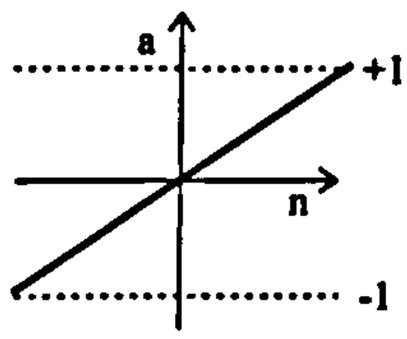

For all n

f(n) = Purelin(n) = n

f(n) = Tansig(n)

(b)

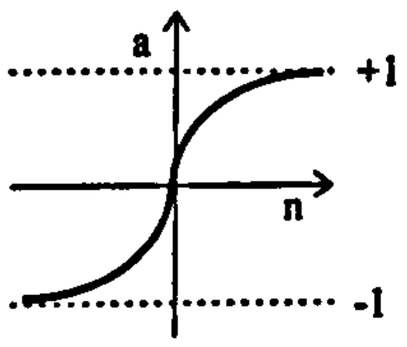

For all n

f(n) = Tansig(n) = tanh(n)

Figures 5.4a,b Transfer functions

f(n) = Logsig(n)

(c)

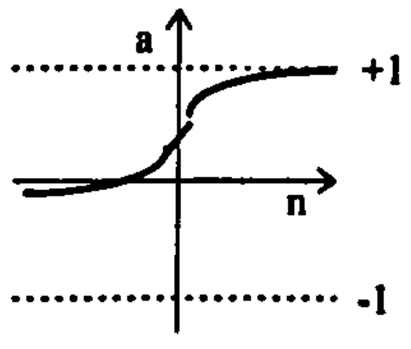

For all n

$$f(n) = \text{Logsig}(n) = \frac{1}{1+e^{-n}}$$

Figure 5.4c Transfer functions

5.4.5 The length of training time

The period of time it takes for all the training data pairs to be presented once to the network and for the weights to be suitably adjusted is known as an 'epoch'. Many epochs are sometimes required to tune the weights so that an acceptable level of error is achieved. The time taken to complete one epoch can be a very limiting factor on the viability of developing an MLP approximation. The tuning of an MLP is terminated when either the weights have been tuned so that the error achieved meets with the satisfaction of the MLP designer or a certain time has elapsed. The completed model will be able to produce output value predictions, when presented with input values which were not included in the training data. The MLP will approximate the functional relationship exhibited by the input and target values which were used to tune the weights and train the MLP. By adjusting the values of the weights and biases in an MLP, many different non-linear, discontinuous, functional relationships can be represented.

5.5 Assessing the relative viability of ANN or polynomial approximator

5.5.1 Introduction

Polynomial approximators could also be used to develop a model of the functional relationship between Global F* and 9 key parameters in meandering compound channels. However, in recent years, it has been suggested that ANN approximators have significant advantages over polynomial approximators. This claim has often been based on evidence obtained from a specific case study. The author decided it was necessary to consider the option of using a polynomial approximator for predicting the Global F* of meandering compound channels as an alternative to the ANN approximator. The

following sections present the theoretical arguments for choosing to develop either a polynomial or ANN approximator.

5.5.2 The basic operational characteristics of a Polynomial approximator

Polynomial approximators are designed by defining a specific functional relationship between the independent (input) variables, $\{x_1, x_2, ...x_i\}$ and the dependent (output) variables, {y}, based on a knowledge of the system to be modelled as shown in Equation 5.2. Box et al [1987] suggested that a polynomial function structure comprising m terms is appropriate for most polynomial approximators where m= k+1.

$$y = b_0 + b_1 X_1 + \cdots b_k X_k \qquad [5.2]$$

where $X = f\{x_1, x_2, ...x_i\}$. The coefficients in Equation 5.2 are calculated by back-substituting all the training pairs, N, typically obtained during the experimental programme. The back-substitution of N training pairs enables the system of equations which is defined in Equation 5.3 to be derived. This system of equations can be solved to find the values for the coefficients.

$$\begin{Bmatrix} y_1 \\ y_2 \\ \cdots \\ y_N \end{Bmatrix} = \begin{bmatrix} 1 & X_{1_1} & \cdots & X_{k_1} \\ 1 & X_{1_2} & \cdots & X_{k_1} \\ \cdots & \cdots & \cdots & \cdots \\ 1 & X_{1_N} & \cdots & X_{k_N} \end{bmatrix} \begin{Bmatrix} b_0 \\ b_1 \\ \cdots \\ b_k \end{Bmatrix} \qquad [5.3]$$

Different matrix solution techniques must be used if there are more, an equal number or fewer training pairs, N, than there are coefficients, m, in the polynomial approximator. These techniques are described in Carpenter [1994].

5.5.3 The similarities and differences between ANN and polynomial approximators

The basic structure of an ANN with its matrix of neurons is very different to the polynomial structure with its defined algebraic structure. However the final configurations for both models are derived by determining the values of coefficients which define the relative importance of nodes in an ANN or terms in a polynomial model respectively. Carpenter [1994] acknowledged this basic similarity and proceeded to formally assess the comparative performance characteristics of the two types of model. He showed that the substantial benefits which are commonly attributed to ANN

approximators have been frequently overstated and misconceived. The common misconceptions that he identified were that:

- ANN approximators are inherently superior to polynomial approximators
- ANN approximators can be trained with fewer data sets than are needed to determine polynomial approximators
- ANN approximators are less sensitive to anomalies in the training data than polynomial approximators
- ANN approximators are easier to derive than polynomial approximators

Carpenter [1994] also demonstrated that ANN approximators were not inherently superior to polynomial approximators and that the choice of one over the other could not be theoretically justified. The choice had to be made by directly comparing each model's capabilities. It can be readily shown that ANN models are just as susceptible to the effects of data incompleteness or inconsistencies as polynomial approximators, see Carpenter [1994]. The ANN's superiority is not proved by comparison of these criteria.

The perception of an ANN's superiority generally is commonly founded on the misconception that that ANNs are easier to derive than polynomial approximators. It is true that polynomial approximators can be difficult to construct. The suitability of the algebraic formulation for the expressions defining the structure of the elements $\{X_1, X_2,....X_k\}$ in Equation 5.3 (in terms of the input variables, $\{x_1 , x_2 ,.....x_i\}$) determines the accuracy of the approximation. For example a typical second order polynomial approximation in two independent input variables, $\{x_1 , x_2\}$ would be defined as in Equation 5.4.

$$y = b_0 + b_1 x_1 + b_2 x_2 + b_3 x_1^2 + b_4 x_1 x_2 + b_5 x_2^2 \qquad [5.4]$$

The structure of the input variable combinations will be dependent upon the physical system requiring approximation. If the exact inter-relationship between the input variables is unknown then it will be a very complicated and time-consuming task to determine the most appropriate structure for the design variables and to produce the most accurate functional approximator. A systematic search of the complete family of possible polynomials will be necessary to develop an optimal approximation. Linear functions would be examined first followed by functions of a higher order.

For ANN approximators, the inter-relationship between input variables, which is defined by the configuration of the neuron connections, can be quickly and efficiently tested by systematically altering the structure of the ANN without needing to know exactly how the changes relate to the actual physics of the system. This is an definite advantage if the system is so complex that very little is know about its fundamental physics. By contrast the designer who develops a successful polynomial approximator will, as a very important bonus, gain an insight into the physical nature of the system being approximated. In practise when comparing the two approaches the benefits associated with the relative ease of deriving the structure of ANN model must be offset by the length of time that is required to train an ANN compared with that needed to derive an equivalent polynomial approximator.

Theoretically comparing the two methods demonstrated that the ANN approximators were not inherently superior. There is no irrefutable technique to determine the relative suitability of each model type for approximating any particular system. This lack of a theoretical method led to the publication by the Department of Trade and Industry (DTI) of DTI [1996] which contained a set of guidelines to enable a designer to chose between implementing either an ANN or a polynomial approximator.

5.5.4 DTI guidelines

In 1996 the DTI published a set of guidelines which were intended to assist interested parties to assess the viability of a ANN model. These guidelines identified the common features associated with successful ANN model implementation. A number of existing ANN models which were acknowledged to be successful were studied to facilitate the identification of these features. The guidelines outlined 4 'pointer' features which could be used to assess the advantages of an ANN model over the other options. The guidelines stated that an ANN approximator may be appropriate if one or more of the following features apply:-

- Only poor quality or incomplete data is available for developing the approximation.
- Different types of input data require integration.
- There are difficulties specifying a knowledge based model for the system concerned.

- The function approximator will need to be adapted when new data becomes available.

5.5.5 The DTI guidelines applied to a Global F* approximator

All 4 features identified in the DTI guidelines are applicable to the problem of developing a method to predict the Global F* of meandering compound channels using the existing experimental data:-

- The data collected from all the available sources world-wide during the Series B extension programme is of generally high quality but it is still affected by experimental noise. Also, there is a level of uncertainty about whether the data relating Global F* to the 9 parameters is complete enough to facilitate an accurate approximation. The data set could be usefully extended by including field data. Currently a large majority of the data is derived from scale models.
- To develop a suitable functional approximator a number of different types of input data, geometric and roughness, must be integrated.
- Although a number of successful models have been developed by using simplified models of the Global F* relationship with the 9 parameters there remains a great deal of difficulty in specifying a knowledge based model for this relationship which includes the effect of all the key parameters.
- The adaptability of an ANN model is a very beneficial feature. The accuracy of a model can be constantly enhanced by being refined through the inclusion of new scale model and field data in the training set as it becomes available.

5.5.6 Conclusions

By applying the DTI guidelines the author determined that an ANN functional approximator was likely to be more suitable than a polynomial approximator for predicting the relationship between Global F* and the 9 key parameters in a meandering compound channel

5.6 The phasing of the ANN development process

The development of the ANN functional approximator to predict the functional relationship between Global F* and the 9 key parameters in a meandering compound channel was divided into six major phases which were recommended by Swingler [1996]. These phases are illustrated in Figure 5.5.

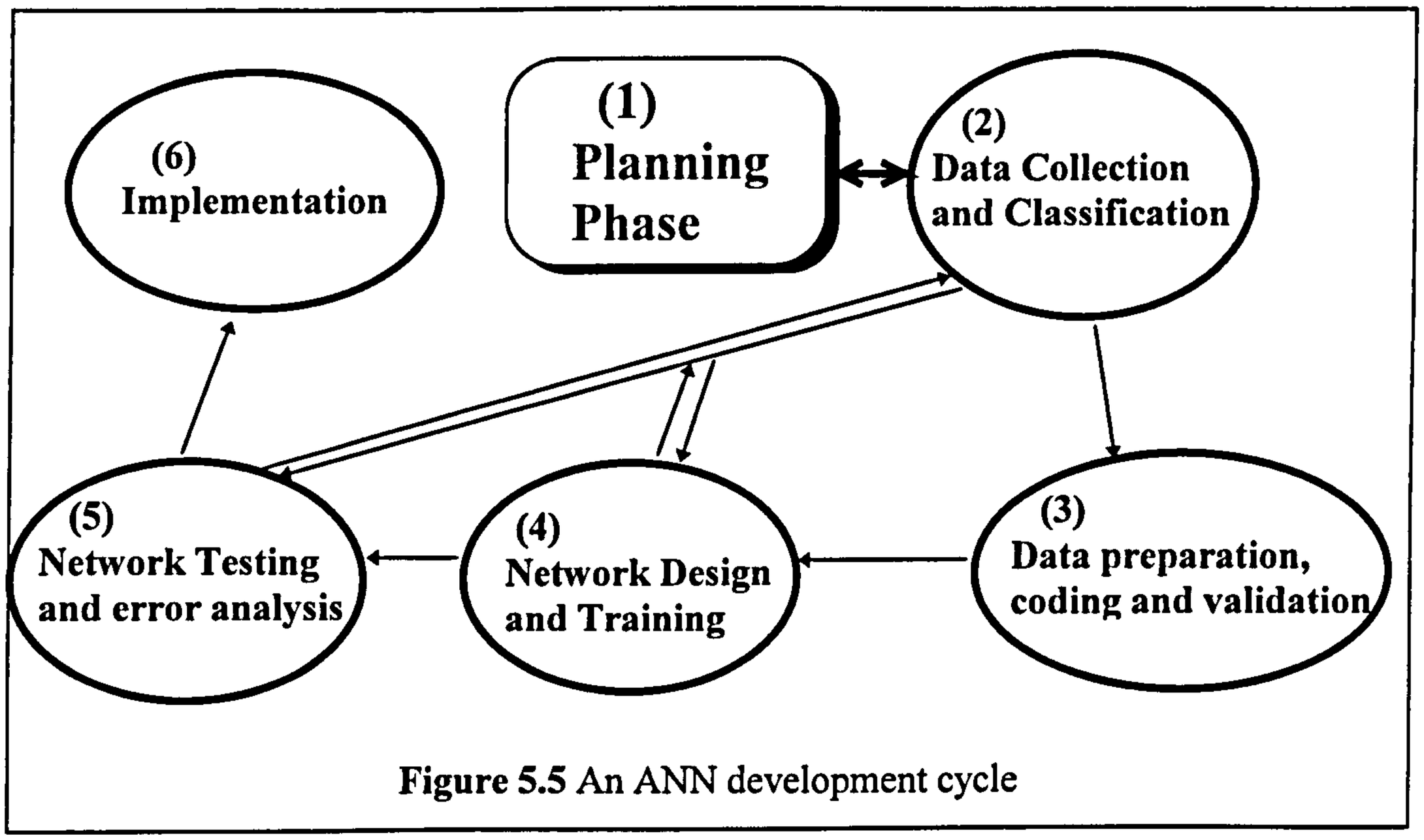

Figure 5.5 An ANN development cycle

5.7 The planning phase

The structure of the planning phase that was adopted is detailed in Figure 5.6.

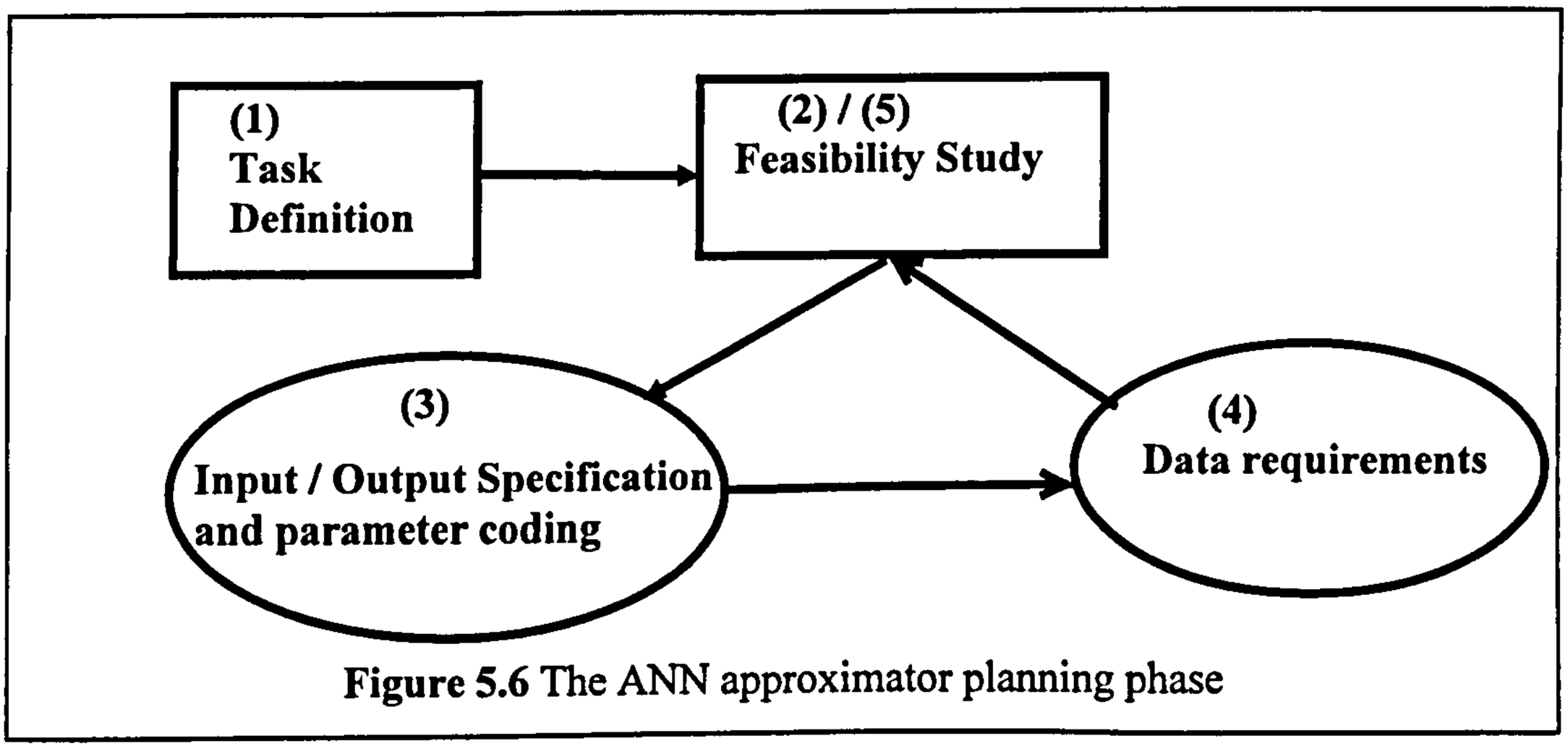

Figure 5.6 The ANN approximator planning phase

Although the DTI guidelines indicated in general that it would be possible to train an ANN approximator to replicate the relationship between Global F* and the 9 parameters

in a meandering compound channel, the author recognised the need to include a detailed planning phase in order to determine whether, on close inspection of the available data, an ANN approximator really was a viable option.

5.7.1 Task Definition

The primary task of the Series B extension programme was to design a deterministic model which could approximate the functional relationship between the Global F* (the target variable) of a meandering compound channel and the 9 key parameters (Input variables). The model was required to generalise the functional relationship exhibited by the raw experimental data which were collected from laboratory and field tests performed on meandering compound channels world-wide.

5.7.2 A Feasibility Study

5.7.2.1 Introduction

An ANN approximator was deemed to be feasible because they had been successfully implemented as functional approximators in many previous case studies, in fields as diverse as Banking and Aerospace Engineering. Two types of physical system have been shown to be particularly suited to being approximated by an ANN. One is a classification system in which the input parameters describe an object requiring recognition and the desired output is an identification of the class or category to which the object belongs. The second is a continuous numeric system in which a description of the relationship between different sets of variables is sought by analysing raw data from a real physical system.

A number of applications for ANN approximators in Hydraulic Engineering have been devised. The majority of these models are based on the second system type in which an ANN effectively acts as a functional approximator of experimental data. Minns [1995] taught a neural network model to describe the relationship between hydraulic flow parameters and the near-bed concentration of suspended sediment using a number of sets of experimental data. The model was compared with a traditional dimensional analysis model and was shown to give more accurate results. Karunanithi et al [1994]

trained an ANN to model the relationship between rainfall intensity and the discharge carried by the Huron River. They showed that their ANN approximator performed better than an equivalent power model derived using dimensional analysis. There are many other successful ANN applications documented in Civil Engineering literature, examples of these applications can be found in Mason *et al.* [1996], Grubert [1995], and Flood I and Kartam N [1994].

5.7.2.2 The importance of scale difference

The author recognised that the accuracy of the final ANN approximator would depend on the amount of high quality data that available for inclusion in the training data set. To obtain the quantity of data required, the results from tests performed on models built at different scales would have to be used. Consequently the author sought a method which could facilitate the direct comparison of flow behaviour in different scale channels and could be incorporated into the development of an ANN approximator.

In Chapter 4 the author presented flow results which showed that similar layer interaction mechanisms are generated in meandering compound channels irrespective of scale. Using plots of Global F* versus relative depth, as shown in Figure 4.58, characteristic 4 flow region behaviour was exhibited whatever the scale of the channel. Channel scale was also shown not to significantly influence the range of magnitude of the layer interaction head loss when measured using Global F*. However, scale changes were shown to effect the relative depths at which the Threshold between flow regions took place (at different flow depths different flow interaction mechanisms dominate).

The author demonstrated that the relative flow characteristics in the main channel and the flood plain channel dictated the magnitude of the relative depths corresponding to the Threshold depths. The author decided to include an additional parameter in the input parameter training set which was a measure of the relative flow characteristics and therefore could be used to account for the effects of scale by acting as a trace to identify trigger values of relative depth and flow characteristic at which transition depths were shown to be achieved. Thus the influence of scale difference would be explicitly accounted for.

5.7.3 Input and Output data specification and coding

Each of the 9 input parameters (listed in Table 5.1) and their corresponding output / target variable, Global F*, were grouped together to form subsets known as a 'Training pair'. Many of the training pairs were gathered together to form data sets to be used for both training and subsequently testing the approximator. The 9 parameters were non-dimensional and could be applied to any channel scale and were therefore included as the input parameters in the training pairs. The novel parameter Relative Reynolds number, Re' (the product of flow velocity and hydraulic depth for the flood plain channel divided by the same product for the main channel) was included as one of the 9 input parameters in the training set in order to act as a trace for transition depth. The author identified the Relative Reynolds number, Re', as the flow characteristic which could identify the effect of scale difference. In Chapter 4 the author showed that when the Relative Reynolds number passes through a magnitude equal to 1 the transition between Zones 2 and 3 was initiated.

Unfortunately the Relative Reynolds number was not useful for identifying Threshold 1/2 because a different measure of relative velocity was shown to control the inception of Threshold between flow regions 1 and 2. The author did not develop an additional trace parameter for Threshold 1/2 in order to avoid over-complicating the training pairs. This was thought to be particularly important because the author expected that two more input parameters, lateral flood plain slope, L and flood bank sinuosity, r_u, would certainly have to be included at some time in the future in a potentially more accurate version of the ANN approximator which was developed during the Series B extension programme. The author felt that leaving out a trace for Threshold 1/2 was more acceptable than for Threshold 2/3 because the difference in the relative depth of Threshold 1/2 was much less significant than the difference of relative depth of Threshold 2/3 in different scale models.

Lateral flood plain slope, S_L, and flood bank sinuosity, r_u, were not included in the ANN approximator developed by the author during the Series B extension programme because no results demonstrating their explicit effect on the magnitude of Global F* were available at the time. The significance of the influence of these two parameters on Global F* variation was, however, well recognised by the author and it is intended that

the ANN approximator will be extended in the future to account for these parameters. The ability of an ANN to be adapted at a later date to include additions to the training pairs and also more training pairs was greater than for polynomial approximators which persuaded the author that an ANN approximator approach to modelling Global F* behaviour was not only feasible but was also the most sensible long-term approach.

The author also decided that it would not be appropriate to use discharge rate, Q, as the target variable in the training set (because it was influenced by head losses due to both bed friction and layer interaction) consequently the author implemented a non-dimensional measure of discharge, Global F*, as an alternative target variable. The target variable had to be dimensionally equivalent to the input and therefore had to be non-dimensional like Global F*. In addition using the Global F* coding ensured that the bed friction head effects which are significantly affected by the scale of the model were separated from the effects of the layer interaction mechanism which were not so significantly affected.

5.7.4 Data requirements

An efficient ANN approximator can only be developed if enough suitable training and test data is available. Mulhall [1995] stated that the minimum size of an ANN training data set was determined by three main criteria:-

- the intrinsic dimensionality of the model.
- the probability distribution of the parameter data.
- the complexity of the system (how well suited the system is to being modelled by interpolating between examples).

Ruelle [1989] suggested that 2^n data pairs would be needed to build a model in n-dimensional space. The Global F* approximator was to be developed using training pairs consisting of 9 independent input parameters and one dependant output variable. The basic model therefore had a dimensionality of 9. Consequently a minimum of 2^9=1024 data pairs were required to comprise an adequate training set.

The Ruelle [1989] estimate predicted the minimum number of training pairs which needed to be included in the training set. However the final number of training pairs in the complete training set was also influenced by the requirement that the training set

must be balanced and contains enough data pairs to cover the required range of input parameter values for the final model. Consequently any data pairs which contain outlier data must not be included in the data set.

Outliers are identified as having vastly different input or output parameter values from the average values of the training data and therefore will tend to bias the final ANN approximator. For normally distributed data elements Chauvenet's criterion may be used to identify outliers. For other data elements which show no typical distribution characteristics the presence of outliers has to be identified by inspection.

The size of the training set may also be affected by the possibility of being able to reduce its dimensions. The training set's dimensionality should be reduced if the data defining the influence of a certain parameter is inadequate or if certain parameters are intrinsically dependant on each other. Reducing the dimensional complexity of a model is desirable because having a lower dimensionality will often benefit a model's ability to generalise. Alternatively Baum E and Haussler D [1989] proposed that the number of pairs in a training set should be predicted using Equation 5.5

$$No.\ of pairs = \frac{1}{ERR} * N \qquad [5.5]$$

where ERR is equal to the RMS error between the targets and outputs and N is equal to the number of weights.

5.7.5 Feasibility reassessed with regard for the generalisation ability of the ANN

An ANN approximator's ability to generalise is the main criterion by which its feasibility will be judged. They can always potentially learn the data they were trained with, this is known as 'grand-mothering', however the ability to subsequently generalise the functional relationship can not be guaranteed even if minimal errors are achieved during training. Consequently a suitable test data set must be extracted from the original experimental data and used to test the generalisation ability of an ANN. Swingler [1996] suggested that a test set which was at least one-fifth of the size of the training set should be created.

During the Series B extension programme 1672 reliable data pairs were collected. Creating a suitable test set would leave 1394 data pairs for the training set which even when not allowing for any dimensional reduction to the input parameters would meet the Ruelle [1989] criterion of a minimum of 1024 data pairs. The author decided it was therefore entirely feasible that an ANN approximator could be developed using this data. However, it was recognised that careful checks would be required throughout the development process to determine if the initial assumptions about the data requirements were correct. Removal of outliers or other data to balance the training set could hinder the feasibility of developing a satisfactory ANN functional approximator.

5.8 Data Collection and Classification

During the Series B extension programme, 8 data sets were collated from 7 experimental and 1 field programme, which illustrated the effect of the 9 key parameters on the hydraulic performance of meandering compound channels. Table 5.2 lists the parameters varied in each experimental programme. Series 8 provided data for a full scale river. Series 3 and 7 represent data from large scale models which were approximately 1:10-1:20 idealised scale models of natural rivers. Series 1,2,4,5,6 provided data for scale models which were approximately 1:100 idealised scale models of natural rivers

Series No.	Experimental Series	Re'	f'	r	S	Mw	RD	AR	SS	X
1	Series B Ext. (G)	√	√	x	x	√	x	√	√	√
2	Series B Ext. (A)	√	√	√	√	x	x	√	x	√
3	Vicksburg	√	√	x	√	√	x	√	x	x
4	Sooky	√	√	√	√	√	x	x	x	x
5	Kiely	√	√	x	x	x	x	x	x	x
6	Aberdeen	√	√	x	√	x	x	x	x	x
7	FCF Series B	√	√	√	x	√	x	√	x	x
8	River Roding	√	√	x	x	x	x	x	x	x

Table 5.2 Experimental data collected during the Series B Extension programme

Each data set included sufficient information to enable the determination of the bed friction characteristics for each one of these models. The provision of suitable bed friction calibration data was essential in determining accurate Global F* values for all states of flow. All the input parameters, excluding main channel shape, φ, varied along a continuous scale. The parameter, φ, was defined as a classifier of cross-sectional

5.9 Data preparation, coding and validation

5.9.1 Preparation and extension of the base data set

A base set of all the available data pairs combined was collected from a selection of data provided by the 8 experimental programmes detailed in Table 5.3. This data set required extension prior to commencing the development and testing phases in order to enable the final ANN approximator to generate predictions of Global F* for low relative flow depths which are critical in field situations. These are the most commonly occurring flood events.

The existing data was extended by plotting a straight line for low relative depths on a typical plot of Global F* versus Relative Depth (RD) for over bank flow in meandering compound channels as shown in Figure 5.7.

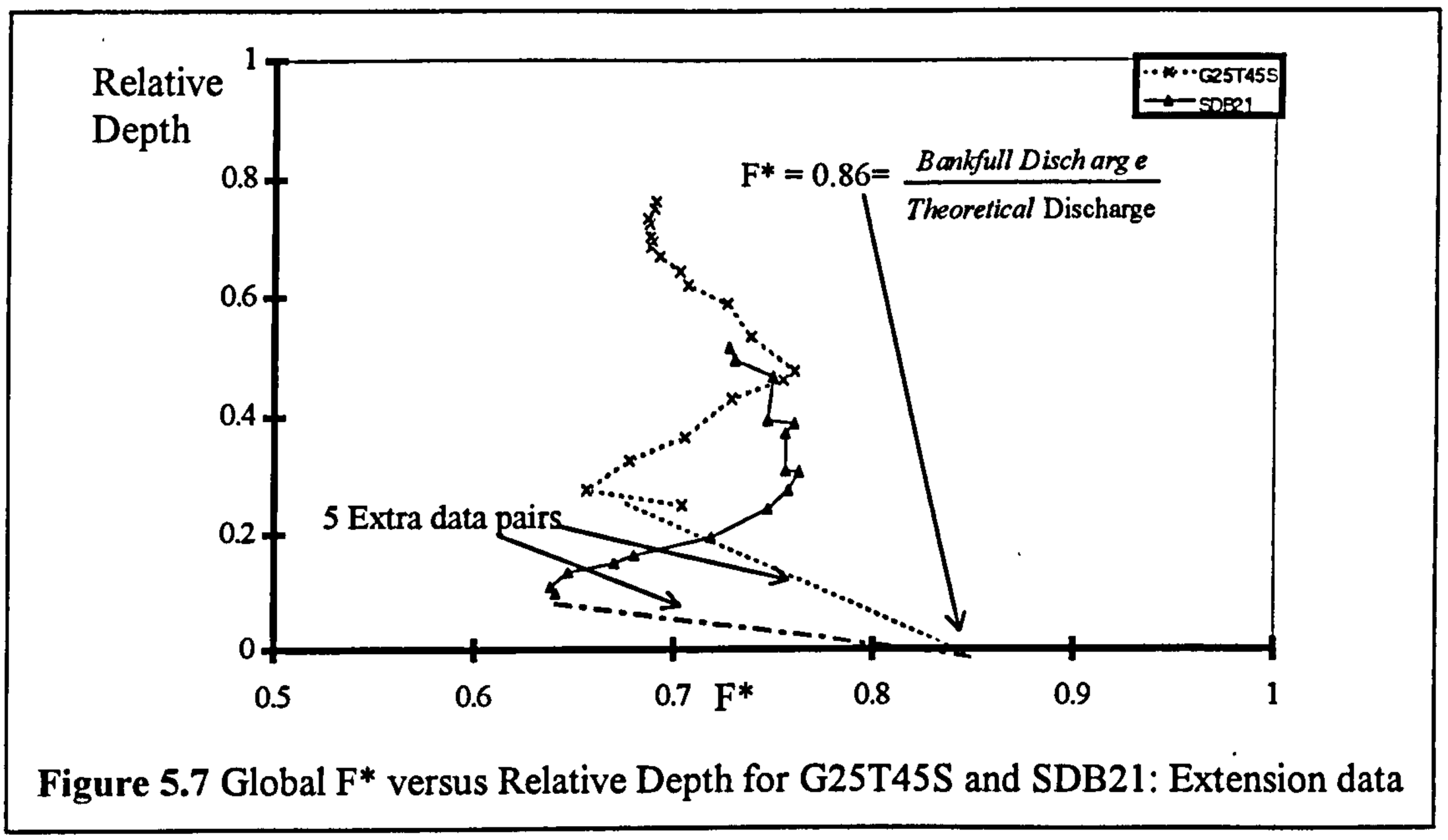

Figure 5.7 Global F* versus Relative Depth for G25T45S and SDB21: Extension data

The straight line was constructed by passing a line through a fixed point defined by the value for Global F* at RD=0. The only difference between the numerator and denominator in the Global F* equation is attributable to the secondary circulation losses generated in the main channel due to its sinuosity. Both the Linearised SCS [1963] method and the Chang [1984] method were used to accurately determine the magnitude of secondary head losses which supplement the basic bed friction head losses when

method and the Chang [1984] method were used to accurately determine the magnitude of secondary head losses which supplement the basic bed friction head losses when inbank discharge measurements were not available. The straight line was pivoted about this point and angled so that it best fits with the limited number of points which were experimentally determined in the lower tail of the Global F* curve (flow region 1) also shown in Figure 5.7.

By measuring from this line, five extra data pairs were added for each data set to the overall experimental data set. The data was not extended for high depths because the behaviour of Global F* with depth was not known and flow in real rivers rarely reach such large relative flow depths. The complete extended data set comprised 1672 data pairs.

5.9.2 Removal of Outliers

The completed training data set was screened (balanced) to identify and remove outlier (extreme value) training pairs. Outlier training pairs contain parameter or target values which are so different from the typical values that there may have been an error in their measurement or the experimental model that they were derived from was unrepresentative of typical models. Whatever the reason, if the outlier pairs were included in the training data sets they could potentially have a significant, deleterious influence on the final accuracy of the trained ANN approximator. Logic dictates that the training pairs which contain parameter values all within similar ranges are more likely to be reliable than the odd pair which lies outside the range. Consequently the outlier training pairs were removed once they had been identified so that they did not bias the ANN approximator.

The outlier data pairs were identified either by inspection or by using Chauvenet's method. Those data pairs which contained input or output parameters which were more than 3 standard deviations from their sample mean were removed. The complete data pair, all ten elements, was removed if only one of its elements was designated an outlier. There was a total of 116 of these outlier data pairs removed from the base data set.

5.9.3 Splitting the experimental data into a test set and training set

The complete extended and balanced basic data set was subsequently split into two separate data sets. One data set was be used to train the ANN functional approximator and the other was used to test the approximator.

The training set data was selected so that it contained data pairs which when grouped together described the greatest possible value ranges for input parameters and the biggest difference between the maximum and minimum parameter values. An ANN approximator will predict the Global F* target values more accurately for a meandering compound channels whose characteristic input parameters are within the same range of the training data than for those whose parameter values are outside this range. The ANN approximator will not necessarily give reliable predictions for channels whose parameter values lie outside the range. The removal of spurious outliers obviously reduces this range so the final range of applicability of the ANN approximator is diminished but the accuracy of the training is increased. There was a natural trade-off between establishing a useful range for the approximator while achieving the best possible accuracy for the ANN which is determined during the development.

The training set which was finally used to train the optimised ANN included all the data pairs from the Series B extension tests performed both in Glasgow and Aberdeen, the Series B tests and the Toebes and Sooky [1967] tests minus 3 sets of model results from tests SDB25, A3N750A and G50N45R, which were removed for inclusion in the test set. All the data pairs from Toebes and Sooky [1967] were eventually removed from the training set because the geometric ratios of these models were dissimilar to those found in natural channels. The author suggests that the associated flow data represented outlier values compared with the rest of the training set and would consequently have an exaggerated and even detrimental effect on the ANN training results. These models exhibited distinctly different patterns of flow behaviour than the others.

The final training set with all the outliers removed consisted of 1378 data pairs which comfortably met the Ruelle [1989] criterion (a minimum of 1024 data pairs for this 9 dimensional approximation). The statistical distribution of Global F* and the 9 parameters in the final training set is given in Table 5.5. The 12 test sets were selected

from the 8 groups of experimental results. The test sets were representative of the whole range of different types and scales of meandering compound channel taken from field and laboratory channels.

	Global F*	RD	Re'	f'	r'	So	Mw	AR	SS
Mean	0.720	0.337	5.716	2.097	1.422	0.0011	1.439	6.191	0.799
St. Dev	0.111	0.206	7.687	1.283	0.214	0.0001	0.256	2.831	0.134
Min.	0.430	0.000	0.147	0.359	1.110	0.0010	1.000	2.670	0.476
Max.	0.974	0.760	40.99	6.530	2.043	0.0013	1.722	14.60	1.000

Table 5.3 The statistical distribution for the training data pairs

In total the 12 complete test sets were selected which contained 184 data pairs. The range of the statistical properties of each parameter in each data set is listed in Table 5.4a-c together with the name of the research team that produced the data. To complicate matters Swingler [1996] presented evidence which showed that an ANN functional approximator predicts desired target values most accurately when the value of the input parameters in the test data pairs is within the same range as the input parameter values in training data pairs. The ANN approximator will generate less reliable predictions for test data pairs where the parameter values lie outside the training data range. The test set was split into three sections according to the test parameters' magnitude in relation to the maximum and minimum parameter values identified in the training set. The performance of the ANN approximator was assessed with regard for the relative value of the parameter values. The first test set comprises those test data pairs which have all their parameter values within the training set range.

Test No.	Mod. Ref.		F*	RD	Re'	f'	r'	So	Mw	AR	SS
1	**G50N45R**	Min.	0.590	0.00	0.22	1.09	1.37	0.0010	1.62	5.33	0.66
		Max.	0.860	0.67	23.8	4.74	1.37	0.0010	1.62	5.33	0.66
	A3N750A	Min.	0.617	0.00	0.71	1.00	1.11	0.0013	1.72	4.57	0.87
		Max.	0.965	0.53	26.1	2.15	1.11	0.0013	1.72	4.57	0.87
	SDKI 301	Min.	0.670	0.09	0.58	0.91	1.22	0.0010	1.56	4.00	1.00
		Max.	0.784	0.44	24.0	2.69	1.22	0.0010	1.56	4.00	1.00
	SDAB102	Min.	0.621	0.11	0.30	0.84	1.41	0.0010	1.20	3.87	0.94
		Max.	0.732	0.58	18.4	1.82	1.41	0.0010	1.20	3.87	0.94

Table 5.4a Test Set 1: Parameter values for the test sets (Within the training set)

The second section comprises the data pairs extracted from the field tests on the River Roding. The third section comprises those test configurations which have some of their parameters outside the training set range.

Test No.	Mod. Ref.		F*	RD	Re'	f'	r'	So	Mw	AR	SS
2	**Roding**	Min.	0.605	0.12	0.60	1.57	1.38	0.0014	1.00	9.51	0.55
	cut	Max.	0.886	0.57	17.2	3.15	1.38	0.0014	1.00	9.51	0.55
	Roding	Min.	0.561	0.12	0.31	0.55	1.38	0.0014	1.00	9.51	0.55
	uncut	Max.	0.775	0.60	10.3	1.13	1.38	0.0014	1.00	9.51	0.55

Table 5.4b Test Set 2: Range of parameter values for the test sets (Field data)

Test No.	Mod. Ref.		F*	RD	Re'	f'	r'	So	Mw	AR	SS
3	**SDB25**	Min.	0.692	0.03	0.25	0.81	1.37	0.0010	1.62	14.6	0.59
		Max.	0.806	0.64	203	3.08	1.37	0.0010	1.62	14.6	0.59
	VB201	Min.	0.712	0.18	0.92	0.98	1.57	0.0010	1.73	5.57	0.71
		Max.	0.758	0.40	5.64	1.49	1.57	0.0010	1.73	5.57	0.71
	VB202	Min.	0.570	0.18	1.91	0.98	1.57	0.0010	1.73	5.57	0.71
		Max.	0.864	0.40	11.7	1.49	1.57	0.0010	1.73	5.57	0.71
	SDAB104	Min.	0.454	0.10	0.22	0.82	2.06	0.0006	1.20	3.87	0.94
		Max.	0.580	0.60	16.7	1.91	2.06	0.0006	1.20	3.87	0.94
	SDSK402	Min.	0.691	0.00	0.20	0.71	1.09	0.0009	2.56	5.50	1.00
		Max.	0.962	0.54	0.61	0.97	1.09	0.0009	2.56	5.50	1.00
	SDSK403	Min.	0.781	0.00	0.28	0.80	1.09	0.0016	2.56	5.50	1.00
		Max.	0.962	0.47	0.62	0.97	1.09	0.0016	2.56	5.50	1.00

Table 5.4c Test Set 3: Range of parameter values for the test sets (Outwith training set)

5.9.4 Scaling the data set

An additional refinement was performed prior to training the ANN approximator and beginning the testing. All input parameter values in the training set were adjusted so that their range was limited between 0 and 1. Prior to scaling, any error in the remaining high valued parameters like AR (maximum = 14.6) would have a greater influence on the accuracy of the ANN than those with low values like So (maximum = 0.0013). A linear, scaling technique was used to set equivalent values for each of the parameter values between 0 and 1. Equation 5.6 shows the formulation which was adopted to scale the parameters (a dummy variable V_i, is used to illustrate the technique). Six of the input parameters were scaled to ensure that they had equal influence. The output parameter Global F* and the input parameters; RD, SS and φ were not scaled because their natural range of values was between 0 and 1.

$$V_i(scaled) = \frac{V_i - \min(V_{i=1...n})}{\max(V_{i=1...n}) - \min(V_{i=1...n})} \quad [5.6]$$

The new statistical properties for the scaled training set, including all 1394 training data pairs, are listed in Table 5.5. The scaled data set was used to train the final, optimised, ANN approximator.

	Global F*	RD	Re'	f'	r'	So	Mw	AR	SS
Mean	0.718	0.334	0.136	0.282	0.336	0.205	0.603	0.293	0.808
St. Dev	0.111	0.204	0.188	0.209	0.232	0.401	0.357	0.237	0.128
Min.	0.430	0.000	0.000	0.000	0.000	0.000	0.000	0.000	0.476
Max.	0.974	0.760	1.000	1.000	1.000	1.000	1.000	1.000	1.000

Table 5.5 Data point statistics for the balanced data set

Before being presented to the completed ANN approximator the test parameters had to also be scaled. The maximum, $\max(V_{1..N})$, and minimum, $\min(V_{1..N})$, parameter values, listed in Table 5.5, were taken from the training set, substituted into Equation 5.6 and used to determine the scaled values of the test parameters. It was these scaled parameters, which comprised the test pairs. They were back-substituted into the ANN approximator to derive predicted values for Global F* and consequently discharge capacity.

5.10 Network Design and Training

5.10.1 The ANN modelling environment

A special type of ANN architecture, a Multi-Layer Perceptron (MLP) model was chosen to form the basis of the Global F* approximator. The MLP software simulation was built using the MATLAB Neural Networks Toolbox which is described in Demuth and Beale [1993]. It was supported on a Viglen 4DX266 personal computer. A back-propagation algorithm was chosen to train the ANN. An MLP was adopted in each of the successful input/output modelling applications described in Section 5.6.2.2 including Minns [1995] and Karunanithi et al [1994].

5.10.2 Optimal number of layers in MLP approximator

Hecht-Neilson [1990] showed that any non-linear, discontinuous function could be modelled using a MLP with 3 layers which complimented the findings of Kurkova [1990] who proved that any function could be approximated by, at most, 4 layers. The most successful applications that the author studied implemented 3 or less layers in their MLP architecture. Consequently, a 3 layer perceptron model was used to approximate the functional relationship between Global F* and the 9 input parameters.

Layer 1, the input layer, contains **m** nodes, Layer 2, the hidden layer, contains **n** nodes and Layer 3, the output layer, contains **p** nodes, as shown in Figure 5.8. The number of nodes in Layer 3, **p**, was set equal to 1. The number of nodes in Layer 1 and Layer 2 were chosen so that an optimal solution for functional approximation of Global F* was obtained after training.

The same transfer function was used for every node in each layer. In Layer 1 linear functions were used, f(n) =n. This was done to ensure all the weighted signals were scaled to the appropriate ranges for input into the subsequent Layers. In Layer 2, the use of asymmetric functions was recommended by Swingler [1996], consequently the Tanh(n) function was used. In Layer 3 the sigmoid function, Logsig(n) was used because it gave an output between 0 and 1 which matched the range of possible values that the dependant variable, Global F* could assume.

5.10.3 Selecting acceptable training error and time for training

The MATLAB Neural Network toolbox measured training error between output and training data in terms of the 'Summed and Squared Error' (SSE). The average RMS was easily calculated by dividing the value for SSE by 1378 (the number of training pairs) and square-rooting. The value of SSE was therefore inter-changeable with RMS. The MLPs which demonstrated the lowest values for SSE consequently produced optimal solutions with regard to modelling the training data.

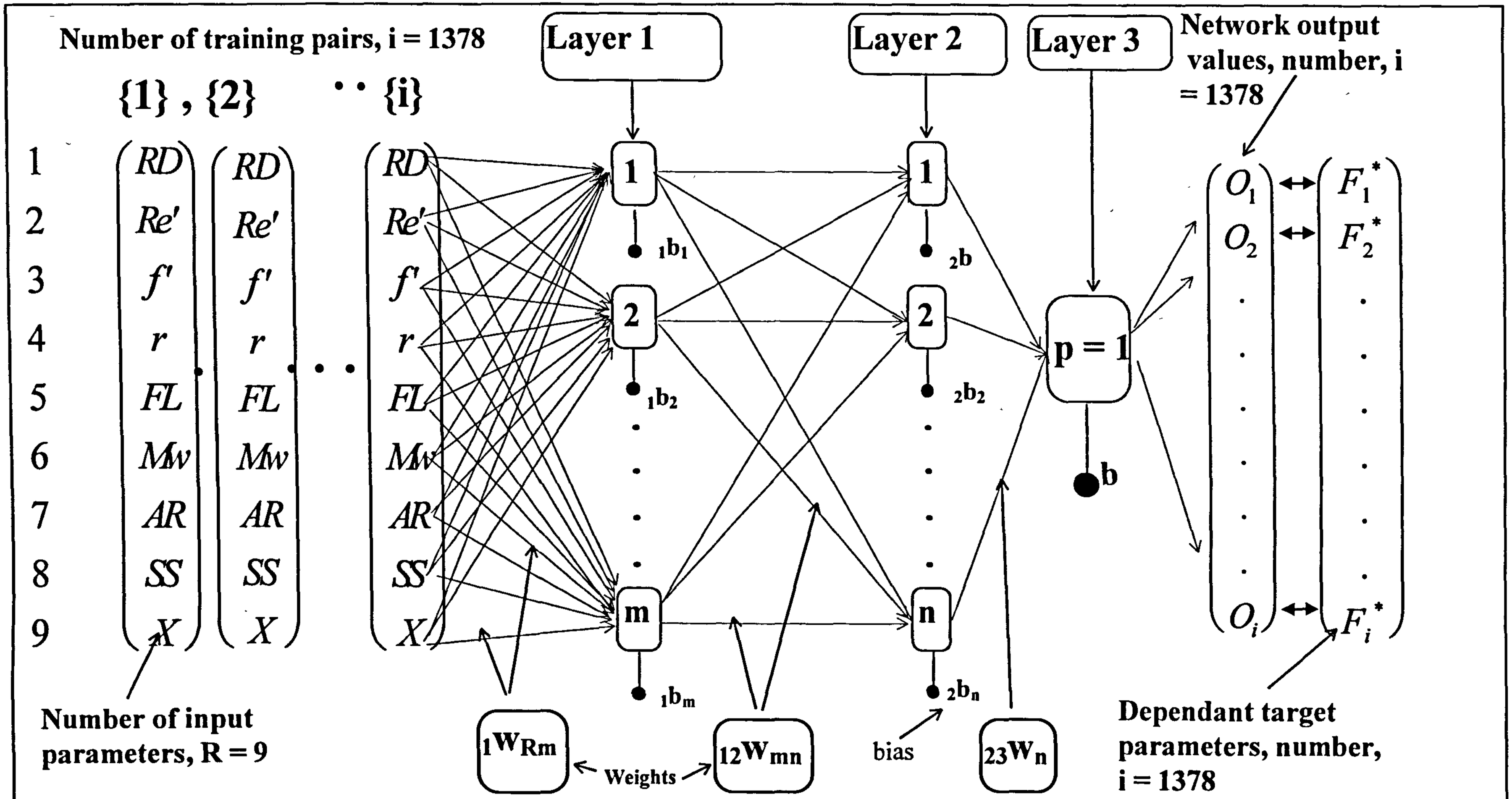

Figure 5.8 A three layer perceptron

However the attainment of the lowest SSE value during training was not the most important criterion by which to judge the MLP's performance. The performance of the MLP was most crucially judged according to its ability to generalise the functional relationship between Global F* and the 9 parameters when applied to the three independent test sets. The percentage difference in Root Mean Squared (RMS) error, averaged over all the training data points, between the predicted target values for Global F* and the measured target values was used to compare MLP architectures.

The choice of MLP architecture was further complicated by the excessive time it took to train some networks. Often many epochs were required before the RMS error values during training fell to acceptable levels. This placed a major constraint on the MLP design specifications because increasing the nodes in each layer increased the time taken to process one epoch exponentially.

Figure 5.9 shows a plot of the SSE value against an epoch for a typical MLP. During the testing programme the author showed that increasing the number of training epochs tended to reduce the value of SSE, however there was clearly an optimum number of epochs after which only slight improvements in the value of SSE were observed.

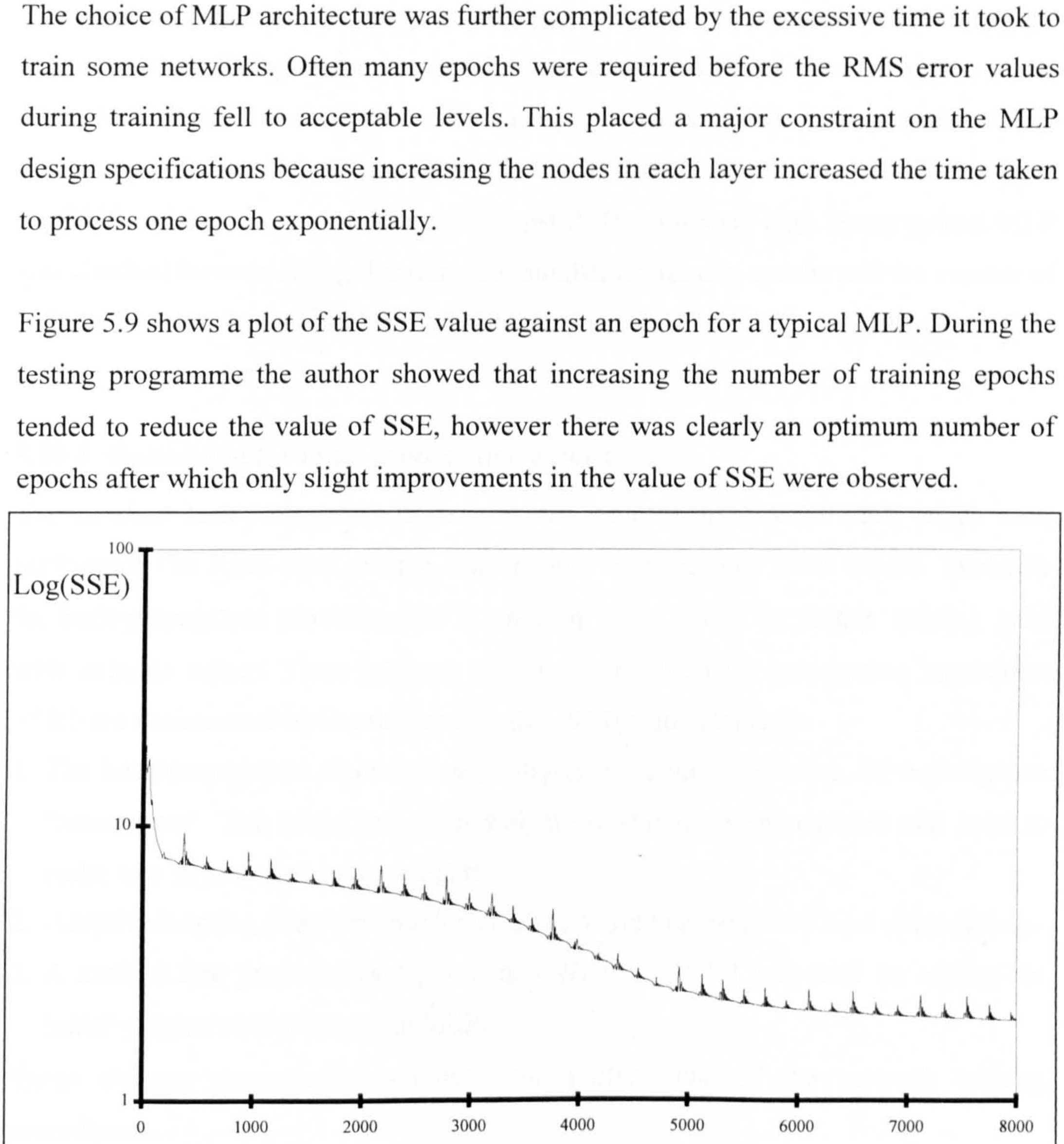

Figure 5.9 Log(Summed and squared errors) versus the number of training epochs

The time restrictions of running a training cycle with many epochs were often restrictive. For instance in a MLP with 10 nodes in Layer 1 and 2 it took 7 hours to process 5000 epochs. Many different MLPs needed to be trained before the optimal structure was identified therefore it was important to put both an epoch and SSE error restriction on training in order to make the trial and error approach feasible in the time available. A number of trials were performed to determine the range of acceptable epochs and SSEs that could be obtained during training.

The number of epochs also had to be carefully controlled to ensure that over-fitting did not occur. Over-fitting is characterised by the manner in which a network approximates a function. If a network function fits each point perfectly but a curve varies wildly between points then it has been over-fitted. Over-fitting was detected in MLPs where the RMS training errors were low and the test RMS error were high. Every trained MLP was checked for over-fitting. Limiting the number of training epochs and the number of weighted connections were identified as being good ways to avoid over-fitting.

5.10.4 Optimising the back-propagation algorithm

The standard back-propagation procedure gave poor results in some trials which were performed. The RMS error did not convergence to sufficiently small values. Typically the back-propagation procedure had a tendency to be biased by certain training pairs with extreme values. Three methods for improving the back-propagation procedures which are summarised by Demuth and Beale [1993] were adopted:

1. The back-propagation algorithm was adapted to make allowances for convergence 'momentum'. The recent trends in weight adjustment were recorded and used to make new adjustments to the weights
2. Adaptive learning rates were implemented to avoid biasing due to local data minima.
3. A method first proposed by Nguyen and Widrow [1992] was used for setting the initial weights and biases of the MLP.

These changes dramatically improved the performance of the network training procedures.

5.10.5 Number of nodes in Layers and the limits in RMS testing error

There is no set method for determining the optimal number of nodes in each layer, as the DTI guidelines [1996] acknowledged. A process of trial and error was used to identify the optimal MLP configuration. Swingler [1996] concurred with the need to adopt a trial and error process and suggested the following basic criteria to assist a designer to optimise an MLP:

- If the training error is low and the test error is high then there are too many weights, a number of nodes must be removed from some of the layers.
- If both the training and test errors are high then there are too few weights, additional nodes must be added to some of the layers.
- If the weights are very large then there are too few weights, a number of nodes must be removed from some of the layers.
- Ensure that the number of nodes in the hidden layer are less than in the input layer to aid the generalisation ability of the network.

Many combinations for the number of hidden layer, **n**, and input layer, **m** nodes were tried before the optimum MLP architecture to approximate the functional relationship between Global F* and the 9 parameters was determined.

5.11 Network Testing and error analysis

5.11.1 Selection of the optimal MLP approximator

Table 5.6 shows the results for 15 different sets of layer combinations and training times. The optimal MLP approximator was identified because it possessed the minimum RMS error values between target and output values for the training data sets. Also it yielded the smallest average (RMS) percentage error when the outputs derived, having presented the input parameters of the three test sets to the MLP approximator, were compared with the target values.

Using this assessment technique MLP12 was identified as the optimal approximator of the relationship between Global F* and the 9 key parameters. MLP12 possessed 12 input nodes and 7 hidden layer nodes and was trained for 8000 epochs. The programme

coding used to construct and train the neural network: MLP12 (using the MATLAB Neural Networks Toolbox) is listed in Appendix A4.

Config. Number	Nodes in Input layer, **m**	Nodes in Hidden layer, **n**	Training epochs	RMS Training	% Error (RMS) Test 1	% Error (RMS) Test 3	% Error (RMS) Test 3
MLP1	8	4	5000	0.047	11.3	23.2	27.2
MLP2	12	4	5000	0.041	7.9	17.2	26.7
MLP3	16	4	5000	0.037	9.7	15.6	23.6
MLP4	8	7	5000	0.035	7.5	16.9	23.5
MLP5	12	7	5000	0.031	7.4	18.4	20.2
MLP6	16	7	5000	0.025	8.6	19.2	20.1
MLP7	8	12	5000	0.029	24.2	18.4	31.7
MLP8	12	12	5000	0.024	7.3	15.6	21.1
MLP10	16	12	5000	0.03	6.9	17.4	22.0
MLP11	12	7	3000	0.031	8.9	14.2	19.2
MLP12	12	7	8000	0.019	6.5	14.2	19.2
MLP13	12	7	12000	0.018	7.2	16.24	25.5
MLP14	12	7	24000	0.0172	7.8	15.5	28.8
MLP15	12	7	50000	0.0134	7.5	18.7	30.2

Table 5.6 A sample of the MLP architectures tested and the training times

Although MLP12 performed better than the other MLPs which were developed it was important to assess in absolute terms the health of MLP12 after training, and the performance of MLP12 when it was used to predict the Global F* values for the various meandering compound channels which were included in the test sets.

5.11.2 Assessment of the health of MLP12 after training

Figure 5.10 shows the comparison between the actual and MLP12 output values of Global F* for the meandering compound flows which was obtained from MLP12 after training. The error spread ±10% with an RMS error value of 4%, which is satisfactory considering the range of experimental error possible in the initial measurements.

The DTI guidelines [1996] stipulated a further important technique for assessing the performance (health) of MLP12 after training. A comparison must be made between the frequency distribution of the magnitude of the weighted links between the nodes within the MLP for the untrained MLP12 and the trained MLP12 respectively.

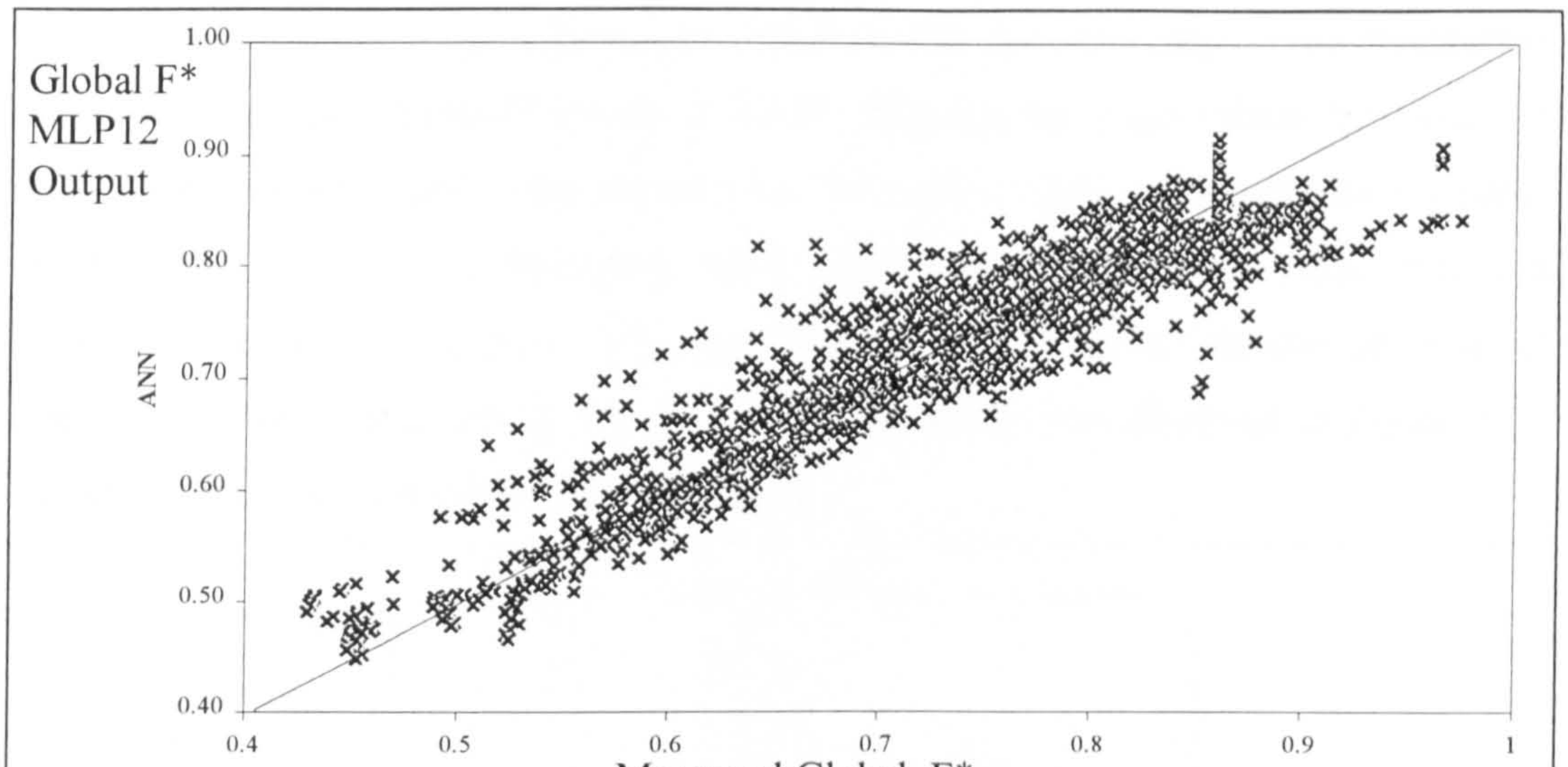

Figure 5.10 Actual F* versus Output F* predicted using the MLP12: Training data

The first criterion for a healthy MLP is that the initial weights are set in the range between +1 and -1. The initial weights for MLP12 are shown in Figure 5.11(a) and they clearly meet the criterion. Figure 5.11(b) shows frequency distribution of weights in the final network, MLP12. The nodal weights were spread in a normal distribution pattern. The majority of the weights had attained low values and maximum values were less than 10. According to Swingler [1996] this was a positive sign that MLP12 is a healthy (high performance) network. If after training the weights had not moved far from their initial values then sufficient learning would not have taken place in the MLP. If a majority of the weights had attained high values then this would have been evidence that the MLP was overfitted.

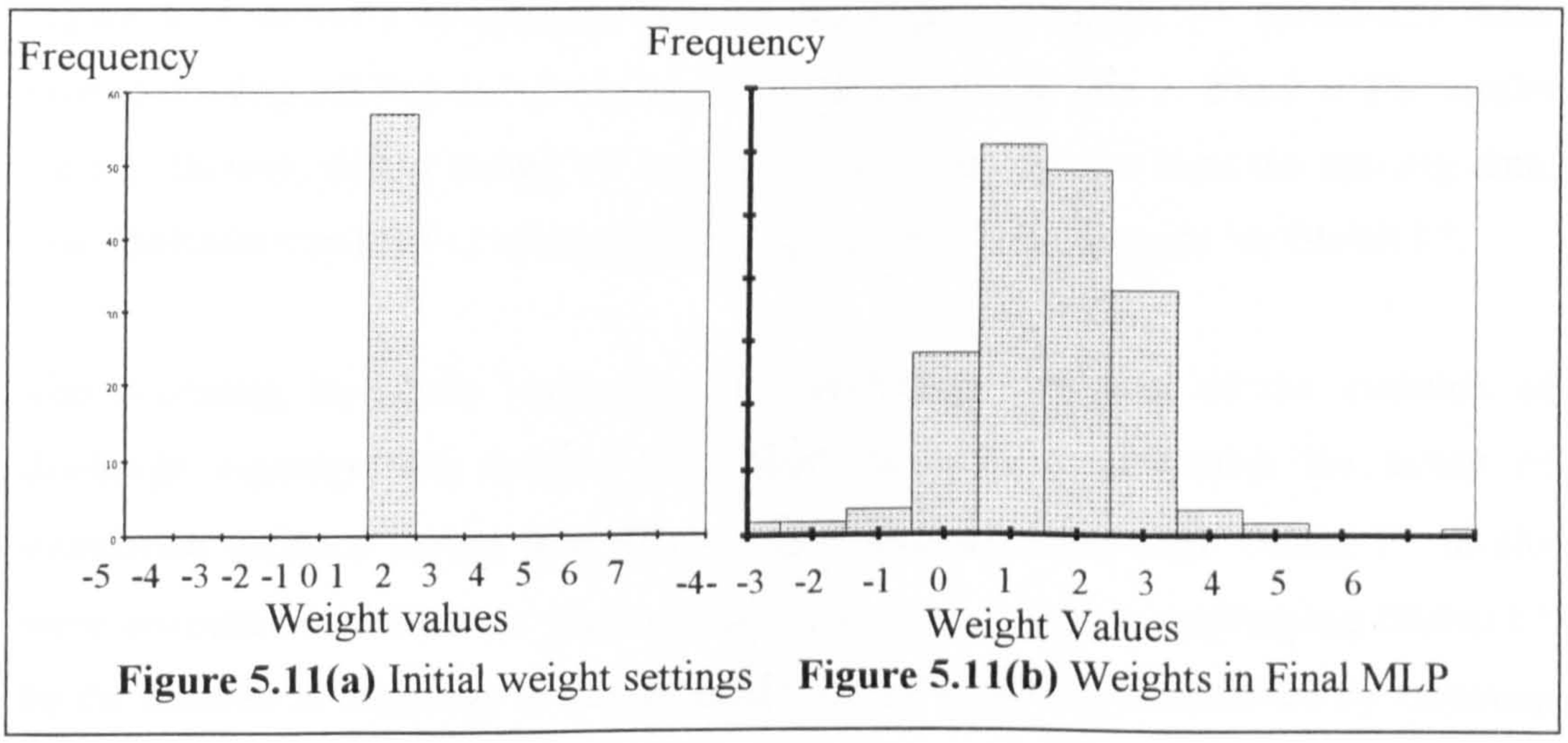

Figure 5.11(a) Initial weight settings **Figure 5.11(b)** Weights in Final MLP

Finally Figure 5.12 shows a histogram which details the percentage error distribution between the output Global F* (predicted by MLP12) and the target values for Global F* which were incorporated in the training set. Swingler [1996] suggested that a healthy MLP would yield a error histogram which would show a frequency peak around a percentage error value of zero which would quickly fall off as the number of errors of greater magnitude diminished. This pattern of behaviour was observed in Figure 5.12 which substantiates that MLP12 was healthy.

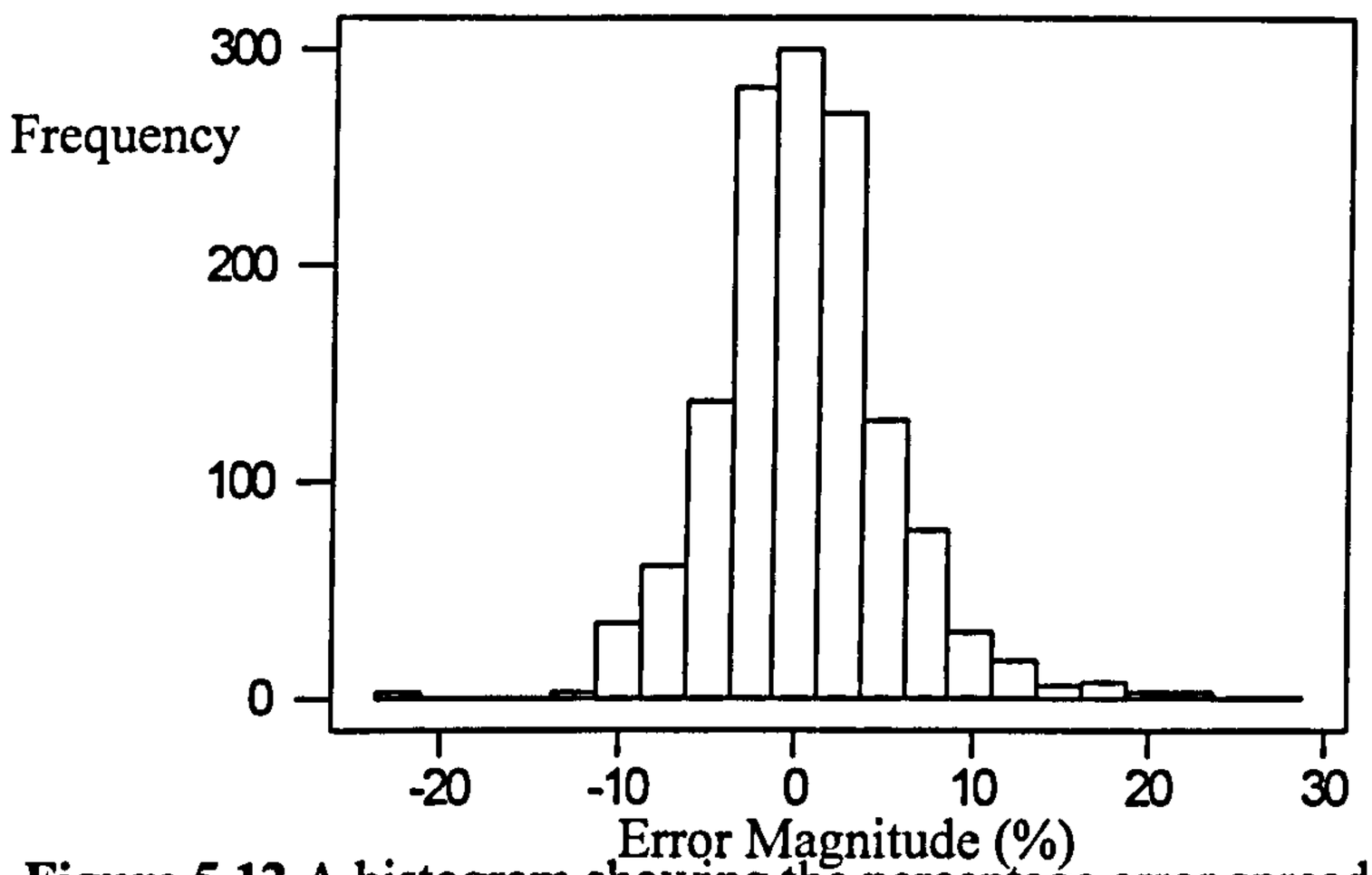

Figure 5.12 A histogram showing the percentage error spread for MLP12

5.11.3 The performance of MLP12 when predicting Global F* for the test sets

5.11.3.1 Introduction

Figure 5.13 shows a comparison between the measured Global F* values and those predicted using MLP12 for all the results contained in test sets 1, 2 and 3. The results are satisfactory, with a spread of data not significantly greater than the training data. This indicates that MLP12 produces generally acceptable predictions for Global F*.

The practising Hydraulic Engineer is predominantly interested in the variation of discharge capacity with relative flow depth in order to determine the extent of inundation suffered during river flood events. Consequently these Global F* results were converted to equivalent measures of discharge capacity by multiplying Global F* by the theoretical discharge in a compound channel which was determined by assuming

only bed friction forces resist the flow. The measured discharge capacity versus relative flow depth results were compared with the values predicted using MLP12.

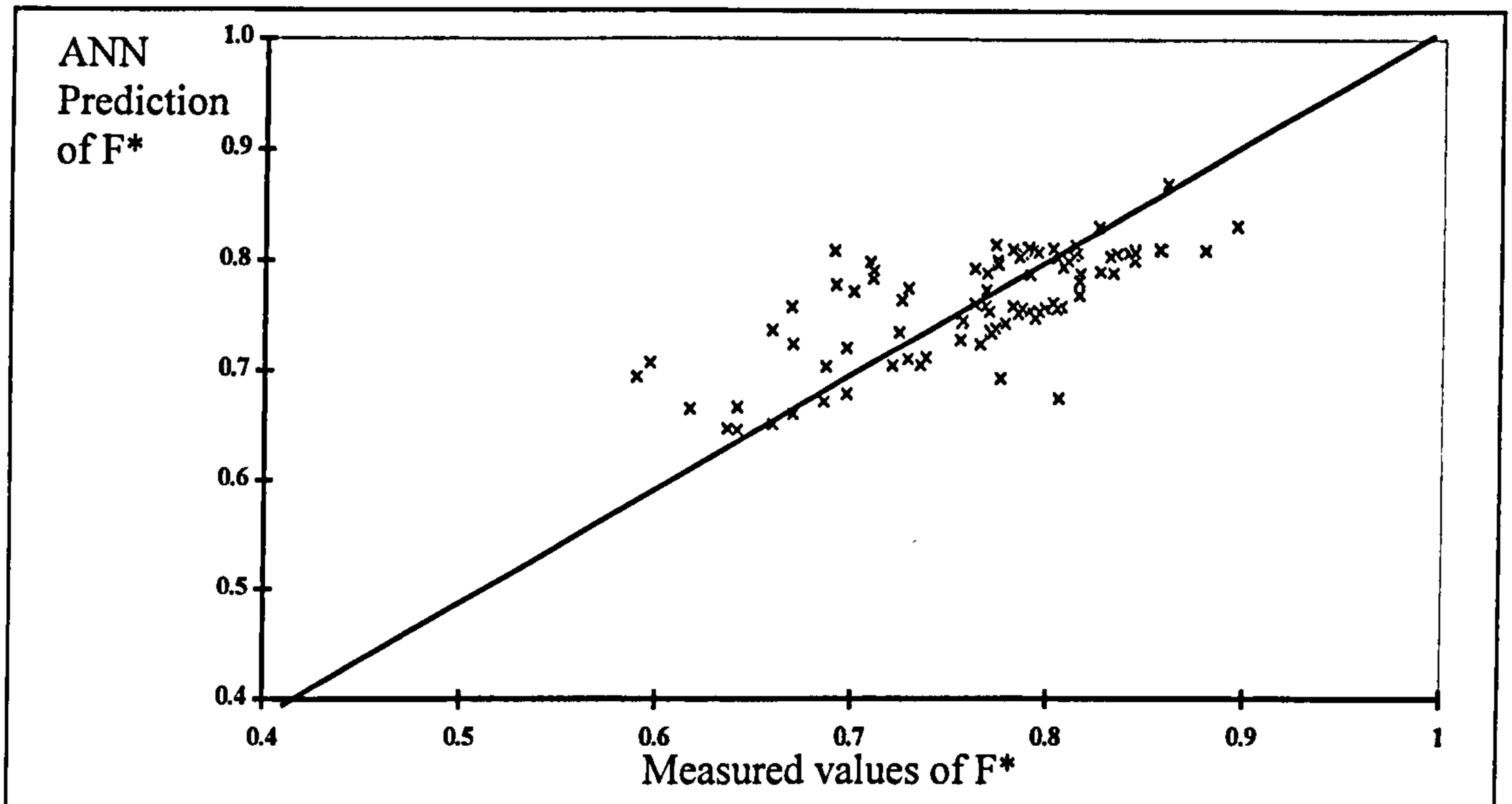

Figure 5.13 Measured F* values versus F* values predicted using the MLP: Test data

Both sets of results were also compared with the values which were predicted using the James and Wark [1] [1992] method (using identical assumptions for the geometric and roughness parameter values). The James and Wark [1] [1992] method was previously the most reliable method available for predicting the discharge capacity of a meandering compound channel. A selection of the discharge capacity and relative flow depth curves from each of the three test sets is presented and the implication of the results discussed.

5.11.3.2 Test set 1 (Training parameters within training range, Small scale models)

Test set 1 contained 4 sets of flow data, each of which possessed a range of values associated with their key parameters which were contained within the maximum and minimum range of the parameter values within the data sets which were used to train MLP12. When the test set 1 input parameters were presented to MLP12, the MLP was able to interpolate to obtain Global F* and hence determine the discharge capacity predictions for these particular models. No extrapolation was necessary.

Figure 5.14 shows plots of relative flow depth versus the measured and predicted discharge capacity for the model: G50N45R, which was tested in Glasgow as part of the

Series B extension (1993-1996) programme. Figures 5.14 and 5.15 show the same plots for SDKI301 and A3N750A which were performed by Kiely [1989] and in Aberdeen during the Series B extension (1993-1996) programme respectively.

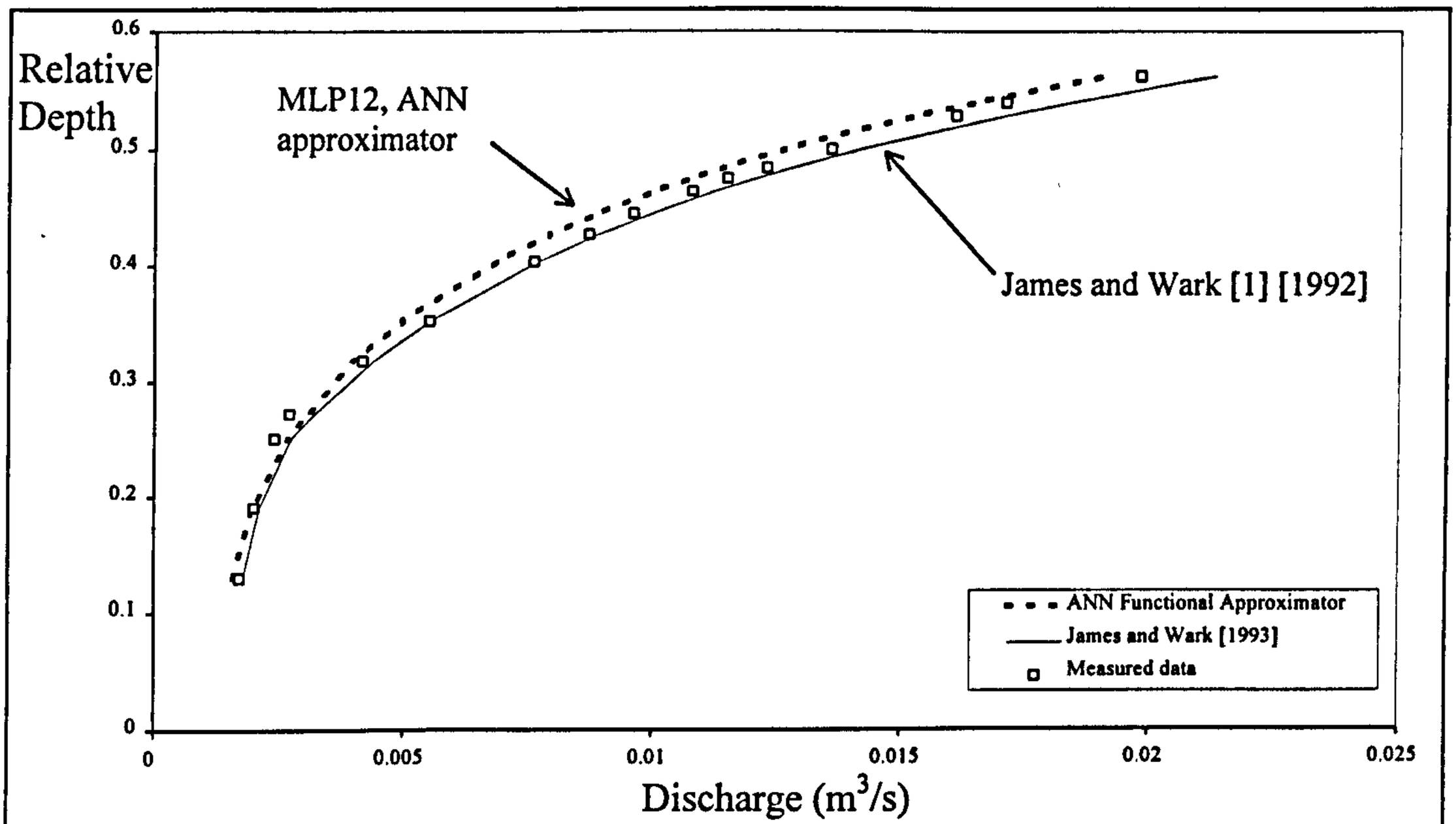

Figure 5.14 Relative depth versus Discharge for G50N45R (Series B ext. (1993-1996))

Figures 5.14 - 5.16 demonstrate that MLP12 predicts the discharge capacity of the G50N90R, SDKI301 and A3N750A more accurately than the James and Wark [1] [1992] method.

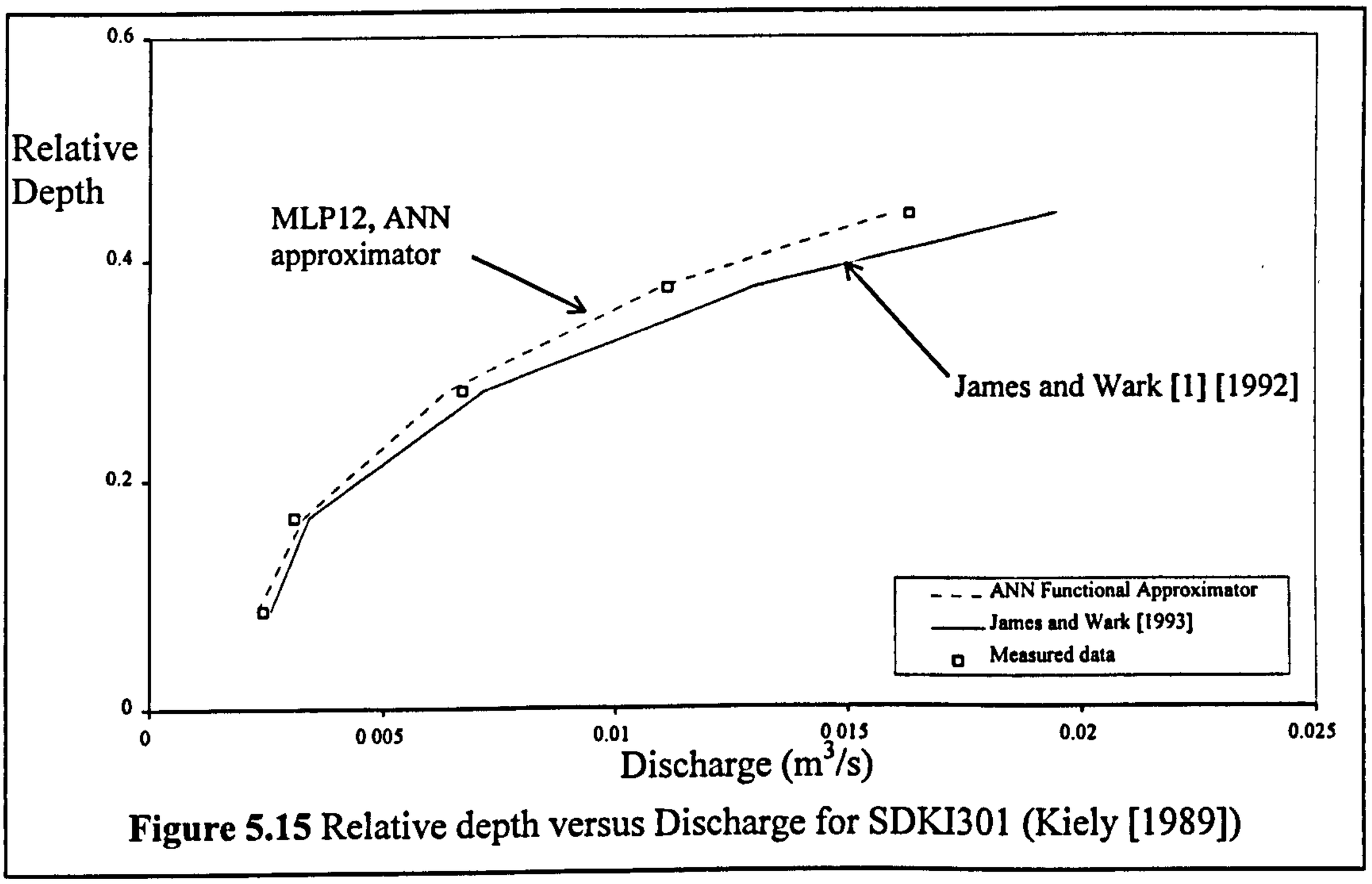

Figure 5.15 Relative depth versus Discharge for SDKI301 (Kiely [1989])

This observation is confirmed by Table 5.7 which compares the percentage difference (RMS) between the measured and predicted discharge capacities. Figures 5.14 - 5.16 also show that the James and Wark [1] [1992] model has a tendency to over-estimates the discharge capacity.

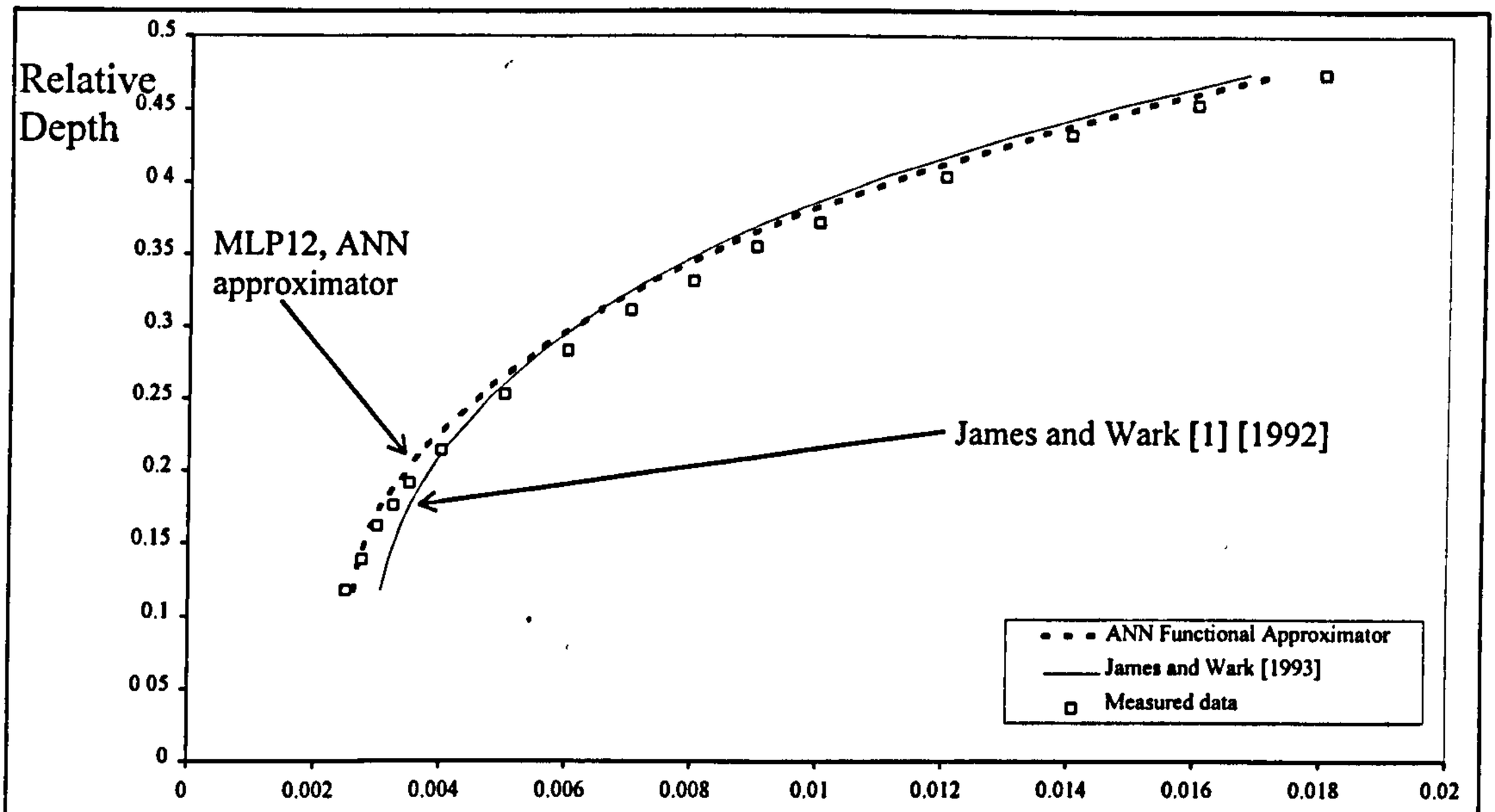

Figure 5.16 Relative depth versus Discharge for A3N750A (Series B ext. (1993-1996))

	MLP12				James and Wark [1] [1992]			
Ref. No.	Mean Q%	Std. Dev.	RMS Q%	Std. Dev.	Mean Q%	Std. Dev.	RMS Q%	Std. Dev.
G50N45R	-4.1	5.2	6.1	4.8	9.8	5.5	9.8	5.5
SDKI301	1.50	4.5	4.1	3.4	2.5	8.8	7.2	4.5
A3N750A	-2.7	3.4	3.1	1.7	6.1	8.6	6.4	4.5

Table 5.7 Comparison between the two discharge prediction methods

The trend is reversed when considering the measured and predicted discharge capacities for SDAB102 which are plotted in Figure 5.17. SDAB102 was tested at Aberdeen in 1991 and was reported by Willetts and Hardwick [1993]. Table 5.8 lists the percentage differences between the measured and predicted discharge capacities results for SDAB102. The James and Wark [1] [1992] method instead of over-predicting the discharge capacity of this channel actually predicts its discharge capacity comparatively accurately. The author suggests that this high level of accuracy can be explained because the results from Aberdeen (1991) were actually used to develop empirical adjustments

which were implemented in the basic James and Wark [1] [1992] method which was developed using the Series B data.

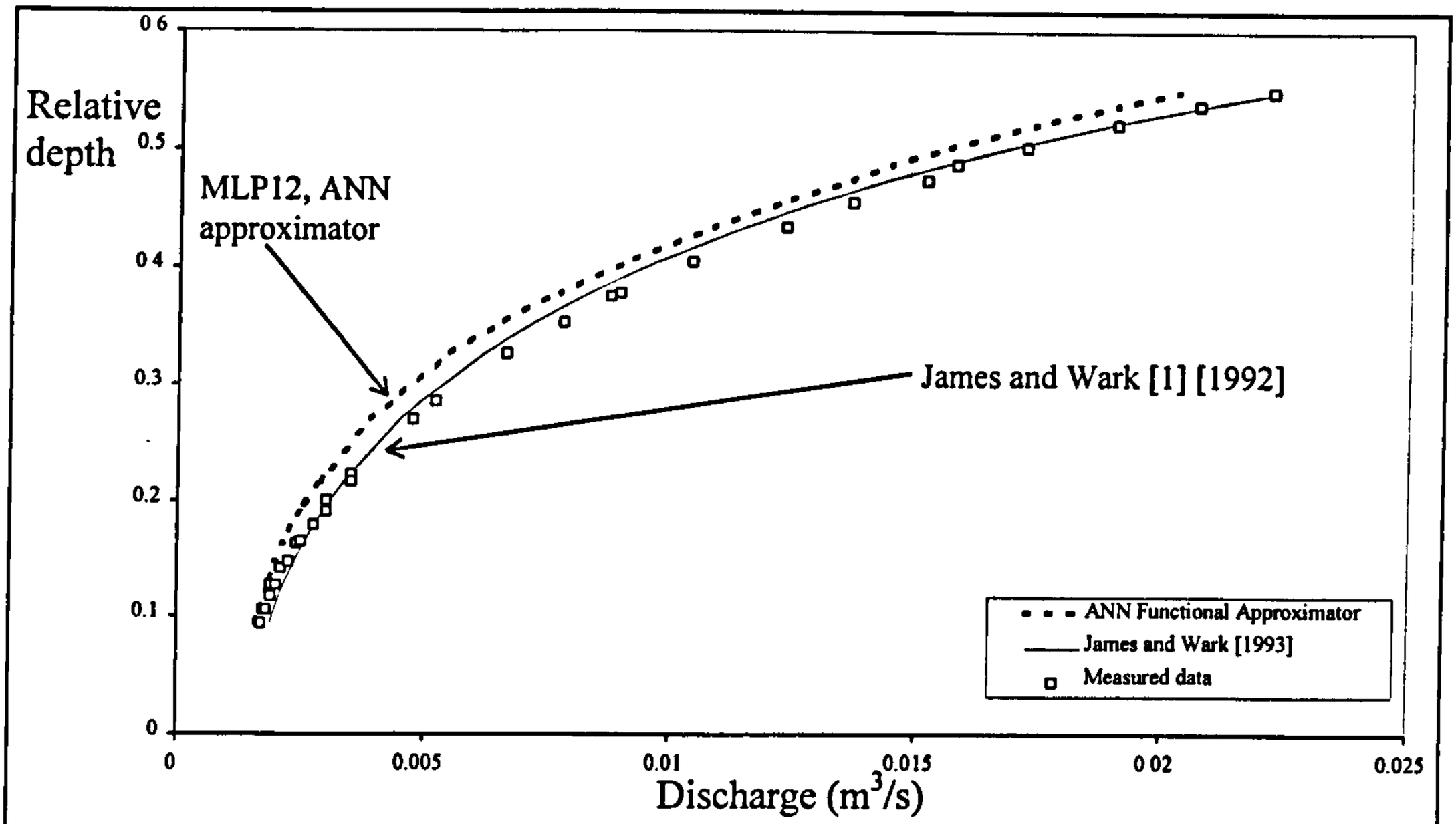

Figure 5.17 Relative depth versus Discharge for SDAB102 (Aberdeen (1991))

	MLP12				James and Wark [1] [1992]			
Ref. No.	Mean Q%	Std. Dev.	RMS Q%	Std. Dev.	Mean Q%	Std. Dev.	RMS Q%	Std. Dev.
SDAB102	-11.4	4.1	16.9	8.7	-2.1	3.6	3.9	2.4

Table 5.8 Comparison between the two discharge prediction methods

The author postulates that the James and Wark [1] [1992] method tends to over-predict discharge capacity when applied to small scale models because is was derived predominantly using the larger scale Series B (1989-1992) data. The Series B models were generally less affected than the smaller scale models by the increases in flow resistance due to layer interaction and so exhibited proportionately larger discharge capacities than the smaller exact scale models. Consequently, because the James and Wark [1] [1992] method was derived by empirically fitting the basic physical (prediction) models to the Series B (1989-1992) data, it over-estimate the discharge capacity predictions for smaller scale models. The exception occurs for the Aberdeen (1991) models for which the James and Wark [1] [1992] method predicts the discharge capacities particularly well. The author attributes this tendency to the further empirical adjustments that were included in the James and Wark [1] [1992] method which were

specifically tailored so that it would fit the Aberdeen (1991) data as well as the Series B (1989-1992) data.

The author postulates that the under-estimation of the discharge capacity of the Aberdeen (1991) test data is attributable to the peculiarities of the Aberdeen (1991) models' configuration. MLP12 was developed using training data which did not account for the extensive variation of relative meander belt width in small scale models. Consequently the author suggests that it is likely that the observed discrepancy is due to this lack of parameter coverage in the training data. Further training of MLP12 with additional data demonstrating the influence of meander belt and the other parameters, flood bank sinuosity and lateral flood plain slope should enable an enhanced MLP12 approximator to make more reliable discharge capacity predictions for models with more outlying parameter values.

In summary however MLP12 was been shown to generate more accurate predictions for the discharge capacity of the meandering compound channels for the majority of models in test set 1, compared with those obtained using the James and Wark [1] [1992] method.

5.11.3.3 Test set 2 (Training parameters outwith training range, Prototype channels)

Test set 2 contained 2 sets of flow data which related to the test results obtained from a study of the discharge capacity of the prototype (field-based) meandering compound channel built on the River Roding, Essex. Care had to be exercised when assessing the performance of the MLP12 prediction methods using test set 2 because the range of values associated with some of the key parameters in these channels extended outwith the maximum and minimum range of the parameter values associated with the data sets which were used to train MLP12. A degree of uncertainty in the predictions also exists because of the difficulty encountered trying to determine realistic roughness coefficients to natural channels. The configuration of the two channels was identical. The only significant difference was due to one channel having mown flood plains and the other the uncut grass.

Sufficient flow data was gathered in order to determine the flow resistance generated in the main channel at bankfull levels. The Manning's n for the main channel was measured in the field as equal to 0.044, it combined both the bed friction and the secondary circulation losses. The flood plains were attributed constant Manning's n values which were equal to 0.035 and 0.05 for the cut and uncut flood plains respectively (chosen to give 'maximum' confidence from the Chow [1959] tables) and were assumed constant over flow depth. The author postulates that the discharge capacity predictions are likely to be accurate for the cut flood plains because the constant Manning's n assumption was more likely to be accurate over the full range of flow depths and flow states for these flood plains. The uncut flood plains were likely to exhibit significant variation from the average Manning's n with varying flow depths. The flow resistance is likely to be very high at low flow depths and until the majority of the vegetation is overtopped after which the value for Manning's n is likely to decrease with increasing flow depth until it achieves a constant value. Unfortunately no field data was gathered during the River Roding studies to enable this variation in Manning's n to be explicitly determined.

Figure 5.18 shows plots of relative flow depth versus discharge capacity for the River Roding (with uncut flood plains).

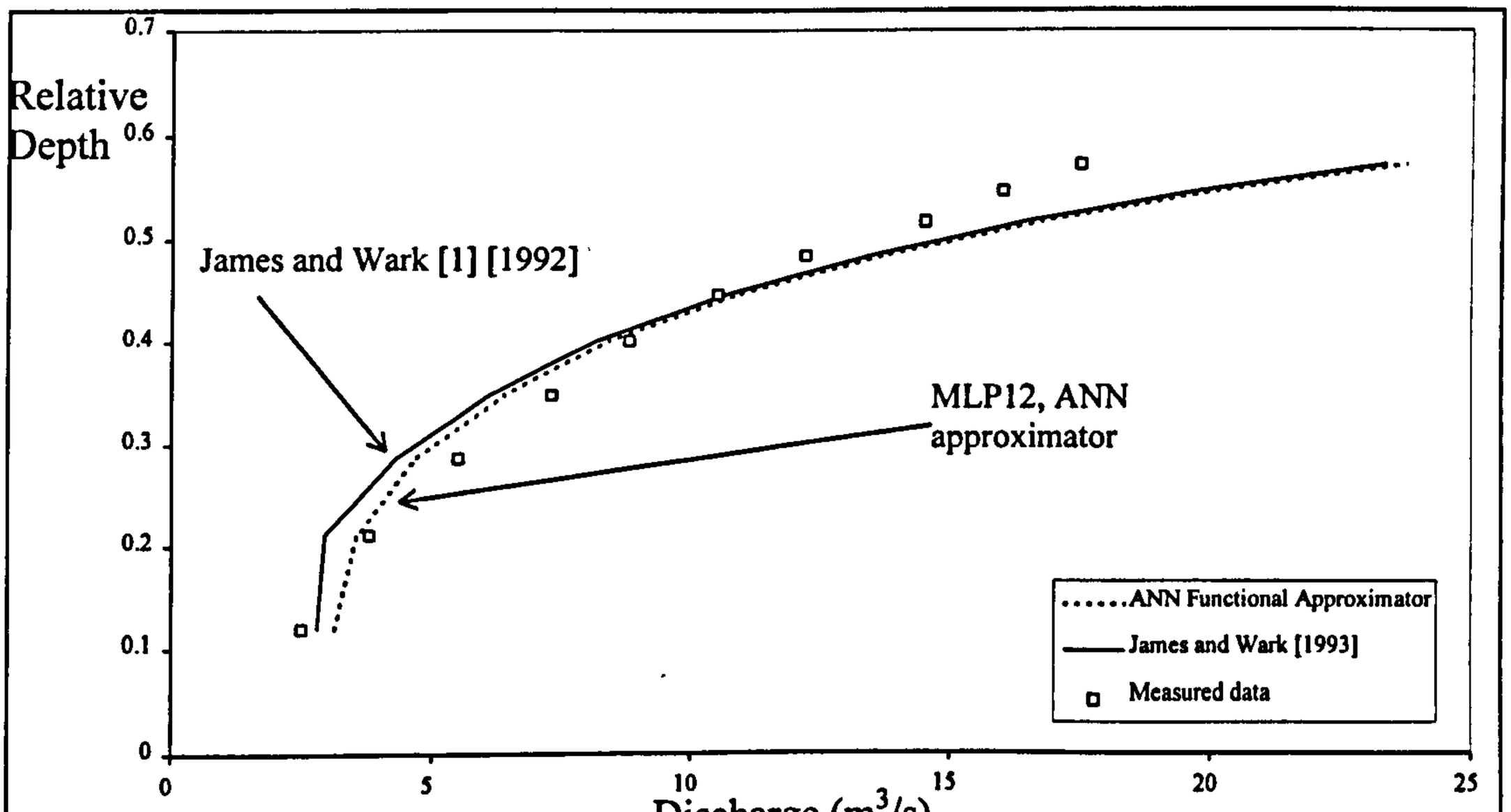

Figure 5.18 Relative depth versus Discharge for the River Roding (Uncut flood plains)

Three values for discharge capacity were plotted which included the measured values and predicted values using both MLP12 and the James and Wark [1] [1992] method. Figure 5.19 shows the differences between the measured discharge capacity and the predicted discharge capacity using MLP12 and the James and Wark [1] methods for the River Roding (with cut flood plains).

Figures 5.18 and 5.19 demonstrate that MLP12 predicts the discharge capacity of the River Roding cut and uncut marginally more accurately than the James and Wark [1] [1992] method. This observation is confirmed by Table 5.9 which shows the mean and RMS percentage differences in discharge capacity for each model when averaging over all flow depths. However both methods displayed significant differences when compared to the measured discharge values.

	MLP12				**James and Wark [1] [1992]**			
Ref. No.	Mean error	Std. Dev.	RMS error	Std. Dev.	Mean error	Std. Dev.	RMS error	Std. Dev.
R. Roding (Uncut)	-8.0	17.5	16.9	11.7	-2.6	19.2	17.6	10.6
R. Roding (Cut)	-5.0	14.9	12.5	8.5	-6.6	13.8	12.5	8.1

Table 5.9 Comparison between the two discharge prediction methods

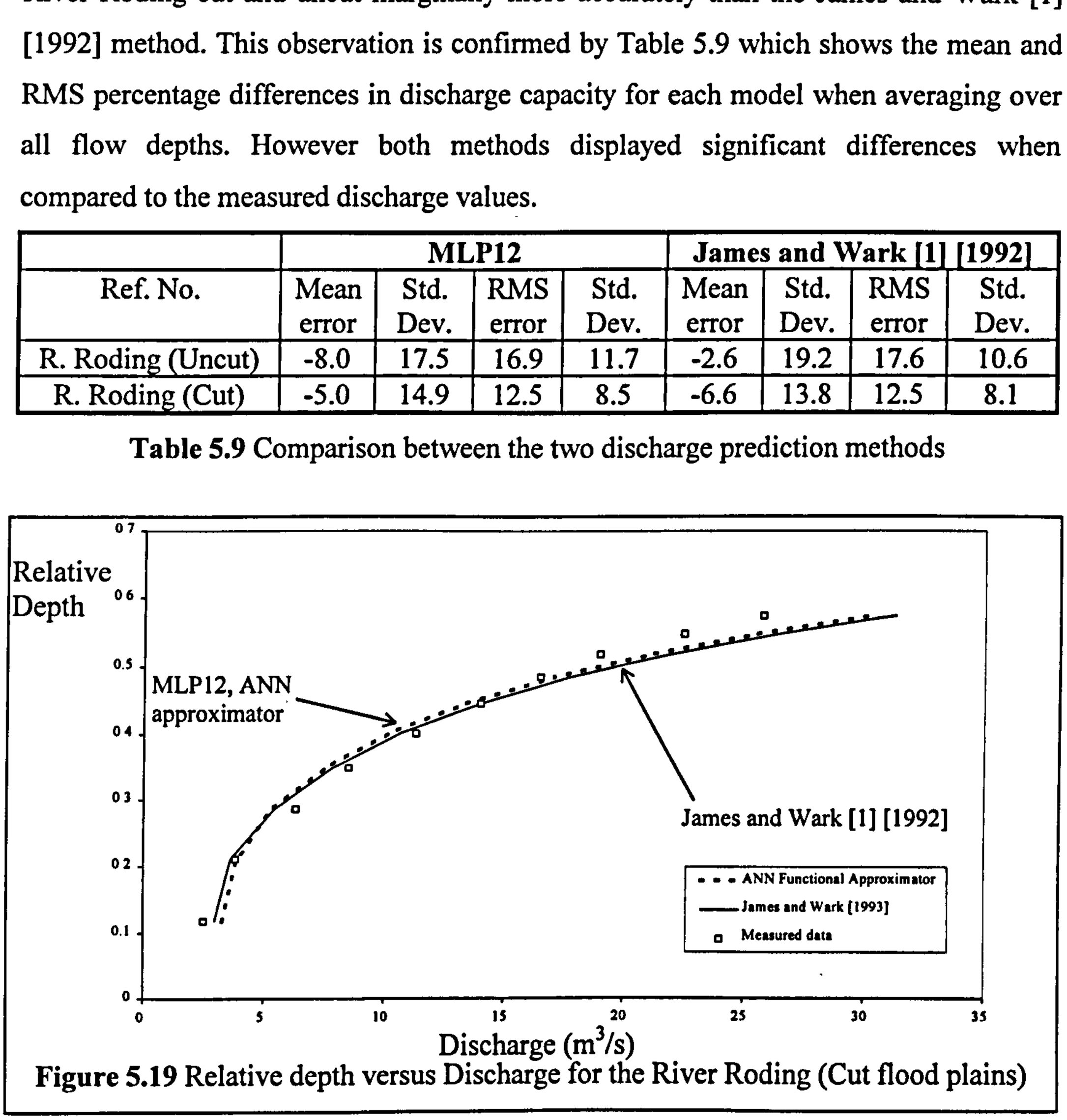

Figure 5.19 Relative depth versus Discharge for the River Roding (Cut flood plains)

The author suggests that the significant discrepancy between the measured and predicted discharges for the River Roding tests, although attributable in part to the deficiency in Manning's n assignment, is also attributable to the lack of allowance for two key

parameters, lateral flood plain slope, S_L, and flood plain channel sinuosity, r_u in both the MLP12 and the James and Wark [1] [1992] methods.

Both methods under-estimate the discharge capacity at low flow depths. The author suggests that this phenomenon occurs because of the presence of a lateral flood plain slope in the River Roding which is likely to have had the effect of reducing the extra flow resistance generated by layer interaction in meandering compound channels at low flow depths (as Sellin [1995] observed). Neither the MLP12 nor the James and Wark [1] [1992] methods cater for the influence of lateral flood plain slope.

Both methods over-estimate the discharge capacity at high flow depths. The author suggests that this phenomenon occurs because at high flow depths (possibly above a certain depth threshold judging by Figures 5.18 and 5.19) the flow resistance caused by the sinuosity of the flood plain begins to have a significant effect. Neither of the models cater for the influence of flood plain sinuosity. The flood plain sinuosity will reduce the average velocity of flow in the flood plain thus lowering the overall discharge capacity. The author also suggests that the influence will be so marked because the reduction in average velocity will also have an impact on the flow layer interaction mechanisms that are generated. The interaction mechanisms were shown in Chapter 4 to depend on the relative flow characteristics in the upper and lower layers in a compound channel.

5.11.3.4 Test set 3 (Training parameters outwith training range, various scale models)

Test set 3 contained 6 sets of flow data. Care had to be exercised when assessing the performance of the MLP12 prediction methods using test set 3 because the range of values associated with some of the key parameters in these channels extended outwith the maximum and minimum range of the parameter values associated with the data sets which were used to train MLP12.

Two representative sets of results from test set 3 are presented. Figure 5.20 shows plots of relative flow depth versus the measured and predicted discharge capacity for the larger scale model: SDB25 (Series B (1989-1992)), predicted using both MLP12 and James and Wark [1] [1992] methods. Figure 5.21 shows plots of relative flow depth

versus the measured and predicted discharge capacity for the larger scale model SDVB201 (Vicksburg [1956]), predicted (using both MLP12 and James and Wark [1] [1992] methods). Significantly the predictions obtained using MLP12 for the test set 3 data exhibit the similar level of accuracy which was achieved when analysing test set 1 but the author notes that parameter values were not very far removed from the range of the training data parameters.

The author concludes that MLP12 is still able to fairly accurately predict the discharge capacity of various compound channels even when the input parameters require extrapolation. However logically there must be a limit to this ability which will have to be determined over time when further suitable data sets are produced. Until then, careful appreciation of the limitations of the MLP12 will enable an Engineer to use it with confidence.

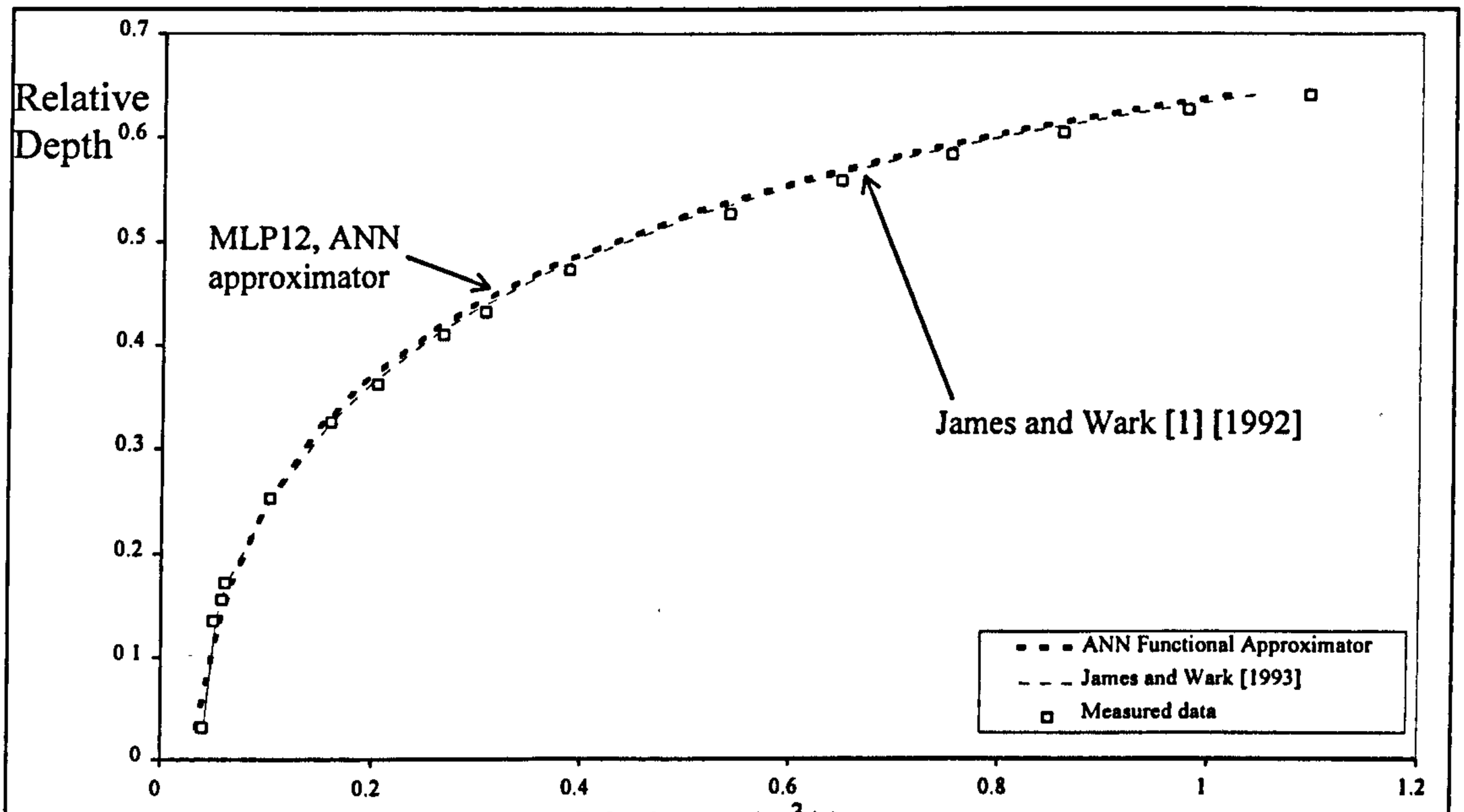

Figure 5.20 Relative depth versus Discharge for SDB25 (Series B (1989-1992))

Table 5.10 shows a comparison of the percentage errors produced by the two prediction methods for tests: SDB25 and SDVB201. The James and Wark [1] [1992] method predicts the discharge capacity of SDB25 with slightly more accuracy than MLP12 method but this was expected because the James and Wark [1] [1992] method was developed using the flow data from SDB25. MLP12 actually predicted the discharge

capacity for SDVB201 with more accuracy than was achieved using the James and Wark [1] [1992] method.

	MLP12				James and Wark [1] [1992]			
Ref. No.	Mean error	Std. Dev.	RMS error	Std. Dev.	Mean error	Std. Dev.	RMS error	Std. Dev.
SDB25	-4.9	7.4	6.2	3.5	-1.8	3.4	3.3	1.4
SDVB201	-3.1	8.9	9.9	7.1	5.6	3.5	5.0	2.4

Table 5.10 Comparison between the two discharge prediction methods

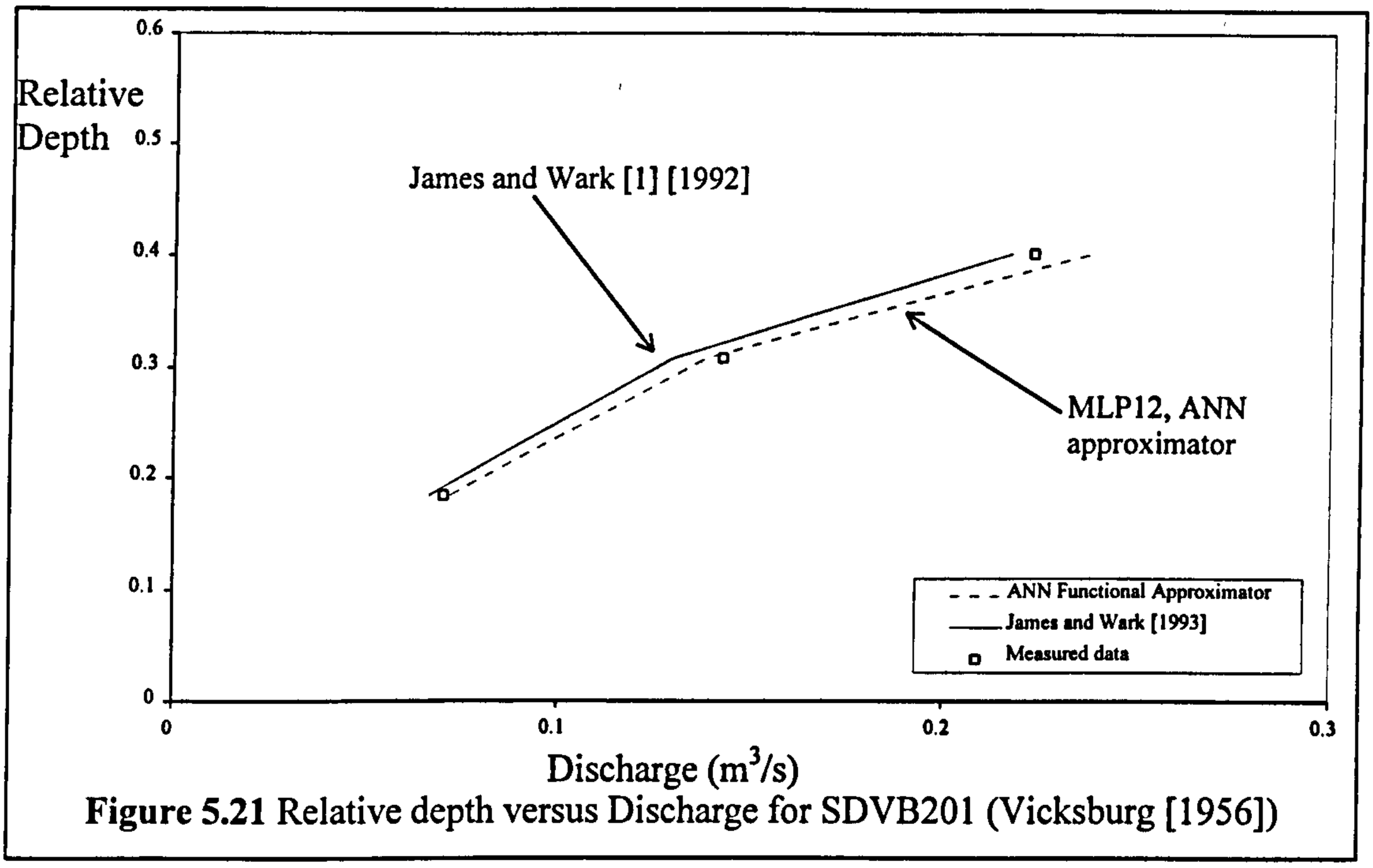

Figure 5.21 Relative depth versus Discharge for SDVB201 (Vicksburg [1956])

5.12 Implementation of the ANN approximator (MLP12)

The neural network: MLP12 is an input/output mapping approximator. Its functional characteristics were established by fine-tuning the weighted connections between the simple functional processing nodes comprising the neural network during training. It can be used whenever predictions for the discharge capacity of a new meandering compound channel are required. The appropriate values for Global F* will be determined for each 9 element input vector (detailing the parameter values in the channels) which are presented to the input/output mapping machine. The author integrated this machine with a 1-dimensional numerical river model so that MLP12 was used to calculate Global F* and hence determine the variation of the conveyance

capacity of a river channel at the intermediate cross-sections in the model. The conveyance predictions for channels with a uniform cross-section were used to analyse a natural river with varying geomorphology by assuming that suitable representative cross-sections could be produced which would (when combined) replicate the actual conveyance characteristic generated in a natural river. Examples of these one dimensional models are presented in Chapter 7.

Any Hydraulic Engineers wishing use the MLP12 approximator can find it on World Wide Web at http://www.civil.gla.ac.uk/. When accessing the ANN approximator (MLP12) the user should understand that it is has been shown to generate accurate predictions for discharge capacity for the majority of meandering compound channel models that is available (with parameter ranges within those used in the training data when formulating it). However MLP12 still needs to be modified to account for lateral flood plain slope, flood plain sinuosity and to make further allowance for scale differences on Threshold 1/2 in the future and can be further improved by training it with additional relevant flow data when it becomes available.

5.13 Summary and conclusions

5.13.1 Development of the Artificial Neural Network approximator

- The author trained an ANN functional approximator to reproduce the relationship between the non-dimensional discharge coefficient, Global F* and 9 influential geometric and roughness parameters using data which was gathered during the Series B extension (1993-1996) programme.
- The author applied the Department of Trade and Industry (DTI) Guidelines [1996] in order to demonstrate that an ANN approximator was more suitable than a polynomial approximator to model the Global F* versus 9 parameter relationship.
- The author showed that an Artificial Neural Network, labelled MLP12, was the optimal functional approximator for the Global F* versus 9 parameter relationship demonstrated by the 1378 training pairs which were collated during the Series B extension (1993-1996) programme. MLP12 incorporated a 3 Layer Perceptron architecture which was trained over 8000 epochs using a back-propagation algorithm.

- The incorporation of the novel parameter Relative Reynolds number, Re', as one of the 9 parameters enabled MLP12 to account for the influence of scale on Threshold 2/3. Relative Reynolds number, Re', was used to identify the flow depths corresponding to Threshold 2/3 in the relative depth versus Global F* plots.
- The author concluded that an independent test set, which consisted of 184 data pairs drawn from a representative selection of small, medium and prototype flow data, was suitable for testing the ANN approximator according to the DTI [1996] criteria.
- The discharge capacity of a meandering compound channel is predicted using the ANN approximator by multiplying the Global F* value, which is produced when the 9 parameters are presented to MLP12, by the theoretical discharge capacity of the channel when bed friction is the only source of flow resistance.

5.13.2 Comparing the performance of the ANN and James and Wark [1] methods

- The ANN approximator, MLP12, generates more accurate predictions for the discharge capacity of meandering compound channels than can be achieved using the James and Wark [1] [1992] method when the parameters of the test set are within the training set parameter range.
- If the parameters of the test set were significantly outwith the training set parameter range then the performance of the MLP12 significantly deteriorates and the James and Wark [1] [1992] method tends to generate more accurate predictions for the discharge capacity.
- MLP12 was tested against the flow data taken from the River Roding. This was the only available set of field data. MLP12 produced marginally more accurate discharge capacity predictions than the James and Wark [1] [1992] method.
- The author noted that there is a significant discrepancy between the predictions produced by both methods and the measured River Roding data. The author proposes that this difference is attributable to the limitations in the bed friction coefficient estimation and the non-inclusion of an allowance for the influence of lateral flood plain slope and flood bank sinuosity in both methods.
- The author notes that the ANN approximator, MLP12, is much simpler to use than the James and Wark [1] [1992] model. It only requires that the 8 parameters

corresponding to the relative depths of interest are presented to the model to determine the Global F* for a meandering compound channel.

- The ANN approximator, MLP12, is supported in a Matlab neural network toolbox software environment as an input/output functional operator and is accessible over the Internet on Web site http://www.civil.gla.ac.uk/.
- The author notes that it will be relatively simple to update MLP12 when additional meandering compound channel flow data is produced. Any new flow data needs to be presented to the ANN approximator in order to train it further. This will integrate the new flow data with the flow behaviour already observed and learnt by the original approximator.

Chapter 6

6. Enhancement of the James and Wark method for predicting the discharge capacity of meandering compound channels

6.1 Introduction

In 1992 Chris James and James Wark produced a semi-empirical, semi-physical method for predicting the discharge capacity of a meandering compound (2-stage) channel. The flow cross-section was sub-divided into 3 zones and correction factors were applied to simplified formulations for predicting zonal discharges in order to account for the contribution of the flow layer interaction losses. The method was developed using sparse flow data gathered during the Series B (1989-1992) programme. This chapter describes the development of an enhanced version of the James and Wark [1] [1992] method which utilises all the new flow data obtained during the Series B extension (1993-1996) programme and accounts in greater detail for the influence of the 11 key parameters on flow behaviour. In order to avoid confusion, the author's enhanced version of the James and Wark [1] [1992] method was named the Enhanced zonal method.

The Enhanced zonal method was developed by the author as part of the Series B extension programme (1993-1996). The Series B extension programme was performed by a collaborative team from the Universities of Glasgow, Aberdeen and Bristol. The team produced results which significantly extended the scope and range of the physical model data that was available for meandering compound channels. The new results revealed further details about the nature of the flow behaviour in meandering compound channels and facilitated the development of the Enhanced zonal prediction method. The Enhanced zonal method predicts the discharge capacity of each flow zone independently in a similar fashion to the James and Wark [1] [1992] method. However an alternative technique was adopted for labelling flow zones, A, B, and C, as shown in Figure 6.1, in

order to avoid confusion with the four flow regions which were shown in Chapter 4 to be characteristic of meandering compound channel flow.

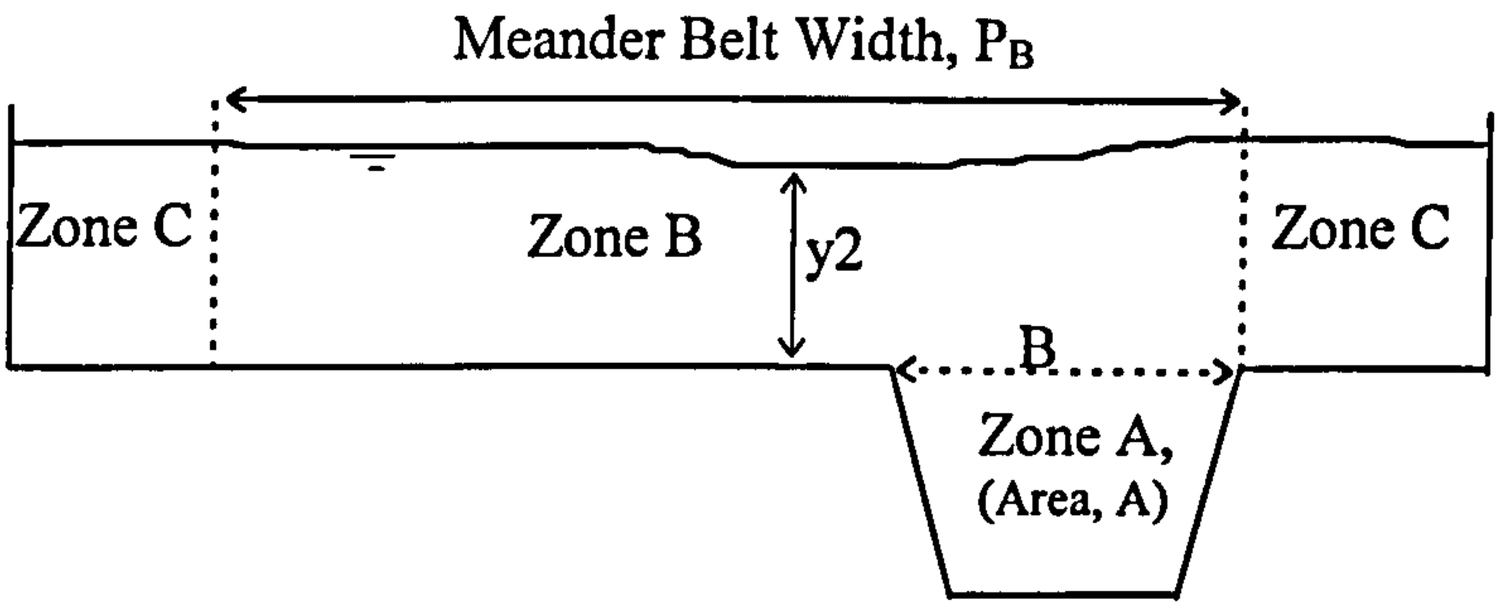

Figure 6.1 Compound channel zonal divisions for the Enhanced zonal method

6.2 Flow behaviour in Zone A (the main channel below bankfull)

6.2.1 The James and Wark [1] [1992] method

The magnitude of discharge in Zone A (below bankfull level) during overbank flow is less than bankfull discharge Q_{bf} (when there is no overbank flow) for the majority of flow depths encountered. If the average Zone A discharge during overbank flow is Q_A then this can be related to the bankfull discharge by a non-dimensional adjustment coefficient, Q_A', as shown in Equation 6.1.

$$Q_A = Q_A' * Q_{bf} \qquad [6.1]$$

The relationship between Q_A' and the relative flow depth, y' (defined using Equation 2.71) was modelled by James and Wark [1] [1992] by performing regression analysis of the Series B extension results and by dividing the flow behaviour into two separate flow regions as illustrated in Figure 6.2. The author will refer to these separate flow regions as flow region A1 (low flow depths) and flow region A2 (high flow depths).

By using the Series B (1989-1992) experimental results for Zone A, James and Wark [1] [1992] demonstrated that in flow region A2 Q_A' increases monotonically with increasing relative depth from a minimum value of Q_A' which is found at low flow depths. James and Wark [1] [1992] developed a method to model the behaviour of Q_A' in flow region A2 which was based on a linear regression fit using the Series B data. They related Q_A' to relative depth (y'/(A/B)) and the four other parameters which were tested during the Series B (1989-1992) programme:- aspect ratio, AR, relative depth, RD, relative

roughness, f', and sinuosity, r. The regression model formulations are shown in Equations 2.66-2.71.

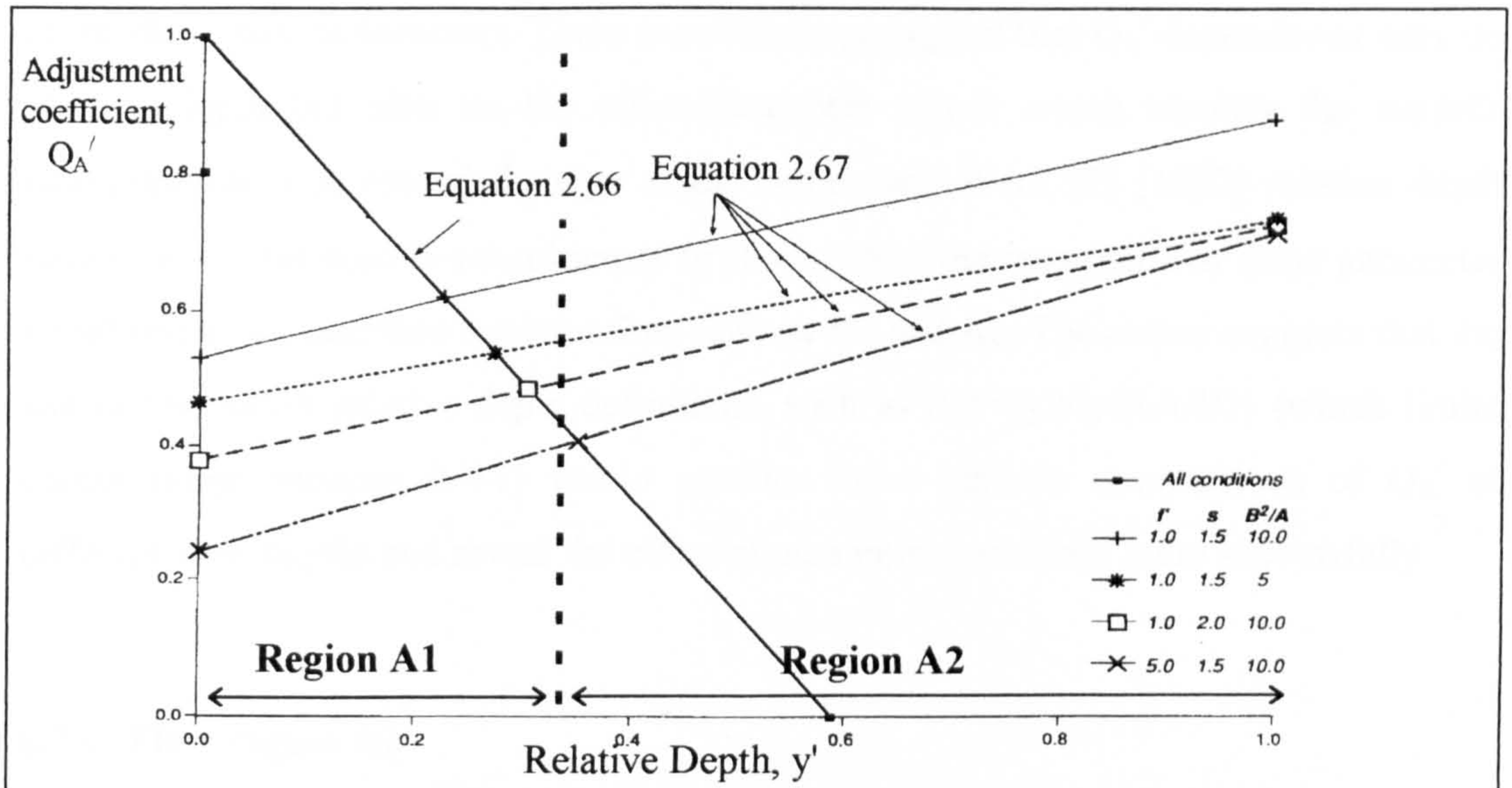

Figure 6.2 Q_A' versus relative depth: Series B data (after James and Wark [1] [1992])

James and Wark [1] [1992] also developed a method to model the behaviour of Q_A' in flow region A1 which was based on a linear regression fit which assumed that Q_A' was solely dependent on relative depth. The regression model formulation is shown in Equation 2.65. The regression fit for flow region A1 was obtained using only two data points to illustrate the characteristic monotonic decrease in the magnitude of Q_A' at low relative depth which is characteristic of flow region A1. Experimental limitations prevented more data points from being obtained within flow region A1. The two data points in flow region 1, which were used in the regression analysis, were determined at bankfull depth, y2 = RD = 0, and at the beginning of flow region A2, which was assumed to coincide with the value of Q_A' which corresponds to the lowest measured relative depth. Q_A' was set equal to 1 when RD=0 by definition. Q_A' and RD was measured directly from the flow region A2 plots.

6.2.2 Limitations of the James and Wark [1] [1992] method

6.2.3 Flow region A1

Figure 6.3 shows some typical plots of Q_A' versus relative depth, y', for G75T45R, G50T45R and G25T45R which were collected at Glasgow during the Series B extension

programme. Figure 6.3 gives an indication that the basic assumption made by James and Wark [1] [1992] for flow region A1, where Q_A' depends solely on the relative depth in all models, may be incorrect. There is evidence to suggest that Q_A' depends not only on relative depth but also on the other parameter values which identify the model's configuration. The extended range of the James and Wark [1] [1992] relative depth definition, y', between $0 \rightarrow \infty$, obscures to some extent the magnitude of these parameter variations at the interface between flow regions A1 and A2. The author suggests that the use of alternative relative depth definitions, such as RD={y2/(y2+A/B)} (which limits output range between $0 \rightarrow 1$) would produce more realistic comparisons of Q_A' at different flow depths and reveal the effect of parameter variations more successfully.

6.2.4 Flow region A2

The limited scope of the Zone A data collected during the Series B (1989-1992) programme in flow region A2 resulted in James and Wark [1] [1992] having to use a linear expression to model flow region A2. However, the author demonstrated (during the Series B extension (1993-1996) programme) that the relationship between Q_A' and relative depth, y', exhibits tendencies to be non-linear. Figure 6.3 shows typical plots of Q_A' versus relative depth (y'/(A/B) for G75T45R, G50T45R and G25T45R.

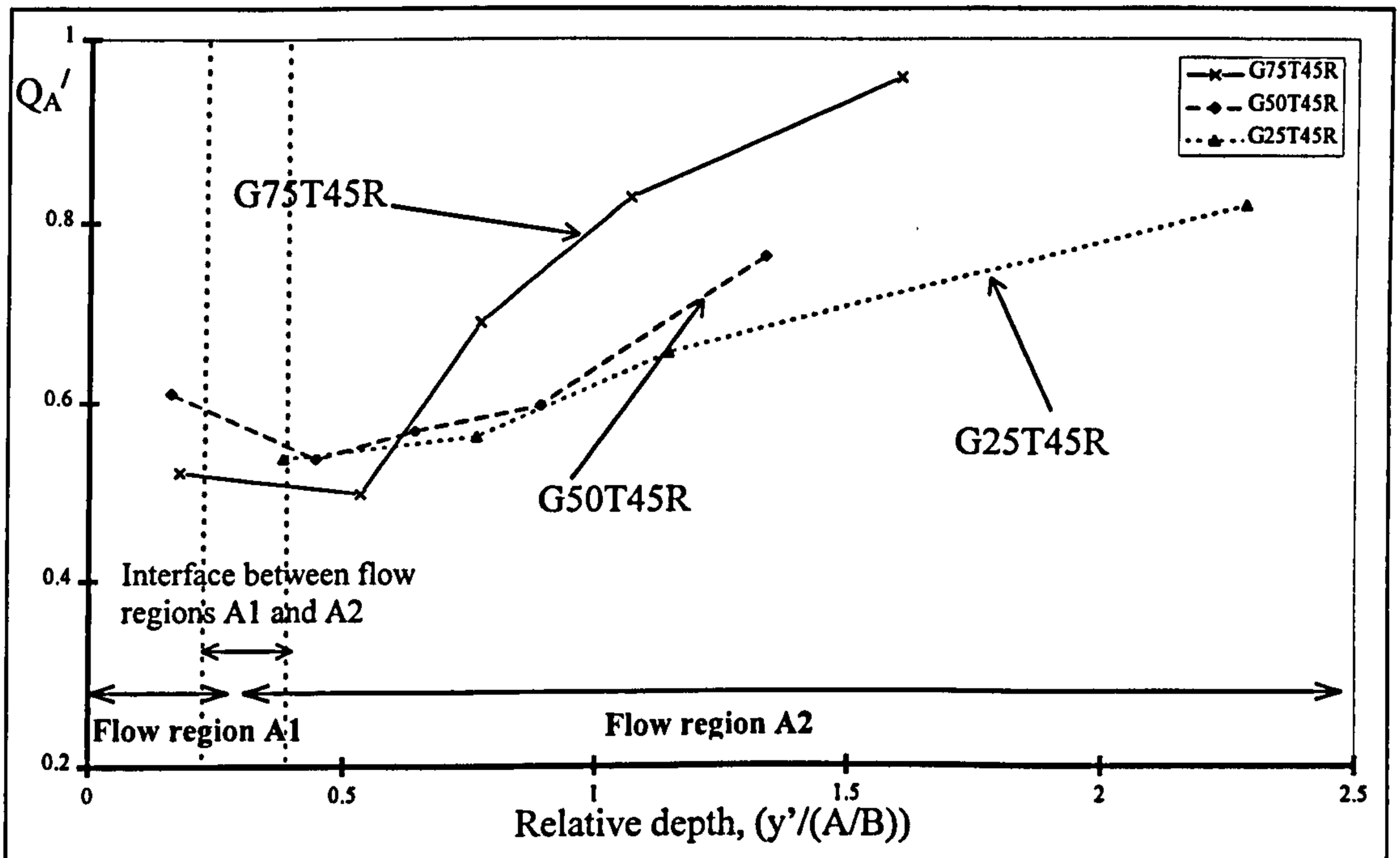

Figure 6.3 Q_A' versus relative depth for G75T45R, G50T45R and G25T45R.

Even though the extended range of relative depth magnitude calculated using the James and Wark [1] [1992] definition, y', obscures the effect, there is evidence, in Figure 6.3, to suggest that there is a complex non-linear dependency between flow behaviour in flow region A2, measured using Q_A', and the other model parameters including relative depth. This reinforces the need to use an alternative relative depth definition, which can limit the output range between 0→1 and illuminate the effect of other parameter variations more successfully.

6.3 The Enhanced zonal method for predicting discharge capacity in Zone A

6.3.1 An alternative definition for relative depth, RD

The alternative definition of relative depth, RD, was adopted by the author to develop the Enhanced zonal method. Instead of using the James and Wark definition of RD = y'/(A/B) a definition of RD = y'/(y'+(A/B)) was used to ensure that the magnitude of RD was limited to within a range between 0 and 1. Adoption of this definition for RD aided the accuracy of the regression fitting procedure by ensuring that the magnitude of RD did not vary significantly between different scale models used in the training data. Figure 6.4 shows plots of Q_A' versus this new definition of relative depth for G75T45R, G50T45R and G25T45R.

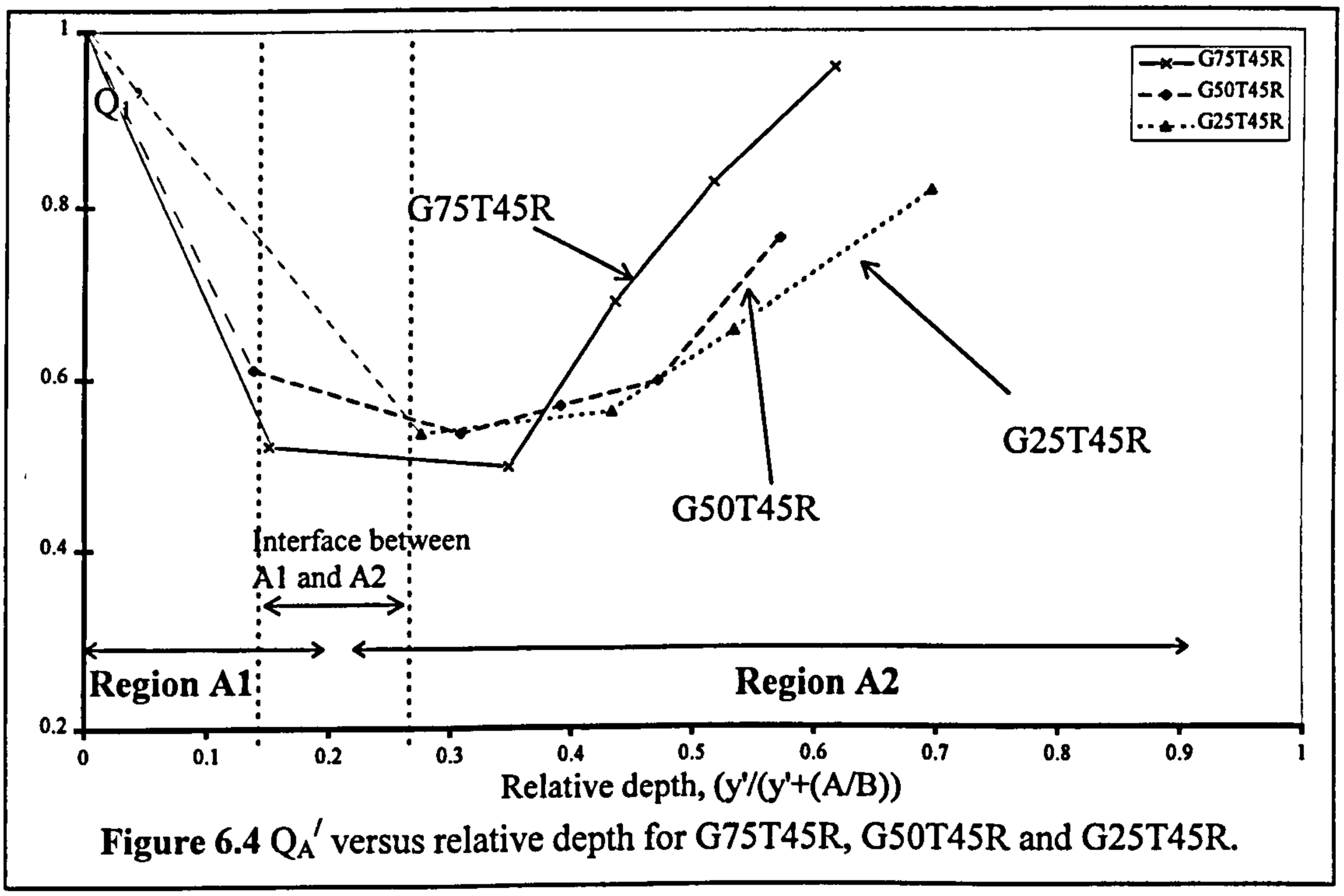

Figure 6.4 Q_A' versus relative depth for G75T45R, G50T45R and G25T45R.

The general patterns of flow behaviour, with non-linearity and multiple parameter dependency, are similar to the ones obtained using the James and Wark [1] definition, but the magnitude of the influence is greater which facilitates the development of suitable regression formulations for predicting the magnitude of Q_A' in flow regions A1 and A2.

6.3.2 Developing a formulation for flow region A1

The author developed a formulation for flow region A1 by fitting a straight line through two data points for Q_{A1}' and RD which could be pre-determined. The first point can be determined because when RD is equal to zero, Q_{A1}' is by definition equal to 1. The second data point can be determined using an observation from Chapter 4. In Chapter 4 it was shown that the flow depth (and hence relative depth) which corresponds to the minimum Global F* value (the end of flow region 1) could be predicted by identifying the flow depth at which the maximum Vertical Shear Force, F_S, is generated between Zones 1 and 2 (as shown in Figure 4.79). Equation 4.8 was used to determine, F_S, at various flow depths. This value of relative depth and the corresponding model parameters are substituted into the appropriate regression model (which was derived for flow region A2 and is detailed in section 6.3.3) in order to determine the corresponding value of Q_{A1}', which is defined as $Q_{A1}'_{min}$. Having determined two values for Q_{A1}', at two relative depths, the formulation for flow region A1 can be derived by re-arranging the typical straight line equation which can be defined when two data points are known. The basic straight line equation is shown in Equation 6.2.

$$Q_{A1}' = m\,(RD) + c \qquad [6.2]$$

To summarise, when RD=0, Q_{A1}' is equal to 1 which implies that c is equal to 1 and when RD is equal to RD_{min}, Q_{A1}' is equal to $Q_{A1}'_{min}$. By substituting these values RD_{min}, $Q_{A1}'_{min}$, and c into Equation 6.2, the value of m can be derived which is presented in Equation 6.3.

$$m = \left(\frac{\left(Q_{A1_{min}}' - 1 \right)}{RD_{min}} \right) \qquad [6.3]$$

The author proposes that Equation 6.4, which is formed by combining Equations 6.2 and 6.3 and knowing that c is equal to 1, is incorporated into the Enhanced zonal method and used to determine the magnitude of Q_{A1}' throughout flow region A1.

$$Q_{A1}^{'} = \left(\frac{\left(Q_{A1_{min}}^{'} - 1 \right)}{RD_{min}} \right) RD + 1 \qquad [6.4]$$

6.3.3 Developing a formulation for flow region A2

6.3.3.1 The key parameters

The author determined the magnitude of Q_{A2}' for between 3 to 6 relative flow depths (ranging between 0.1 and 0.75) in each of the 30 model tests performed in Glasgow during the Series B extension programme. These models provided flow data which demonstrated the influence of 4 key parameters on the Q_{A2}' versus relative depth relationship. These 4 parameters were: scale difference, measured using Re_{CH}, relative roughness, f', main channel aspect ratio, AR, and main channel side slope, S_S. The influence of each parameter is discussed in detail in Section 4.6 and illustrated in Figures 4.47, 4.51, 4.57 and 4.71 respectively.

The Series B extension (1993-1996) programme did schedule model tests to investigate the influence of sinuosity. Unfortunately the results from these tests had not published by the team in Aberdeen at the time of writing. Consequently the author could not include it in the multi-variate regression analysis which he employed to determine empirical adjustments for the basic physical models in the Enhanced zonal method despite it being a key parameter. At the time of writing only the Series B (1989-1992) tests provided data to demonstrate the effect of sinuosity and this data was too limited in extent to be significant in regression analysis. The limited Series B flow data was used to develop basic additional correction factors for the influence of sinuosity which must be used until the flow data becomes available and the empirical adjustments, determined using regression analysis, can upgraded to explicitly include sinuosity.

6.3.3.2 The influence of sinuosity on the adjustment coefficient, Q_A^1 and Q_{A2}'

Figure 6.5 presents plots of Q_A' versus relative depth which were obtained for SDB25 and SDB39 from the Series B (1989-1992) experiments which had sinuosities equal to 1.374 and 2.043 respectively. Figure 6.5 shows that the sinuosity of a main channel

influences both the flow depth at the end of flow region A1 and the magnitude and rate of change of Q_A' with relative depth in Flow region A2. The author suggests that the higher main channel sinuosity in SDB39, compared with SDB25, results in the Reynolds number of the flow is much reduced and therefore more susceptible to interaction with Zone B. This explains why Q_A' is larger in the lower sinuosity channel and increases at a greater rate.

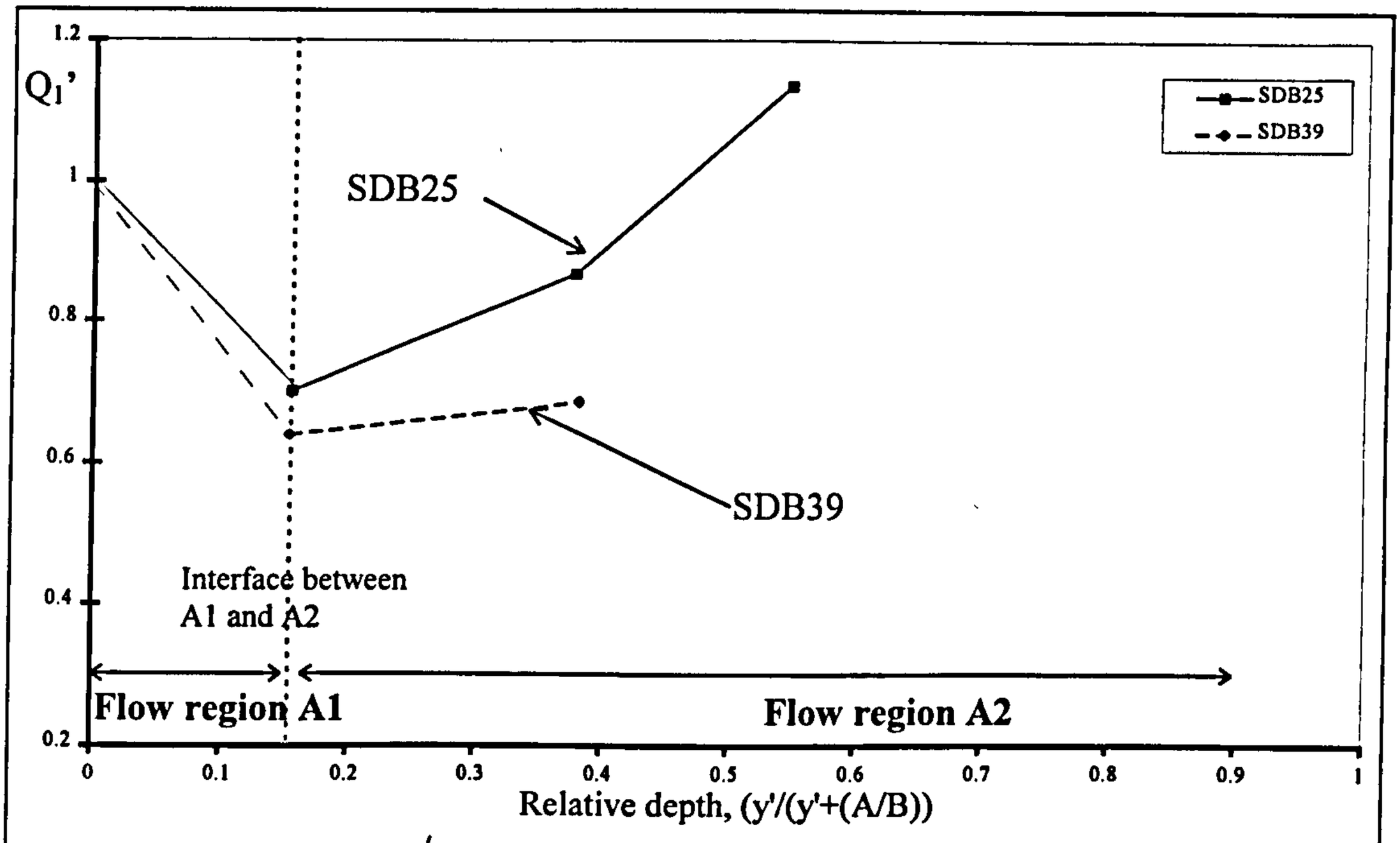

Figure 6.5 Q_A' versus relative depth for SDB25 and SDB39 (r)

6.3.4 Prediction formulation for flow region A2 developed using regression analysis

No evidence was produced in the Series B extension tests to demonstrate that any of the flow data points that were obtained for each separate model should be included in flow region A1. These points would be identified by a local increase in Q_{A2}' (from its maximum value at the beginning of flow region A2) over decreasing flow depths until main channel bankfull depths were achieved. Consequently all the data points were deemed to fall within flow region A2 and were therefore incorporated into the development of a multi-variate regression fit model for flow region A2.

The flow data collected during the Series B extension programme (for all 30 models) and illustrated in Chapters 4 and 6 demonstrate that the relationship between Q_{A2}' and

relative depth is distinctly non-linear. Consequently the author decided that a non-linear multi-variate regression fit to the data would produce the optimum formulation for predicting Q_{A2}'. The author decided that the formulation should take the basic form of Equation 6.5 linking the 5 key parameters tested during the Series B extension programme to the magnitude of Q_{A2}'.

$$Q_{A2}' = f(RD, S_S, AR, f', Re_{CH}) \quad [6.5]$$

Inspection of the characteristic shape of plots of Q_{A2}' versus relative depth suggest that Q_{A2}' could be related to relative depth using a power law to represent the non-linearity that is observed. Various definitions of the formulation of Q_{A2}' were tested using regression analysis. Both additive and multiplicative relationships between the parameters were tried. The additive relationships had similar structures to the original James and Wark [1] [1992] formulations but the multiplicative relationships represented a more logically justifiable method for combining different parameters in a regression analysis. The optimal additive formulation for Q_{A2}', as shown in Equation 6.6, was compared with the multiplicative formulation for Q_{A2}', as shown in Equation 6.7, where a, b, c, d, e, f and g are constants.

$$Q_{A2}' = a*(AR^b)*(S_S{}^C)*(RD^d)*(Re_{CH}{}^e)*(f'^f) \quad [6.6]$$

$$Q_{A2}' = (a*AR+b*S_S+c)*RD^h+(d/Re_{CH}+e*f'+g) \quad [6.7]$$

Table 6.1 lists the pertinent statistical values which were obtained from the regression analysis of the multiplicative formula in Equation 6.6.

Parameter	Value	StdErr	CV(%)	Dependencies
a	3.002e-1	5.898e-2	1.965e+1	0.9965306
b	1.218e-2	2.802e-2	2.300e+2	0.9531405
c	4.746e-2	6.658e-2	1.403e+2	0.7062124
d	9.894e-2	1.896e-2	1.916e+1	0.9966229
e	-8.224e-2	2.551e-2	3.102e+1	0.4077976
g	2.578e-1	3.397e-2	1.318e+1	0.8879224

Table 6.1 Statistical values from the regression fit to the multiplicative formulation

Table 6.1 shows that there are strong parametric dependencies which indicates that the multiplicative formulation is over-parameterised. The parametric standard deviations and CV% values (defined in Section 3.4) were only just within acceptable limits. The RMS percentage error and standard deviation between the measured values for Q_{A2}' and

those obtained by back-substituting the parameter values into Equation 6.6 were equal to 9.97% and 7.38% respectively.

Table 6.2 lists the pertinent statistical values which were obtained from the regression analysis of the optimal additive formulation in Equation 6.7. It shows that there are no strong parametric dependencies, which indicates that the formulation is not over-parameterised and the parametric standard deviations and CV% values are within acceptable limits. The RMS percentage error and standard deviation between the measured values for Q_{A2}' and those obtained by back-substituting the parameter values into Equation 6.7 were equal to 7.57% and 5.84% respectively.

Parameter	Value	StdErr	CV(%)	Dependencies
a	1.311e-2	2.097e-2	1.600e+2	0.9370385
b	4.716e-1	3.306e-1	7.010e+1	0.9722908
c	5.693e-1	3.237e-1	5.686e+1	0.9827107
d	-3.201e+3	3.888e+2	1.215e+1	0.8398216
e	-2.397e-2	8.704e-3	3.631e+1	0.8654549
g	6.870e-1	2.629e-2	3.827e+0	0.9498701
h	2.871e+0	4.146e-1	1.444e+1	0.9670263

Table 6.2 Statistical values from regression fit with 5 parameters

The author concludes that the additive formulation produces the optimal predictive method for Zone A using the data obtained from the Series B and Series B extension experiments, despite the fact that it was a less logical approach for combining parameters. The author decided to adopted the additive formulation for the Enhanced zonal method but recommends that the relative merits of both additive and multiplicative formulations are re-assessed when further pertinent flow data is made available.

The final formulation for Q_{A2}' which was adopted for flow region A2 is given in Equation 6.9. It includes an adjustment factor which is applied on Term 1 in order to account for sinuosity: 'SAF'. The author was aware that no allowance had been made for the influence of sinuosity in the original regression analysis and the value of the superscript, a, was determined by applying Equation 6.8 to the Zone A flow data which was obtained in Series B for SDB25 and SDB39.

$$Q_{A2}' = \overbrace{(1.374/r)^{a}}^{\text{SAF}} * \overbrace{(0.0131*AR+0.472*S_S+0.569)*RD^{2.87}}^{\text{Term 1}} + \overbrace{(-3201/Re_{CH}+-0.024*f'+0.687)}^{\text{Term 2}} \quad [6.8]$$

The Series B extension (1993-1996) data, on which the original formulation was based, was obtained using channels which had a sinuosity, r, equal to 1.374. Consequently the author used the ratio, 1.374/r, to ensure that no adjustment was applied to channels with the same sinuosity as the training set. The coefficient, a, was determined by trial, in order to account for the differences observed in the magnitude of Q_{A2}' in SDB25 and SDB39 as measured in Series B (1989-1992). The optimal magnitude for a was 1.42. The final formulation for Q_{A2}' in the Enhanced zonal method is therefore defined as in Equation 6.9.

$$Q_{A2}' = (1.374/r)^{1.42}*(0.0131*AR+0.472*S_S+0.569)*RD^{2.87} + (-3201/Re_{CH}+-0.024*f'+0.687) \quad [6.9]$$

6.3.5 Combining the flow region A1 and A2 formulations

The variation in the adjustment factor, Q_A', across the whole of range of regions A1 and A2 can be accounted for by choosing the adjustment factor, Q_{A1}' or Q_{A2}', which has the greater value when using both Equations 6.4 and 6.9.

6.3.6 Comparison between the James and Wark [1] [1992] and Enhanced zonal methods

The James and Wark [1] [1992] method predicted the magnitude of Q_A' that was obtained in the Series B (1989-1992) experiments with a reasonable degree of accuracy, as is shown in Figure 6.6. This was expected because the same data was used to develop the regression formulations.

The RMS percentage error and standard deviation between the predicted and measured values of Q_A' were 4.20% and 5.32% respectively. However, comparable levels of accuracy were not achieved when the James and Wark [1] [1992] method was used to compare the predicted and measured values of Q_A' from the Series B extension (1993-1996) data (from Glasgow), as is shown in Figure 6.7. The RMS percentage error and

standard deviation values were 22.7% and 19.0% respectively. This was an unacceptable level of accuracy.

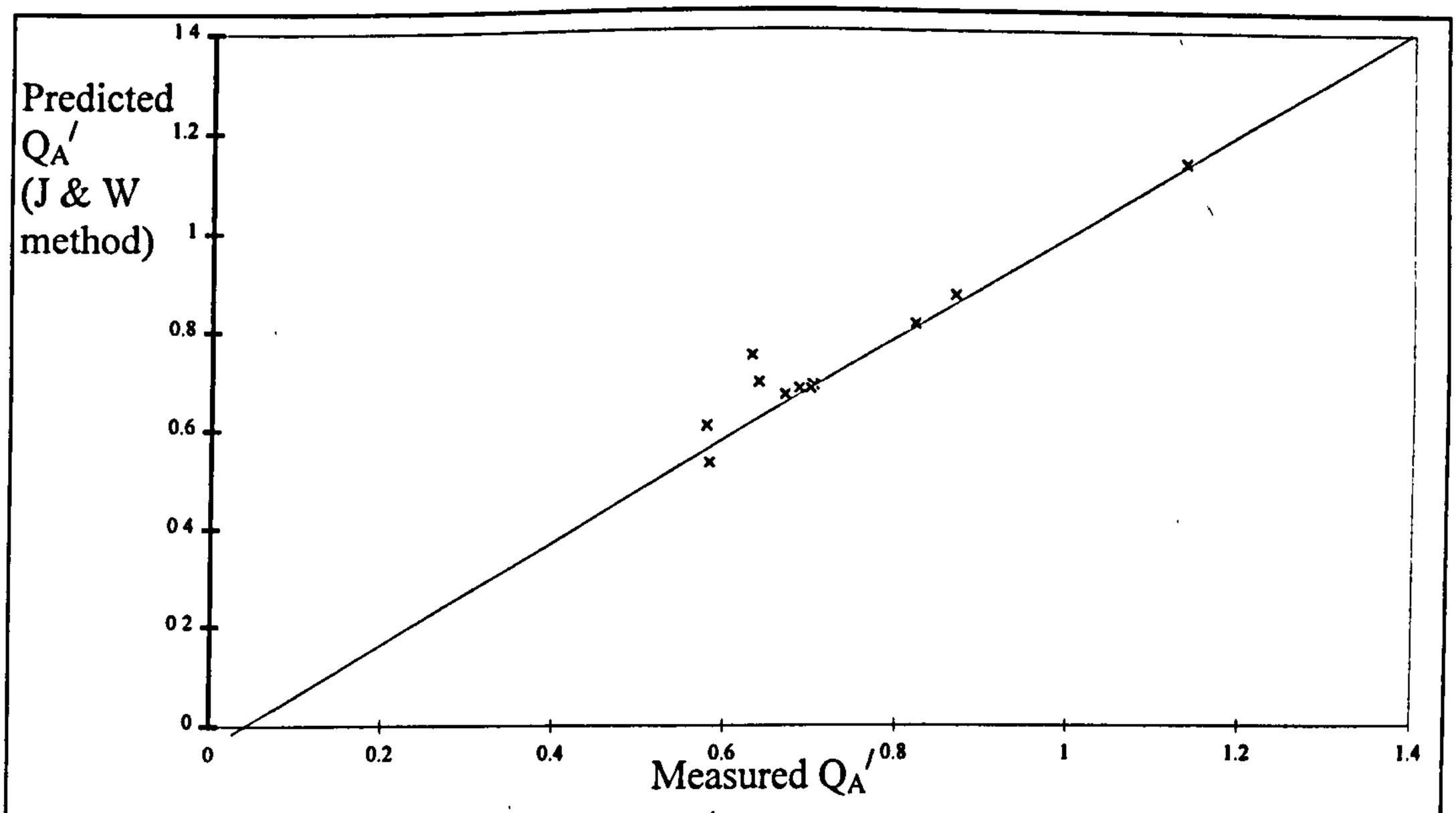

Figure 6.6 Measured versus predicted Q_A' for Series B data (James and Wark [1992])

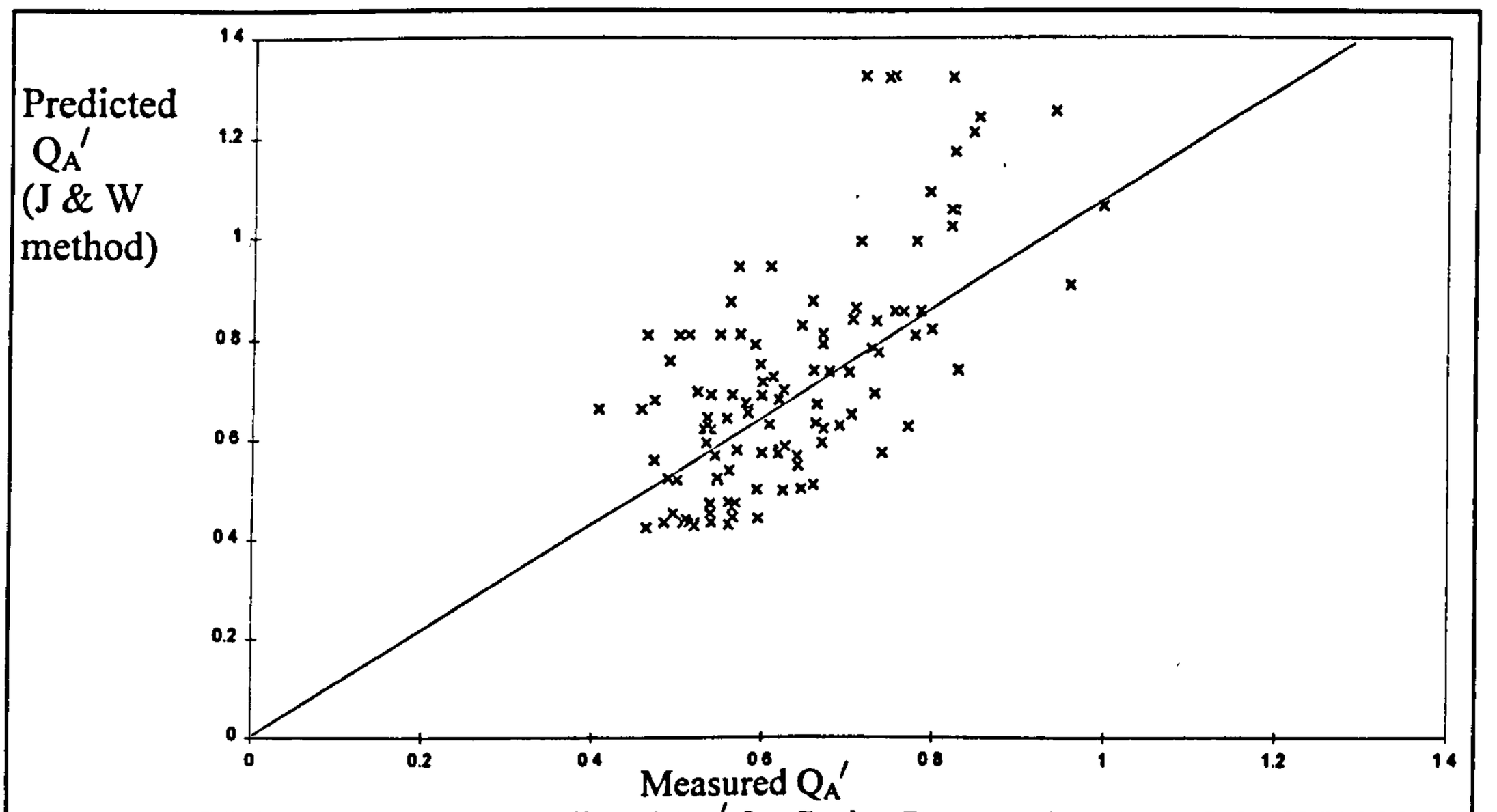

Figure 6.7 Measured versus predicted Q_A' for Series B extension data (J & W [1992])

The differences between the values predicted for Q_A' using the Enhanced zonal method for Zone A and the measured values from the Series B extension (1993-1996) tests are shown in Figure 6.8. The RMS percentage error and standard deviation are 7.1% and 5.5% respectively.

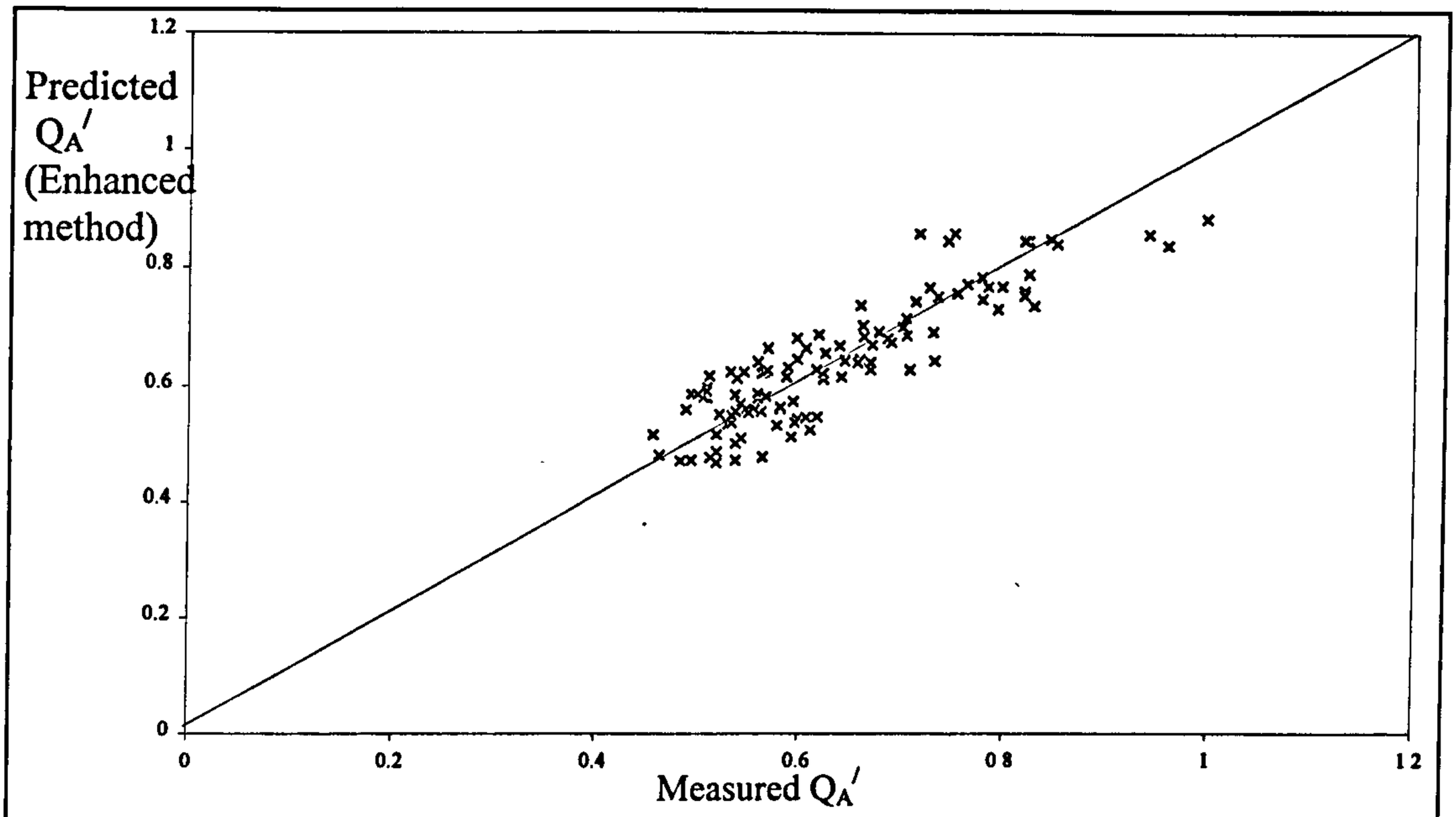

Figure 6.8 Measured versus predicted values for Series B extension data (Enhanced)

Figure 6.9 shows a plot of the predicted and measured values of Q_A' for the Series B (1989-1992) data. The RMS percentage error and standard deviation values were 11.4% and 7.2% respectively.

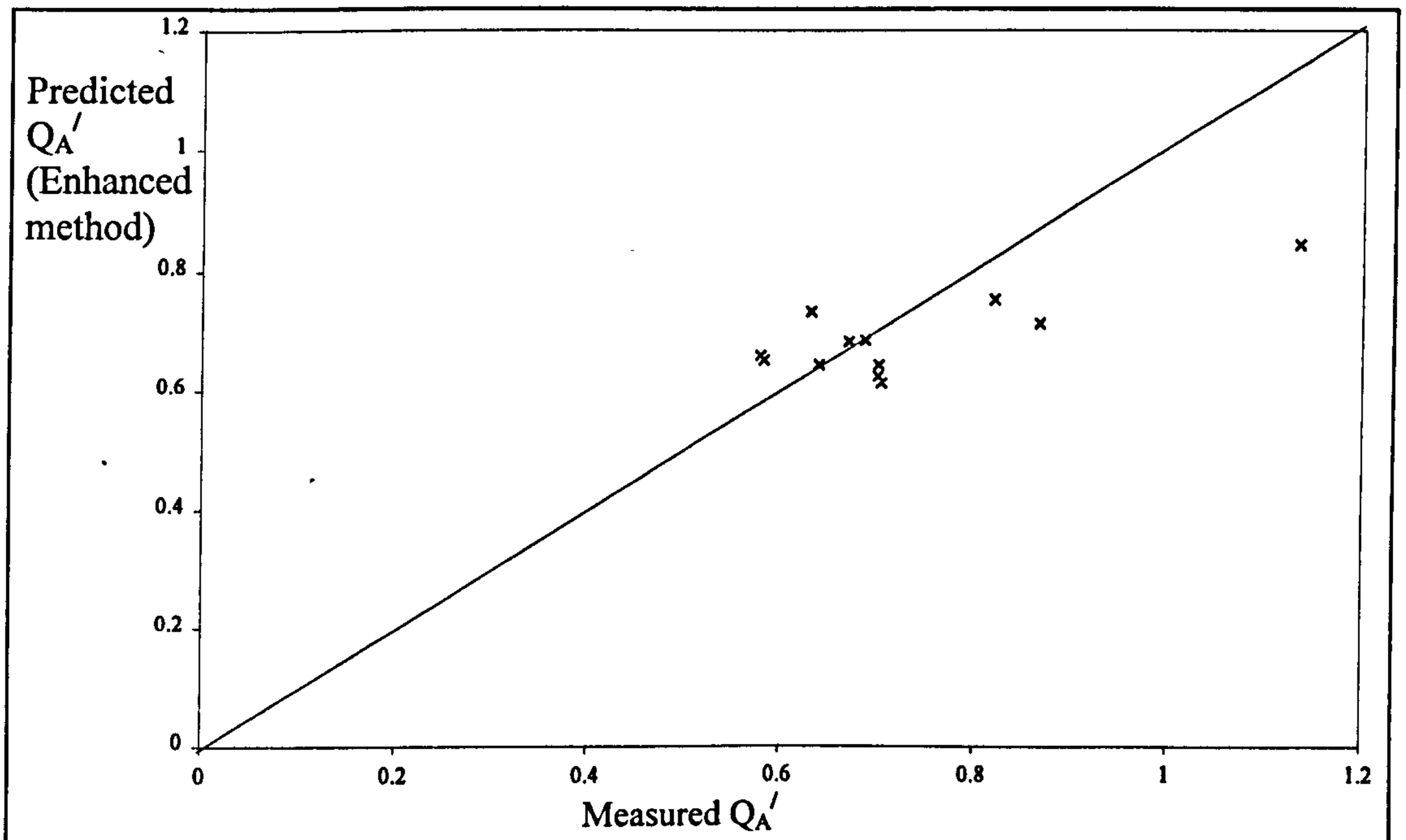

Figure 6.9 Measured versus predicted values for Series B (1989-1992) data

The predictions obtained by applying Equation 6.10 to the Series B data set are not as accurate as the ones obtained using the James and Wark [1] method. However when

they are applied to the Series B extension data they are much more accurate. Therefore the author suggests that the Enhanced zonal method's formulation for predicting Q_A' in both flow region A1 and A2 (which was described by a combination of Equations 6.4 and 6.9) produces generally more accurate predictions than were obtained using the James and Wark [1] [1992] formula, especially when different scale models are considered.

6.4 Flow behaviour in Zone B (above bankfull level)

6.4.1 Critical assessment of the structure of James and Wark [1] [1992]

James and Wark [1] [1992] assumed that the head lost in Zone B when it flows over a meandering main channel could be attributed to bed friction and expansion and contraction losses. They converted existing head loss prediction equations for flow over steps so that they could be applied to meandering compound channels by assuming that two perpendicular trenches (with similar configurations), as shown in Figures 6.10 and 6.11, would induce similar head losses to those generated over a meandering channel.

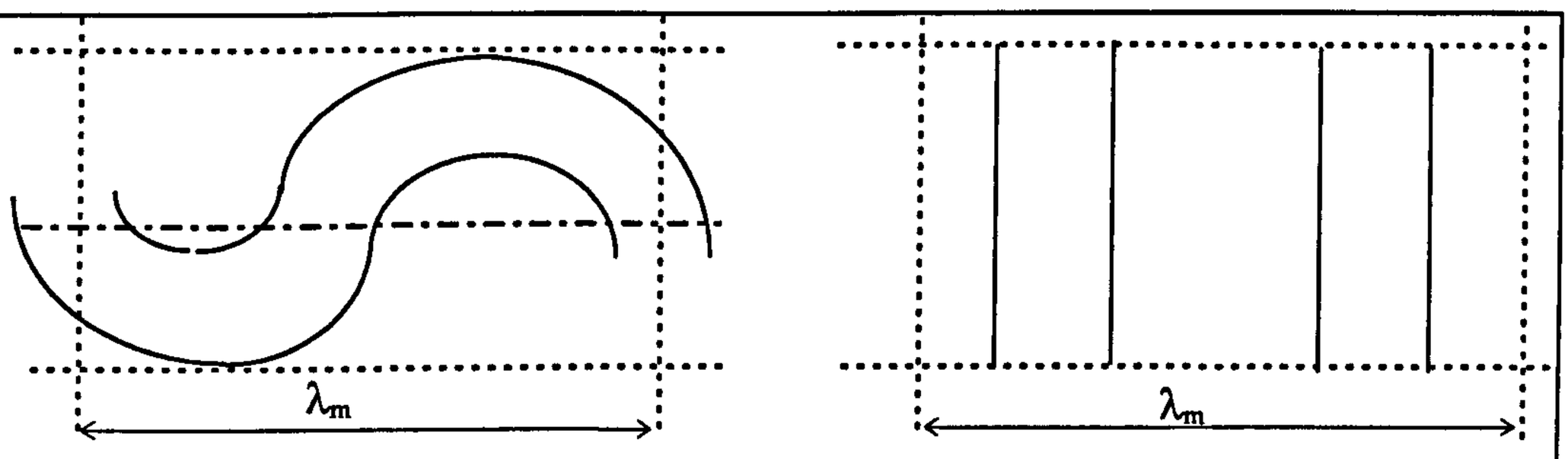

Figure 6.10 The simple trenches which are equivalent to the meandering channel

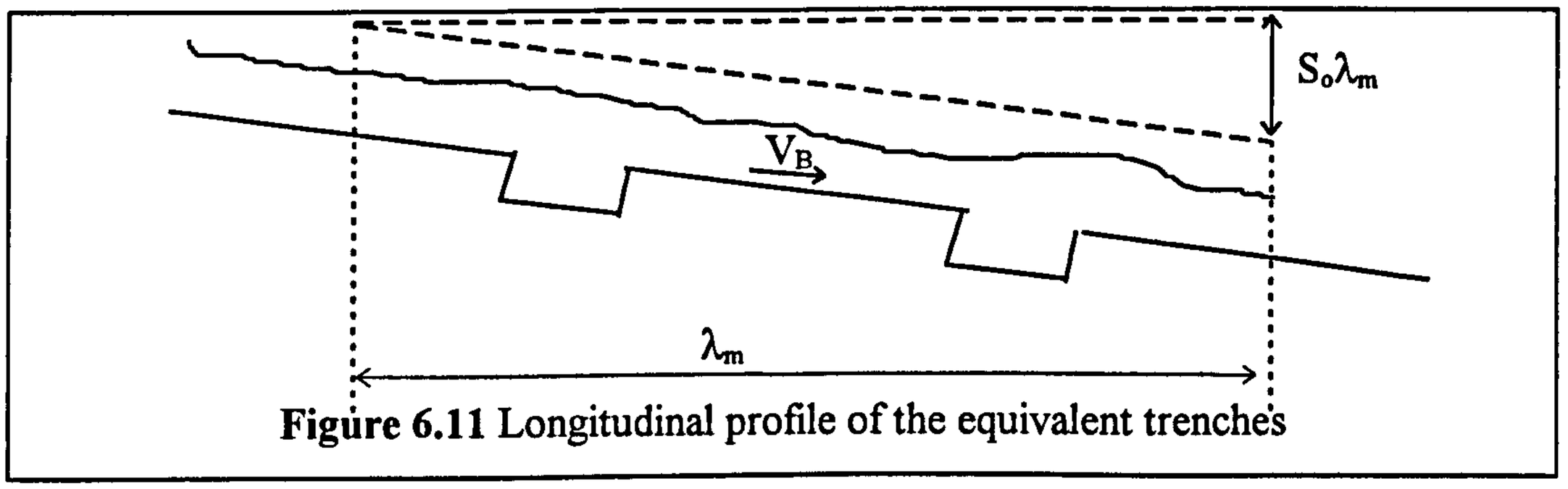

Figure 6.11 Longitudinal profile of the equivalent trenches

By assuming conservation of energy over one wavelength of the main channel the head loss generated in Zone B for uniform flow is defined by Equation 6.10. The term (Ke+Kc) is multiplied by 2 because the flow will expand and contract twice over one main channel wavelength. Equation 6.10 can be re-arranged to derive a definition for Zone B velocity described in Equation 6.11.

$$h_f = \frac{f_B \lambda}{4R_B}\frac{V_B^2}{2g} + (2*(K_e + K_c))\frac{V_B^2}{2g} = S_o \lambda \qquad [6.10]$$

$$V_B = \sqrt{\frac{2gS_o\lambda}{\frac{f_B\lambda}{4R_B} + 2*(K_e + K_c)}} \qquad [6.11]$$

K_e is equal to the head loss coefficient for expansion over a forward facing step which is adjusted to allow for the proximity of the two steps (one backward and one forward facing). The steps are so close that the typical expansion mechanisms associated with flow over a step were interfered with by the opposite step. This alters the magnitude of head loss that is generated and hence the classical head loss formula which was derived for a vertical, isolated step has to be adjusted by an appropriate adjustment factor, C_{we} so that it will still accurately predict the head loss magnitude. Consequently K_e is defined as shown in Equation 6.12.

$$K_e = C_{we} * [1 - y_2[y_2 + h]]^2 \qquad [6.12]$$

K_c is equal to the head loss coefficient for contraction over a backward facing step which is adjusted to allow for the proximity of the two steps (one backward and one forward facing). The steps are so close that the typical contraction mechanism associated with flow over a step were interfered with by the opposite step. This alters the magnitude of head loss that is generated and hence Rouse's [1950] classical head loss formula, $K_{c(Rouse)}$, which was derived for a vertical, isolated step has to be adjusted by an appropriate adjustment factor, C_{we} so that it will still accurately predict the head loss magnitude. Consequently K_C is defined as in Equation 6.13.

$$K_c = C_{we} * K_{c(Rouse)} \qquad [6.13]$$

James and Wark [1] [1992] defined C_{we} in terms of C_{wd} which varies with aspect ratio and C_{SSE} which varies with the tangent of lateral side slope, S_S, as shown in Equations 6.14, 6.15 and 6.16.

$$C_{we} = C_{wd} * C_{SSE} \qquad [6.14]$$

$$C_{wd} = (0.02*[B_2 / A] + 0.69) \qquad [6.15]$$

$$C_{SSE} = (1.0 - S_s/5.7) \quad [6.16]$$

James and Wark [1] [1992] also defined C_{wc} in terms of C_{wd} which varies with aspect ratio and C_{SSE} which varies with the tangent of lateral side slope, S_S as shown in Equation 6.17, 6.18 and 6.19.

$$C_{wc} = C_{wd} * C_{SSC} \quad [6.17]$$

$$C_{wd} = (0.02 * [B_2 / A] + 0.69) \quad [6.18]$$

$$C_{SSC} = (1.0 - S_s/2.5) \quad [6.19]$$

However some of the assumptions underlying the James and Wark [1] [1992] definitions of C_{we} and C_{wc} can be refined and improved. Details of the improvements that can be made are described below:

1. The analysis performed by James and Wark [1] [1992] of the flow data produced by Jasem [1990] indicated that the relationship between C_{wd} and the aspect ratio was identical for both the expansion and contraction of the flow. Results obtained by the author during the Series B extension (1993-1996) programme demonstrated that Jasem's data was inaccurate and therefore the James and Wark [1] (1989-1992) postulation was not accurate
2. James and Wark [1] [1992] also postulated that the Formica [1955] expression for lateral side slope could be directly applied to the trench side slope. Section 4.8 has demonstrated that this assumption results in an almost two fold exaggeration of the influence of side slope.
3. The James and Wark [1] [1992] method incorporated empirical adjustment factors to account for inaccuracies in their definitions for the head loss coefficients K_e and K_c which were incorporated in Equation 6.11. Equation 6.20 details the James and Wark [1] final definition which was derived for $2*(K_e+K_c)$ together with these adjustments.

$$2*(K_e+K_c) = C_{SL} * F_1 * F_2 * (K_e+K_c) \quad [6.20]$$

The author suggests the initial inaccuracies associated with the Equation 6.20 formulation were caused by a lack of allowance for all the influential parameters on expansion and contraction flow which were identified in Section 4.8. Also the underlying assumption that the influence of the two parameters: side slope and aspect ratio were independent was not correct. Further inaccuracies were introduced by the method adopted for the empirical determination of F_1 and F_2 and the lack of physical justification for C_{sl}.

4. James and Wark [1] [1992] defined, C_{sl}, in Equation 6.21, where W_2 is the meander belt width and B is the top width of the main channel. C_{SL} effectively accounts for the twofold multiplication to allow for the two trenches but also includes an arbitrary reduction for the width of the main channel which must be reviewed.

$$C_{sl} = 2\,[W_2 - B] / W_2 \qquad [6.21]$$

5. F_1 and F_2 were determined empirically by fitting the total discharge values which were measured during the Series B [1992] tests to the predicted discharge values which were obtained by applying the basic James and Wark [1] [1992] method. However, F_1 and F_2 were applied as multiplicative factors on only the expansion and contraction term in Equation 6.11. F_1 and F_2 were defined in terms of aspect ratio and sinuosity as shown in Equations 6.22, 6.23 and 6.24.

$$F_1 = 0.1\,B^2 / A \quad \text{for } B^2/A<10 \qquad [6.22]$$

$$F_1 = 1 \quad \text{for } B^2/A > 10 \qquad [6.23]$$

$$F_2 = 1.4 / s \qquad [6.24]$$

Significantly the empirical adjustments were only applied to the Zone B velocity term, but were used to account for the discrepancies between the measured and predicted discharges for the whole compound channel. The discrepancy is not only attributable to errors in Zone B velocity calculation so when the final empirical equation used in the James and Wark [1] [1992] method is applied to determine Zone B velocity in other channels it will tend to yield inaccurate estimates.

6.4.2 The James and Wark [1992] predictions compared with measured velocities

Figures 6.12 and 6.13 show plots of measured and predicted depth-averaged velocities in Zones B and C for SDB21 at 0.05m flow depth (in flow region 2) and at 0.1m flow depth (in flow region 3) respectively. Figures 6.12 and 6.13 show that the James and Wark [1] [1992] method under-estimates the depth-averaged velocity in Zone B across the whole of its width in both flow regions 2 and 3. This behaviour is repeated for the majority of model results gathered during the Series B extension programme.

The author suggests that the discrepancy in Zone B velocity predictions (when using the James and Wark [1] [1992] method) was overlooked because the inaccuracy in discharge capacity prediction comprises only a small percentage of the total discharge. In addition,

some of the deficit in Zone B velocity is compensated for by the over-estimation of velocity in Zone C, which James and Wark [1] [1992] modelled assuming that bed friction was the only source of head loss.

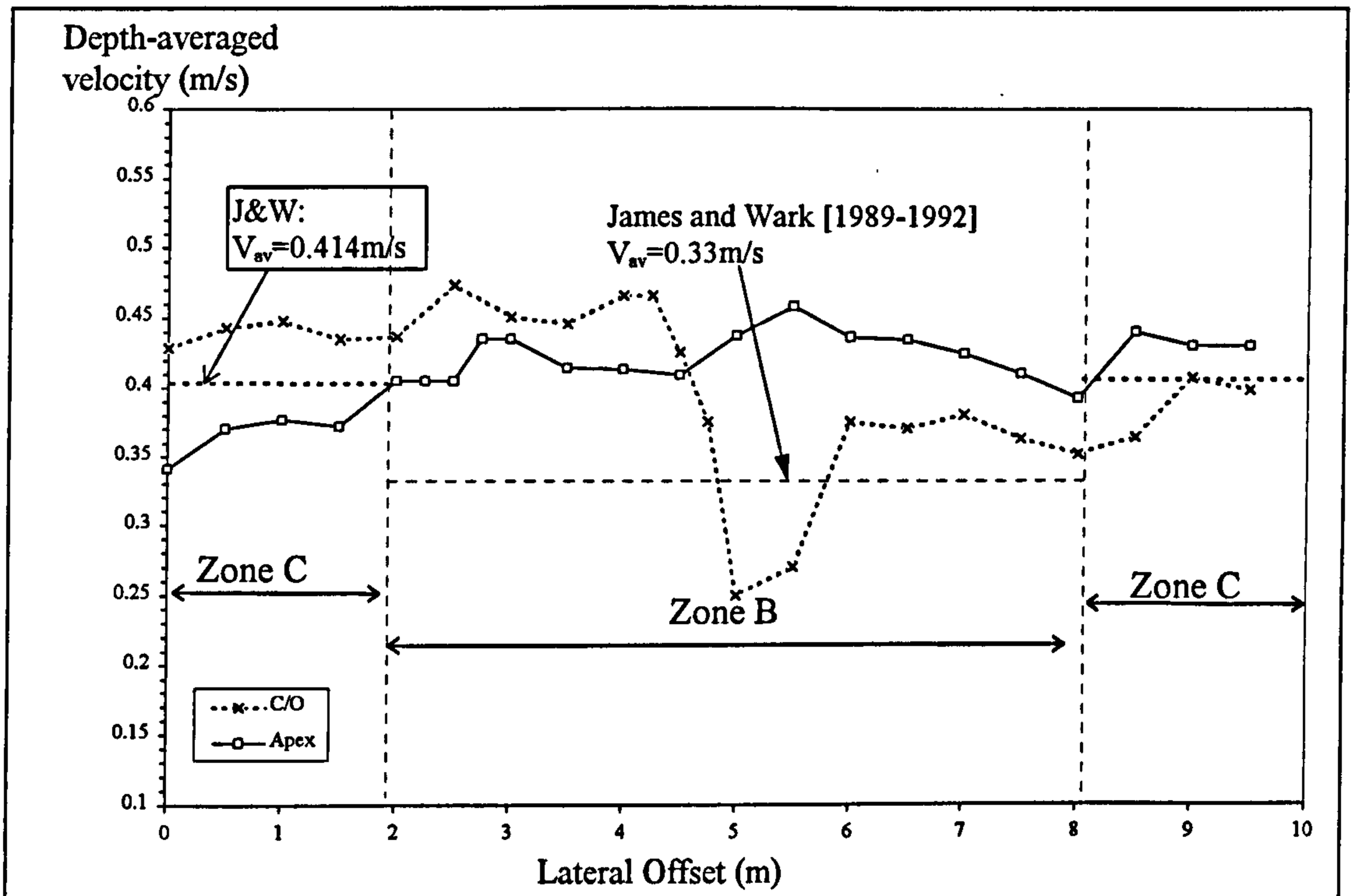

Figure 6.12 Depth-averaged velocity versus lateral offset at 50mm depth (SDB21)

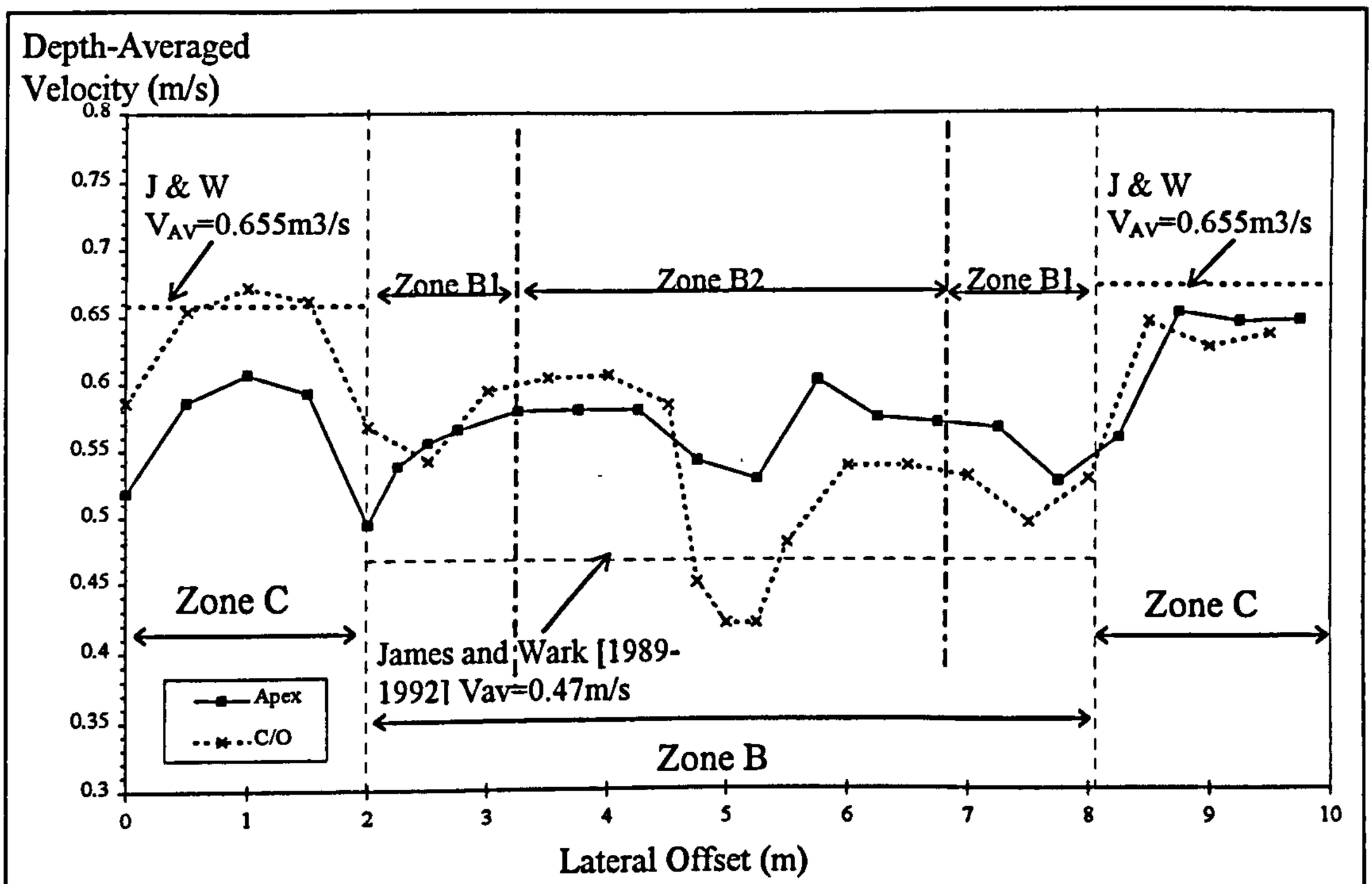

Figure 6.13 Depth-averaged velocity versus lateral offset at 100mm depth (SDB21)

6.4.3 Additional flow features accounted for in the Enhanced zonal method

6.4.3.1 Introduction

The results collected during the Series B extension programme revealed details about the flow behaviour in Zone B which were not explicitly accounted for in the James and Wark [1] [1992] method. The Enhanced zonal method was developed in an attempt to account for the majority of the flow behaviour identified during the Series B extension (1993-1996) programme.

6.4.3.2 The presence of sub-zones in Zone B

The typical plots of depth-averaged velocity across Zone B in Figure 6.12 and 6.13 demonstrate that although one mean depth averaged velocity can be determined for Zone B flow at low flow depths (flow regions 1 and 2), at higher flow regions two distinct sub-zones are generated in Zone B, Zones B1 and B2 as shown in Figure 6.13. Zone B1 is positioned over the apex of the main channel and is characterised by its mean depth-averaged velocity which is significantly reduced from the mean depth-averaged velocity in Zone B2. Zone B2 comprises the rest of Zone B outside the apex zone. These sub-zones are illustrated schematically in Figure 6.14.

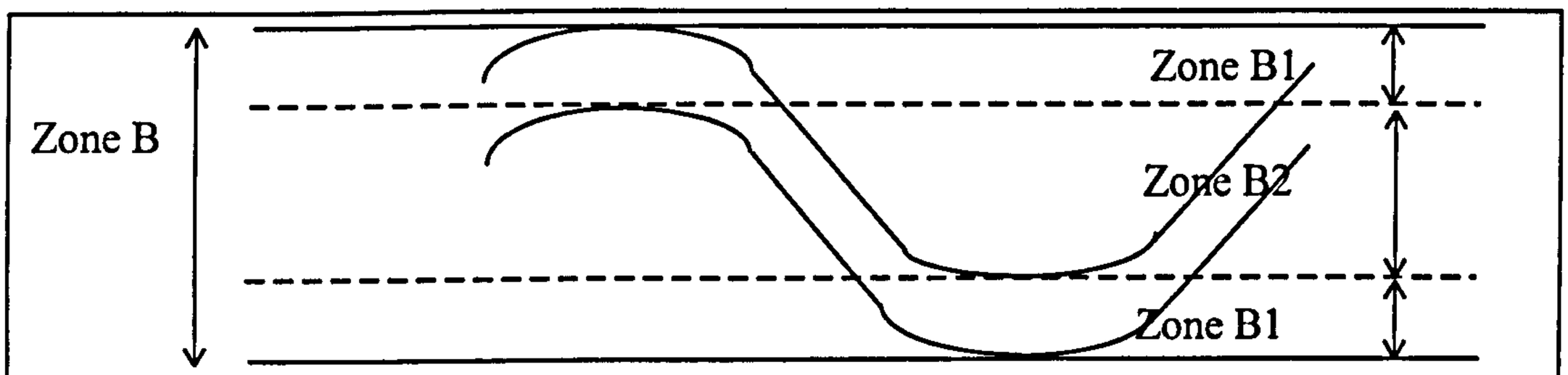

Figure 6.14 Sub-zones in Zone B

6.4.3.3 Layer interaction behaviour in flow regions 1 and 2

Figure 6.12 shows a typical plot of depth-averaged velocity versus flume width in flow regions 1 and 2 (low flow depths) in a larger scale model, SDB21, which was tested during the Series B (1989-1992) programme. The depth-averaged velocities in Zones B1 and B2 are clearly similar to those in Zone C.

The mean depth-averaged velocities between Zones C and B1 in flow regions 1 and 2 were compared for all the models tested during the Series B extension programme in

Glasgow. Figure 6.15 shows a plot which facilitates the comparison between the mean depth-averaged velocities in Zones B2 and B1 in flow regions 1 and 2 for all the models tested during the Series B extension programme in Glasgow.

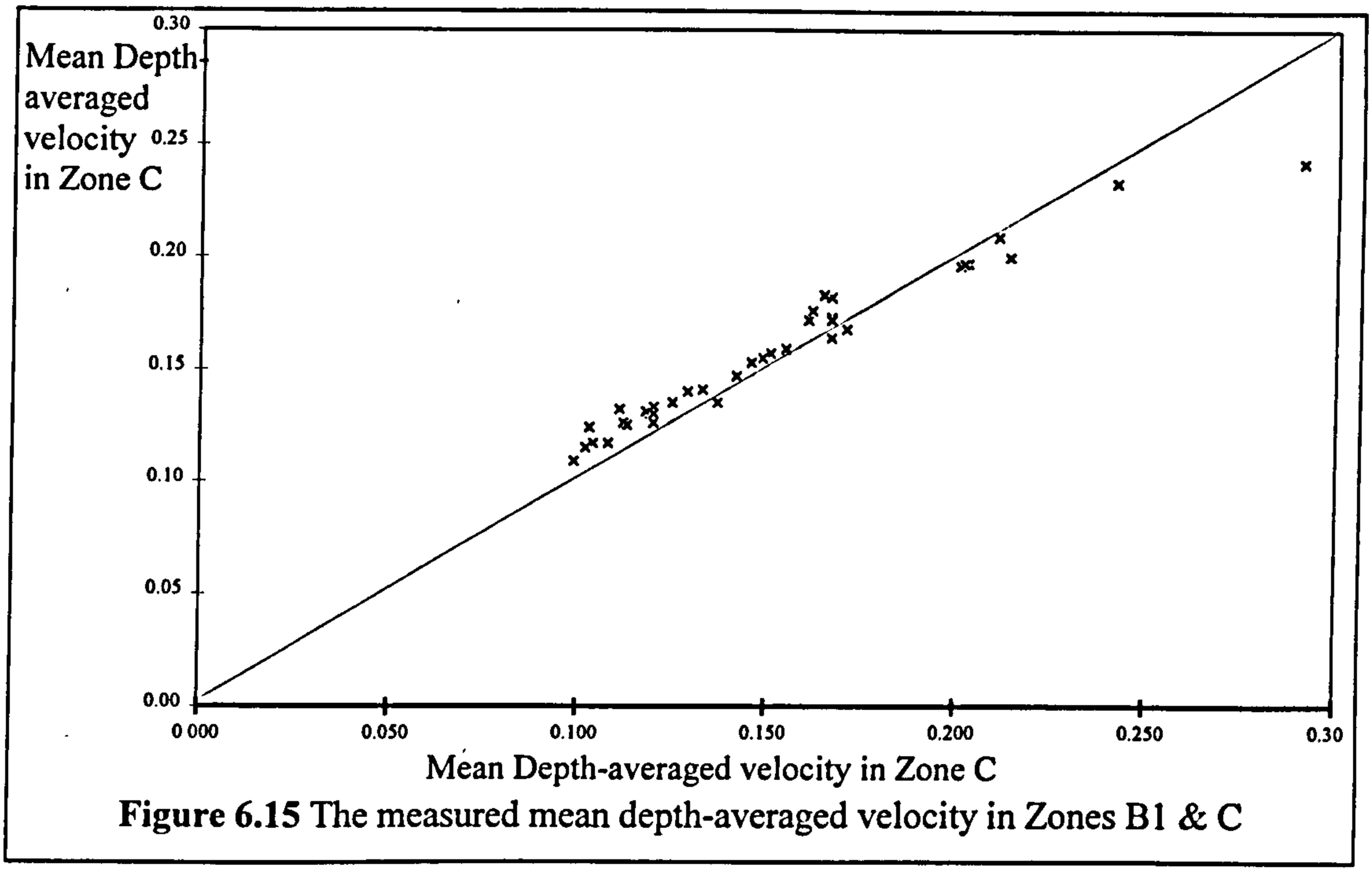

Figure 6.15 The measured mean depth-averaged velocity in Zones B1 & C

Clearly the Zone B flow behaviour in the small scale models tested during the Series B extension (1993-1996) programme, was similar to that observed in the larger scale models in Series B (1989-1992). There is no evidence to suggest that this should not also be true for natural river channels.

The measured Zone C depth-averaged velocities match closely the James and Wark [1] [1992] predicted velocities in flow regions 1 and 2 as illustrated in the representative Figure 6.12. James and Wark [1] [1992] postulated that only bed friction losses are generated in Zone C, at all flow depths. This implies that because the depth averaged velocities in Zones B1, B2 and Zone C are similar, then Zones B1 and B2 must not experience any expansion and contraction head loss at these flow depths. However this contradicts the James and Wark [1] [1992] formulation for Zone B flow velocity which includes an allowance for expansion and contraction losses at all flow depths as shown in Equation 6.11.

The author developed the Enhanced zonal method so that it makes the distinction between the different flow behaviours in Zone B, over all four flow regions. Thus the initial approach adopted in the James and Wark [1] [1992] method was enhanced using the data gathered during the Series B extension (1993-1996) programme.

Closer inspection of Figure 6.15 presents evidence to suggest that the depth-averaged velocity plot in Zone B1 tends to be slightly greater than in Zone C. The author attributed this behaviour to the interaction between the fast flowing main channel (Zone A) water and the Zone B flow. The author suggests that the Zone A exerts a horizontal shear force on the slower moving flood plain water and imposes a small acceleration. However the effect is so negligible that the author did not attempt to account for this acceleration in the Enhanced zonal method. A small underestimate of the discharge would only make the model slightly more conservative.

6.4.3.4 Layer interaction behaviour in flow regions 3 and 4

Figure 6.13 demonstrates that at higher flow depths (in flow region 3) there is by contrast a significant discrepancy between the Zone B1, Zone B2 and Zone C depth averaged velocities. The author demonstrated during the Series B extension programme that the flow behaviour in Zone B in flow region 3, demonstrated by Figure 6.13, was typical of the flow behaviour observed in all the models tested during the Series B extension programme.

The author notes that flow region 3 is initiated when the mean depth-averaged velocity in Zone B attains a certain threshold depth or flow state (indicated by the Relative Reynolds number, Re', equalling 1) significant expansion and contraction flow mechanisms are initiated (as discussed in Chapter 4). The velocity in Zone B is much reduced from that in Zone C, which was calculated by assuming that the only source of flow resistance was bed friction, which implied that there was a significant extra source of flow resistance being generated. Figure 6.13 shows that the James and Wark [1] [1992] method overestimates the magnitude of the expansion and contraction losses in Zone B. It plots the calculated mean depth-averaged flow velocities which are much lower than those measured. The author postulates that improvements in the accuracy of

prediction for the depth-averaged velocity in Zone B in the Enhanced zonal method can be achieved by making allowance for the variation of expansion and contraction behaviour, with flow depth and across the flume, in the Enhanced zonal model.

6.5 The Enhanced zonal method for predicting discharge capacity in Zone B

6.5.1 Introduction

The author chose to develop two different formulations to predict the mean depth averaged velocities in Zones B1 and B2 separately . These formulations were based on the original James and Wark [1] [1992] method, but by treating Zones B1 and B2 separately the observed differences in flow behaviour could be accounted for thus enhancing the original James and Wark [1] [1992] approach. Equation 6.25 shows the formulations included in the Enhanced zonal method for determining the Zone B1 mean depth-averaged velocity. Equation 6.26 shows the formulations included in the Enhanced zonal method for determining the Zone B2 mean depth-averaged velocity. The author also incorporated empirically-determined 'flow region' parameters, F_{B1} and F_{B2}, in order to account for the changes in the magnitude of expansion and contraction head loss in different flow regions. Details of their formulation are given in Section 6.4.4.3.

$$V_{B1} = \sqrt{\frac{2gS_o\lambda}{\frac{f_B\lambda}{4R_{B1}} + F_{B1} * 2 * (K_e + K_c)}} \qquad [6.25]$$

$$V_{B2} = \sqrt{\frac{2gS_o\lambda}{\frac{f_B\lambda}{4R_{B2}} + F_{B2} * 2 * (K_e + K_c)}} \qquad [6.26]$$

Some of the variables g, S_o, λ, f_B in the basic Zone B velocity formulations detailed in Equations 6.25 and 6.26 were assigned identical values in both the Enhanced zonal and James and Wark [1] [1992] methods. However, there were some additional refinements.

1. The definitions for R_{B1} and R_{B2} in the Enhanced zonal method were different to the equivalent definition of R_B in the James and Wark [1] [1992] method. The author specified that R_{B1} and R_{B2} should be defined as being equal to (P_{B1}*y/P_{B1}) and (P_{B2}*y/P_{B2}) respectively, where P_{B1} and P_{B2} were equal to the widths of Zones B1 and B2 respectively and y is equal to the average flow depth throughout Zone B. By

contrast James and Wark [1] [1992] set R_B equal to (P_B*y/(P_{B1}-B)) which had the effect of reducing the perimeter over which the roughness acts. This assumption is only appropriate if the whole of Zone B flows as one entity however the author demonstrated that this was not the case, with two separate but significant flow zones in Zone B being observed. Consequently the new definitions for R_{B1} and R_{B2} was deemed to be more appropriate.

2. The artificial variable, C_{SL}, as defined by James and Wark [1] [1992] was replaced with simply a multiplicative factor equal to 2 in order to account for the two trenches which were assumed to produce the same expansion and contraction head losses as were generated in flow over a meandering compound channel.
3. K_e and K_c were defined using Equations 6.12 and 6.13 once again. However the enhanced definitions for C_{we} and C_{wc}, shown in Equations 6.27 and 6.28 (and derived in section 4.8), were used instead of the James and Wark [1] [1992] definitions (which are given in Equations 6.12 - 6.19). These enhanced definitions account for the inter-dependency of the influence of relative depth, RD, aspect ratio, AR and side slope, S_S.

$$C_{we} = 0.206e^{(-1.31*RD)}AR^{0.693}S_S^{0.369} \quad [6.27]$$

$$C_{we} = 0.189e^{(-3.68*RD)}AR^{0.926}S_S^{0.455} \quad [6.28]$$

6.5.2 Derivation of the 'flow region' parameters, F_{B1} and F_{B2}

The basic combined expansion and contraction head loss coefficient expressions in Equation 6.25 and 6.26 are defined as 2*(K_e+K_c). With the newly refined definitions for K_e and K_c these expressions will produce high accuracy predictions for the head loss coefficients in flow over slots with no flow in them. However in meandering compound channels there is flow in the slots which will resist the expansion and contraction mechanisms until the upper channel flow possesses enough energy (in proportion to the main channel (slot) flow) to start to drive these mechanisms. For meandering compound channels adjustment factors known as 'flow region' parameters have to be included, as in Equations 6.25 and 6.26, in order to adjust the basic head loss coefficient predictions so that they are appropriate for meandering channels.

Examination of the variation in depth-averaged velocity in Zone B within the various flow regions demonstrated that when flow depths correspond to flow regions 1 and 2 minimal expansion and contraction head losses were generated. The velocity plots indicated that the dominant source of flow resistance was bed friction. At these depths the magnitude of the Relative Reynolds number, Re', is less than 1 and the main channel flow had enough energy to resist the expansion and contraction flow mechanisms. The multiplicative adjustment factors, F_{B1} or F_{B2} (which were identified in Equations 6.25 and 6.26) were devised to reflect this lack of expansion and contraction head loss and formulations were sought for them which rapidly tend to zero when Relative Reynolds number fall below 1 and tends to 0. In this way the contribution of the expansion and contraction terms in Equations 6.25 and 6.26 will tend to 0 thus reflecting the small proportion of flow resistance that is contributed to the overall flow resistance at these flow depths by the expansion and contraction head loss mechanisms.

By contrast when the Relative Reynolds number is greater that 1 there is less resistance to the formation of the expansion and contraction flow mechanisms. Consequently a definition for F_{B1} or F_{B2} would need to tend rapidly to larger positive values in order to reflect the more substantial proportion of flow resistance that is contributed by the expansion and contraction mechanisms to the overall flow resistance at these flow depths.

Using the Relative Reynolds number, Re', as a trace variable, the author identified a general expression for the 'flow region' parameter, F, which was expressed in the form shown in Equation 6.29, in order to replicate the observed relationship between Relative Reynolds number variation and the magnitude of expansion and contraction head losses that are generated in Zone B. a and b were set as constants.

$$F = \left(\frac{\mathrm{Re'}}{a + \frac{\mathrm{Re'}}{b}} \right) \qquad [6.29]$$

Figure 6.16 shows plots of F versus Re' for a range of values of a and b. F is much less than 1 when Re' is less than 1 and the main channel flow resists the expansion and contraction losses. By contrast the magnitude of F rises rapidly as Re' exceeds 1 and

continues to increase. This corresponds to the main channel flow being no longer able to resist the expansion and contraction mechanisms.

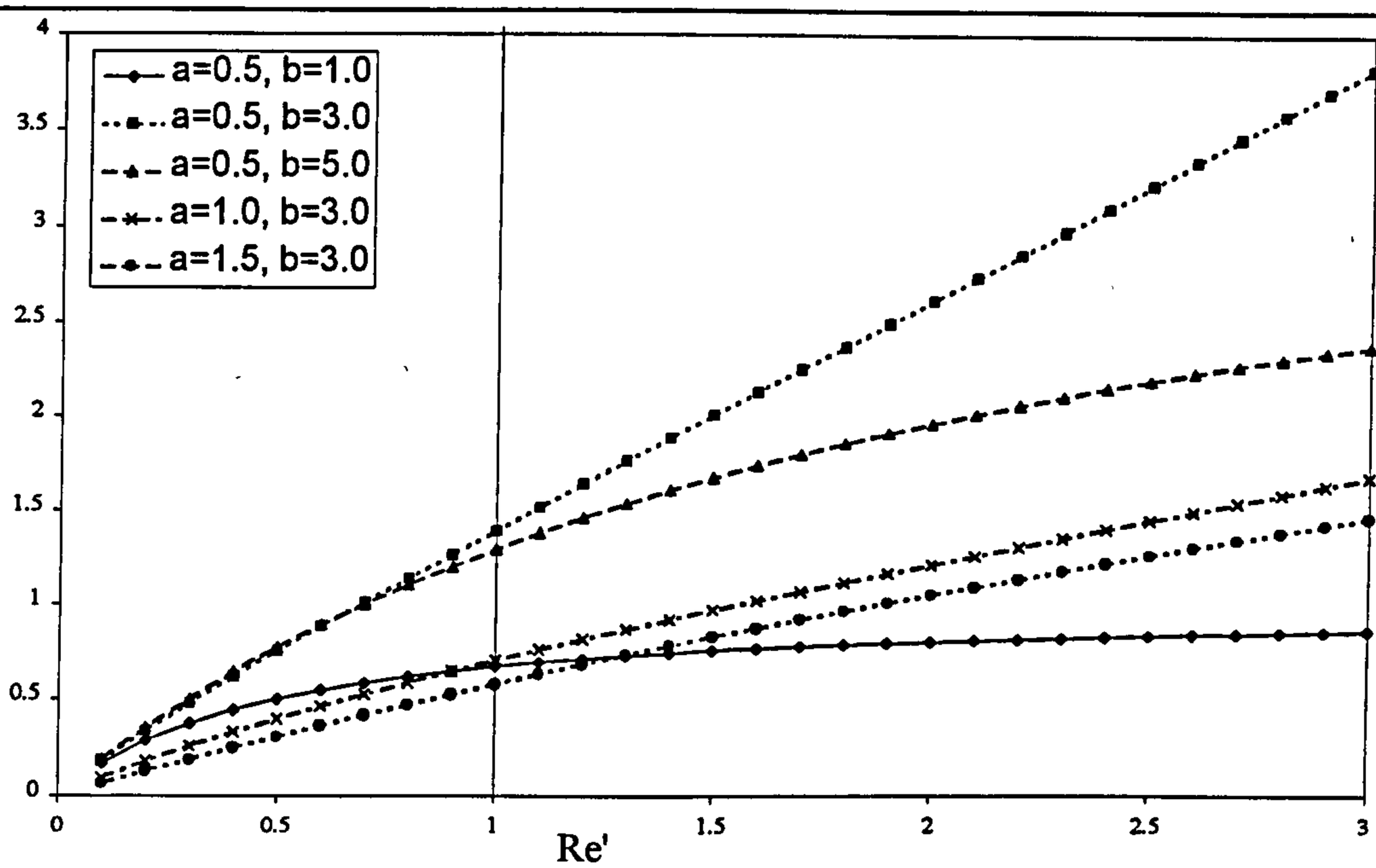

Figure 6.16 Plot of F versus Relative Reynolds number for various a and b

Equation 6.25 which defines the mean depth-averaged velocity in Zone B1 (with F_{B1} defined as in Equations 6.29) was regression fitted to mean depth averaged velocities which were measured in Zone B1, at all flow depths for all available flow data. The flow data which was used was collected from all the models tested during the Series B extension programme. The regression fitting derived values for the constants a and b and hence defined F_{B1}. Table 6.3 lists the pertinent statistical values that were obtained from the regression analysis.

Parameter	Value	StdErr	CV(%)	Dependencies
a	2.370e+0	3.530e-1	1.489e+1	0.7478522
b	6.136e+0	4.046e+0	6.593e+1	0.7478522

Table 6.3 Statistical values from regression fit with V_{B1} flow data

Table 6.3 demonstrates that there are no strong parametric dependencies which show that the relationship is not over-parameterised. The parametric standard deviations and CV% values are within acceptable limits. Consequently the flow region parameter, F_{B1}, is defined as in Equation 6.30

$$F_{B1} = \left(\frac{\mathrm{Re'}}{2.37 + \frac{\mathrm{Re'}}{6.14}} \right) \qquad [6.30]$$

The RMS percentage error and standard deviation between the measured mean depth-averaged velocities for Zone B1 in the Series B extension models (measured V_{B1}) and those obtained by back-substituting the parameter values into Equation 6.25 (predicted V_{B1}) were equal to 10.8% and 6.8% respectively. Figure 6.17 shows a plot of predicted V_{B1} versus measured V_{B1}.

Equation 6.26 which defines the mean depth-averaged velocity in Zone B2 (with F_{B2} defined as in Equations 6.29) was regression fitted to mean depth averaged velocities which were measured in Zone B2 at all flow depths for all available flow data. The flow data which was used was collected from all the models tested during the Series B extension programme. The regression fitting derived values for the constants a and b and hence defined F_{B2}. Table 6.4 lists the pertinent statistical values that were obtained from the regression analysis.

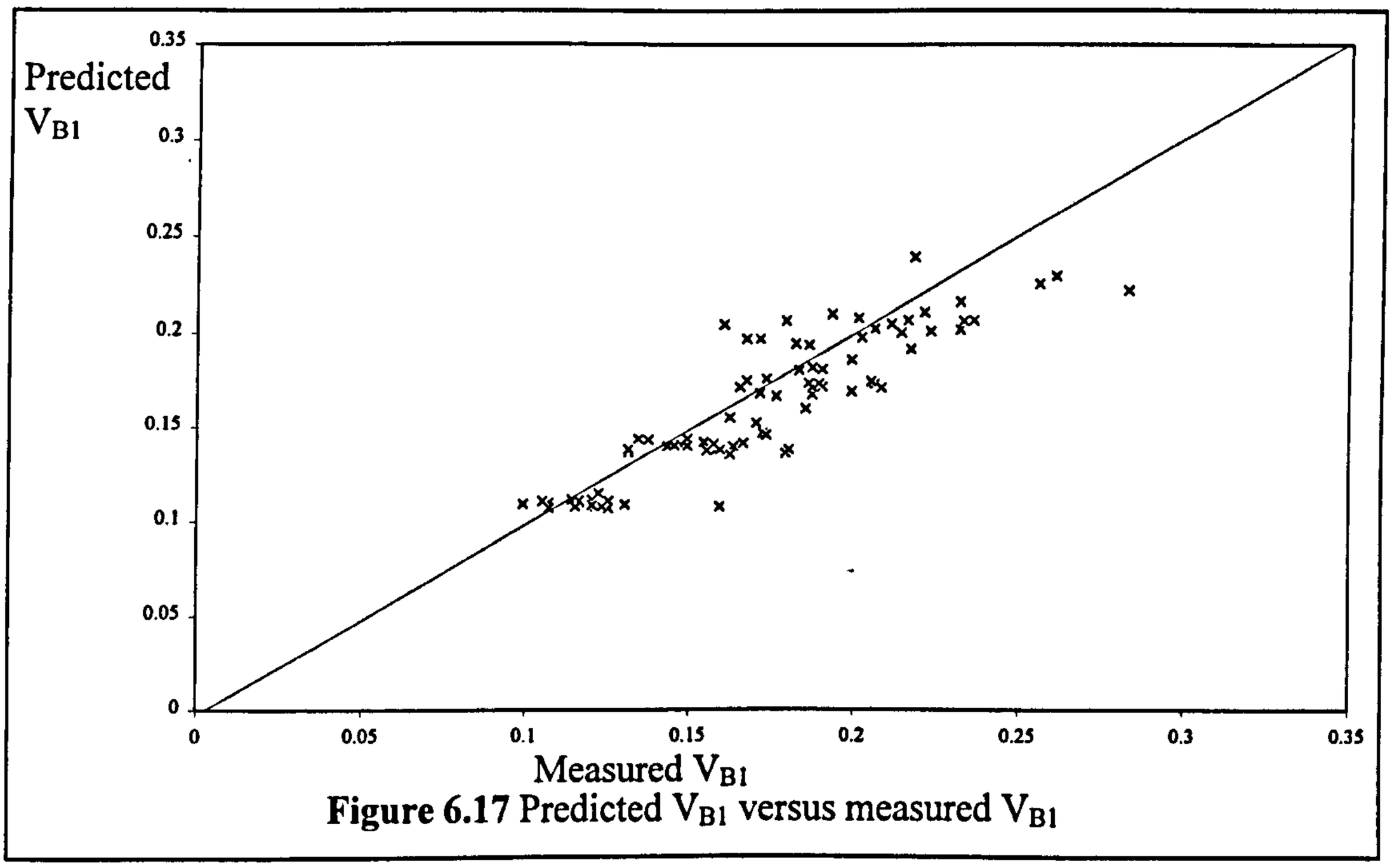

Figure 6.17 Predicted V_{B1} versus measured V_{B1}

Parameter	Value	StdErr	CV(%)	Dependencies
a	1.531e+0	4.396e-1	2.872e+1	0.7356675
b	2.833e+0	1.199e+0	4.233e+1	0.7356675

Table 6.4 Statistical values from regression fit with V_{B2} flow data

Table 6.4 demonstrated that there are no strong parametric dependencies which show that the relationship is not over-parameterised. The parametric standard deviations and CV% values are within acceptable limits. Consequently the flow region parameter, F_{B2} is defined as in Equation 6.31

$$F_{B2} = \left(\frac{\mathrm{Re'}}{1.53 + \frac{\mathrm{Re'}}{2.83}} \right) \qquad [6.31]$$

The RMS percentage error and standard deviation between the measured mean depth-averaged velocities for Zone B2 in the Series B extension models (measured V_{B2}) and those obtained by back-substituting the parameter values into Equation 6.26 (predicted V_{B2}) were equal to 11.0% and 7.1% respectively. Figure 6.18 shows a plot of predicted V_{B2} versus measured V_{B2}.

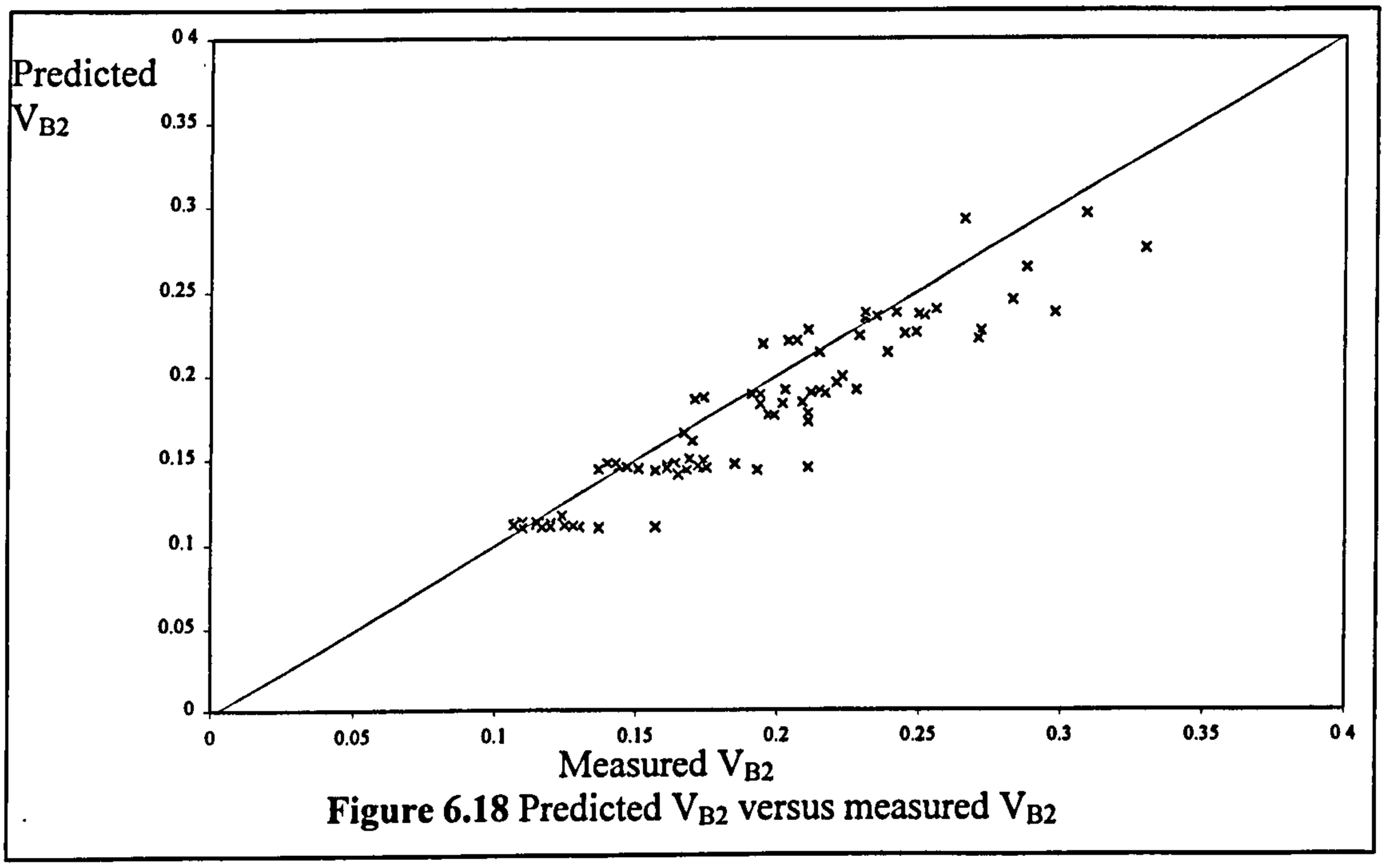

Figure 6.18 Predicted V_{B2} versus measured V_{B2}

6.5.3 The accuracy of the Enhanced zonal method for Zone B velocities

Both the Enhanced zonal method and the James and Wark [1] [1992] method were tested against some of the Series B model results. Figure 6.19 shows a plot of depth-averaged velocity versus flume width for SDB21 at flow depths equal to 0.05m (flow region 2).

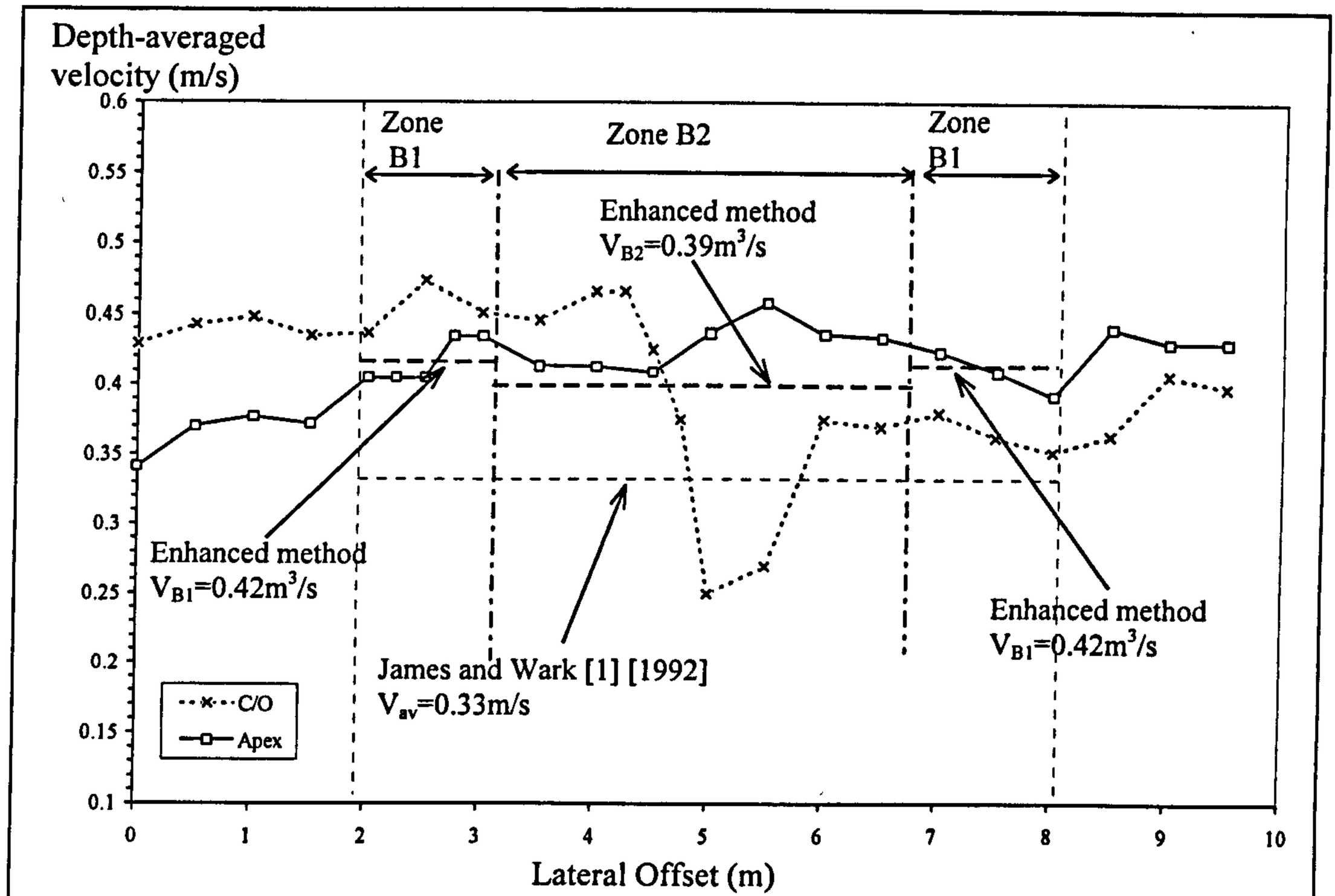

Figure 6.19 Depth-averaged velocity versus lateral offset at 50mm depth (SDB21)

Figure 6.20 shows a plot of depth-averaged velocity versus flume width for SDB21 at flow depths equal to 0.1m (flow region 3).

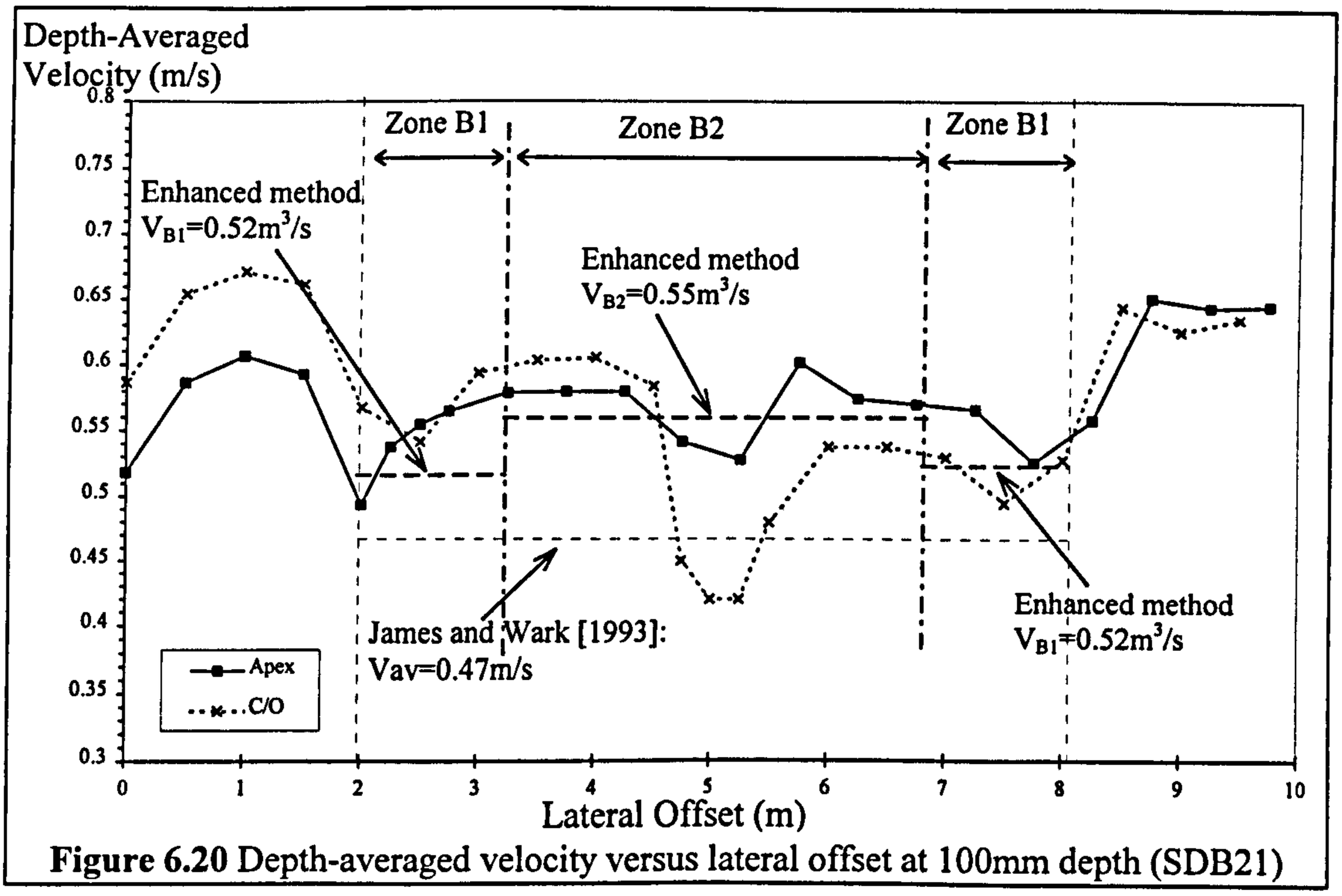

Figure 6.20 Depth-averaged velocity versus lateral offset at 100mm depth (SDB21)

The Enhanced zonal method employs Equations 6.25 and 6.26 in order to determine the mean depth-averaged velocities in Zone B1 and B2 and is based on a much sounder physical basis than the James and Wark [1] [1992] model. Figures 6.19 and 6.20 demonstrate that the Enhanced zonal method predicts the mean depth-averaged velocities in Zone B1 and Zone B2 more accurately than can achieved by using the James and Wark [1] [1992] method.

6.5.4 A refinement identified during the testing of the Enhanced zonal method

Analysis of the Zone B1 velocity predictions demonstrated that the Enhanced zonal method actually predicts the minimum value for Zone B1 velocity, V_{B1}, which occurs at the outside of the Apex. Typical plots, such as Figures 6.19 and 6.20, demonstrated that the depth-averaged velocity varies almost linearly from this minimum value to a value equal to the Zone B2 velocity, V_{B2}, on the inside of the Apex. Consequently in Enhanced zonal method, the discharge conveyed in Zone B1 is calculated using an arithmetic average of the Zone B1 velocity and Zone B2 velocity.

6.6 Flow behaviour in Zone C (Outside the meander belt)

The James and Wark [1] [1992] method recommends that the average velocity for the whole of Zone C can be calculated by assuming that bed friction is the only source of head loss. Consequently one of the standard flow resistance equations, either Manning's n or the Darcy-Weisbach formula, can be used to determine the discharge capacity. Although this postulation is acceptable for wide natural flood plains it is less appropriate for smaller scale physical models.

Figures 6.21 and 6.22 show the depth-averaged velocity in Zone C which was measured in test SDB21 from the Series B (1989-1992) programme at two overbank flow depths: 50mm and 100mm, at a number of lateral offsets across the flume. The James and Wark [1] [1992] estimate for mean depth-averaged velocity gave good predictions for the local velocity in Zone C at the majority of lateral offsets in Zone C. However when the flow depth equalled 100mm, shown in Figure 6.22, there was evidence that a shear zone was developed in Zone C where it interfaces with Zone B1.

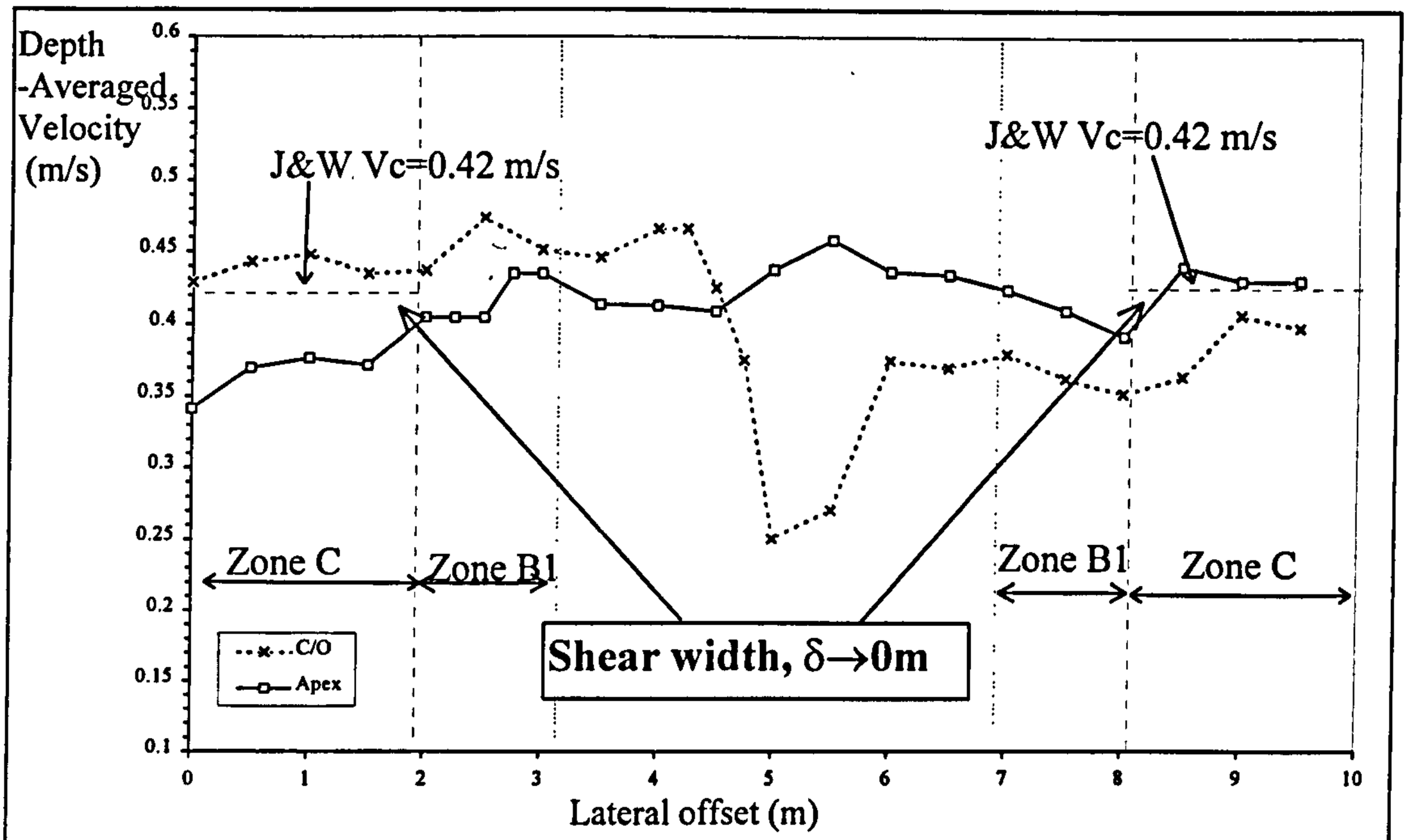

Figure 6.21 Variation of depth-averaged velocity with offset (SDB21, y=50mm)

A zone of vertical shear containing strong vortices with vertical axes parallel to the edge of the meander belt is established between Zones B1 and C. In Figure 6.22 the width of the shear zone is indicated with the symbol, δ. In the shear zone the mean depth-averaged velocity is lower than in the rest of the region.

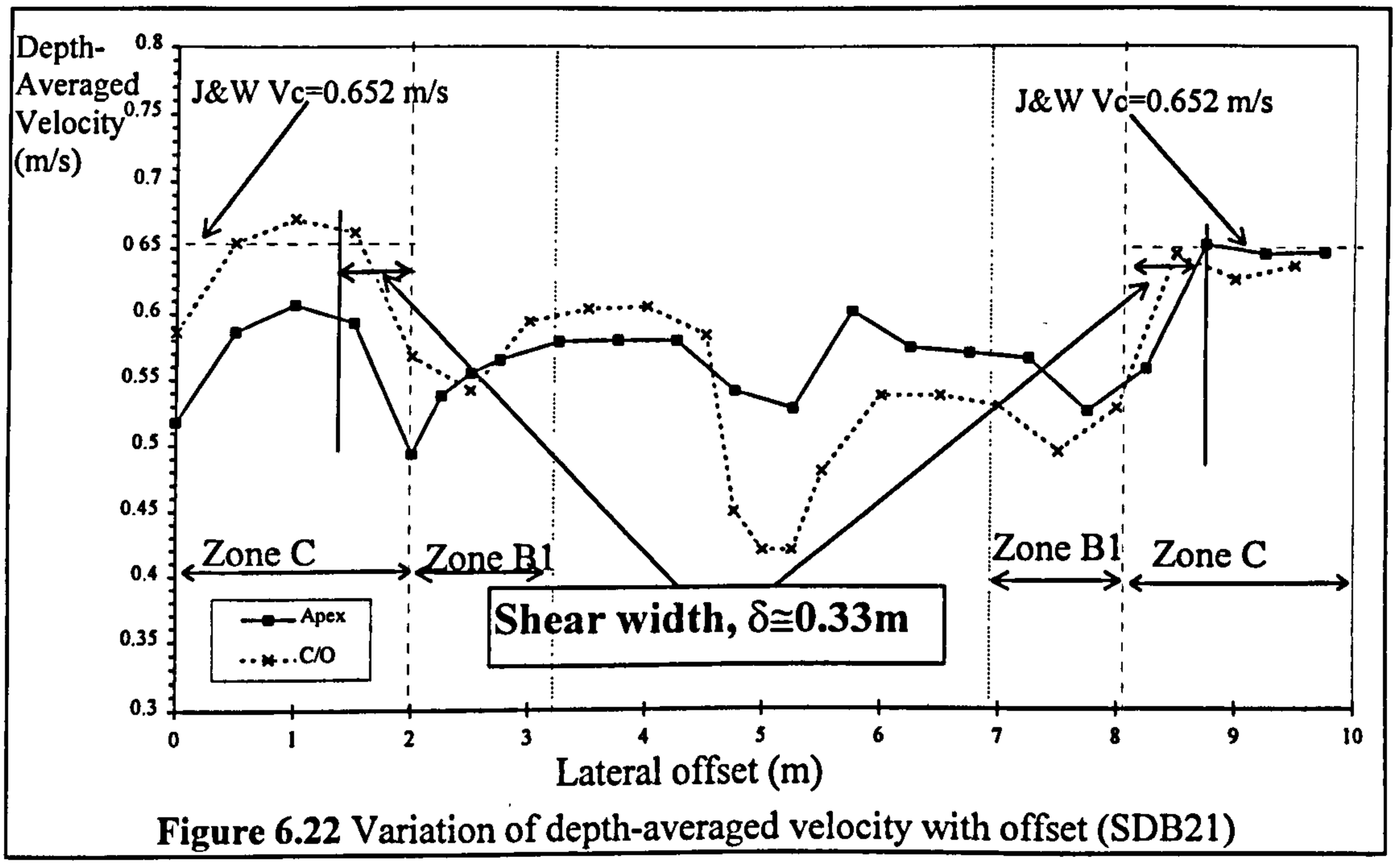

Figure 6.22 Variation of depth-averaged velocity with offset (SDB21)

Consequently the approach adopted in the James and Wark [1] [1992] method, whereby a standard resistance formula is applied to the whole of Zone C, will generate an over-estimation of discharge carried by Zone C.

6.7 The Enhanced zonal method for predicting discharge capacity in Zone C

6.7.1 The influence of flood plain flow depth

The influence of the reduced velocities in the Zone C shear zone will be especially significant in small scale models where the extent of the shear region can comprise a major proportion of the Zone C.

Figure 6.23 compares the mean depth-averaged velocity which was measured in Zone C outwith the shear layer and the velocity which is predicted using the standard resistance equations. It confirms that the mean depth-averaged velocity in Zone C, outwith the shear layer (width δ), can be accurately calculated using the standard resistance formula. The positioning and extent of the shear layer width is clearly illustrated in Figure 6.22.

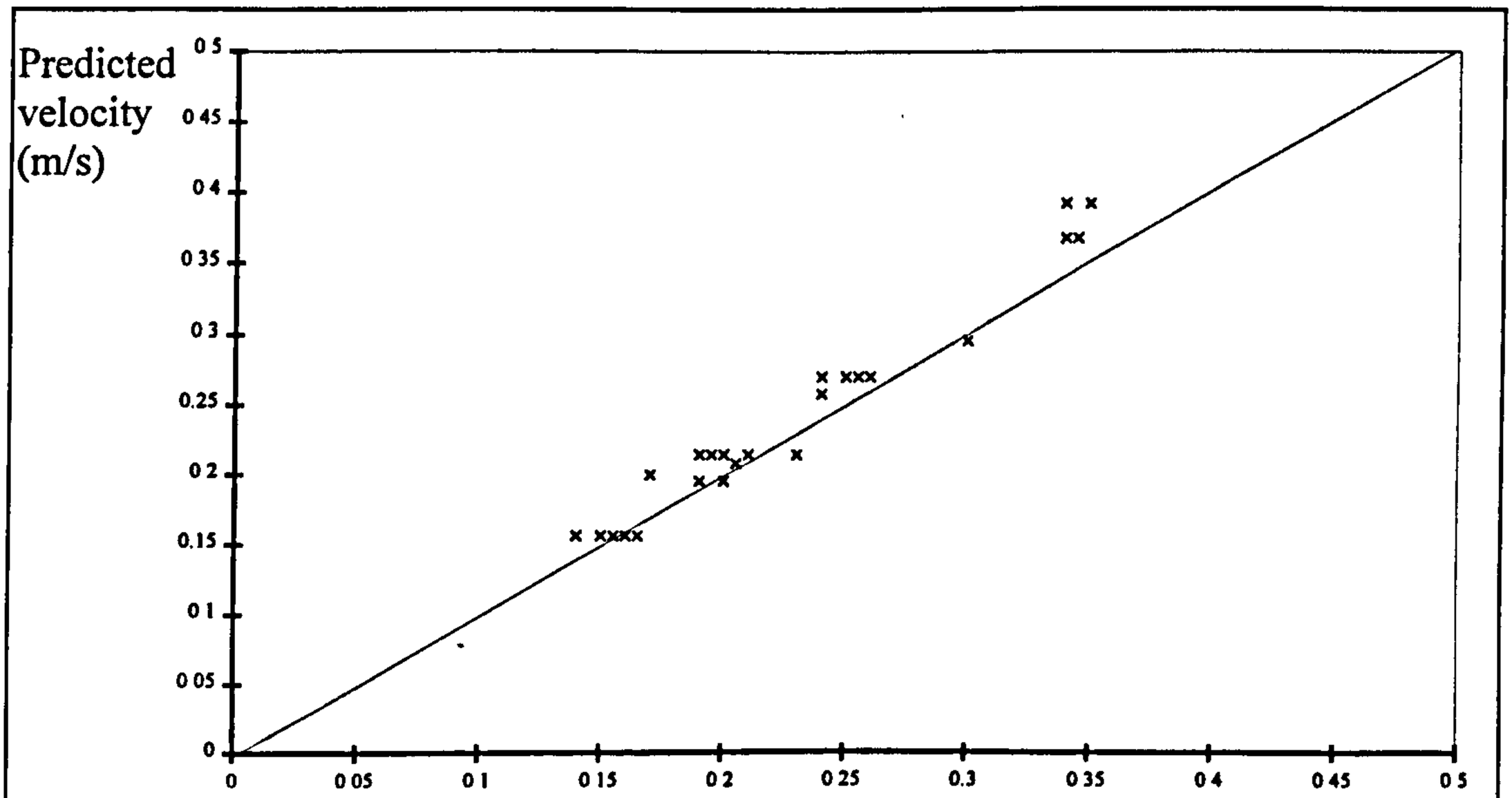

Figure 6.23 Measured versus predicted velocities (outwith the shear zone)

Inside the shear region, δ, the mean depth-averaged velocity can be calculated by taking the arithmetic mean of Zone C (outwith the shear zone) and Zone B1 (at the outside of the apices). The mean depth-averaged velocity in Zone B1 is calculated using Equation

6.25. The author developed an empirical method, as part of the Enhanced zonal method, which determined the width of the shear layer for all flow states and hence calculated the proportion of discharge conveyed within and outwith the shear layer in Zone C.

6.7.2 Determination of shear width for the Enhanced zonal method

Similar shear layers (to the ones generated between Zone B1 and Zone C in meandering compound channels) were observed in straight compound channels where the fast flowing water in the main channel forms a vertical shear layer with the flow on the slower flowing flood plain. The author attempted to extend two existing definitions of shear layer width for co-flowing layers in straight channels so that they could be applied to this situation. Lean and Weare [1979] derived a formulation which related shear width, δ, to the depth averaged lateral turbulent viscosity, ν_t, and the velocity difference, Δu, across the shear layer as shown in Equation 6.32.

$$\frac{\nu_t}{0.01\Delta u} = \delta \qquad [6.32]$$

Samuels [1988] derived an alternative definition for the shear width in straight compound channels, which is shown in Equation 6.33.

$$\delta = 5.7\left(D / gS_{xf} f\right)^{0.25} \nu_t^{0.5} \qquad [6.33]$$

where S_{xf} is the longitudinal friction slope, D is the local flow depth and f is the local Darcy-Weisbach friction factor. The author's attempts to use these methods directly were thwarted by the difficulties in defining suitable values for ν_t. Consequently an alternative empirical method for predicting shear width was developed using the results from the Series B extension (1993-1996) experiments.

In order to facilitate the application of the Enhanced zonal methods formulation to all different scale models, the shear width, δ, was normalised by dividing it by the flood plain flow depth, D, to give a non-dimensional parameter, δ/D.

Equation 6.35 shows an expression for δ/D (in terms of two non-dimensional parameters) the Darcy-Weisbach friction factor, f, and $\Delta u/U^*$ which can be derived by combining Equations 6.32 and 6.33 where the shear velocity, U*, is defined in Equation

6.34 and R is the hydraulic depth (which is set equal to the flood plain flow depth, D) because the flood plains were typically wide and shallow.

$$U^* = (gRS_{xf})^{1/2} \quad [6.34]$$

$$\frac{\delta}{D} = 0.01 * 5.7^2 \left(\frac{1}{f}\right)^{0.5} \frac{\Delta u}{U^*} \quad [6.35]$$

The author postulated that the shear width, in Zone C of a meandering compound channel, will be dependant on the same two non-dimensional parameters. A multi-variate regression analysis was performed on the general form of the shear width equation given in Equation 6.36, where a, b and c are constants.

$$\frac{\delta}{D} = a * \left(\frac{1}{f}\right)^b \left(\frac{\Delta u}{U^*}\right)^c \quad [6.36]$$

Table 6.5 lists the pertinent statistical values that were obtained when Equation 6.36 was regression fitted to the values for δ/D which were measured during the Series B extension programme. The values for δ/D which were measured are listed in Appendix A2. Table 6.5 demonstrates that there are no strong parameter dependencies. This indicates that the relationship is not over-parameterised. The parametric standard deviations and CV% values are within acceptable limits.

Parameter	Value	StdErr	CV(%)	Dependencies
a	3.187e-1	4.458e-2	1.399e+1	0.9894157
b	-5.202e-1	4.648e-2	8.935e+0	0.9906166
c	1.057e-1	3.240e-2	3.064e+1	0.9546556

Table 6.5 Statistical values from regression fit of δ/D to Series B extension data

The geometric progression shown in Equation 6.37 was consequently derived for use in predicting the value of δ/D.

$$\frac{\delta}{D} = 0.317 * \left(\frac{1}{f}\right)^{0.517} \left(\frac{\Delta u}{U^*}\right)^{0.114} \quad [6.37]$$

The RMS percentage error and standard deviation between the measured values for δ/D and those obtained by back-substituting the parameter values into Equation 6.37 were equal to 7.92% and 4.74% respectively. Figure 6.24 shows a plot of the measured shear width versus the shear width yielded by Equation 6.37.

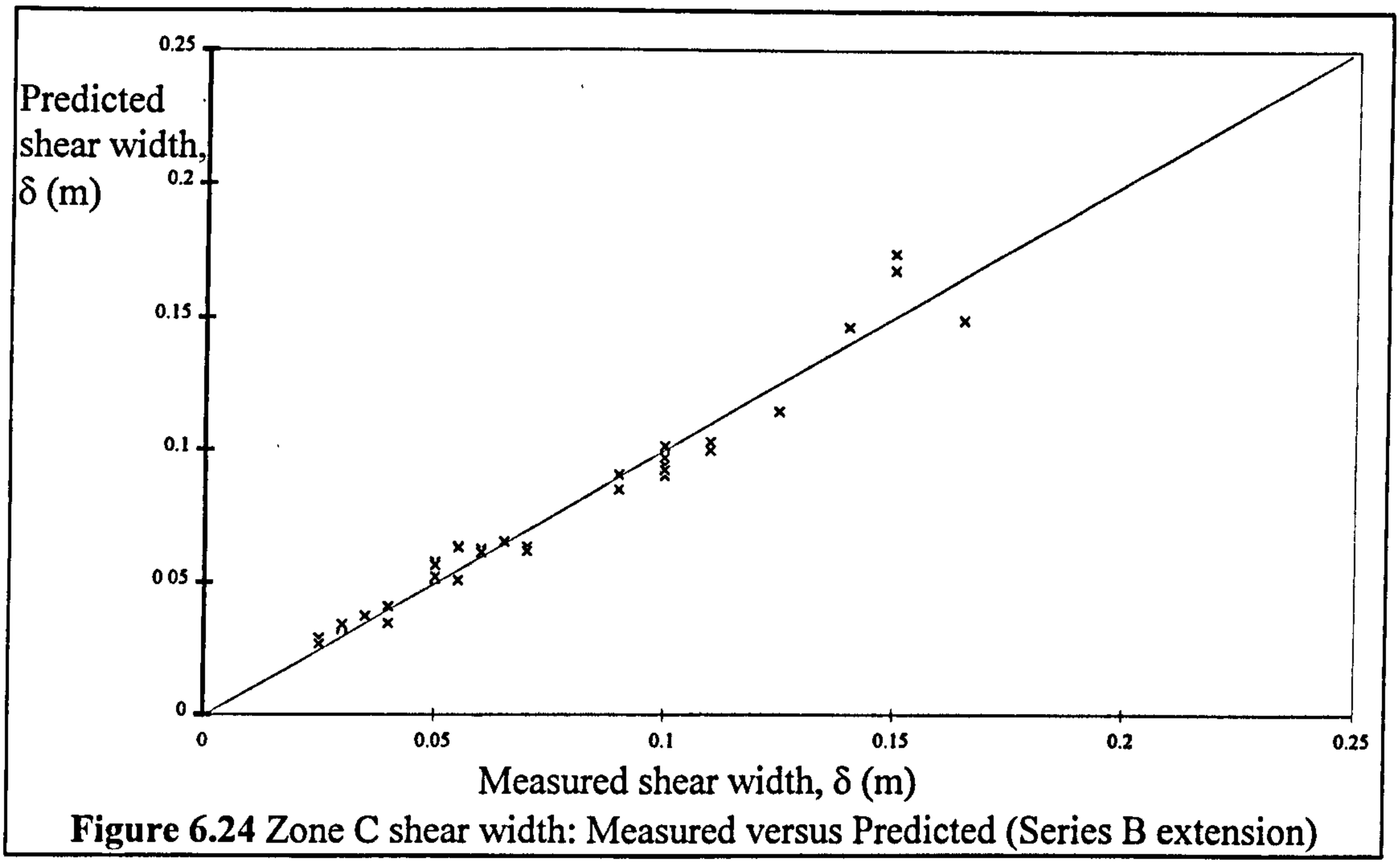

Figure 6.24 Zone C shear width: Measured versus Predicted (Series B extension)

6.7.3 Testing the shear width prediction method using Series B data

The shear width predictions from the Enhanced zonal method were checked against the values measured in the Series B test: SDB21, at 100m flood plain flow depth. The shear width in Zone C (averaged over both Zone C regions) was equal to 0.33m, as shown in Figure 6.22. Equation 6.37 yielded a shear width prediction which was equal to 0.32m (3% error). Further analysis and comparison with the other Series B test results should be performed in the future, when all the results are available, in order to determine whether the same accuracy is achieved for the other tests. In the interim this limited check provided the author with initial confirmation that the method could be used in larger scale models.

6.7.4 Testing the Enhanced zonal method's predictions for Zone C discharge

Standard resistance formulae were used to predict the discharge capacity of the area outwith the shear zone. An arithmetic average of Zone B1 and Zone C (outwith) velocity was used to calculate the average velocity and consequently the discharge capacity inside the shear zone. Figure 6.25 shows a comparison between the discharge in Zone C, measured during the Series B extension programme, and the predicted discharge using the Enhanced zonal method.

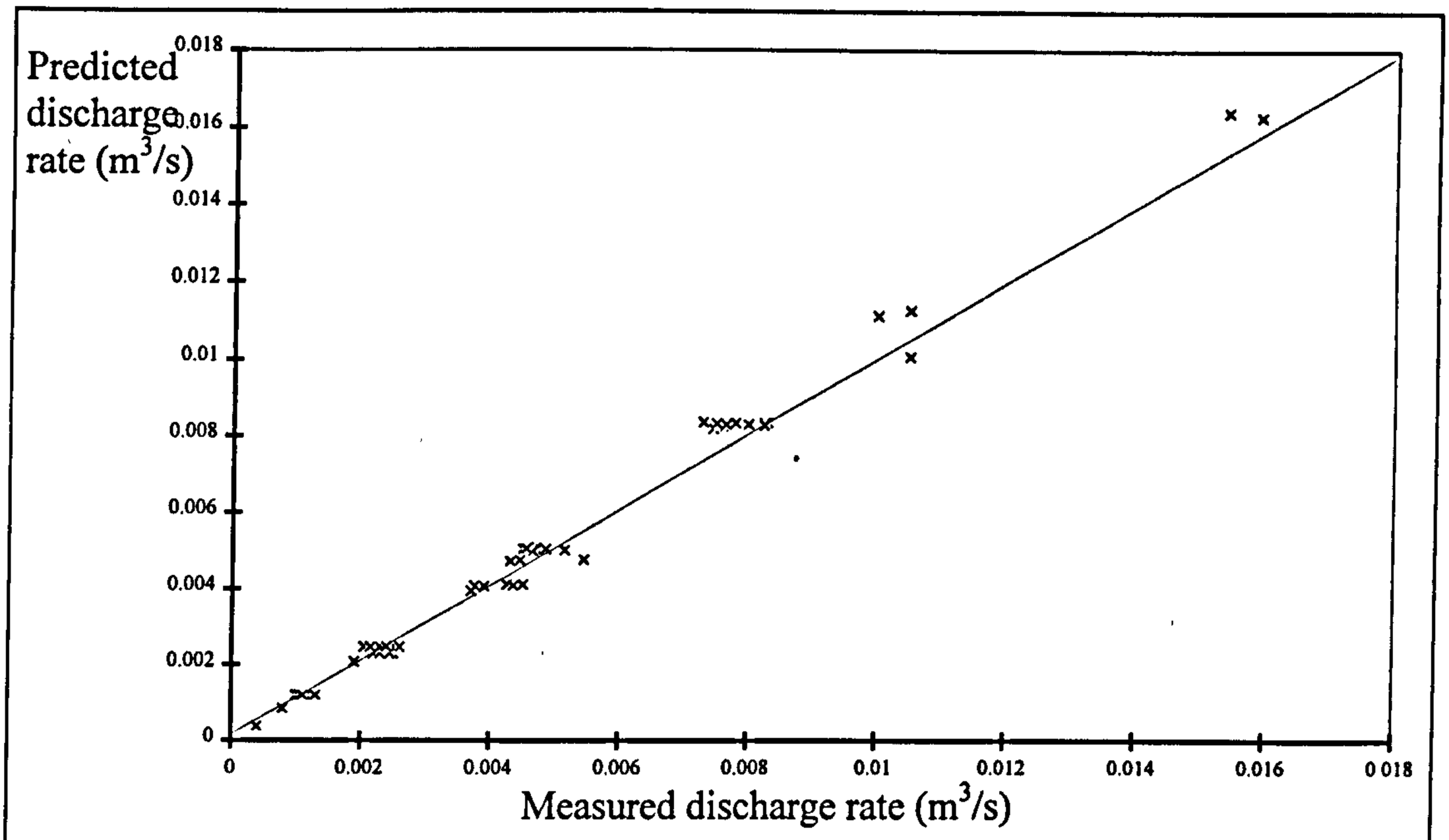

Figure 6.25 Zone C discharge capacity: Measured versus Predicted (Series B extension)

Table 6.6 shows a summary of the percentage differences between the measured and predicted discharges in Zone C.

Zone C Discharge			
Mean	St. Dev.	RMS	St. Dev.
3.2	6.2	7.1	4.4

Table 6.6 Correlation between measured and predicted Zone C discharge

6.8 Testing the Enhanced zonal method for a complete cross-section

6.8.1 Introduction

The author tested the accuracy of the Enhanced zonal method's predictions for total discharge capacity in various meandering compound channels (combining all three zones). Test flow data was only taken from models which possessed reliable bed friction calibration data. The test sets were divided into three distinct groups.

Group 1 consisted of all the available field data / prototype channels. Unfortunately at the time of writing the only available field data was gathered during studies of the River Roding. This data was published by Searle [1985]. Two sets of flow data were collected from the River Roding. One set was collected during year 1984/85 during which time

the flood plain was well maintained (Cut). It was ensured that the grass was kept short on the flood plain. The second set was collected during the year 1983/1984, when the flood plain was not maintained and the grass was left uncut.

Group 2 consisted of large scale model data obtained from Vicksburg [1956] and Series B (1989-1992). These models were large enough to ensure that turbulent flow was still generated in the models at most realistic flow depths. The author postulated that the flow behaviour in these channels were similar to those experienced in real rivers.

Group 3 consisted of a selection of the remaining reliable small scale data which was collected during the Series B extension (1993-1996) programme. This data had to be treated cautiously because scale effects were likely to have a significant influence in these models.

All the discharge capacity predictions that were generated using the Enhanced zonal method were compared with the predictions generated using the original James and Wark [1] [1992] method in order to demonstrate the benefits that can be accrued by using the new Enhanced zonal method.

6.8.2 Group 1: The River Roding data

The flow resistance in the main channel was directly measured, using Manning's n as the friction coefficient and was found to be equal to 0.044 which included an allowance for both bed surface friction and secondary circulation head losses. The author assumed that the same main channel flow resistance was generated for both maintenance conditions of the flood plains, over both years, 1983/84 and 1984/85. The sinuosity of the main channel, r, was equal to 1.4 which was similar to the typical sinuosities in the majority of models used to develop the Enhanced zonal method.

The flow resistance of the flood plain (predominantly friction and blockage resistance) was gauged in terms of Manning's n which was estimated (using the Chow [1959] tables) at n = 0.035 for the well maintained (cut) flood plains. This value corresponded to the maximum value (low maintenance) for short grass on a flood plain. Manning's n

was similarly assessed for the low maintenance flood plains (uncut) and was assigned a value of n= 0.05 which corresponded to the maximum value for high grass. Grass covered the whole flood plain and there was sparse other vegetation so these were reliable first approximation estimates for Manning's n.

Figure 6.26 shows a plot of flow depth versus discharge capacity for cut flood plains which was measured and predicted using the Enhanced zonal and the James and Wark [1] [1992] methods and assuming that the flood plain Manning's n was equal to 0.035.

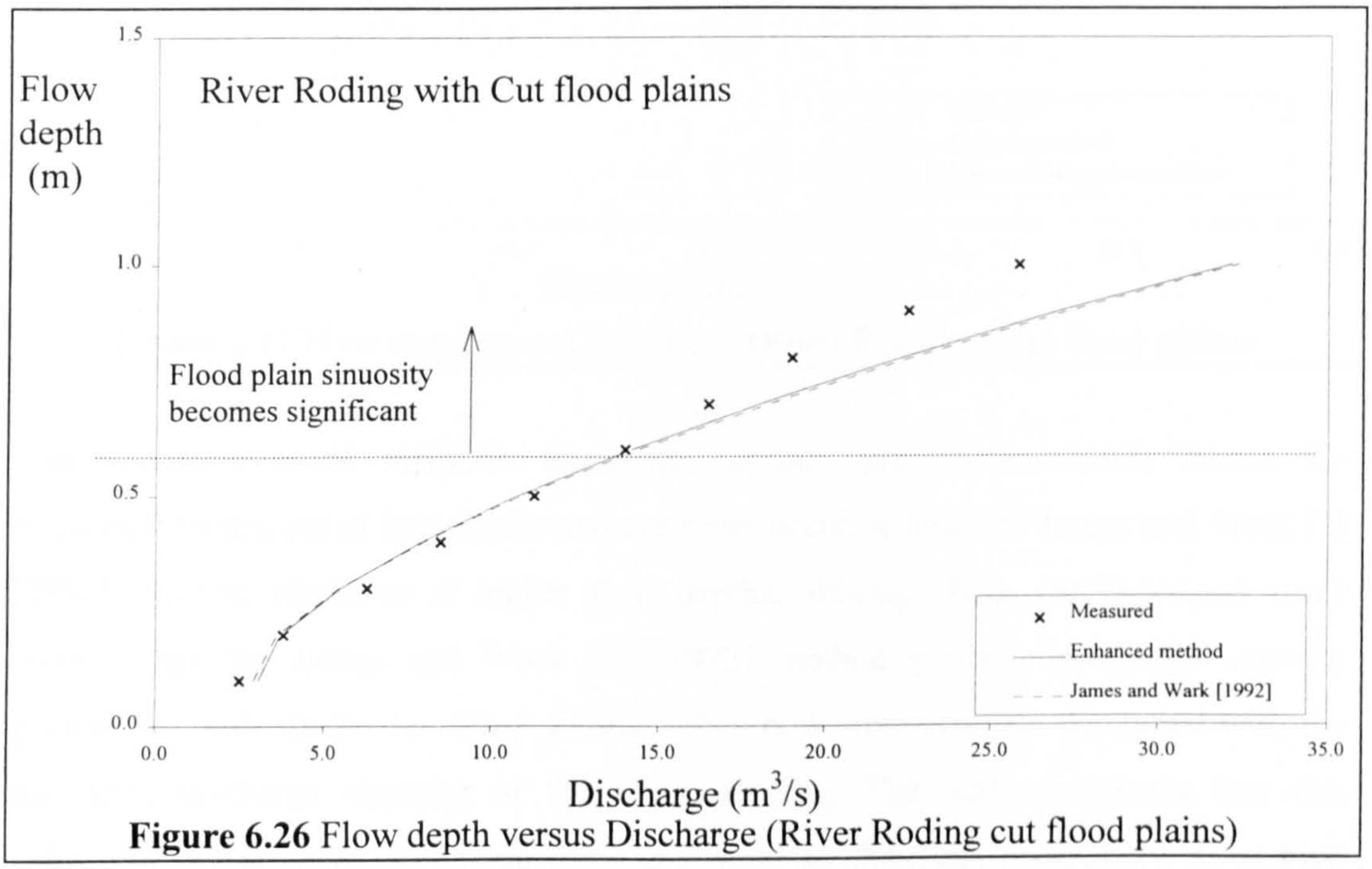

Figure 6.26 Flow depth versus Discharge (River Roding cut flood plains)

Figure 6.27 shows a plot of flow depth versus discharge capacity for the uncut flood plains which was measured and predicted using the Enhanced zonal method and the James and Wark [1] [1992] method and by assuming n= 0.05. Table 6.7 lists the statistical analysis of a selection of results obtained by comparing the measured discharge capacities in the River Roding with those predicted using both the Enhanced zonal and the James and Wark [1] [1992] methods.

	Enhanced zonal method				James and Wark [1][1992] method			
	Mean	St. Dev.	RMS	St. Dev.	Mean	St. Dev.	RMS	St. Dev.
River Roding Cut f/p	6.9	13.7	12.2	8.6	6.9	13.6	12.5	8.1
River Roding Uncut f/p	2.9	16.5	14.0	8.0	4.2	20.9	17.6	10.6

Table 6.7 Difference between the measured and predicted discharges for the River Roding.

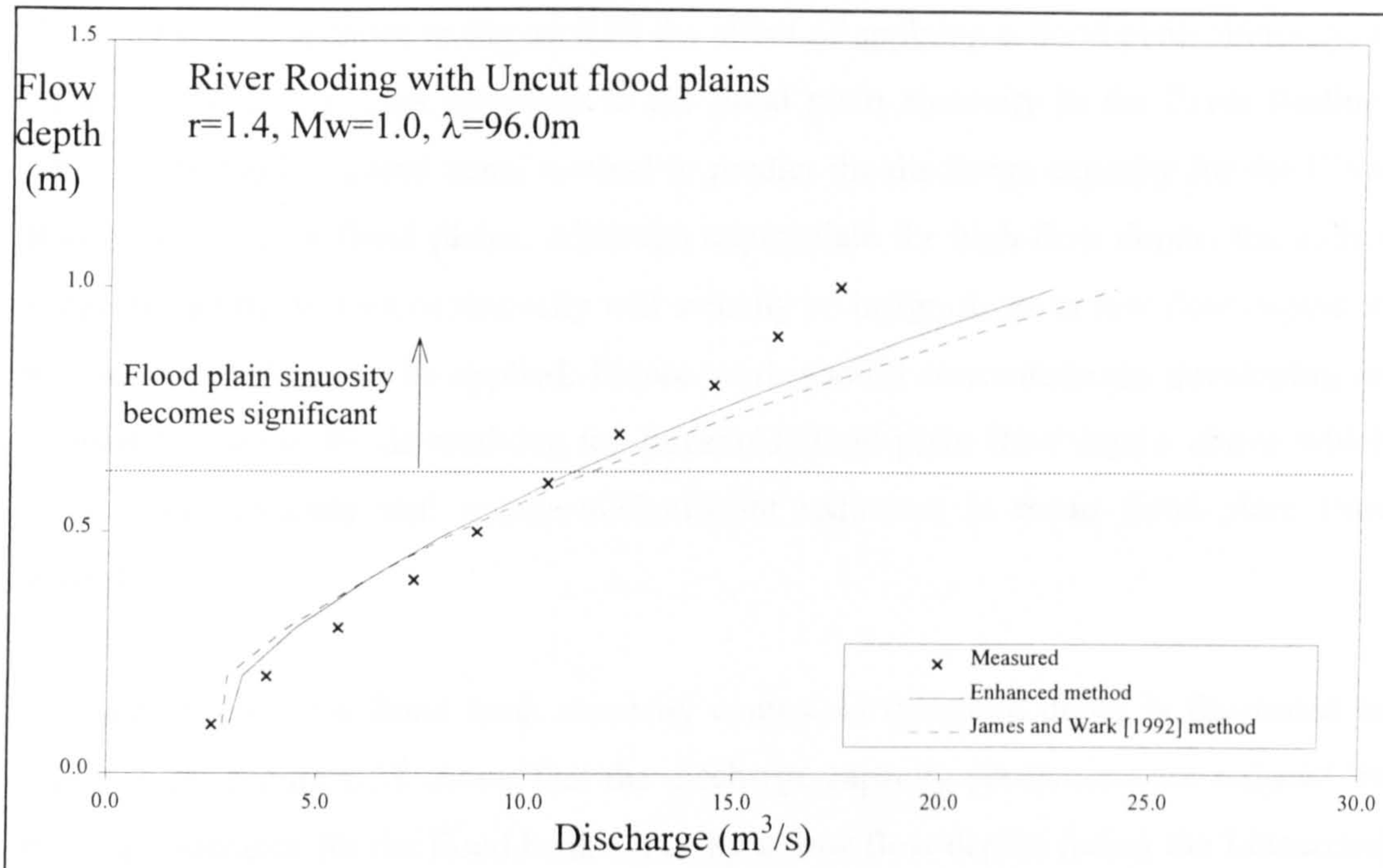

Figure 6.27 Flow depth versus Discharge (River Roding uncut flood plains)

The Enhanced zonal method's discharge capacity predictions closely match the measured discharges at low depths and are more accurate than the James and Wark [1] [1992] method. However at higher flow depths, although both the Enhanced zonal method and the James and Wark [1] [1992] method generate discharge capacity predictions with similar levels of accuracy they both over-estimate compared with the measured discharge capacity of the River Roding. The author suggests that this behaviour is caused by the increasing significance of flood plain sinuosity, r_u, at high flow depths which is not accounted for by either method.

None of the models used to derive the Enhanced zonal method had sinuous flood plains but they are certainly a feature of natural channels and further tests should be performed in the future to explicitly determine the influence of flood plain sinuosity. The author suggests that the sinuosity of the flood banks will induce secondary head losses in the flood plain flow which will supplement the bed friction losses. The capacity of the flood plain will be reduced compared with similar flood plains with straight flood banks at the same flow depths, irrespective of effect on interaction head losses. The author postulates that the resulting reduction in the average Zone B velocities (caused by flood plain sinuosity) will affect the magnitude of the interaction losses and alter the relative depths at which the Thresholds between flow regions are generated.

The author demonstrates in Figure 6.28 the effect of applying a flood plain sinuosity, r_u equal to 1.4 (a first approximation to the flood plain sinuosity in the River Roding) when using the Enhanced zonal method to predict the discharge capacity for the River Roding with uncut flood plains. Although appropriate for high flow depths the author suggests that the impact of sinuosity will actually be insignificant at low flow depths so it should therefore not be applied. Future work should concentrate on developing an explicit technique for determining the threshold flood plain flow depths above which flood bank sinuosity will induce a significant reduction in mean flood plain flow velocity.

The presence of this flood bank sinuosity controlled threshold depth is illustrated in Figure 6.28. Figure 6.28 shows that the discharge capacity predictions are reduced by making allowance for the flood bank sinuosity at low flow depths (using the Linearised SCS [1963] method) and become more inaccurate. However, by contrast, above the threshold depth, the discharge capacity predictions become more accurate.

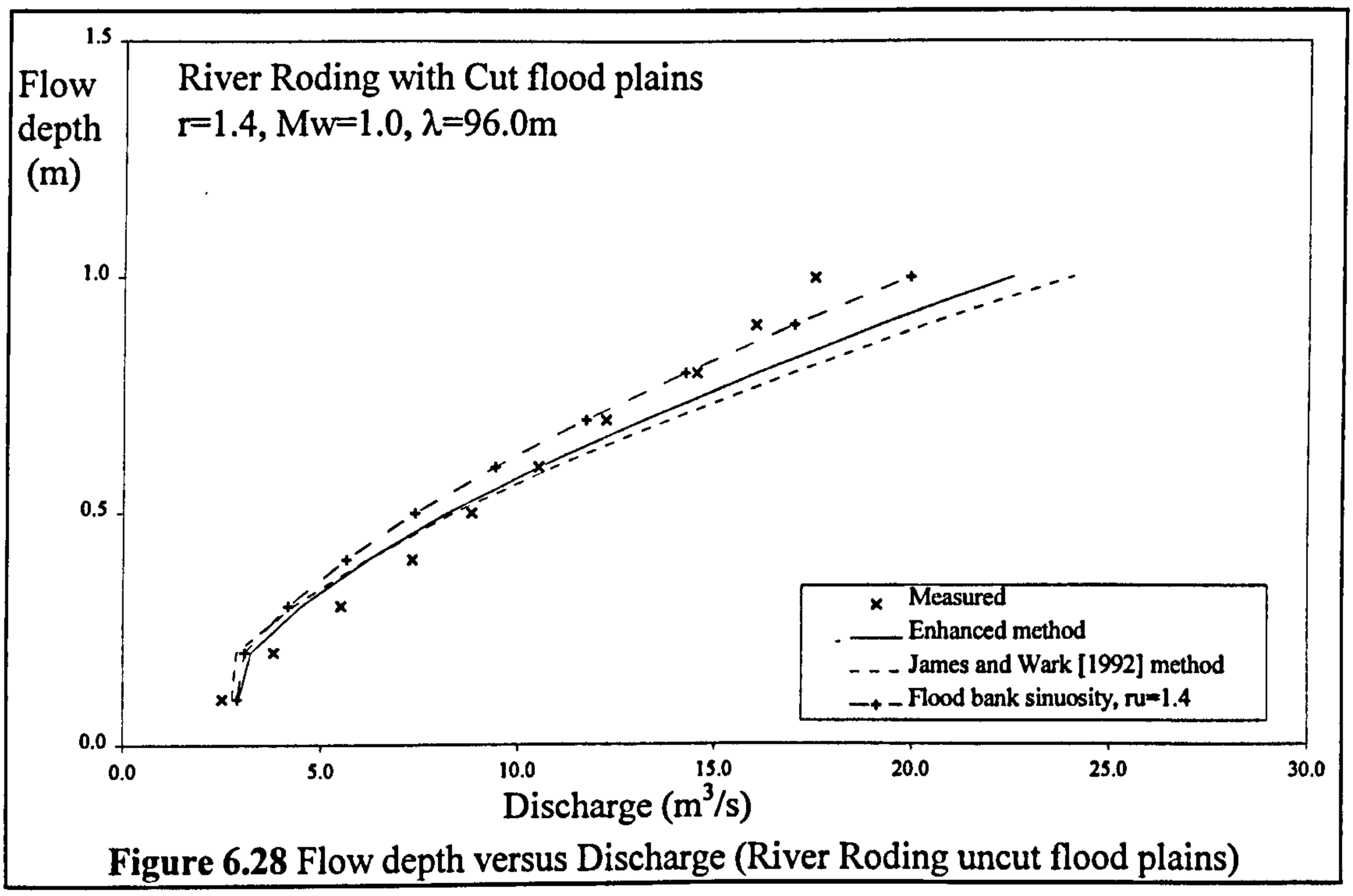

Figure 6.28 Flow depth versus Discharge (River Roding uncut flood plains)

The increase in interaction losses will be countered to some extent by the influence of lateral flood plain slopes, S_L. None of the models sets which were used to derive the Enhanced zonal method incorporated lateral flood plain slopes. However, they are certainly a feature of natural channels and further tests should be performed in the future

to explicitly determine their influence on flow behaviour. In the interim, the author postulates that the presence of lateral flood plain slopes will guide the flood plain flow in the same direction as the main channel so the interaction losses generated by the cross-shearing of the two flow layers will be reduced.

A number of research teams in the Universities of Bristol, England, and Witwatersrand, South Africa, are currently performing experimental tests in order to explicitly demonstrate the influence of flood plain sinuosity (and lateral flood plain slope). When these results are published it will be possible to incorporate more precisely the impact of both in the Enhanced zonal method.

6.8.3 Group 2: Large scale model data

6.8.3.1 Introduction

Two sets of large scale model data were readily available. The flow data obtained during the Series B programme (1989-1992) was detailed and widely regarded as the most reliable data that had been gathered to date. The Vicksburg [1956] data provided significant results to illustrate the influence of various parameters on flow behaviour but the data had to be treated cautiously in quantitative analysis because there was a doubt about the reliability of the bed friction calibration data. Flow data was only available for three flow depths. It was not possible to demonstrate that the typical four region flow behaviour was generated in Vicksburg [1956] models.

6.8.3.2 Series B (1989-1992)

Summary of results

A statistical analysis of the results obtained by comparing the measured discharge capacities of the Series B (1989-1992) models with the discharge capacities predicted using the Enhanced zonal and James and Wark [1] [1992] methods, is presented in Table 6.8.

Table 6.8 demonstrates that the Enhanced zonal method generates more accurate predictions than the James and Wark [1] [1992] method for the majority of models

tested during the Series B (1989-1992) programme. This is further illustrated in Figures 6.29, 6.30 and 6.31 which show plots of flow depth versus the measured and the predicted discharge capacities of SDB25, SDB31 and SDB39. Both SDB25 and SDB31 had natural main channels, main channel sinuosity equal to 1.374 and relative meander belt widths equal to 1.62 and 1.0 respectively. SDB39 had a natural main channel, a main channel sinuosity equal to 2.043 and a relative meander belt width equal to 1.62 and 1.0.

	Enhanced zonal method				James and Wark [1][1992] method			
	Mean	St. Dev.	RMS	St. Dev.	Mean	St. Dev.	RMS	St. Dev.
SDB21	3.3	1.4	3.3	1.4	3.3	5.5	3.9	5.1
SDB25	-2.5	2.6	2.8	2.3	-2.3	2.8	3.3	1.4
SDB31	-6.9	3.0	6.9	3.0	-8.9	6.3	10.1	3.9
SDB34	-5.9	2.6	5.9	2.6	-2.6	2.4	3.2	1.3
SDB39	6.9	8.7	7.9	7.7	-9.5	7.5	11.3	4.2
SDB43	-4.5	6.6	6.6	4.1	-7.4	3.1	7.5	2.6
SDB47	4.5	7.5	7.1	5.1	-15.2	8.6	16.2	6.6

Table 6.8 Difference between the measured and predicted discharges for Series B.

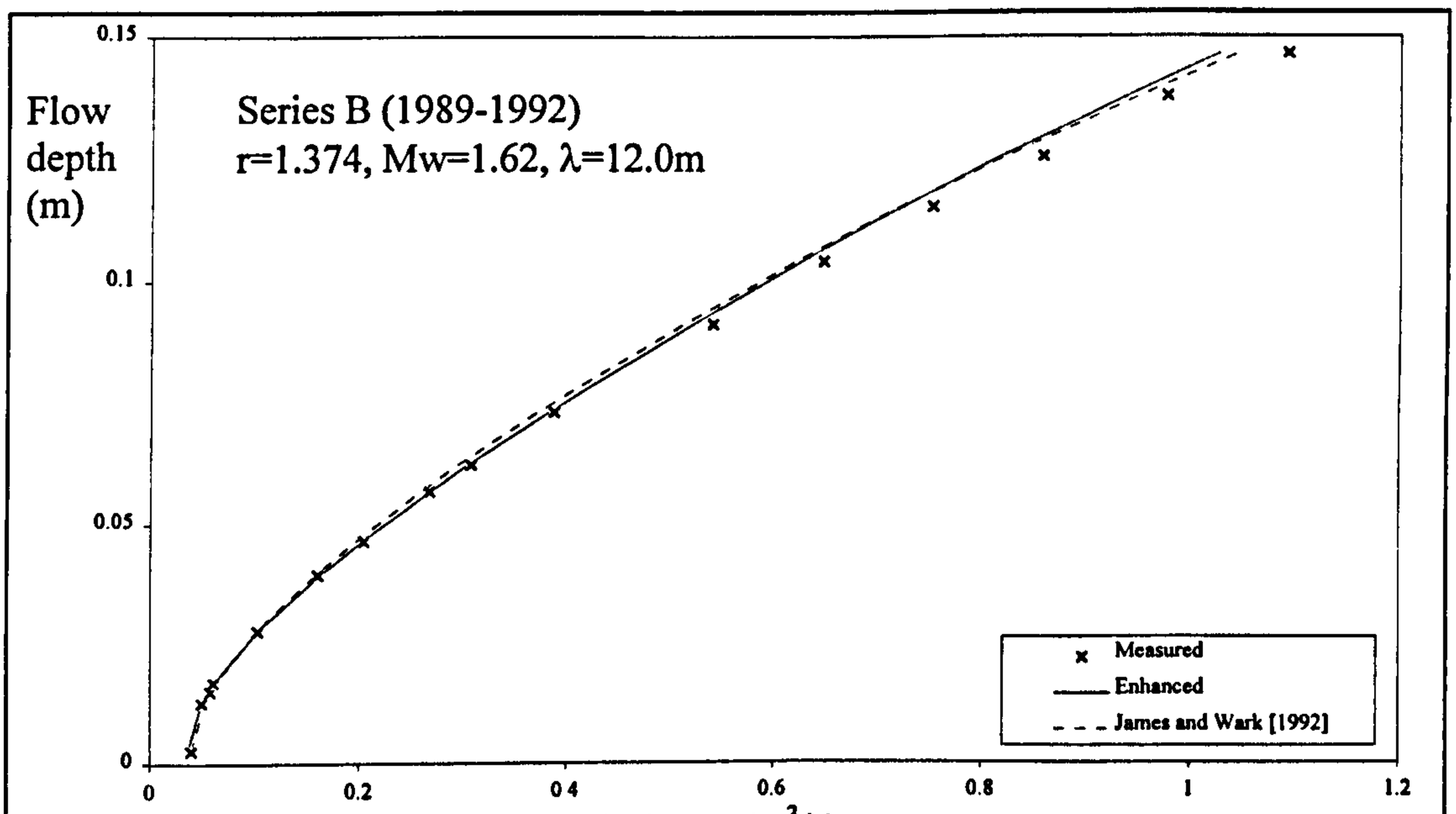

Figure 6.29 Flow depth versus Discharge (SDB25) (Series B (1989-1992))

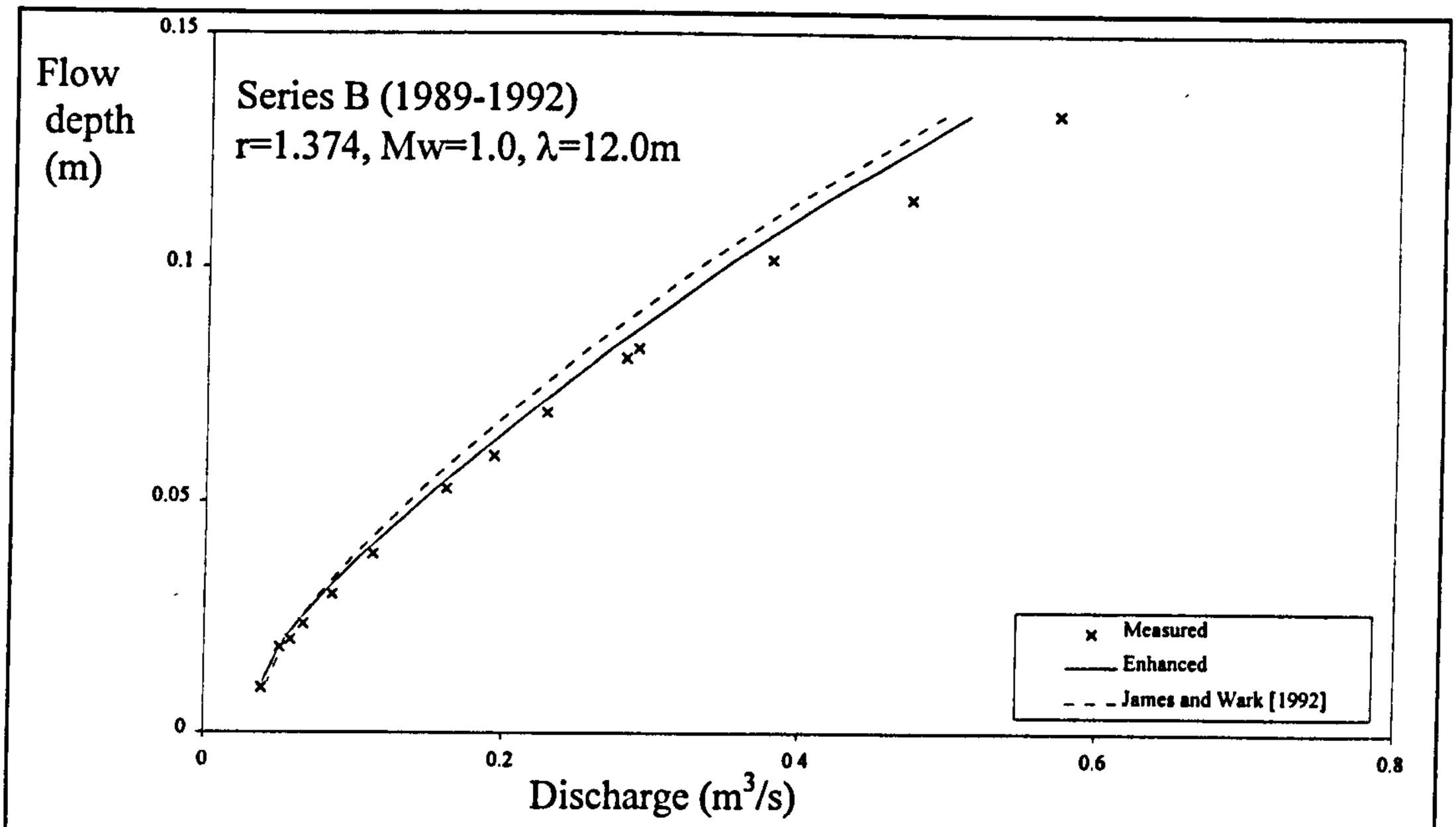

Figure 6.30 Flow depth versus Discharge (SDB31) (Series B (1989-1992))

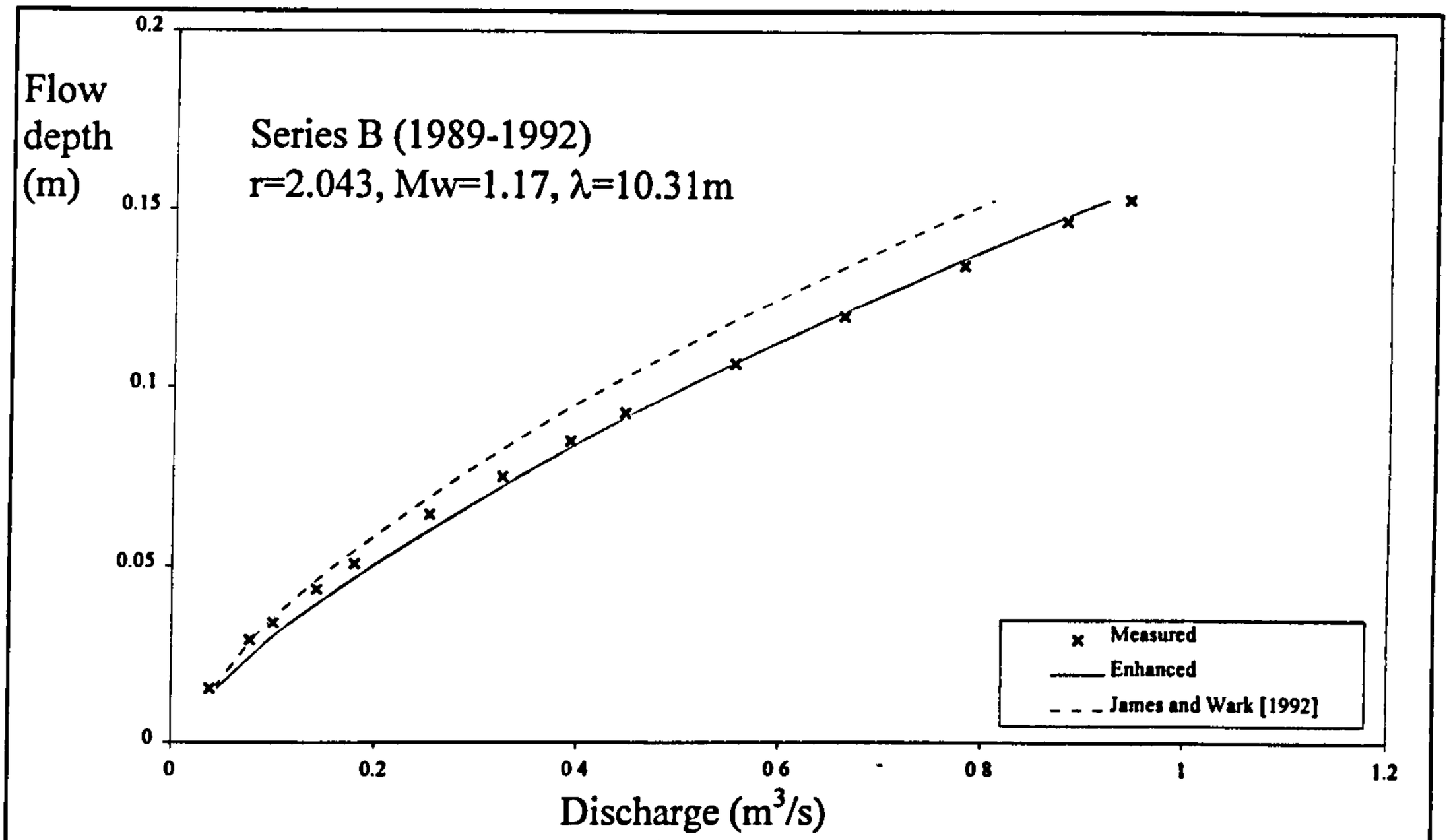

Figure 6.31 Flow depth versus Discharge (SDB39) (Series B (1989-1992))

Close inspection of the results shows that the Enhanced zonal method gives more accurate predictions at lower flow depths than the James and Wark [1] [1992] method. However, at higher flow depths both prediction methods give similar levels of accuracy.

The most significant differences between the performance of the two prediction methods was observed in SDB34 which had a highly roughened flood plain and SDB39 which had a highly sinuous channel and a reduced Zone C width.

Highly roughened flood plains

Both the Enhanced zonal method and the James and Wark [1] [1992] method under-estimate the discharge in SDB34, which had flood plains which were highly roughened with dowel rods. At all flow depths in this model the bed frictional (blockage) resistance dominates flow on the flood plains. Figure 6.32 shows a plan view of the typical pattern of flow velocity vectors that will be generated.

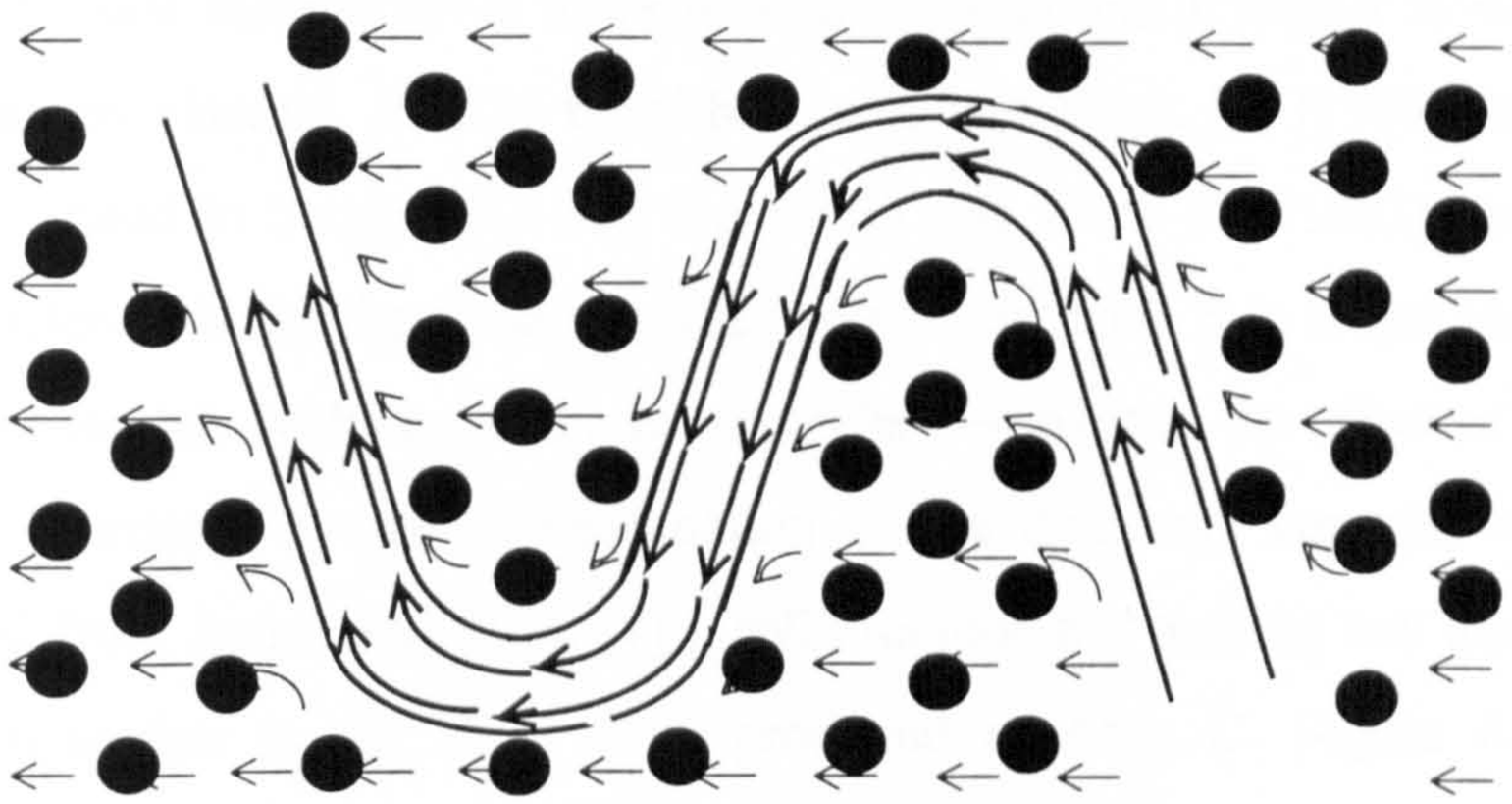

Figure 6.32 Schematic drawing showing the channel with dowel rods

Unlike the majority of meandering compound channel models that have been tested over the years it is clear that the 3 zone split of the cross-section to model the main bodies of interacting flow in a meandering channel, as shown in Figure 6.34, is inappropriate for these channels in flow region 3 and actually a 2 zone split, as shown in Figure 6.34, is more appropriate.

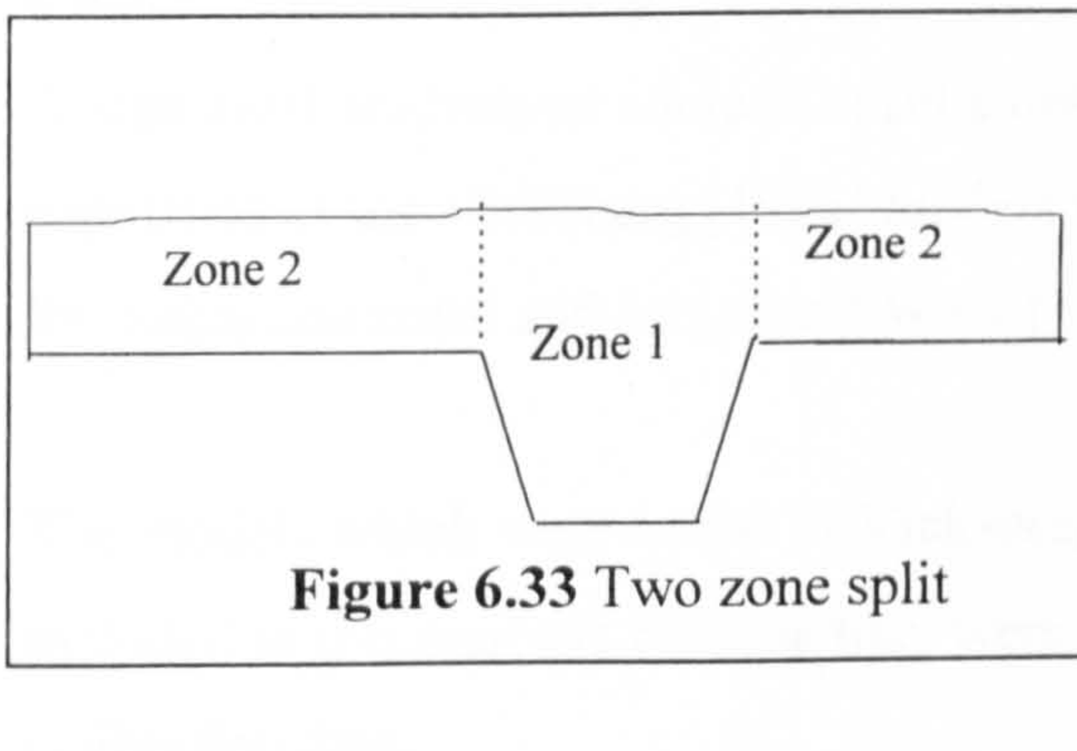

Figure 6.33 Two zone split

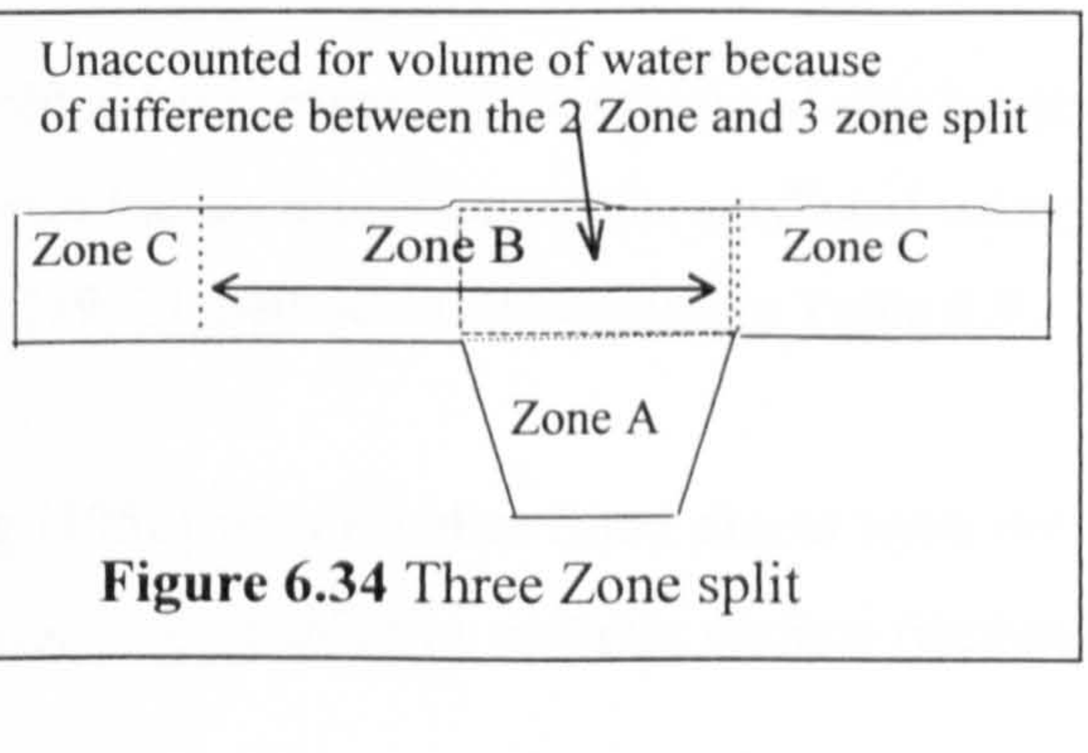

Figure 6.34 Three Zone split

By using the 3 zone split, the same high flow resistance which is appropriate for the flood plains is also applied to the area in Zone 1 (as shown in Figure 6.33) directly above Zone A. In reality this area of water, which is shaded in Figure 6.34, forms a Zone of more free-flowing water in combination with the water in Zone A and acts in a similar fashion to Zone 1 flow in two zone flow behaviour. Consequently, a greater rate of flow passes through this zone (shaded in Figure 6.34) than is accounted for by the Enhanced zonal or James and Wark [1] [1992] methods. This results in the under-estimation of total discharge capacity in these models as shown in Figure 6.30.

Narrow flood plains

The Enhanced zonal method gives more accurate predictions at higher flow depths for the highly sinuous channel, SDB39 than the James and Wark [1] [1992] method. The author demonstrated in Section 6.4 that the James and Wark [1] [1992] method has a tendency to under-estimate the mean averaged velocity in Zone B in larger scale models. However in the models with larger relative meander belt widths, the effect of this under-estimation is countered by the overestimation of the discharge capacity of Zone C, which resulted from James and Wark [1] [1992] method not making any allowance for the velocity reduction in the shear zone produced in Zone C. Figure 6.30 simply illustrated the consequences when the Zone C width becomes reduced or non existent. In these circumstances the counterbalancing does not take place and so the under-estimation of Zone B velocity is significantly reflected by the James and Wark [1] [1992] method which underestimates the total discharge capacity by an amount in proportion to the Zone B velocity deficit.

6.8.3.3 Vicksburg [1956]

A statistical analysis of some of results obtained by comparing the measured discharge capacities of the Vicksburg [1956] models with the discharge capacities predicted using the Enhanced zonal and James and Wark [1] [1992] methods, is presented in Table 6.9.

The models which were tested in Vicksburg [1956] with rougher flood plains were not included in this analysis because they were not accompanied by suitable surface friction calibration data.

	Enhanced zonal method				James and Wark [1] [1992] method			
	Mean	St. Dev.	RMS	St. Dev.	Mean	St. Dev.	RMS	St. Dev.
SDVB201	9.3	2.7	9.3	2.7	-1.2	3.1	2.1	2.2
SDVB204	3.2	6.3	5.9	2.0	-2.1	6.0	5.0	2.4
SDVB207	-1.3	3.6	3.0	1.5	-1.2	5.4	4.5	1.1

Table 6.9 Difference between the measured and predicted discharges for Vicksburg [1956].

Table 6.9 demonstrates that the Enhanced zonal method generates predictions with a similar level of accuracy compared with the James and Wark [1] [1992] method. Figure 6.35 shows plots of flow depth versus measured and predicted flow discharge capacity for SDVB204 in order to illustrate this similarity.

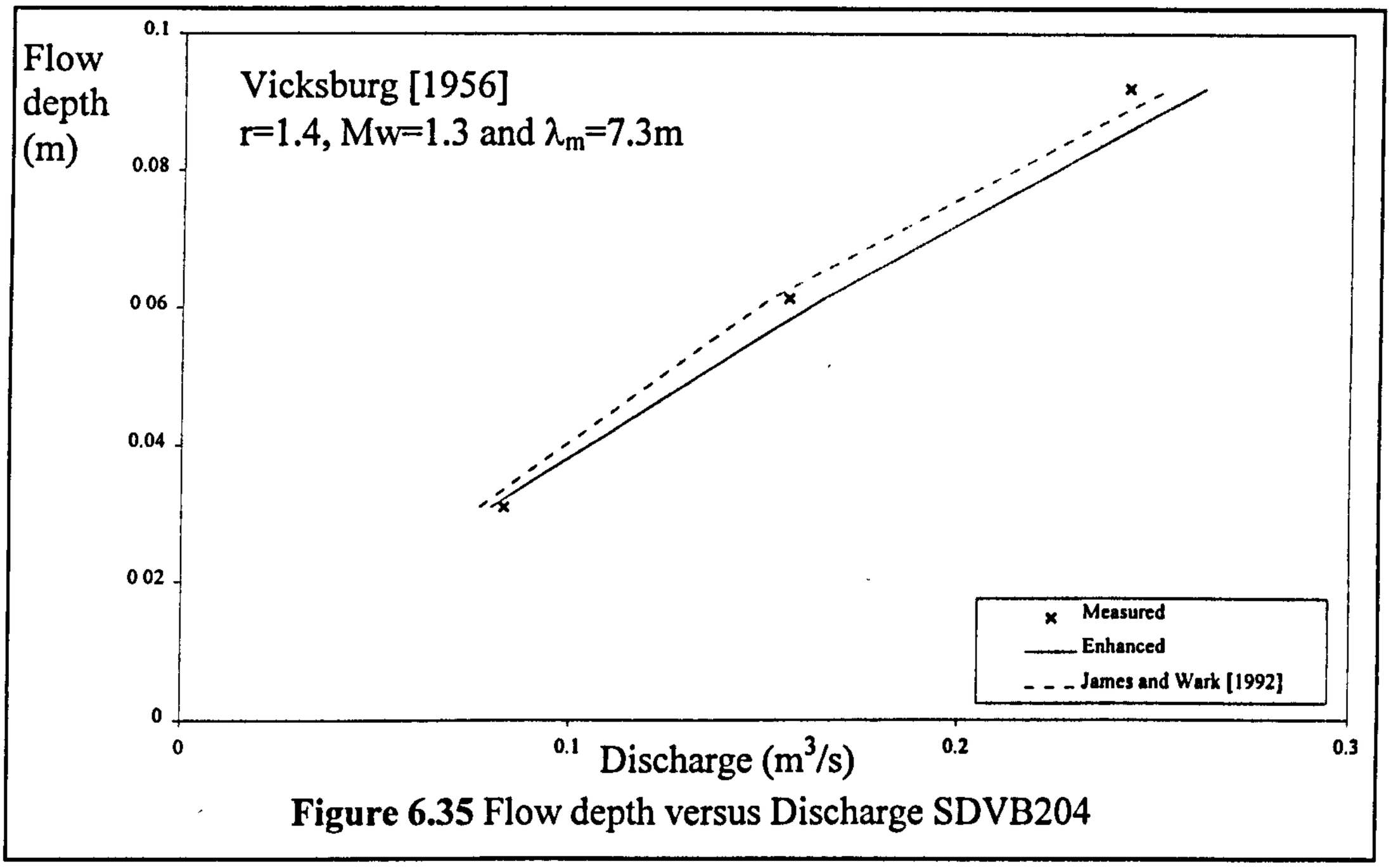

Figure 6.35 Flow depth versus Discharge SDVB204

The small number of data points generated in each model test performed in Vicksburg [1956] and uncertainty about the bed roughness calibration leads the author to suggest that the data should be used carefully when developing or assessing any future discharge capacity prediction methods.

6.8.4 Group 3: Small scale models

6.8.4.1 Introduction

The Enhanced zonal and James and Wark [1] [1992] methods were tested on 5 sets of small scale model data. Listed in chronological order these were: Toebes and Sooky [1967], Kiely [1989], Aberdeen (1991) reported by Willetts and Hardwick [1993], Series B extension (Glasgow), Series B extension (Aberdeen). A distinction is made between the discharge capacity predictions which are generated when the prediction methods are tested on the model flow data which was used to develop them.

6.8.4.2 Toebes and Sooky[1967]

Table 6.10 lists the statistical analysis of a selection of results obtained by comparing the measured discharge capacities in Toebes and Sooky [1967] with those predicted using both the Enhanced zonal and the James and Wark [1] [1992] methods. Apart from SDSK405, the Enhanced zonal and the James and Wark [1] [1992] methods gave accurate predictions for the discharge capacity of these channels. The Enhanced zonal method however gave slightly more accurate results for the majority of the models.

	Enhanced zonal method				James and Wark [1] [1992] method			
	Mean	St. Dev.	RMS	St. Dev.	Mean	St. Dev.	RMS	St. Dev.
SDSK401	-3.3	4.1	4.8	1.6	12.3	4.7	12.3	4.7
SDSK402	-3.0	5.3	4.7	3.5	11.8	4.9	14.8	4.9
SDSK403	-2.2	6.2	6.0	1.4	9.5	5.7	9.5	5.7
SDSK405	-38.4	2.2	38.4	2.2	-29.2	2.2	29.2	2.2
SDSK408	-10.3	4.6	10.3	4.6	1.8	9.6	7.5	5.2
SDSK411	-4.1	6.4	5.9	4.3	5.4	11.3	8.8	8.2

Table 6.10 Difference between the measured and predicted discharges for Series B.

Both methods significantly under-estimate the discharge capacity of SDSK405. The author suggests the discrepancy may be attributable to the very shallow slopes that were used in this model which may have lead to the associated measurements being inaccurate. However the author also considered that both the Enhanced zonal and James and Wark [1] [1992] prediction methods may be inadequate for channels with very shallow slopes such as in SDSK405 which had a flood plain slope which was shallower

than any the other models for which data was collected during the Series B extension (1993-1996) programme.

Much more data must be gathered before this conjecture can be verified. In the interim, the Series B extension (1993-1996) tests in Aberdeen have provided some information demonstrating the influence of flood plain slope, but eventually they only tested relatively steeply sloping flood plain slopes of 1 in 1000 and 1 in 750. Until this data is forthcoming, anyone applying either method to meandering compound channels with shallow flood plain slopes should exercise due care. The two prediction methods have certainly been derived using only data obtained from models with much steeper longitudinal slopes.

Figure 6.36 shows plots of flow depth versus discharge capacity for SDSK402 which demonstrates the typical level of discharge capacity prediction accuracy achieved by both methods.

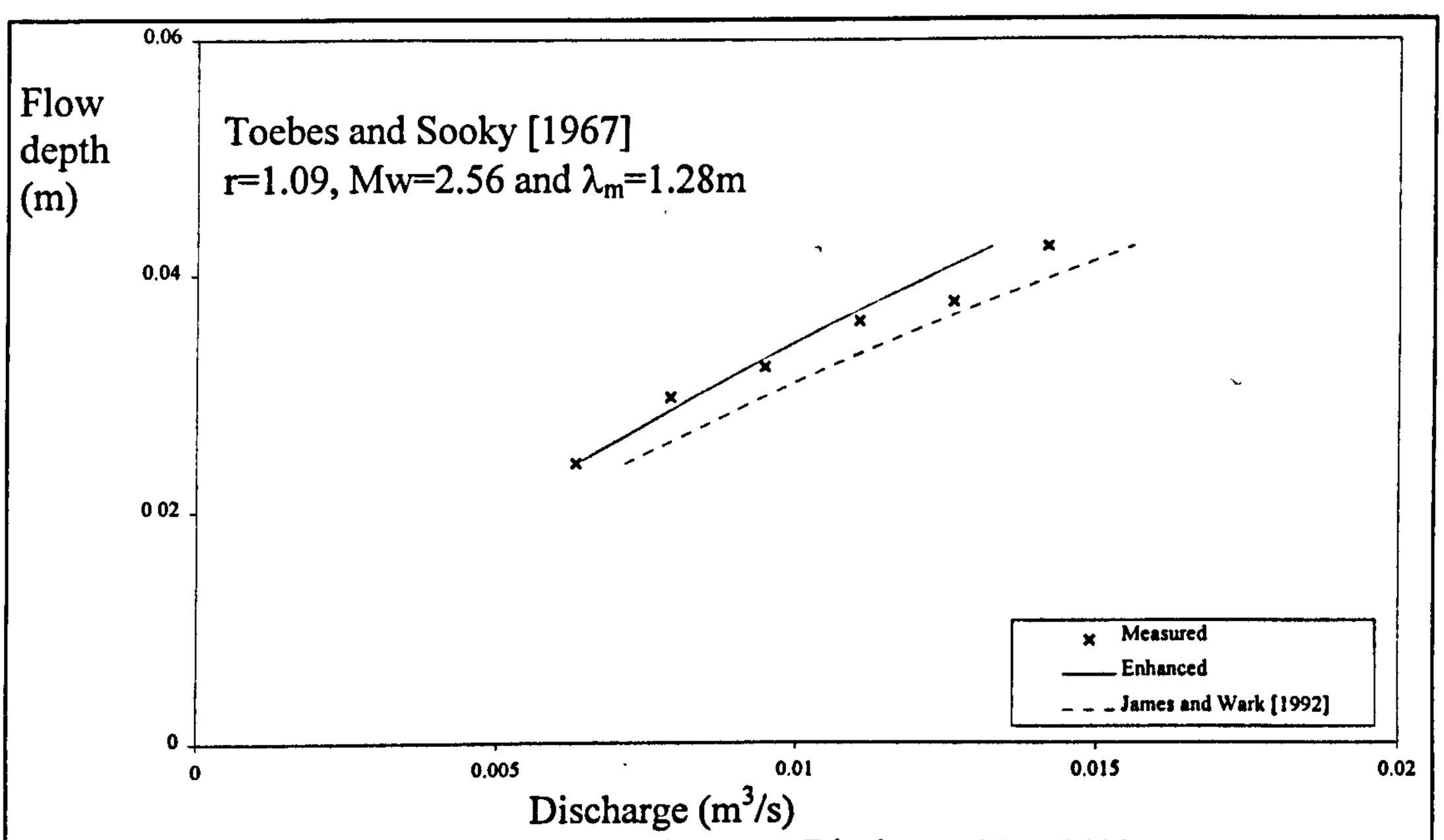

Figure 6.36 Flow depth versus Discharge SDSK403

6.8.4.3 Kiely[1989]

Figure 6.37 shows plots of flow depth versus measured and predicted discharge capacity for the model SDKI301 which was tested by Kiely [1989].

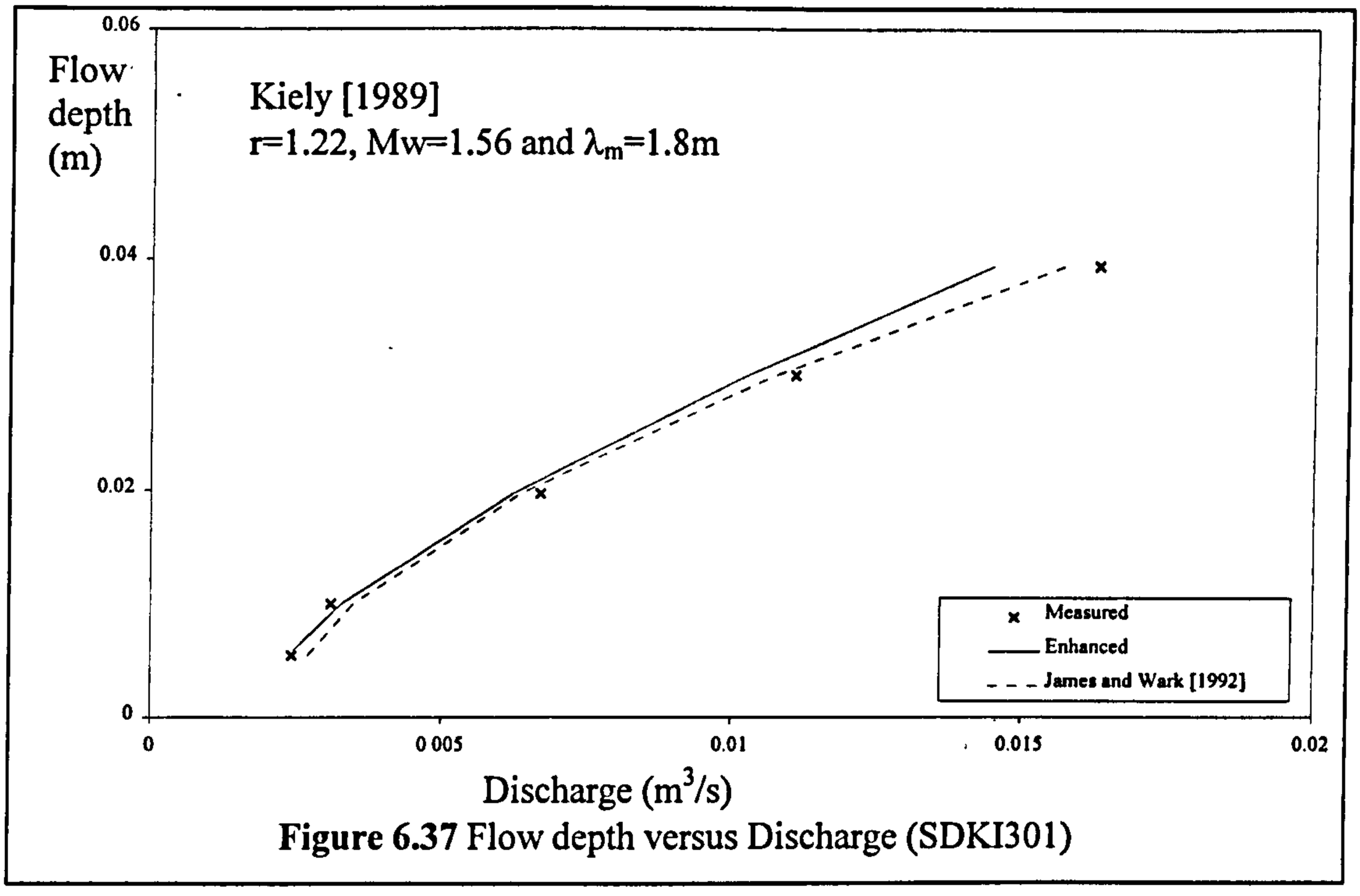

Figure 6.37 Flow depth versus Discharge (SDKI301)

Averaged over all flow depths the Enhanced zonal method gave more accurate predictions for the discharge capacity of SDKI301 than the James and Wark [1] [1992] method. At high flow depths both the Enhanced zonal and James and Wark [1] [1992] methods under-estimate the discharge capacity of SDKI301 with the James and Wark [1] [1992] method yielding slightly more accurate results but by contrast the Enhanced zonal method gives much more accurate predictions at low flow depths.

Table 6.11 lists the statistical analysis of the results obtained by comparing the measured discharge capacities of the Kiely [1989] model with predicted results which were produced by using both the Enhanced zonal method and the James and Wark [1] [1992] methods.

	Enhanced zonal method				James and Wark [1] [1992] method			
	Mean	St. Dev.	RMS	St. Dev.	Mean	St. Dev.	RMS	St. Dev.
SDKI301	4.4	6.5	6.8	3.0	2.5	8.8	7.2	4.5

Table 6.11 Difference between the measured and predicted discharges for Kiely [1989]

6.8.4.4 Aberdeen (1991) (Willetts and Hardwick [1993])

Table 6.12 lists the statistical analysis of a selection of results obtained by comparing the measured discharge capacities with the predicted discharge capacities for the Aberdeen (1991) models using both the Enhanced zonal and James and Wark [1] [1992] methods.

	Enhanced zonal model				James and Wark [1] [1992]			
	Mean	St. Dev.	RMS	St. Dev.	Mean	St. Dev.	RMS	St. Dev.
SDAB101	5.8	7.7	8.8	3.7	7.1	7.7	7.9	6.8
SDAB102	-4.0	2.6	4.1	2.5	-2.1	3.6	3.9	2.4
SDAB104	7.0	6.3	8.5	3.6	7.2	7.9	8.1	6.9

Table 6.12 Difference between the measured and predicted discharges for Series B.

Figure 6.38 shows a typical plot of flow depth versus measured and predicted discharge capacity for SDAB102. The Enhanced zonal method gives a very similar level of accuracy to that obtained using the James and Wark [1] [1992] method even though the James and Wark [1] [1992] method incorporates empirical adjustments which were originally determined using this Aberdeen data.

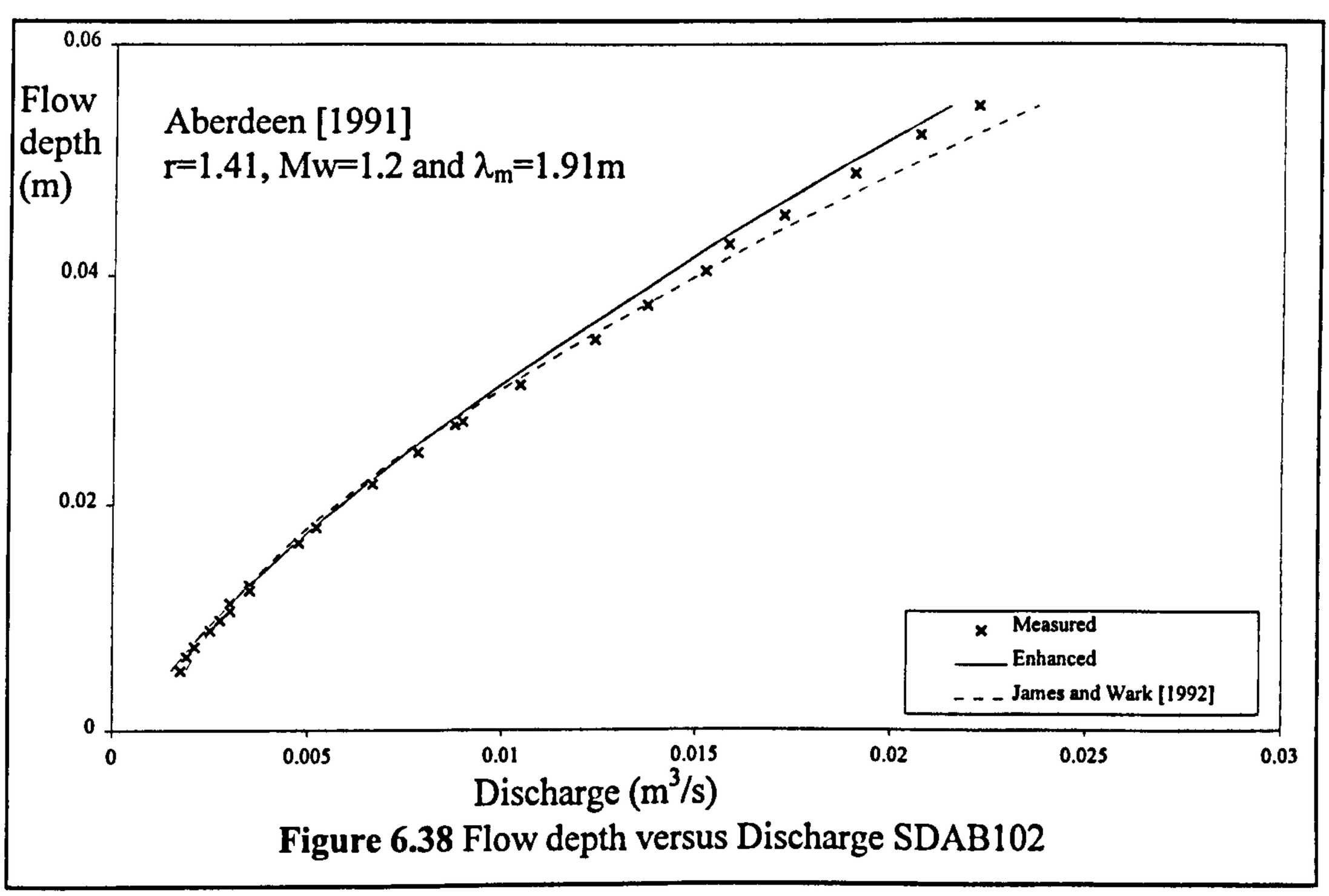

Figure 6.38 Flow depth versus Discharge SDAB102

Both methods generate accurate predictions at both low and high flow depths. The author suggests that the empirical adjustment of the James and Wark [1] [1992] method

significantly improved the accuracy of prediction at low flow depths whereas in other models the Enhanced zonal method has been demonstrated to out-perform the James and Wark [1] [1992] method when determining the discharge capacity of channels at low flow depths.

6.8.4.5 Series B extension (1993-1996) (Glasgow)

Table 6.13 lists the statistical analysis of a selection of results obtained by comparing the measured discharge capacities of the Series B extension (1993-1996) models (Glasgow) with the discharge capacities which were predicted using the Enhanced zonal and James and Wark [1] [1992] methods.

Table 6.13 demonstrates that the Enhanced zonal method generates more accurate predictions than the James and Wark [1] [1992] method. This is to be expected because these results were used extensively to develop the Enhanced zonal method. Figures 6.39, 6.40 and 6.41 show typical plots of flow depth versus measured and predicted discharge capacity for G75T90R, G50T60RA and G25N45R. All three figures demonstrate that both methods are very accurate for models with the general geometric configurations tested in the majority of small-scale experimental programmes.

	Enhanced zonal method				James and Wark [1] [1992] method			
	Mean	St. Dev.	RMS	St. Dev.	Mean	St. Dev.	RMS	St. Dev.
G75T90S	5.3	3.1	5.4	2.9	10.8	4.8	10.8	4.8
G75T90R	5.5	4.3	5.5	4.3	8.0	7.6	8.0	7.6
GR75T90R	8.9	4.4	8.9	4.4	19.3	10.1	19.3	10.1
G75T45R	7.5	5.1	7.5	5.1	8.1	4.5	8.1	4.5
G50T90R	0.1	4.5	3.3	2.9	2.1	6.5	5.7	3.5
G50T60RA	7.2	6.1	7.1	6.1	7.3	4.0	7.3	4.0
G50T45R	0.9	4.0	2.9	2.8	0.3	4.4	3.6	2.4
G50T30R	-2.6	5.6	5.0	3.4	3.8	6.9	6.5	4.3
G50N90R	13.5	2.8	13.5	7.8	15.9	6.6	15.9	6.6
G50N45R	5.2	5.4	5.6	5.0	9.8	5.5	9.8	5.5
G25T90R	5.9	4.1	5.9	4.1	8.8	4.1	8.8	4.1
G25T45R	1.3	5.8	3.2	4.9	1.2	7.5	5.0	5.6
G25T45S	6.9	3.6	6.9	3.6	13.5	2.7	13.5	2.7
G25N90R	5.1	7.9	6.3	6.9	8.4	7.9	9.4	6.3
G25N45R	3.2	7.2	4.9	6.0	5.0	7.9	7.0	6.1
G25T45RN	7.9	3.6	8.4	2.1	15.2	5.3	15.7	3.6
G25T45SN	4.6	9.9	8.9	6.1	15.5	4.6	15.5	4.6

Table 6.13 Difference between the measured and predicted discharges for Series B.

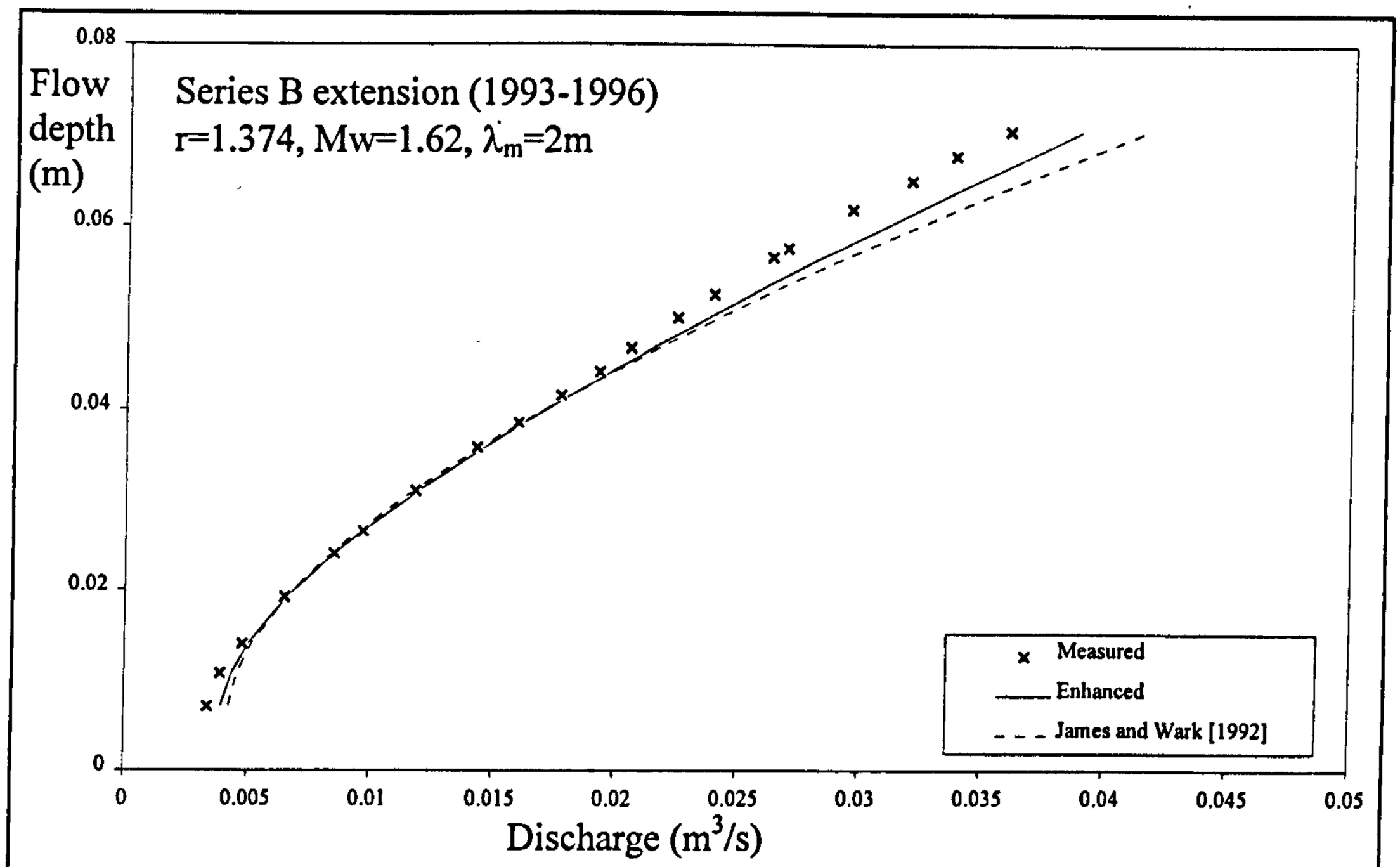

Figure 6.39 Flow depth versus discharge capacity G75T90R

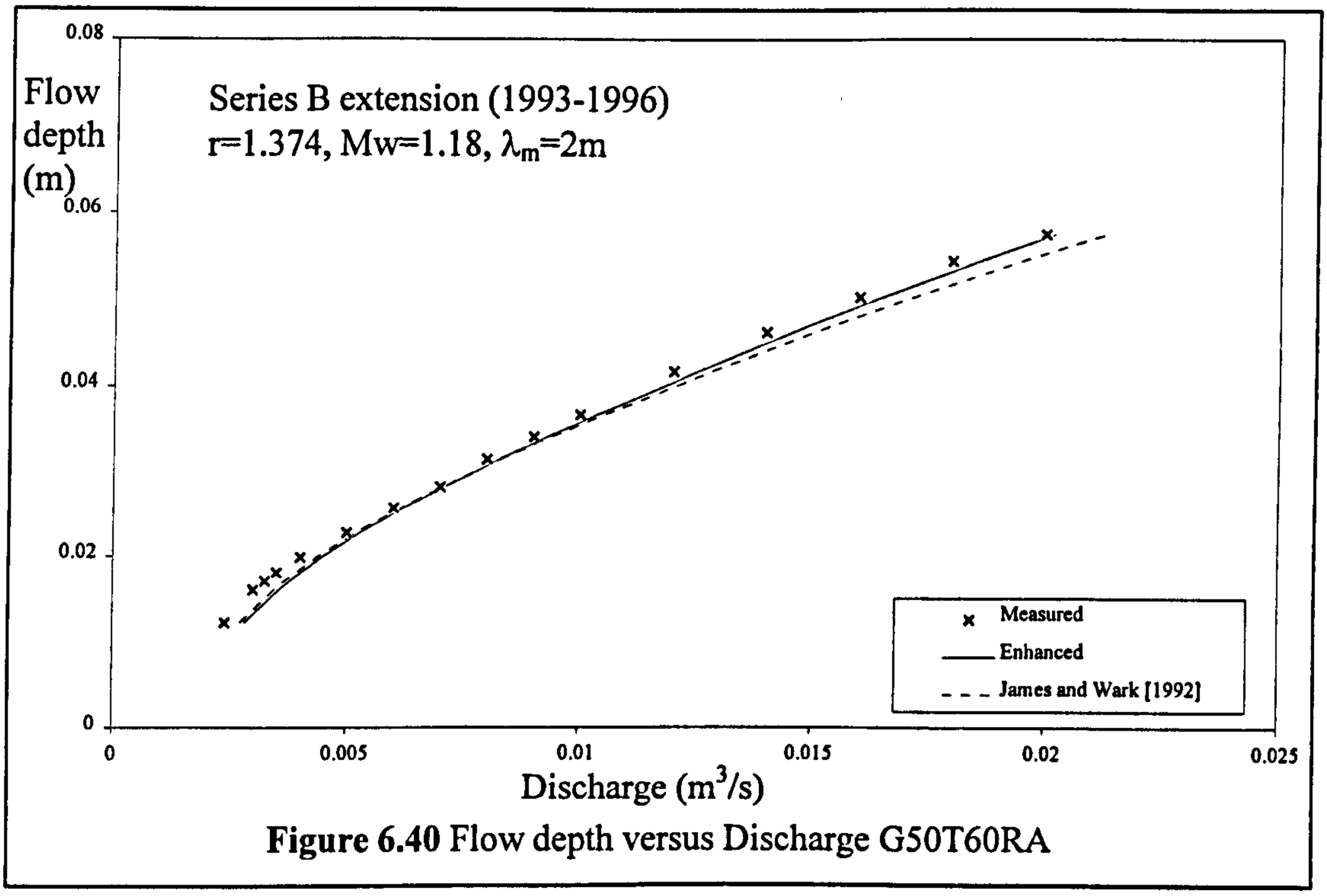

Figure 6.40 Flow depth versus Discharge G50T60RA

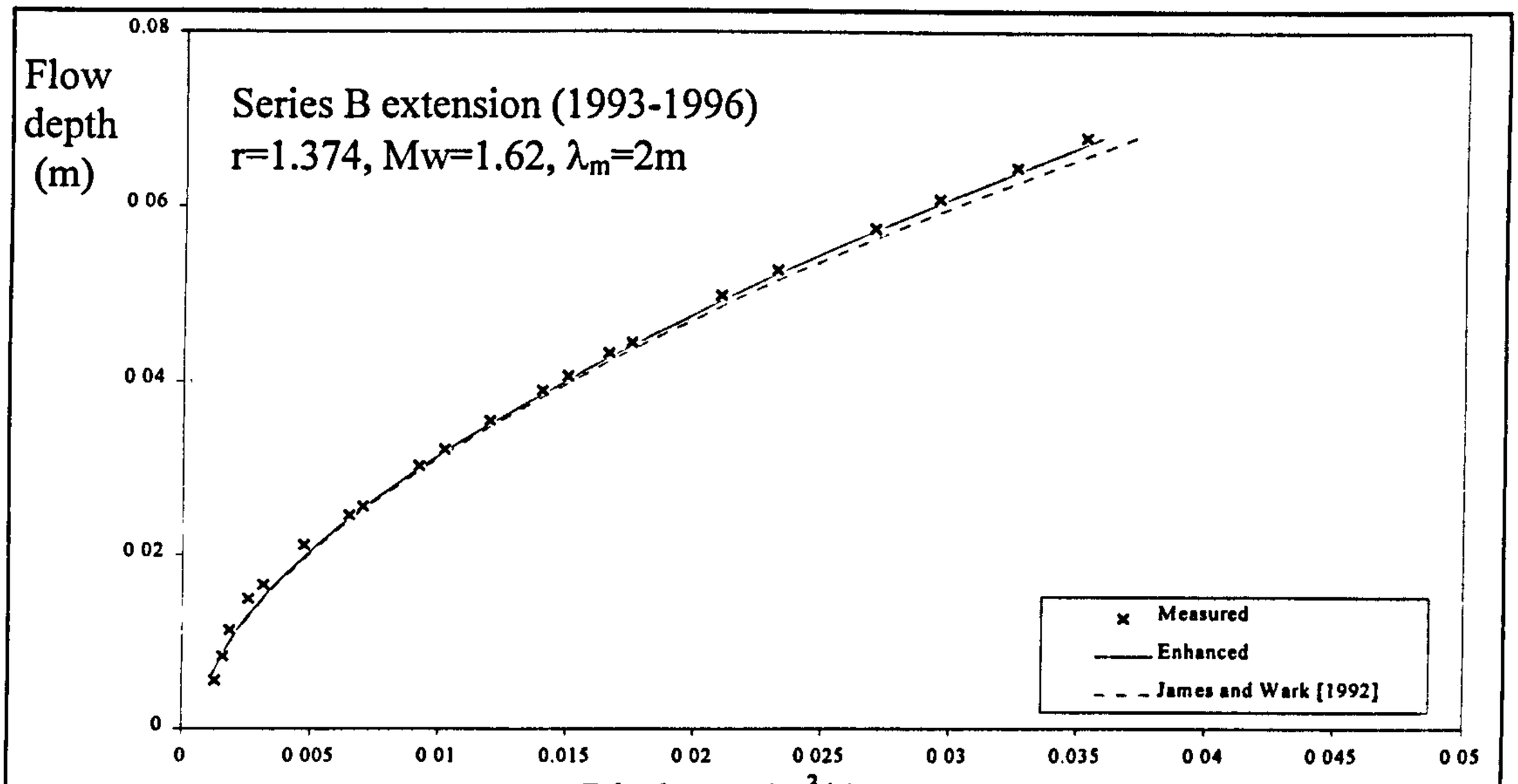

Figure 6.41 Flow depth versus Discharge G25N45R

By contrast the discharge capacity predictions for G25T45RN and G25T45SN did not achieve the same level of accuracy, especially at high flow depths. Although the Enhanced zonal method gives more accurate predictions than the James and Wark [1] [1992] method they still both under-estimate the flow resistance (over-estimate discharge capacity) in these models with narrow flood plains. Figure 6.42 plots flow depth versus measured and predicted discharge capacity for G25T45SN and clearly shows this over-estimate for discharge capacity.

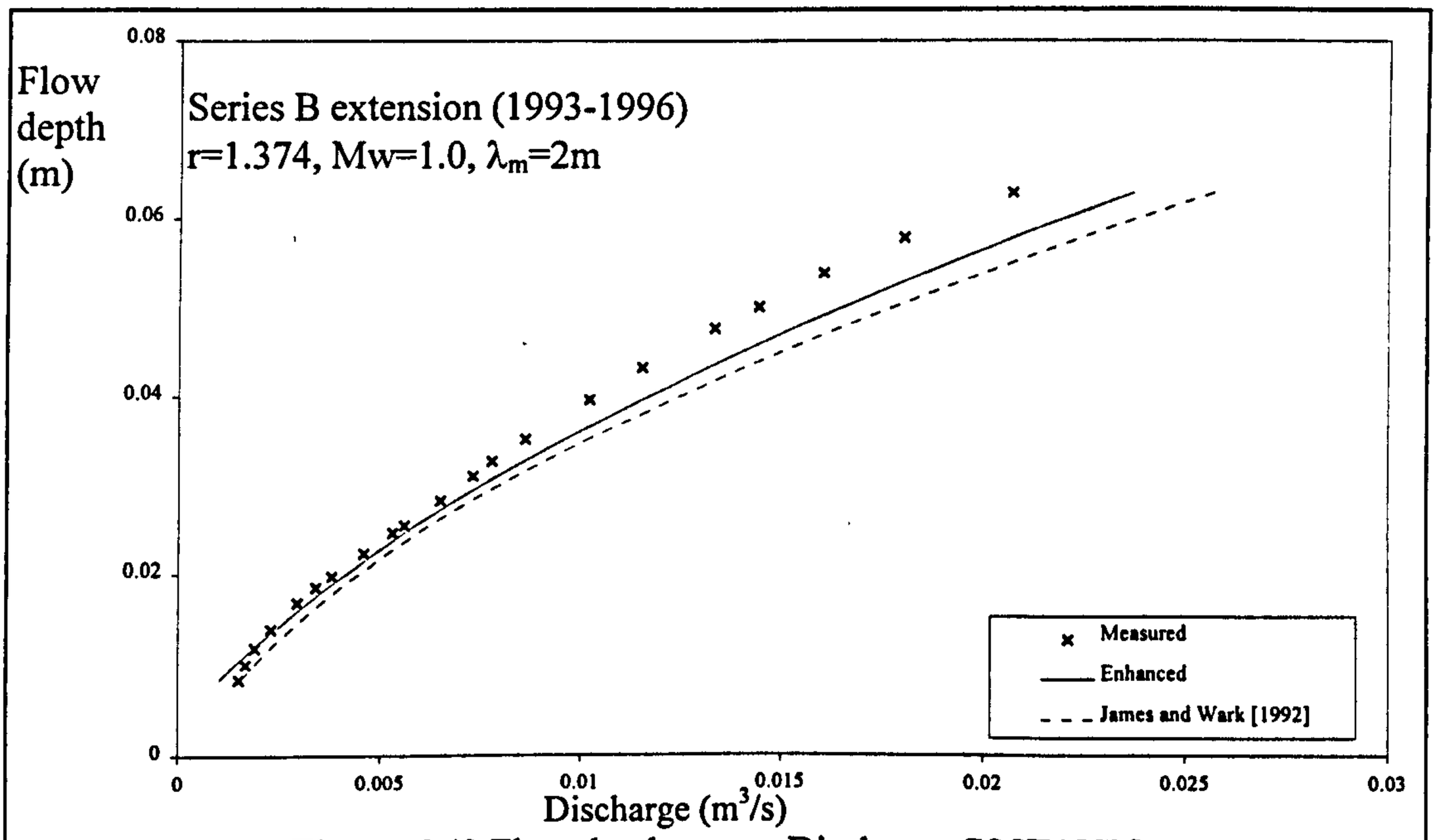

Figure 6.42 Flow depth versus Discharge G25T45SN

Figure 6.43 shows the difference between Enhanced zonal method's predictions for channels for two different models: G25T45S and G25T45SN, which were identical except for their difference in relative meander belt width.

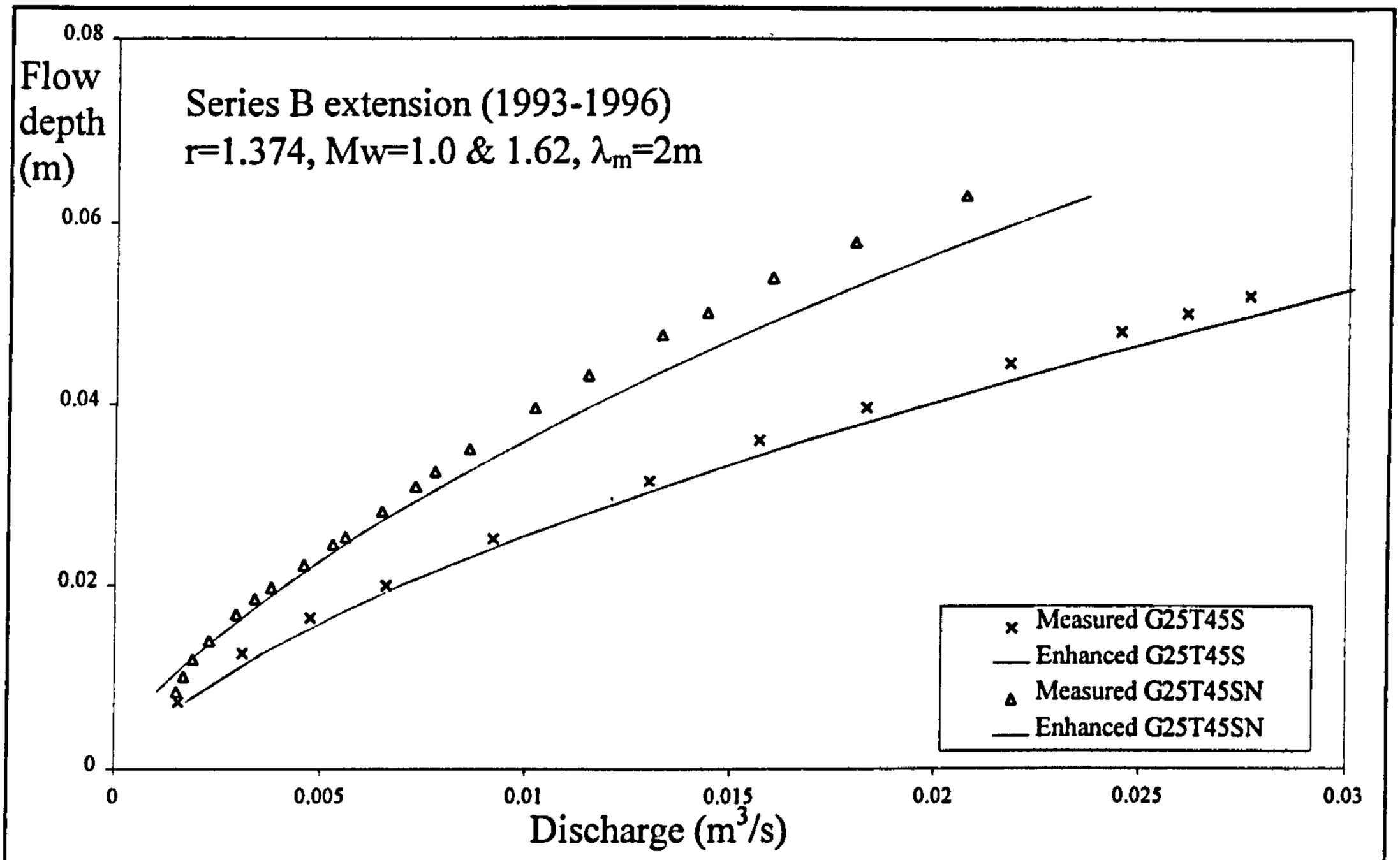

Figure 6.43 Flow depth versus Discharge, G25T45S and G25T45SN

The author postulates that proximity of the flood plain side walls to Zone B will result in the side wall effects significantly interfering with the flow in Zone B in the narrow channel, G25T45SN, thus reducing the mean Zone B velocity in the narrow channel at similar relative depths. The side wall effects will also potentially alter the Threshold depths thus causing an change in flow resistance due to layer interaction. These changes in flow behaviour would explain to some extent the observed reduction in discharge capacity.

Neither the Enhanced zonal method or the James and Wark [1] [1992] method make allowance for any increase in head loss due to side wall effects which would explain why both methods over-estimate the discharge capacity in these channels.

Figure 6.44 shows plots of measured and predicted discharge capacity for two Series B models, SDB25 and SDB31 which also possessed different flood plain widths but were built at a larger scale. The author observes that for these models there is no evidence to

suggest that the discharge capacity predictions generated by the Enhanced zonal and the James and Wark [1] methods under-estimate the flow resistance in any way. In fact it is clear that the enhanced James and Wark [1] [1992] method actually slightly over-estimates the flow resistance method when it is applied to these larger scale models.

The author postulates that when the meandering channel models are larger in scale, the width of Zone B being affected by the side wall effects comprises a smaller proportion of the total width of Zone B. Therefore the proportion of the total flow resistance in Zone B contributed to by the side wall effects will be reduced, causing a smaller divergence between the predicted and measured discharges using the Enhanced zonal and James and Wark [1] [1992] prediction methods.

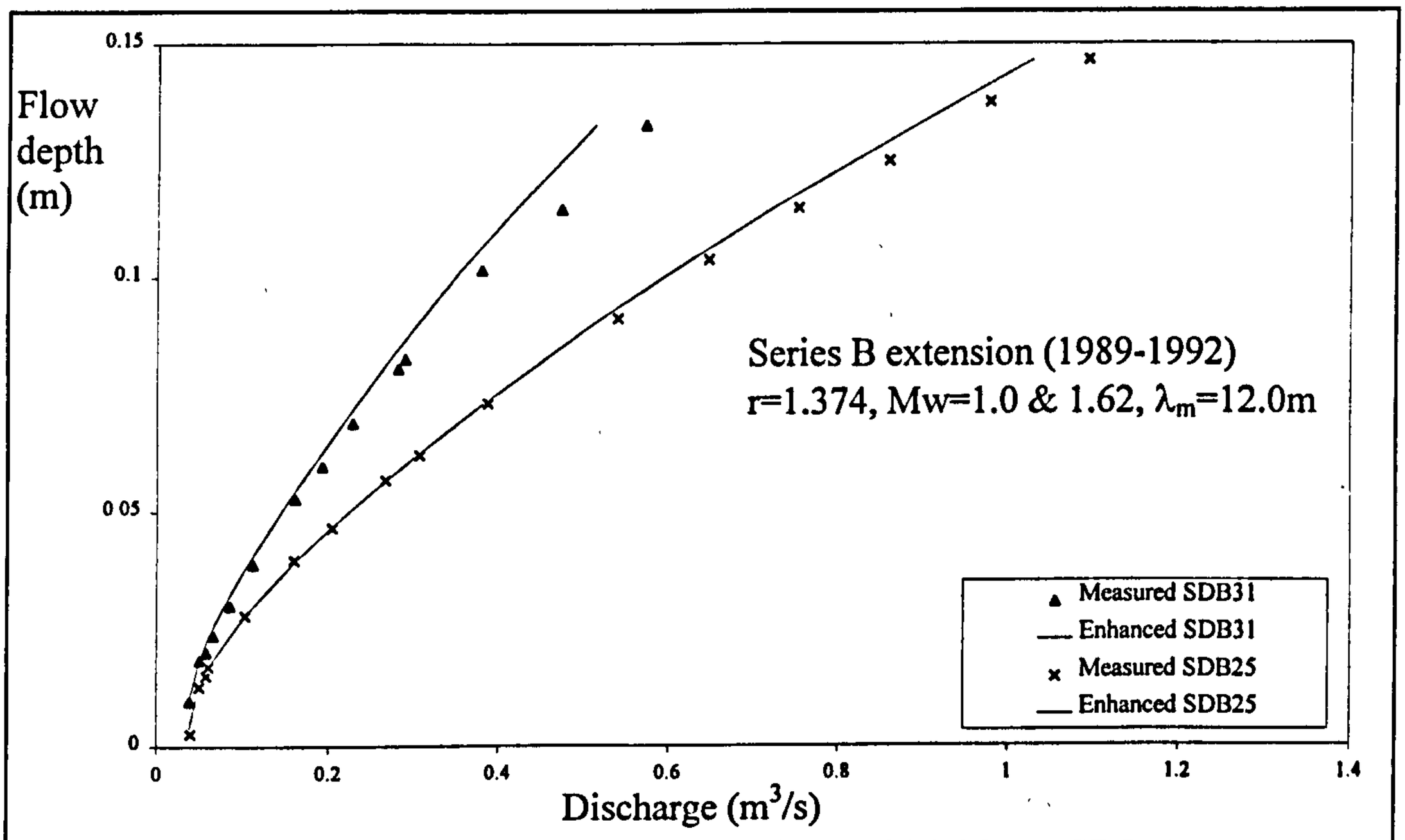

Figure 6.44 Flow depth versus Discharge, SDB25 and SDB31

Further pertinent data with regard to the influence of the relative meander belt width will become available following the publication of the Bristol results. This data will help to determine the precise physics underlying the observed increases in head loss generated by the floodway side wall effects, especially in smaller scale channels. However the author suggests that the provision of this data will not secure a significant improvement in the accuracy of the discharge capacity prediction for channels which are equal or larger than medium scale models like Vicksburg [1956] or Series B (1989-1992). It is possible that the side wall effects will only be significant in small scale

models where the zone of side wall influence is large in proportion to the complete width of the channel. The author suggests that in the interim no allowance needs to be made for side wall effect when applying these prediction methods to natural / prototype channels, which represent the most significant focus for the prediction methods.

6.8.4.6 Series B extension (Aberdeen)

Introduction

Table 6.14 lists the statistical analysis of a selection of results obtained by comparing the measured discharge capacities for the Series B extension models (which were tested in Aberdeen) and the discharge capacities which were predicted using both the Enhanced zonal and James and Wark [1] [1992] methods. Unfortunately at the time of writing no zonal flow data had been published so the Aberdeen results were not included in the data set which was used to develop the Enhanced zonal method.

	Enhanced zonal method				James and Wark [1] [1992] method			
	Mean	St. Dev.	RMS	St. Dev.	Mean	St. Dev.	RMS	St. Dev.
A1T1000S	2.9	7.0	6.2	4.1	4.9	4.8	5.0	4.7
A1T750A	16.8	10.3	16.8	10.3	10.6	4.7	10.6	4.7
A1T1000B	7.4	6.1	7.4	6.1	8.3	4.9	8.3	4.9
A1N1000B	3.3	4.6	4.6	3.3	7.8	4.1	7.8	4.1
A2T1000S	32.4	14.5	32.4	14.5	28.2	3.8	28.2	5.8
A2T750S	30.3	11.6	30.3	11.5	25.5	3.5	25.5	3.5
A2N1000S	10.1	9.8	11.7	7.7	7.5	3.0	7.5	3.0
A2N1000A	5.5	4.9	6.2	4.1	2.9	1.2	2.9	1.1
A2N750B	16.6	6.0	16.6	6.0	10.9	9.4	10.9	9.4
A3T1000S	-1.5	3.9	3.4	2.3	7.0	2.7	7.0	2.7
A3N750S	3.4	4.2	4.6	2.8	12.4	2.8	12.4	2.8
A3N750A	-2.9	4.7	4.9	2.4	6.1	8.6	6.4	8.4
A3N1000B	-11.6	2.9	11.6	2.9	-4.7	5.3	6.5	2.6
A3N750B	3.5	4.9	4.9	3.4	2.5	5.2	4.1	2.3

Table 6.14 Difference between the measured and predicted discharges for Series B.

The Aberdeen tests were divided into 3 sub-groups which were distinguished by having different main channel sinuosities: medium sinuosity channels, r=1.374, low sinuosity channels, r=1.111 and high sinuosity channels, r=1.771.

Medium sinuosity channels, r = 1.374

The series of models, which had main channel sinuosities, r, equal to 1.374, had references like: A1T1000S. The geometric ratios used to define the configurations of these models are detailed in Equations 2.59 - 2.62 and were identical to the Series B extension (1993-1996) models built in Glasgow and similar to those found in real rivers. Both the Enhanced zonal and the James and Wark [1] [1992] methods generate accurate predictions for the discharge capacity of these channels, despite the narrowness of Zone C. The side wall effects appear to have a negligible impact on the accuracy of the prediction methods.

Figures 6.45 show a typical plot of flow depth versus measured and predicted discharge capacity for A1N1000B which was representative of the results obtained for channels with a sinuosity equal to 1.374. The overall level of accuracy of both prediction methods is high at all flow depths with the Enhanced zonal method providing the slightly more accurate predictions especially at low flow depths.

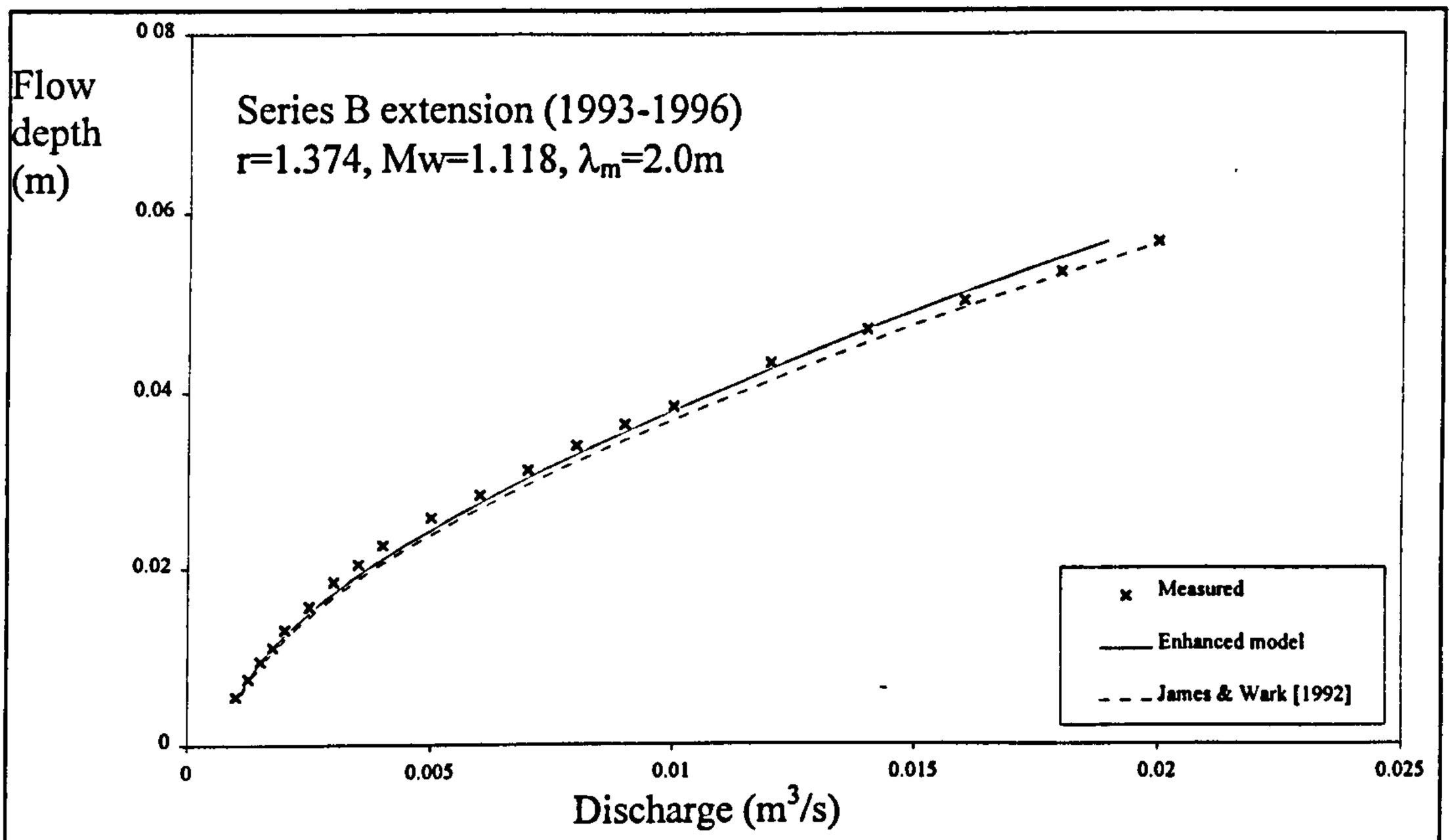

Figure 6.45 Flow depth versus discharge capacity (A1N1000B)

Low sinuosity channels, r = 1.111

The series of models, which had main channel sinuosities, r, equal to 1.111, had references like: A3T1000S. The geometric ratios used to define the configurations of these models are detailed in Equations 2.59 - 2.62 They gave dissimilar values

compared with those associated with real rivers, such as shown by Leopold [1960]. R_c/B and λ_m/R_c are close to 2.4 and 4.6 respectively but in these Aberdeen models R_c/B and λ_m/R_c were equal to 4.2 and 2.8 respectively.

Figures 6.46 show a typical plot of flow depth versus measured and predicted discharge capacity for A3T1000S which was representative of the results obtained for channels with a sinuosity equal to 1.111.

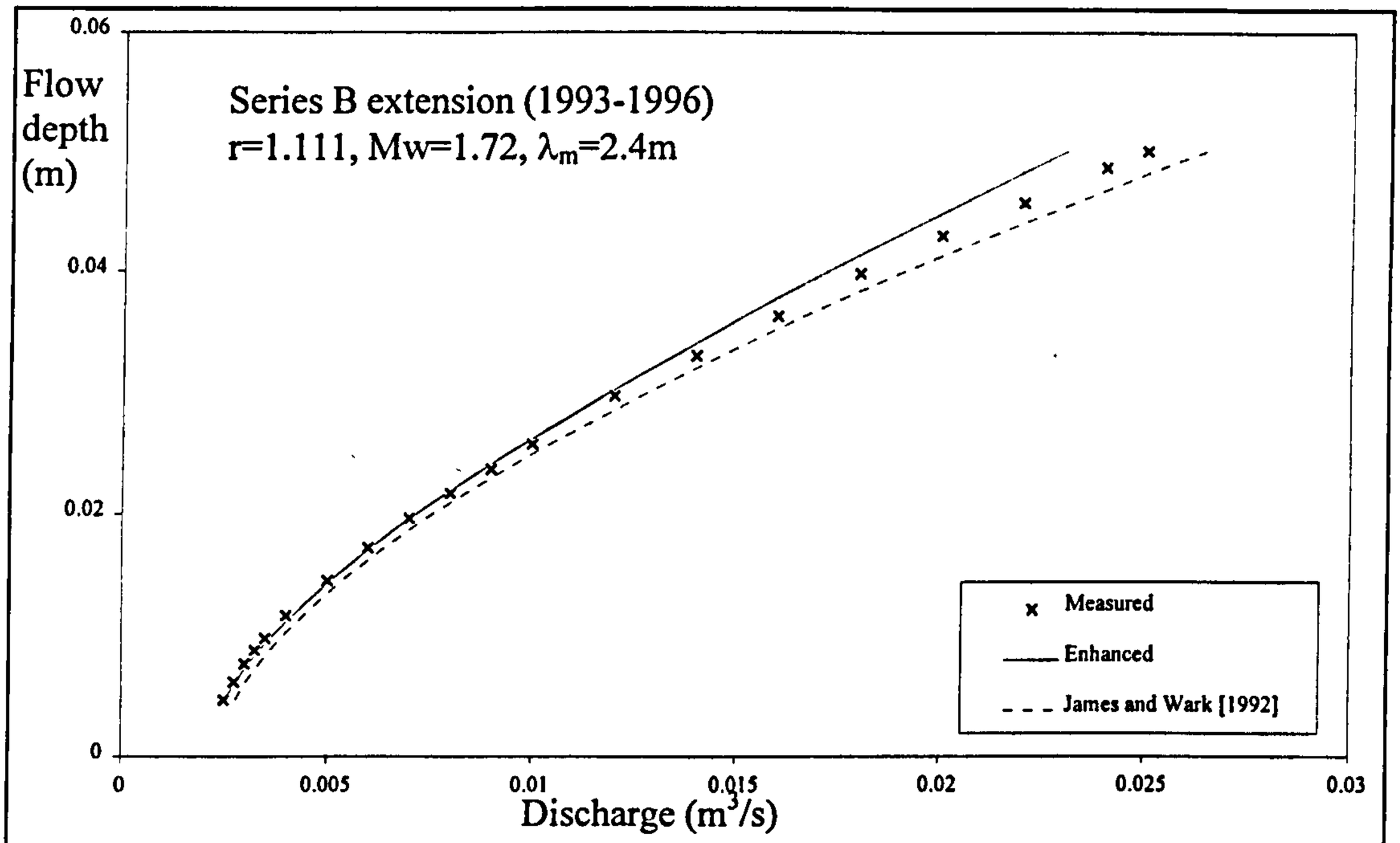

Figure 6.46 Flow depth versus discharge capacity (A3T1000S)

The Enhanced zonal method tends to generate slightly more accurate predictions for discharge capacity than the James and Wark [1] [1992] method when averaged over all flow depths. However, the Enhanced zonal method had a tendency to slightly under-estimate the discharge capacity, especially at higher flow depths. The author postulates that the lower sinuosities result in the main component of mean velocity in the main channel being more aligned to the main component of flood plain velocity in these models compared with the higher sinuosity models. Consequently, the horizontal shearing effect of Zone B over Zone A does not drive the secondary cells which are perpendicular to the main component of main channel flow to such an extent. As a result a smaller proportion of expansion and contraction losses are generated compared. The higher sinuosity channels were predominantly used to develop the Enhanced zonal

method which explains why it tends to over-estimate the flow resistance in the lower sinuosity models. The formulations only make limited allowance for the angle of skew of the main channel.

High sinuosity channels, r = 1.771

The only significant anomalies which were encountered when applying the Enhanced zonal and James and Wark [1] [1992] methods to all the test channel sets collected during the Series B extension (1993-1996) programme were observed when these methods were applied to the series of Aberdeen models with typical reference numbers such as A2T1000S. These models had main channel sinuosities equal to 1.771.

Figures 6.47 and 6.48 show typical plots of flow depth versus measured and predicted discharge capacity for A2N750B and A2T750S which were representative of the results obtained for channels with a sinuosity equal to 1.771.

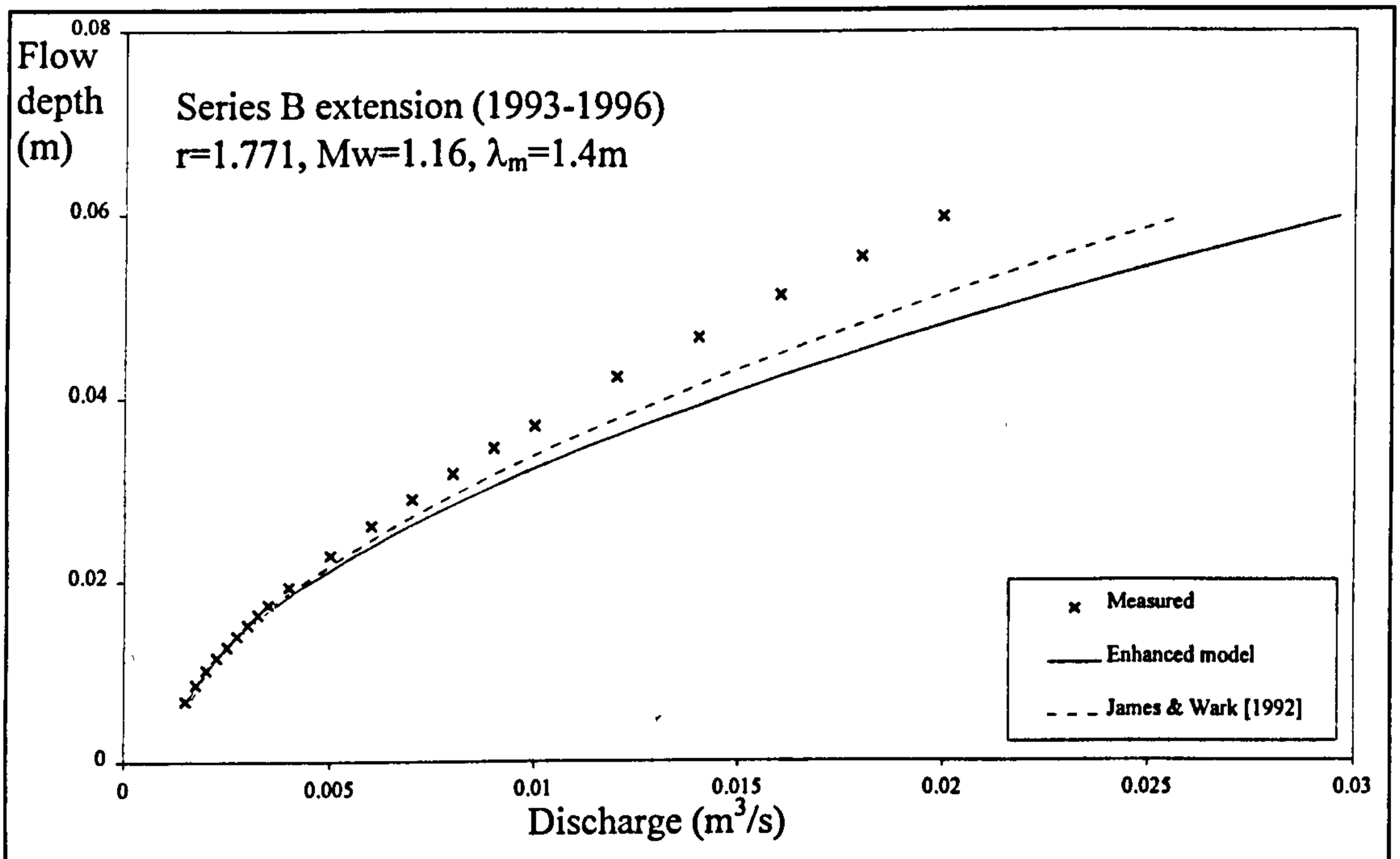

Figure 6.47 Flow depth versus discharge capacity (A2N750B)

Clearly both the Enhanced zonal and James and Wark [1] [1992] methods significantly under-estimate the flow resistance in these high sinuosity, small scale models.

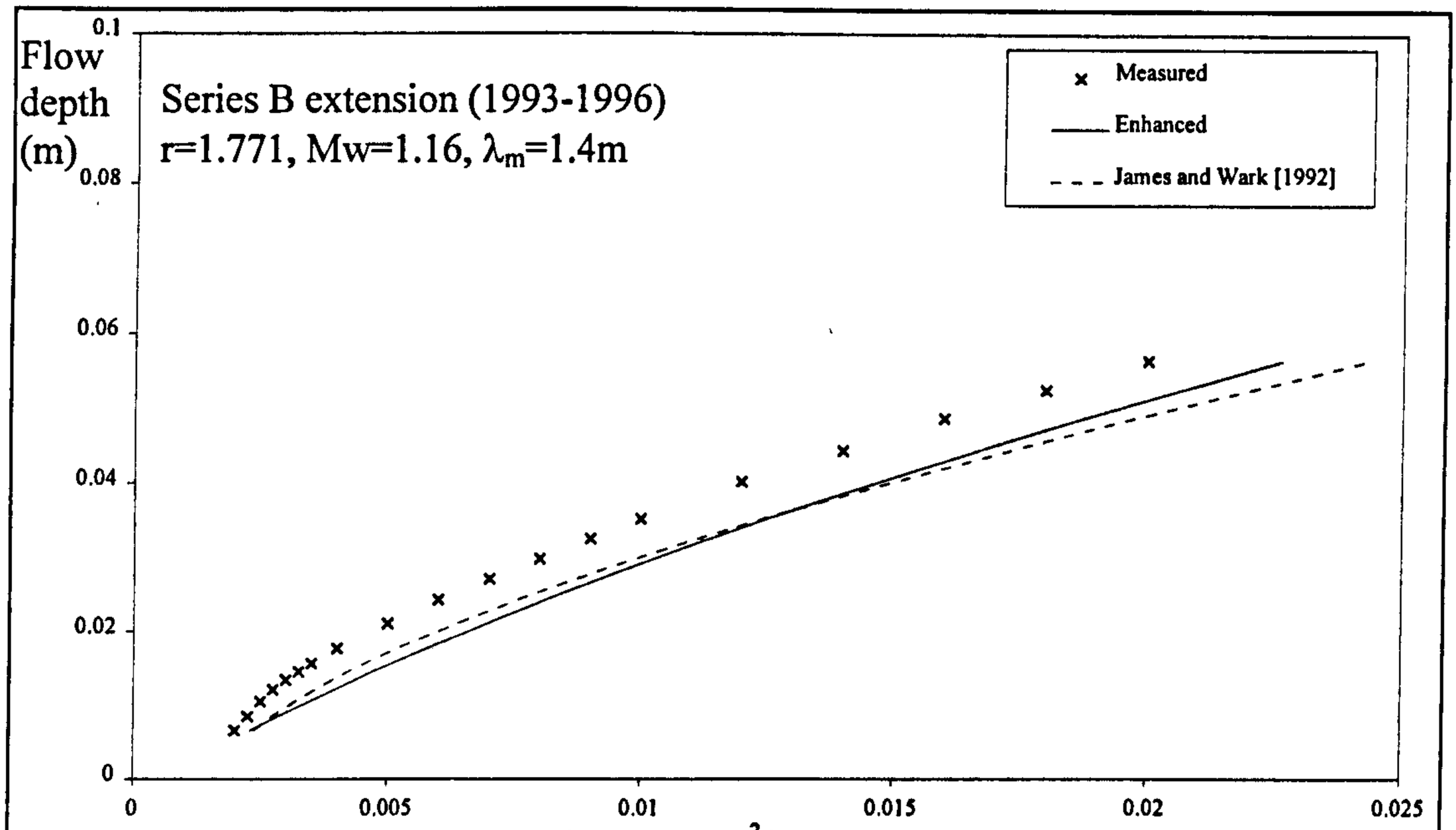

Figure 6.48 Flow depth versus discharge capacity (A2T750S)

The author's initial assumption was that the under-estimation was attributable to the high sinuosity of the main channels. However, inspection of the Series B (1989-1992) results showed that both methods, and especially the Enhanced zonal method produced good discharge capacity predictions for the Series B (1989-1992) models, irrespective of main channel sinuosity variation. Figure 6.29 and 6.31 shows a comparison between the measured and predicted discharge capacities of SDB25 and SDB39 (from Series B (1989-1992) experiments) which had sinuosities equal to 1.374 and 2.043 respectively.

The author notes that both SDB25 and SDB39 had geometric ratios and bend characteristics which were similar to those found in real rivers. By contrast the geometric ratios and bend characteristics in the Aberdeen channels demonstrated that the main channel bends were significantly tighter than in real river channels and in any of the models used to develop the Enhanced zonal method. Instead of possessing standard geometric ratios similar to those associated with real rivers (as identified by Leopold [1960]) where R_c/B and λ_m/R_c are close to 2.4 and 4.6 respectively, in the Aberdeen models R_c/B and λ_m/R_c were equal to 3.9 and 1.8 respectively. These ratio values verify that the bends were much tighter in the Aberdeen models than in nature. The author postulates that it is likely that the tightness of the bends (combined possibly

additional side wall effects which may be significant for these channels) results in greater levels of flow resistance being generated by layer interaction in these models than are typically generated in channels with more realistic geometric ratios.

6.9 The reliability of the Enhanced Zonal method

The author observes that the evidence gathered in Glasgow during the Series B extension (1993-1996) programme demonstrates that the existing Enhanced zonal method can be used to predict the discharge capacity for the majority of meandering compound channels with a higher degree of accuracy than can be achieved using any of the other existing prediction methods, even catering for the influence of high sinuosities in small scale channels.

The author suggests that although further refinements to the Enhanced zonal method will have to be pursued in future research in order to account for abnormally tight bends in small scale models, for now, the discrepancies which arise in discharge capacity predictions for small scale channels with high sinuosities are attributed to the very particular nature of these channels. By contrast, high levels of reliability have been demonstrated during the Series B extension (1993-1996) programme when applying the Enhanced zonal method to larger scale models and prototype channels. Consequently the Enhanced zonal method will be useful to the practising Hydraulic Engineer who wants to apply any discharge prediction method to practical river engineering problems.

6.10 Comparison between the Enhanced zonal, ANN and James and Wark [1] [1992] methods

6.10.1 Introduction

Although the Enhanced zonal method produces more accurate predictions for meandering compound channel discharge capacity than any of the other existing methods, the author wanted to demonstrate whether it was more accurate than the other method he developed during the Series B extension (1993-1996) programme, the ANN approximator. This section compares the discharge capacity predictions generated by the Enhanced zonal, the ANN approximator and the James and Wark [1] [1992] methods.

The author chose the test set for this comparison of prediction methods so that it was limited to the same specific test set which was compiled during the construction of the ANN approximator. This test set was chosen because although limitations in available data meant that a truly independent test set for all three methods was not possible to obtain at this stage in development, it was particularly vital to ensure the test set did not include data which was incorporated in the training set for the ANN approximator. The ANN approximator will have fitted itself very accurately to this data and comparing the relative performance of the other methods would not be realistic because of the likelihood of the excellent agreement between the ANN approximator output and its training set.

6.10.2 A summary of all the test set results

Table 6.15 lists Root Mean Squared (RMS) errors and standard deviations between the predicted and measured discharge capacities.

		Enhanced zonal J & W		Neural Network		James and Wark [1]	
Test Set	Model Reference	RMS error	Std. Dev.	RMS error	Std. Dev.	RMS error	Std. Dev.
	G50N45R (Series B ext. (1993-1996))	5.6	5.0	6.1	4.8	9.8	5.5
1	A3N750A (Series B ext. (1993-1996))	4.9	2.4	3.1	1.7	6.4	8.4
	SDKI 301 (Kiely [1989])	6.8	3.0	4.1	3.4	7.2	4.5
	SDAB102 (Aberdeen (1991))	4.1	2.5	16.9	8.7	3.9	2.4
2	Roding Cut (Field (1983-1986))	12.2	8.6	12.5	8.5	12.5	8.1
	Roding, Uncut (Field (1983-1986))	14.0	8.0	16.9	11.7	17.6	10.6
	SDB25 (Series B (1989-1992))	2.8	2.3	6.2	3.5	3.3	1.4
	SDVB201 (Vicksburg [1956])	5.9	2.0	9.9	8.1	5.0	2.4
3	SDVB202 (Vicksburg [1956])	3.0	1.5	6.1	5.7	4.5	1.1
	SDAB104 (Aberdeen (1991))	8.5	3.6	29.3	11.2	8.1	6.9
	SDSK402 (Toebes and Sooky[1967])	4.7	3.5	8.7	6.7	14.8	4.9

Table 6.15 Difference between the measured and predicted discharges for Series B.

The results are divided into three categories. Category 1 contains model data where the models possessed geometric and roughness parameters which were within the range of the parameters included in the ANN training set. Therefore, the ANN model is most likely to give accurate results for these data sets. Category 2 contains the River Roding

data for which the majority of the parameters were within the range of those used in the ANN training set. Category 3 contains additional model data for which the number of the parameters were outside the range of those used in the ANN training set.

6.10.3 Category 1: Parameters within the training set range

For Category 1 both the Enhanced zonal method and the ANN method produced improved predictions for discharge capacity for all the models except SDAB102. For these models all geometric and roughness parameters of the models fall within the range of the parameters used in the training set for the ANN model.

The ANN actually gives greater prediction accuracy than the Enhanced zonal method for A3N750A and SDKI301. Figure 6.49 shows a plot of flow depth versus all the predicted discharge capacities and the measured discharge capacity for SDKI301.

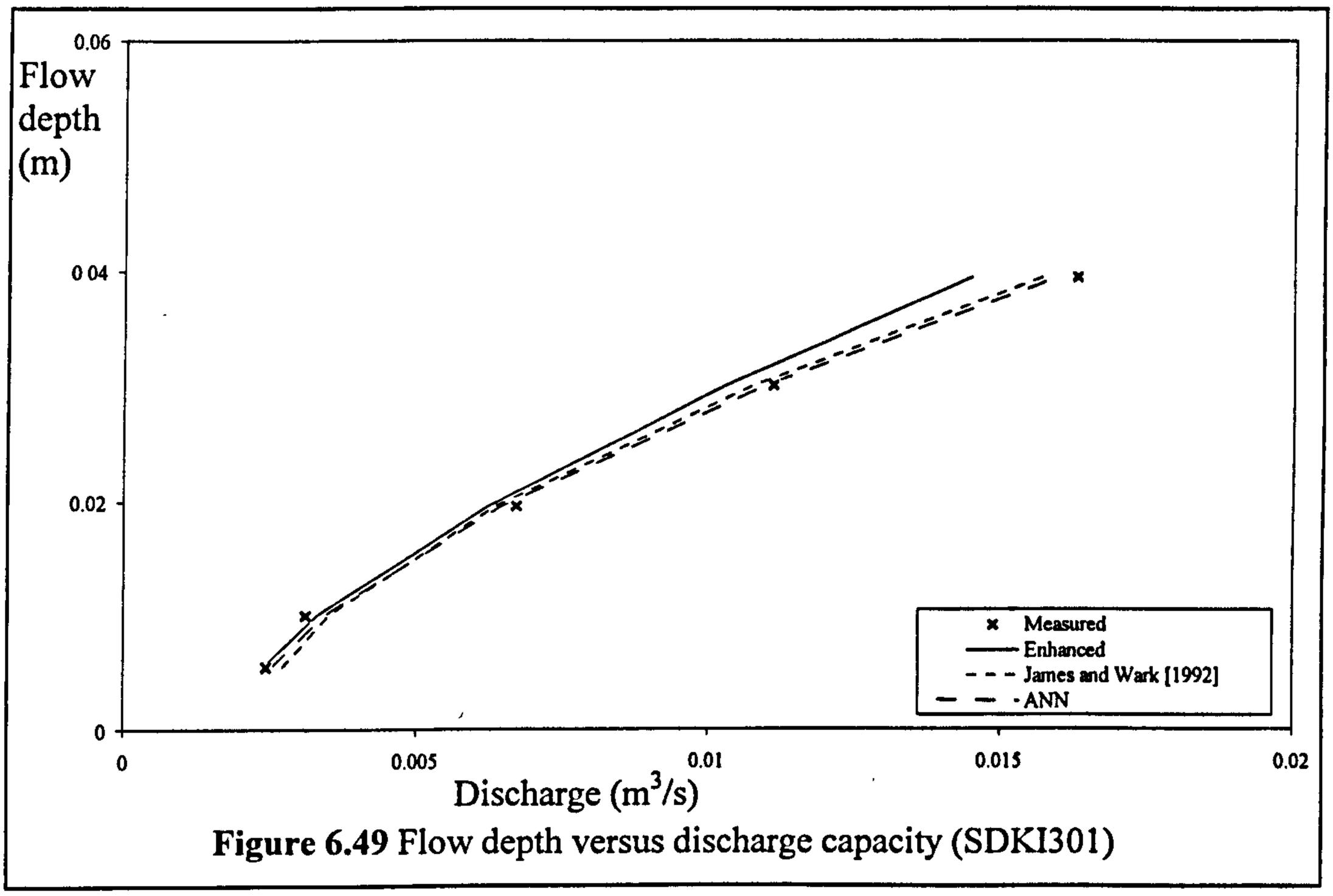

Figure 6.49 Flow depth versus discharge capacity (SDKI301)

Both the ANN and Enhanced zonal method generate almost identical predictions for G50N45R. The Enhanced zonal method generates discharge capacity prediction with greater accuracy for SDAB102 and the ANN was clearly ill-defined for this model.

6.10.4 Category 2: The River Roding

For Category 2 models the ANN method produces only slightly improved levels of discharge prediction accuracy than the James and Wark [1] [1992] method. However, the Enhanced zonal method out-performs both of them. Some of the geometric and roughness parameters of the models fall outside the range of the parameters used in the training set for the ANN model so it was encouraging that the James and Wark [1] [1992] method and the ANN method gave similar result, because it indicates that the ANN is able to extrapolate to a limited extent for parameters outwith the training set.

Figure 6.50 and 6.51 show plots of flow depth versus all the predicted discharge capacities and the measured discharge capacity for the River Roding with both cut and uncut flood plains.

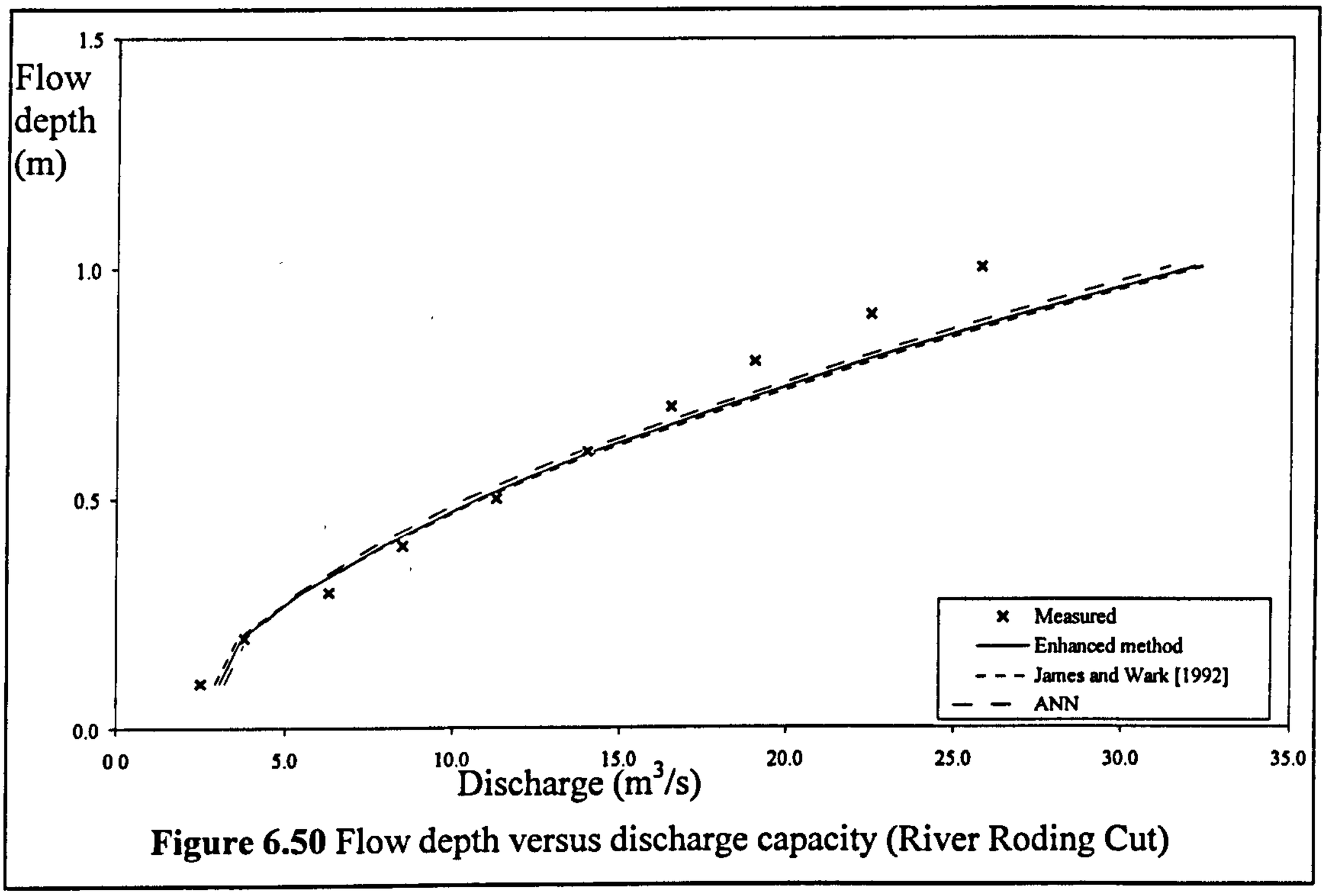

Figure 6.50 Flow depth versus discharge capacity (River Roding Cut)

The ANN approximator and the Enhanced zonal method predicted similar discharge capacities which are more accurate than the James and Wark [1] [1992] prediction at low flow depths in the cut and uncut River Roding. At high flow depth the Enhanced zonal method gives the most accurate results with the ANN and James and Wark [1] [1992] methods giving similar accuracy of results.

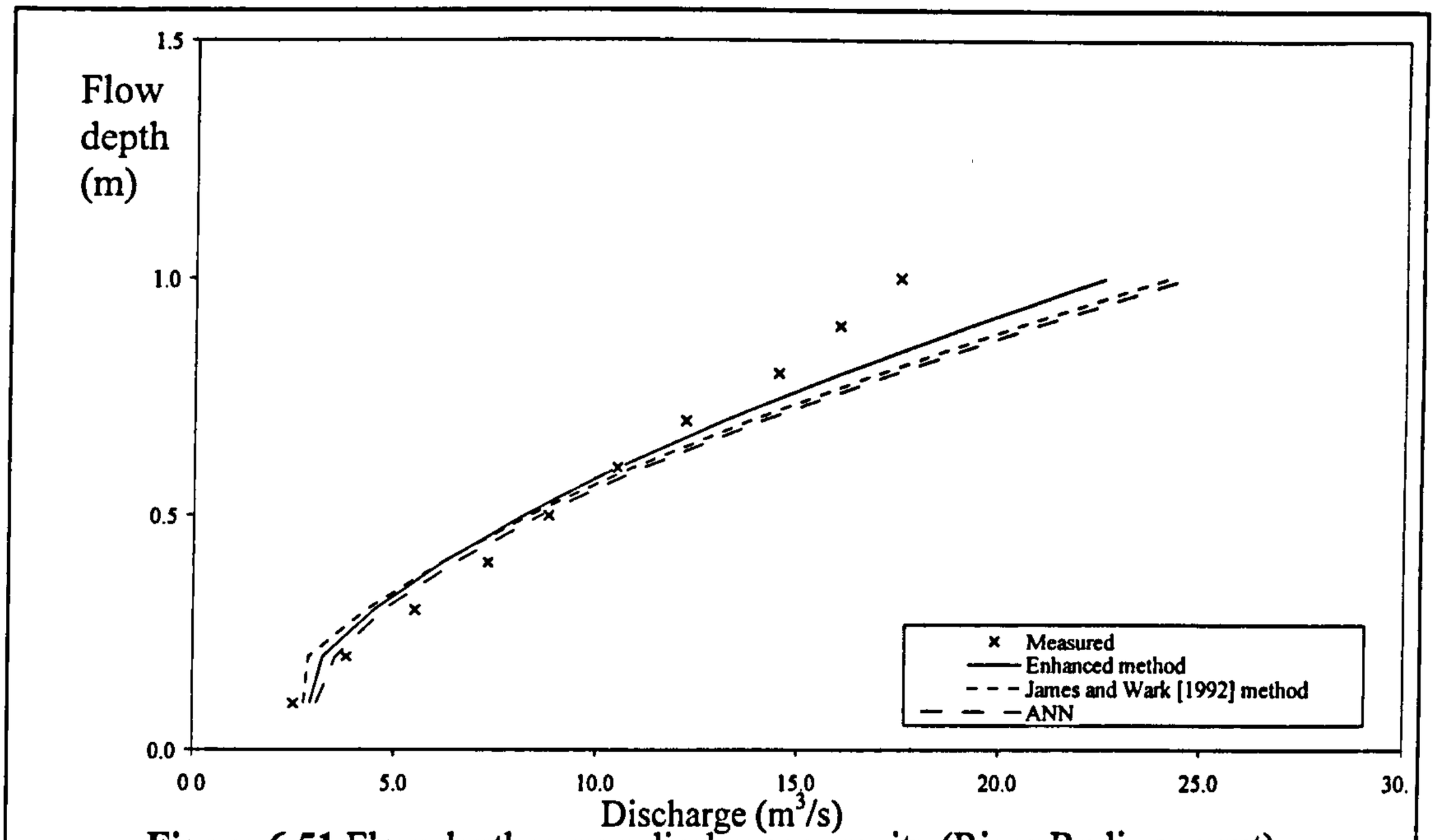

Figure 6.51 Flow depth versus discharge capacity (River Roding uncut)

6.10.5 Category 3: Ranges of input parameters outside that of the training set

The geometric and roughness parameters of the Category 3 models predominantly fall significantly outwith the range of the parameters used in the training set for the ANN model. Figure 6.52 shows a plot of flow depth versus all the predicted discharge capacities and the measured discharge capacity for SDB25 which is characteristic of the results obtained for Category 3.

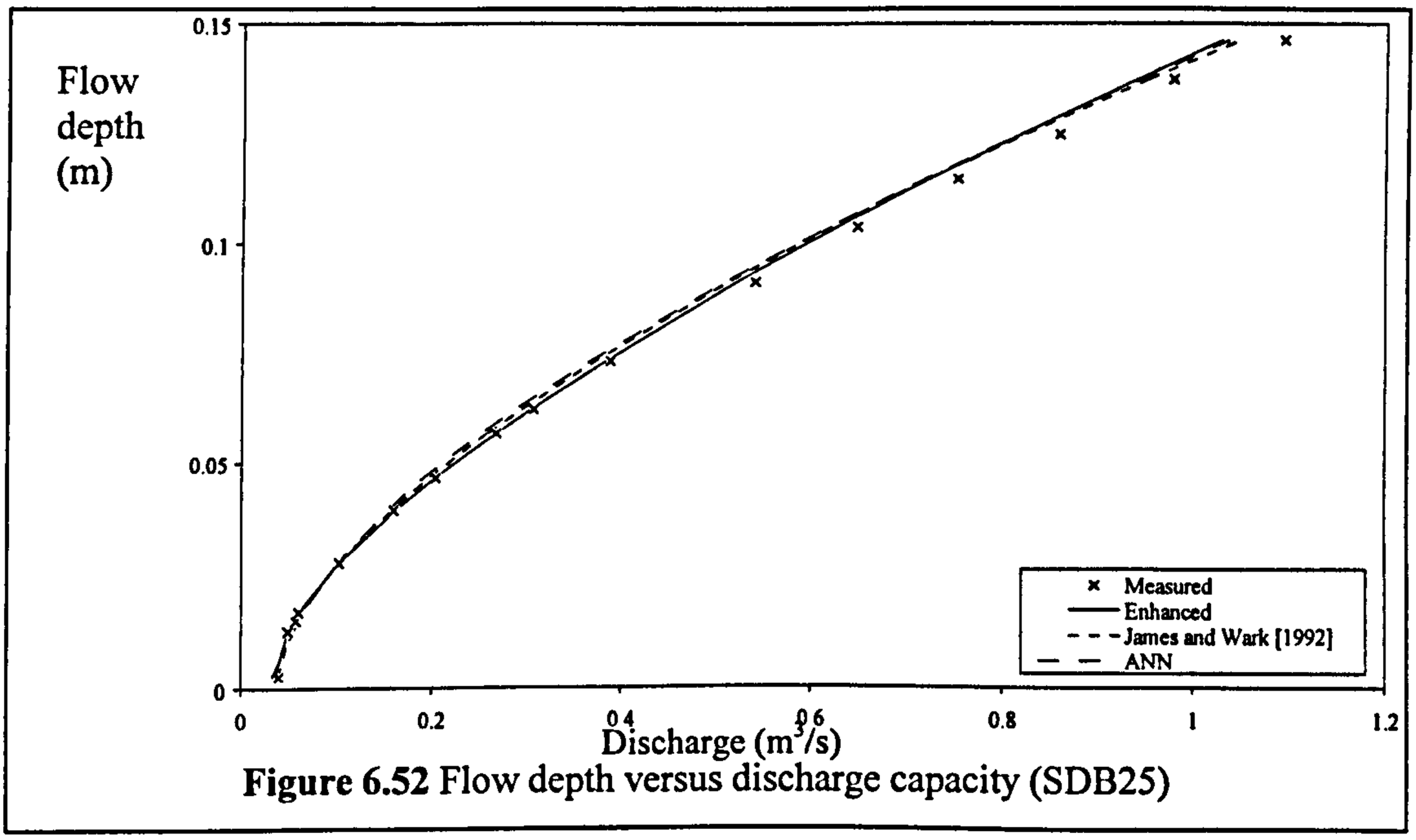

Figure 6.52 Flow depth versus discharge capacity (SDB25)

Both the Enhanced zonal method and the James and Wark [1] [1992] method give better levels of prediction than the ANN model and the Enhanced zonal method gives marginally better predictions than the James and Wark method for this test category.

6.11 Summary and Conclusions

6.11.1 The significance of the Enhanced zonal method

- The author's review of the current discharge capacity prediction methods for uniform meandering compound channels demonstrated that the James and Wark [1] [1992] method produced the most accurate predictions.
- The author noted, following the Series B extension (1993-1996) experiments, that the James and Wark [1] [1992] method was derived using a data set which was limited in range and scope and did not make allowance for the all the intricacies of flow behaviour that the author identified.
- The author therefore developed an Enhanced zonal method which was based on the general structure of the original James and Wark [1] [1992] method but included enhancements for each of the Zone A, B and C discharge formulations.

6.11.2 Zone A

- The author developed an empirical formulation for the Enhanced zonal method to account for the flow resistance due to layer interaction in Zone A. The formulation incorporated a non-dimensional adjustment coefficient Q_A' which was applied to the bankfull discharge capacity of Zone A to cater for the additional interaction losses.
- The author identified that the flow behaviour in Zone A, which was traced by plotting Q_A' versus relative depth, was divided into two characteristic flow regions which were labelled flow regions A1 and A2.
- The author demonstrated that in flow region A1 the magnitude of Q_A' decreases over a small range of flow depths. From a maximum value equal to 1 when relative depth equalled 1, Q_A' decreases to a minimum value which occurs when the flow in the meandering compound channel changes from 2 zone to 3 zone behaviour. The vertical shear interface which existed in flow region 1 between Zones 1 and 2 is disrupted.

- The author demonstrated that in flow region A2, Q_A' increases with increasing relative depths. Q_A' increases non-linearly with relative depth and was shown to be dependant upon 5 other parameters which were tested during the Series B (1989-1992) and Series B extension (1993-1996) programmes and are listed below:-
  a) main channel aspect ratio
  b) main channel side slope
  c) relative main channel and flood plain roughness
  d) main channel Reynolds number
  e) main channel sinuosity
- A multi-variate regression analysis was used to develop a formulation relating Q_A' to the six parameters listed above which is given in Equation 6.10.
- The flow depth corresponding to the end of flow region 1 was derived by the author by determining the flow depth which generates the maximum relative shear force, F_S, for the channel using Equation 4.8. The corresponding value of $Q_{A'min}$ was determined by presenting this flow depth and its associated parameters in Equation 6.10 for flow region A2.
- The author derived a linear expression for Q_A' for flow region A1 which was determined by fitting a straight line between the two predetermined relative depths (RD):- RD = 0 and RD when Q_A' achieved a minimum value.
- The two expressions for defining Q_A' in flow regions A1 and A2, when processed, produced discharge capacity estimates which fitted the flow data for Zone A (which was gathered during the Series B extension (1993-1996)), with greater accuracy than by using the James and Wark [1] [1992] method.

6.11.3 Zone B

- For the Enhanced zonal method, the author adapted the basic physical model defining Zone B velocity which is shown in Equation 6.11 so that it modelled the flow mechanisms in Zone B flow more precisely.
- The author demonstrated that the flow behaviour in Zone B altered radically once the theoretical Relative Reynolds number, Re', exceeded 1. Below Re'=1 Zone B behaved as though bed friction was the only source of flow resistance. Above Re'=1

there is evidence of significant expansion and contraction losses supplementing bed friction.

- The author showed that above Re'=1 (which was labelled Threshold 2/3) the flow in Zone B typically divides into two characteristic sub-zones which he called Zones B1 and B2 as shown in Figure 6.13. The head losses generated are greater in Zone B1 than in Zone B2 so the mean depth averaged velocity is greater in Zone B2.
- The author removed the wetted perimeter reduction in the bed friction term in Equation 6.11 from the basic physical model because data gathered during the Series B extension (1993-1996) demonstrated that it was inappropriate.
- The author defined the expansion and contraction head loss coefficients, K_e and K_c, in Equation 6.11 using two formulations which were derived by the author and defined the adjustment coefficients C_{we} and C_{wc} in terms of aspect ratio, side slope angle and relative depth. The two formulations were presented in Equations 4.14 and 4.15.
- In the Enhanced zonal method, the author used two versions of the basic physical models defined in Equation 6.11, one for Zone B1 and one for Zone B2. Two empirically-determined adjustment coefficients, known as the 'Flow parameters', F_1 and F_2 were derived. They were designed to operate upon the expansion and contraction term and were determined by fitting the basic physical model predictions for Zone B1 and B2 velocity to the measured velocities in these zones (using multi-variate regression analysis). The measured velocities were obtained during the Series B extension (1993-1996) programme.
- Thus the flow parameters, F_1 and F_2, reflect the difference in expansion and contraction losses in Zones B1 and B2 above Threshold 2/3 and because they are defined in terms of Relative Reynolds number, Re', they allowed for the expansion and contractions head losses being negligible below Threshold 2/3.
- The two semi-physical / semi-empirical models which were derived for defining the mean depth averaged velocity in Zones B1 and B2, when processed, produced discharge capacity estimates which fitted the flow data for Zone B with greater accuracy than by using the James and Wark [1] [1992] method.

6.11.4 Zone C

- The author demonstrated that although the majority of Zone C is usually subjected only to bed friction resistance, after the expansion and contraction flow mechanisms are initiated in Zone B1, in flow region 3, then a vertical shear zone is established between Zones C and B1.
- The author developed a formulation which is used to predict the shear zone width, δ, between Zones B1 and C in the Enhanced zonal method. The formulation is presented in Equation 6.37 and was derived by performing multi-variate regression analysis on data gathered during the Series B extension (1993-1996) programme. Shear width, δ, was defined in terms of 3 key parameters:-
  a) the relative velocity in Zones C and B1
  b) the flow depth
  c) flood plain friction factor.
- When the mean velocity in the shear zone was determined and combined with the mean velocity in the rest of Zone C, the discharge capacity estimates produced for Zone C fitted the measured flow data for Zone C with greater accuracy than by using the James and Wark [1] [1992] method.

6.11.5 Comparison between the Enhanced zonal and James and Wark methods

- The author demonstrated that the Enhanced zonal method gave a higher level of accuracy than was achieved by the James and Wark [1] [1992] method for the one set of reliable field data for the River Roding.
- The author demonstrated that the Enhanced zonal method gave a higher level of accuracy than was achieved by the James and Wark [1] [1992] method when tested against the available medium scale model data from the Series B (1989-1992) and Vicksburg [1956] experimental programmes.
- The author demonstrated that the Enhanced method gave a higher level of accuracy than was achieved by the James and Wark [1] [1992] method when tested against the majority of available small scale model data from Toebes and Sooky [1967], Kiely [1989], Aberdeen (1991), Series B extension (1993-1996) (Glasgow) and Series B extension (1993-1996) (Aberdeen).

- The author demonstrated that the Enhanced zonal method was less reliable when tested against meandering compound channels with geometric configurations (especially sinuosity) which are very different from those in natural channels. However the James and Wark [1] [1992] has similar difficulties.

6.11.6 Comparison between the Enhanced zonal, ANN and James and Wark methods

- The author demonstrated that the ANN approximator generates the most accurate predictions for the discharge capacity of a meandering compound channel provided that the geometric and roughness parameters fall within the same range as those used for training the ANN approximator.
- The author demonstrated that the ANN approximator can extrapolate to give reliable discharge capacity predictions even when the parameters are slightly outwith those in the training set.
- The author demonstrated that the accuracy of the ANN approximator method drops well below acceptable tolerances if the geometric and roughness parameters of the channel being assessed are significantly outwith those in the training set.
- The author demonstrated that the Enhanced zonal method generated levels of accuracy which were comparable to the ones obtained using the ANN approximator for the test sets with parameter values within the ANN training set parameter range. However for the test sets with parameter values outside the ANN training set parameter range the Enhanced zonal method generated significantly more accurate predictions than the ANN approximator.
- The author demonstrated that the influence of main channel sinuosity and relative meander belt width is much less significant in larger scale models. The author suggests that users of either the Enhanced zonal method or the ANN approximator that testing to date has demonstrated that they can be confident in the accuracy of the methods when applied to larger scale models.

Chapter 7

7. Case study: Incorporation of discharge capacity prediction methods in novel 1D numerical models to facilitate the design of a flood protection scheme for the River Dane, Cheshire

7.1 Introduction

This chapter chronicles the development and testing by the author of two novel one-dimensional (1D) numerical models for steady and unsteady flows in flooding river channels. These models implement numerical formulations that are similar to the ones used in traditional, industry-standard 1D models. By contrast however, they incorporate the Ackers [1991] and James and Wark [1] [1992] methods instead of the traditionally adopted 'divided channel methods' to produce conveyance characteristics tables for each cross-section along the length of the river being modelled. Inclusion of the Ackers [1991] and James and Wark [1] [1992] method enables the flow resistance generated in natural meandering compound channels by layer interaction to be explicitly accounted for in order to supplement the calculated head lost due to bed friction resistance. The traditional 'divided channel' methods explicitly account for the flow resistance generated by bed friction and only implicitly account for other sources of head loss by including loading to friction factors and by implementing arbitrary perimeter extensions.

In addition a new protocol was developed by the author to assist with the implementation of his novel 1D models when designing compound channel flood protection schemes. The River Dane case study was used as a source of calibration data to validate the 1D models and to demonstrate the operation of the design protocol.

7.2 Historical background to the case study on the River Dane

In the Spring of 1996 the author and Dr A Ervine were asked to perform an investigation into flooding and possible flood protection measures for a site in the Dane valley, Cheshire about 25 miles south-west of Manchester. This area is illustrated in Figure 7.1.

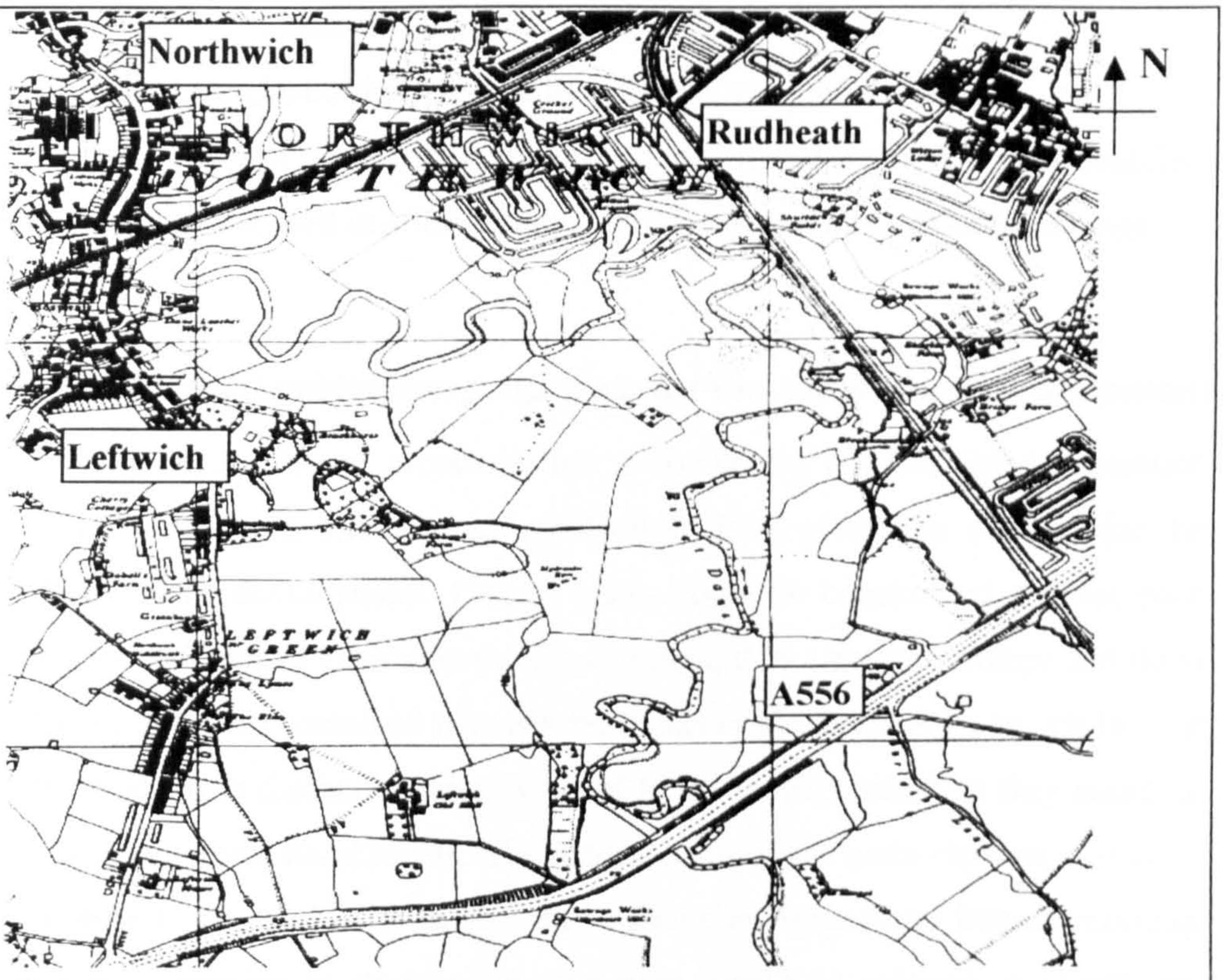

Figure 7.1. Sketch of Dane valley (OS map, 1:10560, Sheet No. SJ67SE)

The flood plains are low-lying, relatively flat and prone to flooding. The town centre of Northwich is just downstream and is also sensitive to flooding. However, to date, the Environment Agency (EA) have objected to proposals for major development on the flood plain of the River Dane. The EA is the Land drainage authority who is charged with controlling development in the flood plains of main rivers such as the Dane.

7.3 Previous flood protection proposals for the River Dane development

An earlier proposal for flood protection, forwarded in 1989, stipulated that the main Dane river channel should be the straightened and dredged to provide the discharge capacity to contain the 1:100 year flood with 600mm freeboard. However, the Environment Agency rejected the proposal for the following reasons:-

- The development would have a detrimental impact on the existing river environment by incorporating a number of radical alterations to the main channel configuration.
- The impact of flood waters downstream, in Northwich town centre, would be exacerbated because of the loss of flood plain storage caused by the straightening and dredging of the main channel.
- The proposed channel would be potentially unstable and prone to erosion.

The author concluded that in retrospect the objections offered by the EA were justified. The design proposals forward in 1989 certainly possessed a number of shortcomings.

7.4 Alternative flood protection proposals for the River Dane development

The author and Dr A. Ervine proposed that a compound channel flood protection scheme would provide an alternate and preferable flood protection scheme for the proposed River Dane development. Distant banks could be constructed and set back from the main river channel to contain the flood waters, thus creating a compound flood channel. The flood plains contained between the banks could, preferably, be left in their natural state if adequate discharge capacity could be provided. Otherwise they could be excavated to reduce river flood levels. The natural state of the main channel would be maintained close to its original form and the negative environmental impact resulting from deepening, widening or straightening the river would be reduced. A significant amount of temporary storage volume would still be provided by the remaining flood plain areas thus ensuring that there would be only a very limited increase in the discharge passed downstream to Northwich after implementing a compound channel when compared with the discharges produced using the more traditional options. The magnitude of remaining compensation storage provided would depend upon the width between the flood banks, as illustrated in Figure 7.2.

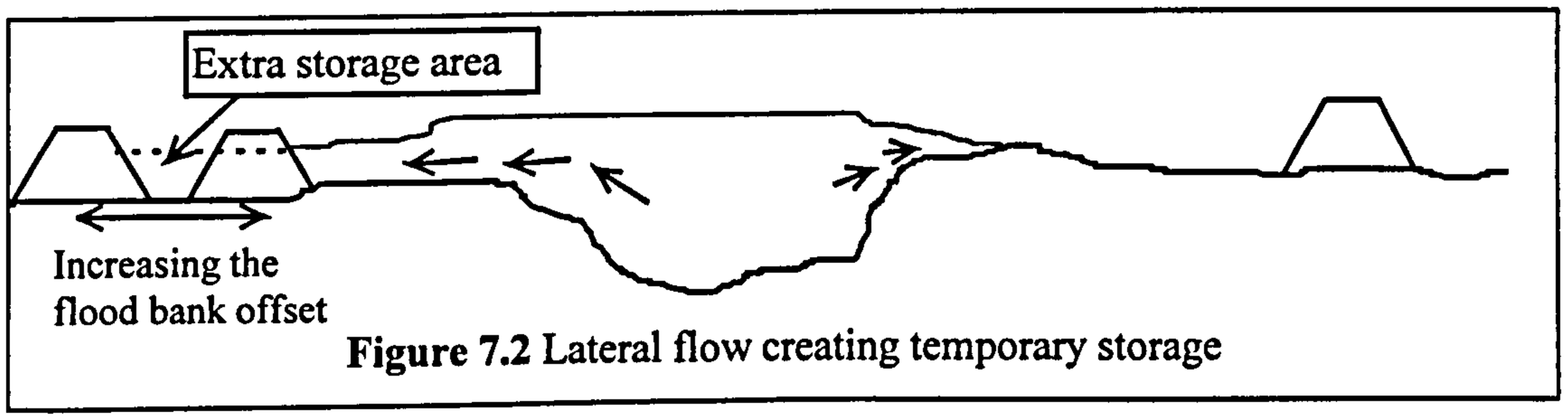

Figure 7.2 Lateral flow creating temporary storage

The negative aspects facing a developer as a result of implementing a distant flood bank scheme were that:-

- the area of flood plain available for development would be reduced, as shown in Figure 7.3.
- no reliable one dimensional numerical model had yet been commercially developed which could accurately model meandering compound channel flow. Therefore the precise impact of building distant flood banks, locally or downstream in Northwich could not be demonstrated to the Environment Agency.

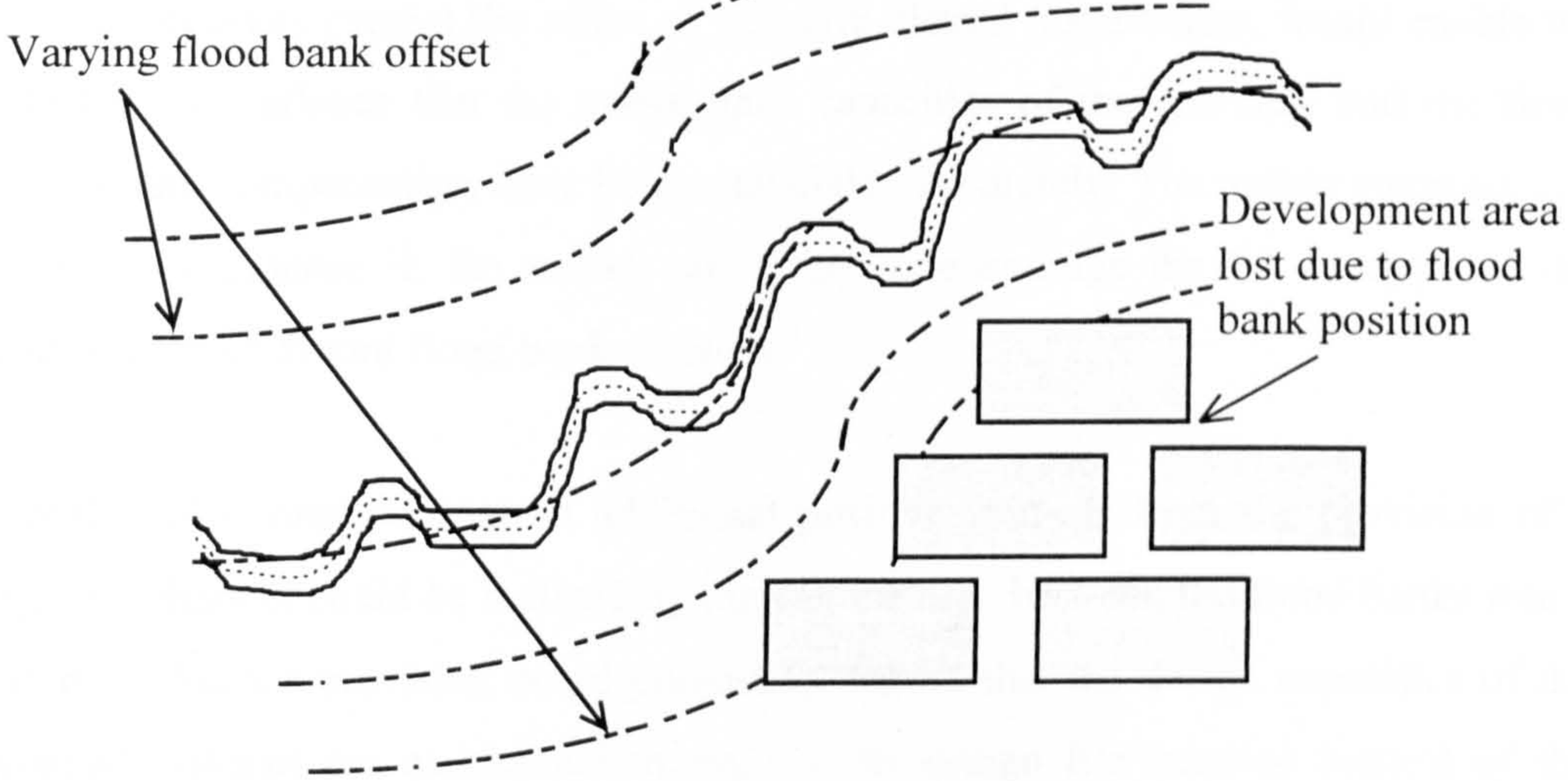

Figure 7.3 Development area affected by flood bank offset

The author acknowledged that the EA were unlikely to approve any compound channel scheme without extensive proof of its viability especially when alternative sites for the development, outside the flood plain, could potentially be found and bearing in mind that the flood plain prior to development was completely natural and unspoilt. The onus was with developers and their Consulting Engineers to demonstrate the viability of any compound channel scheme and to identify benefits for the whole community accruing from the scheme, in order to justify any potential increase in flooding risk that the scheme may engender.

The author proposed that the risk associated with implementing compound channel flood protection measures could be reduced by using the novel steady and unsteady one dimensional numerical models to model the River Dane and to assess the impact of

implementing a compound channel. The novel 1D models explicitly account for the extra head lost due to flow layer interaction in a compound channel thus overcoming the shortcomings and lack of reliability of traditional 1D models. They are unreliable because they account for interaction losses simply by using existing flood data and adjusting the basic friction coefficients until the model matched the calibration data. Typically these very configuration-specific models were subsequently used to analyse various design solutions (with the same adjusted coefficients), even though the adjusted friction coefficients were not appropriate for any alternative channel configurations conceived during the design phase. The author postulated that, the ability of these novel models to precisely predict the effect of building distant flood banks, would enable the EA to have confidence that the conveyance capacities of the channels and the flood water volume compensation were being calculated accurately. The author suggests that their extra confidence in the model was likely to encourage the EA to approve the design of a novel distant flood bank solution.

The author also suggests that an additional positive spin-off from the provision of a compound channel could be realised by turning the area between the flood banks into a linear park. Such a provision could potentially ensure that the design capacities of the compound channel are maintained throughout its design life because control of the hydraulic characteristics of the flood channel could be achieved by the structured management of the park. The author suggests that the funding needed to maintain the park in such a way could be provided in the form of a commuted sum levied from the interested parties, but predominantly the developer. A well-managed park would have the potential for delivering significant enhancements for the environment and providing a valuable amenity for the local communities in Northwich, Rudheath, and Leftwich. It would open previously inaccessible private farmland for use as a public resource.

7.5 A novel one-dimensional numerical model for steady flow

7.5.1 The energy balance equation

An energy balancing technique can be used to determine the water surface level to discharge capacity relationship over most river reaches when they are modelled by a number of representative cross-sections and the boundary conditions are constant. The

Standard Step method, which was described by Chow [1959], calculates the water level (stage), h_i, at adjacent cross-sections, i, progressively up or down a reach (depending on whether sub-critical or super-critical flow prevails) by balancing the specific energy at adjacent cross-sections using the parameters shown in Figure 7.4. Energy balancing has been used as the solution method in a number of commercial 1D models for steady state conditions.

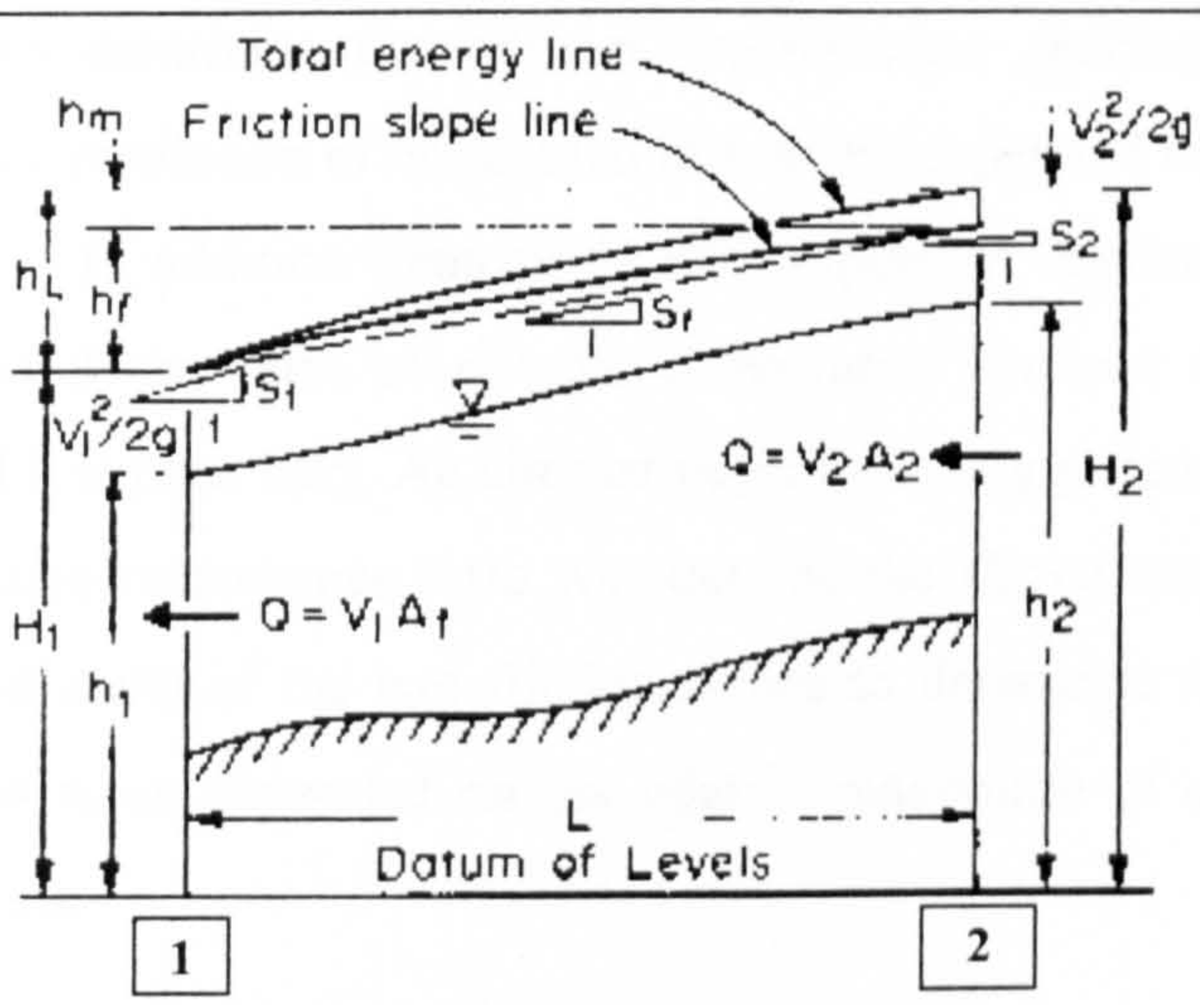

Figure 7.4 Water surface profile for the energy balance method (after Laurenson [1986]

An algebraic expression for the energy balance equation is shown in Equation 7.1. It represents the relationship between the specific energy at adjacent cross-sections 1 and 2 and can be solved at adjacent cross-sections given a discharge rate and a suitable boundary condition (a stage), The model was created and the solution algorithms coded using Fortran77.

$$h_2 = h_1 + \alpha(h_1)\cdot\frac{V_1^2}{2g} - \alpha(h_2)\cdot\frac{V_2^2}{2g} + \Delta x \cdot f(S_{fu}, S_{fd}) + h_e \qquad [7.1]$$

Δx is equal to the distance along the thalweg between the two cross-sections, 1 and 2, $h_{1,2}$ is equal to the magnitude of stage (m) at 1 and 2, g is the gravitational constant, $V_{1,2}$ is equal to the mean depth-averaged velocity at 1 and 2, $f(S_{fu}, S_{fd})$ is the mean friction slope between 1 and 2, h_e is the energy loss when there is a radical difference in cross-sectional geometry between two adjacent sections and $\alpha_{1,2}(h)$ is the energy coefficient at each cross-section and is estimated to make allowance for variations in the velocity field throughout the compound channel cross-section. The numerical solution of the steady state model was designed to incorporate some of the recent refinements which have

been proposed over recent years. In response to Laurenson [1986], the typical mean friction slope was defined as the arithmetic mean of the friction slope at two adjacent cross-sections. Laurenson [1986] tested four options suggested by Cunge *et al* [1980] for determining the mean friction slope against field data. He showed that the arithmetic mean was the most reliable averaging procedure when an optimal cross-section spacing was chosen. It also gave the most consistent results. A method proposed by Samuels [1995] was used to determine the optimal cross-section spacing. Samuels [1995] demonstrated that the resolution of cross-section spacing depended on the magnitude of the flood plain slope. In addition Samuels [1995] stipulated that arithmetic averaging should only be used if the ratio of relative conveyance between cross-sections was greater than 0.8 and less than 1.25. An alternative method, suggested by Pender [1985], was used when relative conveyance ratio was outside the above range. Pender [1985] employed a weighted mean of the two friction slopes to determine the average friction slope. This weighted mean depended on the relative magnitude of conveyance in two adjacent cross-sections.

7.5.2 Incorporating main channel and flood plain interactions

The author modified the methods adopted in traditional one-dimensional (1D) models by using the discharge capacity prediction methods developed during the Series B extension (1993-1996) programme to determine the conveyance characteristics at each cross-section within the basic model and thus explicitly account for the flow resistance generated by layer interaction as well as bed friction. Previously in the traditional models (such as HEC-RAS or MIKE 11) the conveyance characteristics were calculated by assuming that only bed friction resistance was generated. The flow resistance generated by flow layer interaction was accounted for by adding supplements to systematically determined friction coefficients (using Chow's [1959] tables) when applying the model to calibration data.

At the time of performing the River Dane investigation, the Artificial Neural Network (ANN) method (described in Chapter 5) and the Enhanced zonal method (described in Chapter 6) had not been completed. Consequently only the Ackers [1991] method for straight compound channels and the James and Wark [1] [1992] method for meandering

compound channels were initially incorporated into the 1D models. The conveyance characteristics determined in the model for each cross-section (X-S) are listed in Equations 7.2 - 7.4, where h_i is equal to the water surface level, Q_i is equal to the discharge contained within each cross-section, j is the number adjacent river cross-sections, and n is the number of zones comprising each cross-section which are needed to apply either the Ackers [1991] or the James and Wark [1] [1992] methods. The decision about which method to use at each cross-section is determined by considering the sinuosity of the main channel. The Ackers [1991] method is used when the sinuosity, r, is less than 1.09. The James and Wark [1] [1993] method is used when the main channel sinuosity, r, is greater than 1.09.

Conveyance capacity at each X-S, j:

$$K_i \equiv \frac{Q_i}{\sqrt{S_i}} \qquad [7.2]$$

Energy line slope:

$$S_f = \left(\frac{Q_{total}^2}{\left(\sum_{i=1}^{n} K_i \right)^2} \right) \qquad [7.3]$$

Energy coefficient:

$$\alpha' \equiv \frac{\left(\sum_{i=1}^{n} A_i \right)^2}{\left(\sum_{i=1}^{n} K_i \right)^3} \times \sum_{i=1}^{n} \left(\frac{K_i^3}{A_i^2} \right) \qquad [7.4]$$

The conveyance characteristics were incorporated in the 1D model as flow tables, which were linearly interpolated at various intermediate flow depths and discharge rates. They were used to calculate the right-hand side of Equation 7.1 at adjacent cross-sections and known boundary conditions and discharge rates.

7.6 A novel one-dimensional numerical model for unsteady flow

The author also enhanced a one-dimensional numerical model for unsteady flow to explicitly account for the extra flow resistance generated by flow layer interaction in meandering compound channels. The original model was developed by Pender [1985]. An unsteady numerical model is a useful tool for assessing whether the loss in flood water volume storage, which was caused by the construction of the distant flood banks, results in an increase in the maximum discharge that is passed through the compound channel. Thus determining whether the construction of flood banks actually increases the risk of flooding downstream in Northwich.

Pender [1985] used a implicit finite-difference scheme, developed initially by Preissman [1960] to solve the continuity equation, Equation 7.5, and the dynamic equation, Equation 7.6, (generically known as the St Venant equations) when they were applied to a one-dimensional model consisting of a number of representative cross-sections given suitable boundary conditions (rating curves) and a discharge rate hydrograph. The Preissman [1960] scheme is implicit and therefore damps numerical oscillations and avoids instability and have been incorporated in many of the commercially available 1D numerical models that are available today.

$$b\frac{\partial h}{\partial t}+\frac{\partial Q}{\partial x}=q \qquad [7.5]$$

$$\frac{\partial Q}{\partial t}+\frac{\partial}{\partial x}\left(\beta\frac{Q^2}{A}\right)+gA\left(\frac{\partial h}{\partial x}+S_f\right)=0 \qquad [7.6]$$

where Q is equal to discharge rate(m^3/s), b is equal the top width of the channel, A is equal to flow area, β is the momentum coefficient, S_f is the friction slope and q is the lateral inflow per unit width (m^3/s). The supplementary coefficient, β is introduced to simulate quasi two-dimensional flow. The model was created and the solution algorithms coded using Fortran77.

Once again the values of the flow parameters which were required to solve the St Venant equations for 1D unsteady flow were pre-calculated using a combination of the Ackers [1991] method and the James and Wark [1] [1992] method for various stages and discharges at each cross-section and for a full range of possible flow depths. The parameter tables (summarising the conveyance characteristics) produced in this novel manner were applied to the unsteady river model, known as 'Channel' developed by Dr. G. Pender of the Department of Civil Engineering, University of Glasgow.

The original model has been used extensively by Dr Pender for the last 10 years and has proved its value on many river schemes throughout the UK. It has been applied specifically to river/flood plain flows including temporary storage and washland behaviour. The explicit determination of the influence of interaction head losses on the discharge capacity at each cross-section ensured that all channels could be modelled without having to adjust the resistance coefficients during calibration which was the traditional approach.

7.7 Determining geometric and roughness parameters in natural rivers

7.7.1 Introduction

Differing numbers of the key parameters which influence the layer interaction mechanisms in compound channels are included in the Ackers [1991], James & Wark [1] [1992], Artificial Neural Network and the Enhanced zonal discharge prediction methods. Table 3.1 lists the key parameters for meandering compound channels and Section 2.6.3.3 describes the influential parameters in straight compound channels. These parameters can often be defined easily for the uniform small scale physical models but tend to be more difficult to identify and quantify in natural rivers.

The author has established refined definitions for the geometric and roughness parameters which affect flow behaviour in compound channels and are used in the above methods. The refined definitions were developed so that equivalent parameter values could be determined in natural channels whilst maintaining compatibility with the definitions originally defined for the regular channels used in the physical models.

7.7.2 Longitudinal averaging

Each of the James and Wark [1] [1992], Ackers [1991], Artificial Neural Network and the Enhanced zonal methods suffered from the limitation that one average representative cross-section configuration had to be determined for the whole of the reach under investigation to enable the method to be applied. There was also no longitudinal variation of the channel configuration in the model channels used to gather the empirical data on which the methods were based, so the parameters associated with one cross-section represented the configuration over a complete channel reach. Extending this procedure to natural rivers was inevitably prone to inaccuracies because natural rivers exhibit extensive longitudinal variation. It is unlikely that one cross-section can be derived which can be used to determine the interaction losses in a rapidly varying river and even if it can no research has been performed to date to determine this potential relationship.

Incorporation of the methods into a 1D model overcame this problem to some extent. The number of cross-sections that were included in the model were chosen so that the influence of all the significant longitudinal variations were accounted for. In the 1D models the length of river which could be justifiably represented by one cross-section configuration had to be defined. This length was defined as the distance along the thalweg which was equal to half the distance, dx_{xs2}, between 3 adjacent cross-sections, XS1, XS2, XS3 as shown in Figure 7.5. Typical cross-sectional half-point positions are marked on Figure 7.5 as $CS_{1,2}$ and $CS_{2,3}$. All the subsequent parameter values should be calculated by averaging all the intermediate parameter values between cross-sectional half-point positions such as $CS_{1,2}$ and $CS_{2,3}$.

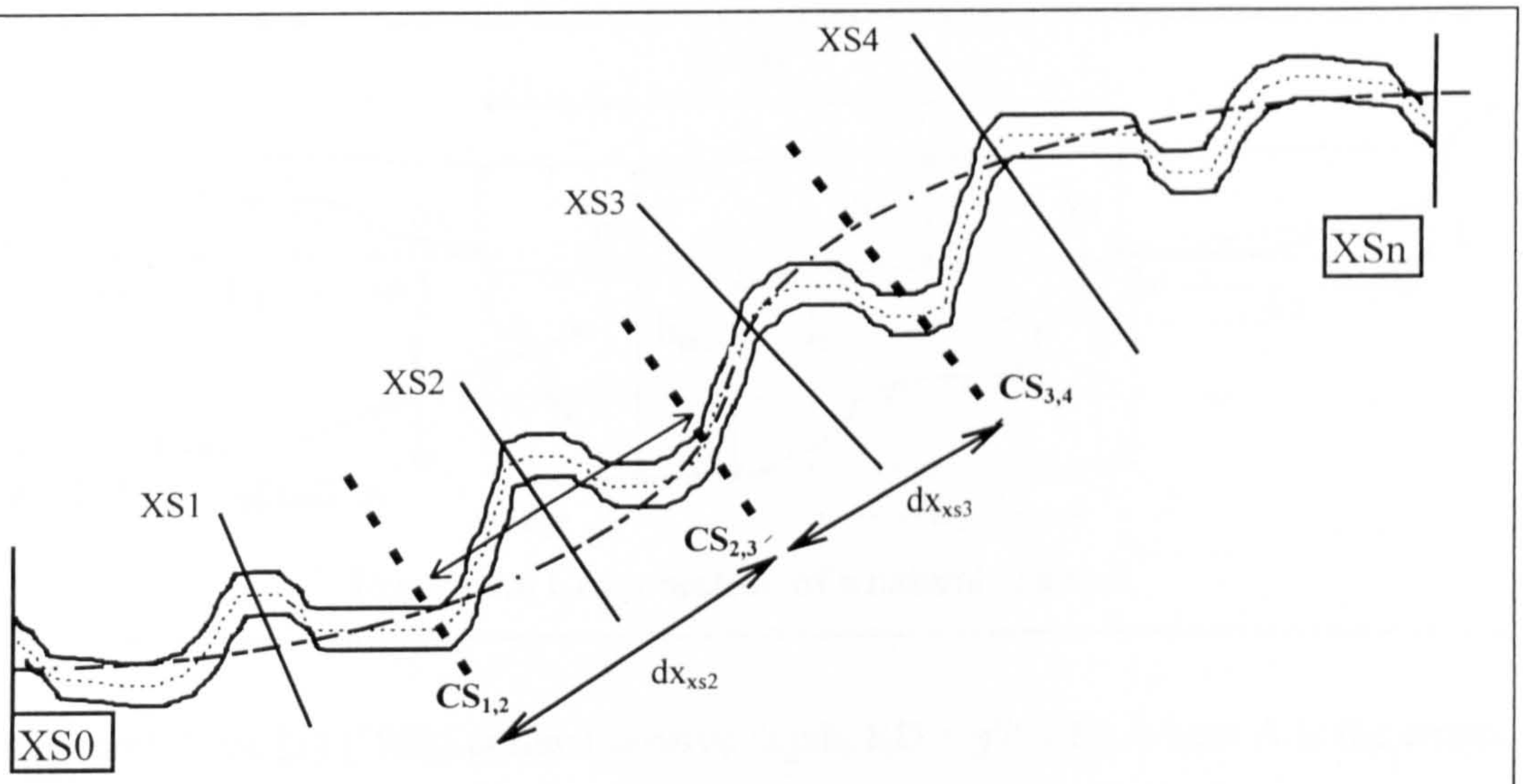

Figure 7.5 Cross-section positions in a natural channel

River Engineers in the UK often use protocols established by Samuels [1990] for spacing cross-sections when developing 1D models. The author acknowledges that further validation work is required to determine whether the cross-sections chosen using this method will give the optimal average sub-reach spacing when determining the representative uniform channels to apply to natural rivers. The author assumed that they would for the River Dane case study.

7.7.3 Relative flow depth, RD

Three different measures of relative depth, RD, have been implemented in the Ackers [1991], James & Wark [1] [1992], Artificial Neural Network and the Enhanced zonal methods for the typical natural channel cross-section shown in Figure 7.6.

Ackers [1991] defined relative flow depth, RD = $(H-h_{max})/H$ where h_{max} is defined as the maximum bankfull depth of the main channel and H is the overall flow depth coinciding with the point of measurement of h_{max}. Clearly the applicability of this definition for relative depth is limited because although h_{max} and H can be easily defined in regular models they are more difficult to define (even inappropriate) in natural channels.

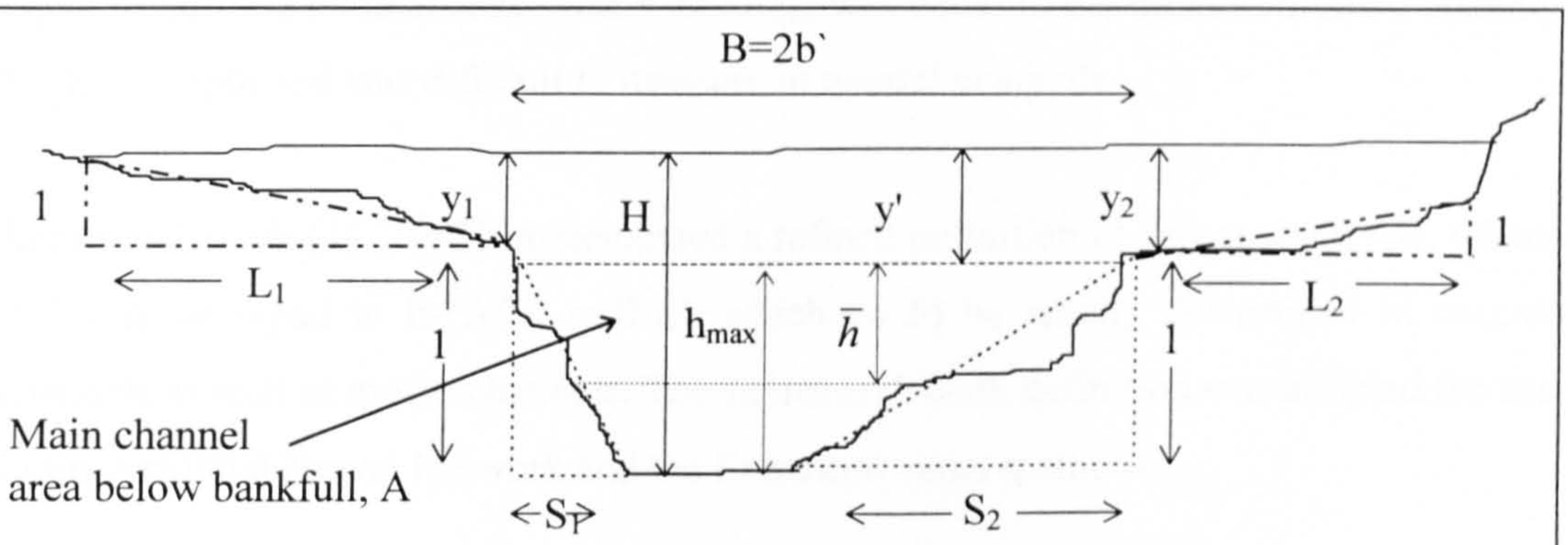

Figure 7.6 Cross-section of a natural channel

James and Wark [1] [1992] defined relative depth, RD = y'/(A/B), where A is the cross-sectional area of the main channel below bankfull level, B is the bankfull top width and y' is the flood plain flow depth. The value for y' was defined as the maximum flood plain flow depth for a particular flood level. These values were easily defined for natural channels and model channels. The disadvantage of this method is that y'/(A/B) tends to ∞ for increasing flow depths. The characteristic 4 flow regions identified by Ackers [1991] extended over a range of relative depths between 0 and 1. The 4 flow regions which were shown to be present in meandering compound channel flow were harder to distinguish when relative depth ranged between 0 and ∞.

An alternative measure of relative depth, which implemented a range of relative depth measurements between 0 and 1 (for presentation clarity) and could be applied equally well to both natural and model channels, was developed for the Artificial Neural Network and Enhanced zonal methods during the Series B extension (1993-1996)

programme. In these methods, relative depth, RD, was defined as equal to y/(y+(A/B)), where y is the arithmetic average of the depth of flow on either side of the flood plain at the top of the main channel, $y=(y_1+ y_2)/2$ and (A/B) is a measure of the average main channel bankfull depth, as shown in Figure 7.6.

7.7.4 Aspect ratio of main channel, AR

Aspect ratio, AR, indicates the width to depth ratio for the main channel which has considerable influence on the interaction mechanisms between layers in compound channels. Ackers [1991] defined main channel aspect ratio, $AR = (2b/h_{max})$ where b was equal to half the main channel width and h_{max} was equal to the maximum main channel bankfull depth and was difficult to measure in natural channels.

James and Wark [1] [1992] implemented a refined definition of aspect ratio, AR, where AR was set equal to $B/(A/B) = B^2/A$ which could be readily determined in natural channels as well as model channels. The James and Wark definition was adopted for use in the Artificial Neural Network and the Enhanced zonal methods.

7.7.5 Relative roughness, f_f/f_c

In natural channels the roughness coefficients are usually assessed in terms of Manning's n for both the main channel and the flood plains. In physical model studies the Darcy-Weisbach friction coefficient, f, is commonly used because the frictional resistance is so dependant on the Reynolds number associated with the flow and the two parameters can be related using the modified smooth law equation. The values for f and n are related by the Equation 7.7.

$$f = \frac{8gn^2}{R^{1/3}} \qquad [7.7]$$

The James and Wark [1] [1992] prediction method and the prediction methods presented in this thesis define relative roughness in terms of the relative Darcy f', which is defined as being equal to $f_{Zone\ B}./ f_{Zone\ A}$. The relative roughness for natural channels is calculated by back-substituting the Manning's n values in Equation 7.7.

$$f_{\text{Zone B}} / f_{\text{Zone A}} \equiv \frac{n^2_{\text{Zone B}} * R_{ZoneA}^{2/3}}{n^2_{\text{Zone A}} * R_{ZoneB}^{2/3}} \quad [7.8]$$

where R is equal to the area of each zone divided by the wetted perimeter of each zone (excluding the division lines).

7.7.6 Sinuosity of the main channel, r

A typical natural river planform is sketched in Figure 7.7. The main channel sinuosity, r, is defined as the ratio of the thalweg length divided by the length measured along a median line that splits the average perpendicular distance between the limits of the meander belt drawn through each bend apex.

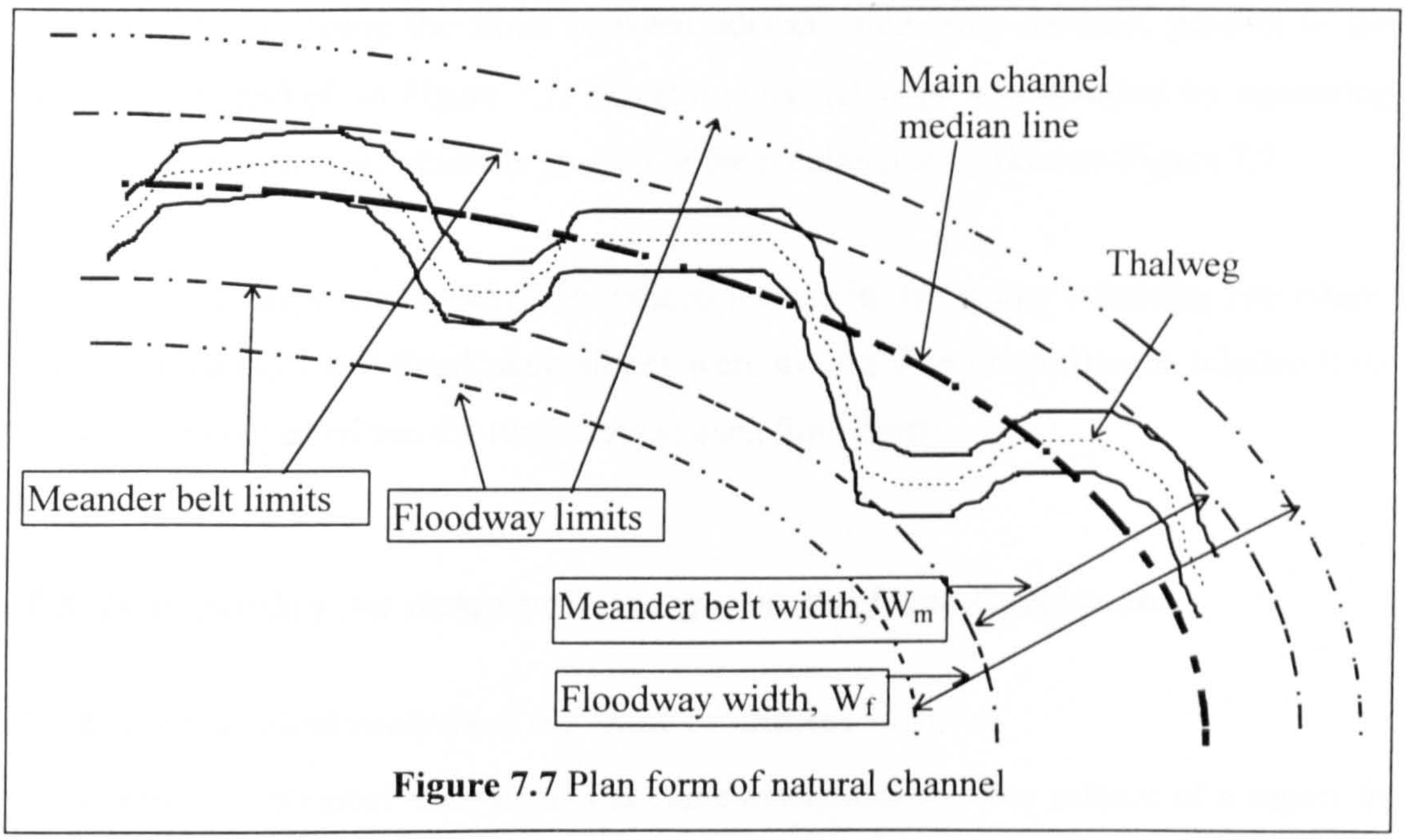

Figure 7.7 Plan form of natural channel

7.7.7 Relative meander belt width, Mw

The relative meander belt width, M_w was set equal to W_f/W_m where W_f is the average distance between the extent of flooding limits (or distant flood banks) and W_m is the average width of the meander belt width, as shown in Figure 7.7.

7.7.8 Main channel side slope angles, S_S

The main channel side slope angles, S_S, are determined at each cross-section. The side slope values are approximated by measuring the angle (in terms of the cotangent, S_S,) made by a construction line extending from the bankfull level to the point of maximum channel depth, as shown in Figure 7.6.

7.7.9 Longitudinal bed slopes, So

Two different longitudinal slopes were chosen, the average longitudinal flood plain slope, S_f, and the average main channel slope, S_{mc}. These were used when applying the prediction formulae to channel cross-sections. The average flood plain slope was obtained by measuring the slope between adjacent mid-cross-sections, parallel to the median line marked on Figure 7.7. The main channel slope was obtained by measuring the slope between cross-sections parallel to the median line marked on Figure 7.7.

An average channel slope had to be defined for use in the energy balancing procedure. The main channel and flood plain slopes were averaged in proportion to relative flow volumes contained within the two layers at each flow depth.

7.8 Determining the design discharges in the Dane Catchment

7.8.1 Hydrological analysis of the Dane catchment

A detailed hydrological analysis of the Dane catchment was the subject of a report in 1989. It was decided that for the study performed by the author in early 1996 the earlier analysis would be accepted. The author acknowledged that further hydrological analyses would be needed before final detailed design was undertaken but this was beyond the scope of the current work. It would be especially important at a later date to incorporate the additional records from the gauging station at Rudheath from 1989-1996. This would extend the original 40 year record to 46 years and may provide better estimates of the 100 year flood.

A sketch-map of the Dane catchment is shown in Figure 7.8. The river rises in the Peak District, flowing west to join the River Wheelock, and from there it heads North West

towards Northwich. The total catchment area is 407.1 km^2. The area for the proposed development is shown hatched, to the South East of Northwich town centre.

Several methods were employed in estimating the mean annual flood $\overline{Q}$ and the one hundred year flood Q_{100}. These methods were suggested by the NRA. Following the publication of the Flood Studies Report (FSR) by NERC in 1975, two basic approaches have evolved in estimating flood flows in rivers with a specified return period. The first approach is a frequency analysis and the second based on a unit hydrograph approach.

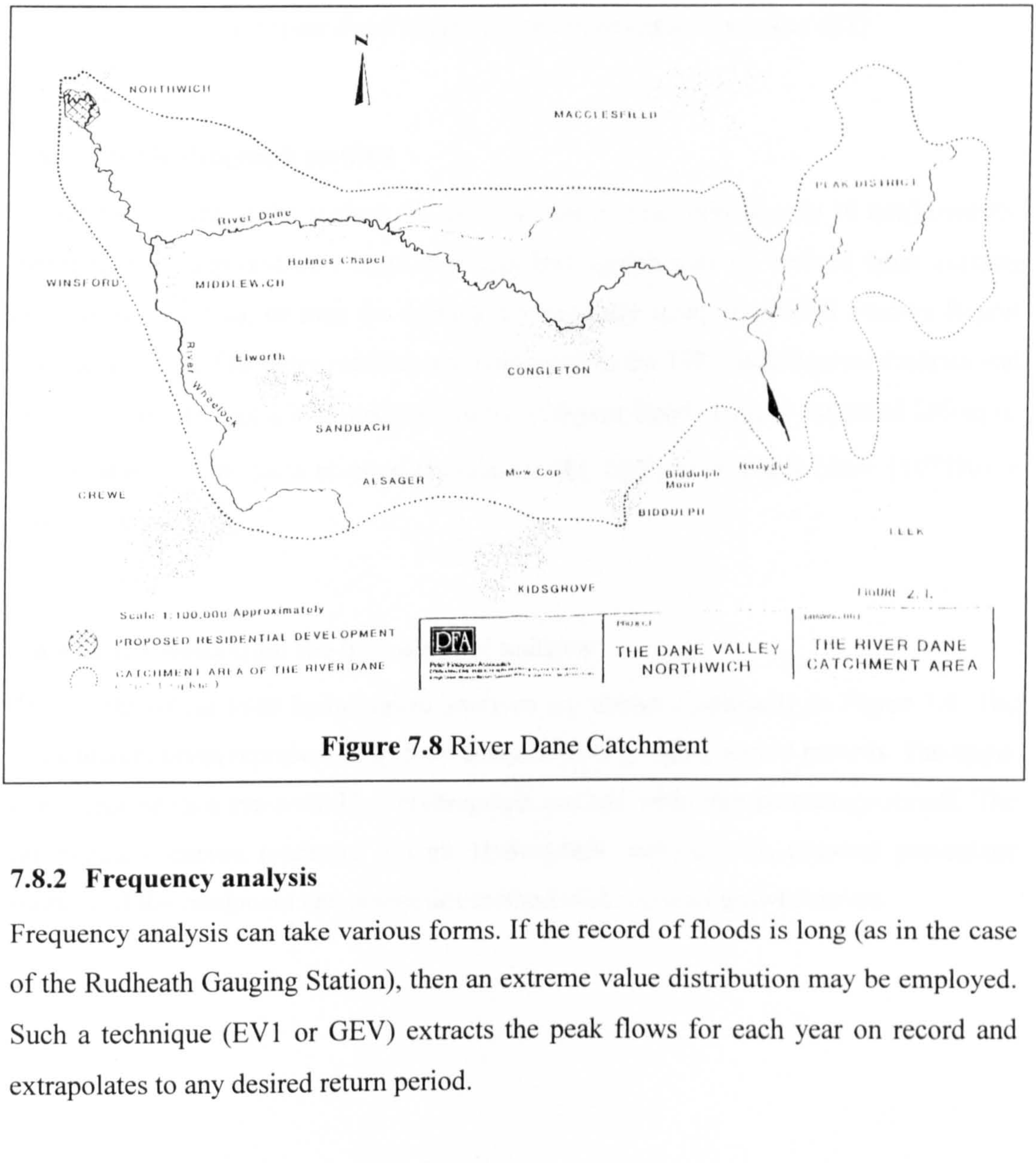

Figure 7.8 River Dane Catchment

7.8.2 Frequency analysis

Frequency analysis can take various forms. If the record of floods is long (as in the case of the Rudheath Gauging Station), then an extreme value distribution may be employed. Such a technique (EV1 or GEV) extracts the peak flows for each year on record and extrapolates to any desired return period.

If a medium or short flood record is available, the mean annual flood $\overline{Q}$ may be estimated from the record available. A flood of 100 year return period, for instance, may then be estimated from regional growth curves, published by NERC (1983), with different extrapolation for each region within the UK.

For very short or no flood records, the method of catchment characteristics may be used where the mean annual flood is estimated using Equation 7.9.

$$\overline{Q} = 0.0201 AREA^{0.94} STMFRQ^{0.27} S1085^{0.16} SOIL^{1.23} RSMD^{1.03} (1+LAKE)^{-0.85} \quad [7.9]$$

The estimate for a 100 year flood is again taken from region curves of $Q/\overline{Q}$.

7.8.3 Unit hydrograph method

A unit hydrograph is the surface run off response to a net rainfall (say 10 mm) over the catchment for a period of 1 hour. The unit hydrograph may be derived from existing rainfall/run off data, or may be derived synthetically using the Flood Studies Report (NERC [1975]). The latter method was employed in the 1989 hydrological analysis and was found to produce a large estimate of the 100-year flood Q_{100} in excess of 200 m^3/s. Other empirical methods such as Benson [1968], Nash [1957] and Shaw [1972]were also employed.

7.8.4 The results from the hydrological analysis

The results of the 1989 hydrological analyses are shown graphically in Figure 7.9. The three lower curves represent frequency analysis from gauging station records. The upper curve represents a synthetic Unit Hydrograph method with high percentage runoff. The intermediate curves represent a Unit Hydrograph method with reduced percentage runoff and the catchment characteristics method with regional growth curves.

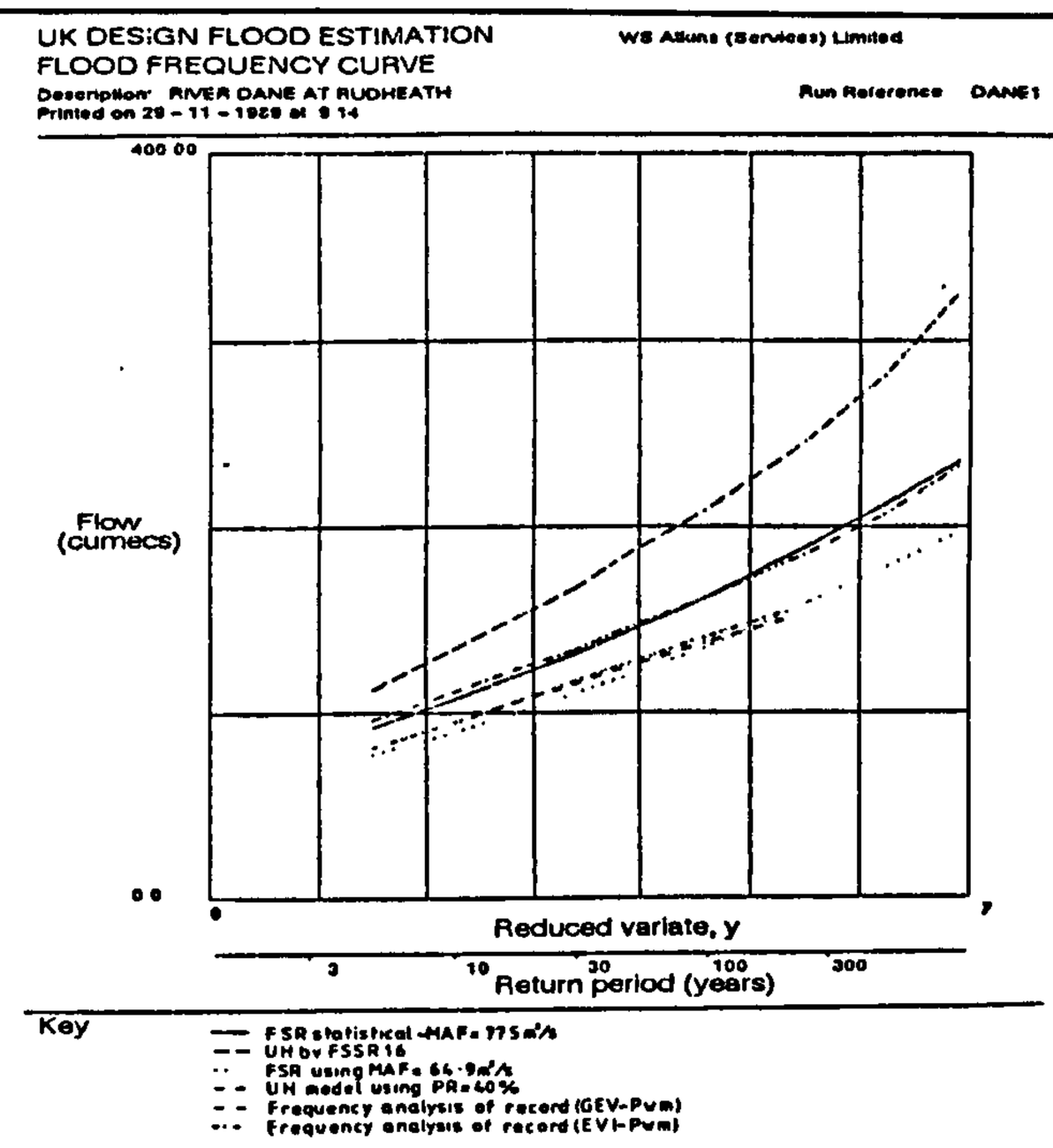

Figure 7.9 Micro-RAS analysis

The middle range values were accepted in the initial analysis, although the rationale for this is not immediately clear. The two accepted curves in Figure 7.9 stem from estimates for an ungauged catchment (usually not the most accurate value) together with a unit hydrograph technique which required to be modified to achieve this accepted value.

The 100 year flood was accepted to be 161.3 m^3/s. This value will also be accepted in this analysis, but it is open to question and really should be the subject of a new hydrological analysis. This corresponds to a mean annual flood around 78 m^3/s which typically would have a return period of 2 to 3 years.

7.9 Development of a steady state numerical model for the River Dane

The author developed a novel one-dimensional model of the River Dane as the first stage of the conceptual design phase. This model incorporated the Ackers [1991] and the James and Wark [1] [1992] methods for determining the appropriate conveyance parameter tables and therefore included the effect of channel / flood plain interaction. The Artificial Neural Network and the Enhanced zonal methods described in Chapters 5 and 6 had not been completed in early 1996 so they were not incorporated in this model. The author suggests that they can easily be incorporated at a later date, at the detailed design phase, in order to benefit from their improved level of discharge capacity prediction accuracy. They can be used to produce alternative conveyance parameter tables instead of the James and Wark [1] [1992] method.

The peak flow from the inflow hydrograph was used in the steady state model. This flow is assumed to be acting at all points along the river. This is a conservative approach but it is suitable for short reaches of river such as that under study.

A numerical model was developed which extended from the confluence of the Weaver upstream to the bridge on the A556 Southern by-pass. A total of 30 surveyed cross-sections were used in the numerical model. These are shown in Figure 7.10.

The cross-sections extended onto the flood plain well beyond the location of distant flood banks and out as far as the limits of natural 1 in 100 year flooding. The accuracy of the main channel cross sectional data is considered to be good. Flood plain level data was obtained from detailed contour maps rather than a detailed survey. This makes the flood plain levels less reliable but accurate enough to give indicative extent of natural flooding. This is less important in the analysis of two-stage channel flooding, where distant flood banks might be only 10-50 m offset from each bend apex.

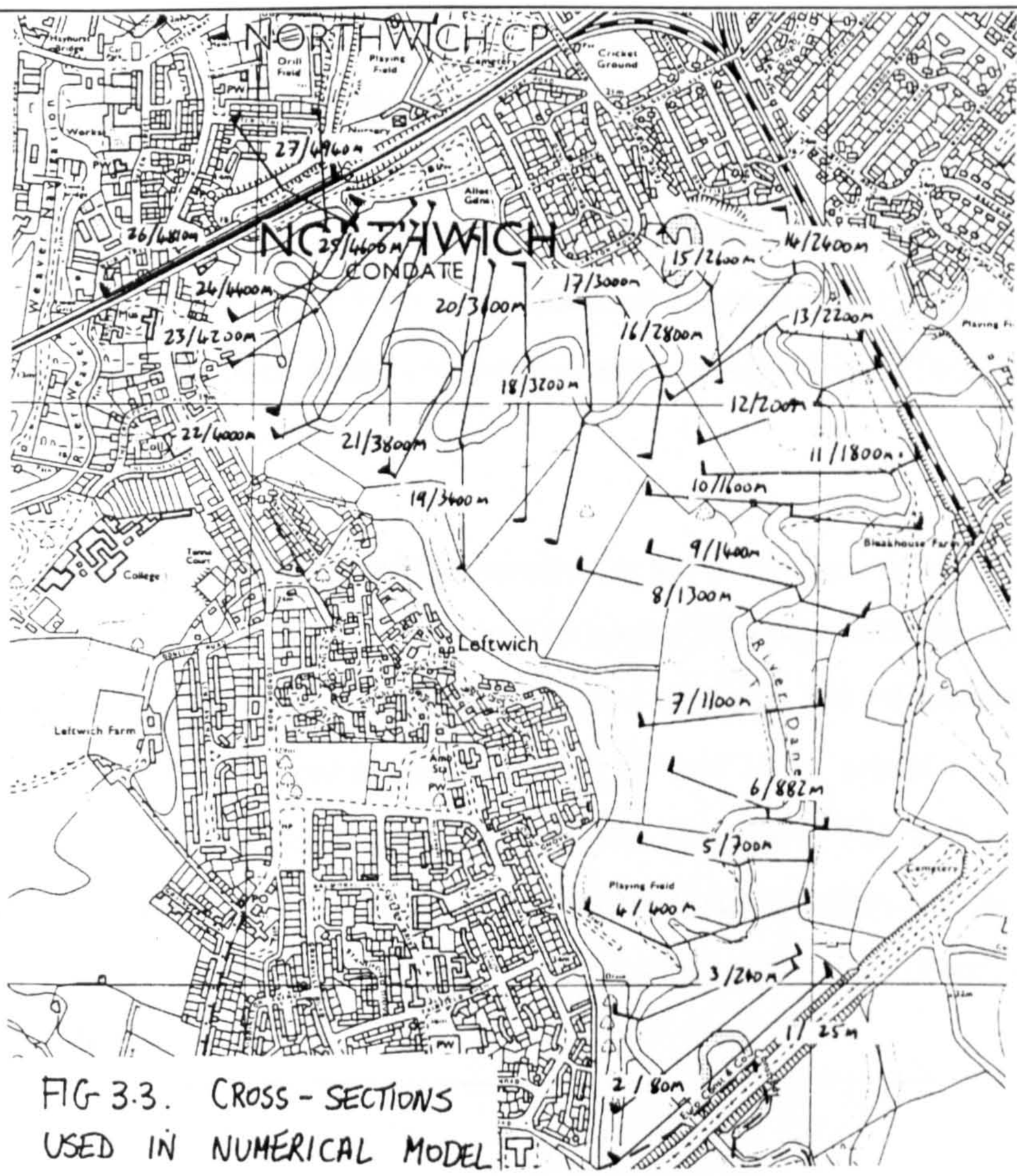

Figure 7.10 Cross-sections for River Dane model

7.10 Calibration of the steady-state numerical model

7.10.1 Introduction

Calibration data was available for only two flood events on the River Dane, in January 1995 and in 1946. Extensive inbank flow data for stage and discharge were obtained from the records at the gauging station in Rudheath, at the upstream boundary of the River Dane site. Stage and discharge data were also obtained for flood events. The downstream levels at the road bridge which marks the confluence between the River Dane and the River Weaver were measured for each flood event.

The roughness coefficients for the main channel and the flood plains had to be determined for input to the model. The tables compiled by Chow [1959] were used to determine the roughness coefficients in terms of Manning's n. Chow's tables specify a

number of categories which correspond to geomorphology and vegetation along the River Dane corridor. An assessment of the River Dane corridor was performed on the 19th of December 1995. Figure 7.11 shows a view of the typical corridor configuration observed on that day. It was noted that the main channel was predominantly clean, winding (with some pools and riffles) and possessed moderate vegetation and shallow slopes at downsteam sections along the reach under consideration. There was a lot of aquatic vegetable matter present.

A study of the river corridor in early 1996 resulted in the author accepting the Manning's n value to be in the range of 0.04 to 0.05 and an earlier estimate of 0.048 was accepted meantime and corroborated using the tables produced by Chow [1959]. Ordnance survey maps dating back over 104 years were collated for the Dane corridor. These maps indicated that the land use has barely changed over the years. The author concluded therefore that this estimate for Manning's n was probably representative of the roughness characteristics which prevailed during the two flood events for which there was reliable flow data, in 1946 and 1995.

Figure 7.11 A typical view of the River Dane and surrounding area

7.10.2 Calibration against the January 1995 flood

The most recent flood data available was obtained by the NRA during the January 1995 flood. The flood peak at Rudheath was estimated to be 107.64 m^3/s and the flood level

was measured at 16.66m AOD. The corresponding confluence level at the Weaver was 10.7m AOD. The resulting flood levels for the January 95 flood along the reach are shown in Figure 7.12. The Rudheath flood level was predicted to be 16.85m AOD which compares reasonably with the 16.66m measured on site.

7.10.3 Calibration against the 1946 flood

The downstream confluence level was approximately 13.5m AOD during the peak of the 1946 event, and the flood discharge rate was estimated to be around 170 m^3/s in the Dane. The Glasgow numerical model was used to simulate this flood event. The predicted flood levels are shown in Figure 7.12 together with both the bank-full levels along the river reach and the measured flooding upstream water levels at Rudheath. It is of interest to note that the Glasgow model predicts an upstream flood level of 17.37m AOD at A556, whereas 17.53m was measured. The models predictions for the 1946 flood once again compares well.

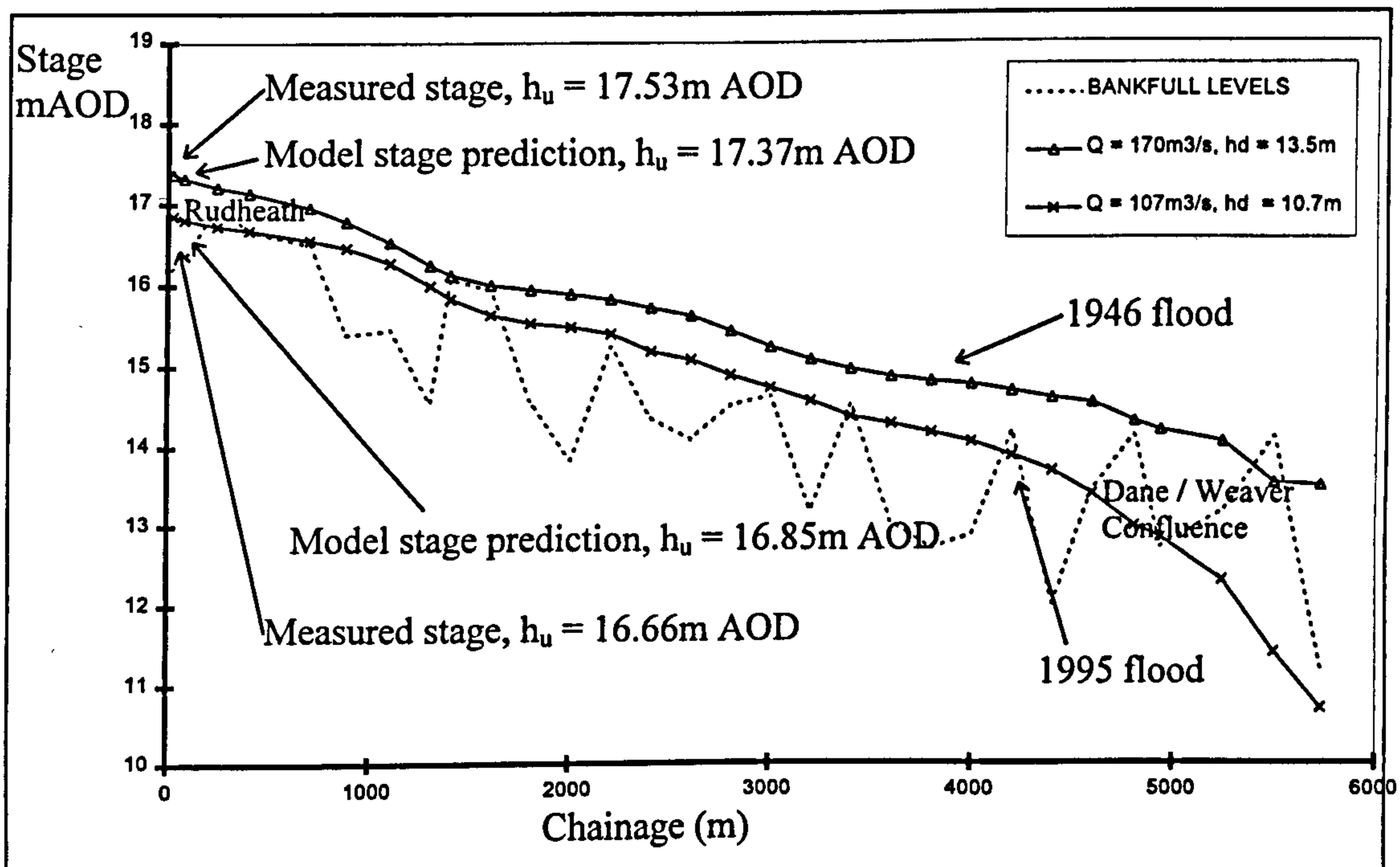

Figure 7.12 Calibrating the steady state model against 1946 and 1995 flood events

7.10.4 Comparison between the Glasgow model and MIKE II

MIKE 11 is an international standard hydraulic model and has a good reputation for handling flood plain flows using a river network analysis. It does not, however,

incorporate latest research findings on river/flood plain interaction which produces energy loss above normal bed friction.

It was decided to compare Mike 11 and the Glasgow model on one graph for the 1 in 100 year estimated flood of 161.3 m^3/s. The results are shown in Figure 7.13. The Glasgow model predicts similar water levels over much of the reach. At Rudheath gauging station Mike II predicts a 17.38m flood level and the Glasgow model a 17.31m AOD. The novel 1D model included an explicit allowance for head losses generated by the main channel and flood plain interaction whereas the MIKE11 model will have incorporated lumped coefficients to allow for this additional source of head loss.

One slight divergence between the MIKE 11 and Glasgow model occurs just upstream and downstream of the railway viaduct around chainage 4600-5400m. The Glasgow model predicts slightly higher water levels.

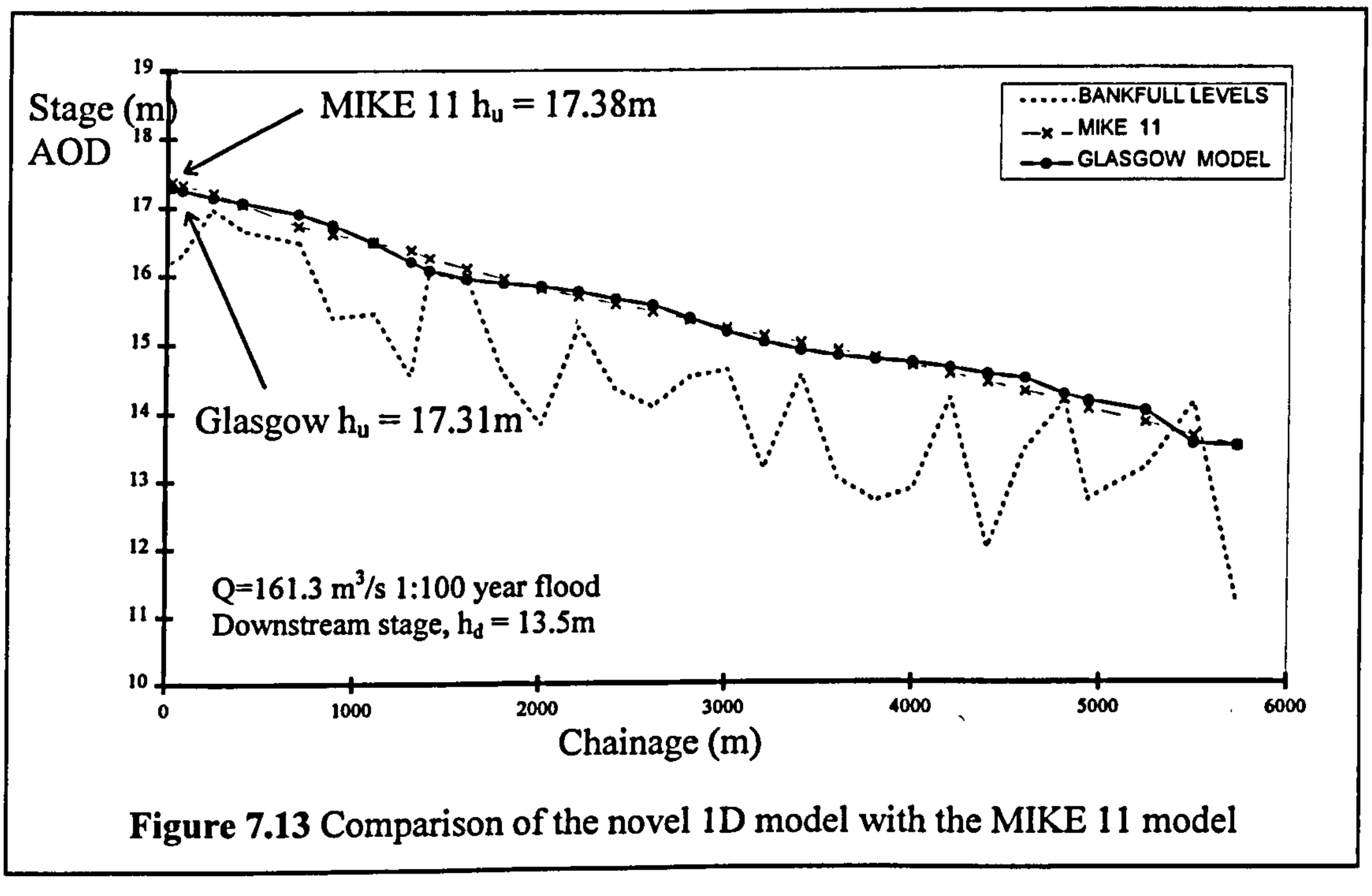

Figure 7.13 Comparison of the novel 1D model with the MIKE 11 model

7.10.5 Conclusions

There was an encouraging similarity between the predicted and the measured water surface levels for the River Dane calibration data. However because of the notorious difficulties associated with assigning Manning's n values and taking field measurements

for water level and discharge capacity, further validation of the model must be performed before a comprehensive appraisal of its accuracy can be delivered which is essential if the model is to be developed further for commercial purposes. In the interim the author concludes that the novel 1D model is reliable enough to pursue the conceptual design of compound channel flood protection schemes for the River Dane.

7.11 Design of a flood protection scheme

7.11.1 The influence of flood plain width

An important choice in the design of a distant flood bank flood protection scheme for the Dane concerns the new width of the flood plain, or the distance apart of the distant flood banks. It was decided to investigate three options. The trial flood banks were positioned at offsets 50m, 30m or 10m outside each bend apex, and an appropriate 1D model was developed. Figure 7.14 shows a sketch of the flood banks offset by 30m. It was important for each option to be compared with the natural flood event i.e. no flood banks. The purpose therefore was to investigate any increases in water level and also the loss of temporary storage on the flood plain.

The case of the 1 in 100 year flood with a natural Manning's n equal to 0.048 and a downstream water level equal to 13.5m is shown in Figure 7.15 for the 10m, 30m, 50m offset and also for no flood banks (the existing configuration).

The water levels along the whole reach follow similar patterns for various compound channel configurations. Consequently plots showing the variation in water level at Rudheath were used to give a clear indication of the exact effect of configuration changes. Figure 7.16 shows the effects of varying the distance between flood banks for differing values of flood plain roughness.

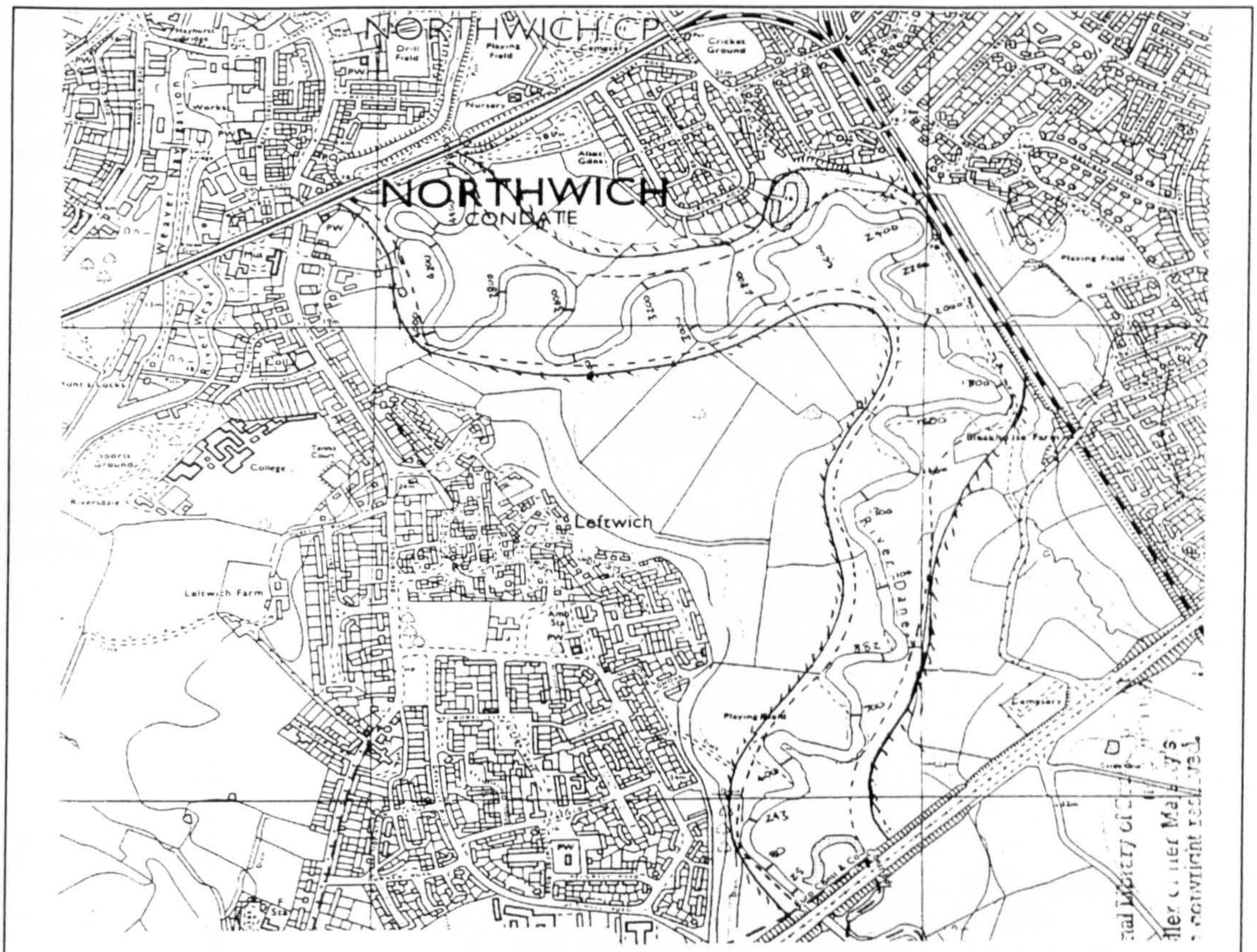

Figure 7.14 Plan view of the proposed scheme (Flood banks offset by 30m)

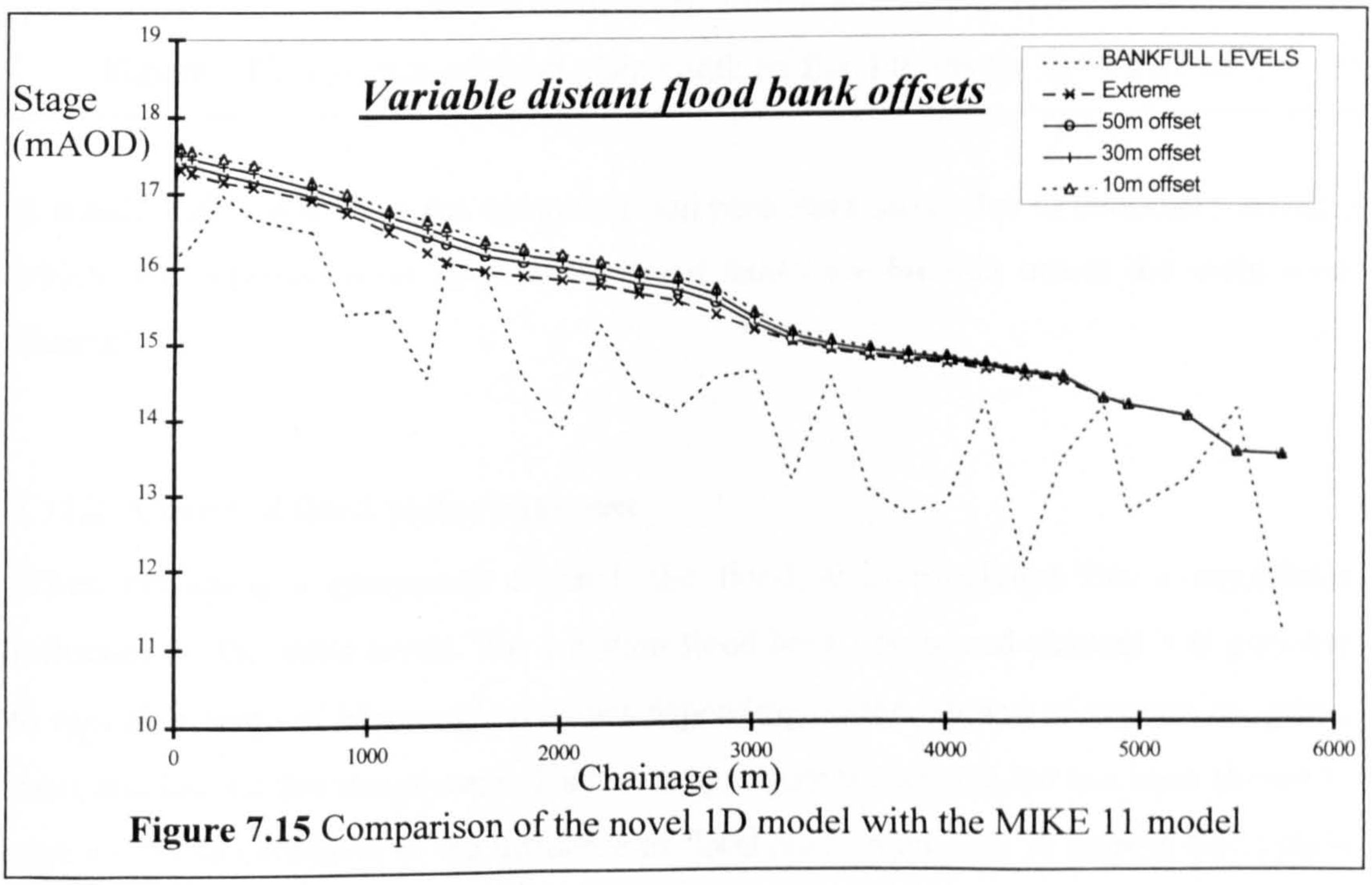

Figure 7.15 Comparison of the novel 1D model with the MIKE 11 model

Figure 7.14 demonstrates that the river flood levels rise as the flood banks are brought closer to the river. 30m distant flood banks give a rise of 0.2m to 0.25m above the natural flood level of 17.31m AOD.

Figure 7.16 demonstrates that for the case of a smooth flood plain n = 0.03 the flood levels can be reduced from the present natural flood level of 17.31m AOD, for all three distant flood bank solutions 10, 30, and 50m.

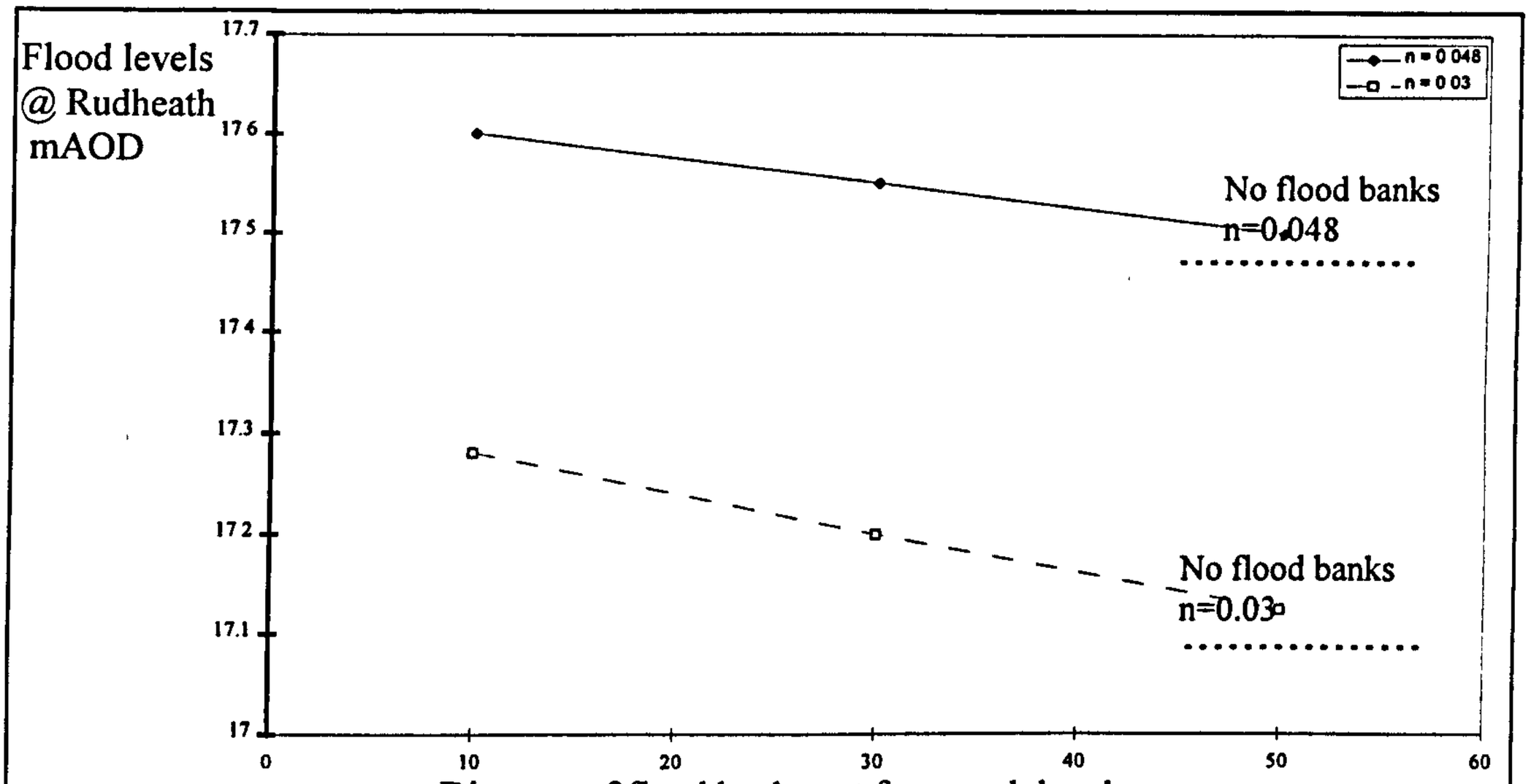

Figure 7.16 Influence of flood plain width on flood levels for Q = 161.3 m^3/s

A steady state model does not compute flood peak attenuation due to temporary storage, which may alleviate level rises as the flood banks are brought nearer the main river channel.

7.11.2 Choice of flood plain roughness

When designing a compound channel, the flood plain roughness has a significant influence on the water levels. For a distant flood bank compound channel it is possible to specify a range of Manning's n values depending on the amount of vegetation, grass, trees and hedges that are present. This is an approximate science but has been shown to give a reliable indication of the influence of flood plain roughness. A smooth flood plain with cut grass and cycle paths may have an n value as low as 0.03. A rougher flood plain with some trees, some bushes, etc. may have a Manning's n value around 0.06.

It was decided therefore to investigate the influence of roughness (or amount of vegetation on the flood plain) on the flood levels. The flood level at Rudheath is again taken as a representative cross section, for the 1 in 100 year flood and a confluence water level 13.5m AOD. Figure 7.17 shows the sensitivity of the existing natural channel to variations of flood plain roughness from n = 0.03 to n = 0.06

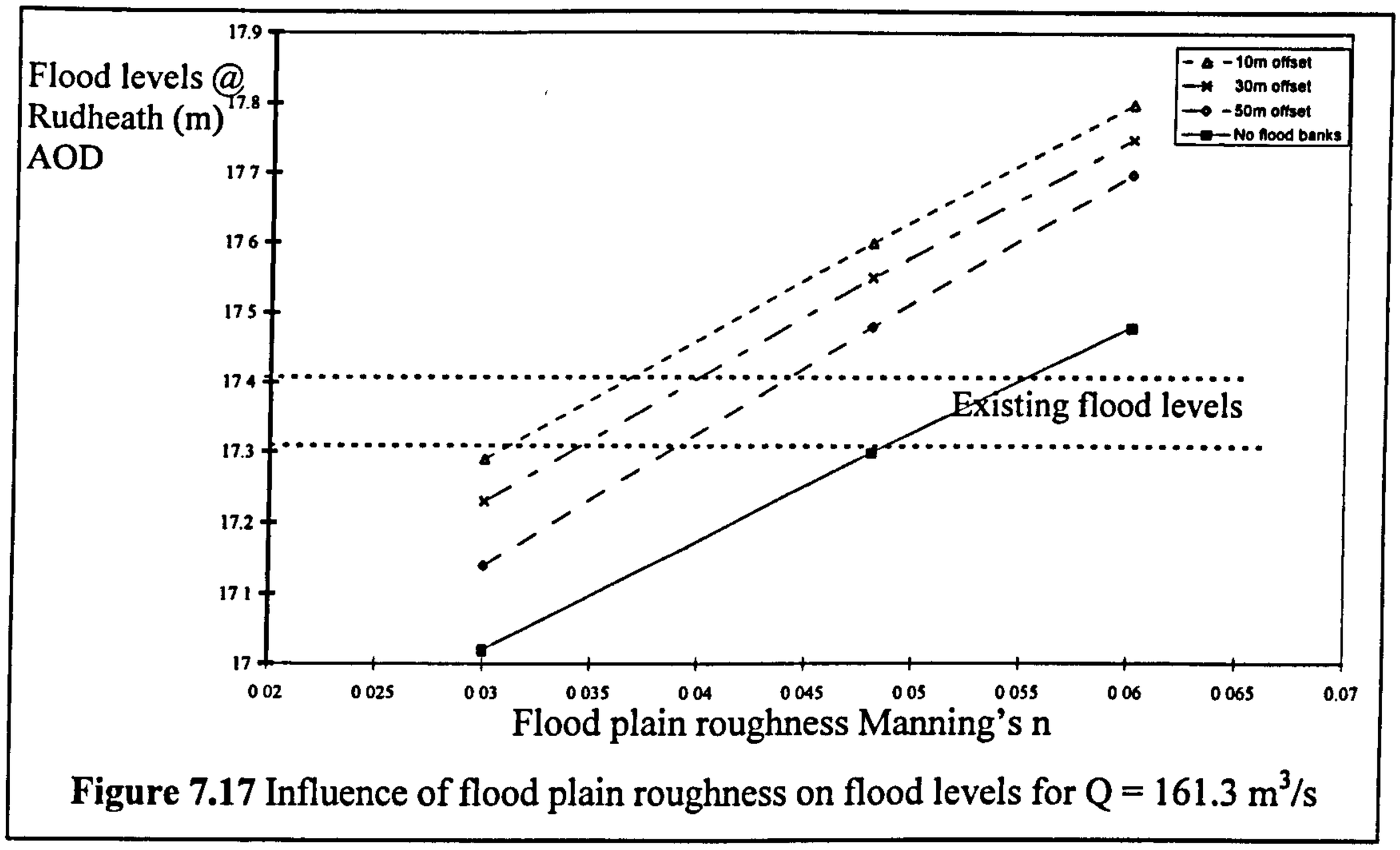

Figure 7.17 Influence of flood plain roughness on flood levels for Q = 161.3 m^3/s

Flood levels increase almost linearly with flood plain roughness. A heavily vegetated flood plain would give flood levels between 0.2 to 0.4m above the existing natural case. A "smooth" flood plain can reduce flooding levels as low as 17.1m AOD which is well below current flood levels. It is not advisable to rely on smooth flood plains to reduce flood levels because of the high level of maintenance required to keep them in the same state. There are many factors which can result in required level of maintenance not being achieved in the long term. It is wise to incorporate additional provisions to cater for any change in level of flood plain vegetation such as increasing the capacity of the flood plains by reducing their level.

The implication here is to opt for "smooth" flood plains to reduce water levels and reduce the amount of temporary storage to be provided elsewhere. This may be less environmentally acceptable.

7.11.3 Reducing the flood plain level

Some two-stage channels (special versions of compound channels) have been used in a number of flood alleviation schemes. The flood plain levels are lowered, a 'slice' is taken off, thus increasing the temporary storage on the flood plains. Examples of these schemes in the UK include the River Ray (Oxfordshire) as shown in Figure 7.18, the River Roding (Essex) and the River Blackwater (Hampshire).

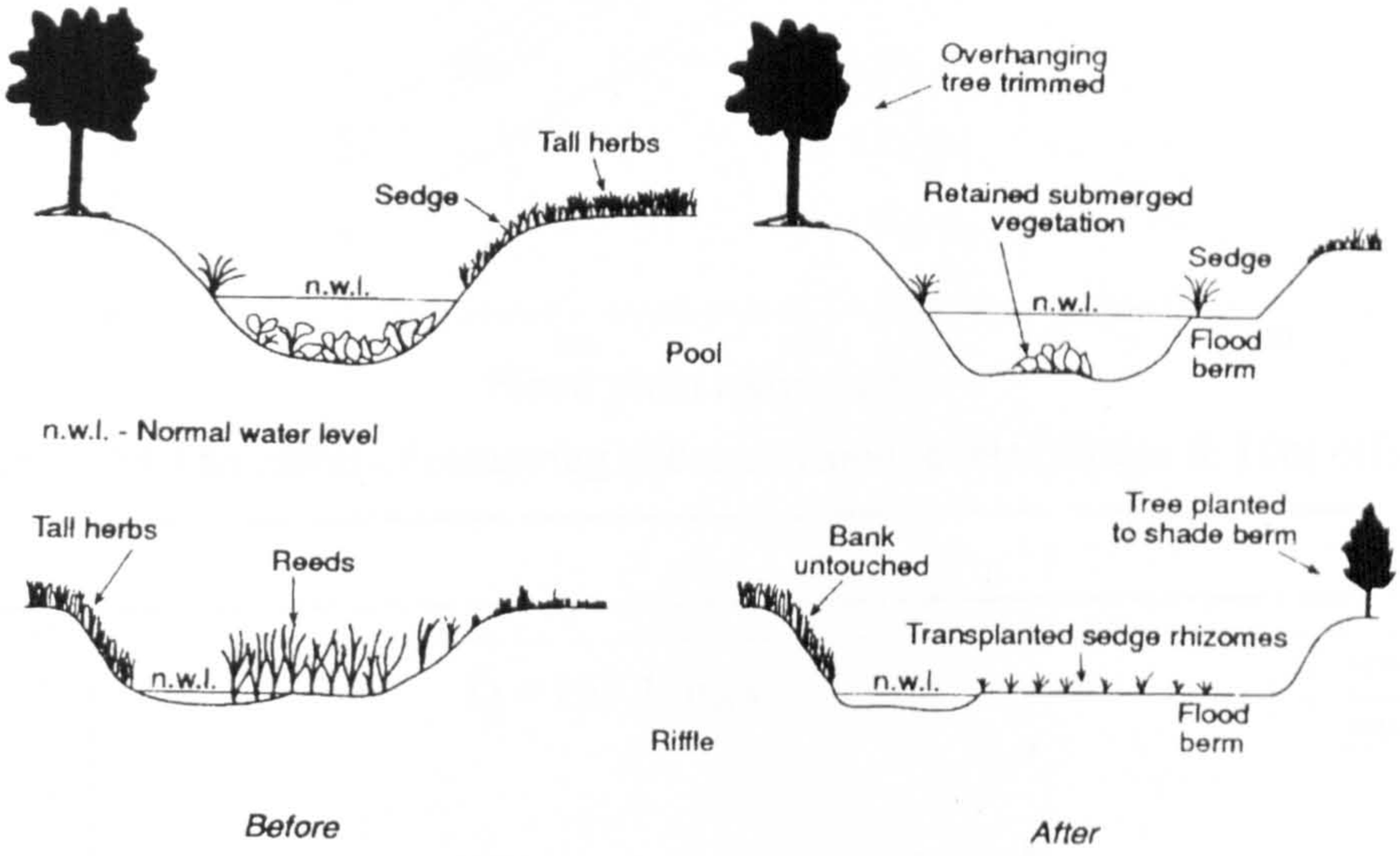

Figure 7.18 River Ray in Oxfordshire (after Brookes [1995])

The procedure is documented in Sellin, Giles and van Beeston [1990]. The 'new' flood plain can be re-grassed, or reeds can be encouraged, as well as a range of other vegetation types. The earth removed may be suitable for the creation of flood banks. Additional storage is also generated (albeit at a lower level) to attenuate peak discharges.

It was decided to investigate the influence of lower flood plain levels for a range of flood plain widths and flood plain roughness values. Modest amounts of flood plain were removed, namely a 0.1m slice and a 0.2m slice. The effect of removing the slices on water levels at Rudheath for the 50m and 10m offset flood banks are shown in Figure 7.19. The results for 30m offset flood banks are shown in Figure 7.20.

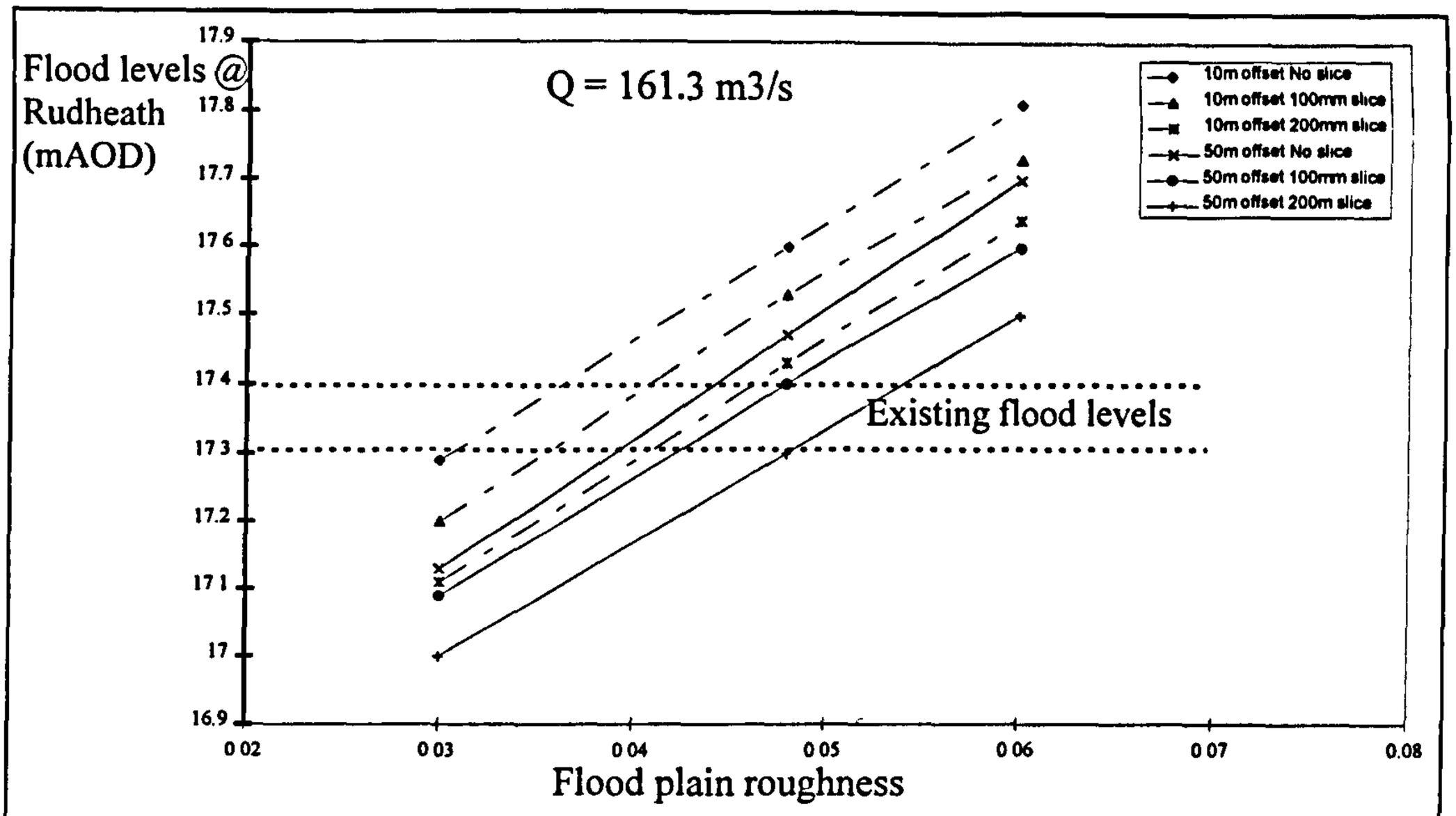

Figure 7.19 The effect of removing slices on flood levels (50mm & 10m offset)

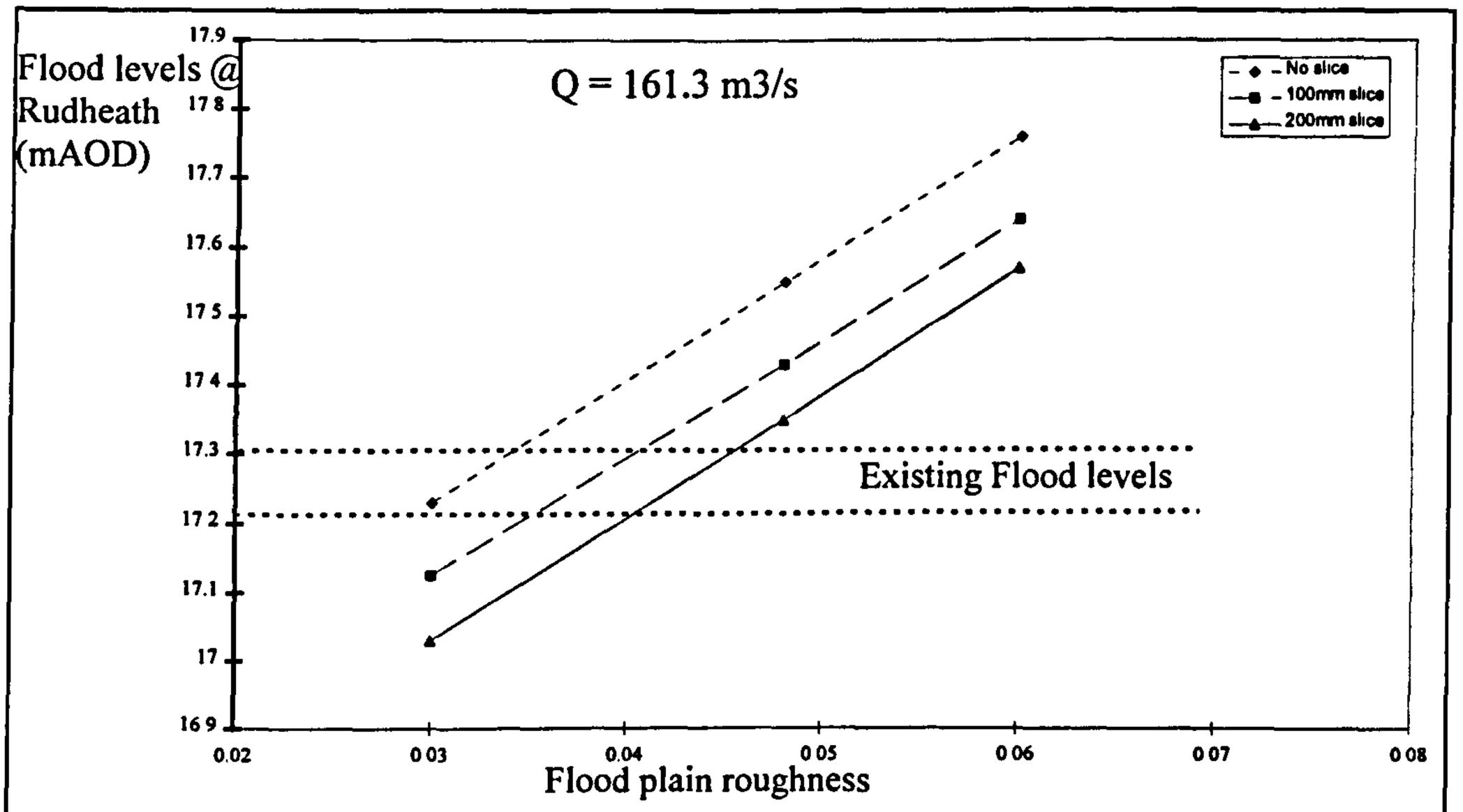

Figure 7.20 The effect of removing slices on flood levels (30m offset)

There is a distinct reduction in flood level as each 0.1m slice is removed. The following general observations can be made:-

- A 200 mm slice from the flood plain reduces flood levels by approximately 0.15-0.2m. A 100 mm slice reduces flood levels by 80-90 mm.
- Existing flood levels (17.35m approx.) can be achieved with a roughened flood plain (n=0.06) for a slice around 300-400mm.

- Reduced flood levels (17.0-17.1m) can be achieved by a combination of a smoother flood plain and a modest slice (200 mm) from the flood plain level.

7.11.4 Volumes of flood compensation

A consequence of the NRA Flood Protection Strategy (1993) is the requirement to compensate (at the same water surface level) for any flood storage lost on flood plains by an equal volume of flood water storage elsewhere. Analysis of such flood storage loss due to development on the flood plain is best carried out following unsteady flow analysis when attenuation is also taken into account. Reasonable estimates can however be obtained by steady state analysis, albeit at a 1 in 100 year flood of 161.3 m^3/s.

Figure 7.21 shows a sketch illustrating the extent of natural flooding and consequently the area of flood plain cut-off by the provision of protective flood banks.

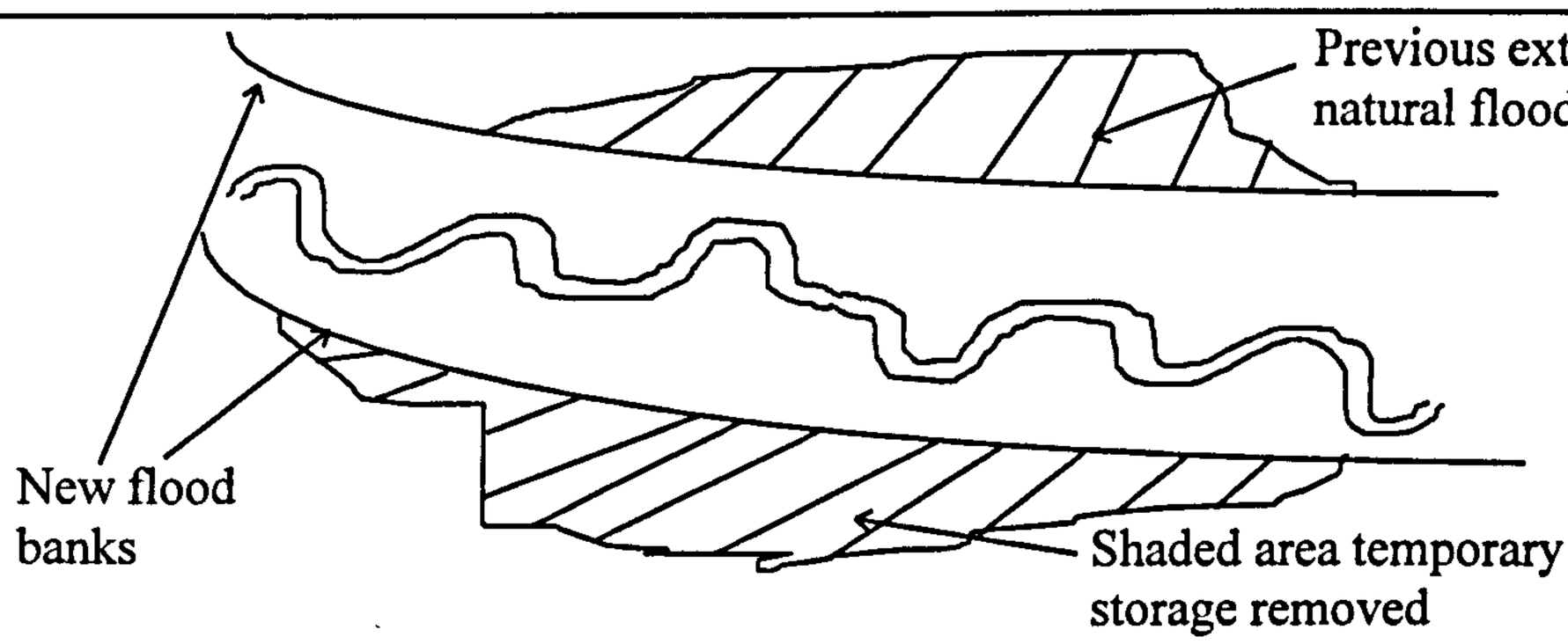

Figure 7.21 Area for temporary flood storage that is lost

Calculations were performed to determine the loss of storage volume along the whole reach for the 1 in 100 year flood with various values assumed for channel roughness, flood bank offset and flood plain 'slice' removal. Table 7.1 shows the values for storage volume (m^3) lost for a channel roughness equal to n=0.047. For the existing natural case of a 1 in 100 year flood with a Manning's n value equal to 0.048 for both channel and flood plain the total storage volume is equal to 1.68×10^6 m^3.

	Depth of flood plain 'slice'		
Flood bank offset	0mm	100m	200mm
50m	175000 m^3	147000 m^3	120000 m^3
30	207000 m^3	183000 m^3	157000 m^3
10	257000 m^3	228000 m^3	206000 m^3

Table 7.1 Lost temporary flood plain storage ($n_f = n_c = 0.048$; $Q = 161.3\ m^3/s$)

When compared with the total volume for the 30m distant flood bank case at the same discharge and roughness values the total storage volume is equal to $1.48 \times 10^6\ m^3$. The volume loss on the flood plain is approximately 200,000 m^3, which should be replaced at a different location along the Dane.

The replacement could be in the form of a temporary storage basin, located possibly upstream of the A556 bridge. Another possibility would be a temporary flood storage basin downstream of the A556 in a designated area of land not used for building purposes. An easier solution might be "slices" from the flood plain itself. Removing a 200mm from the flood plain in the 30m offset option restores 25% of the lost storage volume. This is a significant amount and is well worth consideration.

Unfortunately there are drawbacks associated with excavating the flood plains. Their environmental integrity will be significantly affected although the main channel itself would be largely unaffected. If the EA could be persuaded that the environmental limitations were not insurmountable then a combination of a storage basin and the excavation of the flood plain might be employed to replace the lost storage volume. The EA might be persuaded if the planners could suggest a way in which the environmental diversity of the flood plain could be restored.

The author considered the option of re-planting and re-populating the flood plain areas along with the flood banks and the possibility of turning the whole area into a linear park. Alternatively the flood banks could be placed further apart and the flood plains if carefully managed could be designed to possess lower frictional resistance. Both these alterations would significantly reduce the amount of flood storage volume that is lost.

The author studied the impact that the various flood plain configuration options would have. This was reported in the context of assessing the impact of variations in flood plain roughness, flood bank width and flood plain excavation which were reported in the previous sections. Before a finalised design could be developed various channel combinations would have to be presented to the EA with the idea of negotiating with them to identify the optimal configuration in terms of all their assessment criteria.

7.12 Application of an unsteady state numerical model

7.12.1 Introduction

River flows are usually unsteady, with discharge, Q, and stage, h, varying with time. The steady state model in the previous section was permissible because it assumed the highest peak flow to be acting everywhere along a short river reach. However this was a conservative approach. Unsteady models of the various flood protection options were developed to obtain further valuable information relating to temporary storage effects. In the Dane for instance, temporary storage on the flood plain will reduce or attenuate the upstream flood peak slightly. When flood banks are used there is a slight reduction in temporary storage and hence the flood peak will reduce less than the natural case. This is the purpose and rationale for the EA compensation storage criterion. One way of demonstrating to the EA that there is adequate storage still provided by the flood plain is to prove that the hydrograph peak that reaches Northwich town centre is not higher than before the distant flood banks were built.

7.12.2 The inflow hydrograph

An unsteady numerical model can be used for flood routing provided boundary conditions are known upstream and downstream, as well as detailed cross-sections throughout the river and flood plain. The upstream boundary condition should be in the form of a flood hydrograph with the peak flow corresponding to the 1 in 100 year criterion suggested by the NRA. This is an estimated value of 161.3 m^3/s. Fortunately in the case of the River Dane, there exists a gauging station (Rudheath) at the upstream end of the reach under consideration. Data was made available (from NRA) regarding a

flood hydrograph at Rudheath in January 1995, where the peak flow was estimated to be 107.6 m^3/s. This is shown in Figure 7.22.

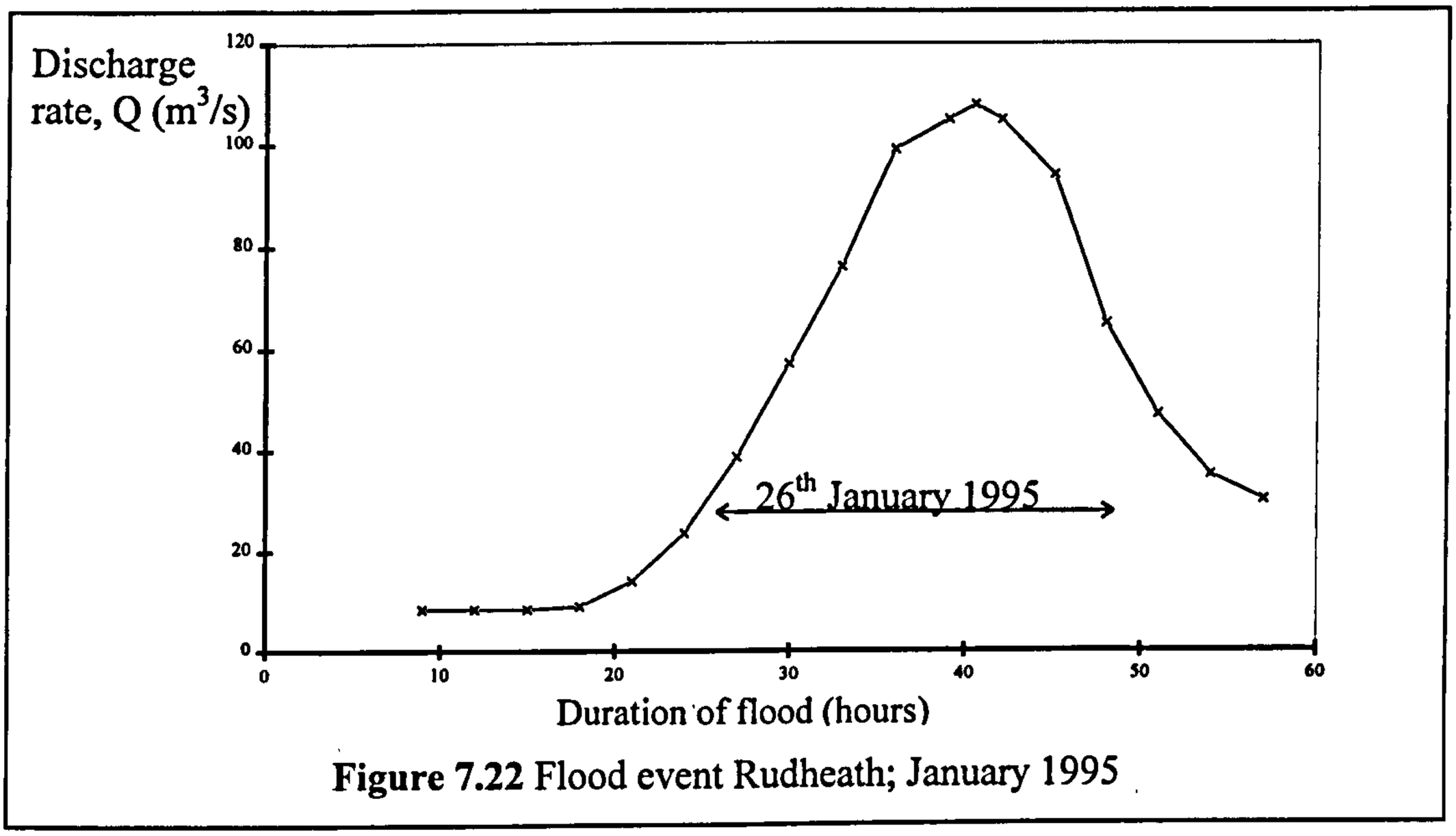

Figure 7.22 Flood event Rudheath; January 1995

Figure 7.22 demonstrates a time base for the entire hydrograph of around 36-40 hours, taking approximately 18 hours to reach the peak flow following commencement. Data was also provided (by NRA) of the 1946 flood at Northwich with an estimated flood of 170 m^3/s. In this case the total hydrograph time base was around 48 hours, with 24 hours to reach the peak. The hydrograph in both cases is reasonably symmetrical.

A reasonable assumption for the 1 in 100 year flood hydrograph would be a peak flow of 161.3 m^3/s with a time base of 36-48 hours. The worst case would be the shorter time base of 36 hours. The result is shown in Figure 7.23, with a symmetrical up-leg and down-leg to the hydrograph.

Ideally the downstream boundary condition should be a rating curve for the Dane-Weaver confluence. This has not be available to the author. Instead, the worst ever measured confluence depth of 13.5m AOD was adopted.

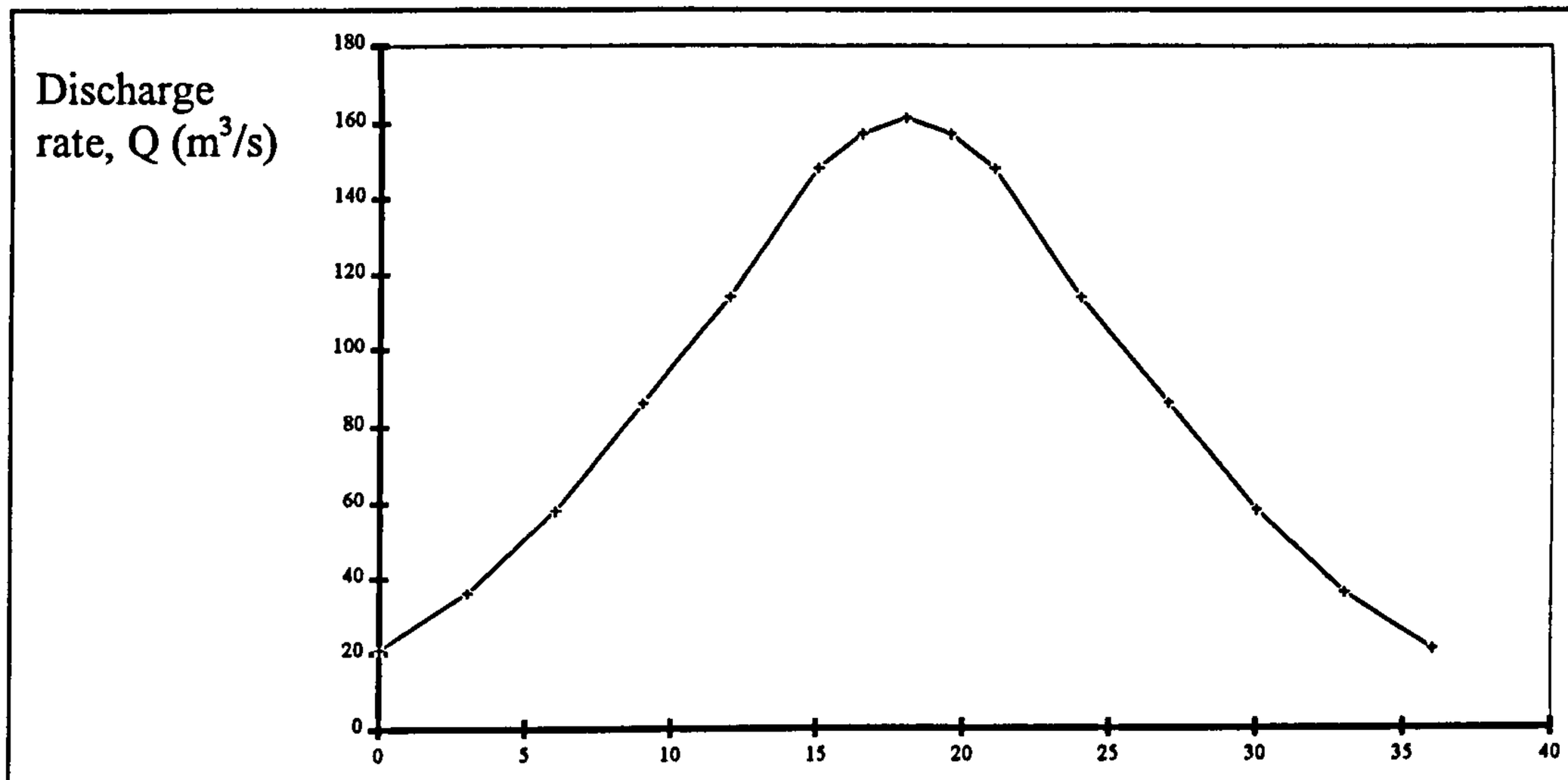

Figure 7.23 Synthetic flood hydrograph for Rudheath 1in 100 year flood

7.12.3 Calibration and Results from the unsteady model

The Glasgow unsteady model was compared with MIKE 11 for the natural channel with n = 0.048 for both the main channel and flood plain. The results are almost identical as shown in Figure 7.24.

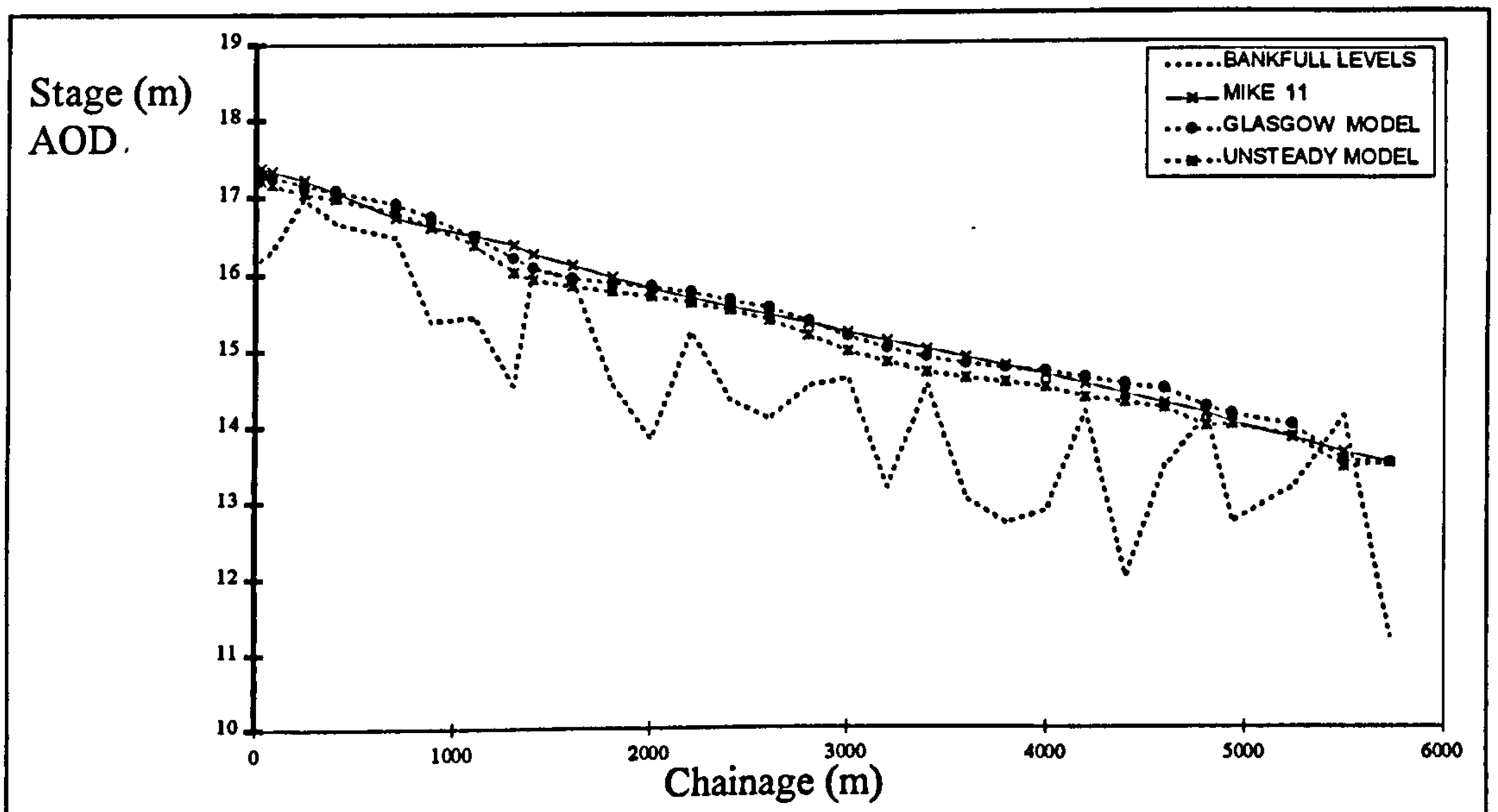

Figure 7.24 Comparison of the novel 1D model with the MIKE 11 model

Figure 7.24 demonstrates that the results from the unsteady model are reliable. The attenuation of the flood peak (as it creates temporary storage on the flood plain) is

shown in Figure 7.25. A reduction in discharge of 3.6 m^3/s due to temporary storage is observed as the flood wave passes from Rudheath to the railway viaduct. This is a small attenuation of the order of 2.2%.

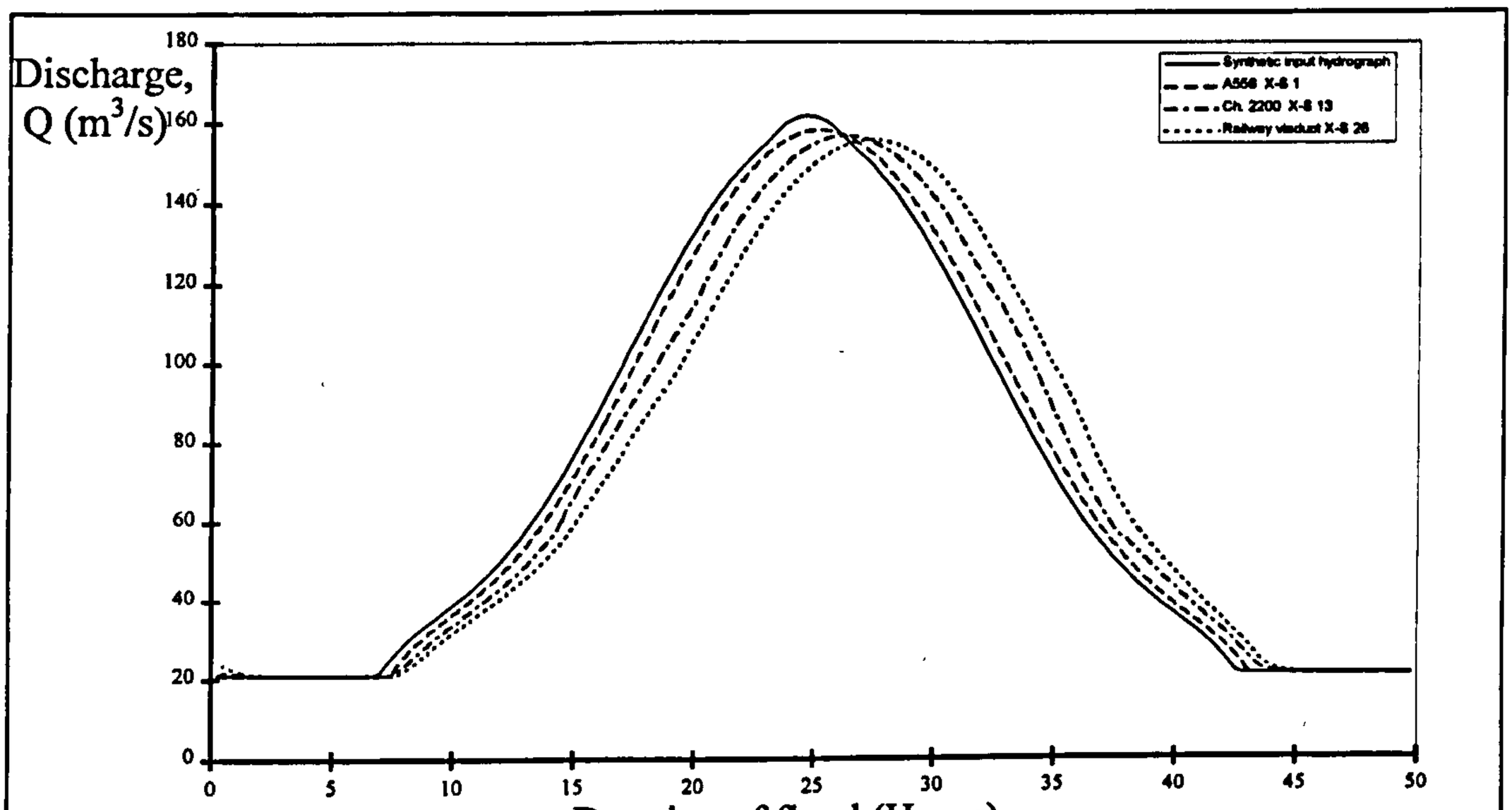

Figure 7.25 Attenuation of flood along the natural River Dane

The effect of various combinations of flood bank offset and flood plain levels at chainage 2200m is shown in Figure 7.26.

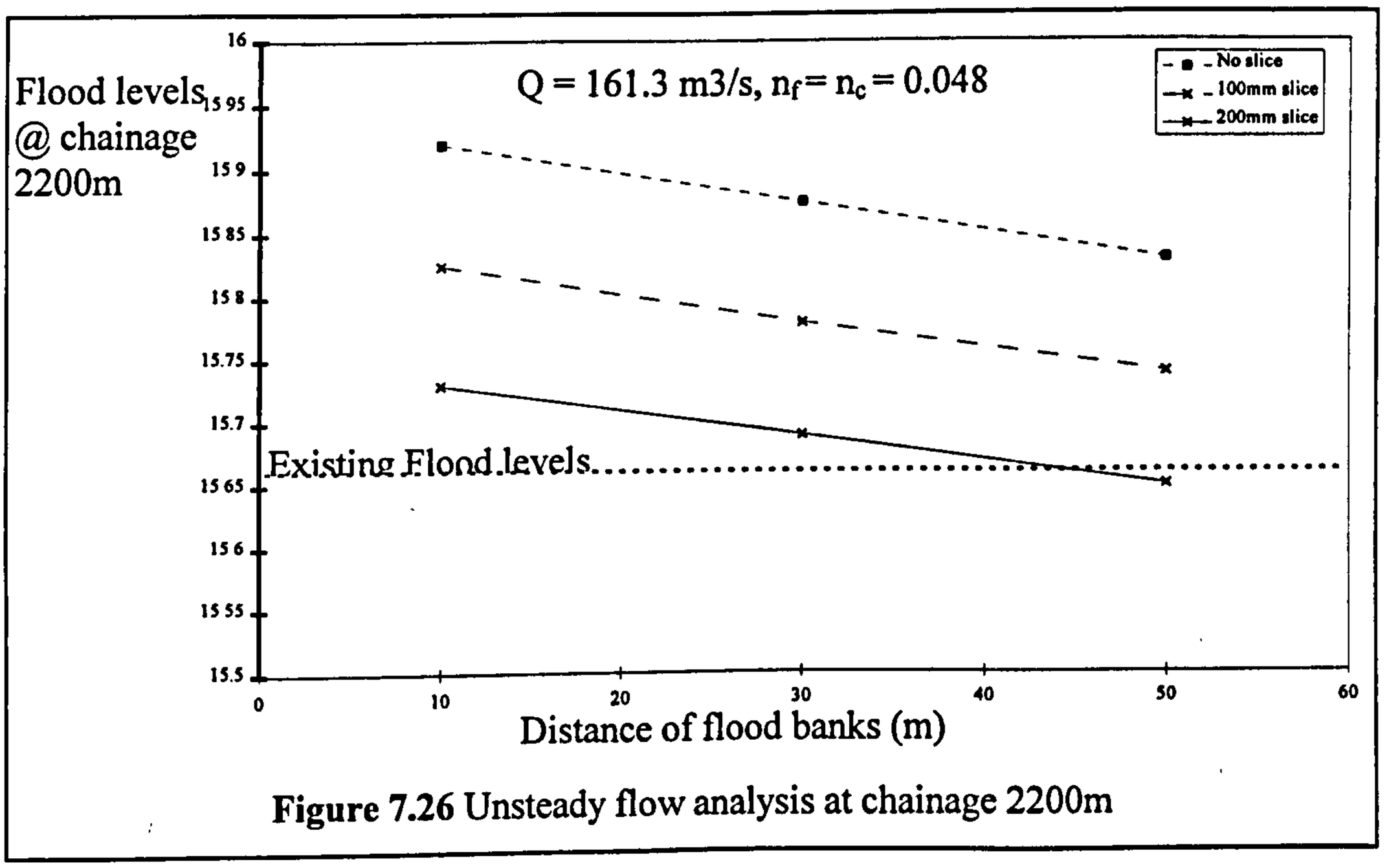

Figure 7.26 Unsteady flow analysis at chainage 2200m

The following observations were developed from the unsteady analysis which was performed for various values Manning's n on the flood plain.

- 30m distant flood banks increase flood levels by 0.2m above the natural case. this is similar to the steady state analysis which predicted 0.2 → 0.25m increase.
- 10m distant flood banks increase flood levels by 0.25m.
- Each 100mm slice removed reduces flood levels by 90mm approximately.
- Flood levels for 30m distant banks are reduced to existing levels by a slice 230 mm deep.
- Flood levels for 10m distant banks are reduced to existing levels by a slice 290 mm deep.

7.13 An idealised physical model of the River Dane

7.13.1 Introduction

The reach of the Dane involved in this study is of the order of 5 to 6 km long. The flows of interest are overbank flows where the river channel interacts with flood plain flow. A minimum Reynolds number criterion for modelling flood plain flow would suggest a minimum physical model scale of the order of 1 to 100. This required a large flume facility such as the National Flood Channel Facility at HR Wallingford which is 50m long and 10m wide and has been used extensively since 1986 Unfortunately the FCF facility was in use until the end of 1997 so that an immediate large scale physical study was not feasible.

In the short time frame involved in this study, it was decided to test a small scale model of 3 to 4 idealised meanders in order to represent two-stage channel flow at the River Dane. The final model is shown in Plate 7.27.

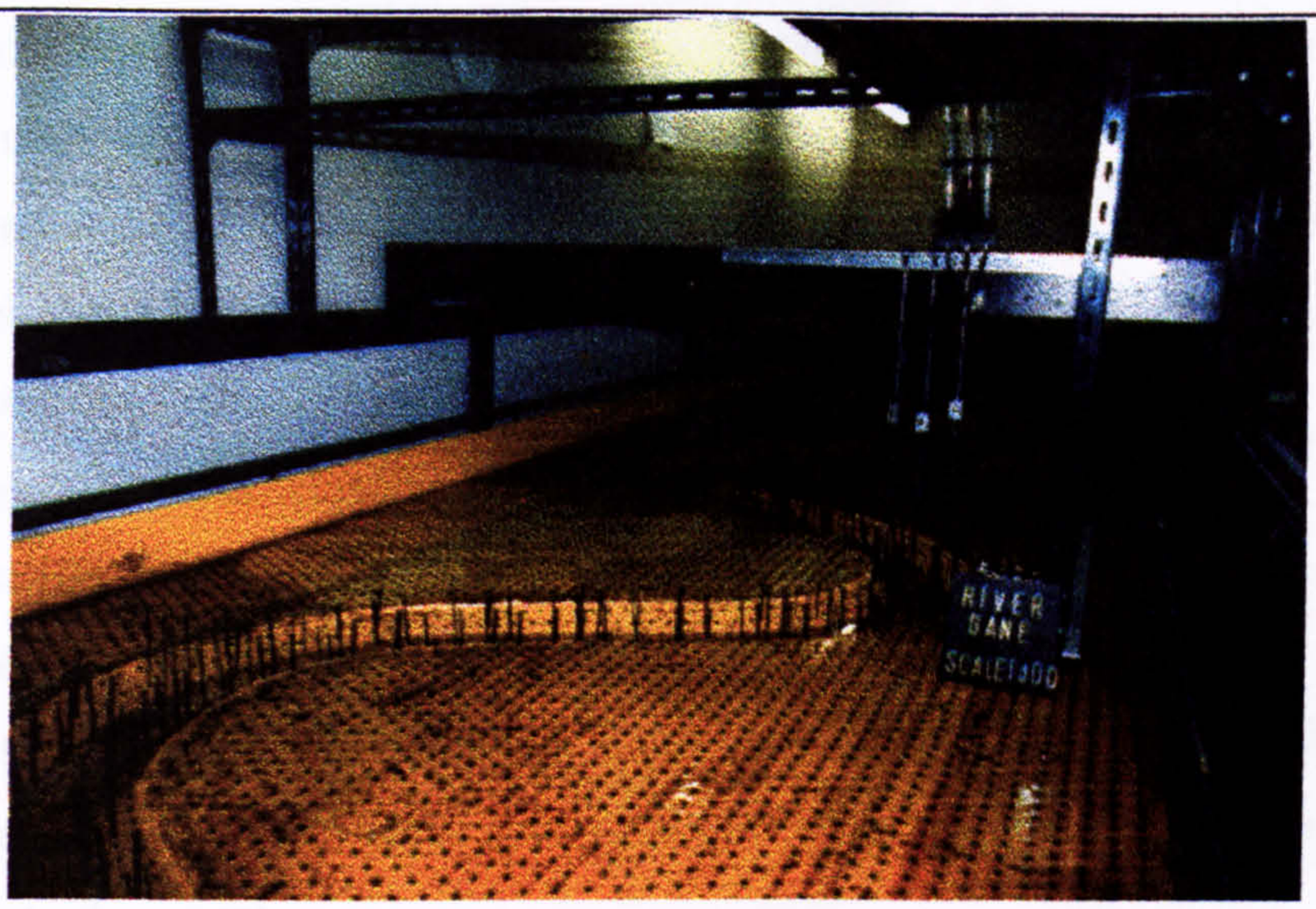

Figure 7.27 The physical model study of the idealised River Dane

7.13.2 The modelling approximations

The purpose of such an investigation is not an accurate representation of flood water levels at the Dane, but instead is a representation of the interaction (or interference) between channel and flood plain flows, for a range of parameters which typify the Dane. The following parameters from the River Dane were incorporated into the physical model:-

- The scale of the model was approximately 1 to 100, with 200 mm top width and 50mm bankfull depth in the main channel. This translates to a 20m wide river with 5m bank-full depth, which is typical of the Dane.
- The side slopes of the model main channel are 37.5° which is a close representation of the River Dane.
- Manning's n for the model's flood plain ranges between 0.0195 (at low flow depths) to 0.014 (at high flow depths). Manning's n for the model's main channel (bankfull) was measured at 0.022. The Manning's n scale ratio, n_r , is equal to $(L_R)^{1/6}$. The model built in Glasgow was approximately an idealised 1 in 100 scale reduction of the natural River Dane which meant that the length scale ratio, L_R was equal to 100. The average Manning's n for the model flood plain is equal to 0.0185 which translates to a roughness of 0.04 for the natural River Dane flood plain. The Manning's n in the main

channel of the model is equal to 0.022 which translates to a roughness of 0.048 for the natural main channel of the River Dane.

- The total width of the physical model is 1.65m, representing a 165m wide two-stage channel at the Dane. This corresponds to flood banks set back approximately 30m from each bend apex.
- The meander wave length in the physical model is 2.0m translating to a meander wavelength of 200m at the Dane. Such a dimension is difficult to measure at the Dane, although typical values appear to be upwards of 250m.
- The longitudinal slope of the model flood plain is 0.001 (1/1000). The River Dane two-stage channel flood plain slope is in the range 1/900 to 1/1300 which is close enough to the model.
- The value of sinuosity is not closely modelled in the physical model. Sinuosity is the ratio of the distance around the thalweg of the main river channel to the linear distance along the two-stage channel. The River Dane sinuosity is 1.8, compared with 1.4 in the physical model. Such a difference can be corrected using data from the EPSRC research programme which has covered sinuosities 2.04, 1.8, 1.4, and 1.1. A correction factor is now available to scale the interference from 1.4 sinuosity up to 1.7.

7.13.3 Results from the physical model

The flume used for the model was 1.65m wide, 0.3m deep and incorporated an 8m long working section, with maximum deliverable discharge rates of up to 100 litres/sec. The physical model results are compared with the results from the steady-state numerical model (with $n_f = n_c = 0.048$) by applying a discharge scale ratio, Q_r, of $100^{5/2}$. The scaled discharges from the physical model results gave fairly close correspondence to the numerical model results and therefore the measured discharges in the natural River Dane.

Differences between the scaled surface roughness in the physical model and in the natural River Dane affected the level of correspondence in hydraulic performance. Figure 7.28 compares the stage-discharge curves obtained from the scaled physical model results and the steady numerical model results. The author has already shown that the steady

numerical model predicts very accurately the stage -discharge relationship of the natural River Dane (for the two calibration tests at least).

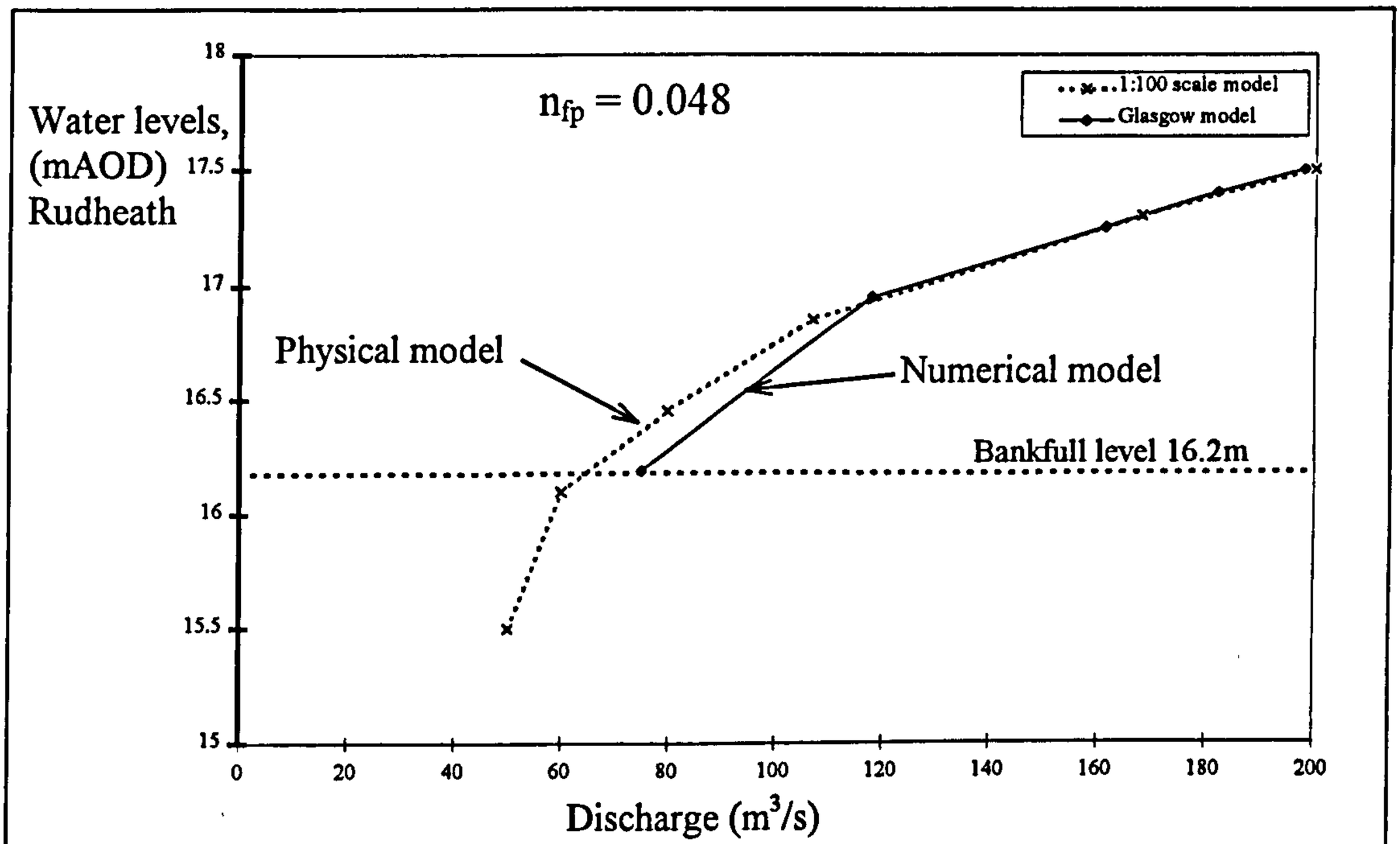

Figure 7.28 Comparison of physical and numerical model results for Rudheath

The physical model results indicate that the discharge corresponding to the level of 17.5m measured at Rudheath in the 1946 flood was around 200m^3/s. There is a discrepancy between the physical model and the natural River Dane of about 8% which is attributable to the difference in roughness and sinuosity. A difference of about 8% reduces discharge magnitude to 185m^3/s which is closer in magnitude to the 170m^3/s value estimated for the 1946 flood. When a discharge equal to 185m^3/s was included in the steady state numerical model then the flood level at Rudheath, which is predicted to be equal to 17.50mAOD which coincides almost exactly with the flood level measured on site in Rudheath in 1946 flood level, was 17.53m. Also when the discharge capacity from the scaled physical model results was determined for a flood level of 16.66mAOD, which was measured at Rudheath in January 1995, the corresponding discharge was equal to 98m^3/s rather than the reported 107 m^3/s for the gauging station on the River Dane. Allowing for the discrepancies in flood plain roughness and sinuosity the discharge magnitude is equivalent to 90 m^3/s. When 90 m^3/s was included in the steady state numerical model a level of 16.57mAOD was predicted at Rudheath. This value coincided almost exactly with the measured value of 16.66mAOD at the gauging station.

7.13.4 The magnitude of interaction losses in the River Dane model

Figure 7.29 shows a plot of relative depth versus F* for the physical model of the River Dane. F* is the ratio of actual discharge to that computed from bed friction alone. The typical four flow region features of overbank flow behaviour are clearly visible.

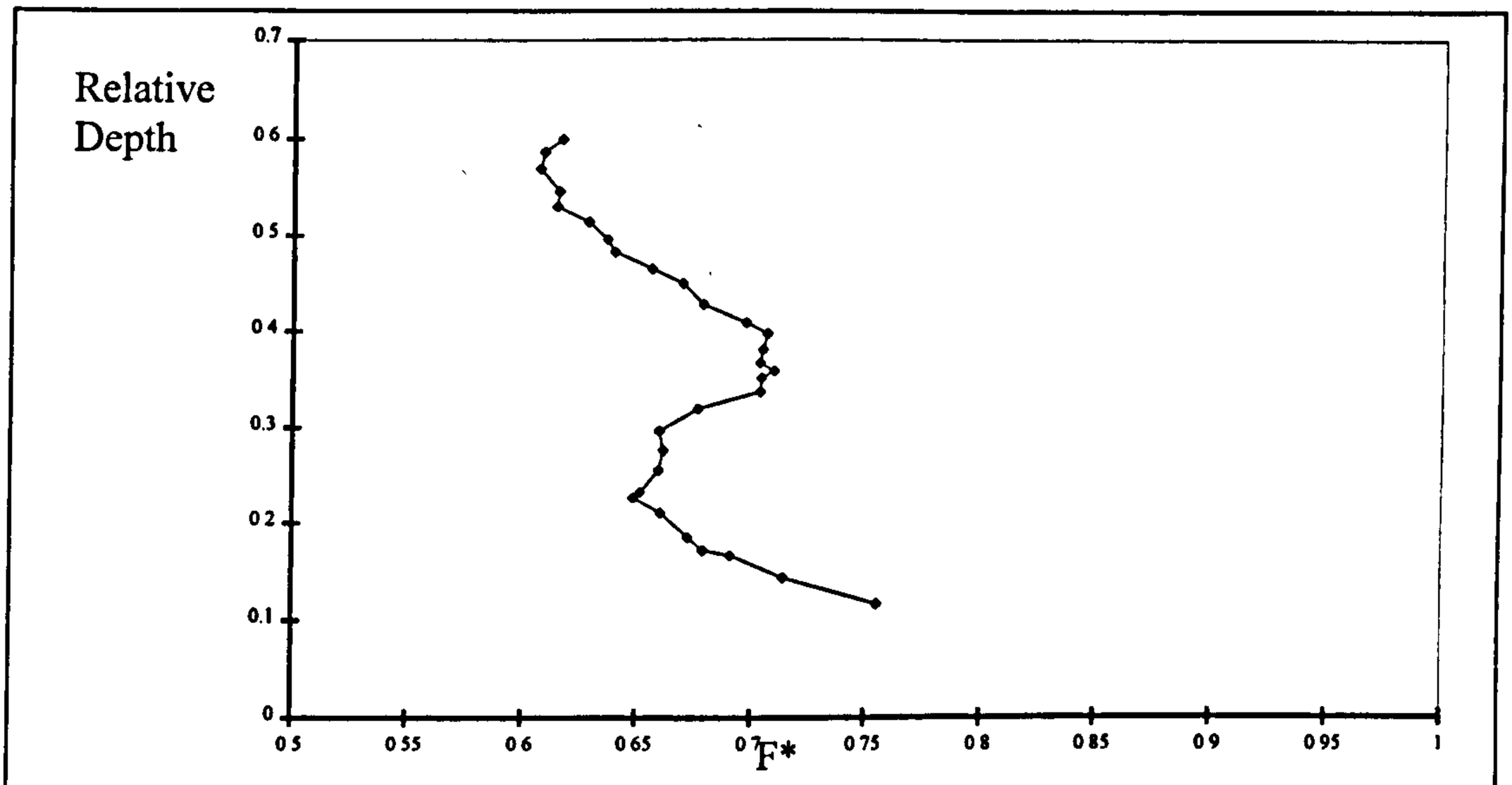

Figure 7.29 F* versus Relative Depth for the physical model

Region 1 exists for relative depths up to 0.2. Region 2 for relative depths up to 0.35. Differences in surface roughness and sinuosity will result in an overall reduction in the magnitude of F* but very little change in the distribution of the 4 flow regions.

For the River Dane Q_{100} is equal to 161.3m^3/s which corresponds to a flow depth of around 0.7m. When compared with the depth of flow in the main river, this corresponds to a typical relative depth of between 0.12 to 0.14. Figure 7.27 reveals an interference estimate for F* to be around 0.8, which is likely to be reduced by 8% to account for differences in roughness and sinuosity so F* will equal approximately 0.74. In Chapter 4 it was demonstrated that this was typical of the magnitude of F* in the meandering compound channels with very rough surfaces which were tested. Consequently the author suggests that the River Dane physical model does behave in a similar fashion to that which would be expected in the natural River Dane.

7.13.5 Flow visualisation

Figure 7.30 shows the injection of dye at a bend apex region and its progress downstream. It is clear that the river channel dominates with most dye trace following the main channel, and only a small proportion entering the flood plain.

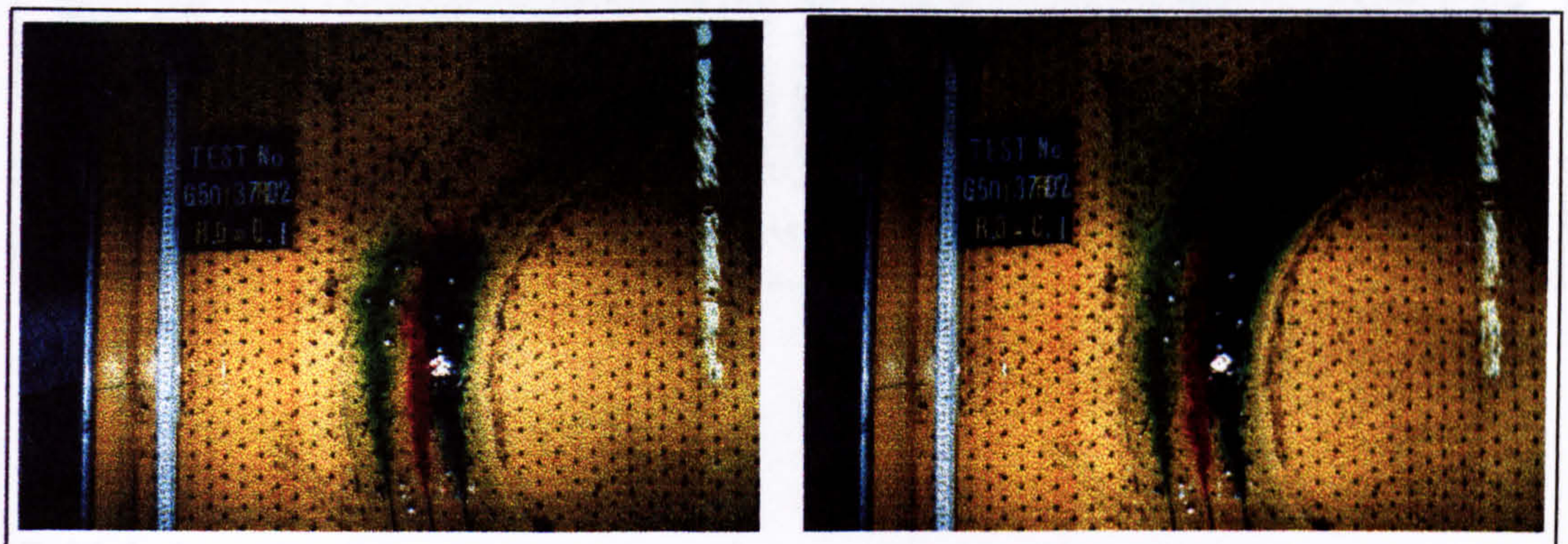

Figure 7.30 Relative depth = 0.1, Apex

This is typical of Flow region 1 behaviour and does not reveal vigorous activity downstream of the bend apex. Figure 7.31 shows dye injection in the "cross-over" region between two bends.

Figure 7.31 Relative depth = 0.1, Cross-over

The dominance of the main channel is confirmed with all flood plain flow entering the main channel, despite the main channel offering 40% more flow resistance than the flood plain. This pattern is reversed at a relative depth of 0.5, as shown in Figure 7.32, Flow region 3 behaviour is exhibited and the flow exits the main channel and enters the flood plain. This is not a realistic example however, as it corresponds to a flood plain flow depth of 5m!

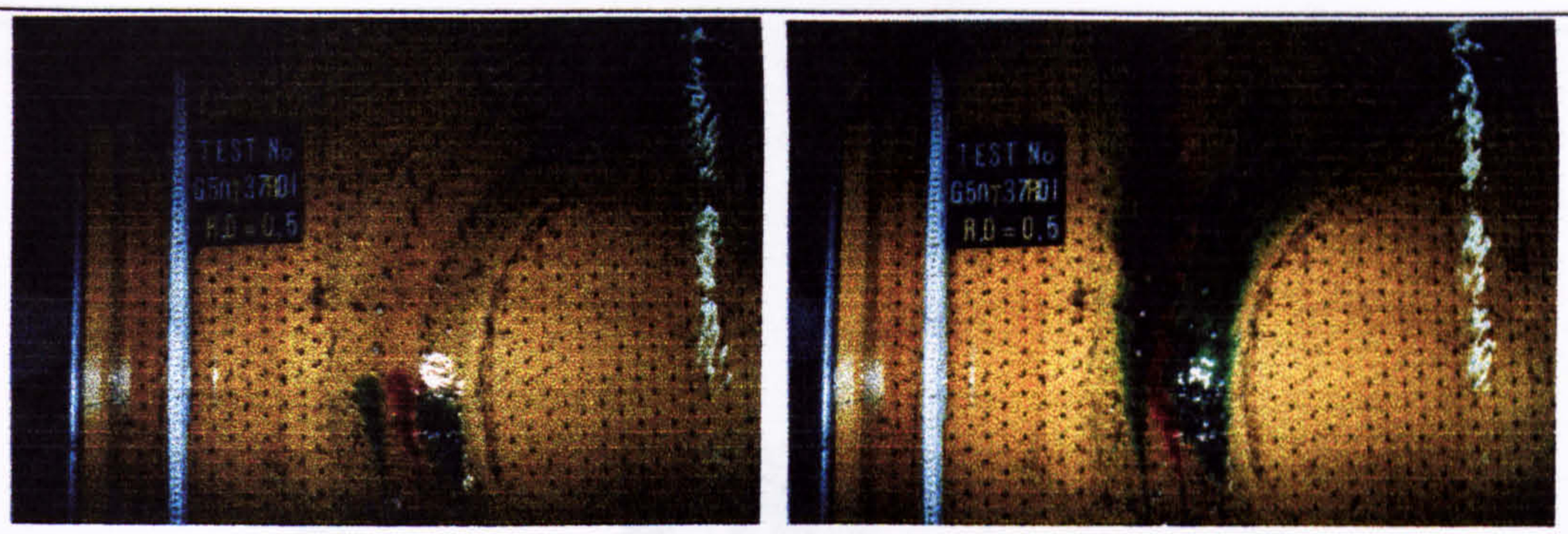

Figure 7.32 Relative depth = 0.5, Apex

7.14 Stability of the River Dane

7.14.1 Introduction

One major area of concern in any flood development plan is the stability of the river. This is particularly true when compound channels with flood banks are being considered, such as the River Dane with its distant flood banks. If the river planform meanders are unstable they could migrate towards the region of the flood banks and eventually undermine them. Consideration was given to the implementation of river bank stabilisation techniques on the River Dane to forestall this problem.

7.14.2 Dane stability near Holmes Chapel

The River Dane has been the subject of several studies concerning its stability. Classic papers by Hooke and Harvey (1983) and Hooke (1987) describe the Dane in detail. The area of study extended over a 14km reach near Holmes Chapel, Cheshire. This was several miles from the new area under investigation, but nevertheless these earlier results gave an indication of the likely stability of the River Dane near Northwich.

The River Dane at Holmes Chapel is a mobile, meandering gravel bed river mixed with sands and silts. The river top width is around 20m with mean annual flow, $\overline{Q}$, of $63m^3/s$. A typical reach is shown in Figure 7.33 revealing river planform movement from 1840 to 1984, a total of 144 years.

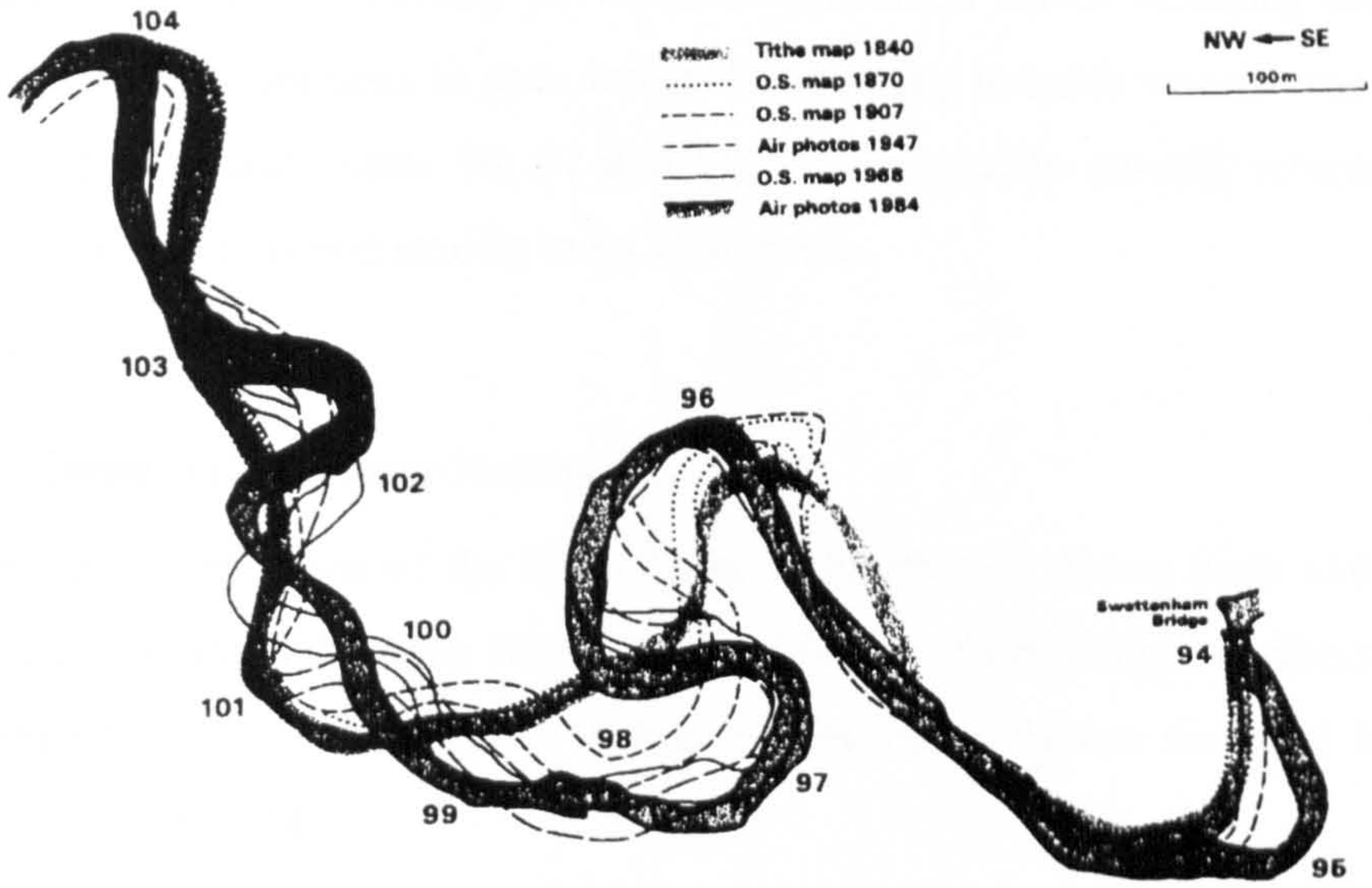

Figure 7.33 River stability near Holmes Chapel (after Hooke J M [1987])

Various observations were made by Hooke J M [1987]:-

- Changes have been characterised by down-valley migration more than lateral migration.
- The sinuosity of the 14km reach has increased by 10% on average, although the sub-reach shown in Figure 7.33 has increased by substantially more than this value.
- Upper limit rates of migration are of the order of 2 to 3 m/year, although the average maximum rates of migration are 0.24 to 0.64 m/year.
- As well as increased sinuosity, the downstream bends are pushed further downstream and upstream bends are pulled in the same direction. Regions just upstream of a bridge for instance, have the greatest number of cut-offs. Bends pushed towards the bridge are constrained by having to pass through it, resulting in a concertina effect in that area.

A distant flood bank flood protection scheme could have been imposed on the River Dane near Holmes Chapel in 1840. Bends with most lateral movement are 96 and 97. At bend 96 lateral movement has been 28m over 144 years and thus a distant flood bank would require to have been 30m outside the 1840 bend apex. Bend 97 is more complex in that it has moved at least 50m laterally but not at a bend apex. If a distant flood bank solution had run from 30m outside bend 95 to 30m outside bend 101, then this large

lateral movement would barely have reached the flood banks. A strong case for having flood banks run from apex to apex rather than curving inwards towards the river. It is of interest to note that bends 96, 97 and 98 will eventually cut-off, returning the river course to a configuration similar to its 1840 route.

7.14.3 Dane stability near Northwich

Ordinance Survey maps of the River Dane at Northwich dating back 110 years, from 1882, were obtained from the National Map Library of Edinburgh. A direct comparison between 1882 and 1992 is shown in Figure 7.34 and is further sketched for additional clarity on Figure 7.34.

The following points can be noted from Figure 7.34:-

- The River Dane has not moved significantly in the last 110 years.
- Most movement has been to straighten and become less meandering. Sinuosity has decreased, although this is a cyclical pattern and may increase again.
- A meander has been removed at the A556 due to bridge construction, (Point A). A meander has been removed at B, and a series of meanders have straightened at C next to a railway. An original meander at D has now been cut-off or moved downstream and is about to cut-off again at E.
- The only significant movement laterally towards distant food banks would be points F and G.

The points F and G identified in the River Dane near Northwich (as shown in Figure 7.34) have moved approximately 20-25m in a period of 110 years, which roughly translates as 0.2m per year. This is in line with Hooke's analysis at Holmes Chapel for lateral movement. If a distant flood bank solution was implemented on the River Dane with the main channel being left untouched, it could be assumed that the current rate of main channel movement would be maintained over the coming years. Consequently if distant flood banks were placed approximately 30m outside each bend apex, they would remain completely unaffected by the river for 150 years even with no bank protection. Nevertheless the use of willows was considered to achieve an enhanced level of bank stability to forestall any possible problems in the long term.

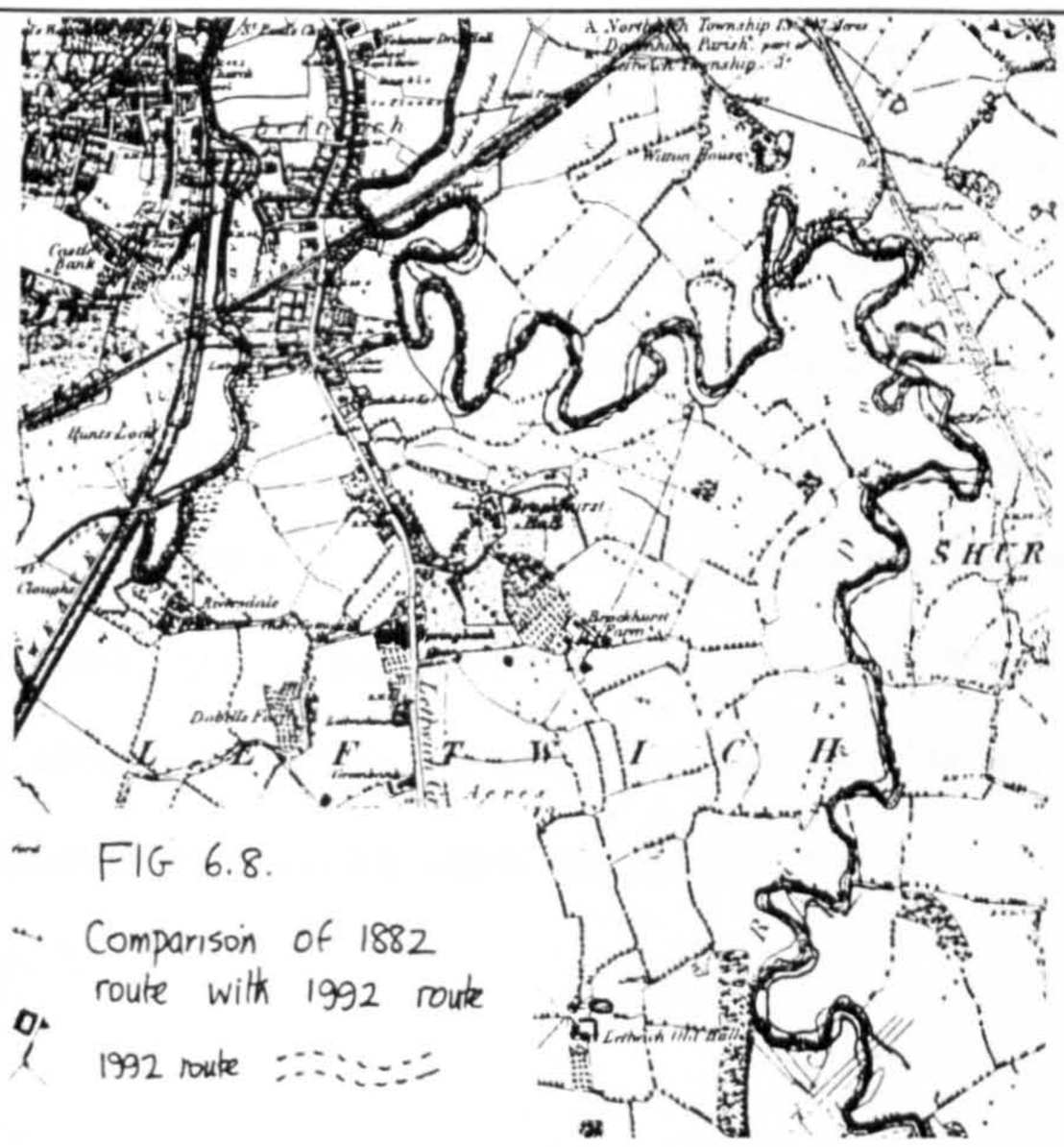

Figure 7.34 R. Dane stability (measured)

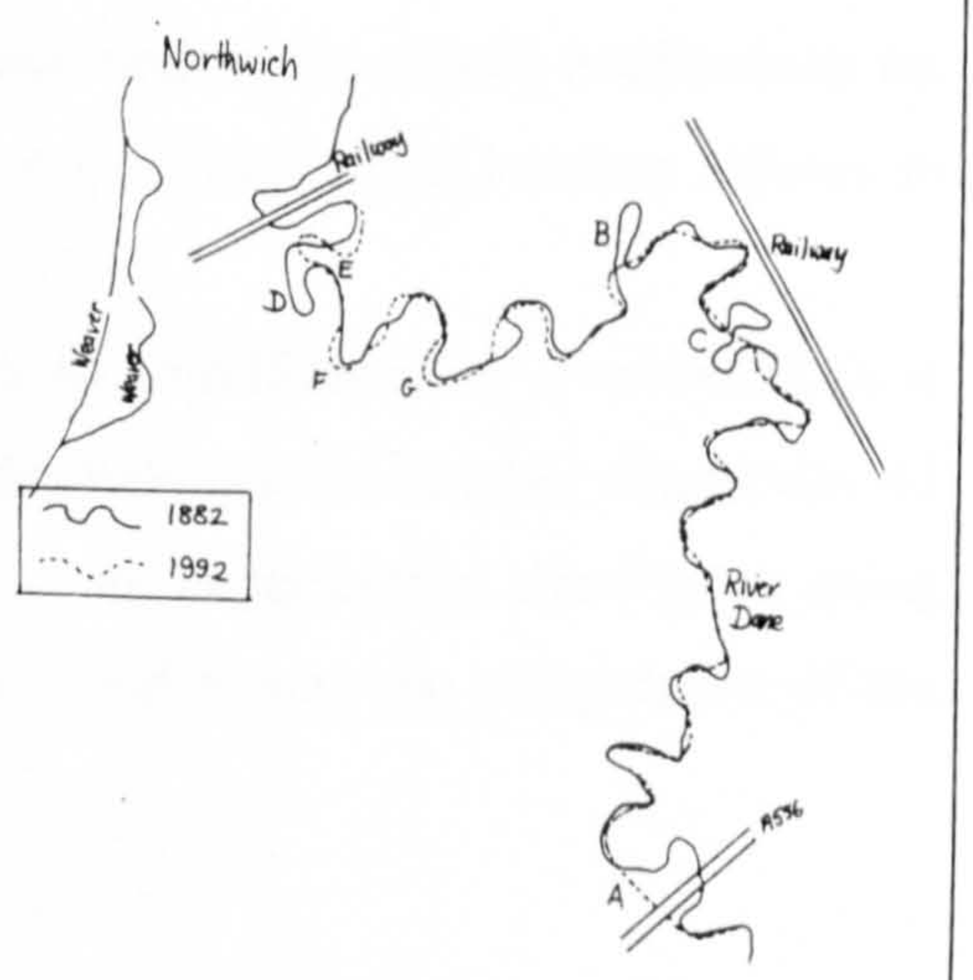

Figure 7.35 R. Dane stability (idealised)

7.14.4 The use of willows as bank protection on the Dane

For some decades Engineers have espoused 'hard' protection methods for rivers including walls, gabions and rock blankets. Recent practice has been to consider 'natural' methods of bank protection including trees, grasses, shrubs, etc. Willows in particular have been widely promoted for river banks, as outlined in "The New Rivers and Wildlife Handbook" RSPB 1994.

The willow is recognised as a key water-tolerant tree which can be used in several forms on the river bank. They can be coppiced to produce short dense and flexible plants also giving a strong anchorage into the bank. Willows can also be used in the form of fascine mattresses and spiling fences. Willows have various effects in the river bank environment:-

- There is a reduction in soil erosion. Vegetation increases flow resistance, lowers velocity near the banks, lowers boundary shear stress and hence produces less erosion.
- Roots from the willows stretch deep into the banks providing natural reinforced earth. Provided roots can go down as far as the low water level, then the tendency for bank slip is significantly reduced as roots cross the plane of the most likely earth slip.

- There is increased bank drainage as less precipitation reaches the soil and also plants draw water from the soil to transpire it to the atmosphere.
- There may be local increases in flow resistance near willows with implications for flood water levels and flood protection. There may be methods of locating willows so as to produce only minimal impact on water levels.

An important step in the Dane Development will be identification of river bends most vulnerable to instability and erosion. This is particularly true for reaches almost devoid of trees and grass. A possible idea might involve an experimental short reach using willows to monitor their effect. Such a proposal would require the co-operation of the NRA.

7.14.5 Basic implementation of regime equations to check stability

River channels adjust to changes in discharge rate, sediment transport rate, or following alterations to the channel. There may be changes to a range of parameters including:-

- the longitudinal channel slope
- the channel width and depth
- the side/lateral slopes of the channel
- the plan form geometry characterised by bend minimum radius of curvature and meander wavelength λ
- sorting of sediment grain sizes downstream

There are at least 8 parameters which can change (8 degrees of freedom). Any numerical model attempting to model stable meanders would therefore need to model each process. Such a model has been developed by Professor Bob Keller, Monash University, Australia and could be employed on the River Dane analysis if required. The model employs a linearly varying planform curvature, regime estimates of meander wavelength λ, river width B, and depth. It also includes models for the inner and outer bank slopes and incorporates an extremal hypotheses for minimum stream power expenditure per unit channel length, and maximum sediment transport efficiency.

An initial estimate for the stability of the Dane at Northwich was performed using simple regime expressions for channel width, depth and meander wavelength. Regime calculations depend on a knowledge of discharge at bankfull depth or a mean annual

flood, $\overline{Q}$. Either of these values may be taken as the dominant discharge forming the channel dimensions. Recent research favours the bankfull discharge. The Dane at Rudheath for instance, has a mean annual flood $\overline{Q}$~ 78 m^3/s and a bankfull discharge of 65-90 m^3/s.

A typical regime estimate of channel width was specified by Hey and Thorne [1986]. The equations that they produced apply to banks of cohesive sand, silt with clay overlying gravel, as is the case at the Dane. The equations apply for bankfull discharge of up to 424 m^3/s and are sub-divided by the degree of vegetation on the banks. Dane vegetation from photographs in Figure 7.27 is probably 'Type III' which corresponds to trees and shrubs, with 5→50% cover. The regime channel width is given by $B = 2.73\ Q^{0.5}$ which is 24-25m wide. This compares almost exactly with the River Dane's measurements. The mean depth of the river channel $\overline{d} = A / B$ should be given by Equation 7.10 and the maximum depth by Equation 7.11.

$$\overline{d} = 0.22\, Q^{0.37}\, D_{50}^{-0.11} \qquad [7.10]$$

$$d_{max} = 0.2\, Q^{0.36}\, D_{50}^{-0.56}\, D_{84}^{0.35} \qquad [7.11]$$

Unfortunately bed material sizes D_{50} and D_{84} for the stretch of the River Dane in Northwich were not known. The meander wavelength, λ, can be characterised by a range of equations. Leopold *et al* [1960] give λ~10.9B whereas Anderson gave $\lambda = 39\, Q^{0.39}$. These equations produce estimates of meander wavelength of 270m and 216m respectively, which compares well with typical wavelengths around 250m in the Dane. The evidence was clear, the River Dane near Northwich although possessing approximately regime dimensions, nevertheless continues to adjust planform through a process of meander cut-offs to cause straightening, followed by new meandering, in a cyclical pattern. Lateral movements can be up to 0.2m per year. Consequently although 30m distant flood banks would be untouched for up to 150 years if the main channel was left unaltered it might nevertheless be prudent to consider bank protection, preferably using natural methods. Hence the suggestion to investigate willows.

7.15 Design Considerations for the Distant Flood bank options

7.15.1 Introduction

A number of additional design features need to be considered if the proposed flood protection scheme and development programme is to be successful. The proposed flood banks are effectively miniature earth dams. The optimisation of their design is crucial to the successful implementation of a compound channel flood protection option. The conditions outside the flood banks in the vicinity of the proposed development area are obviously crucial and were considered at this stage of the design process.

7.15.2 Height and cross-section

A typical cross-section of a suitable flood bank is sketched below in Figure 7.36. It has side slopes of 1 in 3 for soil stability. This value depends on the type of material used. i.e. its angle of inter-granular friction ϕ. For a flood bank typically 1.5m high, the cross sectional area is therefore around $9m^2$, or $18m^2$ both sides, or a total volume of earth around 90,000 m^3 for one length of flood bank on one side of the River Dane.

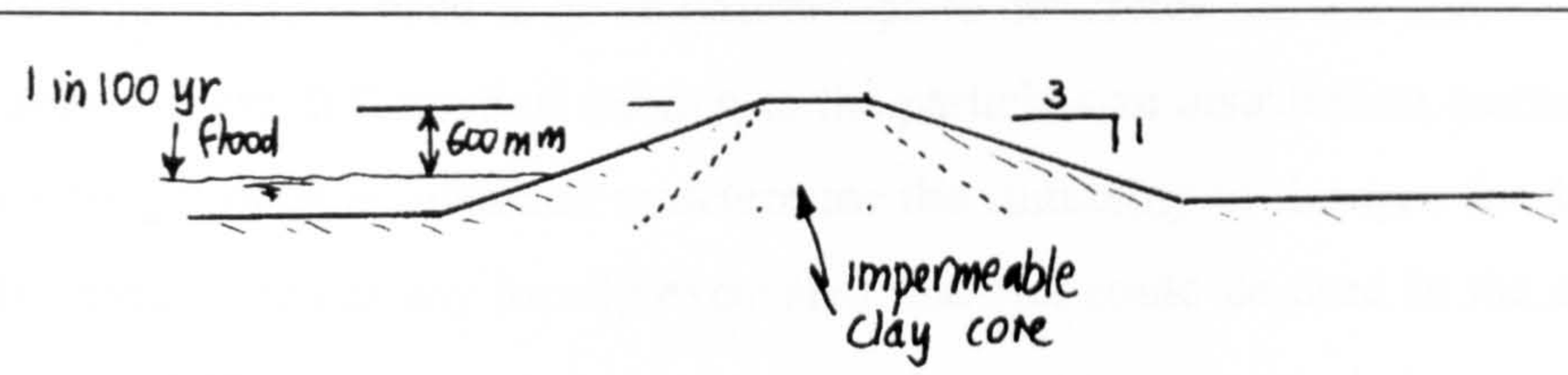

Figure 7.36 Typical cross-section of a flood bank

7.15.3 Permeability of flood banks

It is important that the flood banks are impermeable. This can be achieved by making the entire flood bank from clay. The present in-situ material is a sandy clay which is likely to be to permeable.

7.15.4 Susceptibility of flood banks to erosion; the need for protection

The upper channel flow shown may cause erosion and undermining of the earthen flood banks during peak floods. It is important to consider the use of vegetation cover. Grass is required and the possibility of trees/shrubs should be considered. Trees in this area

will have no appreciable effect on flow resistance. The use of geotextiles should also be considered, as shown in Figure 7.37.

Burrowing animals may also produce a loss of integrity of the flood banks. This might be prevented by the use of geotextiles or geogrids. The polymer variety may be tough enough to guard against burrowing, but this would require careful investigation.

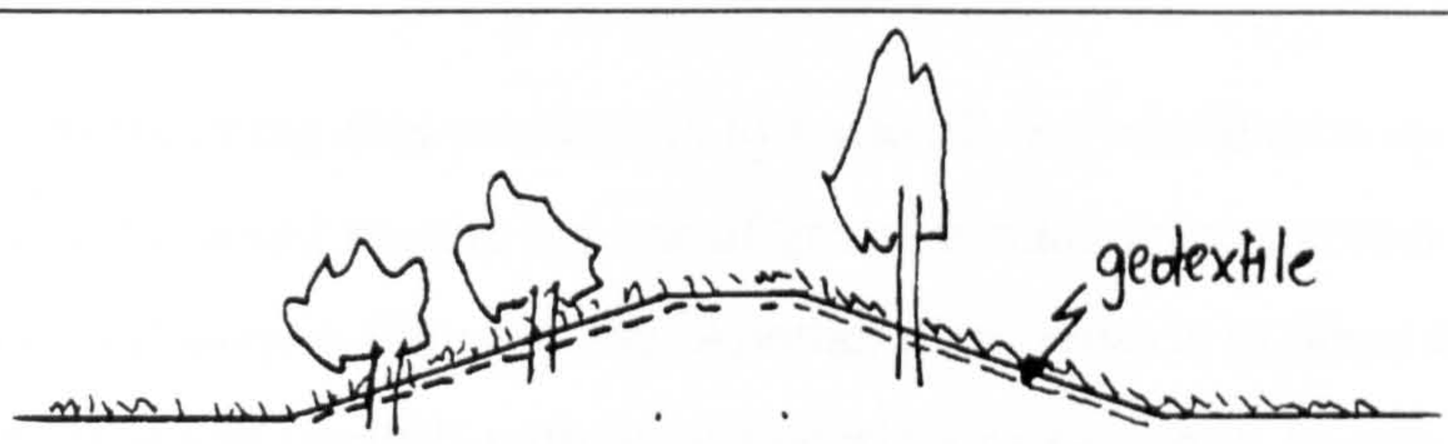

Figure 7.37 Vegetation and geotextiles.

7.16 Conditions in the proposed areas for construction

7.16.1 In-situ borehole tests

In-situ borehole tests need to be commissioned to determine the soil characteristics over the proposed site. Information relating to the particle size distribution, permeability and shear strength must be obtained to determine the suitability of the area for development and to assess whether any locally excavated material could be used in the construction of the flood banks.

7.16.2 Conditions outside the flood banks

Development construction can be carried out either at existing ground levels, or alternatively, the whole area can be infilled with granular fill, up to the level of the top of the flood banks, with the development placed at this level. The choice would depend on the height of the water table and the drainage characteristics of the site.

Construction of a development at the existing ground levels may incur the problem shown in Figure 7.38. The removal of stormwater in the region of the development would be difficult if flood levels in the 2-stage channel are high. A pumping system might be required to remove the rainwater.

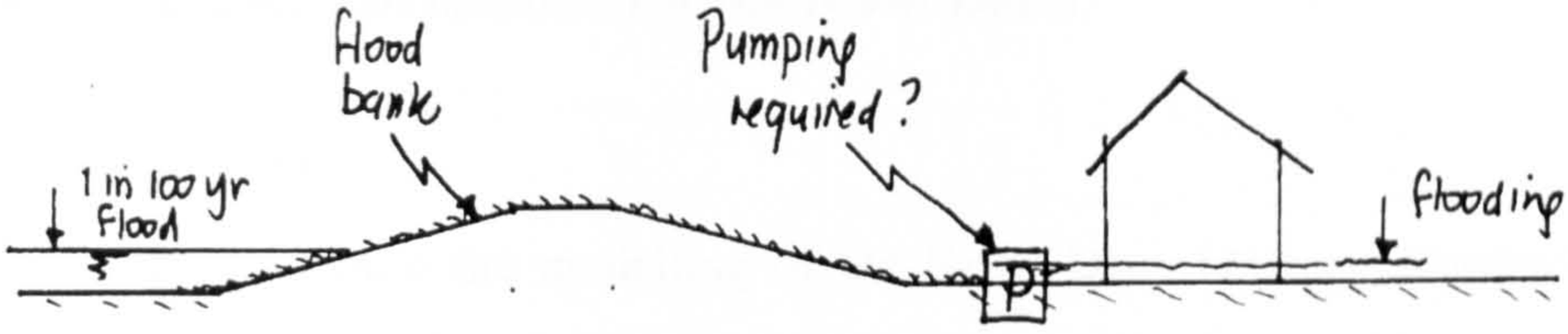

Figure 7.38 Flooding outwith the flood banks.

One method of overcoming this problem is to back-fill the whole area up to the top of the flood banks. This would require the use of granular material to prevent settlement of any construction as shown in Figure 7.39a. Another alternative is to place foundations at existing ground level and backfill with local materials as shown in Figure 7.39b. These alternatives would also ensure that a development was not susceptible to extensive flooding if the flood banks were ever breached.

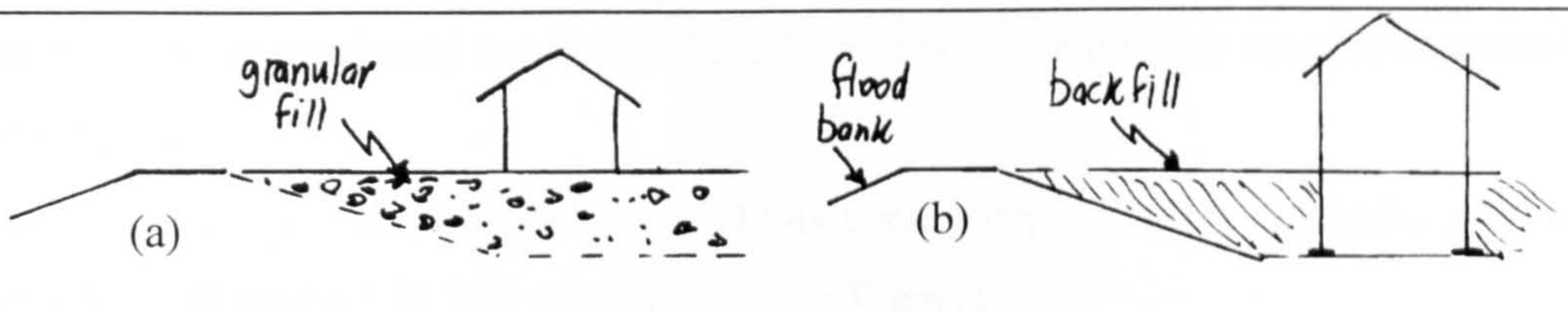

Figure 7.39 Backfill to top of flood banks

7.16.3 A back drain for flood banks

It may be necessary to provide a back-drain for run off from the development which reaches the impermeable clay flood banks, as shown in Figure 7.40

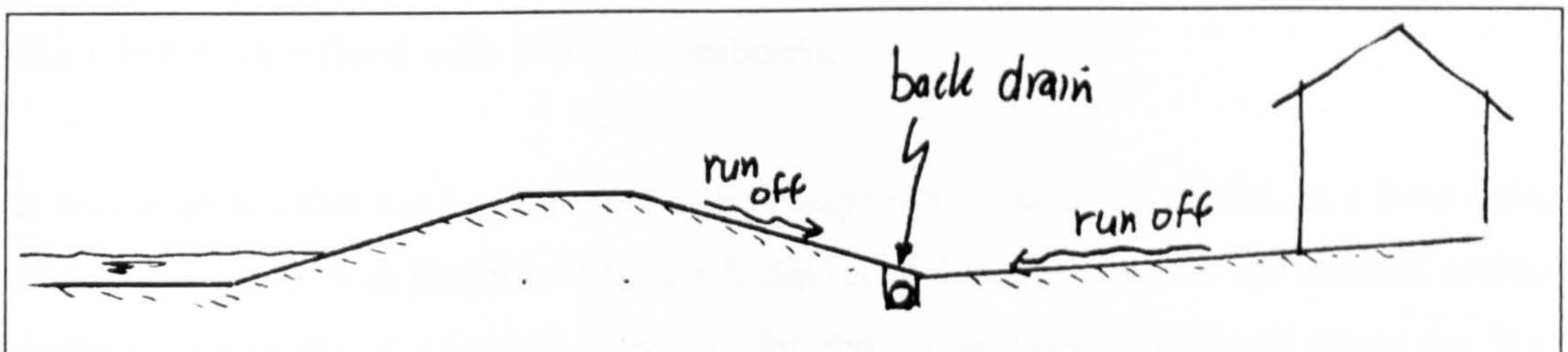

Figure 7.40 Back drain to remove excess water.

7.17 Flood protection options for the River Dane

7.17.1 Introduction

The results obtained from the modelling of the River Dane between Northwich and Rudheath together with other design considerations were used to justify a number of flood protection options for the River Dane. The final option choice will depend to some extent on the EA's rigidity in implementing the criteria for flood (level for level) compensation. Consequently the options proposed attempt to meet the criteria and perform with differing degrees of success. When assessing the various schemes there is a case for arguing that any shortfall in the ability of a particular option to meet the EA's criteria is counterbalanced to some extent by the fact that the analysis carried out in the initial study was conservative in its assumptions in at least four different ways:-

- The 1 in 100 year flood may be less than the present estimate of 161.3 m^3/s.
- The flood plain roughness n = 0.048 should probably have a lower roughness around n = 0.035 to 0.04.
- A confluence water level of 13.5m AOD has been accepted for the analysis. This is likely to be at least a 1 in 200 year flood in the Weaver.
- The numerical model combines high Manning's n values with the James and Wark channel/flood plain interaction model.

The combination of all four effects will probably serve to predict higher water levels for the 1 in 100 year flood than is justified. This in turn produces larger volumes of flood compensation required. The options proposed below nevertheless keep to EA criteria for flood compensation; for no increase in water levels in Northwich town centre; and for the 1 in 100 year flood with 600 mm freeboard.

It was intended that each option would be analysed in detail and costed, at a later date. This initial study was performed to check the reliability of the novel 1D models and to outline various flood protection options for the River Dane. Feedback from the EA would be needed in order to assess the feasibility of implementing compound channel flood protection schemes to meet their strict flood plain development restriction criteria.

7.17.2 Option 1 - Two flood banks a minimum 30m from each bend apex

The analysis has shown that at 30m minimum distance flood banks raise water levels by 0.2 - 0.25m. This increase can be removed by removing a "slice" from the flood plain as sketched in Figure 7.41. The slice would need to be 200-300mm deep, to bring flood levels back down to the before construction levels.

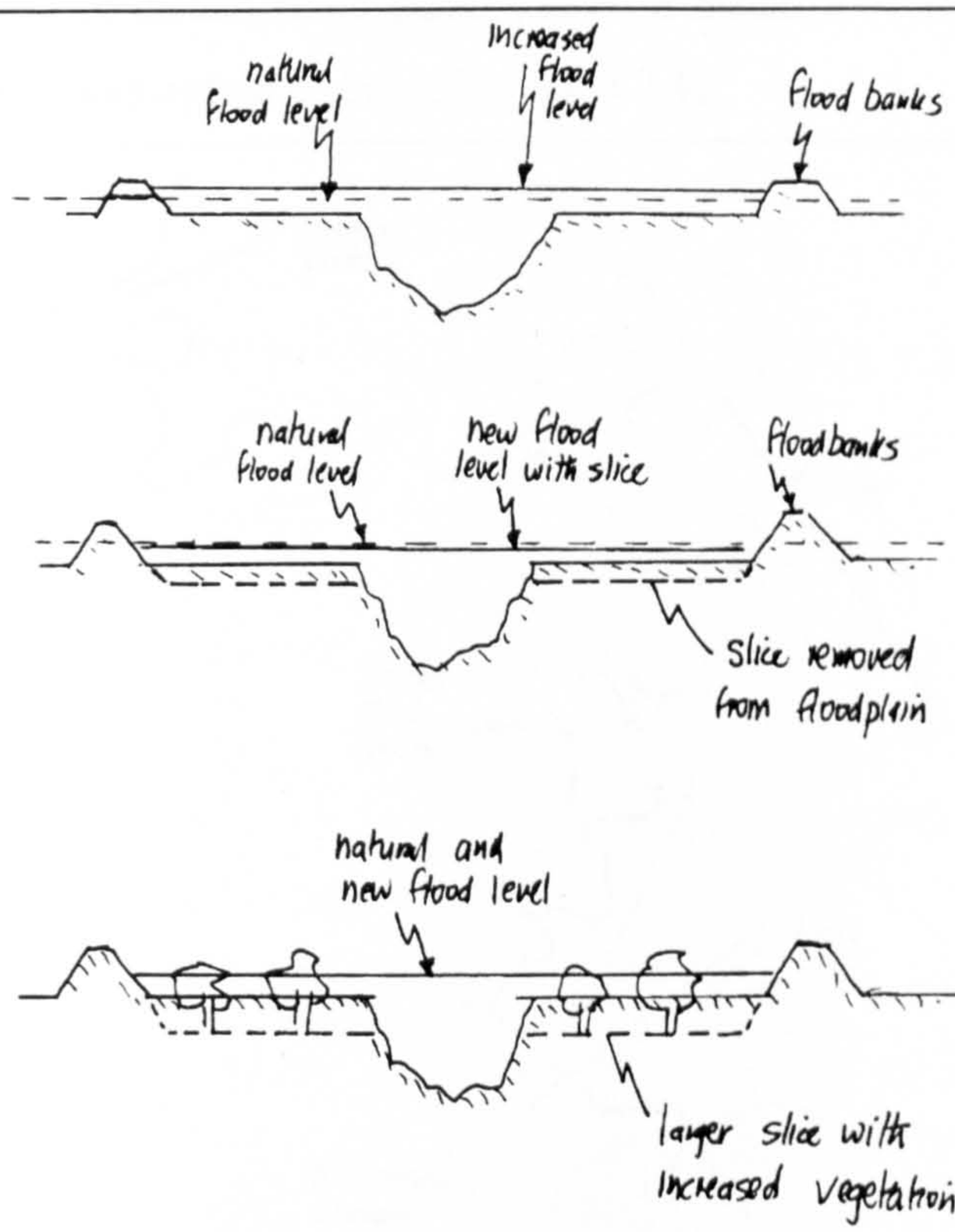

Figure 7.41 Option 1: 'Slices' removed from the flood plain

The major advantage of this method is that additional storage volume is generated by the slice (although it would need to be offset against a lower flood level). In fact a larger "slice" 300-400 mm could be combined with extra vegetation, to bring the water levels back to the existing natural case, and generate even more storage, also shown in Figure 7.41. The additional storage might be allowed as flood compensation storage. From an EA viewpoint this method may go against the "letter" of their flood compensation requirement. i.e. compensation volume is provided, but it is at a lower level than that lost on the flood plain. The EA have implemented similar two-stage channels in the past but normally only where protection was desperately needed for existing development. The merits of this option, using a two-stage channel to protect proposed development,

would have to be discussed in detail with the EA in order to determine whether they thought it was feasible and would sanction it.

7.17.3 Option 2 - Two flood banks with compensation storage

This is again a case of distant flood banks placed a distance of 30m away from each bend apex. A plan of this option is drawn in Figure 7.42.

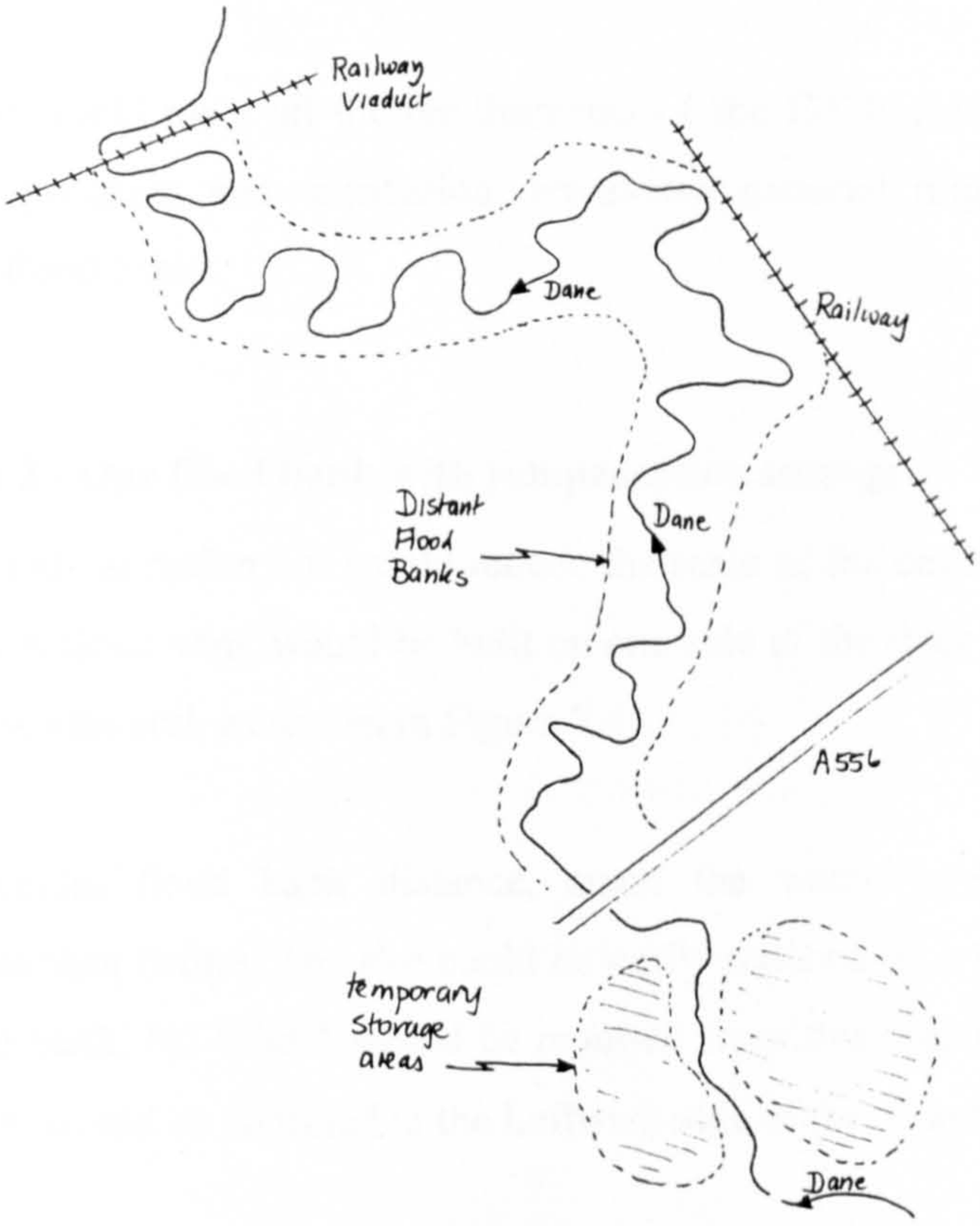

Figure 7.42 Option 2: Distant flood banks (temporary storage, upstream of A556)

This will raise water levels by 0.2 to 0.25m relative to the existing natural case. In this case however there is no slice removed from the flood plain, but instead the flood plain is designed with short, cut grass and tarmac cycle-paths etc., to reduce roughness well below present estimates of n = 0.047. This can reduce the flood level back to existing natural case, and lower, if desired. The advantage of this method is no earthworks to the existing flood plain.

The disadvantage is that temporary flood plain storage needs to be provided elsewhere. A ballpark volume is 200,000 m^3. This might be done upstream of the A556 but would require the purchase of land and the creation of a temporary storage basin of considerable volume and equal to 1000m*285m*0.7m deep. This approach would fulfil the "letter" of the EA requirements, with level for level compensation storage. More detailed calculations could be conducted to refine the volume required, which at present is a crude estimate.

Such a scheme would meet all the requirements of the EA but may be expensive in terms of land purchase and excavation. Excavated material might be suitable for creation of the flood banks.

7.17.4 Option 3 - One flood bank with compensation storage

This is a more radical option but would reduce the scale of the development which can be constructed. A flood bank would be built on one side of the river only, and the other side would remain natural, as shown in Figure 7.43.

For 30m minimum flood bank distance, again the water level would rise but significantly less than before. The rise could be easily reduced by a smooth flood plain inside the flood bank. No "slice" would be required from this side area of flood plain and development would be confined to the Leftwich-side of the flood plain only.

A major advantage of such a scheme is that the flood compensation volume would be effectively halved, to the order of 100,000 m^3. Such a volume might then be provided on the natural unoccupied flood plain, on land already acquired. The temporary storage basin would still be sizeable, of the order of $400m \times 330m \times 0.75m$ deep.

Future calculations would further refine this value. The basin would use natural hollows as much as possible but would still require excavation. There is also the possibility of more than one basin. A sketch of the relative size of basin area (approx. $400m \times 330m$) is shown in Figure 7.43. Excavation of this temporary storage basin may expose the

water table and encourage a wetland area, which could be an environmental feature of the scheme.

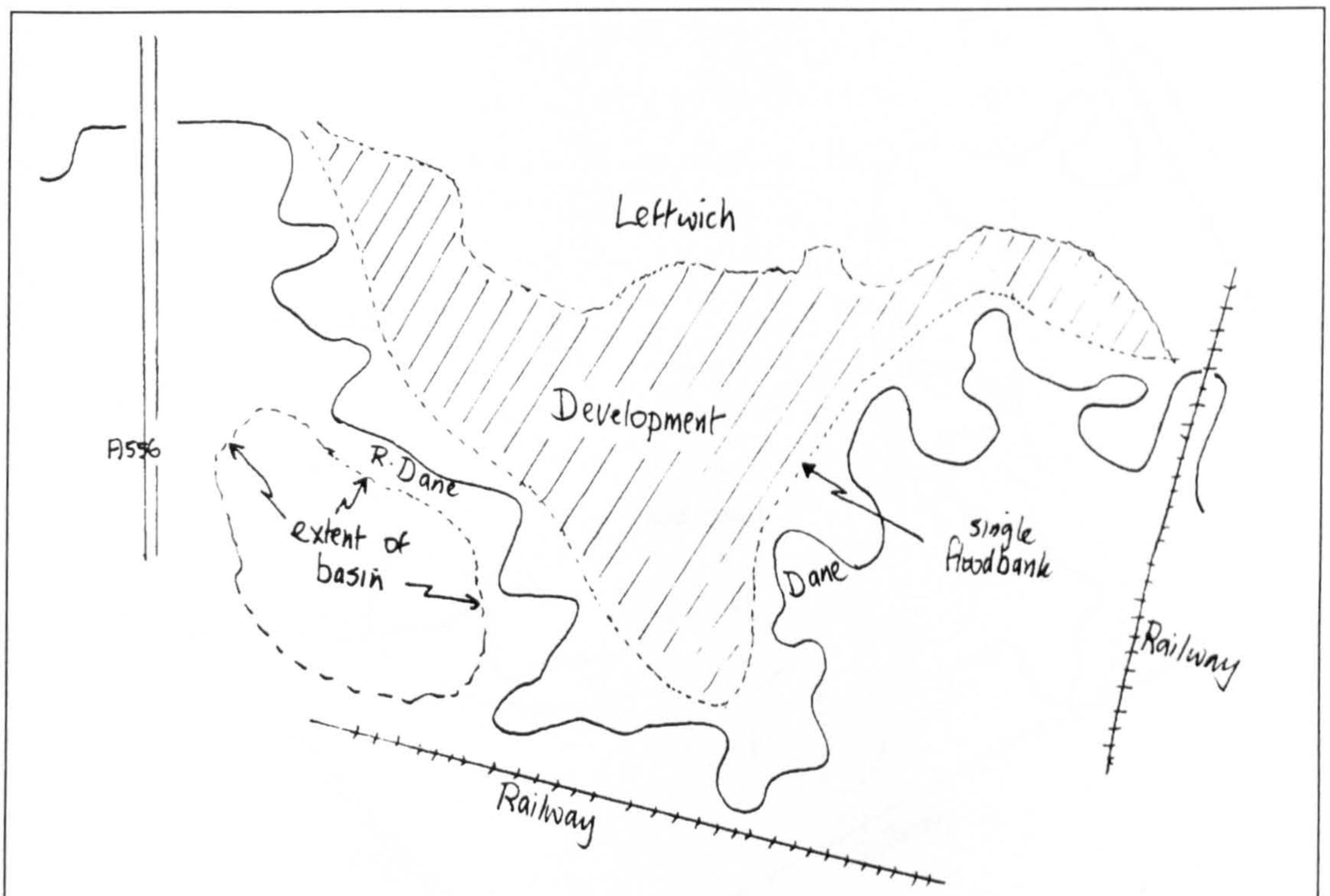

Figure 7.43 Option 3: Single flood bank (temporary storage on opposite bank)

Option 3 would meet EA requirements, be less expensive than option 2, but would drastically reduce the scale of development.

7.17.5 Option 4 - Two flood banks with a lake upstream of the reach

Distant flood banks would be used again probably 30m distant as drawn in Figure 7.44. The 200,000 m^3 compensation storage would be provided by a lake excavated just downstream of the A556. If the lake is to be a permanent feature then it might be excavated to a full 4 to 5m below present ground levels. This would result in a fairly small plan area lake around 200m by 250m. The lake plan area would double if excavation extended only 2 to 2.5m below present ground levels and would increase proportionately as the depths reduced further.

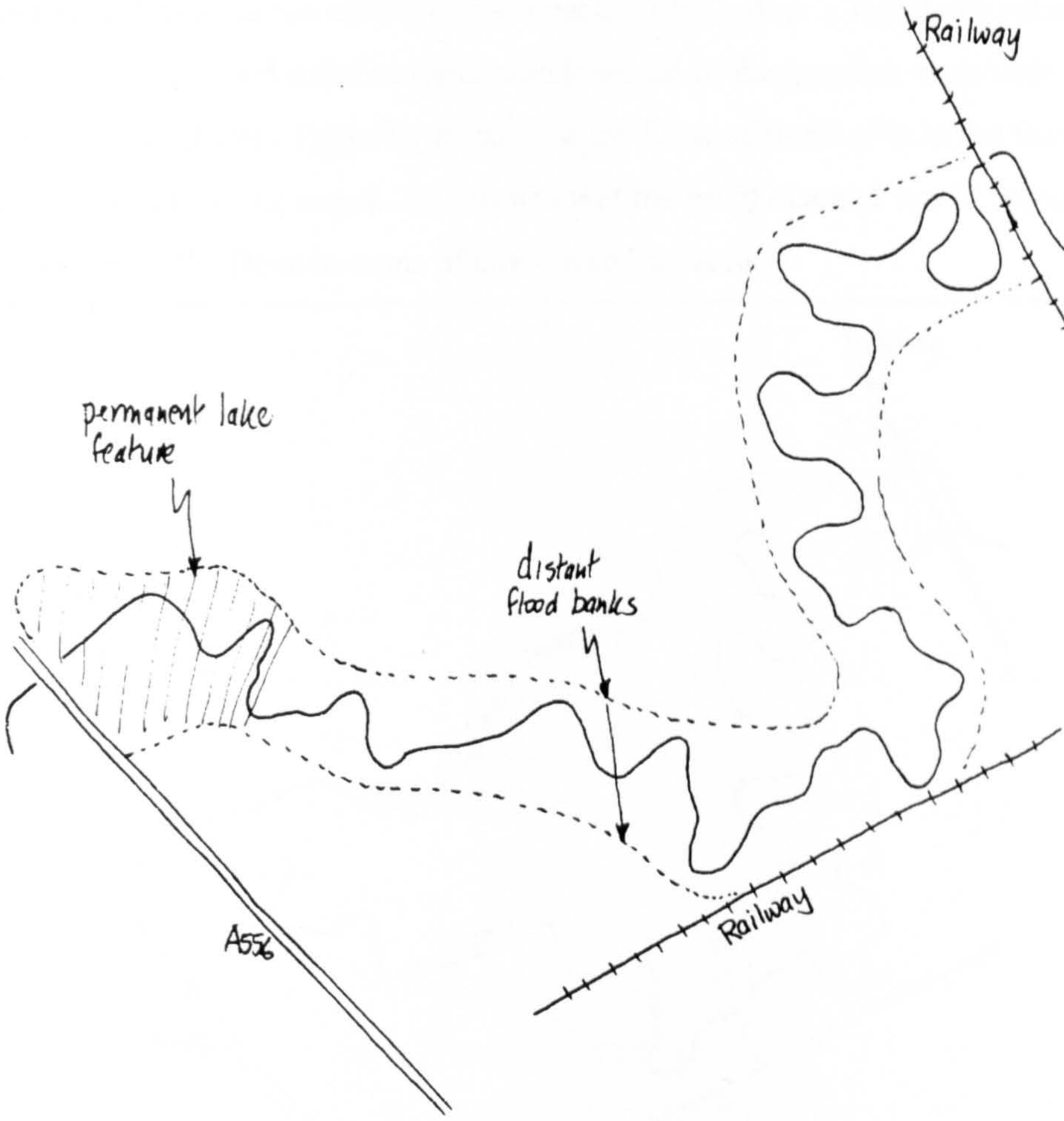

Figure 7.44 Option 4:Permenant lake at A556 with distant flood banks

A deep excavation would ensure the lakes existence for all flows. A shallower excavation would depend on higher river levels or a high ground water table. Rudheath gauging station would be drowned, but higher water levels at lower flows might be possible by using a low weir (producing insignificant water level rise at higher flows). The lake would be useful as an environmental feature including the introduction of a range of flora and fauna and recreational activities. The lake might produce a small rise in water level by $V^2/2g$, which for the 1 in 100 year flood is of the order of 30-40mm. A lowering by 30-40 mm is possible with work to the two stage channel.

7.17.6 Option 5 - The Dane Flood Relief Channel

A completely different kind of option is drawn in Figure 7.45. This is a flood relief channel which makes use of the natural escarpment at Leftwich. Essentially this is a new

river and would remove the need for flood banks. Flows over a threshold value would be diverted into the flood relief channel which would be designed to cope with the 1 in 100 year flood combined. Typically 80 m^3/s in the Dane with 80 m^3/s in the flood relief channel may be a possible target. This means that the relief channel would require to be at least as large as the Dane in terms of cross-sectional area.

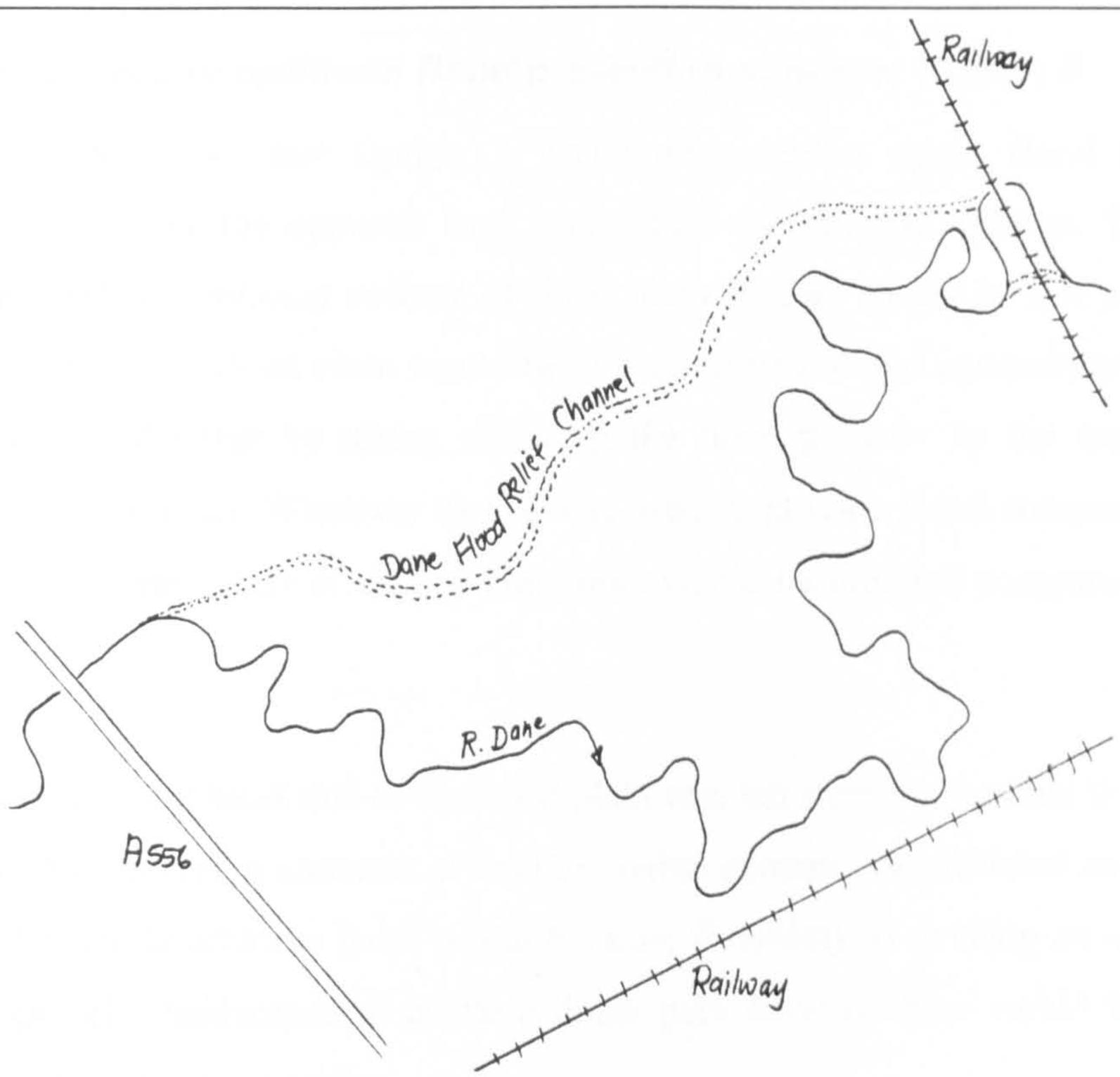

Figure 7.45 Option 5: Flood relief channel

An important feature of such a design would be the flood compensation storage and attenuation of flood peaks moving towards Northwich. At Maidenhead, no compensation storage was required at flood plain level, because the flood relief channel itself provided extra volume, which attenuated the flood peak reaching the downstream end. As well as this, the EA demonstrated that both flood peaks reached the downstream end at different times, reducing the magnitude of the single peak.

Therefore a flood relief channel may be capable of delivering a reduced peak discharge at the railway viaduct by virtue of its own storage volume and because the two flood peaks do not necessarily reach the downstream end at the same time. This would require a detailed computer analysis using an unsteady model.

A flood relief channel would have the advantage of attracting additional wildlife to the Dane Valley, with increased flora and fauna and recreation. The disadvantages might be cost, the need for additional bridges to the development and the marooning of development on an island.

7.18 The choice of optimum flood protection scheme: Option 3

The author considered that Option 3 which advocated a single flood bank with temporary storage on the opposite bank represented the optimal solution. This option would ensure that a minimal volume of flood plain storage would be lost because the right hand side of the flood plain would be left untouched. Flood compensation storage could be provided either by taking slices off the flood plain or by the creation of a temporary storage pond. Whatever choice was used to provide flood compensation the extent and associated costs of excavation works would be minimal compared with the other Options.

The fact that the right hand side of the flood plain was left untouched meant that it could be ensured that minimum amounts of environmental damage was inflicted on the River Dane flood plain. In addition there would be more flexibility to develop an area which could be specially landscaped to create a linear park because there would be a much greater area available to consider.

However, there were a few minor drawbacks associated with Option 3 which had to be considered. Although the ground rises steeply to the right hand side of the main channel, creating natural flood banks, the construction of the flood banks might induce additional erosion damage to these banks during times of flood. The final flood levels associated with the scheme would have to be checked and the local flow condition predicted to assess whether there would be a need to reinforce the natural banks in certain areas. The impact on the railway embankment would have to be carefully assessed.

Despite the drawbacks, on balance, Option 3 definitely appears to represent the optimal solution to enable the development of the River Dane flood plain. In the future, through negotiation with the EA, local planning authorities, and the developers it may well be

possible to refine this initial option to satisfy all parties and to ensure the commissioning of the project.

There was an additional drawback associated with all flood bank solutions. It could be argued that if any flood banks were ever built to protect development on the flood plains, before any construction was started, the ground levels outside the flood bank should be built up so that they coincide with the top of the flood banks. This would be the only way to avoid catastrophe if the flood banks were ever breached. This might seem an extreme measure and an overly cautious one as well as being prohibitively costly but must be considered and discussed with the EA before the project progresses any further.

7.19 Summary and conclusions

7.19.1 The structure of the one-dimensional numerical river models

- The author developed 2 novel one-dimensional numerical models, one for steady and another for unsteady flow. They incorporated the James and Wark [1] [1992] and Ackers [1991] methods for predicting the discharge capacity in compound channels and facilitated the application of these methods for uniform model channels to natural, full-scale, non-uniform river channels.
- The author postulated that the novel one-dimensional models were more reliable than traditional models when calibration data is not available because they could explicitly account for the flow resistance generated by bed friction and flood plain / main channel interaction in meandering compound channels.
- The author postulated that the novel one-dimensional models will be more reliable than traditional models when designing compound channel flood protection schemes. This was due to their ability to explicitly account for flood plain / main channel interaction and the influence of geometric and roughness parameters on the resulting flow resistance.

7.19.2 Analysis of the River Dane using the novel one-dimensional models

- The initial validation of the novel models was performed using calibration data obtained from the River Dane in Cheshire. The novel models predicted stage and discharge capacity relationships for the River Dane which were in close correspondence to the two sets of calibration data that were available from the 1947 and 1995 floods.
- The stage and discharge capacity predictions were of comparable accuracy to those obtained by previous researchers who used a traditional 1D model called MIKE11.
- A scale model of the River Dane was built in Glasgow which was assigned a configuration which possessed similar geometric ratios to those in the natural channel. A comparison was made between the stage-discharge behaviour in the natural channel (during the calibration events) to that in the physical model channel. Making suitable allowance for the scale effects and slight configuration anomalies the author demonstrated that the physical model exhibited similar flow behaviour to that measured in the natural channel.
- A basic stability analysis of the main channel of the River Dane demonstrated that distant flood banks could be constructed which were at minimal risk of being undermined due to movements of the main channel in the next 100years. With the proviso that they are offset at least 10m from the edge of the existing meander belt and that there are neither additional interventions by man on the flow in the River Dane nor major climate change.
- The author observes that a relaxation in the Environment Agency's strict 'level-for-level' flood water volume compensation criteria is needed to make compound channels more viable as flood protection scheme options. The author suggests a minor relaxation of the 'level-for-level' criteria could be negotiated by convincing the Environment Agency that the greater discharge capacity prediction accuracy offered by the new 1D models can enable them not to apply such strict factors of safety when designing of a compound channel flood protection schemes.

7.19.3 Design options for flood protection on the River Dane

- Five design options for a scheme to protect the development in the River Dane were proposed by the author.
- The author identified Option 3, with a single flood bank and temporary storage provided on the opposite bank, as the optimal solution with regard to meeting the Environment Agency's stringent requirements.
- Based on lessons learnt during the River Dane case study, the author proposes that the following 10 point plan should be implemented when designing compound channel flood protection schemes in the future. This will make optimal use of the additional features offered by utilising the novel one-dimensional numerical models:-

1) First perform hydrological analysis. The Environment Agency ask for 6 analyses which include the following methods:- Extremal Value, Unit hydrograph, Catchment Characteristics, MAF regional growth curves and 2 variants.
2) Determine the roughness characteristics of the main river channel. Using available survey data calibrate the numerical model. Adjust Manning's n to match known data (obtain ball park value). Perform gross error check using Chow [1959].
3) Estimate Manning's n value for the flood plain using a combination of Chow [1959] and Acrement and Schneider [1989].
4) Compute conveyance characteristics of each cross section individually using either Ackers [1991], James & Wark [1] [1992], the Artificial Neural Network or the Enhanced zonal methods.
5) Run the model for case of the existing flood plains and distant flood banks.
6) Determine the rise in river water level for distant flood banks.
7) Determine the depth of slice needed to take the water level back to its natural state (no increase in water level).
8) Compute flood storage volume lost on the flood plain and replace storage volume elsewhere, preferably adopting the Environment Agency's 'level for level' strategy.
9) Assess the possibility of including a further slice to increase storage volumes and extra vegetation to retain stored water longer in order to ensure that there is no rise in water level downstream.
10) Ensure there is no increase in flood discharge peak downstream from the scheme and that no detriment is inflicted on third parties.

Chapter 8

8. Summary and conclusions

1. The author utilised the flow data gathered during the Series B extension (1989-1992) programme to develop an enhanced semi-physical / semi-empirical method for predicting the discharge capacity of a uniform meandering compound channel. The method was entitled the Enhanced zonal method and was shown to produce more accurate discharge capacity predictions than the James and Wark [1] [1992] method for the majority of meandering compound channels tested. The Enhanced zonal method was developed by implementing adaptations of the James and Wark [1] [1992] method which was previously the most reliable hand calculation method for determining the discharge capacity in a meandering compound channel.
2. The author also developed an Artificial Neural Network (ANN) functional approximator, known as MLP12, which was trained to replicate the observed relationship between F* and 9 of the key parameters in meandering compound channels. This relationship was revealed by the results gathered during the Series B extension (1993-1996) programme. The resulting ANN approximator was shown to produce more accurate discharge capacity predictions than the James and Wark [1] [1992] method for the majority of channels tested.
3. The ANN approximator produced more accurate discharge capacity predictions than the Enhanced zonal method provided that the range of the parameters in the test channels fell within the range of those used in the original flow data (training) set.
4. However the Enhanced zonal method produced more accurate discharge capacity predictions than the ANN approximator when applied over the whole range of parameters that were tested.
5. Whilst participating in the Series B extension (1993-1996) programme, the author devised a methodology to explicitly compare the flow results from a wide range of different scale meandering compound channels.

6. The author used a non-dimensional discharge parameter known as F* to strip away the contribution of bed friction on overall flow resistance and reveal the contribution of layer interaction.
7. Although the bed friction resistance was greatly influenced by model scale in meandering compound channels, the author showed that the layer interaction mechanisms were similar in different scale models. Different layer interaction mechanisms were generated depending on the relative flow state in the main and flood plain channels.
8. The author devised a novel flow parameter known as Relative flow state, Re', in order to identify the flow depths corresponding to changes in the mechanism of layer interaction. The Relative flow state parameter was defined as the ratio between the Reynolds numbers associated with flow in the main and flood plain channels respectively.
9. The author, in collaboration with parallel teams from Aberdeen and Bristol Universities, took advantage of the fabrication flexibility offered by small scale models in order to test (over a limited two year period) the influence of 11 key geomorphic and roughness parameters on flow behaviour in compound channels.
10. The new comparison methodology developed by the author was used to combine the data gathered during the Series B extension programme with existing data sets derived from equal and larger scale compound channel studies.
11. The author analysed all the new data and re-analysed the existing data in order to determine the precise effect of the key parameters on flow layer interaction in compound channel flow and to assist with the development of new deterministic models for predicting discharge capacity.
12. The plots which were obtained using the available experimental data and by correlating the magnitude of relative depth and the value of F* revealed to the author that the layer interaction mechanisms in meandering compound channels are divided into 4 distinct regions. These regions were distinguishable in the majority of meandering compound channels that were tested, irrespective of scale.
13. In flow region 1 strong lateral turbulent shear is generated by the difference in flow velocity between the fast flowing main channel water (which extends into the flood plain) and the remaining flood plain water which is slow flowing.

14. In flow region 2 the lateral shear action decreases and is replaced by a horizontal shear layer between the flood plain and the main channel (below bankfull). Bed friction dominates the flood plain flow and limited secondary cell production is initiated.
15. In flow region 3 the secondary cell production becomes significant as the flood plain flow expands and contracts as it passes over the main channel. Large quantities of water are expelled from the main channel at the apices.
16. In flow region 4 the proportion of flow resistance contributed by layer interaction diminishes and the compound channels behave more like a simple channels with their value of coherence tending toward 1.
17. No data is currently available to categorically confirm the author's postulation that similar layer interaction mechanisms are generated in full scale, natural channels. There is a glaring need to obtain appropriate field data in order to confirm the author's postulation.
18. The author developed 2 novel one-dimensional (1D) numerical models, one for steady and another for unsteady flow, in order to facilitate the application of the various prediction methods which were developed using regular model channels to irregular natural rivers. Consequently the 1D models included a facility to explicitly determine the head loss contributed by layer interaction as well as bed friction. They were able to explicitly determine the discharge capacity of extensive reaches of natural, full scale, non-uniform river channels rather than predominantly relying on a calibration procedure using field data to achieve optimum accuracy as is usual with existing 1D models.
19. The author also developed a 10 point procedure for designing compound channel flood protection schemes which made use of the new facilities offered by the novel 1D numerical models.
20. The author applied the 10 point procedure and the novel 1D models to a case study of the River Dane in order to illustrate the optimal method by which they could be utilised by a consultant engineer.
21. The environmental benefits that can potentially be accrued by using a distant flood bank solution as a flood protection scheme are illustrated by comparison with the other more traditional solutions that were also plausible for the River Dane case study.

Chapter 9

9. Recommendations for future research

9.1 Laboratory studies and scale model testing

9.1.1 Extension of meandering compound channel data set

- Additional experiments should be performed in order to extend the available data sets which can demonstrate the relationship between stage, discharge, velocity and bed shear stress in meandering compound channels with high main channel sinuosities (between 1.374 and 2.043). In these experiments main channel sinuosity should be varied to include both natural and unnatural bend configurations, such as defined using the geometric ratios defined in Equations 2.60 - 2.63. This is essential in order to determine the reliability of existing data sets. It is also important to determine whether the flow layer interaction mechanisms, and hence the flow resistance, in meandering compound channels are affected by the similarity of the main channel geometries to those found in natural channels. If the similarity of the channel configuration to natural channels is shown to be significant then it must be demonstrated whether the effect is significant in both large and small scale compound channels.
- Further experiments should be performed in order to extend the available data sets which can demonstrate the relationship between stage, discharge, velocity and bed shear stress in meandering compound channels with low sinuosities (between 1.0 and 1.09). These experiments are necessary in order to determine at which sinuosity the flow in a compound channel changes from being typical of straight compound channel flow to being typical of meandering compound channel flow.
- Additional experiments should be performed to determine the precise influence of proximate flood plain banks (measured in terms of relative meander belt width) on the flow behaviour in Zone B and to confirm whether the influence of proximate flood plain banks is predominantly significant in small scale channels.

- Further experiments should be performed in order to extend the available data sets which can demonstrate the relationship between stage, discharge, velocity and bed shear stress for meandering compound channels with variable lateral flood plain slopes. Only a limited number of results were obtained in Bristol during the Series B extension [1993-1996] tests.
- Additional experiments should be performed in order to extend the available data sets which can demonstrate the relationship between stage, discharge, velocity and bed shear stress for meandering compound channels with variable flood bank sinuosity. Only a limited number of results were obtained in Bristol during the Series B extension [1993-1996] tests.
- Further experiments should be performed in order to extend the available data sets which can demonstrate the relationship between stage, discharge, velocity and bed shear stress for meandering compound channels with shallow flood plain slopes. The Series B extension [1993-1996] tested slopes which ranged between 1:750 and 1:1000. Many natural river actually possess much shallower slopes. It is important to determine whether the existing discharge capacity prediction methods are reliable when the river slope is significantly shallower.
- Additional experiments should be performed in order to extend the available data sets which can demonstrate the relationship between stage, discharge, velocity and bed shear stress for meandering compound channels with planform and cross-sectional configurations which vary longitudinally. These experiments will more closely simulate the natural channel situation and can be used to assess the differences resulting from using uniform instead of natural channels. The use of self-formed channels is recommended in order to generate these longitudinal variations.
- Further experiments should be performed in order to extend the available data sets which can demonstrate the relationship between stage, discharge, velocity and bed shear stress for meandering compound channels with increasing numbers of repeating wavelengths, extending the work of Kiely [1989]. These experiments should precisely determine the minimum number of wavelengths needed to establish fully developed flow in a meandering compound channel. This would facilitate the first step to be taken towards developing protocols which can explicitly define the length of a natural channel over which one uniform channel will exhibit similar flow resistance due to layer interaction.

- Additional experiments should be performed in order to obtain detailed measurements of the mean velocities in Zone A (main channel) in the vicinity of Threshold depth A in order to develop improvements to the Vertical shear stress method described in Section 4.7. Special consideration needs to be given to determine the appropriateness of this method for determining Threshold 1/2 in small scale channels with highly sinuous main channels.

9.1.2 Extension slot flow data set

- Further experiments are needed to elaborate more rigorously the influence of relative roughness on the expansion and contraction head losses in flow over a slot.
- Additional experiments are needed to elaborate more rigorously the influence of slot skew angle on the expansion and contraction head losses in flow over a slot.
- The author recommends that further experiments are performed in order to elaborate more clearly the relationship between the main channel (slot) flow velocity and the ability of the slot to resist the expansion and contraction of flood plain flow as it passes over the top.
- Enhanced formulations for the expansion and contraction adjustment coefficients, C_{we} and C_{wc} should be derived using the newly acquired data.

9.2 Further development of the Enhanced zonal method

- The empirical coefficients integral to the Enhanced zonal method should be regularly updated by including complementary zonal flow data from future experimental programmes using further multivariate regression analysis.
- Particular emphasis should be given to including provisions for the 4 main parameters for which only limited data was produced during the Series B extension programme:-

1) main channel sinuosity
2) lateral flood plain slope
3) flood bank sinuosity
4) relative meander belt width

9.3 Further development of the Artificial Neural Network (ANN) models

- The ANN functional approximator; MLP12, which was developed by the author in Glasgow during the Series B extension (1993-1996) programme should be updated to incorporate the additional parametric data relating F* to the original 9 key parameters as it is accumulated.
- The ANN approximator should be extended, by combining revised existing training pairs with newly acquired training pairs, in order to account for the influence of two extra parameters: lateral flood plain slope and flood bank sinuosity for which there was no data at the time of writing this thesis. Bristol are scheduled to publish suitable data as part of the Series B extension (1993-1996) programme. Great care must be taken to avoid potential errors that might be introduced by over-parameterisation.
- The impact of using different training algorithms and/or ANN architectures, such as Radial basis networks, to develop alternative F* versus 9 or 11 parameter functional approximators should be assessed in order to determine whether they will produce improved discharge capacity predictions.
- Further test results are required to determine the viable extrapolation limits for MLP12 when the parameter values of test data falls outside the training range.

9.4 Field data set collection

- Additional field data needs to be gathered in order to facilitate the further validation of the various discharge capacity prediction methods that have been developed.
- Future field data collection should seek to obtain both stage-discharge data and zonal flow data in order to test the validity of the modelling assumptions underlying the various discharge prediction methods.

9.5 Further development / validation of one-dimensional numerical models

- The 2 novel 1D numerical models must be adapted to incorporate the ANN and Enhanced zonal discharge prediction methods which were developed by the author during the Series B extension (1993-1996) programme.
- The fully-adapted 1D numerical models need to be tested on additional case studies to confirm their accuracy and to facilitate any refinements. The author suggests that

they should be tested on the River Blackwater prototype and model channel data which is likely to be published by researchers at Bristol University in the near future.

- The author suggests that the basic 1D models developed during the Series B extension (1993-1996) should be extended for inclusion in some commercially available models, such as HEC-RAS or ISIS.
- The author recognises the need to further develop the procedures for applying the novel 1D models to natural rivers because of the different rationale associated with their application. Because these novel models explicitly account for the layer interaction losses, the range and scope of the calibration data that is needed to enable a Engineer to be confident of their accuracy is likely to be different to that needed when using the traditional 1D models.
- The author suggests that a protocol must be developed to determine the optimal number and positioning of representative uniform cross-sections for inclusion in the 1D models to obtain the most accurate results.
- The reliability of the author's 10 point compound channel design procedure needs to be assessed using further case studies.

9.6 Overcoming the difficulties associated with implementing compound channel flood protection solutions

- A relaxation in the Environment Agency's strict 'level-for-level' flood water volume compensation criteria is needed to make compound channels more viable as flood protection scheme options. The author suggests that new protocols need to be developed, in collaboration with the Environment Agency, in order to quantify what might be considered a more 'reasonable' amount of replacement storage in the specific case of compound channel schemes where extensive conservation benefits can be accrued if they are used as alternatives to traditional methods.
- The author suggests that any attempts to negotiate a relaxation of the 'level-for-level' criteria could be centred around convincing the Environment Agency that the greater discharge capacity prediction accuracy offered by the new 1D models can enable them not to apply such strict factors of safety on the design of compound channel flood protection schemes.

REFERENCES

1. ACKERS P [1991] 'The Hydraulic Design of Straight Compound Channels', Report SR 281, HR Wallingford, October.
2. ACKERS P [1993] 'Flow formulae for straight two-stage channels', Journal of Hydraulic Research. Volume 31, No 4, p 509-531.
3. ACREMENT G J and SCHNEIDER R [1989] 'Guide for selecting Manning's roughness coefficient for natural channels and flood plains', US Geological Survey Water-Supply paper 2339,
4. AGARWAL V C, GARDE R J and RANGA RAJU K G [1984] 'Resistance to flow and sediment transport in curved alluvial channels', Fourth Congress, Asian and Pacific Division, IAHR, Thailand, 11-13 September, pp 207-218.
5. AHMADI R [1979] 'An Experimental Study of Interaction Between Main Channel and Flood Plain Flows', PhD Thesis, Department of Civil Engineering, The University of Alberta, Canada.
6. ALDRIDGE B N and GARRET J M [1973] 'Roughness coefficients for stream channels in Arizona', US Geological Survey Open-file report, p87
7. ALFRINK B J and VAN RIJN L C [1983] 'Two-equation Turbulence model for flow in trenches', Journal. of Hydraulic Engineering, Volume 109, No 3, pp 941 - 958,July
8. ARNOLD U, ROUVE G and STEIN J [1989] 'A Review of Investigations on Compound Open Channel Flow', Hydro-Comp 89, Dubrovnik, Yugoslavia 13-16th June 89, Supplements pp 19,40.
9. ASCE TASK FORCE, [1963] 'Friction factors in open channels.', Journal of the Hydraulics Division, Proceedings of the American society of Civil engineers, Volume. 89, No. HY2, pp 97-141
10. BAGNOLD R A [1960] 'Some aspects of the shape of river meanders', Geological survey professional paper 282-E, Washington
11. BAIRD J I and ERVINE D A [1982] 'Rating Curves for Rivers with Overbank Flow', Proceedings of the. Institution of Civil Engineers, Part 2, 1982, 73, June, pp 465-472.
12. BAIRD J I and ERVINE D A [1984] - 'Resistance to Flow in Channels With Overbank Flood-Plain Flow', Proceedings of the, 1st International. Conference on Channels and Channel Control Structures, Computational Mechanics Centre, Southampton, England, pp 4137-4150.
13. BARBARUTSI S and CHU V H [1991] 'Dye-concentration distribution in shallow re-circulating flows', Journal. of Hydraulic. Eng., Volume 117, No 5, pp 643 - 659
14. BENSON M.A. [1968] 'Uniform flood frequency estimating methods for federal agencies', Water Resources Res. 4,No. 5, pp891-900
15. BAUM E and HAUSSLER D [1989] 'What net size gives valid generalisation?", Neural Computation,1(1), pp151-160
16. BHOWMIK N G and DEMISSIE M [1982] 'Carrying capacity of flood plains', Journal. of the Hydraulic Division, ASCE, Volume. 108, No. HY3, pp 443-452
17. BOX G P AND DRAPER N R [1987] 'Empirical model-building and response surfaces', John Wiley and Sons, New York, N.Y.
18. BROOMHEAD D S and LOWE D [1988] 'Multi-variable functional interpolation and adaptive networks', Complex systems, Vol. 2, pp 321 - 355.

19. BROOKES A [1995] 'Challenges and objectives for Geomorphology in UK river management', Earth surface Processes and Landforms, Volume 20, pp 593 - 610
20. BURNHAM M W [1990] 'Effects of data errors on computed steady-flow profiles', Journal of Hydraulic. Eng., ASCE, Volume. 116, pp 914 - 930
21. CARPENTER W C and BARTHELEMY J F [1994] 'Common misconceptions about neural networks as approximators', Jrnl. of Computing in Civil Engineering, Vol. 8, No. 2, pp 345 - 358
22. CHANG H [1983] 'Energy Expenditure in Curved Open Channels, Journal Hydraulic Engineering, Vol. 109, No 7, July.
23. CHANG H [1984] 'Analysis of River Meanders', Journal of Hydraulic Engineering, Vol. 110
24. CHANG H [1984] 'Regular Meander Path Model', Journal of Hydraulic Engineering, Vol. 110
25. CHANG H [1984] Variation of Flow Resistance Through Curved Channels, Journal of Hydraulic Engineering, Vol. I 10, No 12, pp 1772-1782.
26. CHRISTENSEN B, [1991] 'Calculation of total conveyance in natural channels' discussion', Journal. of the Hydraulic Division., Volume. 117, pp. 1196 -1199
27. CHOW V T [1959] 'Open Channel Hydraulics', McGraw-Hill, London, International Student Edition, ISBN 0-07-Y85906-X.
28. COWAN W L [1956] Estimating Hydraulic Roughness, Agricultural Engineering, Vol. 37, No 7, pp 474-475.
29. CUNGE J A, HOLLY F M and VERWEY A [1980] 'Practical aspects of Computational River Hydraulics', Pitman Publishing, ISBN 0-273-08543-3
30. DEMUTH H and BEALE M [1994] 'Neural Network Toolbox User's Guide: for use with MATLAB', The Mathworks, Inc., Cochituate Place, 24 Prime Park Way, Natick, Mass.
31. DRACOS T and HARDEGGER P [1987] 'Steady uniform flow in prismatic channels with flood plains', Journal. of Hydraulic Research., Volume. 25, pp 169 - 185
32. DEPARTMENT OF TRADE AND INDUSTRY (DTI) guidelines [1994] 'Best Practice Guidelines for Developing Neural Computing Applications', Touche Ross for DTI
33. EINSTEIN H A and BANKS R B, [1950]. Fluid Resistance of composite roughness, Transactions, American Geophysical Union, Volume 31, No 4, pp 606-610.
34. ELLIOTT S and SELLIN R H J [1990] SERC Flood Channel Facility - Skewed Flow Experiments, Journal of Hydraulic Research, Volume 28, No 2, pp 197 - 214.
35. ERVINE A and MACLEOD B [1996] 'Initial report on flooding and flood control on the River Dane at Northwich, Cheshire', Development Land Holdings, February 1996
36. ERVINE D A and BAIRD J 1 [1982] Rating Curves for Rivers with Overbank Flow, Proceedings of the Institution of Civil Engineers, Part 2, 73, June, pp 465,472.
37. ERVINE D A and ELLIS J [1987] Experimental and Computational Aspects of Overbank Flood Plain Flow, Transactions of the Royal Society of Edinburgh : Earth Sciences, 78, pp 315,325.

38. ERVINE D A and JASEM H K [1995] 'Observations on flows in skewed compound flows', Proceedings. of Institution. of Civil. Engineers., Volume. 112, No 3, pp 249 - 259
39. ERVINE D A, WILLETTS B B, SELLIN R H J AND LORENA M [1993] 'Factors affecting conveyance in meandering compound flows', Journal of Hydraulic Eng., Volume. 119, No 12, December, pp 1383 - 1398
40. FARES Y[1989] ' Flow mechanisms in meander cut-off', Ph.D. thesis, University of Glasgow
41. FLOOD I and KARTAM N [1994] 'Neural Networks in Civil engineering. 1: Principles and understanding', Journal. of Computing in Civil. Eng., Volume. 8, No. 2, pp 131 - 148
42. FLOOD I and KARTAM N [1994] 'Neural Networks in Civil engineering. 2: systems and applications', Journal. of Computing in Civil. Eng., Volume. 8, No. 2, pp 149 - 162
43. FORMICA [1955] 'Preliminary test on head losses in channels due to cross-sectional changes', L'Energia elettrica (In Italian), Milano, Vol. 32, No. 7, pp554-568, July
44. FRENCH R H [1986] 'Open channel hydraulics', McGraw-Hill, Singapore.
45. FUJITA M, MICHIUE M and HINOKIDANI O [1991] 'Mathematical simulation of flow and suspended load in open channels with a trench', Proc. of Hydraulic engineering, Japanese society of Civil engineers, 35.
46. FUKUOKA S and FUJITA K [1990] 'Prediction method of flow Resistance in rivers with compound channels and application to river course design', Proceedings. of International. Conference. on river flood hydraulics, pp 113 - 122, 17th September.
47. GABOR D [1960] 'A universal non-linear filter, predictor and simulator which optimises itself by a learning process', Proceedings of the Institution of Electrical engineers (London), Vol. 108, pp 442
48. GARRETT J H [1994] 'Where and why Artificial Neural Networks are applicable in Civil engineering: Editorial', Journal. of Computing in Civil. Eng., Volume. 8, No. 2, pp 129 - 130
49. GREENHILL R K [1992] An Investigation into Compound Meandering Channel Flow, PhD thesis, Department of Civil Engineering, University of Bristol.
50. GREENHILL R K and SELLIN R H J [1993] Development of a Simple Method to Predict Discharges in Compound Meandering Channels, Proceedings. Institution. Civil. Engineers, Water., Maritime & Energy, 101, pp 37-44, Paper 10012.
51. GRUBERT [1995] 'Prediction of Estuarine instabilities with artificial neural networks', Jrnl of Computing in Civil Engineering, Vol. 9, pp 266-274
52. HAYKIN S [1995] 'Neural Networks: A comprehensive Introduction', Maxwell Macmillan International, New York
53. HEY R D and THORNE C R [1986] 'Stable channels with mobile gravel beds', Journal of Hydraulic Engineering, , Vol.112, No.8, pp.671-689
54. HEY R D [1978] 'Determinate hydraulic geometry of river channels', Journal of Hydraulics Division., ASCE, Volume.104, pp 869 - 885, June.
55. HEY R, [1979] 'Flow Resistance in gravel-bed rivers.', Journal. of the hydraulics Division, Volume. 105, No. HY4, pp 365-379.

58. HEY R D [1986] 'River mechanics', J. IWEM , pp 139 - 157

59. HEY R D [1988] 'Mathematical models of channel morphology', Chapter. 5, Modelling geomorphological systems, J Wiley & sons, New York.

60. HEY R D [1990] ' Environmental River Engineering' Journal. IWEM, Volume 4, August

61. HIGGINSON ET AL. [1990] 'Effect of scale distortion in a compound river channel model study', Proceedings. of International. Conference. on River flood hydraulics, Sept. 1990, pp 391-401

62. HIGGINSON N and JOHNSTON H [1988] 'Estimation of friction factor in natural streams', Paper G1, Conference on River Regime, Hydraulics Research Ltd., pp 251-266

63. HIGGINSON N J, JOHNSTON H T and MYERS W R C [1990] The Effect of Scale Distortion in a Compound River Channel Model Study, Paper L2, Proceedings of the International Conference on River Flood Hydraulics, Wallingford, England, 17,20th Sept.

64. HECHT-NEILSON R [1990] 'Neuro-computing', Addison Wesley

65. HOLDEN A P and JAMES C S [1988] 'Discharge computation for compound channels', The Civil engineer in South Africa, pp371 - 376

66. HOLDEN A P and JAMES C S [1989] Boundary Shear Distribution on Flood Plains, Journal of Hydraulic Research, Vol. 27, No 1.

67. HOOKE J M [1987] 'Changes in meander morphology', Proceedings. of Conference on geomorphology, pp 591-605,J Wiley and sons

68. HOOKE J M and HARVEY A M [1983] 'Meander changes in relation to bend morphology and secondary flows', Special Publications. Int. Assoc. of Sedimentologists, Volume. 6, pp 121 - 132

69. HOPFIELD J [1982] 'Neural Networks and physical systems with emergent collective computational facilities', Proc. of the National Academy of Sciences of the USA, Vol. 84, pp8429 - 8433

70. HORTON R E [1933] Separate Roughness Coefficients for Channel Bottom and Sides, Engineering News-Record, Vol. 111, No 22, pp 652-653.

71. HOUSE M A and SANGSTER E K [1991] 'Public perception of river corridor management', Journal. IWEM, Volume 5, pp 312 - 317, June

72. HR Wallingford [1992] Phase A & B Flood Channel Facility Manual, Final Report, HR Wallingford, Report EX 2606 [July]

73. IPPEN A T and DRINKER P A [1962] 'Boundary shear stress in curved trapezoidal channels', Journal of Hydraulic. Division., September, pp143 - 179

74. JAMES and BROWN [1977] Geometric Parameters that Influence flood plain Flow, Hydraulics Laboratory, U S Army Engineer Waterways Experiment Station, Vicksburg, Miss.

75. JAMES C and WARK J [1992] 'Conveyance estimation in Meandering channel", Report SR329, HR Wallingford

76. JAMES C S [1994] 'Evaluation of methods for predicting bend loss in meandering channels', Journal of Hydraulic Eng., ASCE, Volume 120, pp245 - 253,February

77. JANSEN P [1979] 'Principles of river engineering', Pitman, London

78. JASEM H [1990] 'Flow in Skew compound channels', Ph.D. Thesis, University of Glasgow

79. JAYARANTNE B L, TU H, TAMAI N and KAN K [1995] 'Unsteady flow Characteristics in Compound Channels with Vegetated Flood Plains', Proceedings. of IAHR Conference. HYDRA 2000, London, pp 379-384

80. KARUNANITHI N and GRENNEY W [1994] 'Neural networks for river flow prediction', Journal. of Computing in Civil. Eng., Volume. 8, No. 2, pp 129 - 130

81. KAWAHARA Y and TAMAI N [1989] 'Mechanism of lateral momentum transfer in compound channel flows', Proc. of the 23rd IAHR Congress, Ottawa, Aug.

82. KAZEMIPOUR A K and APELT C J [1979] Shape Effects on Resistance to Uniform Flow in Open Channels, Journal of Hydraulic Research, Vol. 17, No 2, pp 129A4&

83. KAZENUPOUR A and APELT I J [1983] Energy Losses in Irregular Chann6, Journal of Hydraulic Engineering, Vol. 109, No 10, pp 1374-1379.

84. KELLER R [1995] 'Prediction of the stable form of meandering compound channels', Monash University, Personal communication

85. KELLER R J and RODI W [1988] 'Prediction of Flow Characteristics in Main Channel/Flood Plain Flows', Journal of Hydraulic Research, Vol. 26, No 4.

86. KIELY G [1989] 'An Experimental study of Overbank Flow in Straight and Meandering Compound Channels', PhD Thesis, Dept of Civil Engineering, University College, Cork.

87. KIELY G [1989] 'Experimental Study of the Mechanisms of Flood Flow in Meandering Channels', Proceedings of the 23rd IAHR Congress, Ottawa, Canada, August.

88. KIELY G [1990] 'Overbank Flow in Meandering Channels the Important Mechanisms', Proceedings of the International Conference on River Flood Hydraulics, Wallingford, 17-20 September.

89. KIELY G, JAVAN M and McKEOGH E J [1989] 'A Comparison of Turbulence Measurements in Straight, Single Meander and Multiple Meander Channels', International. Conference. on Channel Flow and Catchment Runoff, Centennial of Manning's and Kuichlings Rational Formula, University of Virginia, May.

90. KIM J, KLINE S J and JOHNSTON J P [1980] 'Investigation of a re-attaching turbulent shear layer: Flow over a backward facing step', Jrnl. Of Fluids engineering, ASME, Vol. 102, pp 302 - 308

91. KNIGHT A C E [1988] 'Rationalised energy-loss parameters for channels', Journal of Hydraulic Eng., ASCE, Volume 114, pp757 - 765

92. KNIGHT D and DEMETRIOU J, [1983] 'Flood plain and main channel flow interaction.', Journal. of hydraulic engineering, Volume. 109, No. 8, pp1073-1091

93. KNIGHT D and HAMED M, [1984] 'Boundary shear in symmetrical compound channels.', Journal. of Hydraulic engineering, Volume. 110, No. 10, pp 1412-1427

94. KNIGHT D W and SAMUELS P G [1989] 'River Flow Simulation: Research and Developments', Paper 18, I@M Annual Conference.

95. KNIGHT D W and SELLIN R H J [1987] 'The SERC Flood Channel Facility', Journal of the Institution of Water and Environmental Management, Vol. 1, No 2, pp 198-204.

96. KNIGHT D W and SHIONO K [1990] 'Turbulence measurements in a shear layer region of a compound channel', Journal of Hydraulic Research, Volume 26, No 4., pp 175 - 190

97. KNIGHT D W, DEMETRIOU J D and HAMED M E [1983] Hydraulic Analysis of Channels with Flood Plains, Int. Congress Hydraulic Aspects of Floods and Flood Control, September 13-15.

98. KNIGHT D W and LAI C J [1985] 'Turbulent Flow in Compound Channels and Ducts', International. Symp. on 'Refined Flow Modelling and Turbulence Measurements', Iowa, U S A, Sept.

99. KNIGHT D W, SHIONO K and PIRT J [1989] 'Prediction of Depth Mean Velocity and Discharge in Natural Rivers with Overbank Flow', International Conference of Coastal, Estuarine and River Waters, Bradford, England, 19-21 Sept .

100. KNIGHT D W, YUAN Y M and FARES Y R [1992] 'Boundary Shear in Meandering Channels', Proceedings of the. Int. Symposium. on Hydraulic Research in Nature and Laboratory, Wuhan, China, November, 1992.

101. KNIGHT D W and CAO S [1994] 'Boundary shear in the vicinity of river banks', ASCE Conference on Hydraulic engineering, Buffalo, New York, August 1994

102. KOLOSEUS H and DAVIDIAN J, [1958] 'Roughness-concentration effects on flow over hydro-dynamically rough surfaces - laboratory studies of open-channel flow'., Paper 1592-D, Geological survey water-supply, pp 1-21

103. KRISNAMURTHY M and CHRISTENSEN B A [1972] 'Equivalent Roughness for Shallow Channel's, Journal of Hydraulics Division, ASCE, Vol. 98, HY12, pp 2257-2262.

104. KRISHNAPPAN B G and LAU Y L [1986] 'Turbulence Modelling of Flood Plain Flows', Journal of Hydraulic Engineering, Vol. 112, No 4.

105. KURKOVA V [1991] 'Kolmogrov's theorem is relevant', Neural Computation', Vol. 3, pp 617 - 622

106. LAMBERT M and SELLIN R, [1995] 'Velocity distribution in a large scale model of a doubly meandering compound river channel.', Paper 10655, May, pp 1-38

107. LAURENSON E [1986] 'Friction slope averaging in Backwater calculations', Journal. of Hydraulic Eng. ASCE, Volume. 112, pp 1151 - 1163

108. LEAN G H and WEARE J T [1979] 'Modelling Two Dimensional Circulating Flow', Journal Hydraulic Division, Proceedings of the ASCE, Vol. 105, No HV I.

109. LEOPOLD L, BAGNOLD R, WOLMAN M and BRUSH L Jnr., [1960] 'Flow Resistance in sinuous or irregular channels.', Paper 282-D, Geologic survey professional paper, pp 111-133

110. LIMINEROS J T [1970] 'Determination of the manning coefficient from measured bed roughness in Natural channels', Geological Survey water-supply paper 1898-B, Washington

111. LORENA M [1993] 'Meandering compound channels', Ph.D thesis, University of Glasgow

112. LOTTER G K [1933] 'Considerations on Hydraulic Design of Channels with Different Roughness of Walls', Transactions, All-Union Scientific Research Institute, Leningrad, Vol. 9, pp 238-241.

113. LYNESS J F, MYERS W R C and WARK J B [1995] 'A comparative study of the use of the lateral distribution method in modelling flood hydrographs in a compound channel', Proceedings. of IAHR Conference. HYDRA 2000, London, pp 302-307

114.MANSON J R [1994] 'The development of a predictive Procedure for localised three dimensional river flow', Ph.D. Thesis, University of Glasgow

115.MARTIN L A and MYERS W R C [1993] 'Measurement of overbank flow in a compound river channel', Proceedings of the Institution Civil. Engineers Water. Maritime & Energy Volume 101, pp 191 - 193

116.MASON J.C., PRICE R.K. AND TEM'ME A [1996] 'A neural network prediction model of rainfall-runoff using radial basis functions', Jrnl of Hydraulic Research, pp 537-548

117.McCULLOCH W. S. and PITTS W. H. [1943] 'A logical calculus of ideas immanent in nervous activity', Bulletin of Mathematical Biophysics, Vol. 5, pp 115 - 133.

118.McKEOGH E J and KIELY G [1989] 'A Comparison of Velocity Measurements in Straight, Single meander and Multiple Meander Channels', International. Conference. on Channel Flow and Catchment Runoff, Centennial of Manning's and Kuichlings Rational Formula, University of Virginia, May.

119.McKEOGH E J, KIELY G K and JAVAN M [1989] 'Velocity and Turbulence Measurements in a Straight Channel with Interacting flood plains using Laser Doppler Anemometry', Hydraulic & Environment Modelling of Coastal Estuarine and River Waters, Proceedings of the International. Conference, Bradford, 19-21 Sept, pp 429,440.

120.MINNS A W [1995] 'Analysis of experimental data using artificial neural networks', Proceedings. of IAHR Conference. HYDRA 2000, London, 1995, pp 218 - 223

121.MINSKY M L and PAPERT S A [1969] 'Perceptrons', Cambridge MA: MIT Press

122.MULHALL T [1995] 'How much data is needed to train a neural network', Neural Edge, 8, pp 4-5

123.MYERS W R C [1978] 'Momentum Transfer in a Compound Channel', Journal Hydraulic Research, Vol. 16, No2.

124.MYERS W R C [1982] 'Flow Resistance in wide rectangular channels', Journal. of the Hydraulic Division., ASCE, Volume. 108, No HY4, April, pp 471 - 482

125.MYERS W R C [1984] 'Frictional Resistance in channels with flood plains', Proceedings. of 1st International. Conference. on Channels and Channelled control structures, Apr. 1984, pp 73-87

126.MYERS W R C [1987] 'Velocity and Discharge in Compound Channels', Journal of Hydraulic Engineering, Vol. 113, No 6, pp 753,766.

127.MYERS W R C [1990] 'Physical Modelling of a compound River Channel', Proceedings of the International Conference on River Flood Hydraulics, Wallingford, England, 17,20th Sept.

128.MYERS W R C and BRENNAN E K [1990] 'Flow Resistance in compound channels', Journal of Hydraulic Research, Volume. 28, pp 141 - 156

129.MYERS W R C and ELSAWY E N4 [1975] 'Boundary Shear in Channel with flood plain', Journal Hydraulic Division, Proceedings of the, ASCE, Vol. 101, No HY7.

130.NAISH C [1995] 'Towards the development of a discharge prediction method for doubly meandering compound channels', Proceedings. 30th MAFF Conference. of river and coastal engineers, Keele University, 5-7 July

131.NAISH C and SELLIN R H J [1994] 'Scale effects in the hydraulic modelling of compound river channels', Proceedings of the 2nd International conference on hydraulic modelling, Stratford-upon-Avon, pp361-377, 14-16 June

132.NAISH C and SELLIN R H J [1995] 'Scaling of hydraulic roughness for small and large scale river models', Proceedings. of IAHR Conference. HYDRA 2000, London, pp 111-116

133.NAOT D, NEZU I and NAKAGAWA H [1993] 'Calculation of compound open channel flow', Journal. of Hydraulic Eng. ASCE, Volume. 119, no. 12, Dec., pp 1418 - 1426

134.NASH J.E. [1957] 'The form of the instantaneous unit hydrograph', IASH, Pub. No. 45, 3, pp114-121

135.NATIONAL RIVERS AUTHORITY (NRA) [1991] 'Design Method for Straight Compound Channels', R&D Note 44, NRA.

136.NATIONAL RIVERS AUTHORITY (NRA) [1993] 'Flood Defence Strategy', NRA publication.

137.NATIONAL RIVERS AUTHORITY (NRA) [1996] 'Large scale model investigation of a two-stage channel', R&D Note 211.

138.NATURAL ENVIRONMENT RESEARCH COUNCIL (NERC) [1975] 'Flood Studies report', Vol. I and II.

139.NEZU I and RODI W [1985] 'Experimental study on secondary currents in open channel flows', 21st IAHR Congress, Melbourne.

140.NEZU I, TOMINAGA A and NAKAGAWA H [1993] 'Field measurements of secondary currents in straight rivers', Journal of Hydraulic Engineering, May 1993, Vol.119, No.5, pp.598-614

141.NEZU I, [1994] 'Compound open-channel turbulence and its role in river environment - significance of secondary currents.', Ninth congress of the Asian and pacific Division of the international association for hydraulic Research, Singapore

142.NEZU I, KADOTA A and NAKAGAWA H [1995] 'Turbulent Structures of free shear layer over cavity using fibre-optic L.D.A.', Proceedings. of IAHR Conference. HYDRA 2000, London, pp 397-402

143.NEZU I, NAKAGAWA H and ABE T [1995] 'Secondary currents and exchange Processes in compound open-channel flows', Proceedings. of IAHR Conference. HYDRA 2000, London, pp 45-50

144.NGUYEN D and WIDROW B [1990] 'Improving the learning speed of 2-layer neural networks by choosing initial values of adaptive weights', International Joint Conference of Neural Networks, Vol. 3, pp 21 - 26, July

145.PASCHE E and ROUVE G [1985] 'Overbank Flow with Vegetatively Roughened Flood Plains', Journal Hydraulic Engineering, Vol. 111, No 9.

146.PASCHE E, ARNOLD A and ROUVE G [1986] 'Review of Overbank Flow Models', Advancements in Aerodynamics, Fluid Mechanics and Hydraulics, ASCE, June 3-6, Minneapolis, Minnesota.

147.PENDER G [1985] 'The numerical modelling of tide and flood movement in two-dimensional space using implicit finite difference methods', Ph.D. Thesis, University of Strathclyde, Scotland

148.PENDER G, KEOGH D, MANSON J and ADDISON P [1995] 'Verification of a three-dimensional river flow model with experimental data', Proceedings. of IAHR Conference. HYDRA 2000, London, pp 290-295

149.PENNING -ROWSELL E.C. and CHATTERTON J.[1977] 'Benefits of flood alleviation: a manual of assessment techniques' Farnborough, Saxon House, ISBN -x-10-013528-4

150.PREISSMAN A [1960] 'Propagation des Intumescneces dans les Canaux et Rivieres', Proceedings of the 1st Congres de l'Association Francaise de Calcul', Grenoble, France, pp433 - 442

151.PRINOS P and TOWNSEND R D [1983] 'Estimating Discharge in Compound Open Channels', in Proceedings of the 6th Canadian Hydro-technical Conference, Ottawa, Canada. R D Townsend [Ed] Vol. 1, ppl29-146.

152.PRINOS P and TOWNSEND R D [1984] 'Comparison of Methods for Predicting Discharge in Compound Channels', Proceedings of the 1st International Conference on Channels and Channel Control Structures, Southampton.

153.PRINOS P, TOWNSEND R and TAVOULARIS S [1985] 'Structure of Turbulence in Compound Channel Flows, Journal Hydraulic Engineering, Vol. 111, No 9.

154.PRINOS P [1990] 'Turbulence Modelling of Main Channel - flood plain Flows with an algebraic stress model', Proceedings of the of International Conference. on River Flood Hydraulics, Wallingford, pp 164- 172.

155.PURSEGLOVE J. [1989] 'Taming the flood: a history and natural history of rivers and wetlands', Oxford University Press.

156.QUICK M C [1991] 'Reliability of flood discharge estimates', Canadian Journal of Eng., Volume 18, pp 624 - 630

157.RADOJKOVIC B E and DJORDJEVIC B E [1985] 'Computation of Discharge Distribution in Compound Channels', 21st IAHR Congress, Melbourne, Australia, 19,23rd Aug.

158.RAJARATNAM N and AHMADI R M [1979] 'Interaction between main channel and flood plain flows', Journal of Hydraulic Division., Volume. 105, No HY5, pp 573 - 587

159.RAJARATNAM N and AHMADI R M [1981] 'Meandering channels with flood plains', Journal of Hydraulic Research, Volume 19, No 1.

160.RAMSBOTTOM D M [1989] 'Flood Discharge Assessment', Interim Report, Hydraulics Research Ltd, Report SR 195, March.

161.RHODES D G [1995] 'Newton-Raphson solution for gradually varied flow', Paper, Journal. Hydraulic. Research, Volume. 33, no. 2, pp 213-218.

162.ROCHESTER [1956] 'Tests on a cell assembly theory of the action of the brain using a large digital computer', IRE Transactions on Information theory, pp80-93

163.ROUSE H [Ed] [1950] 'Engineering Hydraulics', John Wiley and Sons, New York.

164.ROUVE G and SCHRODER M [1993] 'One - Dimensional Vs Two - Dimensional prediction of compound channel flow', Proceedings. of 1st Inter. Conference. on Hydraulic-science and engineering, Volume. 1, part B, pp 1197 - 1205.

165.ROSENBLATT F [1958] 'The Perceptron: A probabilistic model for information storage and organisation in the brain', Psychological review, Vol. 65, pp 386 - 408.

166.ROZOVSKII I L [1957] 'Flow of Water in Bends of Open Channels', The National Science Foundation Washington D C, The Israel Program for scientific translations

167.RUELLE D [1989] 'Chaotic evolution and strange attractors' Cambridge University press, New York

168.RUMELHART D and McCELLAND J [1986] 'Parallel Distributed Processing', Vols. 1 and 2, Cambridge, MA: the MIT press.

169.SAMUELS P G [1985] 'Modelling of River and Flood Plain Flow using the Finite Element Method', PhD D Thesis, Department of Mathematics, Univ. of Reading

170.SAMUELS P G [1988] 'Lateral Shear Layers in Compound Channels', International. Congress on Fluvial Hydraulics, Budapest

171.SAMUELS P G [1988] 'Stability limits for Preissman's scheme', Journal Hydraulic Engineering, ASCE, Nov.

172.SAMUELS P G [1989] 'Backwater lengths in rivers' Proceedings. Institution Civil. Engineers. Volume 87, pp 571 - 582

173.SAMUELS P G [1989] 'Some Analytical Aspects of Depth Averaged Flow Models', International. Conference Hydraulic and Environmental Modelling of Coastal, Estuarine and River Waters, Bradford, England, 19-21, Sept.

174.SAMUELS P G [1989] 'The hydraulics of two-stage channels - review of current knowledge', Conference. of river engineers, University of Loughborough

175.SAMUELS P G [1990] 'Computation of critical depth in symmetric compound channels.', Discussion, Journal. of hydraulic Research, Volume. 28, No. 1, pp121-123

176.SAMUELS P G [1990] 'Cross-section location in 1-D models', Proceedings. of the International. Conference. in River flood hydraulics, Sept., pp 339 - 350

177.SAMUELS P G [1995] 'Uncertainty in flood level prediction', Proceedings. of IAHR Conference. HYDRA 2000, part 1, pp 567 - 572

178.SARGENT R J [1981] 'Variation of Manning's n roughness coefficient with flow in open river channels' Journal. IWEM, Volume. 4, pp290 - 295, December

179.SEARLE [1985] 'Investigation of the River Roding', Ph.D. Thesis, University of Bristol.

180.SELLIN R H J [1964] 'A Laboratory Investigation into the Interaction Between the Flow in the Channel of a River and that over its Flood Plain', La Houille Blanche/No 7.

181.SELLIN R H J [1990] ' River Roding appraisal', University of Bristol report

182.SELLIN R H J [1991] 'Flow mechanisms in spilling meander channels', Proceedings. of the 1st Conference of river and flood hydraulics

183.SELLIN R H J [1991] 'Towards the identification of flow mechanisms in channels of complex geometry', Proceedings. of 14th Congress of IAHR in Madrid, Sept, pp 1 - 8

184.SELLIN R H J [1995] 'Hydraulic performance of a skewed two-stage flood channel', Journal. of Hydraulic Research., Volume. 33, No. 1, pp 43 - 62

185.SELLIN R H J [1995] 'Turbulent flow Structures and velocity distribution in a two-stage channel bend', Proceedings. of IAHR Conference. HYDRA 2000, London, pp 27-32

186.SELLIN R H J and WILLETTS B [1996] 'Three-dimensional flow and compound channels', Macmillan press

187.SELLIN R H J, ERVINE D A, WILLETTS B B [1993] 'Behaviour of Meandering Two-stage Channels', Proceedings. Institution of Civil Engineers., Water., Maritime & Energy, 101, pp 99-11 1, Paper 10 1 06.

188.SELLIN R H J, GILES A and VAN BEESTEN D P [1990] 'A Post Implementation Appraisal of a Two Stage Channel in the River Roding, Essex', Report submitted to The Thames Division NRA.

189.SERIES B [1993] 'Flow data from the SERC Series A programme: Skew compound channels', University of Bristol

190.SERIES B [1994] 'Flow data from the SERC Series B programme: Meandering compound channels', University of Bristol

191.SHAW E. M AND LYNN P.P. [1972] 'Area rainfall evaluation using two surface fitting techniques', Bulletin IAHS, Vol. 17 (4), pp419-431

192.SHIONO K [1993] 'Numerical modelling for inbank and overbank flows in natural rivers', Proceedings. of 1st Int. Conf. on Hydro-science and engineering, Vol. 1, part B, pp 1265 - 1270

193.SHIONO K and KNIGHT D W [1988] 'Two Dimensional Analytical Solution for a Compound Channel', Third International. Symposium Refined Flow Modelling and Turbulence Measurements Tokyo, Japan, July.

194.SHIONO K and KNIGHT D W [1990] 'Mathematical Models of Flow in Two or Multi-Stage Straight Channels', River Flood Hydraulics Conference, Wallingford, England, 17,20th Sept.

195.SMITH C D [1978] 'Effect of channel meanders on flood stage in valley', Journal. of the Hydraulic Division., ASCE, Volume. 104, No HY1, April, pp 49 - 58

196.SMITH C D [1989] 'Some aspects of flood plain flow in a valley with a meandering channel', Proceedings. of the IAHR Conference., Canada 1989, Fluid hydraulics, pp B355 - B370

197.SMITH G D [1986] Numerical Solution of Partial Differential Equations - Finite Difference Methods, Third Edition Clarendon Press, Oxford.

198.SOIL CONSERVATION SERVICE (SCS) [1963] 'Guide for selecting Roughness Coefficient 'n' Values for Channels', US Department of Agriculture, Soil Conservation Services, Washington.

199.STEIN C J and ROUVE [1989] '2D Depth-Averaged Numerical Predictions of the Flow in a Meandering Channel with Compound Cross Section', Hydrosoft, Vol. 2, No 1, pp 2,7.

200.STEIN C J and ROUVE G [1988] '2D-LVU-Technique for Measuring Flow in a Meandering Channel with Wetted Flood Plains - A New Application and First Results', Proceedings International Conference on Fluvial Hydraulic Budapest, June, pp 5,10.

201.STEPHENSON D and KOLOVOPOULOS [1990] 'Effects of momentum transfer in compound channels', Journal. of Hydraulic Eng., Volume. 116, No 12, pp 1512 - 1522, December

202.SWINGLER K [1996] 'Applying Neural networks: A practical guide', Harcourt Brace and Company, ISBN 0-12-679170-8

203.THOMAS T G and WILLIAMS J R [1995] 'Large eddy simulation of a symmetric trapezoidal channel and flood plain', Proceedings. of IAHR Conference. HYDRA 2000, London, pp 39- 43

204.TOEBES G H and SOOKY A A [1967] 'Hydraulics of meandering rivers with flood plains', Jrnl. of Waterways and Harbours Div., Proc. ASCE, Vol. 93, No WW2, pp213 - 237

205.TOMINAGA A, NEZU I and KOBATAKE [1989] 'Experimental and Numerical Investigations on Turbulent Structure in Compound Open-Channel Flow', Hydro-comp 89, Dubrovnik, Yugoslavia, 13-16th June, pp 244,254

206.TOMINAGA A, and NEZU I [1991] 'Turbulent structure in compound open-channel flows', Journal of Hydraulic Engineering, Jan 1991, Vol.117, No.1, pp.21-41.

207.TOMINAGA A, NAGAO M and NEZU I [1994] 'Experimental study on unsteady flow in open channels with flood plains', Proceedings of the Symposium on fundamentals and advancements in Hydraulic measurements and experimentation, ASCE, pp 396-405

208.TOMINAGA A, LIU J, NAGAO M and NEZU I [1995] 'Hydraulic characteristics of unsteady flow in open channels with flood plains', Proceedings. of IAHR Conference. HYDRA 2000, London, pp 373 - 378

209.TU H, JAYARATNE B L, TAMAI N [1995] 'Velocity Measurements in Unsteady compound Open-Channel Flows', Proceedings. of IAHR Conference. HYDRA 2000, London, pp 385-390

210.UTTLEY A M [1956] 'A theory of the mechanisms of learning based on the compilation of conditional probabilities', Proceedings of the 1st International conference on Cybernetics, Namur, Gauthier-Villars, Paris

211.VICKSBURG [1956] - 'Hydraulic Capacity of Meandering Channels in Straight Floodways', Corps of Engineers US Army, Waterways Experiment Station, Vicksburg, Mississippi,, CWL ITEM 807.

212.WARK J B , JAMES C S and ACKERS P [1994] 'Design of Straight and Meandering channels', R&D Report 13, N.R.A, Rivers House, Bristol, BS12 4UD.

213.WARK J B [1988] 'The Equations of River and Flood plain Flow', A Technical Report submitted to the Dept of Civil Engineering, The University of Glasgow, Dec.

214.WARK J B, SAMUELS P G and ERVINE D A [1990] 'A Practical Method of Estimating Velocity and Discharge in Compound Channels', International Conference on River Flood Hydraulics, Wallingford, Oxfordshire, Sept.

215.WARK J B, RAMSBOTTOM D M and SLADE J E [1991] 'Flood Discharge assessment by the Lateral Distribution Method', Report SR 277, HR Wallingford.

216.WARK J B [1993] 'Discharge assessment in straight and meandering compound channels', Ph.D. Thesis, University of Glasgow

217.WARK J B and JAMES C S [1994] 'An application of a new Procedure for estimating discharges in meandering overbank flows to field data', Proceedings. of the 2nd International. Conference. on river flood hydraulics, J Wiley and sons, pp 405 - 414

218.WIDROW B and HOFF M E [1960] 'Adaptive switching circuits', 'IRE WESCOM' convention record, pp 96 - 104.

219.WILLETTS B B and HARDWICK R I [1993] 'Stage Dependency for Overbank Flow in Meandering Channels', Proceedings. Institution. Civil. Engineers., Water., Maritime & Energy, 101, pp 4554, Paper 10049.

220.WILLETTS B B, ERVINE A D and SELLIN R H J [1993] 'Hydraulics of meandering rivers with adjacent flood plain flow', Proceedings. of 1st Inter. Conference. on Hydro-science and engineering, Volume. 1, part B

221.WILLETTS B B, HARDWICK R I and MACLEAN A G [1990] 'Model Studies of Overbank How from a Meandering Channel', Proceedings of International Conference on River Flood Hydraulics, Wallingford, 17-20 September.

222.WORMLEATON P R , ALLEN J and HADJIPANOS P [1982] 'Discharge assessment in compound channel flow', Journal. of the Hydraulic Division., ASCE, Volume. 108, No HY9, September, pp 975-994

223.YEN B C and YEN C L [1983] 'Flood Flow over Meandering Channels', Proceedings, Rivers '83, River Meandering, ASCE, pp 554-561.

224.ZELLER J [1967] 'Meandering channels in Switzerland', Int. Assoc. Sci. Hydrol., Vol. 75, pp 174 - 186.

225.ZHELEZNYAKOV G V [1965] 'Relative deficit of mean velocity of unstable river flow, kinematic effect in river beds with flood plains', Proc. of 11th Int. Conf. Of IAHR, Leningrad

BIBLIOGRAPHY

1. ACKERS P [1993] 'Hydraulic Design of Two-Stage Channels', Proceedings of the Institution of Civil Engineers, Water, Maritime & Energy, 1992, 96, Dec, pp 247-257.
2. ACKERS P [1993] 'Stage - Discharge for Two-stage channels: The impact of new Research', Journal of IWEM, Volume. 7, pp 52 - 61
3. ANGOLD P G , GURNELL A M and EDWARDS P [1995] 'Information from river corridor surveys', Journal. CIWEM, Volume 9, pp 491 - 498, October
4. ARNOLD U, HOTTAGES J and ROUVE G [1988] 'Combined Digital Image and Finite Element Analysis of Mixing in Compound Open Channel Flow', Proceedings of the 3rd International Symposium Refined How Modelling and Turbulence Measurements, Tokyo.
5. ARNOLD U, PASCHE E, and ROUVE G [1985] 'Mixing in Rivers with compound cross-section', 21st IAHR Congress, Melbourne, Australia, pp 168,172.
6. ARNOLD U, STEIN J and ROUVE G [1989] 'Sophisticated Measurement Techniques for Experimental Investigation of Compound Channel Flow', Hydro-Comp 89, Dubrovnik, Yugoslavia, 13-16th June 89, pp 11,21.
7. BABOVIC V [1995] 'Genetic model induction based on experimental data', Proceedings. IAHR of Conference. HYDRA 2000, London, 1995, pp 212 - 217
8. BAGERELLO B V , FERRO V ET AL [1995] 'Experimental study on flow Resistance law for small diameter plastic pipes', Journal of Irrigation and Drainage Engineering, pp 313 - 316, October
9. BARBARUTSI S, GANOULIS J and CHU V H [1989] 'Experimental investigation of shallow re-circulating flows', Journal. of Hydraulic. Engineering, Volume 115, No 7, pp 906 - 924,July
10. BASARA B and YOUNIS B A [1995] 'Prediction of turbulent flows in dredged trenches', Journal of Hydraulic Research., Volume 33, No 6, pp 813 - 824
11. BATHURST J C [1996] 'Field measurement of boulder flow drag', technical note, Journal. of Hydraulic Engineering, Volume. 122, no. 3, pp 167-169
12. BETTESS R and WHITE W R [1983] 'Meandering and braiding of alluvial channels', Proceedings. of the Institution of Civil Engineers., Volume 75, pp 525 - 538, Sept.
13. BOWMAN M.A., ACREMAN M.L. and PACKMAN J.C. [1990] 'Review of design flood estimation using the FSR rainfall runoff method', Inst. Of Hydrology report, No. 111
14. CAIRNCROSS A M [1990] 'Health impacts in developing countries: New evidence and new prospects', Journal. IWEM, Volume. 4, pp571 - 577, December
15. CHADWICK A and MORFETT J [1986] 'Hydraulics in Civil Engineering', Allen and Unwin, London, ISBN 0-04-627004-3.
16. CHANG H [1988] 'Fluvial Processes in River Engineering', John Wiley and Sons Inc. ISBN 0-471-63139-6.
17. CHOUDHARY M S [1989] 'Simonette river crossing: Extreme flood experience', Canadian Journal of Civil. Engineering, pp 36 - 65
18. CHU V H and BARBARUTSI S [1988] 'Confinement and bed-friction effects in shallow turbulent mixing layers', Journal. of Hydraulic Engineering, Volume 114, No 10, pp 1257 - 1274

19. CHURCH M [1983] 'Pattern of instability in a wandering gravel bed river', Special Publications. International. Association of Sedimentologists, Volume. 6, pp 169 - 180
20. DARBY S E and THORNE C R [1995] 'Prediction of tension crack location and riverbank erosion hazards along destabilised channels', Earth surface Processes and Landforms, Vol. 19, pp 233 - 245
21. DESHENG J and SCHUMM S A [1986] 'A new technique of modelling river morphology', Proceedings. of Conference. on International geomorphology, pp 681 - 690, J Wiley and sons
22. DJORDJEVIC J, PETROVICI J, MAKSIMOVIC C and RADOJKOVIC M [1989] 'Experimental Tracer Investigations in a Compound Laboratory Channel', Hydro-Comp 89, Dubrovnik, Yugoslavia, 13-16th June pp 269-278.
23. DOWNS P W [1995] 'Estimating the probability of river channel adjustment', Earth surface Processes and Landforms, Volume 20, pp 687 - 705
24. DUMA D and GHINDA T [1993] 'A mathematical model for overbank flows in compound channels', Proc. of 1st Int. Conf. on Hydro-science and engineering, Vol. 1, part B, pp 1257 - 1264
25. FALCONER R A [1977] 'Mathematical Modelling of Jet-Forced Circulation in Reservoirs and Harbours', PhD D Thesis, Dept Civil Engineering, Imperial College, London.
26. FERRO V and BAIAMONTE G [1994] 'Flow velocity profiles in gravel-bed rivers', paper, Journal. of Hydraulic engineering, Volume. 120 no.1, pp 60-80
27. FUJITA I, KANDA T, MORITA T and KADOWAKI M [1995] 'Numerical and image analyses of turbulent flow in open channel trench', Proceedings. of IAHR Conference. HYDRA 2000, London, pp 284-289
28. FUKUHARA T and MUROTA A [1990] 'Discharge Assessment in Compound Channel with flood plain roughness, Paper E2, Proceedings of the International Conference on River Flood Hydraulics, Wallingford, England, 17,20th Sept.
29. FUKUOKA S and FUJITA K [1990] 'Prediction method of flow Resistance in rivers with compound channels and application to river course design', Proceedings. of International. Conference. on river flood hydraulics, pp 113 - 122, 17th September.
30. GARCIA M, LOPEZ F AND NINO Y [1995] 'Characterisation of near-bed coherent structures in turbulent open channel flow using synchronised high-speed video and hot film measurements', Experiments in fluids, Volume 19, pp16 - 28
31. GEE D M [1990] 'Large flood plain modelling', Earth surface and Landforms, Vol. 15, pp 513 - 523
32. GOGUS M and ALTINBILEK D, [1994] 'Flow-measurement structures of compound cross section for rivers.', Journal. of irrigation and drainage engineering, Volume. 120, No. 1., pp 110-127
33. GOH A [1995] 'Evaluation of seismic liquefaction using neural networks', Proceedings. of 6th International. Conference. on Civil and structural engineering computing, Cambridge, Publication by Civil - Comp, August, pp 121 - 125
34. GOH A, WONG K and BROMS B [1995] 'Multivariate modelling of FEM data using neural networks', Proceedings. of 6th International. Conference. on Civil and structural engineering computing, Cambridge, Publication. by Civil - comp, August, pp 59 - 64

35. GONCHAROV V N [1962] 'Dynamics of channel flow', Israeli Progress. of Science. Trans., Jerusalem.

36. GOVINDARAJU R S [1992] 'A simplified model for two-dimensional overland flows', Advances in Water Resources, Volume. 15, pp 133 - 141

37. GUPTA A [1983] 'High-magnitude floods and stream channel Response', Special Publications. International. Assoc. of Sedimentologists, Volume. 6, pp 219 - 227

38. HALL M.J. AND HOCKIN D.L. [1980] 'Guide to the design of storage ponds for flood control in partially urbanised catchment areas', CIRIA Tech. Note 100, pp103

39. HAYAT S [1965] 'The Variation of Loss Coefficient with Froude Number in an Open Channel Bend', Thesis presented to the University of Iowa in partial fulfilment of the requirements for the degree of Master of Science.

40. HAYKIN S [1995] 'Neural Networks: A comprehensive Introduction', Maxwell Macmillan International, New York

41. HEAPS N S [1969] 'A Two-dimensional Numerical Sea Model', Philosophical Transactions of the Royal Society Vol. 265, pp 93,137.

42. HENDERSON F M [1966] 'Open Channel Flow', Macmillan, New York.

43. HIGGINS G M , DIELEMAN P J and ABERNETHY C L [1987] 'Trends in irrigation and development and their implications for hydrologists and water Resources engineers', Journal of Hydraulic Research., Volume 87, pp 393 - 406

44. HR WALLINGFORD [1988] 'Assessing the Hydraulic Performance of Environmentally Acceptable Channels', Report EX 1799, HR Wallingford, September.

45. HR Wallingford [1991] 'Phase A & B Flood Channel Facility Manual', Inception Report, HR Wallingford, Report EX 2485 [November]

46. HR Wallingford [1992] 'Phase A & B Flood Channel Facility Manual', Interim Report, HR Wallingford, Report EX 2548 [March]

47. HUNTER S C [1983] 'Mechanics of Continuous Media', 2nd Edition Ellis Horwood Ltd, Chichester, Sussex ISBN 0-470-27384-4.

48. ISHIGAKI T, IMAMOTO H and SHIONO K [1995] 'Coherent structure near the side-wall in open channel flow', Proceedings. of IAHR Conference. HYDRA 2000, London, pp 182-187

49. JAYAWARDENA A and FERNO D [1995] 'Artificial neural networks in hydro-meteorlogical modelling', Proceedings. of 6th International. Conference. on Civil and structural engineering computing, Cambridge, Publication. by Civil - comp, August, pp 115 - 120

50. JIA Y [1990] 'Minimum Froude number and equilibrium of alluvial sand rivers', Earth surface and Landforms, Volume. 15, pp 199 - 209

51. JIONGXIN X [1990] 'An experimental study of complex Response in river channel adjustment downstream from a Reservoir', Earth surface and Landforms, Volume. 15, pp 43 - 53

52. JORDAAN J M Jnr., SCHUTTE S P [1995] 'Form drag of a single recess in a flow boundary', Proceedings. of IAHR Conference. HYDRA 2000, London, pp 403-408

53. KAO J [1996] 'Neural net for determining DEM-based model drainage pattern', Journal. of Irrigation. and Drainage Engineer, April, pp 112 - 121
54. KAWAHARA Y and TAMAI N [1989] 'Proposal of a new algebraic stress model and it applications to compound channel flow', 33rd Japanese conference on Hydraulics, p236-241
55. KELLERHALS R, CHURCH M, BRAY D [1976] 'Classification and analysis of river Processes.', Journal of the Hydraulic Division., Volume. 102 No HY7, pp 813 -827
56. KIKKEWA H, IKEDA S and KITAGAWA A [1976] 'Flow and Bed Topography in Curved Open Channels', Journal of the Hydraulics Division, ASCE, Vol. 102, No HY9, pp 1327-1342.
57. KIRKGOZ M S [1989] 'Turbulent velocity profiles for smooth and rough open channel flow', Journal of Hydraulic Eng., ASCE, Volume 115, pp1543 - 1561
58. KNIGHT D W [1996] 'River channel and flood plain hydraulics', SHSG study group, 18th January, Glasgow
59. KNIGHTON A D and CRYER R [1990] 'Velocity-Discharge relationships in three lowland rivers', Earth surface and Landforms, Volume. 15, pp 501 - 512
60. KONEMANN N [1982] 'Minimum specific energy in compound open channels', Journal. of Hydraulic Eng. ASCE, March, pp 462 - 464
61. KUIPERS and VREUGDENHIL C B [1973] 'Calculation of 2-Dimensional Horizontal Flow', Delft Hydraulics Laboratory, Report S163 part 1.
62. LEHENY R L [1995] 'Simple model for river network', Physical Review E, Volume 52, No 5, pp 5610 - 5620, November
63. LUBINSKI K S [1995] 'A review of mathematical models of river planform changes', Earth surface Processes and Landforms, Volume 20, pp 661 - 670
64. MACBEAN E, PENEL J and SIU K L [1984] 'Uncertainty analysis of a delineated flood plain', Canadian Journal. of Civil. Engineer, Volume. 11, pp 387 - 395
65. MCCARTNEY M P and NADEN P S [1995] 'A Semi-empirical investigation of the influence of flood-plain storage on flood flow', paper, CIWEM, no. 9, pp 239-246
66. MILES G V and WEARE T J [1973] 'On the Representation of Friction in two-dimensional Numerical Models', Numerical Methods in Fluid Dynamics, Proceedings of the International. Conference Univ. of Southampton, England, 26-28 Sept.
67. MIRAJGAOKER A G and CHARLU K L N [1963] 'Natural roughness effects in rigid open channels', Journal of Hydraulic Division., ASCE, Volume 89, pp29 - 44, September
68. MOCKMORE C A [1944] 'Flow Around Bends in Stable Channels', Transactions, ASCE, Vol. 109, pp 593-618.
69. MOSSELMAN E [1995] 'Challenges and objectives for Geomorphology in UK river management', Earth surface Processes and Landforms, Volume 20, pp 137 - 138
70. NALLURI C and JUDY N [1989] 'Flow characteristics in compound channels with vegetated flood plains.', Paper, pp 1-11 complete.
71. ODGAARD A J [1984] 'Shear induced secondary currents in channel flows', Journal of Hydraulic Eng.,

72. ODGAARD J A [1984] 'Flow and Bed Topography in Alluvial Channel Bend', Journal Hydraulic Engineering, Vol. 110, No 4, April.

73. ODGAARD J A [1986] 'Meander Flow Model 1: Development', Journal Hydraulic Engineering, Vol. 112, No 12, Dec.

74. OGINK H J M [1985] 'The Effective Viscosity Coefficient in 2-D Depth Averaged Flow Models', 21st IAHR Congress, Melbourne, Australia.

75. OKOYE J K [1970] 'Characteristics of Transverse Mixing in Open Channel Flows', California Institute of Technology, Pasadena, California, Report No KE-R-23, Nov.

76. ONISHI Y, JAIN S C and KENNEDY J F [1976] 'Effects of Meandering in Alluvial Streams', Journal of the Hydraulics Division, ASCE, Vol. 102, No HY7.

77. PETRYK S and GRANT E U [1978] 'Critical flow in rivers with flood plains', Journal. of Hydraulic Division., Volume. 104, pp 583 - 594

78. PRINOS P [1989] 'Experiments and Numerical Modelling in Compound Open Channel and Duct Flows', Hydro-Comp 89, Dubrovnik, Yugoslavia, 13-16th June, pp 255061

79. RANGA RAJU, K G [1970] 'Resistance relations for alluvial streams', La Houille Blanche, No 1.

80. RHODES D G and KNIGHT D W [1995] 'Lateral shear in a compound duct', Proceedings. of IAHR Conference. HYDRA 2000, London, pp 51-56

81. SATISH M G, GUO Y and RAHMAN M [1991] 'Computation of uniform flow in open channels with flood plains', Canadian Journal of Eng., Volume 18, pp 149 - 155

82. SCHOEMAKER H J [1991] 'Discussion of Series A papers', Journal of Hydraulic Research, Volume 29, No 2., pp 259 - 277

83. SCHRODER M, STEIN C and ROUVE G, [1991] 'Application of the 3D-LDV-Technique on physical model of meandering channel with vegetated flood plain.', 4th International Conference on Laser Anemometry - advances and applications, USA, pp1-9

84. SEAR D A, NEWSON M D and BROOKES A [1995] 'Sediment-related river maintenance: The role of fluvial morphology', Earth surface Processes and Landforms, Volume 20, pp 629 - 647

85. SHUKRY A [1950] 'Flow around Bends in an Open Flume', Transactions ASCE, Vol. 115, pp 75L788.

86. SIMON A [1995] 'Adjustment and recovery of unstable alluvial channels: Identification and approaches for engineering management', Earth surface Processes and Landforms, Volume 20, pp 611 - 628

87. SMART G, [1992]. 'Stage-discharge discontinuity in composite flood channels.', Journal. of Hydraulic Research, Volume. 30, No.6, pp 817-833, discussion pp 574-576

88. TAMAI N and KAWAHARA Y [1989] 'Mechanism of lateral momentum transfer in compound channel flows', Proceedings. of the 1st Conference.. of river and flood hydraulics, PP B463 - 470

89. THORNE C R and THIAGARAJAH R I [1992] 'Future trends and needs in hydraulics', Discussion, Journal of Hydraulic engineering, Volume. 118, no 12, pp 672-677 [closure by Simons D B]

90. TOKYAY N D [1994] 'Computation of discharge and critical depth in compound channels', Proceedings. of the 2nd International. Conference. on river flood hydraulics, J Wiley and sons, pp 393 - 403

91. TONG G D [1982] 'Computation of Turbulent Re-circulating Flow', PhD Thesis, Dept Civil Engineering, Univ. College of Swansea, Univ. of Wales C/Ph/63/82.

92. VAZIRI M [1995] 'Predicting the Caspian sea surface water level using artificial neural networks', Proceedings. of IAHR Conference. HYDRA 2000, London, 1995, pp 556 - 560

93. VREUGDENHIL C B, WUBENGA J H A [1982] 'Computation of Flow Patterns in Rivers', Journal Hydraulic Division, ASCE, Vol. 108, No HY II, Nov.

94. WHARTON G [1995] 'The channel-geometry method: Guidelines and applications', Earth surface Processes and Landforms, Volume 20, pp 649 - 660

95. WHITE W R, BETTESS R and PARIS E [1982] 'Analytical approach to river regime, Journal of Hydraulic Division., Volume. 108, pp 1179 - 1193

96. WILLETTS B B [1992] 'The hydraulics of overbank flow in meandering rivers', Seminar on Multiple Stage Channels, HR Wallingford Ltd., Wallingford, UK.

97. WORDEN K, BALL A and TOMLINSON G [1993] 'Fault location in a framework using neural networks', Smart materials and Structures, Volume. 2, pp 189 - 199

98. WORMLEATON P R [1988] 'Determination of Discharge in Compound Channels using the Dynamic Equation for Lateral Velocity Distribution', International Conference on Fluvial Hydraulics, Budapest.

99. WORMLEATON P R and MERRET D J [1990] 'An improved method of calculation for steady uniform flow in prismatic main channel/flood plain sections', Journal of Hydraulic Research, Volume. 28, pp 157 - 174

100. WORMLEATON P R, and HADJIPANOS P [1985] 'Flow Distribution in Compound Channels', Journal of Hydraulic. Engineering, ASCE, 11 1[2] pp357-361.

101. YEN B C [1971] 'Spatially Varied Open Channel Flow Equations', Department of the Interior, Washington, D C.

102. YEN C and WENZEL C [1970] 'Dynamic Equations for Steady Spatially Varied Flow', Journal Hydraulic Division, ASCE, Vol. 96, No HY3

103. YUEN K W H and KNIGHT D W [1990] 'Critical Flow in a Two Stage Channel', Paper G4, Proceedings of the International. Confer on River Flood Hydraulics, Wallingford, England, 17,20th Sept

104. ZAGHLOUL N [1992] 'A computer model to calculate flow Resistance in open channels with moveable boundaries', Advances in engineering software, Volume. 14, pp 273 - 283

105. ZENG P [1995] 'Artificial Neural Network computing in structural engineering', Proceedings. of 6th International. Conference. on Civil and structural engineering computing, Cambridge, Publication. by Civil - comp, August, pp 37 - 50

Appendix A1: The Series B extension programme in Glasgow Flow data for the whole cross-section

Institution :	**University of Glasgow**
Geometry :	G75T90S
Test No. :	1
Main channel sinuosity :	1.3740 (60^0)
Main channel top width :	0.2m
Main channel aspect ratio :	2.6700
Main channel bank side slope :	90^0 (Trapezoidal)
Main channel cross-sectional shape :	Trapezoidal
Main channel Roughness :	Smooth
Flood plain sinuosity :	1.0
Flood plain roughness :	Smooth
Flood plain lateral slope :	0.0
Flood plain longitudinal slope :	1/1000
Meander belt width : flood plain width :	1.018m/1.650m
Flow :	Inbank / Overbank
Water temperature :	25^0C
Test date :	Summer 1994
File name:	G75T90S.xls

Depth (m)	Dr	Qm (m^3/s)	A(m^2)	R	Re	n	F*	Qm/ Qbf	f	C	k
								Qbf = 0.0044			
0.0427	-0.452	0.0018	0.0085	0.0299	28353	0.0123		0.4091	0.0385	45.2	0.0008
0.0463	-0.408	0.0021	0.0093	0.0316	32265	0.0119		0.4773	0.0351	47.3	0.0006
0.0566	-0.282	0.0029	0.0113	0.0361	40908	0.0117		0.6477	0.0326	49.1	0.0006
0.0654	-0.176	0.0035	0.0131	0.0395	47565	0.0117		0.7955	0.0315	49.9	0.0006
0.0747	-0.066	0.0043	0.0149	0.0428	55326	0.0115		0.9773	0.0295	51.6	0.0005
0.0800	0.063	0.0037	0.0233	0.0128	9190	0.0095	0.6391	0.8409	0.0303	50.9	-0.0001
0.0833	0.100	0.0043	0.0287	0.0158	10557	0.0119	0.6179	0.9695	0.0446	41.9	0.0006
0.0850	0.118	0.0046	0.0315	0.0173	11362	0.0130	0.6058	1.0455	0.0513	39.1	0.0011
0.0872	0.140	0.0053	0.0351	0.0193	13060	0.0137	0.6146	1.2045	0.0547	37.9	0.0015
0.0890	0.157	0.0060	0.0381	0.0208	14756	0.0139	0.6274	1.3636	0.0552	37.7	0.0017
0.0930	0.194	0.0079	0.0447	0.0243	19344	0.0139	0.6615	1.7955	0.0526	38.6	0.0018
0.0950	0.211	0.0089	0.0480	0.0261	21745	0.0140	0.6706	2.0227	0.0518	38.9	0.0018
0.0985	0.239	0.0108	0.0538	0.0291	26287	0.0140	0.6831	2.4545	0.0500	39.6	0.0019
0.1010	0.257	0.0123	0.0579	0.0313	29857	0.0139	0.6917	2.7955	0.0484	40.2	0.0019
0.1030	0.272	0.0135	0.0612	0.0330	32700	0.0140	0.6942	3.0682	0.0477	40.6	0.0019
0.1100	0.318	0.0177	0.0728	0.0389	42552	0.0142	0.6839	4.0227	0.0470	40.9	0.0022
0.1103	0.320	0.0179	0.0732	0.0391	43021	0.0142	0.6851	4.0682	0.0467	41.0	0.0022
0.1158	0.352	0.0215	0.0822	0.0437	51371	0.0144	0.6756	4.8864	0.0462	41.2	0.0024
0.1175	0.362	0.0225	0.0851	0.0452	53661	0.0146	0.6668	5.1136	0.0468	41.0	0.0026
0.1190	0.370	0.0235	0.0876	0.0464	55957	0.0146	0.6633	5.3409	0.0467	41.0	0.0026
0.1210	0.380	0.0249	0.0909	0.0480	59165	0.0147	0.6599	5.6591	0.0465	41.1	0.0027
0.1250	0.400	0.0280	0.0975	0.0513	66251	0.0147	0.6584	6.3636	0.0454	41.6	0.0027
0.1280	0.414	0.0300	0.1025	0.0538	70760	0.0148	0.6481	6.8182	0.0458	41.4	0.0029
0.1314	0.429	0.0330	0.1080	0.0565	77560	0.0147	0.6511	7.5000	0.0443	42.1	0.0028
0.1350	0.444	0.0360	0.1140	0.0594	84292	0.0147	0.6478	8.1818	0.0437	42.4	0.0028
0.1400	0.464	0.0400	0.1223	0.0633	93173	0.0149	0.6386	9.0909	0.0436	42.4	0.0030

Appendix A1 Flow data for the whole cross-section (Series B extension, Glasgow)

Institution :	**University of Glasgow**
Geometry :	G75T90R
Test No. :	2
Main channel sinuosity :	1.3740 (60^0)
Main channel top width :	0.2m
Main channel aspect ratio :	2.6700
Main channel bank side slope :	90^0 (Trapezoidal)
Main channel cross-sectional shape :	Trapezoidal
Main channel Roughness :	Smooth
Floodplain sinuosity :	1.0
Floodplain roughness :	Rough B
Floodplain lateral slope :	0.0
Floodplain longitudinal slope :	1/1000
Meander belt width : floodplain width :	1.018m/1.650m
Flow :	Inbank / Overbank
Water temperature :	25^0C
Test date :	Summer 1994
File name:	G75T90R.xls

Depth (m)	Dr	Qm (m^3/s)	A(m^2)	R	Re	n	F*	Qm/ Qbf	f	C	k
						So		Qm =	0.0044		
0.0373	-0.503	0.0014	0.0075	0.0272	22920	0.0130		0.3182	0.0441	42.2	0.0012
0.0427	-0.431	0.0018	0.0085	0.0299	28353	0.0123		0.4091	0.0385	45.2	0.0008
0.0463	-0.383	0.0021	0.0093	0.0316	32265	0.0119		0.4773	0.0351	47.3	0.0006
0.0566	-0.245	0.0029	0.0113	0.0361	40908	0.0117		0.6477	0.0326	49.1	0.0006
0.0654	-0.128	0.0035	0.0131	0.0395	47565	0.0117		0.7955	0.0315	49.9	0.0006
0.0747	-0.004	0.0043	0.0149	0.0428	55326	0.0115		0.9773	0.0295	51.6	0.0005
0.0820	0.0854	0.0034	0.0266	0.0146	8426	0.0129	0.6740	0.7727	0.0534	38.3	0.0010
0.0857	0.1249	0.0039	0.0327	0.0179	9626	0.0161	0.6640	0.8864	0.0779	31.7	0.0033
0.0890	0.1573	0.0048	0.0381	0.0208	11805	0.0171	0.7033	1.0909	0.0837	30.6	0.0046
0.0942	0.2038	0.0065	0.0467	0.0254	15895	0.0180	0.7461	1.4773	0.0866	30.1	0.0060
0.0990	0.2424	0.0085	0.0546	0.0295	20678	0.0181	0.7822	1.9318	0.0828	30.8	0.0065
0.1015	0.2611	0.0097	0.0587	0.0317	23485	0.0180	0.7971	2.2000	0.0801	31.3	0.0065
0.1060	0.2925	0.0118	0.0662	0.0355	28490	0.0181	0.8023	2.6818	0.0779	31.7	0.0069
0.1108	0.3231	0.0143	0.0741	0.0396	34349	0.0180	0.8028	3.2500	0.0750	32.3	0.0071
0.1135	0.3392	0.0160	0.0785	0.0418	38322	0.0178	0.8112	3.6364	0.0716	33.1	0.0068
0.1165	0.3562	0.0178	0.0835	0.0443	42377	0.0178	0.8073	4.0341	0.0701	33.5	0.0069
0.1191	0.3703	0.0193	0.0878	0.0465	45975	0.0178	0.8025	4.3886	0.0689	33.7	0.0070
0.1217	0.3837	0.0206	0.0921	0.0486	48912	0.0180	0.7850	4.6818	0.0700	33.5	0.0076
0.1250	0.4000	0.0225	0.0975	0.0513	53237	0.0182	0.7716	5.1136	0.0697	33.5	0.0079
0.1275	0.4118	0.0240	0.1016	0.0533	56637	0.0182	0.7625	5.4545	0.0694	33.6	0.0082
0.1315	0.4297	0.0264	0.1082	0.0566	62041	0.0184	0.7466	6.0000	0.0693	33.7	0.0086
0.1325	0.4340	0.0270	0.1099	0.0574	63384	0.0185	0.7424	6.1364	0.0693	33.7	0.0088
0.1368	0.4518	0.0296	0.1170	0.0608	69177	0.0187	0.7248	6.7273	0.0695	33.6	0.0094
0.1400	0.4643	0.0320	0.1223	0.0633	74538	0.0186	0.7222	7.2727	0.0678	34.0	0.0092
0.1428	0.4748	0.0338	0.1269	0.0655	78503	0.0187	0.7125	7.6818	0.0678	34.0	0.0096
0.1455	0.4845	0.0360	0.1313	0.0677	83380	0.0185	0.7124	8.1818	0.0662	34.4	0.0094

Appendix A1 Flow data for the whole cross-section (Series B extension, Glasgow)

Institution :	**University of Glasgow**
Geometry :	GR75T90R
Test No. :	3
Main channel sinuosity :	1.3740 (60^0)
Main channel top width :	0.2m
Main channel aspect ratio :	2.6700
Main channel bank side slope :	90^0 (Trapezoidal)
Main channel cross-sectional shape :	Trapezoidal
Main channel Roughness :	Rough B
Floodplain sinuosity :	1.0
Floodplain roughness :	Rough B
Floodplain lateral slope :	0.0
Floodplain longitudinal slope :	1/1000
Meander belt width : floodplain width :	1.018m/1.650m
Flow :	Inbank / Overbank
Water temperature :	25^0C
Test date :	Autumn 1995
File name:	GR75T90R.xls

Depth (m)	Dr	Qm (m^3/s)	A(m^2)	R	Re	n	F*	Qm/ Qbf	f	C	k
						So		Qbf =	0.0028		
0.0495	-0.340	0.0014	0.0099	0.0331	21050	0.0197		0.5072	0.0946	28.8	0.0094
0.0556	-0.259	0.0017	0.0111	0.0357	25136	0.0187		0.6304	0.0834	30.7	0.0080
0.0672	-0.104	0.0023	0.0134	0.0402	30921	0.0185		0.8333	0.0784	31.6	0.0079
0.0730	-0.027	0.0027	0.0146	0.0422	34821	0.0178		0.9710	0.0715	33.1	0.0068
0.0803	0.0660	0.0024	0.0237	0.0131	5959	0.0152	0.6836	0.8696	0.0764	32.0	0.0022
0.0830	0.0964	0.0028	0.0282	0.0155	6808	0.0179	0.6872	0.9964	0.1003	28.0	0.0048
0.0867	0.1349	0.0035	0.0343	0.0188	8629	0.0198	0.7143	1.2681	0.1155	26.1	0.0076
0.0879	0.1468	0.0038	0.0363	0.0199	9430	0.0199	0.7303	1.3877	0.1152	26.1	0.0080
0.0908	0.1740	0.0046	0.0411	0.0224	11315	0.0206	0.7455	1.6703	0.1177	25.8	0.0094
0.0960	0.2188	0.0064	0.0497	0.0270	15620	0.0206	0.7774	2.3188	0.1108	26.6	0.0102
0.1003	0.2522	0.0083	0.0567	0.0307	20139	0.0200	0.8067	3.0036	0.1001	28.0	0.0097
0.1028	0.2704	0.0093	0.0609	0.0328	22531	0.0201	0.8012	3.3696	0.0987	28.2	0.0102
0.1080	0.3056	0.0115	0.0695	0.0372	27706	0.0203	0.7816	4.1667	0.0967	28.5	0.0111
0.1127	0.3345	0.0138	0.0772	0.0412	33081	0.0202	0.7708	5.0000	0.0927	29.1	0.0114
0.1170	0.3590	0.0160	0.0843	0.0447	38179	0.0202	0.7570	5.7971	0.0899	29.5	0.0117
0.1211	0.3807	0.0181	0.0911	0.0481	43003	0.0203	0.7391	6.5580	0.0886	29.8	0.0122
0.1263	0.4062	0.0210	0.0996	0.0524	49620	0.0203	0:7214	7.6087	0.0862	30.2	0.0126
0.1305	0.4253	0.0232	0.1066	0.0558	54578	0.0205	0.7003	8.4058	0.0864	30.1	0.0135
0.1329	0.4357	0.0251	0.1105	0.0577	58899	0.0201	0.7064	9.0942	0.0822	30.9	0.0127
0.1371	0.4530	0.0275	0.1175	0.0610	64249	0.0203	0.6889	9.9638	0.0821	30.9	0.0134
0.1405	0.4662	0.0296	0.1231	0.0637	68912	0.0203	0.6786	10.725	0.0813	31.1	0.0137
0.1454	0.4842	0.0323	0.1312	0.0676	74818	0.0207	0.6568	11.703	0.0824	30.9	0.0150
0.1515	0.5050	0.0360	0.1412	0.0723	82868	0.0209	0.6382	13.043	0.0825	30.8	0.0160
0.1569	0.5220	0.0397	0.1501	0.0765	90883	0.0210	0.6299	14.384	0.0812	31.1	0.0164
0.1618	0.5365	0.0429	0.1582	0.0802	97720	0.0211	0.6203	15.543	0.0811	31.1	0.0172
0.1660	0.5482	0.0465	0.1652	0.0833	105472	0.0209	0.6243	16.848	0.0782	31.7	0.0166
0.1683	0.5544	0.0482	0.1689	0.0850	109075	0.0209	0.6227	17.464	0.0778	31.8	0.0168
0.1723	0.5647	0.0521	0.1755	0.0880	117427	0.0205	0.6316	18.877	0.0744	32.5	0.0158
0.1750	0.5714	0.0541	0.1800	0.0900	121606	0.0206	0.6298	19.601	0.0743	32.5	0.0161
0.1790	0.5810	0.0581	0.1866	0.0929	130077	0.0203	0.6389	21.051	0.0715	33.1	0.0153

Appendix A1 Flow data for the whole cross-section (Series B extension, Glasgow)

Institution :	**University of Glasgow**
Geometry :	G75T60R
Test No. :	4
Main channel sinuosity :	1.3740 (60^0)
Main channel top width :	0.2m
Main channel aspect ratio :	3.4000
Main channel bank side slope :	60^0 (Trapezoidal)
Main channel cross-sectional shape :	Trapezoidal
Main channel Roughness :	Smooth
Floodplain sinuosity :	1.0
Floodplain roughness :	Rough B
Floodplain lateral slope :	0.0
Floodplain longitudinal slope :	1/1000
Meander belt width : floodplain width :	1.018m/1.650m
Flow :	Inbank / Overbank
Water temperature :	25^0C
Test date :	Spring 1995
File name:	G75T60R.xls

Depth (m)	Dr	Qm (m^3/s)	A(m^2)	R	Re	n	F*	Qm/ Qbf	f	C	k
						So		Qm =	0.0031		
0.0550	-0.232	0.0018	0.0080	0.0332	32724	0.0127		0.5645	0.0395	44.6	0.0011
0.0605	-0.166	0.0021	0.0090	0.0355	37298	0.0124		0.6774	0.0370	46.1	0.0009
0.0655	-0.108	0.0024	0.0099	0.0374	40767	0.0125		0.7742	0.0364	46.4	0.0009
0.0741	-0.010	0.0030	0.0116	0.0407	47401	0.0123		0.9677	0.0346	47.6	0.0009
0.0829	0.1185	0.0029	0.0248	0.0141	7310	0.0142	0.6791	0.9194	0.0654	34.6	0.0016
0.0833	0.1238	0.0029	0.0254	0.0145	7435	0.0146	0.6774	0.9355	0.0686	33.8	0.0019
0.0851	0.1467	0.0031	0.0284	0.0162	7931	0.0166	0.6601	1.0000	0.0850	30.4	0.0036
0.0874	0.1743	0.0036	0.0322	0.0183	9186	0.0177	0.6775	1.1613	0.0937	28.9	0.0050
0.0898	0.2012	0.0043	0.0362	0.0205	10943	0.0182	0.7097	1.3871	0.0947	28.8	0.0057
0.0927	0.2315	0.0052	0.0410	0.0231	13190	0.0186	0.7330	1.6774	0.0957	28.6	0.0067
0.0950	0.2540	0.0060	0.0448	0.0252	15154	0.0188	0.7470	1.9323	0.0951	28.7	0.0072
0.0956	0.2596	0.0062	0.0457	0.0257	15675	0.0189	0.7493	2.0000	0.0951	28.7	0.0074
0.0981	0.2822	0.0074	0.0499	0.0280	18656	0.0184	0.7866	2.3871	0.0873	30.0	0.0068
0.1019	0.3141	0.0090	0.0561	0.0313	22468	0.0186	0.7898	2.8871	0.0861	30.2	0.0074
0.1064	0.3483	0.0110	0.0636	0.0353	27476	0.0187	0.7899	3.5484	0.0834	30.7	0.0079
0.1087	0.3645	0.0122	0.0674	0.0373	30396	0.0186	0.7932	3.9355	0.0810	31.1	0.0079
0.1089	0.3659	0.0124	0.0677	0.0375	30887	0.0184	0.7994	4.0000	0.0795	31.4	0.0076
0.1109	0.3793	0.0134	0.0710	0.0392	33304	0.0185	0.7950	4.3226	0.0787	31.6	0.0078
0.1146	0.4026	0.0155	0.0771	0.0424	38367	0.0183	0.7944	5.0000	0.0756	32.2	0.0078
0.1148	0.4039	0.0156	0.0774	0.0426	38606	0.0183	0.7934	5.0323	0.0756	32.2	0.0078
0.1179	0.4220	0.0175	0.0825	0.0453	43160	0.0182	0.7931	5.6452	0.0728	32.8	0.0077
0.1202	0.4348	0.0189	0.0863	0.0472	46496	0.0181	0.7892	6.0968	0.0715	33.1	0.0077
0.1226	0.4476	0.0203	0.0903	0.0493	49809	0.0182	0.7809	6.5484	0.0709	33.3	0.0079
0.1248	0.4588	0.0218	0.0939	0.0511	53362	0.0181	0.7799	7.0323	0.0692	33.7	0.0078
0.1255	0.4622	0.0221	0.0951	0.0517	54006	0.0182	0.7723	7.1226	0.0700	33.5	0.0081
0.1273	0.4710	0.0232	0.0980	0.0532	56512	0.0183	0.7650	7.4677	0.0698	33.5	0.0083
0.1302	0.4844	0.0251	0.1028	0.0557	61080	0.0182	0.7595	8.0968	0.0684	33.9	0.0083
0.1334	0.4985	0.0275	0.1081	0.0583	66689	0.0181	0.7585	8.8710	0.0662	34.4	0.0080

Appendix A1 Flow data for the whole cross-section (Series B extension, Glasgow)

Institution :	**University of Glasgow**
Geometry :	G75T45R
Test No. :	5
Main channel sinuosity :	1.3740 (60^0)
Main channel top width :	0.2m
Main channel aspect ratio :	4.2600
Main channel bank side slope :	45^0 (Trapezoidal)
Main channel cross-sectional shape :	Trapezoidal
Main channel Roughness :	Smooth
Floodplain sinuosity :	1.0
Floodplain roughness :	Rough B
Floodplain lateral slope :	0.0
Floodplain longitudinal slope :	1/1000
Meander belt width : floodplain width :	1.018m/1.650m
Flow :	Inbank / Overbank
Water temperature :	25^0C
Test date :	Summer 1995
File name:	G75T45R.xls

Depth (m)	Dr	Qm (m^3/s)	A(m^2)	R	Re	n	F*	Qm/ Qbf	f	C	k
						So		Qm =			
								0.0023			
0.0487	-0.304	0.0009	0.0048	0.0256	20353	0.0133		0.3778	0.0468	41.0	0.0013
0.0524	-0.261	0.0011	0.0054	0.0271	23815	0.0124		0.4667	0.0404	44.1	0.0009
0.0567	-0.210	0.0013	0.0060	0.0288	26712	0.0123		0.5556	0.0385	45.2	0.0008
0.0658	-0.105	0.0017	0.0076	0.0323	31416	0.0126		0.7333	0.0393	44.7	0.0010
0.0705	-0.051	0.0019	0.0085	0.0341	34248	0.0127		0.8444	0.0389	44.9	0.0010
0.0743	-0.008	0.0022	0.0092	0.0355	38017	0.0122		0.9778	0.0357	46.9	0.0008
0.0815	0.1218	0.0022	0.0201	0.0117	5734	0.0131	0.7215	0.9778	0.0594	36.3	0.0010
0.0837	0.1558	0.0024	0.0236	0.0137	6239	0.0159	0.6898	1.0667	0.0833	30.7	0.0028
0.0872	0.2065	0.0030	0.0295	0.0170	7767	0.0187	0.6851	1.3333	0.1072	27.1	0.0060
0.0903	0.2461	0.0038	0.0346	0.0199	9803	0.0195	0.7104	1.6889	0.1105	26.7	0.0074
0.0948	0.2964	0.0053	0.0420	0.0240	13604	0.0195	0.7533	2.3556	0.1035	27.5	0.0080
0.0979	0.3282	0.0067	0.0472	0.0268	17212	0.0187	0.7978	2.9911	0.0921	29.2	0.0072
0.1000	0.3478	0.0076	0.0506	0.0287	19391	0.0187	0.8032	3.3778	0.0898	29.6	0.0074
0.1018	0.3638	0.0086	0.0536	0.0304	21897	0.0182	0.8268	3.8222	0.0835	30.7	0.0068
0.1041	0.3830	0.0096	0.0574	0.0324	24380	0.0183	0.8219	4.2667	0.0826	30.8	0.0071
0.1073	0.4080	0.0112	0.0627	0.0353	28341	0.0182	0.8231	4.9778	0.0793	31.5	0.0071
0.1111	0.4351	0.0132	0.0689	0.0386	33260	0.0181	0.8191	5.8667	0.0762	32.1	0.0072
0.1204	0.4920	0.0187	0.0843	0.0468	46632	0.0179	0.8048	8.3111	0.0695	33.6	0.0071
0.1250	0.5161	0.0215	0.0919	0.0507	53342	0.0179	0.7888	9.5556	0.0680	34.0	0.0074
0.1347	0.5602	0.0286	0.1079	0.0589	70205	0.0175	0.7788	12.711	0.0619	35.6	0.0070
0.1419	0.5880	0.0341	0.1198	0.0649	83053	0.0174	0.7659	15.156	0.0593	36.4	0.0069
0.1500	0.6154	0.0404	0.1331	0.0715	97541	0.0175	0.7490	17.956	0.0577	36.9	0.0072

Appendix A1 Flow data for the whole cross-section (Series B extension, Glasgow)

Institution :	**University of Glasgow**
Geometry :	G75T45RN
Test No. :	6
Main channel sinuosity :	1.3740 (60^0)
Main channel top width :	0.2m
Main channel aspect ratio :	4.2600
Main channel bank side slope :	45^0 (Trapezoidal)
Main channel cross-sectional shape :	Trapezoidal
Main channel Roughness :	Smooth
Floodplain sinuosity :	1.0
Floodplain roughness :	Rough B
Floodplain lateral slope :	0.0
Floodplain longitudinal slope :	1/1000
Meander belt width : floodplain width :	1.018m/1.018m
Flow :	Inbank / Overbank
Water temperature :	25^0C
Test date :	Autumn 1995
File name:	G75T45RN.xls

Depth (m)	Dr	Qm (m^3/s)	A(m^2)	R	Re	n	F*	Qm/Qbf	f	C	k
						So		Qm =	0.0023		
0.0487	-0.304	0.0009	0.0048	0.0256	20353	0.0133		0.3778	0.0468	41	0.0013
0.0524	-0.261	0.0011	0.0054	0.0271	23815	0.0124		0.4667	0.0404	44.1	0.0009
0.0567	-0.21	0.0013	0.006	0.0288	26712	0.0123		0.5556	0.0385	45.2	0.0008
0.0658	-0.105	0.0017	0.0076	0.0323	31416	0.0126		0.7333	0.0393	44.7	0.001
0.0705	-0.051	0.0019	0.0085	0.0341	34248	0.0127		0.8444	0.0389	44.9	0.001
0.0743	-0.008	0.0022	0.0092	0.0355	38017	0.0122		0.9778	0.0357	46.9	0.0008
0.0833	0.1509	0.0016	0.0094	0.0059	4670	0.0194	0.5392	0.7289	0.1638	21.9	0.0041
0.0863	0.1942	0.0019	0.0094	0.0059	5249	0.0226	0.5277	0.8222	0.2216	18.8	0.0062
0.0907	0.2509	0.0024	0.0094	0.0059	6828	0.0242	0.5527	1.0756	0.2538	17.6	0.0073
0.093	0.2775	0.0029	0.0094	0.0059	8018	0.0239	0.5793	1.2667	0.2479	17.8	0.0071
0.096	0.3094	0.0033	0.0094	0.0058	9249	0.0246	0.5777	1.4667	0.2642	17.2	0.0076
0.0995	0.3433	0.0042	0.0094	0.0058	11581	0.0235	0.6141	1.8444	0.2419	18	0.0069
0.103	0.374	0.0049	0.0094	0.0058	13698	0.0234	0.6216	2.1911	0.2386	18.1	0.0067
0.1053	0.3926	0.0055	0.0094	0.0058	15238	0.0231	0.6271	2.4444	0.2339	18.3	0.0065
0.1065	0.4019	0.006	0.0094	0.0058	16599	0.0223	0.65	2.6667	0.2169	19	0.006
0.1085	0.4168	0.0065	0.0094	0.0058	17938	0.0222	0.6481	2.8889	0.2165	19	0.0059
0.1125	0.4444	0.0075	0.0094	0.0057	20652	0.0222	0.6402	3.3422	0.2167	19	0.0059
0.116	0.4666	0.0085	0.0094	0.0057	23244	0.0221	0.6354	3.7778	0.2144	19.1	0.0058
0.1185	0.4813	0.0093	0.0094	0.0057	25354	0.0218	0.6364	4.1333	0.2094	19.4	0.0056
0.1202	0.4909	0.0097	0.0094	0.0057	26390	0.022	0.6263	4.3111	0.2132	19.2	0.0057
0.1222	0.5017	0.0105	0.0094	0.0057	28498	0.0215	0.6345	4.6667	0.2042	19.6	0.0054
0.1248	0.5151	0.0112	0.0094	0.0056	30303	0.0217	0.6228	4.9778	0.2072	19.5	0.0055
0.1254	0.5181	0.0114	0.0094	0.0056	30821	0.0216	0.6222	5.0667	0.2065	19.5	0.0055
0.127	0.5259	0.012	0.0094	0.0056	32381	0.0214	0.6237	5.3333	0.2027	19.7	0.0054
0.129	0.5353	0.0127	0.0094	0.0056	34053	0.0214	0.6195	5.6222	0.2019	19.7	0.0053
0.134	0.5573	0.0143	0.0094	0.0056	38266	0.0213	0.6084	6.3556	0.2008	19.8	0.0052
0.1385	0.5753	0.0158	0.0094	0.0056	42055	0.0213	0.5977	7.0222	0.2009	19.8	0.0052
0.1425	0.5902	0.0175	0.0094	0.0055	46360	0.0209	0.6003	7.7778	0.1934	20.1	0.0049
0.147	0.6057	0.0192	0.0094	0.0055	50595	0.0208	0.5942	8.5333	0.1916	20.2	0.0049

Appendix A1 Flow data for the whole cross-section (Series B extension, Glasgow)

Institution :	**University of Glasgow**
Geometry :	G75T37R
Test No. :	7
Main channel sinuosity :	1.3740 (60^0)
Main channel top width :	0.2m
Main channel aspect ratio :	4.2600
Main channel bank side slope :	45^0 (Trapezoidal)
Main channel cross-sectional shape :	Trapezoidal
Main channel Roughness :	Smooth
Floodplain sinuosity :	1.0
Floodplain roughness :	Rough B
Floodplain lateral slope :	0.0
Floodplain longitudinal slope :	1/1000
Meander belt width : floodplain width :	1.018m/1.65m
Flow :	Inbank / Overbank
Water temperature :	25^0C
Test date :	Winter 1995
File name:	G75T37R.xls

Depth (m)	Dr	Qm (m^3/s)	A(m^2)	R	Re	n	F*	Qm/ Qbf	f	C	k
						So		Qm =			
								0.0017			
0.0583	-0.226	0.0009	0.0046	0.0234	19627	0.0119		0.5000	0.0386	45.1	0.0006
0.0625	-0.170	0.0010	0.0052	0.0251	21546	0.0121		0.5882	0.0394	44.6	0.0007
0.0665	-0.117	0.0012	0.0059	0.0267	24509	0.0118		0.7118	0.0367	46.3	0.0006
0.0715	-0.051	0.0014	0.0069	0.0287	26948	0.0121		0.8412	0.0377	45.6	0.0007
0.0740	-0.018	0.0016	0.0073	0.0297	28409	0.0122		0.9176	0.0375	45.7	0.0008
0.0815	0.1465	0.0018	0.0183	0.0107	4723	0.0139	0.7523	1.0588	0.0686	33.8	0.0013
0.0847	0.2039	0.0022	0.0236	0.0137	5855	0.0173	0.7310	1.3176	0.0987	28.2	0.0040
0.0876	0.2496	0.0028	0.0284	0.0164	7373	0.0189	0.7374	1.6647	0.1105	26.6	0.0061
0.0917	0.3060	0.0040	0.0351	0.0203	10494	0.0191	0.7803	2.3806	0.1053	27.3	0.0070
0.0950	0.3456	0.0053	0.0406	0.0233	13613	0.0188	0.8127	3.1000	0.0970	28.4	0.0069
0.0985	0.3829	0.0067	0.0464	0.0265	17237	0.0185	0.8308	3.9412	0.0903	29.5	0.0069
0.1014	0.4107	0.0080	0.0511	0.0292	20514	0.0183	0.8394	4.7059	0.0854	30.3	0.0068
0.1035	0.4294	0.0089	0.0546	0.0311	22767	0.0184	0.8332	5.2353	0.0842	30.5	0.0071
0.1061	0.4509	0.0102	0.0589	0.0334	26016	0.0182	0.8355	6.0000	0.0806	31.2	0.0070
0.1090	0.4730	0.0116	0.0637	0.0360	29489	0.0182	0.8260	6.8235	0.0789	31.5	0.0072
0.1119	0.4935	0.0133	0.0685	0.0386	33700	0.0179	0.8304	7.8235	0.0747	32.4	0.0069
0.1162	0.5210	0.0159	0.0756	0.0424	40094	0.0177	0.8284	9.3529	0.0702	33.4	0.0066
0.1200	0.5430	0.0183	0.0818	0.0457	45950	0.0175	0.8226	10.765	0.0672	34.2	0.0065
0.1239	0.5635	0.0208	0.0883	0.0491	52001	0.0174	0.8122	12.235	0.0652	34.7	0.0065
0.1290	0.5878	0.0244	0.0967	0.0535	60657	0.0173	0.8041	14.353	0.0621	35.6	0.0063
0.1340	0.6090	0.0281	0.1049	0.0577	69471	0.0171	0.7951	16.529	0.0597	36.3	0.0062

Appendix A1 Flow data for the whole cross-section (Series B extension, Glasgow)

Institution :	**University of Glasgow**
Geometry :	G50T90R
Test No. :	8
Main channel sinuosity :	1.3740 (60^0)
Main channel top width :	0.2m
Main channel aspect ratio :	4.0000
Main channel bank side slope :	90^0 (Trapezoidal)
Main channel cross-sectional shape :	Trapezoidal
Main channel Roughness :	Smooth
Flood plain sinuosity :	1.0
Flood plain roughness :	Rough B
Flood plain lateral slope :	0.0
Flood plain longitudinal slope :	1/1000
Meander belt width : flood plain width :	1.018m/1.650m
Flow :	Inbank / Overbank
Water temperature :	25^0C
Test date :	Autumn 1994
File name:	G50T90R.xls

Depth(m)	Dr	Qm (m^3/s)	A(m^2)	R	Re	n	F*	Qm/Qbf	f	C	k
						So		Qm =			
								0.0026			
0.0302	-0.396	0.0010	0.0060	0.0232	17264	0.0133		0.3922	0.0483	40.3	0.0013
0.0334	-0.332	0.0012	0.0067	0.0250	20894	0.0124		0.4863	0.0415	43.5	0.0009
0.0350	-0.300	0.0014	0.0070	0.0259	23643	0.0116		0.5569	0.0360	46.7	0.0005
0.0388	-0.224	0.0017	0.0078	0.0280	27531	0.0113		0.6667	0.0333	48.6	0.0004
0.0470	-0.060	0.0023	0.0094	0.0320	34864	0.0112		0.8941	0.0310	50.3	0.0004
0.0489	-0.022	0.0025	0.0098	0.0328	36985	0.0110		0.9608	0.0299	51.2	0.0003
0.0560	0.1071	0.0022	0.0199	0.0113	5486	0.0131	0.6341	0.8431	0.0600	36.2	0.0010
0.0597	0.1625	0.0028	0.0260	0.0147	7089	0.0162	0.6723	1.0941	0.0839	30.6	0.0031
0.0650	0.2308	0.0042	0.0348	0.0195	10608	0.0178	0.7399	1.6471	0.0926	29.1	0.0052
0.0700	0.2857	0.0062	0.0430	0.0240	15622	0.0173	0.8217	2.4392	0.0812	31.1	0.0050
0.0740	0.3243	0.0080	0.0496	0.0276	20003	0.0171	0.8517	3.1373	0.0761	32.1	0.0050
0.0785	0.3631	0.0100	0.0570	0.0316	24879	0.0174	0.8499	3.9216	0.0750	32.4	0.0056
0.0821	0.3910	0.0116	0.0630	0.0347	28745	0.0178	0.8339	4.5490	0.0758	32.2	0.0064
0.0833	0.3998	0.0123	0.0649	0.0358	30439	0.0176	0.8383	4.8235	0.0741	32.6	0.0062
0.0881	0.4325	0.0149	0.0729	0.0399	36680	0.0177	0.8297	5.8431	0.0718	33.1	0.0065
0.0909	0.4499	0.0165	0.0775	0.0423	40494	0.0177	0.8230	6.4706	0.0707	33.3	0.0067
0.0938	0.4670	0.0182	0.0823	0.0448	44525	0.0178	0.8146	7.1373	0.0698	33.5	0.0069
0.0976	0.4878	0.0205	0.0886	0.0480	49945	0.0179	0.8019	8.0392	0.0690	33.7	0.0072
0.0993	0.4967	0.0216	0.0914	0.0494	52527	0.0179	0.7974	8.4706	0.0684	33.9	0.0073
0.1015	0.5074	0.0230	0.0950	0.0513	55801	0.0179	0.7914	9.0196	0.0678	34.0	0.0074
0.1032	0.5155	0.0240	0.0978	0.0527	58120	0.0180	0.7827	9.4118	0.0681	33.9	0.0077
0.1064	0.5301	0.0262	0.1031	0.0553	63230	0.0180	0.7755	10.275	0.0670	34.2	0.0078
0.1114	0.5511	0.0299	0.1113	0.0594	71775	0.0180	0.7683	11.725	0.0648	34.8	0.0078
0.1183	0.5773	0.0352	0.1227	0.0650	83878	0.0179	0.7564	13.804	0.0627	35.4	0.0080
0.1230	0.5935	0.0390	0.1305	0.0688	92473	0.0179	0.7502	15.294	0.0614	35.7	0.0080

Appendix A1 Flow data for the whole cross-section (Series B extension, Glasgow)

Institution :	**University of Glasgow**
Geometry :	G50T60RA
Test No. :	9
Main channel sinuosity :	1.3740 (60^0)
Main channel top width :	0.2m
Main channel aspect ratio :	4.6700
Main channel bank side slope :	60^0 (Trapezoidal)
Main channel cross-sectional shape :	Trapezoidal
Main channel Roughness :	Smooth
Flood plain sinuosity :	1.0
Flood plain roughness :	Rough B
Flood plain lateral slope :	0.0
Flood plain longitudinal slope :	1/1000
Meander belt width : flood plain width :	1.018m/1.200m
Flow :	Inbank / Overbank
Water temperature :	25^0C
Test date :	Spring 1995
File name:	G50T60RA.xls

Depth	Dr	Qm (m^3/s)	A(m^2)	R	Re	n	F*	Qm/Qbf	f	C	k
						So		Qm =			
								0.0023			
0.0356	-0.292	0.0012	0.0057	0.0257	23331	0.0116		0.5088	0.0360	46.7	0.0005
0.0385	-0.240	0.0014	0.0062	0.0273	27569	0.0109		0.6195	0.0307	50.5	0.0003
0.0431	-0.160	0.0017	0.0071	0.0296	31989	0.0108		0.7522	0.0294	51.7	0.0002
0.0455	-0.118	0.0019	0.0075	0.0308	34022	0.0108		0.8186	0.0292	51.8	0.0003
0.0519	-0.010	0.0023	0.0088	0.0339	39019	0.0110		0.9956	0.0295	51.5	0.0003
0.0626	0.1848	0.0022	0.0210	0.0165	7738	0.0175	0.6046	0.9735	0.0949	28.8	0.0046
0.0646	0.2136	0.0024	0.0234	0.0183	8415	0.0194	0.5945	1.0619	0.1123	26.4	0.0070
0.0674	0.2506	0.0027	0.0268	0.0208	9495	0.0216	0.5806	1.2035	0.1337	24.2	0.0108
0.0699	0.2809	0.0033	0.0298	0.0230	11475	0.0215	0.6168	1.4602	0.1270	24.9	0.0110
0.0731	0.3162	0.0041	0.0336	0.0259	14326	0.0211	0.6551	1.8319	0.1180	25.8	0.0110
0.0759	0.3444	0.0051	0.0370	0.0283	17606	0.0201	0.7024	2.2611	0.1043	27.4	0.0097
0.0790	0.3730	0.0062	0.0407	0.0311	21261	0.0195	0.7337	2.7434	0.0953	28.7	0.0090
0.0830	0.4064	0.0077	0.0455	0.0345	26244	0.0190	0.7590	3.4071	0.0870	30.0	0.0084
0.0860	0.4292	0.0087	0.0491	0.0371	29518	0.0191	0.7534	3.8496	0.0860	30.2	0.0088
0.0890	0.4503	0.0099	0.0527	0.0396	33438	0.0189	0.7579	4.3805	0.0824	30.9	0.0087
0.0917	0.4681	0.0109	0.0560	0.0419	36667	0.0190	0.7506	4.8230	0.0814	31.1	0.0090
0.0945	0.4853	0.0120	0.0593	0.0442	40199	0.0190	0.7441	5.3097	0.0800	31.3	0.0091
0.0970	0.4997	0.0131	0.0623	0.0463	43721	0.0189	0.7427	5.7965	0.0779	31.7	0.0091
0.0985	0.5080	0.0136	0.0641	0.0475	45289	0.0191	0.7319	6.0177	0.0787	31.6	0.0095
0.1003	0.5176	0.0145	0.0663	0.0490	48158	0.0189	0.7342	6.4159	0.0764	32.0	0.0092
0.1020	0.5263	0.0153	0.0683	0.0503	50687	0.0188	0.7326	6.7699	0.0752	32.3	0.0092
0.1039	0.5357	0.0161	0.0706	0.0519	53189	0.0189	0.7255	7.1239	0.0748	32.4	0.0094
0.1055	0.5433	0.0169	0.0725	0.0532	55701	0.0188	0.7246	7.4779	0.0736	32.7	0.0092
0.1080	0.5547	0.0183	0.0755	0.0552	60095	0.0185	0.7277	8.0973	0.0708	33.3	0.0088
0.1108	0.5666	0.0198	0.0788	0.0573	64760	0.0184	0.7271	8.7611	0.0686	33.8	0.0086
0.1135	0.5779	0.0215	0.0821	0.0595	70040	0.0181	0.7316	9.5133	0.0657	34.6	0.0081

Appendix A1 Flow data for the whole cross-section (Series B extension, Glasgow)

Institution :	**University of Glasgow**
Geometry :	G50T60R
Test No. :	10
Main channel sinuosity :	1.3740 (60^0)
Main channel top width :	0.2m
Main channel aspect ratio :	4.6700
Main channel bank side slope :	60^0 (Trapezoidal)
Main channel cross-sectional shape :	Trapezoidal
Main channel Roughness :	Smooth
Floodplain sinuosity :	1.0
Floodplain roughness :	Rough B
Floodplain lateral slope :	0.0
Floodplain longitudinal slope :	1/1000
Meander belt width : floodplain width :	1.018m/1.650m
Flow :	Inbank / Overbank
Water temperature :	25^0C
Test date :	Spring 1995
File name:	G50T60R.xls

Depth	Dr	Qm (m^3/s)	A(m^2)	R	Re	n	F*	Qm/Qbf	f	C	k
						So		Qm =			
								0.0022			
0.0356	-0.2612	0.0012	0.0058	0.0258	23031	0.0119		0.523	0.0375	45.8	0.0006
0.0385	-0.2073	0.0014	0.0063	0.0274	27225	0.0111		0.636	0.0320	49.5	0.0003
0.0431	-0.1232	0.0017	0.0072	0.0298	31607	0.0110		0.773	0.0306	50.7	0.0003
0.0455	-0.0800	0.0019	0.0077	0.0310	34534	0.0107		0.864	0.0288	52.2	0.0002
0.0492	-0.0141	0.0021	0.0084	0.0328	36894	0.0111		0.955	0.0300	51.2	0.0003
0.0566	0.1336	0.0020	0.0194	0.0113	5224	0.0137	0.6484	0.909	0.0653	34.7	0.0012
0.0590	0.1738	0.0024	0.0234	0.0136	6251	0.0157	0.6713	1.091	0.0813	31.1	0.0027
0.0625	0.2261	0.0032	0.0292	0.0168	8281	0.0173	0.7121	1.451	0.0921	29.2	0.0044
0.0650	0.2596	0.0040	0.0333	0.0192	10347	0.0174	0.7597	1.818	0.0888	29.7	0.0047
0.0688	0.3053	0.0056	0.0396	0.0227	14422	0.0167	0.8402	2.545	0.0776	31.8	0.0043
0.0721	0.3406	0.0070	0.0450	0.0257	17960	0.0167	0.8662	3.182	0.0740	32.6	0.0044
0.0755	0.3734	0.0085	0.0506	0.0288	21724	0.0168	0.8732	3.864	0.0720	33.0	0.0047
0.0790	0.4040	0.0102	0.0564	0.0319	25965	0.0168	0.8763	4.636	0.0696	33.6	0.0048
0.0830	0.4354	0.0123	0.0630	0.0355	31170	0.0168	0.8743	5.591	0.0670	34.2	0.0050
0.0877	0.4684	0.0148	0.0708	0.0397	37308	0.0169	0.8575	6.727	0.0657	34.6	0.0053
0.0896	0.4807	0.0158	0.0739	0.0413	39744	0.0170	0.8471	7.182	0.0657	34.6	0.0056
0.0949	0.5121	0.0190	0.0826	0.0460	47512	0.0170	0.8320	8.636	0.0636	35.1	0.0057
0.0985	0.5313	0.0213	0.0886	0.0491	53051	0.0170	0.8215	9.682	0.0622	35.5	0.0058
0.1005	0.5414	0.0228	0.0919	0.0508	56661	0.0169	0.8223	10.364	0.0606	36.0	0.0057
0.1055	0.5647	0.0260	0.1001	0.0550	64258	0.0171	0.8004	11.818	0.0602	36.1	0.0061
0.1080	0.5755	0.0281	0.1043	0.0572	69258	0.0169	0.8031	12.773	0.0581	36.8	0.0058
0.1127	0.5943	0.0315	0.1120	0.0611	77241	0.0169	0.7896	14.318	0.0571	37.1	0.0059
0.1190	0.6173	0.0364	0.1224	0.0663	88646	0.0169	0.7758	16.545	0.0556	37.6	0.0061
0.1247	0.6358	0.0410	0.1318	0.0710	99235	0.0170	0.7650	18.636	0.0545	38.0	0.0062

Appendix A1 Flow data for the whole cross-section (Series B extension, Glasgow)

Institution :	**University of Glasgow**
Geometry :	G50T45R
Test No. :	11
Main channel sinuosity :	1.3740 (60^0)
Main channel top width :	0.2m
Main channel aspect ratio :	5.3300
Main channel bank side slope :	45^0 (Trapezoidal)
Main channel cross-sectional shape :	Trapezoidal
Main channel Roughness :	Smooth
Flood plain sinuosity :	1.0
Flood plain roughness :	Rough B
Flood plain lateral slope :	0.0
Flood plain longitudinal slope :	1/1000
Meander belt width : flood plain width :	1.018m/1.650m
Flow :	Inbank / Overbank
Water temperature :	25^0C
Test date :	Summer 1995
File name:	G50T45R.xls

Depth	Dr	Qm (m^3/s)	A(m^2)	R	Re	n	F*	Qm/Qbf	f	C	k
						So		Qm =			
								0.0019			
0.0346	-0.266	0.0009	0.0047	0.0235	20449	0.0115		0.4865	0.0360	46.7	0.0004
0.0375	-0.214	0.0011	0.0052	0.0250	22907	0.0113		0.5676	0.0345	47.7	0.0004
0.0432	-0.115	0.0013	0.0062	0.0278	26303	0.0118		0.7027	0.0360	46.7	0.0006
0.0460	-0.067	0.0016	0.0067	0.0292	30282	0.0111		0.8378	0.0313	50.1	0.0003
0.0490	-0.017	0.0018	0.0073	0.0306	33916	0.0107		0.9730	0.0288	52.2	0.0002
0.0555	0.1279	0.0019	0.0166	0.0097	5019	0.0133	0.7146	1.0270	0.0648	34.8	0.0010
0.0590	0.1935	0.0022	0.0224	0.0131	5787	0.0189	0.6515	1.1892	0.1192	25.7	0.0055
0.0630	0.2574	0.0029	0.0290	0.0169	7593	0.0195	0.7302	1.5676	0.1163	26.0	0.0068
0.0667	0.3076	0.0041	0.0350	0.0203	10689	0.0191	0.7904	2.2162	0.1055	27.3	0.0070
0.0695	0.3421	0.0054	0.0397	0.0229	14032	0.0180	0.8584	2.9189	0.0899	29.5	0.0059
0.0741	0.3912	0.0073	0.0473	0.0272	18870	0.0180	0.8720	3.9459	0.0844	30.5	0.0062
0.0783	0.4297	0.0093	0.0541	0.0310	23925	0.0177	0.8810	5.0270	0.0786	31.6	0.0061
0.0830	0.4681	0.0118	0.0620	0.0353	30192	0.0175	0.8799	6.3784	0.0736	32.7	0.0061
0.0866	0.4939	0.0138	0.0679	0.0385	35166	0.0175	0.8722	7.4595	0.0709	33.3	0.0061
0.0905	0.5192	0.0160	0.0743	0.0419	40592	0.0172	0.8730	8.6486	0.0667	34.3	0.0058
0.0940	0.5399	0.0180	0.0801	0.0450	45487	0.0171	0.8630	9.7297	0.0648	34.8	0.0059
0.0997	0.5700	0.0218	0.0895	0.0500	54739	0.0171	0.8428	11.784	0.0626	35.4	0.0060
0.1028	0.5847	0.0245	0.0946	0.0527	61306	0.0170	0.8387	13.243	0.0607	36.0	0.0059
0.1080	0.6073	0.0283	0.1032	0.0571	70407	0.0170	0.8244	15.297	0.0588	36.5	0.0060
0.1130	0.6269	0.0315	0.1115	0.0613	77937	0.0170	0.8085	17.027	0.0577	36.9	0.0061
0.1191	0.6483	0.0357	0.1216	0.0665	87736	0.0170	0.7948	19.297	0.0561	37.4	0.0062

Appendix A1 Flow data for the whole cross-section (Series B extension, Glasgow)

Institution :	**University of Glasgow**
Geometry :	GD50T37R (River Dane model)
Test No. :	12
Main channel sinuosity :	1.3740 (60^0)
Main channel top width :	0.2m
Main channel aspect ratio :	5.9900
Main channel bank side slope :	37^0 (Trapezoidal)
Main channel cross-sectional shape :	Trapezoidal
Main channel Roughness :	n = 0.019
Flood plain sinuosity :	1.0
Flood plain roughness :	Rough B
Flood plain lateral slope :	0.0
Flood plain longitudinal slope :	1/1000
Meander belt width : flood plain width :	1.018m/1.650m
Flow :	Inbank / Overbank
Water temperature :	25^0C
Test date :	Spring 1996
File name:	GD50T37R.xls

Depth	Dr	Qm (m^3/s)	A(m^2)	R	Re	n	F*	Qm/Qb f	f	C	k
						So		Qm =	0.0006		
0.0458	-0.070	0.0005	0.0059	0.0267	10650	0.0272		0.8667	0.1942	20.1	0.0239
0.0490	-0.016	0.0006	0.0065	0.0282	10744	0.0294		0.9167	0.2236	18.7	0.0302
0.0566	0.1650	0.0012	0.0176	0.0104	3180	0.0203	0.7553	2.0000	0.1477	23.0	0.0061
0.0584	0.2010	0.0014	0.0205	0.0121	3675	0.0230	0.7142	2.3167	0.1813	20.8	0.0097
0.0600	0.2304	0.0016	0.0232	0.0136	4222	0.0247	0.6910	2.6667	0.2008	19.8	0.0125
0.0604	0.2374	0.0016	0.0238	0.0140	4326	0.0253	0.6790	2.7333	0.2088	19.4	0.0136
0.0614	0.2545	0.0018	0.0255	0.0149	4742	0.0259	0.6723	3.0000	0.2139	19.2	0.0150
0.0634	0.2863	0.0022	0.0288	0.0168	5651	0.0268	0.6603	3.5833	0.2193	18.9	0.0175
0.0647	0.3056	0.0024	0.0309	0.0181	6246	0.0273	0.6485	3.9667	0.2237	18.7	0.0192
0.0652	0.3128	0.0025	0.0318	0.0185	6558	0.0272	0.6515	4.1667	0.2199	18.9	0.0193
0.0672	0.3399	0.0030	0.0351	0.0204	7851	0.0269	0.6594	5.0000	0.2071	19.5	0.0198
0.0691	0.3638	0.0035	0.0382	0.0222	9139	0.0266	0.6616	5.8333	0.1979	19.9	0.0203
0.0711	0.3872	0.0041	0.0415	0.0240	10551	0.0265	0.6600	6.7500	0.1903	20.3	0.0209
0.0735	0.4130	0.0049	0.0455	0.0263	12730	0.0255	0.6765	8.1667	0.1715	21.4	0.0199
0.0755	0.4329	0.0058	0.0488	0.0281	15033	0.0242	0.7040	9.6667	0.1513	22.8	0.0177
0.0771	0.4479	0.0064	0.0514	0.0296	16557	0.0240	0.7045	10.667	0.1457	23.2	0.0176
0.0780	0.4560	0.0068	0.0529	0.0304	17574	0.0236	0.7099	11.333	0.1406	23.6	0.0172
0.0790	0.4647	0.0071	0.0545	0.0313	18432	0.0237	0.7038	11.900	0.1399	23.7	0.0176
0.0808	0.4798	0.0079	0.0575	0.0329	20351	0.0234	0.7051	13.167	0.1340	24.2	0.0173
0.0830	0.4970	0.0089	0.0611	0.0349	22844	0.0230	0.7071	14.817	0.1272	24.8	0.0169
0.0846	0.5088	0.0095	0.0638	0.0364	24367	0.0231	0.6976	15.833	0.1264	24.9	0.0174
0.0875	0.5289	0.0106	0.0686	0.0390	27099	0.0233	0.6786	17.667	0.1260	25.0	0.0186
0.0910	0.5511	0.0122	0.0743	0.0421	31066	0.0232	0.6697	20.333	0.1210	25.5	0.0188
0.0936	0.5662	0.0133	0.0786	0.0444	33767	0.0233	0.6560	22.167	0.1203	25.5	0.0196
0.0968	0.5835	0.0147	0.0839	0.0472	37137	0.0235	0.6397	24.467	0.1198	25.6	0.0207
0.0993	0.5961	0.0160	0.0880	0.0494	40362	0.0233	0.6363	26.667	0.1162	26.0	0.0206
0.1031	0.6139	0.0180	0.0943	0.0527	45215	0.0232	0.6280	30.000	0.1125	26.4	0.0208
0.1066	0.6289	0.0197	0.1001	0.0557	49292	0.0233	0.6141	32.833	0.1119	26.5	0.0218
0.1102	0.6432	0.0220	0.1060	0.0588	54827	0.0230	0.6151	36.667	0.1064	27.2	0.0211
0.1163	0.6650	0.0257	0.1161	0.0639	63643	0.0228	0.6068	42.850	0.1017	27.8	0.0211
0.1210	0.6801	0.0291	0.1238	0.0678	71540	0.0224	0.6086	48.417	0.0962	28.6	0.0203
0.1251	0.6922	0.0324	0.1306	0.0712	79434	0.0218	0.6162	54.000	0.0904	29.5	0.0189

Appendix A1 Flow data for the whole cross-section (Series B extension, Glasgow)

Institution :	**University of Glasgow**
Geometry :	G50T37R
Test No. :	13
Main channel sinuosity :	1.3740 (60^0)
Main channel top width :	0.2m
Main channel aspect ratio :	5.9900
Main channel bank side slope :	37^0 (Trapezoidal)
Main channel cross-sectional shape :	Trapezoidal
Main channel Roughness :	Smooth
Flood plain sinuosity :	1.0
Flood plain roughness :	Rough B
Flood plain lateral slope :	0.0
Flood plain longitudinal slope :	1/1000
Meander belt width : flood plain width :	1.018m/1.650m
Flow :	Inbank / Overbank
Water temperature :	25^0C
Test date :	Spring 1996
File name:	G50T37R.xls

Depth	Dr	Qm (m^3/s)	A(m^2)	R	Re	n	F*	Qm/Qbf	f	C	k
						So		Qm =			
								0.0016			
0.0394	-0.179	0.0009	0.0047	0.0238	20411	0.0117		0.5521	0.0372	45.9	0.0005
0.0422	-0.131	0.0011	0.0052	0.0251	24261	0.0107		0.6871	0.0309	50.4	0.0002
0.0465	-0.058	0.0013	0.0060	0.0270	26346	0.0112		0.7975	0.0329	48.9	0.0004
0.0493	-0.011	0.0016	0.0065	0.0283	30148	0.0106		0.9509	0.0288	52.2	0.0002
0.0572	0.1773	0.0016	0.0186	0.0109	4236	0.0162	0.7062	0.9816	0.0933	29.0	0.0028
0.0584	0.2000	0.0017	0.0205	0.0120	4495	0.0181	0.6800	1.0429	0.1124	26.4	0.0045
0.0623	0.2691	0.0027	0.0270	0.0158	7106	0.0184	0.7728	1.6564	0.1063	27.2	0.0054
0.0649	0.3085	0.0035	0.0313	0.0182	9184	0.0183	0.8138	2.1472	0.1003	28.0	0.0057
0.0678	0.3477	0.0045	0.0361	0.0210	11768	0.0182	0.8425	2.7607	0.0942	28.9	0.0058
0.0721	0.3982	0.0062	0.0431	0.0250	16133	0.0179	0.8671	3.8037	0.0862	30.2	0.0059
0.0749	0.4271	0.0075	0.0478	0.0276	19452	0.0176	0.8826	4.6012	0.0803	31.3	0.0056
0.0789	0.4639	0.0094	0.0544	0.0312	24268	0.0174	0.8825	5.7669	0.0757	32.2	0.0057
0.0833	0.4993	0.0117	0.0616	0.0352	30055	0.0173	0.8777	7.1779	0.0713	33.2	0.0056
0.0877	0.5302	0.0143	0.0689	0.0392	36550	0.0170	0.8758	8.7730	0.0667	34.3	0.0054
0.0928	0.5617	0.0174	0.0773	0.0437	44216	0.0169	0.8616	10.675	0.0635	35.1	0.0054
0.0976	0.5877	0.0206	0.0852	0.0479	52066	0.0167	0.8511	12.638	0.0606	36.0	0.0053
0.1015	0.6066	0.0235	0.0917	0.0513	59136	0.0165	0.8478	14.417	0.0578	36.9	0.0051
0.1063	0.6276	0.0268	0.0996	0.0554	67080	0.0166	0.8286	16.442	0.0568	37.2	0.0053
0.1103	0.6435	0.0300	0.1062	0.0589	74756	0.0165	0.8234	18.405	0.0548	37.8	0.0052
0.1147	0.6594	0.0334	0.1134	0.0625	82829	0.0165	0.8125	20.491	0.0536	38.3	0.0052
0.1189	0.6735	0.0369	0.1204	0.0661	91082	0.0164	0.8043	22.638	0.0524	38.7	0.0052
0.1239	0.6887	0.0412	0.1286	0.0702	101140	0.0164	0.7967	25.276	0.0510	39.2	0.0052

Appendix A1 Flow data for the whole cross-section (Series B extension, Glasgow)

Institution :	**University of Glasgow**
Geometry :	G50T30R
Test No. :	14
Main channel sinuosity :	1.3740 (60^0)
Main channel top width :	0.2m
Main channel aspect ratio :	7.0500
Main channel bank side slope :	30^0 (Trapezoidal)
Main channel cross-sectional shape :	Trapezoidal
Main channel Roughness :	Smooth
Flood plain sinuosity :	1.0
Flood plain roughness :	Rough B
Flood plain lateral slope :	0.0
Flood plain longitudinal slope :	1/1000
Meander belt width : flood plain width :	1.018m/1.650m
Flow :	Inbank / Overbank
Water temperature :	25^0C
Test date :	Autumn 1995
File name:	G50T30R.xls

Depth	Dr	Qm (m^3/s)	A(m^2)	R	Re	n	F*	Qm/Qb f	f	C	k
						So		Qm =			
								0.0013			
0.0417	-0.149	0.0007	0.0041	0.0213	16255	0.0122		0.5600	0.0424	43.0	0.0007
0.0442	-0.104	0.0009	0.0046	0.0224	19873	0.0109		0.7200	0.0330	48.8	0.0003
0.0463	-0.067	0.0010	0.0050	0.0234	21418	0.0108		0.8080	0.0321	49.4	0.0002
0.0488	-0.022	0.0012	0.0054	0.0245	24301	0.0103		0.9600	0.0286	52.3	0.0001
0.0550	0.1499	0.0014	0.0139	0.0081	3668	0.0112	0.8767	1.1280	0.0494	39.9	0.0002
0.0590	0.2410	0.0017	0.0205	0.0118	4480	0.0181	0.7323	1.3840	0.1129	26.4	0.0044
0.0605	0.2703	0.0019	0.0230	0.0132	4783	0.0207	0.6792	1.4800	0.1416	23.5	0.0074
0.0640	0.3306	0.0028	0.0288	0.0165	7261	0.0200	0.7567	2.2560	0.1231	25.2	0.0074
0.0655	0.3535	0.0034	0.0312	0.0179	8740	0.0191	0.8052	2.7200	0.1095	26.8	0.0065
0.0667	0.3707	0.0040	0.0332	0.0190	10371	0.0179	0.8692	3.2320	0.0938	28.9	0.0052
0.0717	0.4336	0.0060	0.0415	0.0235	15315	0.0175	0.8972	4.8000	0.0841	30.5	0.0053
0.0748	0.4666	0.0075	0.0466	0.0264	18949	0.0172	0.9123	5.9600	0.0777	31.8	0.0050
0.0809	0.5215	0.0104	0.0567	0.0318	26271	0.0171	0.9006	8.3200	0.0721	33.0	0.0052
0.0839	0.5446	0.0120	0.0616	0.0345	30211	0.0170	0.8929	9.6000	0.0697	33.6	0.0053
0.0899	0.5846	0.0157	0.0715	0.0398	39262	0.0166	0.8888	12.560	0.0636	35.1	0.0049
0.0942	0.6092	0.0185	0.0786	0.0435	46044	0.0165	0.8790	14.800	0.0607	36.0	0.0049
0.0980	0.6287	0.0210	0.0849	0.0468	52047	0.0165	0.8651	16.800	0.0592	36.4	0.0049
0.1018	0.6463	0.0237	0.0911	0.0500	58493	0.0164	0.8550	18.960	0.0574	37.0	0.0049
0.1055	0.6619	0.0267	0.0972	0.0532	65631	0.0162	0.8539	21.360	0.0548	37.8	0.0047
0.1103	0.6800	0.0307	0.1051	0.0572	75073	0.0160	0.8504	24.560	0.0521	38.8	0.0044
0.1130	0.6897	0.0327	0.1096	0.0595	79726	0.0161	0.8379	26.160	0.0520	38.8	0.0046
0.1168	0.7020	0.0360	0.1159	0.0626	87411	0.0160	0.8331	28.800	0.0505	39.4	0.0045
0.1210	0.7146	0.0400	0.1228	0.0660	96685	0.0158	0.8330	32.000	0.0485	40.2	0.0043

Appendix A1 Flow data for the whole cross-section (Series B extension, Glasgow)

Institution :	**University of Glasgow**
Geometry :	G50N90R
Test No. :	15
Main channel sinuosity :	1.3740 (60^0)
Main channel top width :	0.2m
Main channel aspect ratio :	4.5700
Main channel bank side slope :	90^0 (Natural)
Main channel cross-sectional shape :	Natural
Main channel Roughness :	Smooth
Floodplain sinuosity :	1.0
Floodplain roughness :	Rough B
Floodplain lateral slope :	0.0
Floodplain longitudinal slope :	1/1000
Meander belt width : floodplain width :	1.018m/1.650m
Flow :	Inbank / Overbank
Water temperature :	25^0C
Test date :	Autumn 1994
File name:	G50N90R.xls

Depth	Dr	Qm (m^3/s)	A(m^2)	R	Re	n	F*	Qm/Qbf	f	C	k
						So		Qm =			
								0.0016			
0.0615	-0.225	0.0010	0.0062	0.0242	16760	0.0147		0.5793	0.0584	36.7	0.0023
0.0673	-0.127	0.0012	0.0072	0.0267	19849	0.0145		0.7317	0.0556	37.6	0.0023
0.0711	-0.064	0.0014	0.0080	0.0282	22248	0.0142		0.8537	0.0524	38.7	0.0021
0.0740	-0.016	0.0016	0.0086	0.0293	24686	0.0137		0.9756	0.0479	40.5	0.0017
0.0816	0.1311	0.0017	0.0196	0.0112	4296	0.0163	0.5669	1.0244	0.0936	29.0	0.0029
0.0838	0.1675	0.0018	0.0233	0.0132	4591	0.0205	0.5281	1.0976	0.1391	23.7	0.0071
0.0879	0.2277	0.0026	0.0300	0.0170	6474	0.0225	0.5693	1.5549	0.1550	22.5	0.0110
0.0916	0.2751	0.0035	0.0361	0.0203	8773	0.0228	0.6084	2.1159	0.1495	22.9	0.0125
0.0927	0.2875	0.0038	0.0379	0.0213	9472	0.0229	0.6155	2.2872	0.1480	23.0	0.0129
0.0954	0.3180	0.0050	0.0424	0.0237	12587	0.0208	0.6937	3.0488	0.1184	25.7	0.0101
0.0999	0.3622	0.0067	0.0498	0.0277	16783	0.0204	0.7218	4.0854	0.1078	27.0	0.0100
0.1035	0.3945	0.0085	0.0558	0.0310	21206	0.0195	0.7566	5.1829	0.0950	28.7	0.0089
0.1080	0.4300	0.0106	0.0632	0.0349	26313	0.0193	0.7600	6.4634	0.0894	29.6	0.0090
0.1111	0.4521	0.0122	0.0683	0.0376	30182	0.0191	0.7620	7.4390	0.0854	30.3	0.0088
0.1140	0.4713	0.0135	0.0731	0.0401	33292	0.0193	0.7465	8.2317	0.0855	30.3	0.0095
0.1167	0.4880	0.0148	0.0776	0.0424	36390	0.0194	0.7350	9.0244	0.0850	30.4	0.0099
0.1183	0.4971	0.0158	0.0801	0.0437	38783	0.0192	0.7395	9.6341	0.0822	30.9	0.0095
0.1195	0.5042	0.0165	0.0822	0.0448	40446	0.0192	0.7371	10.061	0.0813	31.1	0.0096
0.1232	0.5242	0.0188	0.0883	0.0479	45898	0.0190	0.7361	11.463	0.0776	31.8	0.0093
0.1251	0.5338	0.0200	0.0914	0.0495	48727	0.0189	0.7341	12.195	0.0761	32.1	0.0092
0.1308	0.5605	0.0240	0.1008	0.0543	58114	0.0185	0.7349	14.634	0.0707	33.3	0.0087
0.1359	0.5819	0.0275	0.1092	0.0585	66225	0.0184	0.7261	16.768	0.0683	33.9	0.0087
0.1414	0.6028	0.0315	0.1183	0.0630	75413	0.0183	0.7182	19.207	0.0659	34.5	0.0086
0.1444	0.6133	0.0340	0.1233	0.0654	81139	0.0181	0.7194	20.732	0.0638	35.1	0.0083
0.1504	0.6328	0.0390	0.1332	0.0702	92482	0.0179	0.7180	23.780	0.0609	35.9	0.0080

Appendix A1 Flow data for the whole cross-section (Series B extension, Glasgow)

Institution :	**University of Glasgow**
Geometry :	G50N60R
Test No. :	16
Main channel sinuosity :	1.3740 (60^0)
Main channel top width :	0.2m
Main channel aspect ratio :	4.9800
Main channel bank side slope :	60^0 (Natural)
Main channel cross-sectional shape :	Natural
Main channel Roughness :	Smooth
Floodplain sinuosity :	1.0
Floodplain roughness :	Rough B
Floodplain lateral slope :	0.0
Floodplain longitudinal slope :	1/1000
Meander belt width : floodplain width :	1.018m/1.650m
Flow :	Inbank / Overbank
Water temperature :	25^0C
Test date :	Spring 1995
File name:	G50N60R.xls

Depth	Dr	Qm (m^3/s)	A(m^2)	R	Re	n	F*	Qm/Qbf	f	C	k
						So		Qm =	0.0015		
0.0723	-0.042	0.0013	0.0075	0.0299	23263	0.0151		0.8667	0.0573	37.0	0.0028
0.0741	-0.014	0.0015	0.0079	0.0306	25421	0.0143		0.9667	0.0514	39.1	0.0022
0.0815	0.1394	0.0018	0.0188	0.0109	4699	0.0143	0.6381	1.2000	0.0726	32.9	0.0015
0.0831	0.1679	0.0019	0.0214	0.0124	4951	0.0171	0.6066	1.2667	0.0986	28.2	0.0036
0.0850	0.1994	0.0020	0.0245	0.0142	5174	0.0207	0.5581	1.3267	0.1384	23.8	0.0076
0.0870	0.2301	0.0024	0.0278	0.0161	6174	0.0215	0.5814	1.5867	0.1440	23.3	0.0092
0.0890	0.2586	0.0028	0.0311	0.0179	7247	0.0222	0.5966	1.8667	0.1479	23.0	0.0108
0.0905	0.2786	0.0033	0.0336	0.0193	8604	0.0213	0.6417	2.2200	0.1328	24.3	0.0099
0.0929	0.3084	0.0041	0.0376	0.0215	10564	0.0210	0.6760	2.7333	0.1240	25.2	0.0098
0.0948	0.3303	0.0048	0.0407	0.0233	12341	0.0205	0.7029	3.2000	0.1160	26.0	0.0095
0.0964	0.3477	0.0056	0.0433	0.0247	14371	0.0196	0.7447	3.7333	0.1034	27.5	0.0083
0.0986	0.3703	0.0064	0.0470	0.0267	16383	0.0197	0.7493	4.2667	0.1014	27.8	0.0087
0.1000	0.3838	0.0071	0.0493	0.0280	18146	0.0192	0.7689	4.7333	0.0955	28.7	0.0081
0.1006	0.3894	0.0075	0.0503	0.0286	19155	0.0188	0.7861	5.0000	0.0910	29.4	0.0075
0.1024	0.4057	0.0083	0.0532	0.0302	21155	0.0187	0.7906	5.5333	0.0885	29.8	0.0076
0.1050	0.4277	0.0094	0.0575	0.0325	23888	0.0188	0.7849	6.2667	0.0874	30.0	0.0080
0.1084	0.4542	0.0110	0.0631	0.0356	27847	0.0188	0.7812	7.3333	0.0846	30.5	0.0082
0.1106	0.4700	0.0122	0.0668	0.0375	30809	0.0186	0.7849	8.1333	0.0814	31.0	0.0080
0.1114	0.4756	0.0128	0.0681	0.0382	32295	0.0184	0.7953	8.5333	0.0785	31.6	0.0076
0.1138	0.4915	0.0141	0.0720	0.0403	35354	0.0184	0.7888	9.3667	0.0772	31.9	0.0077
0.1160	0.5053	0.0155	0.0757	0.0423	38907	0.0181	0.7962	10.333	0.0735	32.7	0.0073
0.1202	0.5296	0.0179	0.0826	0.0459	44721	0.0181	0.7837	11.933	0.0717	33.1	0.0075
0.1238	0.5487	0.0202	0.0885	0.0490	50266	0.0180	0.7785	13.467	0.0692	33.7	0.0074
0.1251	0.5552	0.0211	0.0907	0.0501	52430	0.0179	0.7781	14.067	0.0681	33.9	0.0074
0.1301	0.5785	0.0244	0.0989	0.0544	60297	0.0179	0.7662	16.267	0.0660	34.5	0.0074
0.1332	0.5918	0.0267	0.1041	0.0570	65757	0.0177	0.7640	17.800	0.0640	35.0	0.0073
0.1362	0.6039	0.0288	0.1090	0.0595	70696	0.0177	0.7565	19.200	0.0631	35.3	0.0074
0.1423	0.6264	0.0335	0.1191	0.0646	81689	0.0176	0.7487	22.333	0.0605	36.0	0.0073
0.1476	0.6440	0.0380	0.1278	0.0689	92133	0.0174	0.7472	25.333	0.0580	36.8	0.0070

Appendix A1 Flow data for the whole cross-section (Series B extension, Glasgow)

Institution :	**University of Glasgow**
Geometry :	G50N45R
Test No. :	17
Main channel sinuosity :	1.3740 (60^0)
Main channel top width :	0.2m
Main channel aspect ratio :	5.3300
Main channel bank side slope :	45^0 (Natural)
Main channel cross-sectional shape :	Natural
Main channel Roughness :	Smooth
Floodplain sinuosity :	1.0
Floodplain roughness :	Rough B
Floodplain lateral slope :	0.0
Floodplain longitudinal slope :	1/1000
Meander belt width : floodplain width :	1.018m/1.650m
Flow :	Inbank / Overbank
Water temperature :	25^0C
Test date :	Summer 1995
File name:	G50N45R.xls

Depth	Dr	Qm (m^3/s)	A(m^2)	R	Re	n	F*	Qm/Qbf	f	C	k
						So		Qm =	0.0015		
0.0598	-0.232	0.0007	0.0050	0.0248	15765	0.0163		0.4828	0.0711	33.2	0.0039
0.0643	-0.162	0.0009	0.0057	0.0265	18948	0.0151		0.6207	0.0601	36.1	0.0028
0.0702	-0.072	0.0011	0.0067	0.0287	21335	0.0153		0.7586	0.0599	36.2	0.0030
0.0743	-0.011	0.0014	0.0074	0.0302	24826	0.0143		0.9310	0.0514	39.1	0.0021
0.0806	0.1289	0.0017	0.0167	0.0098	4502	0.0125	0.6856	1.1793	0.0570	37.1	0.0006
0.0838	0.1901	0.0020	0.0220	0.0128	5245	0.0174	0.6414	1.3793	0.1012	27.9	0.0039
0.0875	0.2500	0.0024	0.0281	0.0163	6267	0.0222	0.5895	1.6552	0.1529	22.7	0.0103
0.0890	0.2718	0.0027	0.0306	0.0177	7038	0.0229	0.5964	1.8621	0.1577	22.3	0.0118
0.0925	0.3182	0.0042	0.0364	0.0210	10800	0.0200	0.7239	2.8690	0.1143	26.2	0.0084
0.0955	0.3534	0.0055	0.0413	0.0238	14230	0.0189	0.7903	3.7931	0.0972	28.4	0.0071
0.1005	0.4048	0.0076	0.0496	0.0284	19551	0.0186	0.8152	5.2414	0.0893	29.6	0.0072
0.1030	0.4275	0.0087	0.0537	0.0306	22316	0.0186	0.8159	6.0000	0.0870	30.0	0.0074
0.1051	0.4456	0.0096	0.0572	0.0326	24565	0.0188	0.8071	6.6207	0.0868	30.1	0.0079
0.1075	0.4643	0.0108	0.0611	0.0347	27562	0.0187	0.8096	7.4483	0.0837	30.6	0.0078
0.1090	0.4755	0.0115	0.0636	0.0360	29298	0.0187	0.8039	7.9310	0.0833	30.7	0.0080
0.1103	0.4845	0.0123	0.0657	0.0372	31292	0.0185	0.8124	8.4828	0.0802	31.3	0.0077
0.1125	0.5000	0.0136	0.0694	0.0392	34511	0.0183	0.8141	9.3793	0.0774	31.8	0.0075
0.1170	0.5283	0.0161	0.0768	0.0431	40649	0.0183	0.8018	11.103	0.0750	32.4	0.0078
0.1190	0.5399	0.0171	0.0801	0.0449	43077	0.0185	0.7886	11.793	0.0754	32.3	0.0082
0.1230	0.5614	0.0198	0.0867	0.0484	49656	0.0182	0.7896	13.655	0.0712	33.2	0.0078
0.1250	0.5714	0.0212	0.0900	0.0501	53048	0.0181	0.7892	14.621	0.0694	33.6	0.0077
0.1275	0.5833	0.0228	0.0941	0.0522	56894	0.0181	0.7815	15.724	0.0686	33.8	0.0078
0.1300	0.5946	0.0250	0.0983	0.0544	62211	0.0177	0.7916	17.241	0.0648	34.8	0.0071
0.1318	0.6023	0.0265	0.1012	0.0559	65812	0.0175	0.7943	18.276	0.0630	35.3	0.0069
0.1340	0.6114	0.0280	0.1049	0.0578	69369	0.0176	0.7865	19.310	0.0626	35.4	0.0070
0.1371	0.6235	0.0305	0.1100	0.0604	75305	0.0174	0.7849	21.034	0.0608	35.9	0.0068
0.1400	0.6341	0.0325	0.1148	0.0628	79988	0.0175	0.7736	22.414	0.0607	36.0	0.0071
0.1440	0.6479	0.0360	0.1214	0.0661	88216	0.0173	0.7740	24.828	0.0583	36.7	0.0068
0.1480	0.6606	0.0390	0.1280	0.0694	95153	0.0174	0.7622	26.897	0.0580	36.8	0.0071
0.1518	0.6719	0.0428	0.1342	0.0725	103995	0.0172	0.7682	29.517	0.0554	37.6	0.0066

Appendix A1 Flow data for the whole cross-section (Series B extension, Glasgow)

Institution :	**University of Glasgow**
Geometry :	G50N37R
Test No. :	18
Main channel sinuosity :	1.3740 (60^0)
Main channel top width :	0.2m
Main channel aspect ratio :	5.6400
Main channel bank side slope :	37^0 (Natural)
Main channel cross-sectional shape :	Natural
Main channel Roughness :	Smooth
Floodplain sinuosity :	1.0
Floodplain roughness :	Rough B
Floodplain lateral slope :	0.0
Floodplain longitudinal slope :	1/1000
Meander belt width : floodplain width :	1.018m/1.650m
Flow :	Inbank / Overbank
Water temperature :	25^0C
Test date :	Winter 1995
File name:	G50N37R.xls

Depth	Dr	Qm (m^3/s)	A(m^2)	R	Re	n	F*	Qm/Qbf	f	C	k
						So		Qm =			
								0.0013			
0.0643	-0.158	0.0008	0.0053	0.0259	17449	0.0157		0.6154	0.0656	34.6	0.0033
0.0702	-0.071	0.0011	0.0063	0.0278	20909	0.0148		0.8077	0.0567	37.2	0.0025
0.0743	-0.010	0.0013	0.0070	0.0291	23473	0.0142		0.9615	0.0517	39.0	0.0021
0.0815	0.1549	0.0017	0.0178	0.0104	4460	0.0141	0.7678	1.3077	0.0714	33.1	0.0014
0.0834	0.1916	0.0018	0.0210	0.0122	4739	0.0176	0.6990	1.3923	0.1052	27.3	0.0040
0.0879	0.2668	0.0026	0.0284	0.0164	6771	0.0207	0.6937	2.0000	0.1323	24.4	0.0083
0.0917	0.3202	0.0038	0.0346	0.0200	9775	0.0201	0.7528	2.9000	0.1171	25.9	0.0083
0.0950	0.3607	0.0052	0.0401	0.0230	13432	0.0187	0.8246	4.0000	0.0966	28.5	0.0068
0.0985	0.3986	0.0065	0.0459	0.0262	16723	0.0188	0.8242	5.0000	0.0933	29.0	0.0073
0.1000	0.4131	0.0071	0.0483	0.0276	18108	0.0189	0.8196	5.4231	0.0926	29.1	0.0075
0.1035	0.4457	0.0087	0.0541	0.0308	22255	0.0185	0.8283	6.6923	0.0861	30.2	0.0073
0.1050	0.4584	0.0095	0.0566	0.0321	24260	0.0183	0.8355	7.3077	0.0827	30.8	0.0070
0.1090	0.4896	0.0113	0.0632	0.0357	28777	0.0185	0.8165	8.7077	0.0812	31.1	0.0076
0.1125	0.5141	0.0133	0.0690	0.0388	33678	0.0182	0.8178	10.231	0.0765	32.0	0.0073
0.1162	0.5375	0.0153	0.0751	0.0421	38632	0.0182	0.8057	11.785	0.0743	32.5	0.0074
0.1210	0.5648	0.0182	0.0830	0.0463	45648	0.0180	0.7945	14.000	0.0710	33.2	0.0074
0.1250	0.5851	0.0209	0.0896	0.0498	52187	0.0178	0.7911	16.077	0.0676	34.1	0.0072
0.1290	0.6037	0.0237	0.0962	0.0532	58917	0.0176	0.7856	18.231	0.0649	34.8	0.0070
0.1332	0.6213	0.0269	0.1030	0.0567	66567	0.0174	0.7845	20.692	0.0618	35.6	0.0067
0.1415	0.6521	0.0335	0.1167	0.0637	82148	0.0171	0.7758	25.769	0.0575	36.9	0.0063
0.1496	0.6777	0.0403	0.1301	0.0703	97958	0.0170	0.7667	31.000	0.0547	37.9	0.0062

Appendix A1 Flow data for the whole cross-section (Series B extension, Glasgow)

Institution :	**University of Glasgow**
Geometry :	G25T90R
Test No. :	19
Main channel sinuosity :	1.3740 (60^0)
Main channel top width :	0.2m
Main channel aspect ratio :	8.0000
Main channel bank side slope :	90^0 (Trapezoidal)
Main channel cross-sectional shape :	Trapezoidal
Main channel Roughness :	Smooth
Floodplain sinuosity :	1.0
Floodplain roughness :	Rough B
Floodplain lateral slope :	0.0
Floodplain longitudinal slope :	1/1000
Meander belt width : floodplain width :	1.018m/1.650m
Flow :	Inbank / Overbank
Water temperature :	25^0C
Test date :	Winter 1994
File name:	G25T90R.xls

Depth(m)	Dr	Qm (m^3/s)	A(m^2)	R	Re	n	F*	Qm/Qbf	f	C	k
						So		Qm =			
								0.0009			
0.0203	-0.1880	0.0006	0.0041	0.0169	11211	0.0120		0.7059	0.0441	42.2	0.0006
0.0221	-0.1160	0.0007	0.0044	0.0181	12887	0.0117		0.8235	0.0412	43.6	0.0005
0.0240	-0.0400	0.0008	0.0048	0.0194	14502	0.0117		0.9412	0.0398	44.4	0.0005
0.0335	0.2526	0.0015	0.0189	0.0110	3797	0.0192	0.7529	1.7059	0.1299	24.6	0.0053
0.0363	0.3113	0.0018	0.0236	0.0137	4724	0.0226	0.6910	2.1294	0.1675	21.6	0.0099
0.0378	0.3386	0.0022	0.0261	0.0151	5732	0.0221	0.7228	2.5882	0.1546	22.5	0.0097
0.0417	0.4005	0.0033	0.0326	0.0188	8559	0.0214	0.7615	3.8824	0.1357	24.0	0.0099
0.0440	0.4318	0.0040	0.0364	0.0209	10450	0.0211	0.7742	4.7529	0.1269	24.9	0.0100
0.0457	0.4530	0.0047	0.0392	0.0225	12134	0.0206	0.7925	5.5294	0.1177	25.8	0.0094
0.0474	0.4726	0.0054	0.0420	0.0240	13913	0.0201	0.8069	6.3529	0.1100	26.7	0.0090
0.0499	0.4990	0.0065	0.0461	0.0263	16597	0.0197	0.8175	7.6000	0.1021	27.7	0.0086
0.0520	0.5192	0.0075	0.0496	0.0282	19223	0.0191	0.8334	8.8235	0.0943	28.9	0.0080
0.0560	0.5532	0.0094	0.0561	0.0318	23985	0.0187	0.8345	11.059	0.0870	30.0	0.0077
0.0598	0.5819	0.0113	0.0624	0.0353	28707	0.0186	0.8236	13.294	0.0830	30.7	0.0078
0.0627	0.6013	0.0129	0.0672	0.0379	32665	0.0184	0.8200	15.176	0.0794	31.4	0.0077
0.0673	0.6285	0.0155	0.0748	0.0419	39046	0.0183	0.8072	18.235	0.0757	32.2	0.0077
0.0723	0.6542	0.0187	0.0830	0.0463	46845	0.0180	0.8009	22.000	0.0709	33.3	0.0074
0.0750	0.6667	0.0205	0.0875	0.0486	51200	0.0179	0.7962	24.118	0.0689	33.8	0.0073
0.0807	0.6902	0.0245	0.0969	0.0535	60805	0.0177	0.7864	28.824	0.0652	34.7	0.0071
0.0879	0.7156	0.0302	0.1088	0.0596	74360	0.0173	0.7823	35.529	0.0603	36.1	0.0066
0.0962	0.7401	0.0370	0.1225	0.0665	90283	0.0171	0.7719	43.529	0.0569	37.1	0.0064

Appendix A1 Flow data for the whole cross-section (Series B extension, Glasgow)

Institution :	**University of Glasgow**
Geometry :	G25T60R
Test No. :	20
Main channel sinuosity :	1.3740 (60^0)
Main channel top width :	0.2m
Main channel aspect ratio :	8.6210
Main channel bank side slope :	60^0 (Trapezoidal)
Main channel cross-sectional shape :	Trapezoidal
Main channel Roughness :	Smooth
Floodplain sinuosity :	1.0
Floodplain roughness :	Rough B
Floodplain lateral slope :	0.0
Floodplain longitudinal slope :	1/1000
Meander belt width : floodplain width :	1.018m/1.650m
Flow :	Inbank / Overbank
Water temperature :	25^0C
Test date :	Summer 1995
File name:	G25T60R.xls

Depth	Dr	Qm (m^3/s)	A(m^2)	R	Re	n	F*	Qm/Qbf	f	C	k
						So		Qm =			
								0.0008			
0.0195	-0.2082	0.0005	0.0036	0.1406	10389	0.0124		0.667	0.0475	40.6	0.0008
0.0221	-0.1091	0.0006	0.0041	0.1476	12130	0.0127		0.800	0.0479	40.5	0.0009
0.0235	-0.0562	0.0007	0.0043	0.1659	14347	0.0117		0.960	0.0400	44.3	0.0005
0.0319	0.2293	0.0012	0.0160	0.0095	3097	0.0194	0.6722	1.556	0.1400	23.7	0.0051
0.0333	0.2642	0.0014	0.0184	0.0108	3576	0.0211	0.6672	1.800	0.1577	22.3	0.0071
0.0379	0.3574	0.0022	0.0259	0.0152	5665	0.0234	0.6725	2.867	0.1735	21.3	0.0115
0.0417	0.4180	0.0034	0.0321	0.0188	8788	0.0214	0.7541	4.467	0.1354	24.1	0.0099
0.0427	0.4328	0.0038	0.0338	0.0197	9956	0.0206	0.7867	5.067	0.1229	25.3	0.0089
0.0446	0.4574	0.0046	0.0369	0.0215	12000	0.0196	0.8245	6.120	0.1089	26.8	0.0079
0.0469	0.4856	0.0055	0.0408	0.0237	14340	0.0193	0.8350	7.333	0.1021	27.7	0.0077
0.0502	0.5207	0.0071	0.0462	0.0267	18389	0.0185	0.8658	9.440	0.0894	29.6	0.0068
0.0566	0.5767	0.0101	0.0568	0.0326	26040	0.0181	0.8570	13.467	0.0808	31.2	0.0068
0.0625	0.6178	0.0134	0.0665	0.0379	34315	0.0177	0.8528	17.867	0.0733	32.7	0.0065
0.0669	0.6437	0.0161	0.0738	0.0419	41024	0.0175	0.8469	21.467	0.0689	33.7	0.0063
0.0702	0.6609	0.0184	0.0792	0.0448	46710	0.0172	0.8486	24.533	0.0651	34.7	0.0059
0.0750	0.6831	0.0216	0.0871	0.0490	54537	0.0171	0.8350	28.800	0.0625	35.4	0.0059
0.0764	0.6890	0.0229	0.0894	0.0502	57729	0.0168	0.8433	30.533	0.0601	36.1	0.0055
0.0797	0.7022	0.0255	0.0949	0.0531	64046	0.0166	0.8417	34.000	0.0577	36.9	0.0053
0.0849	0.7209	0.0297	0.1035	0.0575	74163	0.0164	0.8356	39.600	0.0548	37.8	0.0050
0.0892	0.7344	0.0335	0.1105	0.0611	83258	0.0162	0.8357	44.667	0.0522	38.8	0.0047
0.1001	0.7639	0.0433	0.1285	0.0702	106332	0.0160	0.8230	57.733	0.0485	40.2	0.0045

Appendix A1 Flow data for the whole cross-section (Series B extension, Glasgow)

Institution :	**University of Glasgow**
Geometry :	G25T45R
Test No. :	21
Main channel sinuosity :	1.3740 (60^0)
Main channel top width :	0.2m
Main channel aspect ratio :	9.1430
Main channel bank side slope :	45^0 (Trapezoidal)
Main channel cross-sectional shape :	Trapezoidal
Main channel Roughness :	Smooth
Floodplain sinuosity :	1.0
Floodplain roughness :	Rough B
Floodplain lateral slope :	0.0
Floodplain longitudinal slope :	1/1000
Meander belt width : floodplain width :	1.018m/1.650m
Flow :	Inbank / Overbank
Water temperature :	25^0C
Test date :	Summer 1995
File name:	G25T45R.xls

Depth	Dr	Qm (m^3/s)	A(m^2)	R	Re	n	F*	Qm/Qbf	f	C	k
						So		Qm =			
								0.0008			
0.0206	-0.161	0.0005	0.0035	0.0169	10793	0.0125		0.6667	0.0476	40.6	0.0008
0.0231	-0.069	0.0007	0.0040	0.0186	13570	0.0116		0.8667	0.0401	44.2	0.0005
0.0243	-0.026	0.0007	0.0042	0.0194	14798	0.0114		0.9600	0.0383	45.3	0.0004
0.0333	0.2756	0.0014	0.0181	0.0107	3623	0.0192	0.7123	1.8133	0.1312	24.5	0.0052
0.0357	0.3282	0.0016	0.0220	0.0130	4362	0.0223	0.6647	2.1893	0.1665	21.7	0.0093
0.0387	0.3848	0.0024	0.0270	0.0159	6459	0.0213	0.7334	3.2533	0.1417	23.5	0.0089
0.0416	0.4312	0.0035	0.0318	0.0186	9233	0.0196	0.8127	4.6667	0.1140	26.2	0.0074
0.0429	0.4497	0.0040	0.0339	0.0199	10536	0.0192	0.8345	5.3333	0.1066	27.1	0.0070
0.0448	0.4748	0.0047	0.0371	0.0217	12352	0.0190	0.8458	6.2667	0.1012	27.9	0.0069
0.0506	0.5389	0.0071	0.0466	0.0271	18638	0.0183	0.8635	9.5200	0.0880	29.9	0.0067
0.0598	0.6138	0.0118	0.0618	0.0355	30477	0.0177	0.8594	15.733	0.0751	32.3	0.0064
0.0654	0.6485	0.0152	0.0710	0.0406	39007	0.0173	0.8570	20.267	0.0686	33.8	0.0060
0.0675	0.6599	0.0165	0.0745	0.0424	42242	0.0173	0.8519	22.000	0.0671	34.2	0.0060
0.0704	0.6746	0.0185	0.0793	0.0450	47207	0.0171	0.8511	24.667	0.0642	35.0	0.0057
0.0748	0.6946	0.0218	0.0866	0.0489	55351	0.0167	0.8524	29.067	0.0599	36.2	0.0053
0.0778	0.7068	0.0241	0.0915	0.0515	60984	0.0166	0.8500	32.133	0.0578	36.9	0.0051
0.0833	0.7269	0.0288	0.1006	0.0563	72428	0.0162	0.8527	38.400	0.0535	38.3	0.0046
0.0887	0.7440	0.0333	0.1094	0.0608	83247	0.0160	0.8446	44.400	0.0512	39.1	0.0045
0.0887	0.7440	0.0333	0.1094	0.0608	83247	0.0160	0.8446	44.400	0.0512	39.1	0.0045
0.0922	0.7542	0.0368	0.1153	0.0638	91635	0.0158	0.8487	49.067	0.0489	40.1	0.0042
0.0965	0.7655	0.0410	0.1224	0.0675	101517	0.0156	0.8489	54.667	0.0469	40.9	0.0040

Appendix A1 Flow data for the whole cross-section (Series B extension, Glasgow)

Institution :	**University of Glasgow**
Geometry :	G25T45S
Test No. :	22
Main channel sinuosity :	1.3740 (45^0)
Main channel top width :	0.2m
Main channel aspect ratio :	9.1430
Main channel bank side slope :	45^0 (Trapezoidal)
Main channel cross-sectional shape :	Trapezoidal
Main channel Roughness :	Smooth
Floodplain sinuosity :	1.0
Floodplain roughness :	Smooth
Floodplain lateral slope :	0.0
Floodplain longitudinal slope :	1/1000
Meander belt width : floodplain width :	1.018m/1.650m
Flow :	Inbank / Overbank
Water temperature :	25^0C
Test date :	Autumn 1995
File name:	G25T45S.xls

Depth	Dr	Qm (m^3/s)	A(m^2)	R	Re	n	F*	Qm/Qbf	f	C	k
						So		Qm =			
								0.0008			
0.0206	-0.161	0.0005	0.0035	0.0169	10793	0.0125		0.6667	0.0476	40.6	0.0008
0.0231	-0.069	0.0007	0.0040	0.0186	13570	0.0116		0.8667	0.0401	44.2	0.0005
0.0243	-0.026	0.0007	0.0042	0.0194	14798	0.0114		0.9600	0.0383	45.3	0.0004
0.0323	0.2500	0.0016	0.0164	0.0097	4134	0.0144	0.7038	2.0667	0.0767	32.0	0.0016
0.0333	0.2756	0.0017	0.0181	0.0107	4475	0.0158	0.6562	2.2400	0.0891	29.7	0.0025
0.0356	0.3262	0.0024	0.0219	0.0129	6243	0.0156	0.6775	3.1333	0.0819	31.0	0.0026
0.0376	0.3652	0.0031	0.0252	0.0148	8216	0.0151	0.7052	4.1333	0.0727	32.9	0.0023
0.0415	0.4297	0.0048	0.0316	0.0185	12532	0.0145	0.7287	6.3333	0.0621	35.5	0.0020
0.0437	0.4606	0.0060	0.0352	0.0206	15657	0.0139	0.7544	7.9333	0.0551	37.8	0.0017
0.0449	0.4761	0.0066	0.0372	0.0218	17343	0.0137	0.7602	8.8000	0.0528	38.6	0.0016
0.0501	0.5335	0.0092	0.0457	0.0266	24031	0.0139	0.7380	12.267	0.0505	39.4	0.0018
0.0564	0.5891	0.0130	0.0562	0.0324	33708	0.0138	0.7263	17.333	0.0469	40.9	0.0018
0.0609	0.6211	0.0157	0.0636	0.0365	40499	0.0140	0.7065	20.933	0.0465	41.1	0.0020
0.0646	0.6439	0.0183	0.0697	0.0398	47006	0.0140	0.7024	24.400	0.0450	41.8	0.0020
0.0695	0.6702	0.0218	0.0778	0.0442	55684	0.0141	0.6923	29.067	0.0439	42.3	0.0021
0.0730	0.6867	0.0245	0.0836	0.0473	62333	0.0141	0.6880	32.667	0.0429	42.8	0.0021
0.0750	0.6954	0.0261	0.0869	0.0491	66254	0.0141	0.6858	34.800	0.0424	43.0	0.0021
0.0769	0.7033	0.0276	0.0900	0.0507	69911	0.0141	0.6825	36.800	0.0421	43.2	0.0021
0.0829	0.7256	0.0332	0.0999	0.0559	83531	0.0139	0.6872	44.267	0.0396	44.5	0.0020
0.0855	0.7342	0.0358	0.1042	0.0582	89812	0.0138	0.6900	47.733	0.0385	45.2	0.0019
0.0908	0.7503	0.0412	0.1130	0.0627	102751	0.0136	0.6928	54.933	0.0368	46.2	0.0018
0.0953	0.7625	0.0459	0.1204	0.0664	113904	0.0136	0.6933	61.200	0.0357	46.9	0.0017

Appendix A1 Flow data for the whole cross-section (Series B extension, Glasgow)

Institution :	**University of Glasgow**
Geometry :	G25T45SN
Test No. :	23
Main channel sinuosity :	1.3740 (60^0)
Main channel top width :	0.2m
Main channel aspect ratio :	9.1430
Main channel bank side slope :	45^0 (Trapezoidal)
Main channel cross-sectional shape :	Trapezoidal
Main channel Roughness :	Smooth
Floodplain sinuosity :	1.0
Floodplain roughness :	Smooth
Floodplain lateral slope :	0.0
Floodplain longitudinal slope :	1/1000
Meander belt width : floodplain width :	1.018m/1.018m
Flow :	Inbank / Overbank
Water temperature :	25^0C
Test date :	Autumn 1995
File name:	G25T45SN.xls

Depth	Dr	Qm (m^3/s)	A(m^2)	R	Re	n	F*	Qm/Qbf	f	C	k
						So		Qm =			
								0.0008			
0.0206	-0.161	0.0005	0.0035	0.0169	10793	0.0125		0.6667	0.0476	40.6	0.0008
0.0231	-0.069	0.0007	0.0040	0.0186	13570	0.0116		0.8667	0.0401	44.2	0.0005
0.0243	-0.026	0.0007	0.0042	0.0194	14798	0.0114		0.9600	0.0383	45.3	0.0004
0.0335	0.2784	0.0015	0.0183	0.0109	3995	0.0136	0.6955	2.0000	0.0657	34.6	0.0011
0.0351	0.3156	0.0017	0.0210	0.0124	4439	0.0151	0.6423	2.2267	0.0769	31.9	0.0020
0.0369	0.3521	0.0019	0.0240	0.0142	5040	0.0162	0.6050	2.5333	0.0850	30.4	0.0030
0.0390	0.3900	0.0023	0.0275	0.0162	6086	0.0164	0.5990	3.0667	0.0837	30.6	0.0034
0.0419	0.4348	0.0030	0.0322	0.0189	7780	0.0163	0.6018	3.9333	0.0783	31.7	0.0035
0.0435	0.4579	0.0034	0.0349	0.0204	8949	0.0160	0.6102	4.5333	0.0736	32.7	0.0033
0.0448	0.4742	0.0038	0.0370	0.0216	9987	0.0156	0.6224	5.0667	0.0689	33.7	0.0030
0.0472	0.5034	0.0046	0.0410	0.0239	12055	0.0151	0.6377	6.1333	0.0625	35.4	0.0026
0.0494	0.5270	0.0053	0.0446	0.0260	13854	0.0150	0.6404	7.0667	0.0594	36.4	0.0025
0.0502	0.5350	0.0056	0.0460	0.0267	14625	0.0148	0.6454	7.4667	0.0576	36.9	0.0024
0.0530	0.5611	0.0065	0.0506	0.0293	16920	0.0148	0.6407	8.6667	0.0556	37.6	0.0025
0.0558	0.5844	0.0073	0.0552	0.0319	18941	0.0150	0.6237	9.7333	0.0560	37.4	0.0028
0.0575	0.5974	0.0078	0.0580	0.0334	20121	0.0152	0.6121	10.360	0.0566	37.2	0.0030
0.0600	0.6151	0.0086	0.0621	0.0357	22207	0.0153	0.6053	11.467	0.0557	37.5	0.0031
0.0645	0.6433	0.0102	0.0696	0.0397	26203	0.0153	0.5965	13.600	0.0539	38.1	0.0032
0.0681	0.6631	0.0115	0.0755	0.0430	29421	0.0154	0.5880	15.333	0.0530	38.5	0.0033
0.0725	0.6844	0.0133	0.0828	0.0469	33857	0.0153	0.5851	17.733	0.0509	39.3	0.0033
0.0750	0.6954	0.0144	0.0869	0.0491	36554	0.0152	0.5851	19.200	0.0495	39.8	0.0032
0.0788	0.7107	0.0160	0.0932	0.0524	40442	0.0152	0.5803	21.333	0.0484	40.3	0.0032
0.0828	0.7252	0.0180	0.0998	0.0558	45293	0.0150	0.5840	24.000	0.0460	41.3	0.0030
0.0880	0.7420	0.0207	0.1083	0.0603	51786	0.0147	0.5875	27.600	0.0434	42.5	0.0028
0.0931	0.7567	0.0235	0.1167	0.0646	58459	0.0145	0.5909	31.333	0.0412	43.7	0.0025
0.0944	0.7601	0.0242	0.1189	0.0657	60113	0.0145	0.5909	32.267	0.0408	43.9	0.0025
0.0985	0.7704	0.0265	0.1257	0.0691	65530	0.0144	0.5919	35.333	0.0394	44.6	0.0024

Appendix A1 Flow data for the whole cross-section (Series B extension, Glasgow)

Institution :	**University of Glasgow**
Geometry :	G25T45RN
Test No. :	24
Main channel sinuosity :	1.3740 (60^0)
Main channel top width :	0.2m
Main channel aspect ratio :	9.1430
Main channel bank side slope :	45^0 (Trapezoidal)
Main channel cross-sectional shape :	Trapezoidal
Main channel Roughness :	Smooth
Floodplain sinuosity :	1.0
Floodplain roughness :	Rough B
Floodplain lateral slope :	0.0
Floodplain longitudinal slope :	1/1000
Meander belt width : floodplain width :	1.018m/1.018m
Flow :	Inbank / Overbank
Water temperature :	25^0C
Test date :	Autumn 1995
File name:	G25T45RN.xls

Depth	Dr	Qm (m^3/s)	A(m^2)	R	Re	n	F*	Qm/Qbf	f	C	k
						So		Qm =	0.0008		
0.0206	-0.161	0.0005	0.0035	0.0169	10793	0.0125		0.6667	0.0476	40.6	0.0008
0.0231	-0.069	0.0007	0.0040	0.0186	13570	0.0116		0.8667	0.0401	44.2	0.0005
0.0243	-0.026	0.0007	0.0042	0.0194	14798	0.0114		0.9600	0.0383	45.3	0.0004
0.0335	0.2796	0.0012	0.0184	0.0109	3276	0.0164	0.8511	1.6400	0.0954	28.7	0.0028
0.0360	0.3343	0.0014	0.0225	0.0133	3718	0.0196	0.7634	1.8667	0.1276	24.8	0.0061
0.0379	0.3707	0.0016	0.0257	0.0151	4107	0.0217	0.7117	2.0667	0.1488	23.0	0.0091
0.0410	0.4222	0.0020	0.0308	0.0181	5385	0.0218	0.7219	2.7200	0.1418	23.5	0.0101
0.0444	0.4697	0.0027	0.0364	0.0213	6968	0.0217	0.7245	3.5333	0.1335	24.2	0.0109
0.0457	0.4859	0.0030	0.0385	0.0225	7745	0.0213	0.7359	3.9333	0.1262	24.9	0.0105
0.0472	0.5034	0.0033	0.0410	0.0239	8544	0.0212	0.7349	4.3467	0.1227	25.3	0.0107
0.0491	0.5239	0.0037	0.0441	0.0257	9597	0.0211	0.7324	4.8933	0.1187	25.7	0.0109
0.0500	0.5330	0.0039	0.0456	0.0265	10240	0.0208	0.7400	5.2267	0.1140	26.2	0.0105
0.0511	0.5438	0.0042	0.0474	0.0275	10957	0.0206	0.7423	5.6000	0.1106	26.6	0.0103
0.0538	0.5680	0.0050	0.0519	0.0300	12952	0.0200	0.7549	6.6400	0.1007	27.9	0.0095
0.0551	0.5788	0.0054	0.0540	0.0312	14023	0.0196	0.7632	7.2000	0.0958	28.6	0.0090
0.0575	0.5974	0.0061	0.0580	0.0334	15745	0.0194	0.7596	8.1067	0.0918	29.2	0.0089
0.0602	0.6165	0.0068	0.0625	0.0359	17581	0.0194	0.7468	9.0800	0.0897	29.6	0.0092
0.0634	0.6368	0.0079	0.0677	0.0388	20268	0.0190	0.7481	10.507	0.0837	30.6	0.0087
0.0650	0.6462	0.0083	0.0704	0.0402	21310	0.0191	0.7359	11.067	0.0837	30.6	0.0090
0.0680	0.6626	0.0092	0.0753	0.0429	23540	0.0191	0.7221	12.267	0.0820	30.9	0.0092
0.0725	0.6844	0.0107	0.0828	0.0469	27238	0.0190	0.7090	14.267	0.0784	31.6	0.0092
0.0735	0.6889	0.0111	0.0844	0.0477	28225	0.0188	0.7098	14.800	0.0768	32.0	0.0090
0.0752	0.6963	0.0117	0.0872	0.0492	29693	0.0188	0.7053	15.600	0.0756	32.2	0.0090
0.0761	0.7000	0.0120	0.0887	0.0500	30373	0.0188	0.7005	15.973	0.0755	32.2	0.0091
0.0780	0.7076	0.0128	0.0918	0.0517	32382	0.0186	0.7031	17.067	0.0726	32.9	0.0086
0.0808	0.7181	0.0140	0.0965	0.0541	35307	0.0183	0.7039	18.667	0.0693	33.6	0.0082
0.0840	0.7293	0.0152	0.1017	0.0569	38196	0.0182	0.6945	20.267	0.0679	34.0	0.0082
0.0880	0.7420	0.0169	0.1083	0.0603	42279	0.0180	0.6902	22.533	0.0651	34.7	0.0079
0.0910	0.7509	0.0182	0.1133	0.0628	45380	0.0179	0.6867	24.267	0.0632	35.2	0.0077

Appendix A1 Flow data for the whole cross-section (Series B extension, Glasgow)

Institution :	**University of Glasgow**
Geometry :	G25T30R
Test No. :	25
Main channel sinuosity :	1.3740 (60^0)
Main channel top width :	0.2m
Main channel aspect ratio :	10.260
Main channel bank side slope :	30^0 (Trapezoidal)
Main channel cross-sectional shape :	Trapezoidal
Main channel Roughness :	Smooth
Floodplain sinuosity :	1.0
Floodplain roughness :	Rough B
Floodplain lateral slope :	0.0
Floodplain longitudinal slope :	1/1000
Meander belt width : floodplain width :	1.018m/1.650m
Flow :	Inbank / Overbank
Water temperature :	25^0C
Test date :	Winter 1995
File name:	G25T30R.xls

Depth	Dr	Qm (m^3/s)	A(m^2)	R	Re	n	F*	Qm/Qbf	f	C	k
						So		Qm =			
								0.0007			
0.0229	-0.067	0.0006	0.0035	0.0171	12062	0.0114		0.8462	0.0397	44.5	0.0004
0.0241	-0.026	0.0006	0.0037	0.0178	12857	0.0115		0.9231	0.0395	44.6	0.0004
0.0315	0.2500	0.0010	0.0146	0.0087	2682	0.0180	0.7620	1.5385	0.1238	25.2	0.0037
0.0344	0.3253	0.0014	0.0194	0.0115	3741	0.0210	0.7318	2.1538	0.1530	22.6	0.0072
0.0376	0.3925	0.0024	0.0247	0.0146	6390	0.0185	0.8703	3.6923	0.1095	26.8	0.0053
0.0417	0.4613	0.0037	0.0315	0.0185	9803	0.0181	0.9011	5.6923	0.0966	28.5	0.0054
0.0450	0.5063	0.0049	0.0369	0.0217	12932	0.0178	0.9067	7.5385	0.0894	29.6	0.0055
0.0485	0.5465	0.0063	0.0427	0.0250	16559	0.0177	0.9020	9.6923	0.0839	30.6	0.0056
0.0514	0.5752	0.0076	0.0475	0.0277	19908	0.0175	0.8993	11.692	0.0793	31.5	0.0055
0.0535	0.5938	0.0087	0.0509	0.0296	22734	0.0172	0.9061	13.385	0.0748	32.4	0.0052
0.0561	0.6146	0.0100	0.0552	0.0320	26052	0.0171	0.8986	15.385	0.0721	33.0	0.0052
0.0590	0.6355	0.0115	0.0600	0.0347	29860	0.0170	0.8871	17.692	0.0699	33.5	0.0053
0.0619	0.6543	0.0134	0.0648	0.0373	34677	0.0166	0.8971	20.615	0.0647	34.8	0.0048
0.0662	0.6787	0.0160	0.0719	0.0412	41201	0.0165	0.8833	24.615	0.0618	35.6	0.0048
0.0700	0.6977	0.0185	0.0782	0.0446	47433	0.0164	0.8741	28.462	0.0592	36.4	0.0047
0.0739	0.7149	0.0215	0.0846	0.0480	54880	0.0160	0.8765	33.077	0.0554	37.6	0.0043
0.0790	0.7347	0.0254	0.0930	0.0525	64462	0.0158	0.8679	39.077	0.0525	38.7	0.0041
0.0840	0.7516	0.0295	0.1013	0.0568	74447	0.0157	0.8611	45.385	0.0500	39.6	0.0039
0.0905	0.7706	0.0352	0.1120	0.0624	88188	0.0154	0.8539	54.154	0.0472	40.8	0.0037
0.0967	0.7862	0.0408	0.1222	0.0676	101517	0.0154	0.8448	62.769	0.0454	41.6	0.0036

Appendix A1 Flow data for the whole cross-section (Series B extension, Glasgow)

Institution :	**University of Glasgow**
Geometry :	G25N90R
Test No. :	26
Main channel sinuosity :	1.3740 (60^0)
Main channel top width :	0.2m
Main channel aspect ratio :	8.0000
Main channel bank side slope :	90^0 (Natural)
Main channel cross-sectional shape :	Natural
Main channel Roughness :	Smooth
Floodplain sinuosity :	1.0
Floodplain roughness :	Rough B
Floodplain lateral slope :	0.0
Floodplain longitudinal slope :	1/1000
Meander belt width : floodplain width :	1.018m/1.650m
Flow :	Inbank / Overbank
Water temperature :	25^0C
Test date :	Winter 1994
File name:	G25N90R.xls

Depth (m)	Dr	Qm (m^3/s)	A(m^2)	R	Re	n	F*	Qm/ Qbf	f	C	k
						So		Qm =			
								0.0008			
0.0408	-0.285	0.0004	0.0032	0.0147	8162	0.0131		0.4819	0.0553	37.7	0.0011
0.0435	-0.200	0.0005	0.0037	0.0163	9776	0.0130		0.6024	0.0521	38.8	0.0010
0.0495	-0.015	0.0008	0.0049	0.0195	14312	0.0120		0.9639	0.0418	43.3	0.0006
0.0566	0.2089	0.0014	0.0159	0.0093	3641	0.0146	0.8237	1.6747	0.0799	31.3	0.0016
0.0583	0.2492	0.0015	0.0187	0.0109	3921	0.0180	0.7413	1.8072	0.1150	26.1	0.0042
0.0620	0.3243	0.0020	0.0248	0.0144	5128	0.0224	0.6695	2.3735	0.1623	22.0	0.0099
0.0648	0.3719	0.0024	0.0294	0.0170	6331	0.0243	0.6418	2.9398	0.1801	20.9	0.0136
0.0675	0.4118	0.0033	0.0339	0.0195	8536	0.0228	0.6931	3.9759	0.1521	22.7	0.0123
0.0710	0.4565	0.0045	0.0397	0.0227	11593	0.0219	0.7268	5.4217	0.1324	24.3	0.0116
0.0778	0.5261	0.0073	0.0508	0.0289	18662	0.0204	0.7653	8.7952	0.1066	27.1	0.0103
0.0823	0.5633	0.0097	0.0582	0.0329	24672	0.0193	0.7953	11.687	0.0910	29.4	0.0088
0.0855	0.5868	0.0118	0.0636	0.0358	29903	0.0183	0.8238	14.217	0.0801	31.3	0.0074
0.0878	0.6016	0.0132	0.0673	0.0378	33366	0.0180	0.8303	15.904	0.0759	32.2	0.0070
0.0920	0.6269	0.0157	0.0743	0.0416	39497	0.0178	0.8222	18.916	0.0721	33.0	0.0069
0.0945	0.6403	0.0174	0.0784	0.0438	43651	0.0176	0.8243	20.964	0.0689	33.8	0.0066
0.0995	0.6644	0.0205	0.0867	0.0481	51143	0.0176	0.8063	24.699	0.0668	34.3	0.0067
0.1020	0.6753	0.0222	0.0908	0.0502	55231	0.0175	0.8008	26.747	0.0653	34.7	0.0067
0.1070	0.6951	0.0259	0.0991	0.0545	64081	0.0173	0.7950	31.205	0.0621	35.6	0.0065
0.1115	0.7110	0.0294	0.1065	0.0583	72383	0.0172	0.7896	35.422	0.0596	36.3	0.0063
0.1163	0.7260	0.0335	0.1143	0.0623	82050	0.0169	0.7898	40.361	0.0566	37.3	0.0059
0.1183	0.7320	0.0349	0.1177	0.0640	85288	0.0170	0.7803	42.048	0.0568	37.2	0.0062
0.1220	0.7423	0.0380	0.1238	0.0670	92492	0.0170	0.7755	45.783	0.0555	37.6	0.0061

Appendix A1 Flow data for the whole cross-section (Series B extension, Glasgow)

Institution :	**University of Glasgow**
Geometry :	G25N60R
Test No. :	27
Main channel sinuosity :	1.3740 (60^0)
Main channel top width :	0.2m
Main channel aspect ratio :	8.3000
Main channel bank side slope :	60^0 (Natural)
Main channel cross-sectional shape :	Natural
Main channel Roughness :	Smooth
Floodplain sinuosity :	1.0
Floodplain roughness :	Rough B
Floodplain lateral slope :	0.0
Floodplain longitudinal slope :	1/1000
Meander belt width : floodplain width :	1.018m/1.650m
Flow :	Inbank / Overbank
Water temperature :	25^0C
Test date :	Spring 1995
File name:	G25N60R.xls

Depth (m)	Dr	Qm (m^3/s)	A(m^2)	R	Re	n	F*	Qm/ Qbf	f	C	k
						So		Qm =	0.0008		
0.0444	-0.163	0.0006	0.0038	0.0177	12678	0.0116		0.7692	0.0401	44.2	0.0004
0.0472	-0.081	0.0007	0.0043	0.0193	14137	0.0119		0.8974	0.0413	43.6	0.0006
0.0491	-0.026	0.0008	0.0046	0.0203	14705	0.0124		0.9615	0.0444	42.0	0.0008
0.0583	0.2569	0.0016	0.0186	0.0109	4102	0.0171	0.7648	1.9872	0.1038	27.5	0.0035
0.0603	0.3000	0.0018	0.0219	0.0128	4779	0.0195	0.7260	2.3205	0.1271	24.8	0.0060
0.0631	0.3522	0.0022	0.0264	0.0155	5790	0.0222	0.6748	2.8205	0.1552	22.5	0.0100
0.0653	0.3883	0.0028	0.0301	0.0176	7350	0.0217	0.7059	3.5897	0.1426	23.5	0.0100
0.0671	0.4150	0.0033	0.0330	0.0192	8644	0.0216	0.7162	4.2308	0.1371	23.9	0.0103
0.0691	0.4421	0.0040	0.0363	0.0211	10454	0.0210	0.7427	5.1282	0.1248	25.1	0.0098
0.0719	0.4761	0.0050	0.0410	0.0237	13025	0.0205	0.7587	6.4103	0.1150	26.1	0.0096
0.0738	0.4969	0.0058	0.0441	0.0255	15075	0.0200	0.7751	7.4359	0.1068	27.1	0.0091
0.0753	0.5121	0.0066	0.0466	0.0269	17125	0.0193	0.8018	8.4615	0.0973	28.4	0.0081
0.0762	0.5209	0.0071	0.0481	0.0277	18403	0.0189	0.8162	9.1026	0.0925	29.1	0.0075
0.0791	0.5470	0.0085	0.0528	0.0304	21959	0.0185	0.8254	10.897	0.0859	30.2	0.0072
0.0825	0.5742	0.0105	0.0584	0.0335	27020	0.0177	0.8502	13.462	0.0762	32.1	0.0062
0.0845	0.5887	0.0115	0.0617	0.0353	29526	0.0177	0.8427	14.744	0.0749	32.4	0.0063
0.0861	0.5997	0.0125	0.0644	0.0367	32035	0.0174	0.8485	16.026	0.0718	33.1	0.0060
0.0898	0.6228	0.0147	0.0705	0.0400	37514	0.0172	0.8410	18.846	0.0680	34.0	0.0058
0.0903	0.6258	0.0147	0.0713	0.0405	37493	0.0176	0.8320	18.846	0.0704	33.4	0.0063
0.0920	0.6354	0.0158	0.0741	0.0420	40221	0.0174	0.8380	20.256	0.0684	33.9	0.0062
0.0936	0.6440	0.0168	0.0768	0.0434	42689	0.0173	0.8300	21.538	0.0671	34.2	0.0061
0.0963	0.6577	0.0185	0.0812	0.0458	46866	0.0173	0.8252	23.718	0.0654	34.6	0.0061
0.0977	0.6643	0.0195	0.0835	0.0470	49322	0.0172	0.8185	25.000	0.0640	35.0	0.0060
0.0996	0.6730	0.0208	0.0867	0.0487	52497	0.0171	0.8154	26.667	0.0627	35.4	0.0059
0.1004	0.6765	0.0213	0.0880	0.0493	53711	0.0171	0.8118	27.308	0.0626	35.4	0.0059
0.1033	0.6886	0.0230	0.0928	0.0519	57810	0.0173	0.8100	29.487	0.0628	35.4	0.0063
0.1062	0.6999	0.0255	0.0976	0.0544	63886	0.0169	0.8050	32.692	0.0592	36.4	0.0058
0.1078	0.7057	0.0268	0.1002	0.0557	67024	0.0168	0.8028	34.359	0.0580	36.8	0.0056
0.1091	0.7103	0.0280	0.1023	0.0568	69924	0.0166	0.8065	35.897	0.0566	37.2	0.0054
0.1135	0.7249	0.0315	0.1096	0.0606	78281	0.0165	0.7999	40.385	0.0547	37.9	0.0053
0.1148	0.7289	0.0325	0.1117	0.0617	80651	0.0165	0.7965	41.667	0.0544	38.0	0.0053
0.1210	0.7466	0.0375	0.1220	0.0669	92426	0.0165	0.7840	48.077	0.0528	38.5	0.0054
0.1235	0.7531	0.0400	0.1261	0.0689	98318	0.0164	0.7879	51.282	0.0512	39.2	0.0051

Appendix A1 Flow data for the whole cross-section (Series B extension, Glasgow)

Institution :	**University of Glasgow**
Geometry :	G25N45R
Test No. :	28
Main channel sinuosity :	1.3740 (60^0)
Main channel top width :	0.2m
Main channel aspect ratio :	8.5300
Main channel bank side slope :	45^0 (Natural)
Main channel cross-sectional shape :	Natural
Main channel Roughness :	Smooth
Floodplain sinuosity :	1.0
Floodplain roughness :	Rough B
Floodplain lateral slope :	0.0
Floodplain longitudinal slope :	1/1000
Meander belt width : floodplain width :	1.018m/1.650m
Flow :	Inbank / Overbank
Water temperature :	25^0C
Test date :	Summer 1995
File name:	G25N45R.xls

Depth (m)	Dr	Qm (m^3/s)	A(m^2)	R	Re	n	F*	Qm/ Qbf	f	C	k
						So		Qm =			
								0.0008			
0.0477	-0.064	0.0007	0.0043	0.0197	13721	0.0127		0.8800	0.0470	40.9	0.0009
0.0489	-0.031	0.0007	0.0045	0.0203	14259	0.0129		0.9333	0.0476	40.6	0.0010
0.0556	0.1914	0.0013	0.0138	0.0082	3466	0.0124	0.8778	1.7333	0.0602	36.1	0.0006
0.0583	0.2621	0.0016	0.0184	0.0109	4252	0.0167	0.7991	2.1333	0.0987	28.2	0.0031
0.0614	0.3261	0.0019	0.0234	0.0138	4899	0.0219	0.6764	2.4667	0.1569	22.4	0.0090
0.0650	0.3901	0.0026	0.0294	0.0173	6803	0.0233	0.6717	3.4400	0.1645	21.8	0.0122
0.0666	0.4145	0.0032	0.0321	0.0188	8290	0.0221	0.7160	4.2000	0.1438	23.4	0.0109
0.0712	0.4748	0.0047	0.0397	0.0231	12355	0.0211	0.7550	6.2933	0.1227	25.3	0.0104
0.0746	0.5120	0.0065	0.0453	0.0263	16870	0.0192	0.8238	8.6267	0.0976	28.4	0.0079
0.0756	0.5219	0.0070	0.0469	0.0272	18256	0.0188	0.8384	9.3467	0.0926	29.1	0.0074
0.0803	0.5637	0.0092	0.0547	0.0315	23830	0.0185	0.8382	12.267	0.0853	30.3	0.0074
0.0822	0.5786	0.0102	0.0578	0.0332	26363	0.0183	0.8404	13.600	0.0820	30.9	0.0072
0.0855	0.6022	0.0119	0.0633	0.0362	30743	0.0182	0.8352	15.920	0.0784	31.6	0.0071
0.0890	0.6245	0.0140	0.0690	0.0394	35903	0.0179	0.8343	18.667	0.0740	32.6	0.0069
0.0906	0.6339	0.0150	0.0717	0.0408	38398	0.0178	0.8342	20.000	0.0721	33.0	0.0067
0.0932	0.6482	0.0166	0.0760	0.0431	42368	0.0177	0.8291	22.133	0.0700	33.5	0.0067
0.0944	0.6544	0.0175	0.0780	0.0442	44604	0.0175	0.8334	23.333	0.0680	34.0	0.0064
0.0997	0.6794	0.0210	0.0867	0.0489	53205	0.0174	0.8211	28.000	0.0647	34.8	0.0064
0.1026	0.6917	0.0232	0.0915	0.0514	58588	0.0172	0.8210	30.933	0.0621	35.5	0.0061
0.1074	0.7100	0.0270	0.0994	0.0555	67818	0.0169	0.8193	36.000	0.0586	36.6	0.0058
0.1108	0.7217	0.0295	0.1050	0.0584	73817	0.0169	0.8090	39.333	0.0577	36.9	0.0058
0.1145	0.7334	0.0325	0.1111	0.0616	80990	0.0168	0.8035	43.333	0.0561	37.4	0.0058
0.1179	0.7433	0.0352	0.1167	0.0645	87390	0.0168	0.7956	46.933	0.0553	37.7	0.0058
0.1222	0.7548	0.0388	0.1238	0.0681	95872	0.0168	0.7885	51.733	0.0541	38.1	0.0058

Appendix A1 Flow data for the whole cross-section (Series B extension, Glasgow)

Institution :	**University of Glasgow**
Geometry :	G25N30R
Test No. :	29
Main channel sinuosity :	1.3740 (60^0)
Main channel top width :	0.2m
Main channel aspect ratio :	8.9700
Main channel bank side slope :	30^0 (Natural)
Main channel cross-sectional shape :	Natural
Main channel Roughness :	Smooth
Floodplain sinuosity :	1.0
Floodplain roughness :	Rough B
Floodplain lateral slope :	0.0
Floodplain longitudinal slope :	1/1000
Meander belt width : floodplain width :	1.018m/1.650m
Flow :	Inbank / Overbank
Water temperature :	25^0C
Test date :	Winter 1995
File name:	G25N30R.xls

Depth (m)	Dr	Qm (m^3/s)	A(m^2)	R	Re	n	F*	Qm/ Qbf	f	C	k
						So		Qm =			
								0.0007			
0.0452	-0.125	0.0006	0.0036	0.0151	10279	0.0109		0.7639	0.0377	45.6	0.0002
0.0493	-0.018	0.0007	0.0043	0.0175	12717	0.0113		0.9722	0.0384	45.2	0.0003
0.0570	0.2389	0.0014	0.0160	0.0095	3606	0.0156	0.8070	1.8750	0.0897	29.6	0.0022
0.0583	0.2720	0.0015	0.0182	0.0108	4000	0.0175	0.7727	2.0833	0.1091	26.8	0.0038
0.0620	0.3499	0.0021	0.0243	0.0143	5576	0.0206	0.7359	2.9167	0.1372	23.9	0.0076
0.0640	0.3857	0.0025	0.0276	0.0162	6623	0.0216	0.7239	3.4722	0.1439	23.4	0.0094
0.0660	0.4178	0.0033	0.0309	0.0181	8616	0.0200	0.7905	4.5278	0.1200	25.6	0.0078
0.0700	0.4728	0.0046	0.0375	0.0219	12100	0.0197	0.8109	6.3889	0.1092	26.8	0.0081
0.0750	0.5285	0.0069	0.0457	0.0266	17993	0.0184	0.8607	9.5556	0.0893	29.6	0.0068
0.0800	0.5736	0.0090	0.0540	0.0312	23401	0.0186	0.8382	12.500	0.0860	30.2	0.0074
0.0830	0.5967	0.0107	0.0589	0.0340	27725	0.0181	0.8504	14.861	0.0792	31.5	0.0068
0.0875	0.6271	0.0135	0.0663	0.0380	34800	0.0174	0.8637	18.750	0.0709	33.3	0.0061
0.0901	0.6426	0.0148	0.0706	0.0404	38037	0.0176	0.8437	20.556	0.0712	33.2	0.0065
0.0950	0.6686	0.0180	0.0787	0.0447	46004	0.0173	0.8398	25.000	0.0664	34.4	0.0062
0.1000	0.6916	0.0215	0.0870	0.0492	54638	0.0171	0.8338	29.861	0.0625	35.4	0.0059
0.1040	0.7077	0.0245	0.0936	0.0527	61982	0.0169	0.8296	34.028	0.0598	36.2	0.0057
0.1080	0.7223	0.0277	0.1002	0.0561	69764	0.0167	0.8268	38.472	0.0572	37.1	0.0055
0.1100	0.7290	0.0290	0.1035	0.0578	72874	0.0168	0.8154	40.278	0.0574	37.0	0.0057
0.1130	0.7386	0.0316	0.1084	0.0604	79142	0.0166	0.8154	43.889	0.0554	37.6	0.0055
0.1178	0.7525	0.0355	0.1163	0.0645	88437	0.0166	0.8056	49.306	0.0540	38.1	0.0055
0.1224	0.7645	0.0395	0.1239	0.0683	97903	0.0165	0.7999	54.861	0.0525	38.7	0.0054

Appendix A1 Flow data for the whole cross-section (Series B extension, Glasgow)

Institution :	**University of Glasgow**
Geometry :	G10N60R
Test No. :	30
Main channel sinuosity :	1.3740 (60^0)
Main channel top width :	0.2m
Main channel aspect ratio :	15.690
Main channel bank side slope :	60^0 (Natural)
Main channel cross-sectional shape :	Natural
Main channel Roughness :	Smooth
Floodplain sinuosity :	1.0
Floodplain roughness :	Rough B
Floodplain lateral slope :	0.0
Floodplain longitudinal slope :	1/1000
Meander belt width : floodplain width :	1.018m/1.650m
Flow :	Inbank / Overbank
Water temperature :	25^0C
Test date :	Summer 1995
File name:	G10T60R.xls

Depth (m)	Dr	Qm (m^3/s)	A(m^2)	R	Re	n	F*	Qm/ Qbf	f	C	k
						So		Qm =	0.0003		
0.0245	-0.065	0.0003	0.0024	0.0111	6137	0.0109		1.0000	0.0422	43.1	0.0002
0.0337	0.4056	0.0012	0.0169	0.0100	3058	0.0205	0.7803	3.8333	0.1526	22.7	0.0061
0.0356	0.4528	0.0015	0.0200	0.0118	3981	0.0208	0.7831	5.0000	0.1493	22.9	0.0071
0.0378	0.5000	0.0020	0.0236	0.0139	5241	0.0209	0.7851	6.6000	0.1426	23.5	0.0078
0.0388	0.5198	0.0023	0.0253	0.0149	6080	0.0203	0.8093	7.6667	0.1311	24.5	0.0074
0.0414	0.5626	0.0031	0.0296	0.0174	8170	0.0196	0.8338	10.333	0.1159	26.0	0.0070
0.0449	0.6095	0.0045	0.0354	0.0207	11811	0.0181	0.8854	15.000	0.0941	28.9	0.0057
0.0474	0.6368	0.0056	0.0394	0.0230	14659	0.0174	0.9089	18.670	0.0840	30.6	0.0051
0.0525	0.6832	0.0080	0.0479	0.0277	20813	0.0169	0.9128	26.667	0.0738	32.6	0.0047
0.0546	0.6986	0.0090	0.0513	0.0296	23359	0.0168	0.9068	30.000	0.0715	33.1	0.0047
0.0572	0.7160	0.0104	0.0556	0.0320	26912	0.0166	0.9046	34.667	0.0680	34.0	0.0046
0.0592	0.7284	0.0116	0.0590	0.0339	29947	0.0164	0.9052	38.667	0.0652	34.7	0.0044
0.0617	0.7422	0.0131	0.0631	0.0361	33722	0.0162	0.9024	43.667	0.0625	35.4	0.0043
0.0641	0.7539	0.0146	0.0670	0.0383	37483	0.0161	0.9008	48.667	0.0600	36.2	0.0041
0.0674	0.7688	0.0168	0.0725	0.0413	42966	0.0159	0.8949	56.000	0.0573	37.0	0.0040
0.0699	0.7788	0.0187	0.0766	0.0435	47690	0.0156	0.8989	62.333	0.0545	37.9	0.0037
0.0721	0.7870	0.0203	0.0803	0.0454	51641	0.0155	0.8955	67.667	0.0530	38.5	0.0036
0.0744	0.7949	0.0219	0.0841	0.0474	55567	0.0155	0.8868	73.000	0.0522	38.8	0.0036
0.0768	0.8025	0.0240	0.0880	0.0495	60731	0.0153	0.8923	80.000	0.0498	39.7	0.0034
0.0798	0.8113	0.0263	0.0930	0.0522	66327	0.0152	0.8837	87.667	0.0487	40.1	0.0034
0.0825	0.8185	0.0286	0.0974	0.0545	71909	0.0151	0.8814	95.333	0.0473	40.7	0.0032
0.0850	0.8247	0.0305	0.1016	0.0566	76473	0.0152	0.8710	101.67	0.0470	40.9	0.0033
0.0910	0.8381	0.0363	0.1115	0.0617	90410	0.0148	0.8747	121.00	0.0436	42.4	0.0029
0.1011	0.8565	0.0459	0.1281	0.0702	113055	0.0147	0.8621	153.00	0.0410	43.8	0.0028

Appendix A2: The Series B extension (1993-1996) programme in Glasgow

Measured flow data for the three zones

Test no	F/P flow depth	Q_{TOTAL} (Orifice)	Q_{bf} (Theo.)	Q_A (Integrated) (Apex)	Q_A (Integrated) (C/O)	V_{B1} (Meas.)	V_{B2} (Meas.)	Q_B (Integrated)	Q_C (Integrated)
	(m)	(m^3/s)	(m^3/s)	(m^3/s)	(m^3/s)	(m/s)	/m/s)	(m^3/s)	(m^3/s)
G75T90S	0.00833	0.0043	0.0044	0.00230	0.00220	-	-	0.0013	0.0008
G75T90S	0.025	0.0118	0.0044	0.00240	0.00252	0.223	0.215	0.0055	0.0034
G75T90S	0.05	0.028	0.0044	0.00290	0.00292	0.283	0.288	0.0146	0.0093
G75T90R	0.00833	0.0035	0.0044	0.00233	0.00249	-	-	0.0008	0.0004
G75T90R	0.025	0.0091	0.0044	0.00246	0.00228	0.172	0.182	0.0046	0.0023
G75T90R	0.03611	0.0144	0.0044	0.00270	0.00297	0.190	0.215	0.0077	0.0040
G75T90R	0.05	0.0225	0.0044	0.00270	0.00274	0.205	0.228	0.0114	0.0083
GR75T90R	0.0083	0.0028	0.003143	0.00160	0.00160	-	-	0.0007	0.0004
GR75T90R	0.01667	0.005	0.003143	0.00160	0.00160	0.114	0.134	0.0022	0.0011
GR75T90R	0.025	0.0082	0.003143	0.00176	0.00193	0.137	0.160	0.0040	0.0022
GR75T90R	0.0375	0.0138	0.003143	0.00197	0.00210	0.167	0.187	0.0070	0.0051
GR75T90R	0.05	0.02	0.003143	0.00209	0.00222	0.185	0.238	0.0116	0.0075
G75T60R	0.00833	0.0029	0.0031	0.00145	0.00158	-	-	0.0009	0.0005
G75T60R	0.025	0.0082	0.0031	0.00172	0.00177	0.155	0.168	0.0042	0.0026
G75T60R	0.0375	0.0135	0.0031	0.00190	0.00206	0.181	0.203	0.0076	0.0045
G75T60R	0.05	0.0219	0.0031	0.00203	0.00233	0.221	0.246	0.0123	0.0073
G75T45R	0.00833	0.0024	0.0023	0.00130	0.00110	-	-	0.0008	0.0005
G75T45R	0.025	0.0076	0.0023	0.00115	0.00125	0.149	0.155	0.0039	0.0022
G75T45R	0.0361	0.0132	0.0023	0.00152	0.00165	0.175	0.203	0.0073	0.0045
G75T45R	0.05	0.0215	0.0023	0.00169	0.00212	0.196	0.236	0.0116	0.0080
G75T45R	0.075	0.0404	0.0023	0.00191	0.00250	0.256	0.332	0.0242	0.0154
G75T45RN	0.00833	0.00164	0.0023	0.00126	0.00114	-	-	0.0005	0
G75T45RN	0.025	0.0043	0.0023	0.00121	0.00130	0.117	0.131	0.0033	0
G75T45RN	0.05	0.0113	0.0023	0.00145	0.00158	0.169	0.201	0.0099	0
G75T37R	0.00833	0.0021	0.0017	0.00095	0.00085	-	-	0.0008	0.0004
G75T37R	0.01667	0.004	0.0017	0.00095	0.00095	0.102	0.111	0.0019	0.0012
G75T37R	0.025	0.0073	0.0017	0.00089	0.00092	0.143	0.151	0.0038	0.0023
G75T37R	0.0375	0.0134	0.0017	0.00110	0.00120	0.171	0.199	0.0074	0.0045
G75T37R	0.05	0.0216	0.0017	0.00120	0.00136	0.209	0.249	0.0123	0.0076
G50T90R	0.00833	0.0025	0.0026	0.00151	0.00160	-	-	0.0005	0.0004
G50T90R	0.01667	0.00477	0.0026	0.00138	0.00125	0.116	0.126	0.0021	0.0012
G50T90R	0.024	0.008	0.0026	0.00166	0.00158	0.163	0.172	0.0042	0.0025
G50T90R	0.0333	0.0123	0.0026	0.00167	0.00158	0.182	0.192	0.0064	0.0043

Appendix A2 Flow data for the individual zones (Series B extension, Glasgow)

Test no	F/P flow depth	Q_{TOTAL} (Orifice)	Q_{bf} (Theo.)	Q_A (Integrated) (Apex)	Q_A (Integrated) (C/O)	V_{B1} (Meas.)	V_{B2} (Meas.)	Q_B (Integrated)	Q_C (Integrated)
	(m)	(m^3/s)	(m^3/s)	(m^3/s)	(m^3/s)	(m/s)	/m/s)	(m^3/s)	(m^3/s)
G50T60RA	0.00833	0.0018	0.0023	0.00144	0.00140	-	-	0.0004	0.0001
G50T60RA	0.0175	0.0033	0.0023	0.00124	0.00110	0.107	0.114	0.0020	0.0003
G50T60RA	0.0285	0.0069	0.0023	0.00135	0.00140	0.148	0.161	0.0046	0.0008
G50T60RA	0.0525	0.0166	0.0023	0.00160	0.00174	0.193	0.235	0.0121	0.0021
G50T60R	0.0065	0.002	0.0022	0.00130	0.00132	-	-	0.0004	0.0003
G50T60R	0.0167	0.00478	0.0022	0.00132	0.00114	0.115	0.125	0.0021	0.0014
G50T60R	0.024	0.0077	0.0022	0.00120	0.0012	0.147	0.158	0.0038	0.0022
G50T60R	0.0333	0.0123	0.0022	0.00150	0.00145	0.199	0.215	0.0072	0.0045
G50T60R	0.056	0.0265	0.0022	0.00168	0.00174	0.242	0.290	0.0160	0.0105
G50T45R	0.006	0.0019	0.0019	0.00119	0.00113	-	-	0.0005	0.0003
G50T45R	0.01667	0.0041	0.0019	0.00106	0.00098	0.121	0.125	0.0021	0.0013
G50T45R	0.024	0.0073	0.0019	0.00112	0.00104	0.160	0.173	0.0042	0.0023
G50T45R	0.0333	0.0119	0.0019	0.00113	0.00114	0.172	0.188	0.0063	0.0038
G50T45R	0.05	0.0219	0.0019	0.00143	0.00147	0.232	0.263	0.0131	0.0083
G50T30R	0.00833	0.00162	0.0013	0.00082	0.00072	-	-	0.0005	0.0004
G50T30R	0.01667	0.00404	0.0013	0.00076	0.00065	0.130	0.130	0.0022	0.0013
G50T30R	0.024	0.0071	0.0013	0.00089	0.00073	0.162	0.174	0.0042	0.0025
G50T30R	0.0333	0.0119	0.0013	0.00094	0.00089	0.185	0.218	0.0072	0.0044
G50T30R	0.05	0.0224	0.0013	0.00111	0.00103	0.217	0.280	0.0136	0.0083
G50N90R	0.00833	0.0018	0.0016	0.00072	0.00075	-	-	0.0007	0.0004
G50N90R	0.01667	0.00347	0.0016	0.00095	0.00095	0.101	0.103	0.0017	0.0009
G50N90R	0.025	0.0067	0.0016	0.00099	0.00106	0.127	0.142	0.0035	0.0022
G50N90R	0.0375	0.0127	0.0016	0.00102	0.00110	0.168	0.179	0.0068	0.0045
G50N90R	0.05	0.02	0.0016	0.00115	0.00120	0.189	0.210	0.0105	0.0075
G50N60R	0.00833	0.0019	0.0015	0.00080	0.00080	-	-	0.0007	0.0004
G50N60R	0.025	0.0071	0.0015	0.00095	0.00090	0.155	0.155	0.0039	0.0024
G50N60R	0.0361	0.0128	0.0015	0.00108	0.00111	0.185	0.199	0.0072	0.0043
G50N60R	0.05	0.0211	0.0015	0.00118	0.00121	0.202	0.231	0.0115	0.0077
G50N45R	0.00833	0.0019	0.0015	0.00080	0.00096	-	-	0.0007	0.0004
G50N45R	0.01667	0.0034	0.0015	0.00090	0.00080	0.101	0.103	0.0017	0.0009
G50N45R	0.025	0.0074	0.0015	0.00106	0.000946	0.151	0.156	0.0039	0.0023
G50N45R	0.0361	0.0127	0.0015	0.00110	0.00100	0.178	0.199	0.0072	0.0037
G50N45R	0.05	0.0212	0.0015	0.00120	0.00115	0.204	0.225	0.0112	0.0077
G50N45R	0.075	0.0407	0.0015	0.00156	0.00143	0.255	0.302	0.0224	0.0146

Appendix A2 Flow data for the individual zones (Series B extension, Glasgow)

Test no	F/P flow depth	Q_{TOTAL} (Orifice)	Q_{bf} (Theo.)	Q_A (Integrated) (Apex)	Q_A (Integrated) (C/O)	V_{B1} (Meas.)	V_{B2} (Meas.)	Q_B (Integrated)	Q_C (Integrated)
	(m)	(m^3/s)	(m^3/s)	(m^3/s)	(m^3/s)	(m/s)	/m/s)	(m^3/s)	(m^3/s)
G25T90R	0.00833	0.0015	0.0009	0.00049	0.00038	-	-	0.0007	0.0004
G25T90R	0.01667	0.0033	0.0009	0.00051	0.00045	0.102	0.103	0.0017	0.0010
G25T90R	0.025	0.0065	0.0009	0.00058	0.00048	0.131	0.137	0.0035	0.0022
G25T90R	0.0375	0.0129	0.0009	0.00076	0.00064	0.190	0.209	0.0078	0.0047
G25T90R	0.05	0.0205	0.0009	0.00082	0.00066	0.206	0.233	0.0116	0.0071
G25T60R	0.00833	0.0014	0.0008	0.00047	0.00035	-	-	0.0006	0.0004
G25T60R	0.01667	0.0033	0.0008	0.00052	0.00041	0.107	0.109	0.0018	0.0010
G25T60R	0.025	0.0065	0.0008	0.00064	0.00053	0.149	0.152	0.0039	0.0023
G25T60R	0.0375	0.0129	0.0008	0.00072	0.00059	0.187	0.210	0.0078	0.0047
G25T60R	0.05	0.0205	0.0008	0.00081	0.00070	0.211	0.253	0.0125	0.0077
G25T45R	0.00833	0.0014	0.0008	0.00049	0.00037	-	-	0.0006	0.0004
G25T45R	0.01667	0.0035	0.0008	0.00051	0.00039	0.113	0.115	0.0019	0.0011
G25T45R	0.025	0.0069	0.0008	0.00060	0.00045	0.152	0.160	0.0040	0.0023
G25T45R	0.05	0.0219	0.0008	0.00071	0.00060	0.219	0.251	0.0125	0.0075
G25T45S	0.00833	0.0017	0.0008	0.00034	0.00039	-	-	0.0008	0.0005
G25T45S	0.01667	0.0048	0.0008	0.00040	0.00039	0.146	0.151	0.0025	0.0016
G25T45S	0.025	0.0091	0.0008	0.00044	0.00053	0.203	0.211	0.0053	0.0034
G25T45S	0.05	0.0261	0.0008	0.00052	0.00068	0.255	0.302	0.0149	0.0091
G25T45SN	0.00833	0.0015	0.0008	0.00038	0.00045	-	-	0.0012	0
G25T45SN	0.01667	0.0029	0.0008	0.00036	0.00044	0.152	0.157	0.0026	0
G25T45SN	0.025	0.0055	0.0008	0.00040	0.00051	0.175	0.204	0.005	0
G25T45SN	0.05	0.0144	0.0008	0.00052	0.00063	0.232	0.294	0.0143	0
G25T45RN	0.00833	0.0012	0.0008	0.00044	0.00035	-	-	0.0008	0
G25T45RN	0.01667	0.0021	0.0008	0.00048	0.00038	0.104	0.110	0.0018	0
G25T45RN	0.025	0.0039	0.0008	0.00050	0.00040	0.131	0.136	0.0034	0
G25T45RN	0.05	0.0116	0.0008	0.00067	0.00052	0.179	0.227	0.0111	0
G25N90R	0.00833	0.0015	0.0008	0.00049	0.00034	-	-	0.0007	0.0004
G25N90R	0.012	0.002	0.0008	0.00048	0.00038	-	-	0.0010	0.0006
G25N90R	0.01667	0.003	0.0008	0.00057	0.00040	0.105	0.107	0.0018	0.0009
G25N90R	0.025	0.0061	0.0008	0.00060	0.00047	0.139	0.149	0.0037	0.0021
G25N90R	0.0375	0.0131	0.0008	0.00063	0.00051	0.204	0.212	0.0080	0.0047
G25N60R	0.00833	0.0016	0.0008	0.00040	0.00034	-	-	0.0007	0.0004
G25N60R	0.01667	0.0032	0.0008	0.00050	0.00045	0.111	0.115	0.0019	0.0010
G25N60R	0.025	0.0065	0.0008	0.00059	0.00048	0.157	0.164	0.0041	0.0023
G25N60R	0.0375	0.0133	0.0008	0.00071	0.00060	0.205	0.218	0.0082	0.0049
G25N60R	0.05	0.021	0.0008	0.00071	0.00064	0.233	0.253	0.0127	0.0075

Appendix A2 Flow data for the individual zones (Series B extension, Glasgow)

Test no	F/P flow depth	Q_{TOTAL} (Orifice)	Q_{bf} (Theo.)	Q_A (Integrated) (Apex)	Q_A (Integrated) (C/O)	V_{B1} (Meas.)	V_{B2} (Meas.)	Q_B (Integrated)	Q_C (Integrated)
	(m)	(m^3/s)	(m^3/s)	(m^3/s)	(m^3/s)	(m/s)	/m/s)	(m^3/s)	(m^3/s)
G25N45R	0.00833	0.0016	0.0008	0.00046	0.00037	-	-	0.0007	0.0004
G25N45R	0.01667	0.0032	0.0008	0.00052	0.00041	0.100	0.111	0.0018	0.0011
G25N45R	0.025	0.0068	0.0008	0.00059	0.00044	0.141	0.158	0.0039	0.0022
G25N45R	0.05	0.0214	0.0008	0.00079	0.00057	0.221	0.251	0.0125	0.0073
G25N30R	0.00833	0.0015	0.0007	0.00049	0.00030	-	-	0.0007	0.0004
G25N30R	0.012	0.0021	0.0007	0.00043	0.00033	-	-	0.0011	0.0007
G25N30R	0.01667	0.0034	0.0007	0.00042	0.00035	0.099	0.104	0.0017	0.0011
G25N30R	0.025	0.0069	0.0007	0.00061	0.00038	0.152	0.175	0.0043	0.0024
G25N30R	0.0375	0.0135	0.0007	0.00071	0.00040	0.180	0.215	0.0079	0.0046

Appendix A3: Papers published by the author

Using Artificial Neural Networks in Meandering Compound Channels

(IAHR Congress 1997, San Francisco)

BREAC MacLEOD and ALAN ERVINE
University of Glasgow, Glasgow, UK

Summary

This paper describes the development of an Artificial Neural Network (ANN) model to predict the conveyance or discharge capacity of meandering compound channels. An ANN model was trained to approximate the functional relationship between discharge capacity and nine major parameters which influence flow behaviour in meandering compound channels. The training data which exhibits this functional relationship was collated from a range of experimental data sets which have been compiled world-wide. The final training set incorporates data from both large and small scale model experiments as well as field data. The resulting ANN model is at least as good, if not better than any deterministic models developed for this purpose.

Introduction

When a meandering river channel flows overbank, a complex three dimensional mixing process occurs between channel and flood plain, Ervine et al [1]. The difficulties in estimating the stage-discharge relationship for such an overbank flow are well documented. The most successful method developed yet is that of James and Wark [2] who divided the meandering compound channel into 4 flow zones and applied theoretical discharge prediction formulations with empirical adjustments to determine the zonal discharge capacities. The authors have used a different approach and have trained an ANN to approximate the functional relationship between the total discharge capacity of a meandering compound channel and nine major parameters which influence flow behaviour. ANN models have been implemented in many fields as diverse as finance and sociology. Recently a number of applications have been proposed in the field of hydraulic engineering. Minns [3] used a neural network to approximate the bed concentration of suspended sediment and Grubert [4] used ANN to approximate the critical velocity at which interfacial mixing takes place in stratified flow.

The operational characteristics of an ANN

An ANN is an electronic artifice which is designed to mimic the pattern recognition processes exhibited by the human brain. The biological neurons are represented by a set of processing units (nodes) which are arranged in layers and connected to each other by weighted links (representing biological synapses), as shown in Fig 1. The operational characteristics of the nodes are set constant and are chosen to deliver output signals which fall within a specified range of values. The nodes sum the incoming signals and perform a functional transformation on the results to produce the output signals. The training data is presented in pairs to the ANN. Each training pair consists of a set of input and output (target) vectors. The input vectors in the discharge capacity prediction problem comprised the geometric and flow condition parameters in

each of the compound channels. The output vectors were equal to the magnitude of discharge capacity.

The output values which are produced when the input vectors are presented to and processed by the ANN are compared with the target vectors. The ANN is "trained" so that the sum of error between the ANN output values and the target vectors is minimised for the complete set of input values. The values of the weighted links are adjusted using the back-propagation algorithm to train the ANN, as described by Haykin [4].

Experimental Data

The experimental data used in the ANN model have been derived from eight experimental studies into meandering compound flows world-wide. Field data from the River Roding UK, Sellin et al [6] have been used. Large scale flume data from the Flood Channel Facility HR Wallingford, Wark [7] and Vicksburg [8] have been used. Smaller scale flume data from Toebes and Sooky [9]; Kiely [10], Willetts and Hardwick [11] have been used. The most extensive data sets have been collected at Glasgow and Aberdeen Universities (1993-96). They each investigated more than twenty different configurations of meandering compound flows, Macleod [12] and Rameshwaran [13].

Eleven major non-dimensional parameters affecting meandering compound flows have been identified:-

1. Sinuosity of the main channel (r).
2. Relative boundary roughness of flood plain/main channel (f').
3. Meander belt width relative to total floodway width (MW).
4. Aspect ratio of the main channel (AR).
5. Side slopes of the main channel (SS).
6. Cross-sectional shape of the main channel (X).
7. The relative overbank flow depth (RD).
8. Relative Reynolds numbers, flood plain/main channel (Re').
9. Longitudinal bed slope (FL)
10. Lateral slope of flood plain towards the main channel (SL).
11. Sinuosity of the upper flood plain banks (FS).

An absence of data on the last two parameters meant that the neural network model was trained using nine parameters only. Discharge capacity of the compound channel is quantified by a non-dimensional measure F* defined in detail in Ervine et al [1]. F* is the actual discharge in a meandering compound flow, divided by a theoretical discharge, based on bed friction considerations only. In effect it is a measure of channel-flood plain interaction. The resulting equation is of the form

$$F^* = f\left(RD, Re', f', r, FL, Mw, AR, SS, X\right) \qquad (1)$$

During the early stages of data preparation, coding and validation it was decided to sub-divide the available data pairs into two separate groups. One sub-group was used to train the ANN functional approximator and the other data sub-set was used to test the ANN. The test data was selected so that it contained a representative set of data pairs which were derived from a variety model results with a full range of possible geometric configurations. The test data was chosen so that enough data pairs remained to comprise an adequate training data set. Ruelle [14] recommended that a minimum of 1024 data pairs were needed to train an ANN with an input parameter dimensionality of 9. The final training set comprised 1400 data pairs which easily exceeded this minimum number and was therefore adequate.

Results

A 3 layer Perceptron model was chosen as the optimal ANN architecture. This ANN was constructed and trained with the back-propagation algorithm using the MATLAB Neural Networks Toolbox (1993) and supported on a Viglen 4DX266 PC. The complete set of training pairs had to be presented many times (epochs) to the ANN before suitable errors values were achieved. The optimal ANN required 8,000 epochs to achieve a suitable output error. One epoch is the process of presenting the complete training set once to the ANN and adjusting all weighted links accordingly.

Fig. 2 shows the comparison between the actual and ANN output values of F* for the meandering compound flows which was obtained for the optimal ANN during training. The error spread ±10% with an RMS error value of 4%, which is satisfactory considering the range of experimental error possible in the initial measurements.

Fig. 3 shows the result of the neural network model applied to the test data (the data not used for training). The result is satisfactory, with a spread of data not significantly greater than the training data.

The application of the neural network model to three different compound flow situations is shown in Figs 4 to 6. Fig. 4 plots the overbank stage-discharge relationship for a smaller scale model, quasi-natural cross-section and roughened flood plains. Fig. 5 reveals the measured and predicted stage-discharge relationship for a large scale model at HR Wallingford, with flow rates up to 1 m^3/s. Fig. 6 reveals the correlation, for a natural river channel (River Roding, UK) with vegetation on the flood plains cut. It is clear that model data is well predicted using ANN, but less clear for field data where the value of boundary roughness coefficient is not accurately known at every flow depth.

Conclusions

(i) The authors have shown it is possible to develop an artificial neural network model to handle the complexities of meandering compound flows.

(ii) The model is available on the World Wide Web on http://www.civil.gla.ac.uk/

(iii) The model predicts stage and discharge in a meandering compound channel to an accuracy of ±10%.

(iv) The model accuracy for field data depends on good estimates of the boundary friction factors for both river and flood plains.

Acknowledgements

The authors acknowledge the input of the Aberdeen team (Prof. Willetts and Mr. Rameshwaran) and the Bristol team (Prof. Sellin and Ms. Wilson). The research was funded by EPSRC Grant GR/J41048.

References

1. Ervine D.A. et al [1993] 'Factors affecting conveyance in meandering compound flows', Journal of Hydraulic Engineering, Vol. 119, No 12, December, pp 1383 - 1398.
2. James C. and Wark J.B.[1994] 'An application of a new procedure for estimating discharges in meandering overbank flows to field data', Proc. of the 2nd International Conference on River Flood Hydraulics, J Wiley and sons, pp 405 - 414.
3. Minns A.W. [1995] 'Analysis of experimental data using artificial neural networks', Proceedings of IAHR Conference HYDRA 2000, London, 1995, pp 218 - 223.
4. Grubert J.P. [1995] 'Application of neural networks in stratified flow stability analysis', Journal of Hydraulic engineering, Vol. 121, No 7., July.

5. Haykin S [1995] 'Neural Networks: A comprehensive introduction', Maxwell Macmillan International, New York.
6. Sellin R.H.J, Giles A and Beeston D.P (1990) 'Post-Implementation Appraisal of a Two Stage Channel in the River Roding', Jrnl IWEM, 1990, 4, April.
7. Wark J B [1993] - 'Discharge assessment in straight and meandering compound channels', Ph.D. Thesis, University of Glasgow.
8. Vicksburg [1956] 'Hydraulic Capacity of Meandering Channels in Straight Floodways', Corps of Engineers, US Army, Vicksburg, Mississippi, CWL Item 807.
9. Toebes G.H and Sooky A.A. [1967] 'Hydraulics of Meandering Rivers with Flood Plains', Proceedings of the ASCE, Vol. 93, No WW2, pp 213 - 237.
10. Kiely, G.K.. [1990] 'An experimental study of overbank flow in straight and meandering channels', Ph.D. Thesis, University of Cork.
11. Willetts B.B. and Hardwick R.I. [1993] 'Stage Dependency for Overbank Flow in Meandering Channels', Proceedings of the ICE., Water and Maritime , v101, pp 4554.
12. Macleod B [1997] 'The prediction of discharge capacity in meandering compound channels', Ph.D. Thesis, to be presented to the University of Glasgow.
13. Rameshwaran, P. and Willetts, B.B (1996) Personal Communication.
14. Ruelle D [1989] 'Chaotic evolution and strange attractors'. New York: Cambridge University Press.

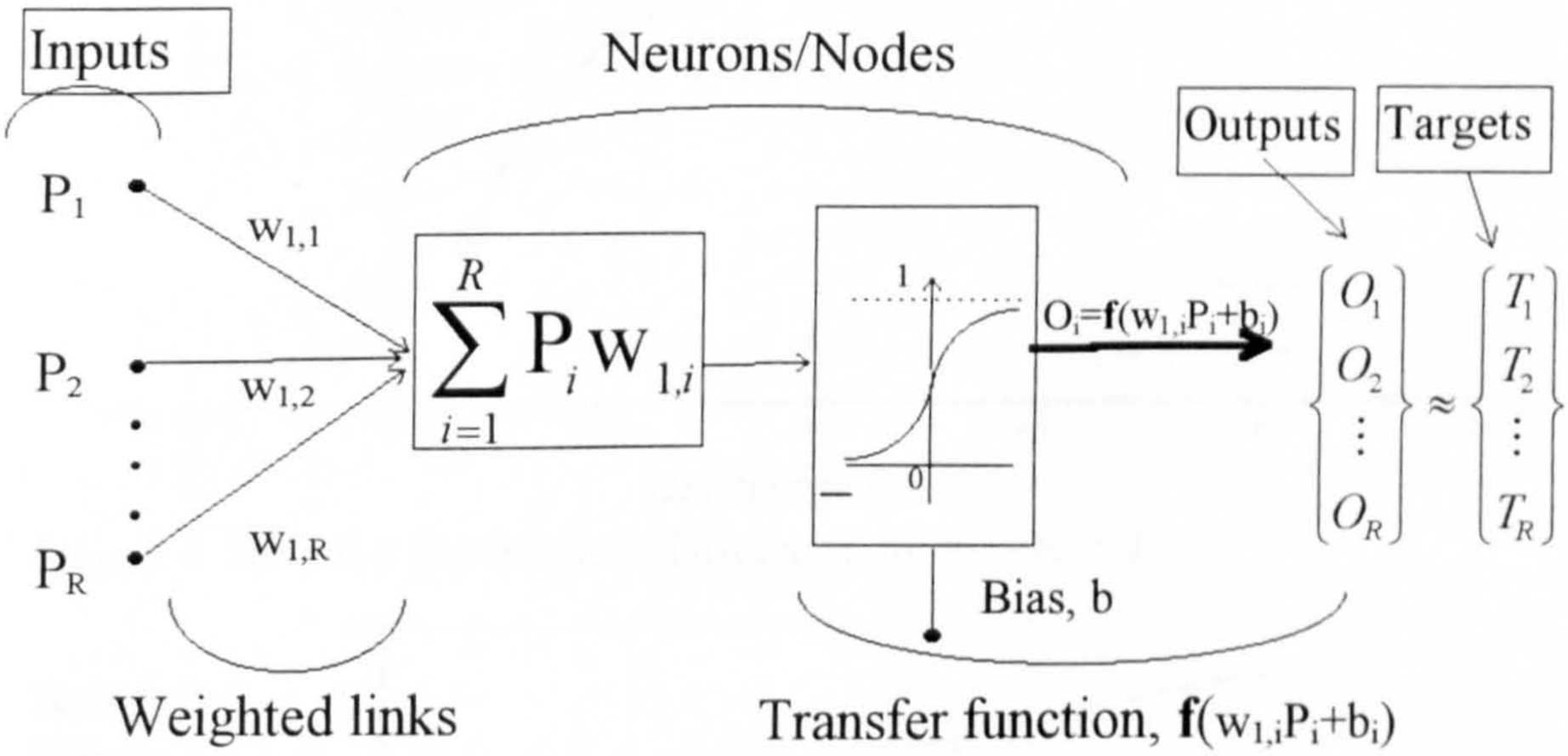

Figure 1 An Artificial Neural Network: The nodes and weighted links

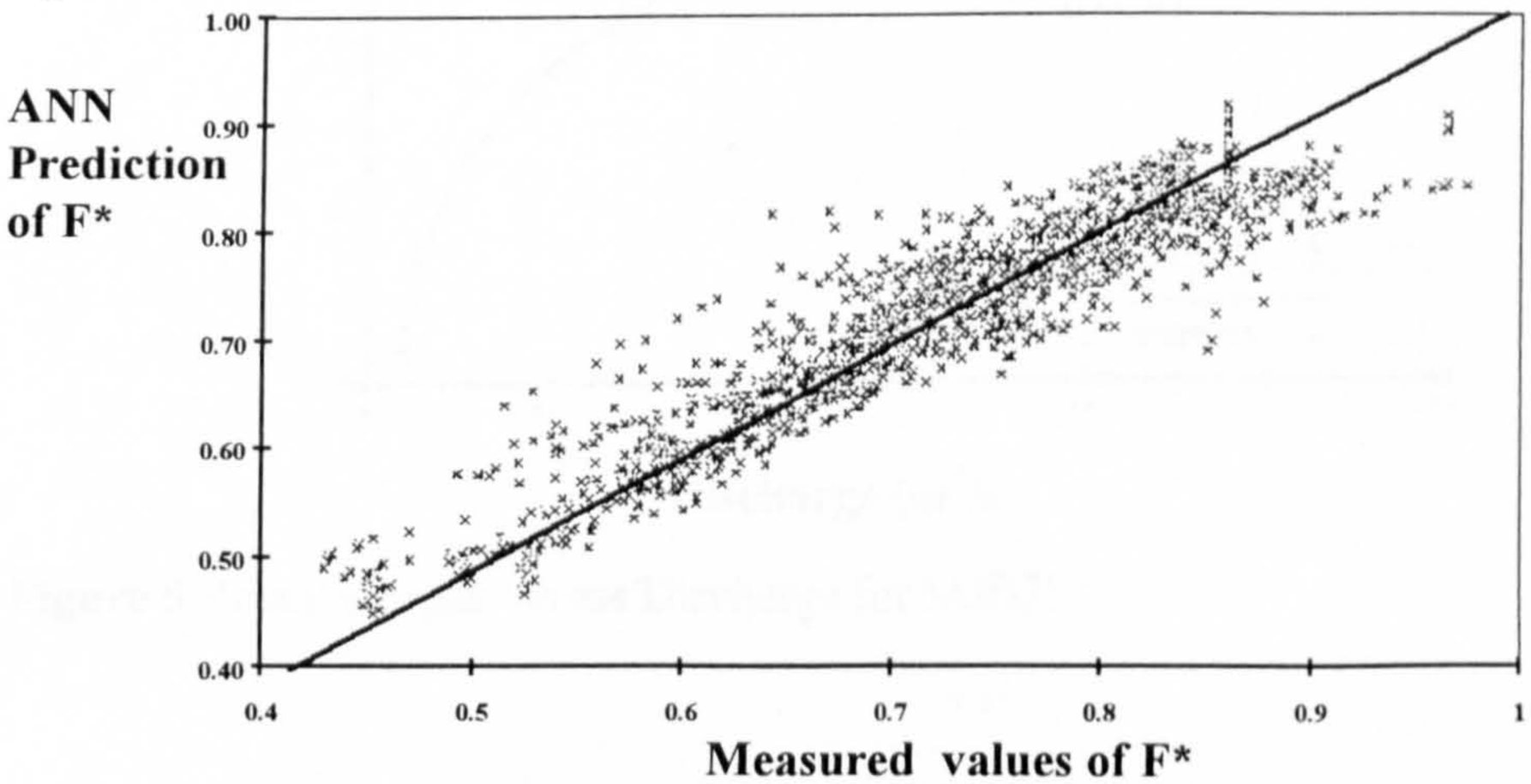

Figure 2 Target F* values versus F* values predicted using the ANN: Training data

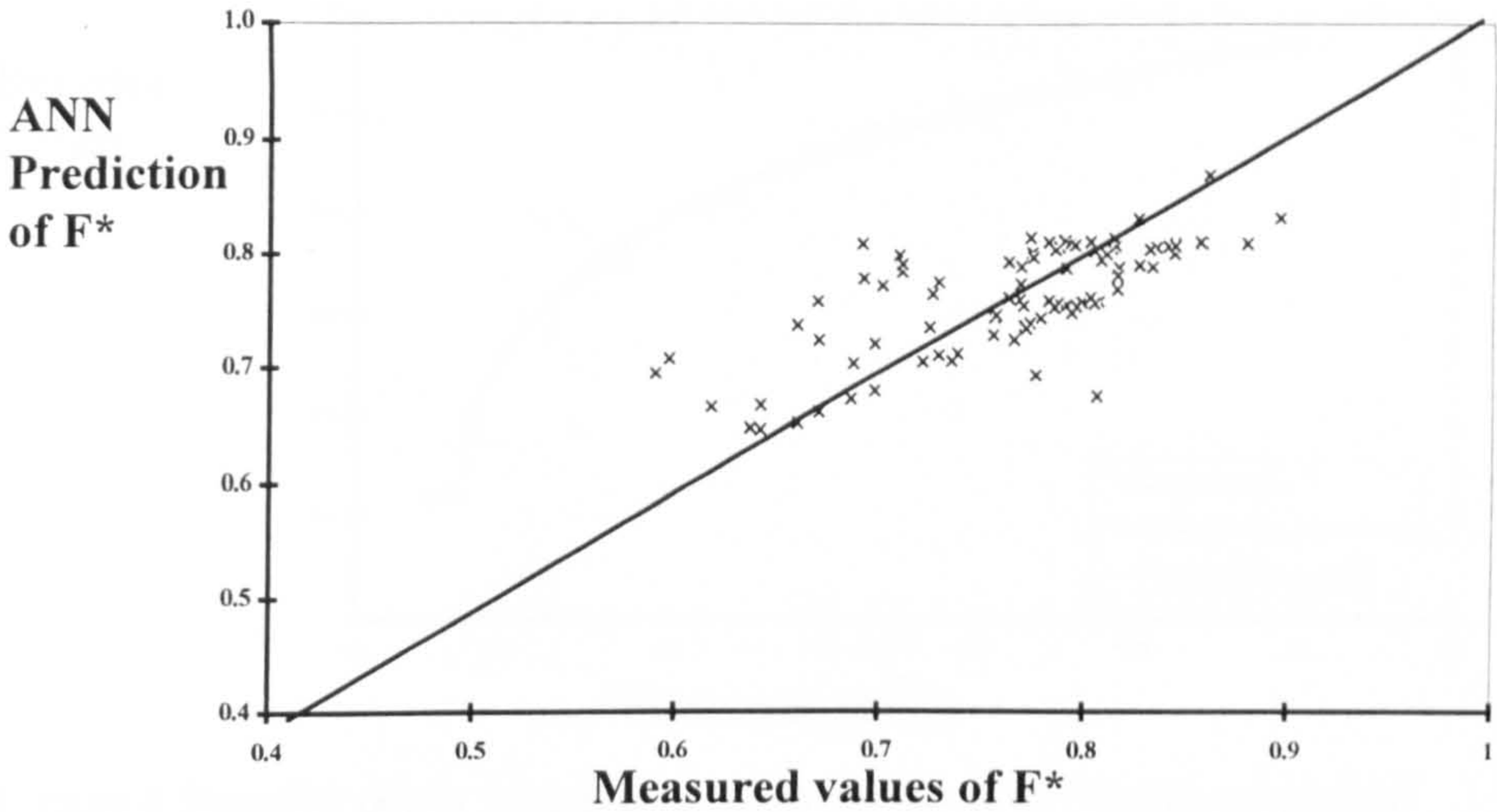

Figure 3 Measured F* values versus F* values predicted using the ANN: Test data

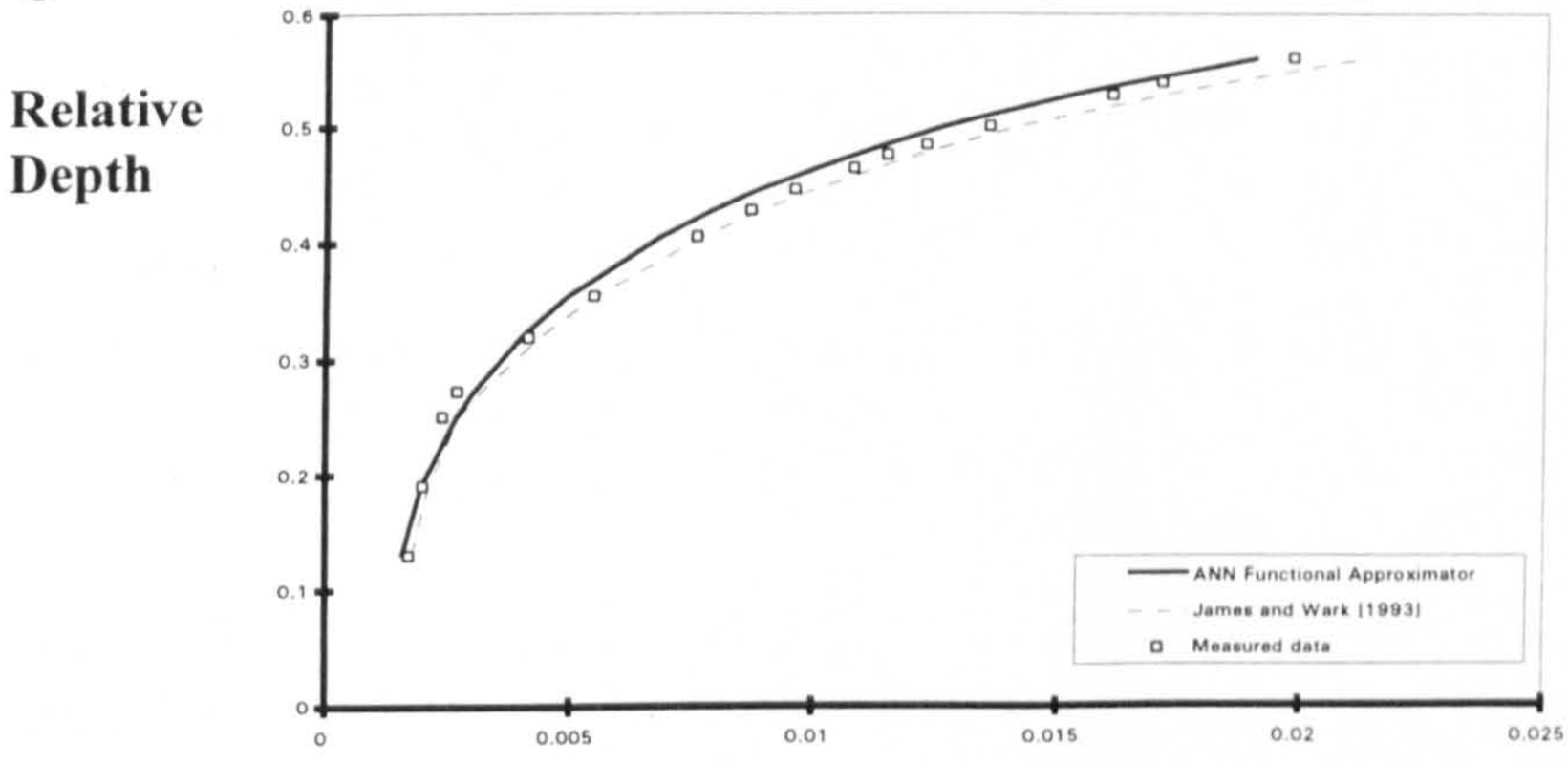

Figure 4 Relative depth versus Discharge for G50N45R

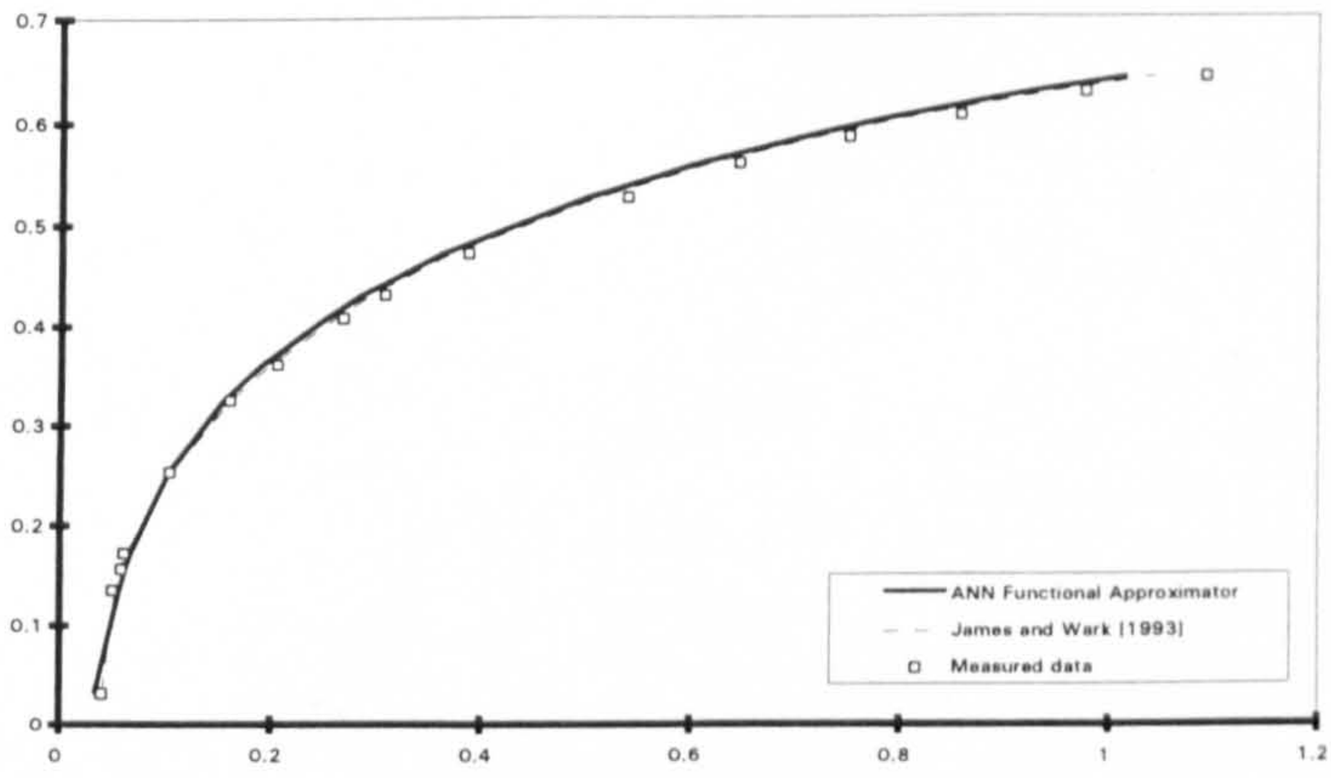

Figure 5 Relative depth versus Discharge for SDB25

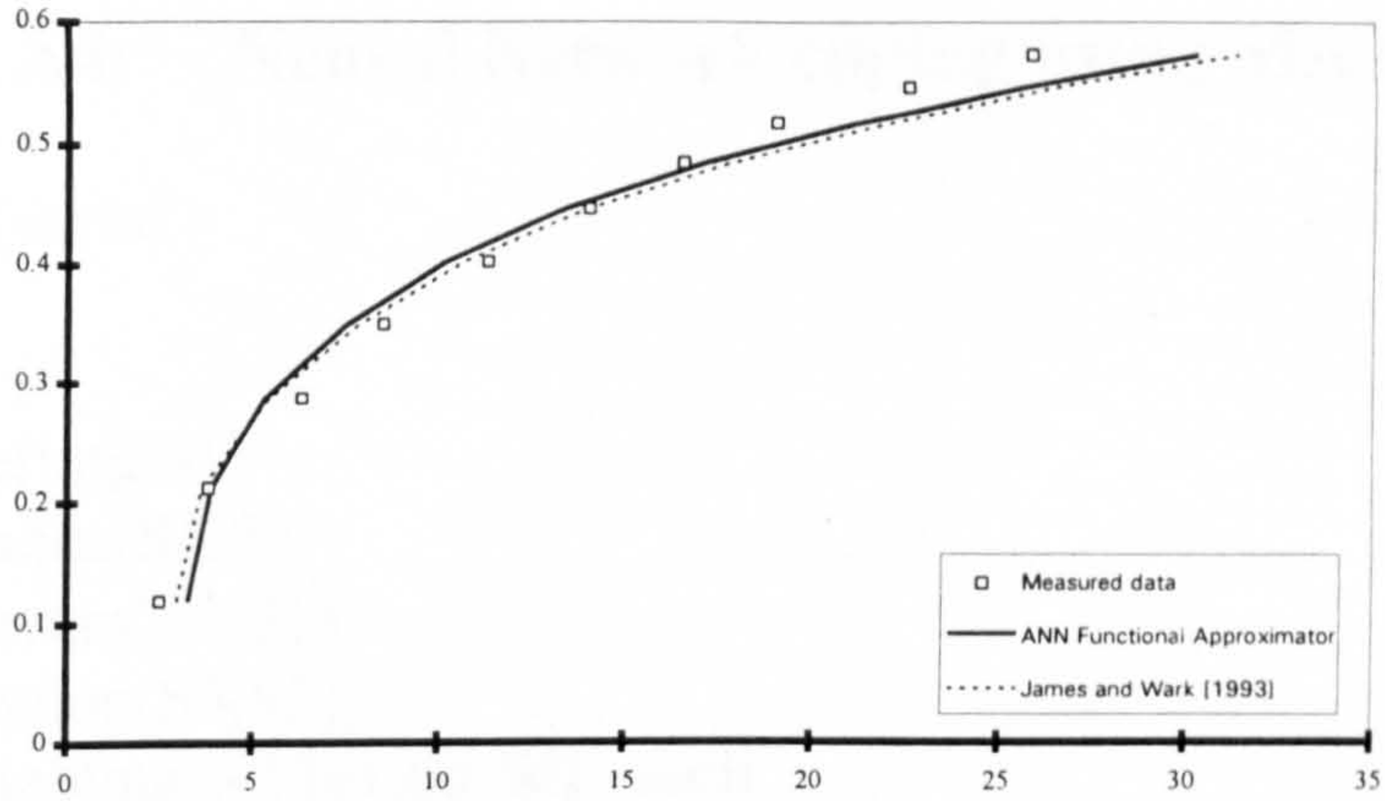

Figure 6 Relative depth versus Discharge for RodCut (Cut flood plains)

Appendix A4: Neural Network coding using MATLAB

```
[R,Q] = size(varis1)
S1 = 12
S2 = 7
[S3,Q] = size(target1)
[W1,B1] = rands(S1,R)
[W2,B2] = nwtan(S2,S1)
[W3,B3] = nwlog(S3,S2)
save h:\1matlab\mat\v12a1.txt W1 -ascii
save h:\1matlab\mat\v12a2.txt W2 -ascii
save h:\1matlab\mat\v12a3.txt W3 -ascii
A1 = purelin(W1*varis1,B1)
A2 = tansig(W2*A1,B2)
A3 = logsig(W3*A2,B3)
disp_freq = 10
momentum = 0.95
max_epoch = 8000
err_goal = 0.001
lr = 0.0005
lr_inc = 1.05
lr_dec = 0.7
err_ratio = 1.04
TP = [disp_freq max_epoch err_goal lr lr_inc lr_dec momentum err_ratio]
[W1,B1,W2,B2,W3,B3,epochs,TR] =
trainbpx(W1,B1,'purelin',W2,B2,'tansig',W3,B3,'logsig',varis1,target1,TP)
A1 = purelin(W1*varis1,B1)
A2 = tansig(W2*A1,B2)
A3 = logsig(W3*A2,B3)
save h:\1matlab\mat\v12a.mat
```